AGGREGATION OF NATURAL COLLOIDAL PARTICLES UNDER SOLAR IRRADIATION

by

Didem Sağlık

B.Sc. in Environmental Engineering, Yildiz Technical University, 2014

Submitted to the Institute of Environmental Sciences

in partial fulfillment of the requirements for the degree of

Master of Science

in

Environmental Technology

Boğaziçi University

2021

AGGREGATION OF NATURAL COLLOIDAL PARTICLES UNDER SOLAR IRRADIATION

APPROVED BY:

Prof. Dr. Miray Bekbölet Thesis Advisor	……...
Prof. Dr. Burak Demirel	……
Assoc. Prof. Dr. Hatice İnan	…….

DATE OF APPROVAL: 22/11/2021

Dedicated to my family…

ACKNOWLEDGEMENTS

I wish to express my sincere gratitude to my thesis advisor Prof. Dr. Miray Bekbölet for her precious guidance, limitless support, patience and valuable contribution throughout this study. She provided me with many opportunities and valuable scientific and personal experiences. It was an honor to study with her. I am so happy to have a chance to study with her due to her admirable perspective on life and magnifical scientific experiences. She is a very special person who I will never forget throughout my life.

I would also like to express my appreciation to the members of my thesis jury; Prof. Dr. Burak Demirel and Assoc. Prof. Dr. Hatice İnan for their valuable time, comments and contributions.

The financial support provided by Boğaziçi University Research Fund to the project 14060 is greatly acknowledged.

I sincerely thank to my colleagues Dr. Nazmiye Cemre Birben, Dr. Nazlı Türkten, Ayşe Hazal Pekcan Çetin, Ezgi Lale for their sharing knowledge with me particularly in laboratory work, never-ending support and friendship.

I would like to thank to my beloved husband Enes Kanpara for his unconditional love, endless patience and encouragement. Last but not least, I am also grateful to my parents Fatma Sağlık and Nurettin Recep Sağlık who believed in me and was always by my side with their patience, tremendouos support, and constant encouragement during my educational life. I am so glad to have you.

ABSTRACT

AGGREGATION OF NATURAL COLLOIDAL PARTICLES UNDER SOLAR IRRADIATION

Aggregation/agglomeration of nanoparticles affects their fate and transport in natural waters. Although nanoparticles behave as colloidal matter expressing aggregation/agglomeration properties under natural water conditions, the role of aggregation/agglomeration during photocatalysis has not been demonstrated clearly so far. The main objective of this study could be described as assessment of the colloidal behavior of the binary system *i.e.*, NOM representative organics and nanoparticles representative of photocatalyst specimens described by following basic experimental procedures prior to, during and under post photo-treatment conditions. To fulfill this aim, dynamic light scattering, sedimentation and turbidity experiments were performed. Aggregation and/or agglomeration of TiO_2 nanoparticles were assessed by using the above indicated physico-chemical parameters in relation to water matrix effects as well as photocatalytic removal efficiencies. Aggregation and/or agglomeration behavior of both matrix components provided information on expected reactivity under irradiation during photocatalysis. Overall evaluation of the systems provided information both during photocatalysis as well as light induced reactions under environmental conditions. Therefore, a broader insight was deduced on the fate of nanoparticles through photocatalysis.

ÖZET

DOĞAL KOLLOİDAL PARTİKÜLLERİN GÜNEŞ IŞINLAMASI ALTINDA KÜMELEŞMESİ

Nanopartiküllerin kümeleşme/yığılmaları doğal sularda geleceklerini ve taşınmalarını etkiler. Nanopartiküller doğal su koşulları altında kümeleşme/yığılma özellikleri ifade eden kolloidal madde gibi davransalar da, fotokataliz sırasında kümeleşme/yığılmanın rolü şu ana kadar olarak gösterilmemiştir. Bu çalışmanın temel amacı, ikili sistemin, yani ışık muamelesi koşulları öncesinde, esnasında ve hemen sonrasında temel deneysel prosedürler takip edilerek tanımlanan fotokatalist numunelerini temsil eden NOM temsili organikler ve nanopartiküllerin kolloidal davranışının değerlendirilmesi olarak tanımlanabilir. Bu amacı yerine getirmek için, dinamik ışık saçılımı, çökelme ve bulanıklık deneyleri uygulanmıştır. TiO_2 nanopartiküllerinin kümeleşme ve/veya yığılması, fotokatalitik giderim verimlerinin yanı sıra, yukarıda belirtilen su anayapısı etkisiyle ilişki içinde olan fiziko-kimyasal parametreler kullanılarak değerlendirilmiştir. Her iki anayapı bileşeninin kümeleşme ve/veya yığılma davranışı, fotokataliz esnasında ışınlama altında beklenen reaktivite hakkında bilgi sağlamıştır. Sistemlerin genel değerlendirmesi, hem fotokataliz hem de çevresel koşullar altında ışıkla uyarılmış reaksiyonlar sırasında bilgi sağlamıştır. Dolayısıyla, fotokataliz vasıtası ile nanopartiküllerin geleceği hakkında daha kapsamlı bir anlayış sonucuna varılmıştır.

TABLE OF CONTENTS

ACKNOWLEDGEMENTS.....iii
ABSTRACT.....iv
ÖZET.....v
TABLE OF CONTENTS.....vi
LIST OF FIGURES.....vii
LIST OF TABLES.....xlv
LIST OF SYMBOLS/ABBREVIATIONS.....xv
1. INTRODUCTION.....1
2. LITERATURE REVIEW.....3
2.1. Colloidal Interactions.....3
2.2. Natural Organic Matter.....7
2.3. Nanoparticles in the Environment.....12
2.4. Assessment of Behavior of Nanoparticles in the Environment.....15
2.4.1. Particle Size Distribution.....16
2.4.2. Sedimentation.....19
2.4.3. Brief Outline of Literature Survey.....19
3. MATERIALS AND METHODS.....23
3.1. Materials.....23
3.1.1. Nanoparticles as Photocatalysts.....23
3.1.2. Organic Matter.....23
3.2. Methodology.....24
3.2.1. Particle Size Distribution using Dynamic Light Scattering Technique.....24
3.2.2. Sedimentation.....24
3.2.3. Turbidity.....25
3.3. Treatment Methodology.....25
3.3.1. Treatment of nanoparticles in the presence of organic matter following photolysis of organic matter.....25
3.3.2. Treatment of nanoparticles in the presence of organic matter following photocatalysis of organic matter.....25
3.3.3. Treatment of sole nanoparticles following light exposure conditions in the absence of organic matter.....26
3.3.4. Treatment of sole nanoparticles under dark conditions in the absence

of organic matter…….....26
3.4. Characterization of Organic Matrix.....……....26
3.4.1. UV-vis Spectroscopic Measurements…….26
3.4.2. Fluorescence Measurements……...26
3.4.3. Dissolved Organic Carbon (DOC) Measurements……...27
3.4.4. Specific parameters…….27
4. RESULTS AND DISCUSSION.....28
4.1. Particle Size Distribution.....…….....28
4.1.1. Mono System: As-is Conditions…….28
4.1.1.1. TiO_2 under "as-is" conditions intensity profile…….28
4.1.1.2. TiO_2 under "as-is" conditions volume profile…….....31
4.1.1.3. TiO_2 under "as-is" conditions surface area profile……....33
4.1.1.4. TiO_2 under "as-is" conditions number profile…….....35
4.1.1.5. N-TiO_2 under "as-is" conditions intensity profile……..37
4.1.1.6. N-TiO_2 under "as-is" conditions volume profile…….....40
4.1.1.7. N-TiO_2 under "as-is" conditions surface area profile……....42
4.1.1.8. N-TiO_2 under "as-is" conditions number profile…….....44
4.1.1.9. Fe-TiO_2 under as-is" conditions intensity profile……...46
4.1.1.10. Fe-TiO_2 under as-is" conditions volume profile……..49
4.1.1.11. Fe-TiO_2 under as-is" conditions surface area profile…….....51
4.1.1.12. Fe-TiO_2 under as-is" conditions number profile……..53
4.1.2. Mono System: As-is Under Dark Conditions……..55
4.1.2.1. "TiO_2 as-is under dark" conditions intensity profile……..55
4.1.2.2. "TiO_2 as-is under dark conditions" volume profile…….....57
4.1.2.3. "TiO_2 as-is under dark conditions" surface area profile……....59
4.1.2.4. "TiO_2 as-is under dark conditions" number profile……...…....61
4.1.2.5. "N-TiO_2 as-is under dark" conditions intensity profile……..63
4.1.2.6. "N-TiO_2 as-is under dark" conditions volume profile……...…....65
4.1.2.7. "N-TiO_2 as-is under dark" conditions surface area profile……....67
4.1.2.8. "N-TiO_2 as-is under dark" conditions number profile……...…....69
4.1.2.9. "Fe-TiO_2 as-is under dark" conditions intensity profile……....71
4.1.2.10. "Fe-TiO_2 as-is under dark" conditions volume profile……....73
4.1.2.11. "Fe-TiO_2 as-is under dark" conditions surface area profile……..75
4.1.2.12. "Fe-TiO_2 as-is under dark" conditions number profile……....77
4.1.3. Mono System: As-is Under Irradiation……...…....79

4.1.3.1. "TiO_2 as-is under irradiation" conditions intensity profile…….....79
4.1.3.2. "TiO_2 as-is under irradiation" conditions volume profile……...81
4.1.3.3. "TiO_2 as-is under irradiation" conditions surface area profile……...…....83
4.1.3.4. "TiO_2 as-is under irradiation" conditions number profile……..85
4.1.3.5. "N-TiO_2 as-is under irradiation" conditions intensity profile…….....87
4.1.3.6. "N-TiO_2 as-is under irradiation" conditions volume profile……..89
4.1.3.7. "N-TiO_2 as-is under irradiation" conditions surface area profile……...91
4.1.3.8. "N-TiO_2 as-is under irradiation" conditions number profile……..93
4.1.3.9. "Fe-TiO_2 as-is under irradiation" conditions intensity profile……...…....95
4.1.3.10. "Fe-TiO_2 as-is under irradiation" conditions volume profile……...97
4.1.3.11. "Fe-TiO_2 as-is under irradiation" conditions surface area profile…….…...99
4.1.3.12. "Fe-TiO_2 as-is under irradiation" conditions number profile…….....101
4.1.4. Binary System: As-is Conditions……...103
4.1.4.1. "TiO_2 and HA" binary system under "as-is" conditions intensity profile…….103
4.1.4.2. "TiO_2 and HA" binary system under "as-is" conditions volume profile…….106
4.1.4.3. "TiO_2 and HA" binary system under "as-is" conditions surface area profile…….108
4.1.4.4. "TiO_2 and HA" binary system under "as-is" conditions number profile ……110
4.1.4.5. "TiO_2 and SRNOM" binary system under "as-is" conditions intensity profile……...112
4.1.4.6. "TiO_2 and SRNOM" binary system under "as-is" conditions volume profile……....114
4.1.4.7. "TiO_2 and SRNOM" binary system under "as-is" conditions surface area profile…….116
4.1.4.8. "TiO_2 and SRNOM" binary system under "as-is" conditions number profile……118
4.1.4.9. "N-TiO_2 and HA" binary system under "as-is" conditions intensity profile……...120
4.1.4.10. "N-TiO_2 and HA" binary system under "as-is" conditions volume profile…….....123
4.1.4.11. "N-TiO_2 and HA" binary system under "as-is" conditions surface area profile……....125

4.1.4.12. "N-TiO_2 and HA" binary system under "as-is" conditions number profile……...…....127
4.1.4.13. "N-TiO_2 and SRNOM" binary system under "as-is" conditions intensity profile…….....129
4.1.4.14. "N-TiO_2 and SRNOM" binary system under "as-is" conditions volume profile…….…..131
4.1.4.15. "N-TiO_2 and SRNOM" binary system under "as-is" conditions surface area profile…….....133
4.1.4.16. "N-TiO_2 and SRNOM" binary system under "as-is" conditions number profile…….…..135
4.1.4.17. "Fe-TiO_2 and HA" binary system under "as-is" conditions intensity profile……137
4.1.4.18. "Fe-TiO_2 and HA" binary system under "as-is" conditions volume profile…….…..140
4.1.4.19. "Fe-TiO_2 and HA" binary system under "as-is" conditions surface area profile…….....142
4.1.4.20. "Fe-TiO_2 and HA" binary system under "as-is" conditions number profile…….…..144
4.1.4.21. "Fe-TiO_2 and SRNOM" binary system under "as-is" conditions intensity profile……146
4.1.4.22. "Fe-TiO_2 and SRNOM" binary system under "as-is" conditions volume profile…….…..148
4.1.4.23. "Fe-TiO_2 and SRNOM" binary system under "as-is" conditions surface area profile…….....150
4.1.4.24. "Fe-TiO_2 and SRNOM" binary system under "as-is" conditions number profile…….…..152
4.1.5. Binary System: As-is Under Dark Conditions……...154
4.1.5.1. "TiO_2 and HA" binary system "as-is" under dark conditions intensity profile…….…….154
4.1.5.2. "TiO_2 and HA" binary system "as-is" under dark conditions volume profile……157
4.1.5.3. "TiO_2 and HA" binary system "as-is" under dark conditions surface area profile……..159
4.1.5.4. "TiO_2 and HA" binary system "as-is" under dark conditions number profile……161

4.1.5.5. "TiO_2 and SRNOM" binary system "as-is" under dark conditions intensity profile……163
4.1.5.6. "TiO_2 and SRNOM" binary system "as-is" under dark conditions volume profile……165
4.1.5.7. "TiO_2 and SRNOM" binary system "as-is" under dark conditions surface area profile……167
4.1.5.8. "TiO_2 and SRNOM" binary system "as-is" under dark conditions number profile……169
4.1.5.9. "N-TiO_2 and HA" binary system "as-is" under dark conditions intensity profile……171
4.1.5.10. "N-TiO_2 and HA" binary system "as-is" under dark conditions volume profile……173
4.1.5.11. "N-TiO_2 and HA" binary system "as-is" under dark conditions surface area profile……175
4.1.5.12. "N-TiO_2 and HA" binary system "as-is" under dark conditions number profile……177
4.1.5.13. "N-TiO_2 and SRNOM" binary system "as-is" under dark conditions intensity profile……179
4.1.5.14. "N-TiO_2 and SRNOM" binary system "as-is" under dark conditions volume profile……181
4.1.5.15. "N-TiO_2 and SRNOM" binary system "as-is" under dark conditions surface area profile……183
4.1.5.16. "N-TiO_2 and SRNOM" binary system "as-is" under dark conditions number profile……185
4.1.5.17. "Fe-TiO_2 and HA" binary system "as-is" under dark conditions intensity profile……187
4.1.5.18. "Fe-TiO_2 and HA" binary system "as-is" under dark conditions volume profile……189
4.1.5.19. "Fe-TiO_2 and HA" binary system "as-is" under dark conditions surface area profile……191
4.1.5.20. "Fe-TiO_2 and HA" binary system "as-is" under dark conditions number profile……193
4.1.5.21. "Fe-TiO_2 and SRNOM" binary system "as-is" under dark conditions intensity profile……195

4.1.5.22. "Fe-TiO_2 and SRNOM" binary system "as-is" under dark conditions volume profile……197
4.1.5.23. "Fe-TiO_2 and SRNOM" binary system "as-is" under dark conditions surface area profile……199
4.1.5.24. "Fe-TiO_2 and SRNOM" binary system "as-is" under dark conditions number profile……201
4.1.6. Binary System: Following Photolysis of Organic Matter……203
4.1.6.1. "TiO_2 and HA_{pho}" binary system following photolysis of organic matter intensity profile……203
4.1.6.2. "TiO_2 and HA_{pho}" binary system following photolysis of organic matter volume profile……206
4.1.6.3. "TiO_2 and HA_{pho}" binary system following photolysis of organic matter surface area profile……208
4.1.6.4. "TiO_2 and HA_{pho}" binary system following photolysis of organic matter number profile……210
4.1.6.5. "TiO_2 and $SRNOM_{pho}$" binary system following photolysis of organic matter intensity profile……212
4.1.6.6. "TiO_2 and $SRNOM_{pho}$" binary system following photolysis of organic matter volume profile……214
4.1.6.7. "TiO_2 and $SRNOM_{pho}$" binary system following photolysis of organic matter surface area profile……216
4.1.6.8. "TiO_2 and $SRNOM_{pho}$" binary system following photolysis of organic matter number profile……218
4.1.6.9. "N-TiO_2 and HA_{pho}" binary system following photolysis of organic matter intensity profile……220
4.1.6.10. "N-TiO_2 and HA_{pho}" binary system following photolysis of organic matter volume profile……222
4.1.6.11. "N-TiO_2 and HA_{pho}" binary system following photolysis of organic matter surface area profile……224
4.1.6.12. "N-TiO_2 and HA_{pho}" binary system following photolysis of organic matter number profile……226
4.1.6.13. "N-TiO_2 and $SRNOM_{pho}$" binary system following photolysis of organic matter intensity profile……228
4.1.6.14. "N-TiO_2 and $SRNOM_{pho}$" binary system following photolysis of organic matter volume profile……230

4.1.6.15. "N-TiO_2 and $SRNOM_{pho}$" binary system following photolysis of organic matter surface area profile……....232
4.1.6.16. "N-TiO_2 and $SRNOM_{pho}$" binary system following photolysis of organic matter number profile……..…..234
4.1.6.17. "Fe-TiO_2 and HA_{pho}" binary system following photolysis of organic matter intensity profile…….236
4.1.6.18. "Fe-TiO_2 and HA_{pho}" binary system following photolysis of organic matter volume profile…….....238
4.1.6.19. "Fe-TiO_2 and HA_{pho}" binary system following photolysis of organic matter surface area profile……....241
4.1.6.20. "Fe-TiO_2 and HA_{pho}" binary system following photolysis of organic matter number profile…….....243
4.1.6.21. "Fe-TiO_2 and $SRNOM_{pho}$" binary system following photolysis of organic matter intensity profile…….245
4.1.6.22. "Fe-TiO_2 and $SRNOM_{pho}$" binary system following photolysis of organic matter volume profile……..…..247
4.1.6.23. "Fe-TiO_2 and $SRNOM_{pho}$" binary system following photolysis of organic matter surface area profile……....249
4.1.6.24. "Fe-TiO_2 and $SRNOM_{pho}$" binary system following photolysis of organic matter number profile……..…..251
4.1.7. Binary System: As-is Under Irradiation…….....253
4.1.7.1. "TiO_2 and HA" binary system "as-is" under irradiation intensity profile……...253
4.1.7.2. "TiO_2 and HA" binary system "as-is" under irradiation volume profile…….255
4.1.7.3. "TiO_2 and HA" binary system "as-is" under irradiation surface area profile……..257
4.1.7.4. "TiO_2 and HA" binary system "as-is" under irradiation number profile…….259
4.1.7.5. "TiO_2 and SRNOM" binary system "as-is" under irradiation intensity profile……...261
4.1.7.6. "TiO_2 and SRNOM" binary system "as-is" under irradiation volume profile…….263
4.1.7.7. "TiO_2 and SRNOM" binary system "as-is" under irradiation surface area profile……..265

4.1.7.8. "TiO_2 and SRNOM" binary system "as-is" under irradiation number profile…….267
4.1.7.9. "N-TiO_2 and HA" binary system "as-is" under irradiation intensity profile……...269
4.1.7.10. "N-TiO_2 and HA" binary system "as-is" under irradiation volume profile…….…..271
4.1.7.11. "N-TiO_2 and HA" binary system "as-is" under irradiation surface area profile……....273
4.1.7.12. "N-TiO_2 and HA" binary system "as-is" under irradiation number profile…….…..275
4.1.7.13. "N-TiO_2 and SRNOM" binary system "as-is" under irradiation intensity profile…….277
4.1.7.14. "N-TiO_2 and SRNOM" binary system "as-is" under irradiation volume profile…….…..279
4.1.7.15. "N-TiO_2 and SRNOM" binary system "as-is" under irradiation surface area profile……....281
4.1.7.16. "N-TiO_2 and SRNOM" binary system "as-is" under irradiation number profile…….…..283
4.1.7.17. "Fe-TiO_2 and HA" binary system "as-is" under irradiation intensity profile…….285
4.1.7.18. "Fe-TiO_2 and HA" binary system "as-is" under irradiation volume profile…….…..287
4.1.7.19. "Fe-TiO_2 and HA" binary system "as-is" under irradiation surface area profile……....289
4.1.7.20. "Fe-TiO_2 and HA" binary system "as-is" under irradiation number profile…….…..291
4.1.7.21. "Fe-TiO_2 and SRNOM" binary system "as-is" under irradiation intensity profile…….293
4.1.7.22. "Fe-TiO_2 and SRNOM" binary system "as-is" under irradiation volume profile…….…..295
4.1.7.23. "Fe-TiO_2 and SRNOM" binary system "as-is" under irradiation surface area profile……....297
4.1.7.24. "Fe-TiO_2 and SRNOM" binary system "as-is" under irradiation number profile…….…..299
4.2. Sedimentation.....……....301

4.2.1. Sedimentation Behavior of Nanoparticles as TiO_2, N-TiO_2 and Fe-TiO_2 under "as-is" Conditions in the Absence of Organic Matter……..303
4.2.1.1. TiO_2 specimen under "as-is" conditions……..303
4.2.1.2. N-TiO_2 specimen under "as-is" conditions……..305
4.2.1.3. Fe-TiO_2 specimen under "as-is" conditions…….....307
4.2.2. Comparative Evaluation of Exponential and Linear Models of TiO_2, N-TiO_2, Fe-TiO_2 "as-is" Conditions…….309
4.2.3. Sedimentation Behavior of Nanoparticles as TiO_2, N-TiO_2 and Fe-TiO_2 "as-is under dark" Conditions in the Absence of Organic Matter……..310
4.2.3.1. TiO_2 specimen "as-is under dark" conditions……...310
4.2.3.2. N-TiO_2 specimen "as-is under dark" conditions……..312
4.2.3.3. Fe-TiO_2 specimen "as-is under dark" conditions…….....314
4.2.4. Comparative Evaluation of Exponential and Linear Models of TiO_2, N-TiO_2, Fe-TiO_2 "as-is under dark" Conditions…….....316
4.2.5. Sedimentation Behavior of Nanoparticles TiO_2, N-TiO_2 and Fe-TiO_2 "as-is under irradiation" in the Absence of Organic Matter……...317
4.2.5.1. TiO_2 specimen "as-is under irradiation" ……...……..317
4.2.5.2. N-TiO_2 specimen "as-is under irradiation" ……...…..319
4.2.5.3. Fe-TiO_2 specimen "as-is under irradiation" …….....321
4.2.6. Comparative Evaluation of Exponential and Linear Models of TiO_2, N-TiO_2, Fe-TiO_2 "as-is under irradiation" Conditions……..323
4.2.7. Sedimentation Behavior of Nanoparticles as TiO_2, N-TiO_2 and Fe-TiO_2 under "as-is" Conditions in the Presence of Organic Matter…….....324
4.2.7.1. "TiO_2 and HA" binary system under "as-is" conditions……...324
4.2.7.2. "TiO_2 and SRNOM" binary system under "as-is" conditions……..326
4.2.7.3. "N-TiO_2 and HA" specimen under "as-is" conditions…….....328
4.2.7.4. "N-TiO_2 and SRNOM" binary system under "as-is" conditions……..330
4.2.7.5. "Fe-TiO_2 and HA" binary system under "as-is" conditions…….....332
4.2.7.6. "Fe-TiO_2 and SRNOM" binary system under "as-is" conditions…….……334
4.2.8. Comparative Evaluation of Exponential and Linear Models of "TiO_2 and HA", "N-TiO_2 and HA", "Fe-TiO_2 and HA" under "as-is" Conditions…….336
4.2.9. Comparative Evaluation of Exponential and Linear Models of "TiO_2 and SRNOM", "N-TiO_2 and SRNOM", "Fe-TiO_2 and SRNOM under "as-is" Conditions……...337

4.2.10. Sedimentation Behavior of Nanoparticles as TiO_2, N-TiO_2 and Fe-TiO_2 "as-is under dark" Conditions in the Presence of Organic Matter……338
4.2.10.1. "TiO_2 and HA" binary system "as-is under dark" conditions……...338
4.2.10.2. "TiO_2 and SRNOM" binary system "as-is under dark" conditions……...340
4.2.10.3. "N-TiO_2 and HA" binary system "as-is under dark" conditions……...342
4.2.10.4. "N-TiO_2 and SRNOM" binary system "as-is under dark" conditions……...344
4.2.10.5. "Fe-TiO_2 and HA" binary system "as-is under dark" conditions……...346
4.2.10.6. "Fe-TiO_2 and SRNOM" binary system "as-is" under dark conditions……...348
4.2.11. Comparative Evaluation of Exponential and Linear Models of "TiO_2 and HA", "N-TiO_2 and HA", "Fe-TiO_2 and HA" "as-is under dark" Conditions…….350
4.2.12. Comparative Evaluation of Exponential and Linear Models of "TiO_2 and SRNOM", "N-TiO_2 and SRNOM", "Fe-TiO_2 and SRNOM" "as-is under dark" Conditions……....351
4.2.13. Sedimentation Behavior of Nanoparticles TiO_2, N-TiO_2 and Fe-TiO_2 "following photolysis of organic matter" in the Presence of Organic Matter….....352
4.2.13.1. "TiO_2 and HA_{pho}" binary system following photolysis of organic matter……352
4.2.13.2. "TiO_2 and $SRNOM_{pho}$" binary system "following photolysis of organic matter" ……..354
4.2.13.3. "N-TiO_2 and HA_{pho}" binary system "following photolysis of organic matter" ……...…….356
4.2.13.4. "N-TiO_2 and $SRNOM_{pho}$" binary system following photolysis of organic matter……358
4.2.13.5. "Fe-TiO_2 and HA_{pho}" binary system "following photolysis of organic matter" …….....360
4.2.13.6. "Fe-TiO_2 and $SRNOM_{pho}$" binary system "following photolysis of organic matter" ……....362
4.2.14. Comparative Evaluation of Exponential and Linear Models of

"TiO_2 and HA_{pho}", "N-TiO_2 and HA_{pho}", "Fe-TiO_2 and HA_{pho}" "following photolysis of organic matter" Conditions…….....364

4.2.15. Comparative Evaluation of Exponential and Linear Models of "TiO_2 and $SRNOM_{pho}$", "N-TiO_2 and $SRNOM_{pho}$", "Fe-TiO_2 and $SRNOM_{pho}$" "following photolysis of organic matter" Conditions…….365

4.2.16. Sedimentation Behavior of Nanoparticles TiO_2, N-TiO_2 and Fe-TiO_2 "as-is under irradiation" in the Presence of Organic Matter…….....366

4.2.16.1. "TiO_2 and HA" binary system "as-is under irradiation" ……...…….366

4.2.16.2. "TiO_2 and SRNOM" binary system "as-is under irradiation" ……...….368

4.2.16.3. "N-TiO_2 and HA" binary system "as-is" under irradiation…….....370

4.2.16.4. "N-TiO_2 and SRNOM" binary system "as-is" under irradiation…….....372

4.2.16.5. "Fe-TiO_2 and HA" binary system "as-is" under irradiation……...374

4.2.16.6. "Fe-TiO_2 and SRNOM" binary system "as-is under irradiation" …...…376

4.2.17. Comparative Evaluation of Exponential and Linear Models of "TiO_2 and HA", "N-TiO_2 and HA", "Fe-TiO_2 and HA" "as-is under irradiation" Conditions……...…....378

4.2.18. Comparative Evaluation of Exponential and Linear Models of "TiO_2 and SRNOM", "N-TiO_2 and SRNOM", "Fe-TiO_2 and SRNOM" "as-is under irradiation" Conditions…….…..379

4.3. Behavior of Nanoparticles as TiO_2, N-TiO_2, and Fe-TiO_2 under "as-is", "as-is dark", and "as-is irradiation" Conditions in the Absence of Organic Matter…….….380

4.3.1. Behavior of TiO_2 under "as-is", "as-is dark", and "as-is irradiation" Conditions…….380

4.3.1.1. Comparative evaluation of selected parameters as hydrodynamic size, hydrodynamic size difference, sedimentation and turbidity variations of TiO_2 under "as-is", "as-is dark", and "as-is irradiation" conditions……...382

4.3.2. Behavior of N-TiO_2 under "as-is", "as-is dark", and "as-is irradiation" Conditions…….384

4.3.2.1. Comparative evaluation of selected parameters as hydrodynamic size, hydrodynamic size difference, sedimentation and turbidity variations of N-TiO_2 under "as-is", "as-is dark", and "as-is irradiation" conditions…….386

4.3.3. Behavior of Fe-TiO_2 under "as-is", "as-is dark", and "as-is irradiation"

Conditions…….388
4.3.3.1. Comparative evaluation of selected parameters as hydrodynamic size, hydrodynamic size difference, sedimentation and turbidity variations of Fe-TiO_2 under “as-is”, “as-is dark”, and “as-is irradiation” conditions……..390
4.4. Behavior of Nanoparticles as TiO_2, N-TiO_2 and Fe-TiO_2 under “as-is”, “as-is dark”, “following photolysis of organic matter”, and “as-is irradiation” Conditions in the Presence of Organic Matter……..392
4.4.1. Behavior of “TiO_2 and HA” Binary System under “as-is”, “as-is dark”, “following photolysis of organic matter”, and “as-is irradiation” Conditions…….392
4.4.1.1. Comparative evaluation of selected parameters as hydrodynamic size, hydrodynamic size difference, sedimentation and turbidity variations of “TiO_2 and HA” binary system under “as-is”, “as-is dark”, “following photolysis of organic matter”, and “as-is irradiation” conditions……...395
4.4.2. Behavior of “TiO_2 and SRNOM” Binary System under “as-is”, “as-is dark”, “following photolysis of organic matter”, and “as-is irradiation” conditions…….398
4.4.2.1. Comparative evaluation of selected parameters as hydrodynamic size, hydrodynamic size difference, sedimentation and turbidity variations of “TiO_2 and SRNOM” binary system under “as-is”, “as-is dark”, “following photolysis of organic matter”, and “as-is irradiation” conditions……...400
4.4.3. Behavior of “N-TiO_2 and HA” Binary System under “as-is”, “as-is dark”, “following photolysis of organic matter”, and “as-is irradiation” conditions…….403
4.4.3.1. Comparative evaluation of selected parameters as hydrodynamic size, hydrodynamic size difference, sedimentation and turbidity variations of “N-TiO_2 and HA” binary system under “as-is”, “as-is dark”, “following photolysis of organic matter”, and “as-is irradiation” conditions……...405
4.4.4. Behavior of “N-TiO_2 and SRNOM” Binary System under “as-is”, “as-is dark”, “following photolysis of organic matter”, and “as-is irradiation” conditions…….408

4.4.4.1. Comparative evaluation of selected parameters as hydrodynamic size, hydrodynamic size difference, sedimentation and turbidity variations of "N-TiO_2 and SRNOM" binary system under "as-is", "as-is dark", "following photolysis of organic matter", and "as-is irradiation" conditions……...410

4.4.5. Behavior of "Fe-TiO_2 and HA" Binary System under "as-is", "as-is dark", "following photolysis of organic matter", and "as-is irradiation" conditions……413

4.4.5.1. Comparative evaluation of selected parameters as hydrodynamic size, hydrodynamic size difference, sedimentation and turbidity variations of "Fe-TiO_2 and HA" binary system under "as-is", "as-is dark", "following photolysis of organic matter", and "as-is irradiation" conditions……...415

4.4.6. Behavior of "Fe-TiO_2 and SRNOM" Binary System under "as-is", "as-is dark", "following photolysis of organic matter", and "as-is irradiation" conditions……418

4.4.6.1. Comparative evaluation of selected parameters as hydrodynamic size, hydrodynamic size difference, sedimentation and turbidity variations of "Fe-TiO_2 and SRNOM" binary system under "as-is", "as-is dark", "following photolysis of organic matter", and "as-is irradiation" conditions……...420

5. CONCLUSION.....……....423

REFERENCES.....426

APPENDIX A: PHYSICO-CHEMICAL AND MORPHOLOGICAL PROPERTIES OF NANOPARTICLES……..435

APPENDIX B: CHARACTERIZATION OF ORGANIC MATRIX……...436

LIST OF FIGURES

Figure 2.1. Particle Stern layer and electrical double layer formation……...4

Figure 2.2. Interactions between repulsive and attractive forces……...4

Figure 2.3. Alteration of characteristics of dry nanoparticle powders in liquid…….....6

Figure 2.4. Operationally defined regional distribution of natural colloids……...7

Figure 2.5. Chemical properties of humic substances…….…..9

Figure 2.6. The model structure of humic acid……..9

Figure 2.7. The model structure of fulvic acid……...9

Figure 2.8. Illustration of TiO_2 photocatalysis and formation of hole-pairs and radicals…….……11

Figure 2.9. Schematic image for crystal structure of anatase and rutile phases of TiO_2……...13

Figure 2.10. Summary of interactions pertaining to environmental compartments in relation to colloidal systems…….....16

Figure 2.11. Size distribution profiles……18

Figure 2.12. Environmental distribution of nanoparticles…….....22

Figure 4.1. TiO_2 under “as-is” conditions intensity profile: Time dependent logN distribution G(d) and multi size distribution C(d)……...…..28

Figure 4.2. TiO_2 under “as-is” conditions intensity profile: Time dependent comparative presentation of log Normal distribution and multi-size distribution of TiO_2 under “as-is” conditions particle size……..29

Figure 4.3. TiO_2 under "as-is" conditions volume profile: Time dependent logN distribution G(d) and multi size distribution C(d)…….....31

Figure 4.4. TiO_2 under "as-is" conditions volume profile: Time dependent comparative presentation of log Normal distribution and multi-size distribution of TiO_2 under "as-is" conditions particle size…….....32

Figure 4.5. TiO_2 under "as-is" conditions surface area profile: Time dependent logN distribution G(d) and multi size distribution C(d)……...…..33

Figure 4.6. TiO_2 under "as-is" conditions surface area profile: Time dependent comparative presentation of log Normal distribution and multi-size distribution of TiO_2 under "as-is" conditions particle size…….34

Figure 4.7. TiO_2 under "as-is" conditions number profile: Time dependent logN distribution G(d) and multi size distribution C(d)…….....35

Figure 4.8. TiO_2 under "as-is" conditions number profile: Time dependent comparative presentation of log Normal distribution and multi-size distribution of TiO_2 under "as-is" conditions particle size…….…..36

Figure 4.9. "N-TiO_2 as-is" intensity profile: Time dependent logN distribution G(d) and multi size distribution C(d)…….....37

Figure 4.10. "N-TiO_2 as-is" intensity profile: Time dependent comparative presentation of log Normal distribution and multi-size distribution of "N-TiO_2 as-is" particle size…….....39

Figure 4.11. "N-TiO_2 as-is" volume profile: Time dependent logN distribution G(d) and multi size distribution C(d)……..40

Figure 4.12. "N-TiO_2 as-is" volume profile: Time dependent comparative presentation of log Normal distribution and multi-size distribution of "N-TiO_2 as-is" particle size…….....41

Figure 4.13. "N-TiO_2 as-is" surface area profile: Time dependent logN distribution G(d) and multi size distribution C(d)……42

Figure 4.14. "N-TiO_2 as-is" surface area profile: Time dependent comparative presentation of log Normal distribution and multi-size distribution of "N-TiO_2 as-is" particle size……43

Figure 4.15. "N-TiO_2 as-is" number profile: Time dependent logN distribution G(d) and multi size distribution C(d)……44

Figure 4.16. "N-TiO_2 as-is" number profile: Time dependent comparative presentation of log Normal distribution and multi-size distribution of "N-TiO_2 as-is" particle size…….....45

Figure 4.17. Fe-TiO_2 under "as-is" conditions intensity profile: Time dependent logN distribution G(d) and multi size distribution C(d)…….…..46

Figure 4.18. Fe-TiO_2 under "as-is" conditions intensity profile: Time dependent comparative presentation of log Normal distribution and multi-size distribution of Fe-TiO_2 under "as-is" conditions particle size…….…..48

Figure 4.19. Fe-TiO_2 under "as-is" conditions volume profile: Time dependent logN distribution G(d) and multi size distribution C(d)…….…..49

Figure 4.20. Fe-TiO_2 under "as-is" conditions volume profile: Time dependent comparative presentation of log Normal distribution and multi-size distribution of Fe-TiO_2 under "as-is" conditions particle size…….…..50

Figure 4.21. Fe-TiO_2 under "as-is" conditions surface area profile: Time dependent logN distribution G(d) and multi size distribution C(d)…….…..51

Figure 4.22. Fe-TiO_2 under "as-is" conditions surface area profile: Time dependent comparative presentation of log Normal distribution and multi-size distribution of Fe-TiO_2 under "as-is" conditions particle size…….52

Figure 4.23. Fe-TiO_2 under "as-is" conditions number profile: Time dependent logN distribution G(d) and multi size distribution C(d)…….…..53

Figure 4.24. Fe-TiO_2 under "as-is" conditions number profile: Time dependent comparative

presentation of log Normal distribution and multi-size distribution of Fe-TiO_2 under "as-is" conditions particle size……..54

Figure 4.25. "TiO_2 as-is under dark" conditions intensity profile: Time dependent logN distribution G(d) and multi size distribution C(d)……..55

Figure 4.26. "TiO_2 as-is under dark" conditions intensity profile: Time dependent comparative presentation of log Normal distribution and multi-size distribution of "TiO_2 as-is under dark" conditions particle size……....56

Figure 4.27. "TiO_2 as-is under dark" conditions volume profile: Time dependent logN distribution G(d) and multi size distribution C(d)…….…..57

Figure 4.28. "TiO_2 as-is under dark" conditions volume profile: Time dependent comparative presentation of log Normal distribution and multi-size distribution of "TiO_2 as-is under dark" conditions particle size…….…..58

Figure 4.29. TiO_2 "as-is under dark" conditions surface area profile: Time dependent logN distribution G(d) and multi size distribution C(d)…….…..59

Figure 4.30. TiO_2 "as-is under dark" conditions surface area profile: Time dependent comparative presentation of log Normal distribution and multi-size distribution of TiO_2 "as-is under dark" conditions particle size……...60

Figure 4.31. "TiO_2 as-is under dark conditions" number profile: Time dependent logN distribution G(d) and multi size distribution C(d)……..61

Figure 4.32. "TiO_2 as-is under dark conditions" number profile: Time dependent comparative presentation of log Normal distribution and multi-size distribution of "TiO_2 as-is under dark conditions" particle size……...…….....62

Figure 4.33. N-TiO_2 "as-is under dark" conditions intensity profile: Time dependent logN distribution G(d) and multi size distribution C(d)…….…..63

Figure 4.34. N-TiO_2 "as-is under dark" conditions intensity profile: Time dependent

comparative presentation of log Normal distribution and multi-size distribution of N-TiO_2 "as-is under dark" conditions particle size……...64

Figure 4.35. N-TiO_2 "as-is under dark" conditions volume profile: Time dependent logN distribution G(d) and multi size distribution C(d)…….…..65

Figure 4.36. N-TiO_2 "as-is under dark" conditions volume profile: Time dependent Comparative presentation of log Normal distribution and multi-size distribution of N-TiO_2 "as-is under dark" conditions particle size……...66

Figure 4.37. N-TiO_2 "as-is under dark" conditions surface area profile: Time dependent logN distribution G(d) and multi size distribution C(d)……..67

Figure 4.38. N-TiO_2 "as-is under dark" conditions surface area profile: Time dependent comparative presentation of log Normal distribution and multi-size distribution of N-TiO_2 "as-is under dark" conditions particle size……..68

Figure 4.39. N-TiO_2 "as-is under dark" conditions number profile: Time dependent logN distribution G(d) and multi size distribution C(d)…….…..69

Figure 4.40. N-TiO_2 "as-is under dark" conditions number profile: Time dependent comparative presentation of log Normal distribution and multi-size distribution of N-TiO_2 "as-is under dark" conditions particle size……..70

Figure 4.41. Fe-TiO_2 "as-is under dark" conditions intensity profile: Time dependent logN distribution G(d) and multi size distribution C(d)…….…..71

Figure 4.42. Fe-TiO_2 "as-is under dark" conditions intensity profile: Time dependent comparative presentation of log Normal distribution and multi-size distribution of Fe-TiO_2 "as-is under dark" conditions particle size……....72

Figure 4.43. Fe-TiO_2 "as-is under dark" conditions volume profile: Time dependent logN distribution G(d) and multi size distribution C(d)…….…..73

Figure 4.44. Fe-TiO_2 "as-is under dark" conditions volume profile: Time dependent

comparative presentation of log Normal distribution and multi-size distribution of Fe-TiO_2 "as-is under dark" conditions particle size……..74

Figure 4.45. Fe-TiO_2 "as-is under dark" conditions surface area profile: Time dependent logN distribution G(d) and multi size distribution C(d)……..75

Figure 4.46. Fe-TiO_2 "as-is under dark" conditions surface area profile: Time dependent comparative presentation of log Normal distribution and multi-size distribution of Fe-TiO_2 "as-is under dark" conditions particle size……..76

Figure 4.47. Fe-TiO_2 "as-is under dark" conditions number profile: Time dependent logN distribution G(d) and multi size distribution C(d)……..77

Figure 4.48. Fe-TiO_2 "as-is under dark" conditions number profile: Time dependent comparative presentation of log Normal distribution and multi-size distribution of Fe-TiO_2 "as-is under dark" conditions particle size……..78

Figure 4.49. "TiO_2 as-is under irradiation" conditions intensity profile: Time dependent logN distribution G(d) and multi size distribution C(d)……..79

Figure 4.50. "TiO_2 as-is under irradiation" conditions intensity profile: Time dependent comparative presentation of log Normal distribution and multi-size distribution of "TiO_2 as-is under irradiation" conditions particle size……...80

Figure 4.51. "TiO_2 as-is under irradiation" volume profile: Time dependent logN distribution G(d) and multi size distribution C(d)……..81

Figure 4.52. "TiO_2 as-is under irradiation" volume profile: Time dependent comparative presentation of log Normal distribution and multi-size distribution of "TiO_2 as-is under irradiation" particle size……82

Figure 4.53. "TiO_2 as-is under irradiation" surface area profile: Time dependent logN distribution G(d) and multi size distribution C(d)……..83

Figure 4.54. "TiO_2 as-is under irradiation" surface area profile: Time dependent comparative

presentation of log Normal distribution and multi-size distribution of "TiO_2 as-is under irradiation" particle size……..84

Figure 4.55. "TiO_2 as-is under irradiation" conditions number profile: Time dependent logN distribution G(d) and multi size distribution C(d)……..85

Figure 4.56. "TiO_2 as-is under irradiation" conditions number profile: Time dependent comparative presentation of log Normal distribution and multi-size distribution of "TiO_2 as-is under irradiation" conditions particle size…….…...86

Figure 4.57. N-TiO_2 "as-is under irradiation" conditions intensity profile: Time dependent logN distribution G(d) and multi size distribution C(d)……..87

Figure 4.58. N-TiO_2 "as-is under irradiation" conditions intensity profile: Time dependent comparative presentation of log Normal distribution and multi-size distribution of N-TiO_2 under irradiation particle size…….88

Figure 4.59. N-TiO_2 "as-is under irradiation" conditions volume profile: Time dependent logN distribution G(d) and multi size distribution C(d)……..89

Figure 4.60. N-TiO_2 "as-is under irradiation" conditions volume profile: Time dependent comparative presentation of log Normal distribution and multi-size distribution of N-TiO_2 "as-is under irradiation" conditions particle size……....90

Figure 4.61. N-TiO_2 "as-is under irradiation" conditions surface area profile: Time dependent logN distribution G(d) and multi size distribution C(d)…….....91

Figure 4.62. N-TiO_2 "as-is under irradiation" conditions surface area profile: Time dependent comparative presentation of log Normal distribution and multi-size distribution of N-TiO_2 "as-is under irradiation" conditions particle size……....92

Figure 4.63. N-TiO_2 "as-is under irradiation" conditions number profile: Time dependent logN distribution G(d) and multi size distribution C(d)…….....93

Figure 4.64. N-TiO_2 "as-is under irradiation" conditions number profile: Time dependent comparative presentation of log Normal distribution and multi-size distribution of N-TiO_2 "as-is under irradiation" conditions particle size……....94

Figure 4.65. Fe-TiO_2 "as-is under irradiation" conditions intensity profile: Time dependent logN distribution G(d) and multi size distribution C(d)…….....95

Figure 4.66. Fe-TiO_2 "as-is under irradiation" conditions intensity profile: Time dependent comparative presentation of log Normal distribution and multi-size distribution of Fe-TiO_2 "as-is under irradiation" conditions particle size……....96

Figure 4.67. Fe-TiO_2 "as-is under irradiation" conditions volume profile: Time dependent logN distribution G(d) and multi size distribution C(d)…….....97

Figure 4.68. Fe-TiO_2 "as-is under irradiation" conditions volume profile: Time dependent comparative presentation of log Normal distribution and multi-size distribution of Fe-TiO_2 "as-is under irradiation" conditions particle size……....98

Figure 4.69. Fe-TiO_2 "as-is under irradiation" conditions surface area profile: Time dependent logN distribution G(d) and multi size distribution C(d)…….....99

Figure 4.70. Fe-TiO_2 "as-is under irradiation" conditions surface area profile: Time dependent comparative presentation of log Normal distribution and multi-size distribution of Fe-TiO_2 "as-is under irradiation" conditions particle size……..100

Figure 4.71. Fe-TiO_2 "as-is" under irradiation" conditions number profile: Time dependent logN distribution G(d) and multi size distribution C(d)……...101

Figure 4.72. Fe-TiO_2 "as-is" under irradiation" conditions number profile: Time dependent comparative presentation of log Normal distribution and multi-size distribution of Fe-TiO_2 "as-is" under irradiation"

conditions particle size……..102

Figure 4.73. "TiO_2 and HA" binary system under "as-is" conditions intensity profile: Time dependent logN distribution G(d) and multi size distribution C(d)…….…..103

Figure 4.74. "TiO_2 and HA" binary system under "as-is" conditions intensity profile: Time dependent comparative presentation of log Normal distribution and multi-size distribution of "TiO_2 and HA" binary system under "as-is" conditions…….…..104

Figure 4.75. "TiO_2 and HA" binary system under "as-is" conditions volume profile: Time dependent logN distribution G(d) and multi size distribution C(d)…….....106

Figure 4.76. "TiO_2 and HA" binary system under "as-is" conditions volume profile: Time dependent comparative presentation of log Normal distribution and multi-size distribution of "TiO_2 and HA" binary system under "as-is" conditions……107

Figure 4.77. "TiO_2 and HA" binary system under "as-is" conditions surface area profile: Time dependent logN distribution G(d) and multi size distribution C(d)……..108

Figure 4.78. "TiO_2 and HA" binary system under "as-is" conditions surface area profile: Time dependent comparative presentation of log Normal distribution and multi-size distribution of "TiO_2 and HA" binary system under "as-is" conditions……109

Figure 4.79. "TiO_2 and HA" binary system under "as-is" conditions number profile: Time dependent logN distribution G(d) and multi size distribution C(d)…….....110

Figure 4.80. "TiO_2 and HA" binary system under "as-is" conditions number profile: Time dependent comparative presentation of log Normal distribution and multi-size distribution of "TiO_2 and HA" binary system under "as-is" conditions…….…...111

Figure 4.81. "TiO_2 and SRNOM" binary system under "as-is" conditions intensity profile:

Time dependent logN distribution G(d) and multi size distribution C(d)…….....112

Figure 4.82. "TiO_2 and SRNOM" binary system under "as-is" conditions intensity profile: Time dependent comparative presentation of log Normal distribution and multi-size distribution of "TiO_2 and SRNOM" binary system under "as-is" conditions……113

Figure 4.83. "TiO_2 and SRNOM" binary system under "as-is" conditions volume profile: Time dependent logN distribution G(d) and multi size distribution C(d)…….....114

Figure 4.84. "TiO_2 and SRNOM" binary system under "as-is" conditions volume profile: Time dependent comparative presentation of log Normal distribution and multi-size distribution of "TiO_2 and SRNOM" binary system under "as-is" conditions……...…….…115

Figure 4.85. "TiO_2 and SRNOM" binary system under "as-is" conditions surface area profile: Time dependent logN distribution G(d) and multi size distribution C(d)……...116

Figure 4.86. "TiO_2 and SRNOM" binary system under "as-is" conditions surface area profile: Time dependent comparative presentation of log Normal distribution and multi-size distribution of "TiO_2 and SRNOM" binary system under "as-is" conditions particle size……....117

Figure 4.87. "TiO_2 and SRNOM" binary system under "as-is" conditions number profile: Time dependent logN distribution G(d) and multi size distribution C(d)…….…..118

Figure 4.88. "TiO_2 and SRNOM" binary system under "as-is" conditions number profile: Time dependent comparative presentation of log Normal distribution and multi-size distribution of "TiO_2 and SRNOM" binary system under "as-is" conditions……....119

Figure 4.89. "N-TiO_2 and HA" binary system under "as-is" conditions intensity profile: Time dependent logN distribution G(d) and multi size

distribution C(d)……....120

Figure 4.90. "N-TiO_2 and HA" binary system under "as-is" conditions intensity profile: Time dependent comparative presentation of log Normal distribution and multi-size distribution of "N-TiO_2 and HA" binary system under "as-is" conditions……...122

Figure 4.91. "N-TiO_2 and HA" binary system under "as-is" conditions volume profile: Time dependent logN distribution G(d) and multi size distribution C(d)……123

Figure 4.92. "N-TiO_2 and HA" binary system under "as-is" conditions volume profile: Time dependent comparative presentation of log Normal distribution and multi-size distribution of "N-TiO_2 and HA" binary system under "as-is" conditions……....124

Figure 4.93. "N-TiO_2 and HA" binary system under "as-is" conditions surface area profile: Time dependent logN distribution G(d) and multi size distribution C(d)……..125

Figure 4.94. "N-TiO_2 and HA" binary system under "as-is" conditions surface area profile: Time dependent comparative presentation of log Normal distribution and multi-size distribution of "N-TiO_2 and HA" binary system under "as-is" conditions…….…..126

Figure 4.95. "N-TiO_2 and HA" binary system under "as-is" conditions number profile: Time dependent logN distribution G(d) and multi size distribution C(d)……127

Figure 4.96. "N-TiO_2 and HA" binary system under "as-is" conditions number profile: Time dependent comparative presentation of log Normal distribution and multi-size distribution of "N-TiO_2 and HA" binary system under "as-is" conditions……....128

Figure 4.97. "N-TiO_2 and SRNOM" binary system under "as-is" conditions intensity profile: Time dependent logN distribution G(d) and multi size distribution C(d)…….….129

Figure 4.98. "N-TiO_2 and SRNOM" binary system under "as-is" conditions intensity profile: Time dependent comparative presentation of log Normal distribution and multi-size distribution of "N-TiO_2 and SRNOM" binary system under "as-is" conditions……..…..130

Figure 4.99. "N-TiO_2 and SRNOM" binary system under "as-is" conditions volume profile: Time dependent logN distribution G(d) and multi size distribution C(d)…….….131

Figure 4.100. "N-TiO_2 and SRNOM" binary system under "as-is" conditions volume profile: Time dependent comparative presentation of log Normal distribution and multi-size distribution of "N-TiO_2 and SRNOM" binary system under "as-is" conditions……..132

Figure 4.101. "N-TiO_2 and SRNOM" binary system under "as-is" conditions surface area profile: Time dependent logN distribution G(d) and multi size distribution C(d)…….133

Figure 4.102. "N-TiO_2 and SRNOM" binary system under "as-is" conditions surface area profile: Time dependent comparative presentation of log Normal distribution and multi-size distribution of "N-TiO_2 and SRNOM" binary system under "as-is" conditions……..134

Figure 4.103. "N-TiO_2 and SRNOM" binary system under "as-is" conditions number profile: Time dependent logN distribution G(d) and multi size distribution C(d)……135

Figure 4.104. "N-TiO_2 and SRNOM" binary system number profile: Time dependent comparative presentation of log Normal distribution and multi-size distribution of "N-TiO_2 and SRNOM" binary system……....136

Figure 4.105. "Fe-TiO_2 and HA" binary system under "as-is" conditions intensity profile: Time dependent logN distribution G(d) and multi size distribution C(d)……137

Figure 4.106. "Fe-TiO_2 and HA" binary system under "as-is" conditions intensity profile: Time dependent comparative presentation of log Normal distribution and multi-size distribution of "Fe-TiO_2 and HA" binary system under "as-is" conditions……..139

Figure 4.107. "Fe-TiO_2 and HA" binary system under "as-is" conditions volume profile: Time dependent logN distribution G(d) and multi size distribution C(d)……140

Figure 4.108. "Fe-TiO_2 and HA" binary system under "as-is" conditions volume profile: Time dependent comparative presentation of log Normal distribution and multi-size distribution of "Fe-TiO_2 and HA" binary system under "as-is" conditions……141

Figure 4.109. "Fe-TiO_2 and HA" binary system under "as-is" conditions surface area profile: Time dependent logN distribution G(d) and multi size distribution C(d)……142

Figure 4.110. "Fe-TiO_2 and HA" binary system under "as-is" conditions surface area profile: Time dependent comparative presentation of log Normal distribution and multi-size distribution of "Fe-TiO_2 and HA" binary system under "as-is" conditions……143

Figure 4.111. "Fe-TiO_2 and HA" binary system under "as-is" conditions number profile: Time dependent logN distribution G(d) and multi size distribution C(d)……144

Figure 4.112. "Fe-TiO_2 and HA" binary system under "as-is" conditions number profile: Time dependent comparative presentation of log Normal distribution and multi-size distribution of "Fe-TiO_2 and HA" binary system under "as-is" conditions……...145

Figure 4.113. "Fe-TiO_2 and SRNOM" binary system under "as-is" conditions intensity profile: Time dependent logN distribution G(d) and multi size distribution C(d)……146

Figure 4.114. "Fe-TiO_2 and SRNOM" binary system under "as-is" conditions intensity profile: Time dependent comparative presentation of log Normal distribution and multi-size distribution of "Fe-TiO_2 and SRNOM" binary system under "as-is" conditions……..…..147

Figure 4.115. "Fe-TiO_2 and SRNOM" binary system under "as-is" conditions volume profile: Time dependent logN distribution G(d) and multi size distribution C(d)……148

Figure 4.116. "Fe-TiO_2 and SRNOM" binary system under "as-is" conditions volume profile: Time dependent comparative presentation of log Normal distribution and multi-size distribution of "Fe-TiO_2 and SRNOM" binary system under "as-is" conditions…….…...149

Figure 4.117. "Fe-TiO_2 and SRNOM" binary system under "as-is" conditions surface area profile: Time dependent logN distribution G(d) and multi size distribution C(d)……150

Figure 4.118. "Fe-TiO_2 and SRNOM" binary system under "as-is" conditions surface area profile: Time dependent comparative presentation of log Normal distribution and multi-size distribution of "Fe-TiO_2 and SRNOM" binary system under "as-is" conditions…….…..151

Figure 4.119. "Fe-TiO_2 and SRNOM" binary system under "as-is" conditions number profile: Time dependent logN distribution G(d) and multi size distribution C(d)……152

Figure 4.120. "Fe-TiO_2 and SRNOM" binary system under "as-is" conditions number profile: Time dependent comparative presentation of log Normal distribution and multi-size distribution of "Fe-TiO_2 and SRNOM" binary system under "as-is" conditions……...153

Figure 4.121. "TiO_2 and HA" binary system "as-is" under dark conditions intensity profile: Time dependent logN distribution G(d) and multi size distribution C(d)……...154

Figure 4.122. "TiO_2 and HA" binary system "as-is" under dark conditions intensity profile: Time dependent comparative presentation of log Normal distribution and multi-size distribution of "TiO_2 and HA" binary system "as-is" under dark conditions……...155

Figure 4.123. "TiO_2 and HA" binary system "as-is" under dark conditions volume profile: Time dependent logN distribution G(d) and multi size distribution C(d)……...157

Figure 4.124. "TiO_2 and HA" binary system "as-is" under dark conditions volume profile: Time dependent comparative presentation of log Normal distribution and multi-size distribution of "TiO_2 and HA" binary system "as-is" under dark conditions……158

Figure 4.125. "TiO_2 and HA" binary system "as-is" under dark conditions surface area profile: Time dependent logN distribution G(d) and multi size distribution C(d)……159

Figure 4.126. "TiO_2 and HA" binary system "as-is" under dark conditions surface area profile: Time dependent comparative presentation of log Normal distribution and multi-size distribution of "TiO_2 and HA" binary system "as-is" under dark conditions……160

Figure 4.127. "TiO_2 and HA" binary system "as-is" under dark conditions number profile: Time dependent logN distribution G(d) and multi size distribution C(d)……...161

Figure 4.128. "TiO_2 and HA" binary system "as-is" under dark conditions number profile: Time dependent comparative presentation of log Normal distribution and multi-size distribution of "TiO_2 and HA" binary system "as-is" under dark conditions…….....162

Figure 4.129. "TiO_2 and SRNOM" binary system "as-is" under dark conditions intensity profile: Time dependent logN distribution G(d) and multi size distribution C(d)……163

Figure 4.130. "TiO_2 and SRNOM" binary system "as-is" under dark conditions intensity

profile: Time dependent comparative presentation of log Normal distribution and multi-size distribution of "TiO_2 and SRNOM" binary system "as-is" under dark conditions……..…..164

Figure 4.131. "TiO_2 and SRNOM" binary system "as-is" under dark conditions volume profile: Time dependent logN distribution G(d) and multi size distribution C(d)……165

Figure 4.132. "TiO_2 and SRNOM" binary system "as-is" under dark conditions volume profile: Time dependent comparative presentation of log Normal distribution and multi-size distribution of "TiO_2 and SRNOM" binary system "as-is" under dark conditions……..…..166

Figure 4.133. "TiO_2 and SRNOM" binary system "as-is" under dark conditions surface area profile: Time dependent logN distribution G(d) and multi size distribution C(d)……167

Figure 4.134. "TiO_2 and SRNOM" binary system "as-is" under dark conditions surface area profile: Time dependent comparative presentation of log Normal distribution and multi-size distribution of "TiO_2 and SRNOM" binary system "as-is" under dark conditions……168

Figure 4.135. "TiO_2 and SRNOM" binary system "as-is" under dark conditions number profile: Time dependent logN distribution G(d) and multi size distribution C(d)……169

Figure 4.136. "TiO_2 and SRNOM" binary system "as-is" under dark conditions number profile: Time dependent comparative presentation of log Normal distribution and multi-size distribution of "TiO_2 and SRNOM" binary system "as-is" under dark conditions……..…..170

Figure 4.137. "N-TiO_2 and HA" binary system "as-is" under dark conditions intensity profile: Time dependent logN distribution G(d) and multi size distribution C(d)……171

Figure 4.138. "N-TiO_2 and HA" binary system "as-is" under dark conditions intensity profile: Time dependent comparative presentation of log Normal distribution and multi-size distribution of "N-TiO_2 and HA" binary system under dark conditions……..172

Figure 4.139. "N-TiO_2 and HA" binary system "as-is" under dark conditions volume profile: Time dependent logN distribution G(d) and multi size distribution C(d)…….173

Figure 4.140. "N-TiO_2 and HA" binary system "as-is" under dark conditions volume profile: Time dependent comparative presentation of log Normal distribution and multi-size distribution of "N-TiO_2 and HA" binary system "as-is" under dark conditions…….174

Figure 4.141. "N-TiO_2 and HA" binary system "as-is" under dark conditions surface area profile: Time dependent logN distribution G(d) and multi size distribution C(d)…….175

Figure 4.142. "N-TiO_2 and HA" binary system "as-is" under dark conditions surface area profile: Time dependent comparative presentation of log Normal distribution and multi-size distribution of "N-TiO_2 and HA" binary system "as-is" under dark conditions…….176

Figure 4.143. "N-TiO_2 and HA" binary system "as-is" under dark conditions number profile: Time dependent logN distribution G(d) and multi size distribution C(d)…….177

Figure 4.144. "N-TiO_2 and HA" binary system "as-is" under dark conditions number profile: Time dependent comparative presentation of log Normal distribution and multi-size distribution of "N-TiO_2 and HA" binary system "as-is" under dark conditions……..178

Figure 4.145. "N-TiO_2 and SRNOM" binary system "as-is" under dark conditions intensity profile: Time dependent logN distribution G(d) and multi size distribution C(d)…….179

Figure 4.146. "N-TiO_2 and SRNOM" binary system "as-is" under dark conditions intensity profile: Time dependent comparative presentation of log Normal distribution and multi-size distribution of "N-TiO_2 and SRNOM" binary system "as-is" under dark conditions……180

Figure 4.147. "N-TiO_2 and SRNOM" binary system "as-is" under dark conditions volume profile: Time dependent logN distribution G(d) and multi size distribution C(d)……181

Figure 4.148. "N-TiO_2 and SRNOM" binary system "as-is" under dark conditions volume profile: Time dependent comparative presentation of log Normal distribution and multi-size distribution of "N-TiO_2 and SRNOM" binary system "as-is" under dark conditions……182

Figure 4.149. "N-TiO_2 and SRNOM" binary system "as-is" under dark conditions surface area profile: Time dependent logN distribution G(d) and multi size distribution C(d)……183

Figure 4.150. "N-TiO_2 and SRNOM" binary system "as-is" under dark conditions surface area profile: Time dependent comparative presentation of log Normal distribution and multi-size distribution of "N-TiO_2 and SRNOM" binary system "as-is" under dark conditions……184

Figure 4.151. "N-TiO_2 and SRNOM" binary system "as-is" under dark conditions number profile: Time dependent logN distribution G(d) and multi size distribution C(d)……185

Figure 4.152. "N-TiO_2 and SRNOM" binary system "as-is" under dark conditions number profile: Time dependent comparative presentation of log Normal distribution and multi-size distribution of "N-TiO_2 and SRNOM" binary system "as-is" under dark conditions……186

Figure 4.153. "Fe-TiO_2 and HA" binary system "as-is" under dark conditions intensity profile: Time dependent logN distribution G(d) and multi size distribution C(d)……187

Figure 4.154. "Fe-TiO_2 and HA" binary system "as-is" under dark conditions intensity profile: Time dependent comparative presentation of log Normal distribution and multi-size distribution of "Fe-TiO_2 and HA" binary system "as-is" under dark conditions……..…..188

Figure 4.155. "Fe-TiO_2 and HA" binary system "as-is" under dark conditions volume profile: Time dependent logN distribution G(d) and multi size distribution C(d)……189

Figure 4.156. "Fe-TiO_2 and HA" binary system "as-is" under dark conditions volume profile: Time dependent comparative presentation of log Normal distribution and multi-size distribution of "Fe-TiO_2 and HA" binary system "as-is" under dark conditions……...190

Figure 4.157. "Fe-TiO_2 and HA" binary system "as-is" under dark conditions surface area profile: Time dependent logN distribution G(d) and multi size distribution C(d)……191

Figure 4.158. "Fe-TiO_2 and HA" binary system "as-is" under dark conditions surface area profile: Time dependent comparative presentation of log Normal distribution and multi-size distribution of "Fe-TiO_2 and HA" binary system "as-is" under dark conditions……..…..192

Figure 4.159. "Fe-TiO_2 and HA" binary system "as-is" under dark conditions number profile: Time dependent logN distribution G(d) and multi size distribution C(d)……193

Figure 4.160. "Fe-TiO_2 and HA" binary system "as-is" under dark conditions number profile: Time dependent comparative presentation of log Normal distribution and multi-size distribution of "Fe-TiO_2 and HA" binary system "as-is" under dark conditions……..…..194

Figure 4.161. "Fe-TiO_2 and SRNOM" binary system "as-is" under dark conditions intensity profile: Time dependent logN distribution G(d) and multi size distribution C(d)……195

Figure 4.162. "Fe-TiO_2 and SRNOM" binary system "as-is" under dark conditions intensity profile: Time dependent comparative presentation of log Normal distribution and multi-size distribution of "Fe-TiO_2 and SRNOM" binary system "as-is" under dark conditions…….196

Figure 4.163. "Fe-TiO_2 and SRNOM" binary system "as-is" under dark conditions volume profile: Time dependent logN distribution G(d) and multi size distribution C(d)……197

Figure 4.164. "Fe-TiO_2 and SRNOM" binary system "as-is" under dark conditions volume profile: Time dependent comparative presentation of log Normal distribution and multi-size distribution of "Fe-TiO_2 and SRNOM" binary system "as-is" under dark conditions……..198

Figure 4.165. "Fe-TiO_2 and SRNOM" binary system "as-is" under dark conditions surface area profile: Time dependent logN distribution G(d) and multi size distribution C(d)…….199

Figure 4.166. "Fe-TiO_2 and SRNOM" binary system "as-is" under dark conditions surface area profile: Time dependent comparative presentation of log Normal distribution and multi-size distribution of "Fe-TiO_2 and SRNOM" binary system "as-is" under dark conditions……...……..200

Figure 4.167. "Fe-TiO_2 and SRNOM" binary system "as-is" under dark conditions number profile: Time dependent logN distribution G(d) and multi size distribution C(d)……201

Figure 4.168. "Fe-TiO_2 and SRNOM" binary system "as-is" under dark conditions number profile: Time dependent comparative presentation of log Normal distribution and multi-size distribution of "Fe-TiO_2 and SRNOM" binary system "as-is" under dark conditions…….202

Figure 4.169. "TiO_2 and HA_{pho}" binary system following photolysis of organic matter intensity profile: Time dependent logN distribution G(d) and multi size distribution C(d)…….203

Figure 4.170. "TiO_2 and HA_{pho}" binary system following photolysis of organic matter intensity profile: Time dependent comparative presentation of log Normal distribution and multi-size distribution of "TiO_2 and HA_{pho}" binary system following photolysis of organic matter……..…..204

Figure 4.171. "TiO_2 and HA_{pho}" binary system following photolysis of organic matter volume profile: Time dependent logN distribution G(d) and multi size distribution C(d)…….206

Figure 4.172. "TiO_2 and HA_{pho}" binary system following photolysis of organic matter volume profile: Time dependent comparative presentation of log Normal distribution and multi-size distribution of "TiO_2 and HA_{pho}" binary system following photolysis of organic matter……..…..207

Figure 4.173. "TiO_2 and HA_{pho}" binary system following photolysis of organic matter surface area profile: Time dependent logN distribution G(d) and multi size distribution C(d)…….208

Figure 4.174. "TiO_2 and HA_{pho}" binary system following photolysis of organic matter surface area profile: Time dependent comparative presentation of log Normal distribution and multi-size distribution of "TiO_2 and HA_{pho}" binary system following photolysis of organic matter……..…...209

Figure 4.175. "TiO_2 and HA_{pho}" binary system following photolysis of organic matter number profile: Time dependent logN distribution G(d) and multi size distribution C(d)…….210

Figure 4.176. "TiO_2 and HA_{pho}" binary system following photolysis of organic matter number profile: Time dependent comparative presentation of log Normal distribution and multi-size distribution of "TiO_2 and HA_{pho}" binary system following photolysis of organic matter……..…..211

Figure 4.177. "TiO_2 and $SRNOM_{pho}$" binary system following photolysis of organic matter intensity profile: Time dependent logN distribution G(d) and multi size distribution C(d)…….212

Figure 4.178. "TiO_2 and $SRNOM_{pho}$" binary system following photolysis of organic matter intensity profile: Time dependent comparative presentation of log Normal distribution and multi-size distribution of "TiO_2 and $SRNOM_{pho}$" binary system following photolysis of organic matter……...213

Figure 4.179. "TiO_2 and $SRNOM_{pho}$" binary system following photolysis of organic matter volume profile: Time dependent logN distribution G(d) and multi size distribution C(d)……214

Figure 4.180. "TiO_2 and $SRNOM_{pho}$" binary system following photolysis of organic matter volume profile: Time dependent comparative presentation of log Normal distribution and multi-size distribution of "TiO_2 and $SRNOM_{pho}$" binary system following photolysis of organic matter……...215

Figure 4.181. "TiO_2 and $SRNOM_{pho}$" binary system following photolysis of organic matter surface area profile: Time dependent logN distribution G(d) and multi size distribution C(d)……..216

Figure 4.182. "TiO_2 and $SRNOM_{pho}$" binary system following photolysis of organic matter surface area profile: Time dependent comparative presentation of log Normal distribution multi-size distribution of "TiO_2 and $SRNOM_{pho}$" binary system following photolysis of organic matter……...217

Figure 4.183. "TiO_2 and $SRNOM_{pho}$" binary system following photolysis of organic matter number profile: Time dependent logN distribution G(d) and multi size distribution C(d)……..218

Figure 4.184. "TiO_2 and $SRNOM_{pho}$" binary system following photolysis of organic matter number profile: Time dependent comparative presentation of log Normal distribution and multi-size distribution of "TiO_2 and $SRNOM_{pho}$" binary system following photolysis of organic matter……...219

Figure 4.185. "N-TiO_2 and HA_{pho}" binary system following photolysis of organic matter intensity profile: Time dependent logN distribution G(d) and multi size distribution C(d)……220

Figure 4.186. "N-TiO_2 and HA_{pho}" binary system following photolysis of organic matter intensity profile: Time dependent comparative presentation of log Normal distribution and multi-size distribution of "N-TiO_2 and HA_{pho}" binary system following photolysis of organic matter……..…...221

Figure 4.187. "N-TiO_2 and HA_{pho}" binary system following photolysis of organic matter volume profile: Time dependent logN distribution G(d) and multi size distribution C(d)……222

Figure 4.188. "N-TiO_2 and HA_{pho}" binary system following photolysis of organic matter volume profile: Time dependent comparative presentation of log Normal distribution and multi-size distribution of "N-TiO_2 and HA_{pho}" binary system following photolysis of organic matter……..…...223

Figure 4.189. "N-TiO_2 and HA_{pho}" binary system following photolysis of organic matter surface area profile: Time dependent logN distribution G(d) and multi size distribution C(d)……..224

Figure 4.190. "N-TiO_2 and HA_{pho}" binary system following photolysis of organic matter surface area profile: Time dependent comparative presentation of log Normal distribution and multi-size distribution of "N-TiO_2 and HA_{pho}" binary system following photolysis of organic matter…….…..…..225

Figure 4.191. "N-TiO_2 and HA_{pho}" binary system following photolysis of organic matter number profile: Time dependent logN distribution G(d) and multi size distribution C(d)……226

Figure 4.192. "N-TiO_2 and HA_{pho}" binary system following photolysis of organic matter number profile: Time dependent comparative presentation of log Normal distribution and multi-size distribution of "N-TiO_2 and HA_{pho}" binary system following photolysis of organic matter……..…...227

Figure 4.193. "N-TiO_2 and $SRNOM_{pho}$" binary system following photolysis of organic matter intensity profile: Time dependent logN distribution G(d) and multi size distribution C(d)……228

Figure 4.194. "N-TiO_2 and $SRNOM_{pho}$" binary system following photolysis of organic matter intensity profile: Time dependent comparative presentation of log Normal distribution and multi-size distribution of "N-TiO_2 and $SRNOM_{pho}$" binary system following photolysis of organic matter……...229

Figure 4.195. "N-TiO_2 and $SRNOM_{pho}$" binary system following photolysis of organic matter volume profile: Time dependent logN distribution G(d) and multi size distribution C(d)……230

Figure 4.196. "N-TiO_2 and $SRNOM_{pho}$" binary system following photolysis of organic matter volume profile: Time dependent comparative presentation of log Normal distribution and multi-size distribution of "N-TiO_2 and $SRNOM_{pho}$" binary system following photolysis of organic matter……...231

Figure 4.197. "N-TiO_2 and $SRNOM_{pho}$" binary system following photolysis of organic matter surface area profile: Time dependent logN distribution G(d) and multi size distribution C(d)……232

Figure 4.198. "N-TiO_2 and $SRNOM_{pho}$" binary system following photolysis of organic matter surface area profile: Time dependent comparative presentation of log Normal distribution and multi-size distribution of "N-TiO_2 and $SRNOM_{pho}$" binary system following photolysis of organic matter……233

Figure 4.199. "N-TiO_2 and $SRNOM_{pho}$" binary system following photolysis of organic matter number profile: Time dependent logN distribution G(d) and multi size distribution C(d)……234

Figure 4.200. "N-TiO_2 and $SRNOM_{pho}$" binary system following photolysis of organic matter number profile: Time dependent comparative presentation of log Normal distribution and multi-size distribution of "N-TiO_2 and $SRNOM_{pho}$" binary system following photolysis of organic matter……...235

Figure 4.201. "Fe-TiO_2 and HA_{pho}" binary system following photolysis of organic matter intensity profile: Time dependent logN distribution G(d) and multi size distribution C(d)……236

Figure 4.202. "Fe-TiO_2 and HA_{pho}" binary system following photolysis of organic matter intensity profile: Time dependent comparative presentation of log Normal distribution and multi-size distribution of "Fe-TiO_2 and HA_{pho}" binary system following photolysis of organic matter……...237

Figure 4.203. "Fe-TiO_2 and HA_{pho}" binary system following photolysis of organic matter volume profile: Time dependent logN distribution G(d) and multi size distribution C(d)……238

Figure 4.204. "Fe-TiO_2 and HA_{pho}" binary system following photolysis of organic matter volume profile: Time dependent comparative presentation of log Normal distribution and multi-size distribution of "Fe-TiO_2 and HA_{pho}" binary system following photolysis of organic matter……...240

Figure 4.205. "Fe-TiO_2 and HA_{pho}" binary system following photolysis of organic matter surface area profile: Time dependent logN distribution G(d) and multi size distribution C(d)……241

Figure 4.206. "Fe-TiO_2 and HA_{pho}" binary system following photolysis of organic matter surface area profile: Time dependent comparative presentation of log Normal distribution and multi-size distribution of "Fe-TiO_2 and HA_{pho}" binary system following photolysis of organic matter……...242

Figure 4.207. "Fe-TiO_2 and HA_{pho}" binary system following photolysis of organic matter number profile: Time dependent logN distribution G(d) and multi size distribution C(d)……243

Figure 4.208. "Fe-TiO_2 and HA_{pho}" binary system following photolysis of organic matter number profile: Time dependent comparative presentation of log Normal distribution and multi-size distribution of "Fe-TiO_2 and HA_{pho}" binary system following photolysis of organic matter……...244

Figure 4.209. "Fe-TiO_2 and $SRNOM_{pho}$" binary system following photolysis of organic matter intensity profile: Time dependent logN distribution G(d) and multi size distribution C(d)……245

Figure 4.210. "Fe-TiO_2 and $SRNOM_{pho}$" binary system following photolysis of organic matter intensity profile: Time dependent comparative presentation of log Normal distribution and multi-size distribution of "Fe-TiO_2 and $SRNOM_{pho}$" binary system following photolysis of organic matter……...246

Figure 4.211. "Fe-TiO_2 and $SRNOM_{pho}$" binary system following photolysis of organic matter volume profile: Time dependent logN distribution G(d) and multi size distribution C(d)…….247

Figure 4.212. "Fe-TiO_2 and $SRNOM_{pho}$" binary system following photolysis of organic matter volume profile: Time dependent comparative presentation of log Normal distribution and multi-size distribution of "Fe-TiO_2 and $SRNOM_{pho}$" binary system following photolysis of organic matter……..…..248

Figure 4.213. "Fe-TiO_2 and $SRNOM_{pho}$" binary system following photolysis of organic matter surface area profile: Time dependent logN distribution G(d) and multi size distribution C(d)……249

Figure 4.214. "Fe-TiO_2 and $SRNOM_{pho}$" binary system following photolysis of organic matter surface area profile: Time dependent comparative presentation of log Normal distribution and multi-size distribution of "Fe-TiO_2 and $SRNOM_{pho}$" binary system following photolysis of organic matter……....250

Figure 4.215. "Fe-TiO_2 and $SRNOM_{pho}$" binary system following photolysis of organic matter number profile: Time dependent logN distribution G(d) and multi size distribution C(d)…….251

Figure 4.216. "Fe-TiO_2 and $SRNOM_{pho}$" binary system following photolysis of organic matter number profile: Time dependent comparative presentation of log Normal distribution and multi-size distribution of "Fe-TiO_2 and $SRNOM_{pho}$" binary system following photolysis of organic matter……....252

Figure 4.217. "TiO_2 and HA" binary system "as-is" under irradiation intensity profile: Time dependent logN distribution G(d) and multi size distribution C(d)……...253

Figure 4.218. "TiO_2 and HA" binary system "as-is" under irradiation intensity profile: Time dependent comparative presentation of log Normal distribution and multi-size distribution of "TiO_2 and HA" binary system "as-is" under irradiation……..….254

Figure 4.219. "TiO_2 and HA" binary system "as-is" under irradiation volume profile: Time dependent logN distribution G(d) and multi size distribution C(d)……...255

Figure 4.220. "TiO_2 and HA" binary system "as-is" under irradiation volume profile: Time dependent comparative presentation of log Normal distribution and multi-size distribution of "TiO_2 and HA" binary system "as-is" under irradiation……..….256

Figure 4.221. "TiO_2 and HA" binary system "as-is" under irradiation surface area profile: Time dependent logN distribution G(d) and multi size distribution C(d)……...257

Figure 4.222. "TiO_2 and HA" binary system "as-is" under irradiation surface area profile: Time dependent comparative presentation of log Normal distribution and multi-size distribution of "TiO_2 and HA" binary system "as-is" under irradiation……..….258

Figure 4.223. "TiO_2 and HA" binary system "as-is" under irradiation number profile: Time dependent logN distribution G(d) and multi size distribution C(d)……...259

Figure 4.224. "TiO_2 and HA" binary system "as-is" under irradiation number profile: Time dependent comparative presentation of log Normal distribution and multi-size distribution of "TiO_2 and HA" binary system "as-is" under irradiation……..….260

Figure 4.225. "TiO_2 and SRNOM" binary system "as-is" under irradiation intensity profile: Time dependent logN distribution G(d) and multi size distribution C(d)……...261

Figure 4.226. "TiO_2 and SRNOM" binary system "as-is" under irradiation intensity profile: Time dependent comparative presentation of log Normal distribution and multi-size distribution of "TiO_2 and SRNOM" binary system "as-is" under irradiation……262

Figure 4.227. "TiO_2 and SRNOM" binary system "as-is" under irradiation volume profile: Time dependent logN distribution G(d) and multi size distribution C(d)……...263

Figure 4.228. "TiO_2 and SRNOM" binary system "as-is" under irradiation volume profile: Time dependent comparative presentation of log Normal distribution and multi-size distribution of "TiO_2 and SRNOM" binary system "as-is" under irradiation……264

Figure 4.229. "TiO_2 and SRNOM" binary system "as-is" under irradiation surface area profile: Time dependent logN distribution G(d) and multi size distribution C(d)……...265

Figure 4.230. "TiO_2 and SRNOM" binary system "as-is" under irradiation surface area profile: Time dependent comparative presentation of log Normal distribution and multi-size distribution of "TiO_2 and SRNOM" binary system "as-is" under irradiation…….....266

Figure 4.231. "TiO_2 and SRNOM" binary system "as-is" under irradiation number profile: Time dependent logN distribution G(d) and multi size distribution C(d)……...267

Figure 4.232. "TiO_2 and SRNOM" binary system "as-is" under irradiation number profile: Time dependent comparative presentation of log Normal distribution and multi-size distribution of "TiO_2 and SRNOM" binary system "as-is" under irradiation……268

Figure 4.233. "N-TiO_2 and HA" binary system "as-is" under irradiation intensity profile: Time dependent logN distribution G(d) and multi size distribution C(d)……...269

Figure 4.234. "N-TiO_2 and HA" binary system "as-is" under irradiation intensity profile: Time dependent comparative presentation of log Normal distribution and multi-size distribution of "N-TiO_2 and HA" binary system "as-is" under

irradiation intensity profile…….270

Figure 4.235. "N-TiO_2 and HA" binary system "as-is" under irradiation volume profile: Time dependent logN distribution G(d) and multi size distribution C(d)……...271

Figure 4.236. "N-TiO_2 and HA" binary system "as-is" under irradiation volume profile: Time dependent comparative presentation of log Normal distribution and multi-size distribution of "N-TiO_2 and HA" binary system "as-is" under irradiation…….….272

Figure 4.237. "N-TiO_2 and HA" binary system "as-is" under irradiation surface area profile: Time dependent logN distribution G(d) and multi size distribution C(d)……...273

Figure 4.238. "N-TiO_2 and HA" binary system "as-is" under irradiation surface area profile: Time dependent comparative presentation of log Normal distribution and multi-size distribution of "N-TiO_2 and HA" binary system "as-is" under irradiation…….….274

Figure 4.239. "N-TiO_2 and HA" binary system "as-is" under irradiation number profile: Time dependent logN distribution G(d) and multi size distribution C(d)……...275

Figure 4.240. "N-TiO_2 and HA" binary system "as-is" under irradiation number profile: Time dependent comparative presentation of log Normal distribution and multi-size distribution of "N-TiO_2 and HA" binary system "as-is" under irradiation…….….276

Figure 4.241. "N-TiO_2 and SRNOM" binary system "as-is" under irradiation intensity profile: Time dependent logN distribution G(d) and multi size distribution C(d)……...277

Figure 4.242. "N-TiO_2 and SRNOM" binary system "as-is" under irradiation intensity profile: Time dependent comparative presentation of log Normal distribution and multi-size distribution of "N-TiO_2 and SRNOM" binary system "as-is" under irradiation…….….278

Figure 4.243. "N-TiO_2 and SRNOM" binary system "as-is" under irradiation volume profile:

Time dependent logN distribution G(d) and multi size distribution C(d)……...279

Figure 4.244. "N-TiO_2 and SRNOM" binary system "as-is" under irradiation volume profile: Time dependent comparative presentation of log Normal distribution and multi-size distribution of "N-TiO_2 and SRNOM" binary system "as-is" under irradiation…….280

Figure 4.245. "N-TiO_2 and SRNOM" binary system "as-is" under irradiation surface area profile: Time dependent logN distribution G(d) and multi size distribution C(d)……..281

Figure 4.246. "N-TiO_2 and SRNOM" binary system "as-is" under irradiation surface area profile: Time dependent comparative presentation of log Normal distribution and multi-size distribution of "N-TiO_2 and SRNOM" binary system "as-is" under irradiation…….……....282

Figure 4.247. "N-TiO_2 and SRNOM" binary system "as-is" under irradiation number profile: Time dependent logN distribution G(d) and multi size distribution C(d)……...283

Figure 4.248. "N-TiO_2 and SRNOM" binary system "as-is" under irradiation number profile: Time dependent comparative presentation of log Normal distribution and multi-size distribution of "N-TiO_2 and SRNOM" binary system "as-is" under irradiation…….….284

Figure 4.249. "Fe-TiO_2 and HA" binary system "as-is" under irradiation intensity profile: Time dependent logN distribution G(d) and multi size distribution C(d)……...285

Figure 4.250. "Fe-TiO_2 and HA" binary system "as-is" under irradiation intensity profile: Time dependent comparative presentation of log Normal distribution and multi-size distribution of "Fe-TiO_2 and HA" binary system "as-is" under irradiation…….….286

Figure 4.251. "Fe-TiO_2 and HA" binary system "as-is" under irradiation volume profile: Time dependent logN distribution G(d) and multi size distribution C(d)……...287

Figure 4.252. "Fe-TiO_2 and HA" binary system "as-is" under irradiation volume profile: Time dependent comparative presentation of log Normal distribution and multi-size distribution of "Fe-TiO_2 and HA" binary system "as-is" under irradiation……..….288

Figure 4.253. "Fe-TiO_2 and HA" binary system "as-is" under irradiation surface area profile: Time dependent logN distribution G(d) and multi size distribution C(d)……...289

Figure 4.254. "Fe-TiO_2 and HA" binary system "as-is" under irradiation surface area profile: Time dependent comparative presentation of log Normal distribution and multi-size distribution of "Fe-TiO_2 and HA" binary system "as-is" under irradiation…….….290

Figure 4.255. "Fe-TiO_2 and HA" binary system "as-is" under irradiation number profile: Time dependent logN distribution G(d) and multi size distribution C(d)……...291

Figure 4.256. "Fe-TiO_2 and HA" binary system "as-is" under irradiation number profile: Time dependent comparative presentation of log Normal distribution and multi-size distribution of "Fe-TiO_2 and HA" binary system "as-is" under irradiation…….292

Figure 4.257. "Fe-TiO_2 and SRNOM" binary system "as-is" under irradiation intensity profile: Time dependent logN distribution G(d) and multi size distribution C(d)…….……...293

Figure 4.258. "Fe-TiO_2 and SRNOM" binary system "as-is" under irradiation intensity profile: Time dependent comparative presentation of log Normal distribution and multi-size distribution of "Fe-TiO_2 and SRNOM" binary system "as-is" under irradiation…….….294

Figure 4.259. "Fe-TiO_2 and SRNOM" binary system "as-is" under irradiation volume profile: Time dependent logN distribution G(d) and multi size distribution C(d)……...295

Figure 4.260. "Fe-TiO_2 and SRNOM" binary system "as-is" under irradiation volume profile: Time dependent comparative presentation of log Normal distribution and multi-size distribution of "Fe-TiO_2 and SRNOM" binary system "as-is" under

irradiation…….….296

Figure 4.261. "Fe-TiO_2 and SRNOM" binary system "as-is" under irradiation surface area profile: Time dependent logN distribution G(d) and multi size distribution C(d)…….297

Figure 4.262. "Fe-TiO_2 and SRNOM" binary system "as-is" under irradiation surface area profile: Time dependent comparative presentation of log Normal distribution and multi-size distribution of "Fe-TiO_2 and SRNOM" binary system "as-is" under irradiation…….298

Figure 4.263. "Fe-TiO_2 and SRNOM" binary system "as-is" under irradiation number profile: Time dependent logN distribution G(d) and multi size distribution C(d)……...299

Figure 4.264. "Fe-TiO_2 and SRNOM" binary system "as-is" under irradiation number profile: Time dependent comparative presentation of log Normal distribution and multi-size distribution of "Fe-TiO_2 and SRNOM" binary system "as-is" under irradiation…….300

Figure 4.265. Sedimentation behavior of TiO_2 under "as-is" conditions, a) UV-vis absorbance variations b) Normalized absorbance with respect to time……...303

Figure 4.266. Sedimentation behavior of N-TiO_2 under "as-is" conditions, a) UV-vis absorbance variations b) Normalized absorbance with respect to time…….…...305

Figure 4.267. Sedimentation behavior of Fe-TiO_2 under "as-is" conditions, a) UV-vis absorbance variations b) Normalized absorbance with respect to time…….…...307

Figure 4.268. Sedimentation behavior of TiO_2 "as-is under dark" conditions, a) UV-vis absorbance variations b) Normalized absorbance with respect to time…….…...310

Figure 4.269. Sedimentation behavior of N-TiO_2 "as-is under dark" conditions, a) UV-vis absorbance variations b) Normalized absorbance with respect to time…….…...312

Figure 4.270. Sedimentation behavior of Fe-TiO_2 "as-is under dark" conditions, a) UV-vis

absorbance variations b) Normalized absorbance with respect to time……...314

Figure 4.271. Sedimentation behavior of TiO_2 "as-is under irradiation", a) UV-vis absorbance variations b) Normalized absorbance with respect to time……...317

Figure 4.272. Sedimentation behavior of N-TiO_2 "as-is under irradiation", a) UV-vis absorbance variations b) Normalized absorbance with respect to time……...319

Figure 4.273. Sedimentation behavior of Fe-TiO_2 "as-is under irradiation", a) UV-vis absorbance variations b) Normalized absorbance with respect to time……...321

Figure 4.274. Sedimentation behavior of "TiO_2 and HA" under "as-is" conditions, a) UV-vis absorbance variations b) Normalized absorbance with respect to time……...324

Figure 4.275. Sedimentation behavior of "TiO_2 and SRNOM" under "as-is" conditions, a) UV-vis absorbance variations b) Normalized absorbance with respect to time……326

Figure 4.276. Sedimentation behavior of "N-TiO_2 and HA" under "as-is" conditions, a) UV-vis absorbance variations b) Normalized absorbance with respect to time……328

Figure 4.277. Sedimentation behavior of "N-TiO_2 and SRNOM" under "as-is" conditions, a) UV-vis absorbance variations b) Normalized absorbance with respect to time……330

Figure 4.278. Sedimentation behavior of "Fe-TiO_2 and HA" under "as-is" conditions, a) UV-vis absorbance variations b) Normalized absorbance with respect to time……332

Figure 4.279. Sedimentation behavior of "Fe-TiO_2 and SRNOM" under "as-is" conditions, a) UV-vis absorbance variations b) Normalized absorbance with respect to time……334

Figure 4.280. Sedimentation behavior of "TiO_2 and HA" "as-is" under dark conditions,

a) UV-vis absorbance variations b) Normalized absorbance with respect to time……338

Figure 4.281. Sedimentation behavior of "TiO_2 and SRNOM" "as-is under dark" conditions, a) UV-vis absorbance variations b) Normalized absorbance with respect to time……340

Figure 4.282. Sedimentation behavior of "N-TiO_2 and HA" "as-is under dark" conditions, a) UV-vis absorbance variations b) Normalized absorbance with respect to time……342

Figure 4.283. Sedimentation behavior of "N-TiO_2 and SRNOM" "as-is under dark" conditions, a) UV-vis absorbance variations b) Normalized absorbance with respect to time……344

Figure 4.284. Sedimentation behavior of "Fe-TiO_2 and HA" "as-is under dark" conditions, a) UV-vis absorbance variations b) Normalized absorbance with respect to time……346

Figure 4.285. Sedimentation behavior of "Fe-TiO_2 and SRNOM" "as-is under dark" conditions, a) UV-vis absorbance variations b) Normalized absorbance with respect to time……348

Figure 4.286. Sedimentation behavior of "TiO_2 and HA_{pho}" binary system following photolysis of organic matter, a) UV-vis absorbance variations b) Normalized absorbance with respect to time……352

Figure 4.287. Sedimentation behavior of "TiO_2 and $SRNOM_{pho}$" binary system following photolysis of organic matter, a) UV-vis absorbance variations b) Normalized absorbance with respect to time……..354

Figure 4.288. Sedimentation behavior of "N-TiO_2 and HA_{pho}" "following photolysis of organic matter", a) UV-vis absorbance variations b) Normalized absorbance with respect to time……356

Figure 4.289. Sedimentation behavior of "N-TiO_2 and $SRNOM_{pho}$" "following photolysis of organic matter", a) UV-vis absorbance variations b) Normalized absorbance with respect to time…….358

Figure 4.290. Sedimentation behavior of "Fe-TiO_2 and HA_{pho}" "following photolysis of organic matter", a) UV-vis absorbance variations b) Normalized absorbance with respect to time…….360

Figure 4.291. Sedimentation behavior of "Fe-TiO_2 and $SRNOM_{pho}$" "following photolysis of organic matter", a) UV-vis absorbance variations b) Normalized absorbance with respect to time…….362

Figure 4.292. Sedimentation behavior of "TiO_2 and HA" "as-is under irradiation", a) UV-vis absorbance variations b) Normalized absorbance with respect to time……...366

Figure 4.293. Sedimentation behavior of "TiO_2 and SRNOM" "as-is under irradiation", a) UV-vis absorbance variations b) Normalized absorbance with respect to time…….368

Figure 4.294. Sedimentation behavior of "N-TiO_2 and HA" "as-is under irradiation", a) UV-vis absorbance variations b) Normalized absorbance with respect to time…….370

Figure 4.295. Sedimentation behavior of "N-TiO_2 and SRNOM" "as-is" under irradiation, a) UV-vis absorbance variations b) Normalized absorbance with respect to time…….372

Figure 4.296. Sedimentation behavior of "Fe-TiO_2 and HA" "as-is" under irradiation, a) UV-vis absorbance variations b) Normalized absorbance with respect to time…….374

Figure 4.297. Sedimentation behavior of "Fe-TiO_2 and SRNOM" "as-is under irradiation", a) UV-vis absorbance variations b) Normalized absorbance with respect to time…….376

Figure 4.298. Hydrodynamic size variations of TiO_2 under “as-is”, “as-is dark” and “as-is irradiation” conditions……380

Figure 4.299. Sedimentation profiles of TiO_2 under “as-is”, “as-is dark” and “as-is irradiation” conditions……...381

Figure 4.300. Turbidity profiles of TiO_2 under “as-is”, “as-is dark” and “as-is irradiation” conditions……...381

Figure 4.301. TiO_2 under “as-is” conditions. Comparative evaluation of selected parameters as hydrodynamic size, hydrodynamic size difference, sedimentation and turbidity variations……382

Figure 4.302. TiO_2 “as-is” under dark conditions. Comparative evaluation of selected parameters as hydrodynamic size, hydrodynamic size difference, sedimentation and turbidity variations……383

Figure 4.303. TiO_2 “as-is” under irradiation. Comparative evaluation of selected parameters as hydrodynamic size, hydrodynamic size difference, sedimentation and turbidity variations……383

Figure 4.304. Hydrodynamic size variations of N-TiO_2 under “as-is”, “as-is dark” and “as-is irradiation” conditions……384

Figure 4.305. Sedimentation profiles of N-TiO_2 under “as-is”, “as-is dark” and “as-is irradiation” conditions……...385

Figure 4.306. Turbidity profiles of N-TiO_2 under “as-is”, “as-is dark” and “as-is irradiation” conditions……...385

Figure 4.307. N-TiO_2 under “as-is” conditions. Comparative evaluation of selected parameters as hydrodynamic size, hydrodynamic size difference, sedimentation and turbidity variations……386

Figure 4.308. N-TiO_2 “as is” under dark conditions. Comparative evaluation of selected

parameters as hydrodynamic size, hydrodynamic size difference, sedimentation and turbidity variations……...387

Figure 4.309. N-TiO_2 “as-is” under irradiation. Comparative evaluation of selected parameters as hydrodynamic size, hydrodynamic size difference, sedimentation and turbidity variations……387

Figure 4.310. Hydrodynamic size variations of Fe-TiO_2 under “as-is”, “as-is dark” and “as-is irradiation” conditions……388

Figure 4.311. Sedimentation profiles of Fe-TiO_2 under “as-is”, “as-is dark” and “as-is irradiation” conditions……...388

Figure 4.312. Turbidity profiles of Fe-TiO_2 under “as-is”, “as-is dark” and “as-is irradiation” conditions……...389

Figure 4.313. Fe-TiO_2 under “as-is” conditions. Comparative evaluation of selected parameters as hydrodynamic size, hydrodynamic size difference, sedimentation and turbidity variations……390

Figure 4.314. Fe-TiO_2 “as-is” under dark conditions. Comparative evaluation of selected parameters as hydrodynamic size, hydrodynamic size difference, sedimentation and turbidity variations……391

Figure 4.315. Fe-TiO_2 “as-is” under irradiation. Comparative evaluation of selected parameters as hydrodynamic size, hydrodynamic size difference, sedimentation and turbidity variations……391

Figure 4.316. Hydrodynamic size variations of TiO_2 and HA binary system under “as-is”, “as-is dark”, “following photolysis of organic matter”, and “as-is irradiation” conditions…….392

Figure 4.317. Sedimentation profiles of TiO_2 and HA binary system under “as-is”, “as-is dark”, “following photolysis of organic matter”, and “as-is irradiation” conditions…….393

Figure 4.318. Turbidity profiles of TiO_2 and HA binary system under “as-is”, “as-is dark”, “following photolysis of organic matter”, and “as-is irradiation” conditions……..394

Figure 4.319. “TiO_2 and HA” binary system under “as-is” conditions. Comparative evaluation of selected parameters as hydrodynamic size, hydrodynamic size difference, sedimentation and turbidity variations…….……395

Figure 4.320. “TiO_2 and HA” binary system “as-is” under dark conditions. Comparative evaluation of selected parameters as hydrodynamic size, hydrodynamic size difference, sedimentation and turbidity variations……..…..396

Figure 4.321. “TiO_2 and HA_{pho}” binary system following photolysis of organic matter. Comparative evaluation of selected parameters as hydrodynamic size, hydrodynamic size difference, sedimentation and turbidity variations……...396

Figure 4.322. “TiO_2 and HA” binary system “as-is” under irradiation. Comparative evaluation of selected parameters as hydrodynamic size, hydrodynamic size difference, sedimentation and turbidity variations……...397

Figure 4.323. Hydrodynamic size variations of TiO_2 and SRNOM binary system under “as-is”, “as-is dark”, “following photolysis of organic matter”, and “as-is irradiation” conditions…….….398

Figure 4.324. Sedimentation profiles of TiO_2 and SRNOM binary system under “as-is”, “as-is dark”, “following photolysis of organic matter”, and “as-is irradiation” conditions…….….399

Figure 4.325. Turbidity profiles of TiO_2 and SRNOM binary system under “as-is”, “as-is dark” and “as-is irradiation” conditions…….…..399

Figure 4.326. “TiO_2 and SRNOM” binary system under “as-is” conditions. Comparative evaluation of selected parameters as hydrodynamic size, hydrodynamic size difference, sedimentation and turbidity variations…….400

Figure 4.327. “TiO_2 and SRNOM” binary system “as-is” under dark conditions. Comparative

evaluation of selected parameters as hydrodynamic size, hydrodynamic size difference, sedimentation and turbidity variations…….401

Figure 4.328. "TiO_2 and $SRNOM_{pho}$" binary system following photolysis of organic matter. Comparative evaluation of selected parameters as hydrodynamic size, hydrodynamic size difference, sedimentation and turbidity variations……..401

Figure 4.329. "TiO_2 and SRNOM" "as-is" under irradiation. Comparative evaluation of selected parameters as hydrodynamic size, hydrodynamic size difference, sedimentation and turbidity variations…….….402

Figure 4.330. Hydrodynamic size variations of N-TiO_2 and HA binary system under "as-is", "as-is dark", "following photolysis of organic matter", and "as-is irradiation" conditions…….403

Figure 4.331. Sedimentation profiles of N-TiO_2 and HA binary system under "as-is", "as-is dark", "following photolysis of organic matter", and "as-is irradiation" conditions…….....404

Figure 4.332. Turbidity profiles of N-TiO_2 and HA binary system under "as-is", "as-is dark" and "as-is irradiation" conditions…….404

Figure 4.333. "N-TiO_2 and HA" binary system under "as-is" conditions. Comparative evaluation of selected parameters as hydrodynamic size, hydrodynamic size difference, sedimentation and turbidity variations…….…..405

Figure 4.334. "N-TiO_2 and HA" binary system "as-is" under dark conditions. Comparative evaluation of selected parameters as hydrodynamic size, hydrodynamic size difference, sedimentation and turbidity variations…….406

Figure 4.335. "N-TiO_2 and HA_{pho}" binary system following photolysis of organic matter. Comparative evaluation of selected parameters as hydrodynamic size, hydrodynamic size difference, sedimentation and turbidity variations……..407

Figure 4.336. "N-TiO_2 and HA" binary system "as-is" under irradiation. Comparative evaluation

of selected parameters as hydrodynamic size, hydrodynamic size difference, sedimentation and turbidity variations……..…..407

Figure 4.337. Hydrodynamic size variations of N-TiO_2 and SRNOM binary system under "as-is", "as-is dark", "following photolysis of organic matter", and "as-is irradiation" conditions…….….408

Figure 4.338. Sedimentation profiles of N-TiO_2 and SRNOM binary system under "as-is", "as-is dark", "following photolysis of organic matter", and "as-is irradiation" conditions…….409

Figure 4.339. Turbidity profiles of N-TiO_2 and SRNOM binary system under "as-is", "as-is dark", "following photolysis of organic matter", and "as-is irradiation" conditions…….....409

Figure 4.340. "N-TiO_2 and SRNOM" binary system under "as-is" conditions. Comparative evaluation of selected parameters as hydrodynamic size, hydrodynamic size difference, sedimentation and turbidity variations…….410

Figure 4.341. "N-TiO_2 and SRNOM" binary system "as-is" under dark conditions. Comparative evaluation of selected parameters as hydrodynamic size, hydrodynamic size difference, sedimentation and turbidity variations…….411

Figure 4.342. "N-TiO_2 and $SRNOM_{pho}$" binary system following photolysis of organic matter. Comparative evaluation of selected parameters as hydrodynamic size, hydrodynamic size difference, sedimentation and turbidity variations……..411

Figure 4.343. "N-TiO_2 and SRNOM" binary system "as-is" under irradiation. Comparative evaluation of selected parameters as hydrodynamic size, hydrodynamic size difference, sedimentation and turbidity variations…….412

Figure 4.344. Hydrodynamic size variations of Fe-TiO_2 and HA binary system under "as-is", "as-is dark", "following photolysis of organic matter", and "as-is irradiation" conditions……...413

Figure 4.345. Sedimentation profiles of Fe-TiO_2 and HA binary system under "as-is", "as-is dark", "following photolysis of organic matter", and "as-is irradiation" conditions……...414

Figure 4.346. Turbidity profiles of Fe-TiO_2 and HA binary system under "as-is", "as-is dark", "following photolysis of organic matter", and "as-is irradiation" conditions…….....414

Figure 4.347. "Fe-TiO_2 and HA" binary system under "as-is" conditions. Comparative evaluation of selected parameters as hydrodynamic size, hydrodynamic size difference, sedimentation and turbidity variations……..…….…..415

Figure 4.348. "Fe-TiO_2 and HA" binary system "as-is" under dark conditions. Comparative evaluation of selected parameters as hydrodynamic size, hydrodynamic size difference, sedimentation and turbidity variations…….416

Figure 4.349. "Fe-TiO_2 and HA_{pho}" binary system following photolysis of organic matter. Comparative evaluation of selected parameters as hydrodynamic size, hydrodynamic size difference, sedimentation and turbidity variations……..416

Figure 4.350. "Fe-TiO_2 and HA" binary system "as-is" under irradiation. Comparative evaluation of selected parameters as hydrodynamic size, hydrodynamic size difference, sedimentation and turbidity variations…….……417

Figure 4.351. Hydrodynamic size variations of Fe-TiO_2 and SRNOM binary system under "as-is", "as-is dark", "following photolysis of organic matter", and "as-is irradiation" conditions…….…….418

Figure 4.352. Sedimentation profiles of Fe-TiO_2 and SRNOM binary system under "as-is", "as-is dark", "following photolysis of organic matter", and "as-is irradiation" conditions…….419

Figure 4.353. Turbidity profiles of Fe-TiO_2 and SRNOM binary system under "as-is", "as-is dark", "following photolysis of organic matter", and "as-is irradiation" conditions…….....419

Figure 4.354. "Fe-TiO_2 and SRNOM" binary system under "as-is" conditions. Comparative evaluation of selected parameters as hydrodynamic size, hydrodynamic size difference, sedimentation and turbidity variations…….420

Figure 4.355. "Fe-TiO_2 and SRNOM" binary system "as-is" under dark conditions. Comparative evaluation of selected parameters as hydrodynamic size, hydrodynamic size difference, sedimentation and turbidity variations…..…….421

Figure 4.356. "Fe-TiO_2 and $SRNOM_{pho}$" binary system following photolysis of organic matter. Comparative evaluation of selected parameters as hydrodynamic size, hydrodynamic size difference, sedimentation and turbidity variations……...422

Figure 4.357. "Fe-TiO_2 and SRNOM" binary system "as-is" under irradiation. Comparative evaluation of selected parameters as hydrodynamic size, hydrodynamic size difference, sedimentation and turbidity variations…….422

LIST OF TABLES

Table 4.1. TiO_2 under "as-is" conditions intensity profile: Time dependent mean diameter, range and min-max diameter difference with respect to log normal and multi-size distribution……30

Table 4.2. Polydispersity of TiO_2 under "as-is" conditions…….....30

Table 4.3. TiO_2 under "as-is" conditions volume profile: Time dependent mean diameter, range and min-max diameter difference with respect to log normal and multi-size distribution……31

Table 4.4. TiO_2 under "as-is" conditions surface area profile: Time dependent mean diameter, range and min-max diameter difference with respect to log normal and multi-size distribution……33

Table 4.5. TiO_2 under "as-is" conditions number profile: Time dependent mean diameter, range and min-max diameter difference with respect to log normal and multi-size distribution……35

Table 4.6. N-TiO_2 under "as-is" conditions intensity profile: Time dependent mean diameter, range and min-max diameter difference with respect to log normal and multi-size distribution…….37

Table 4.7. Polydispersity of "N-TiO_2 under "as-is" conditions" ……...……..38

Table 4.8. N-TiO_2 under "as-is" conditions volume profile: Time dependent mean diameter, range and min-max diameter difference with respect to log normal and multi-size distribution…….....40

Table 4.9. N-TiO_2 under "as-is" conditions surface area profile: Time dependent mean diameter, range and min-max diameter difference with respect to log normal and multi-size distribution…….……42

Table 4.10. N-TiO_2 under "as-is" conditions number profile: Time dependent mean diameter, range and min-max diameter difference with respect to log normal and multi-size distribution……...44

Table 4.11. Fe-TiO_2 under "as-is" conditions intensity profile: Time dependent mean diameter, range and min-max diameter difference with respect to log normal and multi-size distribution…….....46

Table 4.12. Polydispersity of Fe-TiO_2 under "as-is" conditions……..47

Table 4.13. Fe-TiO_2 under "as-is" conditions volume profile: Time dependent mean diameter, range and min-max diameter difference with respect to log normal and multi-size distribution…….....49

Table 4.14. Fe-TiO_2 under "as-is" conditions surface area profile: Time dependent mean diameter, range and min-max diameter difference with respect to log normal and multi-size distribution…….....51

Table 4.15. Fe-TiO_2 under "as-is" conditions number profile: Time dependent mean diameter, range and min-max diameter difference with respect to log normal and multi-size distribution…….....53

Table 4.16. TiO_2 "as-is" under dark conditions intensity profile: Time dependent mean diameter, range and min-max diameter difference with respect to log normal and multi-size distribution…….....55

Table 4.17. Polydispersity of TiO_2 "as-is" under dark conditions……...56

Table 4.18. TiO_2 "as-is" under dark conditions volume profile: Time dependent mean diameter, range and min-max diameter difference with respect to log normal and multi-size distribution…….....57

Table 4.19. TiO_2 "as-is under dark" conditions surface area profile: Time dependent mean diameter, range and min-max diameter difference with respect to log normal and multi-size distribution…….....59

Table 4.20. TiO_2 "as-is" under dark conditions number profile: Time dependent mean diameter, range and min-max diameter difference with respect to log normal and multi-size distribution…….....61

Table 4.21. N-TiO_2 "as-is" under dark conditions intensity profile: Time dependent mean diameter, range and min-max diameter difference with respect to log normal and multi-size distribution…….....63

Table 4.22. Polydispersity of N-TiO_2 "as-is" under dark conditions……...64

Table 4.23. N-TiO_2 "as-is under dark" conditions volume profile: Time dependent mean diameter, range and min-max diameter difference with respect to log normal and multi-size distribution…….....65

Table 4.24. N-TiO_2 "as-is under dark" conditions surface area profile: Time dependent mean diameter, range and min-max diameter difference with respect to log normal and multi-size distribution…….……..67

Table 4.25. N-TiO_2 "as-is under dark" conditions number profile: Time dependent mean diameter, range and min-max diameter difference with respect to log normal and multi-size distribution…….....69

Table 4.26. Fe-TiO_2 "as-is under dark" conditions intensity profile: Time dependent mean diameter, range and min-max diameter difference with respect to log normal and multi-size distribution…….....71

Table 4.27. Polydispersity of Fe-TiO_2 "as-is under dark" conditions……..72

Table 4.28. Fe-TiO_2 "as-is under dark" conditions volume profile: Time dependent mean diameter, range and min-max diameter difference with respect to log normal and multi-size distribution…….....73

Table 4.29. Fe-TiO_2 "as-is under dark" conditions surface area profile: Time dependent mean diameter, range and min-max diameter difference with respect to log normal and multi-size distribution…….…75

Table 4.30. Fe-TiO_2 "as-is under dark" conditions number profile: Time dependent mean diameter, range and min-max diameter difference with respect to log normal and multi-size distribution…….....77

Table 4.31. "TiO_2 as-is under irradiation" conditions intensity profile: Time dependent mean diameter, range and min-max diameter difference with respect to log normal and multi-size distribution…….….79

Table 4.32. Polydispersity of "TiO_2 as-is under irradiation" conditions……..80

Table 4.33. TiO_2 as-is under irradiation" volume profile: Time dependent mean diameter, range and min-max diameter difference with respect to log normal and multi-size distribution…….….81

Table 4.34. TiO_2 "as-is" under irradiation" surface area profile: Time dependent mean diameter, range and min-max diameter difference with respect to log normal and multi-size distribution…….....83

Table 4.35. TiO_2 "as-is" under irradiation conditions number profile: Time dependent mean diameter, range and min-max diameter difference with respect to log normal and multi-size distribution…….….85

Table 4.36. N-TiO_2 "as-is under irradiation" conditions intensity profile: Time dependent mean diameter, range and min-max diameter difference with respect to log normal and multi-size distribution…….……..87

Table 4.37. Polydispersity of N-TiO_2 "as-is under irradiation" conditions……..88

Table 4.38. N-TiO_2 "as-is under irradiation" conditions volume profile: Time dependent mean diameter, range and min-max diameter difference with respect to log normal and multi-size distribution…….……..89

Table 4.39. N-TiO_2 "as-is under irradiation" conditions surface area profile: Time dependent mean diameter, range and min-max diameter difference with respect to log normal and multi-size distribution…….……..91

Table 4.40. N-TiO_2 "as-is under irradiation" conditions number profile: Time dependent mean diameter, range and min-max diameter difference with respect to log normal and multi-size distribution……..……..93

Table 4.41. Fe-TiO_2 "as-is under irradiation" conditions intensity profile: Time dependent mean diameter, range and min-max diameter difference with respect to log normal and multi-size distribution…….……..95

Table 4.42. Polydispersity of Fe-TiO_2 "as-is under irradiation" conditions…….....96

Table 4.43. Fe-TiO_2 "as-is under irradiation" conditions volume profile: Time dependent mean diameter, range and min-max diameter difference with respect to log normal and multi-size distribution…….……..97

Table 4.44. Fe-TiO_2 "as-is under irradiation" conditions surface area profile: Time dependent mean diameter, range and min-max diameter difference with respect to log normal and multi-size distribution…….……99

Table 4.45. Fe-TiO_2 "as-is" under irradiation" conditions number profile: Time dependent mean diameter, range and min-max diameter difference with respect to log normal and multi-size distribution…….101

Table 4.46. "TiO_2 and HA" binary system under "as-is" conditions intensity profile: Time dependent mean diameter, range and min-max diameter difference with respect to log normal and multi-size distribution…….……...105

Table 4.47. Polydispersity of "TiO_2 and HA" binary system under "as-is" conditions…….....105

Table 4.48. "TiO_2 and HA" binary system under "as-is" conditions volume profile: Time dependent mean diameter, range and min-max diameter difference with respect to log normal and multi-size distribution……106

Table 4.49. "TiO_2 and HA" binary system under "as-is" conditions surface area profile: Time dependent mean diameter, range and min-max diameter difference with respect to log normal and multi-size distribution…….……..108

Table 4.50. "TiO_2 and HA" binary system under "as-is" conditions number profile: Time dependent mean diameter, range and min-max diameter difference with respect to log normal and multi-size distribution……...110

Table 4.51. "TiO_2 and SRNOM" binary system under "as-is" conditions intensity profile: Time dependent mean diameter, range and min-max diameter difference with respect to log normal and multi-size distribution……...112

Table 4.52. Polydispersity of "TiO_2 and SRNOM" binary system under "as-is" conditions…….....113

Table 4.53. "TiO_2 and SRNOM" binary system under "as-is" conditions volume profile: Time dependent mean diameter, range and min-max diameter difference with respect to log normal and multi-size distribution……...114

Table 4.54. "TiO_2 and SRNOM" binary system under "as-is" conditions surface area profile: Time dependent mean diameter, range and min-max diameter difference with respect to log normal and multi-size distribution……...116

Table 4.55. "TiO_2 and SRNOM" binary system under "as-is" conditions number profile: Time dependent mean diameter, range and min-max diameter difference with respect to log normal and multi-size distribution……118

Table 4.56. "N-TiO_2 and HA" binary system under "as-is" conditions intensity profile: Time dependent mean diameter, range and min-max diameter difference with respect to log normal and multi-size distribution……....120

Table 4.57. Polydispersity of "N-TiO_2 and HA" binary system under "as-is" conditions…….....121

Table 4.58. "N-TiO_2 and HA" binary system under "as-is" conditions volume profile: Time dependent mean diameter, range and min-max diameter difference with respect to log normal and multi-size distribution……123

Table 4.59. "N-TiO_2 and HA" binary system under "as-is" conditions surface area profile: Time dependent mean diameter, range and min-max diameter difference with respect to log normal and multi-size distribution……125

Table 4.60. "N-TiO_2 and HA" binary system under "as-is" conditions number profile: Time dependent mean diameter, range and min-max diameter difference with respect to log normal and multi-size distribution…….....127

Table 4.61. "N-TiO_2 and SRNOM" binary system under "as-is" conditions intensity profile: Time dependent mean diameter, range and min-max diameter difference with respect to log normal and multi-size distribution……129

Table 4.62. Polydispersity of "N-TiO_2 and SRNOM" binary system under "as-is" conditions…....130

Table 4.63. "N-TiO_2 and SRNOM" binary system under "as-is" conditions volume profile: Time dependent mean diameter, range and min-max diameter difference with respect to log normal and multi-size distribution……131

Table 4.64. "N-TiO_2 and SRNOM" binary system under "as-is" conditions surface area profile: Time dependent mean diameter, range and min-max diameter difference with respect to log normal and multi-size distribution…….…....133

Table 4.65. "N-TiO_2 and SRNOM" binary system under "as-is" conditions number profile: Time dependent mean diameter, range and min-max diameter difference with respect to log normal and multi-size distribution……...……135

Table 4.66. "Fe-TiO_2 and HA" binary system under "as-is" conditions intensity profile: Time dependent mean diameter, range and min-max diameter difference with respect to log normal and multi-size distribution……..…….137

Table 4.67. Polydispersity of "Fe-TiO_2 and HA" binary system under "as-is" conditions…….……138

Table 4.68. "Fe-TiO_2 and HA" binary system under "as-is" conditions volume profile: Time dependent mean diameter, range and min-max diameter difference with respect to log normal and multi-size distribution…….....140

Table 4.69. "Fe-TiO_2 and HA" binary system under "as-is" conditions surface area profile: Time dependent mean diameter, range and min-max diameter difference with respect to log normal and multi-size distribution……142

Table 4.70. "Fe-TiO_2 and HA" binary system under "as-is" conditions number profile: Time dependent mean diameter, range and min-max diameter difference with respect to log normal and multi-size distribution…….....144

Table 4.71. "Fe-TiO_2 and SRNOM" binary system under "as-is" conditions intensity profile: Time dependent mean diameter, range and min-max diameter difference with respect to log normal and multi-size distribution……146

Table 4.72. Polydispersity of "Fe-TiO_2 and SRNOM" binary system under "as-is" conditions……147

Table 4.73. "Fe-TiO_2 and SRNOM" binary system under "as-is" conditions volume profile: Time dependent mean diameter, range and min-max diameter difference with respect to log normal and multi-size distribution……148

Table 4.74. "Fe-TiO_2 and SRNOM" binary system under "as-is" conditions surface area profile: Time dependent mean diameter, range and min-max diameter difference with respect to log normal and multi-size distribution……....150

Table 4.75. "Fe-TiO_2 and SRNOM" binary system under "as-is" conditions number profile: Time dependent mean diameter, range and min-max diameter difference with respect to log normal and multi-size distribution……152

Table 4.76. "TiO_2 and HA" binary system "as-is" under dark conditions intensity profile: Time dependent mean diameter, range and min-max diameter difference with respect to log normal and multi-size distribution…….....156

Table 4.77. Polydispersity of "TiO_2 and HA" binary system "as-is" under dark conditions…….....156

Table 4.78. "TiO_2 and HA" binary system "as-is" under dark conditions volume profile: Time dependent mean diameter, range and min-max diameter difference with respect to log normal and multi-size distribution…….....157

Table 4.79. "TiO_2 and HA" binary system "as-is" under dark conditions surface area profile: Time dependent mean diameter, range and min-max diameter difference with respect to log normal and multi-size distribution……159

Table 4.80. "TiO_2 and HA" binary system "as-is" under dark conditions number profile: Time dependent mean diameter, range and min-max diameter difference with respect to log normal and multi-size distribution…….....161

Table 4.81. "TiO_2 and SRNOM" binary system "as-is" under dark conditions intensity profile: Time dependent mean diameter, range and min-max diameter difference with respect to log normal and multi-size distribution……163

Table 4.82. Polydispersity of "TiO_2 and SRNOM" binary system "as-is" under dark conditions.....164

Table 4.83. "TiO_2 and SRNOM" binary system "as-is" under dark conditions volume profile: Time dependent mean diameter, range and min-max diameter difference with respect to log normal and multi-size distribution……165

Table 4.84. "TiO_2 and SRNOM" binary system "as-is" under dark conditions surface area profile: Time dependent mean diameter, range and min-max diameter difference with respect to log normal and multi-size distribution……....167

Table 4.85. "TiO_2 and SRNOM" binary system "as-is" under dark conditions number profile: Time dependent mean diameter, range and min-max diameter difference with respect to log normal and multi-size distribution……169

Table 4.86. "N-TiO_2 and HA" binary system "as-is" under dark conditions intensity profile: Time dependent mean diameter, range and min-max diameter difference with respect to log normal and multi-size distribution……171

Table 4.87. Polydispersity of "N-TiO_2 and HA" binary system "as-is" under dark conditions….....172

Table 4.88. "N-TiO_2 and HA" binary system "as-is" under dark conditions volume profile: Time dependent mean diameter, range and min-max diameter difference with respect to log normal and multi-size distribution……173

Table 4.89. "N-TiO_2 and HA" binary system "as-is" under dark conditions surface area profile:

Time dependent mean diameter, range and min-max diameter difference with respect to log normal and multi-size distribution…….…….....175

Table 4.90. "N-TiO_2 and HA" binary system "as-is" under dark conditions number profile: Time dependent mean diameter, range and min-max diameter difference with respect to log normal and multi-size distribution……...….177

Table 4.91. "N-TiO_2 and SRNOM" binary system "as-is" under dark conditions intensity profile: Time dependent mean diameter, range and min-max diameter difference with respect to log normal and multi-size distribution…….....179

Table 4.92. Polydispersity of "N-TiO_2 and SRNOM" binary system "as-is" under dark conditions…….….180

Table 4.93. "N-TiO_2 and SRNOM" binary system "as-is" under dark conditions volume profile: Time dependent mean diameter, range and min-max diameter difference with respect to log normal and multi-size distribution…….....181

Table 4.94. "N-TiO_2 and SRNOM" binary system "as-is" under dark conditions surface area profile: Time dependent mean diameter, range and min-max diameter difference with respect to log normal and multi-size distribution……183

Table 4.95. "N-TiO_2 and SRNOM" binary system "as-is" under dark conditions number profile: Time dependent mean diameter, range and min-max diameter difference with respect to log normal and multi-size distribution…….....185

Table 4.96. "Fe-TiO_2 and HA" binary system "as-is" under dark conditions intensity profile: Time dependent mean diameter, range and min-max diameter difference with respect to log normal and multi-size distribution……187

Table 4.97. Polydispersity of "Fe-TiO_2 and HA" binary system "as-is" under dark conditions.……188

Table 4.98. "Fe-TiO_2 and HA" binary system "as-is" under dark conditions volume profile: Time dependent mean diameter, range and min-max diameter difference with

respect to log normal and multi-size distribution……189

Table 4.99. "Fe-TiO_2 and HA" binary system "as-is" under dark conditions surface area profile: Time dependent mean diameter, range and min-max diameter difference with respect to log normal and multi-size distribution…….……..…..191

Table 4.100. "Fe-TiO_2 and HA" binary system "as-is" under dark conditions number profile: Time dependent mean diameter, range and min-max diameter difference with respect to log normal and multi-size distribution…….....193

Table 4.101. "Fe-TiO_2 and SRNOM" binary system "as-is" under dark conditions intensity profile: Time dependent mean diameter, range and min-max diameter difference with respect to log normal and multi-size distribution……..195

Table 4.102. Polydispersity of "Fe-TiO_2 and SRNOM" binary system "as-is" under dark conditions……196

Table 4.103. "Fe-TiO_2 and SRNOM" binary system "as-is" under dark conditions volume profile: Time dependent mean diameter, range and min-max diameter difference with respect to log normal and multi-size distribution……..197

Table 4.104. "Fe-TiO_2 and SRNOM" binary system "as-is" under dark conditions surface area profile: Time dependent mean diameter, range and min-max diameter difference with respect to log normal and multi-size distribution……..199

Table 4.105. "Fe-TiO_2 and SRNOM" binary system "as-is" under dark conditions number profile: Time dependent mean diameter, range and min-max diameter difference with respect to log normal and multi-size distribution……..201

Table 4.106. "TiO_2 and HA_{pho}" binary system following photolysis of organic matter intensity profile: Time dependent mean diameter, range and min-max diameter difference with respect to log normal and multi-size distribution……..205

Table 4.107. Polydispersity of "TiO_2 and HA_{pho}" binary system following photolysis of organic matter……...205

Table 4.108. "TiO_2 and HA_{pho}" binary system following photolysis of organic matter volume profile: Time dependent mean diameter, range and min-max diameter difference with respect to log normal and multi-size distribution……..206

Table 4.109. "TiO_2 and HA_{pho}" binary system following photolysis of organic matter surface area profile: Time dependent mean diameter, range and min-max diameter difference with respect to log normal and multi-size distribution…….208

Table 4.110. "TiO_2 and HA_{pho}" binary system following photolysis of organic matter number profile: Time dependent mean diameter, range and min-max diameter difference with respect to log normal and multi-size distribution……..210

Table 4.111. "TiO_2 and $SRNOM_{pho}$" binary system following photolysis of organic matter intensity profile: Time dependent mean diameter, range and min-max diameter difference with respect to log normal and multi-size distribution…….212

Table 4.112. Polydispersity of "TiO_2 and $SRNOM_{pho}$" binary system following photolysis of organic matter…….213

Table 4.113. "TiO_2 and $SRNOM_{pho}$" binary system following photolysis of organic matter volume profile: Time dependent mean diameter, range and min-max diameter difference with respect to log normal and multi-size distribution…….214

Table 4.114. "TiO_2 and $SRNOM_{pho}$" binary system following photolysis of organic matter surface area profile: Time dependent mean diameter, range and min-max diameter difference with respect to log normal and multi-size distribution……..216

Table 4.115. "TiO_2 and $SRNOM_{pho}$" binary system following photolysis of organic matter number profile: Time dependent mean diameter, range and min-max diameter difference with respect to log normal and multi-size distribution…….218

Table 4.116. "N-TiO_2 and HA_{pho}" binary system following photolysis of organic matter intensity profile: Time dependent mean diameter, range and min-max diameter difference with respect to log normal and multi-size distribution……..220

Table 4.117. Polydispersity of "N-TiO_2 and HA_{pho}" binary system following photolysis of organic matter…….....221

Table 4.118. "N-TiO_2 and HA_{pho}" binary system following photolysis of organic matter volume profile: Time dependent mean diameter, range and min-max diameter difference with respect to log normal and multi-size distribution…….222

Table 4.119. "N-TiO_2 and HA_{pho}" binary system following photolysis of organic matter surface area profile: Time dependent mean diameter, range and min-max diameter difference with respect to log normal and multi-size distribution……..224

Table 4.120. "N-TiO_2 and HA_{pho}" binary system following photolysis of organic matter number profile: Time dependent mean diameter, range and min-max diameter difference with respect to log normal and multi-size distribution…….226

Table 4.121. "N-TiO_2 and $SRNOM_{pho}$" binary system following photolysis of organic matter intensity profile: Time dependent mean diameter, range and min-max diameter difference with respect to log normal and multi-size distribution…….....228

Table 4.122. Polydispersity of "N-TiO_2 and $SRNOM_{pho}$" binary system following photolysis of organic matter…….…….229

Table 4.123. "N-TiO_2 and $SRNOM_{pho}$" binary system following photolysis of organic matter volume profile: Time dependent mean diameter, range and min-max diameter difference with respect to log normal and multi-size distribution…….....230

Table 4.124. "N-TiO_2 and $SRNOM_{pho}$" binary system following photolysis of organic matter surface area profile: Time dependent mean diameter, range and min-max diameter difference with respect to log normal and multi-size distribution……..232

Table 4.125. "N-TiO_2 and $SRNOM_{pho}$" binary system following photolysis of organic matter number profile: Time dependent mean diameter, range and min-max diameter difference with respect to log normal and multi-size distribution…….....234

Table 4.126. "Fe-TiO_2 and HA_{pho}" binary system following photolysis of organic matter

intensity profile: Time dependent mean diameter, range and min-max diameter difference with respect to log normal and multi-size distribution……...236

Table 4.127. Polydispersity of "Fe-TiO_2 and HA_{pho}" binary system following photolysis of organic matter…….….237

Table 4.128. "Fe-TiO_2 and HA_{pho}" binary system following photolysis of organic matter volume profile: Time dependent mean diameter, range and min-max diameter difference with respect to log normal and multi-size distribution…….238

Table 4.129. "Fe-TiO_2 and HA_{pho}" binary system following photolysis of organic matter surface area profile: Time dependent mean diameter, range and min-max diameter difference with respect to log normal and multi-size distribution……..241

Table 4.130. "Fe-TiO_2 and HA_{pho}" binary system following photolysis of organic matter number profile: Time dependent mean diameter, range and min-max diameter difference with respect to log normal and multi-size distribution…….243

Table 4.131. "Fe-TiO_2 and $SRNOM_{pho}$" binary system following photolysis of organic matter intensity profile: Time dependent mean diameter, range and min-max diameter difference with respect to log normal and multi-size distribution…….....245

Table 4.132. Polydispersity of "Fe-TiO_2 and $SRNOM_{pho}$" binary system following photolysis of organic matter……..246

Table 4.133. "Fe-TiO_2 and $SRNOM_{pho}$" binary system following photolysis of organic matter volume profile: Time dependent mean diameter, range and min-max diameter difference with respect to log normal and multi-size distribution…….....247

Table 4.134. "Fe-TiO_2 and $SRNOM_{pho}$" binary system following photolysis of organic matter surface area profile: Time dependent mean diameter, range and min-max diameter difference with respect to log normal and multi-size distribution…….....249

Table 4.135. "Fe-TiO_2 and $SRNOM_{pho}$" binary system following photolysis of organic matter

number profile: Time dependent mean diameter, range and min-max diameter difference with respect to log normal and multi-size distribution…….....251

Table 4.136. "TiO_2 and HA" binary system "as-is" under irradiation intensity profile: Time dependent mean diameter, range and min-max diameter difference with respect to log normal and multi-size distribution……..253

Table 4.137. Polydispersity of "TiO_2 and HA" binary system "as-is" under irradiation……254

Table 4.138. "TiO_2 and HA" binary system "as-is" under irradiation volume profile: Time dependent mean diameter, range and min-max diameter difference with respect to log normal and multi-size distribution…….255

Table 4.139. "TiO_2 and HA" binary system "as-is" under irradiation surface area profile: Time dependent mean diameter, range and min-max diameter difference with respect to log normal and multi-size distribution…….257

Table 4.140. "TiO_2 and HA" binary system "as-is" under irradiation number profile: Time dependent mean diameter, range and min-max diameter difference with respect to log normal and multi-size distribution……..259

Table 4.141. "TiO_2 and SRNOM" binary system "as-is" under irradiation intensity profile: Time dependent mean diameter, range and min-max diameter difference with respect to log normal and multi-size distribution…….....261

Table 4.142. Polydispersity of "TiO_2 and SRNOM" binary system "as-is" under irradiation……262

Table 4.143. "TiO_2 and SRNOM" binary system "as-is" under irradiation volume profile: Time dependent mean diameter, range and min-max diameter difference with respect to log normal and multi-size distribution…….....263

Table 4.144. "TiO_2 and SRNOM" binary system "as-is" under irradiation surface area profile: Time dependent mean diameter, range and min-max diameter difference with respect to log normal and multi-size distribution…….....265

Table 4.145. "TiO_2 and SRNOM" binary system "as-is" under irradiation number profile: Time dependent mean diameter, range and min-max diameter difference with respect to log normal and multi-size distribution……..267

Table 4.146. "N-TiO_2 and HA" binary system "as-is" under irradiation intensity profile: Time dependent mean diameter, range and min-max diameter difference with respect to log normal and multi-size distribution……..269

Table 4.147. Polydispersity of "N-TiO_2 and HA" binary system "as-is" under irradiation intensity profile……270

Table 4.148. "N-TiO_2 and HA" binary system "as-is" under irradiation volume profile: Time dependent mean diameter, range and min-max diameter difference with respect to log normal and multi-size distribution…….....271

Table 4.149. "N-TiO_2 and HA" binary system "as-is" under irradiation surface area profile: Time dependent mean diameter, range and min-max diameter difference with respect to log normal and multi-size distribution…….....273

Table 4.150. "N-TiO_2 and HA" binary system "as-is" under irradiation number profile: Time dependent mean diameter, range and min-max diameter difference with respect to log normal and multi-size distribution…….....275

Table 4.151. "N-TiO_2 and SRNOM" binary system "as-is" under irradiation intensity profile: Time dependent mean diameter, range and min-max diameter difference with respect to log normal and multi-size distribution…….....277

Table 4.152. Polydispersity of "N-TiO_2 and SRNOM" binary system "as-is" under irradiation……278

Table 4.153. "N-TiO_2 and SRNOM" binary system "as-is" under irradiation volume profile: Time dependent mean diameter, range and min-max diameter difference with respect to log normal and multi-size distribution……..279

Table 4.154. "N-TiO_2 and SRNOM" binary system "as-is" under irradiation surface area profile:

Time dependent mean diameter, range and min-max diameter difference with respect to log normal and multi-size distribution……..281

Table 4.155. "N-TiO_2 and SRNOM" binary system "as-is" under irradiation number profile: Time dependent mean diameter, range and min-max diameter difference with respect to log normal and multi-size distribution……..283

Table 4.156. "Fe-TiO_2 and HA" binary system "as-is" under irradiation intensity profile: Time dependent mean diameter, range and min-max diameter difference with respect to log normal and multi-size distribution……..285

Table 4.157. Polydispersity of "Fe-TiO_2 and HA" binary system "as-is" under irradiation……...286

Table 4.158. "Fe-TiO_2 and HA" binary system "as-is" under irradiation volume profile: Time dependent mean diameter, range and min-max diameter difference with respect to log normal and multi-size distribution…….....287

Table 4.159. "Fe-TiO_2 and HA" binary system "as-is" under irradiation surface area profile: Time dependent mean diameter, range and min-max diameter difference with respect to log normal and multi-size distribution…….....289

Table 4.160. "Fe-TiO_2 and HA" binary system "as-is" under irradiation number profile: Time dependent mean diameter, range and min-max diameter difference with respect to log normal and multi-size distribution…….291

Table 4.161. "Fe-TiO_2 and SRNOM" binary system "as-is" under irradiation intensity profile: Time dependent mean diameter, range and min-max diameter difference with respect to log normal and multi-size distribution……...……...293

Table 4.162. Polydispersity of "Fe-TiO_2 and SRNOM" binary system "as-is" under irradiation.....294

Table 4.163. "Fe-TiO_2 and SRNOM" binary system "as-is" under irradiation volume profile: Time dependent mean diameter, range and min-max diameter difference with respect to log normal and multi-size distribution…….....295

Table 4.164. "Fe-TiO_2 and SRNOM" binary system "as-is" under irradiation surface area profile: Time dependent mean diameter, range and min-max diameter difference with respect to log normal and multi-size distribution……..297

Table 4.165. "Fe-TiO_2 and SRNOM" binary system "as-is" under irradiation number profile: Time dependent mean diameter, range and min-max diameter difference with respect to log normal and multi-size distribution…….....299

Table 4.166. TiO_2 under "as-is" conditions, kinetic model parameters……..304

Table 4.167. N-TiO_2 under "as-is" conditions, kinetic model parameters…….306

Table 4.168. Fe-TiO_2 under "as-is" conditions, kinetic model parameters……....308

Table 4.169. Comparative presentation of sedimentation kinetics of NPs under "as-is" conditions at λ=550 nm……309

Table 4.170. TiO_2 "as-is under dark" conditions, kinetic model parameters…….....311

Table 4.171. N-TiO_2 "as-is under dark" conditions, kinetic model parameters…….....313

Table 4.172. Fe-TiO_2 "as-is under dark" conditions, kinetic model parameters…….....315

Table 4.173. Comparative presentation of sedimentation kinetics of NPs under "as-is under dark" conditions at λ= 550 nm……..316

Table 4.174. TiO_2 "as-is under irradiation", kinetic model parameters…….318

Table 4.175. N-TiO_2 "as-is under irradiation", kinetic model parameters…….....319

Table 4.176. Fe-TiO_2 "as-is under irradiation", kinetic model parameters…….....322

Table 4.177. Comparative presentation of sedimentation kinetics of NPs under "as-is irradiation" conditions at λ=550 nm……...323

Table 4.178. "TiO_2 and HA" under "as-is" conditions, kinetic model parameters…….....325

Table 4.179. "TiO_2 and SRNOM" under "as-is" conditions, kinetic model parameters…….....327

Table 4.180. "N-TiO_2 and HA" under "as-is" conditions, kinetic model parameters…….....329

Table 4.181. "N-TiO_2 and SRNOM" under "as-is" conditions, kinetic model parameters……331

Table 4.182. "Fe-TiO_2 and HA" under "as-is" conditions, kinetic model parameters……333

Table 4.183. "Fe-TiO_2 and SRNOM" under "as-is" conditions, kinetic model parameters……...335

Table 4.184. Comparative presentation of sedimentation kinetics of NPs under "as-is" conditions at λ=550 nm……336

Table 4.185. Comparative presentation of sedimentation kinetics of NPs under "as-is" conditions at λ=550 nm……337

Table 4.186. "TiO_2 and HA" "as-is under dark" conditions, kinetic model parameters…….……339

Table 4.187. "TiO_2 and SRNOM" "as-is under dark" conditions, kinetic model parameters…..…...341

Table 4.188. "N-TiO_2 and HA" "as-is under dark" conditions, kinetic model parameters…….……343

Table 4.189. "N-TiO_2 and SRNOM" "as-is under dark" conditions, kinetic model parameters……345

Table 4.190. "Fe-TiO_2 and HA" "as-is under dark" conditions, kinetic model parameters……347

Table 4.191. "Fe-TiO_2 and SRNOM" "as-is" under dark conditions, kinetic model parameters……349

Table 4.192. Comparative presentation of sedimentation kinetics of NPs under "as-is under dark" conditions at λ=550 nm……..350

Table 4.193. Comparative presentation of sedimentation kinetics of NPs under "as-is under dark" conditions at λ=550 nm……..351

Table 4.194. "TiO_2 and HA_{pho}" binary system following photolysis of organic matter, kinetic model parameters…….353

Table 4.195. "TiO_2 and $SRNOM_{pho}$" binary system following photolysis of organic matter, kinetic model parameters…….355

Table 4.196. "N-TiO_2 and HA_{pho}" binary system following photolysis of organic matter, kinetic model parameters…….357

Table 4.197. "N-TiO_2 and $SRNOM_{pho}$" binary system following photolysis of organic matter, kinetic model parameters…….359

Table 4.198. "Fe-TiO_2 and HA_{pho}" binary system following photolysis of organic matter, kinetic model parameters…….361

Table 4.199. "Fe-TiO_2 and $SRNOM_{pho}$" binary system following photolysis of organic matter, kinetic model parameters…….363

Table 4.200. Comparative presentation of sedimentation kinetics of NPs under "following photolysis of organic matter" conditions at λ=550 nm…….....364

Table 4.201. Comparative presentation of sedimentation kinetics of NPs under "following photolysis of organic matter" conditions at λ=550 nm…….....365

Table 4.202. "TiO_2 and HA" "as-is" under irradiation, kinetic model parameters…….……367

Table 4.203. "TiO_2 and SRNOM" "as-is" under irradiation, kinetic model parameters…….…...369

Table 4.204. "N-TiO_2 and HA" "as-is" under irradiation, kinetic model parameters…….…...371

Table 4.205. "N-TiO_2 and SRNOM" "as-is" under irradiation, kinetic model parameters…….…...373

Table 4.206. “Fe-TiO_2 and HA” “as-is” under irradiation, kinetic model parameters……...375

Table 4.207. “Fe-TiO_2 and SRNOM” “as-is” under irradiation, kinetic model parameters……...377

Table 4.208. Comparative presentation of sedimentation kinetics of NPs under “as-is” irradiation conditions at λ=550 nm…….....378

Table 4.209. Comparative presentation of sedimentation kinetics of NPs under “as-is” irradiation conditions at λ=550 nm…….....379

Table A. Nanoparticle characterizations…….....435

Table B. Specified and specific UV-vis spectroscopic parameters and NPOC of HA samples.....436

LIST OF SYMBOLS / ABBREVIATIONS

Symbol	Explanation	Unit
A/A_o	Normalized absorbance	
A_λ	Absorbance at specific wavelength at time t	
$A_{\lambda o}$	Absorbance at specific wavelength at time 0	
°C	Celsius	
C	Concentration	
C_0	Initial concentration	
C/C_0	Normalized concentration	
C(d)	Multi-size distribution	
cm	Centimeter	
CO_2	Carbon dioxide	
d	Particle size	nm
$\overline{D}$	Diffusion coefficient	
$\bar{d}$	Average diameter	
d_a	Area average	
d_n	Number average	
d_w	Weight average	
E_{bg}	Band-gap energy	eV
e^-	Electron	
e_{cb}^-	Photogenerated electron	
Fe	Iron	
FI_{sync}	Fluorescence intensity in synchronous scan mode	
g	Gram	
G(d)	LogN distribution	
h	Planck's constant	$6.63x10^{-34}$ m^2 kg/s
h^+	Photogenerated hole	
H^+	Hydrogen ion	
H_2O	Water	
H_2O_2	Hydrogen peroxide	

HA_{pho}	Humic acid subjected to photolysis	
$HO^{\bullet}$	Hydroxyl radical	
k	Rate constant	min^{-1}
λ	Wavelength	nm
λ_{emis}	Emission wavelength	nm
λ_{exc}	Excitation wavelength	nm
L	Liter	
m	Meter	
M	Particle mass	
M^2	Particle mass square	
N	Nitrogen	
P	Shape factor	
μm	Micrometer	
mg	Milligram	
mL	Milliliter	
mW	Miliwatt	
ν	Frequency of the light	s^{-1}
nm	Nanometer	
O_2	Oxygen	
O_3	Ozone	
$O_2^{\bullet -}$	Superoxide radical anion	
pK_a	p function of acid dissociation constant	
%	Percentage	
pH	p function of hydrogen ion concentration	
pH_{zpc}	pH of point of zero charge condition	
Ti	Titanium	
t	Time	min
TiO_2	Titanium dioxide	
W	Watt	

Abbreviation	Explanation	
AOPs	Advanced oxidation processes	
BET	Brunauer-Emmett-Teller	
CB	Conduction band	
$Color_{436}$	Absorbance at 436 nm	
DLS	Dynamic light scattering	
DLVO	Derjaguin, Landau, Verwey and Overbeek	
DOM	Dissolved organic matter	
DOC	Dissolved organic carbon	mg/L
E2/E3	Ratio of $UV_{254}/Color_{436}$	
FA	Fulvic acid	
FI	Fluorescence intensity	
FI_{emis}	Fluorescence emission	
HA	Humic acid	
HS	Humic substances	
IHSS	International Humic Substance Society	
min	Minute	
NP	Nanoparticle	
NPOC	Non-purgeable organic carbon	mg Org C/L
NTU	Nephelometric turbidity unit	
NOM	Natural organic matter	
PSD	Particle size distribution	
ROS	Reactive oxygen species	
$SCoA_{436}$	Specific color absorbance at 436 nm	L/m mg
SFI	Specific fluorescence intensity	
SFI_{sync}	Specific fluorescence intensity in synchronous scan mode	
SFI_{emis}	Specific fluorescence intensity in emission scan mode	
SRNOM	Suwannee River natural organic matter	
$SRNOM_{pho}$	Suwannee River natural organic matter subjected to photolysis	
$SUVA_{254}$	Specific UV Absorbance at 254 nm	L/m mg
$SUVA_{280}$	Specific UV Absorbance at 280 nm	L/m mg
$SUVA_{365}$	Specific UV Absorbance at 365 nm	L/m mg

TOC	Total organic carbon
UV	Ultraviolet
UV_{254}	Absorbance at 254 nm
UV_{280}	Absorbance at 280 nm
UV_{365}	Absorbance at 365 nm
UV-vis	Ultraviolet-visible
VB	Valence band

1. INTRODUCTION

Natural organic matter (NOM) defined as all of the broken-down organic material that comes from plants and animals in the environment. The natural colloidal composition of natural water could be described with the presence of macro molecules and their aggregates (organic matter, DOM sub-fractions, *etc*...), inorganic colloids (clays, oxides, *etc*…), bio colloids (algae, bacteria *etc*...), and aggregates (composed of particles, macromolecules, biocolloids *etc*…) (Colombo et al., 2015; Hufschmid et al., 2017; Zhou et al., 2012).

In many cases a colloidal system consists of two distinct phases: a dispersed phase (or internal phase) and a continuous phase (or dispersion medium). Colloidal system can be solid in liquid, liquid in liquid, liquid in gas, *etc*... depending upon the form of dispersed phase and dispersion medium. Basic definition of aggregates and agglomerates depends on the behavior of primary particles occurring in different geometrical forms. Aggregates are defined as clusters of particles expressing surface area smaller than the sum of the primary particles. Whereas, agglomerates are formed by edge to edge, corner to corner and edge to corner interactions of the primary particles. In colloidal stability, the interactions between colloidal particles play a crucial role and lead to a wealth of significant and interesting kind of dispersion behavior (Henglein, 1861; Martínez et al., 2011).

Photocatalytic reaction system is generally consisted of a photocatalyst *i.e.* TiO_2 and a substrate *e.g.* NOM namely humic substances (HS) composed of humic (HA) and fulvic acids (FA). Photocatalysis proceeds via surface oriented reactions therefore, pre adsorption of the substrate onto photocatalyst is required. Since light exposure initiates the photocatalytic reactions, photolytic reactions of substrate should also be encountered (Kisch, 2015; Pichat, 2013; Sharpless et al., 2014).

Photolysis is a chemical process by which chemical bonds are broken as the result of transfer of light energy (direct photolysis) or radiant energy (indirect photolysis) to these bonds. Numerous chemical and environmental factors including the light adsorption properties and reactivity of the chemical, and the intensity of solar radiation affect the rate of photolysis.

Photocatalytic treatment of NOM and its analog compounds has been studied for decades by Bekbolet and colleagues. NOM is considered as one of the major colloidal component of natural water matrix. NOM delivers extensive reactions that could be considered as important most significantly to human health. Moreover, it should be indicated that the dissolved fraction of NOM

as defined by the fraction passing 0.45 μm filter and described as dissolved organic matter (DOM) would be more significant due to the diversity in chemical composition in aqueous phase.

Based on the literature survey findings, it was clearly stated that colloidal behavior of both inorganic and organic components displayed various reactions under solar irradiation in nanoscale conditions. The main objective of this study is to investigate the colloidal behavior of the binary system prior to, during and under post photo-treatment conditions. Following individual assessments, binary systems composed of humic fractions and nanoparticles (NPs) were subjected to evaluation by respective indicative parameters. Hence, overall evaluation of the systems provided information both during photocatalysis as well as light induced reactions under environmental conditions.

2. LITERATURE REVIEW

The colloidal constituents of natural waters could be described with the presence of macro molecular organics (natural organic matter (NOM), dissolved organic matter (DOM) and sub-fractions, *etc*...), inorganic colloids (clays, oxides, *etc*…), bio colloids (algae, bacteria *etc*...), and aggregates of these components formed through various interactions (Colombo et al., 2015; Hufschmid et al., 2017; Zhou et al., 2012).

In many cases a colloidal system consists of two distinct phases: a dispersed phase (or internal phase) and a continuous phase (or dispersion medium). From a general perspective, a colloidal system can be solid in liquid, liquid in liquid, liquid in gas, *etc*... depending upon the form of dispersed phase and dispersion medium. Basic definition of aggregates and agglomerates depends on the behavior of primary particles occurring in different geometrical forms. Aggregates are defined as clusters of particles expressing surface area smaller than the sum of the primary particles. Whereas, agglomerates are formed by edge to edge, corner to corner and edge to corner interactions of the primary particles. In colloidal stability, the interactions between colloidal particles play a crucial role and lead to a wealth of significant and interesting kind of dispersion behavior (Henglein, 1861; Martínez et al., 2011).

2.1. Colloidal Interactions

Colloid science is known to the scientific community for 150 years. In terms of length scales, the colloidal regime is approximately considered between 1 nm and 1,000 nm (Velev et al., 2009). It covers the size range between simple molecules and objects visible in a light microscope.

In colloidal stability, the interactions between colloidal particles play a crucial role and lead to a wealth of significant and interesting kind of dispersion behavior (Henglein, 1861; Martínez et al., 2011). Interactions between nano- and micro-sized inorganic colloid particles of fixed shape (hard matter), as well as interactions between hard and soft matter (surfactants, proteins and polymers) have a great importance in the field of nanotechnology and holds the key to the stability, fabrication and properties of the nanomaterials. Therefore, studying the interactions in the colloidal domain has an importance not only for their bio-medical applications but also for the improvement and betterment of many daily-use industrial products (Bharti, 2014). Repulsive and attractive forces influence the individual particles in a hydrophobic solution. The repulsive forces derive from the electrical double

layer, whereas the principle attractive forces derive from van der Waals forces of intermolecular attraction which affects the colloids to agglomerate or separate (Figure 2.1).

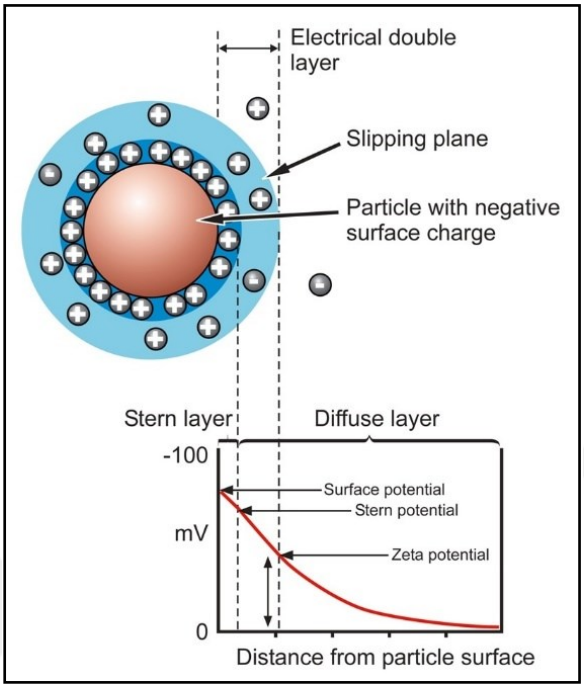


Figure 2.1. Particle Stern layer and electrical double layer formation (Hendricks, 2006).

According to theories developed by Derjaguin, Landau, Verwey and Overbeek (DLVO), interactions between these forces contribute to the overall stability of a colloidal dispersion (Benefield et al., 1982; Hendricks, 2006). Interactions between repulsive and attractive forces are presented in Figure 2.2.

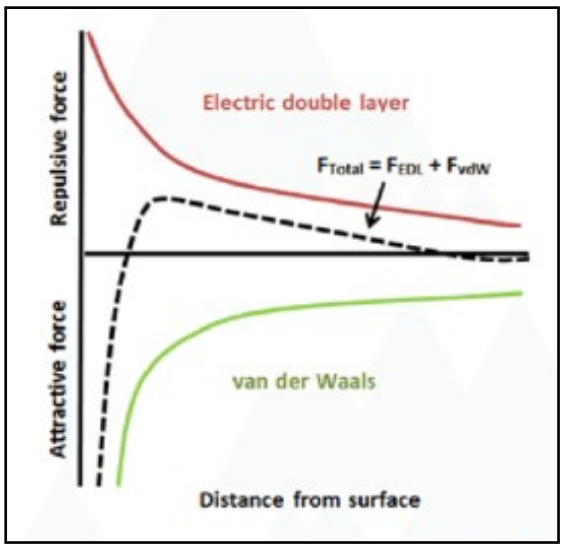


Figure 2.2. Interactions between repulsive and attractive forces (Hendricks, 2006).

Charged colloids are held apart as a result of their electrical charge, basically similarly charges repel and opposite charges attract each other. The magnitude of this charge on a colloidal particle cannot be measured directly; however, a value of the potential at some distance from the particle can be calculated from a measurement of the electrophoretic mobility of the particle. Electrophoretic mobility is defined as the solute's behavior as a response to the applied electrical field in which cations move toward the negatively charged cathode, and anions move toward the positively charged anode as expected whereas neutral species remain stationary.

Zeta potential is the potential that exists at the plane of shear between the bulk liquid and an envelope of water that moves with the particle. Although the exact location of this shearing plane is not known, it is generally thought to lie in the diffuse layer. The magnitude of the zeta potential refers to a rough measure of the stability of a colloidal particle. High zeta potentials suggest strong forces of separation and stable colloidal systems, lower zeta potentials are associated with less stable systems (Benefield et al., 1982).

Since they affect key colloid properties such as rheology, film gloss, surface area and packing density, the particle size and particle size distribution (PSD) of materials express great importance. Additionally, some precautions need to be taken to prevent particles from sticking together (aggregating) due to inter-particle collisions in the liquid medium in order to prevent the aggregation of fine particles into much larger, undesirable units. This can be attained by creating an interparticle electrical and/or steric energy barrier. For very fine particles, to prevent aggregation, a combination of both electrical and steric barriers can be needed (Venkataraman, 2005).

Behavior of primary particles occurring in different geometrical forms directly result on either aggregate or agglomerate formations. Aggregates are defined as clusters of particles expressing surface area smaller than the sum of the primary particles held by strong chemical forces. Whereas, agglomerates are formed by edge to edge, corner to corner and edge to corner interactions of the primary particles brought together by weak van der Waals forces. Size of the agglomerates vary in shape and depend on solution conditions, temperature, viscosity *etc*... Moreover, density of agglomerates directly depends on particle size distribution of the primary particles. Primary particles initially form agglomerate by adhesive forces followed by aggregation. Formation of agglomerates leads to destabilization of the colloidal systems. Though agglomerates could easily be broken by mechanical means, aggregates are comprised of strongly bonded particles through a process that is generally regarded as reversible under certain conditions (Piccolo, 2001). The alteration of

characteristics of dry nanoparticle powders when added to a liquid is illustrated in Figure 2.3 (Jiang et al, 2009).

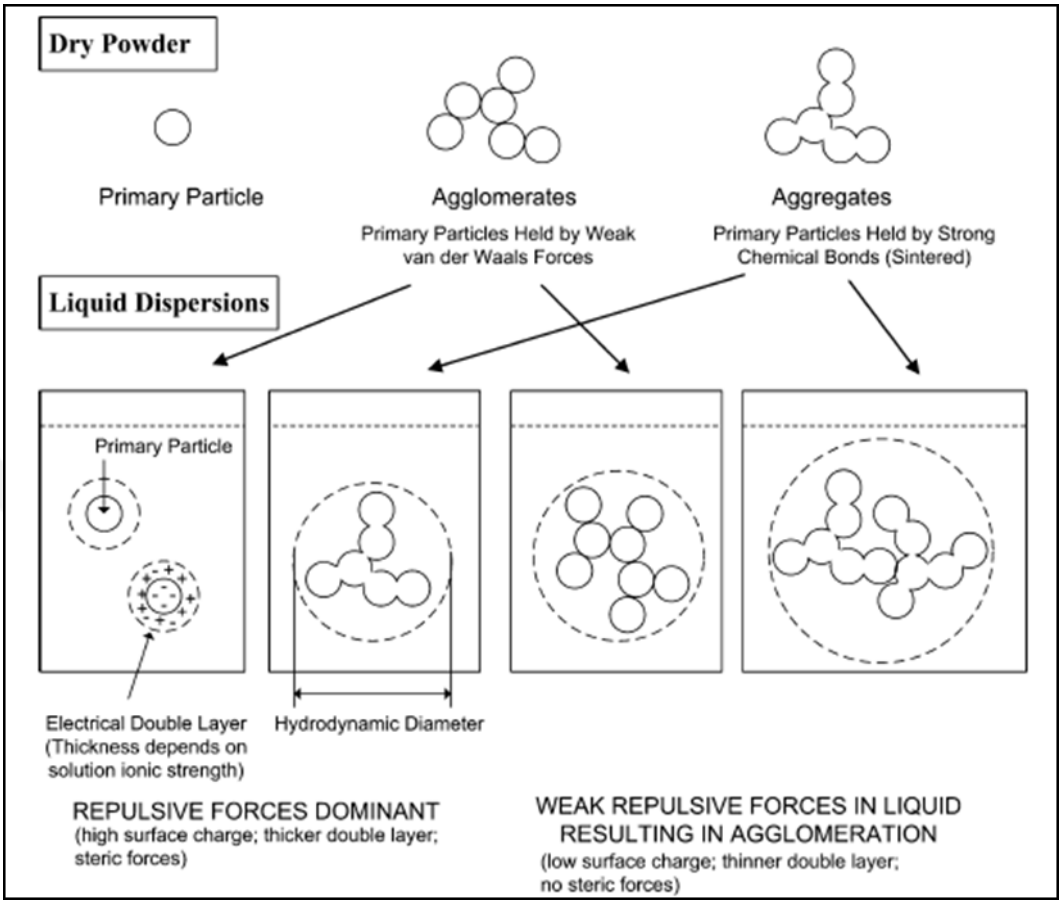


Figure 2.3. Alteration of characteristics of dry nanoparticle powders in liquid (Jiang et al, 2009).

On the other hand, amorphous particles without any specifically defined shape are recognized as a bulk material remaining in the colloidal system.

From a general perspective, natural colloids express size domains with respect to an operationally defined cut-off filtration through 0.45 μm filters as presented in Figure 2.4. The size of natural colloids ranges in between 1 nm to 1 μm. Depending on the main characteristics, main sub-groups could be defined as inorganic fractions (clays, oxides, sulfides, carbonates, phosphates, *etc.*,) and organic fractions (*eg*. macro molecules). Moreover, bio-colloids as composed of viruses, bacteria and algae express size ranges extended to regions greater than 0.45 μm. It should be indicated that particulate matter is also operationally defined as particles of expressing sizes greater than 0.45 μm. Aggregate sizes range from few nanometers to 10 μm that is considerably close to size of inorganic colloids. Size of nanoparticles can be considered as within this range as 1 nm to 100 nm.

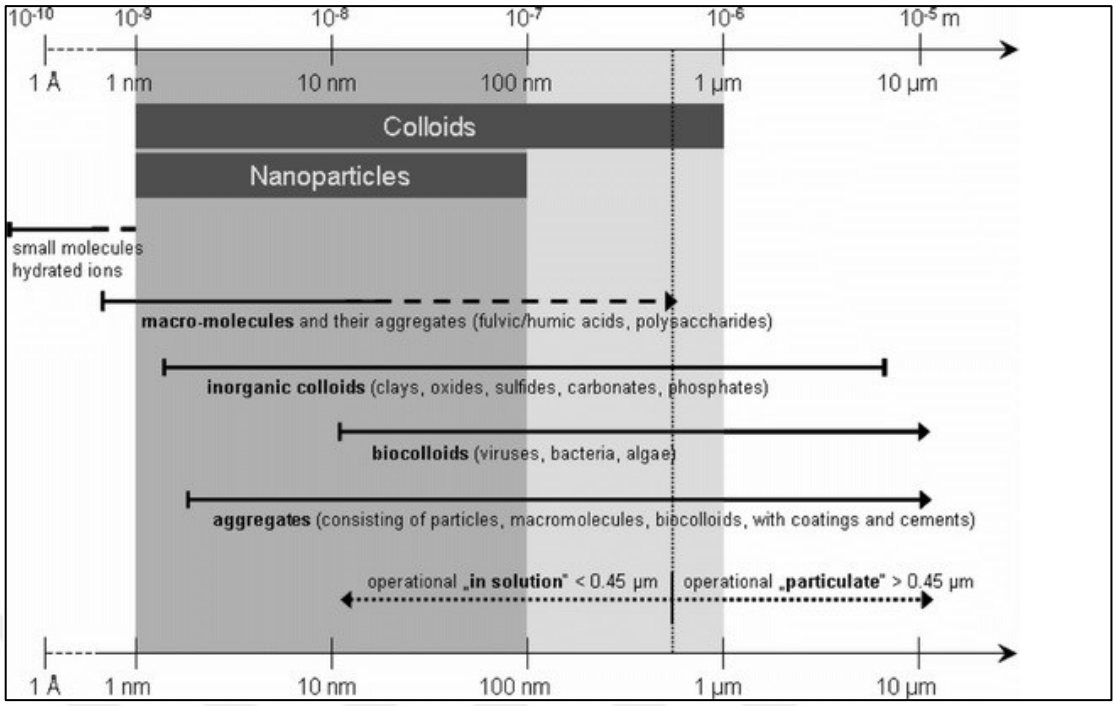


Figure 2.4. Operationally defined regional distribution of natural colloids (Christian et al., 2008).

Besides, specific regions organo-mineral associations could play significant roles in the environment resulting from interactive chemistry between mineral surfaces and organic molecules and local environmental conditions such as hydrology, pH, and ionic strength.

2.2. Natural Organic Matter

NOM is considered as one of the major colloidal component of natural water matrix. NOM indicates extensive reactions that could be considered as important most significantly to human health. Moreover, it should also be indicated that the dissolved fraction of NOM as defined by the fraction passing through 0.45 µm filter and described as DOM would be more significant due to the diversity in chemical composition in aqueous phase. DOM in the environment can be classified into two main classes, humic substances (HS) and non-humic substances including hydrocarbons, carbohydrates, aminoacids *etc*. HS are defined as composed of chemically complex, non-biochemical organic components, which are largely hydrophilic, amorphous, dark colored and resistant to chemical and biological degradation are among the most widely distributed organic materials on the earth (Stevenson, 1982). Due to ill-defined molecular properties, HS are preferentially expressed by conceptual models rather than chemical structures composed of various units (Senesi, 1999; Stevenson, 1994; Wershaw, 1999). Distinction between fractions of HS could be attributed to the basic chemical properties as, molecular weight and size distribution profiles, functional groups (carboxylic and phenolic groups), aromaticity and aliphatic character.

Furthermore, HS are formed in both terrestrial and aquatic systems. The origin of HS is derived from plants, animals and microbial residues. Hence, they are parts of soil and/or sediment, or they are dissolved in ground or surface water. HS are divided into three components: humic acid (HA), fulvic acid (FA) and humin depending on the solubility in alkali or acid solutions. HA is the fraction of HS that is not soluble in water under acidic conditions (pH < 2) but becomes soluble at higher pH values. HAs are completely soluble only in strongly basic solution, the solubility of HAs increase with increasing pH and decrease with increasing inert electrolyte concentration (Kipton et al., 1992). FA is the fraction of HS that is soluble in water under all pH values. Humin is the fraction of HS that is not soluble in water at any pH conditions. FAs are light yellow to yellow-brown in color, HAs are dark brown to black in color, and humins are black in color. HAs, FAs and humins are not so much different from each other. They are all part of a heterogeneous supramolecular system and the differences between the classes are due to the variations in chemical composition, acidity, size, molecular weight, degree of hydrophobicity and self-associations of molecules. The chemical properties of HS are presented in Figure 2.5 (Stevenson, 1982).

Depending on the source, location and extraction method, HS differ in composition. The elemental composition ranges comprise the three types of HS, the carbon content of a humic material could be arranged in the following series, FA < HA < Humin (vanLoon and Duffy, 2000). HAs contain more hydrogen, carbon, nitrogen and sulfur than fulvic acids. Additionally, researches have shown that humins are similar to HAs except that they are strongly bound to metals and clays, rendering them insoluble (Gaffney et al., 1996). The range of elemental composition of HS is 40-60 % carbon, 30-50 % oxygen, 4-5 % hydrogen, 1-4 % nitrogen, 1-2 % sulfur and 0- 0.3 % phosphorus. With the aim of exhibiting the general structure and function of HA and FA, two models are presented in Figure 2.6. and Figure 2.7.

Despite the origin and environmental conditions of their formation, HS generally demonstrate similar elemental and functional group composition. However, HS formed under different climatic regimes and natural soils contain different ranges of aromaticity and carboxylic and phenolic functional group contents. The complex aromatic component of soil HS has been reported to range from 35 to 92 % (Hatcher et al., 1981).

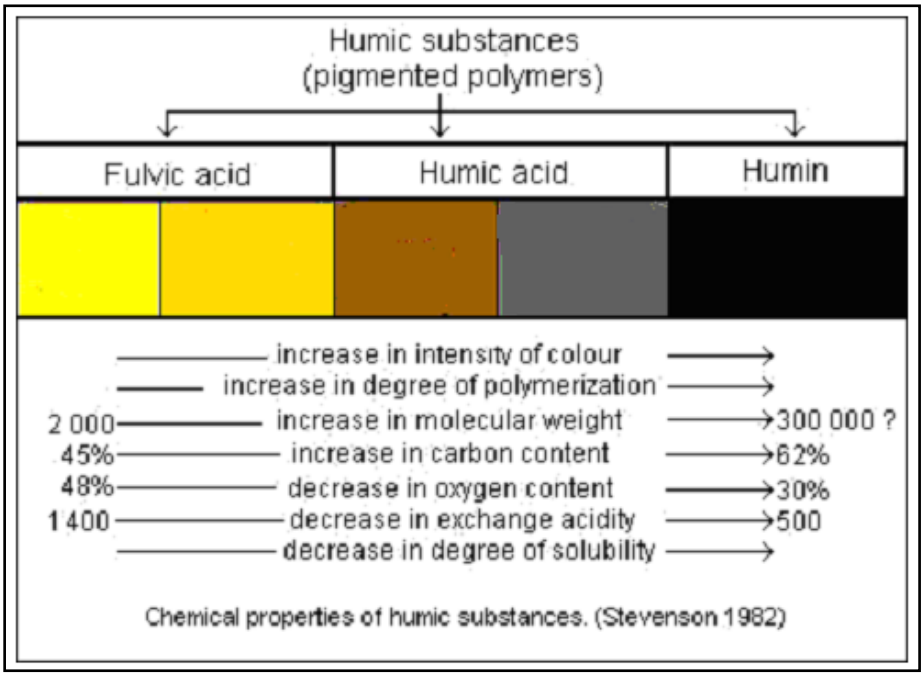


Figure 2.5. Chemical properties of humic substances (Stevenson, 1982).

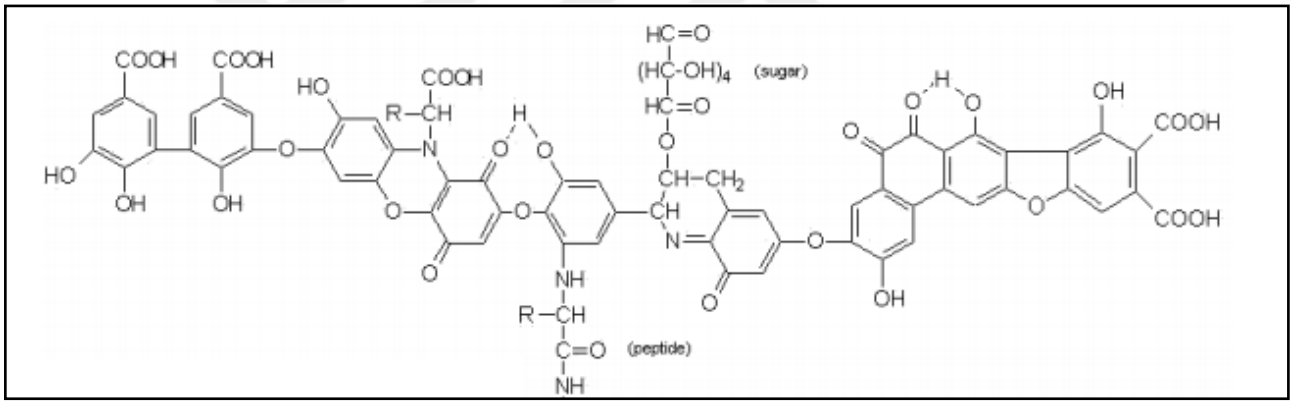


Figure 2.6. The model structure of humic acid (Stevenson, 1982).

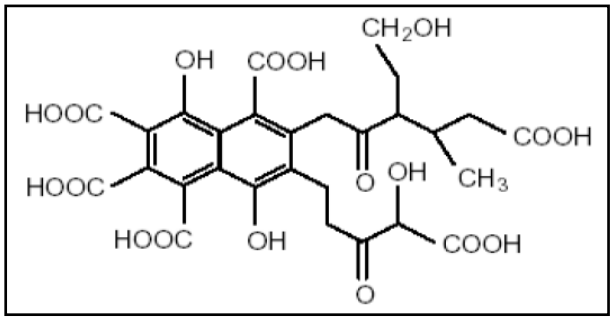


Figure 2.7. The model structure of fulvic acid (Buffle, 1988).

Humic substances may cause problems in drinking water since they impart undesirable color to the water that is not aesthetically pleasing to domestic consumers and also unsuitable for the paper, beverage and textile industries. Moreover, they have adverse effects in consequence of contributing

to bacterial growth in water distribution systems resulting in fouling potential of membranes and ion exchange resins. As a result of the decomposition of plant and animal remainders, HS can cause many environmental and health problems due to their reactions with oxidizing agents used for disinfection purposes. Thus, formed disinfection by-products mainly trihalomethanes in case of chlorination express carcinogenic and mutagenic properties. The removal of these substances from wastewater treatment facilities is an environmentally significant issue. HS forming from the end products of plant tissue decay are stable to biological oxidation. As HA cannot be adequately eliminated with conventional treatment procedures used in drinking water systems, in order to remove humic acid from water, many different treatment technologies such as enhanced coagulation, advanced oxidation methods (Kitis et al., 2007), adsorption (Peng et al., 2006; Uyguner and Bekbolet, 2007), biofiltration (Melin et al., 1999; Sobecka et al., 2006), membrane processes (Petala et al., 2006), and photocatalysis (Bekbolet et al., 1998; Selcuk et al., 2003; Murray et al., 2004) were applied. Nonetheless, conventional coagulation and flocculation process followed by filtration methods are inadequate to remove TOC by more than 10-50 % (Wang et al., 2000). Maintenance of residual sludge containing high aluminum concentration formed by this coagulation/flocculation process constitutes additional concerns. HA biodegradation (Wang et al., 2000) and surface activated carbon adsorption processes are relatively slow and ineffective.

Additionally, the conventional water treatment methods used for the successful removal of the natural organic colloidal matter, application of advanced oxidation processes (AOPs) more specifically photocatalysis had gained widespread attention (Matilainen et al., 2010). AOPs depend on the use of highly reactive oxidizing species (ROS) mainly hydroxyl radical ($HO^{\bullet}$) in order to decompose organic matters into innocuous components (Rashed et al., 2007). AOPs operating by reactions of ROS which are generated by means of chemical, photocatalytic and electro-chemical reactions are more effective techniques to remove organic pollutants from wastewaters when compared to direct chemical oxidation (*e.g.* ozonation) (Rajeswari et al., 2009). The major advantage of photocatalysis could be based on the observed performance as a substitute for the energy-intensive conventional treatment methods. Furthermore, photocatalysis could lead to complete mineralization of the humic components by the formation of inoffensive end products *i.e.* CO_2 and H_2O under specified operational conditions at ambient temperature and pressure environments.

AOPs are known to be innovative water and wastewater treatment technologies in which the main mechanism is production of highly reactive oxygen species (ROS) (H_2O_2, $OH^{\bullet}$, $O_2^{\bullet -}$) that are able to degrade even the refractory organic molecules into biodegradable compounds. Among these reactive oxygen species, hydroxyl radical is one of the most powerful oxidizing agents (Redox

potential, E=2.80 V) and has the ability to non-selectively oxidize a wide range of pollutants effectively. AOPs are mainly expressed by light-homogeneous AOPs (UV/O_3, UV/H_2O_2 and $UV/H_2O_2/O_3$, photo-Fenton), dark-homogeneous AOPs (US, O_3, US/O_3, US/H_2O_2, US/ H_2O_2/O_3, Fenton), light-heterogeneous AOPs (electro-Fenton, UV/TiO_2 photocatalysis, electrodialysis and electrochemical oxidation processes) and dark heterogeneous AOPs (n-zVI) (Oppenländer, 2003).

Heterogeneous photocatalytic reaction system is generally consisted of a photocatalyst and a substrate which is generally an organic matter. Photocatalysis proceeds via surface oriented reactions therefore, pre adsorption of the substrate onto photocatalyst is required. Since light exposure initiates the photocatalytic reactions, photolytic reactions of substrate should also be encountered (Kisch, 2015; Pichat, 2013; Sharpless et al., 2014). Specifically, if energy of the photon is equal or greater than the band gap of the photocatalyst, when a semiconductor photocatalyst is exposed to light, the photon is absorbed by the photocatalyst. The photoexcitation of an electron from the valence band to the conduction band occurs in the semiconductor photocatalyst upon absorption of the photon which is shown in Figure 2.8 (Pichat, 2013). TiO_2 is almost the most ideal photocatalyst because of its decent photocatalytic properties, ease of production and low cost (Gupta and Tripathi, 2011).

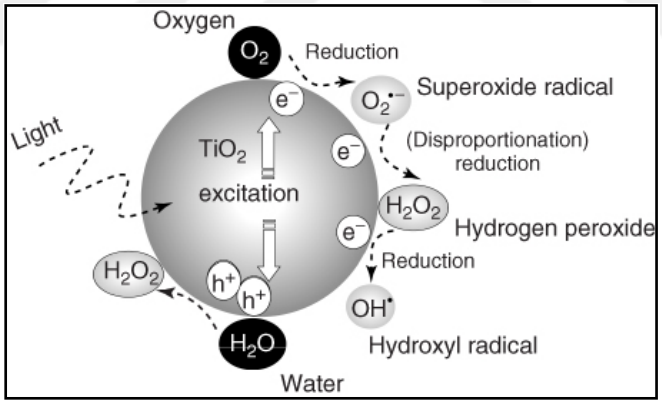


Figure 2.8. Illustration of TiO_2 photocatalysis and formation of hole-pairs and radicals (Pichat, 2013).

In TiO_2/UV light process, a titanium peroxide semiconductor absorbs UV light and generates hydroxyl radicals. Specifically, during UV illumination of TiO_2, conduction band electrons and valence band holes are initially yielded (Eq. 2.1). In order to yield superoxide radical anions, band electrons interact with surface adsorbed molecular oxygen (Eq. 2.2), while band holes interact with water to produce hydroxyl radical (Eq. 2.3) (Crittenden et al., 2005).

$$TiO_2 + h\nu \rightarrow e_{cb}^- + h^+ \quad (2.1)$$

$$e_{cb}^- + O_2 \rightarrow O_2^{-\bullet} \quad (2.2)$$

$$h^+ + H_2O \rightarrow H^+ + HO^\bullet \quad (2.3)$$

Organic compounds can undergo oxidative degradation through their reactions with valence bond holes, hydroxyl and peroxide radicals and also reductive cleavage through their reactions with electrons. So far, TiO_2/UV light process has been extensively used for wastewater treatment. The key advantages of this process are the operation at ambient conditions. Besides, TiO_2 is efficient to oxidize organic compounds into harmless compounds such as CO_2 and H_2O (Chatterjee and Dasgupta, 2005). The major factors affecting TiO_2/UV light process are: initial organic load, amount of catalyst, reactor's design, UV irradiation time, temperature, solution's pH, light intensity and presence of ionic species. However, it should be considered that due to the opacity offered by the catalyst particles, the use of excessive amounts of catalyst may reduce the amount of energy being transferred into the medium (Pichat, 2013).

2.3. Nanoparticles in the Environment

Since NPs are defined as particles with at least one dimension <100 nm could be accepted as a sub-set of colloidal particles (SCENIHR, 2005) and due to the nano-scale primary particle sizes of photocatalyst, most of the used photocatalysts are considered as NPs. Therefore, the colloidal matrix of natural waters is altered through the emergence of NP into the environment. Christian and co-workers discussed in detail the NP descriptions by using TiO_2 as an example (Christian et al., 2008). The explanations were based on the properties of TiO_2 with a primary particle size of 30 nm (± 10 nm) and crystal structure composition as 75 % anatase and 25 % rutile. Particle size distribution could be regarded as a mixture of small (anatase) and large (rutile) or vice-versa. The diversity in particle sizes could affect the aggregation, agglomeration and even precipitation of TiO_2. However, various counter ions and most significantly organic matter act as barriers preventing the particle-particle interaction through charge stabilization.

TiO_2 NPs has the highest production rate according to the wide usage areas. However, in scientific view photocatalytic properties of TiO_2 NPs has the top attention (Gupta and Tripathi, 2011). TiO_2 is a transition metal oxide and mostly produced in rutile and anatase crystal structures. According to Zhang and colleagues anatase structure can be transformed to the rutile phase after reaching a certain particle size and becomes more stable (Zhang et al., 2000).

Band gap energies of anatase and rutile structures are 3.2 and 3.02 eV, respectively. This band gap energy difference causes high photoactivity for anatase and light reflecting properties for rutile structure. When an electron excited from valance band to conduction band upon exposure to UV illumination, an electron-hole (e^-/h^+) pair as a redox couple is generated. If this e^-/h^+ pair recombines photocatalytic efficiency is lost as is in the brookite phase due to its low redox potential. But for the anatase phase this band gap energy is enough to protect e^-/h^+ pair. Basically, crystal structure of anatase and rutile phases of TiO_2 is presented in Figure 2.9 (Diebold, 2003).

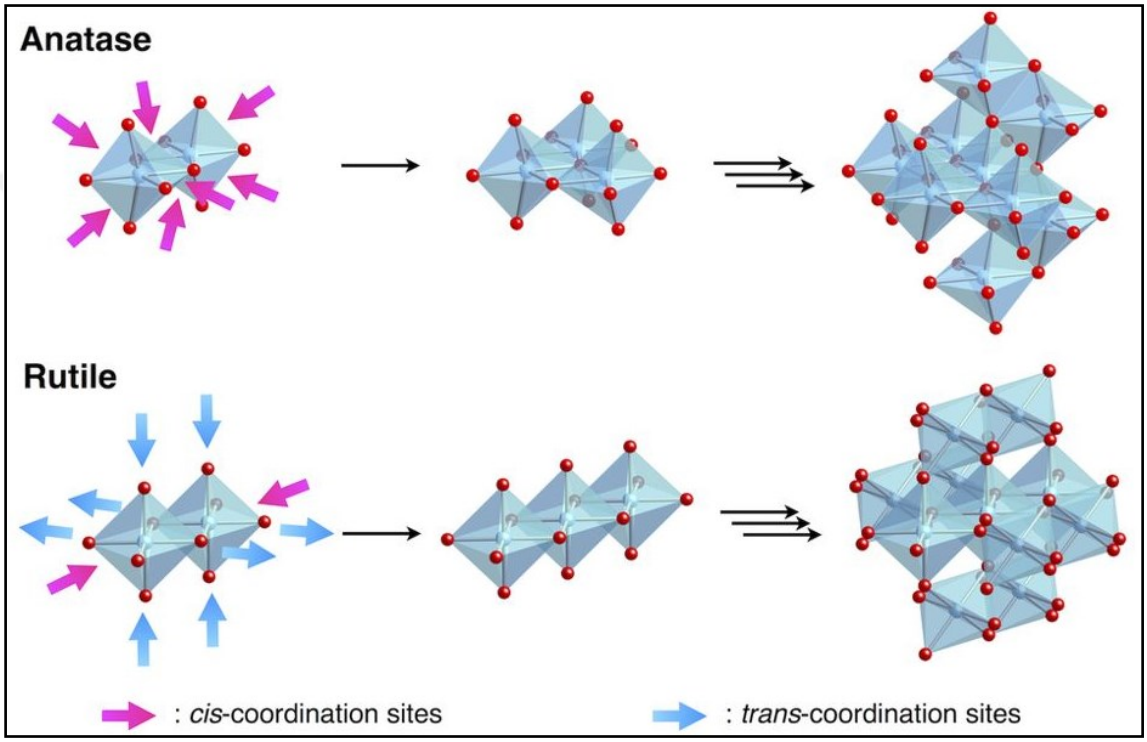


Figure 2.9. Schematic image for crystal structure of anatase and rutile phases of TiO_2 (Diebold, 2003).

Doping with transition metal cations adds additional energy levels within the band gap of a semiconductor. Eventually, the energy needed for electron transition from valance band to conduction band has been reduced but this also can cause an increase in the rate of recombination between photogenerated e^-/h^+. Photocatalytic effect occurs when the trapped electron and hole are transferred to the surface of the photocatalyst, to prevent this e^-/h^+ recombination metal ions must be doped near the surface of NP so, it can trap the electron or hole.

Cationic doping leads to the localized d-states deep in the band-gap of TiO_2 usually acting as the recombination centers for photoexcited electrons and holes that create lower photocatalytic activity (Wang et al., 2009). In recent years, the metal ion-doped into TiO_2 technique has been widely

investigated. Noble metals, *e.g.* Pt, are most frequently researched (Linsebigler et al., 1995; Sakthivel et al., 2004). Other metals, *e.g.* Au, Pd, and Ru have been mentioned to be useful for photocatalytic reactions (Sakthivel et al., 2004). The transitional metal ions, *e.g.* Fe have been utilized to increase the photocatalytic activity (Hoffmann et al., 1995). Conversely, anionic doping leads to the p-states near the valence band much like other deep donor levels in semiconductors to develop visible-light reactive photocatalysts *e.g.* N-doped TiO_2 (Wang et al., 2009; Zhang et al., 2009b).

Aggregation of metal oxide nanoparticles used as photocatalysts has been demonstrated to influence the photocatalysis by retardation/inhibition of the formation of ROS (Budarz et al., 2017; Hotze et al., 2010; Jassby et al., 2012; Melcher et al., 2017). Upon introduction to aquatic environments, nanoparticle behavior is dependent on particle-specific properties (*e.g.*, size, shape, chemical composition, surface charge, and coating), particle state (free or matrix incorporated), the surrounding solution chemistry (*e.g.*, pH, ionic strength, ionic composition, natural organic matter content), and hydrodynamic conditions (Diaz et al., 2015; Lee et al., 2016; Petosa et al., 2010; Raza et al., 2016; Wang et al., 2016). Stability of nanoparticles deserved special attention with respect to their behavior in aquatic systems as well as during water treatment (Zhang et al., 2008). Recently, due the extensive release of nanoparticles to the environment their role in natural systems attracted special attention (Al-Kattan et al., 2014; Petersen et al., 2014; Sillanpää et al., 2011). It is reported that behavior of nanoparticles could be elucidated considering various reaction mechanims based on the matrix components covering the light effect (Sun et al., 2014; Zou et al., 2013). Thus, a binary system could be defined as "substrate and photocatalyst" since both of the components display colloidal behavior in aqueous slurry systems (Wang and Keller, 2009; Wagoner et al., 1997).

Dark adsorption phenomenon is considered as a complementary approach to the overall understanding of the surface coverage by Bekbolet and co-workers (Bekbolet et al., 2002; Uyguner and Bekbolet, 2005a). The surfaces of the stationary particles have a profound effect on their sorptive properties for organic molecules. Almost all stationary particle surfaces are covered with an organic coating namely humic moiety that imparts a negative charge to the surface under natural water conditions. Considering a reaction medium composed of humic molecules and the oxide surface of TiO_2 possessing an almost neutral pH_{zpc} (pH_{zpc} = 6.3), similar surface attractions would be reasonable (Jaffrezic-Renault et al., 1986). At pH values close to the pH_{zpc}, the surface of TiO_2 is equally positively and negatively charged (Eq. 2.4-2.6). The chemistry of the TiO_2 is dominated by surface hydroxyl groups.

$$TiO_2 + H_2O \rightarrow Ti\text{-}OH + H^+ \quad (2.4)$$

$$Ti\text{-}OH + H^+ \rightarrow TiOH_2^+ \quad pH<pH_{zpc} \quad (2.5)$$

$$Ti\text{-}OH \rightarrow Ti\text{-}O^- + H^+ \quad pH>pH_{zpc} \quad (2.6)$$

On the other hand, humic matter contains carboxylic (pK_a 3-5) and phenolic functional groups (pK_a >8) (Manahan, 2000). pH dependent deprotonation of these groups leads to surface charge development. Under natural water conditions (pH~7) deprotonation of carboxylic groups predominate over phenolic groups (Senesi, 1999). Between the carboxyl and hydroxyl groups of the HS versus surface hydroxyl groups of the TiO_2, ligand exchange mechanism is expected. Specific interactions could also be functional between metal oxide surface hydroxyl groups or adsorbed water and the oxygen of adsorbed carboxyl or hydroxyl groups of organic acids including HA. Ligand exchange is highly affected by the pH value of the adjacent solution. As a rule, as pH value decreases, adsorption of HS onto TiO_2 surfaces increases, passing a maximum at pH 4.3- to 4.7, corresponding to pK_a values of most abundant carboxylic acids. As a result, the high molecular weight HS may sorb preferentially (Nikolaou et al., 2007).

2.4. Assessment of Behavior of Nanoparticles in the Environment

Besides the naturally present inorganic colloidal materials, release of nanomaterials to the environment results in various interactions that could be assessed through agglomeration and aggregation phenomena. Recent interest is focused to the understanding of the behavior of these interacting species and their fate in natural environments (Joo and Zhao, 2017).

Below presented Figure 2.10. covers all contacts in between living and non-living components open to exposure to both incident solar irradiation as well as sedimentary layers in water column. In aquatic ecosystems, nanoparticles dissolve and accumulate in organisms. Metal oxide nanoparticles (MNPs) such as TiO_2, ZnO, and CeO_2 can aggregate rapidly and may be exposed to physically, chemically and biologically tranformations in the air, soils and waters (Joo and Zhao, 2017). Suspended or aggregated nanoparticles and other contaminants reach sediments influenced by suspension-feeding invertebrates (Montes et al., 2012). Various kinds of suspension-feeders live in sediments. Also, as can be seen from Figure 2.10, under direct action of natural sunlight, metal oxide nanoparticles have been shown to induce ROS, and Cl^- ions released from dissolution add to toxicity.

Natural colloidal particles could contribute to all inter and intra interactions resulting in eco-toxicological effects under dynamic conditions. Under these circumstances, major nanoparticle

behavior should be assessed through particle size distribution profiles as well as sedimentation tendencies both in the presence and absence of organic matter. Most of the literature findings refer to simulated heterogeneous environmental conditions. Moreover, unavoidable role of contaminants should also be addressed.

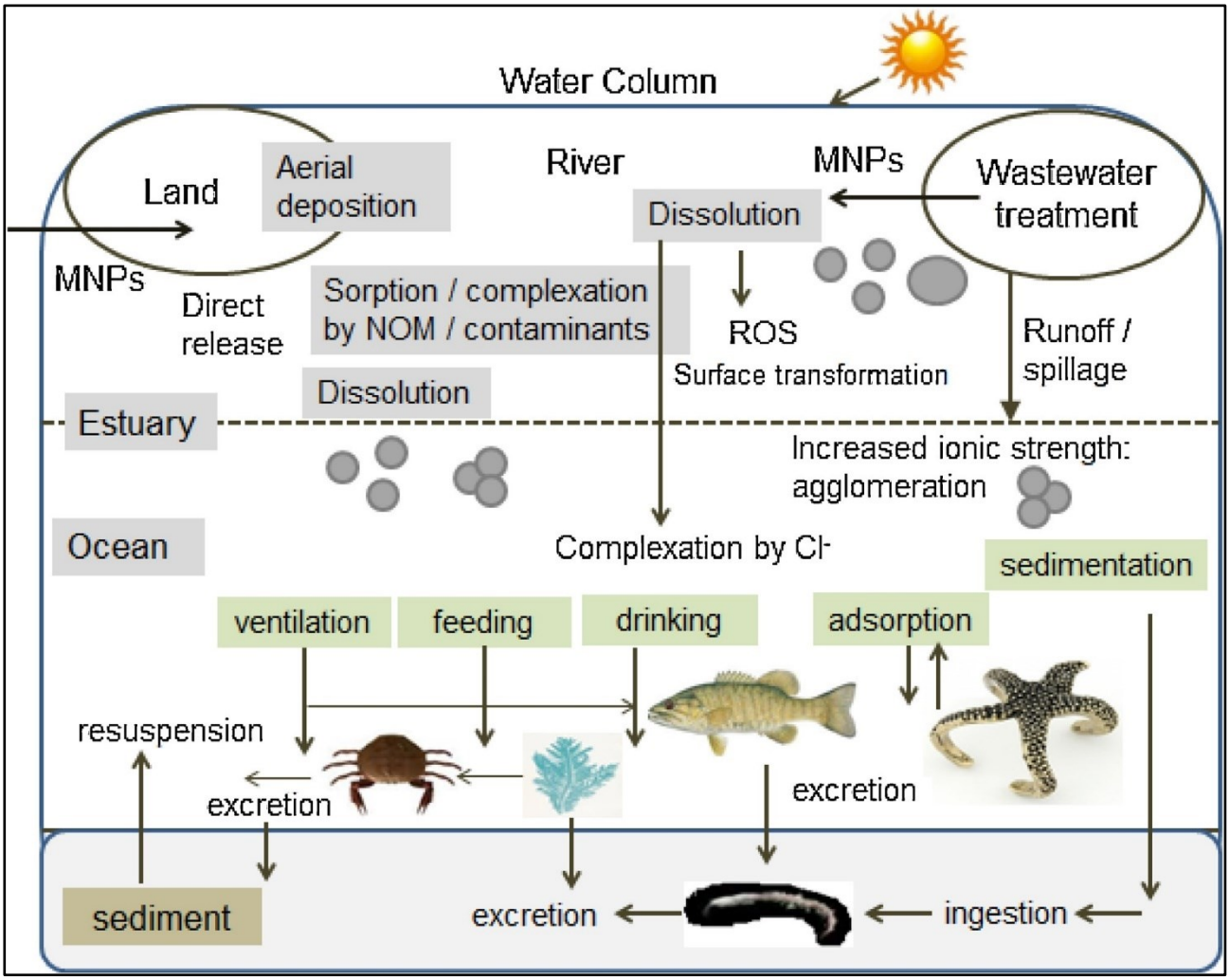


Figure 2.10. Summary of interactions pertaining to environmental compartments in relation to colloidal systems (Joo and Zhao, 2017).

Excluding all interfering and co-existing presence of contaminants and natural habitats, simple systems composed of selected nanoparticles and NOM representatives express the major importance in elucidation of the system.

2.4.1. Particle Size Distribution

Dynamic light scattering (DLS) technique demonstrates the intensity of scattered light as a function of distribution of particle size. The hydrodynamic size distribution obtained from the

analysis of DLS data are primarily intensity weighted distributions (Hassan et al., 2015). In intensity weighted distributions, each particle's contribution in the distribution associates with the intensity of light scattered by the particle. Particle size distribution can be converted into volume or number weighted distributions by means of some algorithms. The conversion of relative distributions of intensity to volume or number can be performed using the Mie theory (Bohren et al., 1983). When compared the data obtained from other methods such as number or volume distributions, the intensity of light scattered by the particle should be taken into account. The intensity of light scattered by particles is proportional to the number of particles, particle mass square, and the shape factor which is a function of particle size and scattering vector (Eq. 2.7). Considering these factors, the average diffusion coefficient ($\overline{D}$) obtained by DLS can be written as

$$\overline{D}=\frac{\sum i\ N_i M_i^2 P(q,R) D_i}{\sum i\ N_i M_i^2 P(q,R)} \tag{2.7}$$

where; N is the number of particles, M is particle mass, P (q,R) is shape factor which is a function of particle size and scattering vector.

Since the diffusion coefficient is weighted by particle mass square (M^2), the average diffusion coefficient of a polydisperse population obtained by DLS is prone to large sizes. Also, the particle scattering power depends on the refractive index of the particles. In other words, if the particle refractive index is known, the distribution by weight or number can be determined. If the limiting case of particles that are small compared with the wavelength of light, the shape factor can be equal to the unity. Therefore, the measured diffusion coefficient becomes the z-average diffusion coefficient. The diffusion coefficient is inversely proportional to the diameter, M is proportional to d^3, thus, the average diameter ($\overline{d}$) obtained by DLS can be written as in Eq. 2.8-2.11,

number average; $\overline{d}=\frac{\sum i\ N_i d_i^6}{\sum i\ N_i d_i^5}$ (2.8)

number average; $d_n=\frac{\sum i\ N_i d_i}{\sum i\ N_i}$ (2.9)

area average; $d_a=\frac{\sum i\ N_i d_i^3}{\sum i\ N_i d_i^2}$ (2.10)

weight average diameter, $d_w=\frac{\sum i\ N_i d_i^4}{\sum i\ N_i d_i^3}$ (2.11)

By definition, the number-average (d_n), area average (d_a) and weight-average (d_w) diameter of polydisperse spherical particles should follow the order

$$d_n \leq d_a \leq d_w \leq \bar{d}$$

From a general perspective, particle size distribution data can be presented numerically (tabular format) or graphically. Graphical presentation could be presented displayed using two types: differential and cumulative.

Differential Distribution: The differential distribution shows the relative amount at each size. This distribution is unimodal (single peaked) but not monodisperse (all one size).

Cumulative Distribution: The cumulative undersize distribution shows the relative amount at or below a particular size (Figure 2.11) (Modi et al., 2018).

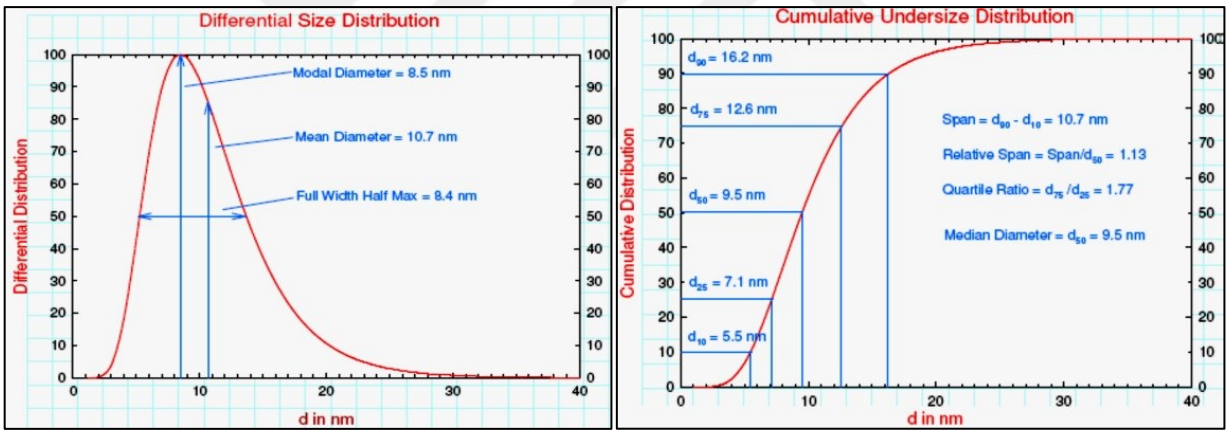


Figure 2.11. Size distribution profiles (Modi et al., 2018).

Interpretation of size distribution profiles could also be mono-model or multi model depending on the sample properties. In either case, sample specification could only be assessed under the specified environmental conditions. The role of interfering species *e.g*. ionic strength and /or presence of organic matrix directly affect the hydrodynamic size. Photocatalyst specimens as nanoparticles are mainly described by aggregate sizes and/or hydrodynamic sizes in relation to primary crystal sizes that could also be visualized by scanning electron microscopic/ transmission electron microscopic images. As an example, TiO_2 photocatalyst primary crystal size is derived from X-ray crystallographic analysis and calculated by Bragg equation as 35 nm however aqueous TiO_2 dispersions display aggregate sizes greater than 100 nm as a result of homo interactions and surface hydroxylation. Therefore, particle size distribution profiles express hydrodynamic sizes effective

during treatment. On the other hand, surface area properties should be directly related to the hydrodynamic size of the nano TiO_2 specimen (Suttiponparnit et al., 2011). Moreover, DLS methodology assumes particles as spherical rather than considering actual crystallographic shapes.

2.4.2. Sedimentation

Sedimentation is defined as time-dependent deposition of particles due to gravity. Sedimentation is considered as an important mechanism for particles with aerodynamic diameters 0.5 μm – 5 μm. Gravitational sedimentation generally limited to particles expressing larger size, on the other hand, smaller particles tend to settle very slowly due to Brownian motion. Very small particles < 0.1 mm could practically express no sedimentation efficiency. Time dependent change in particle size could be visualized by UV-vis absorbance spectroscopy to assess the sedimentation rate under controlled conditions. Along with dynamic light scattering techniques, simple absorbance measurements at specific wavelengths could also reveal information about the behavior of nanoparticles in the environment under the specified circumstances.

Larger particles (with identical specific mass) express sedimentation rates faster than smaller particles. In case that particles are typically smaller than about diameters 10-100 nm, sedimentation velocities in the earth's gravitational field are very small. Results attained by sedimentation experiments would be erroneous and centrifugation should be performed.

2.4.3. Brief Outline of Literature Survey

Brunelli and colleagues studied the agglomeration behavior of commercially available pristine n-TiO_2 in synthetic fresh water samples. Four different concentrations (0.01, 0.1, 1.0 and 10 mg/L) were tested and experiments were carried out over 50 h. The results of the n-TiO_2 agglomeration recorded at selected times (0.2, 25 and 50 h) and the average size of 0.1 mg/L concentration of n-TiO_2 suspended in artificial fresh water was reported 221±3 nm after 0.2 h (Brunelli et al., 2013). While the average size of n-TiO_2 agglomerates generally increased with time over the initial hours (up to 25 h), the average size of agglomerates of most samples was found at 50 h similar or lower than those at 25 h. From the point of Brunelli and colleagues view, different agglomeration behavior may be mainly attributed to the initial concentration and secondly, the duration of the experiment (Brunelli et al., 2013).

Lee and colleagues investigated the effect of HA on n- TiO_2 aggregation in deionized water. Two different concentrations of HA (0.57 and 5.7 mg/L) were used and experiments were conducted over a 12 h period. It was found that, in the absence of HA, the average hydrodynamic diameter was 195 nm. However, in the presence of HA (0.57 and 5.7 mg/L), the initial hydrodynamic diameter was 175 nm and 194 nm, respectively. In addition, at 12 h, the average diameter of n-TiO_2 was 176.7 nm for the concentration of 0.57 mg/L HA and 193.2 nm for the concentration of 5.7 mg/L, respectively. It was concluded that at both 0 and 12 h, the hydrodynamic diameter of n-TiO_2 in the presence of HA (5.7 mg/L) was not significantly different compared to the hydrodynamic diameter in the absence of HA, whereas significant differences were observed at lower HA concentration (0.57 mg/L) at both 0 h and 12 h (Lee et al., 2016).

Erhayem and Sohn examined the effect of NOOM type (HA, FA and NOM) from the same source on NOOM adsorption onto nano-TiO_2 and on the consequent effects on nano-TiO_2 stability in the presence of environmentally relevant cations and anions. The results indicated that nano-TiO_2 suspended in Milli-Q water was stable for experimental time in the absence of NOOM. However, for nano-TiO_2 suspended in 10 mg/L SRFA, SRNOM, or SRHA, 35, 73, or 80 % loss of λ_{378} absorbance within 60 min was observed. Different pH values and a constant ionic strength of 100 mmol/L were evaluated, the order of the extent of sedimentation of nano-TiO_2 suspended in NOOM was SRHA > SRNOM > SRFA. The sedimentation of coated NPs was greatest near neutral (6.5-7) pH for all NOOM types. It was concluded that the extent of NOOM adsorption onto nano-TiO_2 could be mostly dependent on the type of NOOM at a given solution pH and ionic strength (Erhayem and Sohn, 2014a, b).

Romanello and de Cortalezzi investigated in detail the aggregation rates, aggregate size and aggregate morphology of nanoTiO_2 under various conditions resembling natural waters *i.e.* inert electrolytes, divalent cations, and NOM (Romanello and de Cortalezzi, 2013). The stabilization of nanoparticles was described by DLVO theory describing NOM exerting a stabilizing effect.

Moreover, the effect of UV irradiation (5 mW/cm^2) onto n-TiO_2 nanoparticle stability was expressed by aggregation rates as an increase from <0.001 nm/s before irradiation to 0.027 nm/s after 50 h irradiation, resulting in aggregates with a hydrodynamic diameter of 623 nm (Sun et al., 2014). Aggregation rate was also reported as dependent on irradiation period that was attributed to the excessive formation of surface hydroxyl groups.

As a basic approach, effect of varying particle sizes, morphologies, and crystal structures of TiO_2 was elucidated in terms of colloidal stability as agglomeration with reference to anatase and rutile phases both in the presence and absence of NOM (Zhou et al., 2013). It should also be kept in mind that properties like surface area, primary particle size, and crystal phase of titanium dioxide nanoparticles primarily affect dispersion properties prior to further evaluation of aggregation/agglomeration behavior (Suttiponparnit et al., 2011).

A comparison of aggregation behavior in aqueous humic acids from different origins was elucidated by the formation of amphiphilic structures as related to HA and solvent interactions resulting from intermolecular, rather than intramolecular, rearrangements (Young and von Wandruszka, 2001). Contrary to the effective role of NOM on the aggregation/agglomeration behavior of TiO_2, NOM could also take part on the disagglomeration phenomena (Loosli et al., 2014). Reported results indicated that both NOM and sub-fractions of NOM expressed disagglomeration via electrostatic forces and steric interactions leading to fragmentation. It should also be indicated that spontaneous aggregation of sole HA depending on pH conditions effective on conformational changes in humic structure could be verified by Atomic Force Methodology (Colombo et al., 2015).

Effects of HA on aggregation of nano-TiO_2 was evaluated by sedimentation experiments that were conducted by recording absorbance at λ=508 nm. The concentrations of suspended particles decreased by only approximately 20 % in 180 min the reason of which was attributed to the adsorption of NOM forming electrostatic double layer on the surface of TiO_2 particles (Li et al., 2015). The theoretical background had been reviewed and documented in detail by Petosa and colleagues (Petosa et al., 2010). Colloidal forces leading to particle deposition and aggregation behavior were related to particle-particle and surface interactions resulting in diverse effects on environmental transport systems. Recently Zhao and colleagues also performed sedimentation experiments by visible spectroscopy (absorbance measurements performed at λ=508 nm) to elucidate the electrostatic interactions between TiO_2 and humic materials under various pH conditions (Zhao et al., 2019). Furthermore, influence of morphology *i.e.* ellipsoidal and spherical shaped of TiO_2 particles were evaluated by DLS methodology under simulated environmental conditions (Raza et al., 2016). FA was used as the model NOM compound along with the ionic strength effect on the aggregation kinetics under neutral pH conditions. DLS histograms indicated condition dependent variations in aggregate sizes. The presence of counter ions also expressed distinct effects on particle size distribution profiles.

As also presented previously in Figure 2.10, in the below given schematic representation (Figure 2.12) the presence and fate of engineered nanoparticles (*e.g.* TiO_2) in aquatic environments has been thoroughly investigated (Abbas et al., 2020; Heilgeist et al., 2021). Homo- and hetero-aggregation/agglomeration phenomena were described with reference to the literature findings revealing the importance of all interactions and pertaining reactions to be elucidated. The role of solar irradiation, thereby formation of ROS in the presence of natural organic matter *i.e*. NOM, diretly effect the successively and simultaneously preceeding reactions in aqueous medium. Among all processes covering the role of common anions and cations, suspended particle matter (SPM) as well as microbiological systems (biota), physicochemical characteristics and size distribution profiles of TiO_2 nano-particles dictate the major routes leading to final deposition on sediments as "sinks" although erosion should still be considered as a backward reaction pathway.

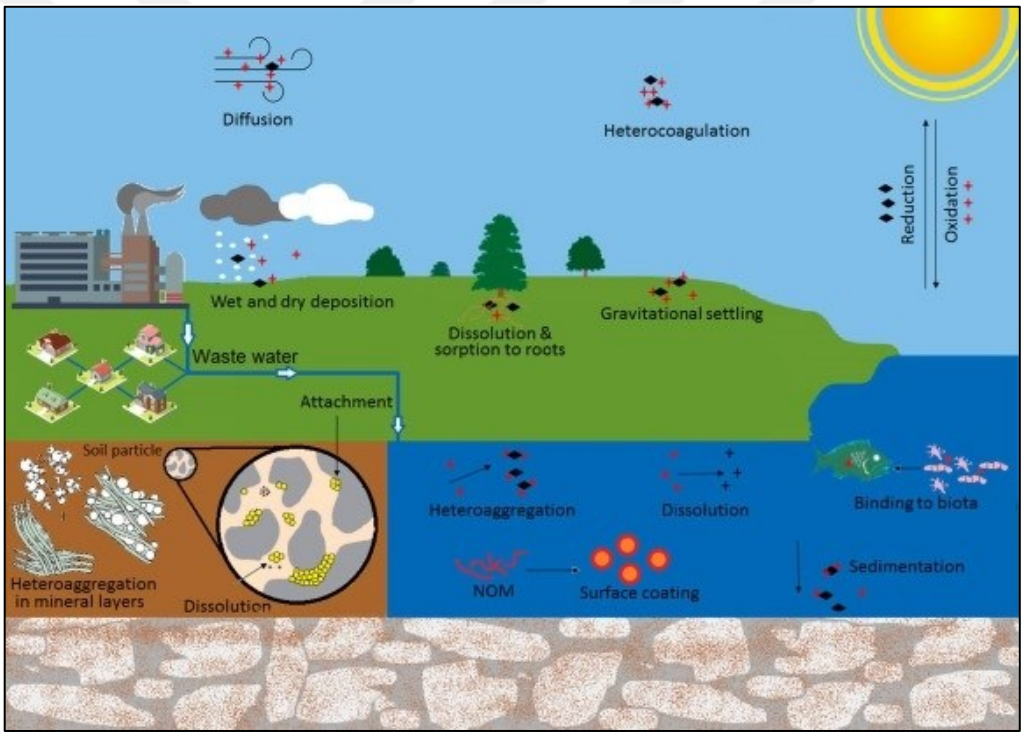


Figure 2.12. Environmental distribution of nanoparticles (Abbas et al., 2020).

Based on the above presented fundamental knowledge, elucidation of physicochemical interactions governing mono and binary systems composed of particle-organics and particle-particle interactions under conditions representative of aquatic environments deserves specific attention. Therefore, the primary objective of this study was to elucidate the interactions between NOM representative organics and nanoparticles representative of photocatalyst specimens described by following basic experimental procedures, *i.e.* dynamic light scattering, sedimentation and turbidity. It should also be emphasized that since the organic matrix is prone to photolytic as well as photocatalytic interactions, experimental design was also focused on these conditions.

3. MATERIALS AND METHODS

3.1. Materials

3.1.1. Nanoparticles as Photocatalysts

Three different photocatalyst specimens were used as examples of nanoparticles. Commercial TiO_2 P-25 was supplied from Degussa/Evonik. TiO_2 was also used for the preparation of N-TiO_2 and Fe-TiO_2 and specimens. N-TiO_2 and Fe-TiO_2 nanomaterials were prepared by Turkten and co-workers at Yildiz Technical University (Birben et al., 2015; Yalcin et al., 2010). Preparation of doped TiO_2 specimens were carried out utilizing an incipient wet impregnation method. Detailed information about morphological and physicochemical properties was presented in Appendix A Section. Aforementioned TiO_2 based nanoparticles were further utilized as semiconductor photocatalyst specimens in photocatalytic treatment of organic matter. The loading of the nanoparticles was kept constant as 0.25 mg/mL under all conditions.

3.1.2. Organic Matter

Two types of organic matter were used throughout the experimental study. Commercially available HA was supplied from Aldrich (Aldrich Co. Ltd., USA). Suwannee River Natural Organic Matter (SRNOM) was purchased from International Humic Substances Society (IHSS) (IHSS HA).

Stock humic acid solution with a concentration of 1000 mg/L was prepared by adding 1 g HA into 1 L of ultra pure water and dissolved by sonication in order to obtain homogenous solution. In a similar manner, stock SRNOM solution with a concentration of 200 mg/L was prepared by adding 0.1 g SRNOM into 500 mL of ultra pure water and dissolved by sonication in order to attain homogenous solution. Thus, prepared stock solutions were stored in amber glass bottles and were protected from light. Working solutions as 20 mg/L HA and 10 mg/L SRNOM were prepared from respective stock solutions by dilution. HA and SRNOM solutions were filtered from 0.45 μm Millipore cellulose acetate membrane filters. Ultra pure water was prepared by using Millipore Milli-Q system and used in the preparation of all aqueous solutions. The characterization of the organic matter either as sole or upon respective treatment options, was performed according to the methodology outlined by Bekbolet and co-workers. Detailed information was given in supplementary section (Appendix B).

3.2. Methodology

Mono and binary systems were described as follows:

Mono system: Aqueous solution of 0.25 mg/mL TiO_2, N-TiO_2 and Fe-TiO_2 nanoparticles were prepared by sonication for 1 minute and stirred for 4 minutes using a magnetic stirrer. Thus, prepared dispersions were directly taken for analysis. Following a similar manner, 20 mg/L HA and 10 mg/L SRNOM were also subjected to particle size analysis, sedimentation and turbidity measurements.

Binary system: Binary system solutions composed of TiO_2, N-TiO_2 and Fe-TiO_2 nanoparticles and organic matter *i.e.* HA or SRNOM namely and referred to as "TiO_2 and HA", "TiO_2 and SRNOM", "N-TiO_2 and HA", "N-TiO_2 and SRNOM", "Fe-TiO_2 and HA", "Fe-TiO_2 and SRNOM" were sonicated for 1 minute and stirred for 4 minutes using magnetic stirrer. Thus, prepared dispersions were directly taken to immediate particle size analysis, sedimentation and turbidity measurements.

3.2.1. Particle Size Distribution using DLS Technique

Particle size distribution of TiO_2 specimens was measured by time-resolved particle size analyzer based on dynamic light scattering technique using DLS, 90 Plus, Brookhaven Instrument Corp. The DLS was operated with a 15 mW solid state laser at a wavelength of 635 nm and light scattering was detected at an angle of 90°. Intensity, volume, surface area, number weighted distributions were measured using log normal and multimodal size distribution modes. The sample was placed into disposable polystyrene cuvette using a pasteur pipette. Particle size distribution measurements of aqueous all suspensions composed of mono- and binary systems were recorded every 30 min for 2 h.

3.2.2. Sedimentation

Sedimentation experiments were performed by time resolved optical absorbance measurements under specified experimental conditions simultaneously with DLS measurements. Aqueous nanoparticle suspension was sonicated for 1 minute and stirred for 4 minutes using magnetic stirrer. UV-vis absorbance scan spectra were recorded using quartz UV-vis cuvette with optimal path length of 1.0 cm every 30 min for 2 h. Sedimentation profiles of all nanoparticle suspensions were measured by Shimadzu UV-100 instrument.

3.2.3. Turbidity

Turbidity experiments were carried out using an HACH portable turbidity meter in a range of 0.01 to 1000 NTU. Turbidity measurements of aqueous all nanoparticle suspensions in a 16 mL glass cuvette were recorded every 30 min over a 2 h period. Turbidity measurements were also performed simultaneously with particle size analysis, and sedimentation.

3.3. Treatment Methodology

Following elucidation of mono and binary systems under as-is conditions, effect of light exposure on sole nanoparticles, and sole organic matter (photolysis) and binary systems (photocatalysis) were also investigated. Sole nanoparticles were similarly treated under dark conditions.

3.3.1. Treatment of Nanoparticles in the Presence of Organic Matter Following Photolysis of Organic Matter

Organic matter, *i.e.* HA or SRNOM was exposed to simulated solar irradiation for one hour in solar simulator (ATLAS Suntest CPS+, light intensity: 250 W/m^2). Following photolysis of organic matter, 50 mL of irradiated organic matter was mixed with 0.25 mg/mL of TiO_2, N-TiO_2 and Fe-TiO_2 nanoparticles and sonicated for 1 minute and stirred for 4 minutes by magnetic stirrer to ensure a homogenous mixture. Then, samples were subjected to particle size analysis, sedimentation and turbidity measurements.

3.3.2. Treatment of Nanoparticles in the Presence of Organic Matter Following Photocatalysis of Organic Matter

Organic matter, *i.e*. HA or SRNOM, were subjected to photocatalytic treatment using TiO_2, N-TiO_2 and Fe-TiO_2 and photocatalyst nanoparticles. All samples were sonicated for 30 seconds to ensure a homogenous mixture. After that, samples were exposed to simulated solar irradiation using ATLAS Suntest CPS+ for certain reaction periods depending on organic matter removal efficiency data *i.e*. 30 minutes for TiO_2 and N-TiO_2, 60 minutes for Fe-TiO_2. Following irradiation, samples were directly taken for particle size analysis, sedimentation and turbidity measurements according to the procedures described in sections 3.2.1.; 3.2.2. and 3.2.3.

3.3.3. Treatment of Sole Nanoparticles Following Light Exposure Conditions in the Absence of Organic Matter

0.25 mg/mL of TiO_2, N-TiO_2, and Fe-TiO_2 in aqueous medium was sonicated for 30 seconds to ensure a homogenous mixture. After that, samples were exposed to irradiation for one hour in solar simulator (ATLAS Suntest CPS+) under light exposure conditions. Irradiated samples were directly taken to particle size analysis, sedimentation and turbidity measurements.

3.3.4. Treatment of Sole Nanoparticles under Dark Conditions in the Absence of Organic Matter

0.25 mg/mL of TiO_2, N-TiO_2, and Fe-TiO_2 in aqueous medium was sonicated for 30 seconds to ensure a homogenous mixture. After that, samples were kept under dark conditions for one hour in solar simulator (ATLAS Suntest CPS+) to ensure similar reaction conditions. Thus, obtained samples were directly taken particle size analysis, sedimentation and turbidity measurements.

3.4. Characterization of Organic Matrix

3.4.1. UV-vis Spectroscopic Measurements

UV-vis absorption spectra of HA and SRNOM solutions were recorded on a Perkin Elmer Lambda 35 UV-vis double beam spectrophotometer with Hellma quartz cuvettes of 1.0 cm optical path length. Several UV-vis absorbance values were selected and defined as specified UV-vis parameters *i.e.,* $Color_{436,}$ UV_{365}, UV_{280} and UV_{254}. The specified parameters are clarified as follows; $Color_{436}$: Color forming moieties, absorbance at 436 nm; $UV3_{65}$: Organic matter content, absorbance at 365 nm; UV_{280}: Organic matter content, absorbance at 280 nm, and UV_{254}: Organic matter content, absorbance at 254 nm.

3.4.2. Fluorescence Measurements

Fluorescence spectra in emission and synchronous scan modes were recorded on a Perkin Elmer LS 55 Luminescence Spectrometer equipped with a 150 W Xenon arc lamp and a red sensitive photomultiplier tube. 1-cm path length quartz cells were used in order to place the samples in the instrument. For all measurements, a scan speed of 400 nm min^{-1} with a slit width opening of 10 nm was set and used. Synchronous scan spectra of samples were recorded in the excitation wavelength

range of 200-600 nm with the bandwidth of $\Delta\lambda$=18 nm between the excitation and emission monochromators (Bekbolet and Sen-Kavurmaci, 2015; Uyguner and Bekbolet, 2005b). The emission spectra were scanned at λ_{emis} 450 nm to that at λ_{emis} 500 nm following excitation at λ_{exc} 370 nm.

3.4.3. Dissolved Organic Carbon (DOC) Measurements

Dissolved Organic Carbon (mg OrgC/L) measurements of organic matter were performed on a Shimadzu TOC VWP Total Organic Carbon Analyzer. Calibration of the instrument was done using potassium hydrogen phthalate in the concentration range of 0-25 mg C/L.

3.4.4. Specific Parameters

Specific UV-vis parameters as $SCoA_{436}$, $SUVA_{365}$, $SUVA_{280}$, and $SUVA_{254}$ (L/m mg) were calculated by normalization of absorbance values of the specified UV-vis parameters ($Color_{436}$, UV_{365}, UV_{280} and UV_{254}) to the DOC contents. Moreover, specific fluorescence parameters were attained through normalization of fluorescence intensities (FI_{emis} and FI_{sync}) in terms of emission scan and synchronous scan modes. Specific fluorescence parameters of SFI_{emis} and SFI_{sync} were calculated through normalization of maximum fluorescence intensities at 450 nm for emission scan mode and at 470 nm for synchronous scan mode to DOC concentrations.

4. RESULTS AND DISCUSSION

Results and Discussion part covers particle size distribution (Section 4.1), sedimentation (Section 4.2) and comparative evaluation in cooperating turbidity results (Section 4.3).

4.1. Particle Size Distribution

All of the species will be presented as mono system and binary system composed of "TiO_2 and HA", "TiO_2 and SRNOM", "N-TiO_2 and HA", "N-TiO_2 and SRNOM", "Fe-TiO_2 and HA", "Fe-TiO_2 and SRNOM" under various conditions such as "as-is", "as-is under dark", "following photolysis of organic matter", and "as-is under irradiation".

4.1.1. Mono System: As-is Conditions

The elucidation of the hydrodynamic particle size of the nanoparticles were presented under "as-is" conditions separately *i.e.* TiO_2, N-TiO_2 and Fe-TiO_2. Basically, data represented time dependent hydrodynamic size variations in terms of intensity, volume, surface area, and number parameters. Particle size distribution will be presented in two modes as mono-size and multi-size distribution.

4.1.1.1. TiO_2 under "as-is" conditions intensity profile. Time dependent logN distribution G(d) and multi size distribution C(d) of TiO_2 "as-is" intensity profile was presented in Figure 4.1.

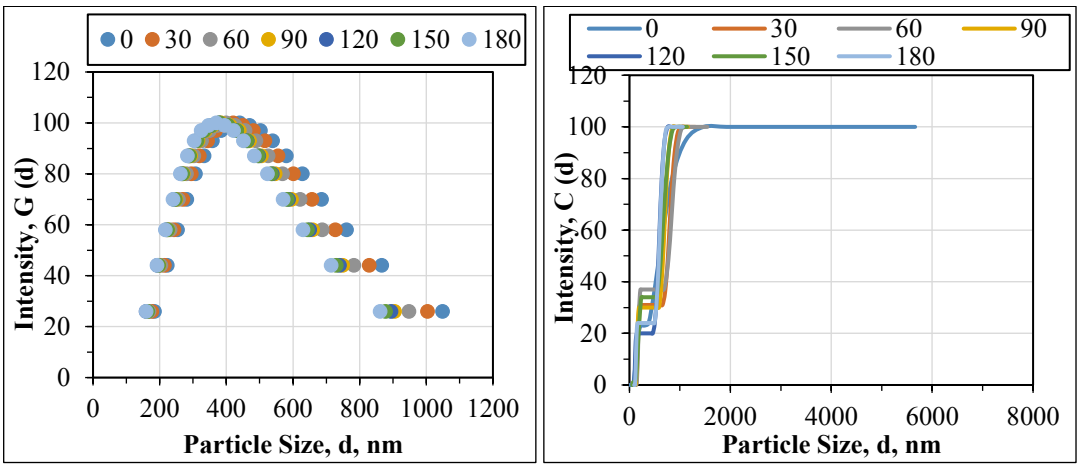


Figure 4.1. TiO_2 under "as-is" conditions intensity profile: Time dependent logN distribution G(d) and multi size distribution C(d).

Time dependent comparative presentation of log Normal distribution and multi-size distribution of TiO_2 under "as-is" conditions particle size was presented in Figure 4.2.

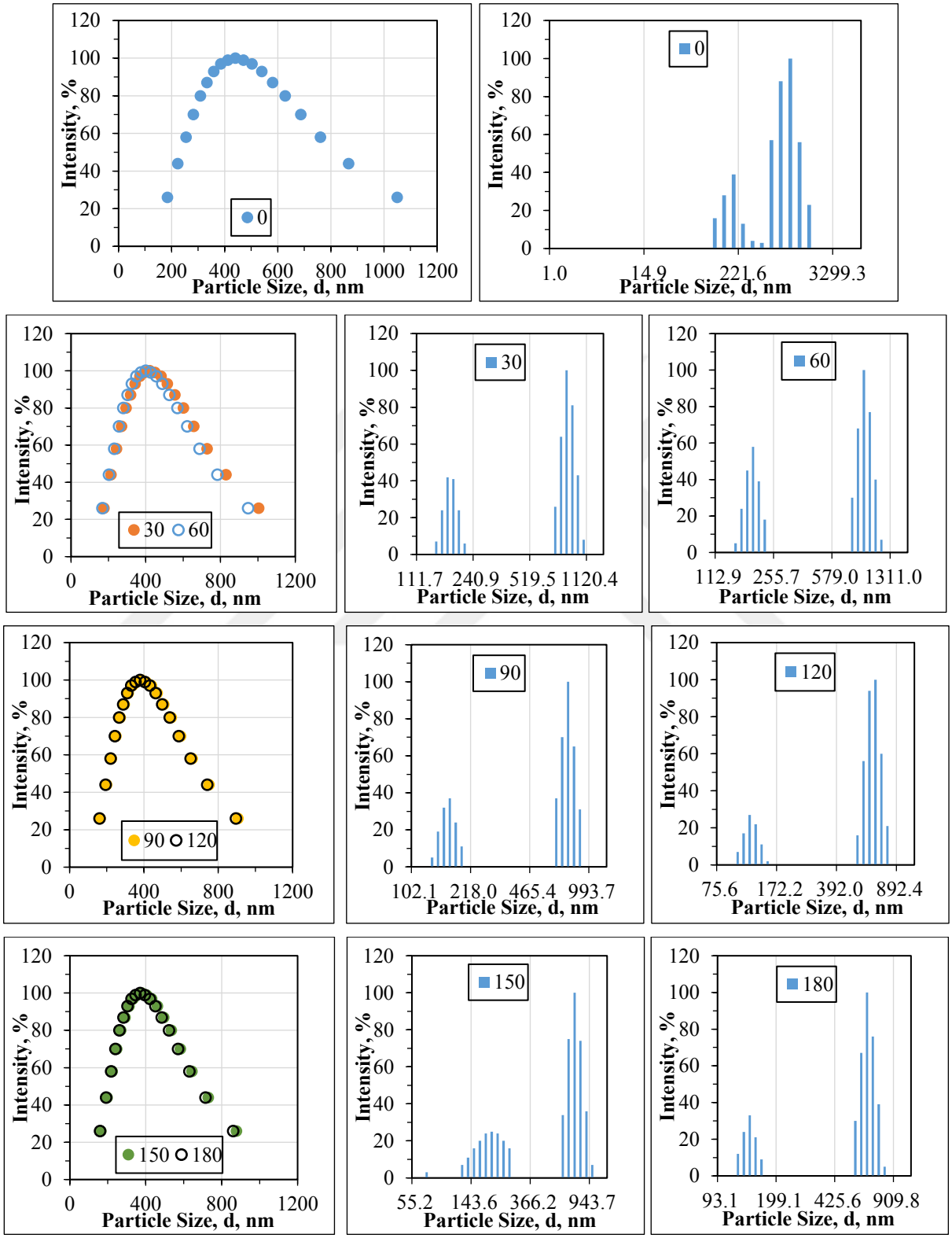


Figure 4.2. TiO_2 under "as-is" conditions intensity profile: Time dependent comparative presentation of log Normal distribution and multi-size distribution of TiO_2 under "as-is" conditions particle size.

Based on the data presented in Figure 4.1 and 4.2., time dependent mean diameter, range and min-max diameter difference with respect to log normal and multi-size distribution of TiO_2 under "as-is" conditions intensity profile was presented in Table 4.1.

Table 4.1. TiO_2 under "as-is" conditions intensity profile: Time dependent mean diameter, range and min-max diameter difference with respect to log normal and multi-size distribution.

TiO_2	time, min						
	0	30	60	90	120	150	180
Log Normal distribution							
Mean, nm	439.6	420.9	399.2	384.7	378.2	379.4	370.3
Range	184.1-1049.5	176.5-1003.8	168.1-947.8	163.6-904.7	160.0-894.0	163.9-878.3	159.2-861.5
Difference	865.4	827.3	779.7	741.1	734.0	714.4	702.3
Multi-size distribution							
Max 1, nm	169.2	164.0	184.4	160.9	114.1	66.6	136.2
Max 2, nm	855.1	823.9	871.2	733.7	642.2	184.8	622.3
Max 3, nm	-	-	-	-	-	710.4	-
Range	1.0 - 5662.2	111.7-1306.6	112.9-1543.8	102.1-1156.5	75.6-1052.0	55.2-1140.4	93.1-1059.1
Difference	5661.2	1194.9	1430.9	1054.4	976.4	1085.2	966.0

According to log normal distribution, initial hydrodynamic size of TiO_2 under "as-is" conditions was attained as 439.6 nm. During 180 min, the hydrodynamic size of TiO_2 followed a slowly decreasing trend and detected to 370.3 nm. Accordingly, with respect to time hydrodynamic size difference decreased from 865.4 nm to 702.3 nm. However, considering multi-size distribution, two max diameters were obtained as 169.2 nm and 855.1 nm for TiO_2 under "as-is" conditions following initial period of time. Upon 180 min, two max diameters were attained as 136.2 nm and 622.3 nm. Also, the hydrodynamic size differences were observed in between 5661.2 nm and 966.0 nm with respect to time. Although hydrodynamic particle sizes were observed as coinciding peaks according to the log normal distribution, peaks were monitored distinctly different as bimodal in multi-size distribution until 180 min.

Polydispersity of TiO_2 under "as-is" conditions was presented in Table 4.2. No significant variation was observed over period of 180 min. Simply an average value of 0.312 could be regarded as suitable for expressing polydispersity.

Table 4.2. Polydispersity of TiO_2 under "as-is" conditions.

TiO_2	Polydispersity						
	0	30	60	90	120	150	180
	0.323	0.322	0.318	0.310	0.314	0.297	0.301

4.1.1.2. TiO_2 under "as-is" conditions volume profile. Time dependent logN distribution G(d) and multi size distribution C(d) of TiO_2 under "as-is" conditions volume profile was given in Figure 4.3. Time dependent mean diameter, range and min-max diameter difference with respect to log normal and multi-size distribution of TiO_2 under "as-is" conditions volume profile was given in Table 4.3.

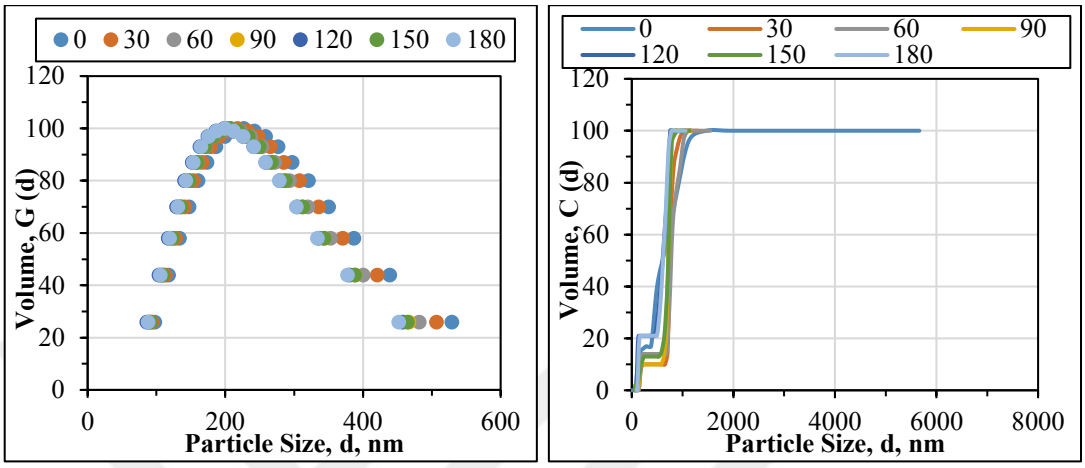


Figure 4.3. TiO_2 under "as-is" conditions volume profile: Time dependent logN distribution G(d) and multi size distribution C(d).

Table 4.3. TiO_2 under "as-is" conditions volume profile: Time dependent mean diameter, range and min-max diameter difference with respect to log normal and multi-size distribution.

TiO_2	time, min						
	0	30	60	90	120	150	180
Log Normal distribution							
Mean, nm	226.9	217.6	207.9	203.5	198.4	205.7	199.2
Range	97.3-528.8	93.5-506.7	89.7-481.7	88.7-466.8	86.0-457.6	91.2-464.3	87.8-451.9
Difference	431.5	413.2	392.0	378.1	371.6	373.1	364.1
Multi-size distribution							
Max 1, nm	98.6	164.0	184.4	149.2	114.1	66.6	136.2
Max 2, nm	498.3	763.0	802.9	160.9	757.0	143.6	724.4
Max 3, nm	1120.2	-	1025.9	733.7	-	156.2	-
Max 4, nm	-	-	-	-	-	169.9	-
Max 5, nm	-	-	-	-	-	184.8	-
Max 6, nm	-	-	-	-	-	780.9	-
Range	1.0-5662.2	111.7-1306.6	112.9-1543.8	102.1-1156.5	75.6-1052.0	55.2-1140.4	93.1-1059.1
Difference	5661.2	1194.9	1430.9	1054.4	976.4	1085.2	966.0

In terms of volume distribution, initial hydrodynamic size of TiO_2 under "as-is" conditions was obtained as 226.9 nm and reached to 199.2 nm over period of 180 min. Considering multi-size distribution, six max diameters were attained upon 150 min. Initial size difference was recorded as 5661.2 nm and decreased to 966.0 nm at the end of 180 min. In a similar manner, time dependent

comparative presentation of log Normal distribution and multi-size distribution of TiO_2 under "as-is" conditions volume profile was demonstrated in Figure 4.4.

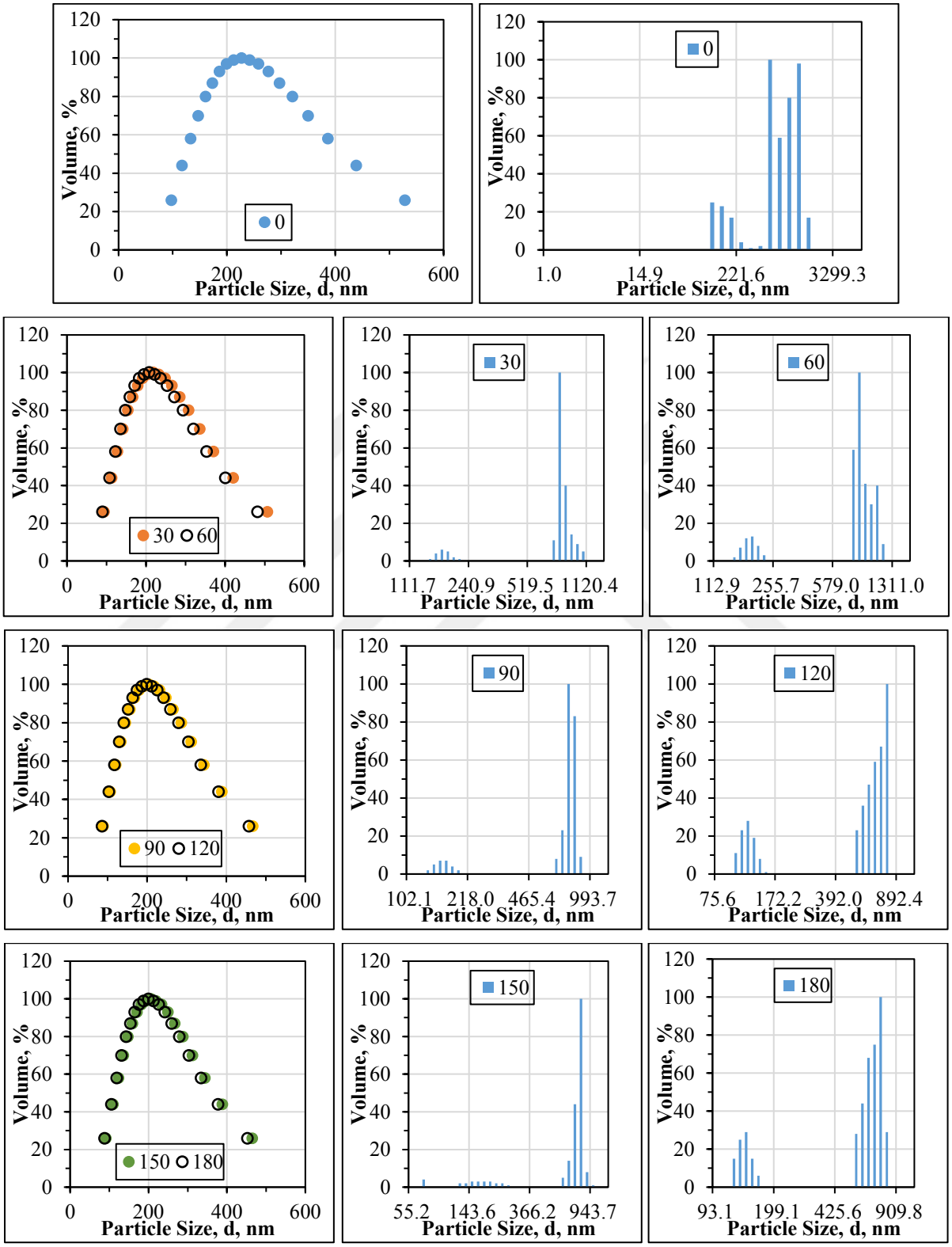


Figure 4.4. TiO_2 under "as-is" conditions volume profile: Time dependent comparative presentation of log Normal distribution and multi-size distribution of TiO_2 under "as-is" conditions particle size.

4.1.1.3. TiO_2 under "as-is" conditions surface area profile. Time dependent logN distribution G(d) and multi size distribution C(d) of TiO_2 under "as-is" conditions surface area profile was presented in Figure 4.5. Time dependent mean diameter, range and min-max diameter difference with respect to log normal and multi-size distribution of TiO_2 under "as-is" conditions surface area profile was displayed in Table 4.4.

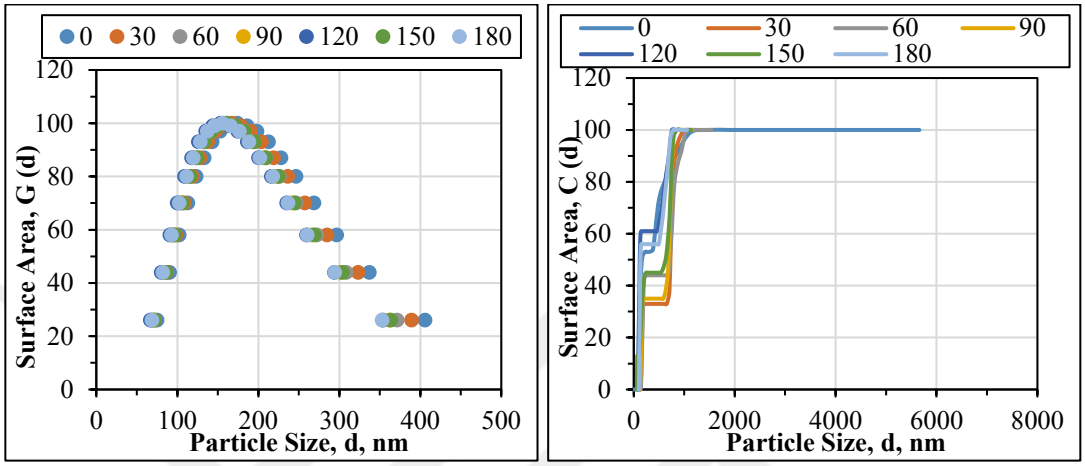


Figure 4.5. TiO_2 under "as-is" conditions surface area profile: Time dependent logN distribution G(d) and multi size distribution C(d).

Table 4.4. TiO_2 under "as-is" conditions surface area profile: Time dependent mean diameter, range and min-max diameter difference with respect to log normal and multi-size distribution.

TiO_2	time, min						
	0	30	60	90	120	150	180
Log Normal distribution							
Mean, nm	174.1	167.2	160.1	157.7	153.3	161.1	155.4
Range	74.7-405.8	71.8-389.1	69.1-371.1	68.8-361.8	66.4-353.5	71.4-363.5	68.5-352.7
Difference	331.1	317.3	302.0	293.0	287.1	292.1	284.2
Multi-size distribution							
Max 1, nm	98.6	164.0	184.4	149.2	114.1	66.6	136.2
Max 2, nm	498.3	763.0	802.9	733.7	757.0	143.6	724.4
Max 3, nm	855.1	-	-	-	-	156.2	-
Max 4, nm	-	-	-	-	-	780.9	-
Range	1.0-5662.2	111.7-1306.6	112.9-1543.8	102.1-1156.5	75.6-1052.0	55.2-1140.4	93.1-1059.1
Difference	5661.2	1194.9	1430.9	1054.4	976.4	1085.2	966.0

In terms of surface area profile, hydrodynamic particle size of TiO_2 under "as-is" conditions exhibited a slightly decreasing trend and obtained an average diameter as 161.3 nm. Size difference was obtained between 284.2 nm and 331.1 nm. For comparison purposes, initially three bimodal peaks were monitored as 98.6 nm, 498.3 nm and 855.1 nm, and also two peaks were observed upon

180 min. Time dependent comparative presentation of log Normal distribution and multi-size distribution of TiO_2 under "as-is" conditions surface area profile was exhibited in Figure 4.6.

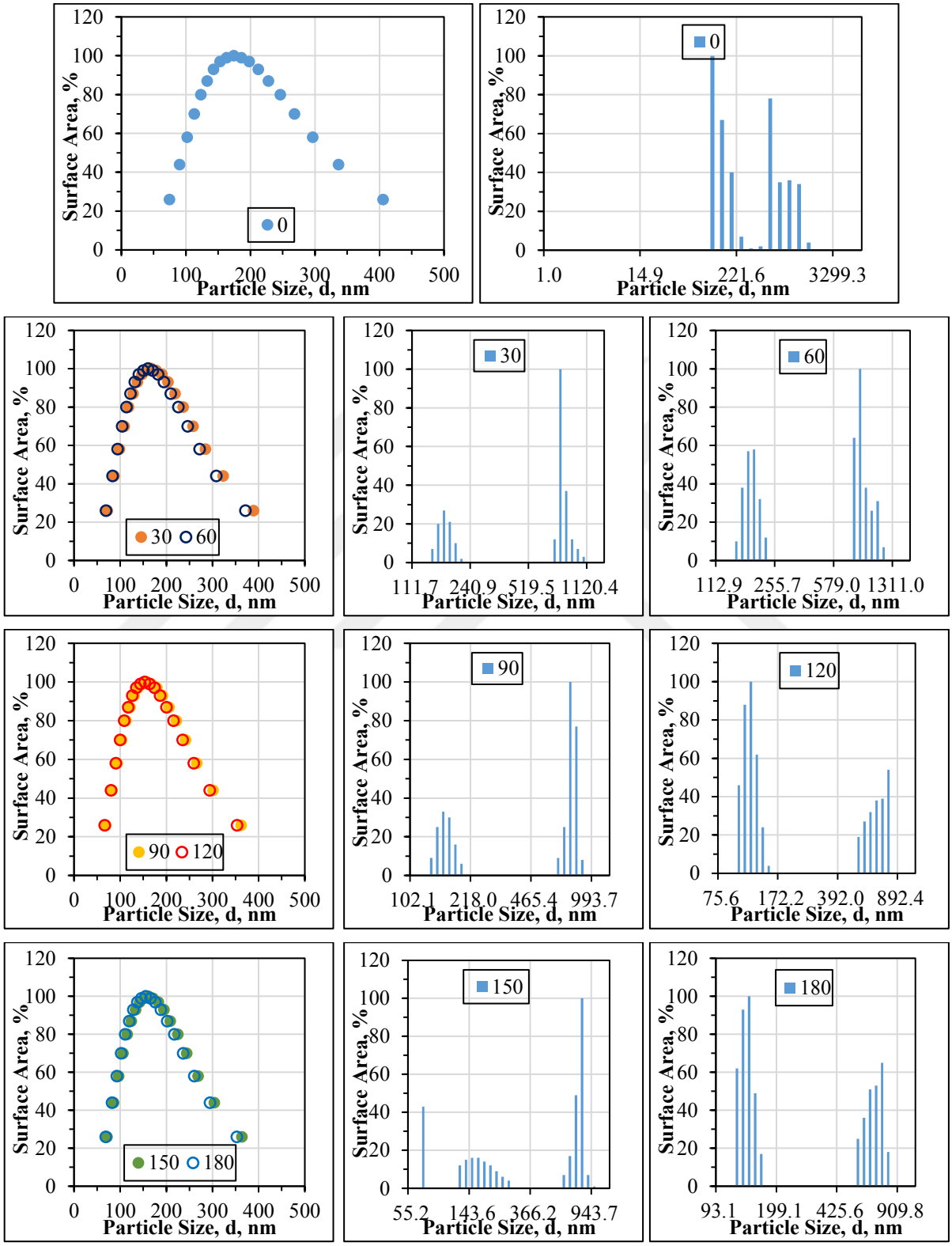


Figure 4.6. TiO_2 under "as-is" conditions surface area profile: Time dependent comparative presentation of log Normal distribution and multi-size distribution of TiO_2 under "as-is" conditions particle size.

4.1.1.4. TiO_2 under "as-is" conditions number profile. Time dependent logN distribution G(d) and multi size distribution C(d) of TiO_2 under "as-is" conditions number profile was presented in Figure 4.7. Time dependent mean diameter, range and min-max diameter difference with respect to log normal and multi-size distribution of TiO_2 under "as-is" conditions number profile was shown in Table 4.5.

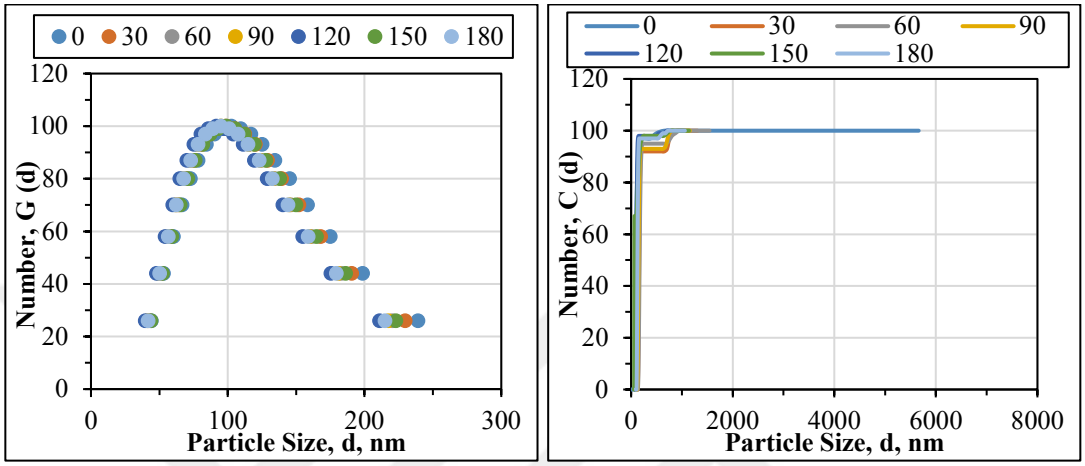


Figure 4.7. TiO_2 under "as-is" conditions number profile: Time dependent logN distribution G(d) and multi size distribution C(d).

Table 4.5. TiO_2 under "as-is" conditions number profile: Time dependent mean diameter, range and min-max diameter difference with respect to log normal and multi-size distribution.

TiO_2	time, min						
	0	30	60	90	120	150	180
Log Normal distribution							
Mean, nm	102.6	98.6	95.0	94.8	91.5	98.7	94.7
Range	44.0-239.1	42.4-229.6	41.0-220.2	41.3-217.4	39.7-210.9	43.7-222.8	41.7-214.8
Difference	195.1	187.2	179.2	176.1	171.2	179.1	173.1
Multi-size distribution							
Max 1, nm	98.6	164.0	169.9	149.2	105.1	66.6	126.2
Max 2, nm	498.3	763.0	802.9	733.7	501.7	121.3	576.7
Max 3, nm	-	-	-	-	544.7	132.0	622.3
Max 4, nm	-	-	-	-	591.4	780.9	671.4
Max 5, nm	-	-	-	-	642.2	-	724.4
Max 6, nm	-	-	-	-	697.2	-	-
Max 7, nm	-	-	-	-	757.0	-	-
Range	1.0-5662.2	111.7-1306.6	112.9-1543.8	102.1-1156.5	75.6-1052.0	55.2-1140.4	93.1-1059.1
Difference	5661.2	1194.9	1430.9	1054.4	976.4	1085.2	966.0

According to log normal distribution, TiO_2 under "as-is" conditions did not exhibit drastic changes along 180 min. Simply an average hydrodynamic diameter could be accepted as 96.6 nm.

Also, initially two peaks were observed in multi-size distribution and reached to seven bimodal peaks upon 120 min. Time dependent comparative presentation of log Normal distribution and multi-size distribution of TiO_2 under "as-is" conditions number profile was presented in Figure 4.8.

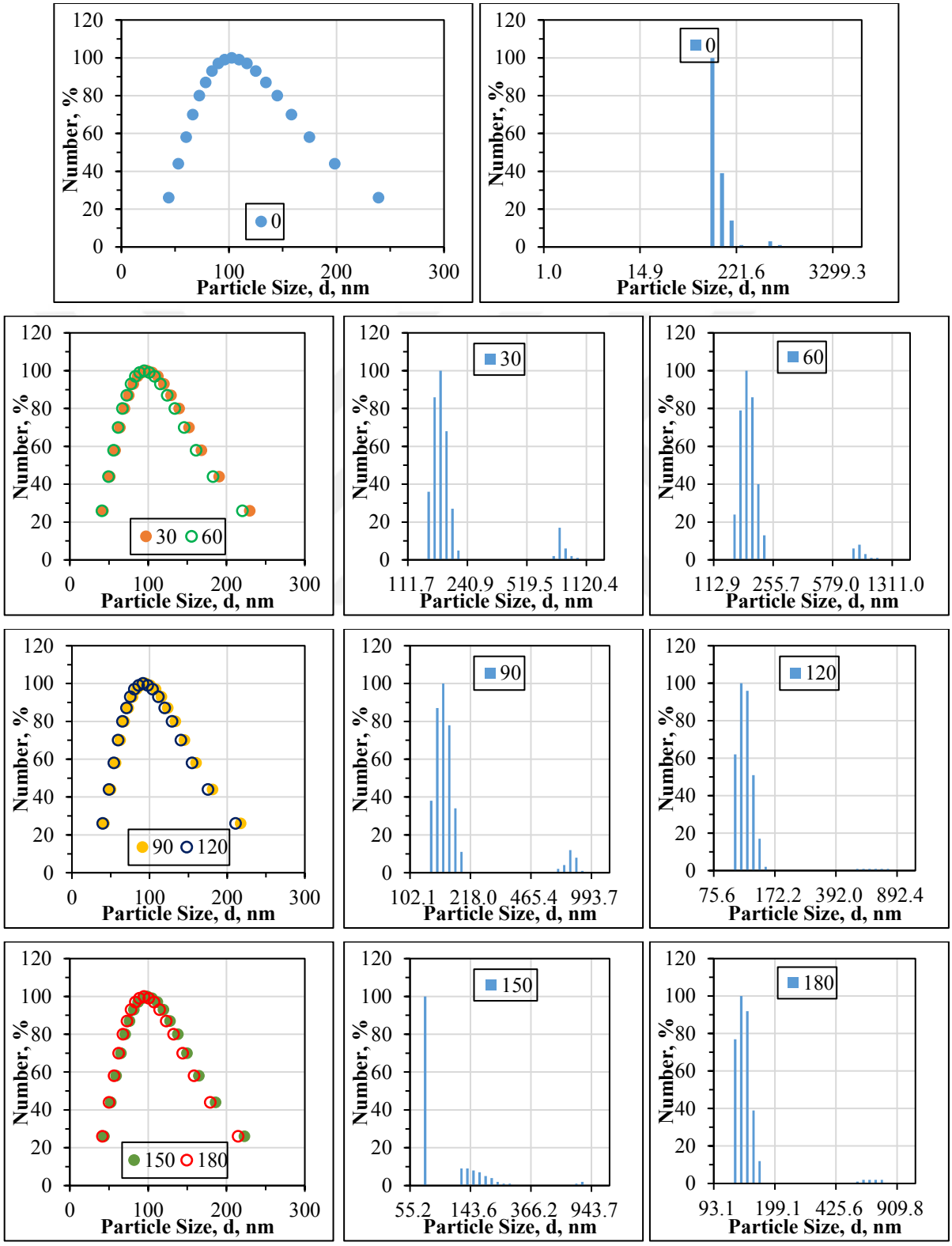


Figure 4.8. TiO_2 under "as-is" conditions number profile: Time dependent comparative presentation of log Normal distribution and multi-size distribution of TiO_2 under "as-is" conditions particle size.

4.1.1.5. N-TiO_2 under "as-is" conditions intensity profile. As explained for TiO_2 under "as-is" conditions intensity profile (Figure 4.1), a similar approach was followed for N-TiO_2 under "as-is" conditions intensity profile. Time dependent logN distribution G(d) and multi size distribution C(d) of N-TiO_2 under "as-is" conditions intensity profile was displayed in Figure 4.9. Time dependent mean diameter, range and min-max diameter difference with respect to log normal and multi-size distribution of N-TiO_2 under "as-is" conditions intensity profile was shown in Table 4.6. Also, time dependent polydispersity of N-TiO_2 under "as-is" conditions was exhibited in Table 4.7.

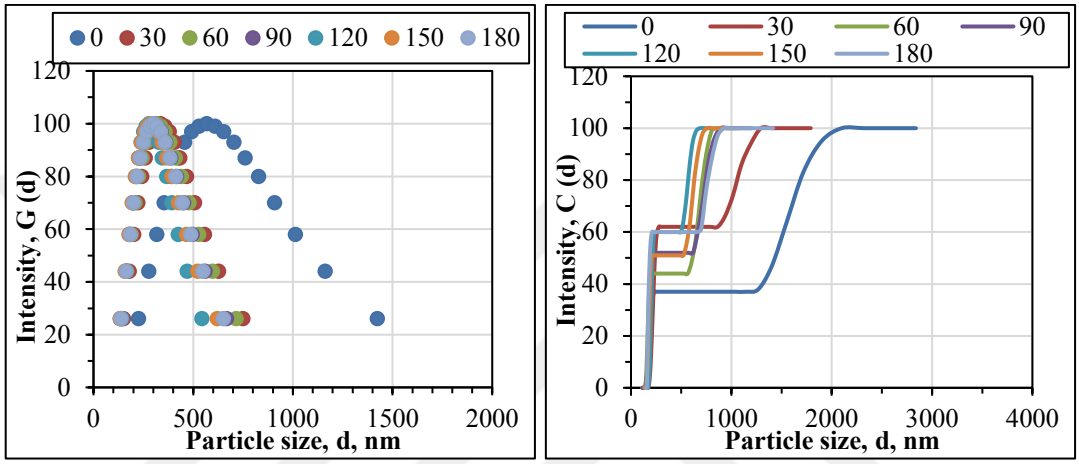


Figure 4.9. N-TiO_2 under "as-is" conditions intensity profile: Time dependent logN distribution G(d) and multi size distribution C(d).

Table 4.6. N-TiO_2 under "as-is" conditions intensity profile: Time dependent mean diameter, range and min-max diameter difference with respect to log normal and multi-size distribution.

N-TiO_2	time, min						
	0	30	60	90	120	150	180
Log Normal distribution							
Mean, nm	567.9	336.0	316.5	300.6	279.4	288.4	299.6
Range	226.5-1423.9	150.7-749.2	140.0-715.2	135.4-667.3	143.2-544.9	134.0-620.5	137.8-651.3
Difference	1197.4	598.5	575.2	531.9	401.7	486.5	513.5
Multi-size distribution							
Max 1, nm	187.8	235.7	171.0	189.2	200.8	180.8	209.7
Max 2, nm	1717.2	1100.8	699.0	771.5	584.7	630.0	862.9
Range	113.6-2839.6	133.6-1790.8	112.1-1066.3	112.7-1202.5	145.7-805.8	132.3-975.2	147.3-1415.8
Difference	2726.0	1657.2	954.2	1089.8	660.1	842.9	1268.5

In a similar manner to data described TiO_2 under "as-is" conditions intensity profile (Table 4.1) time dependent mean diameter, range and min-max diameter difference with respect to log normal and multi-size distribution of N-TiO_2 under "as-is" conditions intensity profile was presented.

According to log normal distribution and in terms of intensity profile, it could be inferred that initial hydrodynamic particle size of N-TiO_2 under "as-is" conditions was obtained as 567.9 nm. Upon 30 min, hydrodynamic particle size revealed roughly 20 % decrease and recorded as 336.0 nm, and minor variations was observed until the end of 180 min. Upon 180 min, hydrodynamic particle size of N-TiO_2 under "as-is" conditions was attained as 299.6 nm. On the other hand, according to log normal distribution, size difference decreased from 1197.4 nm to 513.5 nm according to time variations.

However, in terms of multi-size distribution, initially two max diameters were attained as 187.8 nm and 1717.2 nm, and remained until the end of 180 min period. On the other hand, according to multi-size distribution, initial size difference between max and min diameter was obtained as 2726.0 nm and detected to 1268.5 nm upon period of 180 min.

For comparison purposes, it could be asserted that contrary to slight variations detected for hydrodynamic particle sizes of TiO_2 under "as-is" conditions, N-TiO_2 under "as-is" conditions demonstrated drastic changes according to time variations. Due to the fact that hydrodynamic particle sizes were obtained as coinciding peaks according to the log normal distribution, max diameters were attained distinctly different as bimodal in multi-size distribution until 180 min period. On the other hand, considering size differences, N-TiO_2 under "as-is" conditions intensity profile revealed higher size differences in comparison to TiO_2 under "as-is" conditions intensity profile (Table 4.1). The reason could be attributed to the variations in hydrodynamic particle sizes.

As explained for TiO_2 under "as-is" conditions (Table 4.2), time dependent polydispersity of N-TiO_2 under "as-is" conditions were displayed in Table 4.7. It could be deduced that a sharp decrease was observed in the first 30 min (0.366 to 0.268) and a fluctuating trend was monitored until the end of 180 min reacging a polydispersity value 0.250. Considering all values form a general point of view, an average value of 0.264 could be regarded as appropriate for expressing polydispersity.

Table 4.7. Polydispersity of N-TiO_2 under "as-is" conditions.

N-TiO_2	Polydispersity						
	0	30	60	90	120	150	180
	0.366	0.268	0.278	0.265	0.179	0.242	0.250

Time dependent comparative presentation of log Normal distribution and multi-size distribution of N-TiO_2 under "as-is" conditions intensity profile was displayed in Figure 4.10. As indicated for TiO_2 under "as-is" conditions intensity profile (Figure 4.2), a similar approach was also followed for

presentation of N-TiO_2 under "as-is" conditions intensity profile. Therefore, below given comparative intensity distribution profiles expressed time dependent variations in hydrodynamic particle size.

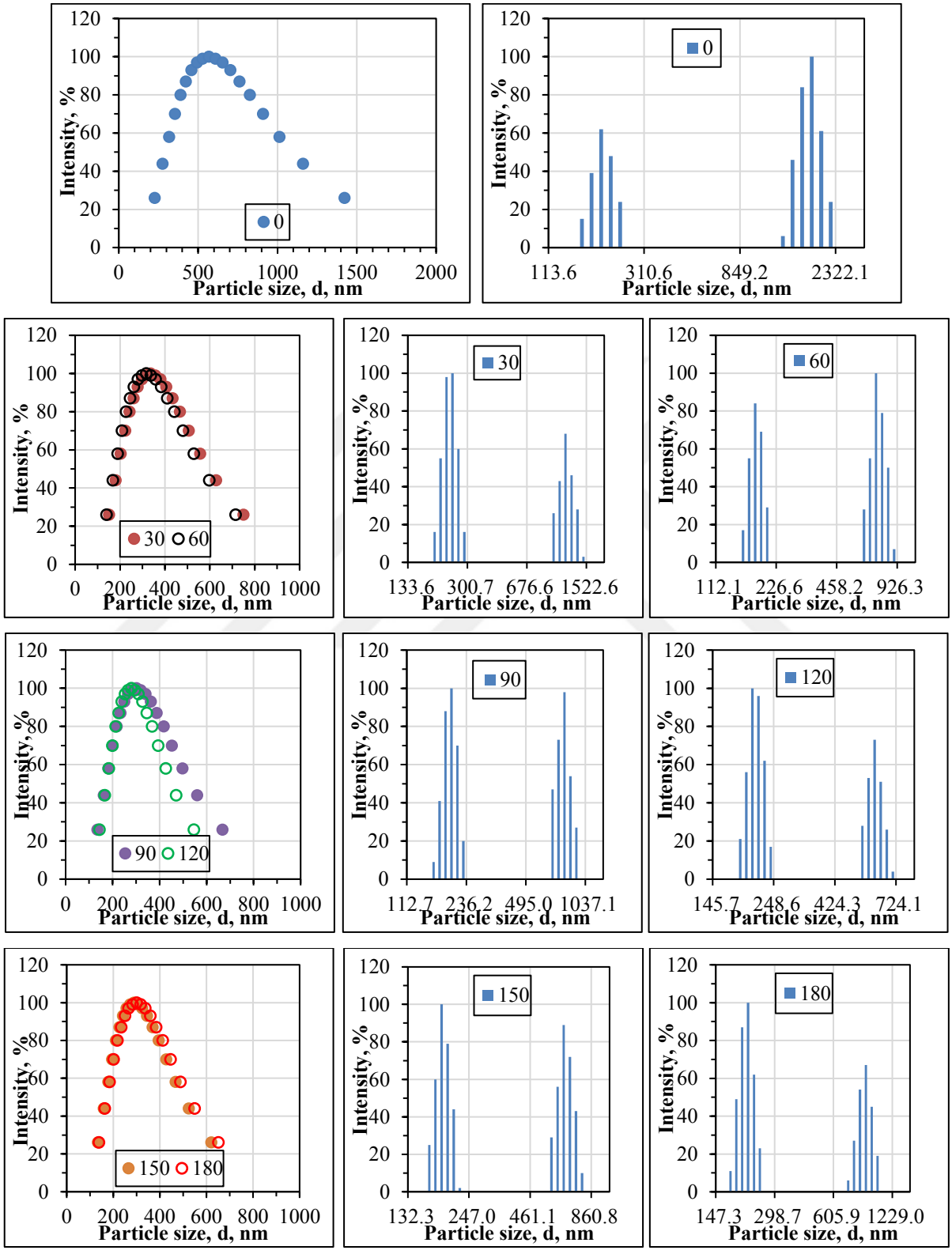


Figure 4.10. N-TiO_2 under "as-is" conditions intensity profile: Time dependent comparative presentation of log Normal distribution and multi-size distribution of N-TiO_2 under "as-is" conditions.

4.1.1.6. N-TiO_2 under "as-is" conditions volume profile. Time dependent logN distribution G(d) and multi size distribution C(d) of N-TiO_2 under "as-is" conditions volume profile was given in Figure 4.11. Also, time dependent mean diameter, range and min-max diameter difference with respect to log normal and multi-size distribution of N-TiO_2 under "as-is" conditions volume profile was displayed in Table 4.8.

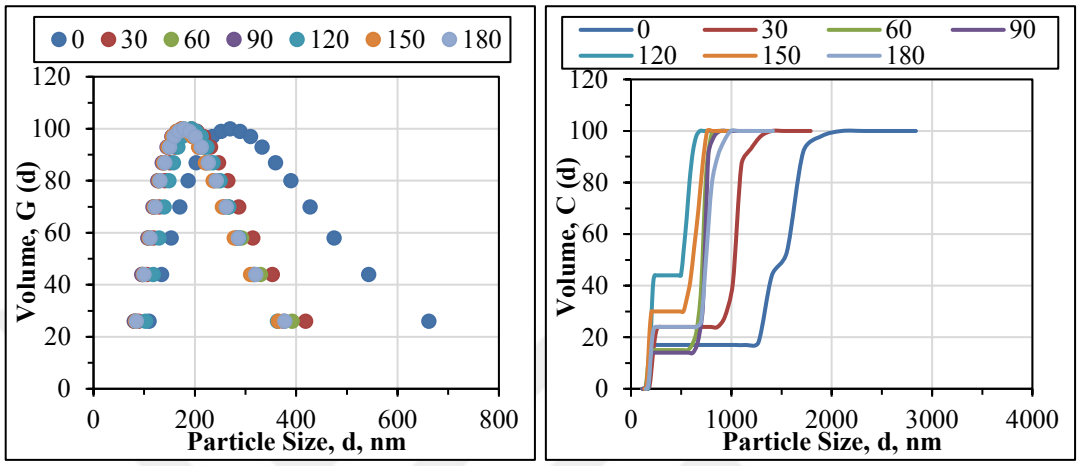


Figure 4.11. N-TiO_2 under "as-is" conditions volume profile: Time dependent logN distribution G(d) and multi size distribution C(d).

Table 4.8. N-TiO_2 under "as-is" conditions volume profile: Time dependent mean diameter, range and min-max diameter difference with respect to log normal and multi-size distribution.

N-TiO_2	time, min						
	0	30	60	90	120	150	180
Log Normal distribution							
Mean, nm	269.9	193.0	178.1	173.9	193.1	174.6	178.7
Range	110.1-662.1	89.0-418.8	80.9-392.0	80.5-375.5	102.6-363.4	83.5-364.8	84.6-377.5
Difference	552.0	329.8	311.1	295.0	260.8	281.3	292.9
Multi-size distribution							
Max 1, nm	187.8	217.4	171.0	175.7	200.8	180.8	209.7
Max 2, nm	1717.2	235.7	749.9	189.2	584.7	713.8	804.0
Max 3, nm	-	1100.8	-	771.5	-	-	-
Range	113.6-2839.6	133.6-1790.8	112.1-1066.3	112.7-1202.5	145.7-805.8	132.3-975.2	147.3-1415.8
Difference	2726.0	1657.2	954.2	1089.8	660.1	842.9	1268.5

Considering log normal distribution, it could be inferred that a continuous decrease was monitored upon period of 180 min. Size difference decreased from 552.0 nm to 292.9 nm. However, initially two peaks were observed as 187.8 nm and 1717.2 nm, and upon 30 min, three peaks were monitored as 217.4 nm, 235.7 nm, 1100.8 nm. On the other hand, size difference decreased from 2726.0 nm to 1268.5 in terms of multi-size distribution along 180 min.

Time dependent comparative presentation of log Normal distribution and multi-size distribution of N-TiO_2 under "as-is" conditions volume profile was given in Figure 4.12.

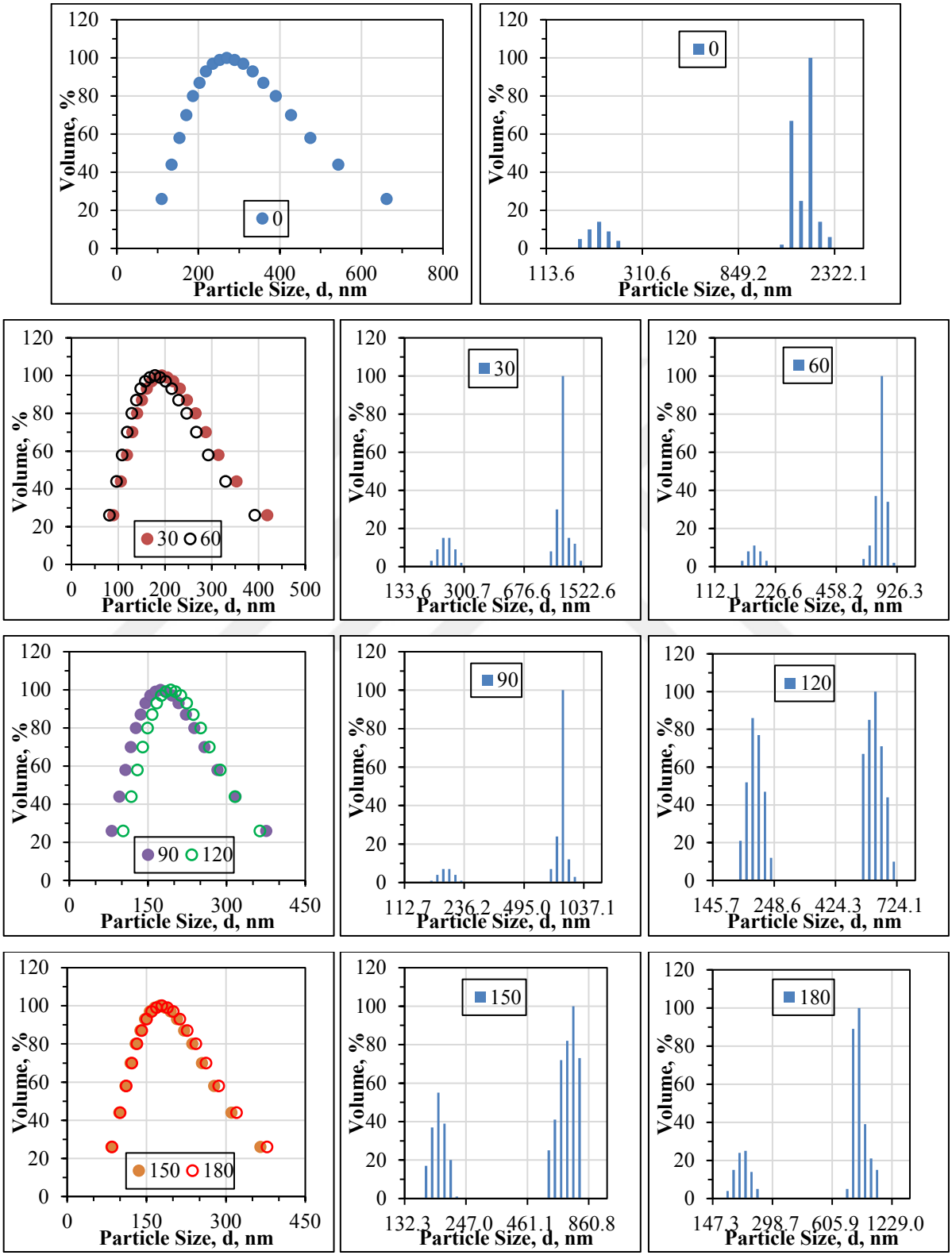


Figure 4.12. N-TiO_2 under "as-is" conditions volume profile: Time dependent comparative presentation of log Normal distribution and multi-size distribution of N-TiO_2 under "as-is" conditions.

4.1.1.7. N-TiO_2 under "as-is" conditions surface area profile. In a similar manner to data described N-TiO_2 under "as-is" conditions volume profile (Figure 4.11), time dependent logN distribution G(d) and multi size distribution C(d) of N-TiO_2 under "as-is" conditions surface area profile was demonstrated in Figure 4.13. Time dependent mean diameter, range and min-max diameter difference with respect to log normal and multi-size distribution of N-TiO_2 under "as-is" conditions surface area profile was exhibited in Table 4.9.

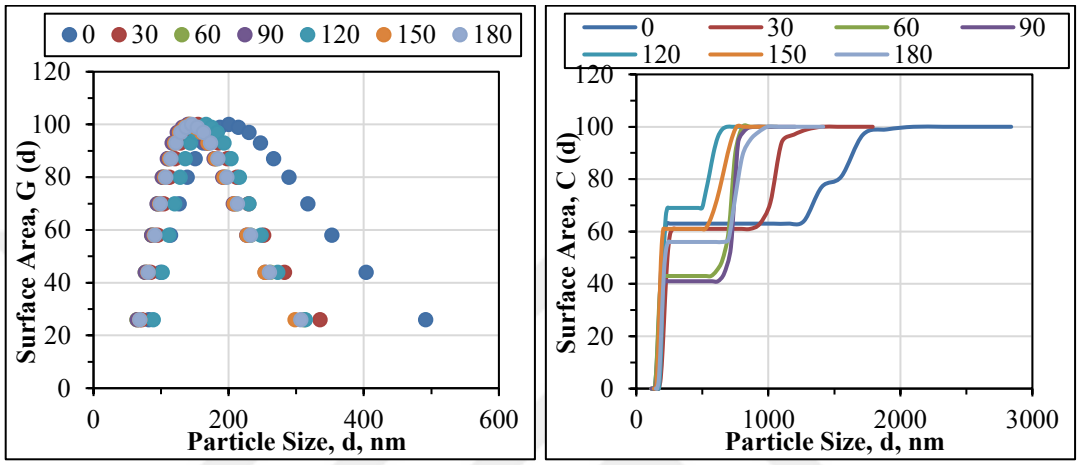


Figure 4.13. N-TiO_2 under "as-is" conditions surface area profile: Time dependent logN distribution G(d) and multi size distribution C(d).

Table 4.9. N-TiO_2 under "as-is" conditions surface area profile: Time dependent mean diameter, range and min-max diameter difference with respect to log normal and multi-size distribution.

N-TiO_2	time, min						
	0	30	60	90	120	150	180
Log Normal distribution							
Mean, nm	200.5	154.7	141.5	139.7	166.5	142.8	145.3
Range	81.7-491.7	71.3-335.5	64.3-311.5	64.7-301.6	88.5-313.4	68.4-298.5	68.8-307.0
Difference	410.0	264.2	247.2	236.9	224.9	230.1	238.2
Multi-size distribution							
Max 1, nm	187.8	217.4	171.0	175.7	200.8	180.8	195.4
Max 2, nm	1404.3	1100.8	749.9	771.5	584.7	713.8	804.0
Max 3, nm	1717.2	-	-	-	-	-	-
Range	113.6-2839.6	133.6-1790.8	112.1-1066.3	112.7-1202.5	145.7-805.8	132.3-975.2	147.3-1415.8
Difference	2726.0	1657.2	954.2	1089.8	660.1	842.9	1268.5

Initial hydrodynamic size of N-TiO_2 under "as-is" conditions was obtained as 200.5 nm. During 180 min, the hydrodynamic size of N-TiO_2 followed a rapidly decreasing trend and detected to 145.3 nm. Initial size difference between max and min diameter was attained as 410.0 nm and decreased to 238.2 nm upon 180 min experimental duration. However, considering multi-size distribution, initially

three peaks were attained. Time dependent comparative presentation of log Normal distribution and multi-size distribution of N-TiO_2 under "as-is" conditions surface area profile was demonstrated in Figure 4.12.

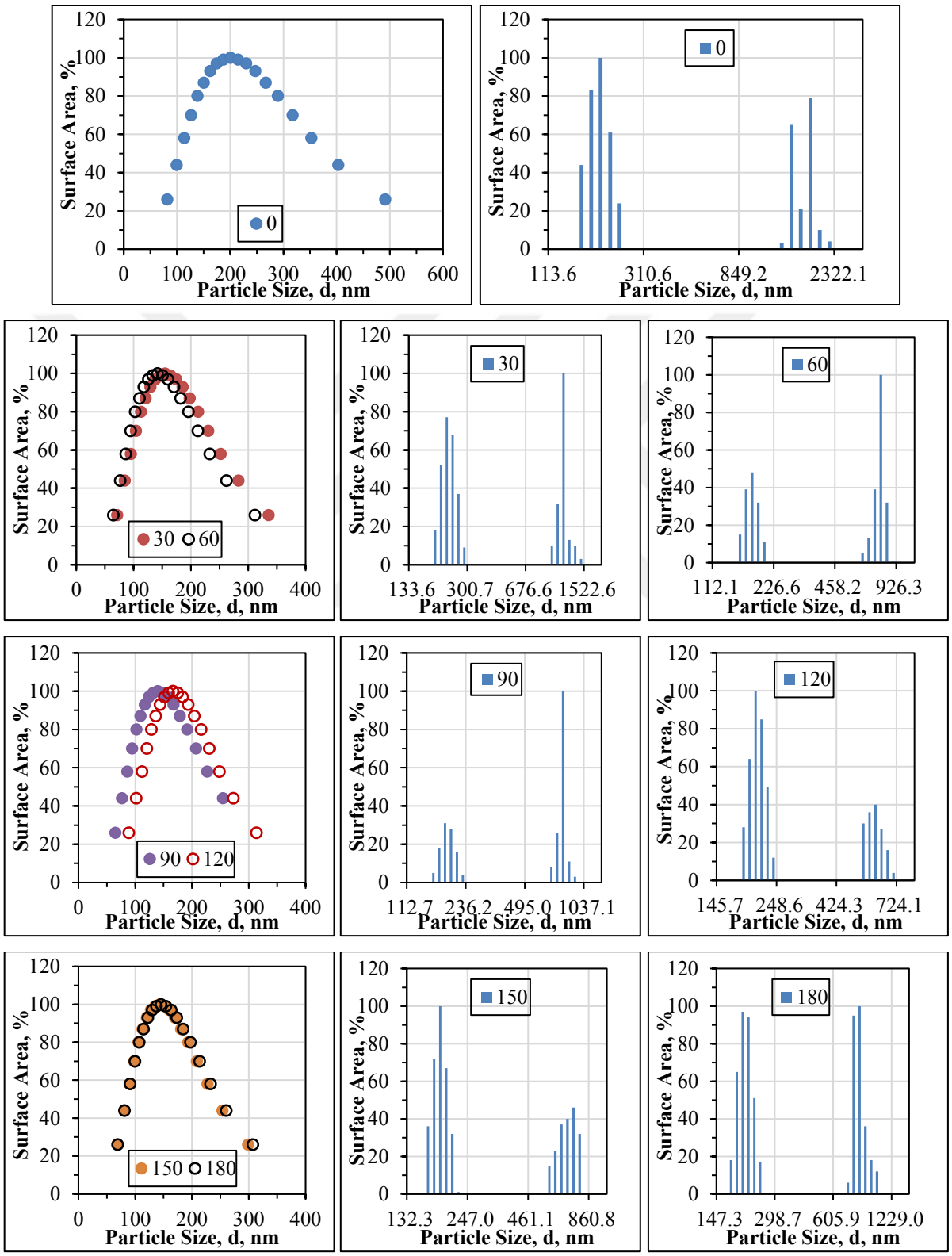


Figure 4.14. N-TiO_2 under "as-is" conditions surface area profile: Time dependent comparative presentation of log Normal distribution and multi-size distribution of N-TiO_2 under "as-is" conditions.

4.1.1.8. N-TiO_2 under "as-is" conditions number profile. Time dependent logN distribution G(d) and multi size distribution C(d) of N-TiO_2 under "as-is" conditions number profile was exhibited in Figure 4.15. Also, time dependent mean diameter, range and min-max diameter difference with respect to log normal and multi-size distribution of N-TiO_2 under "as-is" conditions number profile was given in Table 4.10.

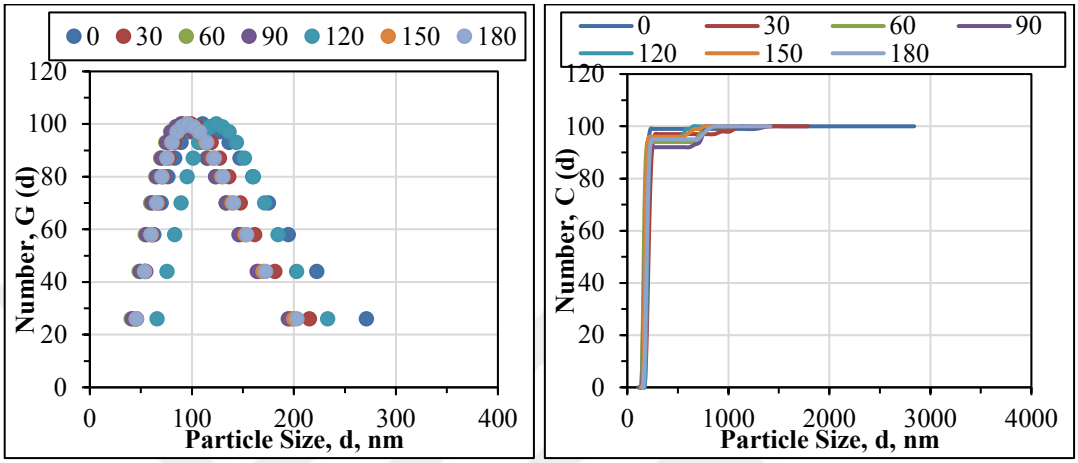


Figure 4.15. N-TiO_2 under "as-is" conditions number profile: Time dependent logN distribution G(d) and multi size distribution C(d).

Table 4.10. N-TiO_2 under "as-is" conditions number profile: Time dependent mean diameter, range and min-max diameter difference with respect to log normal and multi-size distribution.

N-TiO_2	time, min						
	0	30	60	90	120	150	180
Log Normal distribution							
Mean, nm	110.6	99.3	89.4	90.1	123.9	95.6	96.1
Range	45.1-271.2	45.8-215.4	40.6-196.7	41.7-194.6	65.8-233.2	45.7-199.8	45.5-203.0
Difference	226.1	169.6	156.1	152.9	167.4	154.1	157.5
Multi-size distribution							
Max 1, nm	169.8	217.4	171.0	175.7	200.8	180.8	195.4
Max 2, nm	1404.3	1100.8	749.9	771.5	554.3	630.0	749.1
Max 3, nm	1717.2	-	-	-	584.7	670.6	-
Max 4, nm	-	-	-	-	-	713.8	-
Range	113.6-2839.6	133.6-1790.8	112.1-1066.3	112.7-1202.5	145.7-805.8	132.3-975.2	147.3-1415.8
Difference	2726.0	1657.2	954.2	1089.8	660.1	842.9	1268.5

In terms of log normal distribution, it could be deduced that a sharp decrease was monitored until 120 min. Upon period of 120 min, dramatic increases that may be due to possible aggregation of nanoparticles were observed. Accordingly, a rapid decrease remained until the end of 180 min. In terms of multi-size distribution, initially three peaks were recorded and two peaks were observed until

120 min. Upon 120 min, three peaks were monitored and two peaks were attained upon 180 min. Time dependent comparative presentation of log Normal distribution and multi-size distribution of N-TiO_2 under "as-is" conditions number profile was presented in Figure 4.16.

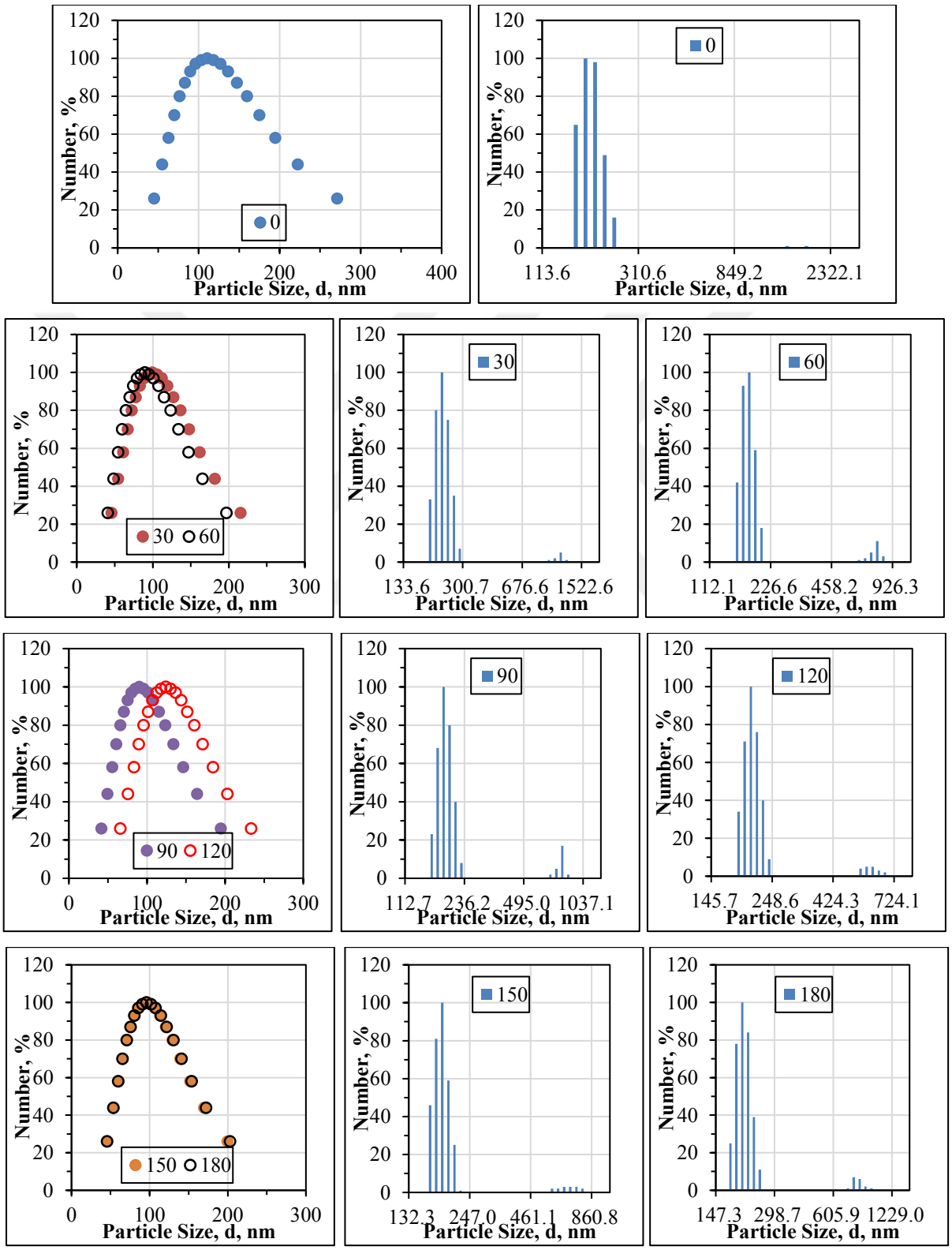


Figure 4.16. N-TiO_2 under "as-is" conditions number profile: Time dependent comparative presentation of log Normal distribution and multi-size distribution of N-TiO_2 under "as-is" conditions.

4.1.1.9. Fe-TiO_2 under as-is" conditions intensity profile. As expressed for TiO_2 under "as-is" conditions intensity profile (Figure 4.1), and N-TiO_2 under "as-is" conditions intensity profile (Figure 4.9), a similar approach was followed for Fe-TiO_2 under "as-is" conditions intensity profile. Time dependent logN distribution G(d) and multi size distribution C(d) of Fe-TiO_2 under "as-is" conditions intensity profile was demonstrated in Figure 4.17. Time dependent mean diameter, range and min-max diameter difference with respect to log normal and multi-size distribution of Fe-TiO_2 under "as-is" conditions intensity profile was displayed in and Table 4.11.

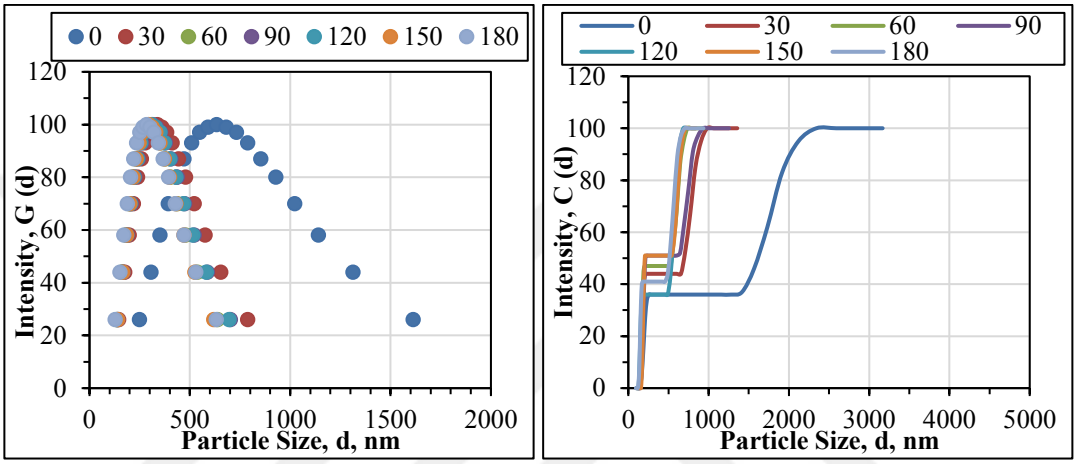


Figure 4.17. Fe-TiO_2 under "as-is" conditions intensity profile: Time dependent logN distribution G(d) and multi size distribution C(d).

Table 4.11. Fe-TiO_2 under "as-is" conditions intensity profile: Time dependent mean diameter, range and min-max diameter difference with respect to log normal and multi-size distribution.

Fe-TiO_2	time, min						
	0	30	60	90	120	150	180
Log Normal distribution							
Mean, nm	633.6	338.3	293.7	313.6	309.5	294.8	283.8
Range	248.9-1612.8	145.1-788.4	135.0-638.9	140.1-702.2	137.6-696.1	140.4-619.2	127.4-632.5
Difference	1363.9	643.3	503.9	562.1	558.5	478.8	505.1
Multi-size distribution							
Max 1, nm	209.5	180.0	177.2	183.3	157.1	185.6	146.1
Max 2, nm	1915.9	835.7	644.1	804.9	599.4	638.2	567.5
Max 3, nm	-	-	-	-	-	-	609.6
Range	126.7-3168.1	102.2-1357.1	110.1-968.2	117.6-1254.6	98.3-837.7	140.2-845.0	95.1-935.8
Difference	3041.4	1254.9	858.1	1137.0	739.4	704.8	840.7

In a similar manner to data depicted TiO_2 under "as-is" conditions intensity profile (Table 4.1) and N-TiO_2 under "as-is" conditions intensity profile (Table 4.6), time dependent mean diameter, range and min-max diameter difference with respect to log normal and multi-size distribution of Fe-

TiO_2 under "as-is" conditions intensity profile was demonstrated. According to log normal distribution and in terms of intensity profile, initial hydrodynamic particle size of Fe-TiO_2 under "as-is" conditions was recorded as 633.6 nm. Upon 30 min, hydrodynamic particle size revealed approximately 50 % decrease and detected as 338.3 nm, and continuous decrease was observed until the end of 180 min. Upon 180 min, hydrodynamic particle size of Fe-TiO_2 under "as-is" conditions were attained as 283.8 nm. On the other hand, according to log normal distribution, size difference decreased from 1363.9 nm to 505.1 nm with respect to time.

However, in terms of multi-size distribution, two max diameters were obtained until 180 min. Upon 180 min, three max diameters were attained as 146.1 nm, 567.5 nm, and 609.6 nm for Fe-TiO_2 under "as-is" conditions. On the other hand, according to multi-size distribution, initial size difference between max and min diameter was attained as 3041.4 nm and detected to 840.7 nm upon period of 180 min.

For comparison purposes, it could be deduced that contrary to minor variations detected for hydrodynamic particle sizes of TiO_2 under "as-is" conditions, and in a similar manner to N-TiO_2 under "as-is" conditions, Fe-TiO_2 under "as-is" conditions also displayed dramatic changes according to time variations. Due to the fact that hydrodynamic particle sizes were attained as coinciding peaks according to the log normal distribution, max diameters were obtained particularly different as bimodal in multi-size distribution until 180 min.

As elucidated for TiO_2 under "as-is" conditions (Table 4.2) and N-TiO_2 under "as-is" conditions (Table 4.7), time dependent polydispersity of Fe-TiO_2 under "as-is" conditions were presented in Table 4.12. It could be stated that continuously decreasing trend was monitored over the period of 180 min. Simply an average value of 0.282 could be regarded as suitable for expressing polydispersity.

Table 4.12. Polydispersity of Fe-TiO_2 under "as-is" conditions.

Fe-TiO_2	Polydispersity						
	0	30	60	90	120	150	180
	0.381	0.303	0.250	0.271	0.275	0.226	0.268

As explained for TiO_2 under "as-is" conditions intensity profile (Figure 4.2), and N-TiO_2 under "as-is" conditions intensity profile (Figure 4.10), a similar approach was followed for Fe-TiO_2 under "as-is" conditions intensity profile. Time dependent comparative presentation of log Normal

distribution and multi-size distribution of Fe-TiO_2 under “as-is” conditions intensity profile was presented in Figure 4.18.

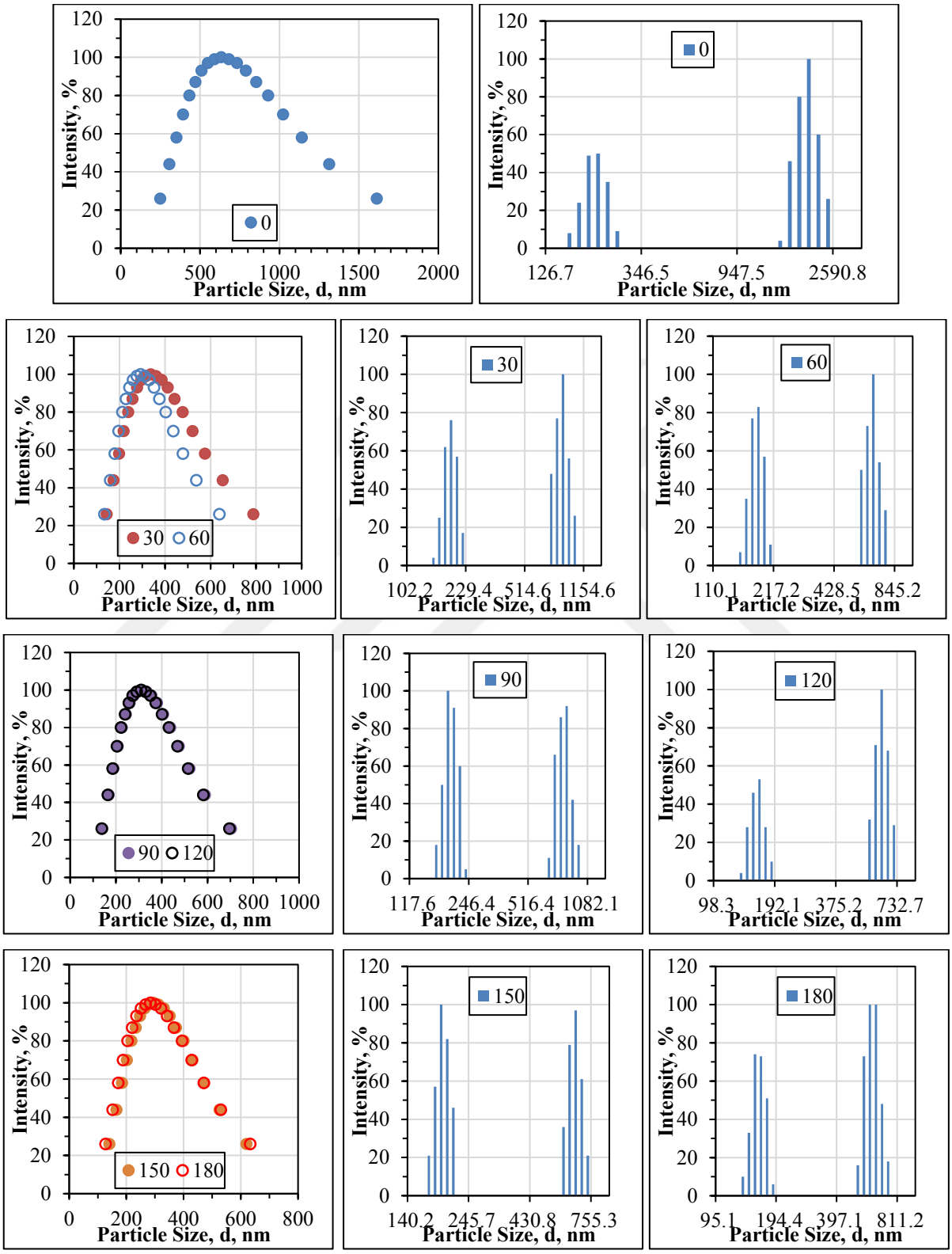


Figure 4.18. Fe-TiO_2 under “as-is” conditions intensity profile: Time dependent comparative presentation of log Normal distribution and multi-size distribution of Fe-TiO_2 under “as-is” conditions particle size.

4.1.1.10. Fe-TiO_2 under as-is" conditions volume profile. Time dependent logN distribution G(d) and multi size distribution C(d), mean diameter, range and min-max diameter difference with respect to log normal and multi-size distribution of Fe-TiO_2 under "as-is" conditions volume profile was exhibited in Figure 4.19 and Table 4.13, respectively.

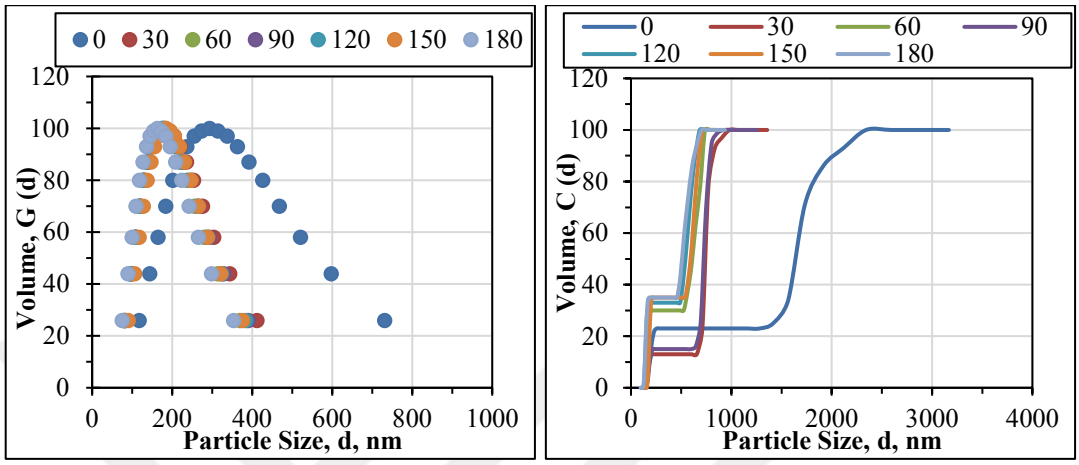


Figure 4.19. Fe-TiO_2 under "as-is" conditions volume profile: Time dependent logN distribution G(d) and multi size distribution C(d).

Table 4.13. Fe-TiO_2 under "as-is" conditions volume profile: Time dependent mean diameter, range and min-max diameter difference with respect to log normal and multi-size distribution.

Fe-TiO_2	time, min						
	0	30	60	90	120	150	180
Log Normal distribution							
Mean, nm	293.4	181.5	175.0	179.1	175.5	184.7	163.2
Range	117.7-731.0	79.8-412.5	82.8-369.9	82.2-390.2	80.1-384.2	90.7-376.2	75.3-353.9
Difference	613.3	332.7	287.1	308.0	304.1	285.5	278.6
Multi-size distribution							
Max 1, nm	189.5	166.0	165.5	183.3	147.0	185.6	146.1
Max 2, nm	1732.5	180.0	737.8	747.5	157.1	638.2	528.4
Max 3, nm	-	770.8	-	-	599.4	-	-
Range	126.7-3168.1	102.2-1357.1	110.1-968.2	117.6-1254.6	98.3-837.7	140.2-845.0	95.1-935.8
Difference	3041.4	1254.9	858.1	1137.0	739.4	704.8	840.7

Considering log normal distribution, hydrodynamic particle size revealed a sharp decrease in the first 30 min. Accordingly, continuous decrease was attained upon 180 min. Size difference decreased from 613.3 nm to 278.6 nm. For comparison purposes, two peaks were observed and coinciding peaks that were observed in log normal distribution were seen as bimodal until 180 min. Also, size difference of multi-size distribution was in accordance with variations of hydrodynamic size. Time

dependent comparative presentation of log Normal distribution and multi-size distribution of Fe-TiO_2 under “as-is” conditions volume profile was given in Figure 4.20.

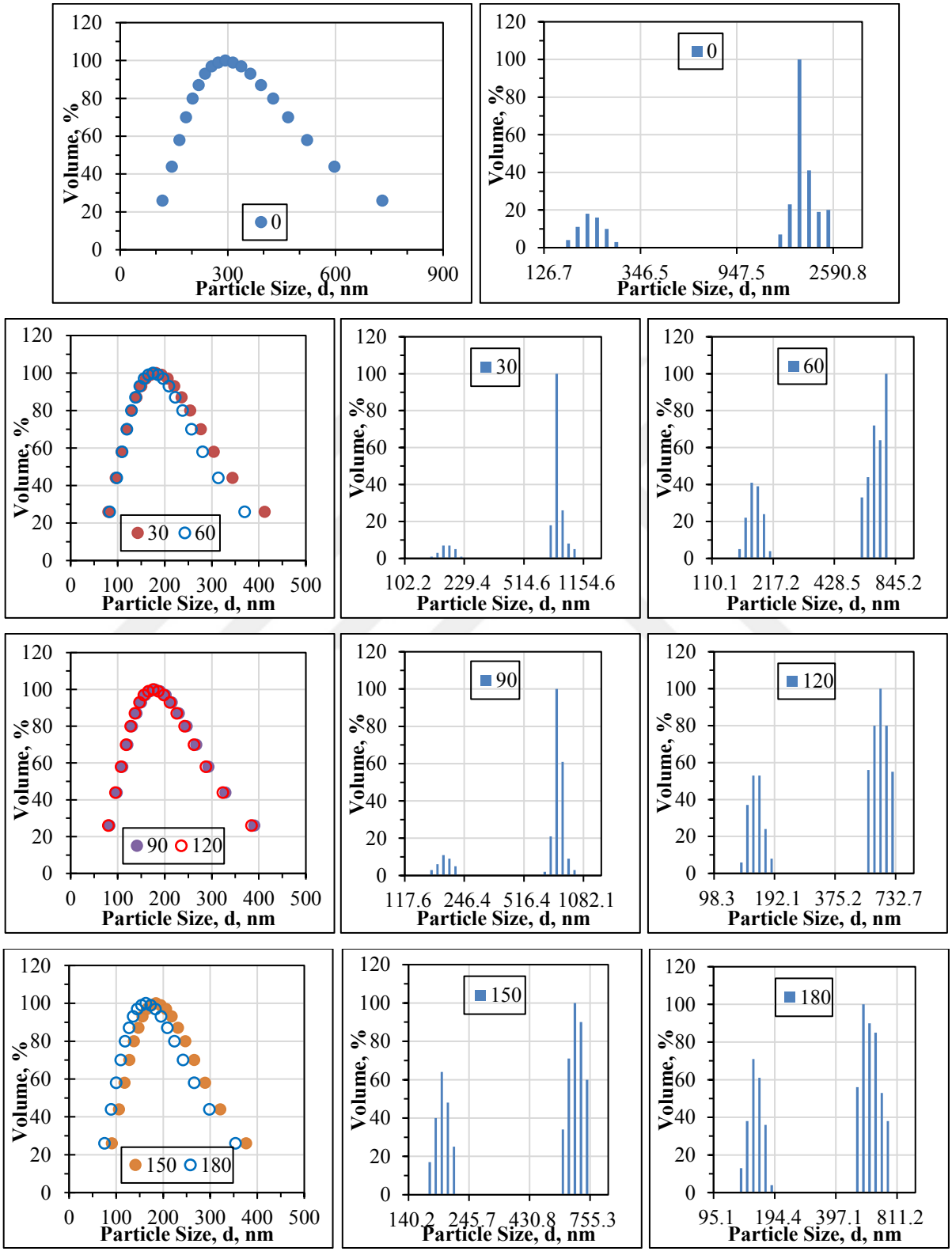


Figure 4.20. Fe-TiO_2 under “as-is” conditions volume profile: Time dependent comparative presentation of log Normal distribution and multi-size distribution of Fe-TiO_2 under “as-is” conditions particle size.

4.1.1.11. Fe-TiO_2 under as-is" conditions surface area profile. Time dependent logN distribution G(d) and multi size distribution C(d), mean diameter, range and min-max diameter difference with respect to log normal and multi-size distribution of Fe-TiO_2 under "as-is" conditions surface area profile was demonstrated in Figure 4.21 and Table 4.14, respectively.

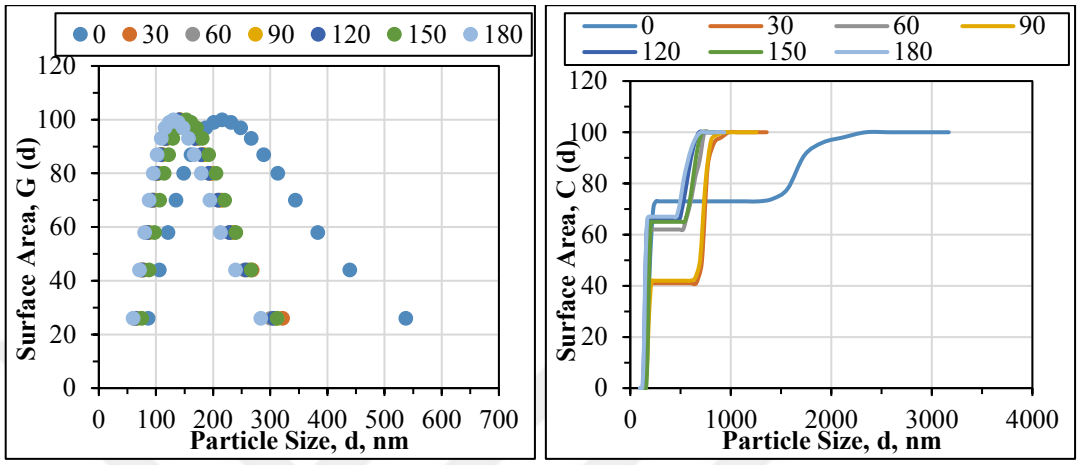


Figure 4.21. Fe-TiO_2 under "as-is" conditions surface area profile: Time dependent logN distribution G(d) and multi size distribution C(d).

Table 4.14. Fe-TiO_2 under "as-is" conditions surface area profile: Time dependent mean diameter, range and min-max diameter difference with respect to log normal and multi-size distribution.

Fe-TiO_2	time, min						
	0	30	60	90	120	150	180
Log Normal distribution							
Mean, nm	215.6	141.5	142.2	143.1	139.9	153.2	130.8
Range	86.5-537.2	62.2-321.5	67.3-300.7	65.7-311.9	63.9-306.2	75.2-312.0	60.3-283.6
Difference	450.7	259.3	233.4	246.2	242.3	236.8	223.3
Multi-size distribution							
Max 1, nm	189.5	166.0	165.5	183.3	147.0	185.6	146.1
Max 2, nm	1732.5	770.8	644.1	747.5	599.4	638.2	528.4
Max 3, nm	-	-	737.8	-	-	-	-
Range	126.7-3168.1	102.2-1357.1	110.1-968.2	117.6-1254.6	98.3-837.7	140.2-845.0	95.1-935.8
Difference	3041.4	1254.9	858.1	1137.0	739.4	704.8	840.7

Hydrodynamic particle size of Fe-TiO_2 under "as-is" conditions revealed almost % 50 difference with respect to time. It could be inferred that hydrodynamic size was initially 215.6 nm and detected to 130.8 nm upon 180 min. From a general perspective, calculated size difference was in accordance with variations recorded in hydrodynamic size. However, max diameters could be easily seen in multi-size distribution and it could be inferred that two peaks were observed along 180 min. Size

difference revealed a sharp decrease and dropped from 3041.4 nm to 840.7 nm upon 180 min (Figure 4.22).

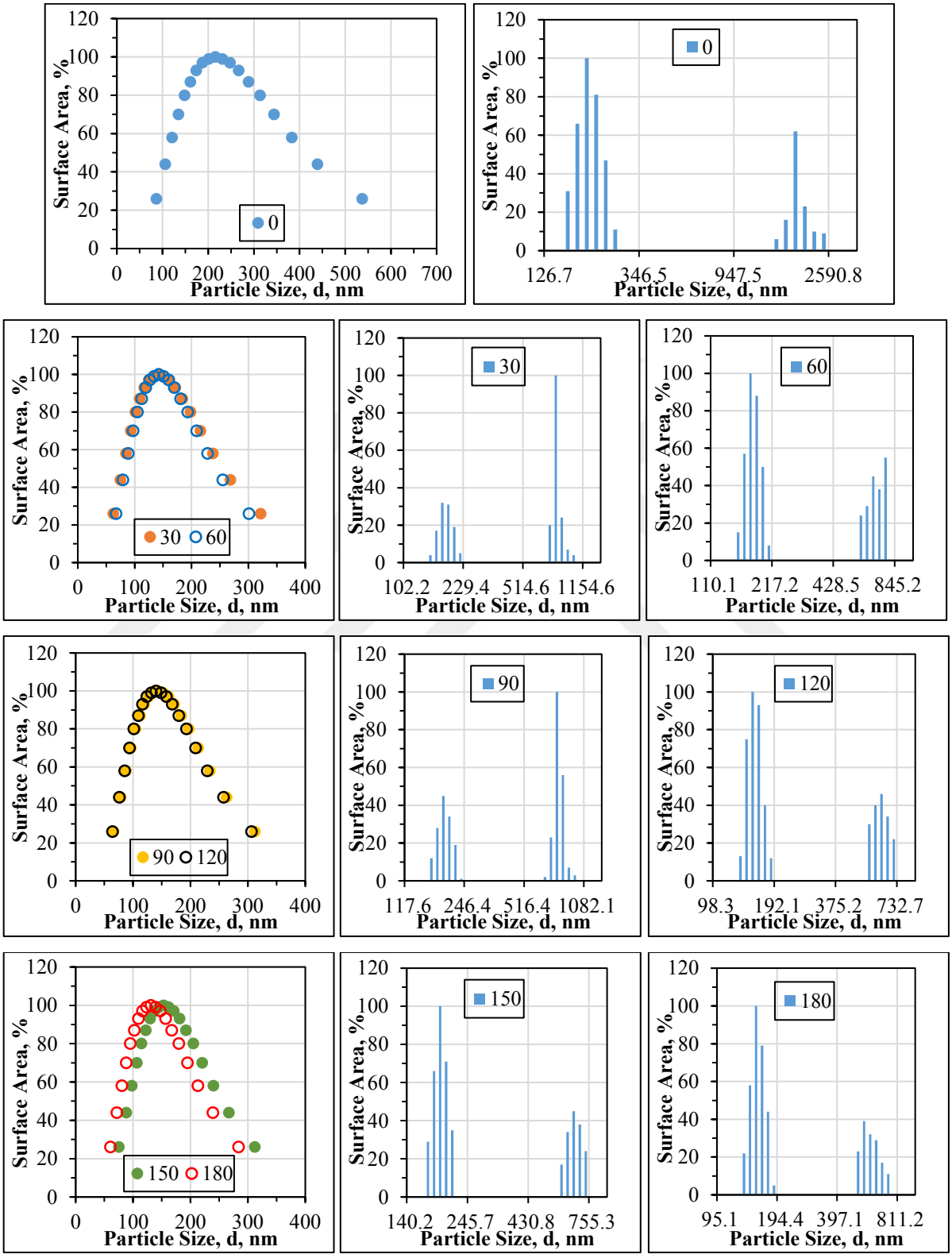


Figure 4.22. Fe-TiO_2 under "as-is" conditions surface area profile: Time dependent comparative presentation of log Normal distribution and multi-size distribution of Fe-TiO_2 under "as-is" conditions particle size.

4.1.1.12. Fe-TiO_2 under "as-is" conditions number profile. Time dependent logN distribution G(d) and multi size distribution C(d) of Fe-TiO_2 under "as-is" conditions number profile was given in Figure 4.23. Time dependent mean diameter, range and min-max diameter difference with respect to log normal and multi-size distribution of Fe-TiO_2 under "as-is" conditions number profile was given in Table 4.15.

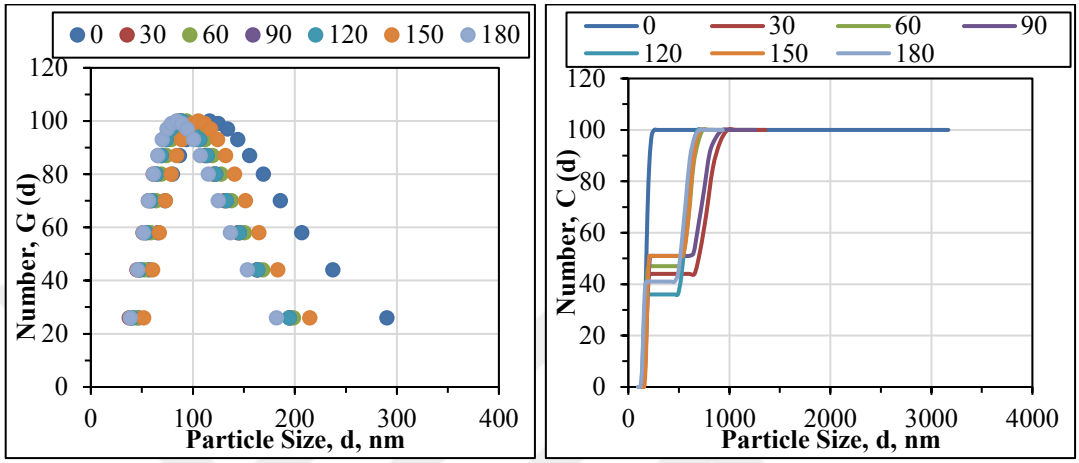


Figure 4.23. Fe-TiO_2 under "as-is" conditions number profile: Time dependent logN distribution G(d) and multi size distribution C(d).

Table 4.15. Fe-TiO_2 under "as-is" conditions number profile: Time dependent mean diameter, range and min-max diameter difference with respect to log normal and multi-size distribution.

Fe-TiO_2	time, min						
	0	30	60	90	120	150	180
Log Normal distribution							
Mean, nm	116.5	86.0	94.0	91.4	88.8	105.4	84.0
Range	46.7-290.2	37.8-195.4	44.5-198.7	42.0-199.2	40.6-194.5	51.7-214.6	38.7-182.1
Difference	243.5	157.6	154.2	157.2	153.9	162.9	143.4
Multi-size distribution							
Max 1, nm	189.5	180.0	177.2	183.3	157.1	185.6	146.1
Max 2, nm	1732.5	835.7	644.1	804.9	599.4	638.2	567.5
Max 3, nm	-	-	-	-	-	-	609.6
Range	126.7-3168.1	102.2-1357.1	110.1-968.2	117.6-1254.6	98.3-837.7	140.2-845.0	95.1-935.8
Difference	3041.4	1254.9	858.1	1137.0	739.4	704.8	840.7

In terms of number profile, hydrodynamic particle size of Fe-TiO_2 under "as-is" conditions did not display significant variations with respect to time. However, rapid increase was observed between 30 and 60 min, also 120 and 150 min. The reason could be attributed to possible aggregation behavior of nanoparticles. Size difference decreased from 243.5 nm to 143.4 nm. Also, in terms of multi-size distribution, two peaks were observed upon 180 min (Figure 4.24). Time dependent comparative

presentation of log Normal distribution and multi-size distribution of Fe-TiO_2 under "as-is" conditions number profile was demonstrated in Figure 4.24.

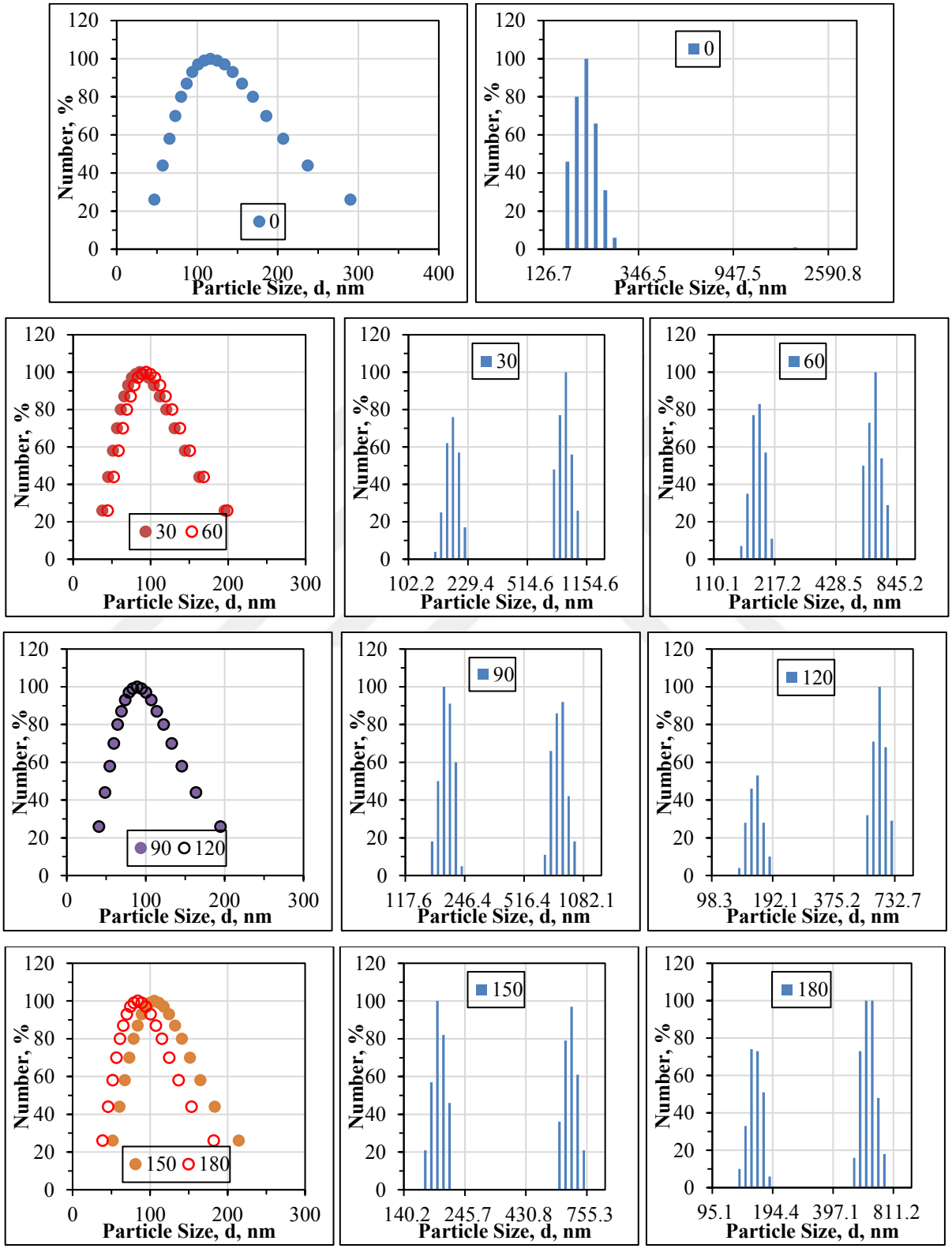


Figure 4.24. Fe-TiO_2 under "as-is" conditions number profile: Time dependent comparative presentation of log Normal distribution and multi-size distribution of Fe-TiO_2 under "as-is" conditions particle size.

4.1.2. Mono System: As-is Under Dark Conditions

As explained for mono system under "as-is" conditions, a similar approach was followed for elucidation of the hydrodynamic particle size of the nanoparticles "as-is under dark" conditions.

4.1.2.1. TiO_2 "as-is" under dark conditions intensity profile. Time dependent logN distribution G(d) and multi size distribution C(d) of TiO_2 "as-is under dark" conditions intensity profile was presented in Figure 4.25. Time dependent mean diameter, range and min-max diameter difference with respect to log normal and multi-size distribution of TiO_2 "as-is" under dark conditions intensity profile and polydispersity were demonstrated in Table 4.16 and Table 4.17., respectively.

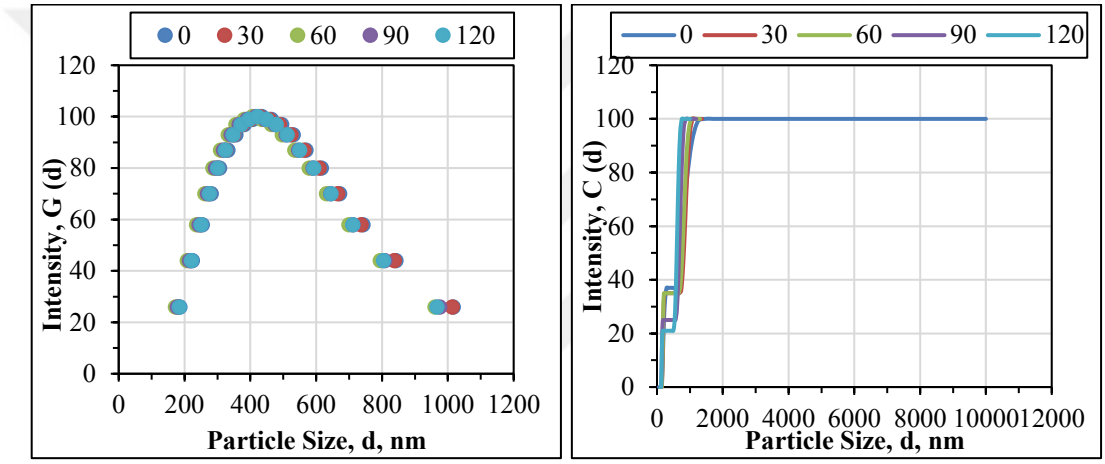


Figure 4.25. TiO_2 "as-is" under dark conditions intensity profile: Time dependent logN distribution G(d) and multi size distribution C(d).

Table 4.16. TiO_2 "as-is" under dark conditions intensity profile: Time dependent mean diameter, range and min-max diameter difference with respect to log normal and multi-size distribution.

TiO_2	time, min				
	0	30	60	90	120
Log Normal distribution					
Mean, nm	434.2	427.4	406.7	416.5	421.5
Range	185.5-1016.4	180.2-1013.5	172.2-960.7	177.8-975.3	183.8-966.2
Difference	830.9	833.3	788.5	797.5	782.4
Multi-size distribution					
Max 1, nm	211.8	180.9	181.5	156.1	149.8
Max 2, nm	899.0	195.6	895.2	703.3	657.1
Max 3, nm	-	928.2	-	-	-
Range	58.6-10.000	113.4-1370.0	115.0-1309.0	107.1-1191.2	105.4-1002.5
Difference	9941.4	1256.6	1194.0	1084.1	897.1

In terms of intensity distribution, the hydrodynamic size of TiO_2 "as-is" under dark conditions did not display significant variations, initial conditions was attained as 434.2 nm and dropped to 421.5 nm along 120 min. Considering multi-size distribution, two max diameters were attained upon 120 min. Time dependent comparative presentation of log Normal distribution and multi-size distribution of TiO_2 "as-is" under dark conditions intensity profile was presented in Figure 4.26.

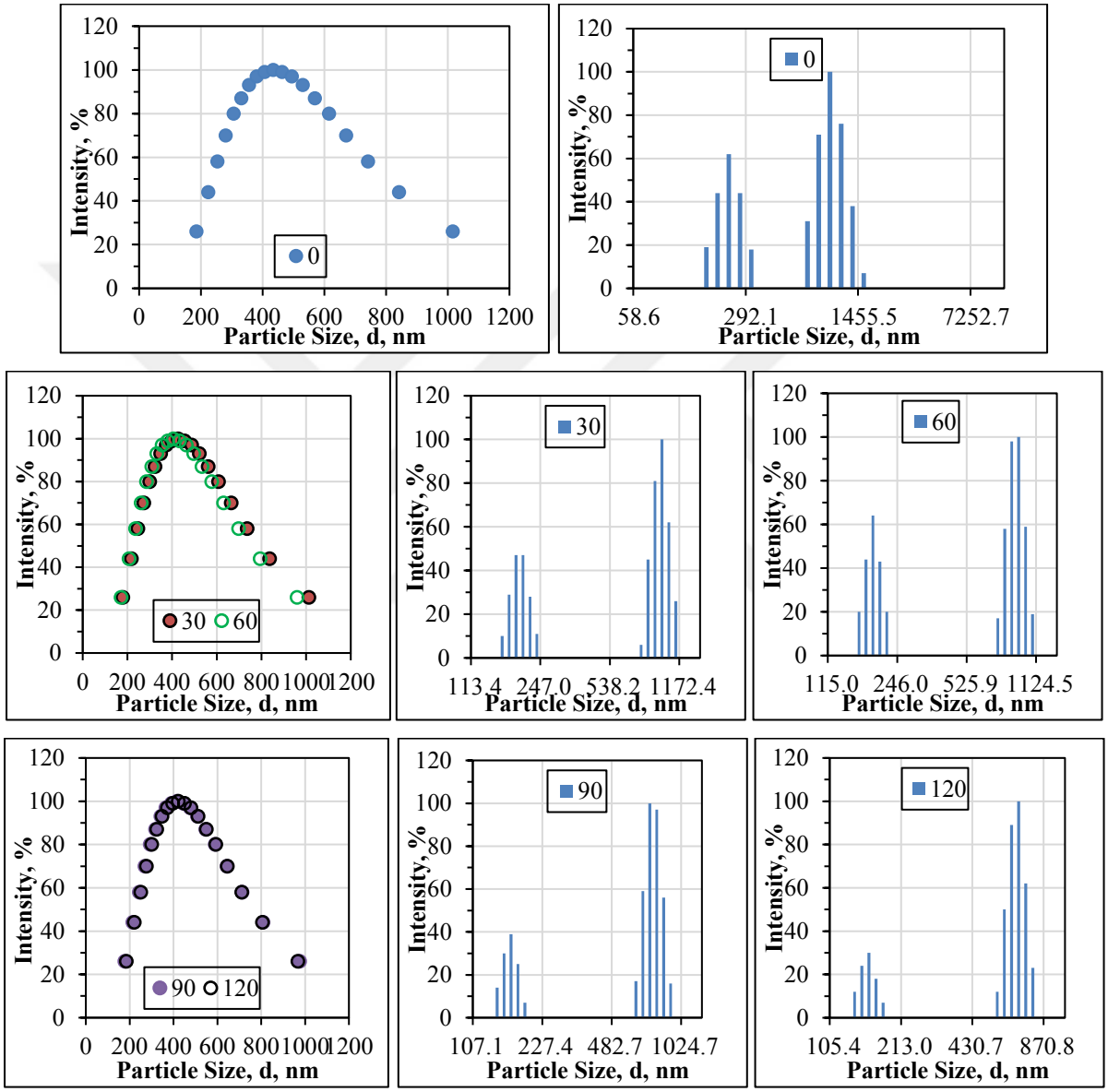


Figure 4.26. TiO_2 "as-is" under dark conditions intensity profile: Time dependent comparative presentation of log Normal distribution and multi-size distribution of TiO_2 "as-is" under dark conditions particle size.

Table 4.17. Polydispersity of TiO_2 "as-is" under dark conditions.

TiO_2	Polydispersity				
	0	30	60	90	120
	0.306	0.317	0.314	0.307	0.290

4.1.2.2. TiO_2 "as-is" under dark conditions volume profile. Time dependent logN distribution G(d) and multi size distribution C(d) of TiO_2 "as-is" under dark conditions volume profile was exhibited in Figure 4.27. Time dependent mean diameter, range and min-max diameter difference with respect to log normal and multi-size distribution of TiO_2 "as-is" under dark conditions volume profile was presented in Table 4.18.

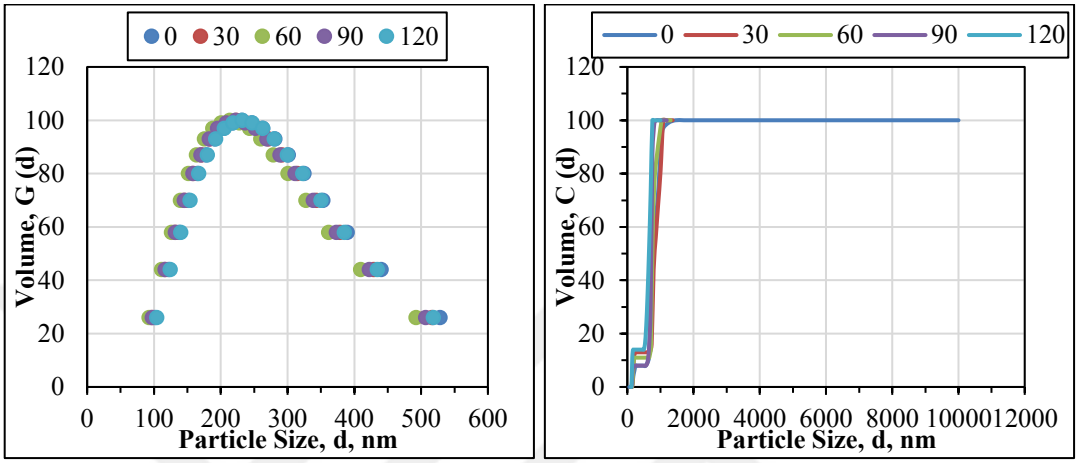


Figure 4.27. TiO_2 "as-is" under dark conditions volume profile: Time dependent logN distribution G(d) and multi size distribution C(d).

Table 4.18. TiO_2 "as-is" under dark conditions volume profile: Time dependent mean diameter, range and min-max diameter difference with respect to log normal and multi-size distribution.

TiO_2	time, min				
	0	30	60	90	120
Log Normal distribution					
Mean, nm	231.4	222.9	213.5	221.7	232.0
Range	101.3-528.2	96.3-516.0	92.6-492.2	97.1-506.5	103.9-518.3
Difference	426.9	419.7	399.6	409.4	414.4
Multi-size distribution					
Max 1, nm	211.8	180.9	181.5	144.8	149.8
Max 2, nm	765.6	794.4	769.0	156.1	756.5
Max 3, nm	1055.6	1084.6	-	758.3	-
Range	58.6-10.000	113.4-1370.0	115.0-1309.0	107.1-1191.2	105.4-1002.5
Difference	9941.4	1256.6	1194.0	1084.1	897.1

Considering log normal distribution, initial hydrodynamic size of TiO_2 "as-is" under dark conditions was monitored as 231.4 nm. Along 120 min, the hydrodynamic size of TiO_2 did not show a big alteration and detected to 232.0 nm. It could also be deduced that hydrodynamic size difference dropped from 426.9 nm to 414.4 nm with respect to time. For comparison purposes, in terms of multi-size distribution it could also be inferred that three peaks were observed as 211.8 nm, 765.6

nm, and 1055.6 nm for TiO_2 "as-is" under dark conditions following initial period of time. Upon 120 min, two max diameters were obtained as 149.8 nm and 756.5 nm. Also, the hydrodynamic size differences were attained in between 9941.4 nm and 897.1 nm with respect to time. Due to the fact that hydrodynamic particle sizes were detected as coinciding peaks according to the log normal distribution, peaks were observed distinctly different as bimodal in multi-size distribution until 120 min.

Time dependent comparative presentation of log Normal distribution and multi-size distribution of TiO_2 "as-is" under dark conditions volume profile was demonstrated in Figure 4.28.

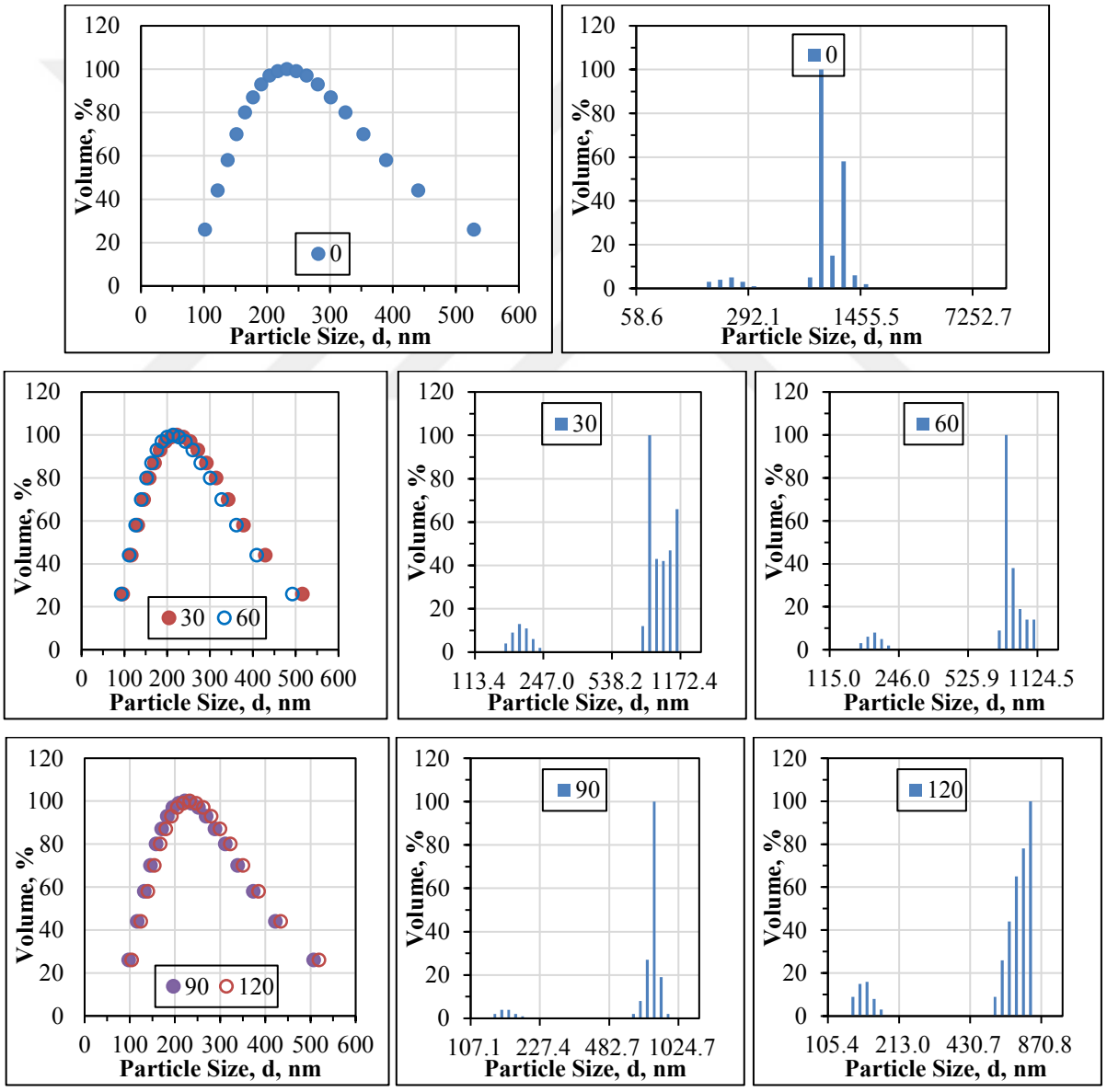


Figure 4.28. TiO_2 "as-is" under dark conditions volume profile: Time dependent comparative presentation of log Normal distribution and multi-size distribution of TiO_2 "as-is" under dark conditions particle size.

4.1.2.3. TiO_2 "as-is" under dark conditions surface area profile. As explained for TiO_2 "as-is" under dark conditions volume profile (Figure 4.27), a similar approach was followed for "TiO_2 as-is under dark conditions" surface area profile. Time dependent logN distribution G(d) and multi size distribution C(d) of TiO_2 "as-is" under dark conditions surface area profile was displayed in Figure 4.29.

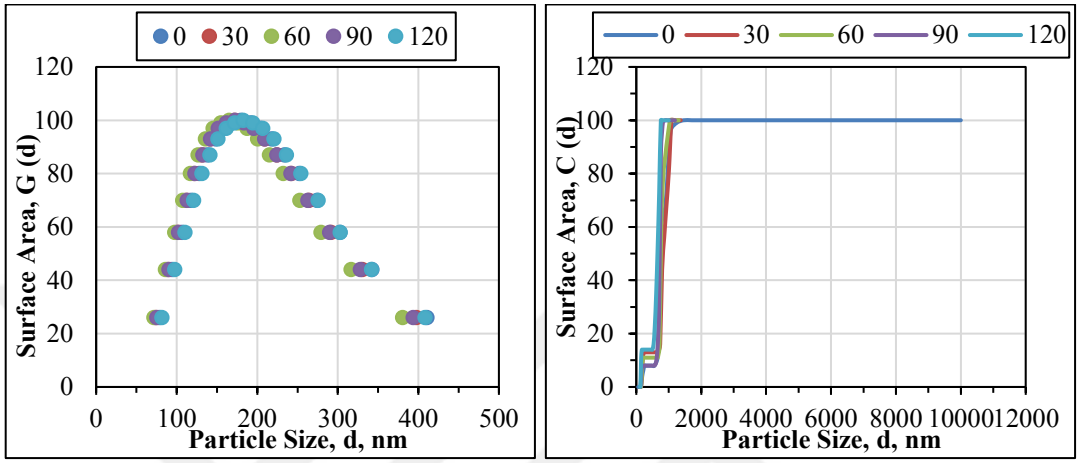


Figure 4.29. TiO_2 "as-is" under dark conditions surface area profile: Time dependent logN distribution G(d) and multi size distribution C(d).

Also, as explained for TiO_2 "as-is" under dark conditions volume profile (Table 4.18), following a similar trend, time dependent mean diameter, range and min-max diameter difference with respect to log normal and multi-size distribution of TiO_2 "as-is" under dark conditions surface area profile was exhibited in Table 4.19.

Table 4.19. TiO_2 "as-is" under dark conditions surface area profile: Time dependent mean diameter, range and min-max diameter difference with respect to log normal and multi-size distribution.

TiO_2	time, min				
	0	30	60	90	120
Log Normal distribution					
Mean, nm	179.9	171.8	165.0	172.3	182.8
Range	78.8-410.6	74.2-397.8	71.6-380.4	75.4-393.6	81.8-408.3
Difference	331.8	323.6	308.8	318.2	326.5
Multi-size distribution					
Max 1, nm	211.8	180.9	181.5	144.8	149.8
Max 2, nm	765.6	794.4	769.0	156.1	756.5
Max 3, nm	1055.6	1084.6	-	758.3	-
Range	58.6-10.000	113.4-1370.0	115.0-1309.0	107.1-1191.2	105.4-1002.5
Difference	9941.4	1256.6	1194.0	1084.1	897.1

Under the specified “as-is under dark” conditions represented by surface area profile; it could be deduced that continuous decrease in hydrodynamic particle size was monitored until 90 min. However, upon 90 and 120 min, a minor difference was observed in hydrodynamic particle size. The reason could be attributed to the aggregation of particles. For comparison purposes, initially three bimodal peaks were monitored as 211.8 nm, 765.6 nm and 1055.6 nm. Upon 120 min, two max diameters were observed as 149.8 nm and 756.5 nm.

Time dependent comparative presentation of log Normal distribution and multi-size distribution of TiO_2 “as-is” under dark conditions surface area profile was exhibited in Figure 4.30.

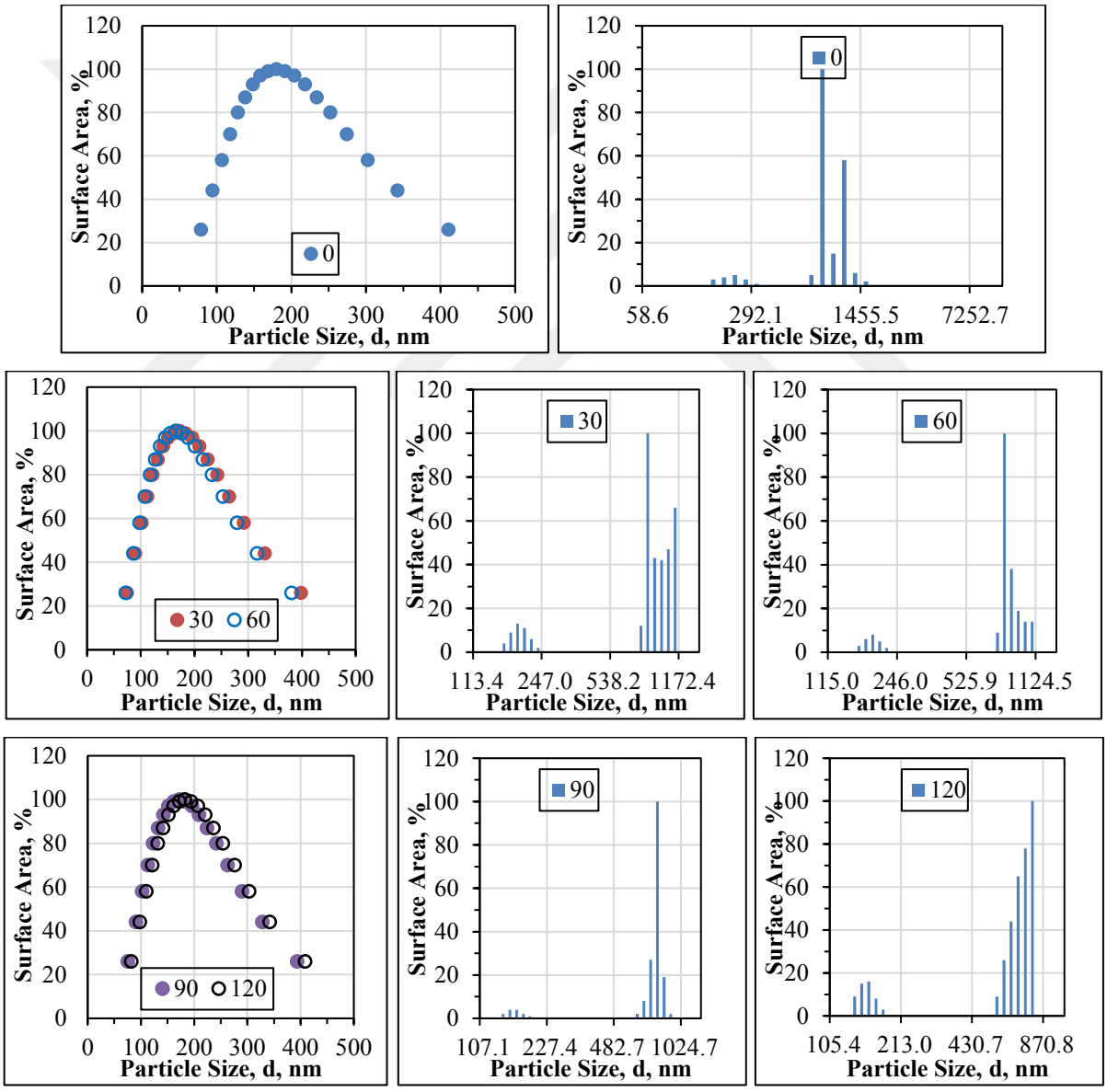


Figure 4.30. TiO_2 “as-is” under dark conditions surface area profile: Time dependent comparative presentation of log Normal distribution and multi-size distribution of TiO_2 “as-is” under dark conditions particle size.

4.1.2.4. TiO_2 "as-is" under dark conditions number profile. Time dependent logN distribution G(d) and multi size distribution C(d) of TiO_2 "as-is" under dark conditions number profile was given in Figure 4.31. Also, time dependent mean diameter, range and min-max diameter difference with respect to log normal and multi-size distribution of TiO_2 "as-is" under dark conditions number profile was displayed in Table 4.20.

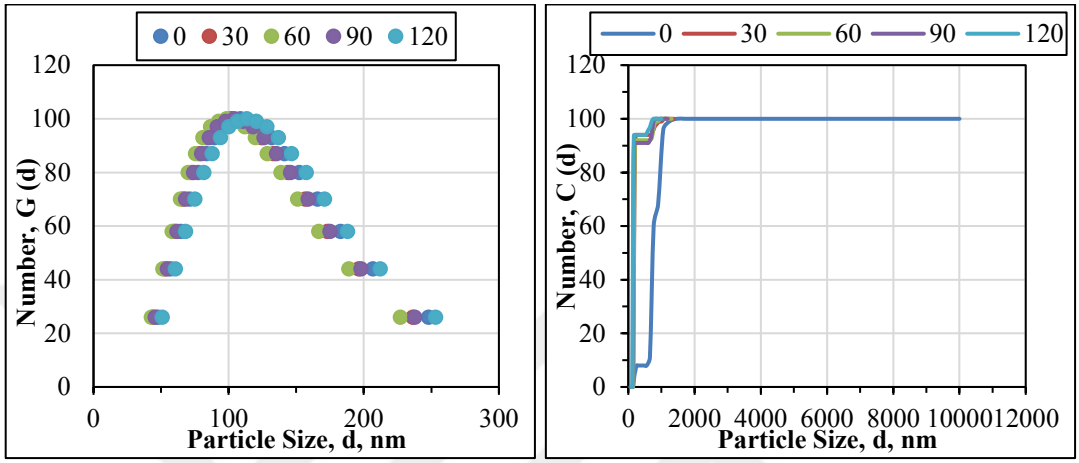


Figure 4.31. TiO_2 "as-is" under dark conditions number profile: Time dependent logN distribution G(d) and multi size distribution C(d).

Table 4.20. TiO_2 "as-is" under dark conditions number profile: Time dependent mean diameter, range and min-max diameter difference with respect to log normal and multi-size distribution.

TiO_2	time, min				
	0	30	60	90	120
Log Normal distribution					
Mean, nm	108.7	102.1	98.6	104.1	113.4
Range	47.6-248.1	44.1-236.3	42.8-227.2	45.6-237.7	50.8-253.3
Difference	200.5	192.2	184.4	192.1	202.5
Multi-size distribution					
Max 1, nm	211.8	180.9	181.5	144.8	139.6
Max 2, nm	765.6	794.4	769.0	758.3	612.4
Max 3, nm	1055.6	-	-	-	657.1
Max 4, nm	-	-	-	-	705.0
Max 5, nm	-	-	-	-	756.5
Range	58.6-10.000	113.4-1370.0	115.0-1309.0	107.1-1191.2	105.4-1002.5
Difference	9941.4	1256.6	1194.0	1084.1	897.1

In terms of number profile, it could be deduced that hydrodynamic particle size of TiO_2 "as-is" under dark conditions revealed a slightly decreasing trend until 90 min. Upon 90 min and 120 min, due to possible aggregation of nanoparticles, increase in hydrodynamic size was monitored. This

variation was supported by hydrodynamic size differences. Accordingly, initial hydrodynamic size difference decreased from 200.5 nm to 184.4 nm, and increased to 202.5 nm upon 120 min. For comparison purposes, although hydrodynamic particle sizes were detected as coinciding peaks according to the log normal distribution, peaks were observed particularly different as bimodal in multi-size distribution until 120 min. Initially, three peaks were observed as 211.8 nm, 765.6 nm, 1055.6 nm, two peaks were monitored upon 30 min, 60 min and 90 min. However, upon 120 min, five peaks were monitored as 139.6 nm, 612.4 nm, 657.1 nm, 705.0 nm, 756.5 nm. Time dependent comparative presentation of log Normal distribution and multi-size distribution of TiO_2 "as-is" under dark conditions number profile was exhibited in Figure 4.32.

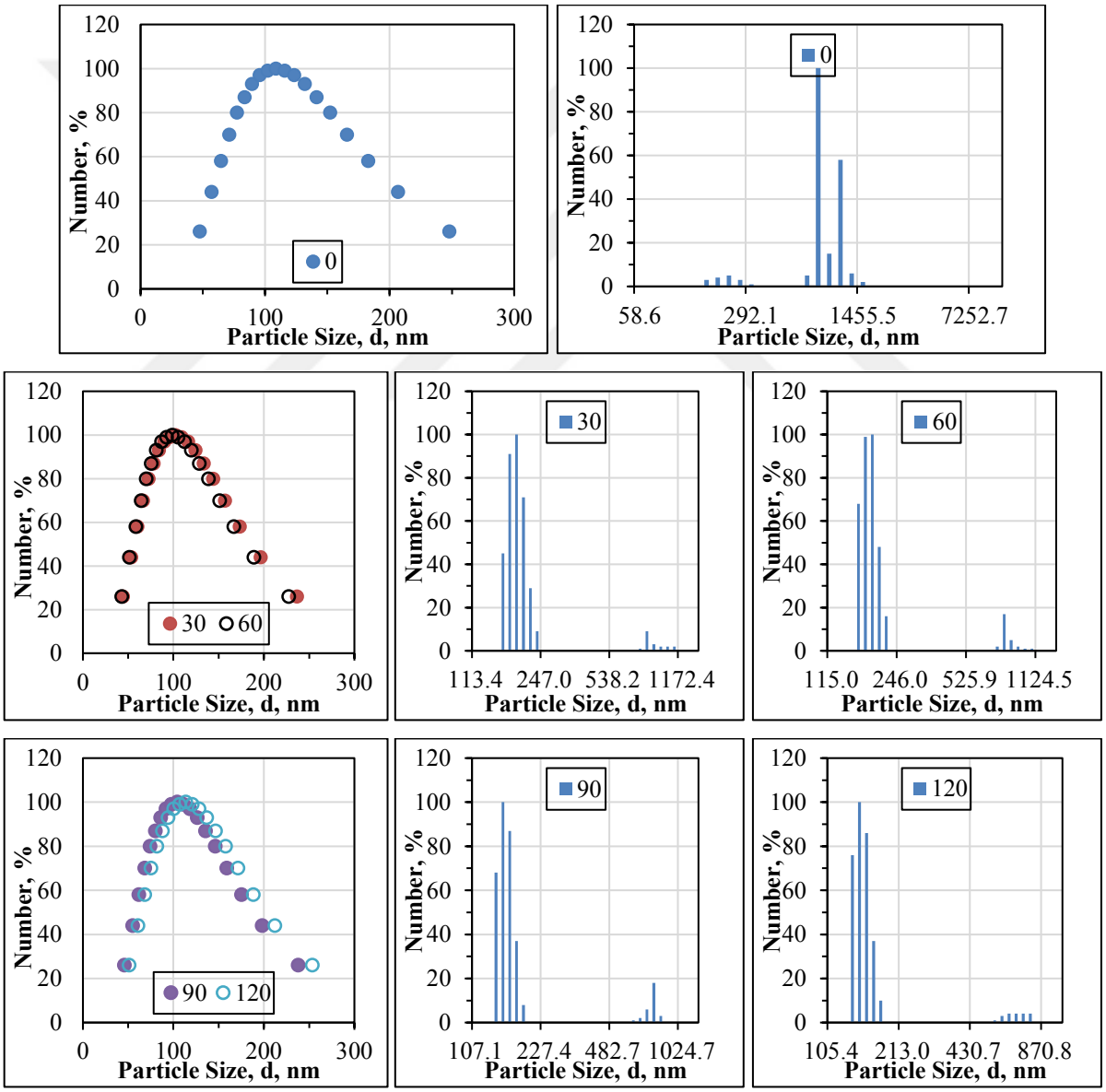


Figure 4.32. TiO_2 "as-is" under dark conditions number profile: Time dependent comparative presentation of log Normal distribution and multi-size distribution of TiO_2 "as-is" under dark conditions particle size.

4.1.2.5. N-TiO_2 "as-is" under dark conditions intensity profile. Time dependent logN distribution G(d) and multi size distribution C(d) of N-TiO_2 "as-is" under dark conditions intensity profile was presented in Figure 4.33. Time dependent mean diameter, range and min-max diameter difference with respect to log normal and multi-size distribution of N-TiO_2 "as-is" under dark conditions intensity profile was displayed in Table 4.21.

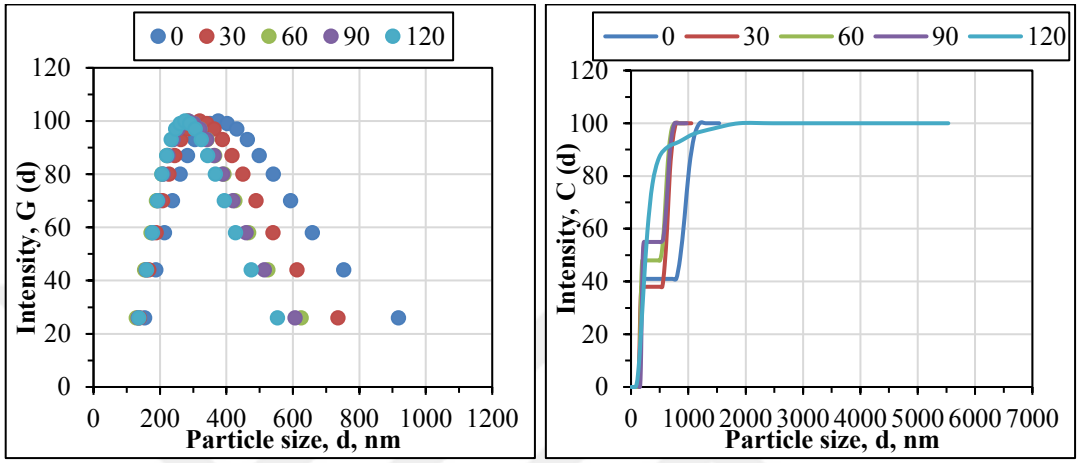


Figure 4.33. N-TiO_2 "as-is" under dark conditions intensity profile: Time dependent logN distribution G(d) and multi size distribution C(d).

Table 4.21. N-TiO_2 "as-is" under dark conditions intensity profile: Time dependent mean diameter, range and min-max diameter difference with respect to log normal and multi-size distribution.

N-TiO_2	time, min				
	0	30	60	90	120
Log Normal distribution					
Mean, nm	375.7	319.4	284.2	285.7	275.1
Range	153.8-917.5	138.7-735.8	129.2-625.1	134.4-607.1	136.6-554.1
Difference	763.7	597.1	495.9	472.7	417.5
Multi-size distribution					
Max 1, nm	175.4	157.4	171.3	187.4	286.0
Max 2, nm	1013.4	679.1	621.1	673.0	1099.5
Range	106.3-1538.7	101.5-1053.1	106.6-932.9	138.3-969.7	1.0-5533.9
Difference	1432.4	951.6	826.3	831.4	5532.9

In terms of intensity profile, hydrodynamic particle size variations of N-TiO_2 "as-is" under dark conditions demonstrated a rapid decrease upon period of 120 min. Initial hydrodynamic size was recorded as 375.7 nm and decreased to 275.1 nm with respect to 120 min. Hydrodynamic size altered almost 50 % and decreased from 763.7 nm to 417.5 nm. For comparison purposes, two peaks were monitored along 120 min according to multi-size distribution.

Time dependent comparative presentation of log Normal distribution and multi-size distribution of N-TiO_2 "as-is" under dark conditions intensity profile was presented in Figure 4.34. Also, time dependent polydispersity of N-TiO_2 under "as-is" conditions was exhibited in Table 4.22 and it could be inferred that a significant variation was observed with respect to time. Polydispersity of N-TiO_2 "as-is" under dark conditions was recorded between 0.343 and 0.199 upon 120 min.

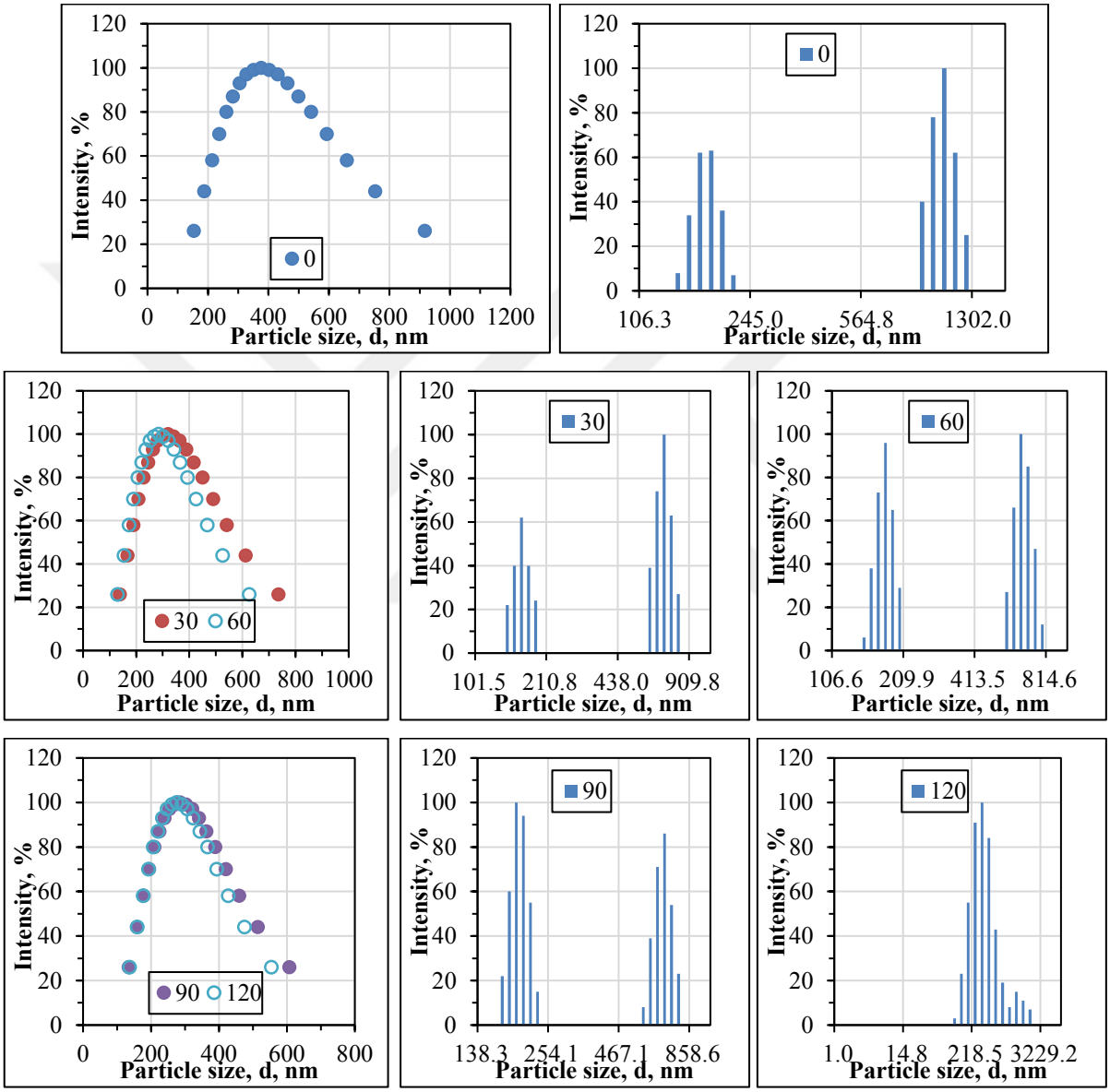


Figure 4.34. N-TiO_2 "as-is" under dark conditions intensity profile: Time dependent comparative presentation of log Normal distribution and multi-size distribution of N-TiO_2 "as-is" under dark conditions particle size.

Table 4.22. Polydispersity of N-TiO_2 "as-is" under dark conditions.

N-TiO_2	Polydispersity				
	0	30	60	90	120
	0.343	0.293	0.258	0.234	0.199

4.1.2.6. N-TiO_2 "as-is" under dark conditions volume profile. As explained for N-TiO_2 "as-is" under dark conditions intensity profile (Figure 4.33), a similar approach was followed for N-TiO_2 "as-is" under dark conditions volume profile. Time dependent logN distribution G(d) and multi size distribution C(d) of N-TiO_2 "as-is" under dark conditions volume profile was given in Figure 4.35. Time dependent mean diameter, range and min-max diameter difference with respect to log normal and multi-size distribution of N-TiO_2 "as-is" under dark conditions volume profile was exhibited in Table 4.23.

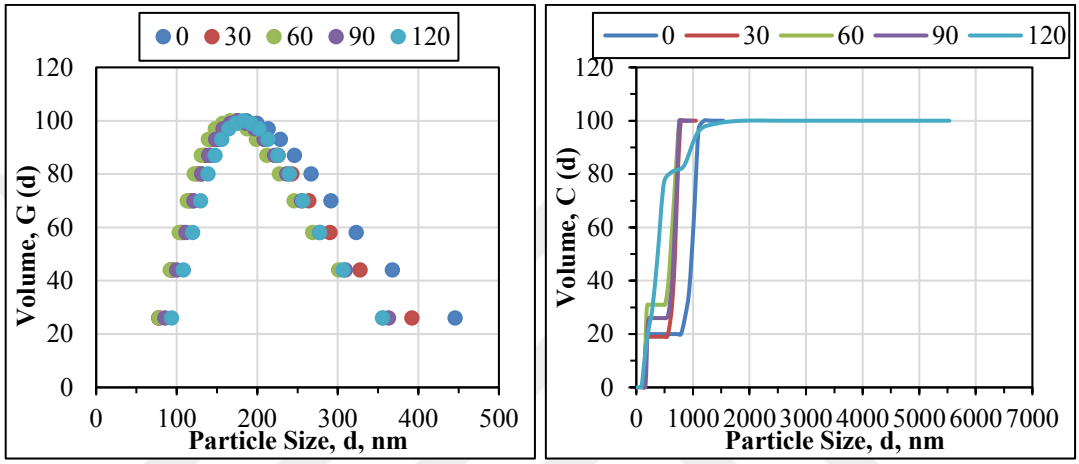


Figure 4.35. N-TiO_2 "as-is" under dark conditions volume profile: Time dependent logN distribution G(d) and multi size distribution C(d).

Table 4.23. N-TiO_2 "as-is" under dark conditions volume profile: Time dependent mean diameter, range and min-max diameter difference with respect to log normal and multi-size distribution.

N-TiO_2	time, min				
	0	30	60	90	120
Log Normal distribution					
Mean, nm	186.7	174.5	166.6	176.0	182.5
Range	78.2-445.6	77.7-391.9	77.9-356.3	85.4-363.1	93.7-355.4
Difference	367.4	314.2	278.4	277.7	261.7
Multi-size distribution					
Max 1, nm	161.3	157.4	171.3	187.4	490.1
Max 2, nm	1101.7	730.6	711.3	760.1	1099.5
Range	106.3-1538.7	101.5-1053.1	106.6-932.9	138.3-969.7	1.0-5533.9
Difference	1432.4	951.6	826.3	831.4	5532.9

In terms of volume profile, it could be deduced that no significant variation was monitored in hydrodynamic size along 120 min. Initial hydrodynamic size was recorded as 186.7 nm whereas a slight decrease was observed upon 120 min and detected to 182.5 nm. Size difference revealed drastic

changes, initially monitored as 367.4 nm and detected to 261.7 at the end of 120 min period. For comparison purposes, considering multi-size distribution, it could be inferred that two peaks were observed upon 120 min. Due to multi-size distribution, possible coinciding peaks that were attained by log normal distribution could be easily discriminated and seen from Figure 4.36.

As described for N-TiO_2 "as-is" under dark conditions intensity profile (Figure 4.34), a similar approach was followed for N-TiO_2 "as-is" under dark conditions volume profile. Time dependent comparative presentation of log Normal distribution and multi-size distribution of N-TiO_2 "as-is" under dark conditions volume profile was displayed in Figure 4.36.

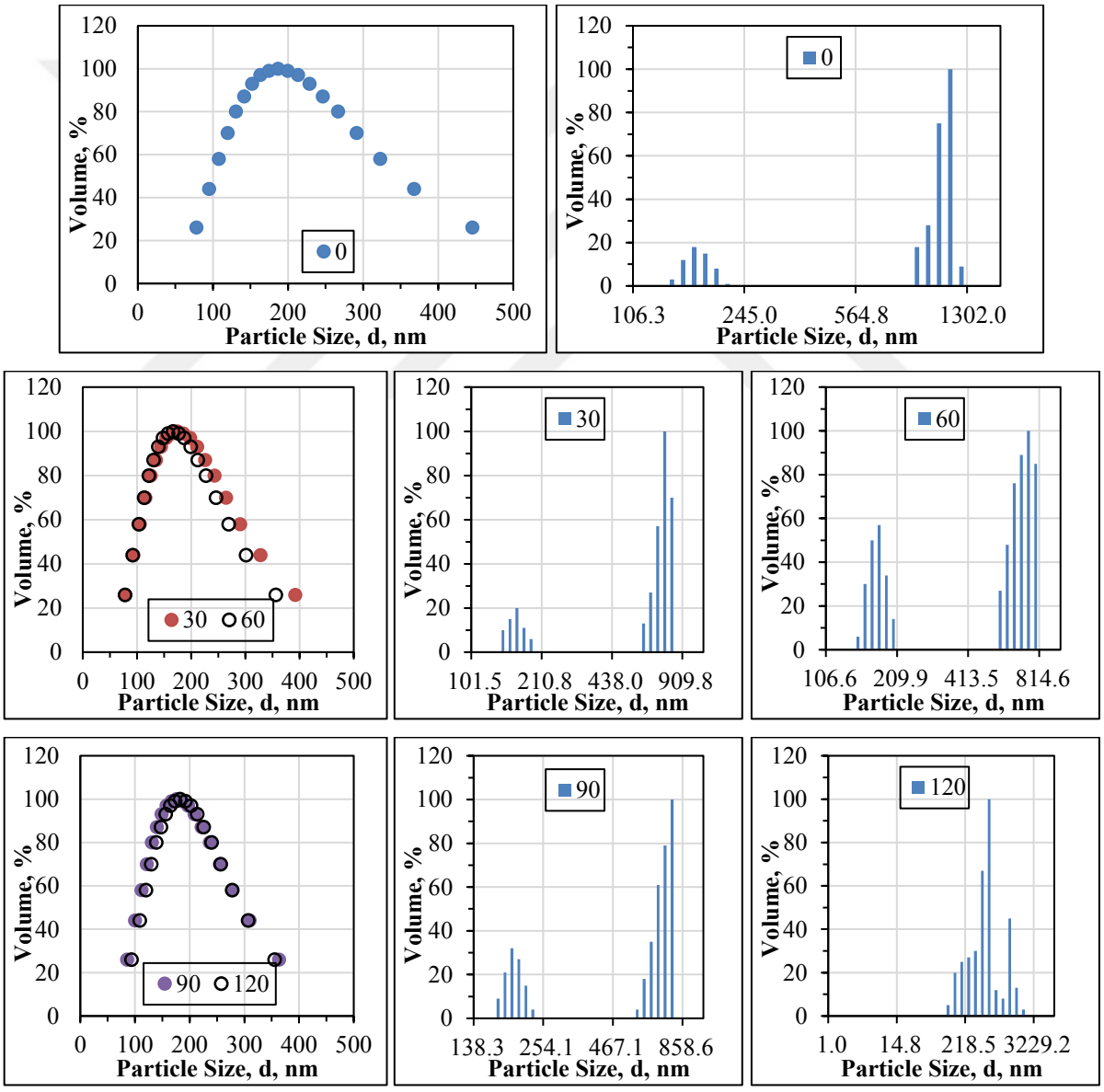


Figure 4.36. N-TiO_2 "as-is" under dark conditions volume profile: Time dependent comparative presentation of log Normal distribution and multi-size distribution of N-TiO_2 "as-is" under dark conditions particle size.

4.1.2.7. N-TiO_2 "as-is" under dark conditions surface area profile. As explained for N-TiO_2 "as-is" under dark conditions volume profile (Figure 4.35), a similar approach was followed for N-TiO_2 "as-is" under dark conditions surface area profile. Time dependent logN distribution G(d) and multi size distribution C(d) of N-TiO_2 "as-is" under dark conditions surface area profile was presented in Figure 4.37. Time dependent mean diameter, range and min-max diameter difference with respect to log normal and multi-size distribution of N-TiO_2 "as-is" under dark conditions surface area profile was demonstrated in Table 4.24.

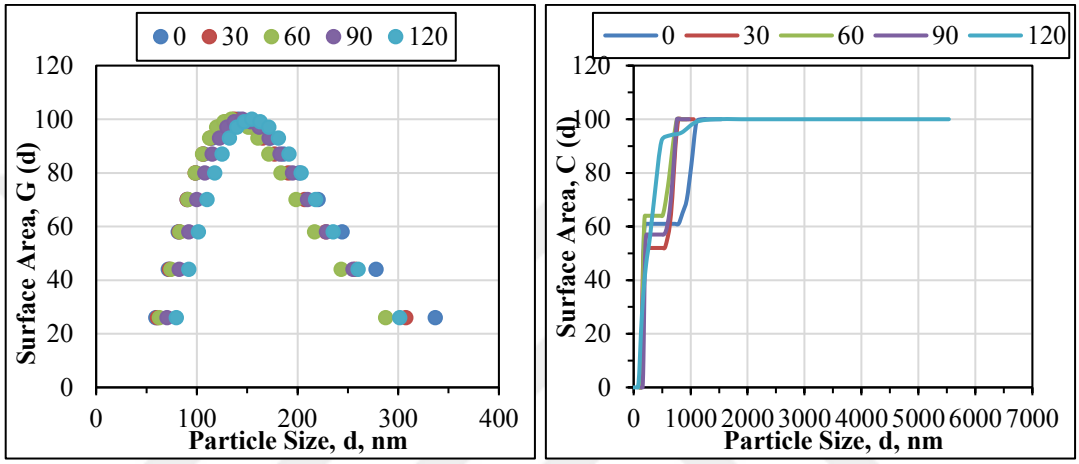


Figure 4.37. N-TiO_2 "as-is" under dark conditions surface area profile: Time dependent logN distribution G(d) and multi size distribution C(d).

Table 4.24. N-TiO_2 "as-is" under dark conditions surface area profile: Time dependent mean diameter, range and min-max diameter difference with respect to log normal and multi-size distribution.

N-TiO_2	time, min				
	0	30	60	90	120
Log Normal distribution					
Mean, nm	141.2	137.1	134.5	145.1	154.8
Range	59.2-336.9	61.0-307.7	62.9-287.7	70.3-299.2	79.5-301.6
Difference	277.7	246.7	224.8	228.9	222.1
Multi-size distribution					
Max 1, nm	161.3	157.4	171.3	187.4	127.5
Max 2, nm	1101.7	730.6	711.3	760.1	490.1
Max 3, nm	-	-	-	-	1099.5
Range	106.3-1538.7	101.5-1053.1	106.6-932.9	138.3-969.7	1.0-5533.9
Difference	1432.4	951.6	826.3	831.4	5532.9

In terms of surface area profile, it could be inferred that hydrodynamic particle size of N-TiO_2 "as-is" under dark conditions initially revealed as 141.2 nm and decreased until 90 min. Upon 90 and

120 min, a slight increase was observed, the reason could be ascribed to aggregation behavior of nanoparticles. Also, size difference did not demonstrate a significant variation with respect to time. Initial size difference was recorded as 277.7 nm and detected to 222.1 nm at the end of 120 min period. For comparison purposes, in terms of multi-size distribution, it could be deduced that two peaks were observed until 120 min. Upon 120 min, three max diameters were obtained.

Following a similar manner, time dependent comparative presentation of log Normal distribution and multi-size distribution of N-TiO_2 "as-is" under dark conditions surface area profile was displayed in Figure 4.38.

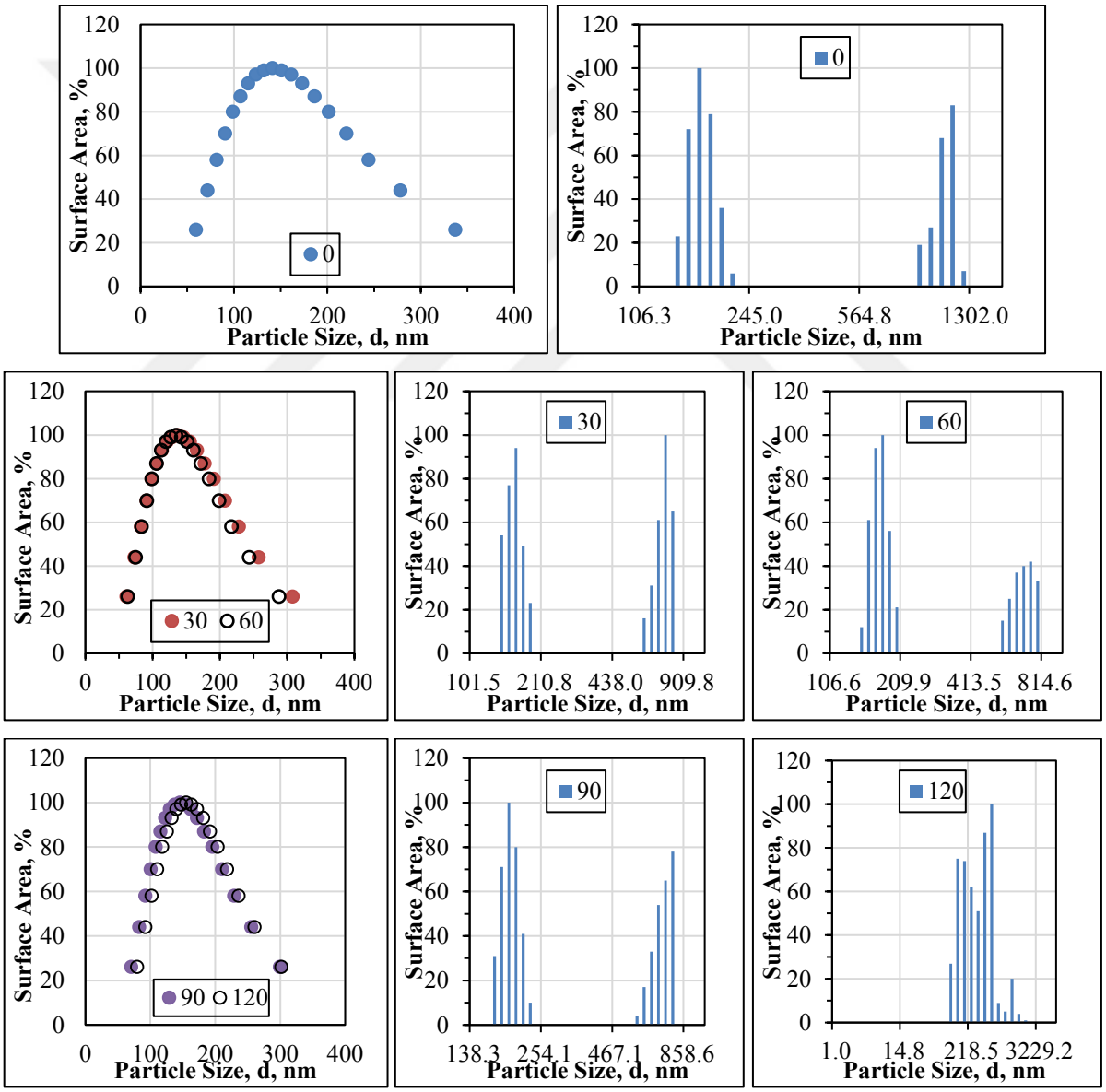


Figure 4.38. N-TiO_2 "as-is" under dark conditions surface area profile: Time dependent comparative presentation of log Normal distribution and multi-size distribution of N-TiO_2 "as-is" under dark conditions particle size.

4.1.2.8. N-TiO_2 "as-is" under dark conditions number profile. As elucidated for N-TiO_2 "as-is" under dark conditions surface area profile (Figure 4.37), a similar trend was followed for N-TiO_2 "as-is under dark" conditions number profile. Time dependent logN distribution G(d) and multi size distribution C(d) of N-TiO_2 "as-is" under dark conditions number profile was exhibited in Figure 4.39. Time dependent mean diameter, range and min-max diameter difference with respect to log normal and multi-size distribution of N-TiO_2 "as-is" under dark conditions number profile was presented in Table 4.25.

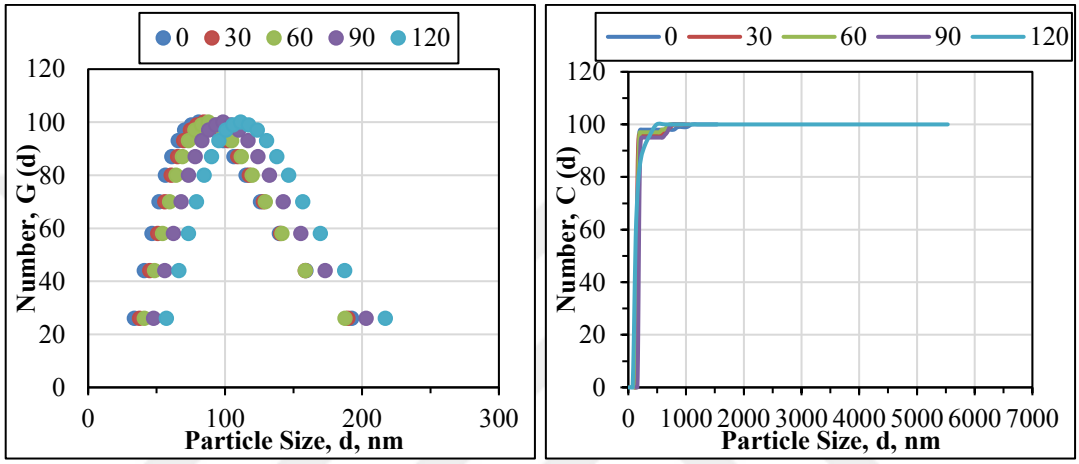


Figure 4.39. N-TiO_2 "as-is" under dark conditions number profile: Time dependent logN distribution G(d) and multi size distribution C(d).

Table 4.25. N-TiO_2 "as-is" under dark conditions number profile: Time dependent mean diameter, range and min-max diameter difference with respect to log normal and multi-size distribution.

N-TiO_2	time, min				
	0	30	60	90	120
Log Normal distribution					
Mean, nm	80.7	84.5	87.7	98.5	111.5
Range	33.8-192.6	37.6-189.7	41.0-187.7	47.7-203.1	57.2-217.1
Difference	158.8	152.1	146.7	155.4	159.9
Multi-size distribution					
Max 1, nm	161.3	157.4	160.1	187.4	127.5
Max 2, nm	1013.4	730.6	621.1	760.1	-
Max 3, nm	1101.7	-	-	-	-
Range	106.3-1538.7	101.5-1053.1	106.6-932.9	138.3-969.7	1.0-5533.9
Difference	1432.4	951.6	826.3	831.4	5532.9

Considering log normal distribution, initial hydrodynamic particle size of N-TiO_2 "as-is" under dark conditions revealed as 80.7 nm and detected to 111.5 nm upon period of 120 min. A rapid increase was monitored during 120 min. The reason could be attributed to aggregation behavior of

N-TiO_2 nanoparticles. Initial size difference was observed as 158.8 nm and no significant alteration was monitored along 120 min period. Considering multi-size distribution, initially three peaks were attained and two peaks were obtained until the end of 120 min. Coinciding peaks were attained by log normal distribution could easily be discriminated due to multi-size distribution.

Likewise expressed so far, a similar approach was also followed for N-TiO_2 "as-is" under dark conditions number profile. Time dependent comparative presentation of log Normal distribution and multi-size distribution of N-TiO_2 "as-is" under dark conditions number profile was given in Figure 4.40.

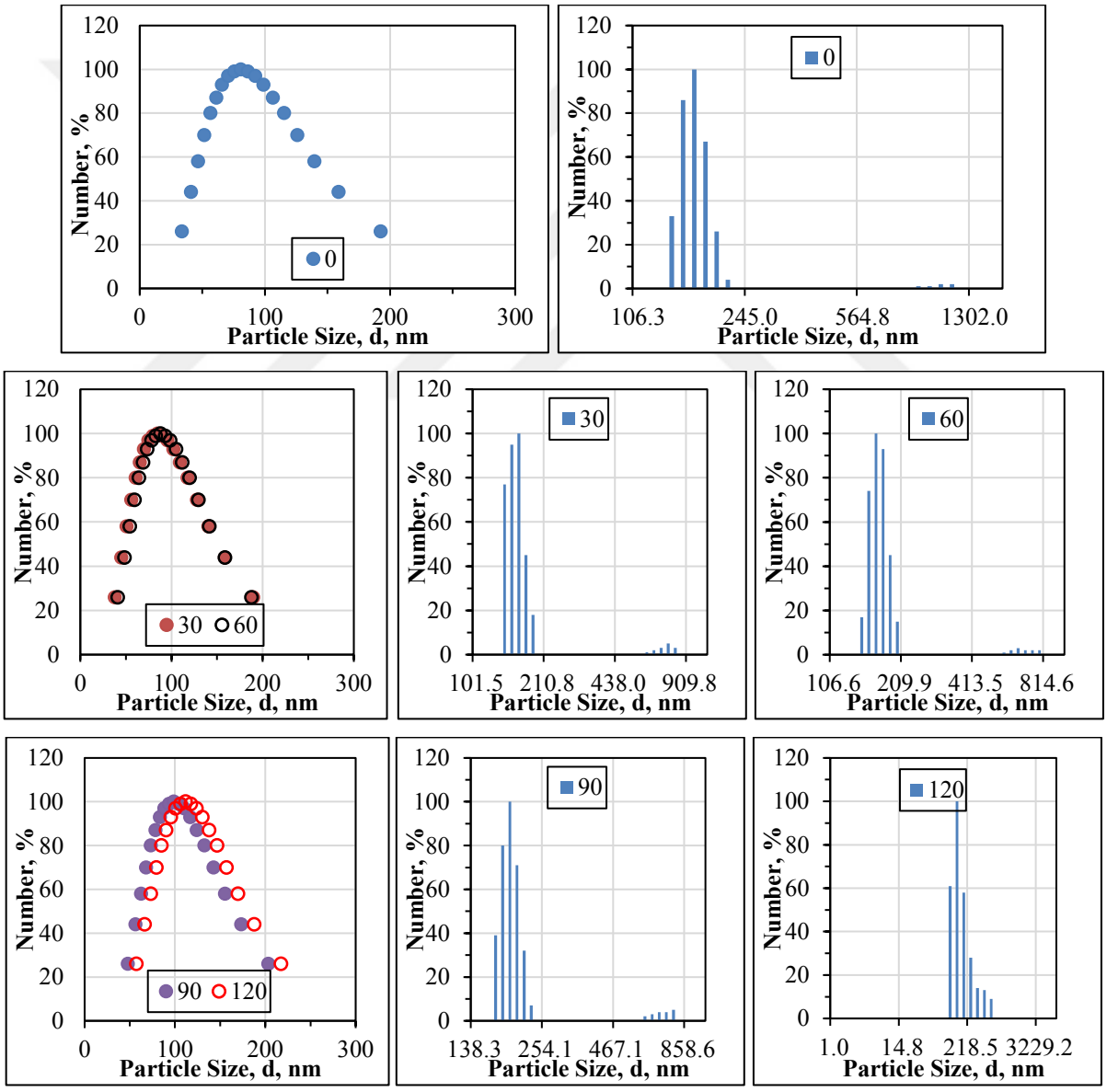


Figure 4.40. N-TiO_2 "as-is" under dark conditions number profile: Time dependent comparative presentation of log Normal distribution and multi-size distribution of N-TiO_2 "as-is" under dark conditions particle size.

4.1.2.9. Fe-TiO_2 "as-is" under dark conditions intensity profile. Time dependent logN distribution G(d) and multi size distribution C(d) of Fe-TiO_2 "as-is" under dark conditions intensity profile was given in Figure 4.41 and related parameters were given in Table 4.26.

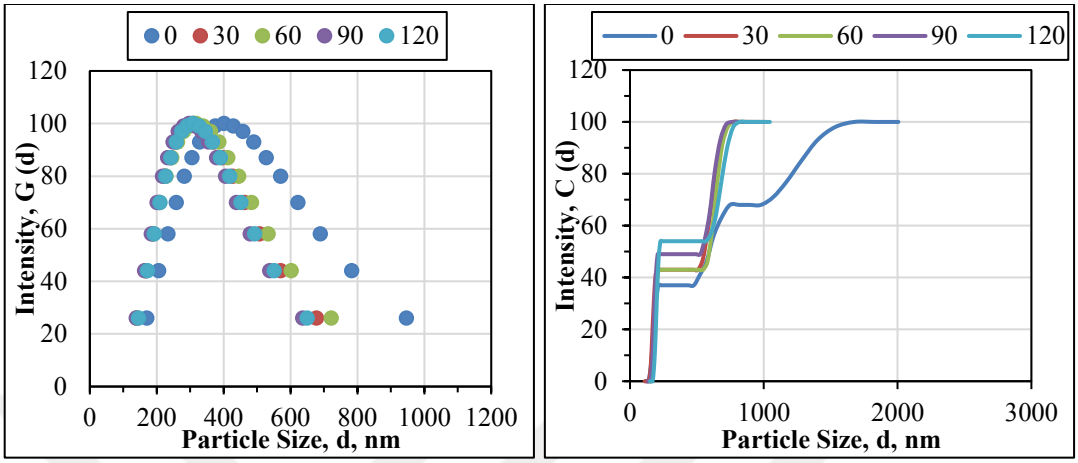


Figure 4.41. Fe-TiO_2 "as-is" under dark conditions intensity profile: Time dependent logN distribution G(d) and multi size distribution C(d).

Table 4.26. Fe-TiO_2 "as-is" under dark conditions intensity profile: Time dependent mean diameter, range and min-max diameter difference with respect to log normal and multi-size distribution.

Fe-TiO_2	time, min				
	0	30	60	90	120
Log Normal distribution					
Mean, nm	401.2	309.3	318.3	297.2	308.1
Range	170.1-946.4	141.1-678.1	140.4-721.5	138.8-636.3	145.9-650.4
Difference	776.3	537.0	581.1	497.5	504.5
Multi-size distribution					
Max 1, nm	177.8	178.5	191.1	182.8	202.1
Max 2, nm	624.6	626.0	650.2	634.0	682.9
Max 3, nm	1401.0	-	-	-	-
Range	113.5-2006.1	109.6-1019.8	142.7-922.7	134.0-979.8	149.1-1045.6
Difference	1892.6	910.2	780.0	845.8	896.5

In terms of intensity profile, initial hydrodynamic particle size of Fe-TiO_2 "as-is" under dark conditions detected as 401.2 nm and revealed a sharp decline in the first 30 min. Accordingly, a slight decrease was observed upon period of 120 min and hydrodynamic size was obtained as 308.1 nm at the end of 120 min. Size difference was in accordance with hydrodynamic size during 120 min, and at first it was recorded as 776.3 nm and reached to 504.5 nm upon 120 min. However, considering multi-size distribution, two peaks were monitored with respect to time.

Time dependent comparative presentation of log Normal distribution and multi-size distribution of Fe-TiO_2 "as-is" under dark conditions intensity profile was exhibited in Figure 4.42. Also, polydispersity of Fe-TiO_2 "as-is" under dark conditions were presented in Table 4.27. It could be concluded that a sharp decrease was observed in the first 30 min and continuous decrease was detected upon 120 min.

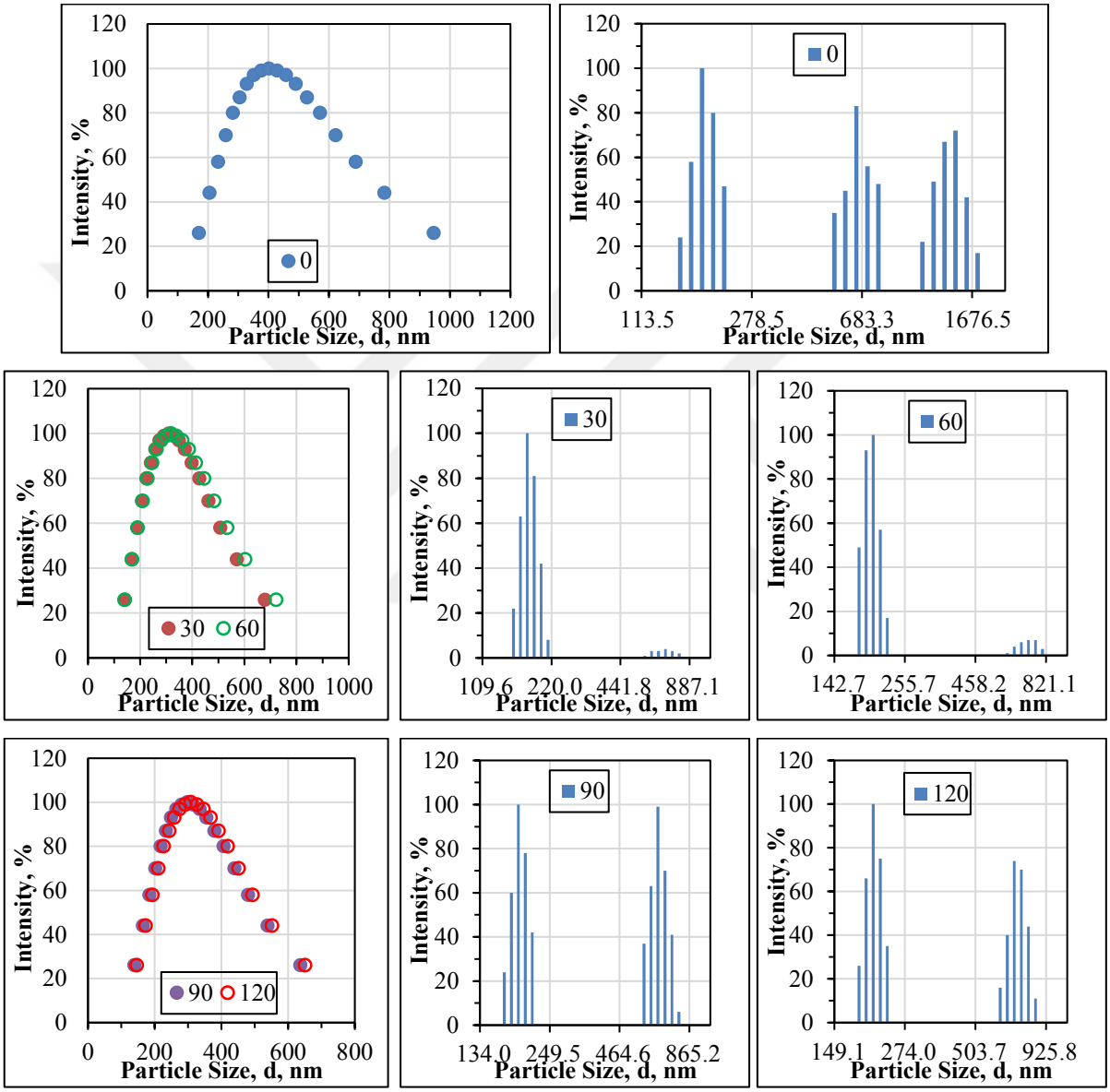


Figure 4.42. Fe-TiO_2 "as-is" under dark conditions intensity profile: Time dependent comparative presentation of log Normal distribution and multi-size distribution of Fe-TiO_2 "as-is" under dark conditions particle size.

Table 4.27. Polydispersity of Fe-TiO_2 "as-is" under dark conditions.

Fe-TiO_2	Polydispersity				
	0	30	60	90	120
	0.313	0.256	0.281	0.239	0.229

4.1.2.10. Fe-TiO_2 "as-is" under dark conditions volume profile. Time dependent logN distribution G(d) and multi size distribution C(d) of Fe-TiO_2 "as-is" under dark conditions volume profile was presented in Figure 4.43. Time dependent mean diameter, range and min-max diameter difference with respect to log normal and multi-size distribution of Fe-TiO_2 "as-is" under dark conditions volume profile was demonstrated in Table 4.28.

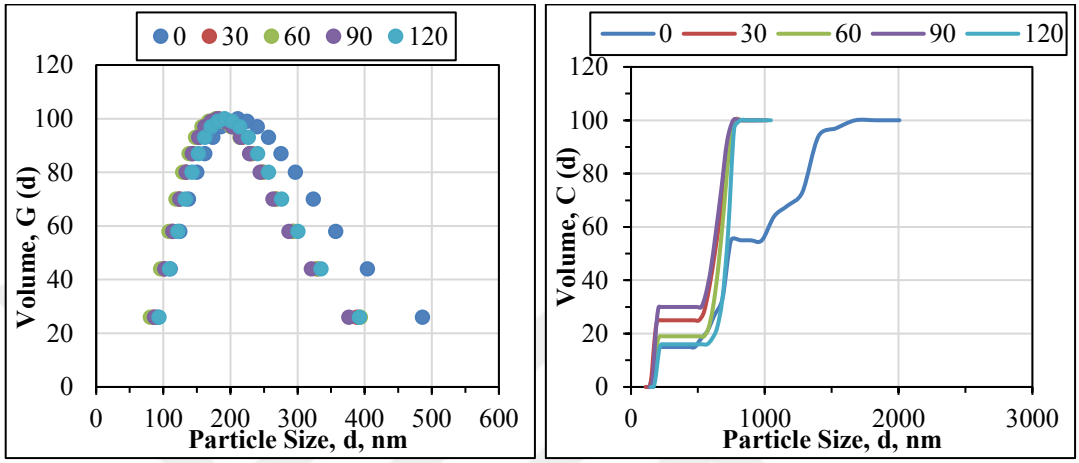


Figure 4.43. Fe-TiO_2 "as-is" under dark conditions volume profile: Time dependent logN distribution G(d) and multi size distribution C(d).

Table 4.28. Fe-TiO_2 "as-is" under dark conditions volume profile: Time dependent mean diameter, range and min-max diameter difference with respect to log normal and multi-size distribution.

Fe-TiO_2	time, min				
	0	30	60	90	120
Log Normal distribution					
Mean, nm	211.1	182.2	178.3	181.2	191.6
Range	91.7-486.0	85.5-388.4	80.7-393.6	87.2-376.7	93.5-392.4
Difference	394.3	302.9	312.9	289.5	298.9
Multi-size distribution					
Max 1, nm	177.8	166.5	191.1	182.8	202.1
Max 2, nm	522.0	178.5	730.7	718.0	771.3
Max 3, nm	747.4	719.7	-	-	-
Max 4, nm	1070.3	-	-	-	-
Max 5, nm	1401.0	-	-	-	-
Max 6, nm	1676.5	-	-	-	-
Range	113.5-2006.1	109.6-1019.8	142.7-922.7	134.0-979.8	149.1-1045.6
Difference	1892.6	910.2	780.0	845.8	896.5

According to log normal distribution, a continuous decrease was observed for Fe-TiO_2 "as-is" under dark conditions volume profile. Initial hydrodynamic particle size of Fe-TiO_2 "as-is" under dark conditions was monitored as 211.1 nm and detected to 191.6 upon 120 min. Size difference

between max and min diameter was attained between 394.3 nm and 298.9 nm along 120 min. For comparison purposes, in terms of multi-size distribution, continuously stirred sample demonstrated six peaks as 177.8 nm, 522.0 nm, 747.4 nm, 1070.3 nm, 1401.0 nm, and 1676.5 nm. Upon 30 min, three peaks were observed and two peaks were monitored until the end of 120 min.

As elucidated for Fe-TiO_2 "as-is" under dark conditions intensity profile (Figure 4.42), a similar approach was followed for Fe-TiO_2 "as-is" under dark conditions volume profile. Time dependent comparative presentation of log Normal distribution and multi-size distribution of Fe-TiO_2 "as-is" under dark conditions volume profile was displayed in Figure 4.44.

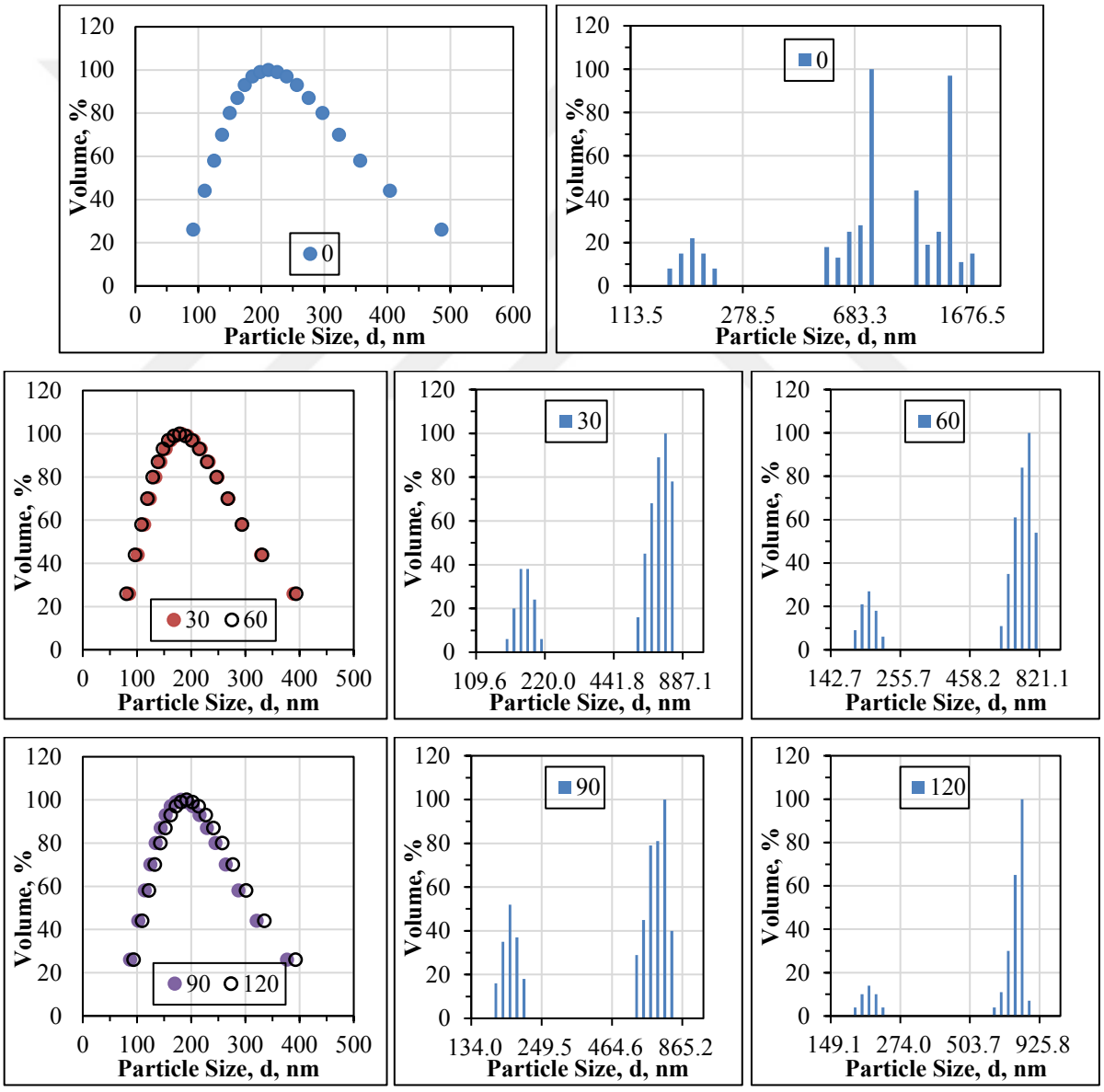


Figure 4.44. Fe-TiO_2 "as-is" under dark conditions volume profile: Time dependent comparative presentation of log Normal distribution and multi-size distribution of Fe-TiO_2 "as-is" under dark conditions particle size.

4.1.2.11. Fe-TiO_2 "as-is" under dark conditions surface area profile. As explained for Fe-TiO_2 "as-is" under dark conditions intensity profile (Figure 4.41) and volume profile (Figure 4.43), a similar approach was followed for Fe-TiO_2 "as-is" under dark conditions surface area profile. Time dependent logN distribution G(d) and multi size distribution C(d) of Fe-TiO_2 "as-is" under dark conditions surface area profile was displayed in Figure 4.45. Time dependent mean diameter, range and min-max diameter difference with respect to log normal and multi-size distribution of Fe-TiO_2 "as-is" under dark conditions surface area profile was given in Table 4.29.

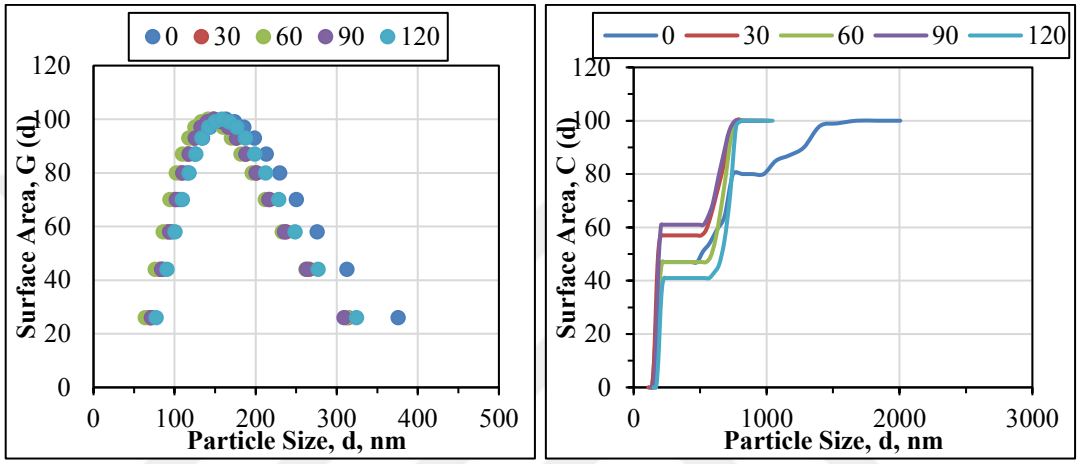


Figure 4.45. Fe-TiO_2 "as-is" under dark conditions surface area profile: Time dependent logN distribution G(d) and multi size distribution C(d).

Table 4.29. Fe-TiO_2 "as-is" under dark conditions surface area profile: Time dependent mean diameter, range and min-max diameter difference with respect to log normal and multi-size distribution.

Fe-TiO_2	time, min				
	0	30	60	90	120
Log Normal distribution					
Mean, nm	163.3	147.5	141.4	148.7	158.4
Range	71.0-375.9	69.2-314.3	64.0-312.2	71.5-309.1	77.3-324.5
Difference	304.9	245.1	248.2	237.6	247.2
Multi-size distribution					
Max 1, nm	177.8	166.5	191.1	182.8	202.1
Max 2, nm	522.0	719.7	730.7	634.0	771.3
Max 3, nm	747.4	-	-	718.0	-
Max 4, nm	1070.3	-	-	-	-
Max 5, nm	1401.0	-	-	-	-
Max 6, nm	1676.5	-	-	-	-
Range	113.5-2006.1	109.6-1019.8	142.7-922.7	134.0-979.8	149.1-1045.6
Difference	1892.6	910.2	780.0	845.8	896.5

Considering log normal distribution, hydrodynamic particle size of Fe-TiO_2 "as-is" under dark conditions did not display a significant variation in terms of surface area profile with respect to time. Initial hydrodynamic particle size was attained as 163.3 nm and decreased to 158.4 nm upon 120 min. Accordingly, initial size difference was obtained as 304.9 nm and detected to 247.2 nm upon 120 min. However, considering multi-size distribution, initially six max diameters were obtained as explained for volume profile, and two max diameters were observed until the end of 120 min.

Time dependent comparative presentation of log Normal distribution and multi-size distribution of Fe-TiO_2 "as-is" under dark conditions surface area profile was exhibited in Figure 4.46.

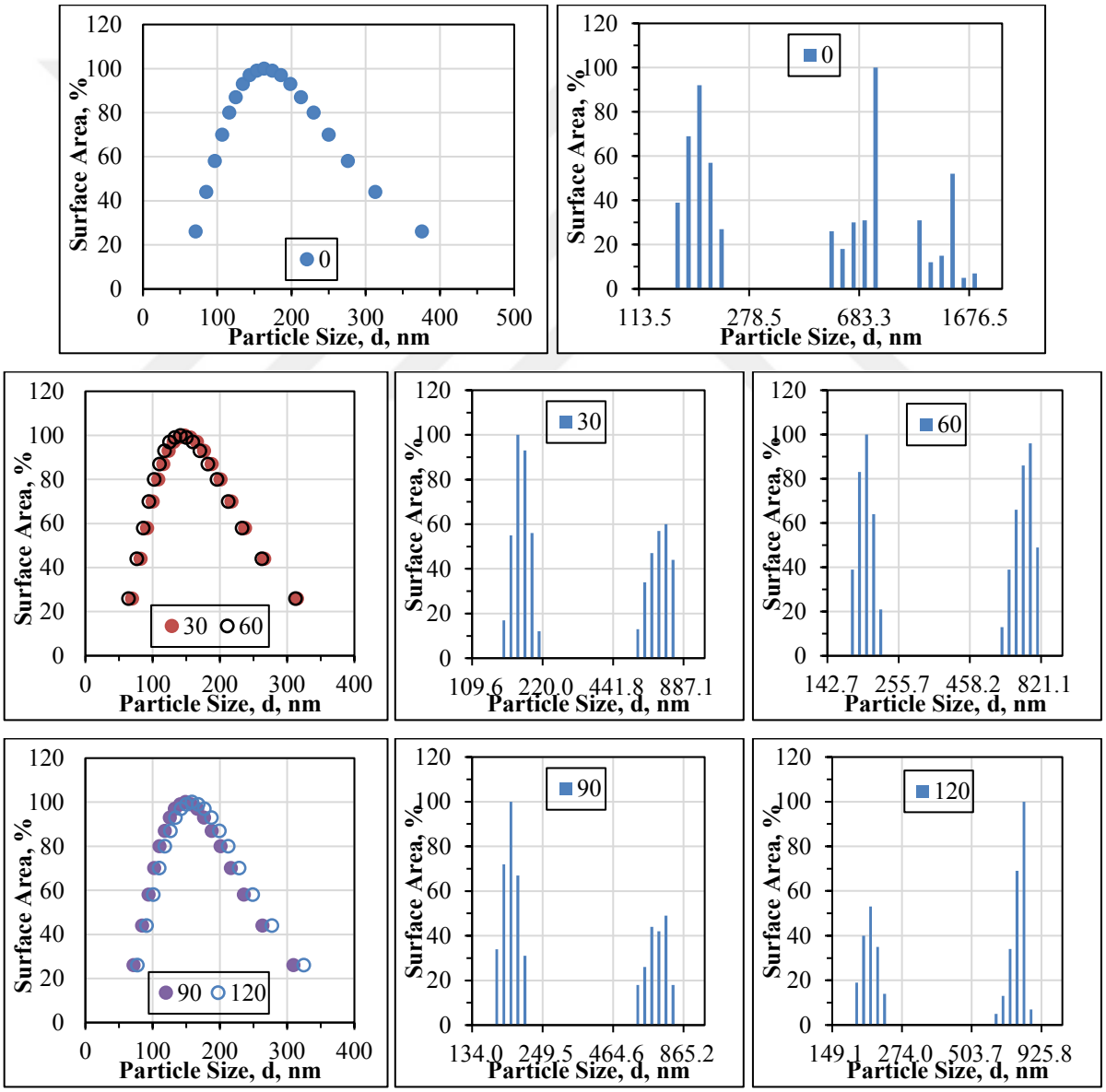


Figure 4.46. Fe-TiO_2 "as-is" under dark conditions surface area profile: Time dependent comparative presentation of log Normal distribution and multi-size distribution of Fe-TiO_2 "as-is" under dark conditions particle size.

4.1.2.12. Fe-TiO_2 "as-is" under dark conditions number profile. Time dependent logN distribution G(d) and multi size distribution C(d) of Fe-TiO_2 "as-is" under dark conditions number profile was given in Figure 4.47. Time dependent mean diameter, range and min-max diameter difference with respect to log normal and multi-size distribution of Fe-TiO_2 "as-is" under dark conditions number profile was presented in Table 4.30.

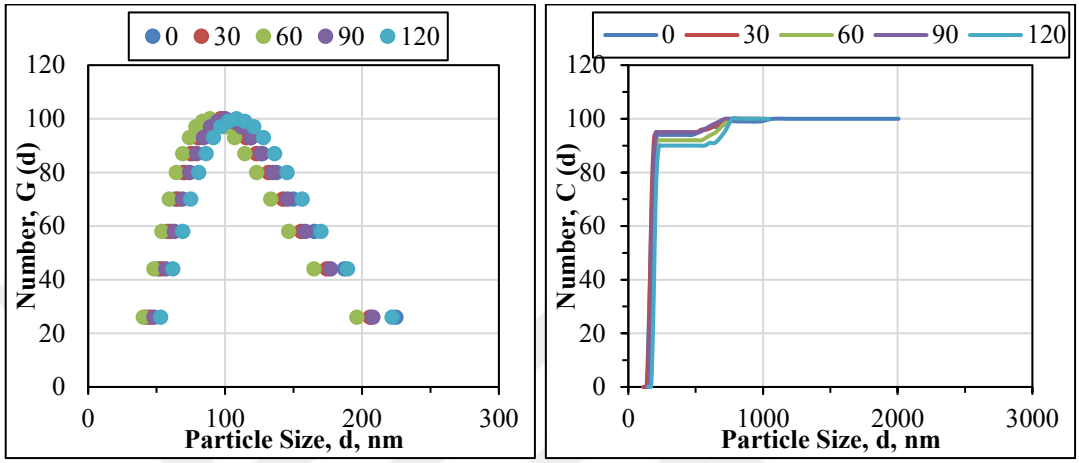


Figure 4.47. Fe-TiO_2 "as-is" under dark conditions number profile: Time dependent logN distribution G(d) and multi size distribution C(d).

Table 4.30. Fe-TiO_2 "as-is" under dark conditions number profile: Time dependent mean diameter, range and min-max diameter difference with respect to log normal and multi-size distribution.

Fe-TiO_2	time, min				
	0	30	60	90	120
Log Normal distribution					
Mean, nm	97.7	96.6	88.9	100.1	108.3
Range	42.5-224.9	45.3-205.9	40.3-196.4	48.1-208.0	52.9-221.9
Difference	182.4	160.6	156.1	159.9	169.0
Multi-size distribution					
Max 1, nm	177.8	166.5	191.1	182.8	202.1
Max 2, nm	522.0	671.2	689.3	634.0	771.3
Max 3, nm	624.6	-	730.7	-	-
Max 4, nm	747.4	-	-	-	-
Max 5, nm	1070.3	-	-	-	-
Max 6, nm	1401.0	-	-	-	-
Range	113.5-2006.1	109.6-1019.8	142.7-922.7	134.0-979.8	149.1-1045.6
Difference	1892.6	910.2	780.0	845.8	896.5

In a similar manner to data depicted Fe-TiO_2 "as-is" under dark conditions surface area profile (Table 4.29), time dependent mean diameter, range and min-max diameter difference with respect to log normal and multi-size distribution of Fe-TiO_2 "as-is" under dark conditions number profile was

elucidated and it could be inferred that no significant alteration was monitored upon 120 min. Initial hydrodynamic size was attained as 97.7 nm and following a slight increase, it was reached to 108.3 nm at the end of 120 min. Also, size difference was in accordance with hydrodynamic size and decreased from 182.4 nm to 169.0 nm with respect to time. However, in terms of multi-size distribution, it could be deduced that initially six peaks were observed and two peaks were monitored until the end of 120 min.

Time dependent comparative presentation of log Normal distribution and multi-size distribution of Fe-TiO_2 "as-is" under dark conditions number profile was given in Figure 4.48.

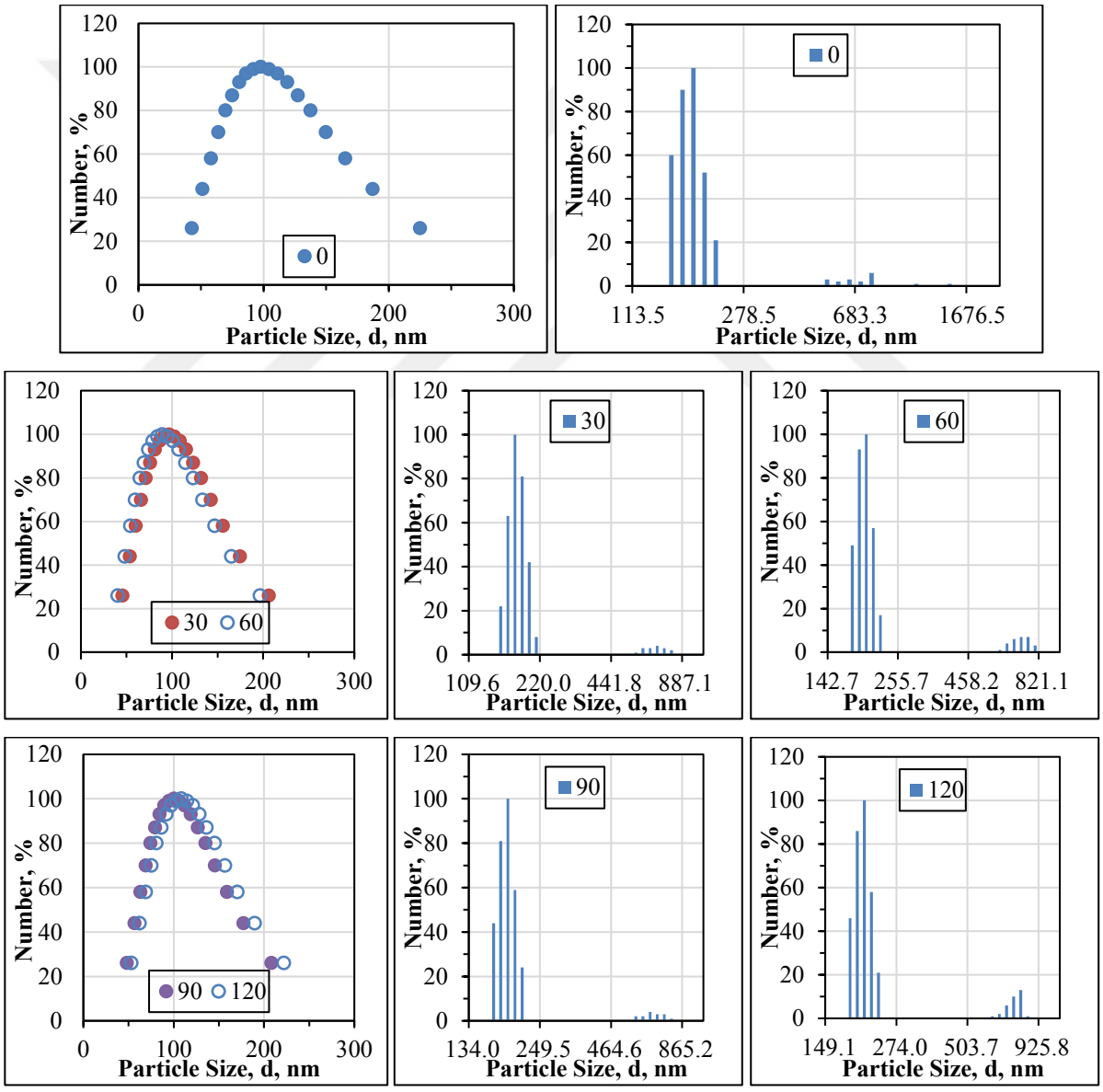


Figure 4.48. Fe-TiO_2 "as-is" under dark conditions number profile: Time dependent comparative presentation of log Normal distribution and multi-size distribution of Fe-TiO_2 "as-is" under dark conditions particle size.

4.1.3. Mono System: As-is Under Irradiation

The clarification of the hydrodynamic particle size of the nanoparticles were demonstrated under "as-is" under irradiation conditions.

4.1.3.1. TiO_2 "as-is" under irradiation conditions intensity profile. Time dependent logN distribution G(d) and multi size distribution C(d), and mean diameter, range and min-max diameter difference with respect to log normal and multi-size distribution of TiO_2 "as-is" under irradiation conditions intensity profile was exhibited in Figure 4.49 and Table 4.31., respectively.

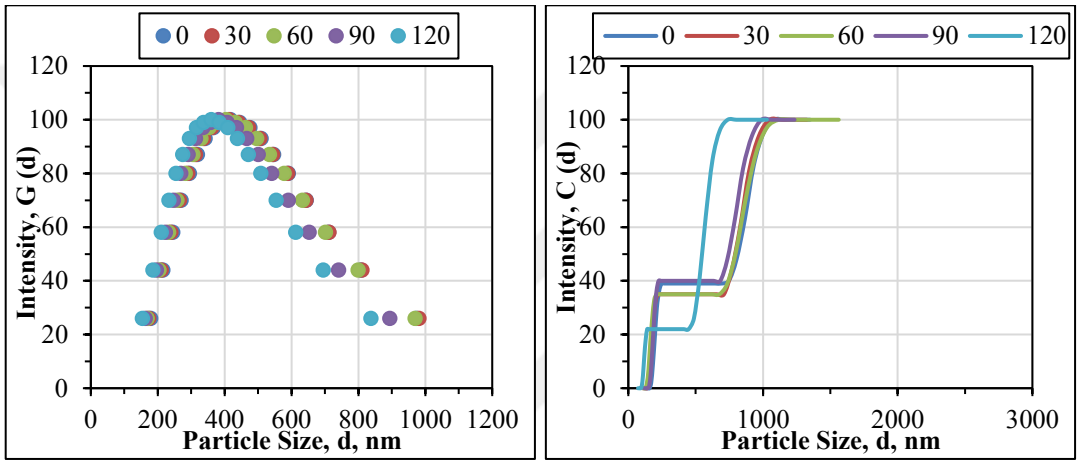


Figure 4.49. TiO_2 "as-is" under irradiation conditions intensity profile: Time dependent logN distribution G(d) and multi size distribution C(d).

Table 4.31. TiO_2 "as-is" under irradiation conditions intensity profile: Time dependent mean diameter, range and min-max diameter difference with respect to log normal and multi-size distribution.

TiO_2	time, min				
	0	30	60	90	120
Log Normal distribution					
Mean, nm	417.4	413.0	403.9	381.9	359.7
Range	178.9-973.7	173.9-980.9	168.2-969.9	163.1-894.3	154.4-838.0
Difference	794.8	807.0	801.7	731.2	683.6
Multi-size distribution					
Max 1, nm	196.7	174.9	177.1	193.8	118.5
Max 2, nm	931.5	189.0	869.3	852.4	574.9
Max 3, nm	-	897.1	-	-	-
Range	126.1-1348.9	109.6-1324.1	107.2-1562.1	115.4-1234.4	71.9-1028.8
Difference	1222.8	1214.5	1454.9	1119.0	956.9

Both for log normal distribution and multi-size distribution, TiO_2 "as-is" under irradiation revealed a continuously decreasing trend in terms of intensity profile upon 120 min. Time dependent comparative presentation of log Normal distribution and multi-size distribution of TiO_2 "as-is" under irradiation conditions intensity profile was given in Figure 4.50. Also, it could be easily seen that polydispersity did not demonstrate a significant change along 120 min (Table 4.32).

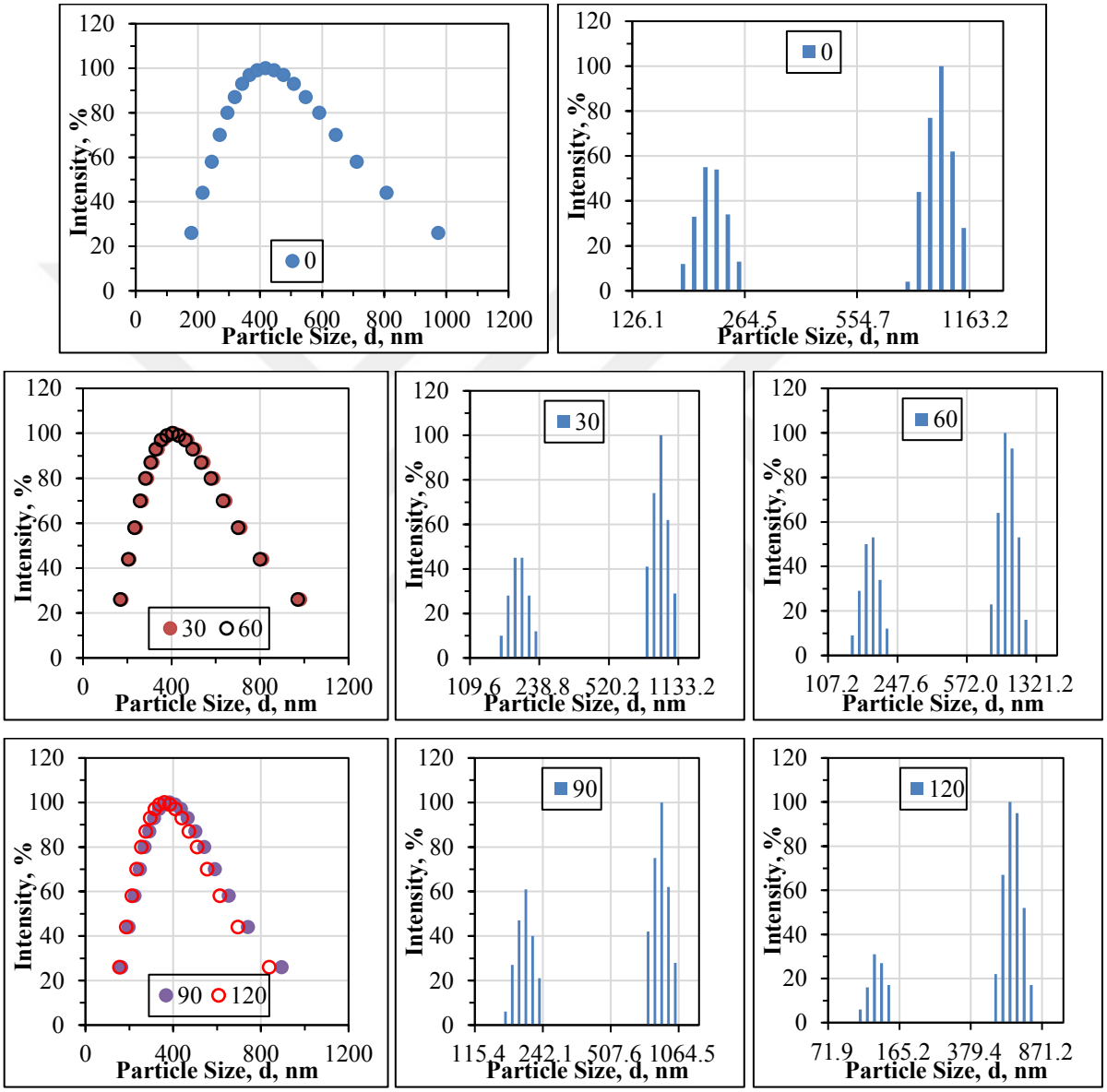


Figure 4.50. TiO_2 "as-is" under irradiation conditions intensity profile: Time dependent comparative presentation of log Normal distribution and multi-size distribution of TiO_2 "as-is" under irradiation conditions particle size.

Table 4.32. Polydispersity of TiO_2 "as-is" under irradiation conditions.

TiO_2	Polydispersity				
	0	30	60	90	120
	0.304	0.318	0.328	0.307	0.303

4.1.3.2. TiO_2 "as-is" under irradiation conditions volume profile. As elucidated for TiO_2 "as-is" under irradiation conditions intensity profile, a similar approach was followed for time dependent logN distribution G(d) and multi size distribution C(d) of TiO_2 "as-is" under irradiation conditions volume profile (Figure 4.51).

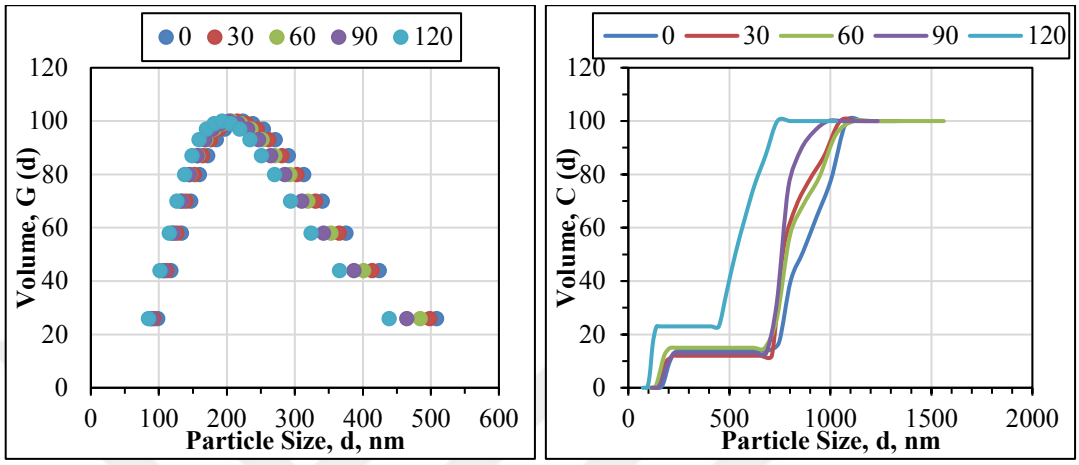


Figure 4.51. TiO_2 "as-is" under irradiation volume profile: Time dependent logN distribution G(d) and multi size distribution C(d).

Time dependent mean diameter, range and min-max diameter difference with respect to log normal and multi-size distribution of TiO_2 "as-is" under irradiation conditions volume profile was presented in Table 4.33.

Table 4.33. TiO_2 "as-is" under irradiation volume profile: Time dependent mean diameter, range and min-max diameter difference with respect to log normal and multi-size distribution.

TiO_2	time, min				
	0	30	60	90	120
Log Normal distribution					
Mean, nm	223.5	215.0	206.5	203.4	193.1
Range	98.3-508.6	92.8-498.3	88.1-484.2	89.1-464.5	85.0-438.7
Difference	410.3	405.5	396.1	375.4	353.7
Multi-size distribution					
Max 1, nm	211.8	174.9	162.9	193.8	118.5
Max 2, nm	803.3	767.8	799.5	791.6	529.1
Max 3, nm	1080.2	1048.3	1027.8	-	737.8
Range	126.1-1348.9	109.6-1324.1	107.2-1562.1	115.4-1234.4	71.9-1028.8
Difference	1222.8	1214.5	1454.9	1119.0	956.9

In terms of volume profile, it could be inferred that hydrodynamic particle size of TiO_2 "as-is" under irradiation expressed a continuously decreasing trend according to time variations. Sample was

immediately subjected to recording after irradiation revealed hydrodynamic size as 223.5 nm and detected to 193.1 nm upon period of 120 min. Accordingly, hydrodynamic size differences were altered in between 410.3 nm and 353.7 nm along 120 min. However, it could be deduced that due to multi-size distribution mode, possible coinciding particles could be easily discriminated. Three peaks were attained until 90 min. Upon 90 min, two peaks were obtained and three peaks remained until the end of 120 min.

Likewise expressed so far, time dependent comparative presentation of log Normal distribution and multi-size distribution of TiO_2 "as-is" under irradiation conditions volume profile was exhibited in Figure 4.52.

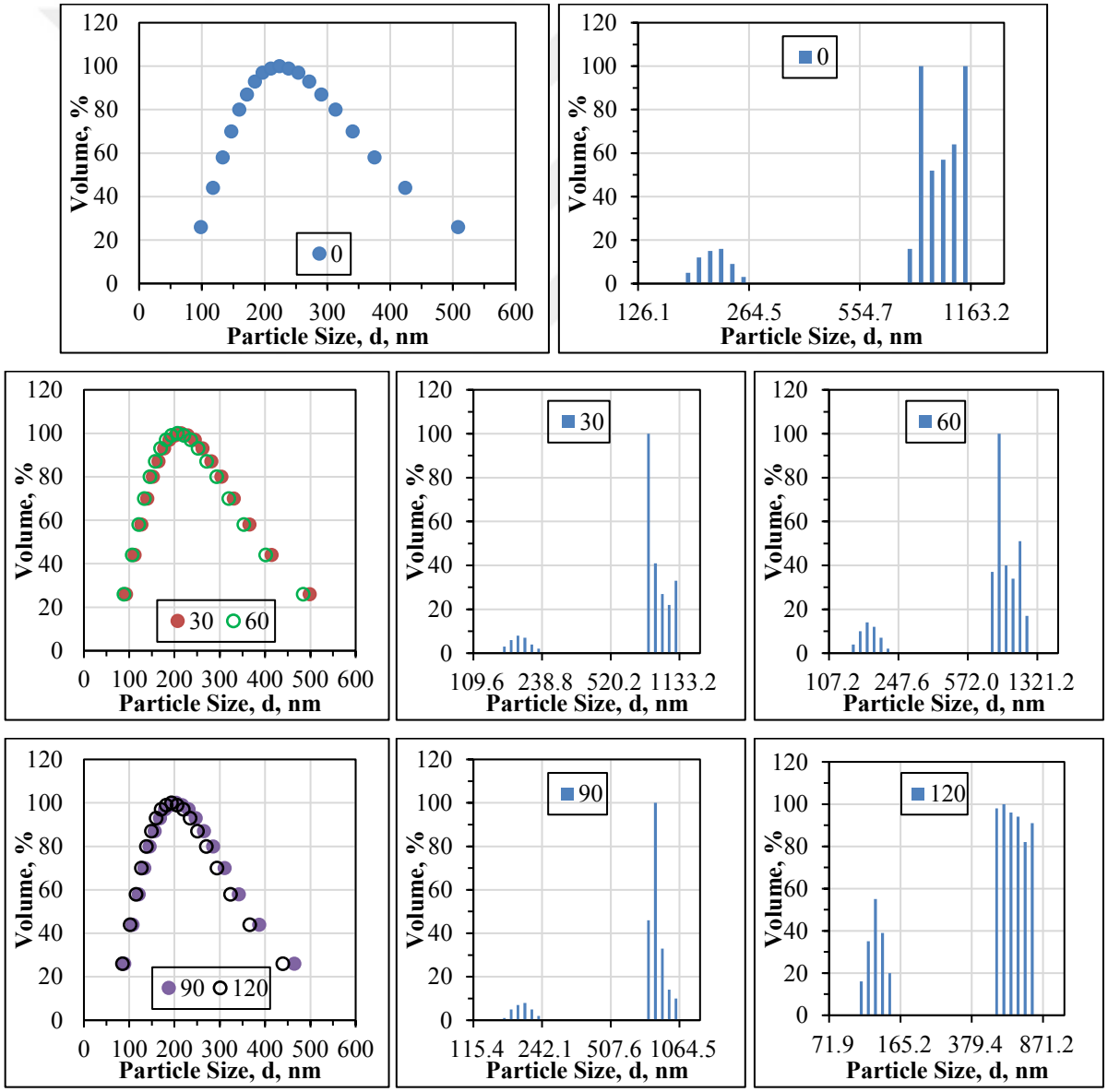


Figure 4.52. TiO_2 "as-is" under irradiation volume profile: Time dependent comparative presentation of log Normal distribution and multi-size distribution of TiO_2 "as-is" under irradiation particle size.

4.1.3.3. TiO_2 "as-is" under irradiation conditions surface area profile. Time dependent logN distribution G(d) and multi size distribution C(d) of TiO_2 "as-is" under irradiation conditions surface area profile was displayed in Figure 4.53.

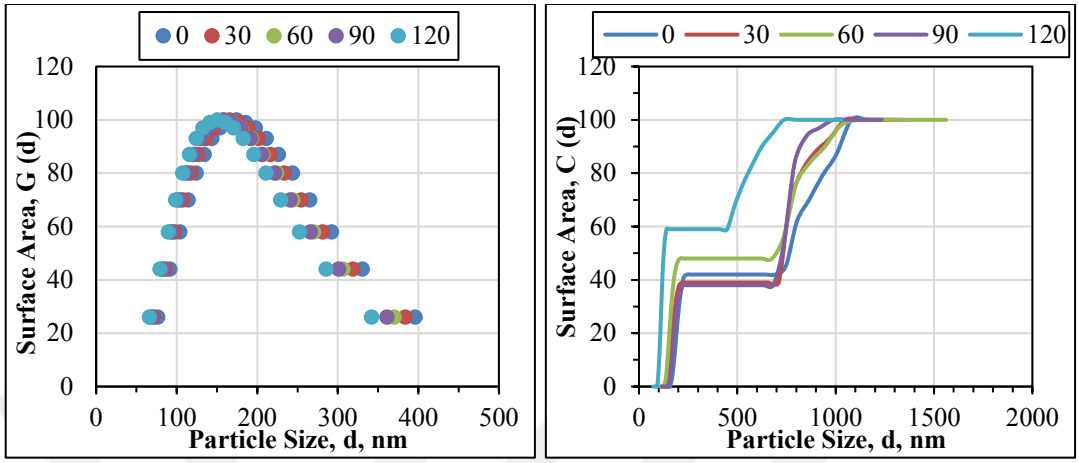


Figure 4.53. TiO_2 "as-is" under irradiation surface area profile: Time dependent logN distribution G(d) and multi size distribution C(d).

In a similar manner, time dependent mean diameter, range and min-max diameter difference with respect to log normal and multi-size distribution of TiO_2 "as-is" under irradiation conditions surface area profile was shown in Table 4.34.

Table 4.34. TiO_2 "as-is" under irradiation surface area profile: Time dependent mean diameter, range and min-max diameter difference with respect to log normal and multi-size distribution.

TiO_2	time, min				
	0	30	60	90	120
Log Normal distribution					
Mean, nm	174.1	165.6	157.9	158.1	150.6
Range	76.5-396.2	71.4-383.8	67.4-370.3	69.2-361.0	66.3-342.1
Difference	319.7	312.4	302.9	291.8	275.8
Multi-size distribution					
Max 1, nm	196.7	174.9	162.9	193.8	118.5
Max 2, nm	803.3	767.8	799.5	791.6	486.9
Max 3, nm	1080.2	1048.3	1027.8	-	737.8
Range	126.1-1348.9	109.6-1324.1	107.2-1562.1	115.4-1234.4	71.9-1028.8
Difference	1222.8	1214.5	1454.9	1119.0	956.9

Considering log normal distribution, initial hydrodynamic size of TiO_2 "as-is" under irradiation conditions was examined as 174.1 nm. During 120 min, the hydrodynamic size of TiO_2 displayed a drastic change and decreased to 150.6 nm. Correspondingly, hydrodynamic size also expressed a

distinct variation from 319.7 nm to 275.8 nm. For comparison purposes, in terms of multi-size distribution it could also be deduced that three peaks were observed as 196.7 nm, 803.3 nm, and 1080.2 nm for TiO_2 "as-is" under irradiation conditions following initial period of time. Upon 120 min, three max diameters were attained as 118.5 nm, 486.9 and 737.8 nm.

As elucidated for TiO_2 "as-is" under irradiation conditions volume profile (Figure 4.52), following a similar trend, time dependent comparative presentation of log Normal distribution and multi-size distribution of TiO_2 "as-is" under irradiation conditions surface area profile was exhibited in Figure 4.54.

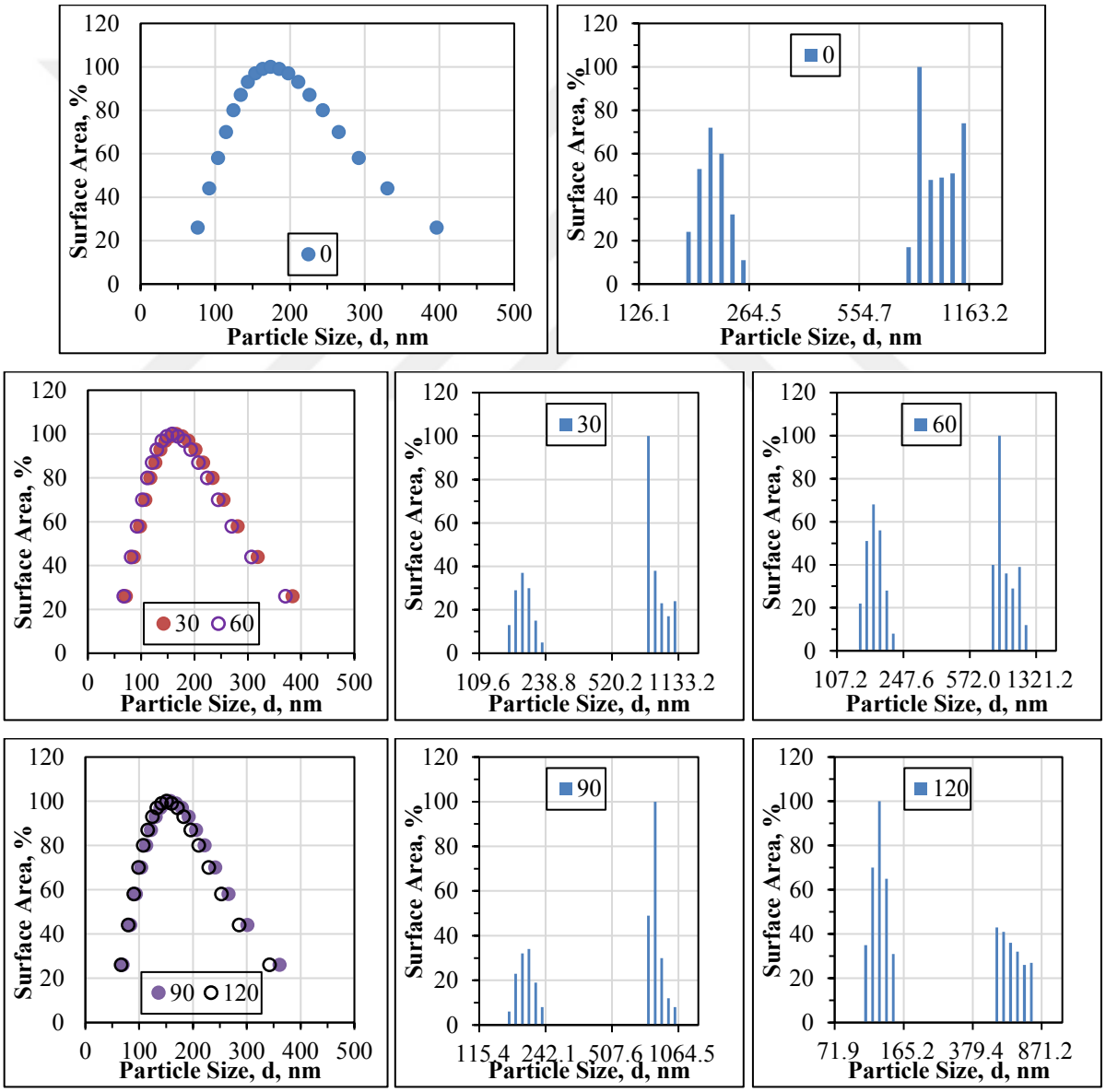


Figure 4.54. TiO_2 "as-is" under irradiation surface area profile: Time dependent comparative presentation of log Normal distribution and multi-size distribution of TiO_2 "as-is" under irradiation particle size.

4.1.3.4. TiO_2 "as-is" under irradiation conditions number profile. As expressed for TiO_2 "as-is" under irradiation conditions surface area profile (Figure 4.53), time dependent logN distribution G(d) and multi size distribution C(d) of TiO_2 "as-is" under irradiation conditions number profile was presented Figure 4.55.

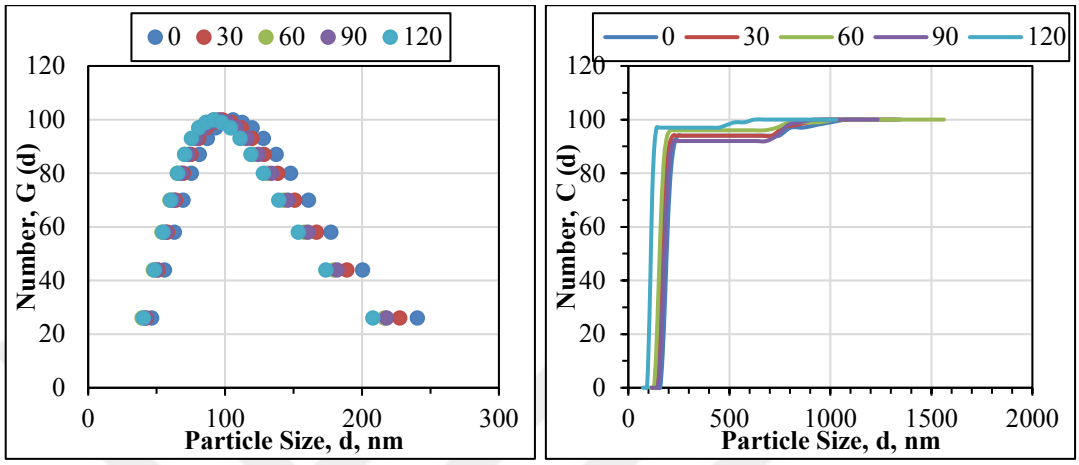


Figure 4.55. TiO_2 "as-is" under irradiation conditions number profile: Time dependent logN distribution G(d) and multi size distribution C(d).

In a similar manner, time dependent mean diameter, range and min-max diameter difference with respect to log normal and multi-size distribution of TiO_2 "as-is" under irradiation conditions number profile was exhibited in Table 4.35.

Table 4.35. TiO_2 "as-is" under irradiation conditions number profile: Time dependent mean diameter, range and min-max diameter difference with respect to log normal and multi-size distribution.

TiO_2	time, min				
	0	30	60	90	120
Log Normal distribution					
Mean, nm	105.7	98.2	92.3	95.5	91.5
Range	46.4-240.4	42.4-227.6	39.4-216.5	41.8-218.1	40.3-208.0
Difference	194.0	185.2	177.1	176.3	167.7
Multi-size distribution					
Max 1, nm	196.7	174.9	162.9	180.0	118.5
Max 2, nm	803.3	767.8	799.5	791.6	486.9
Range	126.1-1348.9	109.6-1324.1	107.2-1562.1	115.4-1234.4	71.9-1028.8
Difference	1222.8	1214.5	1454.9	1119.0	956.9

In terms of number profile and with respect to log normal distribution, hydrodynamic particle size variations with respect to time revealed a sharp decrease and detected 105.7 nm to 91.5 nm.

Variations in hydrodynamic size supported by hydrodynamic particle size difference and decreased 194.0 nm to 167.7 nm upon period of 120 min. For comparison purposes, according to multi-size distribution, it could be inferred that two peaks were observed for TiO_2 "as-is" under irradiation conditions in terms of number profile. Also, size differences were decreased from 1222.8 nm to 956.9 nm with respect to time.

Following a similar manner, time dependent comparative presentation of log Normal distribution and multi-size distribution of TiO_2 "as-is" under irradiation conditions number profile was presented in Figure 4.56.

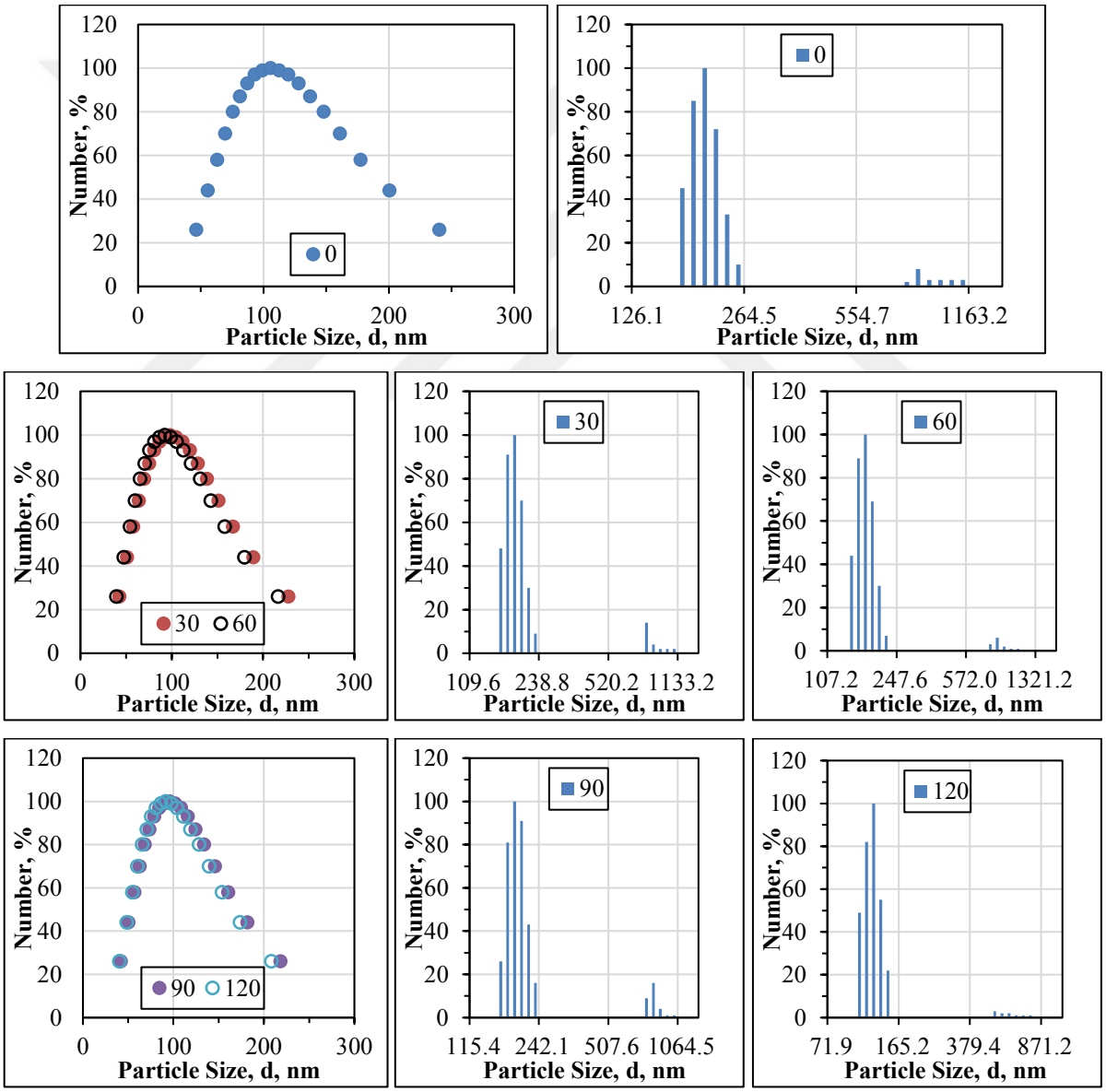


Figure 4.56. TiO_2 "as-is" under irradiation conditions number profile: Time dependent comparative presentation of log Normal distribution and multi-size distribution of TiO_2 "as-is" under irradiation conditions particle size.

4.1.3.5. N-TiO_2 "as-is" under irradiation conditions intensity profile. As elucidated for TiO_2 "as-is" under irradiation conditions (Figure 4.49), a similar approach was followed for N-TiO_2 "as-is" under irradiation conditions. Time dependent logN distribution G(d) and multi size distribution C(d) of N-TiO_2 "as-is" under irradiation conditions intensity profile was displayed in Figure 4.57 and related parameters was given in Table 4.36.

Polydispersity of N-TiO_2 "as-is" under irradiation conditions were presented in Table 4.37. Initially a sharp decrease was observed and upon 30 min, no significant variation was monitored until 120 min.

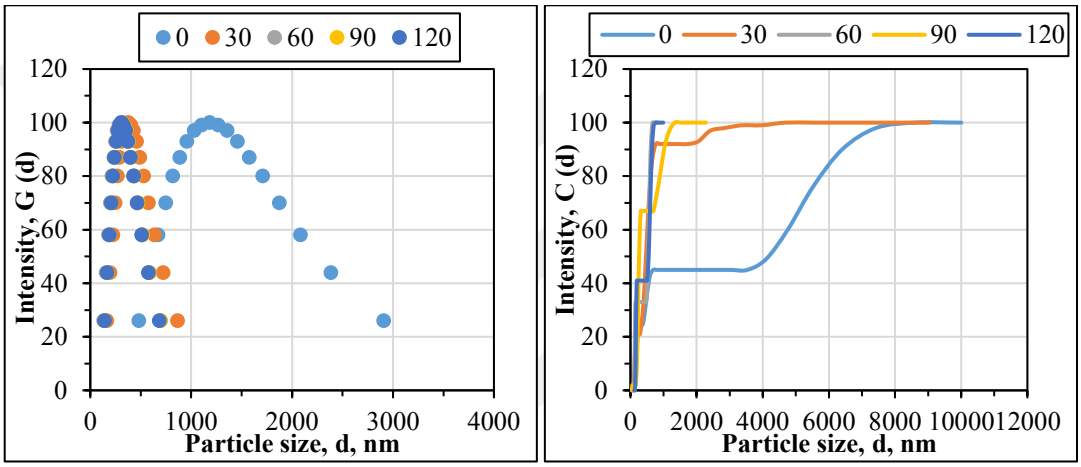


Figure 4.57. N-TiO_2 "as-is" under irradiation conditions intensity profile: Time dependent logN distribution G(d) and multi size distribution C(d).

Table 4.36. N-TiO_2 "as-is" under irradiation conditions intensity profile: Time dependent mean diameter, range and min-max diameter difference with respect to log normal and multi-size distribution.

N-TiO_2	time, min				
	0	30	60	90	120
Log Normal distribution					
Mean, nm	1182.7	376.8	303.6	316.0	310.8
Range	481.2-2906.7	163.8-866.7	132.0-698.4	143.3-696.7	141.0-685.1
Difference	2425.5	702.9	566.4	553.4	544.1
Multi-size distribution					
Max 1, nm	180.6	124.5	132.4	56.1	166.3
Max 2, nm	511.3	548.7	585.5	240.3	613.0
Max 3, nm	5517.4	2418.9	-	1030.2	-
Max 4, nm	-	4676.9	-	-	-
Range	85.9-10.000	46.3-9042.5	94.5-820.7	33.0-2278.7	110.1-991.3
Difference	9914.1	8996.2	726.2	2245.7	881.2

Initial hydrodynamic size of N-TiO_2 “as-is” under irradiation conditions revealed a drastic change. Upon 30 min, continuous decrease was observed until 120 min. However, in terms of multi-size distribution, it could be deduced that four max diameters were attained during 120 min. Time dependent comparative presentation of log Normal distribution and multi-size distribution of N-TiO_2 “as-is” under irradiation conditions intensity profile was presented in Figure 4.58.

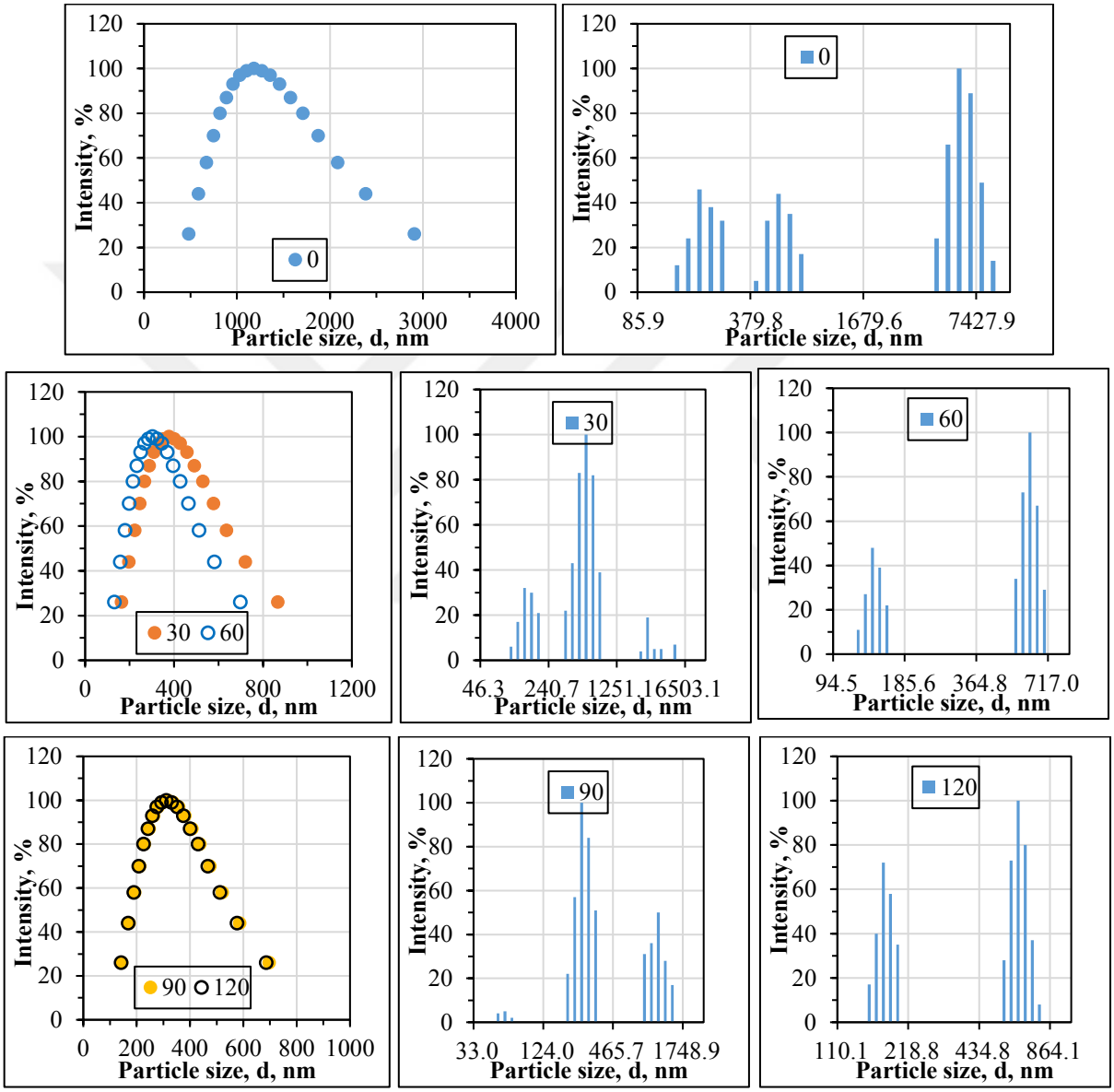


Figure 4.58. N-TiO_2 “as-is” under irradiation conditions intensity profile: Time dependent comparative presentation of log Normal distribution and multi-size distribution of N-TiO_2 “as-is” under irradiation particle size.

Table 4.37. Polydispersity of N-TiO_2 “as-is” under irradiation conditions.

N-TiO_2	Polydispersity				
	0	30	60	90	120
	0.348	0.292	0.292	0.260	0.260

4.1.3.6. N-TiO_2 "as-is" under irradiation conditions volume profile. Time dependent logN distribution G(d) and multi size distribution C(d) of N-TiO_2 "as-is" under irradiation conditions volume profile was presented in Figure 4.57. Time dependent mean diameter, range and min-max diameter difference with respect to log normal and multi-size distribution of N-TiO_2 "as-is" under irradiation conditions volume profile was demonstrated in Table 4.38.

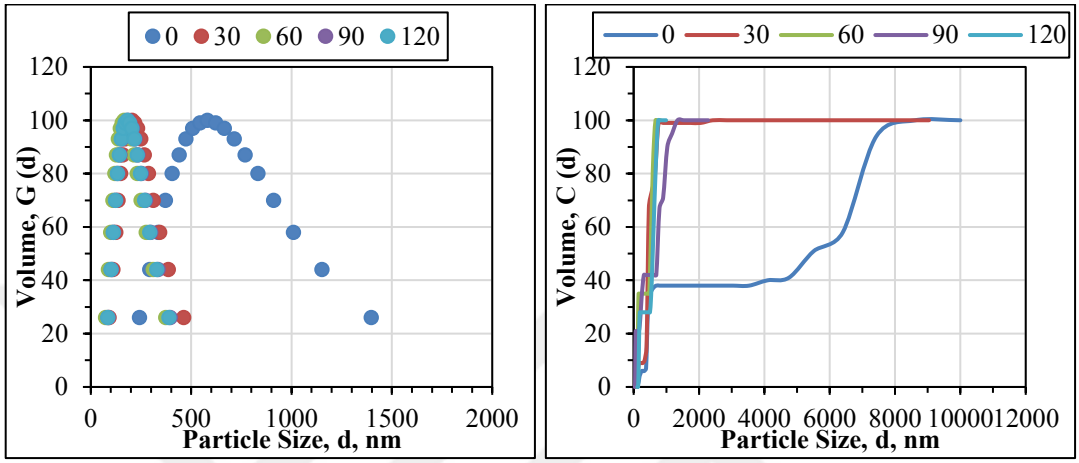


Figure 4.59. N-TiO_2 "as-is" under irradiation conditions volume profile: Time dependent logN distribution G(d) and multi size distribution C(d).

Table 4.38. N-TiO_2 "as-is" under irradiation conditions volume profile: Time dependent mean diameter, range and min-max diameter difference with respect to log normal and multi-size distribution.

N-TiO_2	time, min				
	0	30	60	90	120
Log Normal distribution					
Mean, nm	581.7	206.3	166.3	184.6	181.7
Range	242.1-1397.4	92.0-462.6	74.2-372.8	86.1-395.9	84.8-389.4
Difference	1155.3	370.6	298.6	309.8	304.6
Multi-size distribution					
Max 1, nm	180.6	124.5	132.4	49.1	166.3
Max 2, nm	440.7	465.3	585.5	240.3	656.5
Max 3, nm	5517.4	763.0	-	790.6	-
Max 4, nm	7427.9	2051.3	-	1030.2	-
Max 5, nm	-	2418.9	-	1342.2	-
Max 6, nm	-	4676.9	-	-	-
Range	85.9-10.000	46.3-9042.5	94.5-820.7	33.0-2278.7	110.1-991.3
Difference	9914.1	8996.2	726.2	2245.7	881.2

In terms of volume profile, initial hydrodynamic particle size of N-TiO_2 "as-is" under irradiation conditions were recorded as 581.7 nm. Upon 30 min, drastic changes were observed and

hydrodynamic size decreased to 206.3 nm. Upon 120 min, hydrodynamic particle size was 181.7 nm. Initial size difference between max and min diameter was attained as 1155.3 nm and detected to 304.6 nm upon period of 120 min. Considering multi-size distribution, initially four peaks were observed. Upon 30 min, six max diameters were obtained, two peaks were attained upon 60 min. Upon 90 min, five peaks were observed and two max diameters were monitored at the end of 120 min.

As explained for N-TiO_2 "as-is" under irradiation conditions intensity profile (Figure 4.58), a similar approach followed for N-TiO_2 "as-is" under irradiation conditions volume profile. Time dependent comparative presentation of log Normal distribution and multi-size distribution of N-TiO_2 "as-is" under irradiation conditions volume profile was demonstrated in Figure 4.60.

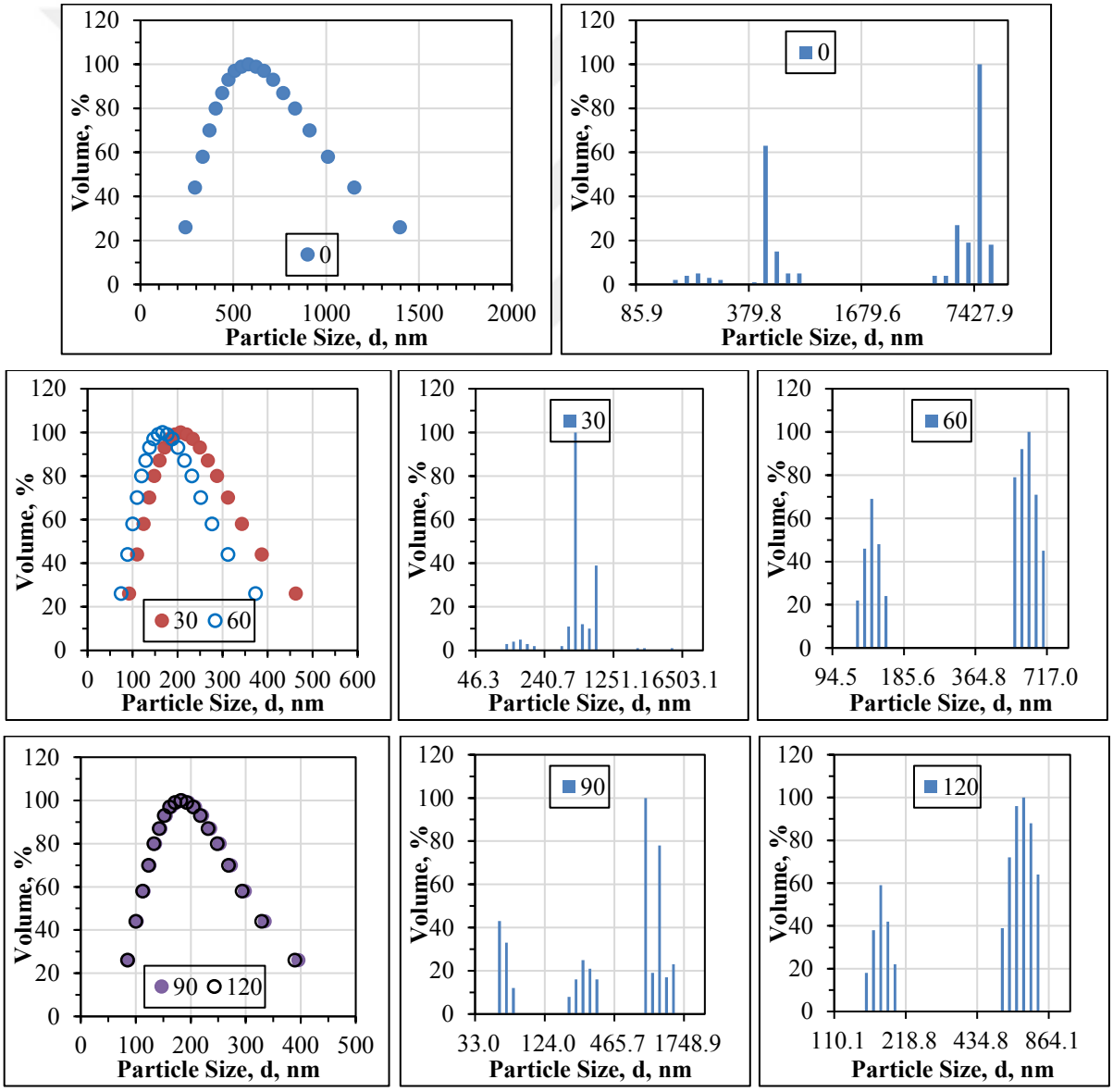


Figure 4.60. N-TiO_2 "as-is" under irradiation conditions volume profile: Time dependent comparative presentation of log Normal distribution and multi-size distribution of N-TiO_2 "as-is" under irradiation conditions particle size.

4.1.3.7. N-TiO_2 "as-is" under irradiation conditions surface area profile. Time dependent logN distribution G(d) and multi size distribution C(d) of N-TiO_2 "as-is" under irradiation conditions surface area profile was given in Figure 4.61. Time dependent mean diameter, range and min-max diameter difference with respect to log normal and multi-size distribution of N-TiO_2 "as-is" under irradiation conditions surface area profile was displayed in Table 4.39.

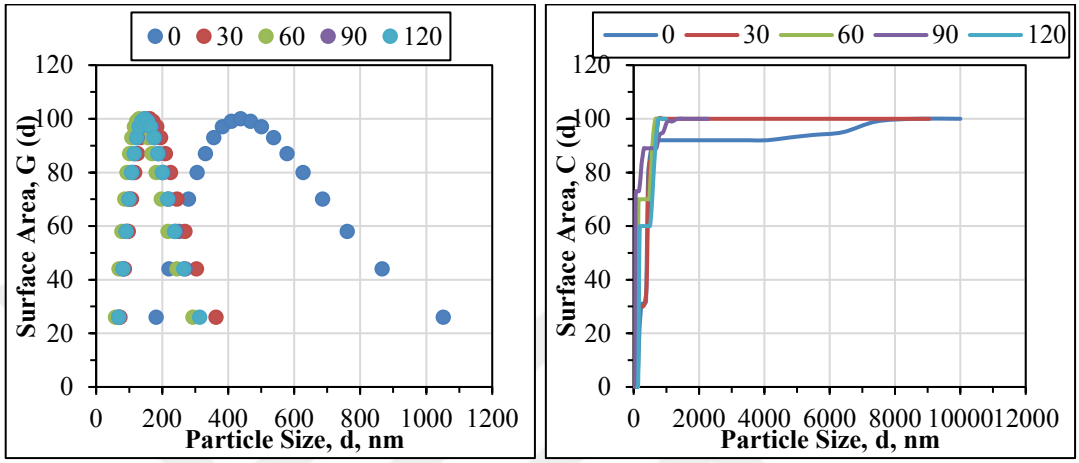


Figure 4.61. N-TiO_2 "as-is" under irradiation conditions surface area profile: Time dependent logN distribution G(d) and multi size distribution C(d).

Table 4.39. N-TiO_2 "as-is" under irradiation conditions surface area profile: Time dependent mean diameter, range and min-max diameter difference with respect to log normal and multi-size distribution.

N-TiO_2	time, min				
	0	30	60	90	120
Log Normal distribution					
Mean, nm	437.9	162.2	130.7	148.9	146.6
Range	182.3-1052.0	72.3-363.6	58.3-293.0	69.5-319.3	68.4-314.1
Difference	869.7	291.3	234.7	249.8	245.7
Multi-size distribution					
Max 1, nm	180.6	124.5	132.4	49.1	166.3
Max 2, nm	440.7	465.3	585.5	240.3	613.0
Max 3, nm	5517.4	763.0	-	790.6	-
Max 4, nm	7427.9	-	-	1030.2	-
Range	85.9-10.000	46.3-9042.5	94.5-820.7	33.0-2278.7	110.1-991.3
Difference	9914.1	8996.2	726.2	2245.7	881.2

According to log normal distribution, initial hydrodynamic particle size of N-TiO_2 "as-is" under irradiation conditions revealed as 437.9 nm. Upon 30 min, a sharp decrease was observed and detected to 162.2 nm. Correspondingly, continuous decrease was attained and detected to 146.6 nm

upon period of 120 min. Initial size difference between max and min diameter revealed as 869.7 nm and dropped to 245.7 nm upon 120 min. However, possible coinciding peaks that were monitored in log normal distribution could be easily discriminated by multi-size distribution. According to multi-size distribution, initially four peaks were observed and two peaks were obtained upon period of 120 min.

As explained for N-TiO_2 "as-is" under irradiation conditions volume profile (Figure 4.60), a similar approach was followed for N-TiO_2 "as-is" under irradiation conditions surface area profile. Time dependent comparative presentation of log Normal distribution and multi-size distribution of N-TiO_2 "as-is" under irradiation conditions surface area profile was exhibited in Figure 4.62.

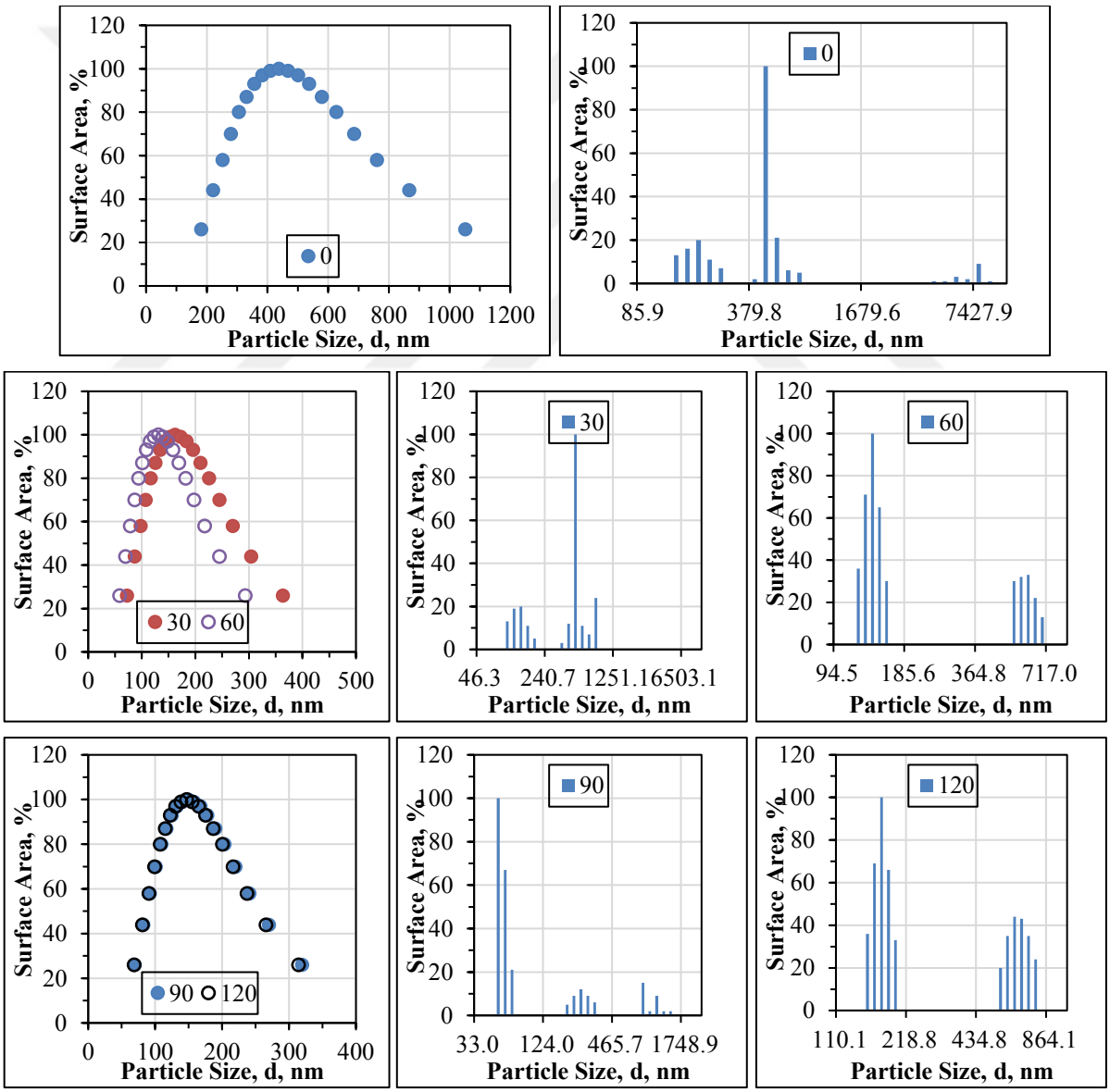


Figure 4.62. N-TiO_2 "as-is" under irradiation conditions surface area profile: Time dependent comparative presentation of log Normal distribution and multi-size distribution of N-TiO_2 "as-is" under irradiation conditions particle size.

4.1.3.8. N-TiO_2 "as-is" under irradiation conditions number profile. Time dependent logN distribution G(d) and multi size distribution C(d) of N-TiO_2 "as-is" under irradiation conditions number profile was demonstrated in Figure 4.63. Also, time dependent mean diameter, range and min-max diameter difference with respect to log normal and multi-size distribution of N-TiO_2 "as-is" under irradiation conditions number profile was exhibited in Table 4.40.

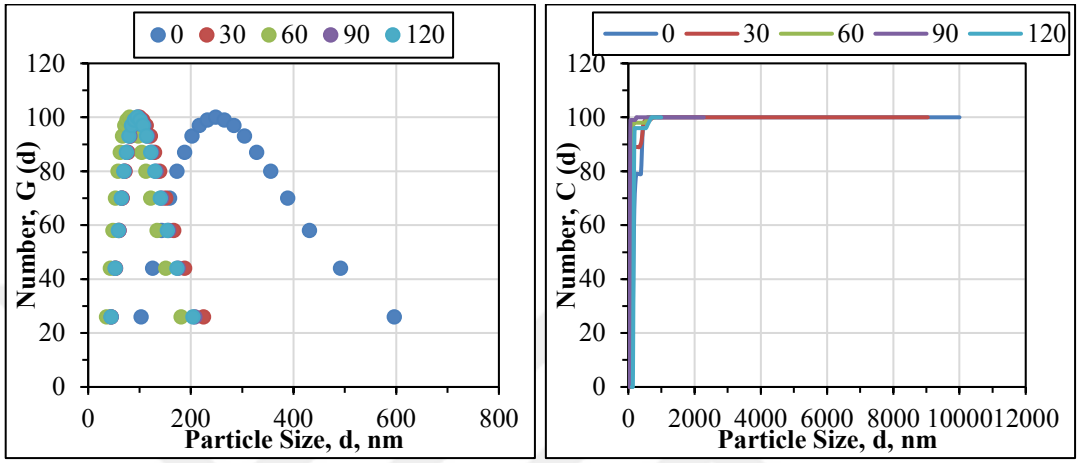


Figure 4.63. N-TiO_2 "as-is" under irradiation conditions number profile: Time dependent logN distribution G(d) and multi size distribution C(d).

Table 4.40. N-TiO_2 "as-is" under irradiation conditions number profile: Time dependent mean diameter, range and min-max diameter difference with respect to log normal and multi-size distribution.

N-TiO_2	time, min				
	0	30	60	90	120
Log Normal distribution					
Mean, nm	248.2	100.2	80.8	96.9	95.4
Range	103.3-596.3	44.7-224.6	36.0-181.1	45.2-207.7	44.5-204.4
Difference	493.0	179.9	145.1	162.5	159.9
Multi-size distribution					
Max 1, nm	134.2	105.6	132.4	49.1	166.3
Max 2, nm	440.7	465.3	511.5	240.3	572.3
Max 3, nm	-	763.0	547.2	-	613.0
Max 4, nm	-	-	585.5	-	656.5
Range	85.9-10.000	46.3-9042.5	94.5-820.7	33.0-2278.7	110.1-991.3
Difference	9914.1	8996.2	726.2	2245.7	881.2

In terms of number profile, it could be deduced that initially ~ 60 % decrease in hydrodynamic particle size. Initial hydrodynamic particle size was attained as 248.2 nm. Upon period of 30 min, hydrodynamic particle size was obtained as 100.2 nm and no significant variation was monitored

until the end of 120 min. Accordingly, initial size difference between min and max diameter revealed as 493.0 nm and detected to 159.9 nm with respect to time. Considering multi-size distribution, it could be inferred that initially two max diameters were observed and four peaks were obtained until the end of 120 min. Also, size difference decreased from 9914.1 nm to 881.2 nm upon period of 120 min.

As explained for N-TiO_2 "as-is" under irradiation conditions surface area profile (Figure 4.62), a similar approach was followed for N-TiO_2 "as-is" under irradiation conditions number profile. Time dependent comparative presentation of log Normal distribution and multi-size distribution of N-TiO_2 "as-is" under irradiation conditions number was given in Figure 4.64.

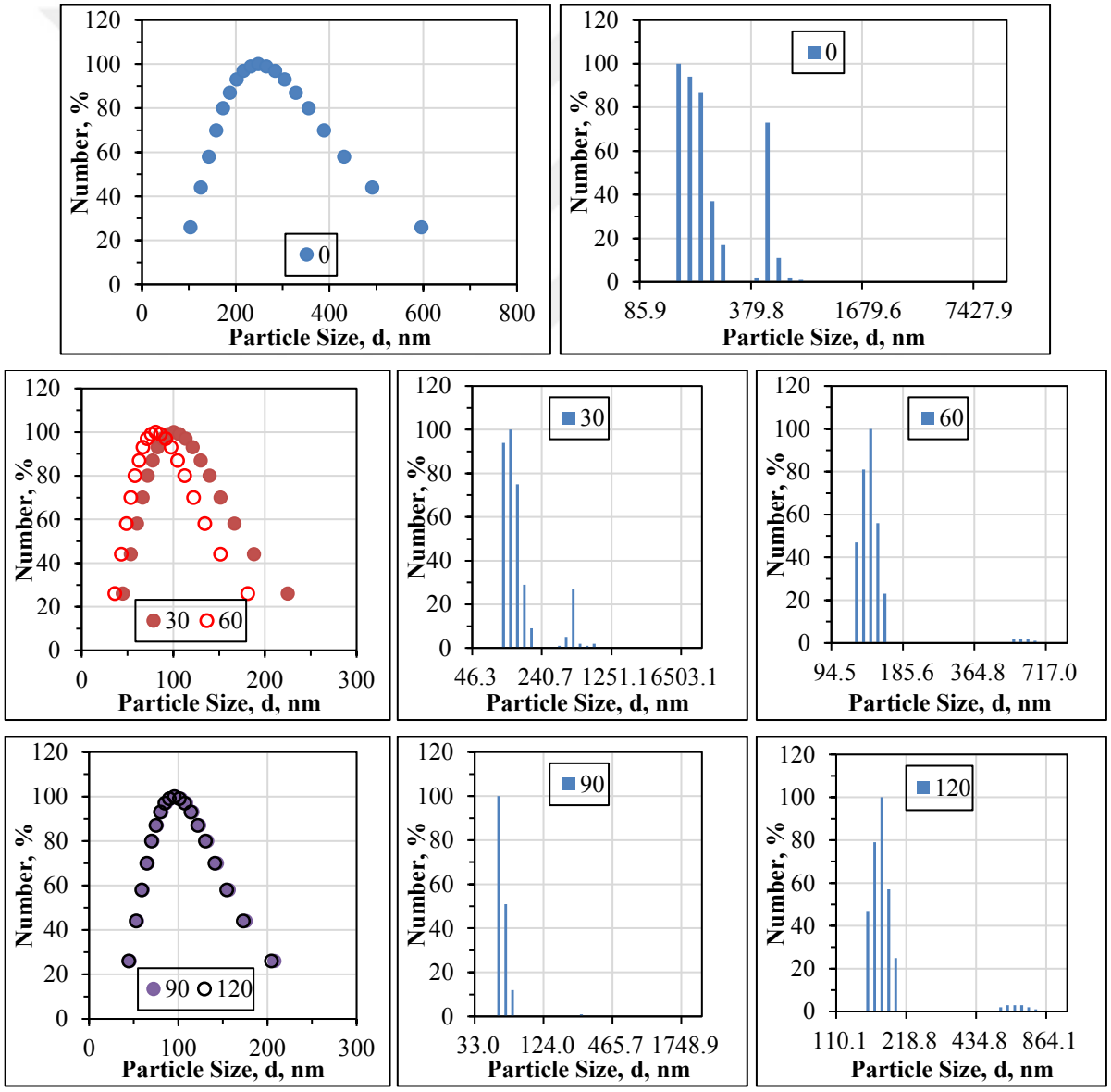


Figure 4.64. N-TiO_2 "as-is" under irradiation conditions number profile: Time dependent comparative presentation of log Normal distribution and multi-size distribution of N-TiO_2 "as-is" under irradiation conditions particle size.

4.1.3.9. Fe-TiO_2 "as-is" under irradiation conditions intensity profile. As explained for N-TiO_2 "as-is" under irradiation conditions (Figure 4.57), a similar approach was followed for Fe-TiO_2 "as-is" under irradiation conditions. Time dependent logN distribution G(d) and multi size distribution C(d) of Fe-TiO_2 "as-is" under irradiation conditions intensity profile was exhibited in Figure 4.65. Time dependent mean diameter, range and min-max diameter difference with respect to log normal and multi-size distribution of Fe-TiO_2 "as-is" under irradiation conditions intensity profile was presented in Table 4.41.

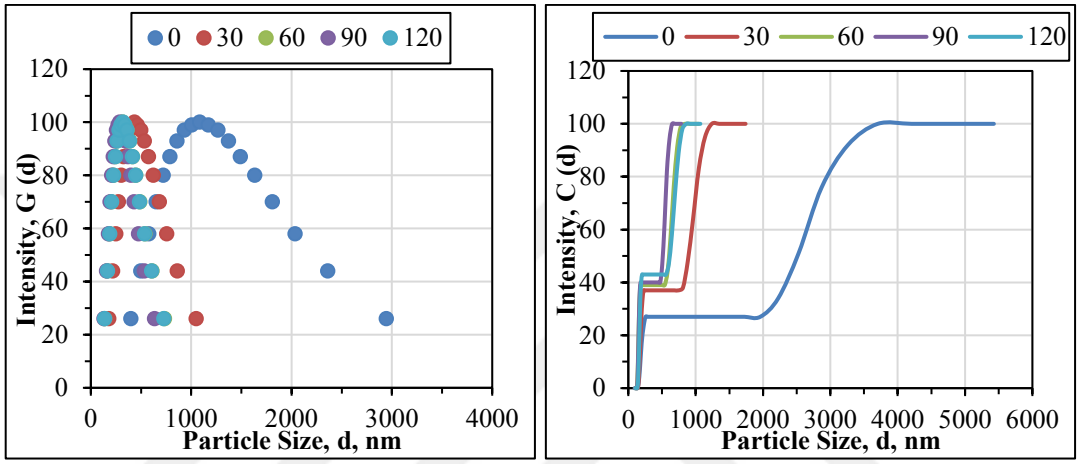


Figure 4.65. Fe-TiO_2 "as-is" under irradiation conditions intensity profile: Time dependent logN distribution G(d) and multi size distribution C(d).

Table 4.41. Fe-TiO_2 "as-is" under irradiation conditions intensity profile: Time dependent mean diameter, range and min-max diameter difference with respect to log normal and multi-size distribution.

Fe-TiO_2	time, min				
	0	30	60	90	120
Log Normal distribution					
Mean, nm	1085.6	434.0	316.9	289.0	318.6
Range	400.2-2944.9	179.5-1049.3	136.5-735.4	131.4-635.4	139.3-728.6
Difference	2544.7	869.8	598.9	504.0	589.3
Multi-size distribution					
Max 1, nm	197.9	191.6	156.1	160.0	176.8
Max 2, nm	2871.2	1046.2	673.7	572.7	694.5
Range	92.1-5428.1	115.2-1741.0	100.7-1044.7	102.4-787.7	106.8-1069.8
Difference	5336.0	1625.8	944.0	685.3	963.0

In terms of intensity profile, initial hydrodynamic size was recorded as 1085.6 nm. However, upon 30 min, almost 55 % decrease and then continuously decrease was observed until the end of

period. For comparison purposes, it could be inferred that two peaks were monitored along 120 min. Also, polydispersity of Fe-TiO_2 "as-is" under irradiation conditions was displayed in Table 4.42 and revealed a continuously decreasing trend during 120 min. Time dependent comparative presentation of log Normal distribution and multi-size distribution of Fe-TiO_2 "as-is" under irradiation conditions intensity profile was given in Figure 4.66.

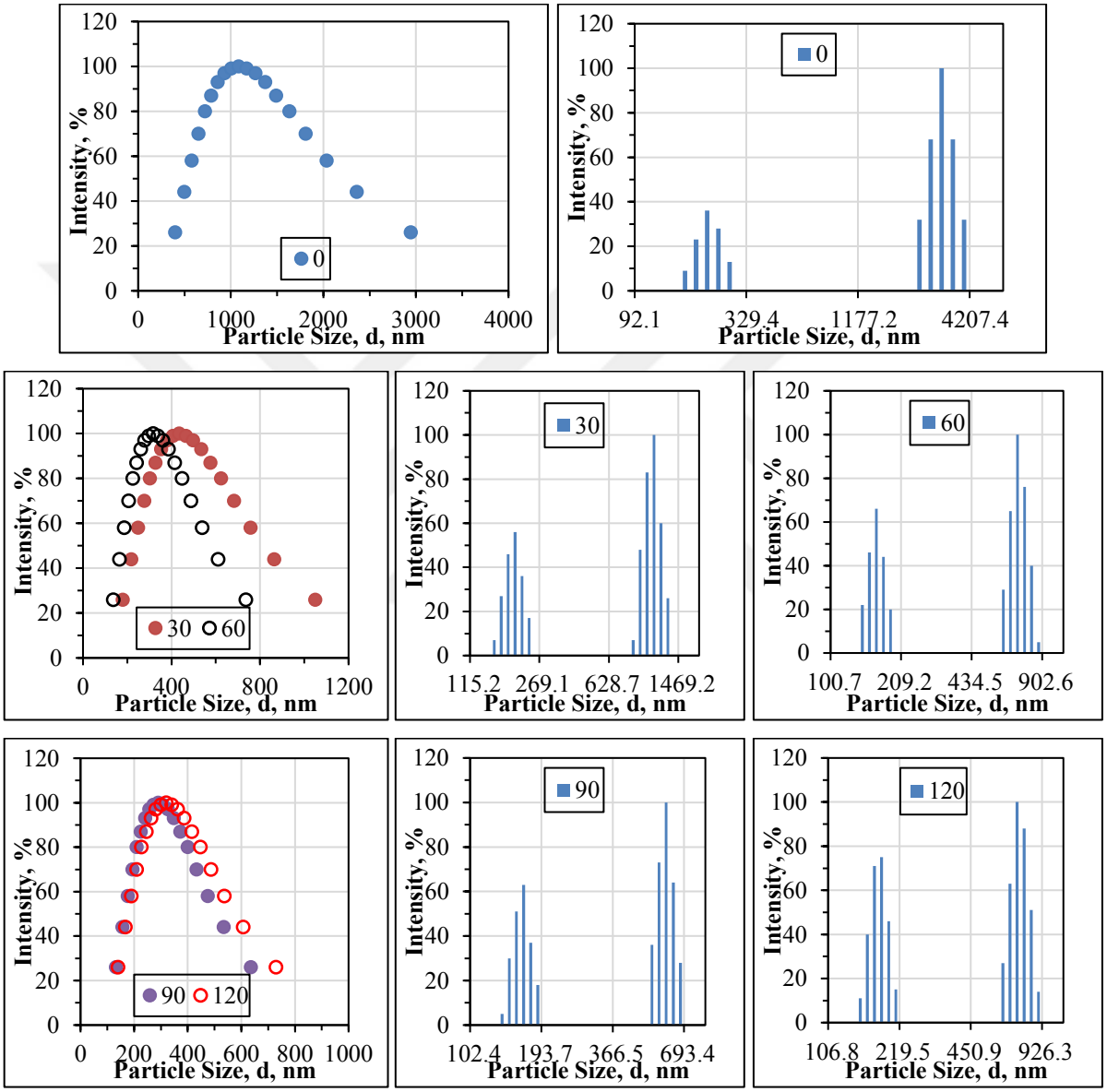


Figure 4.66. Fe-TiO_2 "as-is" under irradiation conditions intensity profile: Time dependent comparative presentation of log Normal distribution and multi-size distribution of Fe-TiO_2 "as-is" under irradiation conditions particle size.

Table 4.42. Polydispersity of Fe-TiO_2 "as-is" under irradiation conditions.

Fe-TiO_2	Polydispersity				
	0	30	60	90	120
	0.445	0.334	0.299	0.258	0.288

4.1.3.10. Fe-TiO_2 "as-is" under irradiation conditions volume profile. Time dependent logN distribution G(d) and multi size distribution C(d) of Fe-TiO_2 "as-is" under irradiation conditions volume profile was demonstrated in Figure 4.67. Time dependent mean diameter, range and min-max diameter difference with respect to log normal and multi-size distribution of Fe-TiO_2 "as-is" under irradiation conditions volume profile was displayed in Table 4.43.

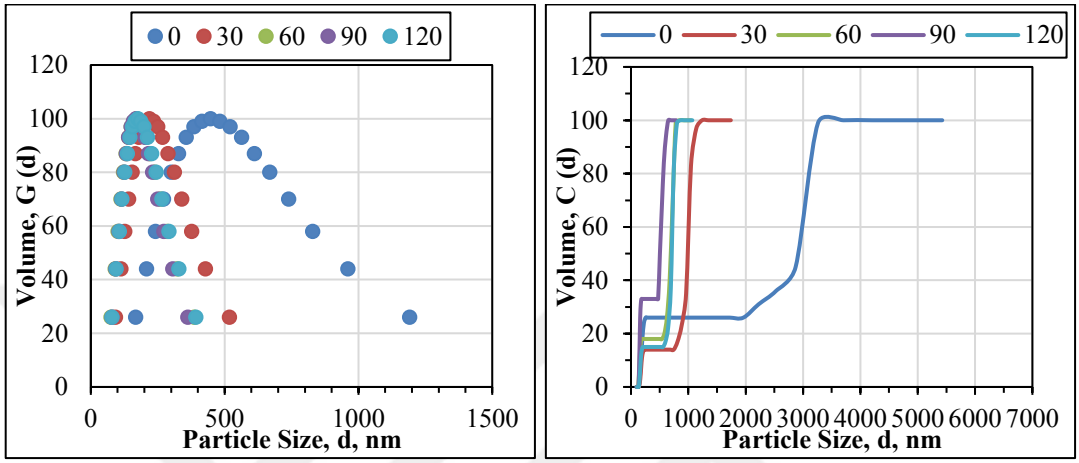


Figure 4.67. Fe-TiO_2 "as-is" under irradiation conditions volume profile: Time dependent logN distribution G(d) and multi size distribution C(d).

Table 4.43. Fe-TiO_2 "as-is" under irradiation conditions volume profile: Time dependent mean diameter, range and min-max diameter difference with respect to log normal and multi-size distribution.

Fe-TiO_2	time, min				
	0	30	60	90	120
Log Normal distribution					
Mean, nm	448.0	219.3	171.1	169.5	176.1
Range	168.3-1192.2	92.9-518.0	75.6-387.2	79.3-362.4	79.0-392.4
Difference	1023.9	425.1	311.6	283.1	313.4
Multi-size distribution					
Max 1, nm	197.9	176.0	156.1	160.0	164.5
Max 2, nm	3261.2	191.6	779.8	537.3	746.4
Max 3, nm	-	1046.2	-	572.7	-
Range	92.1-5428.1	115.2-1741.0	100.7-1044.7	102.4-787.7	106.8-1069.8
Difference	5336.0	1625.8	944.0	685.3	963.0

As elucidated for Fe-TiO_2 "as-is" under irradiation conditions intensity profile (Table 4.41), a similar approach was followed for Fe-TiO_2 "as-is" under irradiation conditions volume profile. It could be deduced that hydrodynamic particle size approximately 50 % decreased upon 30 min. Initial hydrodynamic particle size was recorded as 448.0 nm and reached to 219.3 nm upon 30 min.

Accordingly, continuously decrease was monitored with slight variations until the end of 120 min. Also, difference between max and min diameter was attained as 1023.9 nm and detected to 313.4 nm upon 120 min. However, in terms of multi-size distribution, initially two peaks were monitored and three peaks were attained upon 30 min. Size difference was obtained as 5336.0 nm and detected to 963.0 nm upon 120 min.

As explained for Fe-TiO_2 "as-is" under irradiation conditions intensity profile (Figure 4.66), time dependent comparative presentation of log Normal distribution and multi-size distribution of Fe-TiO_2 "as-is" under irradiation conditions volume profile was displayed in Figure 4.68.

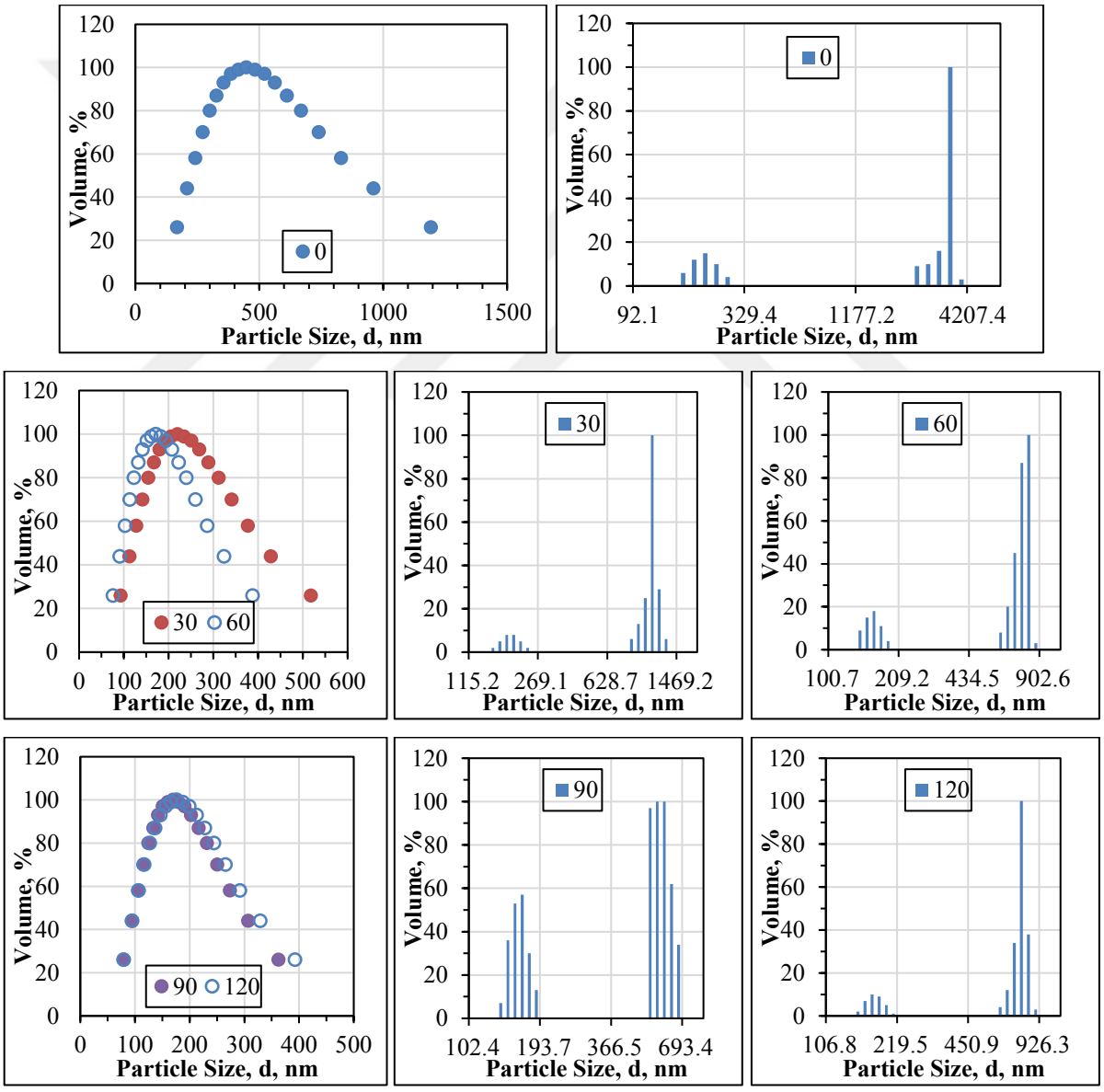


Figure 4.68. Fe-TiO_2 "as-is" under irradiation conditions volume profile: Time dependent comparative presentation of log Normal distribution and multi-size distribution of Fe-TiO_2 "as-is" under irradiation conditions particle size.

4.1.3.11. Fe-TiO_2 "as-is" under irradiation conditions surface area profile. As described for Fe-TiO_2 "as-is" under irradiation conditions volume profile (Figure 4.67), a similar approach was followed for Fe-TiO_2 "as-is" under irradiation conditions surface area profile. Time dependent logN distribution G(d) and multi size distribution C(d) of Fe-TiO_2 "as-is" under irradiation conditions surface area profile was displayed in Figure 4.69. Time dependent mean diameter, range and min-max diameter difference with respect to log normal and multi-size distribution of Fe-TiO_2 "as-is" under irradiation conditions surface area profile was exhibited in Table 4.44.

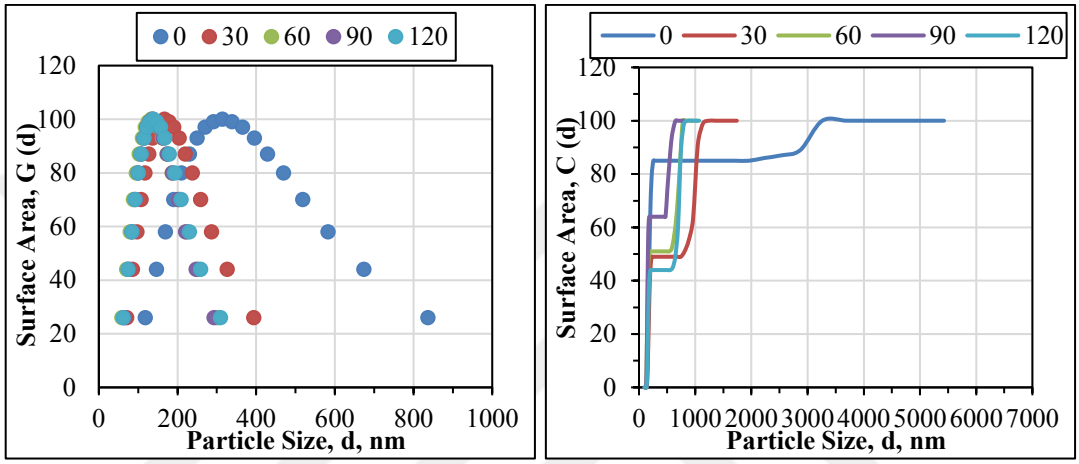


Figure 4.69. Fe-TiO_2 "as-is" under irradiation conditions surface area profile: Time dependent logN distribution G(d) and multi size distribution C(d).

Table 4.44. Fe-TiO_2 "as-is" under irradiation conditions surface area profile: Time dependent mean diameter, range and min-max diameter difference with respect to log normal and multi-size distribution.

Fe-TiO_2	time, min				
	0	30	60	90	120
Log Normal distribution					
Mean, nm	314.4	166.9	133.8	137.0	138.9
Range	118.1-836.7	70.7-394.2	59.1-302.7	64.1-292.8	62.3-309.5
Difference	718.6	323.5	243.6	228.7	247.2
Multi-size distribution					
Max 1, nm	197.9	176.0	156.1	160.0	164.5
Max 2, nm	3261.2	1046.2	779.8	504.1	746.4
Range	92.1-5428.1	115.2-1741.0	100.7-1044.7	102.4-787.7	106.8-1069.8
Difference	5336.0	1625.8	944.0	685.3	963.0

In terms of surface area profile, it could be inferred that hydrodynamic particle size of Fe-TiO_2 "as-is" under irradiation conditions was obtained as 314.4 nm. Upon 30 min, a sharp decrease was

observed and slight variations remained until the end of 120 min. On the other hand, difference between max and min diameter revealed roughly 50 % decrease in the first 30 min. Upon 30 min, continuously decrease was monitored along 120 min. However, in terms of multi-size distribution, two max diameters were attained during 120 min.

In a similar manner, time dependent comparative presentation of log Normal distribution and multi-size distribution of Fe-TiO_2 "as-is" under irradiation conditions surface area profile was demonstrated in Figure 4.70.

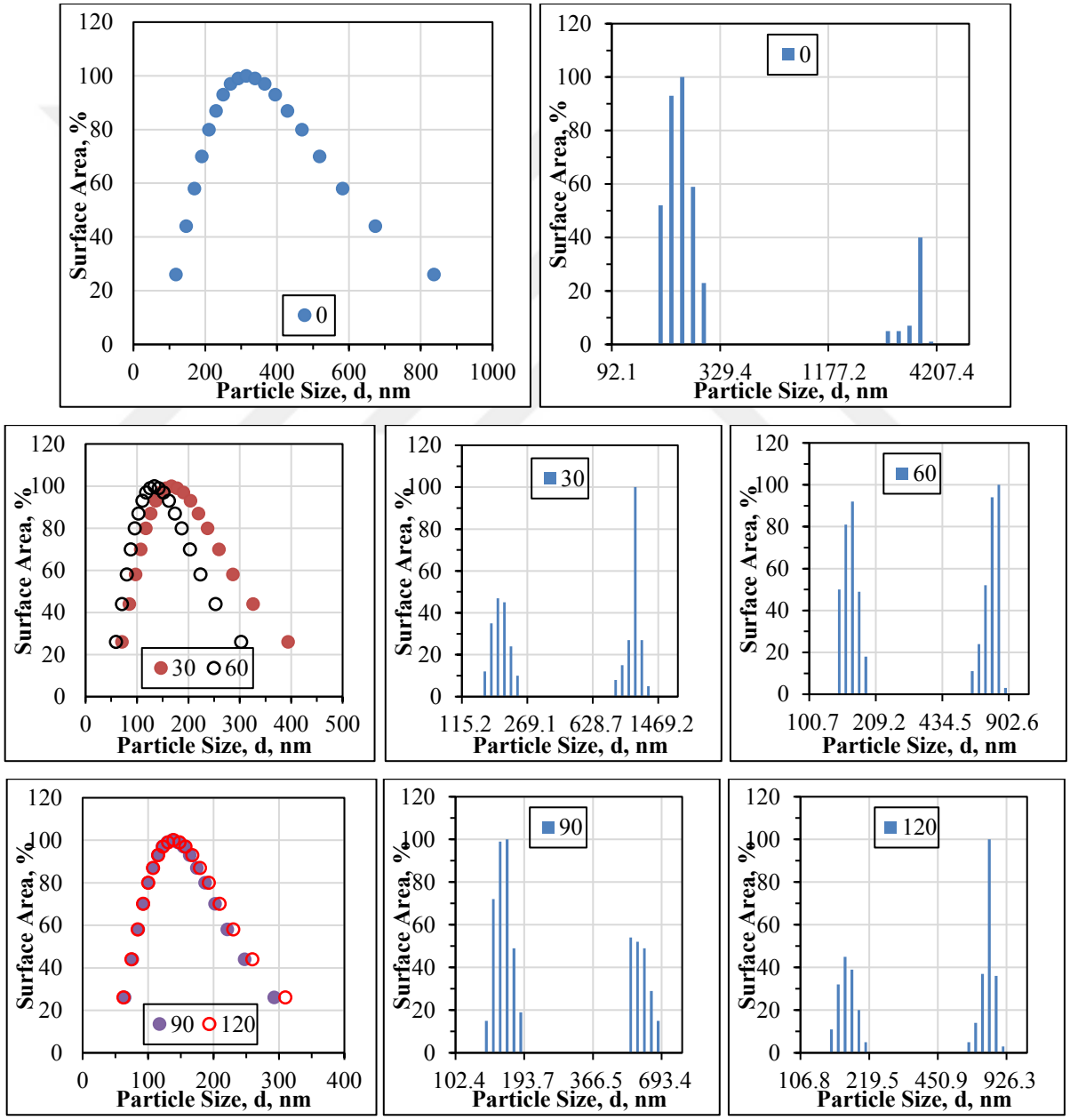


Figure 4.70. Fe-TiO_2 "as-is" under irradiation conditions surface area profile: Time dependent comparative presentation of log Normal distribution and multi-size distribution of Fe-TiO_2 "as-is" under irradiation conditions particle size.

4.1.3.12. Fe-TiO_2 "as-is" under irradiation conditions number profile. In a similar manner to data depicted Fe-TiO_2 "as-is" under irradiation conditions surface area profile (Figure 4.69), time dependent logN distribution G(d) and multi size distribution C(d) of Fe-TiO_2 "as-is" under irradiation conditions number profile was given in Figure 4.71. Time dependent mean diameter, range and min-max diameter difference with respect to log normal and multi-size distribution of Fe-TiO_2 "as-is" under irradiation conditions number profile was shown in Table 4.45.

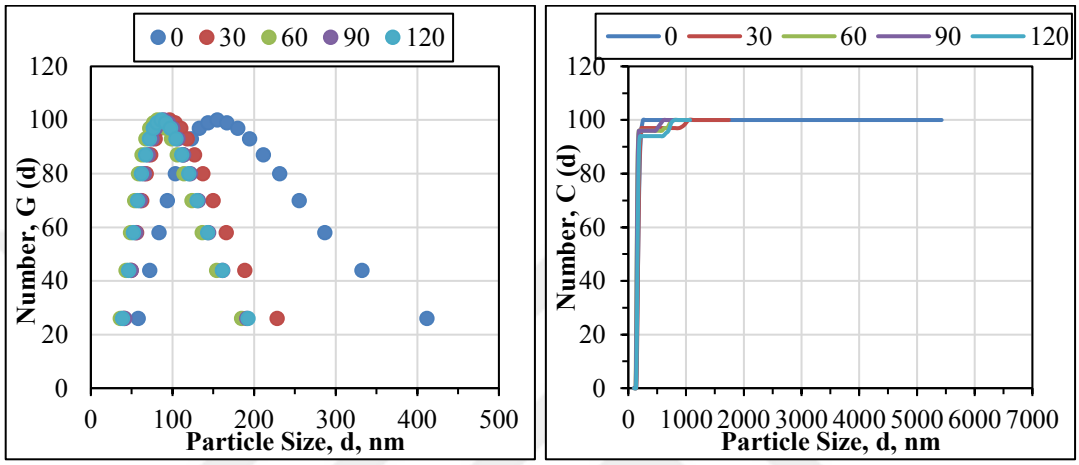


Figure 4.71. Fe-TiO_2 "as-is" under irradiation conditions number profile: Time dependent logN distribution G(d) and multi size distribution C(d).

Table 4.45. Fe-TiO_2 "as-is" under irradiation conditions number profile: Time dependent mean diameter, range and min-max diameter difference with respect to log normal and multi-size distribution.

Fe-TiO_2	time, min				
	0	30	60	90	120
Log Normal distribution					
Mean, nm	154.9	96.7	81.7	89.4	86.4
Range	58.2-412.1	40.9-228.4	36.1-184.9	41.8-191.1	38.8-192.6
Difference	353.9	187.5	148.8	149.3	153.8
Multi-size distribution					
Max 1, nm	174.2	176.0	145.1	150.1	164.5
Max 2, nm	-	1046.2	724.8	504.1	746.4
Range	92.1-5428.1	115.2-1741.0	100.7-1044.7	102.4-787.7	106.8-1069.8
Difference	5336.0	1625.8	944.0	685.3	963.0

In terms of number profile, it could be deduced that hydrodynamic particle size of Fe-TiO_2 "as-is" under irradiation conditions was attained as 154.9 nm. Upon 30 min, approximately 40 % decrease was monitored and slight variations remained until the end of 120 min. On the other hand, in the first

30 min, roughly 50 % decrease was obtained in terms of difference between max and min diameter. Upon 30 min, continuously decrease was observed along 120 min. For comparison purposes, in terms of multi-size distribution, two max diameters were attained during 120 min. Due to multi-size distribution, possible coinciding peaks were easily discriminated from hydrodynamic particle size that was attained by log normal distribution.

Following a similar manner, time dependent comparative presentation of log Normal distribution and multi-size distribution of Fe-TiO_2 "as-is" under irradiation conditions number profile was presented in Figure 4.72.

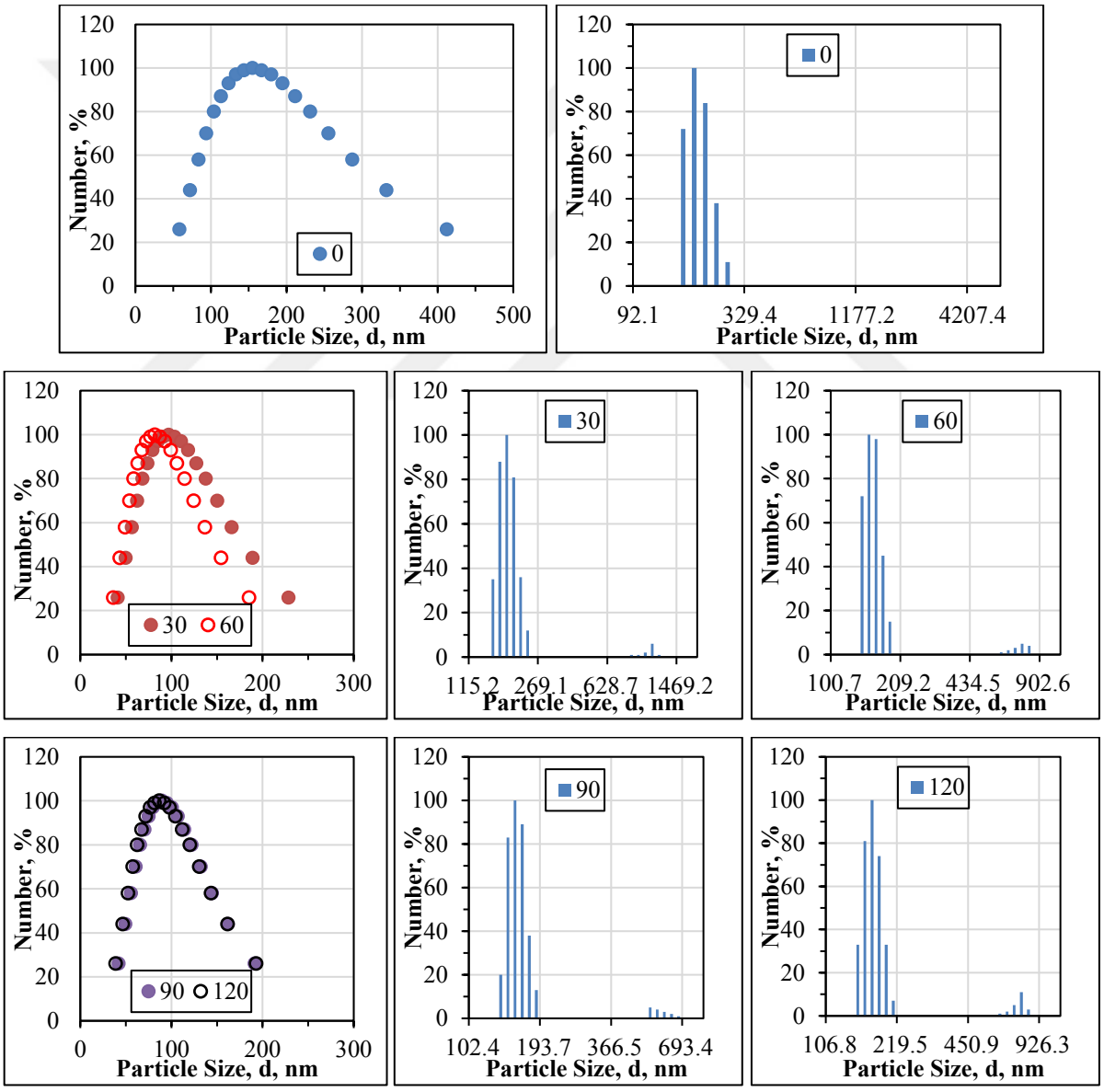


Figure 4.72. Fe-TiO_2 "as-is" under irradiation conditions number profile: Time dependent comparative presentation of log Normal distribution and multi-size distribution of Fe-TiO_2 "as-is" under irradiation conditions particle size.

4.1.4. Binary System: As-is Conditions

As explained for mono system under "as-is" conditions (Section 4.1.1), in a similar manner, the explication of the hydrodynamic particle size of the nanoparticles were also presented under "as-is" conditions separately *i.e.* "TiO_2 and HA" binary system, "TiO_2 and SRNOM" binary system, "N-TiO_2 and HA" binary system, "N-TiO_2 and SRNOM" binary system, "Fe-TiO_2 and HA" binary system, "Fe-TiO_2 and SRNOM" binary system. Simply, data represented time dependent hydrodynamic size variations in terms of intensity, volume, surface area, and number parameters. Particle size distribution will be presented in two modes as mono-size and multi-size distribution.

4.1.4.1. "TiO_2 and HA" binary system under "as-is" conditions intensity profile. Time dependent logN distribution G(d) and multi size distribution C(d) of TiO_2 and HA" binary system under "as-is" conditions intensity profile was exhibited in Figure 4.73.

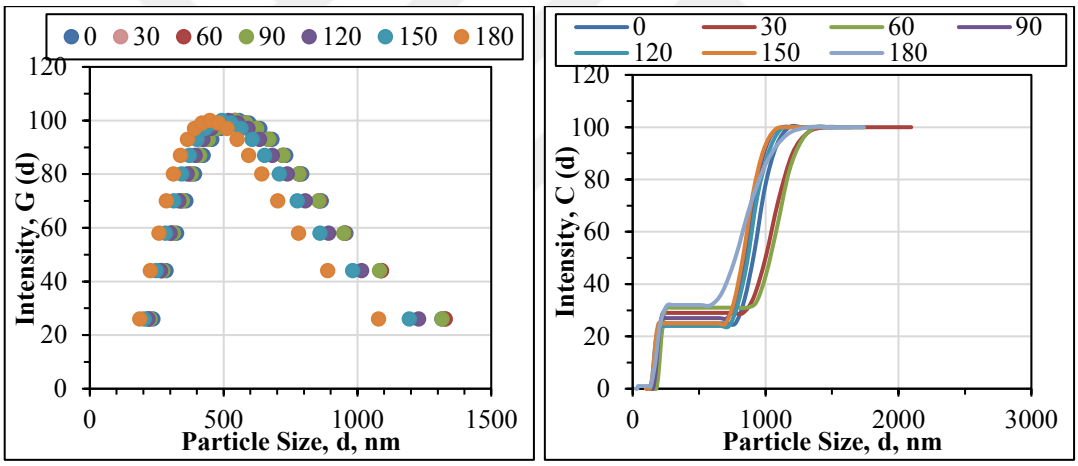


Figure 4.73. "TiO_2 and HA" binary system under "as-is" conditions intensity profile: Time dependent logN distribution G(d) and multi size distribution C(d).

In a similar manner to data depicted TiO_2 under "as-is" conditions intensity profile (Figure 4.1), log normal distribution G(d) and multi size distribution C(d) of "TiO_2 and HA" binary system under "as-is" conditions intensity profile was demonstrated with respect to time. It could be seen that hydrodynamic particle size of "TiO_2 and HA" binary system under "as-is" conditions displayed a slightly decreasing trend according to time variations. In terms of log normal distribution, it could be inferred that certain peaks were observed coinciding max diameters. However, due to multi-size distribution, each max diameter could be easily separated. Also, size difference could be seen from both of two modes. Time dependent comparative presentation of log Normal distribution and multi-

size distribution of "TiO_2 and HA" binary system under "as-is" conditions intensity profile was displayed in Figure 4.74.

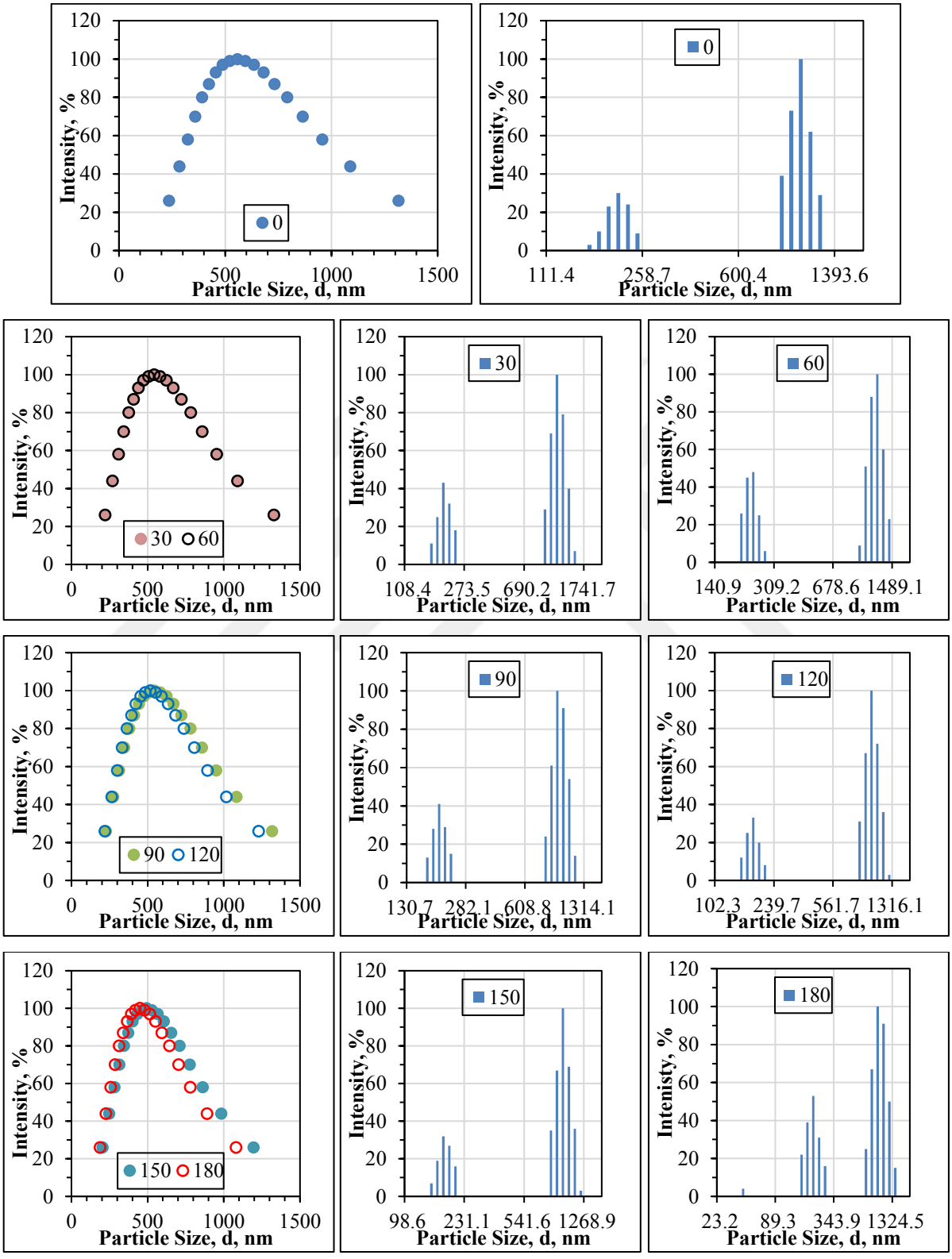


Figure 4.74. "TiO_2 and HA" binary system under "as-is" conditions intensity profile: Time dependent comparative presentation of log Normal distribution and multi-size distribution of "TiO_2 and HA" binary system under "as-is" conditions.

Based on the data displayed in Figure 4.73 and 4.74., time dependent mean diameter, range and min-max diameter difference with respect to log normal and multi-size distribution of "TiO_2 and HA" binary system under "as-is" conditions intensity profile was exhibited in Table 4.46.

Table 4.46. "TiO_2 and HA" binary system under "as-is" conditions intensity profile: Time dependent mean diameter, range and min-max diameter difference with respect to log normal and multi-size distribution.

TiO_2 and HA	time, min						
	0	30	60	90	120	150	180
Log Normal distribution							
Mean, nm	557.2	542.0	544.4	517.9	511.5	493.2	448.5
Range	236.0-1315.7	221.2-1328.0	225.2-1316.0	218.3-1228.8	210.5-1243.1	203.6-1194.6	186.5-1078.9
Difference	1079.7	1106.8	1090.8	1010.5	1032.6	991.0	892.4
Multi-size distribution							
Max 1, nm	200.9	188.9	225.8	192.0	170.5	164.4	39.8
Max 2, nm	995.1	1096.4	1176.3	894.5	936.2	902.7	200.6
Max 3, nm	-	-	-	-	-	-	883.9
Range	111.4-1649.2	108.4-2095.9	140.9-1742.5	130.7-1532.8	102.3-1560.4	98.6-1504.5	23.2-1734.6
Difference	1537.8	1987.5	1601.6	1402.1	1458.1	1405.9	1711.4

According to log normal distribution, initial hydrodynamic size of "TiO_2 and HA" binary system under "as-is" conditions was obtained as 557.2 nm. During 180 min, the hydrodynamic size of "TiO_2 and HA" followed a slightly decreasing trend and detected to 448.5 nm. Correspondingly, hydrodynamic size difference decreased from 1079.7 nm to 892.4 nm with respect to time. However, in terms of multi-size distribution, two max diameters were obtained as 200.9 nm and 995.1 nm for "TiO_2 and HA" binary system under "as-is" conditions following initial period of time. Two peaks were observed until 180 min. Upon 180 min, one peak was obtained as 883.9 nm. Initial size difference between max and min diameter was attained as 1537.8 nm and reached to 1711.4 nm at the end of 180 min.

Polydispersity of "TiO_2 and HA" binary system under "as-is" conditions was given in Table 4.47. It could be inferred that slowly decreasing trend was monitored over period of 180 min. Simply an average value of 0.331 could be regarded as suitable for expressing polydispersity.

Table 4.47. Polydispersity of "TiO_2 and HA" binary system under "as-is" conditions.

TiO_2 and HA	Polydispersity						
	0	30	60	90	120	150	180
	0.314	0.346	0.334	0.318	0.338	0.335	0.329

4.1.4.2. "TiO_2 and HA" binary system under "as-is" conditions volume profile. Time dependent logN distribution G(d) and multi size distribution C(d) of "TiO_2 and HA" binary system under "as-is" conditions volume profile was exhibited in Figure 4.75 and related parameters were given in Table 4.48.

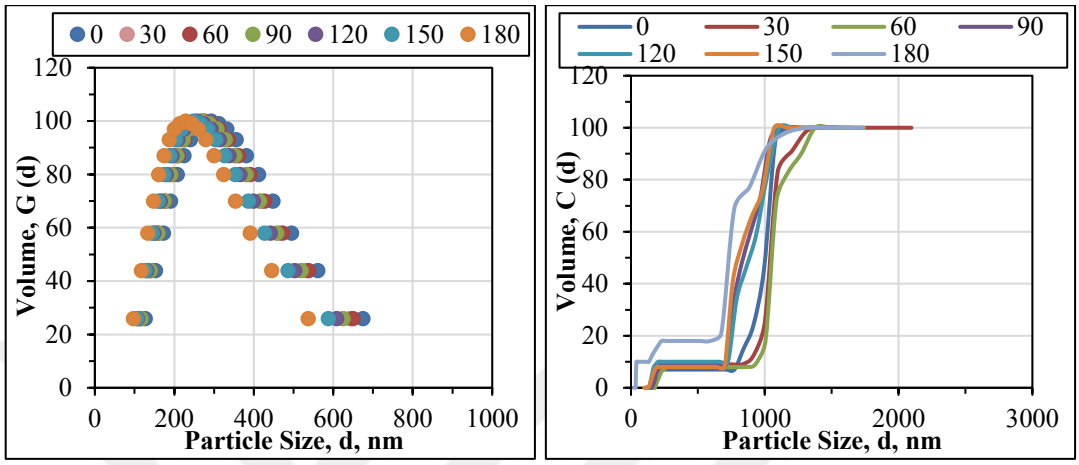


Figure 4.75. "TiO_2 and HA" binary system under "as-is" conditions volume profile: Time dependent logN distribution G(d) and multi size distribution C(d).

Table 4.48. "TiO_2 and HA" binary system under "as-is" conditions volume profile: Time dependent mean diameter, range and min-max diameter difference with respect to log normal and multi-size distribution.

TiO_2 and HA	time, min						
	0	30	60	90	120	150	180
Log Normal distribution							
Mean, nm	292.7	267.9	275.2	269.9	256.4	248.6	228.6
Range	127.0-674.5	111.9-641.6	116.6-649.9	116.6-625.1	108.0-608.7	105.1-588.1	97.3-537.1
Difference	547.5	529.7	533.3	508.5	500.7	483.0	439.8
Multi-size distribution							
Max 1, nm	184.7	188.9	208.8	192.0	170.5	164.4	39.8
Max 2, nm	200.9	1096.4	225.8	766.9	789.6	761.3	175.3
Max 3, nm	1082.5	-	1087.4	1043.3	1019.4	-	200.6
Max 4, nm	-	-	-	-	-	-	772.4
Max 5, nm	-	-	-	-	-	-	1011.5
Range	111.4-1649.2	108.4-2095.9	140.9-1742.5	130.7-1532.8	102.3-1560.4	98.6-1504.5	23.2-1734.6
Difference	1537.8	1987.5	1601.6	1402.1	1458.1	1405.9	1711.4

Hydrodynamic size of "TiO_2 and HA" exhibited a slightly decreasing trend with respect to time. Size difference was decreased from 547.5 nm to 439.8 nm during 180 min. Considering multi-size distribution, initially three peaks were monitored and five peaks were observed upon 180 min.

Time dependent comparative presentation of log Normal distribution and multi-size distribution of "TiO_2 and HA" binary system under "as-is" conditions volume profile was given in Figure 4.76.

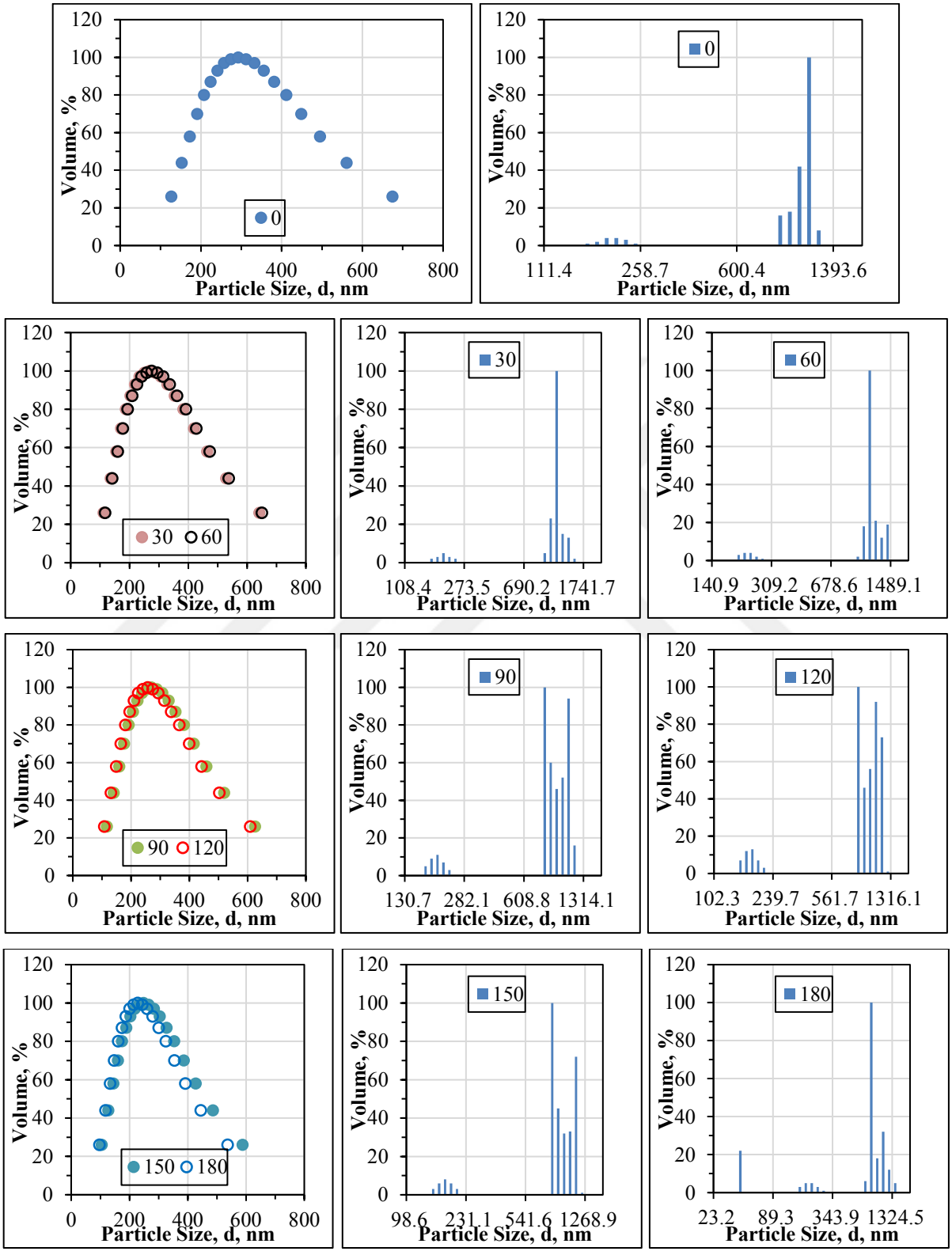


Figure 4.76. "TiO_2 and HA" binary system under "as-is" conditions volume profile: Time dependent comparative presentation of log Normal distribution and multi-size distribution of "TiO_2 and HA" binary system under "as-is" conditions.

4.1.4.3. "TiO_2 and HA" binary system under "as-is" conditions surface area profile. Time dependent logN distribution G(d) and multi size distribution C(d) of "TiO_2 and HA" binary system under "as-is" conditions surface area profile was exhibited in Figure 4.77. Time dependent mean diameter, range and min-max diameter difference with respect to log normal and multi-size distribution of "TiO_2 and HA" binary system under "as-is" conditions surface area profile was demonstrated in Table 4.49.

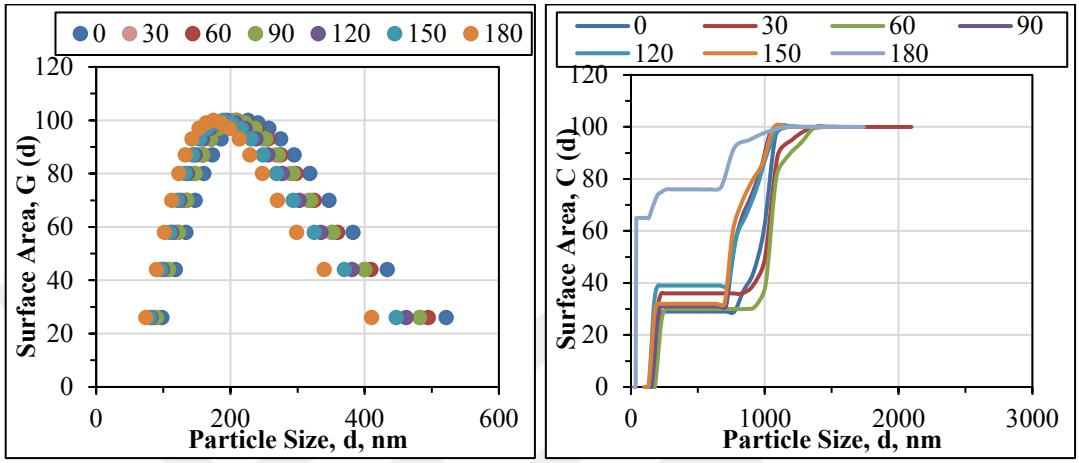


Figure 4.77. "TiO_2 and HA" binary system under "as-is" conditions surface area profile: Time dependent logN distribution G(d) and multi size distribution C(d).

Table 4.49. "TiO_2 and HA" binary system under "as-is" conditions surface area profile: Time dependent mean diameter, range and min-max diameter difference with respect to log normal and multi-size distribution.

TiO_2 and HA	time, min						
	0	30	60	90	120	150	180
Log Normal distribution							
Mean, nm	226.3	202.1	209.5	208.0	194.5	189.0	174.6
Range	98.2-521.4	84.4-484.0	88.7-494.7	89.8-481.7	81.9-461.7	79.9-447.1	74.3-410.2
Difference	423.2	399.6	406.0	391.9	379.8	367.2	335.9
Multi-size distribution							
Max 1, nm	184.7	188.9	208.8	192.0	170.5	164.4	39.8
Max 2, nm	200.9	1096.4	1087.4	766.9	789.6	761.3	175.3
Max 3, nm	1082.5	-	-	1043.3	1019.4	1070.2	772.4
Max 4, nm	-	-	-	-	-	-	1011.5
Range	111.4-1649.2	108.4-2095.9	140.9-1742.5	130.7-1532.8	102.3-1560.4	98.6-1504.5	23.2-1734.6
Difference	1537.8	1987.5	1601.6	1402.1	1458.1	1405.9	1711.4

In terms of surface area profile, continuous decrease was observed until the end of period. Also, three peaks were observed in terms of multi-size distribution along 180 min. Time dependent

comparative presentation of log Normal distribution and multi-size distribution of "TiO_2 and HA" binary system under "as-is" conditions surface area was presented in Figure 4.78.

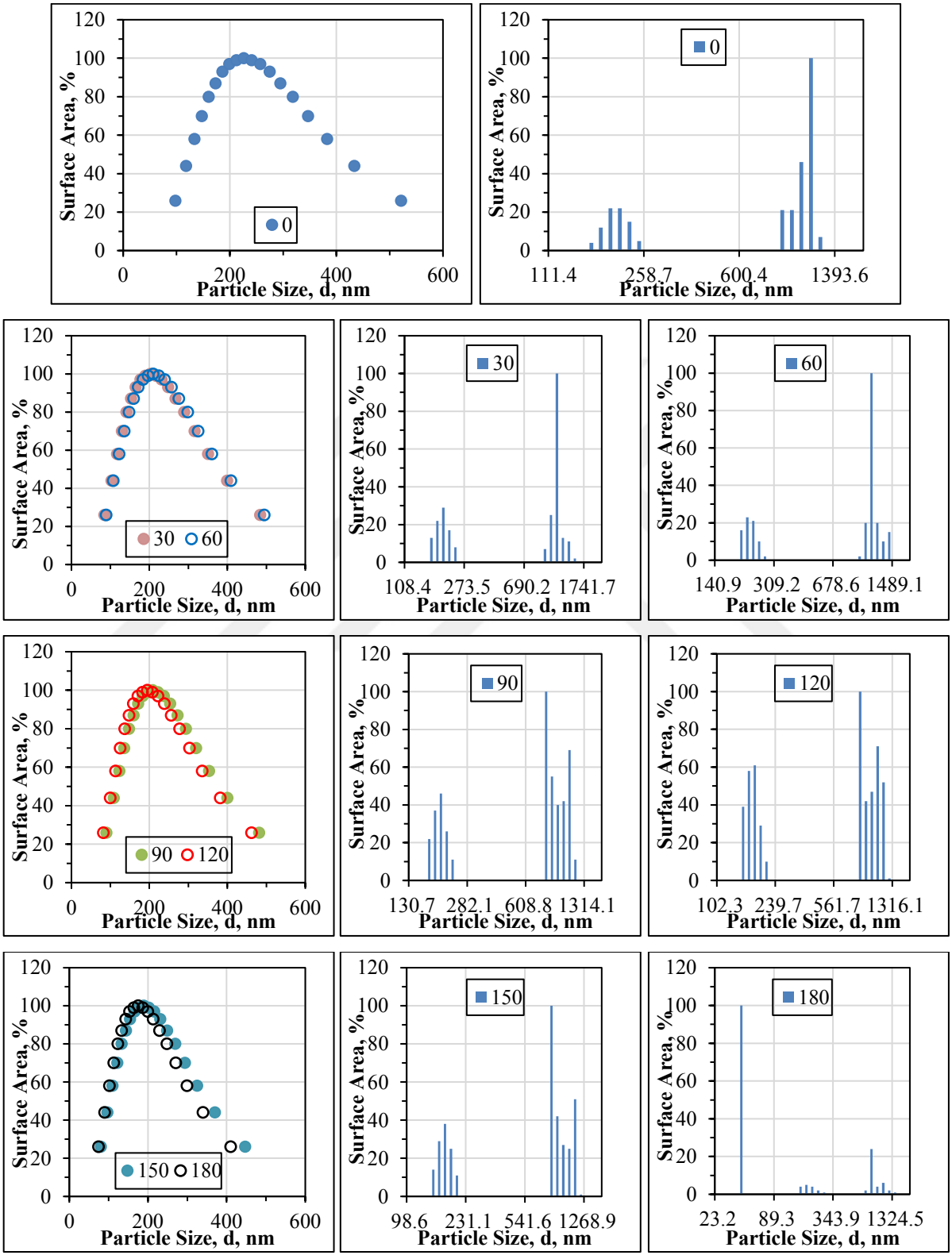


Figure 4.78. "TiO_2 and HA" binary system under "as-is" conditions surface area profile: Time dependent comparative presentation of log Normal distribution and multi-size distribution of "TiO_2 and HA" binary system under "as-is" conditions.

4.1.4.4. "TiO_2 and HA" binary system under "as-is" conditions number profile. Time dependent logN distribution G(d) and multi size distribution C(d) of "TiO_2 and HA" binary system under "as-is" conditions number profile was displayed in Figure 4.79. Time dependent mean diameter, range and min-max diameter difference with respect to log normal and multi-size distribution of "TiO_2 and HA" binary system under "as-is" conditions number profile was given in Table 4.50.

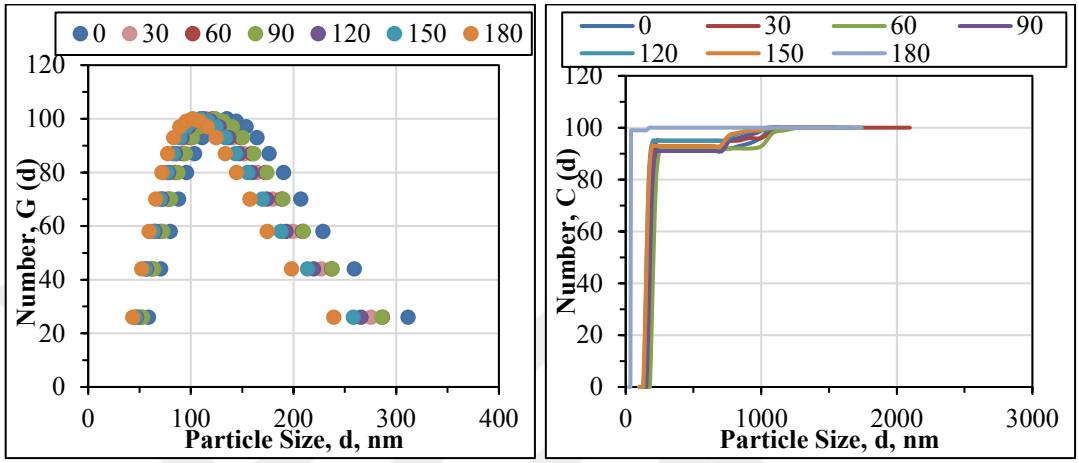


Figure 4.79. "TiO_2 and HA" binary system under "as-is" conditions number profile: Time dependent logN distribution G(d) and multi size distribution C(d).

Table 4.50. "TiO_2 and HA" binary system under "as-is" conditions number profile: Time dependent mean diameter, range and min-max diameter difference with respect to log normal and multi-size distribution.

TiO_2 and HA	time, min						
	0	30	60	90	120	150	180
Log Normal distribution							
Mean, nm	135.2	115.0	121.4	123.5	111.9	109.2	101.9
Range	58.7-311.5	48.0-275.5	51.4-286.7	53.3-286.0	47.1-265.7	46.2-258.4	43.4-239.3
Difference	252.8	227.5	235.3	232.7	218.6	212.2	195.9
Multi-size distribution							
Max 1, nm	184.7	188.9	208.8	192.0	156.6	164.4	39.8
Max 2, nm	1082.5	1096.4	1087.4	766.9	789.6	761.3	-
Max 3, nm	-	-	-	1043.3	1019.4	1070.2	-
Range	111.4-1649.2	108.4-2095.9	140.9-1742.5	130.7-1532.8	102.3-1560.4	98.6-1504.5	23.2-1734.6
Difference	1537.8	1987.5	1601.6	1402.1	1458.1	1405.9	1711.4

In terms of number profile, hydrodynamic particle size of "TiO_2 and HA" binary system under "as-is" conditions revealed a slowly decreasing trend along 180 min. However, in terms of multi-size distribution, two peaks were obtained during 180 min. Time dependent comparative presentation of

log Normal distribution and multi-size distribution of "TiO_2 and HA" binary system under "as-is" conditions number profile was exhibited in Figure 4.80.

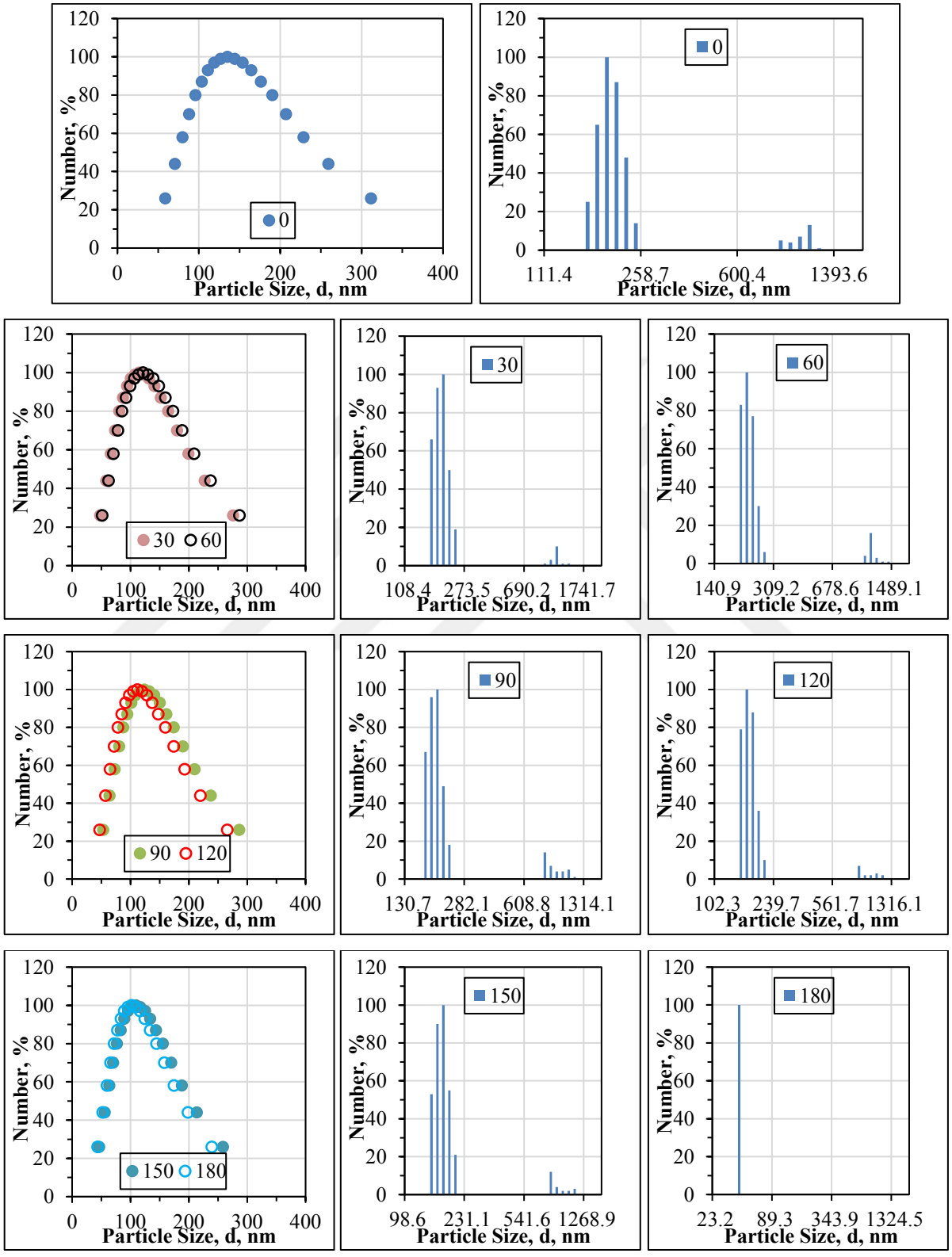


Figure 4.80. "TiO_2 and HA" binary system under "as-is" conditions number profile: Time dependent comparative presentation of log Normal distribution and multi-size distribution of "TiO_2 and HA" binary system under "as-is" conditions.

4.1.4.5. "TiO_2 and SRNOM" binary system under "as-is" conditions intensity profile. Time dependent logN distribution G(d) and multi size distribution C(d) of "TiO_2 and SRNOM" binary system under "as-is" conditions intensity profile was displayed in Figure 4.81. Time dependent mean diameter, range and min-max diameter difference with respect to log normal and multi-size distribution of "TiO_2 and SRNOM" binary system under "as-is" conditions intensity profile was given in Table 4.51.

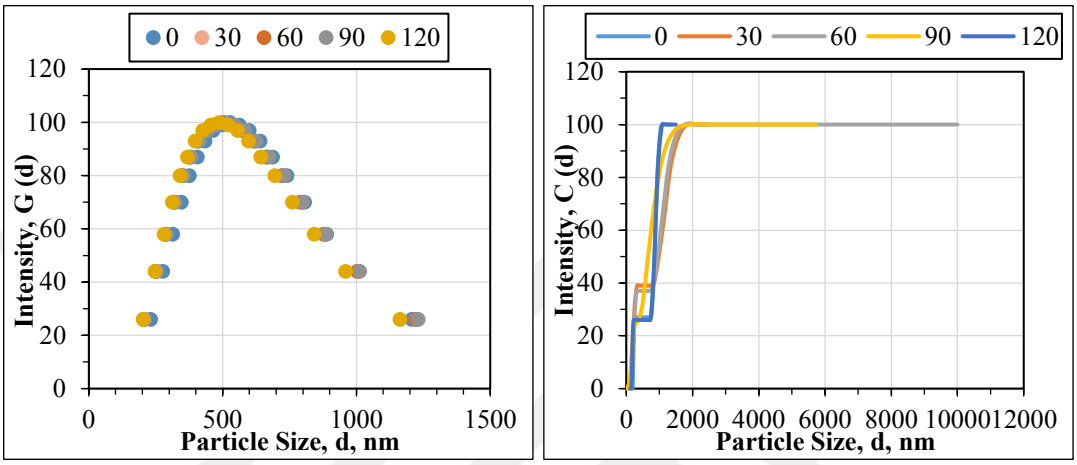


Figure 4.81. "TiO_2 and SRNOM" binary system under "as-is" conditions intensity profile: Time dependent logN distribution G(d) and multi size distribution C(d).

Table 4.51. "TiO_2 and SRNOM" binary system under "as-is" conditions intensity profile: Time dependent mean diameter, range and min-max diameter difference with respect to log normal and multi-size distribution.

TiO_2 and SRNOM	time, min				
	0	30	60	90	120
Log Normal distribution					
Mean, nm	527.8	500.4	508.4	487.2	502.0
Range	230.7-1207.2	204.7-1223.2	210.0-1230.8	204.1-1162.9	211.2-1193.1
Difference	976.5	1018.5	1020.8	958.8	981.9
Multi-size distribution					
Max 1, nm	224.9	31.2	87.6	170.0	188.1
Max 2, nm	914.9	238.9	226.0	860.8	924.7
Max 3, nm	-	1337.3	1283.7	-	-
Range	161.0-1366.1	16.7-2501.8	63.9-10.000	1.0-5710.7	116.6-1491.1
Difference	1205.1	2485.1	9936.1	5709.7	1374.5

According to log normal distribution, initial hydrodynamic size of "TiO_2 and SRNOM" binary system under "as-is" conditions was attained as 527.8 nm and detected to 502.0 nm upon 180 min. In terms of multi-size distribution, initially two max diameters were obtained. Time dependent

comparative presentation of log Normal distribution and multi-size distribution of "TiO_2 and SRNOM" binary system under "as-is" conditions intensity profile was exhibited in Figure 4.82. Polydispersity of "TiO_2 and SRNOM" binary system under "as-is" conditions was presented in Table 4.52. It could be inferred that slowly increasing trend was observed along 120 min. Simply an average value of 0.322 could be regarded as appropriate for expressing polydispersity.

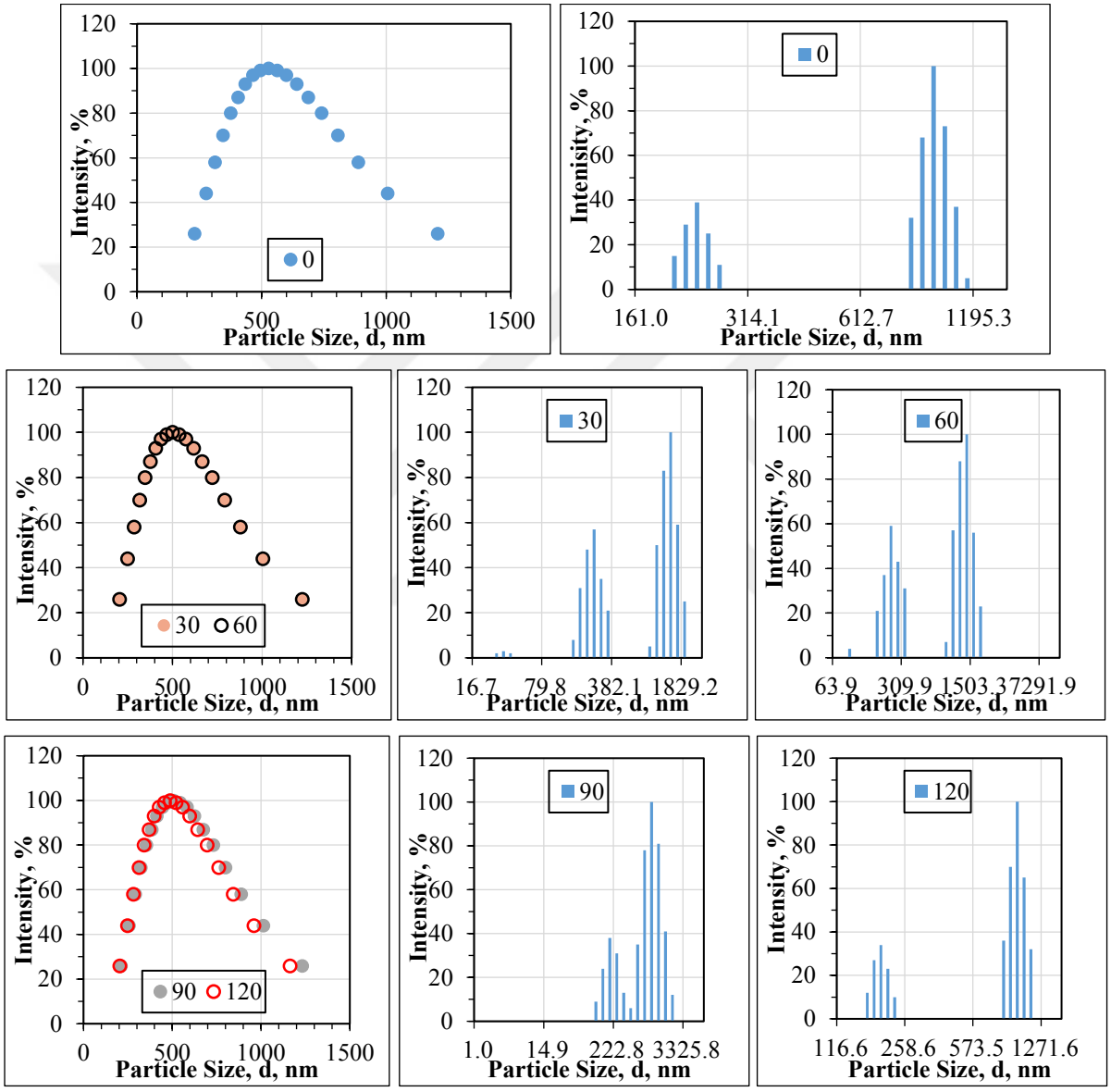


Figure 4.82. "TiO_2 and SRNOM" binary system under "as-is" conditions intensity profile: Time dependent comparative presentation of log Normal distribution and multi-size distribution of "TiO_2 and SRNOM" binary system under "as-is" conditions.

Table 4.52. Polydispersity of "TiO_2 and SRNOM" binary system under "as-is" conditions.

TiO_2 and SRNOM	Polydispersity				
	0	30	60	90	120
	0.288	0.343	0.335	0.323	0.319

4.1.4.6. "TiO_2 and SRNOM" binary system under "as-is" conditions volume profile. Time dependent logN distribution G(d) and multi size distribution C(d) of "TiO_2 and SRNOM" binary system under "as-is" conditions volume profile was exhibited in Figure 4.83. Also, time dependent mean diameter, range and min-max diameter difference with respect to log normal and multi-size distribution of "TiO_2 and SRNOM" binary system under "as-is" conditions volume profile was displayed in Table 4.53.

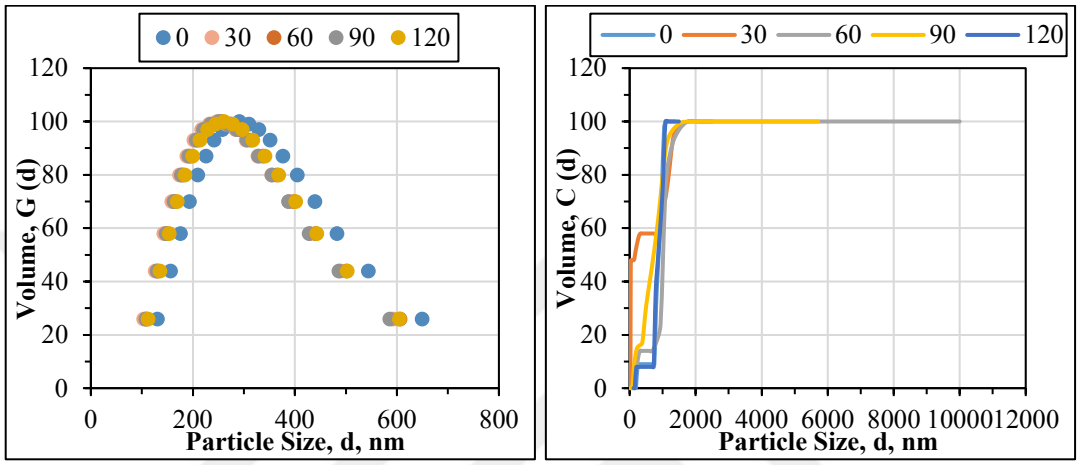


Figure 4.83. "TiO_2 and SRNOM" binary system under "as-is" conditions volume profile: Time dependent logN distribution G(d) and multi size distribution C(d).

Table 4.53. "TiO_2 and SRNOM" binary system under "as-is" conditions volume profile: Time dependent mean diameter, range and min-max diameter difference with respect to log normal and multi-size distribution.

TiO_2 and SRNOM	time, min				
	0	30	60	90	120
Log Normal distribution					
Mean, nm	291.6	248.3	256.4	251.4	261.0
Range	130.8-649.8	103.9-593.2	108.4-606.3	107.9-586.0	112.5-605.4
Difference	519.0	489.3	497.9	478.1	492.9
Multi-size distribution					
Max 1, nm	224.9	26.7	87.6	129.8	188.1
Max 2, nm	800.5	204.3	226.0	501.3	788.6
Max 3, nm	1045.7	238.9	1096.2	1128.0	1084.4
Max 4, nm	-	1337.3	-	-	-
Range	161.0-1366.1	16.7-2501.8	63.9-10.000	1.0-5710.7	116.6-1491.1
Difference	1205.1	2485.1	9936.1	5709.7	1374.5

As elucidated for "TiO_2 and SRNOM" binary system under "as-is" conditions intensity profile (Table 4.51), a similar approach was followed for "TiO_2 and SRNOM" binary system under "as-is"

conditions volume profile. Initial hydrodynamic particle size was recorded as 291.6 nm and continuous decrease was observed with slight variations until the end of 120 min. Also, initial size difference was attained as 519.0 nm and detected to 492.9 nm upon 120 min. However, in terms of multi-size distribution, initially three peaks were observed and four peaks were obtained upon 30 min. Two max diameters were recorded until the end of 120 min.

As explained for "TiO_2 and SRNOM" binary system under "as-is" conditions intensity profile (Figure 4.82), time dependent comparative presentation of log Normal distribution and multi-size distribution of "TiO_2 and SRNOM" binary system under "as-is" conditions volume profile was demonstrated in Figure 4.84.

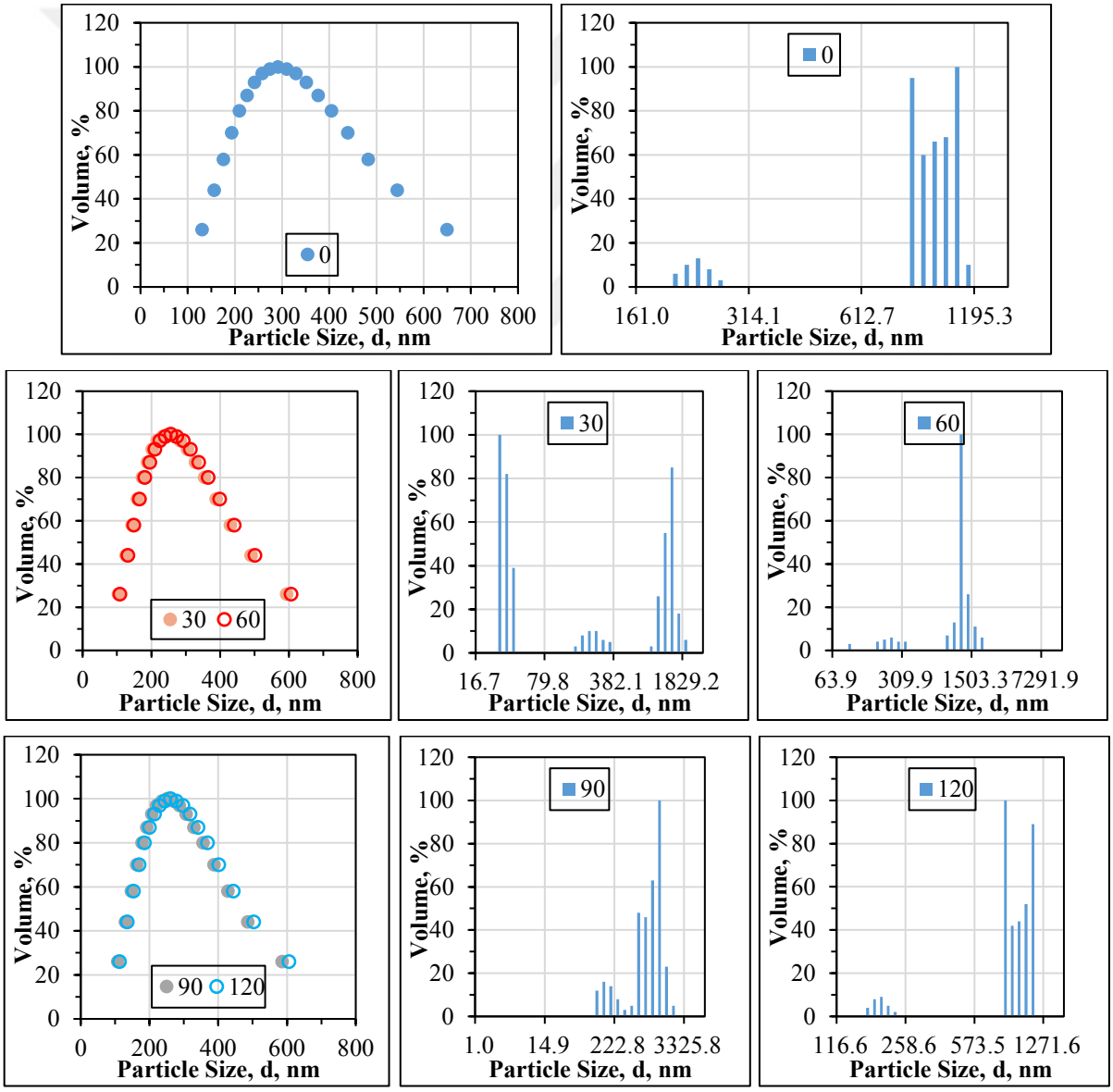


Figure 4.84. "TiO_2 and SRNOM" binary system under "as-is" conditions volume profile: Time dependent comparative presentation of log Normal distribution and multi-size distribution of "TiO_2 and SRNOM" binary system under "as-is" conditions.

4.1.4.7. "TiO_2 and SRNOM" binary system under "as-is" conditions surface area profile. Likewise expressed so far, a similar approach was also followed for "TiO_2 and SRNOM" binary system under "as-is" conditions surface area profile. Time dependent logN distribution G(d) and multi size distribution C(d) of "TiO_2 and SRNOM" binary system under "as-is" conditions surface area profile was given in Figure 4.85. Also, time dependent mean diameter, range and min-max diameter difference with respect to log normal and multi-size distribution of "TiO_2 and SRNOM" binary system under "as-is" conditions surface area profile was demonstrated in Table 4.54.

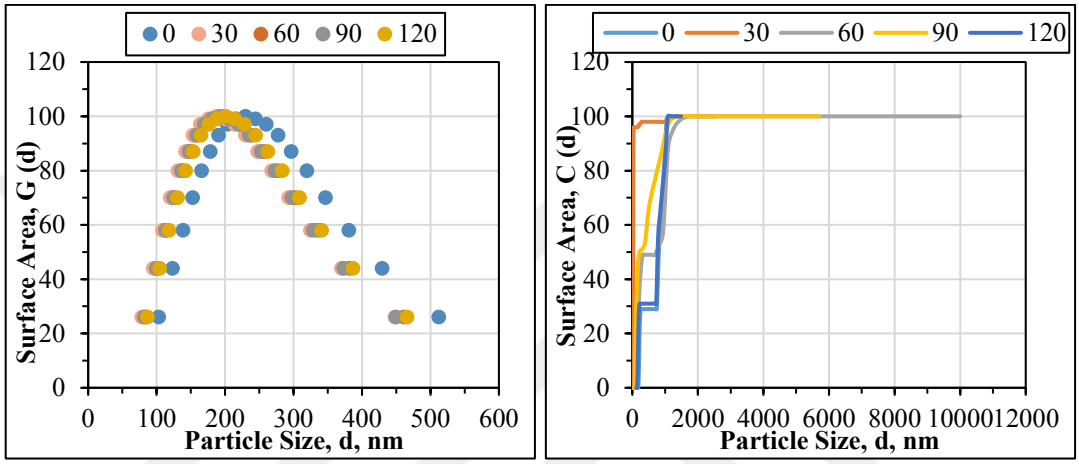


Figure 4.85. "TiO_2 and SRNOM" binary system under "as-is" conditions surface area profile: Time dependent logN distribution G(d) and multi size distribution C(d).

Table 4.54. "TiO_2 and SRNOM" binary system under "as-is" conditions surface area profile: Time dependent mean diameter, range and min-max diameter difference with respect to log normal and multi-size distribution.

TiO_2 and SRNOM	time, min				
	0	30	60	90	120
Log Normal distribution					
Mean, nm	230.0	187.6	194.9	193.0	200.9
Range	103.2-512.5	78.5-448.2	82.4-461.1	82.8-449.8	86.6-466.0
Difference	409.3	369.7	378.7	367.0	379.4
Multi-size distribution					
Max 1, nm	224.9	26.7	87.6	129.8	173.7
Max 2, nm	800.5	149.3	226.0	501.3	188.1
Max 3, nm	914.9	174.7	1096.2	1128.0	788.6
Max 4, nm	1045.7	204.3	-	-	1084.4
Max 5, nm	-	238.9	-	-	-
Max 6, nm	-	279.4	-	-	-
Max 7, nm	-	1337.3	-	-	-
Range	161.0-1366.1	16.7-2501.8	63.9-10.000	1.0-5710.7	116.6-1491.1
Difference	1205.1	2485.1	9936.1	5709.7	1374.5

According to log normal distribution, it could be seen that hydrodynamic particle size of "TiO_2 and SRNOM" binary system under "as-is" conditions displayed a slowly decreasing trend according to time variations. Initial hydrodynamic size was obtained as 230.0 nm and detected to 200.9 nm upon 120 min. Size difference decreased from 409.3 nm to 379.4 nm upon 120 min. For comparison purposes, in terms of multi-size distribution, initially four peaks were observed and seven peaks were attained upon 30 min. Also, four max diameters were obtained upon 120 min.

Time dependent comparative presentation of log Normal distribution and multi-size distribution of "TiO_2 and SRNOM" binary system under "as-is" conditions surface area profile was demonstrated in Figure 4.86.

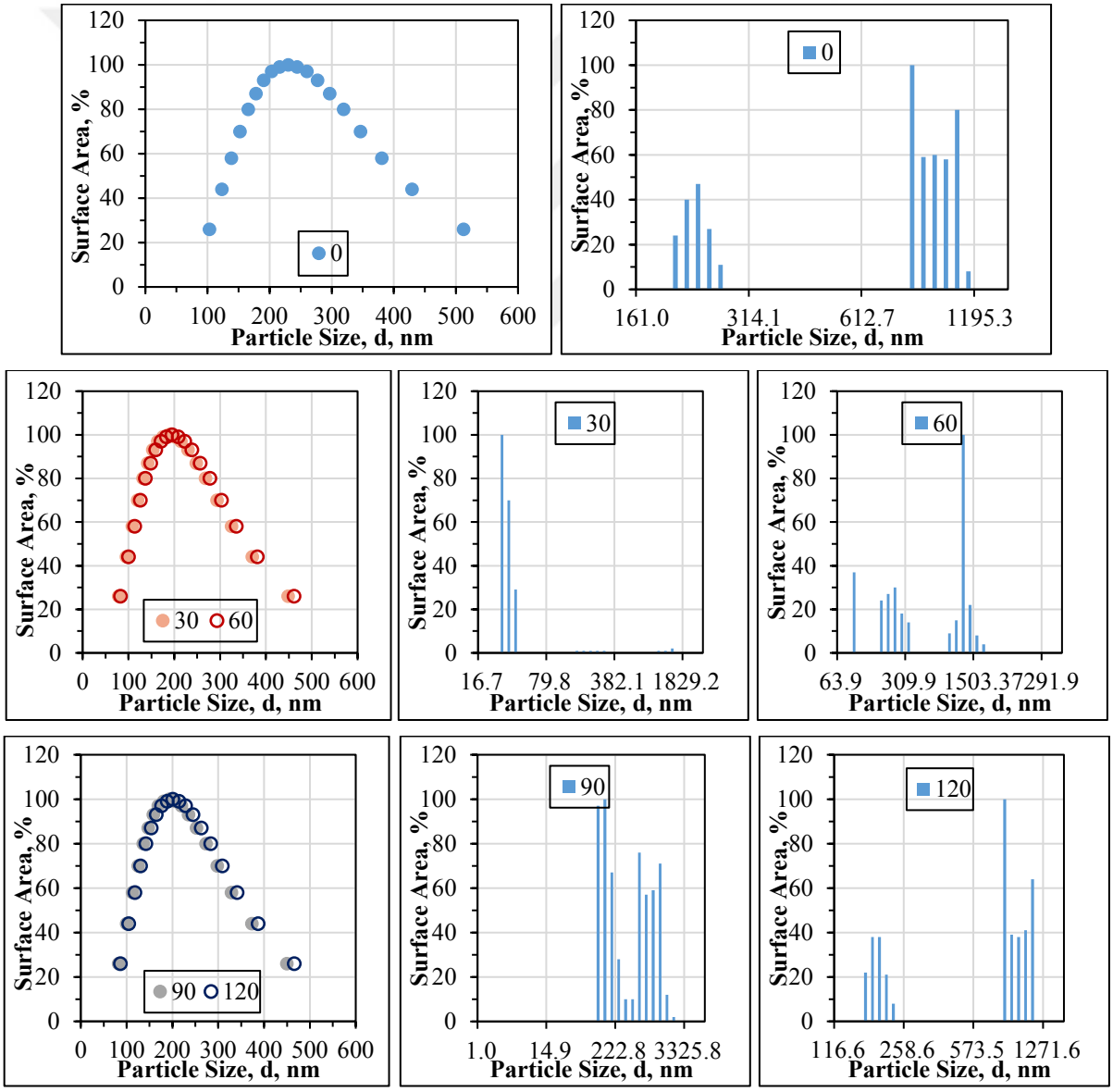


Figure 4.86. "TiO_2 and SRNOM" binary system under "as-is" conditions surface area profile: Time dependent comparative presentation of log Normal distribution and multi-size distribution of "TiO_2 and SRNOM" binary system under "as-is" conditions particle size.

4.1.4.8. "TiO_2 and SRNOM" binary system under "as-is" conditions number profile. Time dependent logN distribution G(d) and multi size distribution C(d) of "TiO_2 and SRNOM" binary system under "as-is" conditions number profile was displayed in Figure 4.87. Time dependent mean diameter, range and min-max diameter difference with respect to log normal and multi-size distribution of "TiO_2 and SRNOM" binary system under "as-is" conditions number profile was exhibited in Table 4.55.

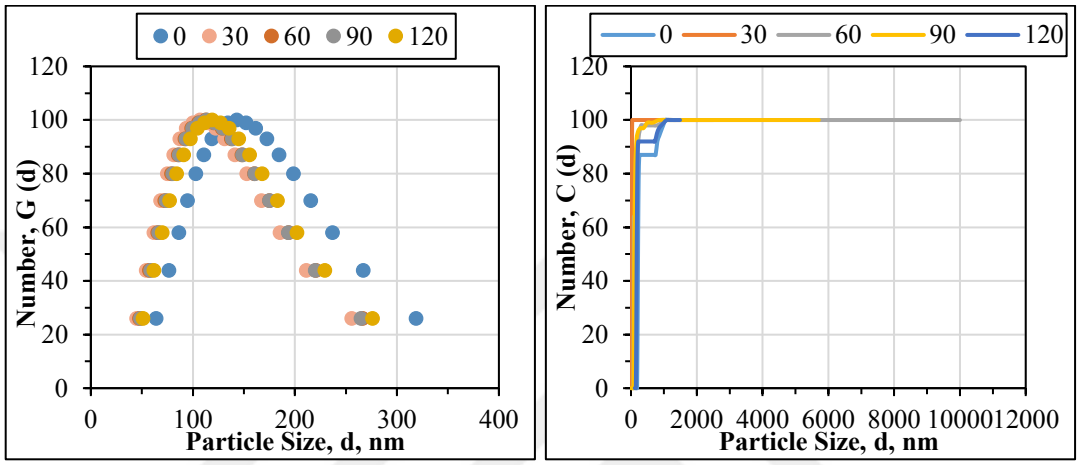


Figure 4.87. "TiO_2 and SRNOM" binary system under "as-is" conditions number profile: Time dependent logN distribution G(d) and multi size distribution C(d).

Table 4.55. "TiO_2 and SRNOM" binary system under "as-is" conditions number profile: Time dependent mean diameter, range and min-max diameter difference with respect to log normal and multi-size distribution.

TiO_2 and SRNOM	time, min				
	0	30	60	90	120
Log Normal distribution					
Mean, nm	143.1	107.1	112.7	113.7	119.0
Range	64.2-318.8	44.8-255.9	47.7-266.6	48.8-265.0	51.3-276.1
Difference	254.6	211.1	218.9	216.2	224.8
Multi-size distribution					
Max 1, nm	224.9	26.7	87.6	99.0	173.7
Max 2, nm	800.5	-	164.8	501.3	788.6
Max 3, nm	1045.7	-	1096.2	-	1084.4
Range	161.0-1366.1	16.7-2501.8	63.9-10.000	1.0-5710.7	116.6-1491.1
Difference	1205.1	2485.1	9936.1	5709.7	1374.5

In terms of number profile, it could be inferred that hydrodynamic particle size of "TiO_2 and SRNOM" binary system under "as-is" conditions was obtained as 143.1 nm. Upon 30 min, roughly 25 % decrease was observed and slight alterations remained until 120 min. On the other hand, in the

first 30 min, approximately 15 % decrease was attained in terms of difference between max and min diameter. Initial size difference was obtained as 254.6 nm and detected to 224.8 nm upon 120 min. Upon 30 min, slight variations were monitored until the end of 120 min. For comparison purposes, in terms of multi-size distribution, initially three max diameters were attained. Upon 30 min, one peak was observed and three peaks were monitored upon 60 min. Upon 90 min, two peaks were obtained and three peaks remained until the end of 120 min.

Time dependent comparative presentation of log Normal distribution and multi-size distribution of "TiO_2 and SRNOM" binary system under "as-is" conditions number profile was shown in Figure 4.88.

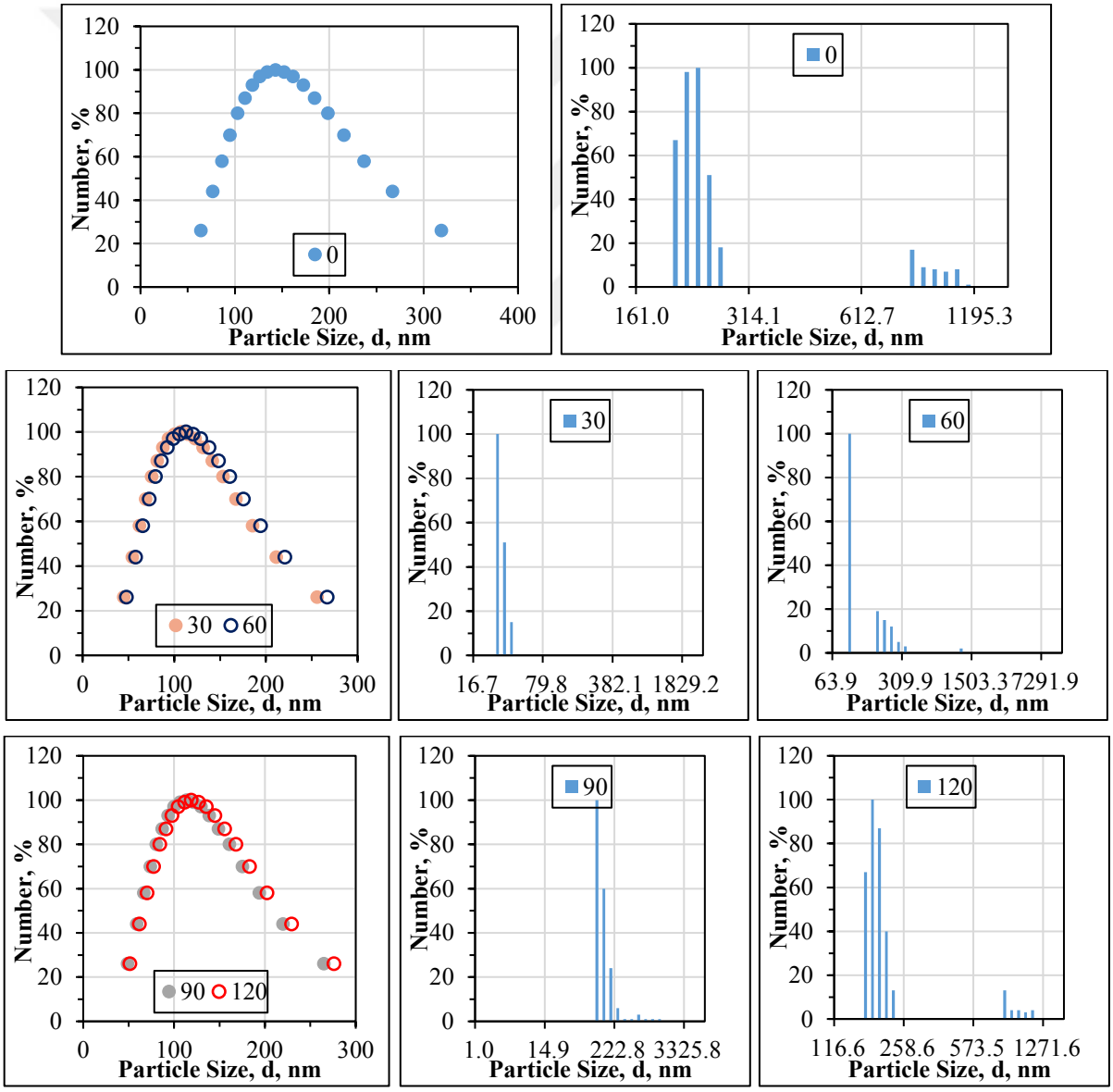


Figure 4.88. "TiO_2 and SRNOM" binary system under "as-is" conditions number profile: Time dependent comparative presentation of log Normal distribution and multi-size distribution of "TiO_2 and SRNOM" binary system under "as-is" conditions.

4.1.4.9. "N-TiO_2 and HA" binary system under "as-is" conditions intensity profile. As explained for "TiO_2 and HA" binary system under "as-is" conditions intensity profile (Figure 4.73), a similar approach was followed for "N-TiO_2 and HA" binary system under "as-is" conditions intensity profile. Time dependent logN distribution G(d) and multi size distribution C(d) of "N-TiO_2 and HA" binary system under "as-is" conditions intensity profile was presented in Figure 4.89. In a similar manner to data represented "TiO_2 and HA" binary system under "as-is" conditions, time dependent mean diameter, range and min-max diameter difference with respect to log normal and multi-size distribution of "N-TiO_2 and HA" binary system under "as-is" conditions intensity profile was exhibited in Table 4.56. Also, polydispersity of "N-TiO_2 and HA" binary system under "as-is" conditions was displayed in Table 4.57.

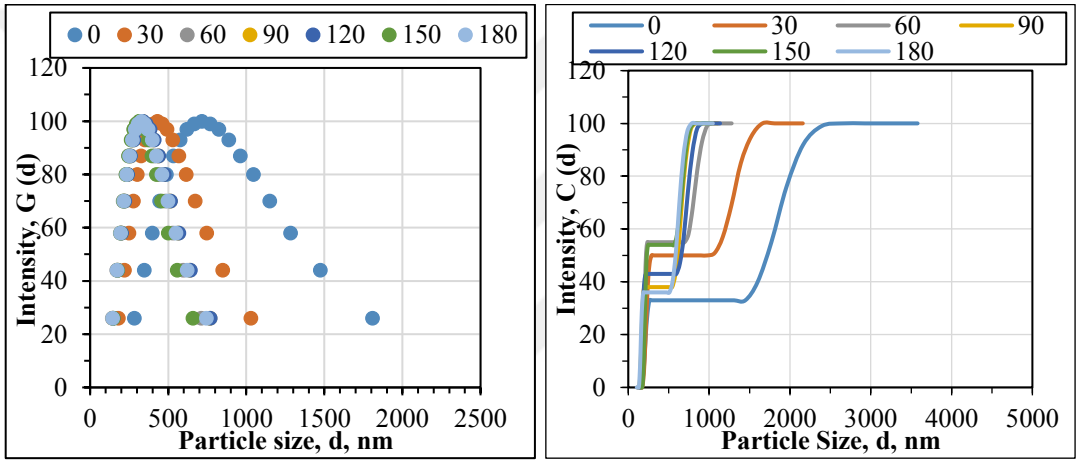


Figure 4.89. "N-TiO_2 and HA" binary system under "as-is" conditions intensity profile: Time dependent logN distribution G(d) and multi size distribution C(d).

Table 4.56. "N-TiO_2 and HA" binary system under "as-is" conditions intensity profile: Time dependent mean diameter, range and min-max diameter difference with respect to log normal and multi-size distribution.

N-TiO_2 and HA	time, min						
	0	30	60	90	120	150	180
Log Normal distribution							
Mean, nm	715.9	431.8	319.6	336.0	338.1	313.5	328.0
Range	283.4-1808.5	181.1-1029.8	143.3-713.0	147.3-766.6	148.3-770.5	149.2-658.8	144.3-745.6
Difference	1525.1	848.7	569.7	619.3	622.2	509.6	601.3
Multi-size distribution							
Max 1, nm	214.1	220.8	205.7	172.9	174.6	204.8	160.6
Max 2, nm	1957.4	1392.6	851.9	671.9	736.9	679.5	631.6
Range	143.2-3579.3	130.5-2159.0	146.7-1278.5	112.6-1107.9	113.3-1135.1	151.8-1033.9	104.2-1046.1
Difference	3436.1	2028.5	1131.8	995.3	1021.8	882.1	941.9

In a similar manner to data represented "TiO_2 and HA" binary system under "as-is" conditions intensity profile (Table 4.46), time dependent mean diameter, range and min-max diameter difference with respect to log normal and multi-size distribution of "N-TiO_2 and HA" binary system under "as-is" conditions intensity profile was exhibited. According to log normal distribution and in terms of intensity profile, initial hydrodynamic particle size of "N-TiO_2 and HA" binary system under "as-is" conditions was detected as 715.9 nm. Upon 30 min, a sharp decrease was monitored and hydrodynamic particle size was recorded as 431.8 nm, and continuous decrease was observed until the end of 180 min. Upon 180 min, hydrodynamic particle size of "N-TiO_2 and HA" binary system under "as-is" conditions was recorded as 328.0 nm. Also, according to log normal distribution, size difference decreased from 1525.1 nm to 601.3 nm according to time variations.

However, in terms of multi-size distribution, two max diameters were obtained as 214.1 nm and 1957.4 nm for "N-TiO_2 and HA" binary system under "as-is" conditions following initial period of time and remained until the end of 180 min. On the other hand, according to multi-size distribution, initial size difference between max and min diameter was attained as 3436.1 nm and detected to 941.9 nm at the end of 180 min.

For comparison purposes, it could be deduced that contrary to minor alterations verified for hydrodynamic particle sizes of "TiO_2 and HA" binary system under "as-is" conditions, "N-TiO_2 and HA" binary system under "as-is" conditions exhibited a significant change according to time variations. Due to the fact that hydrodynamic particle sizes were detected as coinciding peaks according to the log normal distribution, max diameters were attained particularly different as bimodal in multi-size distribution until 180 min.

Following a similar manner to data described "TiO_2 and HA" binary system under "as-is" conditions (Table 4.47), polydispersity of "N-TiO_2 and HA" binary system under "as-is" conditions was displayed (Table 4.57). It could be inferred that gradually decreasing trend was monitored until 60 min. Upon 60 min, a sharp decrease was observed and slight alterations remained until the end of 180 min. Basically an average value of 0.292 could be regarded as suitable for expressing polydispersity.

Table 4.57. Polydispersity of "N-TiO_2 and HA" binary system under "as-is" conditions.

N-TiO_2 and HA	Polydispersity						
	0	30	60	90	120	150	180
	0.374	0.322	0.269	0.286	0.285	0.226	0.283

Time dependent comparative presentation of log Normal distribution and multi-size distribution of "N-TiO_2 and HA" binary system under "as-is" conditions was given in Figure 4.90.

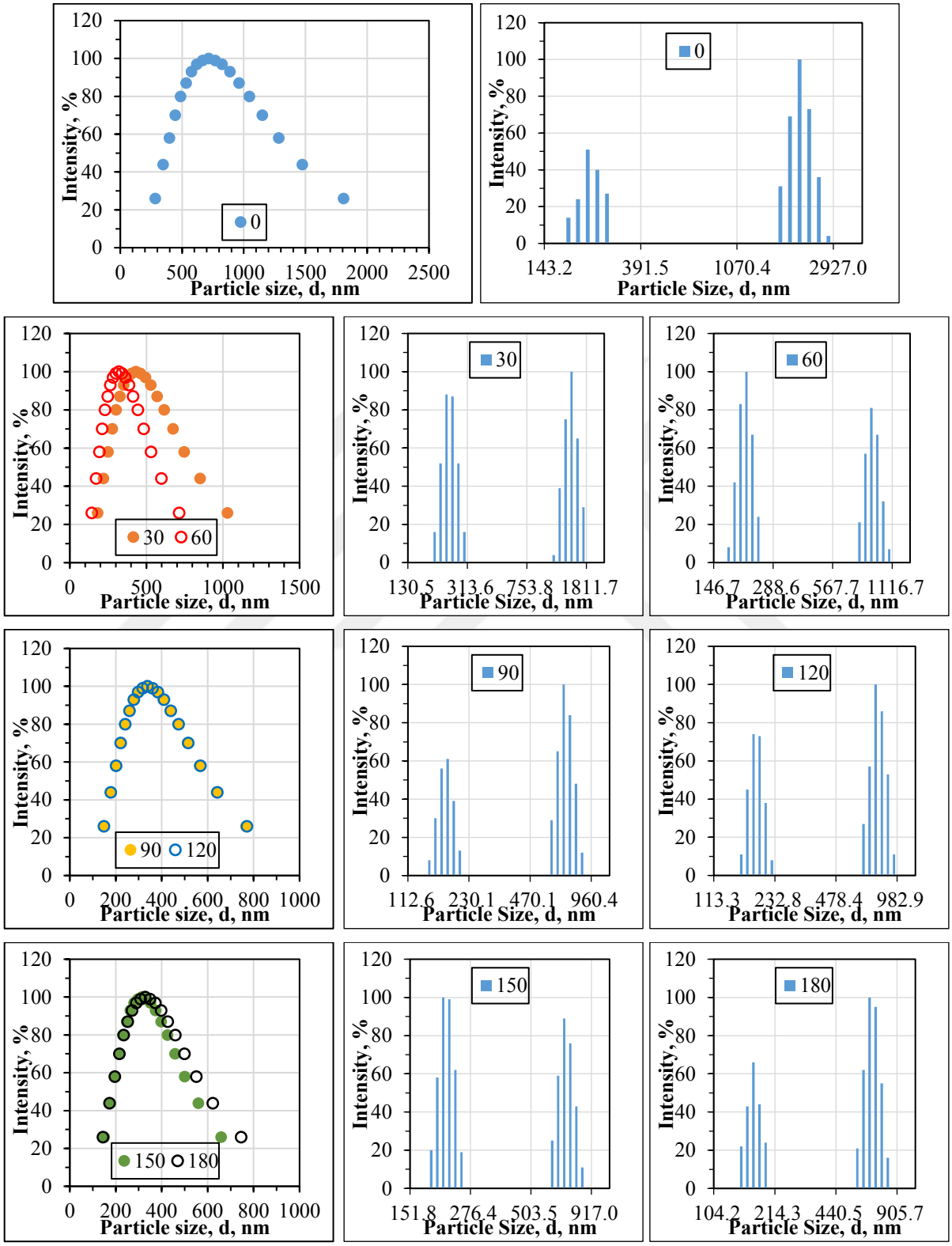


Figure 4.90. "N-TiO_2 and HA" binary system under "as-is" conditions intensity profile: Time dependent comparative presentation of log Normal distribution and multi-size distribution of "N-TiO_2 and HA" binary system under "as-is" conditions.

4.1.4.10. "N-TiO_2 and HA" binary system under "as-is" conditions volume profile. Time dependent logN distribution G(d) and multi size distribution C(d) of "N-TiO_2 and HA" binary system under "as-is" conditions volume profile was displayed in Figure 4.91. Time dependent mean diameter, range and min-max diameter difference with respect to log normal and multi-size distribution of "N-TiO_2 and HA" binary system under "as-is" conditions volume profile was presented in Table 4.58.

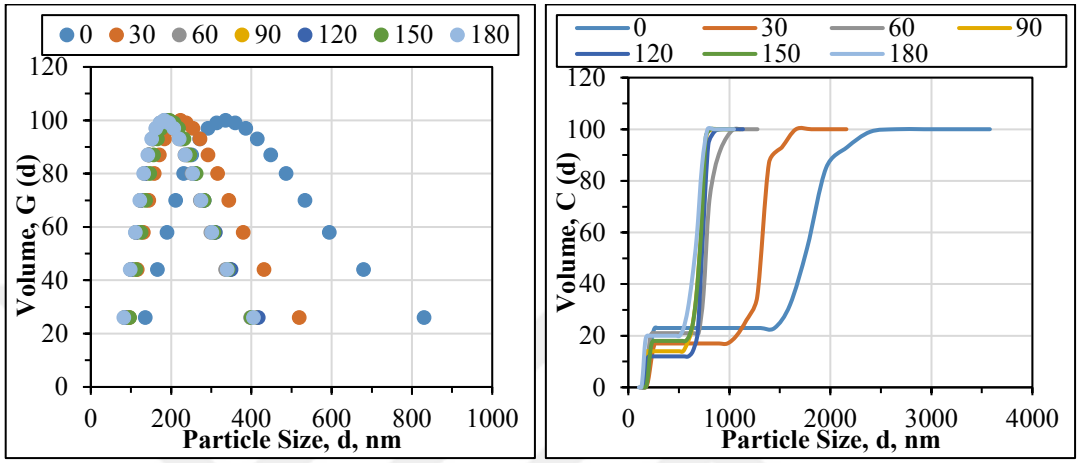


Figure 4.91. "N-TiO_2 and HA" binary system under "as-is" conditions volume profile: Time dependent logN distribution G(d) and multi size distribution C(d).

Table 4.58. "N-TiO_2 and HA" binary system under "as-is" conditions volume profile: Time dependent mean diameter, range and min-max diameter difference with respect to log normal and multi-size distribution.

N-TiO_2 and HA	time, min						
	0	30	60	90	120	150	180
Log Normal distribution							
Mean, nm	335.8	223.2	183.5	186.4	187.8	196.3	183.0
Range	135.8-830.2	95.9-519.7	84.5-398.3	83.9-414.3	84.6-417.0	96.3-400.1	82.6-405.1
Difference	694.4	423.8	313.8	330.4	332.4	303.8	322.5
Multi-size distribution							
Max 1, nm	214.1	220.8	205.7	161.0	174.6	204.8	160.6
Max 2, nm	1957.4	1392.6	796.2	172.9	736.9	766.1	729.6
Max 3, nm	-	1659.6	-	775.1	-	-	-
Range	143.2-3579.3	130.5-2159.0	146.7-1278.5	112.6-1107.9	113.3-1135.1	151.8-1033.9	104.2-1046.1
Difference	3436.1	2028.5	1131.8	995.3	1021.8	882.1	941.9

In terms of volume profile, it could be deduced that hydrodynamic particle size of "N-TiO_2 and HA" binary system under "as-is" conditions was recorded as 335.8 nm and roughly 50 % decrease was observed upon 180 min. Time dependent comparative presentation of log Normal distribution

and multi-size distribution of "N-TiO_2 and HA" binary system under "as-is" conditions volume profile was exhibited in Figure 4.92.

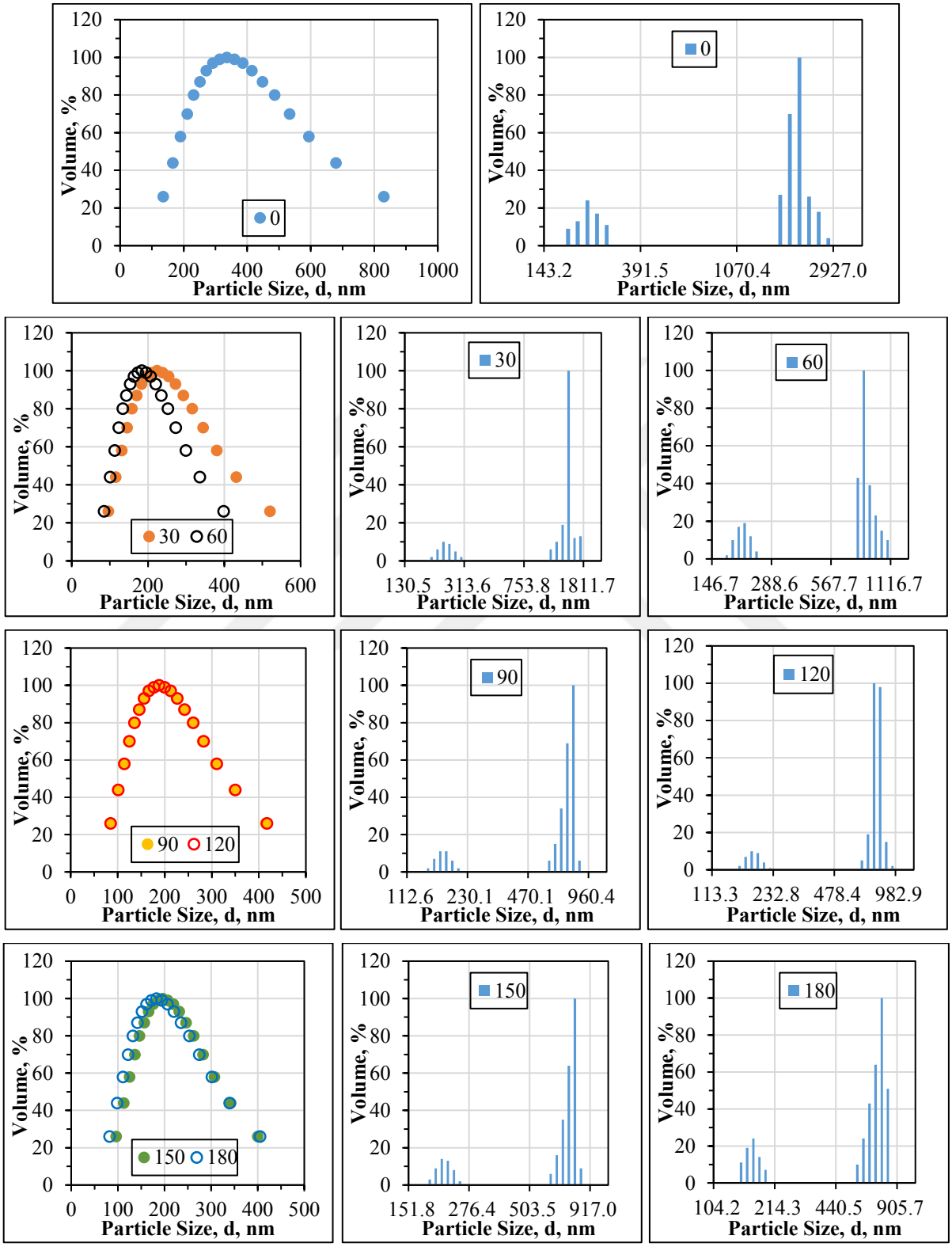


Figure 4.92. "N-TiO_2 and HA" binary system under "as-is" conditions volume profile: Time dependent comparative presentation of log Normal distribution and multi-size distribution of "N-TiO_2 and HA" binary system under "as-is" conditions.

4.1.4.11. "N-TiO_2 and HA" binary system under "as-is" conditions surface area profile. Time dependent logN distribution G(d) and multi size distribution C(d) of "N-TiO_2 and HA" binary system under "as-is" conditions surface area profile was presented in Figure 4.93. Time dependent mean diameter, range and min-max diameter difference with respect to log normal and multi-size distribution of "N-TiO_2 and HA" binary system under "as-is" conditions surface area profile was demonstrated in Table 4.59.

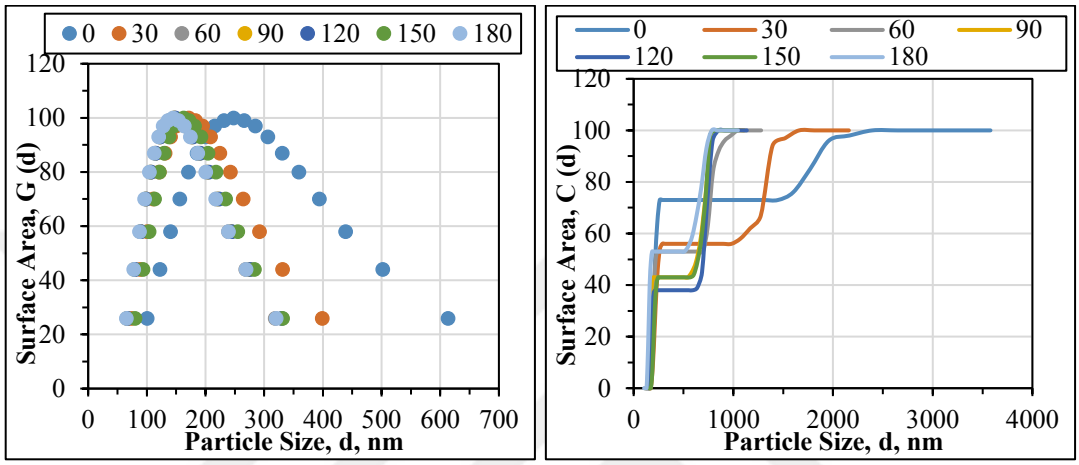


Figure 4.93. "N-TiO_2 and HA" binary system under "as-is" conditions surface area profile: Time dependent logN distribution G(d) and multi size distribution C(d).

Table 4.59. "N-TiO_2 and HA" binary system under "as-is" conditions surface area profile: Time dependent mean diameter, range and min-max diameter difference with respect to log normal and multi-size distribution.

N-TiO_2 and HA	time, min						
	0	30	60	90	120	150	180
Log Normal distribution							
Mean, nm	248.1	171.4	147.0	147.3	148.5	162.8	144.9
Range	100.4-613.4	73.6-399.1	67.7-319.0	66.3-327.3	66.9-329.6	79.9-331.7	65.4-320.7
Difference	513.0	325.5	251.3	261.0	262.7	251.8	255.3
Multi-size distribution							
Max 1, nm	214.1	220.8	205.7	161.0	174.6	204.8	160.6
Max 2, nm	1957.4	1392.6	796.2	775.1	736.9	766.1	729.6
Range	143.2-3579.3	130.5-2159.0	146.7-1278.5	112.6-1107.9	113.3-1135.1	151.8-1033.9	104.2-1046.1
Difference	3436.1	2028.5	1131.8	995.3	1021.8	882.1	941.9

In terms of surface area profile, initial hydrodynamic size was attained as 248.1 nm. However, upon 30 min, almost 30 % decrease and then continuous decrease was monitored upon 180 min. In terms of multi-size distribution, two peaks were observed along 180 min. Time dependent

comparative presentation of log Normal distribution and multi-size distribution of "N-TiO_2 and HA" binary system under "as-is" conditions surface area profile was given in Figure 4.94.

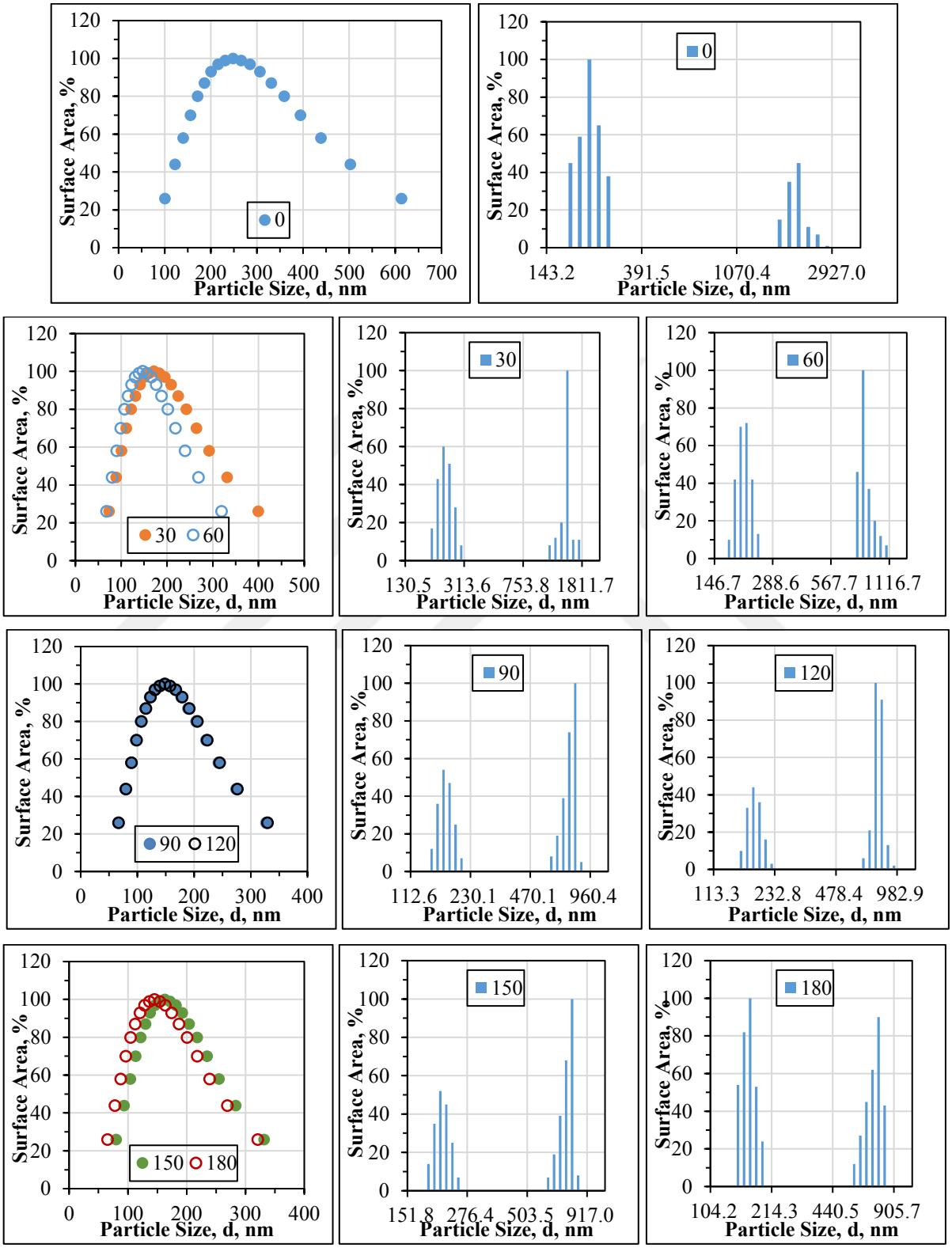


Figure 4.94. "N-TiO_2 and HA" binary system under "as-is" conditions surface area profile: Time dependent comparative presentation of log Normal distribution and multi-size distribution of "N-TiO_2 and HA" binary system under "as-is" conditions.

4.1.4.12. "N-TiO_2 and HA" binary system under "as-is" conditions number profile. Time dependent logN distribution G(d) and multi size distribution C(d) of "N-TiO_2 and HA" binary system under "as-is" conditions number profile was given in Figure 4.95. Time dependent mean diameter, range and min-max diameter difference with respect to log normal and multi-size distribution of "N-TiO_2 and HA" binary system under "as-is" conditions number profile was displayed in Table 4.60.

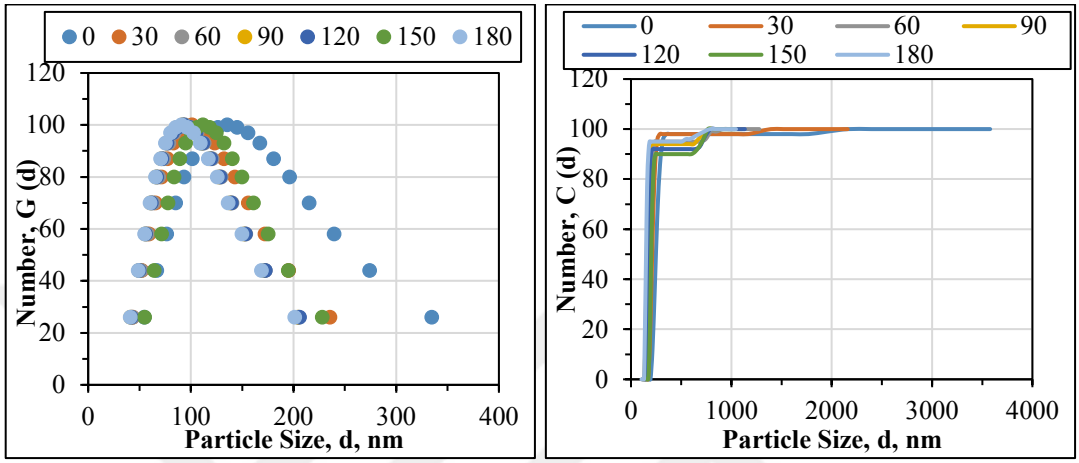


Figure 4.95. "N-TiO_2 and HA" binary system under "as-is" conditions number profile: Time dependent logN distribution G(d) and multi size distribution C(d).

Table 4.60. "N-TiO_2 and HA" binary system under "as-is" conditions number profile: Time dependent mean diameter, range and min-max diameter difference with respect to log normal and multi-size distribution.

N-TiO_2 and HA	time, min						
	0	30	60	90	120	150	180
Log Normal distribution							
Mean, nm	135.4	101.1	94.3	91.9	92.8	111.9	90.8
Range	54.8-334.8	43.4-235.4	43.4-204.6	41.4-204.3	41.8-206.0	54.9-228.1	41.0-201.1
Difference	280.0	192.0	161.2	162.9	164.2	173.2	160.1
Multi-size distribution							
Max 1, nm	214.1	220.8	192.3	161.0	174.6	204.8	160.6
Max 2, nm	1770.1	1392.6	796.2	775.1	736.9	766.1	729.6
Max 3, nm	1957.4	-	-	-	-	-	-
Range	143.2-3579.3	130.5-2159.0	146.7-1278.5	112.6-1107.9	113.3-1135.1	151.8-1033.9	104.2-1046.1
Difference	3436.1	2028.5	1131.8	995.3	1021.8	882.1	941.9

Hydrodynamic particle size variations with respect to time revealed a sharp decrease and detected between 135.4 nm and 90.8 nm. For comparison purposes, according to multi-size distribution, initially three peaks were observed and two peaks were monitored until 180 min. Time

dependent comparative presentation of log Normal distribution and multi-size distribution of "N-TiO_2 and HA" binary system under "as-is" conditions number profile was presented in Figure 4.96.

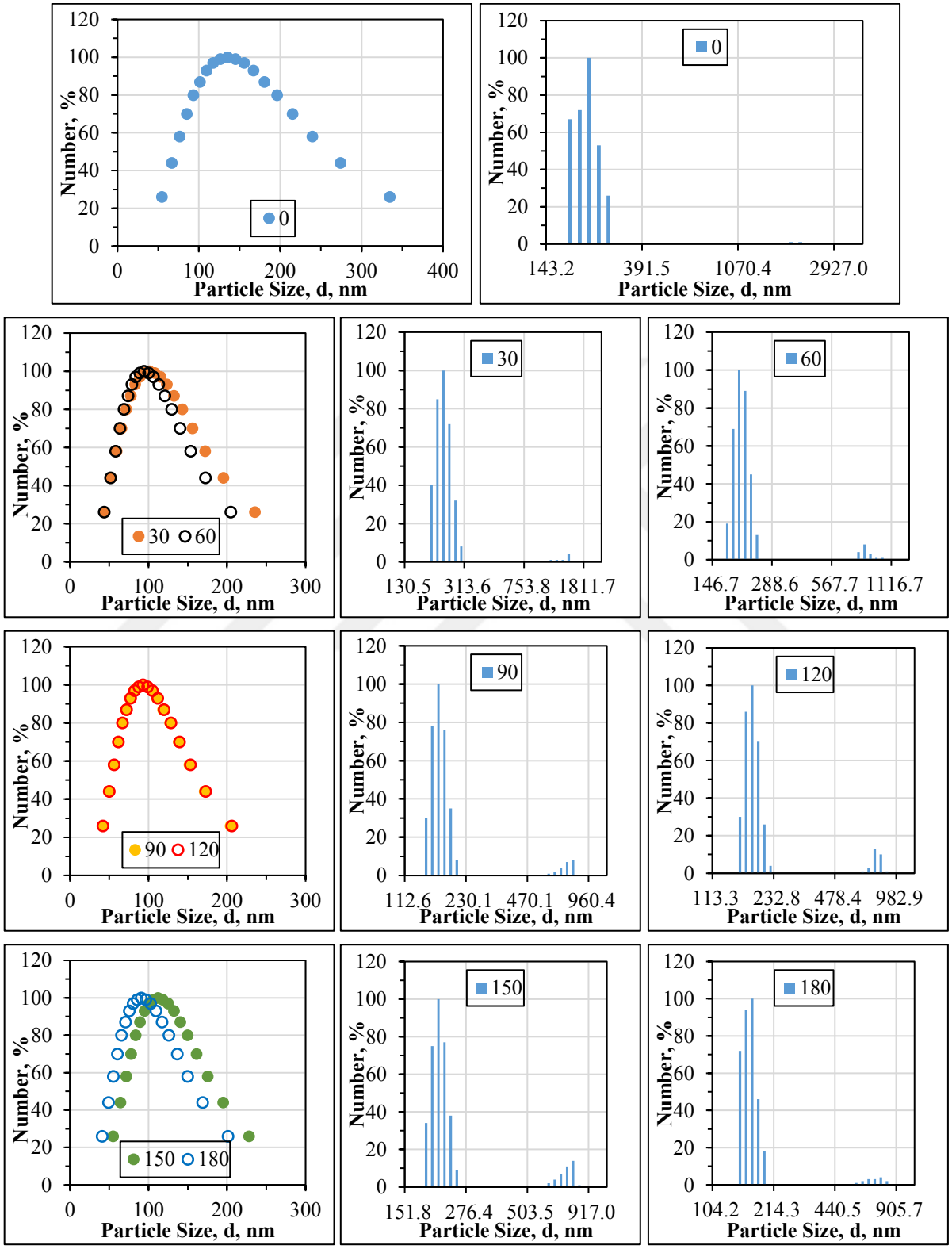


Figure 4.96. "N-TiO_2 and HA" binary system under "as-is" conditions number profile: Time dependent comparative presentation of log Normal distribution and multi-size distribution of "N-TiO_2 and HA" binary system under "as-is" conditions.

4.1.4.13. "N-TiO_2 and SRNOM" binary system under "as-is" conditions intensity profile. In a similar manner to data depicted "N-TiO_2 and HA" binary system under "as-is" conditions intensity profile (Figure 4.89), time dependent logN distribution G(d) and multi size distribution C(d) of "N-TiO_2 and SRNOM" binary system under "as-is" conditions intensity profile was shown in Figure 4.97. Time dependent mean diameter, range and min-max diameter difference with respect to log normal and multi-size distribution of "N-TiO_2 and SRNOM" binary system under "as-is" conditions intensity profile was given in Table 4.61.

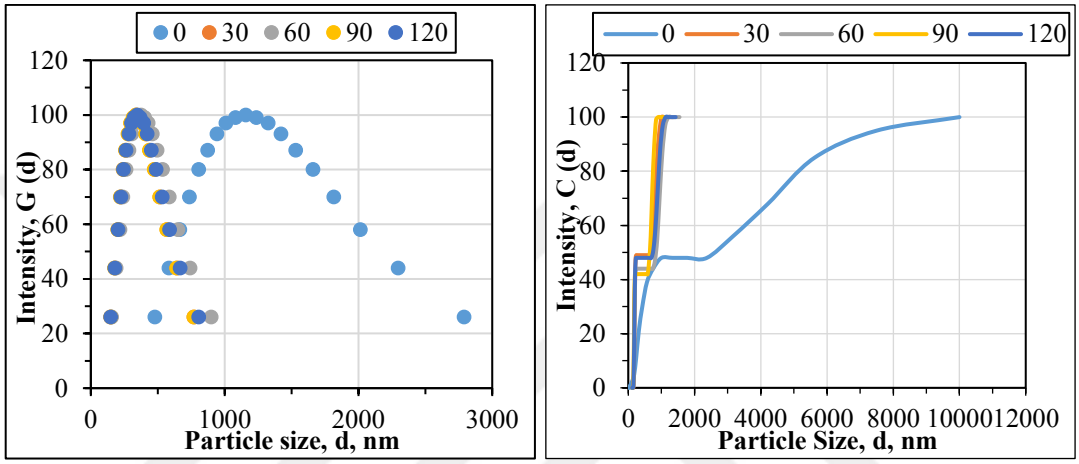


Figure 4.97. "N-TiO_2 and SRNOM" binary system under "as-is" conditions intensity profile: Time dependent logN distribution G(d) and multi size distribution C(d).

Table 4.61. "N-TiO_2 and SRNOM" binary system under "as-is" conditions intensity profile: Time dependent mean diameter, range and min-max diameter difference with respect to log normal and multi-size distribution.

N-TiO_2 and SRNOM	time, min				
	0	30	60	90	120
Log Normal distribution					
Mean, nm	1157.7	340.0	375.9	338.0	346.3
Range	480.2-2791.1	149.9-771.0	157.2-899.1	148.3-770.4	148.7-806.3
Difference	2310.8	621.1	741.9	622.1	657.6
Multi-size distribution					
Max 1, nm	421.7	189.7	185.3	174.0	195.6
Max 2, nm	5623.4	863.3	947.6	726.0	887.1
Range	1.0-10.000	120.4-1360.0	113.6-1546.0	113.3-1114.5	112.0-1430.1
Difference	9999.0	1239.6	1432.4	1001.2	1318.1

Hydrodynamic particle size of "N-TiO_2 and SRNOM" revealed a sharp decrease, initial hydrodynamic particle size was recorded as 1157.7 nm and decreased to 346.3 nm upon 120 min. In terms of multi-size distribution, two peaks were observed along 120 min. Time dependent

comparative presentation of log Normal distribution and multi-size distribution of "N-TiO_2 and SRNOM" binary system under "as-is" conditions intensity profile was given in Figure 4.98. Also, time dependent polydispersity of "N-TiO_2 and SRNOM" binary system under "as-is" conditions was presented in Table 4.62 and it could be deduced that a continuous decrease was monitored with respect to time.

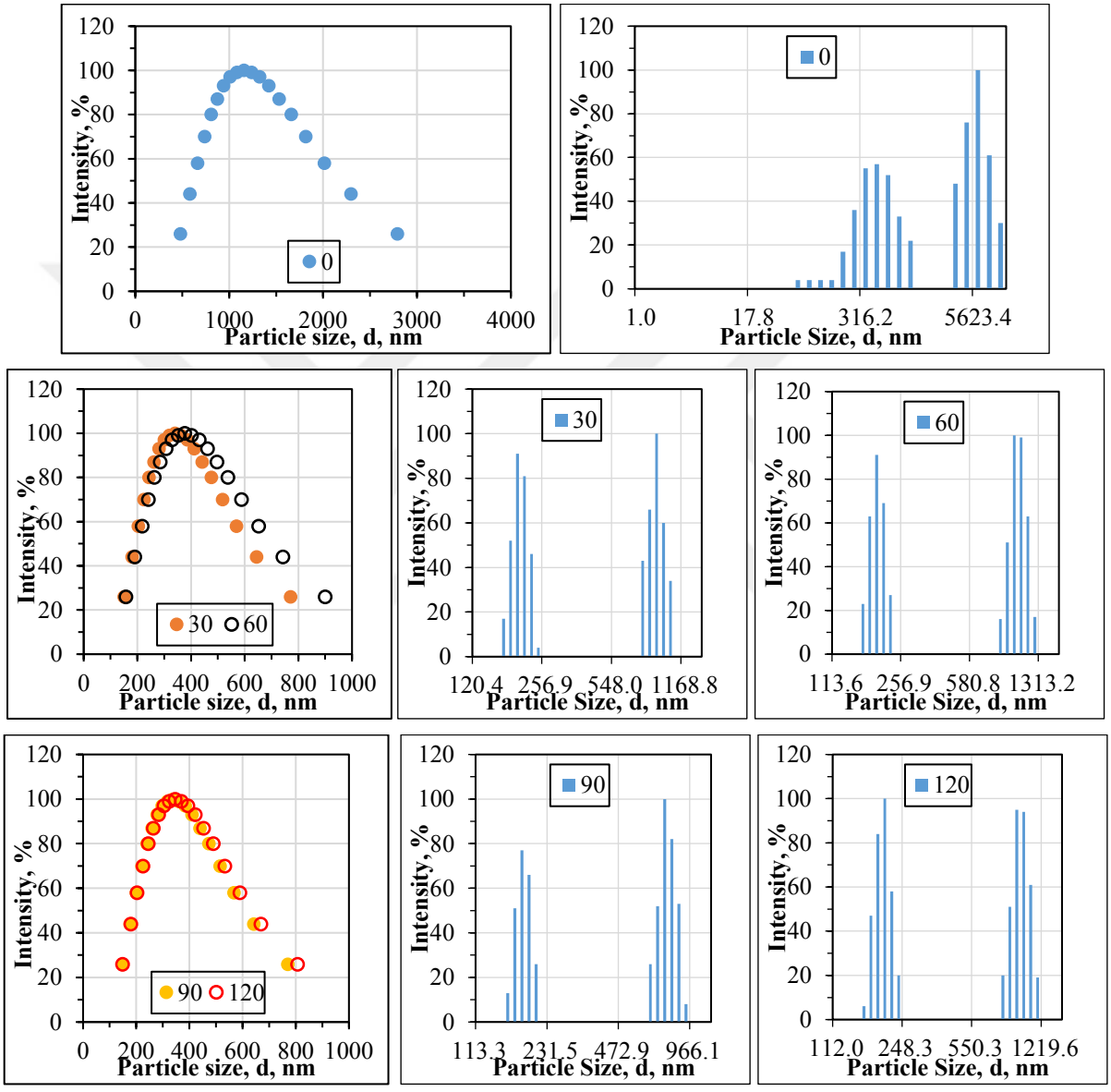


Figure 4.98. "N-TiO_2 and SRNOM" binary system under "as-is" conditions intensity profile: Time dependent comparative presentation of log Normal distribution and multi-size distribution of "N-TiO_2 and SRNOM" binary system under "as-is" conditions.

Table 4.62. Polydispersity of "N-TiO_2 and SRNOM" binary system under "as-is" conditions.

N-TiO_2 and SRNOM	Polydispersity				
	0	30	60	90	120
	0.331	0.281	0.325	0.285	0.302

4.1.4.14. "N-TiO_2 and SRNOM" binary system under "as-is" conditions volume profile. As explained for "N-TiO_2 and SRNOM" binary system under "as-is" conditions intensity profile (Figure 4.97), a similar approach was followed for "N-TiO_2 and SRNOM" binary system under "as-is" conditions volume profile. Time dependent logN distribution G(d) and multi size distribution C(d) of "N-TiO_2 and SRNOM" binary system under "as-is" conditions volume profile was presented in Figure 4.99. Time dependent mean diameter, range and min-max diameter difference with respect to log normal and multi-size distribution of "N-TiO_2 and SRNOM" binary system under "as-is" conditions volume profile was demonstrated in Table 4.63.

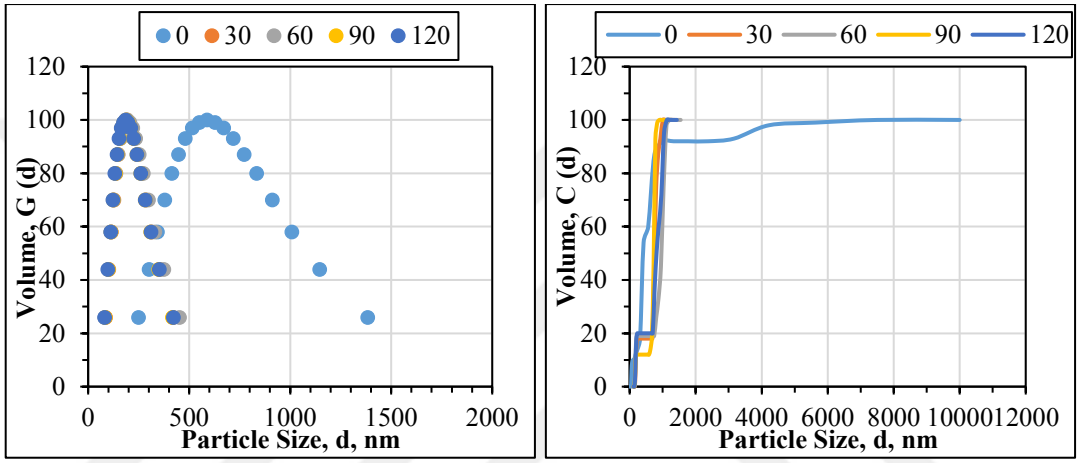


Figure 4.99. "N-TiO_2 and SRNOM" binary system under "as-is" conditions volume profile: Time dependent logN distribution G(d) and multi size distribution C(d).

Table 4.63. "N-TiO_2 and SRNOM" binary system under "as-is" conditions volume profile: Time dependent mean diameter, range and min-max diameter difference with respect to log normal and multi-size distribution.

N-TiO_2 and SRNOM	time, min				
	0	30	60	90	120
Log Normal distribution					
Mean, nm	587.9	190.4	193.4	187.8	186.0
Range	249.7-1384.3	86.2-420.4	82.8-451.7	84.6-417.0	81.9-422.4
Difference	1134.6	334.2	368.9	332.4	340.5
Multi-size distribution					
Max 1, nm	56.2	189.7	185.3	174.0	195.6
Max 2, nm	421.7	800.3	804.9	779.7	756.6
Max 3, nm	749.9	1004.5	1028.1	-	1040.2
Max 4, nm	4217.0	-	-	-	-
Max 5, nm	7498.9	-	-	-	-
Range	1.0-10.000	120.4-1360.0	113.6-1546.0	113.3-1114.5	112.0-1430.1
Difference	9999.0	1239.6	1432.4	1001.2	1318.1

According to volume profile, it could be deduced that hydrodynamic particle size of "N-TiO_2 and SRNOM" binary system under "as-is" conditions demonstrated a rapidly decreasing trend with respect to time. In terms of log normal distribution, initial hydrodynamic particle size was recorded as 587.9 nm and reached to 186.0 nm upon 120 min. Also, size difference decreased from 1134.6 nm to 340.5 nm upon 120 min. For comparison purposes, in terms of multi-size distribution, initially five max diameters were attained. Upon 30 min, three peaks were obtained until 90 min. Upon 90 min, two max diameters were observed and three peaks were attained until the end of 120 min. Time dependent comparative presentation of log Normal distribution and multi-size distribution of "N-TiO_2 and SRNOM" binary system under "as-is" conditions volume profile was demonstrated in Figure 4.100.

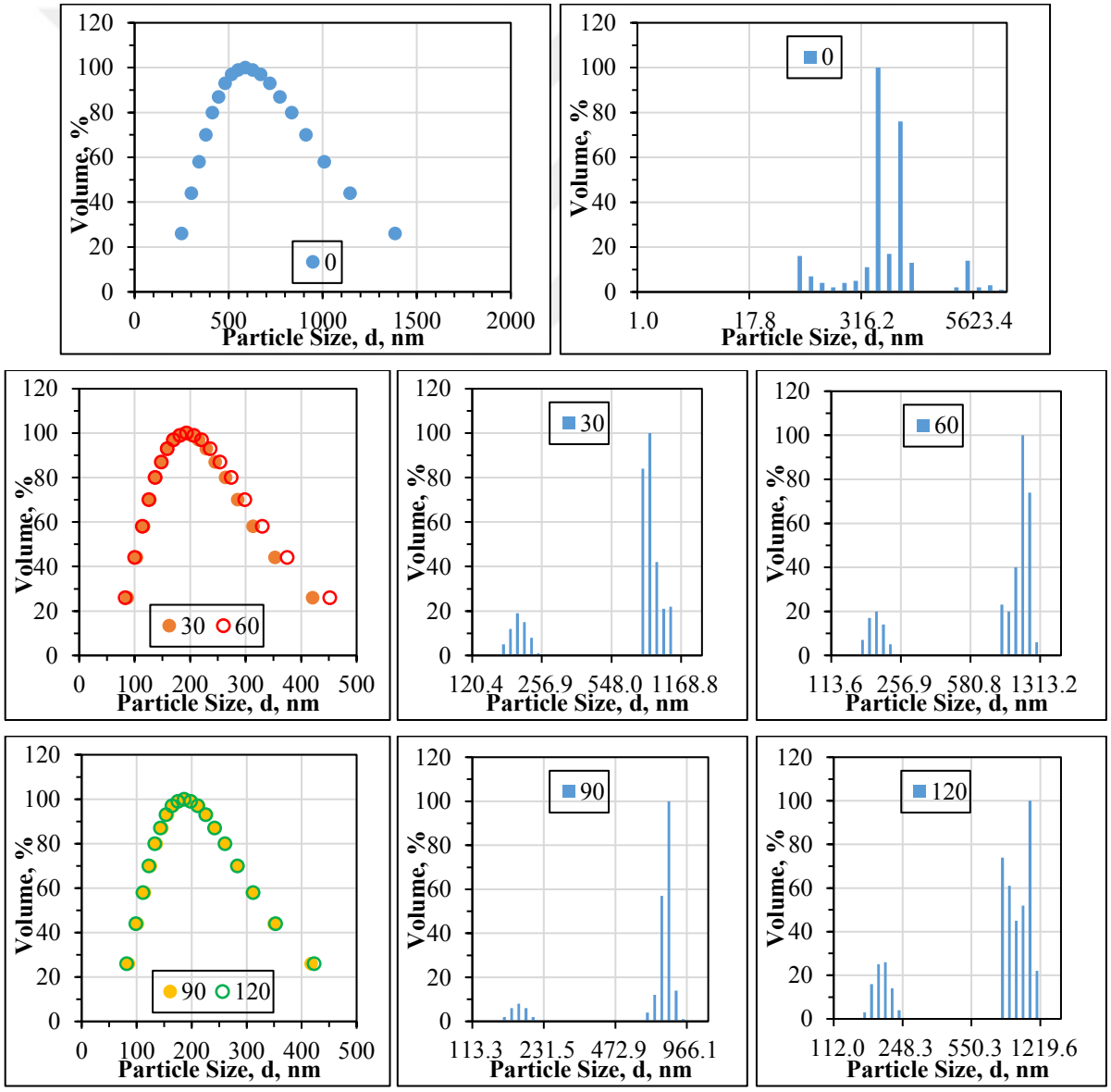


Figure 4.100. "N-TiO_2 and SRNOM" binary system under "as-is" conditions volume profile: Time dependent comparative presentation of log Normal distribution and multi-size distribution of "N-TiO_2 and SRNOM" binary system under "as-is" conditions.

4.1.4.15. "N-TiO_2 and SRNOM" binary system under "as-is" conditions surface area profile. As explained for "N-TiO_2 and SRNOM" binary system under "as-is" conditions intensity profile (Figure 4.97) and volume profile (Figure 4.99), a similar approach was followed for "N-TiO_2 and SRNOM" binary system under "as-is" conditions surface area profile. Time dependent logN distribution G(d) and multi size distribution C(d) of "N-TiO_2 and SRNOM" binary system under "as-is" conditions surface area profile was demonstrated in Figure 4.101. Also, time dependent mean diameter, range and min-max diameter difference with respect to log normal and multi-size distribution of "N-TiO_2 and SRNOM" binary system under "as-is" conditions surface area profile was displayed in Table 4.64.

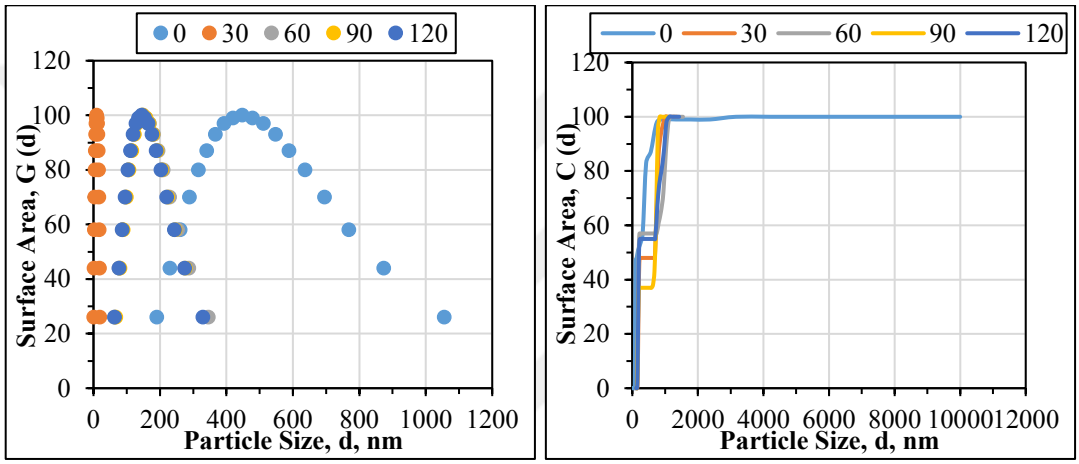


Figure 4.101. "N-TiO_2 and SRNOM" binary system under "as-is" conditions surface area profile: Time dependent logN distribution G(d) and multi size distribution C(d).

Table 4.64. "N-TiO_2 and SRNOM" binary system under "as-is" conditions surface area profile: Time dependent mean diameter, range and min-max diameter difference with respect to log normal and multi-size distribution.

N-TiO_2 and SRNOM	time, min				
	0	30	60	90	120
Log Normal distribution					
Mean, nm	448.3	150.9	148.3	148.5	145.1
Range	190.4-1055.7	68.3-333.4	63.5-346.2	66.9-329.6	63.9-329.4
Difference	865.3	265.1	282.7	262.7	265.5
Multi-size distribution					
Max 1, nm	56.2	189.7	185.3	174.0	180.6
Max 2, nm	421.7	800.3	804.9	779.7	756.6
Max 3, nm	479.9	-	1028.1	-	1040.2
Max 4, nm	4217.0	-	-	-	-
Range	1.0-10.000	120.4-1360.0	113.6-1546.0	113.3-1114.5	112.0-1430.1
Difference	9999.0	1239.6	1432.4	1001.2	1318.1

According to log normal distribution, initial hydrodynamic particle size of "N-TiO_2 and SRNOM" binary system under "as-is" conditions was attained as 448.3 nm. During 120 min, hydrodynamic particle size of "N-TiO_2 and SRNOM" followed a rapidly decreasing trend and detected to 145.1 nm. However, in terms of multi-size distribution, four max diameters were obtained as 56.2 nm, 421.7 nm, 479.9 nm and 4217.0 nm for "N-TiO_2 and SRNOM" binary system under "as-is" conditions following initial period of time. Upon 30 min, two peaks were observed and upon 60 min, three peaks were attained. Upon 90 min, two peaks were monitored and three peaks were obtained until the end of 120 min period. Time dependent comparative presentation of log Normal distribution and multi-size distribution of "N-TiO_2 and SRNOM" binary system under "as-is" conditions surface area profile was presented in Figure 4.102.

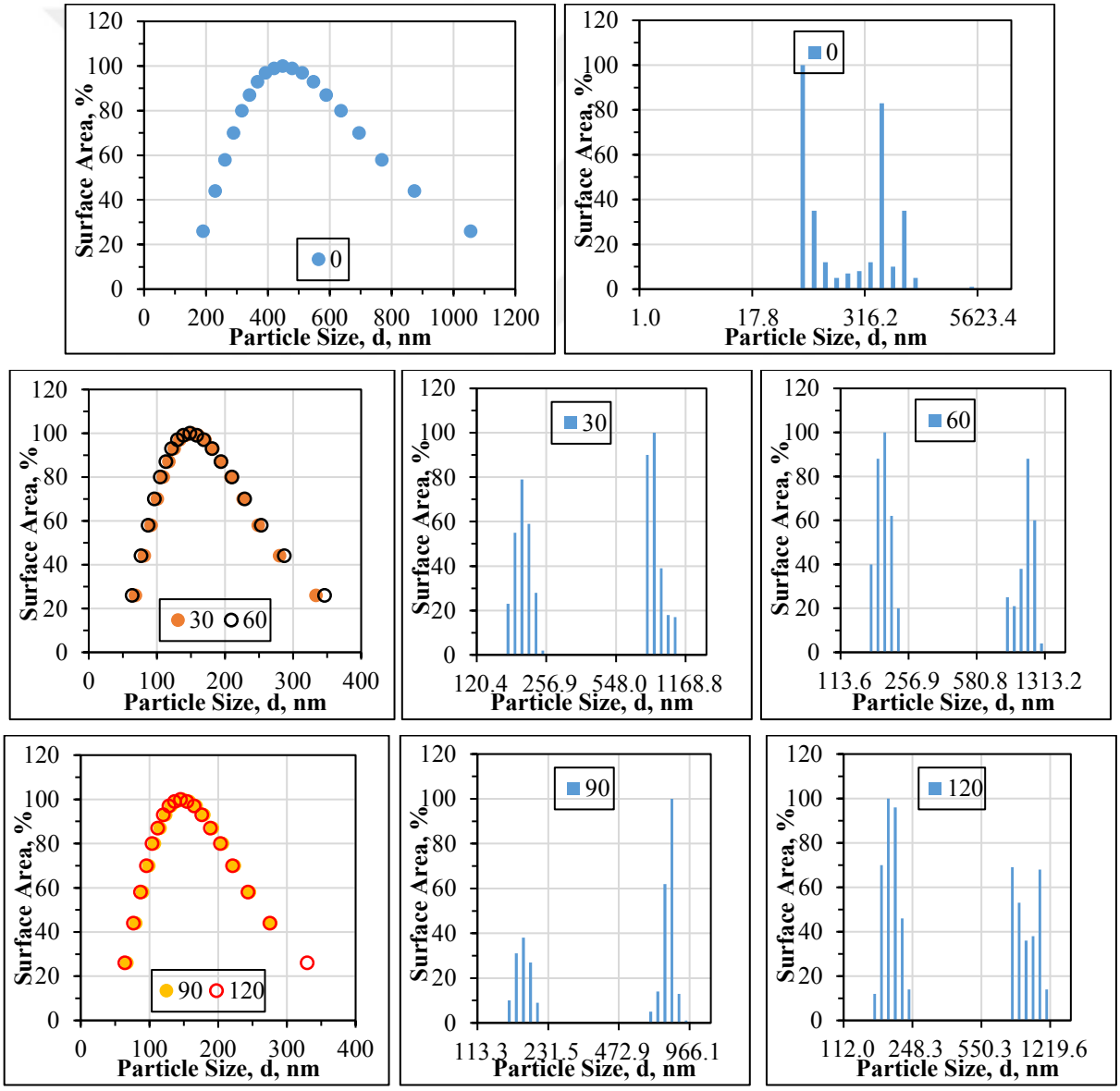


Figure 4.102. "N-TiO_2 and SRNOM" binary system under "as-is" conditions surface area profile: Time dependent comparative presentation of log Normal distribution and multi-size distribution of "N-TiO_2 and SRNOM" binary system under "as-is" conditions.

4.1.4.16. "N-TiO_2 and SRNOM" binary system under "as-is" conditions number profile. Likewise expressed so far, a similar approach was also followed for "N-TiO_2 and SRNOM" binary system under "as-is" conditions number profile. Time dependent logN distribution G(d) and multi size distribution C(d) of "N-TiO_2 and SRNOM" binary system under "as-is" conditions number profile was demonstrated in Figure 4.103. Time dependent mean diameter, range and min-max diameter difference with respect to log normal and multi-size distribution of "N-TiO_2 and SRNOM" binary system under "as-is" conditions number profile was presented in Table 4.65.

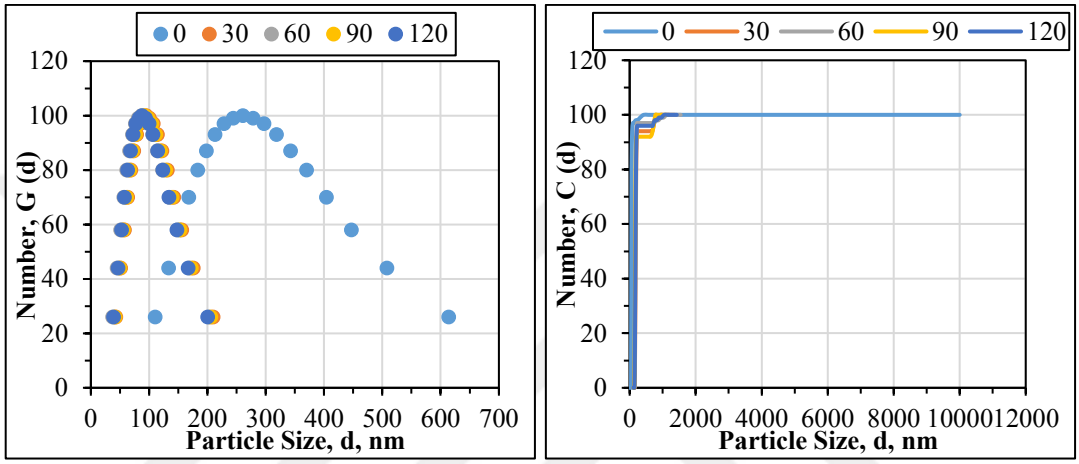


Figure 4.103. "N-TiO_2 and SRNOM" binary system under "as-is" conditions number profile: Time dependent logN distribution G(d) and multi size distribution C(d).

Table 4.65. "N-TiO_2 and SRNOM" binary system under "as-is" conditions number profile: Time dependent mean diameter, range and min-max diameter difference with respect to log normal and multi-size distribution.

N-TiO_2 and SRNOM	time, min				
	0	30	60	90	120
Log Normal distribution					
Mean, nm	260.7	94.9	87.1	92.8	88.2
Range	110.7-613.9	43.0-209.6	37.3-203.5	41.8-206.0	38.9-200.4
Difference	503.2	166.6	166.2	164.2	161.5
Multi-size distribution					
Max 1, nm	56.2	189.7	170.8	174.0	180.6
Max 2, nm	421.7	741.9	1028.1	779.7	756.6
Max 3, nm	-	800.3	-	-	1040.2
Range	1.0-10.000	120.4-1360.0	113.6-1546.0	113.3-1114.5	112.0-1430.1
Difference	9999.0	1239.6	1432.4	1001.2	1318.1

In terms of number profile, it could be inferred that initial hydrodynamic particle size of "N-TiO_2 and SRNOM" binary system under "as-is" conditions was attained as 260.7 nm. Upon 30 min,

approximately 65 % decrease was monitored and slight variations remained until 120 min. On the other hand, initial size difference was revealed a sharp decrease and decreased from 503.2 nm to 166.6 nm in the first 30 min. Upon 30 min, slight variations were monitored until the end of 120 min. For comparison purposes, in terms of multi-size distribution, initially two max diameters were attained. Upon 30 min, three peaks were monitored. However, upon 60 min, two peaks were obtained until 120 min. Upon 120 min, three peaks were observed.

Time dependent comparative presentation of log Normal distribution and multi-size distribution of "N-TiO_2 and SRNOM" binary system under "as-is" conditions number profile was shown in Figure 4.104.

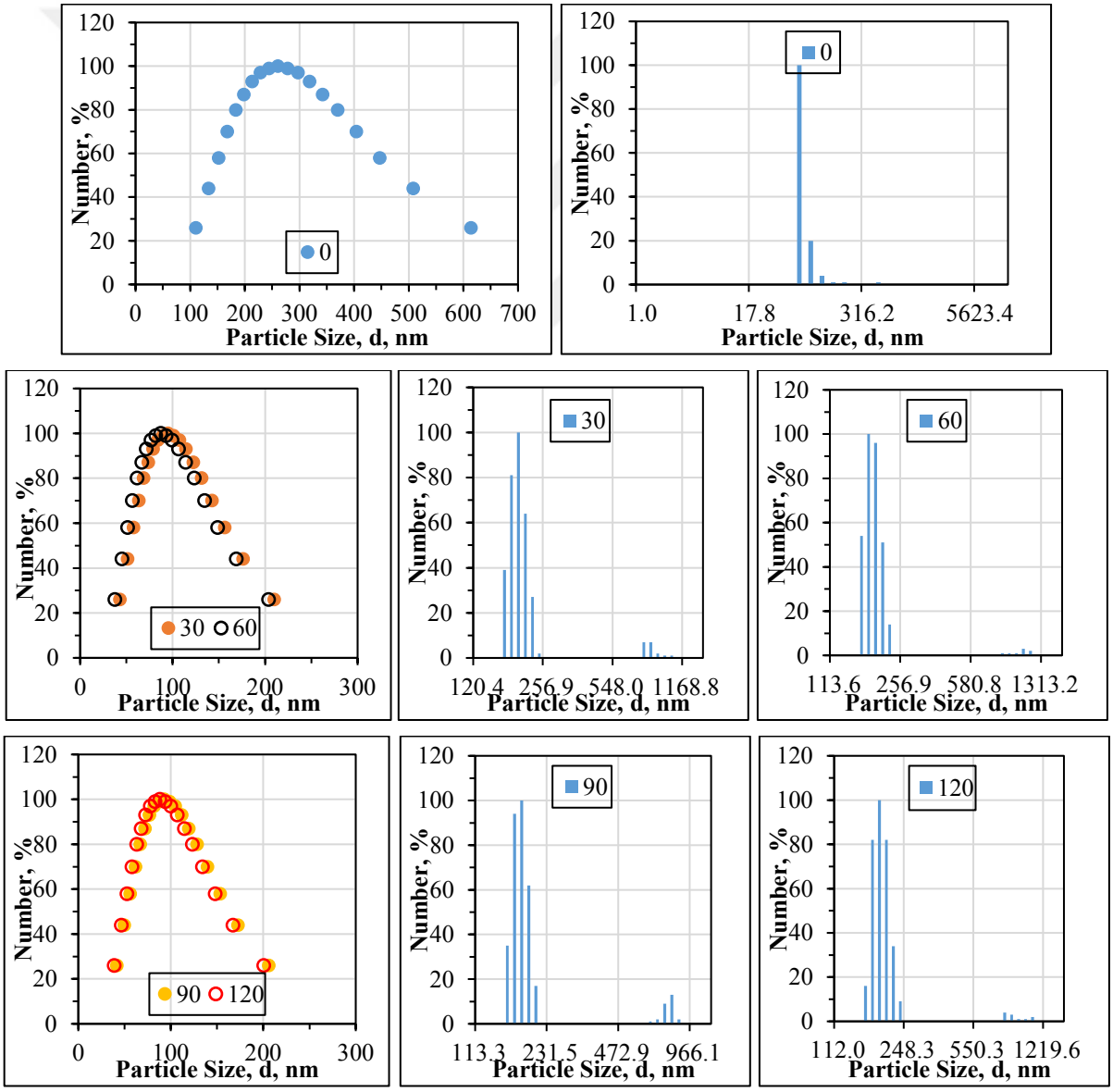


Figure 4.104. "N-TiO_2 and SRNOM" binary system number profile: Time dependent comparative presentation of log Normal distribution and multi-size distribution of "N-TiO_2 and SRNOM" binary system.

4.1.4.17. "Fe-TiO_2 and HA" binary system under "as-is" conditions intensity profile. As elucidated for "N-TiO_2 and HA" binary system under "as-is" conditions intensity profile (Figure 4.89), a similar approach was followed for "Fe-TiO_2 and HA" binary system under "as-is" conditions intensity profile. Time dependent logN distribution G(d) and multi size distribution C(d) of "Fe-TiO_2 and HA" binary system under "as-is" conditions intensity profile was presented in Figure 4.105. Time dependent mean diameter, range and min-max diameter difference with respect to log normal and multi-size distribution of "Fe-TiO_2 and HA" binary system under "as-is" conditions intensity profile was exhibited in Table 4.66. Also, polydispersity of "Fe-TiO_2 and HA" binary system under "as-is" conditions was demonstrated in Table 4.67.

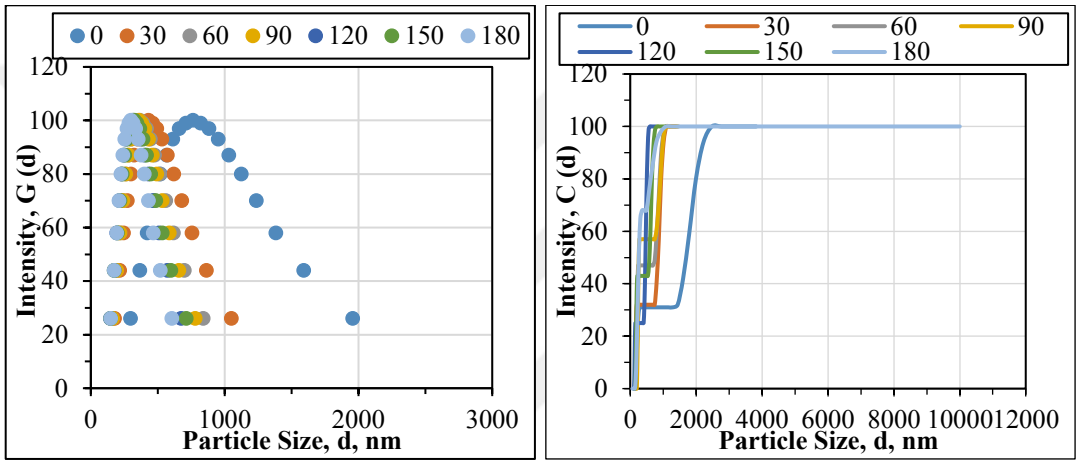


Figure 4.105. "Fe-TiO_2 and HA" binary system under "as-is" conditions intensity profile: Time dependent logN distribution G(d) and multi size distribution C(d).

Table 4.66. "Fe-TiO_2 and HA" binary system under "as-is" conditions intensity profile: Time dependent mean diameter, range and min-max diameter difference with respect to log normal and multi-size distribution.

Fe-TiO_2 and HA	time, min						
	0	30	60	90	120	150	180
Log Normal distribution							
Mean, nm	764.4	430.9	366.8	358.3	315.7	325.1	300.6
Range	298.3-1958.7	176.6-1051.5	160.1-840.3	164.3-781.5	147.5-675.9	148.2-713.3	149.3-605.2
Difference	1660.4	874.9	680.2	617.2	528.4	565.1	455.9
Multi-size distribution							
Max 1, nm	203.7	168.8	204.7	241.2	134.9	187.6	260.7
Max 2, nm	227.0	936.0	931.4	964.6	490.5	658.0	791.1
Max 3, nm	1992.2	-	-	-	-	-	-
Range	118.3-3822.0	114.4-1381.5	130.0-1467.4	173.4-1433.3	97.7-770.8	115.2-1071.8	62.6-10.000
Difference	3703.7	1267.1	1337.4	1259.9	673.1	956.6	9937.4

In a similar manner to data described "TiO_2 and HA" binary system under "as-is" conditions intensity profile (Table 4.46) and "N-TiO_2 and HA" binary system under "as-is" conditions intensity profile (Table 4.56), time dependent mean diameter, range and min-max diameter difference with respect to log normal and multi-size distribution of "Fe-TiO_2 and HA" binary system under "as-is" conditions intensity profile was presented. According to log normal distribution and in terms of intensity profile, initial hydrodynamic particle size of "Fe-TiO_2 and HA" binary system under "as-is" conditions was recorded as 764.4 nm. Upon 30 min, a rapid decrease was observed and hydrodynamic size was detected as 430.9 nm and continuous decrease was monitored until the end of 180 min. Upon 180 min, hydrodynamic particle size of "Fe-TiO_2 and HA" binary system under "as-is" conditions was detected as 300.6 nm. According to log normal distribution, size difference decreased from 1660.4 nm to 455.9 nm according to time variations. However, in terms of multi-size distribution, three max diameters were attained as 203.7 nm, 227.0 nm, and 1992.2 nm for "Fe-TiO_2 and HA" binary system under "as-is" conditions following initial period of time and two peaks were observed until the end of 180 min. On the other hand, according to multi-size distribution, initial size difference between max and min diameter was obtained as 3703.7 nm and reached to 9937.4 nm at the end of 180 min.

For comparison purposes, it could be stated that contrary to slight variations recorded for hydrodynamic particle sizes of "TiO_2 and HA" binary system under "as-is" conditions, and in a similar manner to "N-TiO_2 and HA" binary system under "as-is" conditions, "Fe-TiO_2 and HA" binary system under "as-is" conditions also demonstrated a significant variation with respect to time. Due to the fact that hydrodynamic particle sizes were recorded as coinciding peaks according to the log normal distribution, max diameters were obtained distinctly different as bimodal in multi-size distribution until 180 min.

Following a similar manner, polydispersity of "Fe-TiO_2 and HA" binary system under "as-is" conditions was demonstrated. It could be asserted that slowly decreasing trend was observed until 60 min. Upon 60 min, a sharp decline was monitored and minor variations remained until the end of 180 min. Simply an average value of 0.280 could be regarded as appropriate for expressing polydispersity of "Fe-TiO_2 and HA" binary system under "as-is" conditions.

Table 4.67. Polydispersity of "Fe-TiO_2 and HA" binary system under "as-is" conditions.

Fe-TiO_2 and HA	Polydispersity						
	0	30	60	90	120	150	180
	0.387	0.342	0.289	0.252	0.239	0.256	0.198

Time dependent comparative presentation of log Normal distribution and multi-size distribution of "Fe-TiO_2 and HA" binary system under "as-is" conditions was given in Figure 4.106.

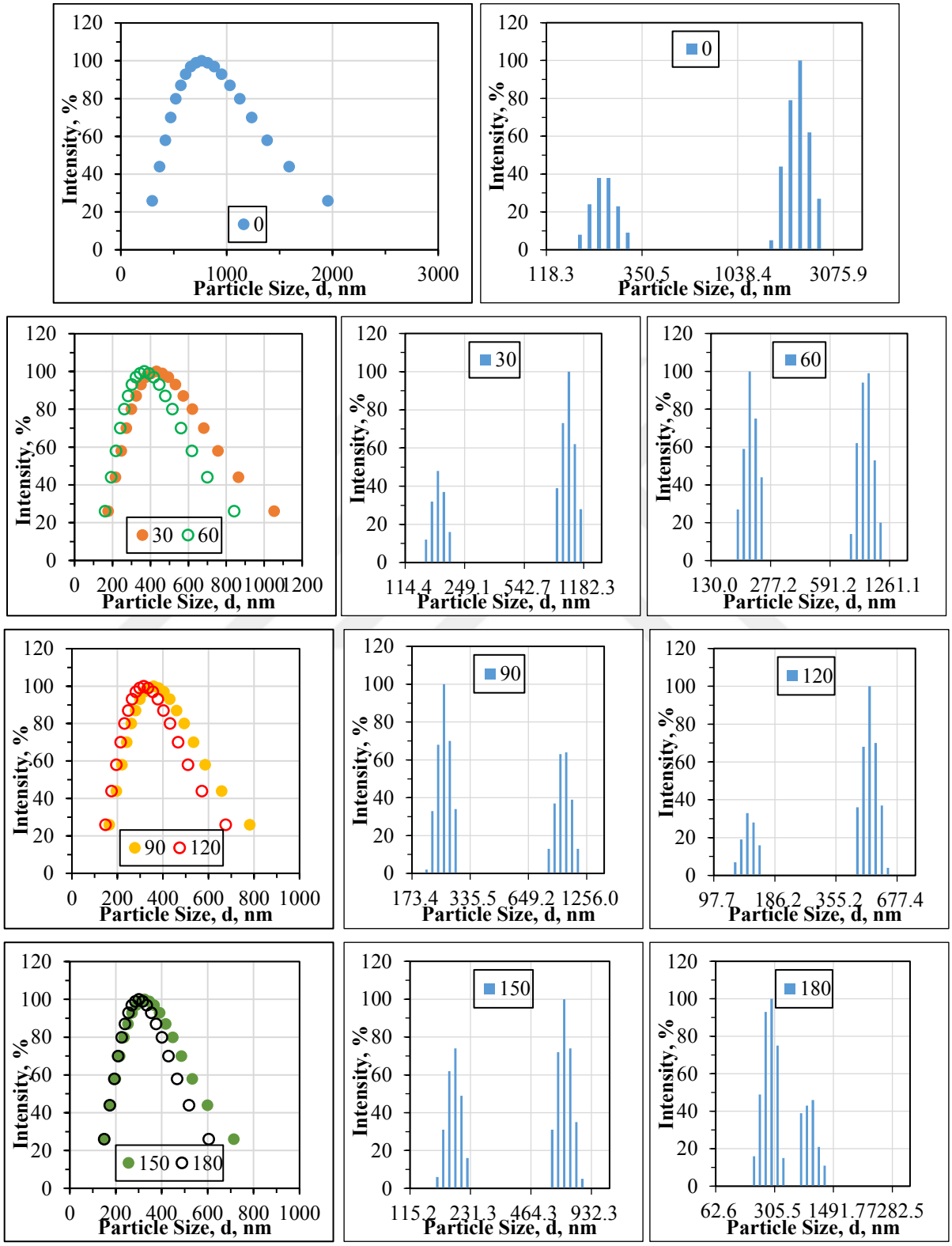


Figure 4.106. "Fe-TiO_2 and HA" binary system under "as-is" conditions intensity profile: Time dependent comparative presentation of log Normal distribution and multi-size distribution of "Fe-TiO_2 and HA" binary system under "as-is" conditions.

4.1.4.18. "Fe-TiO_2 and HA" binary system under "as-is" conditions volume profile. Time dependent logN distribution G(d) and multi size distribution C(d) of "Fe-TiO_2 and HA" binary system under "as-is" conditions volume profile was exhibited in Figure 4.107. Time dependent mean diameter, range and min-max diameter difference with respect to log normal and multi-size distribution of "Fe-TiO_2 and HA" binary system under "as-is" conditions volume profile was displayed in Table 4.68.

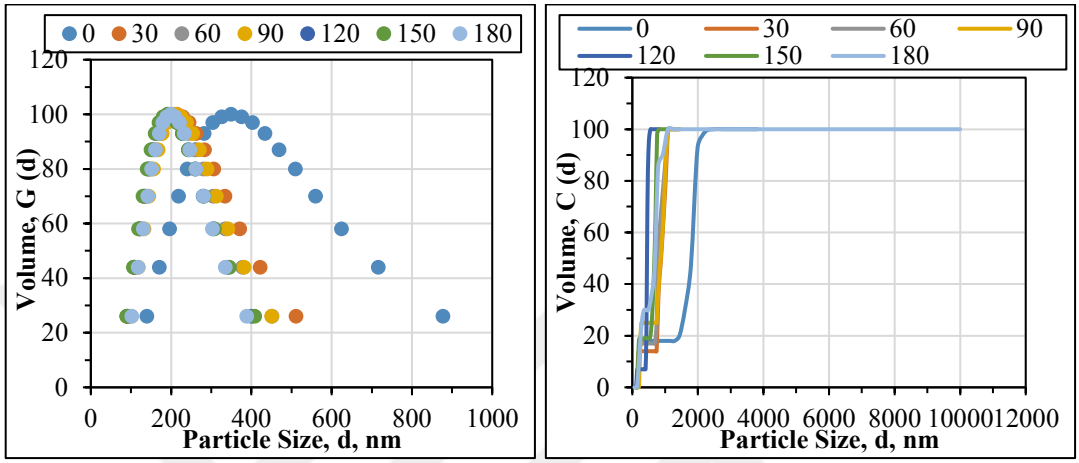


Figure 4.107. "Fe-TiO_2 and HA" binary system under "as-is" conditions volume profile: Time dependent logN distribution G(d) and multi size distribution C(d).

Table 4.68. "Fe-TiO_2 and HA" binary system under "as-is" conditions volume profile: Time dependent mean diameter, range and min-max diameter difference with respect to log normal and multi-size distribution.

Fe-TiO_2 and HA	time, min						
	0	30	60	90	120	150	180
Log Normal distribution							
Mean, nm	349.8	214.5	202.2	212.7	192.5	191.3	199.4
Range	139.4-877.7	90.0-511.5	90.6-451.4	100.4-450.9	92.6-400.2	89.7-408.1	102.4-388.3
Difference	738.3	421.5	360.8	350.5	307.6	318.4	285.9
Multi-size distribution							
Max 1, nm	203.7	168.8	204.7	241.2	134.9	175.0	222.5
Max 2, nm	1992.2	801.0	800.5	791.3	459.8	187.6	260.7
Max 3, nm	-	1093.7	1083.8	1030.4	-	756.4	791.1
Max 4, nm	-	-	-	-	-	-	1086.3
Range	118.3-3822.0	114.4-1381.5	130.0-1467.4	173.4-1433.3	97.7-770.8	115.2-1071.8	62.6-10.000
Difference	3703.7	1267.1	1337.4	1259.9	673.1	956.6	9937.4

Hydrodynamic particle size variations detected between 349.8 nm and 199.4 nm. According to multi-size distribution, initially two peaks were monitored and four peaks were observed upon 180

min. Time dependent comparative presentation of log Normal distribution and multi-size distribution of "Fe-TiO_2 and HA" binary system under "as-is" conditions was given in Figure 4.108.

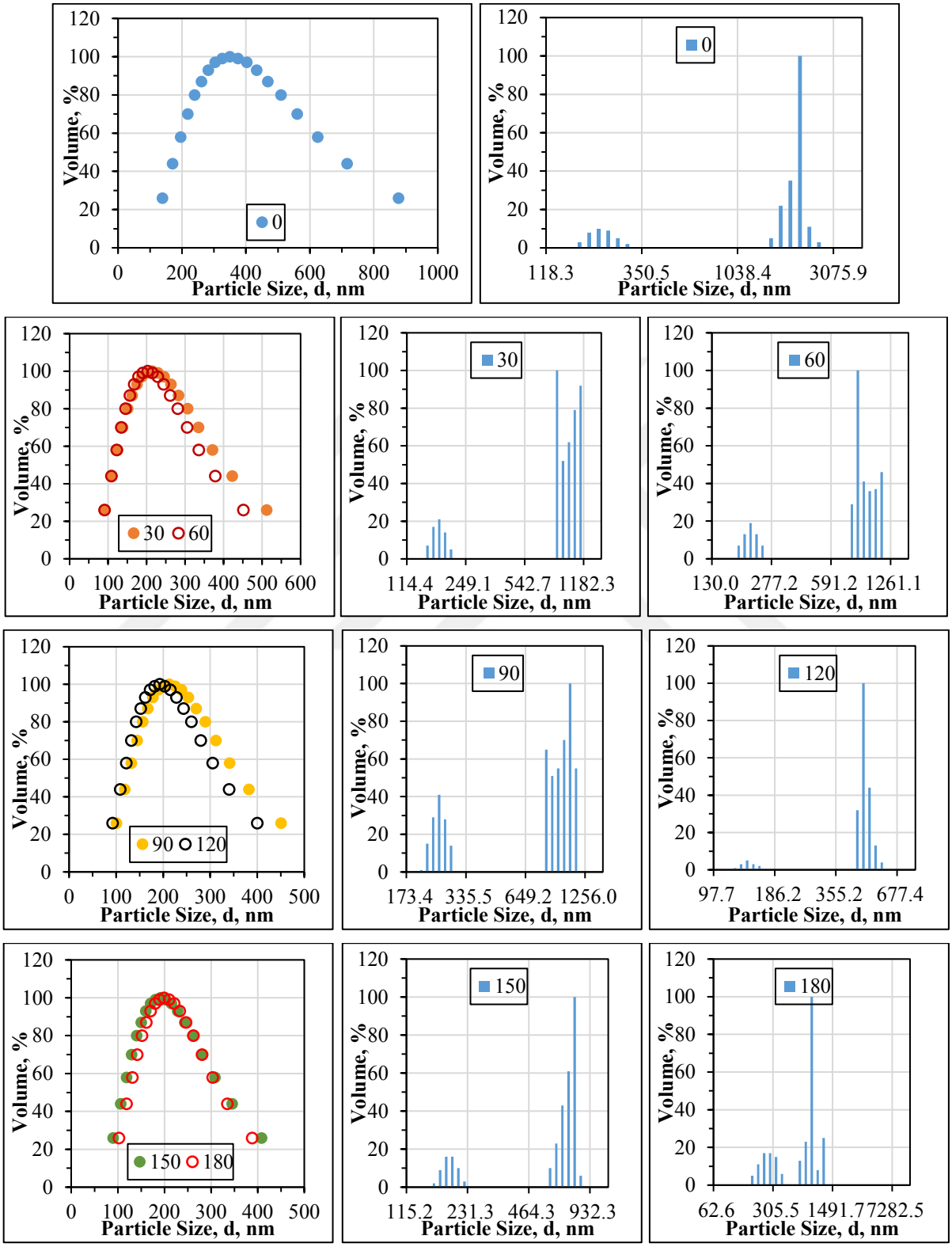


Figure 4.108. "Fe-TiO_2 and HA" binary system under "as-is" conditions volume profile: Time dependent comparative presentation of log Normal distribution and multi-size distribution of "Fe-TiO_2 and HA" binary system under "as-is" conditions.

4.1.4.19. "Fe-TiO_2 and HA" binary system under "as-is" conditions surface area profile. Time dependent logN distribution G(d) and multi size distribution C(d) of "Fe-TiO_2 and HA" binary system under "as-is" conditions surface area profile was presented in Figure 4.109. Time dependent mean diameter, range and min-max diameter difference with respect to log normal and multi-size distribution of "Fe-TiO_2 and HA" binary system under "as-is" conditions surface area profile was demonstrated in Table 4.69.

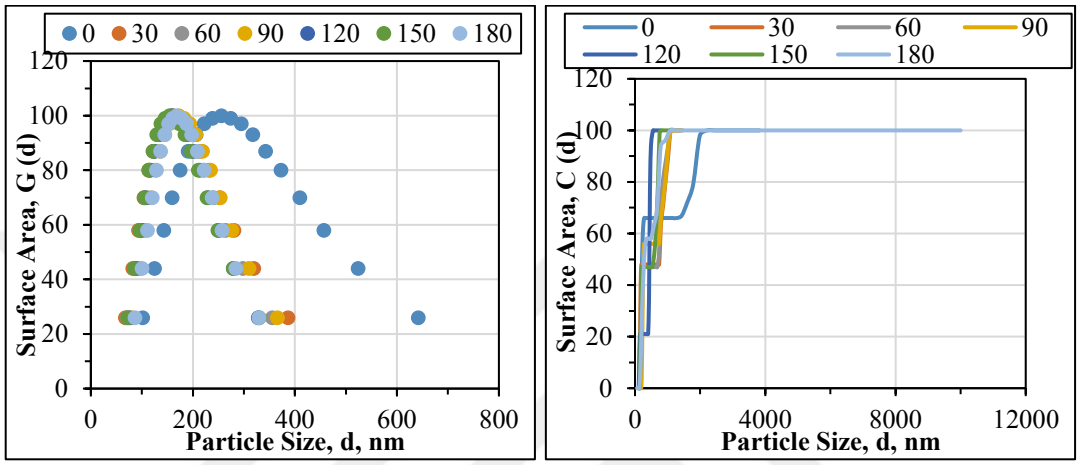


Figure 4.109. "Fe-TiO_2 and HA" binary system under "as-is" conditions surface area profile: Time dependent logN distribution G(d) and multi size distribution C(d).

Table 4.69. "Fe-TiO_2 and HA" binary system under "as-is" conditions surface area profile: Time dependent mean diameter, range and min-max diameter difference with respect to log normal and multi-size distribution.

Fe-TiO_2 and HA	time, min						
	0	30	60	90	120	150	180
Log Normal distribution							
Mean, nm	255.9	162.3	159.3	172.7	158.0	154.7	169.2
Range	102.0-642.0	68.1-387.0	71.4-355.7	81.5-366.0	76.0-328.4	72.5-330.1	86.9-329.5
Difference	540.0	318.9	284.3	284.5	252.4	257.6	242.6
Multi-size distribution							
Max 1, nm	203.7	168.8	204.7	241.2	134.9	175.0	222.5
Max 2, nm	1992.2	801.0	800.5	791.3	459.8	756.4	791.1
Max 3, nm	-	1093.7	1083.8	1030.4	-	-	1086.3
Range	118.3-3822.0	114.4-1381.5	130.0-1467.4	173.4-1433.3	97.7-770.8	115.2-1071.8	62.6-10.000
Difference	3703.7	1267.1	1337.4	1259.9	673.1	956.6	9937.4

In terms of surface area profile, initial hydrodynamic particle size of "Fe-TiO_2 and HA" was obtained as 255.9 nm. Upon 30 min, ~45 % decrease was observed. In terms of multi-size distribution, initially two peaks and upon 30 min, three peaks were observed. Time dependent comparative

presentation of log Normal distribution and multi-size distribution of "Fe-TiO_2 and HA" binary system under "as-is" conditions surface area profile was given in Figure 4.110.

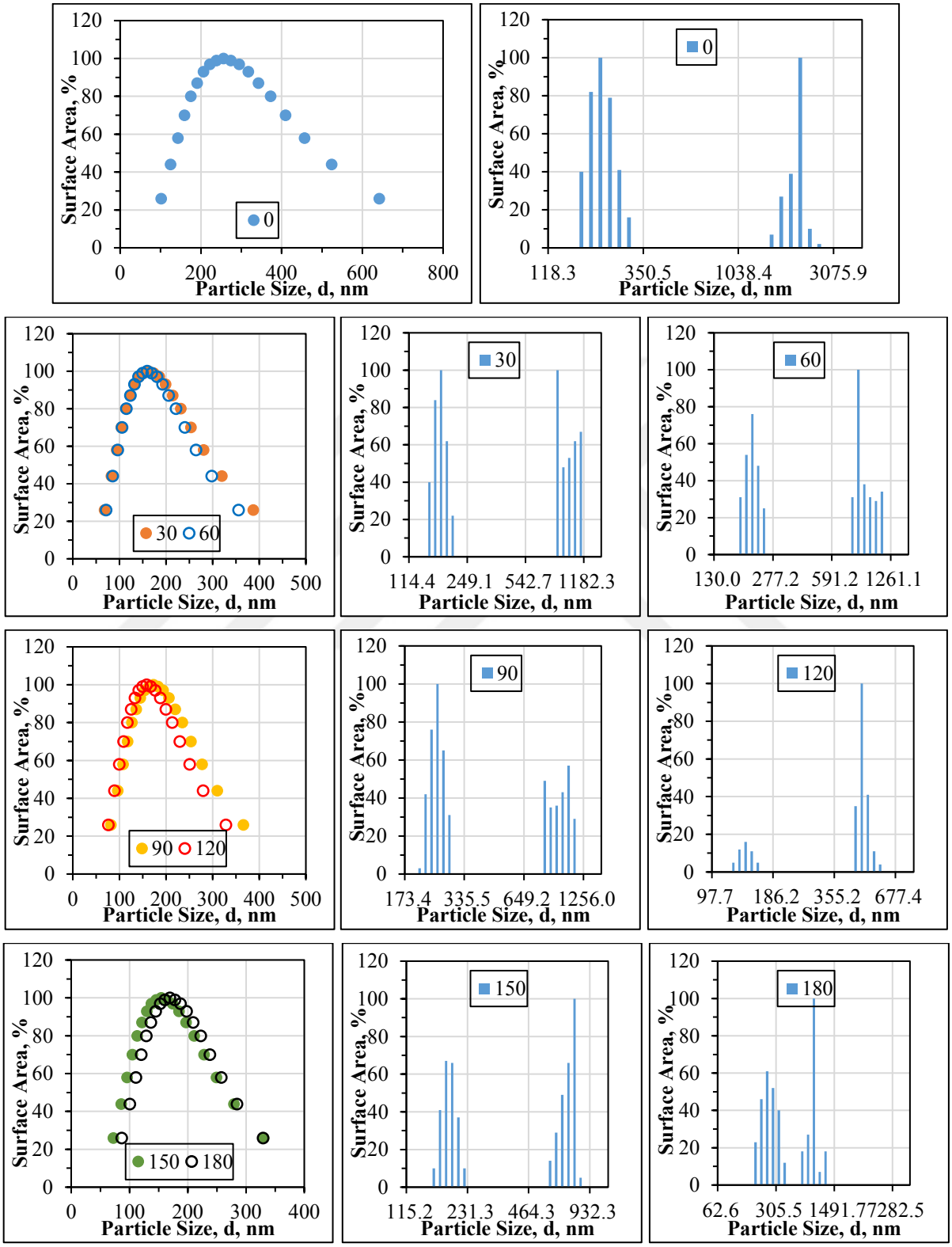


Figure 4.110. "Fe-TiO_2 and HA" binary system under "as-is" conditions surface area profile: Time dependent comparative presentation of log Normal distribution and multi-size distribution of "Fe-TiO_2 and HA" binary system under "as-is" conditions.

4.1.4.20. "Fe-TiO_2 and HA" binary system under "as-is" conditions number profile. Time dependent logN distribution G(d) and multi size distribution C(d) of "Fe-TiO_2 and HA" binary system under "as-is" conditions number profile was exhibited in Figure 4.111. Time dependent mean diameter, range and min-max diameter difference with respect to log normal and multi-size distribution of "Fe-TiO_2 and HA" binary system under "as-is" conditions number profile was presented in Table 4.70.

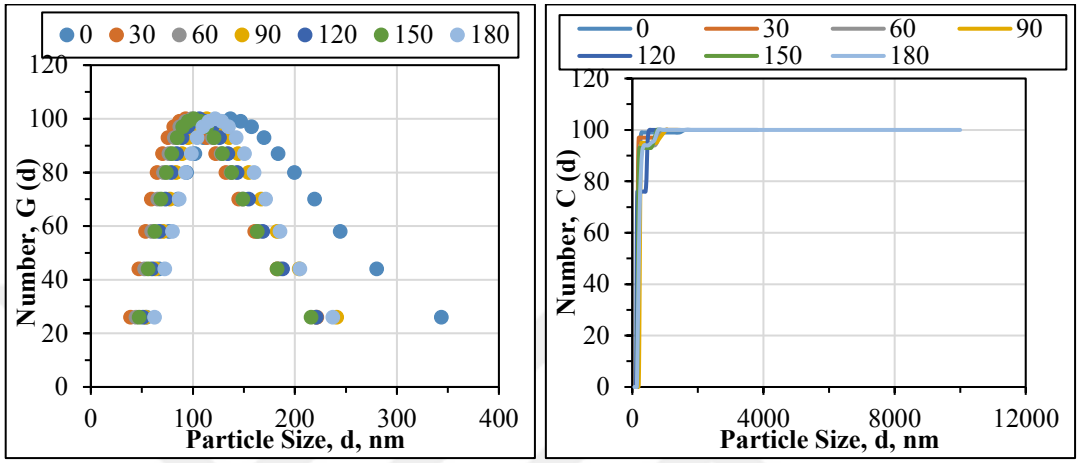


Figure 4.111. "Fe-TiO_2 and HA" binary system under "as-is" conditions number profile: Time dependent logN distribution G(d) and multi size distribution C(d).

Table 4.70. "Fe-TiO_2 and HA" binary system under "as-is" conditions number profile: Time dependent mean diameter, range and min-max diameter difference with respect to log normal and multi-size distribution.

Fe-TiO_2 and HA	time, min						
	0	30	60	90	120	150	180
Log Normal distribution							
Mean, nm	136.9	92.9	98.9	113.8	106.4	101.2	121.9
Range	54.6-343.5	39.0-221.5	44.3-220.9	53.7-241.2	51.2-221.1	47.5-216.0	62.6-237.3
Difference	288.9	182.5	176.6	187.5	169.9	168.5	174.7
Multi-size distribution							
Max 1, nm	182.7	168.8	204.7	241.2	134.9	175.0	189.9
Max 2, nm	1992.2	801.0	800.5	791.3	459.8	756.4	791.1
Range	118.3-3822.0	114.4-1381.5	130.0-1467.4	173.4-1433.3	97.7-770.8	115.2-1071.8	62.6-10.000
Difference	3703.7	1267.1	1337.4	1259.9	673.1	956.6	9937.4

In terms of number profile, hydrodynamic particle size of "Fe-TiO_2 and HA" binary system under "as-is" conditions displayed a sharp decrease following initial period of time and slight increases were observed until 180 min. In terms of multi-size distribution, two max diameters were obtained along 180 min. Time dependent comparative presentation of log Normal distribution and multi-size

distribution of "Fe-TiO_2 and HA" binary system under "as-is" conditions number profile was presented in Figure 4.112.

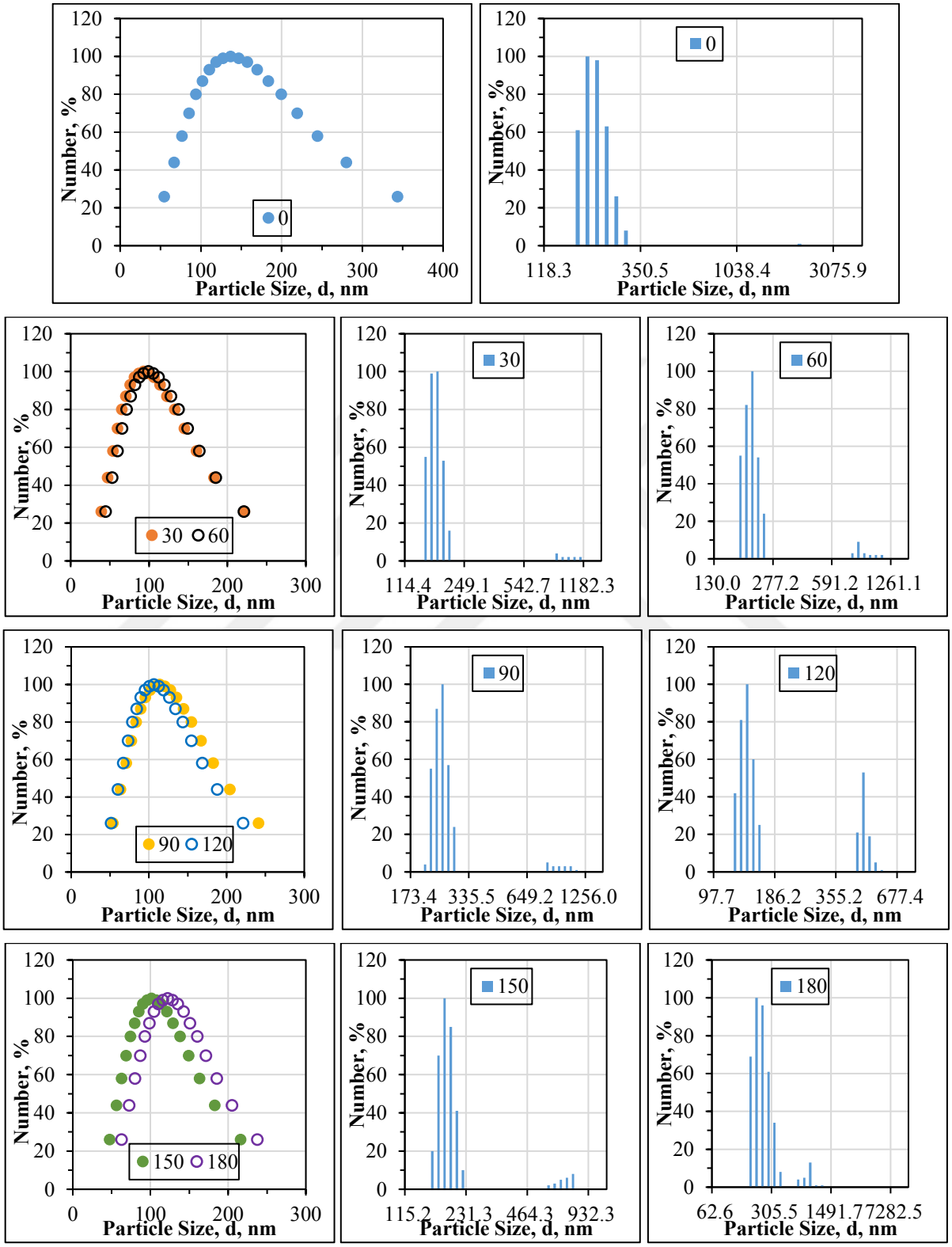


Figure 4.112. "Fe-TiO_2 and HA" binary system under "as-is" conditions number profile: Time dependent comparative presentation of log Normal distribution and multi-size distribution of "Fe-TiO_2 and HA" binary system under "as-is" conditions.

4.1.4.21. "Fe-TiO_2 and SRNOM" binary system under "as-is" conditions intensity profile. Time dependent logN distribution G(d) and multi size distribution C(d) of "Fe-TiO_2 and SRNOM" binary system under "as-is" conditions intensity profile was displayed in Figure 4.113. Time dependent mean diameter, range and min-max diameter difference with respect to log normal and multi-size distribution of "Fe-TiO_2 and SRNOM" binary system under "as-is" conditions intensity profile was exhibited in Table 4.71.

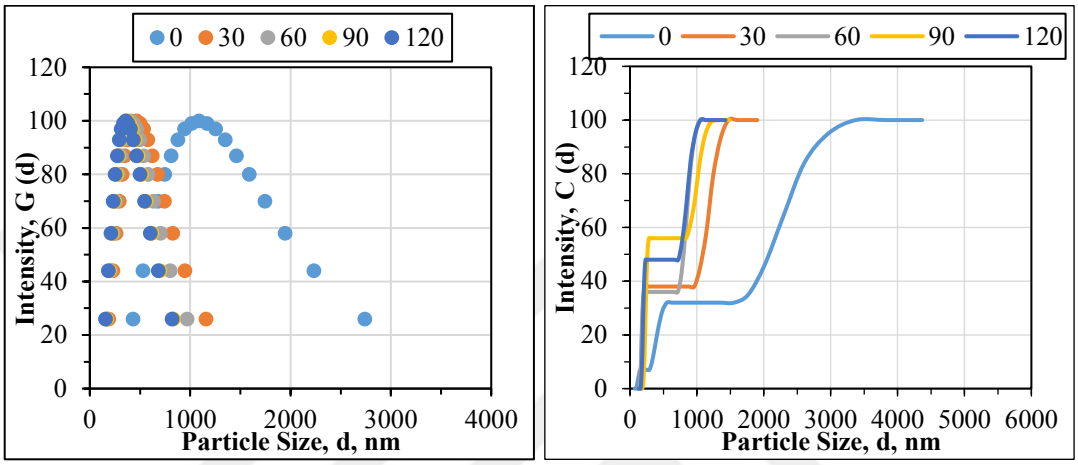


Figure 4.113. "Fe-TiO_2 and SRNOM" binary system under "as-is" conditions intensity profile: Time dependent logN distribution G(d) and multi size distribution C(d).

Table 4.71. "Fe-TiO_2 and SRNOM" binary system under "as-is" conditions intensity profile: Time dependent mean diameter, range and min-max diameter difference with respect to log normal and multi-size distribution.

Fe-TiO_2 and SRNOM	time, min				
	0	30	60	90	120
Log Normal distribution					
Mean, nm	1088.8	466.4	407.7	372.9	357.2
Range	432.7-2739.7	187.9-1157.8	171.0-971.8	166.6-834.5	155.7-819.2
Difference	2307.0	969.9	800.8	667.9	663.5
Multi-size distribution					
Max 1, nm	133.4	189.7	181.9	245.7	199.3
Max 2, nm	426.7	1241.7	897.4	1039.9	906.9
Max 3, nm	2604.9	-	-	-	-
Range	69.9-4367.9	123.8-1903.2	115.3-1312.2	148.3-1491.6	126.5-1428.7
Difference	4298.0	1779.4	1196.9	1343.3	1302.2

In terms of intensity profile, initial hydrodynamic particle size of "Fe-TiO_2 and SRNOM" binary system under "as-is" conditions detected as 1088.8 nm and displayed a sharp decrease in the first 30 min. Accordingly, continuous decrease was monitored upon 120 min. Considering multi-size

distribution, initially three peaks were observed and two peaks remained until 120 min. Time dependent comparative presentation of log Normal distribution and multi-size distribution of "Fe-TiO_2 and SRNOM" binary system under "as-is" conditions intensity profile was presented in Figure 4.114. Also, polydispersity of "Fe-TiO_2 and SRNOM" binary system under "as-is" conditions was given in Table 4.72. It could be concluded that continuous decrease was monitored upon 120 min.

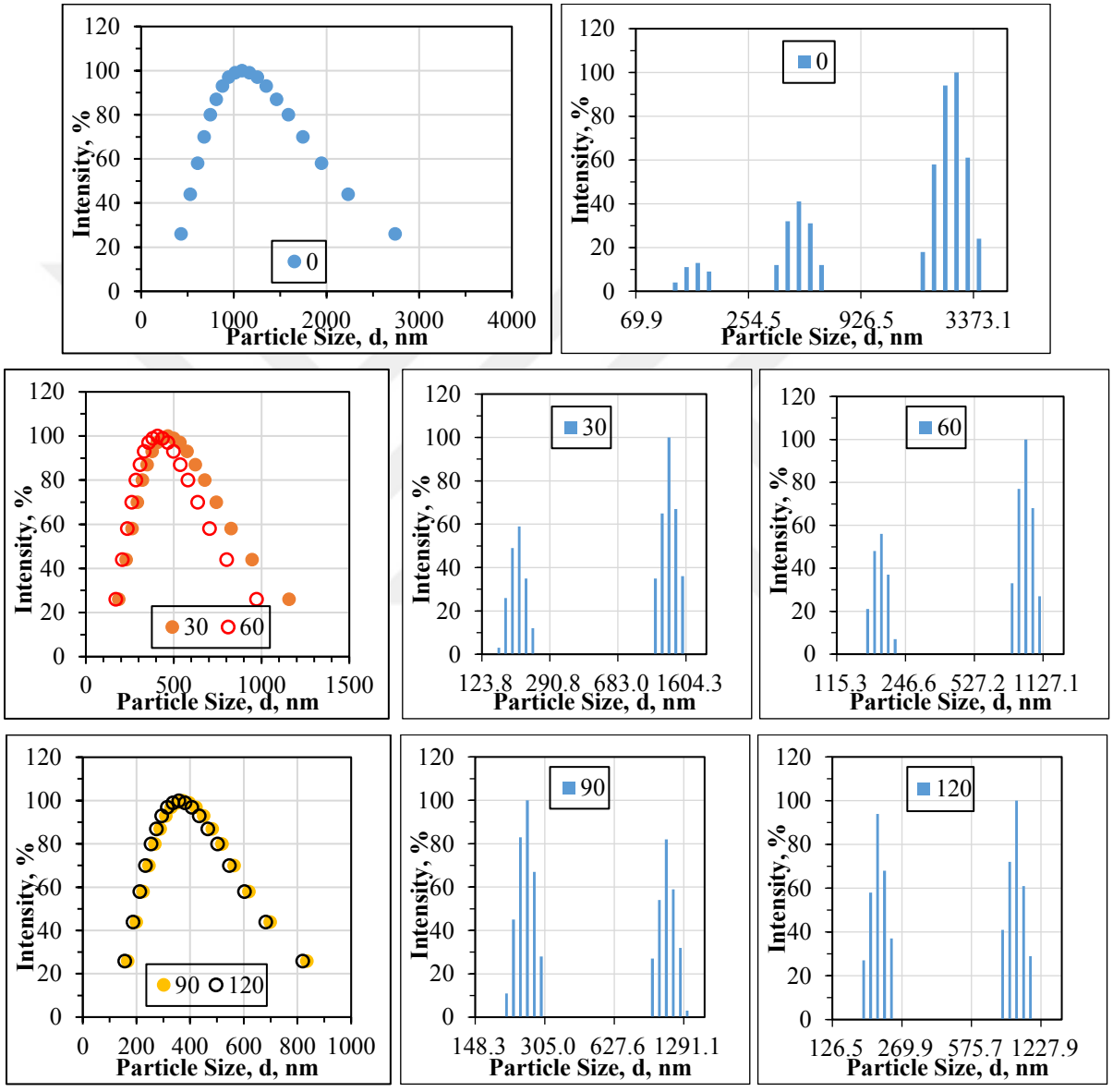


Figure 4.114. "Fe-TiO_2 and SRNOM" binary system under "as-is" conditions intensity profile: Time dependent comparative presentation of log Normal distribution and multi-size distribution of "Fe-TiO_2 and SRNOM" binary system under "as-is" conditions.

Table 4.72. Polydispersity of "Fe-TiO_2 and SRNOM" binary system under "as-is" conditions.

Fe-TiO_2 and SRNOM	Polydispersity				
	0	30	60	90	120
	0.370	0.357	0.322	0.271	0.290

4.1.4.22. "Fe-TiO_2 and SRNOM" binary system under "as-is" conditions volume profile. Time dependent logN distribution G(d) and multi size distribution C(d) of "Fe-TiO_2 and SRNOM" binary system under "as-is" conditions volume profile was exhibited in Figure 4.115. Time dependent mean diameter, range and min-max diameter difference with respect to log normal and multi-size distribution of "Fe-TiO_2 and SRNOM" binary system under "as-is" conditions volume profile was demonstrated in Table 4.73.

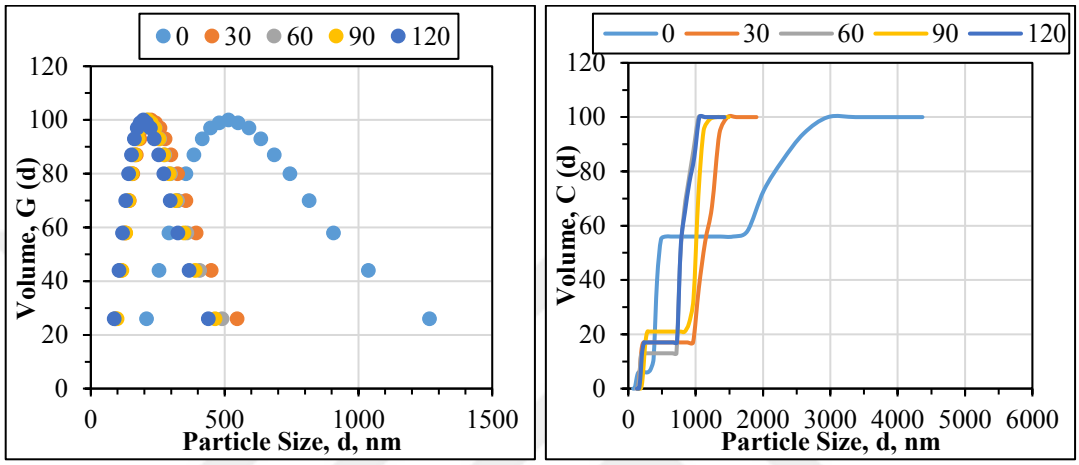


Figure 4.115. "Fe-TiO_2 and SRNOM" binary system under "as-is" conditions volume profile: Time dependent logN distribution G(d) and multi size distribution C(d).

Table 4.73. "Fe-TiO_2 and SRNOM" binary system under "as-is" conditions volume profile: Time dependent mean diameter, range and min-max diameter difference with respect to log normal and multi-size distribution.

Fe-TiO_2 and SRNOM	time, min				
	0	30	60	90	120
Log Normal distribution					
Mean, nm	514.3	225.6	210.9	213.0	196.5
Range	208.9-1266.2	92.9-547.5	90.6-490.8	97.8-464.0	87.9-439.2
Difference	1057.3	454.6	400.2	366.2	351.3
Multi-size distribution					
Max 1, nm	117.2	174.2	168.6	245.7	199.3
Max 2, nm	426.7	189.7	181.9	1039.9	779.4
Max 3, nm	2011.7	1046.8	770.8	-	1055.3
Max 4, nm	-	1352.4	1044.7	-	-
Range	69.9-4367.9	123.8-1903.2	115.3-1312.2	148.3-1491.6	126.5-1428.7
Difference	4298.0	1779.4	1196.9	1343.3	1302.2

According to log normal distribution, it could be inferred that hydrodynamic particle size of "Fe-TiO_2 and SRNOM" binary system under "as-is" conditions demonstrated a rapidly decreasing trend

according to time variations. Initial hydrodynamic particle size was attained as 514.3 nm, revealed approximately 50 % decrease and detected to 196.5 nm upon 120 min. In terms of log normal distribution, size difference decreased from 1057.3 nm to 351.3 nm upon 120 min. For comparison purposes, in terms of multi-size distribution, initially three peaks were monitored and four peaks were attained upon 30 min and 60 min. Upon 90 min, two peaks were monitored. Also, three max diameters were attained upon 120 min period. In terms of multi-size distribution, size difference decreased from 4298.0 nm to 1302.2 nm. Time dependent comparative presentation of log Normal distribution and multi-size distribution of "Fe-TiO_2 and SRNOM" binary system under "as-is" conditions volume profile was displayed in Figure 4.116.

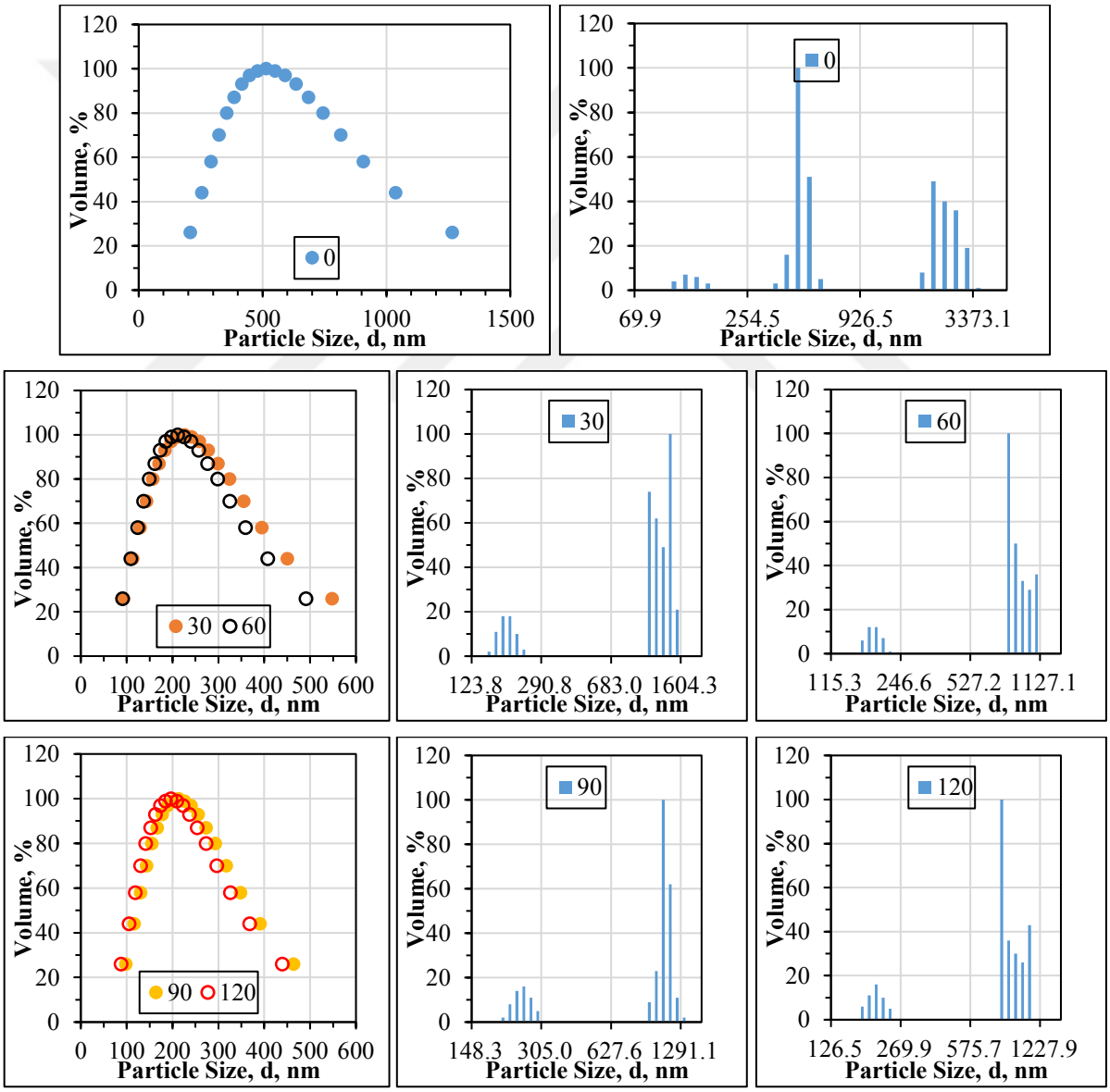


Figure 4.116. "Fe-TiO_2 and SRNOM" binary system under "as-is" conditions volume profile: Time dependent comparative presentation of log Normal distribution and multi-size distribution of "Fe-TiO_2 and SRNOM" binary system under "as-is" conditions.

4.1.4.23. "Fe-TiO_2 and SRNOM" binary system under "as-is" conditions surface area profile. Time dependent logN distribution G(d) and multi size distribution C(d) of "Fe-TiO_2 and SRNOM" binary system under "as-is" conditions surface area profile was displayed in Figure 4.117. Time dependent mean diameter, range and min-max diameter difference with respect to log normal and multi-size distribution of "Fe-TiO_2 and SRNOM" binary system under "as-is" conditions surface area profile was demonstrated in Table 4.74.

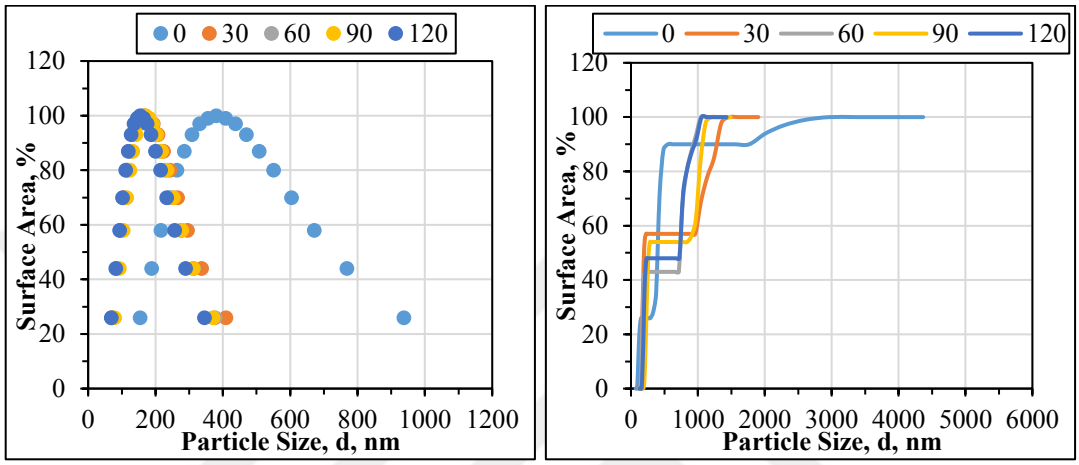


Figure 4.117. "Fe-TiO_2 and SRNOM" binary system under "as-is" conditions surface area profile: Time dependent logN distribution G(d) and multi size distribution C(d).

Table 4.74. "Fe-TiO_2 and SRNOM" binary system under "as-is" conditions surface area profile: Time dependent mean diameter, range and min-max diameter difference with respect to log normal and multi-size distribution.

Fe-TiO_2 and SRNOM	time, min				
	0	30	60	90	120
Log Normal distribution					
Mean, nm	381.0	168.7	162.0	170.3	154.8
Range	154.8-938.1	69.5-409.5	69.6-377.1	78.2-370.9	69.2-345.8
Difference	783.3	340.0	307.5	292.7	276.6
Multi-size distribution					
Max 1, nm	117.2	174.2	168.6	245.7	199.3
Max 2, nm	426.7	1046.8	770.8	1039.9	779.4
Max 3, nm	2011.7	1352.4	1044.7	-	1055.3
Range	69.9-4367.9	123.8-1903.2	115.3-1312.2	148.3-1491.6	126.5-1428.7
Difference	4298.0	1779.4	1196.9	1343.3	1302.2

In a similar manner to data depicted "Fe-TiO_2 and SRNOM" binary system under "as-is" conditions volume profile (Figure 4.115), log normal distribution G(d) and multi size distribution C(d) of "Fe-TiO_2 and SRNOM" binary system under "as-is" conditions surface area profile was

displayed with respect to time. It could be seen that hydrodynamic particle size of "Fe-TiO_2 and SRNOM" binary system under "as-is" conditions exhibited a sharp decrease following initial period of time and minor variations remained until 120 min. Initial hydrodynamic particle size was obtained as 381.0 nm and decreased to 154.8 during 120 min. Size difference revealed a sharp decrease in the first 30 min and continuously decreasing trend was attained until 120 min. However, in terms of multi-size distribution, three max diameters were observed until the end of 120 min. In terms of multi-size distribution, size difference decreased from 4298.0 nm to 1302.2 nm. Time dependent comparative presentation of log Normal distribution and multi-size distribution of "Fe-TiO_2 and SRNOM" binary system under "as-is" conditions surface area profile was demonstrated in Figure 4.118.

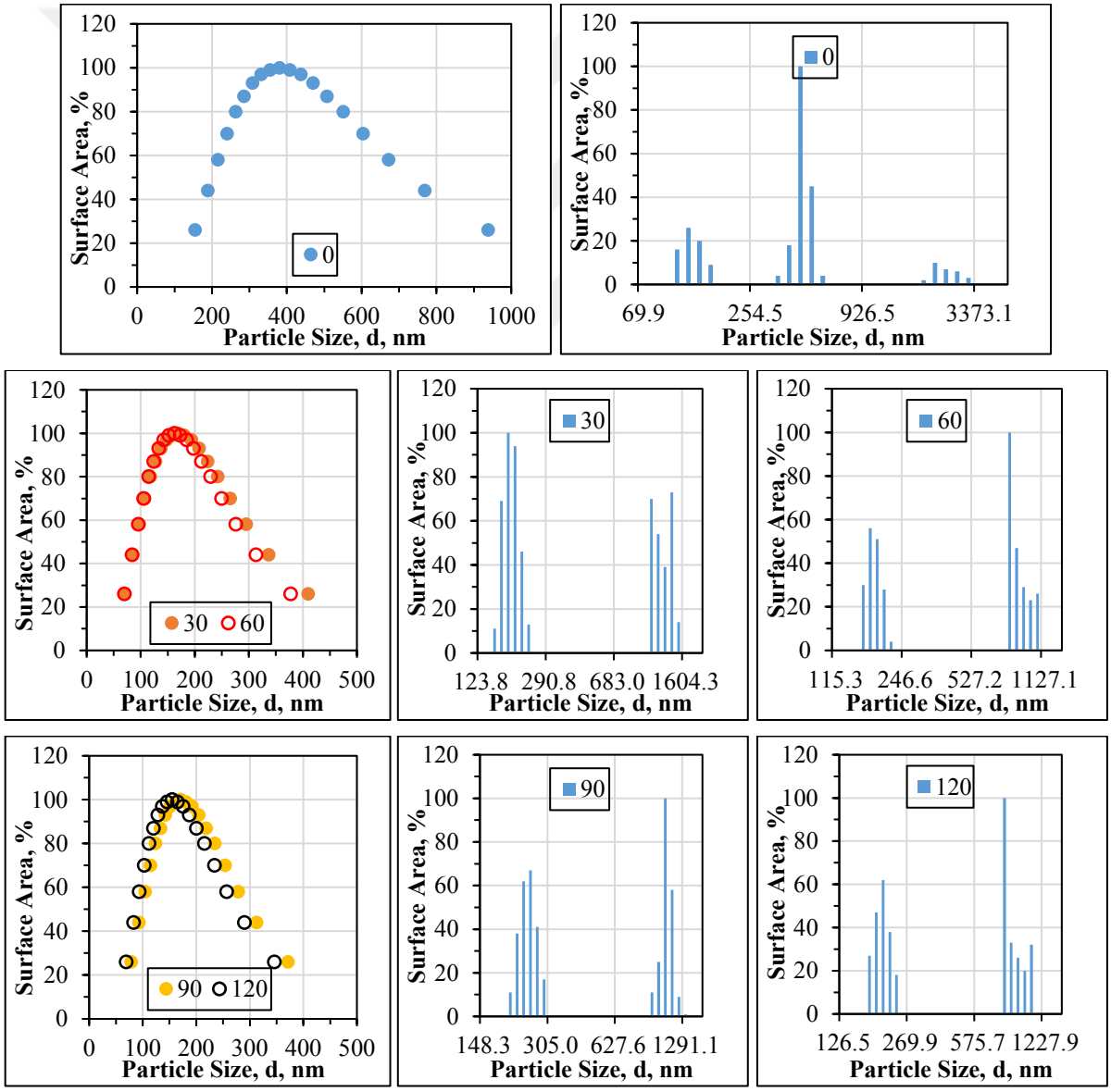


Figure 4.118. "Fe-TiO_2 and SRNOM" binary system under "as-is" conditions surface area profile: Time dependent comparative presentation of log Normal distribution and multi-size distribution of "Fe-TiO_2 and SRNOM" binary system under "as-is" conditions.

4.1.4.24. "Fe-TiO_2 and SRNOM" binary system under "as-is" conditions number profile. Time dependent logN distribution G(d) and multi size distribution C(d) of "Fe-TiO_2 and SRNOM" binary system under "as-is" conditions number profile was given in Figure 4.119. Time dependent mean diameter, range and min-max diameter difference with respect to log normal and multi-size distribution of "Fe-TiO_2 and SRNOM" binary system under "as-is" conditions number profile was displayed in Table 4.75.

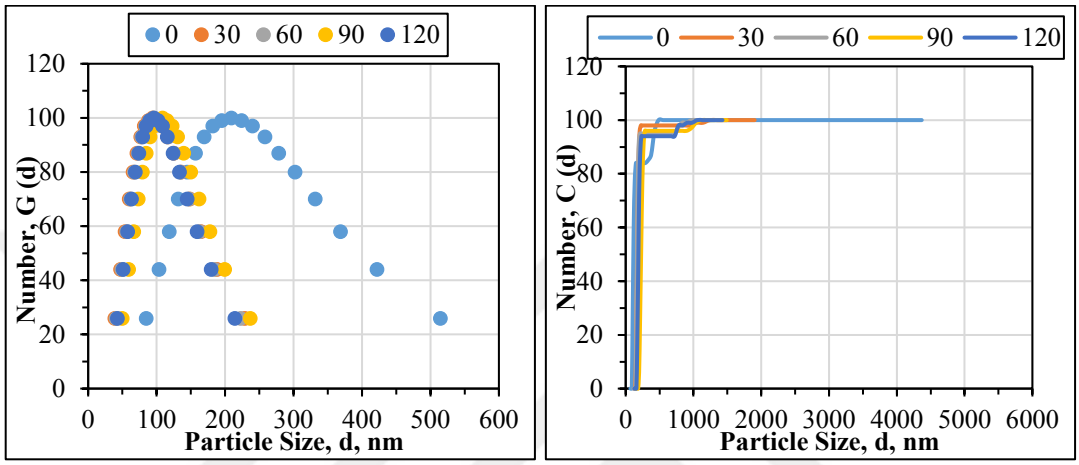


Figure 4.119. "Fe-TiO_2 and SRNOM" binary system under "as-is" conditions number profile: Time dependent logN distribution G(d) and multi size distribution C(d).

Table 4.75. "Fe-TiO_2 and SRNOM" binary system under "as-is" conditions number profile: Time dependent mean diameter, range and min-max diameter difference with respect to log normal and multi-size distribution.

Fe-TiO_2 and SRNOM	time, min				
	0	30	60	90	120
Log Normal distribution					
Mean, nm	209.1	94.3	95.6	108.8	96.0
Range	84.9-514.8	38.9-229.0	41.1-222.6	50.0-237.0	42.9-214.4
Difference	429.9	190.1	181.5	187.0	171.5
Multi-size distribution					
Max 1, nm	117.2	174.2	168.6	228.6	199.3
Max 2, nm	426.7	1046.8	770.8	1039.9	779.4
Max 3, nm	-	-	-	-	1055.3
Range	69.9-4367.9	123.8-1903.2	115.3-1312.2	148.3-1491.6	126.5-1428.7
Difference	4298.0	1779.4	1196.9	1343.3	1302.2

As explained for "Fe-TiO_2 and SRNOM" binary system under "as-is" conditions surface area profile (Table 4.74), a similar approach was followed for "Fe-TiO_2 and SRNOM" binary system under "as-is" conditions number profile. It could be inferred that hydrodynamic particle size roughly 50 %

decreased upon 30 min. Initial hydrodynamic particle size was recorded as 209.1 nm and reached to 94.3 nm upon 30 min. Correspondingly, minor increase was monitored with slight variations until the end of 120 min. Also, difference between max and min diameter was obtained as 429.9 nm and detected to 171.5 nm upon period of 120 min. However, in terms of multi-size distribution, initially two max diameters were observed and three peaks were attained upon 120 min.

As explained for "Fe-TiO_2 and SRNOM" binary system under "as-is" conditions surface area profile (Figure 4.118), time dependent comparative presentation of log Normal distribution and multi-size distribution of "Fe-TiO_2 and SRNOM" binary system under "as-is" conditions number profile was presented in Figure 4.120.

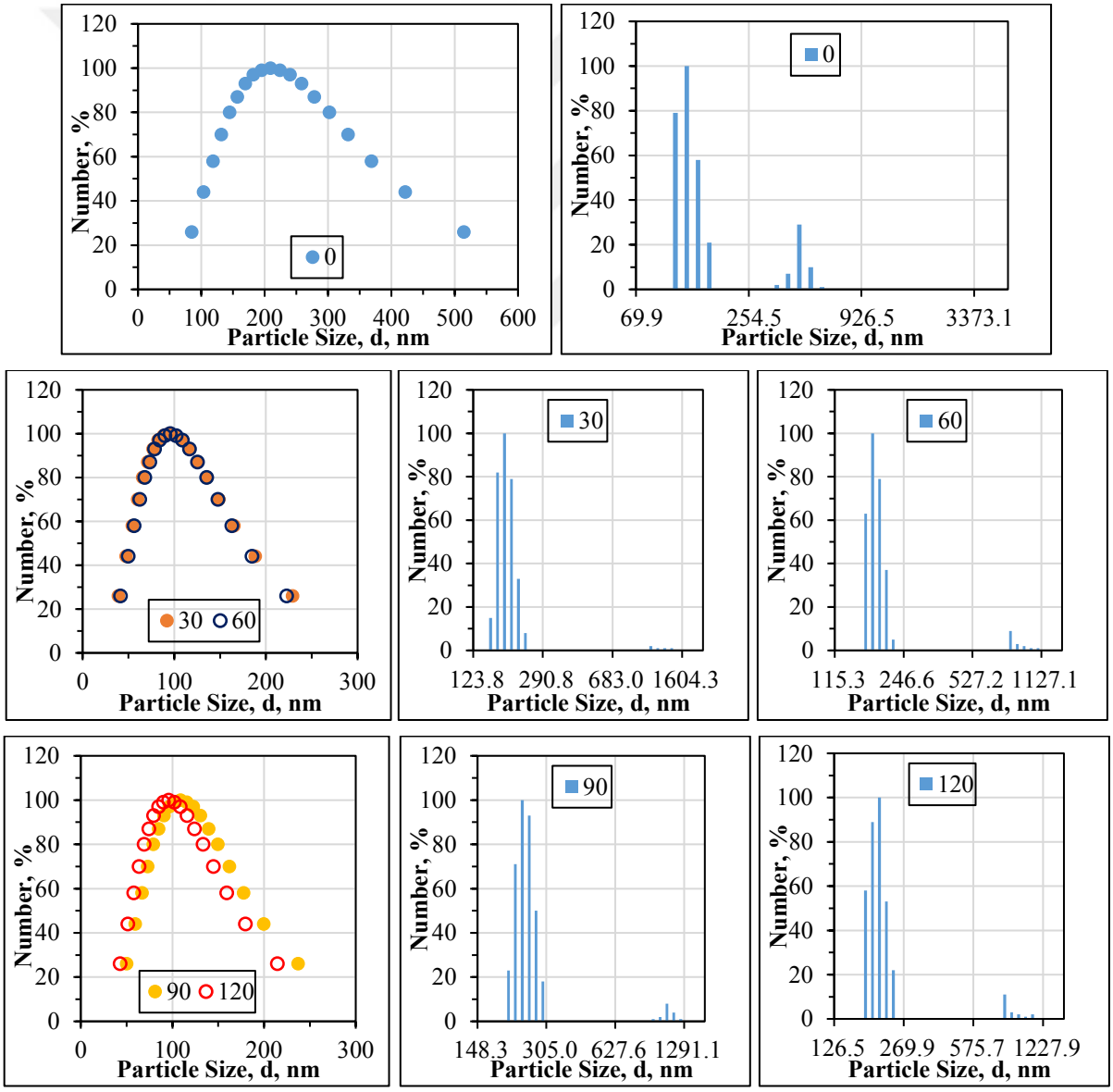


Figure 4.120. "Fe-TiO_2 and SRNOM" binary system under "as-is" conditions number profile: Time dependent comparative presentation of log Normal distribution and multi-size distribution of "Fe-TiO_2 and SRNOM" binary system under "as-is" conditions.

4.1.5. Binary System: As-is Under Dark Conditions

As explained for binary system under "as-is" (Section 4.1.4), a similar approach was followed for elucidation of the hydrodynamic particle size of binary system "as-is" under dark conditions. The elucidation of the hydrodynamic particle size of the nanoparticles were also exhibited "as-is" under dark conditions separately *i.e.* "TiO_2 and HA" binary system "as-is" under dark conditions, "N-TiO_2 and HA" binary system "as-is" under dark conditions, and "Fe-TiO_2 and HA" binary system "as-is" under dark conditions. Basically, data represented time dependent hydrodynamic size variations in terms of intensity, volume, surface area, and number parameters. Particle size distribution will be presented in two modes as mono-size and multi-size distribution.

4.1.5.1. "TiO_2 and HA" binary system "as-is" under dark conditions intensity profile. Time dependent logN distribution G(d) and multi size distribution C(d) of "TiO_2 and HA" binary system "as-is" under dark conditions intensity profile was given in Figure 4.121. Time dependent mean diameter, range and min-max diameter difference with respect to log normal and multi-size distribution of "TiO_2 and HA" binary system "as-is" under dark conditions intensity profile was displayed in Table 4.76. Also, polydispersity of "TiO_2 and HA" binary system "as-is" under dark conditions was demonstrated in Table 4.77.

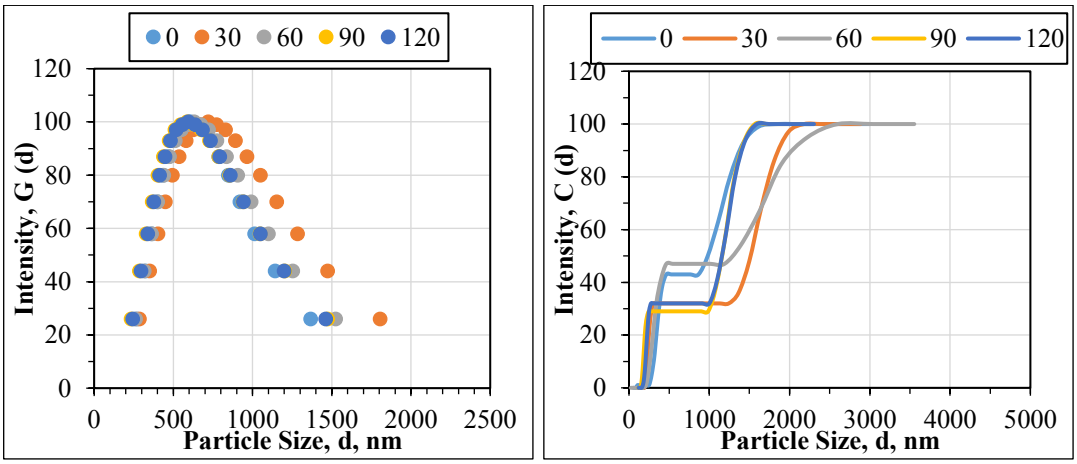


Figure 4.121. "TiO_2 and HA" binary system "as-is" under dark conditions intensity profile: Time dependent logN distribution G(d) and multi size distribution C(d).

In a similar manner to data described "TiO_2 and HA" binary system under "as-is" conditions intensity profile (Figure 4.73), log normal distribution G(d) and multi size distribution C(d) of "TiO_2 and HA" binary system "as-is" under dark conditions intensity profile was demonstrated according to time variations. Hydrodynamic particle size of "TiO_2 and HA" binary system "as-is" under dark

conditions exhibited a fluctuating trend with respect to time. In terms of log normal distribution, it could be deduced that certain peaks were monitored as coinciding max diameters. However, due to multi-size distribution, each peak could be easily discriminated. Time dependent comparative presentation of log Normal distribution and multi-size distribution of "TiO_2 and HA" binary system "as-is" under dark conditions intensity profile was presented in Figure 4.122.

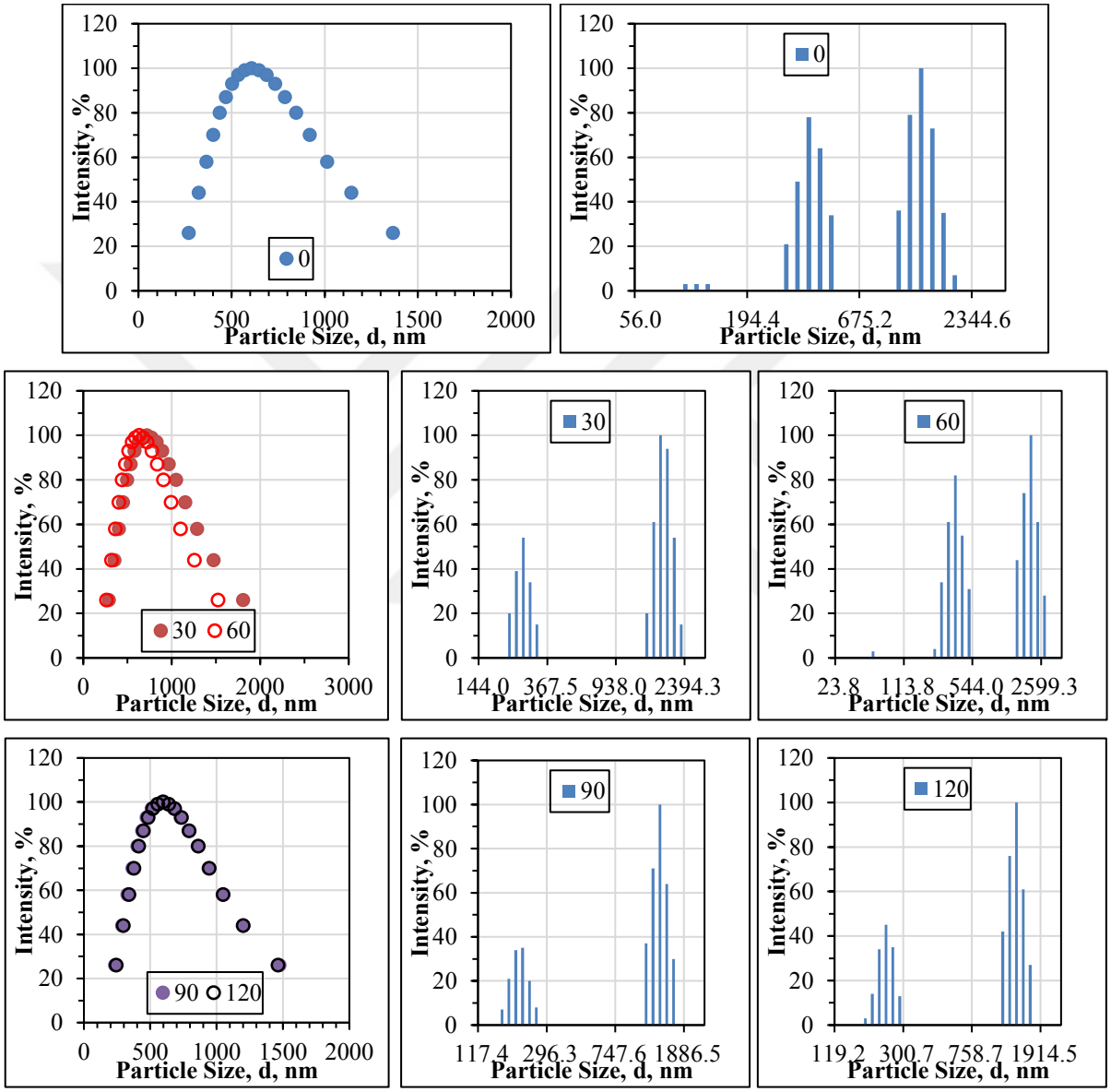


Figure 4.122. "TiO_2 and HA" binary system "as-is" under dark conditions intensity profile: Time dependent comparative presentation of log Normal distribution and multi-size distribution of "TiO_2 and HA" binary system "as-is" under dark conditions.

Based on the data presented in Figure 4.121 and 4.122., time dependent mean diameter, range and min-max diameter difference with respect to log normal and multi-size distribution of "TiO_2 and HA" binary system "as-is" under dark conditions intensity profile was displayed in Table 4.76.

Table 4.76. "TiO_2 and HA" binary system "as-is" under dark conditions intensity profile: Time dependent mean diameter, range and min-max diameter difference with respect to log normal and multi-size distribution.

TiO_2 and HA	time, min				
	0	30	60	90	120
Log Normal distribution					
Mean, nm	608.2	719.8	630.7	587.0	595.7
Range	270.6-1143.0	286.9-1474.2	261.0-1254.6	233.9-1202.6	242.7-1199.5
Difference	1096.0	1519.0	1263.3	1239.4	1219.7
Multi-size distribution					
Max 1, nm	92.1	252.6	52.1	204.6	227.8
Max 2, nm	104.3	1645.8	340.2	1302.8	1322.1
Max 3, nm	118.2	-	1901.1	-	-
Max 4, nm	362.3	-	-	-	-
Max 5, nm	1258.2	-	-	-	-
Range	56.0-3007.5	144.0-2887.8	23.8-3553.9	117.4-2270.2	119.2-2303.8
Difference	2951.5	2743.8	3530.1	2152.8	2184.6

According to log normal distribution and in terms of intensity profile, initial hydrodynamic particle size of "TiO_2 and HA" binary system "as-is" under dark conditions was attained as 608.2 nm. During 120 min, hydrodynamic size of "TiO_2 and HA" binary system "as-is" under dark conditions followed a fluctuating trend and detected to 595.7 nm. On the other hand, initial size difference was recorded as 1096.0 nm and reached to 1219.7 nm upon period of 120 min. However, in terms of multi-size distribution, five max diameters were obtained as 92.1 nm, 104.3 nm, 118.2 nm, 362.3 nm, and 1258.2 nm following initial period of time. Upon 30 min, two peaks were observed and upon 60 min, three peaks were monitored. Upon 90 min, two peaks were obtained until the end of 120 min period.

As described for "TiO_2 and HA" binary system under "as-is" conditions (Table 4.47), polydispersity of "TiO_2 and HA" binary system "as-is" under dark conditions was demonstrated in Table 4.77. It could be asserted that "TiO_2 and HA" binary system "as-is" under dark conditions displayed an inconsistent according to time variations. Simply an average value of 0.338 (0.367 to 0.274) could be regarded as appropriate for expressing polydispersity.

Table 4.77. Polydispersity of "TiO_2 and HA" binary system "as-is" under dark conditions.

TiO_2 and HA	Polydispersity				
	0	30	60	90	120
	0.274	0.367	0.333	0.367	0.347

4.1.5.2. "TiO_2 and HA" binary system "as-is" under dark conditions volume profile. Time dependent logN distribution G(d) and multi size distribution C(d) of "TiO_2 and HA" binary system "as-is" under dark conditions, and time dependent mean diameter, range and min-max diameter difference with respect to log normal and multi-size distribution of "TiO_2 and HA" binary system "as-is" under dark conditions volume profile were given in Figure 4.123 and Table 4.78.

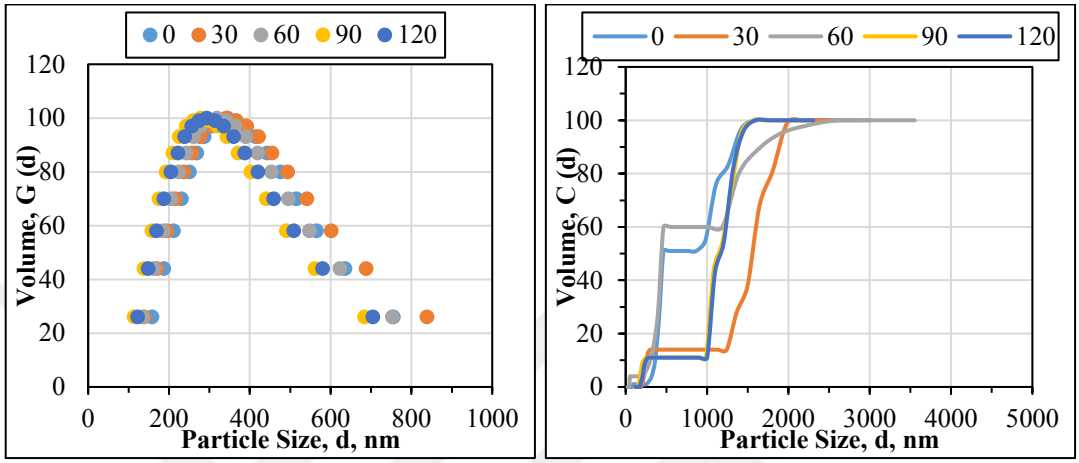


Figure 4.123. "TiO_2 and HA" binary system "as-is" under dark conditions volume profile: Time dependent logN distribution G(d) and multi size distribution C(d).

Table 4.78. "TiO_2 and HA" binary system "as-is" under dark conditions volume profile: Time dependent mean diameter, range and min-max diameter difference with respect to log normal and multi-size distribution.

TiO_2 and HA	time, min				
	0	30	60	90	120
Log Normal distribution					
Mean, nm	345.3	341.8	319.0	278.6	293.6
Range	157.9-755.3	139.3-838.9	135.1-753.1	113.5-684.0	122.4-704.4
Difference	597.4	699.6	618.0	570.5	582.0
Multi-size distribution					
Max 1, nm	92.1	252.6	52.1	186.5	227.8
Max 2, nm	104.3	1645.8	465.2	1082.6	1098.7
Max 3, nm	464.7	1985.1	1390.4	1429.1	1322.1
Max 4, nm	1110.9	-	-	-	-
Max 5, nm	1425.0	-	-	-	-
Range	56.0-3007.5	144.0-2887.8	23.8-3553.9	117.4-2270.2	119.2-2303.8
Difference	2951.5	2743.8	3530.1	2152.8	2184.6

According to log normal distribution, it could be deduced that hydrodynamic particle size of "TiO_2 and HA" binary system "as-is" under dark conditions revealed a slowly decreasing trend

according to time variations. Initial hydrodynamic size was obtained as 345.3 nm and detected to 293.6 nm upon 120 min. Also, in terms of log normal distribution, size difference decreased from 597.4 nm to 582.0 nm upon 120 min. For comparison purposes, in terms of multi-size distribution, initially five max diameters were monitored and three max diameters remained until the end of 120 min. Initial size difference was recorded as 2951.5 nm and decreased to 2184.6 nm during 120 min.

In a similar manner to "TiO_2 and HA" binary system "as-is" under dark conditions intensity profile, time dependent comparative presentation of log Normal distribution and multi-size distribution of "TiO_2 and HA" binary system "as-is" under dark conditions volume profile was demonstrated in Figure 4.124.

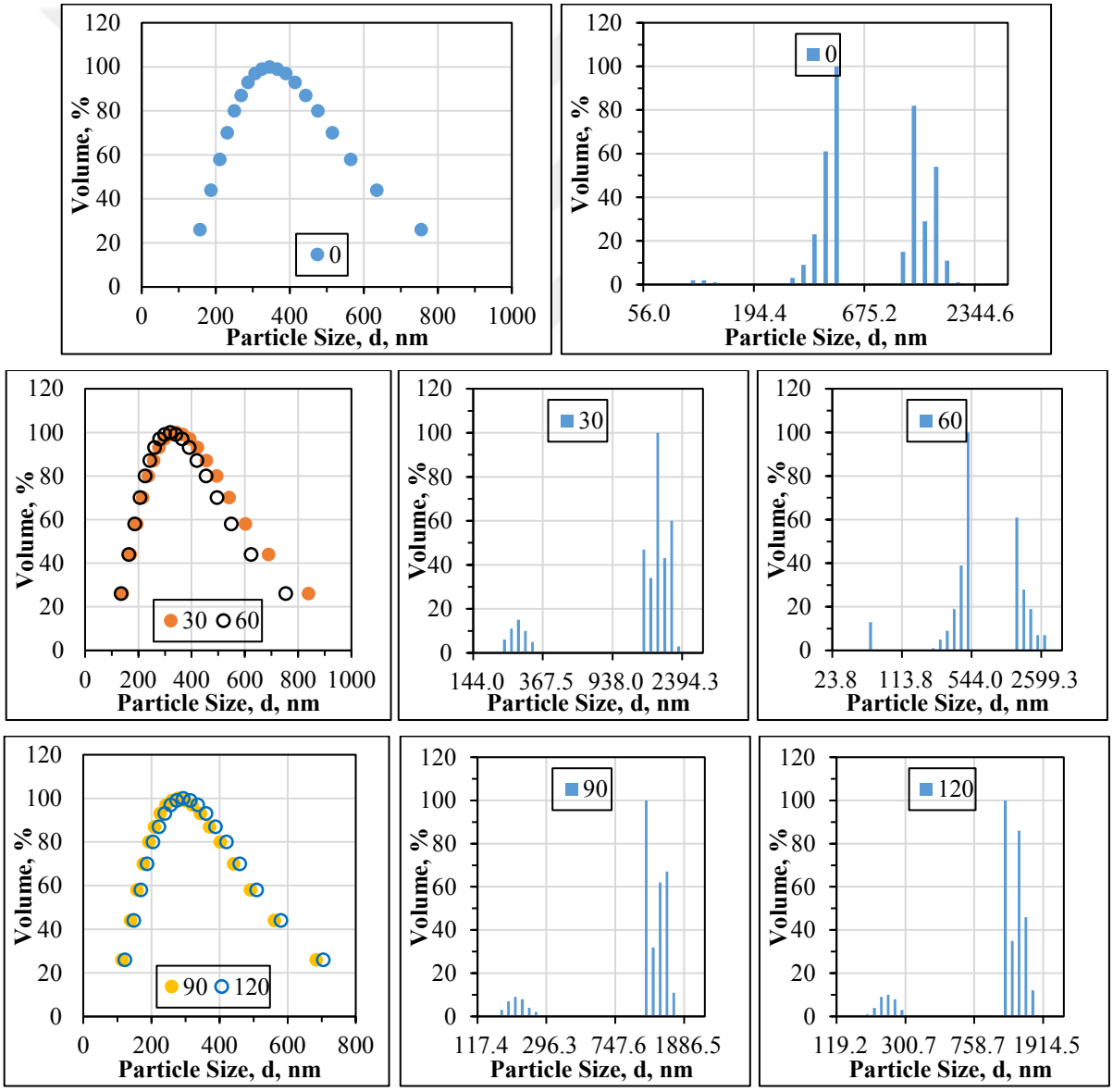


Figure 4.124. "TiO_2 and HA" binary system "as-is" under dark conditions volume profile: Time dependent comparative presentation of log Normal distribution and multi-size distribution of "TiO_2 and HA" binary system "as-is" under dark conditions.

4.1.5.3. "TiO_2 and HA" binary system "as-is" under dark conditions surface area profile. Time dependent logN distribution G(d) and multi size distribution C(d) of "TiO_2 and HA" binary system "as-is" under dark conditions surface area profile was demonstrated in Figure 4.125. Time dependent mean diameter, range and min-max diameter difference with respect to log normal and multi-size distribution of "TiO_2 and HA" binary system "as-is" under dark conditions surface area profile was presented in Table 4.79.

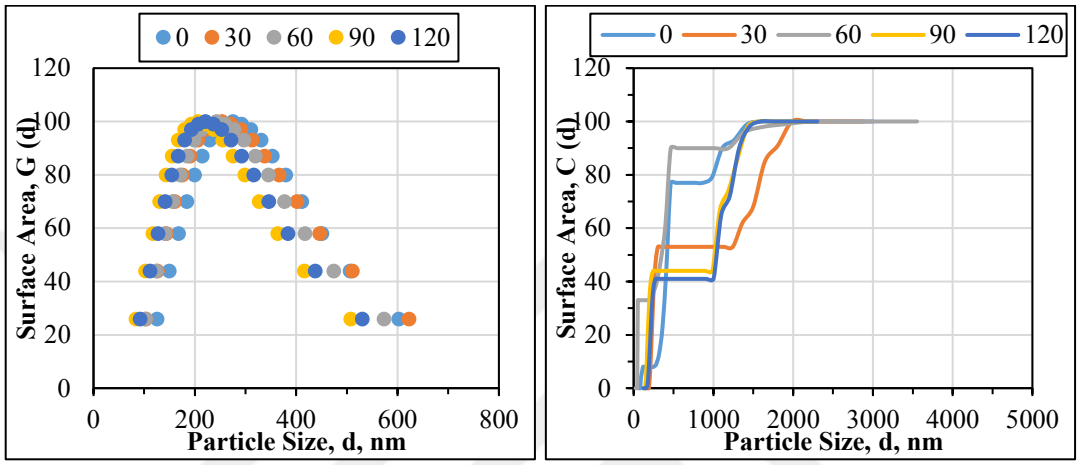


Figure 4.125. "TiO_2 and HA" binary system "as-is" under dark conditions surface area profile: Time dependent logN distribution G(d) and multi size distribution C(d).

Table 4.79. "TiO_2 and HA" binary system "as-is" under dark conditions surface area profile: Time dependent mean diameter, range and min-max diameter difference with respect to log normal and multi-size distribution.

TiO_2 and HA	time, min				
	0	30	60	90	120
Log Normal distribution					
Mean, nm	275.3	253.7	242.9	206.7	221.2
Range	125.9-602.3	103.4-622.7	102.9-573.4	84.2-507.6	92.2-530.7
Difference	476.4	519.3	470.5	423.4	438.5
Multi-size distribution					
Max 1, nm	92.1	252.6	52.1	186.5	227.8
Max 2, nm	464.7	1364.5	465.2	1082.6	1098.7
Max 3, nm	1110.9	1645.8	1390.4	1302.8	1322.1
Max 4, nm	1425.0	1985.1	-	-	-
Range	56.0-3007.5	144.0-2887.8	23.8-3553.9	117.4-2270.2	119.2-2303.8
Difference	2951.5	2743.8	3530.1	2152.8	2184.6

According to log normal distribution, it could be deduced that hydrodynamic particle size of "TiO_2 and HA" binary system "as-is" under dark conditions displayed a slowly decreasing trend with

respect to time. Initial hydrodynamic particle size was obtained as 275.3 nm and decreased to 253.7 nm upon 30 min. Accordingly, minor variations were monitored hydrodynamic particle size was detected to 221.2 nm upon period of 120 min. In terms of log normal distribution, size difference between max and min diameter decreased from 476.4 nm to 438.5 nm upon 120 min. For comparison purposes, in terms of multi-size distribution, four max diameters were observed following initial period of time and upon 30 min. Also, three max diameters were attained until the end of 120 min. In terms of multi-size distribution, size difference decreased from 2951.5 nm to 2184.6 nm. Time dependent comparative presentation of log Normal distribution and multi-size distribution of "TiO_2 and HA" binary system "as-is" under dark conditions surface area profile was demonstrated in Figure 4.126.

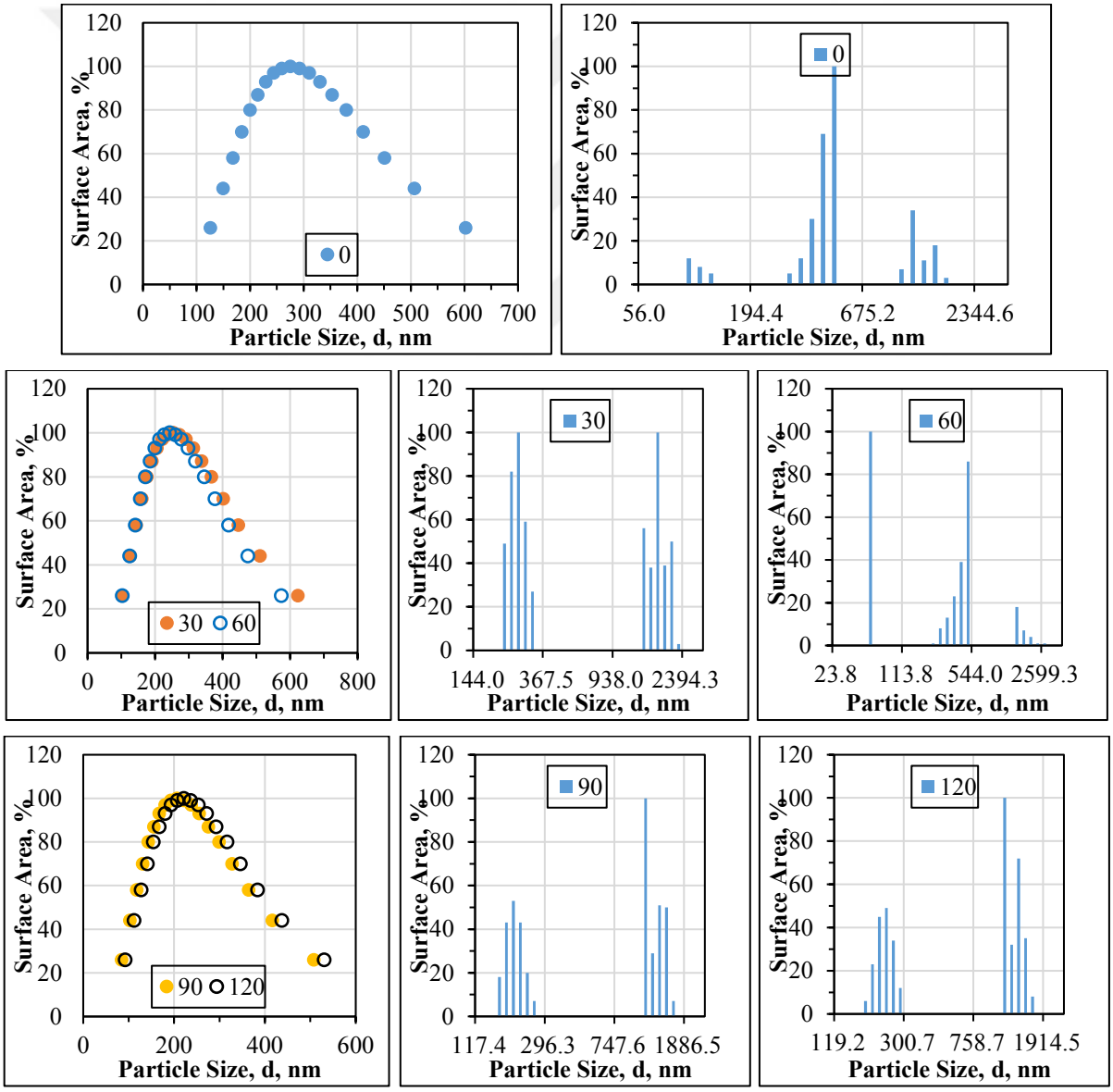


Figure 4.126. "TiO_2 and HA" binary system "as-is" under dark conditions surface area profile: Time dependent comparative presentation of log Normal distribution and multi-size distribution of "TiO_2 and HA" binary system "as-is" under dark conditions.

4.1.5.4. "TiO_2 and HA" binary system "as-is" under dark conditions number profile. Time dependent logN distribution G(d) and multi size distribution C(d) of "TiO_2 and HA" binary system "as-is" under dark conditions number profile was exhibited in Figure 4.127. Also, time dependent mean diameter, range and min-max diameter difference with respect to log normal and multi-size distribution of "TiO_2 and HA" binary system "as-is" under dark conditions number profile was displayed in Table 4.80.

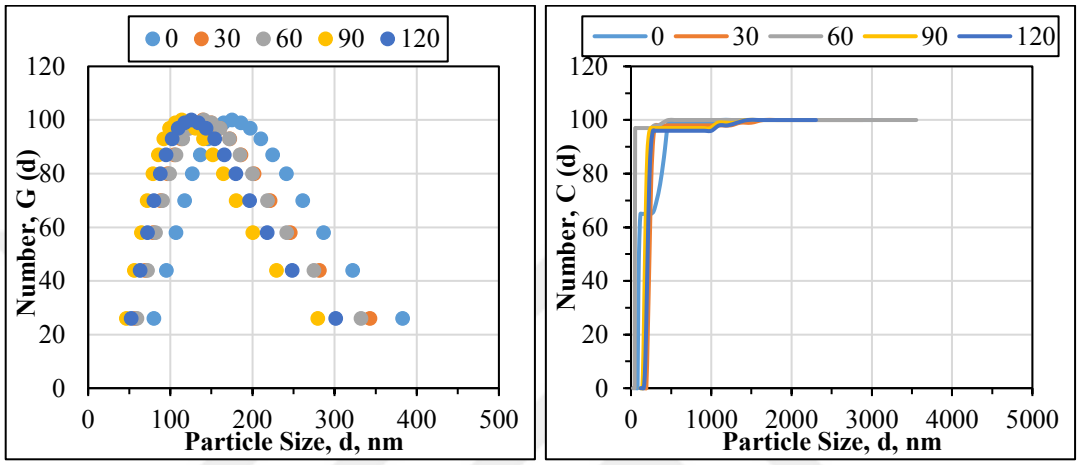


Figure 4.127. "TiO_2 and HA" binary system "as-is" under dark conditions number profile: Time dependent logN distribution G(d) and multi size distribution C(d).

Table 4.80. "TiO_2 and HA" binary system "as-is" under dark conditions number profile: Time dependent mean diameter, range and min-max diameter difference with respect to log normal and multi-size distribution.

TiO_2 and HA	time, min				
	0	30	60	90	120
Log Normal distribution					
Mean, nm	175.1	139.8	140.8	113.9	125.6
Range	80.0-383.0	57.0-343.2	59.6-332.4	46.4-279.6	52.3-301.3
Difference	303.0	286.2	272.8	233.2	249.0
Multi-size distribution					
Max 1, nm	92.1	252.6	52.1	186.5	207.6
Max 2, nm	464.7	1364.5	340.2	1082.6	1098.7
Max 3, nm	1110.9	1645.8	397.8	1302.8	1322.1
Max 4, nm	1425.0	-	465.2	1429.1	-
Range	56.0-3007.5	144.0-2887.8	23.8-3553.9	117.4-2270.2	119.2-2303.8
Difference	2951.5	2743.8	3530.1	2152.8	2184.6

According to log normal distribution, initial hydrodynamic particle size of "TiO_2 and HA" binary system "as-is" under dark conditions was obtained as 175.1 nm. Along 120 min, hydrodynamic size

of "TiO_2 and HA" binary system "as-is" under dark conditions followed a slightly decreasing trend and detected to 125.6 nm. Size difference was monitored between 303.0 nm and 249.0 nm. However, in terms of multi-size distribution, four max diameters were attained as 92.1 nm, 464.7 nm, 1110.9 nm and 1425.0 nm for "TiO_2 and HA" binary system "as-is" under dark conditions following initial period of time. Three peaks were observed upon 30 min and four peaks were monitored upon 60 and 90 min. Three peaks were attained until the end of 120 min.

Time dependent comparative presentation of log Normal distribution and multi-size distribution of "TiO_2 and HA" binary system "as-is" under dark conditions number profile was demonstrated in Figure 4.128.

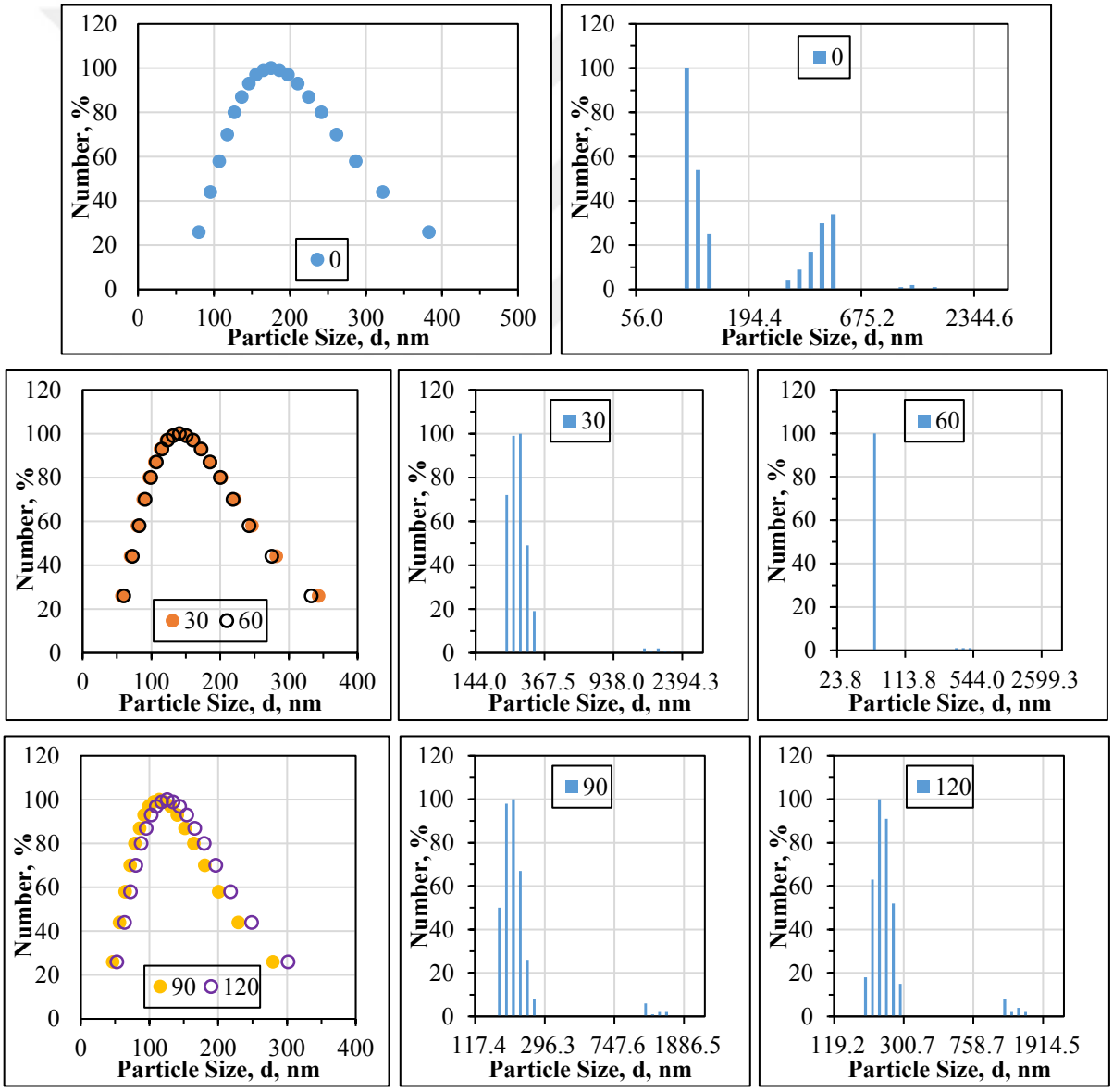


Figure 4.128. "TiO_2 and HA" binary system "as-is" under dark conditions number profile: Time dependent comparative presentation of log Normal distribution and multi-size distribution of "TiO_2 and HA" binary system "as-is" under dark conditions.

4.1.5.5. "TiO_2 and SRNOM" binary system "as-is" under dark conditions intensity profile. Time dependent logN distribution G(d) and multi size distribution C(d) of "TiO_2 and SRNOM" binary system "as-is" under dark conditions intensity profile was presented in Figure 4.129. Time dependent mean diameter, range and min-max diameter difference with respect to log normal and multi-size distribution of "TiO_2 and SRNOM" binary system "as-is" under dark conditions intensity profile was given in Table 4.81.

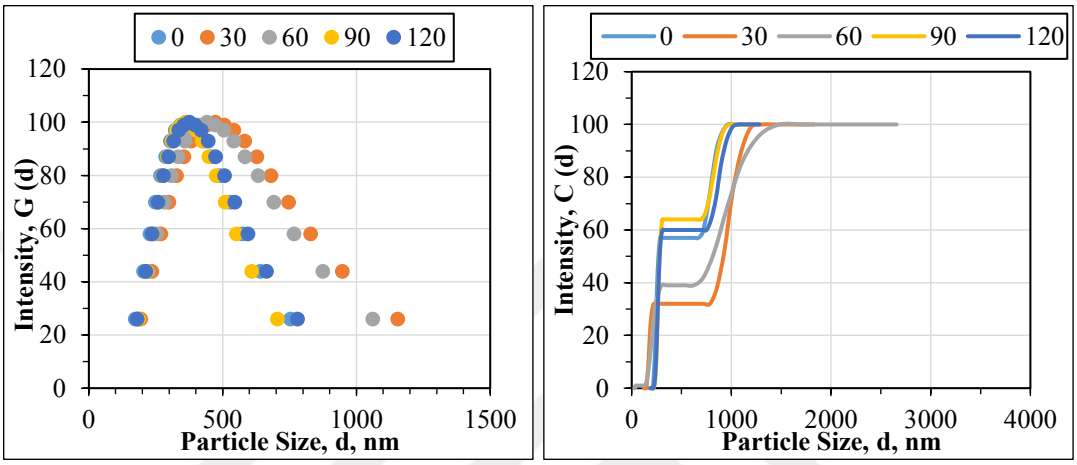


Figure 4.129. "TiO_2 and SRNOM" binary system "as-is" under dark conditions intensity profile: Time dependent logN distribution G(d) and multi size distribution C(d).

Table 4.81. "TiO_2 and SRNOM" binary system "as-is" under dark conditions intensity profile: Time dependent mean diameter, range and min-max diameter difference with respect to log normal and multi-size distribution.

TiO_2 and SRNOM	time, min				
	0	30	60	90	120
Log Normal distribution					
Mean, nm	362.4	472.7	441.7	363.3	375.9
Range	174.1-754.4	193.6-1154.1	183.8-1061.4	187.1-705.3	181.2-779.7
Difference	580.3	960.5	877.6	518.2	598.5
Multi-size distribution					
Max 1, nm	252.7	186.7	224.9	274.2	274.2
Max 2, nm	853.7	1011.7	1111.8	825.1	897.5
Max 3, nm	-	-	-	874.3	-
Range	175.4-1230.1	122.3-1827.9	25.4-2658.3	193.7-1238.0	192.1-1280.9
Difference	1054.7	1705.6	2632.9	1044.3	1088.8

In terms of intensity profile, it could be inferred that hydrodynamic particle size of "TiO_2 and SRNOM" binary system "as-is" under dark conditions displayed a fluctuating trend according to time variations. In terms of multi-size distribution, it could be deduced that two peaks were observed upon

120 min. Time dependent comparative presentation of log Normal distribution and multi-size distribution of "TiO_2 and SRNOM" binary system "as-is" under dark conditions intensity profile was displayed in Figure 4.130. Also, polydispersity of "TiO_2 and SRNOM" binary system "as-is" under dark conditions was given in Table 4.82. It could be concluded that a rapid increase was observed in the first 30 min and continuously decreasing trend was detected until 120 min.

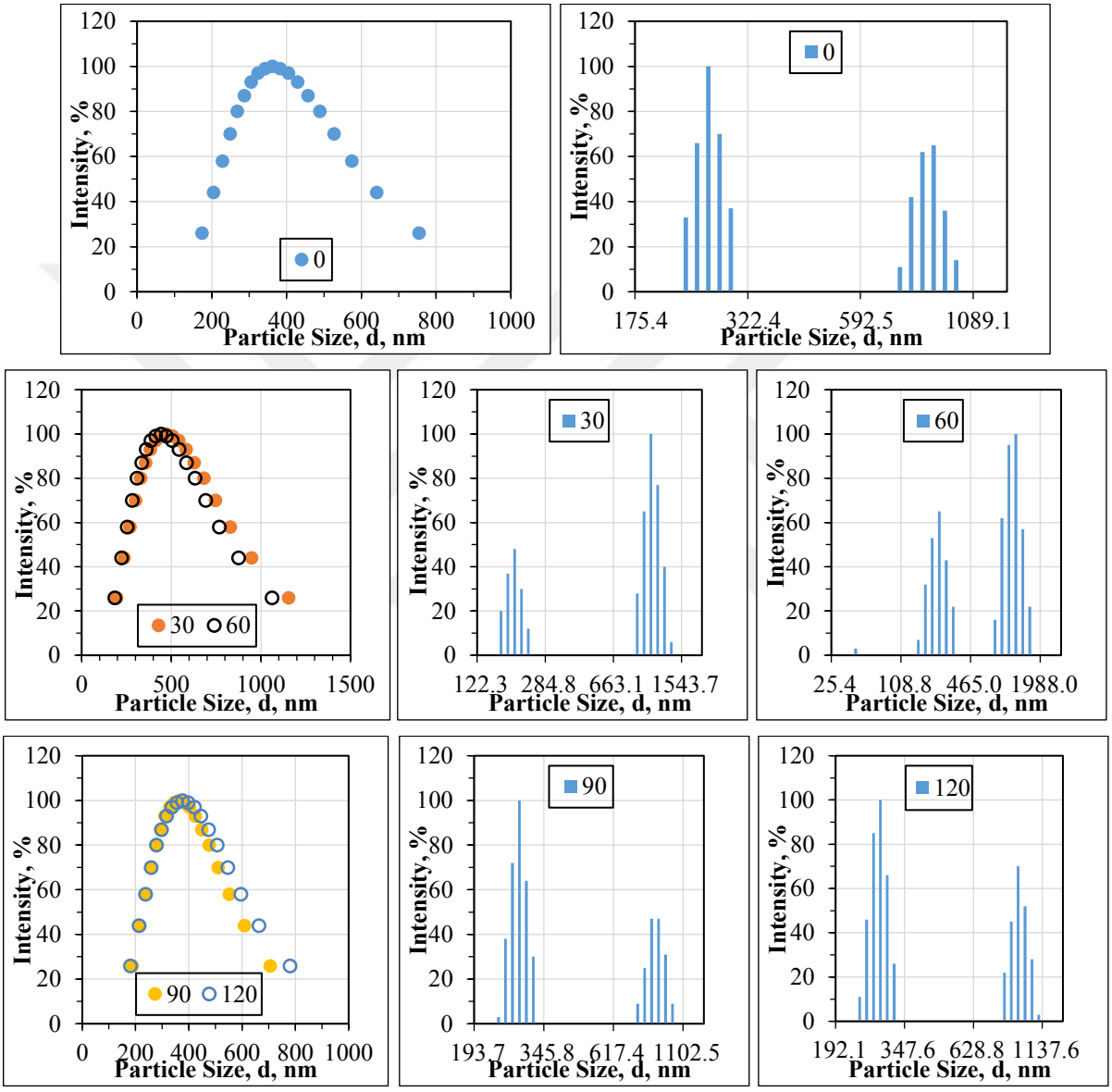


Figure 4.130. "TiO_2 and SRNOM" binary system "as-is" under dark conditions intensity profile: Time dependent comparative presentation of log Normal distribution and multi-size distribution of "TiO_2 and SRNOM" binary system "as-is" under dark conditions.

Table 4.82. Polydispersity of "TiO_2 and SRNOM" binary system "as-is" under dark conditions.

TiO_2 and SRNOM	Polydispersity				
	0	30	60	90	120
	0.220	0.342	0.328	0.177	0.217

4.1.5.6. "TiO_2 and SRNOM" binary system "as-is" under dark conditions volume profile. As described for "TiO_2 and SRNOM" binary system "as-is" under dark conditions intensity profile (Figure 4.129), a similar approach was followed for "TiO_2 and SRNOM" binary system "as-is" under dark conditions volume profile. Time dependent logN distribution G(d) and multi size distribution C(d) of "TiO_2 and SRNOM" binary system "as-is" under dark conditions volume profile was shown in Figure 4.131. Time dependent mean diameter, range and min-max diameter difference with respect to log normal and multi-size distribution of "TiO_2 and SRNOM" binary system "as-is" under dark conditions volume profile was displayed in Table 4.83.

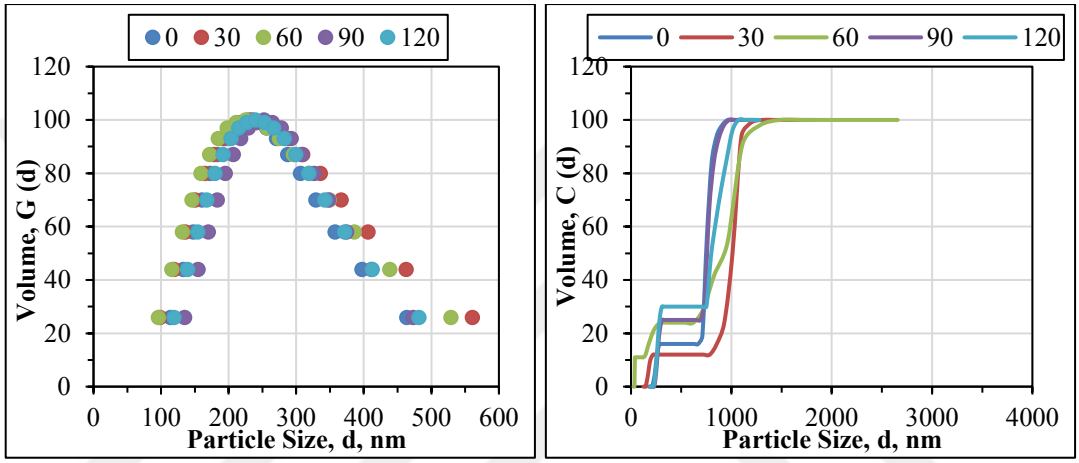


Figure 4.131. "TiO_2 and SRNOM" binary system "as-is" under dark conditions volume profile: Time dependent logN distribution G(d) and multi size distribution C(d).

Table 4.83. "TiO_2 and SRNOM" binary system "as-is" under dark conditions volume profile: Time dependent mean diameter, range and min-max diameter difference with respect to log normal and multi-size distribution.

TiO_2 and SRNOM	time, min				
	0	30	60	90	120
Log Normal distribution					
Mean, nm	229.9	235.0	225.6	252.5	239.6
Range	113.9-463.8	98.5-560.8	96.1-529.3	134.8-473.0	119.2-481.6
Difference	349.9	462.3	433.2	338.2	362.4
Multi-size distribution					
Max 1, nm	252.7	171.5	39.3	274.2	274.2
Max 2, nm	755.9	186.7	194.5	778.6	797.1
Max 3, nm	-	1100.9	224.9	-	897.5
Max 4, nm	-	-	831.4	-	-
Max 5, nm	-	-	1111.8	-	-
Range	175.4-1230.1	122.3-1827.9	25.4-2658.3	193.7-1238.0	192.1-1280.9
Difference	1054.7	1705.6	2632.9	1044.3	1088.8

In terms of volume profile, it could be inferred that hydrodynamic particle size of "TiO_2 and SRNOM" binary system "as-is" under dark conditions revealed as 229.9 nm. Upon 30 min, slightly increase was observed and minor variations remained until 120 min. On the other hand, in the first 30 min, approximately 25 % increase was obtained in terms of difference between max and min diameter. Initial size difference was attained as 349.9 nm and detected to 362.4 nm upon 120 min. For comparison purposes, in terms of multi-size distribution, initially two peaks were attained. Upon 30 min, three peaks were observed and five peaks were monitored upon 60 min. Time dependent comparative presentation of log Normal distribution and multi-size distribution of "TiO_2 and SRNOM" binary system "as-is" under dark conditions volume profile was demonstrated in Figure 4.132.

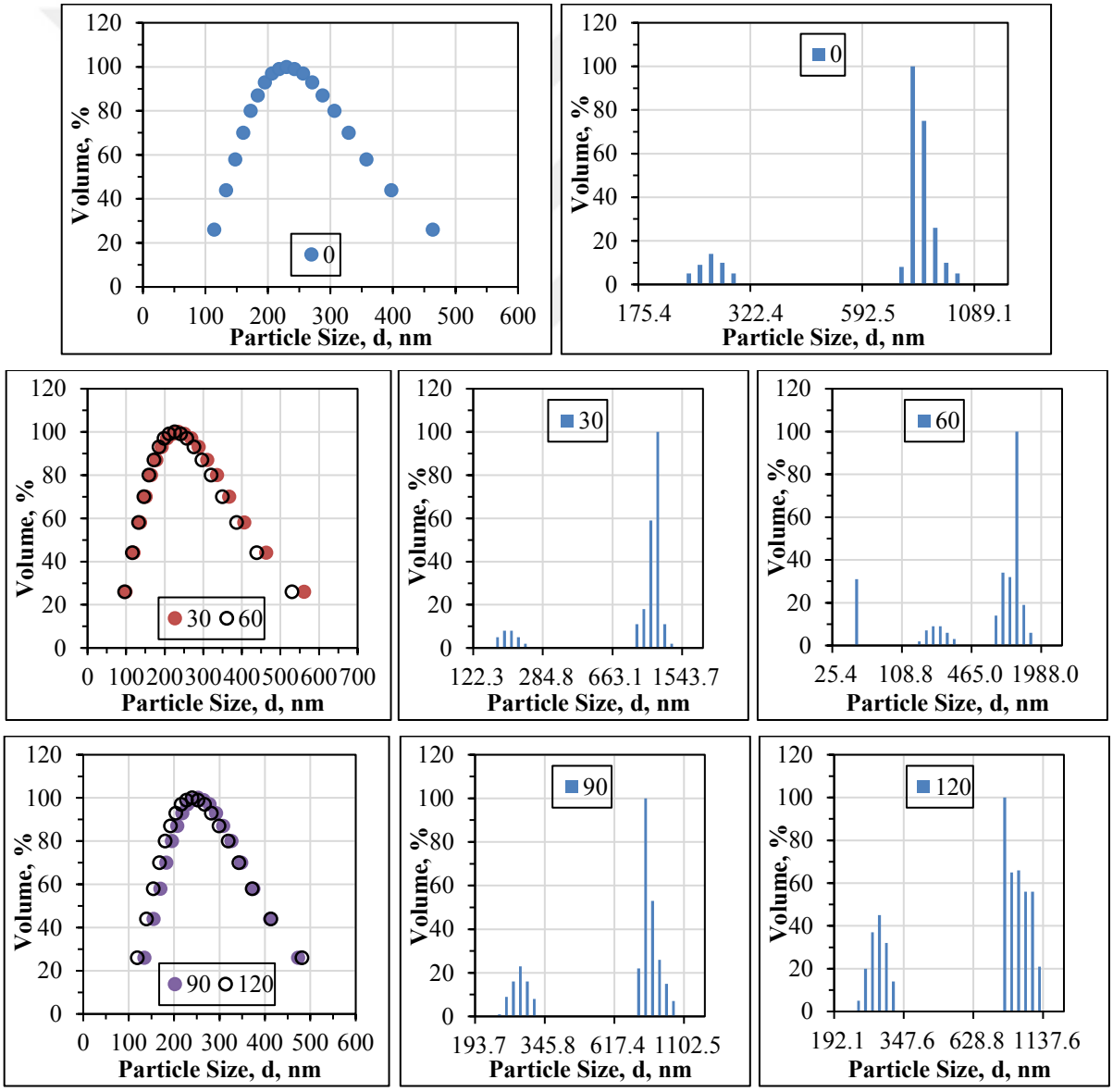


Figure 4.132. "TiO_2 and SRNOM" binary system "as-is" under dark conditions volume profile: Time dependent comparative presentation of log Normal distribution and multi-size distribution of "TiO_2 and SRNOM" binary system "as-is" under dark conditions.

4.1.5.7. "TiO_2 and SRNOM" binary system "as-is" under dark conditions surface area profile. Time dependent logN distribution G(d) and multi size distribution C(d) of "TiO_2 and SRNOM" binary system "as-is" under dark conditions surface area profile was presented in Figure 4.133. Time dependent mean diameter, range and min-max diameter difference with respect to log normal and multi-size distribution of "TiO_2 and SRNOM" binary system "as-is" under dark conditions surface area profile was demonstrated in Table 4.84.

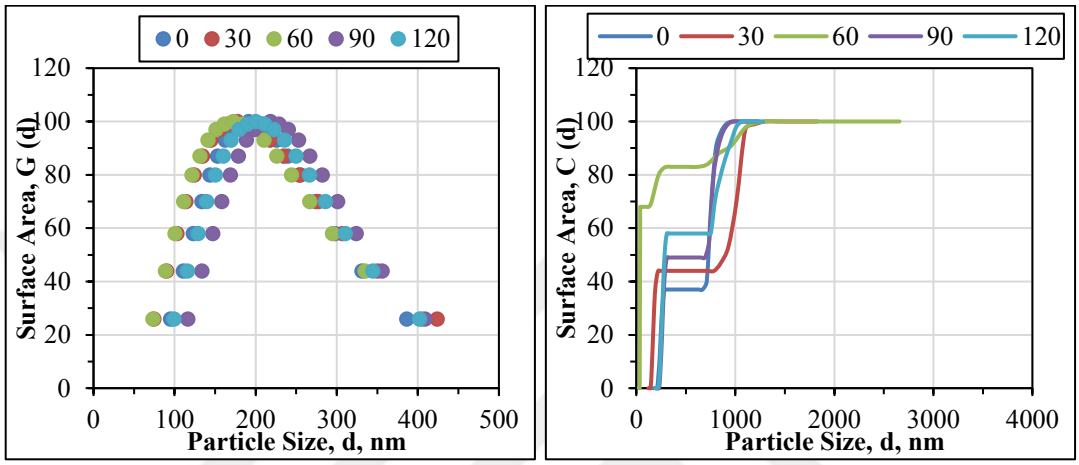


Figure 4.133. "TiO_2 and SRNOM" binary system "as-is" under dark conditions surface area profile: Time dependent logN distribution G(d) and multi size distribution C(d).

Table 4.84. "TiO_2 and SRNOM" binary system "as-is" under dark conditions surface area profile: Time dependent mean diameter, range and min-max diameter difference with respect to log normal and multi-size distribution.

TiO_2 and SRNOM	time, min				
	0	30	60	90	120
Log Normal distribution					
Mean, nm	191.6	177.7	172.4	218.3	200.1
Range	94.9-386.6	74.5-424.0	73.5-404.5	116.6-408.9	99.5-402.2
Difference	291.7	349.5	331.0	292.3	302.7
Multi-size distribution					
Max 1, nm	252.7	186.7	39.3	274.2	274.2
Max 2, nm	755.9	1100.9	194.5	778.6	797.1
Max 3, nm	-	-	831.4	-	-
Max 4, nm	-	-	1111.8	-	-
Range	175.4-1230.1	122.3-1827.9	25.4-2658.3	193.7-1238.0	192.1-1280.9
Difference	1054.7	1705.6	2632.9	1044.3	1088.8

In terms of surface area profile, it could be inferred that initial hydrodynamic particle size of "TiO_2 and SRNOM" binary system "as-is" under dark conditions revealed as 191.6 nm. Upon 30 min,

approximately 10 % decrease was monitored and minor variations remained until 120 min. On the other hand, initial size difference displayed a rapid increase and increased from 291.7 nm to 349.5 nm in the first 30 min. Upon 30 min, slight variations were observed until the end of 120 min. For comparison purposes, in terms of multi-size distribution, initially two max diameters were obtained until 60 min. Upon 60 min, four peaks were observed and two peaks were monitored until the end of 120 min.

Time dependent comparative presentation of log Normal distribution and multi-size distribution of "TiO_2 and SRNOM" binary system "as-is" under dark conditions surface area profile was given in Figure 4.134.

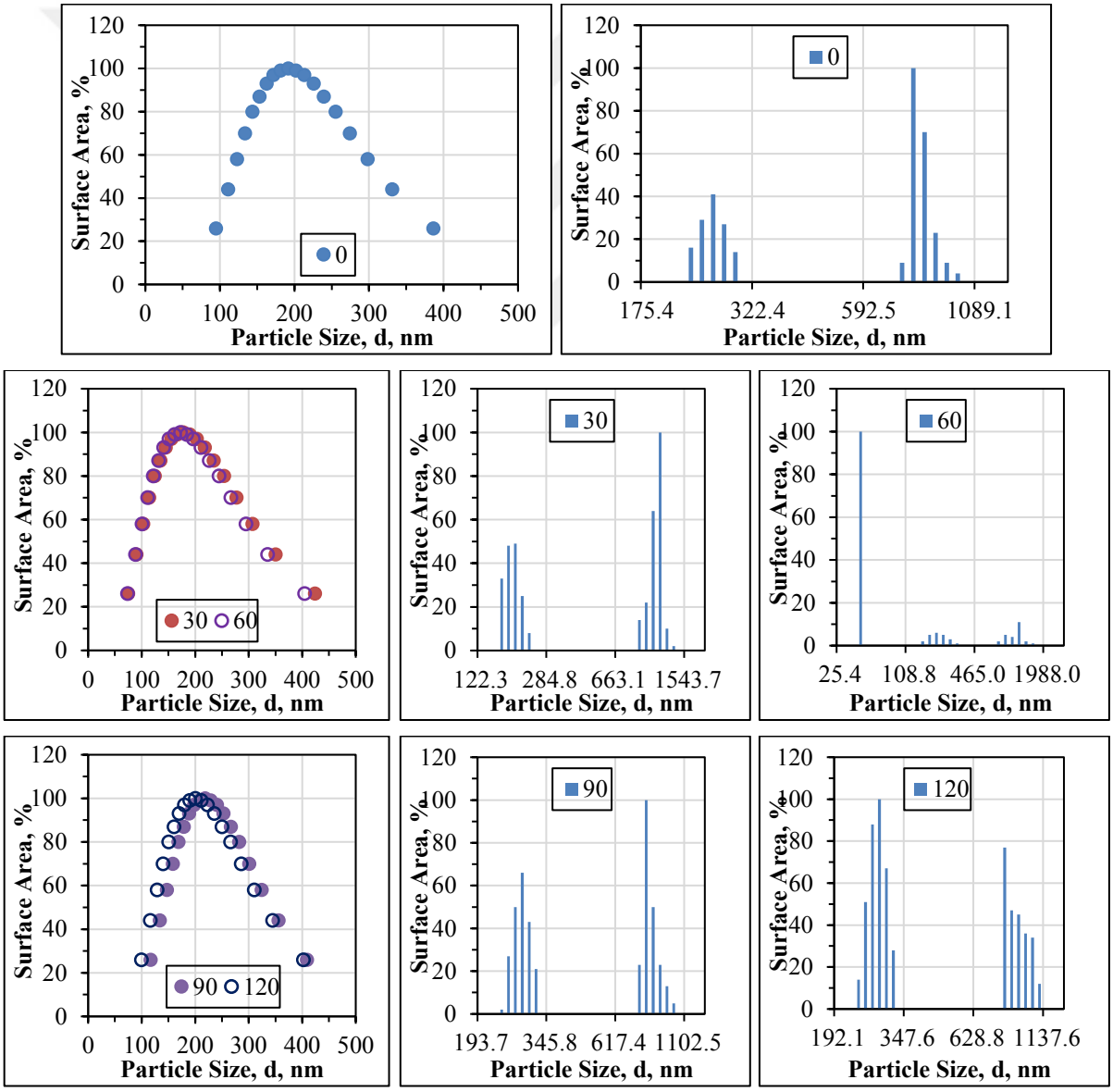


Figure 4.134. "TiO_2 and SRNOM" binary system "as-is" under dark conditions surface area profile: Time dependent comparative presentation of log Normal distribution and multi-size distribution of "TiO_2 and SRNOM" binary system "as-is" under dark conditions.

4.1.5.8. "TiO_2 and SRNOM" binary system "as-is" under dark conditions number profile. Time dependent logN distribution G(d) and multi size distribution C(d) of "TiO_2 and SRNOM" binary system "as-is" under dark conditions number profile was displayed in Figure 4.135. Time dependent mean diameter, range and min-max diameter difference with respect to log normal and multi-size distribution of "TiO_2 and SRNOM" binary system "as-is" under dark conditions number profile was presented in Table 4.85.

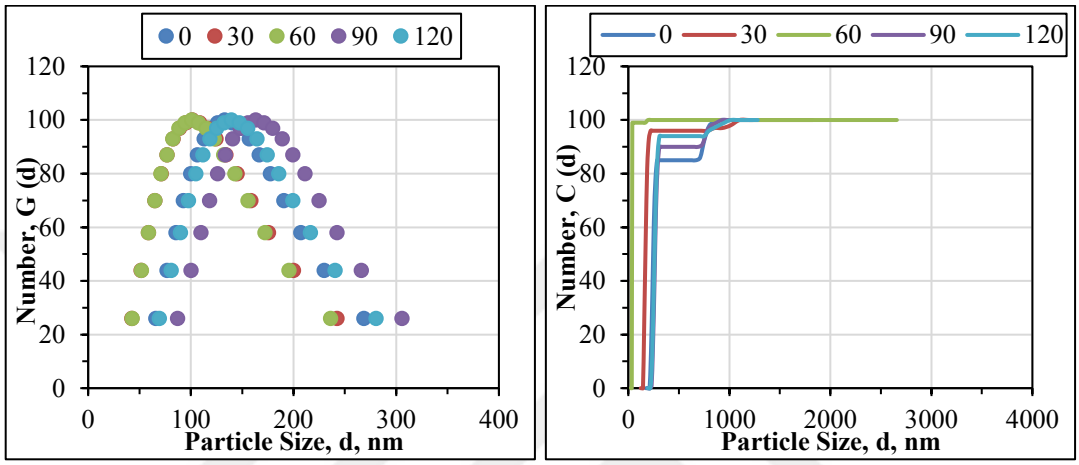


Figure 4.135. "TiO_2 and SRNOM" binary system "as-is" under dark conditions number profile: Time dependent logN distribution G(d) and multi size distribution C(d).

Table 4.85. "TiO_2 and SRNOM" binary system "as-is" under dark conditions number profile: Time dependent mean diameter, range and min-max diameter difference with respect to log normal and multi-size distribution.

TiO_2 and SRNOM	time, min				
	0	30	60	90	120
Log Normal distribution					
Mean, nm	133.1	101.6	100.7	163.2	139.5
Range	66.0-268.6	42.6-242.5	42.9-236.3	87.2-305.7	69.4-280.5
Difference	202.6	199.9	193.4	218.5	211.1
Multi-size distribution					
Max 1, nm	252.7	171.5	39.3	274.2	274.2
Max 2, nm	755.9	1100.9	-	778.6	797.1
Range	175.4-1230.1	122.3-1827.9	25.4-2658.3	193.7-1238.0	192.1-1280.9
Difference	1054.7	1705.6	2632.9	1044.3	1088.8

According to log normal distribution, initial hydrodynamic particle size of "TiO_2 and SRNOM" binary system "as-is" under dark conditions was obtained as 133.1 nm. During 120 min, hydrodynamic size of "TiO_2 and SRNOM" binary system "as-is" under dark conditions followed a fluctuating trend and detected to 139.5 nm. Also, in terms of log normal distribution, size difference

was obtained as 202.6 nm following initial period of time and slight variations remained until the end of 120 min. However, in terms of multi-size distribution, two max diameters were attained as 252.7 and 755.9 nm for "TiO_2 and SRNOM" binary system "as-is" under dark conditions following initial period of time. One peak was observed upon 60 min and two peaks remained until the end of 120 min. Also, in terms of multi-size distribution, size difference was attained as 1054.7 nm following initial period of time and reached to 1088.8 nm at the end of 120 min.

Time dependent comparative presentation of log Normal distribution and multi-size distribution of "TiO_2 and SRNOM" binary system "as-is" under dark conditions number profile was presented in Figure 4.136.

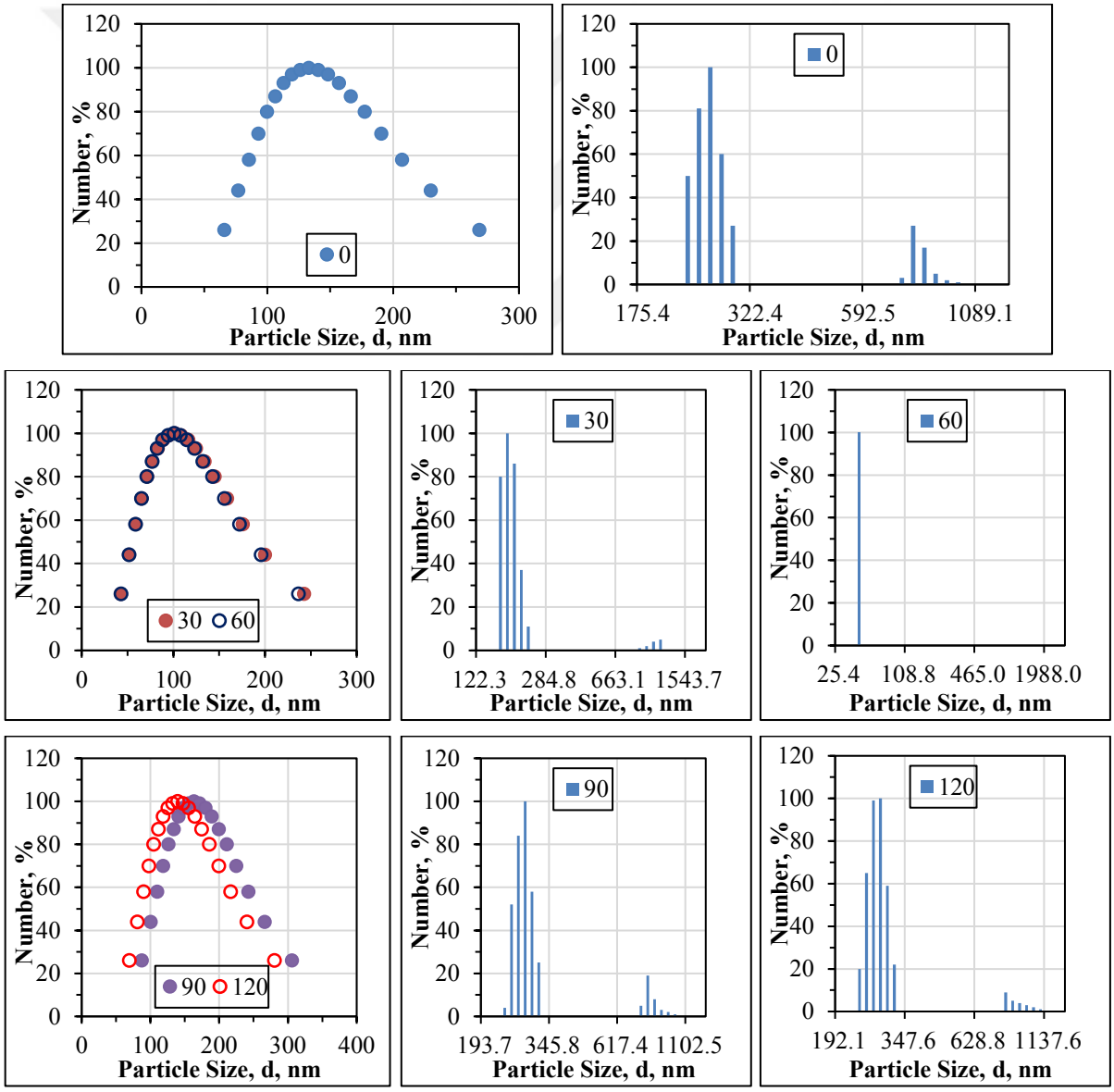


Figure 4.136. "TiO_2 and SRNOM" binary system "as-is" under dark conditions number profile: Time dependent comparative presentation of log Normal distribution and multi-size distribution of "TiO_2 and SRNOM" binary system "as-is" under dark conditions.

4.1.5.9. "N-TiO_2 and HA" binary system "as-is" under dark conditions intensity profile. Time dependent logN distribution G(d) and multi size distribution C(d) of "N-TiO_2 and HA" binary system "as-is" under dark conditions intensity profile was demonstrated in Figure 4.137. Time dependent mean diameter, range and min-max diameter difference with respect to log normal and multi-size distribution of "N-TiO_2 and HA" binary system "as-is" under dark conditions intensity profile was exhibited in Table 4.86.

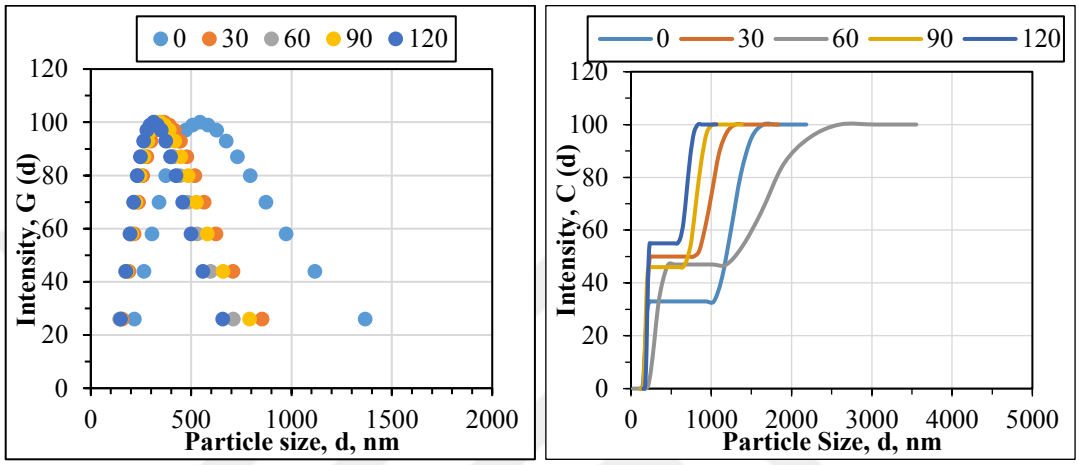


Figure 4.137. "N-TiO_2 and HA" binary system "as-is" under dark conditions intensity profile: Time dependent logN distribution G(d) and multi size distribution C(d).

Table 4.86. "N-TiO_2 and HA" binary system "as-is" under dark conditions intensity profile: Time dependent mean diameter, range and min-max diameter difference with respect to log normal and multi-size distribution.

N-TiO_2 and HA	time, min				
	0	30	60	90	120
Log Normal distribution					
Mean, nm	544.5	366.3	320.7	344.8	313.4
Range	216.7-1367.9	157.1-854.0	144.7-710.7	150.4-790.8	149.2-658.2
Difference	1151.2	696.9	566.0	640.4	509.0
Multi-size distribution					
Max 1, nm	191.1	198.0	340.2	192.5	205.6
Max 2, nm	1367.3	1096.1	1901.1	875.6	738.3
Range	108.9-2184.4	118.5-1831.4	23.8-3553.9	122.2-1379.4	151.7-1063.8
Difference	2075.5	1712.9	3530.1	1257.2	912.1

According to log normal distribution, hydrodynamic size of "N-TiO_2 and HA" binary system "as-is" under dark conditions was recorded as 544.5 nm. Upon 30 min, a sharp decrease was observed and hydrodynamic size was detected to 366.3 nm. However, considering multi-size distribution, two peaks were obtained as 191.1 nm and 1367.3 nm following initial period of time.

Time dependent comparative presentation of log Normal distribution and multi-size distribution of "N-TiO_2 and HA" binary system "as-is" under dark conditions intensity profile was demonstrated in Figure 4.138. Also, polydispersity of "N-TiO_2 and HA" binary system "as-is" under dark conditions was presented in Table 4.87 and a continuous decrease (0.368 to 0.226) was monitored along 120 min.

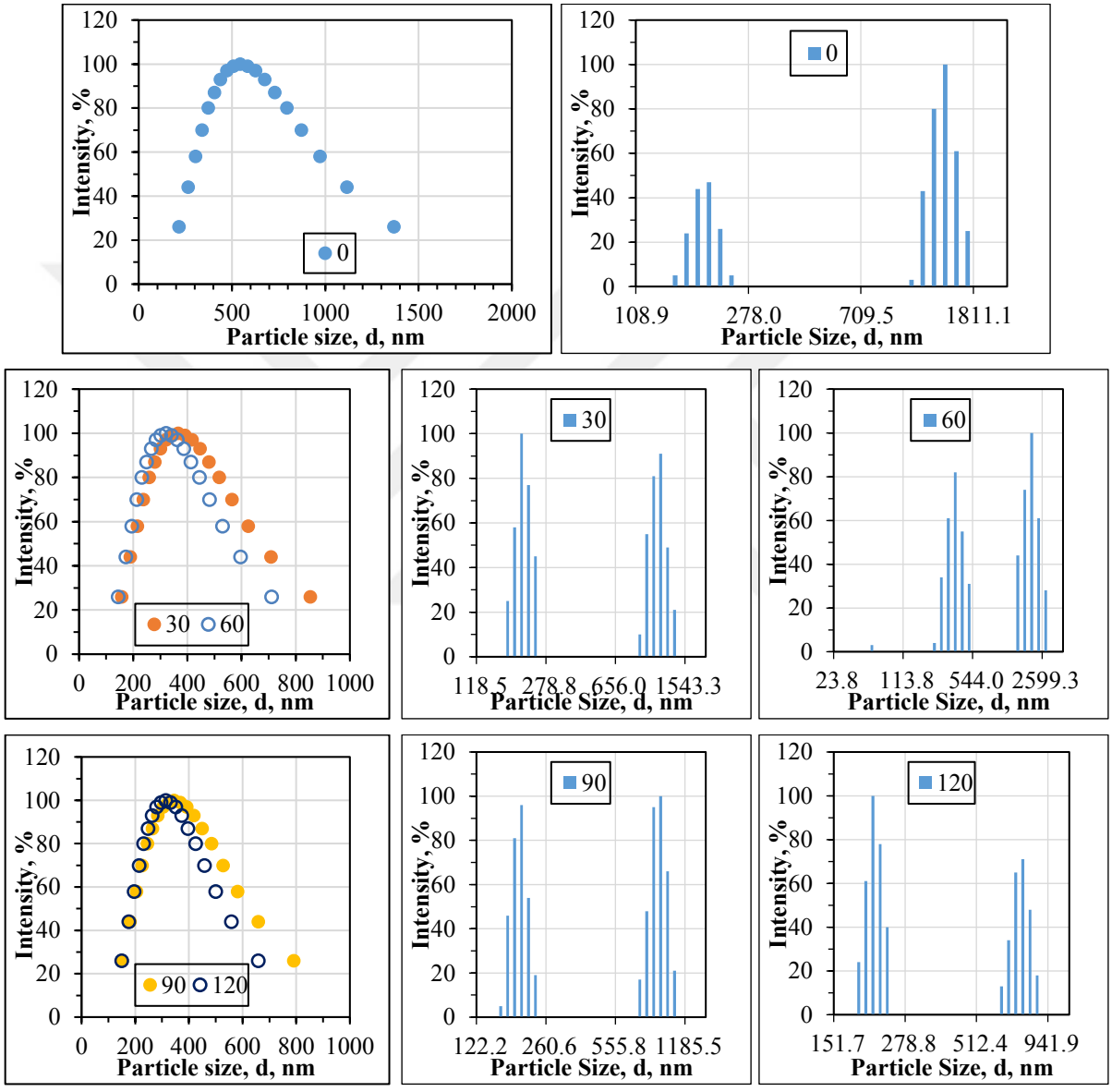


Figure 4.138. "N-TiO_2 and HA" binary system "as-is" under dark conditions intensity profile: Time dependent comparative presentation of log Normal distribution and multi-size distribution of "N-TiO_2 and HA" binary system under dark conditions.

Table 4.87. Polydispersity of "N-TiO_2 and HA" binary system "as-is" under dark conditions.

N-TiO_2 and HA	Polydispersity				
	0	30	60	90	120
	0.368	0.303	0.264	0.290	0.226

4.1.5.10. "N-TiO_2 and HA" binary system "as-is" under dark conditions volume profile. In a similar manner to data represented "N-TiO_2 and HA" binary system "as-is" under dark conditions intensity profile (Figure 4.137), time dependent logN distribution G(d) and multi size distribution C(d) of "N-TiO_2 and HA" binary system "as-is" under dark conditions volume profile was displayed in Figure 4.139. Time dependent mean diameter, range and min-max diameter difference with respect to log normal and multi-size distribution of "N-TiO_2 and HA" binary system "as-is" under dark conditions volume profile was presented in Table 4.88.

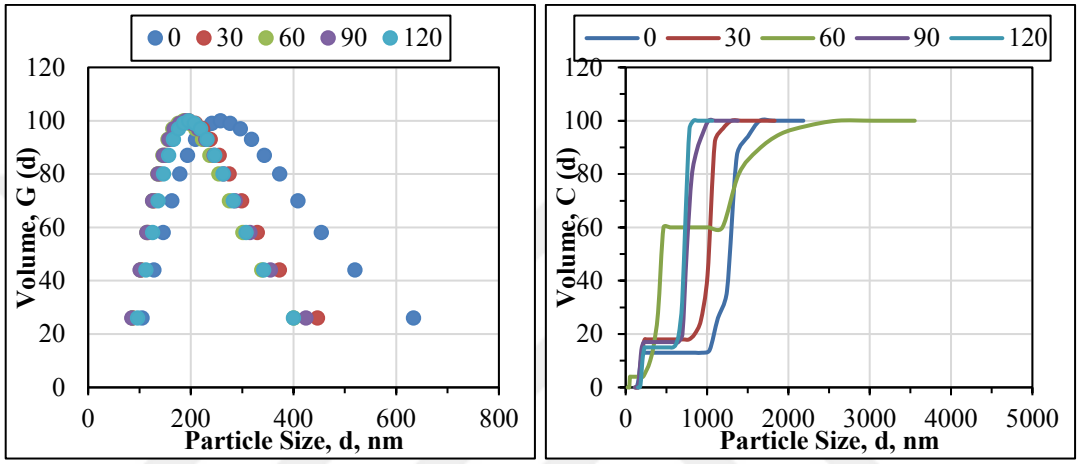


Figure 4.139. "N-TiO_2 and HA" binary system "as-is" under dark conditions volume profile: Time dependent logN distribution G(d) and multi size distribution C(d).

Table 4.88. "N-TiO_2 and HA" binary system "as-is" under dark conditions volume profile: Time dependent mean diameter, range and min-max diameter difference with respect to log normal and multi-size distribution.

N-TiO_2 and HA	time, min				
	0	30	60	90	120
Log Normal distribution					
Mean, nm	257.9	196.4	185.9	189.8	196.4
Range	104.9-634.0	86.4-446.5	86.3-400.8	84.9-424.0	96.4-400.0
Difference	529.1	360.1	314.5	339.1	303.6
Multi-size distribution					
Max 1, nm	174.0	198.0	52.1	192.5	205.6
Max 2, nm	1133.6	1096.1	465.2	752.5	738.3
Max 3, nm	1367.3	-	1390.4	-	-
Range	108.9-2184.4	118.5-1831.4	23.8-3553.9	122.2-1379.4	151.7-1063.8
Difference	2075.5	1712.9	3530.1	1257.2	912.1

According to log normal distribution, it could be asserted that hydrodynamic particle size of "N-TiO_2 and HA" binary system "as-is" under dark conditions revealed a slowly decreasing trend with

respect to time. Initial hydrodynamic size was attained as 257.9 nm and detected to 196.4 nm upon 120 min. Also, in terms of log normal distribution, size difference decreased from 529.1 nm to 303.6 nm upon 120 min. For comparison purposes, in terms of multi-size distribution, initially three max diameters were observed and two max diameters remained until the end of 120 min. Initial size difference was recorded as 2075.5 nm and decreased to 912.1 nm during 120 min.

In a similar manner to "N-TiO_2 and HA" binary system "as-is" under dark conditions intensity profile (Figure 4.138), time dependent comparative presentation of log Normal distribution and multi-size distribution of "N-TiO_2 and HA" binary system "as-is" under dark conditions volume profile was displayed in Figure 4.140.

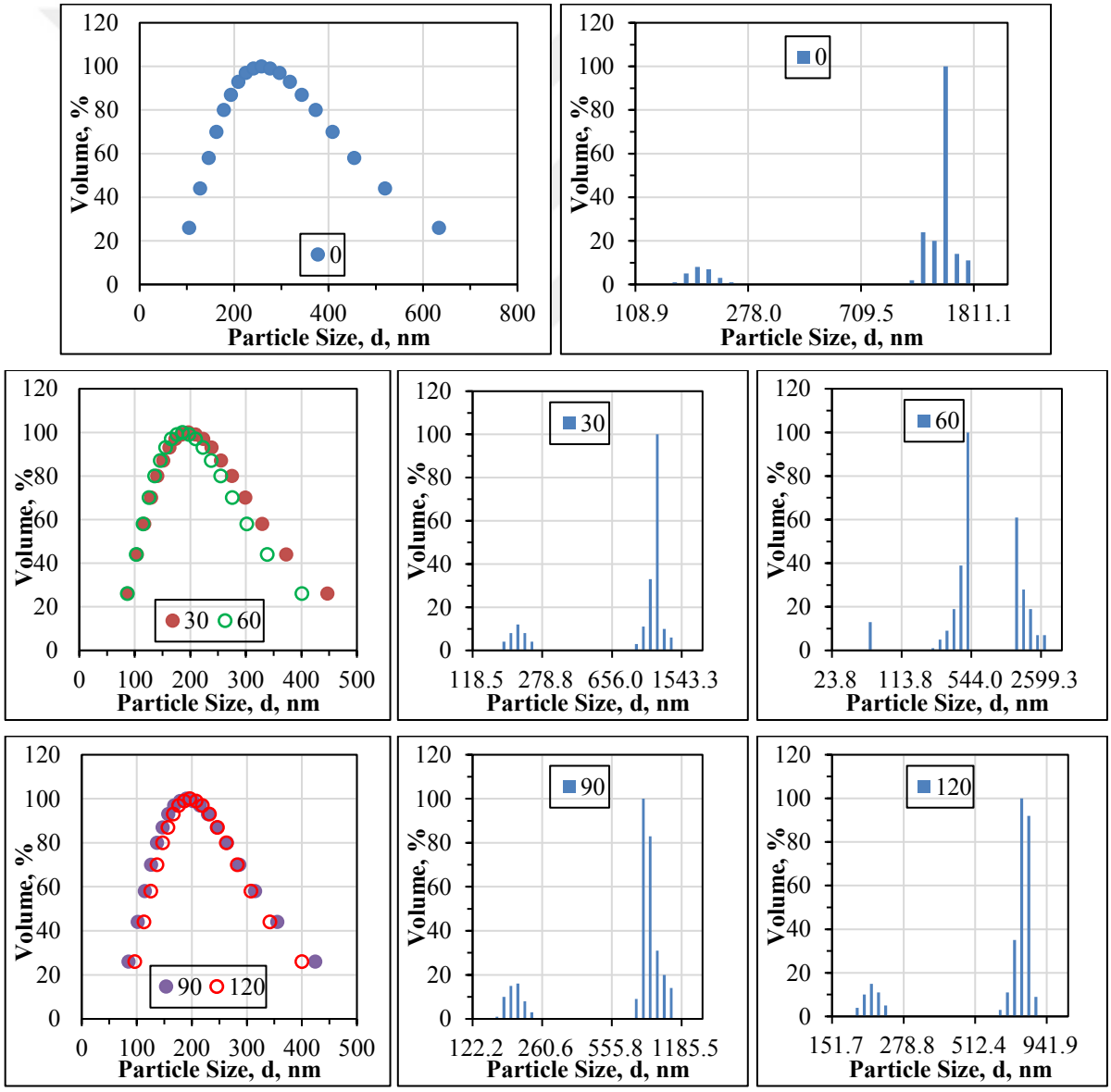


Figure 4.140. "N-TiO_2 and HA" binary system "as-is" under dark conditions volume profile: Time dependent comparative presentation of log Normal distribution and multi-size distribution of "N-TiO_2 and HA" binary system "as-is" under dark conditions.

4.1.5.11. "N-TiO_2 and HA" binary system "as-is" under dark conditions surface area profile. In a similar manner to data represented "N-TiO_2 and HA" binary system "as-is" under dark conditions volume profile (Figure 4.139), time dependent logN distribution G(d) and multi size distribution C(d) of "N-TiO_2 and HA" binary system "as-is" under dark conditions surface area profile was given in Figure 4.141. Time dependent mean diameter, range and min-max diameter difference with respect to log normal and multi-size distribution of "N-TiO_2 and HA" binary system "as-is" under dark conditions surface area profile was shown in Table 4.89.

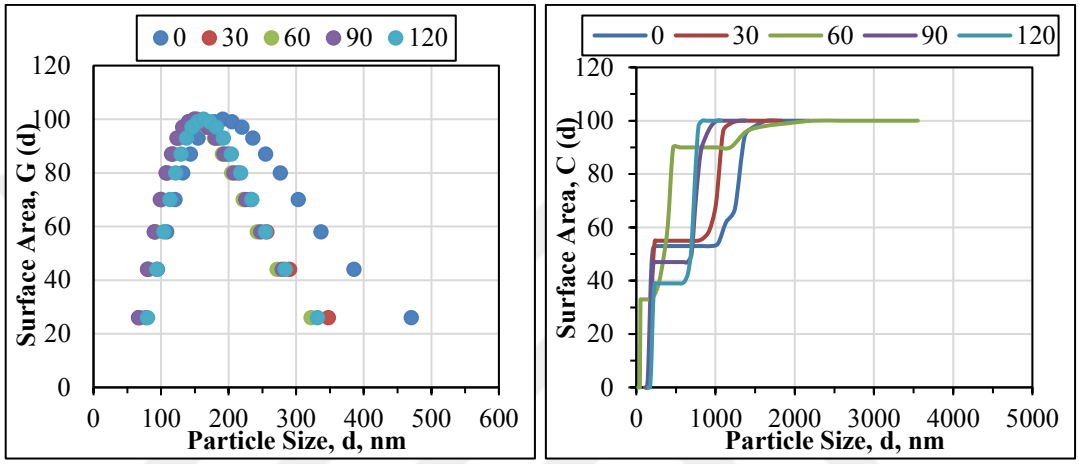


Figure 4.141. "N-TiO_2 and HA" binary system "as-is" under dark conditions surface area profile: Time dependent logN distribution G(d) and multi size distribution C(d).

Table 4.89. "N-TiO_2 and HA" binary system "as-is" under dark conditions surface area profile: Time dependent mean diameter, range and min-max diameter difference with respect to log normal and multi-size distribution.

N-TiO_2 and HA	time, min				
	0	30	60	90	120
Log Normal distribution					
Mean, nm	191.3	153.0	149.5	149.4	162.9
Range	77.8-470.2	67.3-347.9	69.4-322.3	66.9-333.9	80.0-331.7
Difference	392.4	280.6	252.9	267.0	251.7
Multi-size distribution					
Max 1, nm	174.0	198.0	52.1	178.4	205.6
Max 2, nm	1133.6	1096.1	465.2	752.5	738.3
Max 3, nm	1367.3	-	1390.4	-	-
Range	108.9-2184.4	118.5-1831.4	23.8-3553.9	122.2-1379.4	151.7-1063.8
Difference	2075.5	1712.9	3530.1	1257.2	912.1

In terms of surface area profile, it could be stated that hydrodynamic particle size of "N-TiO_2 and HA" binary system "as-is" under dark conditions revealed a slightly decreasing trend according

to time variations. Hydrodynamic particle size was recorded as 191.3 nm following initial period of time and detected to 162.9 nm upon period of 120 min. Accordingly, hydrodynamic size difference was recorded between 392.4 nm and 251.7 nm along 120 min. However, in terms of multi-size distribution, three peaks were observed following initial period of time and two peaks were monitored upon 120 min.

Time dependent comparative presentation of log Normal distribution and multi-size distribution of "N-TiO_2 and HA" binary system "as-is" under dark conditions surface area profile was demonstrated in Figure 4.142.

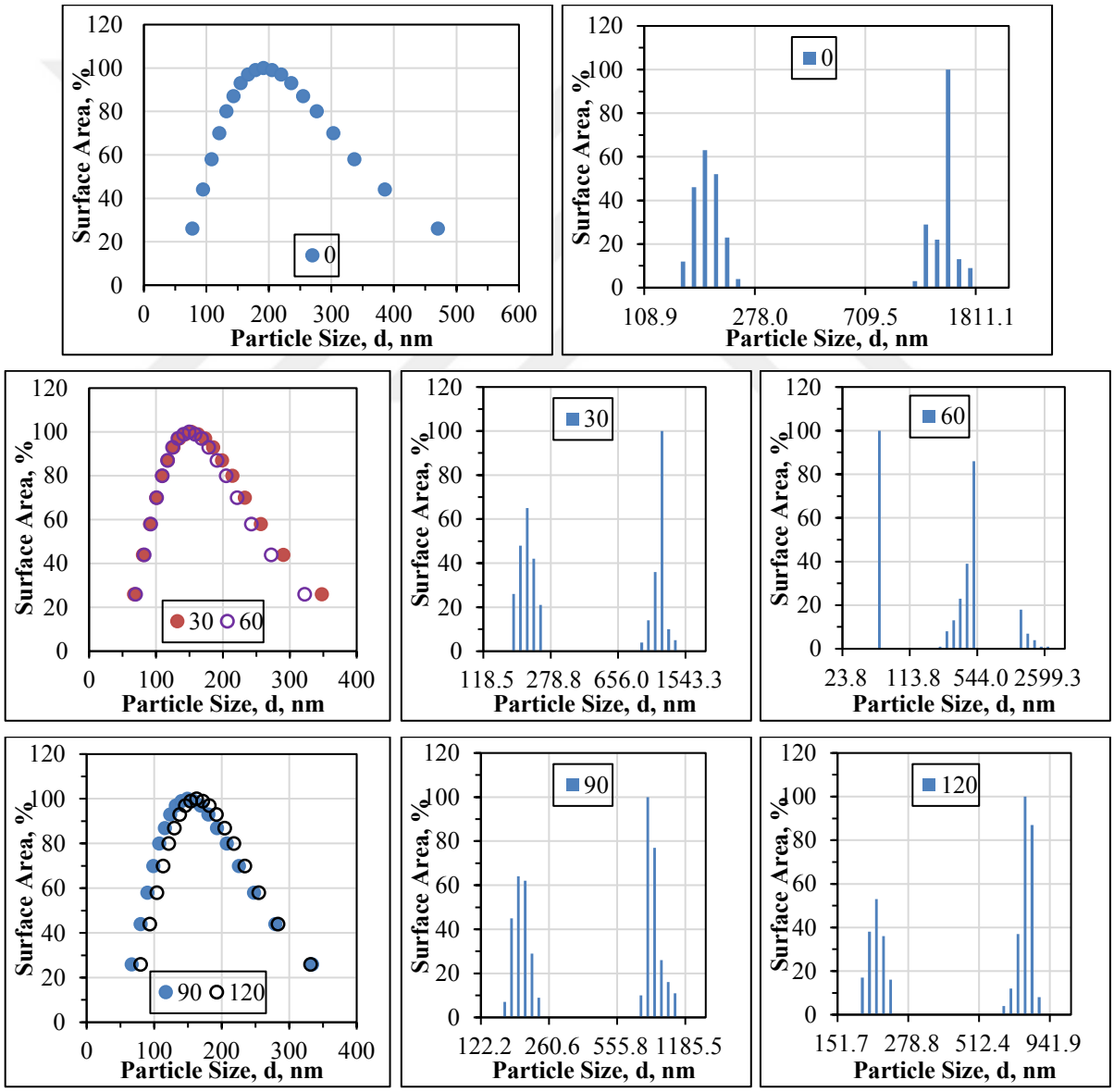


Figure 4.142. "N-TiO_2 and HA" binary system "as-is" under dark conditions surface area profile: Time dependent comparative presentation of log Normal distribution and multi-size distribution of "N-TiO_2 and HA" binary system "as-is" under dark conditions.

4.1.5.12. "N-TiO_2 and HA" binary system "as-is" under dark conditions number profile. As explained for "N-TiO_2 and HA" binary system "as-is" under dark conditions intensity profile (Figure 4.137), volume profile (Figure 4.139) and surface area profile (Figure 4.141), a similar approach was followed for "N-TiO_2 and HA" binary system "as-is" under dark conditions number profile. Time dependent logN distribution G(d) and multi size distribution C(d) of "N-TiO_2 and HA" binary system "as-is" under dark conditions number profile was displayed in Figure 4.143. Time dependent mean diameter, range and min-max diameter difference with respect to log normal and multi-size distribution of "N-TiO_2 and HA" binary system "as-is" under dark conditions number profile was given in Table 4.90.

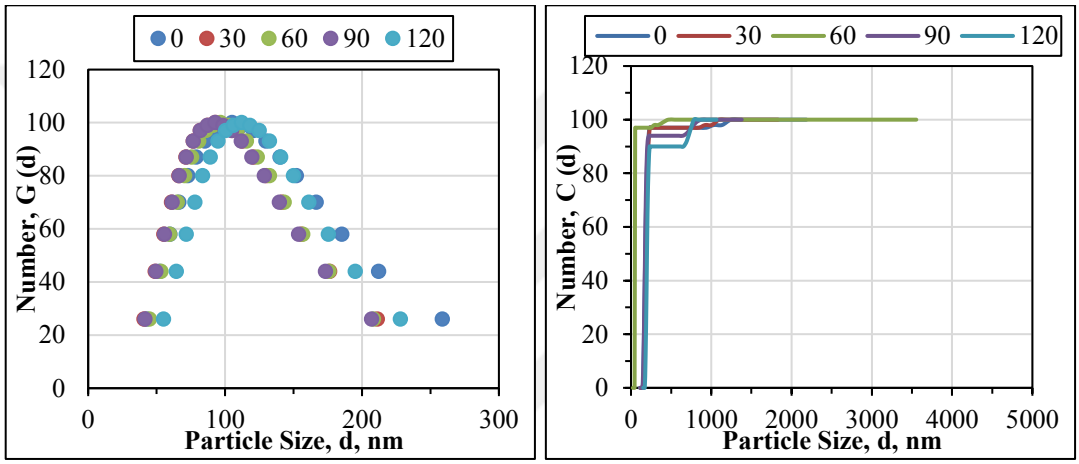


Figure 4.143. "N-TiO_2 and HA" binary system "as-is" under dark conditions number profile: Time dependent logN distribution G(d) and multi size distribution C(d).

Table 4.90. "N-TiO_2 and HA" binary system "as-is" under dark conditions number profile: Time dependent mean diameter, range and min-max diameter difference with respect to log normal and multi-size distribution.

N-TiO_2 and HA	time, min				
	0	30	60	90	120
Log Normal distribution					
Mean, nm	105.2	92.9	96.7	92.7	112.1
Range	42.8-258.6	40.9-211.3	44.8-208.4	41.5-207.1	55.0-228.2
Difference	215.8	170.4	163.6	165.6	173.2
Multi-size distribution					
Max 1, nm	174.0	198.0	52.1	178.4	205.6
Max 2, nm	1367.3	1096.1	340.2	752.5	738.3
Max 3, nm	-	-	397.8	-	-
Max 4, nm	-	-	465.2	-	-
Range	108.9-2184.4	118.5-1831.4	23.8-3553.9	122.2-1379.4	151.7-1063.8
Difference	2075.5	1712.9	3530.1	1257.2	912.1

In a similar manner to data depicted "N-TiO_2 and HA" binary system "as-is" under dark conditions surface area profile (Figure 4.142), log normal distribution G(d) and multi size distribution C(d) of "N-TiO_2 and HA" binary system "as-is" under dark conditions number profile was demonstrated with respect to time. It could be seen that initial hydrodynamic size of "N-TiO_2 and HA" binary system "as-is" under dark conditions displayed a sharp decrease and minor variations remained until 120 min. In terms of multi-size distribution, two max diameters were obtained following initial period of time. Upon 60 min, four peaks were monitored. Upon 90 min, two peaks were observed until the end of 120 min period. Time dependent comparative presentation of log Normal distribution and multi-size distribution of "N-TiO_2 and HA" binary system "as-is" under dark conditions number profile was given in Figure 4.144.

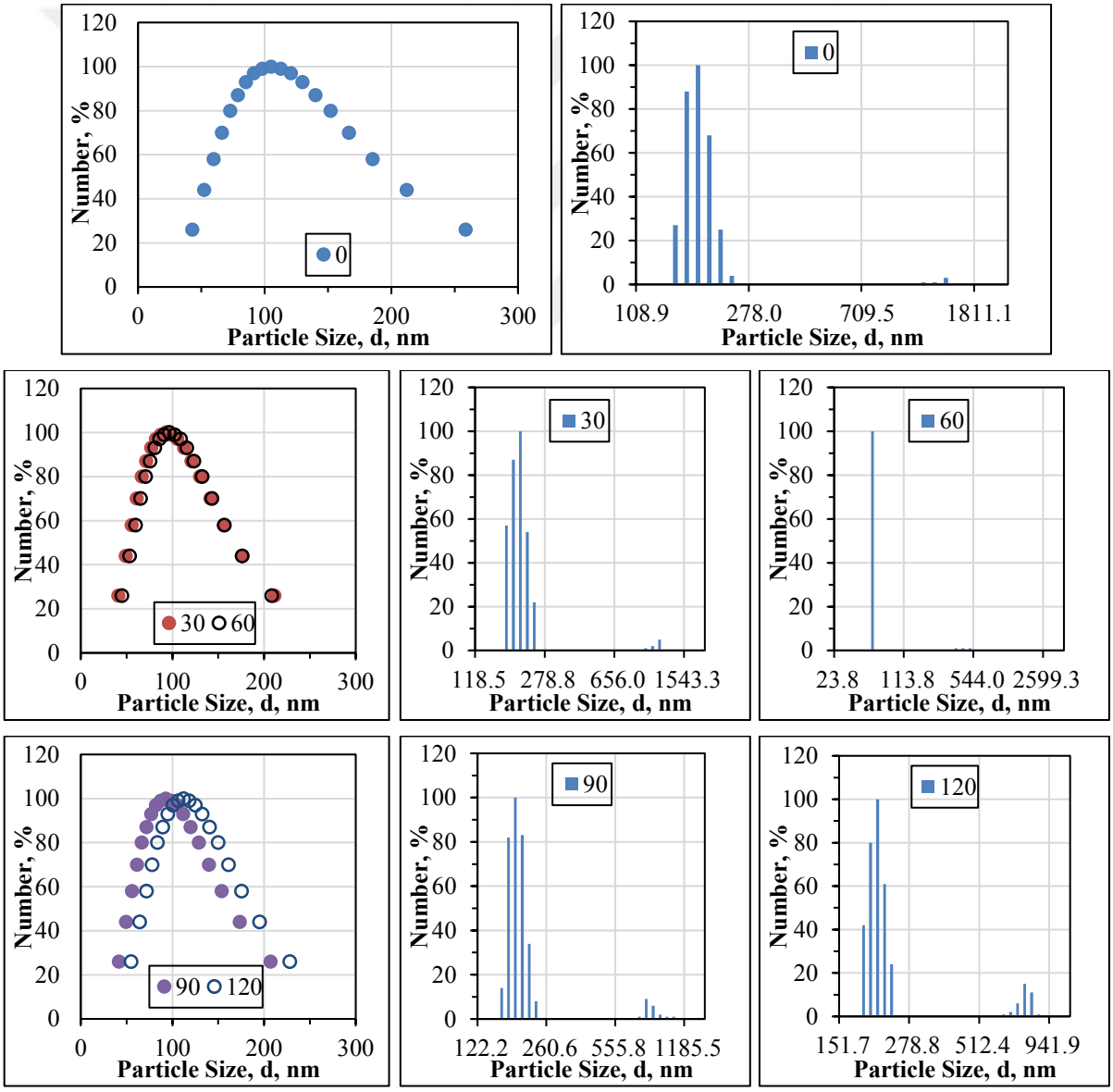


Figure 4.144. "N-TiO_2 and HA" binary system "as-is" under dark conditions number profile: Time dependent comparative presentation of log Normal distribution and multi-size distribution of "N-TiO_2 and HA" binary system "as-is" under dark conditions.

4.1.5.13. "N-TiO_2 and SRNOM" binary system "as-is" under dark conditions intensity profile. In a similar manner to data represented "N-TiO_2 and HA" binary system "as-is" under dark conditions intensity profile (Figure 4.137), time dependent logN distribution G(d) and multi size distribution C(d) of "N-TiO_2 and SRNOM" binary system "as-is" under dark conditions intensity profile was shown in Figure 4.145. Time dependent mean diameter, range and min-max diameter difference with respect to log normal and multi-size distribution of "N-TiO_2 and SRNOM" binary system "as-is" under dark conditions intensity profile was presented in Table 4.91.

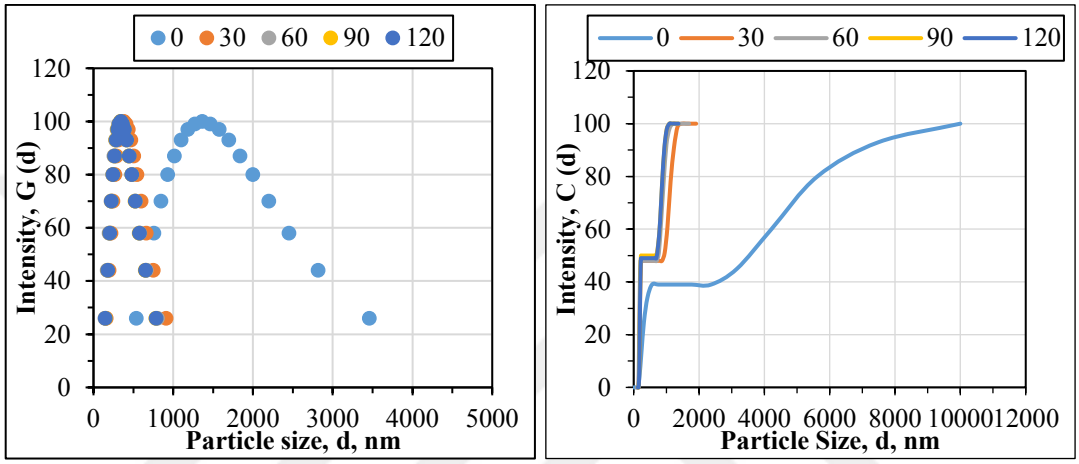


Figure 4.145. "N-TiO_2 and SRNOM" binary system "as-is" under dark conditions intensity profile: Time dependent logN distribution G(d) and multi size distribution C(d).

Table 4.91. "N-TiO_2 and SRNOM" binary system "as-is" under dark conditions intensity profile: Time dependent mean diameter, range and min-max diameter difference with respect to log normal and multi-size distribution.

N-TiO_2 and SRNOM	time, min				
	0	30	60	90	120
Log Normal distribution					
Mean, nm	1365.3	382.7	339.3	342.5	343.8
Range	538.7-3460.6	161.0-909.4	143.7-801.1	150.3-780.4	150.1-787.5
Difference	2921.9	748.4	657.4	630.1	637.4
Multi-size distribution					
Max 1, nm	316.2	195.7	173.6	191.1	191.9
Max 2, nm	5623.4	1130.6	918.4	869.6	873.0
Range	1.0-10.000	115.7-1913.5	102.6-1696.7	121.3-1369.9	121.8-1375.3
Difference	9999.0	1797.8	1594.1	1248.6	1253.5

In terms of intensity profile, initial hydrodynamic particle size of "N-TiO_2 and SRNOM" binary system "as-is" under dark conditions detected as 1365.3 nm and revealed a sharp decrease in the first 30 min. Considering multi-size distribution, two peaks were monitored according to time variations.

Time dependent comparative presentation of log Normal distribution and multi-size distribution of "N-TiO_2 and SRNOM" binary system "as-is" under dark conditions intensity profile was presented in Figure 4.146. Also, polydispersity of "N-TiO_2 and SRNOM" binary system "as-is" under dark conditions was exhibited in Table 4.92, a sharp decline was monitored in the first 30 min and continuous decrease was detected upon 120 min.

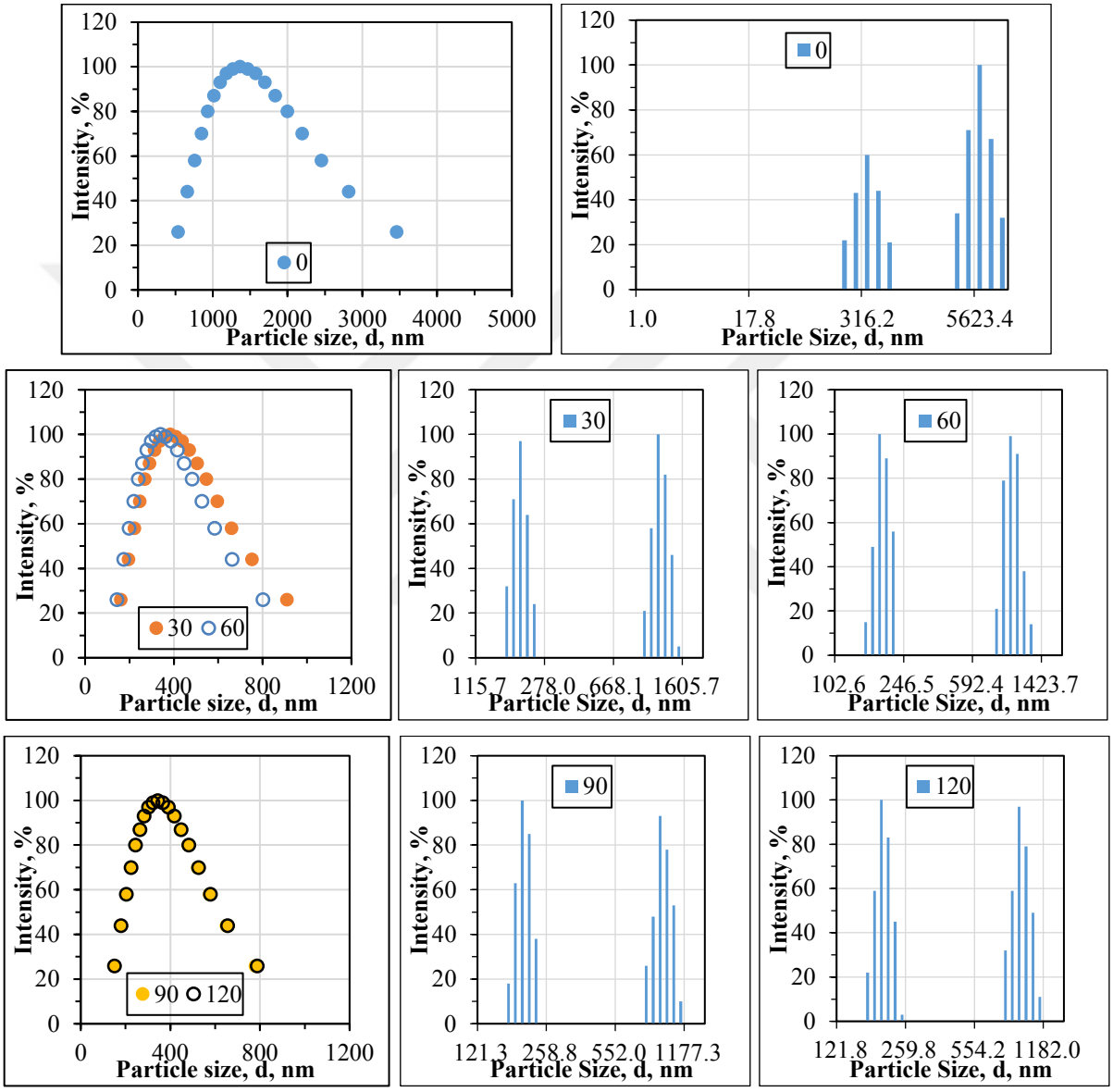


Figure 4.146. "N-TiO_2 and SRNOM" binary system "as-is" under dark conditions intensity profile: Time dependent comparative presentation of log Normal distribution and multi-size distribution of "N-TiO_2 and SRNOM" binary system "as-is" under dark conditions.

Table 4.92. Polydispersity of "N-TiO_2 and SRNOM" binary system "as-is" under dark conditions.

N-TiO_2 and SRNOM	Polydispersity				
	0	30	60	90	120
	0.377	0.319	0.313	0.285	0.289

4.1.5.14. "N-TiO_2 and SRNOM" binary system "as-is" under dark conditions volume profile. In a similar manner to data depicted "N-TiO_2 and SRNOM" binary system "as-is" under dark conditions intensity profile (Figure 4.145), time dependent logN distribution G(d) and multi size distribution C(d) of "N-TiO_2 and SRNOM" binary system "as-is" under dark conditions volume profile was displayed in Figure 4.147. Time dependent mean diameter, range and min-max diameter difference with respect to log normal and multi-size distribution of "N-TiO_2 and SRNOM" binary system "as-is" under dark conditions volume profile was presented in Table 4.93.

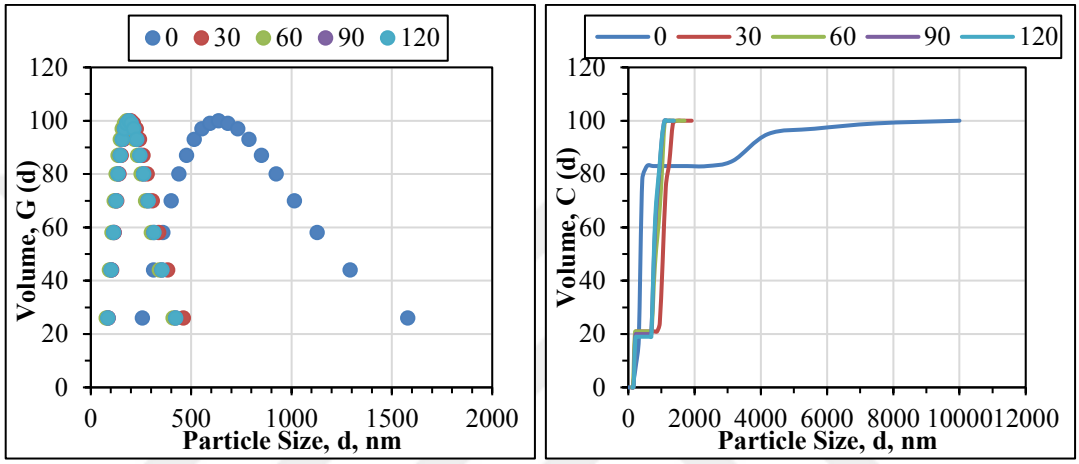


Figure 4.147. "N-TiO_2 and SRNOM" binary system "as-is" under dark conditions volume profile: Time dependent logN distribution G(d) and multi size distribution C(d).

Table 4.93. "N-TiO_2 and SRNOM" binary system "as-is" under dark conditions volume profile: Time dependent mean diameter, range and min-max diameter difference with respect to log normal and multi-size distribution.

N-TiO_2 and SRNOM	time, min				
	0	30	60	90	120
Log Normal distribution					
Mean, nm	636.9	199.0	178.3	190.3	189.6
Range	256.7-1579.9	85.8-461.6	77.4-410.8	85.7-422.5	84.9-423.1
Difference	1323.2	375.8	333.4	336.8	338.2
Multi-size distribution					
Max 1, nm	421.7	195.7	173.6	191.1	191.9
Max 2, nm	4217.0	1130.6	770.6	806.1	750.3
Max 3, nm	7498.9	1347.4	1094.4	1011.8	1015.8
Range	1.0-10.000	115.7-1913.5	102.6-1696.7	121.3-1369.9	121.8-1375.3
Difference	9999.0	1797.8	1594.1	1248.6	1253.5

In terms of intensity profile, initial hydrodynamic particle size of "N-TiO_2 and SRNOM" binary system "as-is" under dark conditions detected as 636.9 nm and revealed a rapid decrease in the first

30 min. Accordingly, slight variations remained until 120 min. Initial hydrodynamic particle size was recorded as 636.9 nm and reached to 189.6 nm upon period of 120 min. In terms of log normal distribution, size difference revealed a sharp decrease in the first 30 min and detected to 338.2 nm at the end of 120 min period. Considering multi-size distribution, three max diameters were monitored during 120 min. In terms of multi-size distribution, size difference between max and min diameter was decreased from 9999 nm to 1253.5 nm along 120 min. As explained for "N-TiO_2 and SRNOM" binary system "as-is" under dark conditions intensity profile (Figure 4.146), time dependent comparative presentation of log Normal distribution and multi-size distribution of "N-TiO_2 and SRNOM" binary system "as-is" under dark conditions volume profile was demonstrated in Figure 4.148.

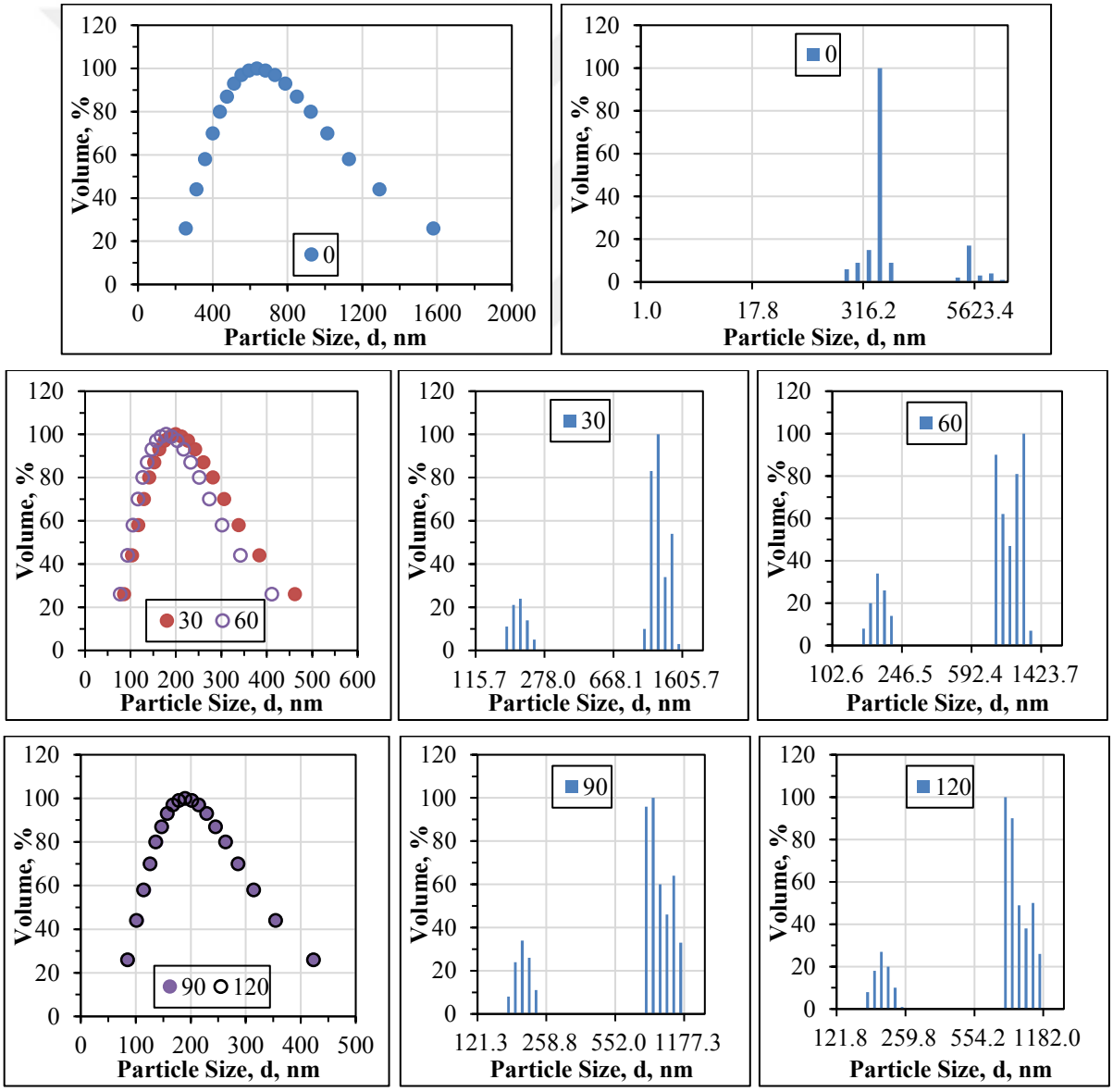


Figure 4.148. "N-TiO_2 and SRNOM" binary system "as-is" under dark conditions volume profile: Time dependent comparative presentation of log Normal distribution and multi-size distribution of "N-TiO_2 and SRNOM" binary system "as-is" under dark conditions.

4.1.5.15. "N-TiO_2 and SRNOM" binary system "as-is" under dark conditions surface area profile. In a similar manner to data depicted "N-TiO_2 and SRNOM" binary system "as-is" under dark conditions volume profile (Figure 4.147), time dependent logN distribution G(d) and multi size distribution C(d) of "N-TiO_2 and SRNOM" binary system "as-is" under dark conditions surface area profile was given in Figure 4.149. Time dependent mean diameter, range and min-max diameter difference with respect to log normal and multi-size distribution of "N-TiO_2 and SRNOM" binary system "as-is" under dark conditions surface area profile was displayed in Table 4.94.

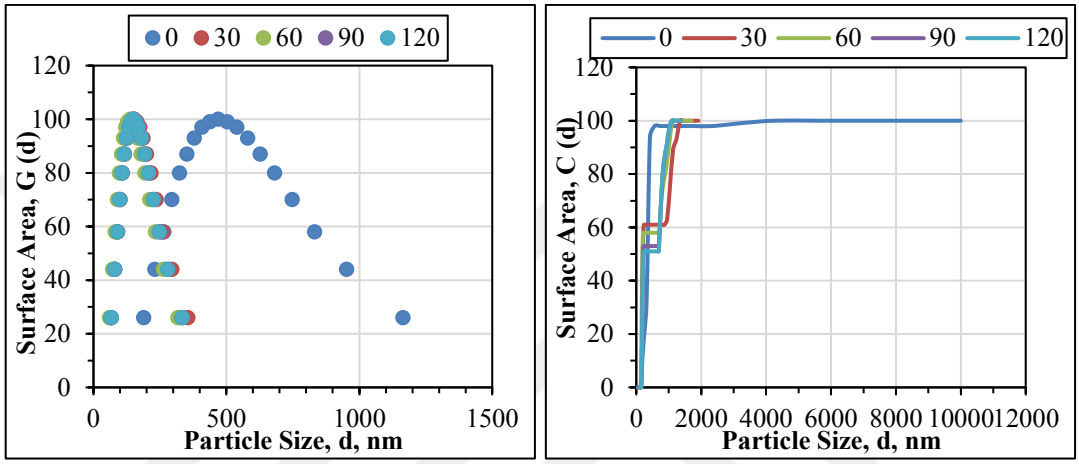


Figure 4.149. "N-TiO_2 and SRNOM" binary system "as-is" under dark conditions surface area profile: Time dependent logN distribution G(d) and multi size distribution C(d).

Table 4.94. "N-TiO_2 and SRNOM" binary system "as-is" under dark conditions surface area profile: Time dependent mean diameter, range and min-max diameter difference with respect to log normal and multi-size distribution.

N-TiO_2 and SRNOM	time, min				
	0	30	60	90	120
Log Normal distribution					
Mean, nm	469.5	153.2	137.9	150.5	149.4
Range	189.3-1164.5	66.0-355.3	59.9-317.6	67.8-334.0	66.9-333.4
Difference	975.2	289.3	257.7	266.2	266.5
Multi-size distribution					
Max 1, nm	421.7	195.7	173.6	191.1	191.9
Max 2, nm	4217.0	1130.6	770.6	747.3	750.3
Max 3, nm	-	1347.4	1094.4	1011.8	1015.8
Range	1.0-10.000	115.7-1913.5	102.6-1696.7	121.3-1369.9	121.8-1375.3
Difference	9999.0	1797.8	1594.1	1248.6	1253.5

According to log normal distribution and in terms of surface area profile, initial hydrodynamic particle size of "N-TiO_2 and SRNOM" binary system "as-is" under dark conditions was detected as

469.5 nm. Upon 30 min, roughly 65 % decline was observed and minor variations remained until 120 min. On the other hand, initial size difference was revealed a dramatic decrease and decreased from 975.2 nm to 289.3 nm in the first 30 min. Upon period of 30 min, minor alterations were monitored until the end of 120 min. For comparison purposes, in terms of multi-size distribution, initially two peaks were obtained. Upon 30 min, three max diameters were observed and remained until the end of 120 min.

Time dependent comparative presentation of log Normal distribution and multi-size distribution of "N-TiO_2 and SRNOM" binary system "as-is" under dark conditions surface area profile was displayed in Figure 4.150.

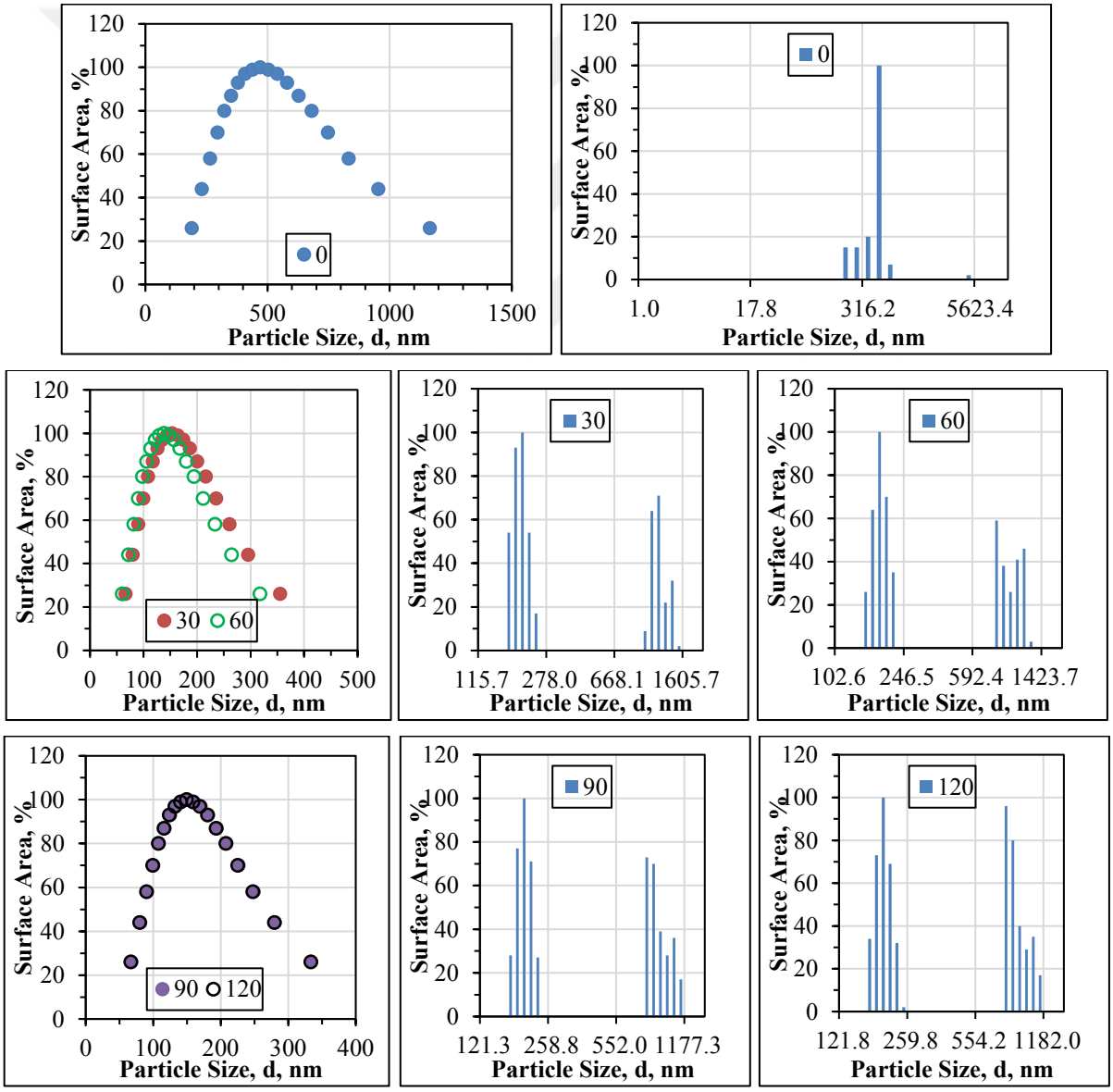


Figure 4.150. "N-TiO_2 and SRNOM" binary system "as-is" under dark conditions surface area profile: Time dependent comparative presentation of log Normal distribution and multi-size distribution of "N-TiO_2 and SRNOM" binary system "as-is" under dark conditions.

4.1.5.16. "N-TiO_2 and SRNOM" binary system "as-is" under dark conditions number profile. In a similar manner to data represented "N-TiO_2 and SRNOM" binary system "as-is" under dark conditions surface area profile (Figure 4.149), time dependent logN distribution G(d) and multi size distribution C(d) of "N-TiO_2 and SRNOM" binary system "as-is" under dark conditions number profile was demonstrated in Figure 4.151. Time dependent mean diameter, range and min-max diameter difference with respect to log normal and multi-size distribution of "N-TiO_2 and SRNOM" binary system "as-is" under dark conditions number profile was exhibited in Table 4.95.

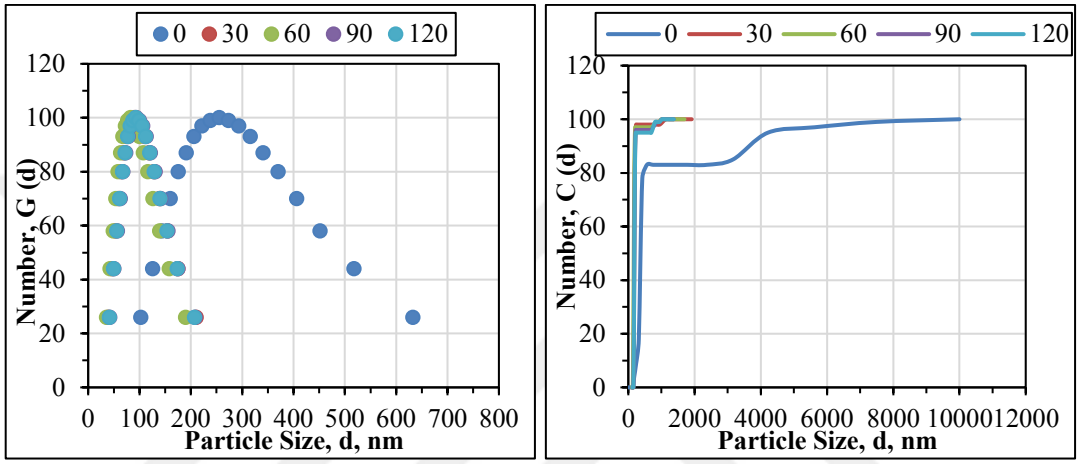


Figure 4.151. "N-TiO_2 and SRNOM" binary system "as-is" under dark conditions number profile: Time dependent logN distribution G(d) and multi size distribution C(d).

Table 4.95. "N-TiO_2 and SRNOM" binary system "as-is" under dark conditions number profile: Time dependent mean diameter, range and min-max diameter difference with respect to log normal and multi-size distribution.

N-TiO_2 and SRNOM	time, min				
	0	30	60	90	120
Log Normal distribution					
Mean, nm	255.1	90.8	82.4	94.0	92.8
Range	102.8-632.7	39.1-210.6	35.8-189.8	42.4-208.8	41.6-207.1
Difference	529.9	171.5	154.0	166.4	165.5
Multi-size distribution					
Max 1, nm	421.7	179.3	173.6	191.1	191.9
Max 2, nm	4217.0	1035.7	770.6	747.3	750.3
Max 3, nm	7498.9	1130.6	-	-	-
Range	1.0-10.000	115.7-1913.5	102.6-1696.7	121.3-1369.9	121.8-1375.3
Difference	9999.0	1797.8	1594.1	1248.6	1253.5

According to log normal distribution, initial hydrodynamic particle size of "N-TiO_2 and SRNOM" binary system "as-is" under dark conditions was obtained as 255.1 nm. Along 120 min,

hydrodynamic particle size of "N-TiO_2 and SRNOM" binary system "as-is" under dark conditions followed a rapidly decreasing trend and detected to 92.8 nm. In terms of log normal distribution, initial size difference was detected as 529.9 nm and decreased to 165.5 nm at the end of 120 min. According to multi-size distribution, three peaks were monitored as 421.7 nm, 4217.0 nm, and 7498.9 nm for "N-TiO_2 and SRNOM" binary system "as-is" under dark conditions following initial period of time. Upon period of 60 min, two peaks were observed until the end of 120 min. As explained for "N-TiO_2 and SRNOM" binary system "as-is" under dark conditions surface area profile, time dependent comparative presentation of log Normal distribution and multi-size distribution of "N-TiO_2 and SRNOM" binary system "as-is" under dark conditions number profile was demonstrated in Figure 4.152.

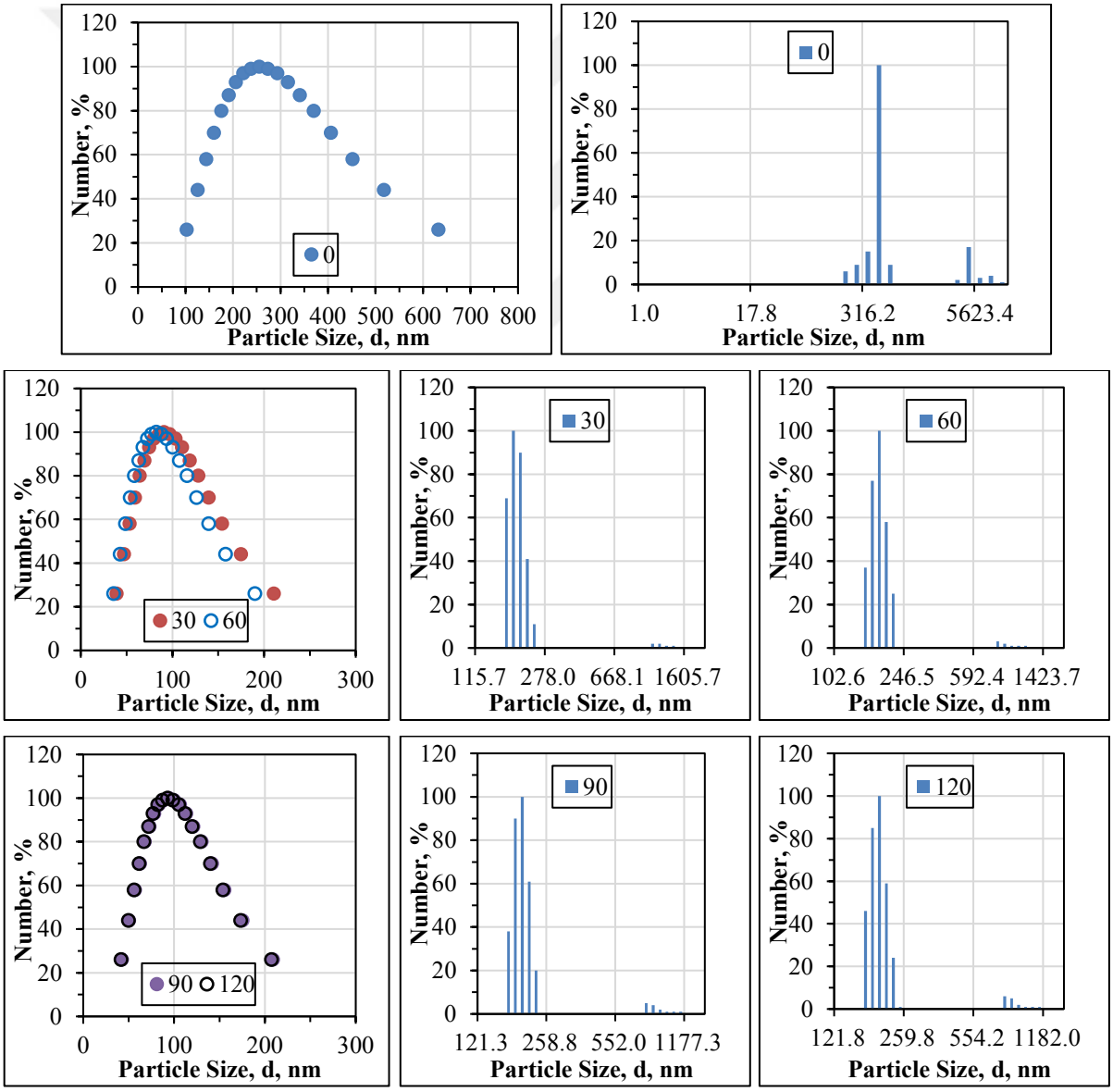


Figure 4.152. "N-TiO_2 and SRNOM" binary system "as-is" under dark conditions number profile: Time dependent comparative presentation of log Normal distribution and multi-size distribution of "N-TiO_2 and SRNOM" binary system "as-is" under dark conditions.

4.1.5.17. "Fe-TiO_2 and HA" binary system "as-is" under dark conditions intensity profile. As elucidated for "N-TiO_2 and HA" binary system "as-is" under dark conditions intensity profile (Figure 4.137), a similar approach was followed for "Fe-TiO_2 and HA" binary system "as-is" under dark conditions intensity profile. Time dependent logN distribution G(d) and multi size distribution C(d) of "Fe-TiO_2 and HA" binary system "as-is" under dark conditions intensity profile was presented in Figure 4.153. Time dependent mean diameter, range and min-max diameter difference with respect to log normal and multi-size distribution of "Fe-TiO_2 and HA" binary system "as-is" under dark conditions intensity profile was displayed in Table 4.96.

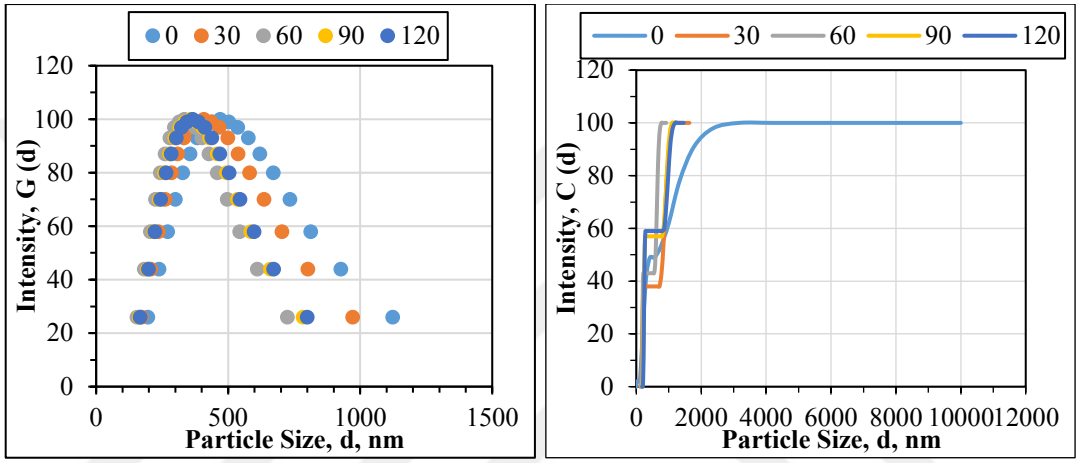


Figure 4.153. "Fe-TiO_2 and HA" binary system "as-is" under dark conditions intensity profile: Time dependent logN distribution G(d) and multi size distribution C(d).

Table 4.96. "Fe-TiO_2 and HA" binary system "as-is" under dark conditions intensity profile: Time dependent mean diameter, range and min-max diameter difference with respect to log normal and multi-size distribution.

Fe-TiO_2 and HA	time, min				
	0	30	60	90	120
Log Normal distribution					
Mean, nm	469.6	407.6	334.4	357.8	365.1
Range	196.3-1123.5	171.1-971.3	154.3-724.5	163.3-784.3	166.8-799.2
Difference	927.2	800.2	570.2	621.0	632.4
Multi-size distribution					
Max 1, nm	1.8	189.6	191.1	240.9	245.8
Max 2, nm	2.4	915.5	650.2	963.3	982.8
Max 3, nm	3.2	-	-	-	1049.9
Max 4, nm	237.1	-	-	-	-
Max 5, nm	1333.5	-	-	-	-
Range	1.0-10.000	115.3-1635.3	142.7-922.7	173.2-1431.3	176.7-1460.4
Difference	9999.0	1520.0	780.0	1258.1	1283.7

In terms of intensity profile, initial hydrodynamic size was obtained as 469.6 nm. In terms of multi-size distribution, initially five peaks were attained. Time dependent comparative presentation of log Normal distribution and multi-size distribution, and also polydispersity of "Fe-TiO_2 and HA" binary system "as-is" under dark conditions intensity profile was presented in Figure 4.154 and Table 4.97. An average value of 0.281 could be regarded as suitable for expressing polydispersity.

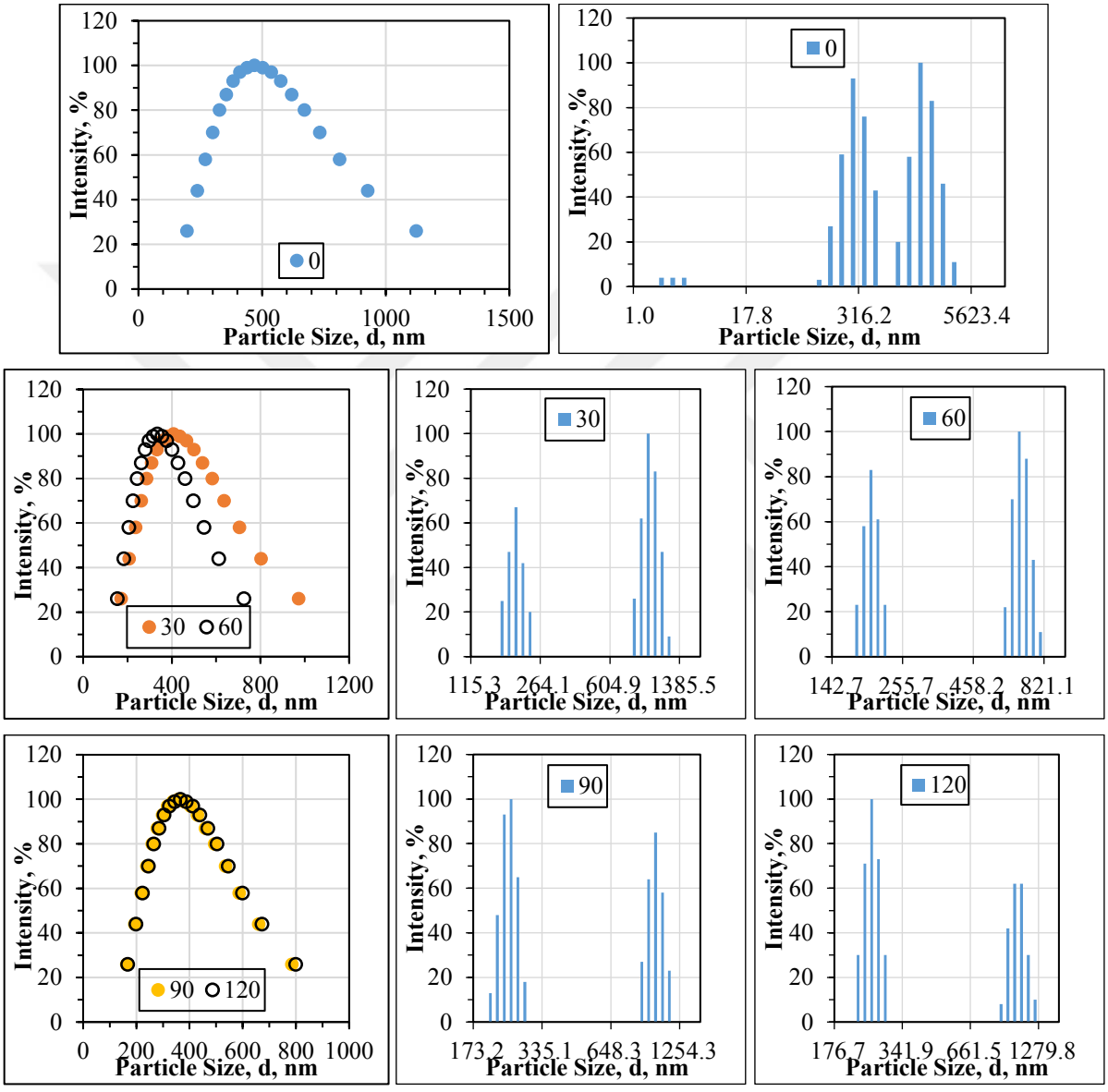


Figure 4.154. "Fe-TiO_2 and HA" binary system "as-is" under dark conditions intensity profile: Time dependent comparative presentation of log Normal distribution and multi-size distribution of "Fe-TiO_2 and HA" binary system "as-is" under dark conditions.

Table 4.97. Polydispersity of "Fe-TiO_2 and HA" binary system "as-is" under dark conditions.

Fe-TiO_2 and HA	Polydispersity				
	0	30	60	90	120
	0.325	0.321	0.247	0.256	0.255

4.1.5.18. "Fe-TiO_2 and HA" binary system "as-is" under dark conditions volume profile. In a similar manner to data depicted "Fe-TiO_2 and HA" binary system "as-is" under dark conditions intensity profile (Figure 4.153), time dependent logN distribution G(d) and multi size distribution C(d) of "Fe-TiO_2 and HA" binary system "as-is" under dark conditions volume profile was displayed in Figure 4.155. Time dependent mean diameter, range and min-max diameter difference with respect to log normal and multi-size distribution of "Fe-TiO_2 and HA" binary system "as-is" under dark conditions volume profile was presented in Table 4.98.

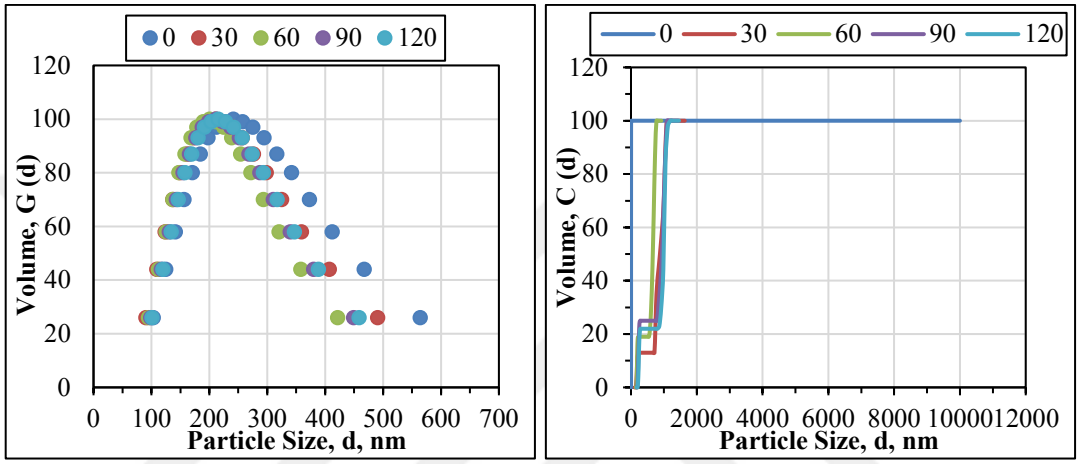


Figure 4.155. "Fe-TiO_2 and HA" binary system "as-is" under dark conditions volume profile: Time dependent logN distribution G(d) and multi size distribution C(d).

Table 4.98. "Fe-TiO_2 and HA" binary system "as-is" under dark conditions volume profile: Time dependent mean diameter, range and min-max diameter difference with respect to log normal and multi-size distribution.

Fe-TiO_2 and HA	time, min				
	0	30	60	90	120
Log Normal distribution					
Mean, nm	241.5	211.0	200.4	210.9	215.6
Range	103.4-564.1	90.7-490.8	95.2-421.9	99.0-449.4	101.3-458.7
Difference	460.7	400.1	326.7	350.4	357.4
Multi-size distribution					
Max 1, nm	1.8	189.6	191.1	225.5	245.8
Max 2, nm	-	775.6	730.7	240.9	1049.9
Max 3, nm	-	1080.5	-	1029.0	-
Range	1.0-10.000	115.3-1635.3	142.7-922.7	173.2-1431.3	176.7-1460.4
Difference	9999.0	1520.0	780.0	1258.1	1283.7

As explained for "Fe-TiO_2 and HA" binary system "as-is" under dark conditions intensity profile (Table 4.96), a similar approach was followed for "Fe-TiO_2 and HA" binary system "as-is" under

dark conditions volume profile. It could be deduced that hydrodynamic particle size roughly 10 % decreased upon 30 min. Initial hydrodynamic particle size was recorded as 241.5 nm and detected to 211.0 nm upon 30 min. Accordingly, minor increase was observed with slight variations until the end of 120 min. However, in terms of multi-size distribution, initially one peak was observed, three peaks were monitored upon 30 min, and two peaks were obtained upon 120 min.

As described for "Fe-TiO_2 and HA" binary system "as-is" under dark conditions intensity profile (Figure 4.154), time dependent comparative presentation of log Normal distribution and multi-size distribution of "Fe-TiO_2 and HA" binary system "as-is" under dark conditions volume profile was demonstrated in Figure 4.156.

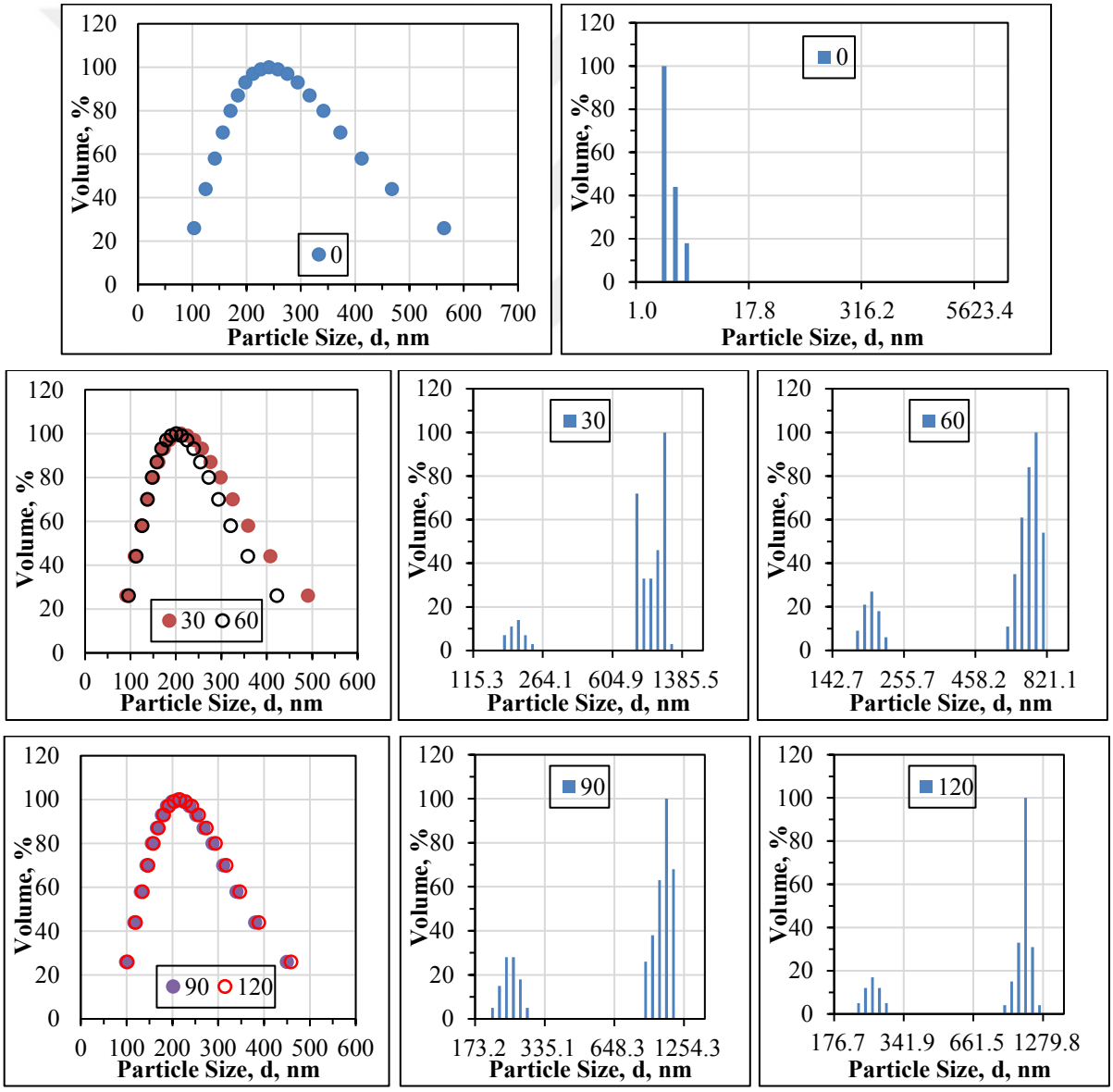


Figure 4.156. "Fe-TiO_2 and HA" binary system "as-is" under dark conditions volume profile: Time dependent comparative presentation of log Normal distribution and multi-size distribution of "Fe-TiO_2 and HA" binary system "as-is" under dark conditions.

4.1.5.19. "Fe-TiO_2 and HA" binary system "as-is" under dark conditions surface area profile. In a similar manner to data depicted "Fe-TiO_2 and HA" binary system "as-is" under dark conditions volume profile (Figure 4.155), time dependent logN distribution G(d) and multi size distribution C(d) of "Fe-TiO_2 and HA" binary system "as-is" under dark conditions surface area profile was exhibited in Figure 4.157. Time dependent mean diameter, range and min-max diameter difference with respect to log normal and multi-size distribution of "Fe-TiO_2 and HA" binary system "as-is" under dark conditions surface area profile was displayed in Table 4.99.

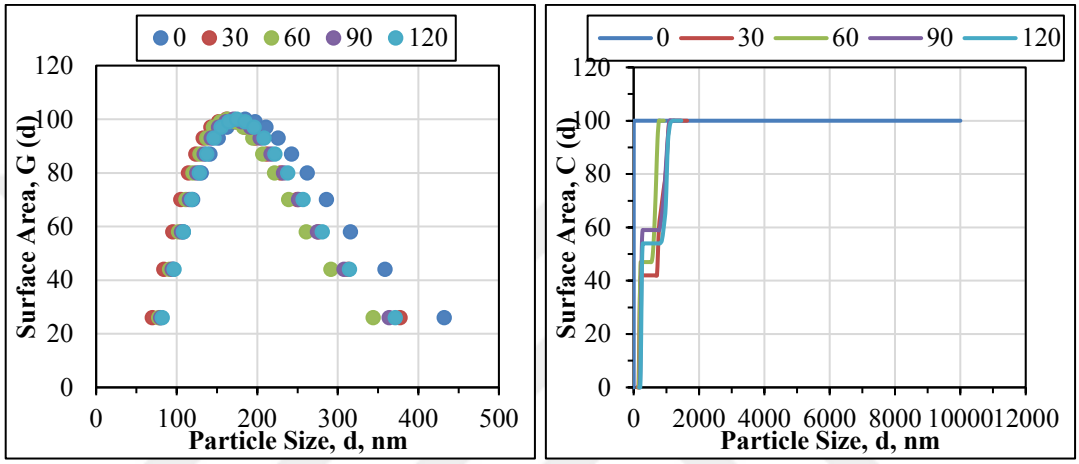


Figure 4.157. "Fe-TiO_2 and HA" binary system "as-is" under dark conditions surface area profile: Time dependent logN distribution G(d) and multi size distribution C(d).

Table 4.99. "Fe-TiO_2 and HA" binary system "as-is" under dark conditions surface area profile: Time dependent mean diameter, range and min-max diameter difference with respect to log normal and multi-size distribution.

Fe-TiO_2 and HA	time, min				
	0	30	60	90	120
Log Normal distribution					
Mean, nm	185.1	162.1	163.3	170.7	174.6
Range	79.2-432.4	69.7-377.2	77.6-343.8	80.1-363.7	82.0-371.5
Difference	353.2	307.5	266.2	283.6	289.5
Multi-size distribution					
Max 1, nm	1.8	189.6	191.1	225.5	245.8
Max 2, nm	-	775.6	730.7	1029.0	1049.9
Max 3, nm	-	1080.5	-	-	-
Range	1.0-10.000	115.3-1635.3	142.7-922.7	173.2-1431.3	176.7-1460.4
Difference	9999.0	1520.0	780.0	1258.1	1283.7

In terms of surface area profile, it could be seen that hydrodynamic particle size of "Fe-TiO_2 and HA" binary system "as-is" under dark conditions revealed a slight decrease following initial period

of time and minor increase remained until 120 min. Initial hydrodynamic size was attained as 185.1 nm and detected to 174.6 upon 120 min. According to log normal distribution, size difference between max and min diameter revealed a minor decrease in the first 30 min and continuous decrease was obtained until 120 min. However, in terms of multi-size distribution, initially one peak was observed, upon 30 min three peaks were monitored, and two peaks were observed until the end of 120 min. In terms of multi-size distribution, size difference decreased from 9999.0 nm to 1283.7 nm.

Time dependent comparative presentation of log Normal distribution and multi-size distribution of "Fe-TiO_2 and HA" binary system "as-is" under dark conditions surface area profile was exhibited in Figure 4.158.

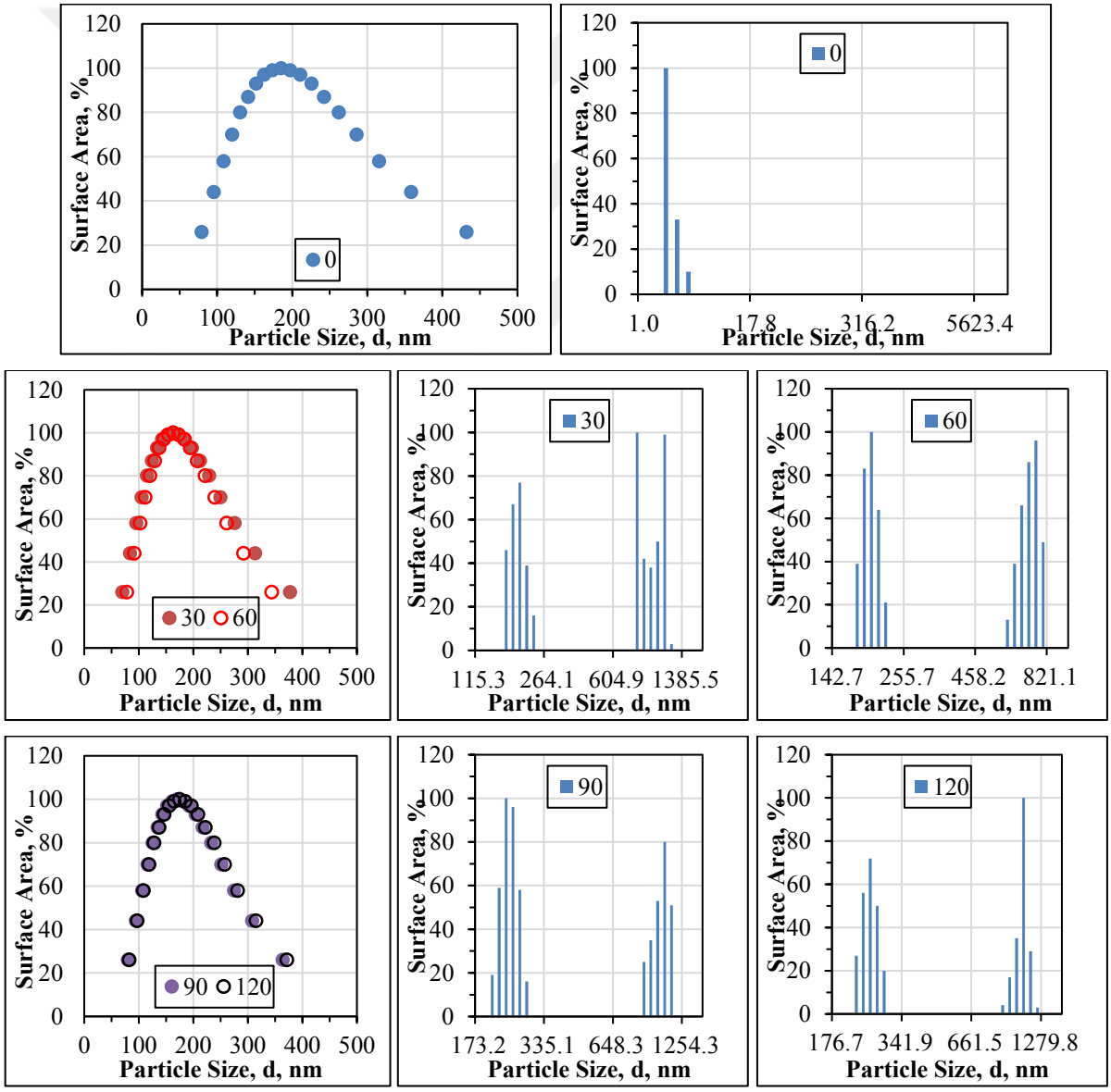


Figure 4.158. "Fe-TiO_2 and HA" binary system "as-is" under dark conditions surface area profile: Time dependent comparative presentation of log Normal distribution and multi-size distribution of "Fe-TiO_2 and HA" binary system "as-is" under dark conditions.

4.1.5.20. "Fe-TiO_2 and HA" binary system "as-is" under dark conditions number profile. Time dependent logN distribution G(d) and multi size distribution C(d) of "Fe-TiO_2 and HA" binary system "as-is" under dark conditions number profile was exhibited in Figure 4.159. Time dependent mean diameter, range and min-max diameter difference with respect to log normal and multi-size distribution of "Fe-TiO_2 and HA" binary system "as-is" under dark conditions number profile was demonstrated in Table 4.100.

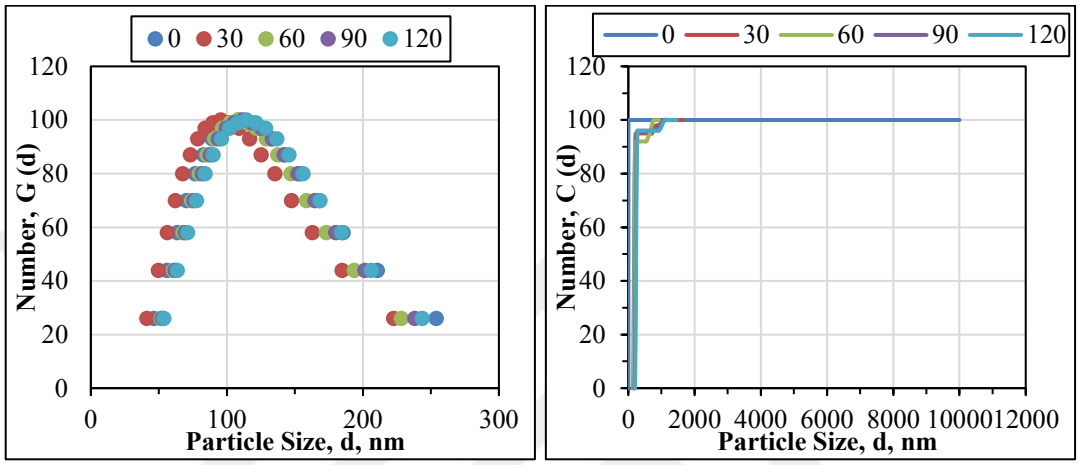


Figure 4.159. "Fe-TiO_2 and HA" binary system "as-is" under dark conditions number profile: Time dependent logN distribution G(d) and multi size distribution C(d).

Table 4.100. "Fe-TiO_2 and HA" binary system "as-is" under dark conditions number profile: Time dependent mean diameter, range and min-max diameter difference with respect to log normal and multi-size distribution.

Fe-TiO_2 and HA	time, min				
	0	30	60	90	120
Log Normal distribution					
Mean, nm	108.7	95.7	108.4	111.8	114.5
Range	46.5-254.0	41.2-222.7	51.5-228.3	52.5-238.2	53.8-243.7
Difference	207.5	181.5	176.8	185.7	189.9
Multi-size distribution					
Max 1, nm	1.8	174.5	191.1	225.5	245.8
Max 2, nm	-	775.6	689.3	1029.0	1049.9
Max 3, nm	-	1080.5	730.7	-	-
Range	1.0-10.000	115.3-1635.3	142.7-922.7	173.2-1431.3	176.7-1460.4
Difference	9999.0	1520.0	780.0	1258.1	1283.7

Considering log normal distribution and in terms of number profile, initial hydrodynamic particle size of "Fe-TiO_2 and HA" binary system "as-is" under dark conditions was recorded as 108.7 nm. During 120 min, hydrodynamic particle size of "Fe-TiO_2 and HA" binary system "as-is" under dark

conditions displayed a fluctuating trend. Initial hydrodynamic particle size was recorded as 108.7 nm and detected to 114.5 nm at the end of 120 min. Also, size difference decreased from 207.5 nm to 189.9 nm during 120 min. For comparison purposes, in terms of multi-size distribution, initially one peak was monitored. Upon period of 30 min, three peaks were observed, and two peaks were attained until the end of 120 min.

As explained for "Fe-TiO_2 and HA" binary system "as-is" under dark conditions surface area profile, following a similar manner, time dependent comparative presentation of log Normal distribution and multi-size distribution of "Fe-TiO_2 and HA" binary system "as-is" under dark conditions number profile was given in Figure 4.160.

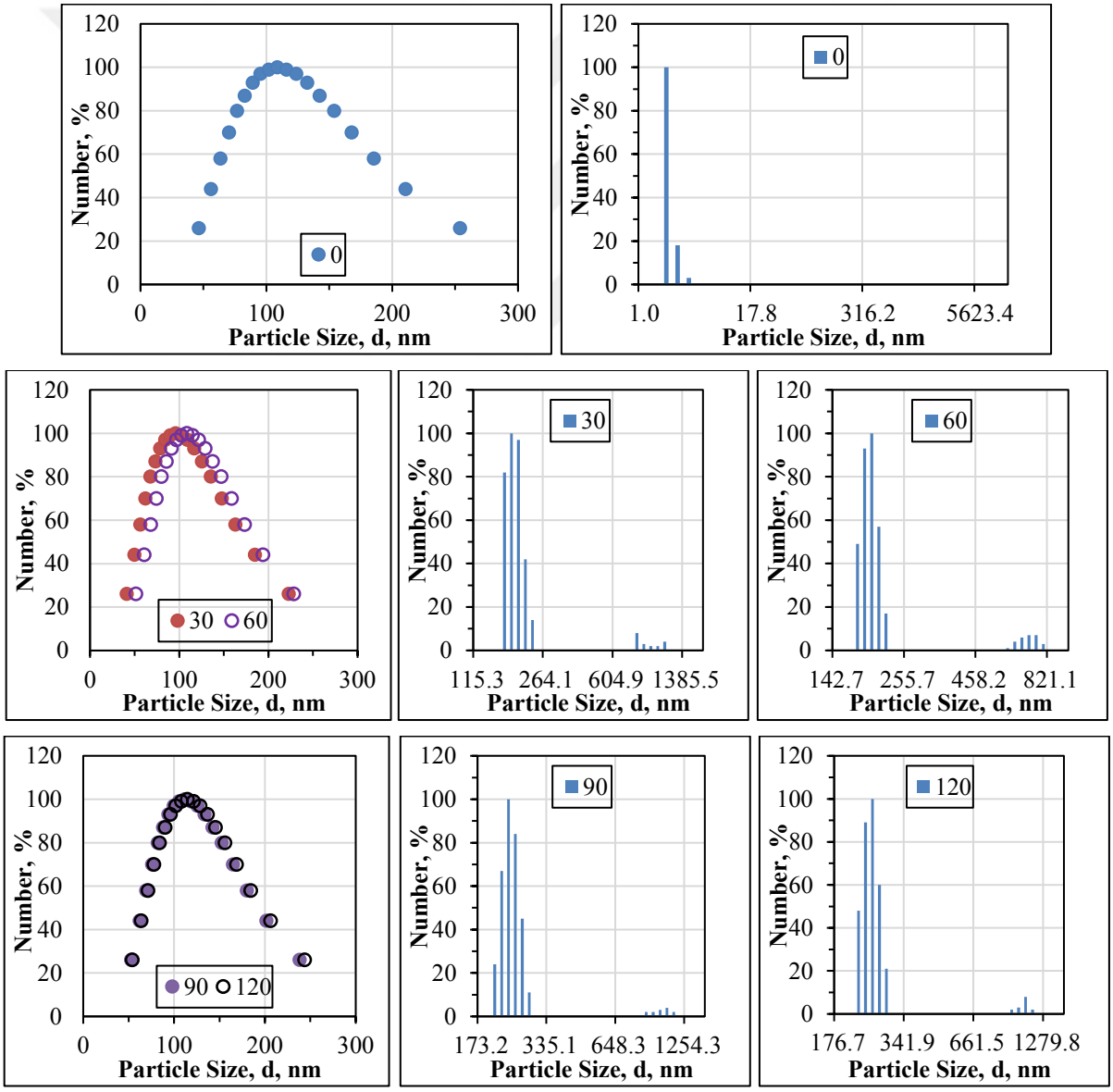


Figure 4.160. "Fe-TiO_2 and HA" binary system "as-is" under dark conditions number profile: Time dependent comparative presentation of log Normal distribution and multi-size distribution of "Fe-TiO_2 and HA" binary system "as-is" under dark conditions.

4.1.5.21. "Fe-TiO_2 and SRNOM" binary system "as-is" under dark conditions intensity profile. As explained for "Fe-TiO_2 and HA" binary system "as-is" under dark conditions intensity profile (Figure 4.153), a similar approach was followed for "Fe-TiO_2 and SRNOM" binary system "as-is" under dark conditions intensity profile. Time dependent logN distribution G(d) and multi size distribution C(d) of "Fe-TiO_2 and SRNOM" binary system "as-is" under dark conditions intensity profile was shown in Figure 4.161. Time dependent mean diameter, range and min-max diameter difference with respect to log normal and multi-size distribution of "Fe-TiO_2 and SRNOM" binary system "as-is" under dark conditions intensity profile was given in Table 4.101. Polydispersity of "Fe-TiO_2 and SRNOM" binary system "as-is" under dark conditions was displayed in Figure 4.102.

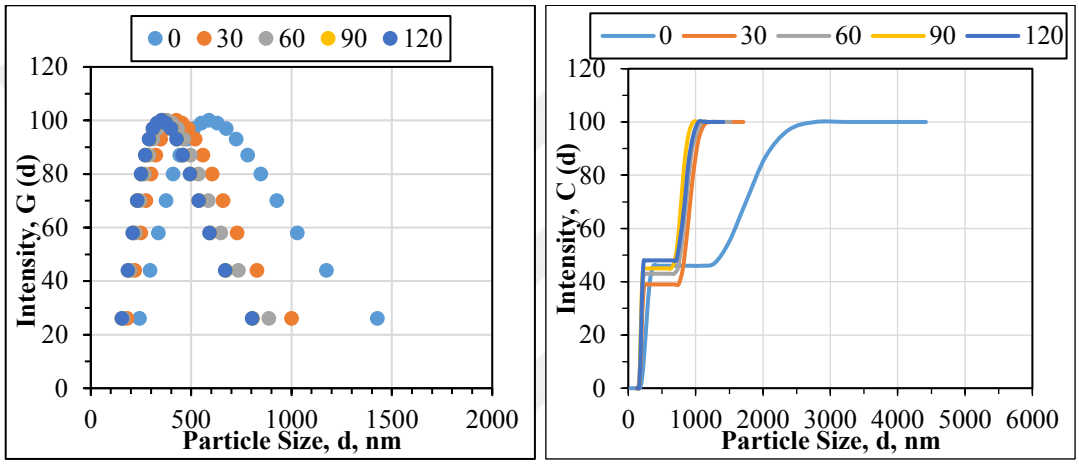


Figure 4.161. "Fe-TiO_2 and SRNOM" binary system "as-is" under dark conditions intensity profile: Time dependent logN distribution G(d) and multi size distribution C(d).

Table 4.101. "Fe-TiO_2 and SRNOM" binary system "as-is" under dark conditions intensity profile: Time dependent mean diameter, range and min-max diameter difference with respect to log normal and multi-size distribution.

Fe-TiO_2 and SRNOM	time, min				
	0	30	60	90	120
Log Normal distribution					
Mean, nm	589.3	425.7	378.8	354.0	352.3
Range	243.1-1428.4	181.1-1000.6	161.7-887.4	155.5-806.1	154.3-804.0
Difference	1185.3	819.5	725.7	650.6	649.7
Multi-size distribution					
Max 1, nm	49.8	198.0	201.6	191.3	196.6
Max 2, nm	273.0	956.0	935.9	838.9	894.4
Max 3, nm	2039.4	-	-	-	-
Range	31.3-4419.6	120.4-1707.7	114.5-1519.9	125.4-1192.8	124.8-1409.1
Difference	4388.3	1587.3	1405.4	1067.4	1284.3

In terms of intensity profile, initial hydrodynamic size of "Fe-TiO_2 and SRNOM" was recorded as 589.3 nm. Upon 30 min, ~ 20 % decrease was monitored. In terms of multi-size distribution, initially three peaks were attained and two peaks were observed until 120 min. Time dependent comparative presentation of log Normal distribution and multi-size distribution of "Fe-TiO_2 and SRNOM" binary system "as-is" under dark conditions intensity profile was shown in Figure 4.162.

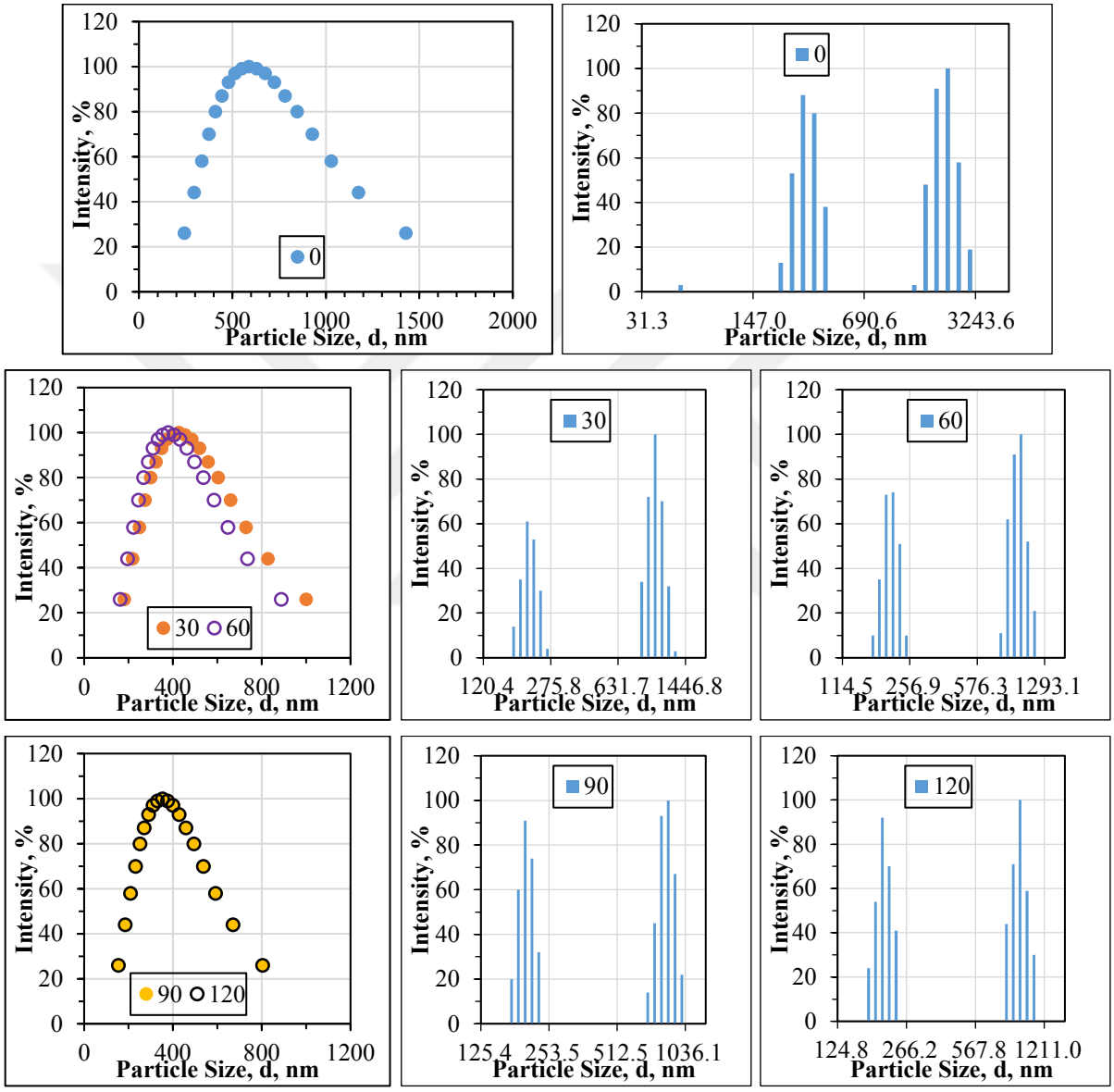


Figure 4.162. "Fe-TiO_2 and SRNOM" binary system "as-is" under dark conditions intensity profile: Time dependent comparative presentation of log Normal distribution and multi-size distribution of "Fe-TiO_2 and SRNOM" binary system "as-is" under dark conditions.

Table 4.102. Polydispersity of "Fe-TiO_2 and SRNOM" binary system "as-is" under dark conditions.

Fe-TiO_2 and SRNOM	Polydispersity				
	0	30	60	90	120
	0.336	0.310	0.307	0.284	0.286

4.1.5.22. "Fe-TiO_2 and SRNOM" binary system "as-is" under dark conditions volume profile. In a similar manner to data depicted "Fe-TiO_2 and SRNOM" binary system "as-is" under dark conditions intensity profile (Figure 4.161), time dependent logN distribution G(d) and multi size distribution C(d) of "Fe-TiO_2 and SRNOM" binary system "as-is" under dark conditions volume profile was presented in Figure 4.163. Time dependent mean diameter, range and min-max diameter difference with respect to log normal and multi-size distribution of "Fe-TiO_2 and SRNOM" binary system "as-is" under dark conditions volume profile was exhibited in Table 4.103.

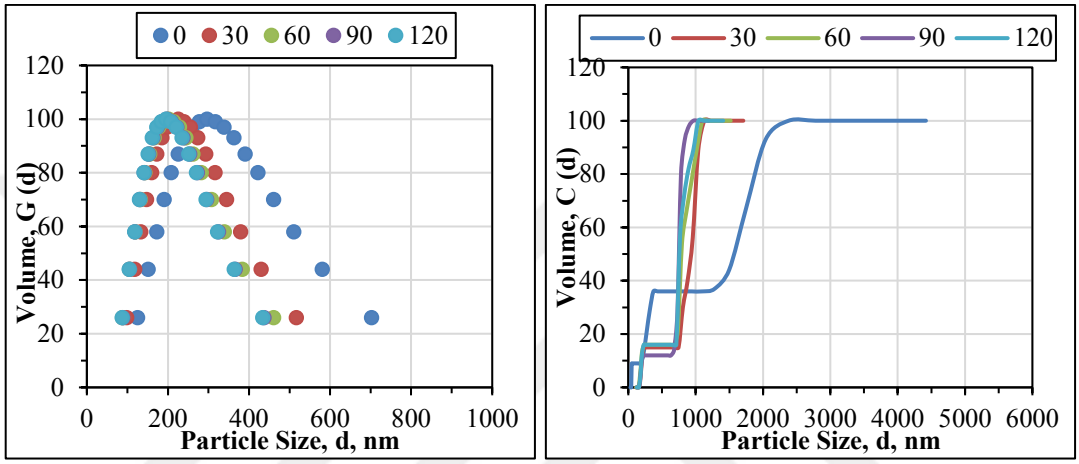


Figure 4.163. "Fe-TiO_2 and SRNOM" binary system "as-is" under dark conditions volume profile: Time dependent logN distribution G(d) and multi size distribution C(d).

Table 4.103. "Fe-TiO_2 and SRNOM" binary system "as-is" under dark conditions volume profile: Time dependent mean diameter, range and min-max diameter difference with respect to log normal and multi-size distribution.

Fe-TiO_2 and SRNOM	time, min				
	0	30	60	90	120
Log Normal distribution					
Mean, nm	296.6	225.2	201.6	196.9	195.3
Range	125.2-702.3	98.2-516.6	88.2-460.7	88.8-436.9	87.8-434.2
Difference	577.1	418.4	372.5	348.1	346.4
Multi-size distribution					
Max 1, nm	49.8	198.0	185.9	191.3	196.6
Max 2, nm	318.7	810.0	796.3	781.9	768.7
Max 3, nm	2039.4	1038.6	1014.7	-	1040.8
Range	31.3-4419.6	120.4-1707.7	114.5-1519.9	125.4-1192.8	124.8-1409.1
Difference	4388.3	1587.3	1405.4	1067.4	1284.3

According to volume profile, hydrodynamic particle size of "Fe-TiO_2 and SRNOM" binary system "as-is" under dark conditions displayed a slowly decreasing trend with respect to time. In

terms of log normal distribution, initial hydrodynamic size was attained as 296.6 nm and detected to 195.3 nm upon 120 min. Also, in terms of log normal distribution, size difference between max and min diameter decreased from 577.1 nm to 346.4 nm upon 120 min. For comparison purposes, in terms of multi-size distribution, initially three max diameters were observed as 49.8 nm, 318.7 nm, and 2039.4 nm. Upon 90 min, two peaks were attained as 191.3 nm and 781.9 nm. Upon 120 min, three peaks were monitored as 196.6 nm, 768.7 nm and 1040.8 nm. In terms of multi-size distribution, size difference decreased from 4388.3 nm to 1284.3 nm according to time variations. Time dependent comparative presentation of log Normal distribution and multi-size distribution of "Fe-TiO_2 and SRNOM" binary system "as-is" under dark conditions volume profile was demonstrated in Figure 4.164.

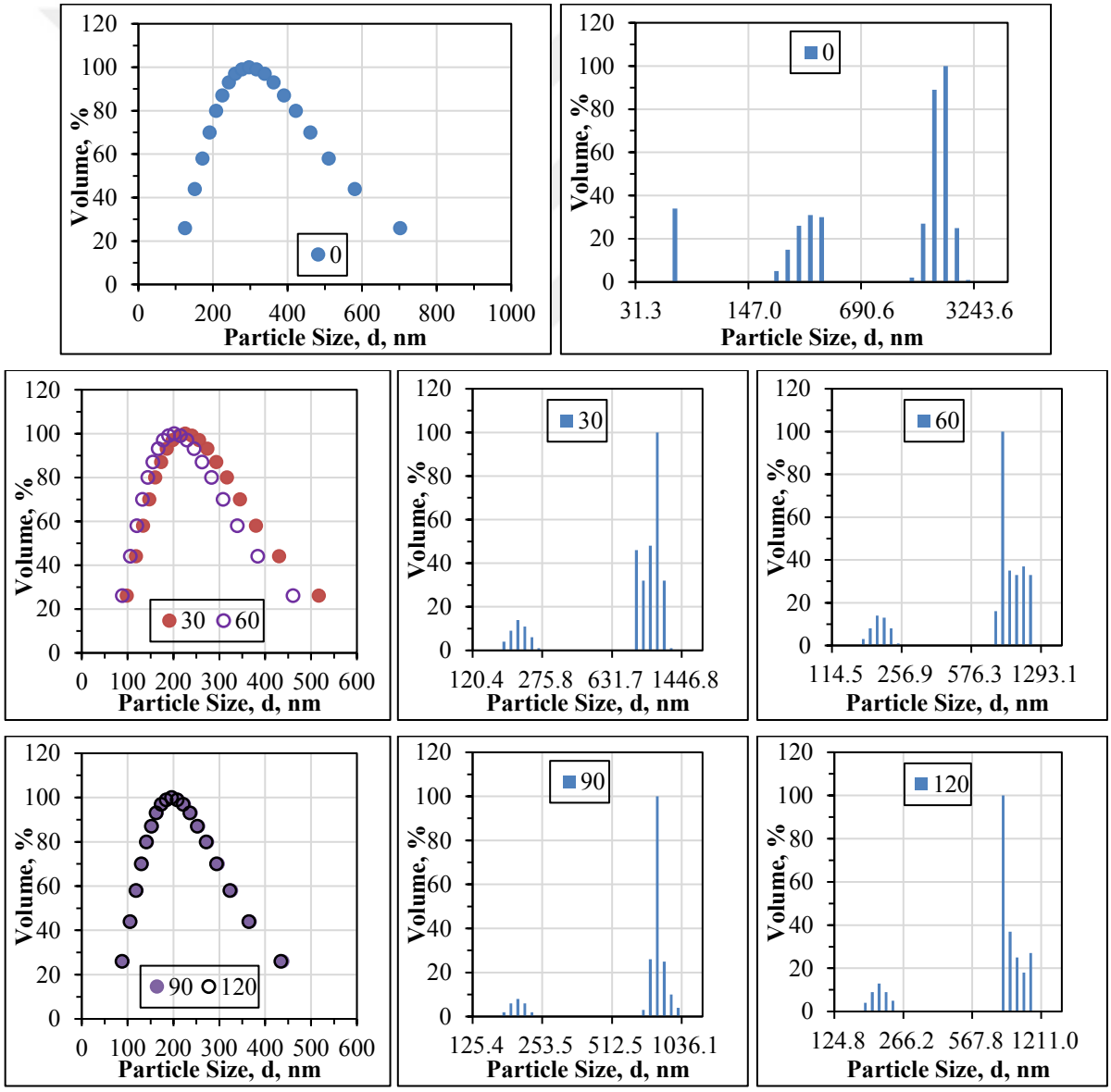


Figure 4.164. "Fe-TiO_2 and SRNOM" binary system "as-is" under dark conditions volume profile: Time dependent comparative presentation of log Normal distribution and multi-size distribution of "Fe-TiO_2 and SRNOM" binary system "as-is" under dark conditions.

4.1.5.23. "Fe-TiO_2 and SRNOM" binary system "as-is" under dark conditions surface area profile.

In a similar manner to data represented "Fe-TiO_2 and SRNOM" binary system "as-is" under dark conditions volume profile (Figure 4.163), time dependent logN distribution G(d) and multi size distribution C(d) of "Fe-TiO_2 and SRNOM" binary system "as-is" under dark conditions surface area profile was demonstrated in Figure 4.165. Accordingly, time dependent mean diameter, range and min-max diameter difference with respect to log normal and multi-size distribution of "Fe-TiO_2 and SRNOM" binary system "as-is" under dark conditions surface area profile was exhibited in Table 4.104.

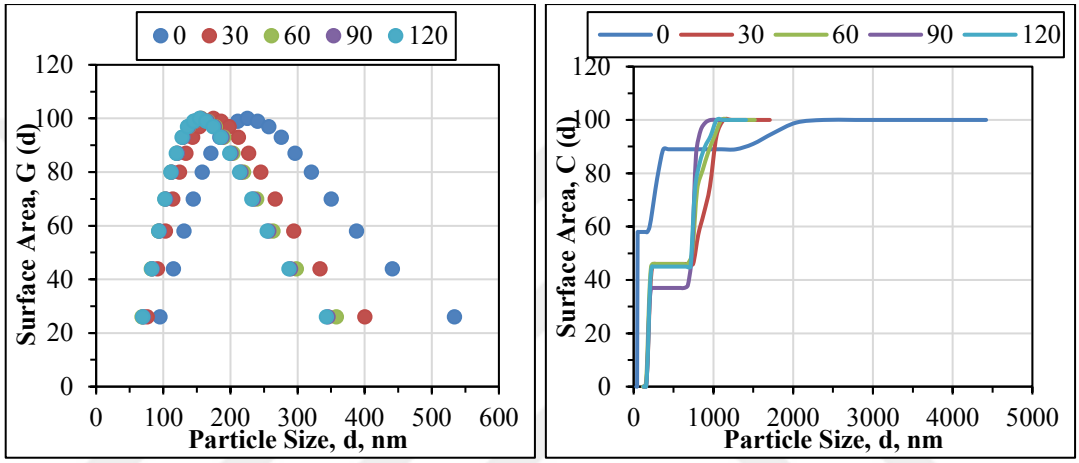


Figure 4.165. "Fe-TiO_2 and SRNOM" binary system "as-is" under dark conditions surface area profile: Time dependent logN distribution G(d) and multi size distribution C(d).

Table 4.104. "Fe-TiO_2 and SRNOM" binary system "as-is" under dark conditions surface area profile: Time dependent mean diameter, range and min-max diameter difference with respect to log normal and multi-size distribution.

Fe-TiO_2 and SRNOM	time, min				
	0	30	60	90	120
Log Normal distribution					
Mean, nm	225.4	174.6	156.7	155.8	154.2
Range	95.2-533.7	76.1-400.4	68.6-357.9	70.2-345.5	69.4-343.0
Difference	438.5	324.3	289.3	275.3	273.6
Multi-size distribution					
Max 1, nm	49.8	198.0	185.9	191.3	196.6
Max 2, nm	273.0	810.0	796.3	781.9	768.7
Max 3, nm	318.7	1038.6	1014.7	-	1040.8
Max 4, nm	1747.1	-	-	-	-
Max 5, nm	2039.4	-	-	-	-
Range	31.3-4419.6	120.4-1707.7	114.5-1519.9	125.4-1192.8	124.8-1409.1
Difference	4388.3	1587.3	1405.4	1067.4	1284.3

In terms of surface area profile, hydrodynamic particle size of "Fe-TiO_2 and SRNOM" binary system "as-is" under dark conditions was recorded as 225.4 nm. Upon 30 min, a sharp decrease was monitored and continuous decrease remained until 120 min. On the other hand, in the first 30 min, roughly 25 % decline was observed in size difference between max and min diameter. Initial size difference was attained as 438.5 nm and detected to 273.6 nm upon 120 min. For comparison purposes, in terms of multi-size distribution, initially five max diameters were obtained. Upon 30 min, three peaks were observed and remained until the end of 120 min period. Time dependent comparative presentation of log Normal distribution and multi-size distribution of "Fe-TiO_2 and SRNOM" binary system "as-is" under dark conditions surface area profile was exhibited in Figure 4.166.

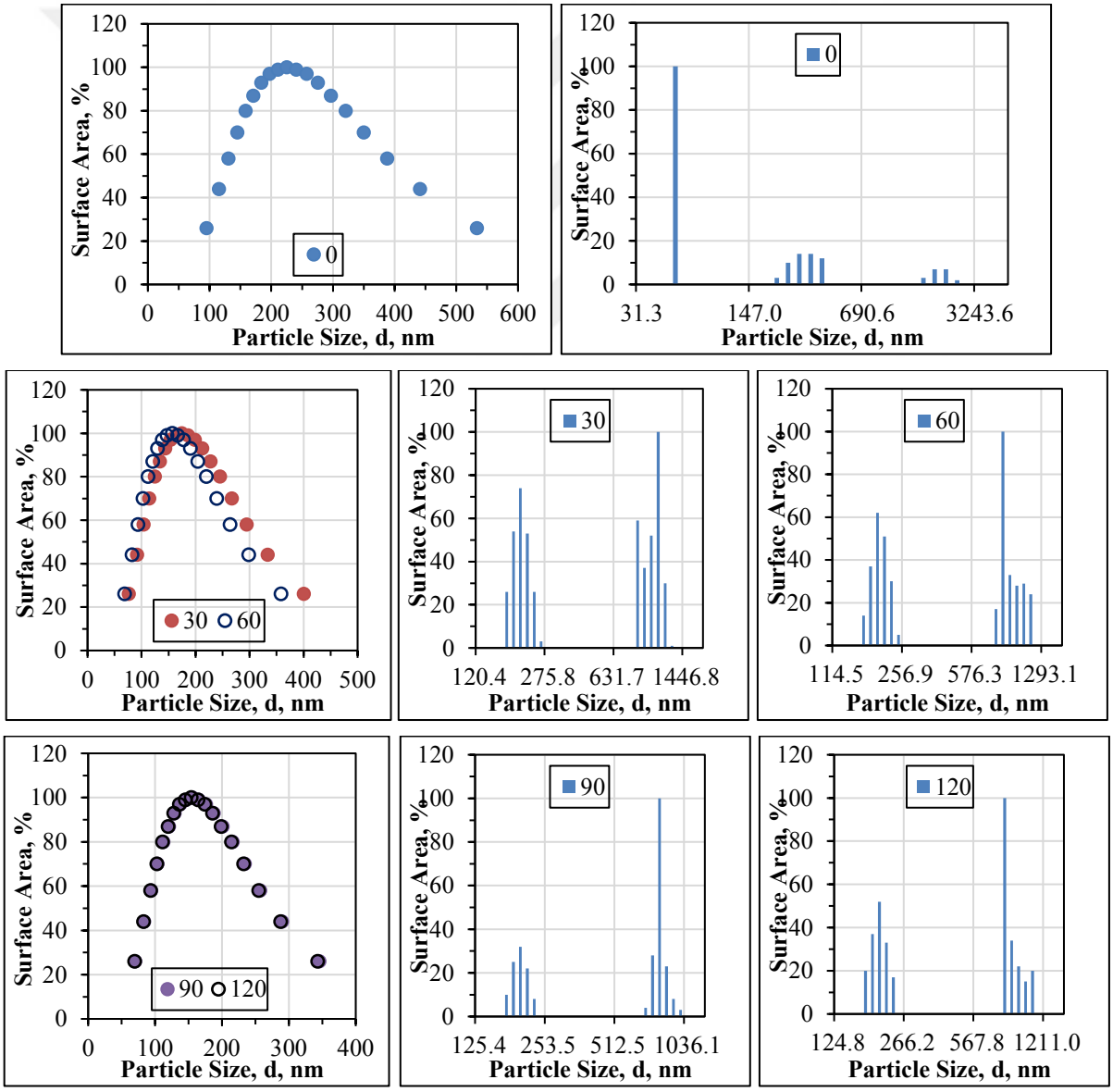


Figure 4.166. "Fe-TiO_2 and SRNOM" binary system "as-is" under dark conditions surface area profile: Time dependent comparative presentation of log Normal distribution and multi-size distribution of "Fe-TiO_2 and SRNOM" binary system "as-is" under dark conditions.

4.1.5.24. "Fe-TiO_2 and SRNOM" binary system "as-is" under dark conditions number profile. As elucidated for "Fe-TiO_2 and SRNOM" binary system "as-is" under dark conditions surface area profile (Figure 4.165), time dependent logN distribution G(d) and multi size distribution C(d) of "Fe-TiO_2 and SRNOM" binary system "as-is" under dark conditions number profile was given in Figure 4.167. Time dependent mean diameter, range and min-max diameter difference with respect to log normal and multi-size distribution of "Fe-TiO_2 and SRNOM" binary system "as-is" under dark conditions number profile was shown in Table 4.105.

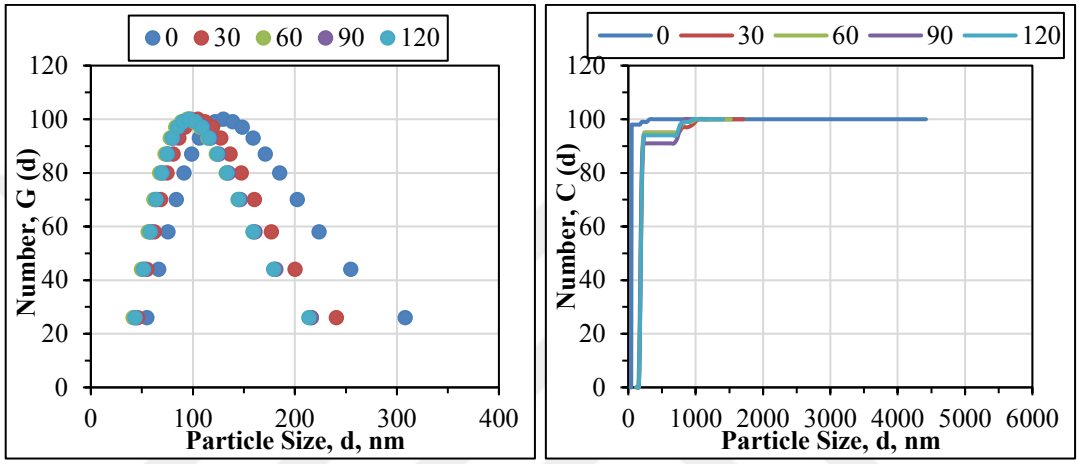


Figure 4.167. "Fe-TiO_2 and SRNOM" binary system "as-is" under dark conditions number profile: Time dependent logN distribution G(d) and multi size distribution C(d).

Table 4.105. "Fe-TiO_2 and SRNOM" binary system "as-is" under dark conditions number profile: Time dependent mean diameter, range and min-max diameter difference with respect to log normal and multi-size distribution.

Fe-TiO_2 and SRNOM	time, min				
	0	30	60	90	120
Log Normal distribution					
Mean, nm	130.1	104.9	94.6	97.4	96.2
Range	54.9-308.1	45.8-240.7	41.4-216.1	43.9-216.1	43.3-213.9
Difference	253.2	194.9	174.7	172.2	170.6
Multi-size distribution					
Max 1, nm	49.8	198.0	185.9	191.3	196.6
Max 2, nm	-	810.0	796.3	781.9	768.7
Max 3, nm	-	1038.6	-	-	-
Range	31.3-4419.6	120.4-1707.7	114.5-1519.9	125.4-1192.8	124.8-1409.1
Difference	4388.3	1587.3	1405.4	1067.4	1284.3

In terms of number profile, hydrodynamic particle size of "Fe-TiO_2 and SRNOM" binary system "as-is" under dark conditions revealed a rapid decrease following initial period of time. Initial

hydrodynamic size was recorded as 130.1 nm and decreased to 96.2 nm upon 120 min. According to log normal distribution, size difference was observed between 253.2 nm and 170.6 nm upon period of 120 min. However, in terms of multi-size distribution, initially one peak was observed and three peaks were attained upon 30 min. Also, upon 60 min, two peaks were monitored until the end of 120 min.

In a similar manner to data depicted "Fe-TiO_2 and SRNOM" binary system "as-is" under dark conditions surface area profile (Figure 4.166), time dependent comparative presentation of log Normal distribution and multi-size distribution of "Fe-TiO_2 and SRNOM" binary system "as-is" under dark conditions number profile was demonstrated in Figure 4.168.

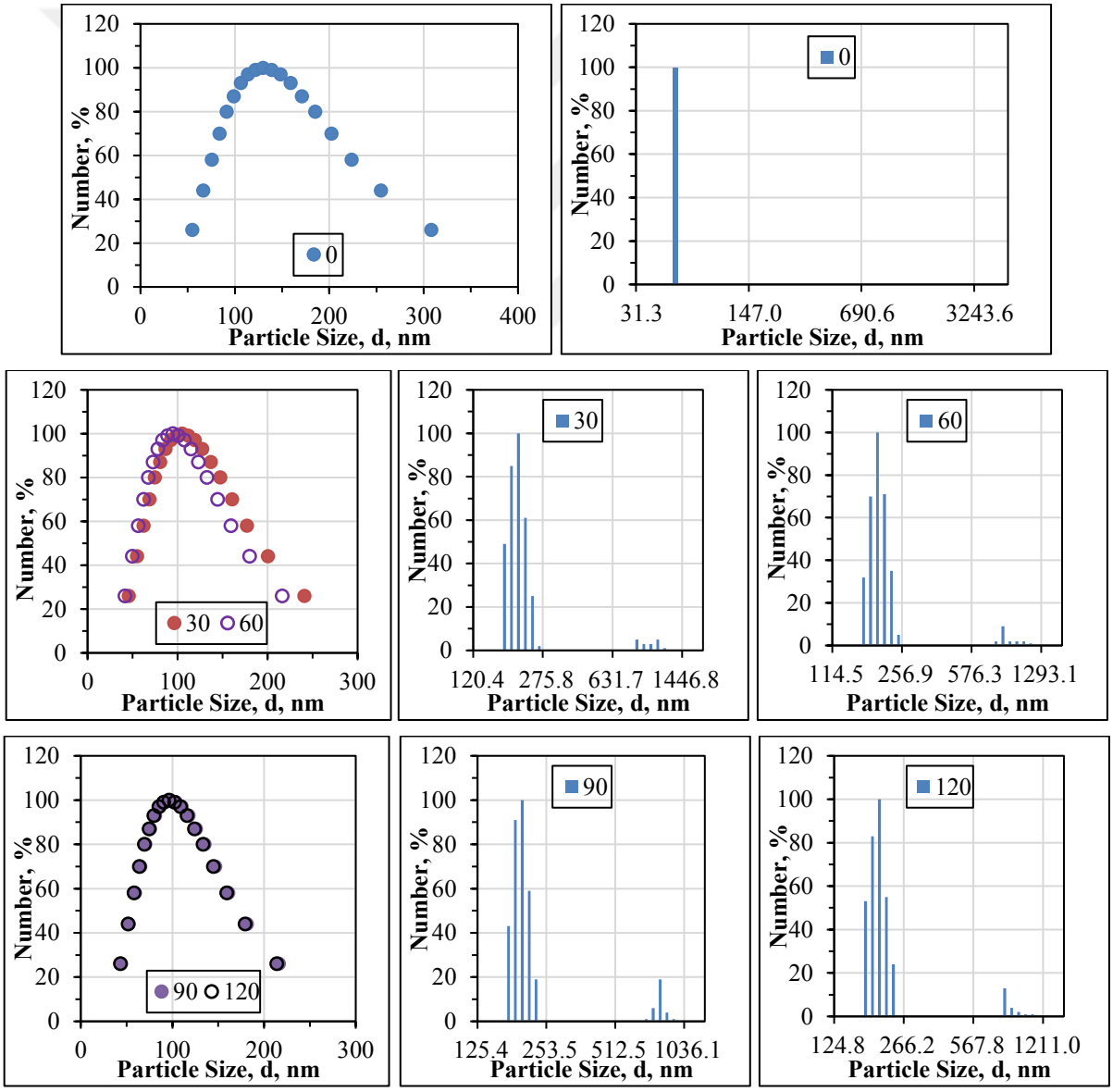


Figure 4.168. "Fe-TiO_2 and SRNOM" binary system "as-is" under dark conditions number profile: Time dependent comparative presentation of log Normal distribution and multi-size distribution of "Fe-TiO_2 and SRNOM" binary system "as-is" under dark conditions.

4.1.6. Binary System: Following Photolysis of Organic Matter

As elucidated for binary system under "as-is" conditions (Section 4.1.4), in a similar manner, the explication of the hydrodynamic particle size of the nanoparticles were also presented following photolysis of organic matter separately *i.e.* "TiO_2 and HA_{pho}" binary system following photolysis of organic matter, "TiO_2 and $SRNOM_{pho}$" binary system following photolysis of organic matter, "N-TiO_2 and HA_{pho}" binary system following photolysis of organic matter, "N-TiO_2 and $SRNOM_{pho}$" binary system following photolysis of organic matter, "Fe-TiO_2 and HA_{pho}" binary system following photolysis of organic matter, "Fe-TiO_2 and $SRNOM_{pho}$" binary system following photolysis of organic matter. Simply, data represented time dependent hydrodynamic size variations in terms of intensity, volume, surface area, and number parameters. Particle size distribution will be presented in two modes as mono-size and multi-size distribution.

4.1.6.1. "TiO_2 and HA_{pho}" binary system following photolysis of organic matter intensity profile. Time dependent logN distribution G(d) and multi size distribution C(d) of "TiO_2 and HA_{pho}" binary system following photolysis of organic matter intensity profile was demonstrated in Figure 4.169.

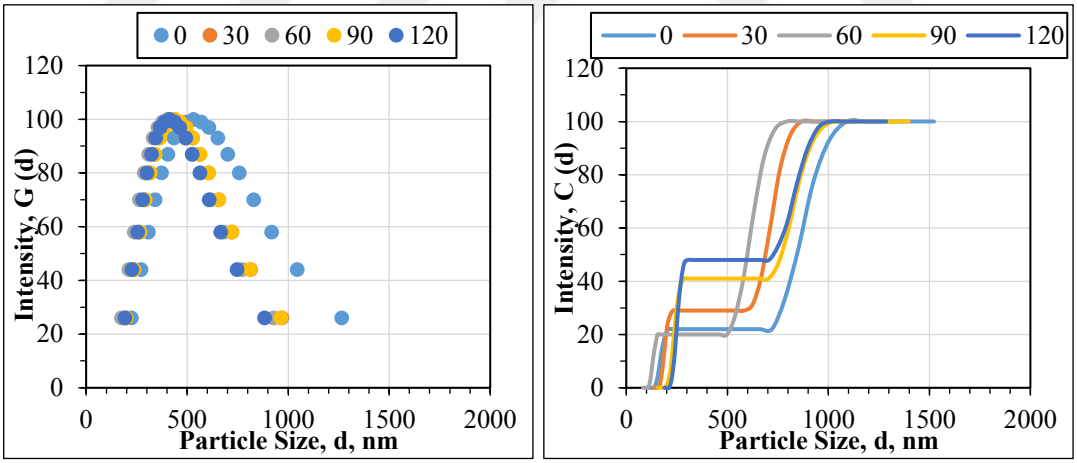


Figure 4.169. "TiO_2 and HA_{pho}" binary system following photolysis of organic matter intensity profile: Time dependent logN distribution G(d) and multi size distribution C(d).

In a similar manner to data represented "TiO_2 and HA" binary system under "as-is" conditions intensity profile (Figure 4.73), log normal distribution G(d) and multi size distribution C(d) of "TiO_2 and HA_{pho}" binary system following photolysis of organic matter intensity profile was displayed according to time variations. It could be seen that hydrodynamic particle size of "TiO_2 and HA_{pho}" binary system following photolysis of organic matter exhibited a continuously decreasing trend with respect to time. In terms of log normal distribution, it could be deduced that coinciding peaks could

be easily seen upon initial period of time. However, due to multi-size distribution, each max diameter could be easily discriminated. Also, size difference between max and min diameter could be seen both from log Normal distribution and multi-size distribution. In a similar manner to data described "TiO_2 and HA" binary system under "as-is" conditions (Figure 4.74), time dependent comparative presentation of log Normal distribution and multi-size distribution of "TiO_2 and HA_{pho}" binary system following photolysis of organic matter intensity profile was presented in Figure 4.170. Time dependent mean diameter, range and min-max diameter difference with respect to log normal and multi-size distribution of "TiO_2 and HA_{pho}" binary system following photolysis of organic matter intensity profile was demonstrated in Table 4.106.

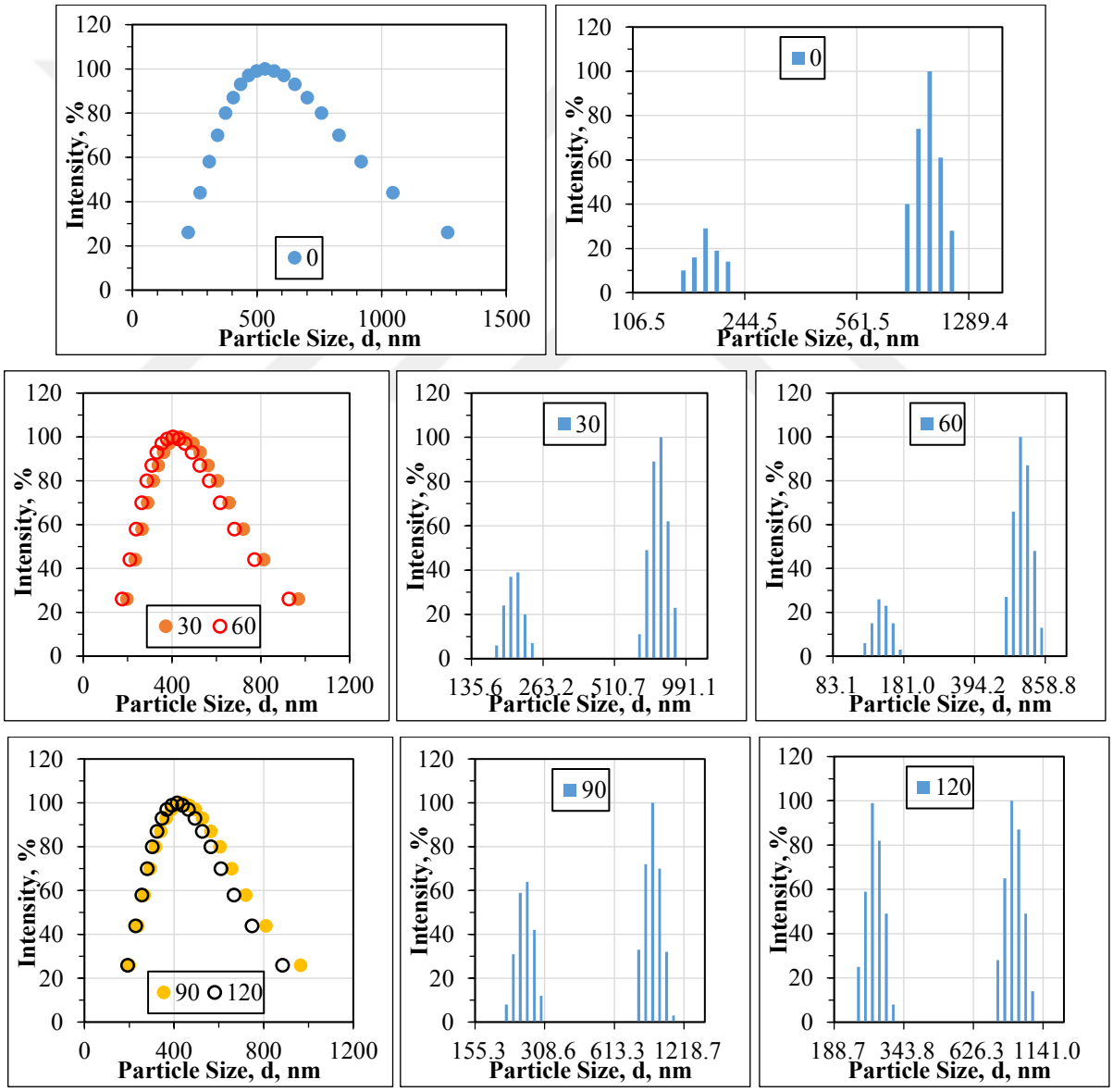


Figure 4.170. "TiO_2 and HA_{pho}" binary system following photolysis of organic matter intensity profile: Time dependent comparative presentation of log Normal distribution and multi-size distribution of "TiO_2 and HA_{pho}" binary system following photolysis of organic matter.

Table 4.106. "TiO_2 and HA_{pho}" binary system following photolysis of organic matter intensity profile: Time dependent mean diameter, range and min-max diameter difference with respect to log normal and multi-size distribution.

TiO_2 and HA	time, min				
	0	30	60	90	120
Log Normal distribution					
Mean, nm	532.4	437.2	403.5	438.4	412.7
Range	224.0-1265.1	197.2-969.4	175.5-927.6	199.4-964.0	192.7-883.9
Difference	1041.1	772.2	752.1	764.6	691.2
Multi-size distribution					
Max 1, nm	175.3	201.9	132.5	251.2	254.7
Max 2, nm	924.6	760.2	628.9	864.5	845.4
Range	106.5-1522.7	135.6-1131.6	83.1-1003.5	155.3-1398.1	188.7-1286.4
Difference	1416.2	996.0	920.4	1242.8	1097.7

In terms of intensity profile, initial hydrodynamic particle size of "TiO_2 and HA_{pho}" binary system following photolysis of organic matter was attained as 532.4 nm. Upon 30 min, a rapid decrease was observed and hydrodynamic particle size was recorded as 437.2 nm. Accordingly, a continuous decrease was monitored until the end of 120 min. Upon 120 min, hydrodynamic particle size was detected as 412.7 nm. According to log normal distribution, size difference was obtained between 1041.1 nm and 691.2 nm along 120 min. For comparison purposes, according to multi-size distribution, two max diameters were observed along 120 min. It could be deduced that "TiO_2 and HA_{pho}" binary system following photolysis of organic matter intensity profile revealed higher values in time dependent hydrodynamic particle size, and dramatic changes in time dependent min-max diameter differences in comparison to "TiO_2 and HA" binary system under "as-is" conditions intensity profile (Table 4.46).

Following a similar manner, polydispersity of "TiO_2 and HA_{pho}" binary system following photolysis of organic matter was displayed in Table 4.107. It could be concluded that a sharp decrease was observed following initial period of time and slight variations remained until the end of 120 min. Simply an average value of 0.274 could be accepted as suitable for expressing polydispersity.

Table 4.107. Polydispersity of "TiO_2 and HA_{pho}" binary system following photolysis of organic matter.

TiO_2 and HA	Polydispersity				
	0	30	60	90	120
	0.319	0.264	0.292	0.258	0.239

4.1.6.2. "TiO_2 and HA_{pho}" binary system following photolysis of organic matter volume profile. In a similar manner to data represented "TiO_2 and HA_{pho}" binary system following photolysis of organic matter intensity profile (Figure 4.169), time dependent logN distribution G(d) and multi size distribution C(d) of "TiO_2 and HA_{pho}" binary system following photolysis of organic matter volume profile was demonstrated in Figure 4.171. Time dependent mean diameter, range and min-max diameter difference with respect to log normal and multi-size distribution of "TiO_2 and HA_{pho}" binary system following photolysis of organic matter volume profile was exhibited in Table 4.108.

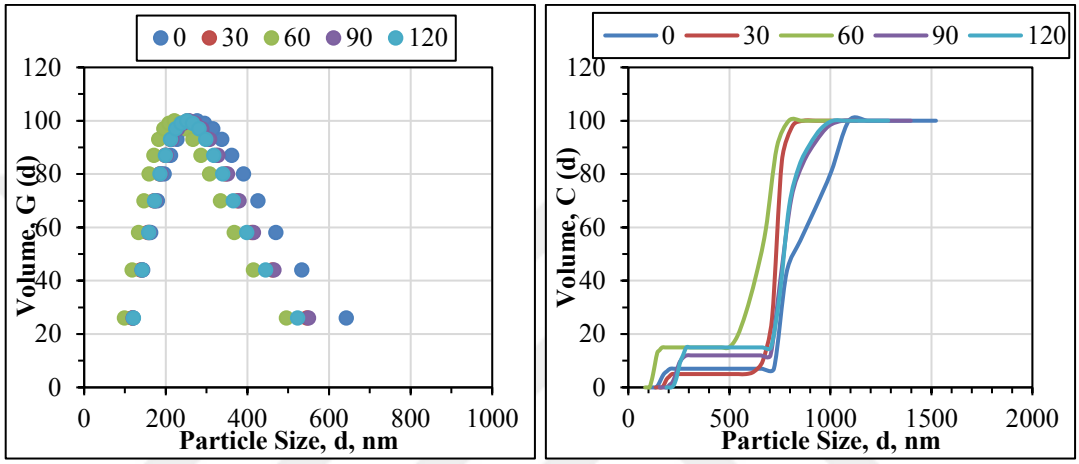


Figure 4.171. "TiO_2 and HA_{pho}" binary system following photolysis of organic matter volume profile: Time dependent logN distribution G(d) and multi size distribution C(d).

Table 4.108. "TiO_2 and HA_{pho}" binary system following photolysis of organic matter volume profile: Time dependent mean diameter, range and min-max diameter difference with respect to log normal and multi-size distribution.

TiO_2 and HA	time, min				
	0	30	60	90	120
Log Normal distribution					
Mean, nm	276.8	253.3	221.2	257.1	251.5
Range	119.3-642.1	117.4-546.3	98.7-495.5	120.3-549.8	121.0-523.1
Difference	522.8	428.9	396.8	429.5	402.1
Multi-size distribution					
Max 1, nm	175.3	188.9	132.5	234.5	254.7
Max 2, nm	783.0	760.2	734.9	251.2	796.1
Max 3, nm	1091.9	-	-	807.2	-
Range	106.5-1522.7	135.6-1131.6	83.1-1003.5	155.3-1398.1	188.7-1286.4
Difference	1416.2	996.0	920.4	1242.8	1097.7

As explained for "TiO_2 and HA_{pho}" binary system following photolysis of organic matter intensity profile (Table 4.106), a similar approach was followed for "TiO_2 and HA_{pho}" binary system

following photolysis of organic matter volume profile. It could be inferred that hydrodynamic particle size approximately 10 % decreased upon 30 min. Initial hydrodynamic particle size was recorded as 276.8 nm and decreased to 251.5 nm upon 30 min. Correspondingly, slight increase was monitored with minor variations until the end of 120 min. However, in terms of multi-size distribution, initially three peaks were observed, two peaks were monitored upon 30 and 60 min, and two peaks were attained upon 120 min. As described for "TiO_2 and HA_{pho}" binary system following photolysis of organic matter intensity profile (Figure 4.170), time dependent comparative presentation of log Normal distribution and multi-size distribution of "TiO_2 and HA_{pho}" binary system following photolysis of organic matter volume profile was exhibited in Figure 4.172.

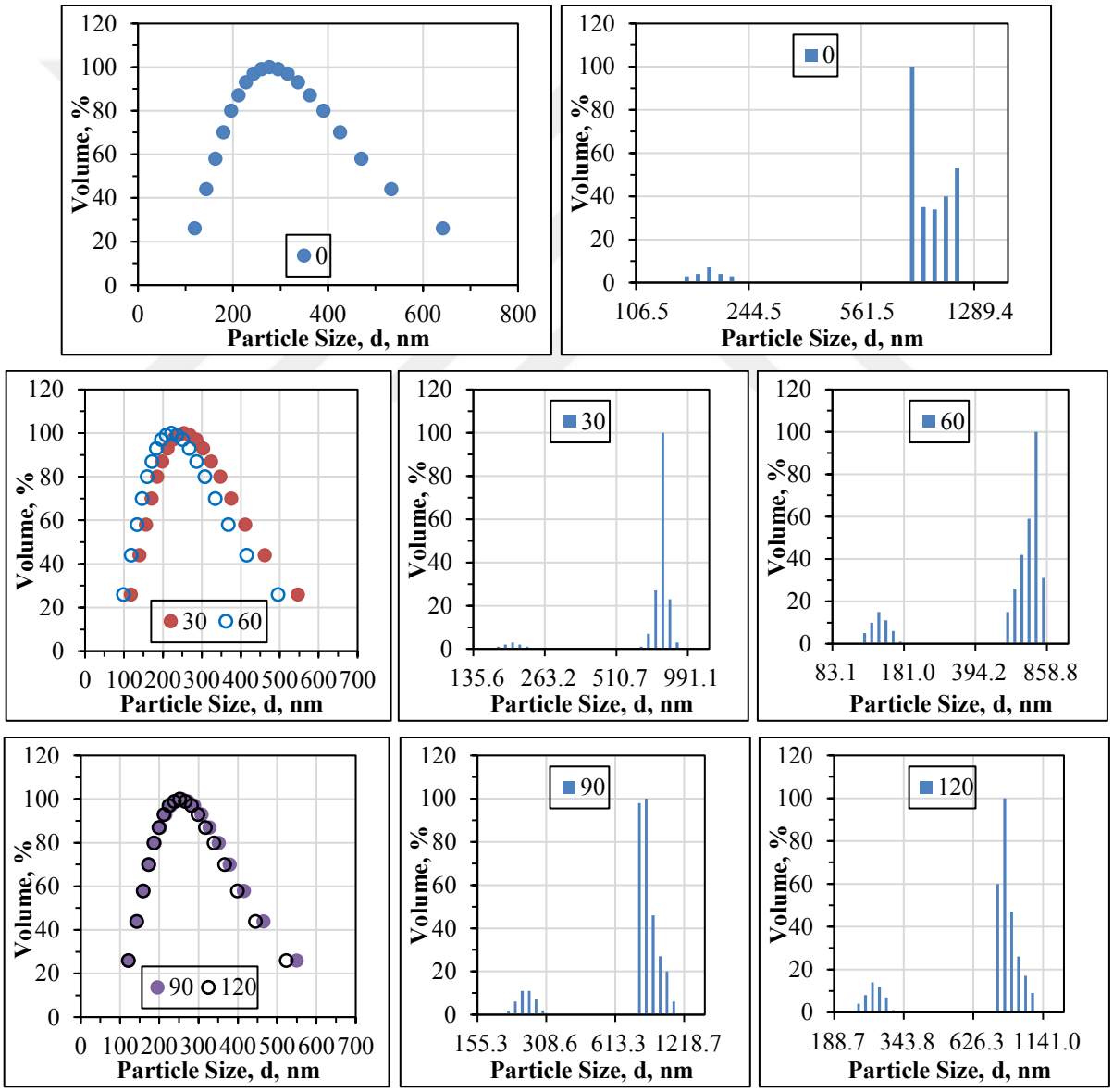


Figure 4.172. "TiO_2 and HA_{pho}" binary system following photolysis of organic matter volume profile: Time dependent comparative presentation of log Normal distribution and multi-size distribution of "TiO_2 and HA_{pho}" binary system following photolysis of organic matter.

4.1.6.3. "TiO_2 and HA_{pho}" binary system following photolysis of organic matter surface area profile.

Time dependent logN distribution G(d) and multi size distribution C(d) of "TiO_2 and HA_{pho}" binary system following photolysis of organic matter surface area profile was demonstrated in Figure 4.173. Time dependent mean diameter, range and min-max diameter difference with respect to log normal and multi-size distribution of "TiO_2 and HA_{pho}" binary system following photolysis of organic matter volume profile was displayed in Table 4.109.

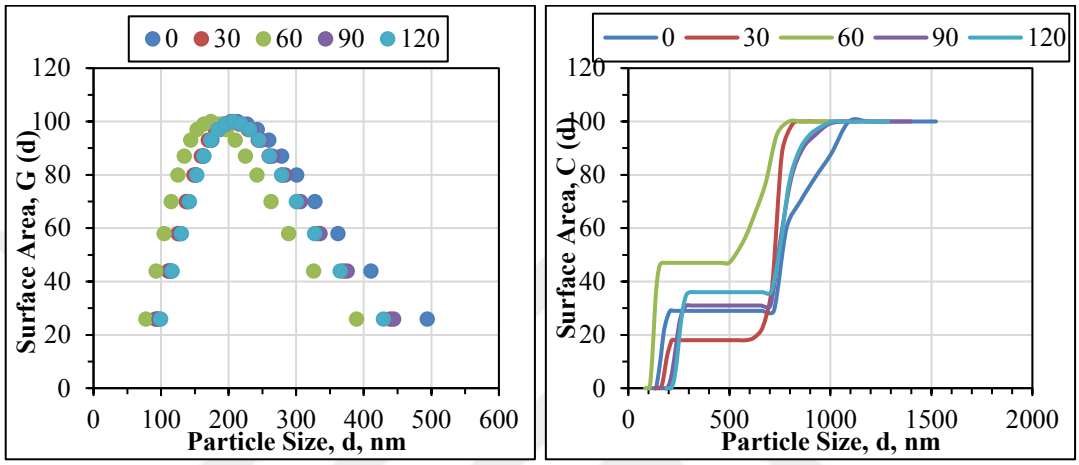


Figure 4.173. "TiO_2 and HA_{pho}" binary system following photolysis of organic matter surface area profile: Time dependent logN distribution G(d) and multi size distribution C(d).

Table 4.109. "TiO_2 and HA_{pho}" binary system following photolysis of organic matter surface area profile: Time dependent mean diameter, range and min-max diameter difference with respect to log normal and multi-size distribution.

TiO_2 and HA	time, min				
	0	30	60	90	120
Log Normal distribution					
Mean, nm	213.1	203.6	173.9	207.7	206.3
Range	91.9-494.3	94.4-439.1	77.6-389.6	97.2-444.1	99.2-429.1
Difference	402.4	344.7	312.0	346.9	329.9
Multi-size distribution					
Max 1, nm	175.3	188.9	132.5	234.5	254.7
Max 2, nm	783.0	760.2	734.9	251.2	796.1
Max 3, nm	1091.9	-	-	753.6	-
Range	106.5-1522.7	135.6-1131.6	83.1-1003.5	155.3-1398.1	188.7-1286.4
Difference	1416.2	996.0	920.4	1242.8	1097.7

According to log normal distribution, initial hydrodynamic particle size of "TiO_2 and HA_{pho}" binary system following photolysis of organic matter was obtained as 213.1 nm. During 120 min, hydrodynamic particle size of "TiO_2 and HA_{pho}" binary system following photolysis of organic matter

followed a slightly decreasing trend and detected to 206.3 nm. In terms of log normal distribution, size difference decreased from 402.4 nm to 329.9 nm upon period of 120 min. However, in terms of multi-size distribution, three max diameters were attained as 175.3 nm, 783.0 nm, and 1091.9 nm for "TiO_2 and HA_{pho}" binary system following photolysis of organic matter following initial period of time. Upon 30 min and 60 min, two peaks were observed and remained until the end of 120 min. In terms of multi-size distribution, size difference decreased from 1416.2 nm to 1097.7 nm upon 120 min. Time dependent comparative presentation of log Normal distribution and multi-size distribution of "TiO_2 and HA_{pho}" binary system following photolysis of organic matter surface area profile was displayed in Figure 4.174.

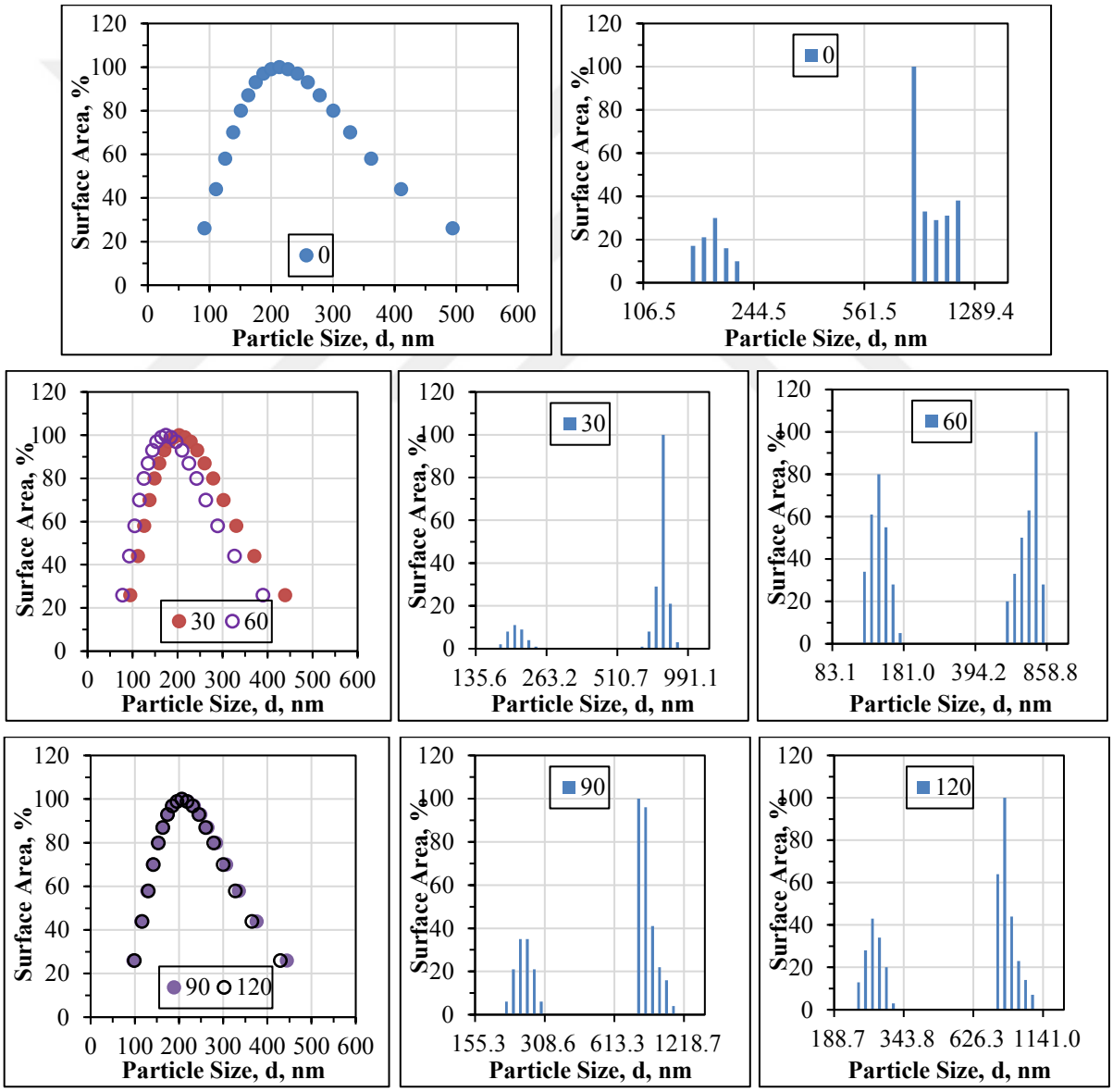


Figure 4.174. "TiO_2 and HA_{pho}" binary system following photolysis of organic matter surface area profile: Time dependent comparative presentation of log Normal distribution and multi-size distribution of "TiO_2 and HA_{pho}" binary system following photolysis of organic matter.

4.1.6.4. "TiO_2 and HA_{pho}" binary system following photolysis of organic matter number profile. In a similar manner to data described "TiO_2 and HA_{pho}" binary system following photolysis of organic matter surface area profile (Figure 4.173), time dependent logN distribution G(d) and multi size distribution C(d) of "TiO_2 and HA_{pho}" binary system following photolysis of organic matter number profile was displayed in Figure 4.175. Time dependent mean diameter, range and min-max diameter difference with respect to log normal and multi-size distribution of "TiO_2 and HA_{pho}" binary system following photolysis of organic matter number profile was exhibited in Table 4.110.

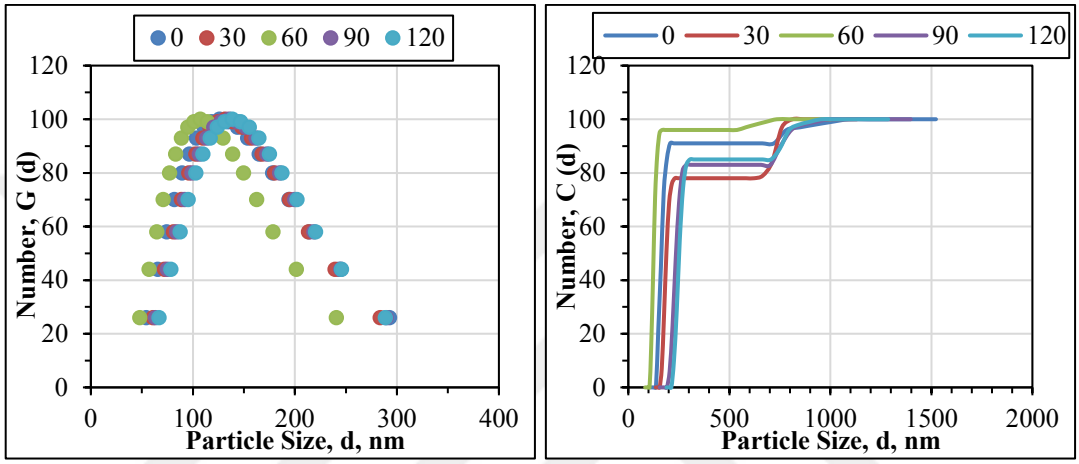


Figure 4.175. "TiO_2 and HA_{pho}" binary system following photolysis of organic matter number profile: Time dependent logN distribution G(d) and multi size distribution C(d).

Table 4.110. "TiO_2 and HA_{pho}" binary system following photolysis of organic matter number profile: Time dependent mean diameter, range and min-max diameter difference with respect to log normal and multi-size distribution.

TiO_2 and HA	time, min				
	0	30	60	90	120
Log Normal distribution					
Mean, nm	126.3	131.5	107.5	135.6	138.8
Range	54.4-292.9	61.0-283.7	48.0-240.8	63.4-289.8	66.8-288.7
Difference	238.5	222.7	192.8	226.4	221.9
Multi-size distribution					
Max 1, nm	175.3	188.9	132.5	234.5	254.7
Max 2, nm	783.0	760.2	734.9	753.6	796.1
Range	106.5-1522.7	135.6-1131.6	83.1-1003.5	155.3-1398.1	188.7-1286.4
Difference	1416.2	996.0	920.4	1242.8	1097.7

According to log normal distribution and in terms of number profile, it could be asserted that hydrodynamic particle size of "TiO_2 and HA_{pho}" binary system following photolysis of organic matter demonstrated minor variations with respect to time. Initial hydrodynamic particle size was attained

as 126.3 nm and reached to 138.8 nm upon period of 120 min. Also, in terms of log normal distribution, size difference decreased from 238.5 nm to 221.9 nm upon 120 min. For comparison purposes, in terms of multi-size distribution, two max diameters were monitored until the end of 120 min period.

As explained for "TiO_2 and HA_{pho}" binary system following photolysis of organic matter surface area profile (Figure 4.174), a similar approach followed for "TiO_2 and HA_{pho}" binary system following photolysis of organic matter number profile. Time dependent comparative presentation of log Normal distribution and multi-size distribution of "TiO_2 and HA_{pho}" binary system following photolysis of organic matter number profile was displayed in Figure 4.176.

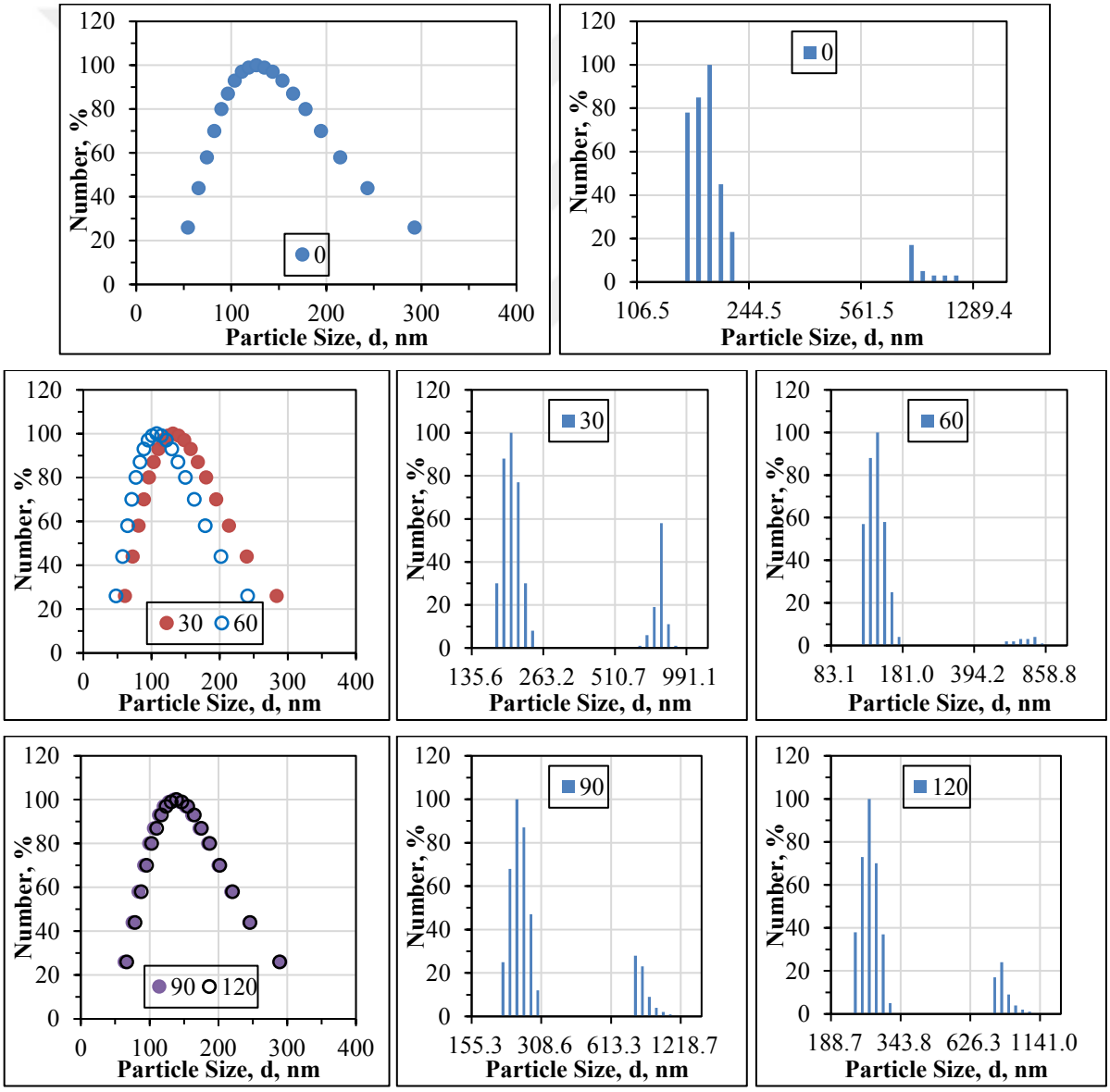


Figure 4.176. "TiO_2 and HA_{pho}" binary system following photolysis of organic matter number profile: Time dependent comparative presentation of log Normal distribution and multi-size distribution of "TiO_2 and HA_{pho}" binary system following photolysis of organic matter.

4.1.6.5. "TiO_2 and $SRNOM_{pho}$" binary system following photolysis of organic matter intensity profile. Time dependent logN distribution G(d) and multi size distribution C(d) of "TiO_2 and $SRNOM_{pho}$" binary system following photolysis of organic matter intensity profile was given in Figure 4.177. Time dependent mean diameter, range and min-max diameter difference with respect to log normal and multi-size distribution of "TiO_2 and $SRNOM_{pho}$" binary system following photolysis of organic matter intensity profile was presented in Table 4.111.

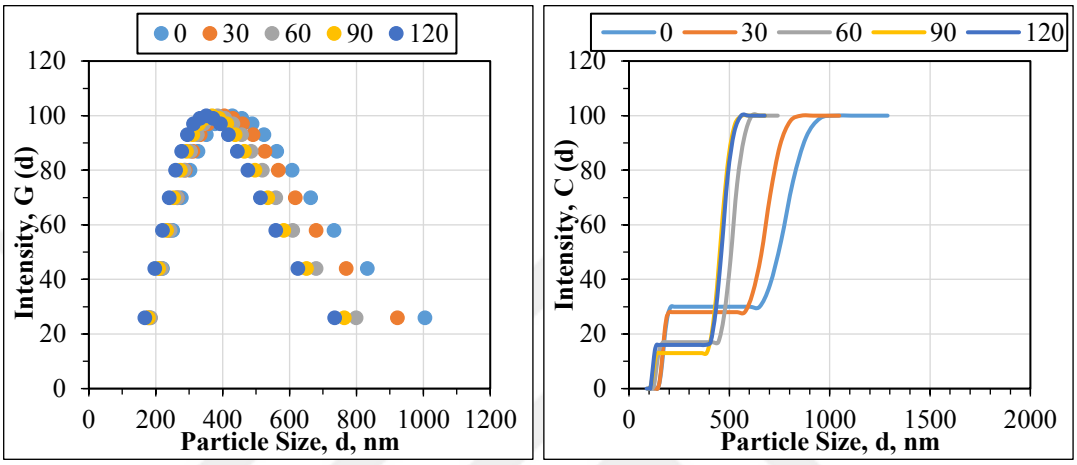


Figure 4.177. "TiO_2 and $SRNOM_{pho}$" binary system following photolysis of organic matter intensity profile: Time dependent logN distribution G(d) and multi size distribution C(d).

Table 4.111. "TiO_2 and $SRNOM_{pho}$" binary system following photolysis of organic matter intensity profile: Time dependent mean diameter, range and min-max diameter difference with respect to log normal and multi-size distribution.

TiO_2 and SRNOM	time, min				
	0	30	60	90	120
Mean, nm	428.7	404.7	384.6	368.9	351.2
Log Normal distribution					
Range	182.8-1005.0	177.5-922.6	185.2-798.8	178.1-763.9	167.7-735.6
Difference	822.2	745.1	613.6	585.8	567.9
Multi-size distribution					
Max 1, nm	179.3	174.9	141.0	125.9	128.8
Max 2, nm	817.4	703.7	150.3	466.6	492.0
Max 3, nm	-	-	538.7	-	-
Range	113.7-1288.5	125.5-1047.6	96.2-741.3	92.2-678.3	87.8-676.9
Difference	1174.8	922.1	645.1	586.1	589.1

Hydrodynamic size of "TiO_2 and $SRNOM_{pho}$" binary system following photolysis of organic matter revealed a continuous decrease along 120 min. In terms of multi-size distribution, two peaks were attained excluding 60 min. Three peaks were obtained upon 60 min. Time dependent

comparative presentation of log Normal distribution and multi-size distribution of "TiO_2 and $SRNOM_{pho}$" binary system following photolysis of organic matter intensity profile was given in Figure 4.178. Polydispersity of "TiO_2 and $SRNOM_{pho}$" binary system following photolysis of organic matter was shown in Table 4.112, an average value of 0.250 could be excepted as suitable.

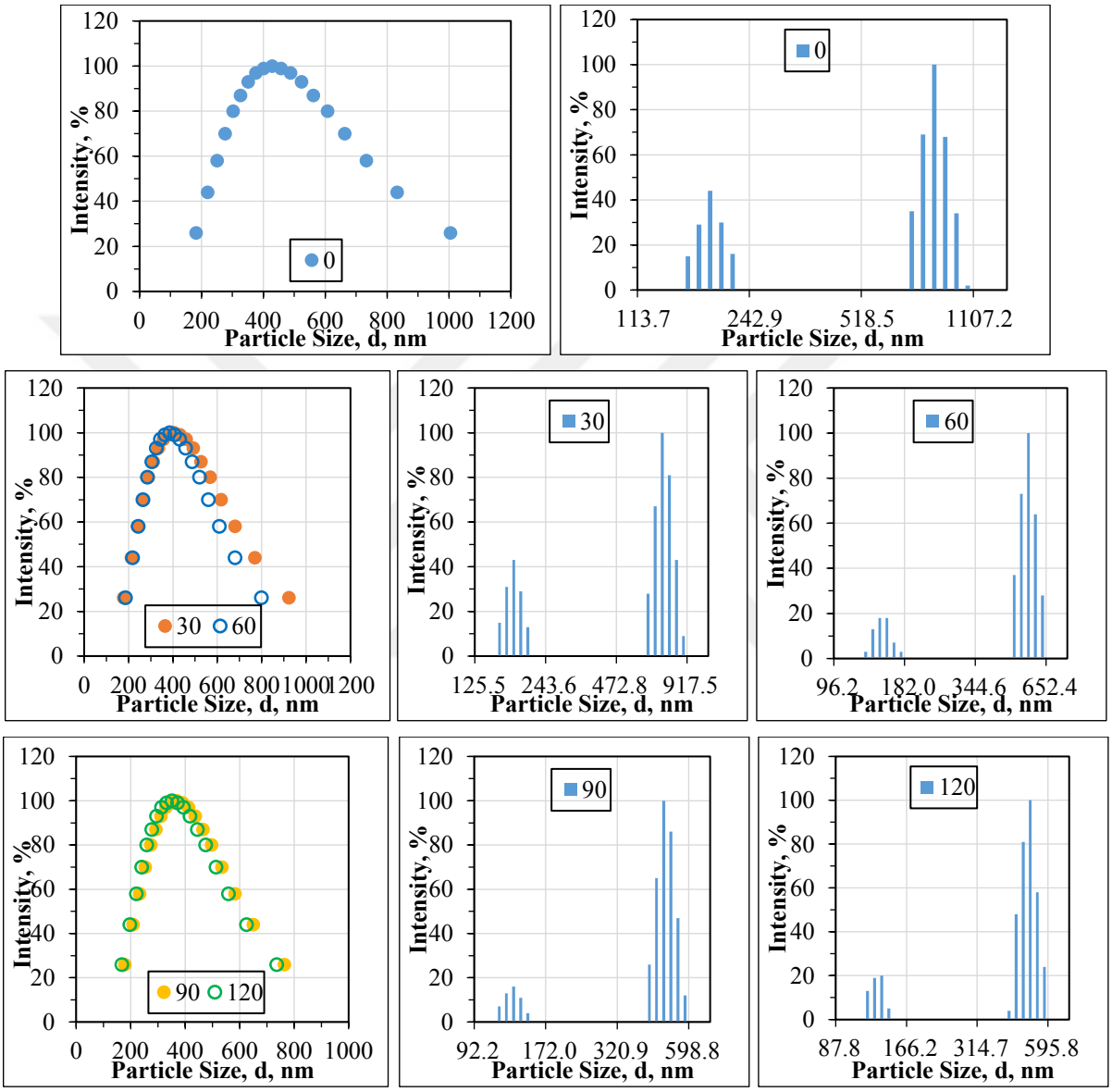


Figure 4.178. "TiO_2 and $SRNOM_{pho}$" binary system following photolysis of organic matter intensity profile: Time dependent comparative presentation of log Normal distribution and multi-size distribution of "TiO_2 and $SRNOM_{pho}$" binary system following photolysis of organic matter.

Table 4.112. Polydispersity of "TiO_2 and $SRNOM_{pho}$" binary system following photolysis of organic matter.

TiO_2 and SRNOM	Polydispersity				
	0	30	60	90	120
	0.308	0.285	0.218	0.216	0.224

4.1.6.6. "TiO_2 and $SRNOM_{pho}$" binary system following photolysis of organic matter volume profile.

As explained for "TiO_2 and $SRNOM_{pho}$" binary system following photolysis of organic matter intensity profile (Figure 4.177), a similar approach was followed for "TiO_2 and $SRNOM_{pho}$" binary system following photolysis of organic matter volume profile. Time dependent logN distribution G(d) and multi size distribution C(d) of "TiO_2 and $SRNOM_{pho}$" binary system following photolysis of organic matter volume profile was exhibited in Figure 4.179. Time dependent mean diameter, range and min-max diameter difference with respect to log normal and multi-size distribution of "TiO_2 and $SRNOM_{pho}$" binary system following photolysis of organic matter volume profile was displayed in Table 4.113.

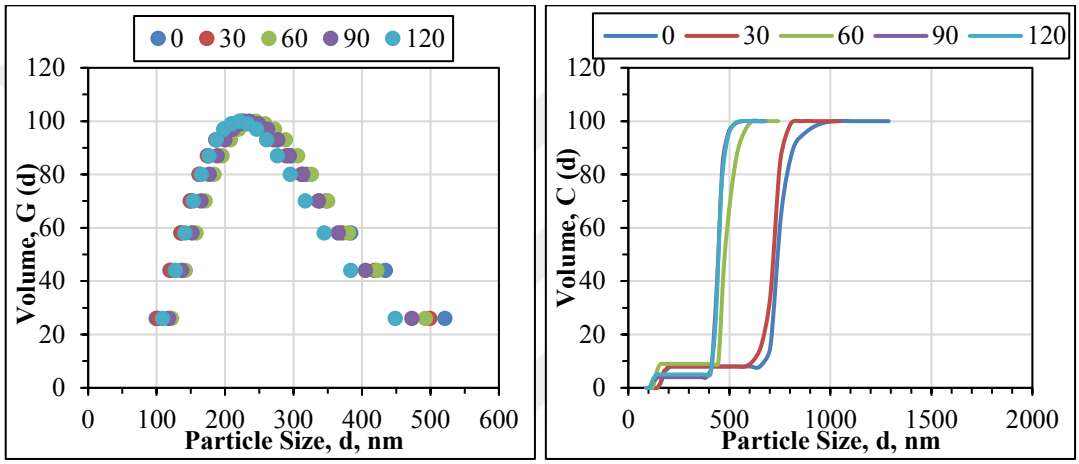


Figure 4.179. "TiO_2 and $SRNOM_{pho}$" binary system following photolysis of organic matter volume profile: Time dependent logN distribution G(d) and multi size distribution C(d).

Table 4.113. "TiO_2 and $SRNOM_{pho}$" binary system following photolysis of organic matter volume profile: Time dependent mean diameter, range and min-max diameter difference with respect to log normal and multi-size distribution.

TiO_2 and SRNOM	time, min				
	0	30	60	90	120
Log Normal distribution					
Mean, nm	227.8	224.7	244.8	235.6	220.9
Range	99.6-521.0	101.2-499.1	121.6-492.6	117.4-472.8	108.8-448.6
Difference	421.4	397.9	371.0	355.4	339.8
Multi-size distribution					
Max 1, nm	179.3	174.9	141.0	118.3	113.3
Max 2, nm	757.7	752.0	474.2	125.9	120.8
Max 3, nm	-	-	-	466.6	128.8
Max 4, nm	-	-	-	-	461.5
Range	113.7-1288.5	125.5-1047.6	96.2-741.3	92.2-678.3	87.8-676.9
Difference	1174.8	922.1	645.1	586.1	589.1

According to log normal distribution and in terms of volume profile, hydrodynamic particle size of "TiO_2 and $SRNOM_{pho}$" binary system following photolysis of organic matter revealed a slight decrease, initial hydrodynamic particle size was attained as 227.8 nm and decreased to 220.9 nm upon 120 min. Also, according to log normal distribution, size difference between max and min diameter was obtained between 421.4 nm and 339.8 nm upon 120 min. In terms of multi-size distribution, two peaks were observed following initial period of time and remained until 90 min. Upon period of 90 min, three peaks were monitored and four peaks were obtained at the end of 120 min. Time dependent comparative presentation of log Normal distribution and multi-size distribution of "TiO_2 and $SRNOM_{pho}$" binary system following photolysis of organic matter volume profile was demonstrated in Figure 4.180.

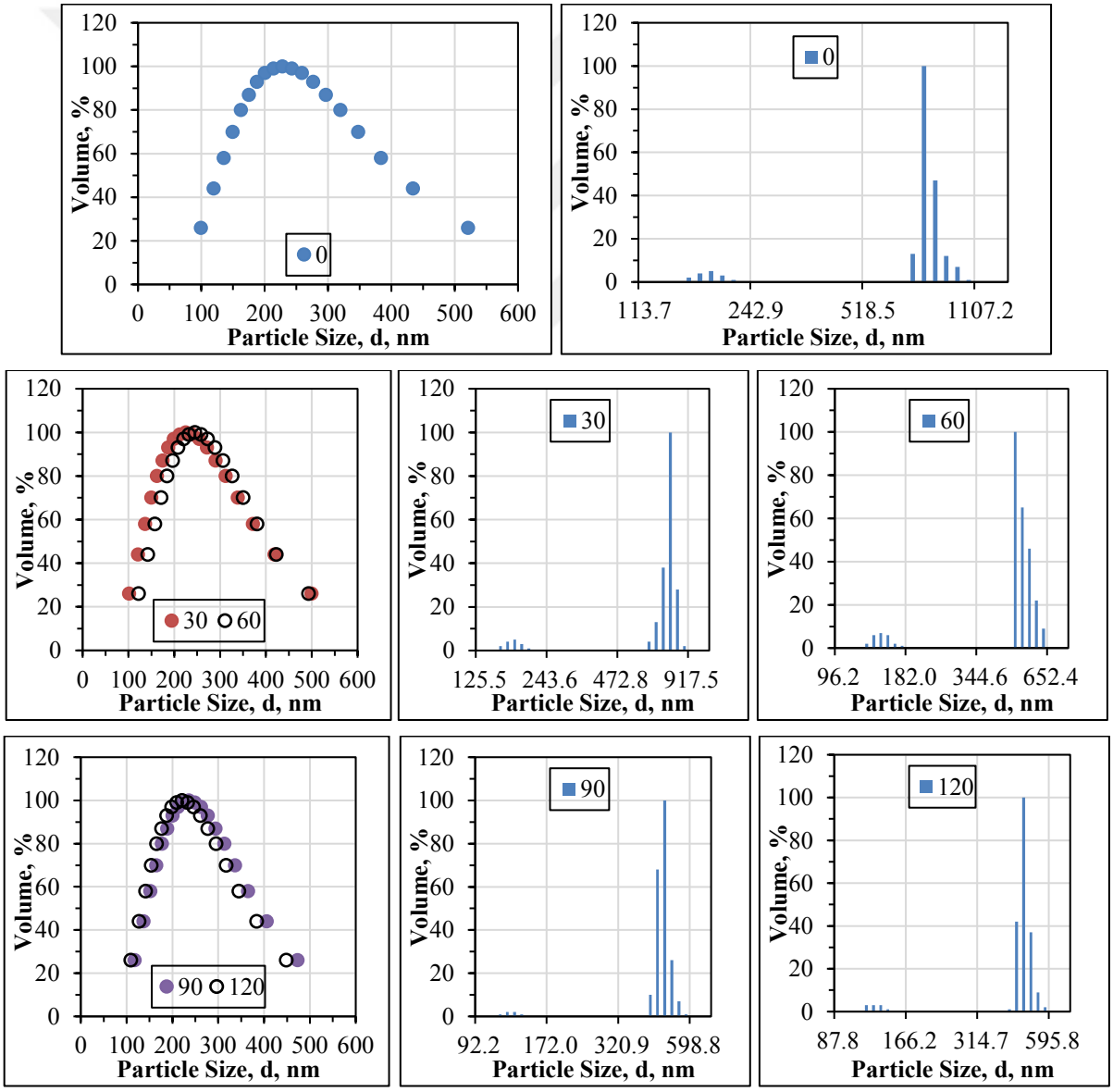


Figure 4.180. "TiO_2 and $SRNOM_{pho}$" binary system following photolysis of organic matter volume profile: Time dependent comparative presentation of log Normal distribution and multi-size distribution of "TiO_2 and $SRNOM_{pho}$" binary system following photolysis of organic matter.

4.1.6.7. "TiO_2 and $SRNOM_{pho}$" binary system following photolysis of organic matter surface area profile. Time dependent logN distribution G(d) and multi size distribution C(d) of "TiO_2 and $SRNOM_{pho}$" binary system following photolysis of organic matter surface area profile was demonstrated in Figure 4.181. Time dependent mean diameter, range and min-max diameter difference with respect to log normal and multi-size distribution of "TiO_2 and $SRNOM_{pho}$" binary system following photolysis of organic matter surface area profile was presented in Table 4.114.

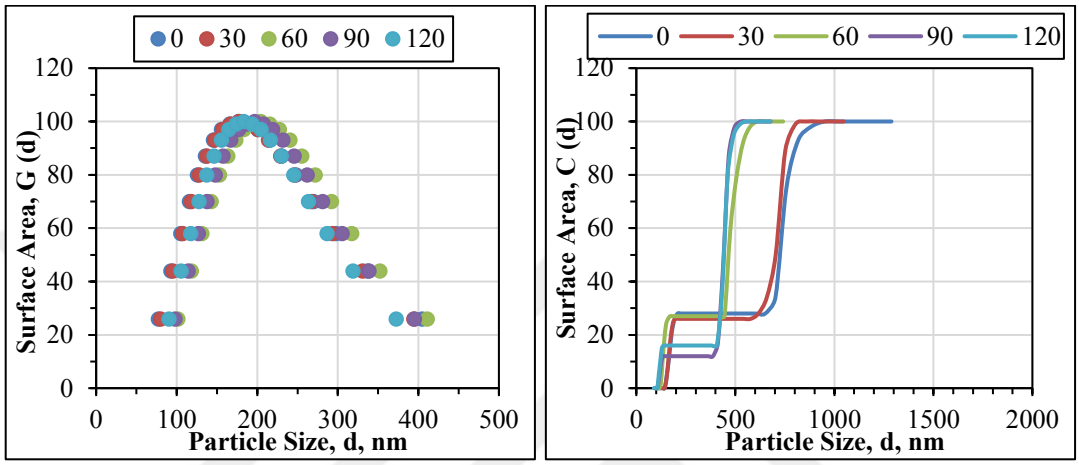


Figure 4.181. "TiO_2 and $SRNOM_{pho}$" binary system following photolysis of organic matter surface area profile: Time dependent logN distribution G(d) and multi size distribution C(d).

Table 4.114. "TiO_2 and $SRNOM_{pho}$" binary system following photolysis of organic matter surface area profile: Time dependent mean diameter, range and min-max diameter difference with respect to log normal and multi-size distribution.

TiO_2 and SRNOM	time, min				
	0	30	60	90	120
Log Normal distribution					
Mean, nm	176.9	177.6	204.3	196.9	183.5
Range	77.4-404.6	80.0-394.5	101.5-411.1	98.1-395.2	90.4-372.7
Difference	327.2	314.5	309.6	297.1	282.3
Multi-size distribution					
Max 1, nm	179.3	174.9	141.0	118.3	120.8
Max 2, nm	757.7	752.0	474.2	125.9	461.5
Max 3, nm	-	-	-	466.6	-
Range	113.7-1288.5	125.5-1047.6	96.2-741.3	92.2-678.3	87.8-676.9
Difference	1174.8	922.1	645.1	586.1	589.1

In terms of surface area profile, it could be deduced that hydrodynamic particle size of "TiO_2 and $SRNOM_{pho}$" binary system following photolysis of organic matter displayed a fluctuating trend with respect to time. Initial hydrodynamic particle size was recorded as 176.9 nm and detected to 183.5

nm at the end of 120 min period. Also, in terms of log normal distribution, size difference was recorded between 327.2 nm and 282.3 nm along 120 min. According to multi-size distribution, two max diameters were observed following initial period of time and remained until 90 min. Upon period of 90 min, three peaks were monitored and two max diameters were observed upon 120 min. On the other hand, in terms of multi-size distribution, size difference was decreased from 1174.8 nm to 589.1 nm upon period of 120 min. In a similar manner to data represented "TiO_2 and $SRNOM_{pho}$" binary system following photolysis of organic matter volume profile (Figure 4.180), time dependent comparative presentation of log Normal distribution and multi-size distribution of "TiO_2 and $SRNOM_{pho}$" binary system following photolysis of organic matter surface area profile was demonstrated in Figure 4.182.

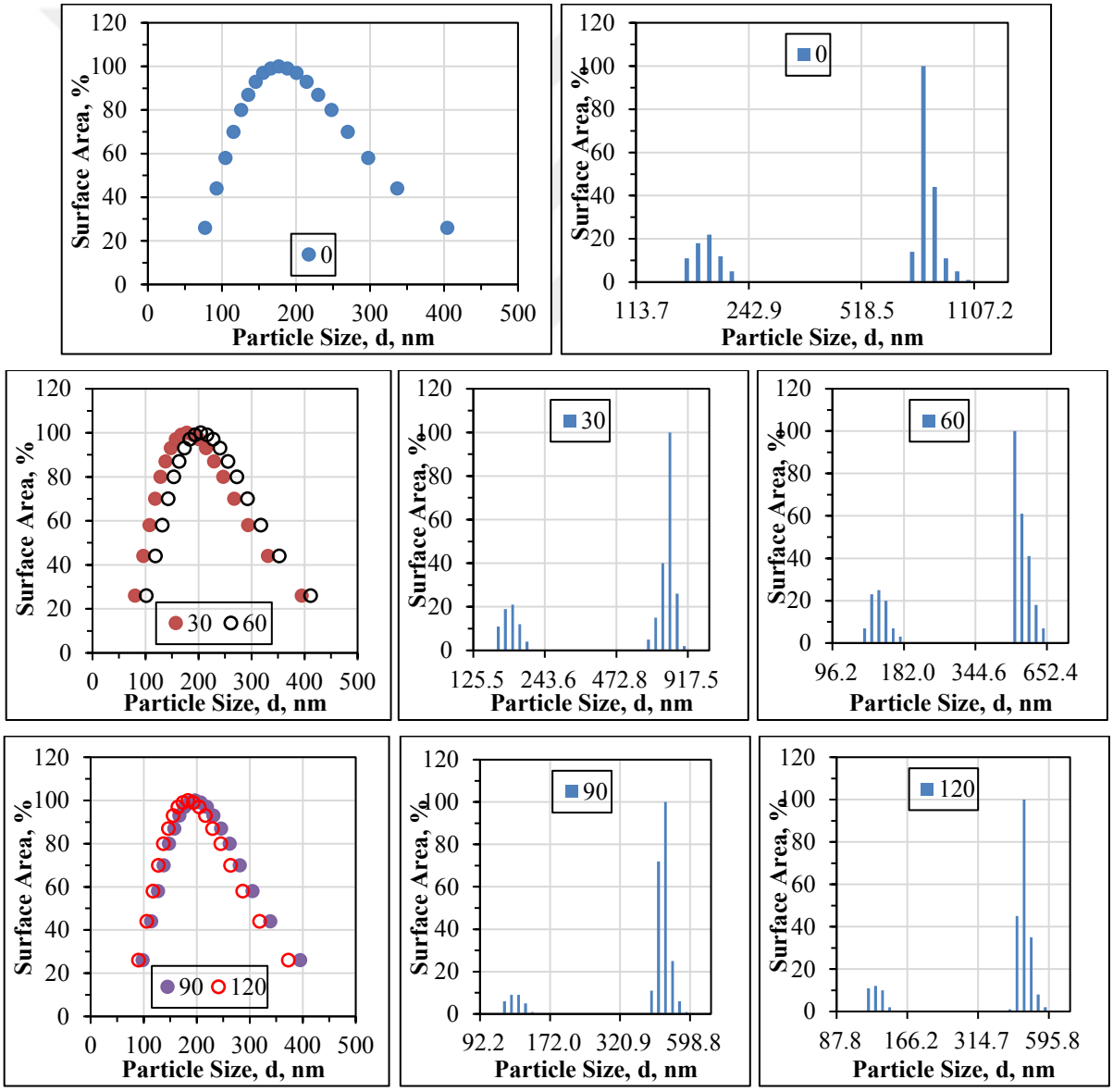


Figure 4.182. "TiO_2 and $SRNOM_{pho}$" binary system following photolysis of organic matter surface area profile: Time dependent comparative presentation of log Normal distribution and multi-size distribution of "TiO_2 and $SRNOM_{pho}$" binary system following photolysis of organic matter.

4.1.6.8. "TiO_2 and $SRNOM_{pho}$" binary system following photolysis of organic matter number profile.

Time dependent logN distribution G(d) and multi size distribution C(d) of "TiO_2 and $SRNOM_{pho}$" binary system following photolysis of organic matter number profile was shown in Figure 4.183. Time dependent mean diameter, range and min-max diameter difference with respect to log normal and multi-size distribution of "TiO_2 and $SRNOM_{pho}$" binary system following photolysis of organic matter number profile was given in Table 4.115.

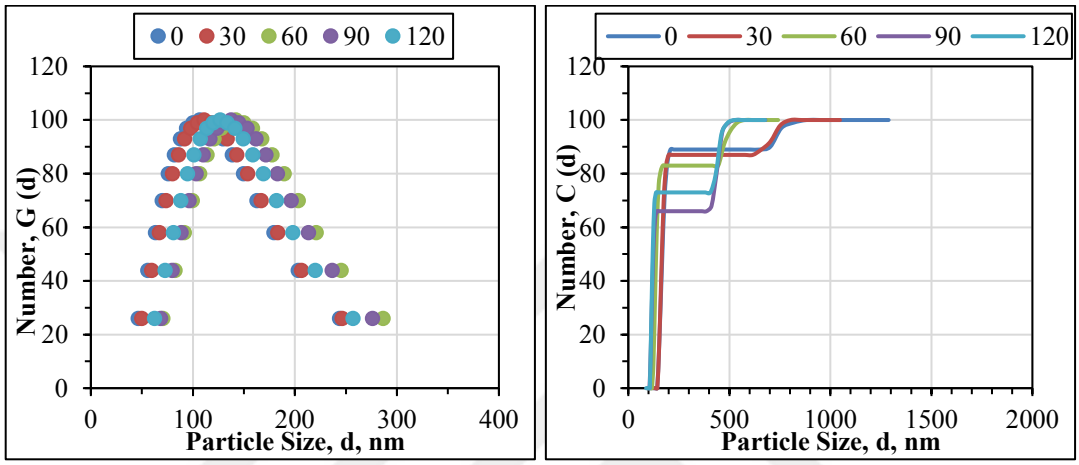


Figure 4.183. "TiO_2 and $SRNOM_{pho}$" binary system following photolysis of organic matter number profile: Time dependent logN distribution G(d) and multi size distribution C(d).

Table 4.115. "TiO_2 and $SRNOM_{pho}$" binary system following photolysis of organic matter number profile: Time dependent mean diameter, range and min-max diameter difference with respect to log normal and multi-size distribution.

TiO_2 and SRNOM	time, min				
	0	30	60	90	120
Log Normal distribution					
Mean, nm	106.7	111.0	142.3	137.6	126.7
Range	46.6-244.0	50.0-246.4	70.7-286.4	68.5-276.1	62.4-257.2
Difference	197.4	196.4	215.7	207.6	194.8
Multi-size distribution					
Max 1, nm	179.3	163.7	132.3	118.3	113.3
Max 2, nm	757.7	752.0	474.2	466.6	120.8
Max 3, nm	-	-	-	-	461.5
Range	113.7-1288.5	125.5-1047.6	96.2-741.3	92.2-678.3	87.8-676.9
Difference	1174.8	922.1	645.1	586.1	589.1

In terms of number profile, it could be stated that hydrodynamic particle size of "TiO_2 and $SRNOM_{pho}$" binary system following photolysis of organic matter exhibited a fluctuating trend according to time variations. In terms of log normal distribution, initial hydrodynamic particle size

was recorded as 106.7 nm and detected to 126.7 nm upon period of 120 min. Initial size difference was attained as 197.4 nm and reached to 194.8 nm at the end of 120 min. In terms of multi-size distribution, it could be asserted that two peaks were observed until 120 min. Upon 120 min, three peaks were monitored. As described for "TiO_2 and $SRNOM_{pho}$" binary system following photolysis of organic matter surface area profile (Figure 4.182), a similar approach was followed for "TiO_2 and $SRNOM_{pho}$" binary system following photolysis of organic matter number profile. Time dependent comparative presentation of log Normal distribution and multi-size distribution of "TiO_2 and $SRNOM_{pho}$" binary system following photolysis of organic matter number profile was presented in Figure 4.184.

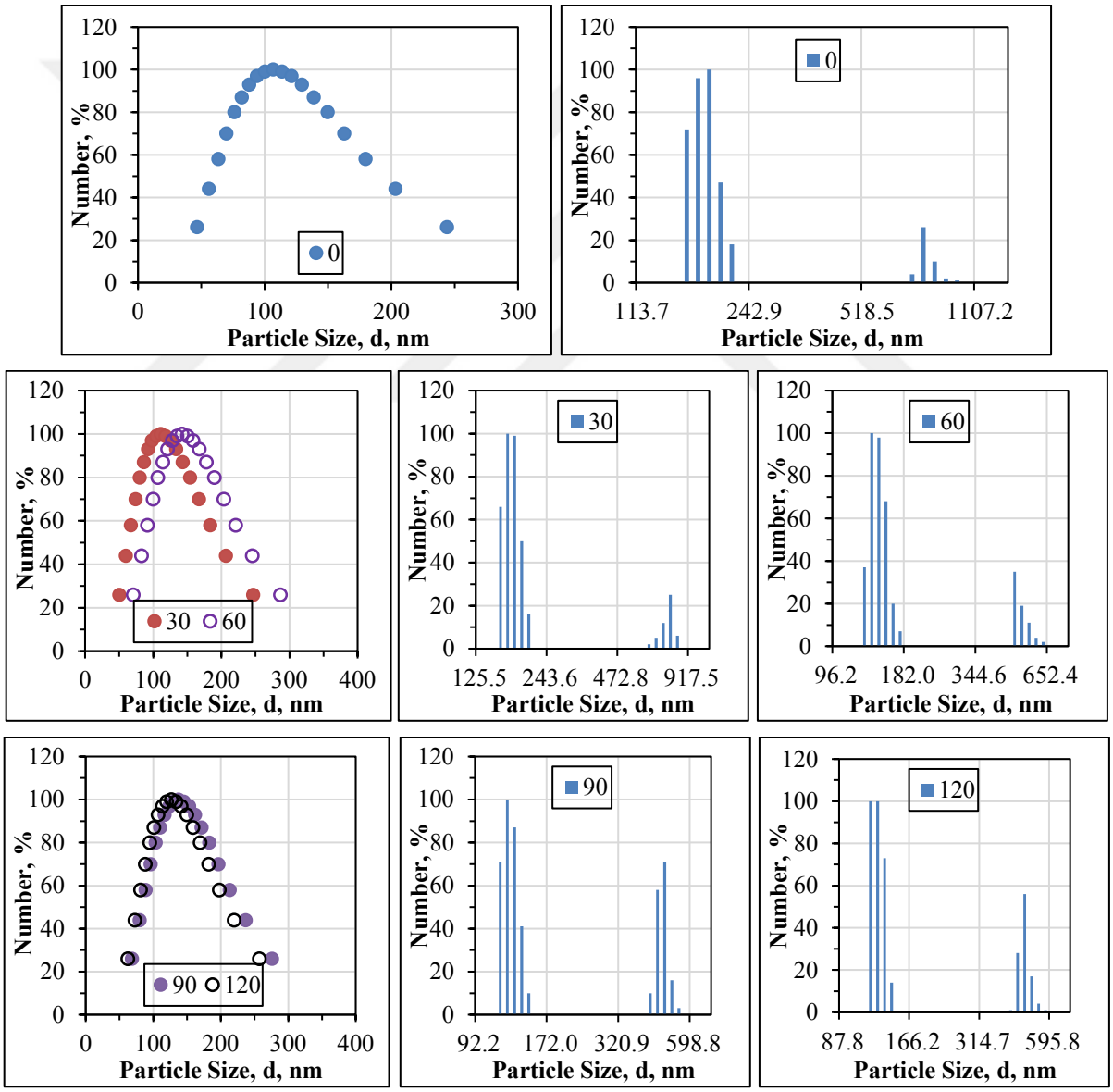


Figure 4.184. "TiO_2 and $SRNOM_{pho}$" binary system following photolysis of organic matter number profile: Time dependent comparative presentation of log Normal distribution and multi-size distribution of "TiO_2 and $SRNOM_{pho}$" binary system following photolysis of organic matter.

4.1.6.9. "N-TiO_2 and HA_{pho}" binary system following photolysis of organic matter intensity profile. Time dependent logN distribution G(d) and multi size distribution C(d) of "N-TiO_2 and HA_{pho}" binary system following photolysis of organic matter intensity profile was demonstrated in Figure 4.185. Time dependent mean diameter, range and min-max diameter difference with respect to log normal and multi-size distribution of "N-TiO_2 and HA_{pho}" binary system following photolysis of organic matter intensity profile was displayed in Table 4.116.

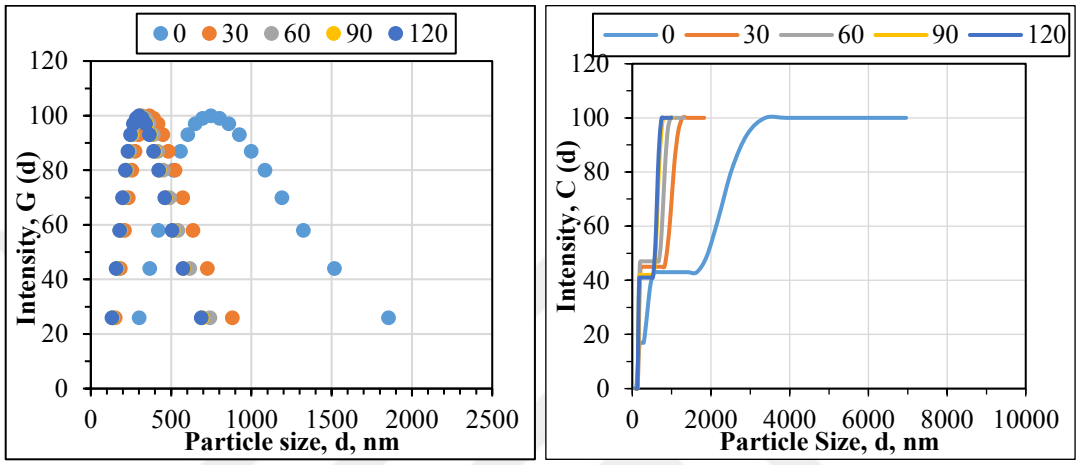


Figure 4.185. "N-TiO_2 and HA_{pho}" binary system following photolysis of organic matter intensity profile: Time dependent logN distribution G(d) and multi size distribution C(d).

Table 4.116. "N-TiO_2 and HA_{pho}" binary system following photolysis of organic matter intensity profile: Time dependent mean diameter, range and min-max diameter difference with respect to log normal and multi-size distribution.

N-TiO_2 and HA	time, min				
	0	30	60	90	120
Log Normal distribution					
Mean, nm	747.4	365.6	319.2	306.0	301.4
Range	301.1-1855.1	151.8-880.7	137.2-742.7	135.1-693.3	131.9-688.5
Difference	1554.0	728.9	605.5	558.2	556.6
Multi-size distribution					
Max 1, nm	140.5	177.2	175.3	158.0	155.1
Max 2, nm	446.6	1066.9	839.3	667.1	647.3
Max 3, nm	2530.3	-	-	-	-
Range	68.2-6959.6	103.4-1828.2	120.8-1312.9	102.6-1027.5	101.0-993.7
Difference	6891.4	1724.8	1192.1	924.9	892.7

Hydrodynamic size of "N-TiO_2 and HA_{pho}" binary system was attained as 747.4 nm. Upon 30 min, a rapid decrease was monitored and hydrodynamic size was obtained as 365.6 nm. In terms of multi-size distribution, initially three peaks were obtained. Time dependent comparative presentation

of log Normal distribution and multi-size distribution of "N-TiO_2 and HA_{pho}" binary system following photolysis of organic matter intensity profile was presented in Figure 4.186. Polydispersity of "N-TiO_2 and HA_{pho}" binary system following photolysis of organic matter was given in Table 4.117 and continuous decrease was observed along 120 min.

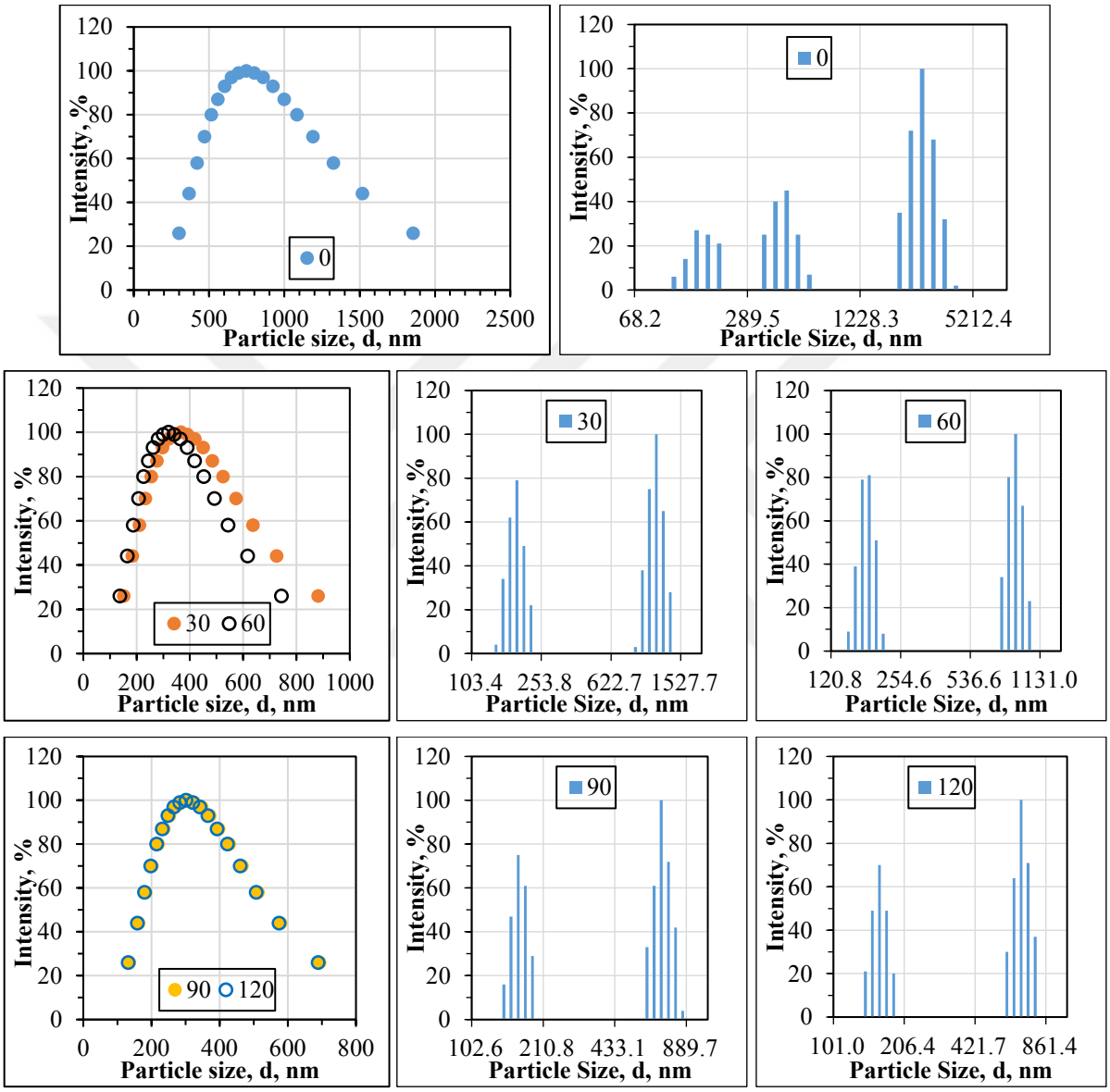


Figure 4.186. "N-TiO_2 and HA_{pho}" binary system following photolysis of organic matter intensity profile: Time dependent comparative presentation of log Normal distribution and multi-size distribution of "N-TiO_2 and HA_{pho}" binary system following photolysis of organic matter.

Table 4.117. Polydispersity of "N-TiO_2 and HA_{pho}" binary system following photolysis of organic matter.

N-TiO_2 and HA	Polydispersity				
	0	30	60	90	120
	0.357	0.331	0.301	0.280	0.287

4.1.6.10. "N-TiO_2 and HA_{pho}" binary system following photolysis of organic matter volume profile.

Time dependent logN distribution G(d) and multi size distribution C(d) of "N-TiO_2 and HA_{pho}" binary system following photolysis of organic matter volume profile was exhibited in Figure 4.187. Time dependent mean diameter, range and min-max diameter difference with respect to log normal and multi-size distribution of "N-TiO_2 and HA_{pho}" binary system following photolysis of organic matter volume profile was presented in Table 4.118.

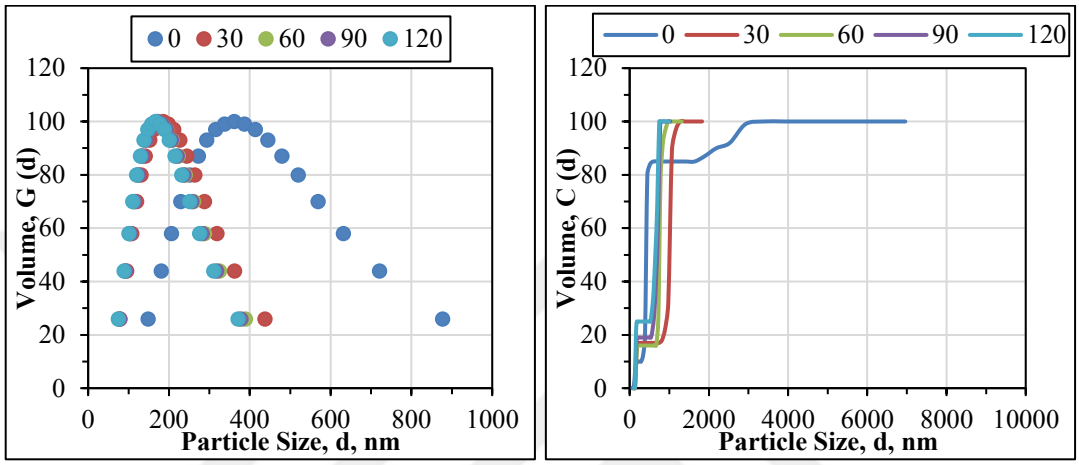


Figure 4.187. "N-TiO_2 and HA_{pho}" binary system following photolysis of organic matter volume profile: Time dependent logN distribution G(d) and multi size distribution C(d).

Table 4.118. "N-TiO_2 and HA_{pho}" binary system following photolysis of organic matter volume profile: Time dependent mean diameter, range and min-max diameter difference with respect to log normal and multi-size distribution.

N-TiO_2 and HA	time, min				
	0	30	60	90	120
Log Normal distribution					
Mean, nm	361.5	186.0	171.7	171.6	166.9
Range	148.9-877.4	79.1-437.5	75.7-389.6	77.8-378.6	75.0-371.4
Difference	728.5	358.4	313.9	300.8	296.4
Multi-size distribution					
Max 1, nm	140.5	177.2	162.7	158.0	155.1
Max 2, nm	446.6	1066.9	779.0	770.4	746.7
Max 3, nm	2923.8	-	-	-	-
Max 4, nm	3903.9	-	-	-	-
Range	68.2-6959.6	103.4-1828.2	120.8-1312.9	102.6-1027.5	101.0-993.7
Difference	6891.4	1724.8	1192.1	924.9	892.7

According to log normal distribution and in terms of volume profile, hydrodynamic particle size of "N-TiO_2 and HA_{pho}" binary system following photolysis of organic matter was obtained as 361.5

nm. Upon 30 min, a sharp decrease was observed and minor variations remained until the end of 120 min. On the other hand, in the first 30 min, approximately 50 % decline was monitored in size difference between max and min diameter. Initial size difference was obtained as 728.5 nm and detected to 296.4 nm upon period of 120 min. For comparison purposes, in terms of multi-size distribution, four max diameters were recorded as 140.5 nm, 446.6 nm, 2923.8 nm, and 3903.9 nm following initial period of time. Upon 30 min, two peaks were monitored and remained until the end of 120 min period. Time dependent comparative presentation of log Normal distribution and multi-size distribution of "N-TiO_2 and HA_{pho}" binary system following photolysis of organic matter intensity profile was demonstrated in Figure 4.188.

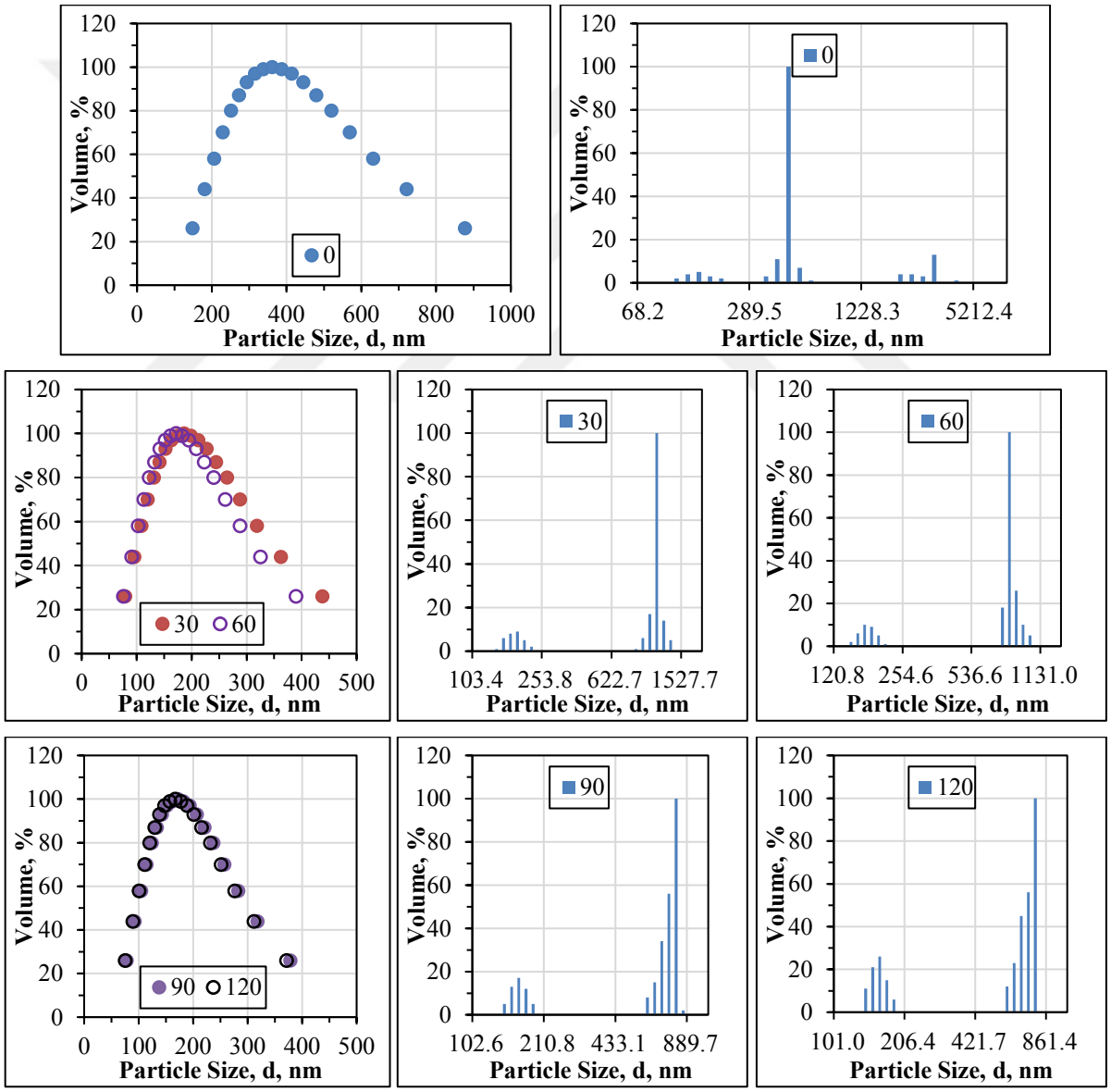


Figure 4.188. "N-TiO_2 and HA_{pho}" binary system following photolysis of organic matter volume profile: Time dependent comparative presentation of log Normal distribution and multi-size distribution of "N-TiO_2 and HA_{pho}" binary system following photolysis of organic matter.

4.1.6.11. "N-TiO_2 and HA_{pho}" binary system following photolysis of organic matter surface area profile. Time dependent logN distribution G(d) and multi size distribution C(d) of "N-TiO_2 and HA_{pho}" binary system following photolysis of organic matter surface area profile was given in Figure 4.189. Time dependent mean diameter, range and min-max diameter difference with respect to log normal and multi-size distribution of "N-TiO_2 and HA_{pho}" binary system following photolysis of organic matter surface area profile was shown in Table 4.119.

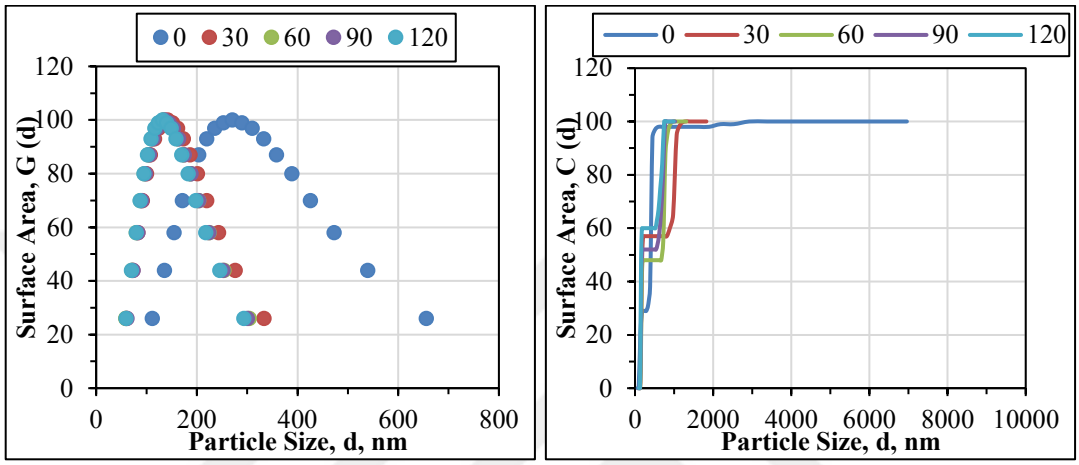


Figure 4.189. "N-TiO_2 and HA_{pho}" binary system following photolysis of organic matter surface area profile: Time dependent logN distribution G(d) and multi size distribution C(d).

Table 4.119. "N-TiO_2 and HA_{pho}" binary system following photolysis of organic matter surface area profile: Time dependent mean diameter, range and min-max diameter difference with respect to log normal and multi-size distribution.

N-TiO_2 and HA	time, min				
	0	30	60	90	120
Log Normal distribution					
Mean, nm	270.4	141.9	134.0	136.1	131.7
Range	111.4-656.2	60.3-333.8	59.1-304.0	61.7-300.4	59.2-293.2
Difference	544.8	273.5	244.9	238.7	234.0
Multi-size distribution					
Max 1, nm	140.5	162.0	162.7	158.0	155.1
Max 2, nm	446.6	1066.9	779.0	770.4	746.7
Max 3, nm	2923.8	-	-	-	-
Range	68.2-6959.6	103.4-1828.2	120.8-1312.9	102.6-1027.5	101.0-993.7
Difference	6891.4	1724.8	1192.1	924.9	892.7

As described for "N-TiO_2 and HA_{pho}" binary system following photolysis of organic matter volume profile (Table 4.118), a similar approach was followed for "N-TiO_2 and HA_{pho}" binary system following photolysis of organic matter surface area profile. It could be asserted that hydrodynamic

particle size approximately 50 % decreased upon 30 min. Initial hydrodynamic particle size was obtained as 270.4 nm and detected to 141.9 nm upon 30 min. Correspondingly, slight variations were observed until the end of 120 min. Also, size difference was recorded between 544.8 nm and 234.0 nm along 120 min. For comparison purposes, in terms of multi-size distribution, initially three max diameters were attained and two peaks were monitored until the end of 120 min. As elucidated for "N-TiO_2 and HA_{pho}" binary system following photolysis of organic matter volume profile (Figure 4.188), time dependent comparative presentation of log Normal distribution and multi-size distribution of "N-TiO_2 and HA_{pho}" binary system following photolysis of organic matter surface area profile was demonstrated in Figure 4.190.

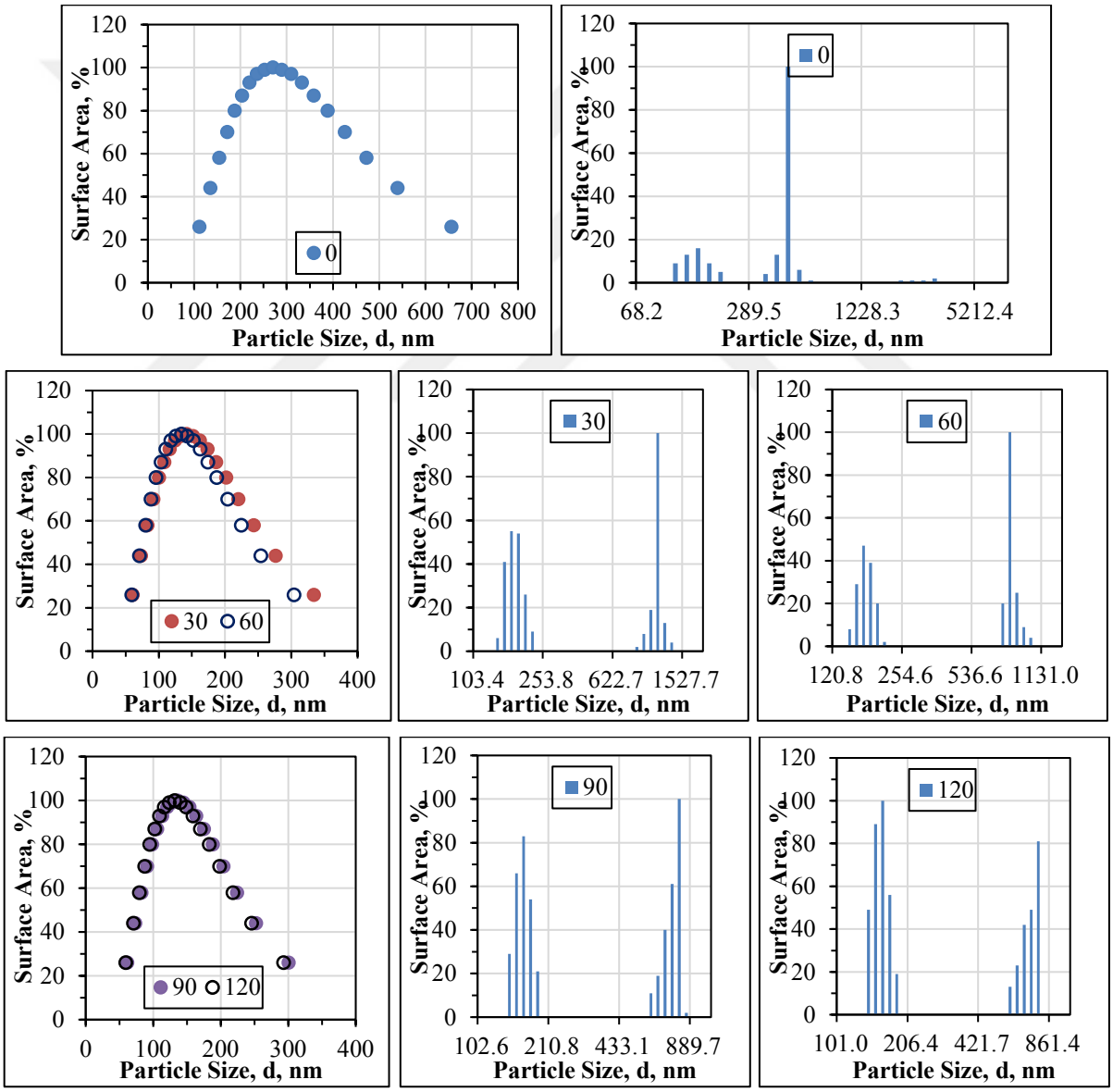


Figure 4.190. "N-TiO_2 and HA_{pho}" binary system following photolysis of organic matter surface area profile: Time dependent comparative presentation of log Normal distribution and multi-size distribution of "N-TiO_2 and HA_{pho}" binary system following photolysis of organic matter.

4.1.6.12. "N-TiO_2 and HA_{pho}" binary system following photolysis of organic matter number profile. Time dependent logN distribution G(d) and multi size distribution C(d) of "N-TiO_2 and HA_{pho}" binary system following photolysis of organic matter number profile was demonstrated in Figure 4.191. Time dependent mean diameter, range and min-max diameter difference with respect to log normal and multi-size distribution of "N-TiO_2 and HA_{pho}" binary system following photolysis of organic matter number profile was presented in Table 4.120.

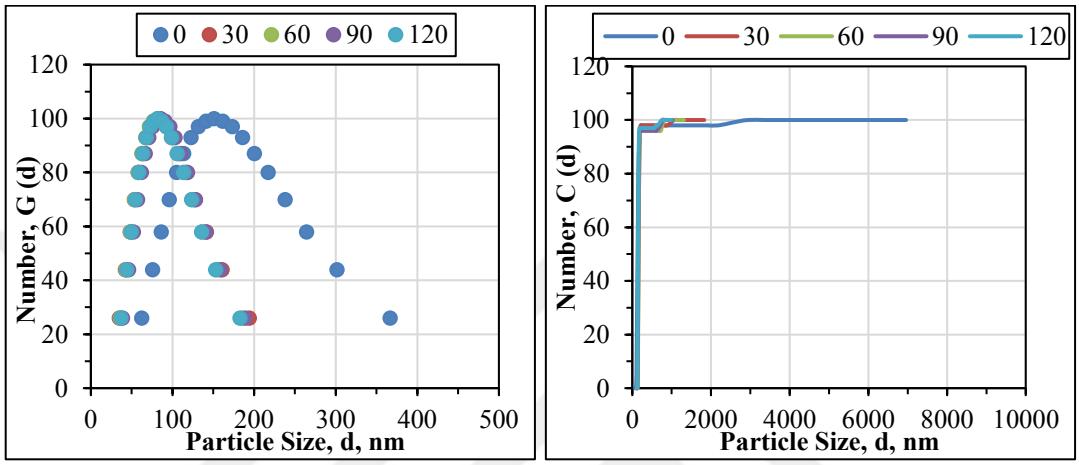


Figure 4.191. "N-TiO_2 and HA_{pho}" binary system following photolysis of organic matter number profile: Time dependent logN distribution G(d) and multi size distribution C(d).

Table 4.120. "N-TiO_2 and HA_{pho}" binary system following photolysis of organic matter number profile: Time dependent mean diameter, range and min-max diameter difference with respect to log normal and multi-size distribution.

N-TiO_2 and HA	time, min				
	0	30	60	90	120
Log Normal distribution					
Mean, nm	151.2	82.6	81.6	85.7	82.1
Range	62.3-367.0	35.1-194.4	36.0-185.1	38.8-189.1	36.9-182.7
Difference	304.7	159.3	149.1	150.3	145.8
Multi-size distribution					
Max 1, nm	121.6	162.0	162.7	158.0	144.4
Max 2, nm	446.6	1066.9	779.0	770.4	746.7
Range	68.2-6959.6	103.4-1828.2	120.8-1312.9	102.6-1027.5	101.0-993.7
Difference	6891.4	1724.8	1192.1	924.9	892.7

In a similar manner to data depicted "N-TiO_2 and HA_{pho}" binary system following photolysis of organic matter surface area profile (Figure 4.189), log normal distribution G(d) and multi size distribution C(d) of "N-TiO_2 and HA_{pho}" binary system following photolysis of organic matter number profile was exhibited with respect to time. It could be seen that hydrodynamic particle size

of "N-TiO_2 and HA_{pho}" binary system following photolysis of organic matter displayed a continuously decreasing trend according to time variations. In terms of log normal distribution, it could be inferred that coinciding peaks could be seen upon 30 min. Initial hydrodynamic particle size was detected as 151.2 nm and decreased to 82.1 nm upon 120 min. However, due to multi-size distribution, each max diameter could be easily discriminated. It could be asserted that two max diameters were observed upon period of 120 min.

Time dependent comparative presentation of log Normal distribution and multi-size distribution of "N-TiO_2 and HA_{pho}" binary system following photolysis of organic matter number profile was presented in Figure 4.192.

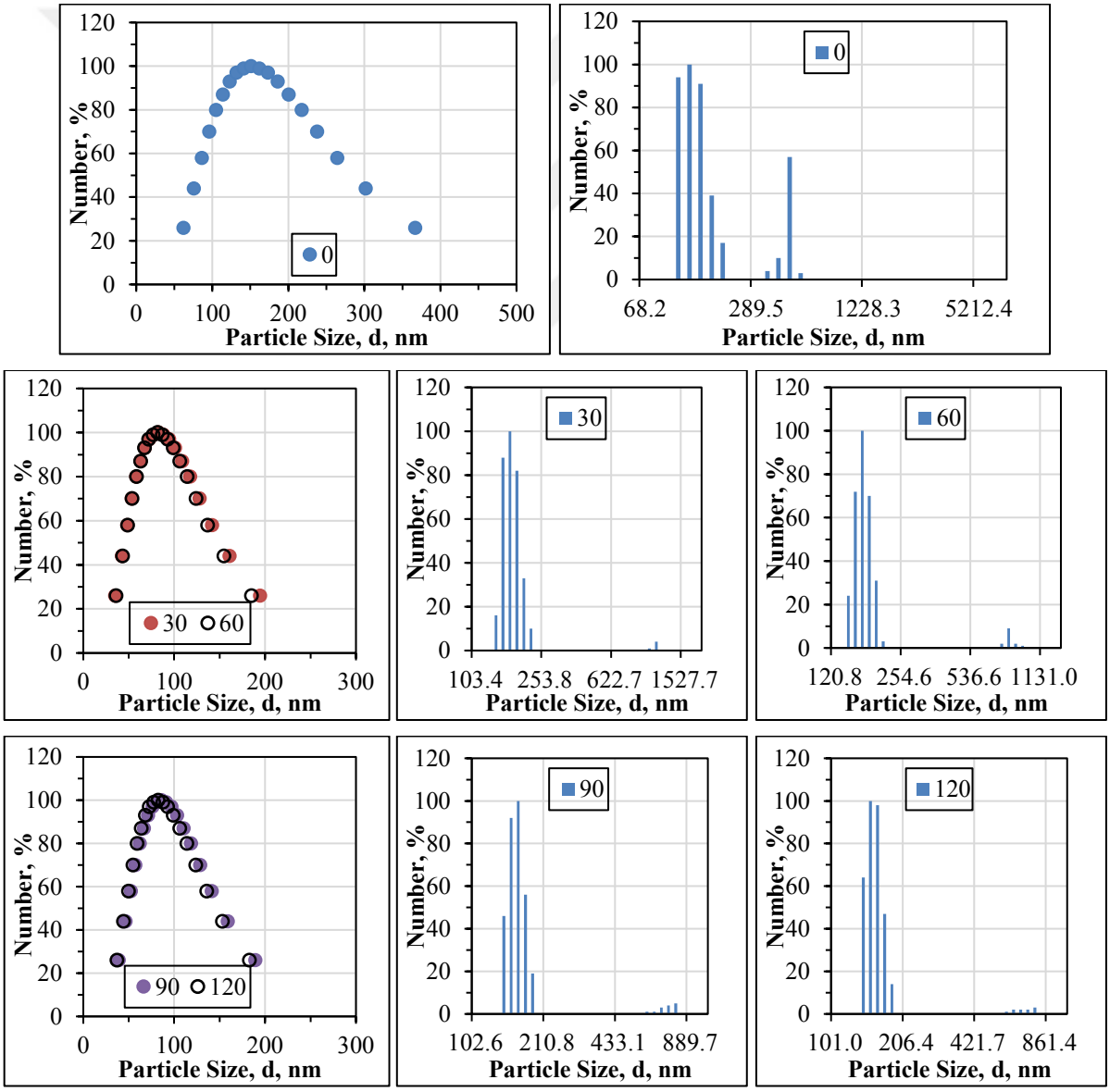


Figure 4.192. "N-TiO_2 and HA_{pho}" binary system following photolysis of organic matter number profile: Time dependent comparative presentation of log Normal distribution and multi-size distribution of "N-TiO_2 and HA_{pho}" binary system following photolysis of organic matter.

4.1.6.13. "N-TiO_2 and $SRNOM_{pho}$" binary system following photolysis of organic matter intensity profile. Time dependent logN distribution G(d) and multi size distribution C(d) of "N-TiO_2 and $SRNOM_{pho}$" binary system following photolysis of organic matter intensity profile was presented in Figure 4.193. Time dependent mean diameter, range and min-max diameter difference with respect to log normal and multi-size distribution of "N-TiO_2 and $SRNOM_{pho}$" binary system following photolysis of organic matter intensity profile was displayed in Table 4.121. Also, polydispersity of "N-TiO_2 and $SRNOM_{pho}$" binary system following photolysis of organic matter was given in Table 4.122 and continuous decrease was observed along 120 min.

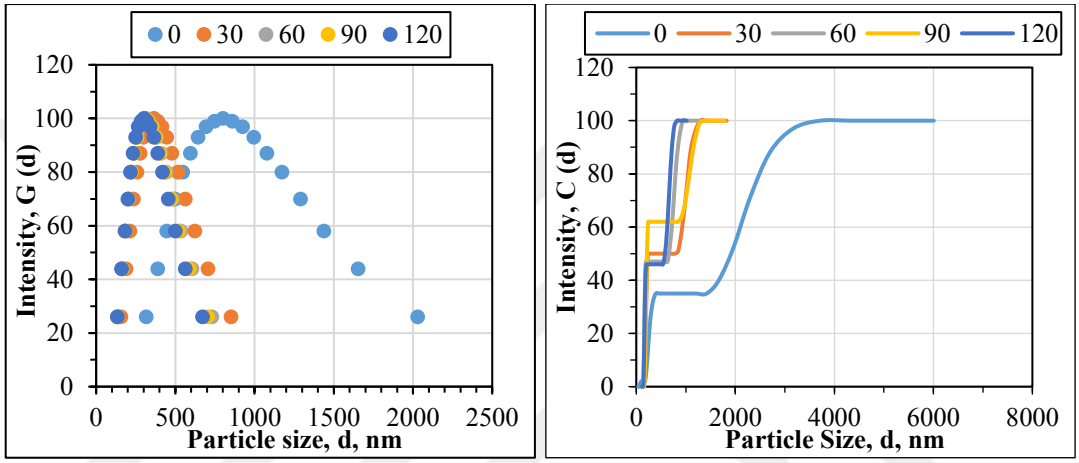


Figure 4.193. "N-TiO_2 and $SRNOM_{pho}$" binary system following photolysis of organic matter intensity profile: Time dependent logN distribution G(d) and multi size distribution C(d).

Table 4.121. "N-TiO_2 and $SRNOM_{pho}$" binary system following photolysis of organic matter intensity profile: Time dependent mean diameter, range and min-max diameter difference with respect to log normal and multi-size distribution.

N-TiO_2 and SRNOM	time, min				
	0	30	60	90	120
Log Normal distribution					
Mean, nm	801.2	364.8	313.3	311.1	301.7
Range	316.3-2029.5	156.1-852.5	134.4-730.5	137.2-705.2	135.4-672.5
Difference	1713.2	696.4	596.1	568.0	537.1
Multi-size distribution					
Max 1, nm	73.3	197.2	163.5	204.0	174.9
Max 2, nm	83.8	1091.7	802.8	1082.0	666.4
Max 3, nm	95.8	-	-	-	-
Max 4, nm	285.7	-	-	-	-
Max 5, nm	2296.3	-	-	-	-
Range	35.5-6008.9	118.1-1824.0	101.4-1294.1	123.7-1784.8	106.9-1016.7
Difference	5973.4	1705.9	1192.7	1661.1	909.8

Initial hydrodynamic size of "N-TiO_2 and $SRNOM_{pho}$" was attained as 801.2 nm and detected to 301.7 nm upon 120 min. Initially five peaks were observed as bimodal. Time dependent comparative presentation of log Normal distribution and multi-size distribution of "N-TiO_2 and $SRNOM_{pho}$" following photolysis of organic matter intensity profile was exhibited in Figure 4.194.

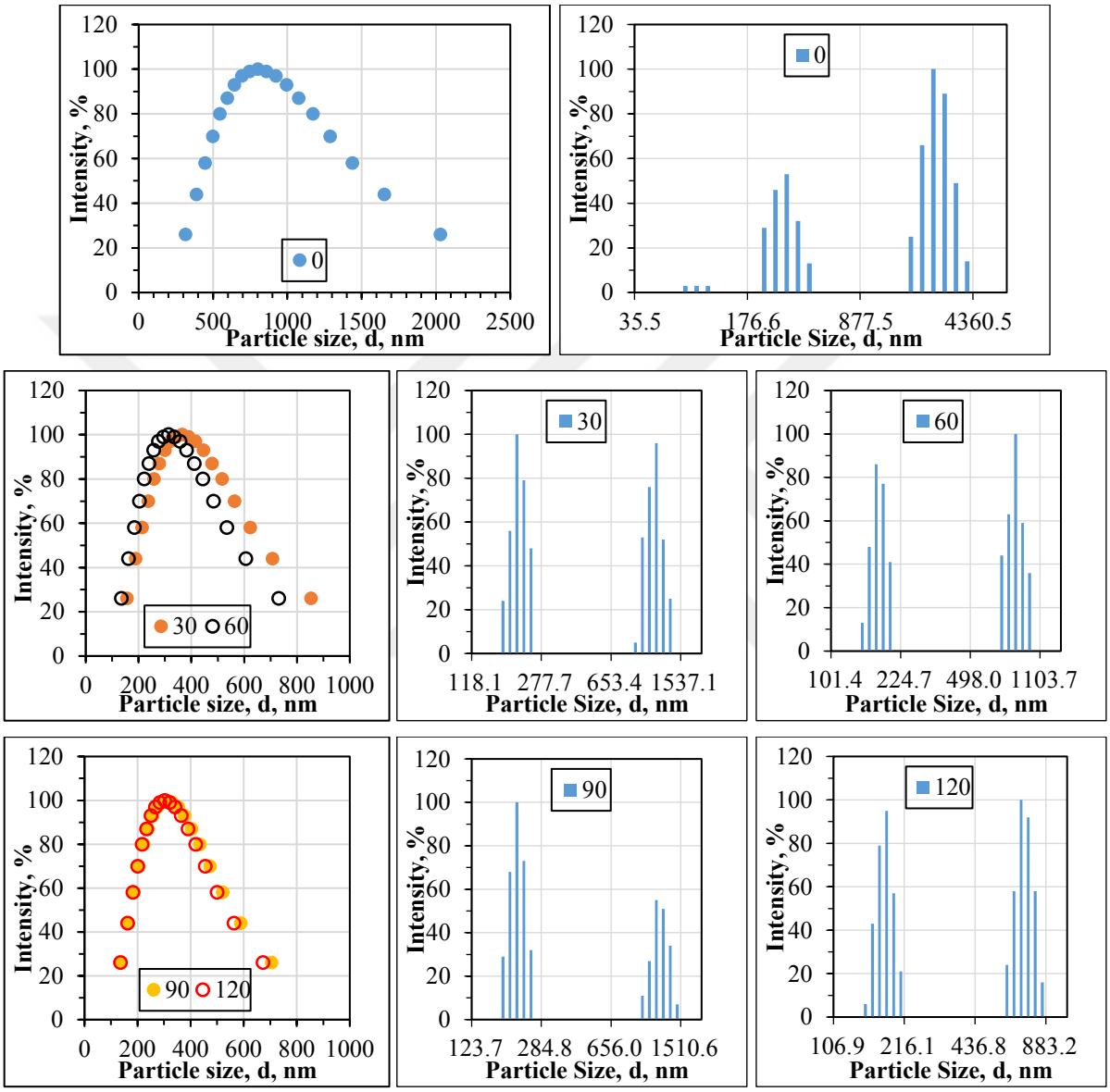


Figure 4.194. "N-TiO_2 and $SRNOM_{pho}$" binary system following photolysis of organic matter intensity profile: Time dependent comparative presentation of log Normal distribution and multi-size distribution of "N-TiO_2 and $SRNOM_{pho}$" binary system following photolysis of organic matter.

Table 4.122. Polydispersity of "N-TiO_2 and $SRNOM_{pho}$" binary system following photolysis of organic matter.

N-TiO_2 and SRNOM	Polydispersity				
	0	30	60	90	120
	0.376	0.305	0.303	0.281	0.268

4.1.6.14. "N-TiO_2 and $SRNOM_{pho}$" binary system following photolysis of organic matter volume profile. As explained for "N-TiO_2 and $SRNOM_{pho}$" binary system following photolysis of organic matter intensity profile (Figure 4.193), a similar approach was followed for "N-TiO_2 and $SRNOM_{pho}$" binary system following photolysis of organic matter volume profile. Time dependent logN distribution G(d) and multi size distribution C(d) of "N-TiO_2 and $SRNOM_{pho}$" binary system following photolysis of organic matter volume profile was displayed in Figure 4.195. Time dependent mean diameter, range and min-max diameter difference with respect to log normal and multi-size distribution of "N-TiO_2 and $SRNOM_{pho}$" binary system following photolysis of organic matter volume profile was demonstrated in Table 4.123.

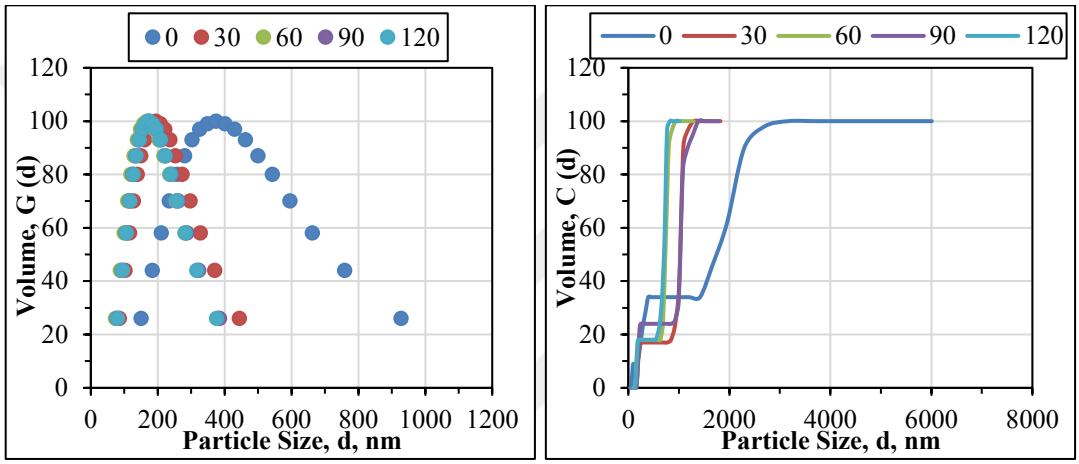


Figure 4.195. "N-TiO_2 and $SRNOM_{pho}$" binary system following photolysis of organic matter volume profile: Time dependent logN distribution G(d) and multi size distribution C(d).

Table 4.123. "N-TiO_2 and $SRNOM_{pho}$" binary system following photolysis of organic matter volume profile: Time dependent mean diameter, range and min-max diameter difference with respect to log normal and multi-size distribution.

N-TiO_2 and SRNOM	time, min				
	0	30	60	90	120
Log Normal distribution					
Mean, nm	374.1	194.9	168.0	174.3	173.4
Range	150.9-927.5	85.5-444.1	73.9-382.0	78.9-384.8	80.0-376.2
Difference	776.6	358.6	308.1	305.9	296.2
Multi-size distribution					
Max 1, nm	73.3	197.2	163.5	204.0	174.9
Max 2, nm	285.7	1091.7	802.8	1082.0	767.2
Max 3, nm	393.7	-	-	-	-
Max 4, nm	2296.3	-	-	-	-
Range	35.5-6008.9	118.1-1824.0	101.4-1294.1	123.7-1784.8	106.9-1016.7
Difference	5973.4	1705.9	1192.7	1661.1	909.8

According to intensity profile, it could be stated that hydrodynamic particle size of "N-TiO_2 and $SRNOM_{pho}$" binary system following photolysis of organic matter revealed a sharp decrease in the first 30 min. Accordingly, continuous decrease remained until the end of 120 min. On the other hand, in terms of log normal distribution, size difference was attained as 776.6 nm and decreased to 296.2 nm upon 120 min. For comparison purposes, in terms of multi-size distribution, initially four max diameters were recorded and two max diameters remained until the end of 120 min. Time dependent comparative presentation of log Normal distribution and multi-size distribution of "N-TiO_2 and $SRNOM_{pho}$" binary system following photolysis of organic matter volume profile was exhibited in Figure 196.

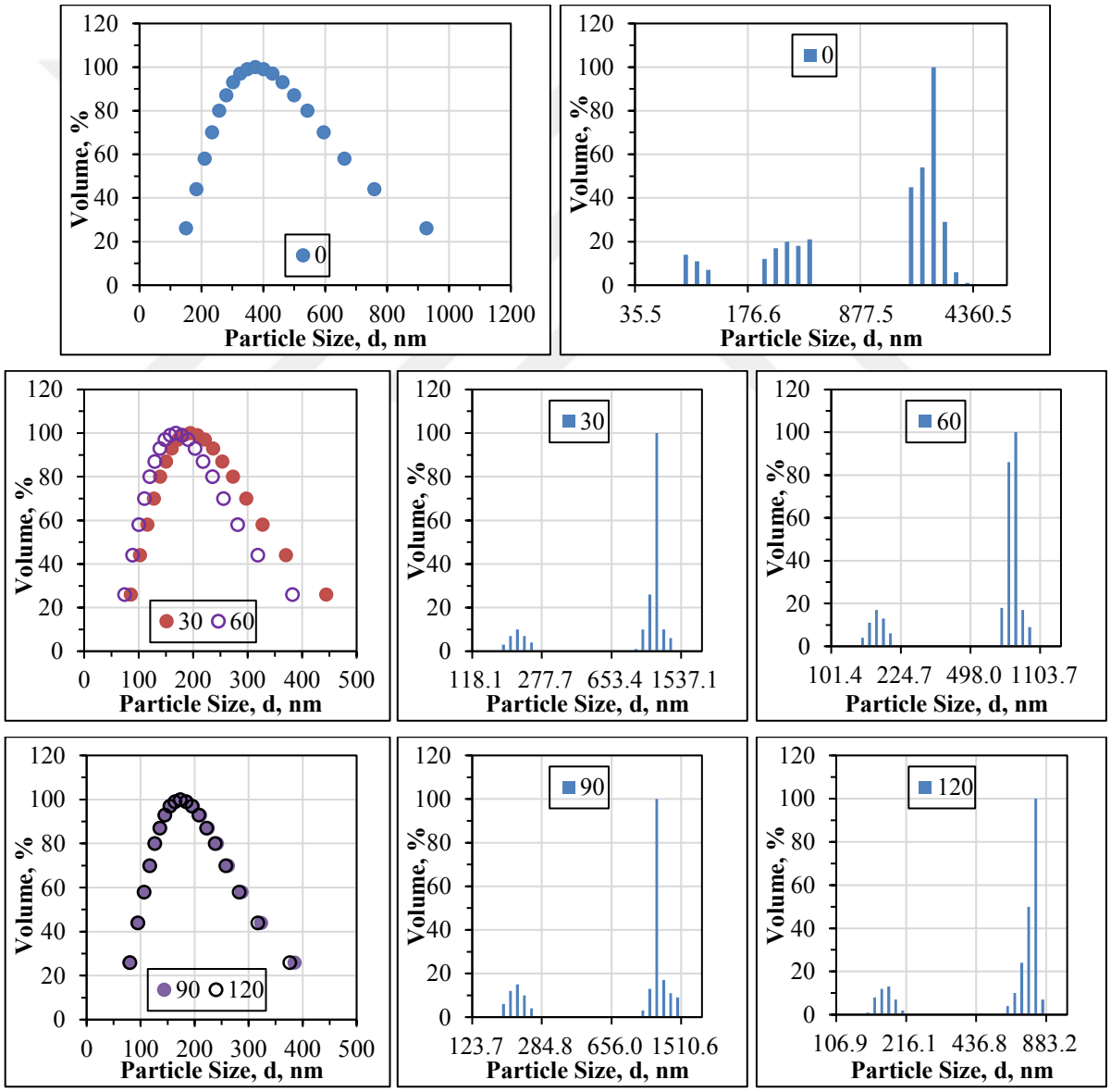


Figure 4.196. "N-TiO_2 and $SRNOM_{pho}$" binary system following photolysis of organic matter volume profile: Time dependent comparative presentation of log Normal distribution and multi-size distribution of "N-TiO_2 and $SRNOM_{pho}$" binary system following photolysis of organic matter.

4.1.6.15. "N-TiO_2 and $SRNOM_{pho}$" binary system following photolysis of organic matter surface area profile. Time dependent logN distribution G(d) and multi size distribution C(d) of "N-TiO_2 and $SRNOM_{pho}$" binary system following photolysis of organic matter surface area profile was presented in Figure 4.197. Time dependent mean diameter, range and min-max diameter difference with respect to log normal and multi-size distribution of "N-TiO_2 and $SRNOM_{pho}$" binary system following photolysis of organic matter surface area profile was given in Table 4.124.

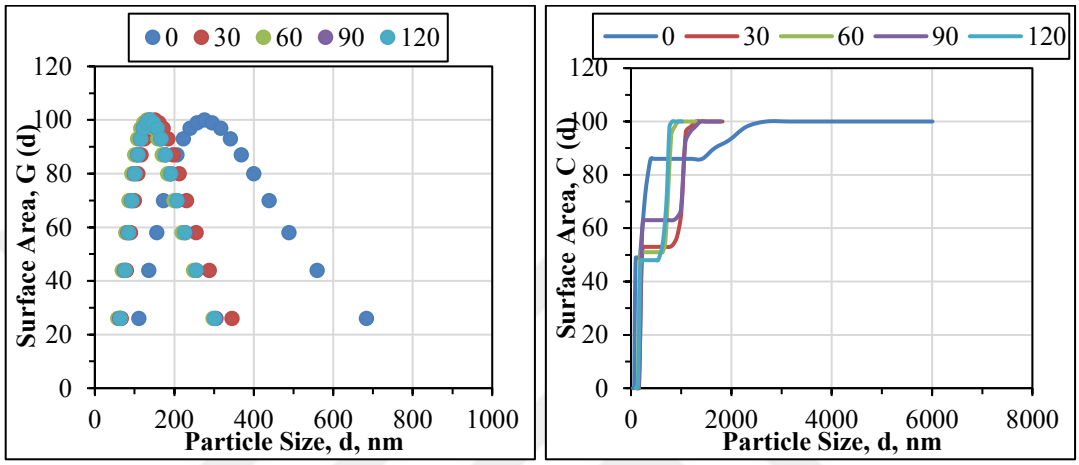


Figure 4.197. "N-TiO_2 and $SRNOM_{pho}$" binary system following photolysis of organic matter surface area profile: Time dependent logN distribution G(d) and multi size distribution C(d).

Table 4.124. "N-TiO_2 and $SRNOM_{pho}$" binary system following photolysis of organic matter surface area profile: Time dependent mean diameter, range and min-max diameter difference with respect to log normal and multi-size distribution.

N-TiO_2 and SRNOM	time, min				
	0	30	60	90	120
Log Normal distribution					
Mean, nm	275.9	151.6	130.9	138.2	139.0
Range	111.3-683.9	66.5-345.6	57.6-297.7	62.6-305.2	64.1-301.4
Difference	572.6	279.1	240.1	242.6	237.3
Multi-size distribution					
Max 1, nm	73.3	197.2	163.5	204.0	163.1
Max 2, nm	285.7	1091.7	802.8	1082.0	767.2
Max 3, nm	2296.3	-	-	-	-
Range	35.5-6008.9	118.1-1824.0	101.4-1294.1	123.7-1784.8	106.9-1016.7
Difference	5973.4	1705.9	1192.7	1661.1	909.8

As explained for "N-TiO_2 and $SRNOM_{pho}$" binary system following photolysis of organic matter volume profile (Table 4.123), a similar approach was followed for "N-TiO_2 and $SRNOM_{pho}$" binary system following photolysis of organic matter volume profile. It could be deduced that hydrodynamic

particle size roughly 45 % decreased in the first 30 min. Initial hydrodynamic particle size was obtained as 275.9 nm and detected to 151.6 nm upon 30 min. Correspondingly, minor variations remained until the end of 120 min. Considering multi-size distribution, initially three max diameters were observed as 73.3 nm, 285.7 nm, and 2296.3 nm, and two max diameters remained until the end of 120 min.

As elucidated for "N-TiO_2 and $SRNOM_{pho}$" binary system following photolysis of organic matter volume profile (Figure 4.196), time dependent comparative presentation of log Normal distribution and multi-size distribution of "N-TiO_2 and $SRNOM_{pho}$" binary system following photolysis of organic matter surface area profile was given in Figure 4.198.

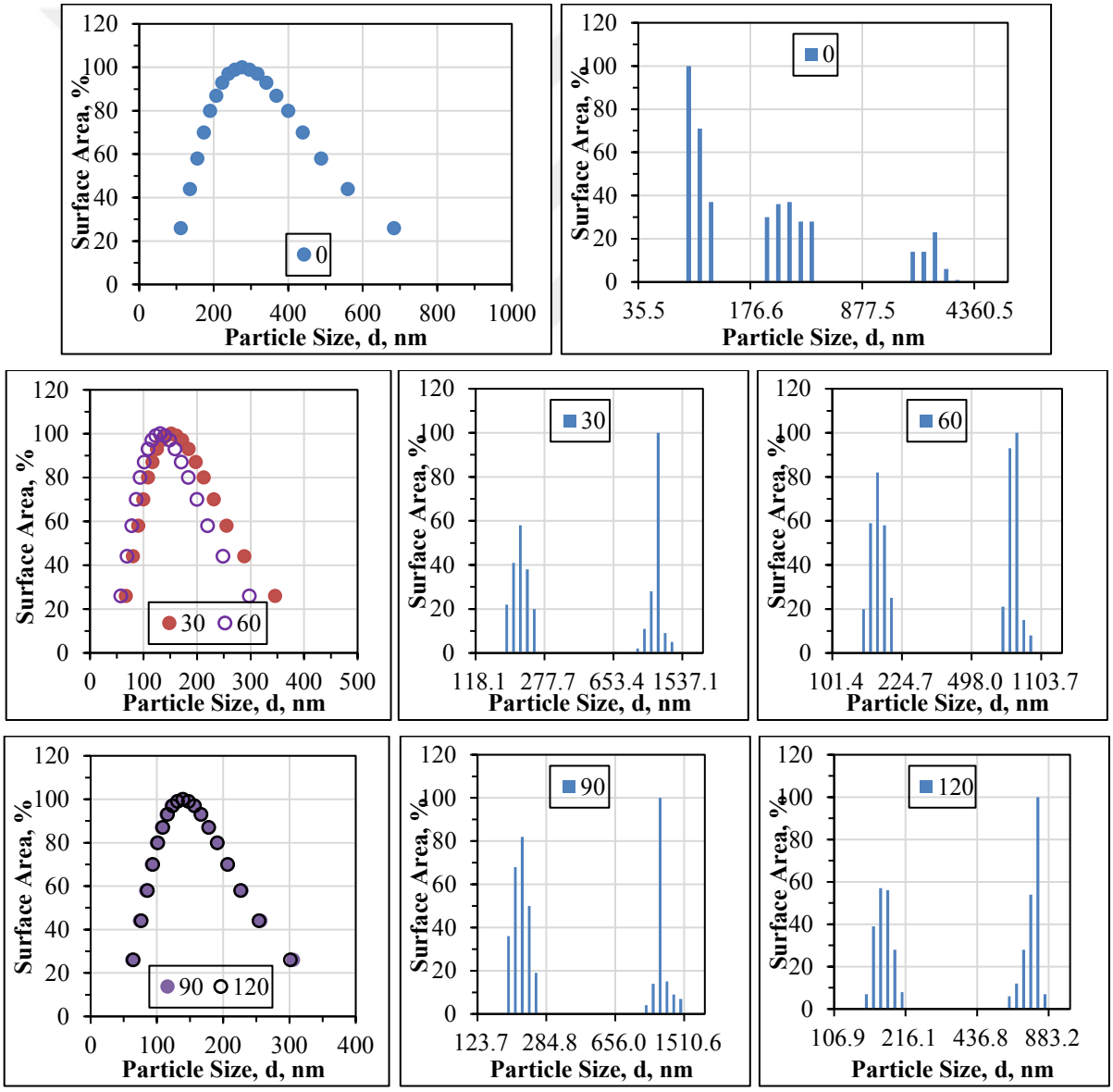


Figure 4.198. "N-TiO_2 and $SRNOM_{pho}$" binary system following photolysis of organic matter surface area profile: Time dependent comparative presentation of log Normal distribution and multi-size distribution of "N-TiO_2 and $SRNOM_{pho}$" binary system following photolysis of organic matter.

4.1.6.16. "N-TiO_2 and $SRNOM_{pho}$" binary system following photolysis of organic matter number profile. Likewise expressed so far, time dependent logN distribution G(d) and multi size distribution C(d) of "N-TiO_2 and $SRNOM_{pho}$" binary system following photolysis of organic matter number profile was exhibited in Figure 4.199. Also, time dependent mean diameter, range and min-max diameter difference with respect to log normal and multi-size distribution of "N-TiO_2 and $SRNOM_{pho}$" binary system following photolysis of organic matter number profile was presented in Table 4.125.

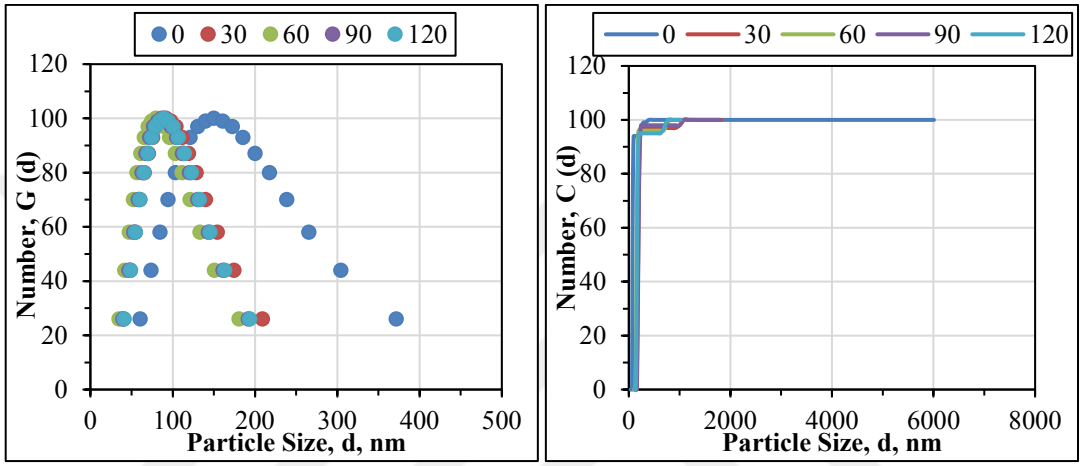


Figure 4.199. "N-TiO_2 and $SRNOM_{pho}$" binary system following photolysis of organic matter number profile: Time dependent logN distribution G(d) and multi size distribution C(d).

Table 4.125. "N-TiO_2 and $SRNOM_{pho}$" binary system following photolysis of organic matter number profile: Time dependent mean diameter, range and min-max diameter difference with respect to log normal and multi-size distribution.

N-TiO_2 and SRNOM	time, min				
	0	30	60	90	120
Log Normal distribution					
Mean, nm	150.0	91.8	79.5	87.0	89.2
Range	60.5-371.9	40.3-209.3	35.0-180.8	39.4-192.0	41.2-193.6
Difference	311.4	169.0	145.8	152.6	152.4
Multi-size distribution					
Max 1, nm	73.3	197.2	163.5	204.0	163.1
Max 2, nm	207.3	1091.7	741.4	1082.0	767.2
Max 3, nm	-	-	802.8	-	-
Range	35.5-6008.9	118.1-1824.0	101.4-1294.1	123.7-1784.8	106.9-1016.7
Difference	5973.4	1705.9	1192.7	1661.1	909.8

In terms of number profile, it could be deduced that a rapid decrease was observed in the first 30 min. Accordingly, a continuous decrease remained until the end of 120 min. Initial hydrodynamic

particle size was attained as 150.0 nm and detected to 89.2 nm upon 120 min. According to log normal distribution, a sharp decrease was observed in size difference in the first 30 min. It could be stated that initial size difference was obtained as 311.4 nm and detected to 152.4 nm at the end of 120 min. However, considering multi-size distribution, two max diameters were attained as 73.3 nm and 207.3 nm until 60 min. Upon 60 min, three peaks were observed and two peaks remained until the end of 120 min. According to multi-size distribution, size difference decreased from 5973.4 nm to 909.8 nm upon period of 120 min. Time dependent comparative presentation of log Normal distribution and multi-size distribution of "N-TiO_2 and $SRNOM_{pho}$" binary system following photolysis of organic matter number profile was demonstrated in Figure 4.200.

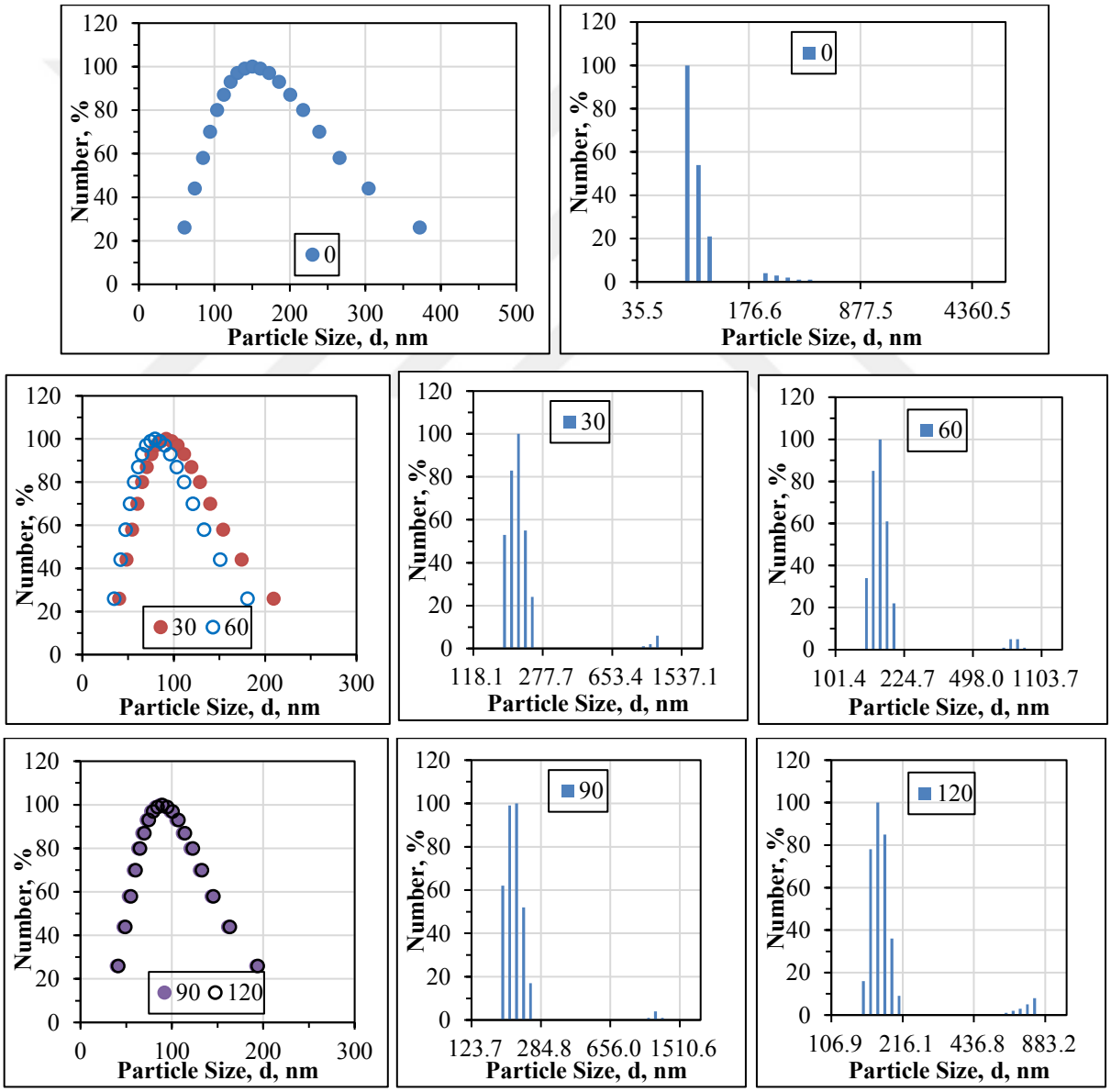


Figure 4.200. "N-TiO_2 and $SRNOM_{pho}$" binary system following photolysis of organic matter number profile: Time dependent comparative presentation of log Normal distribution and multi-size distribution of "N-TiO_2 and $SRNOM_{pho}$" binary system following photolysis of organic matter.

4.1.6.17. "Fe-TiO_2 and HA_{pho}" binary system following photolysis of organic matter intensity profile.

Time dependent logN distribution G(d) and multi size distribution C(d) of "Fe-TiO_2 and HA_{pho}" binary system following photolysis of organic matter intensity profile was presented in Figure 4.201. Time dependent mean diameter, range and min-max diameter difference with respect to log normal and multi-size distribution of "Fe-TiO_2 and HA_{pho}" binary system following photolysis of organic matter intensity profile was exhibited in Table 4.126.

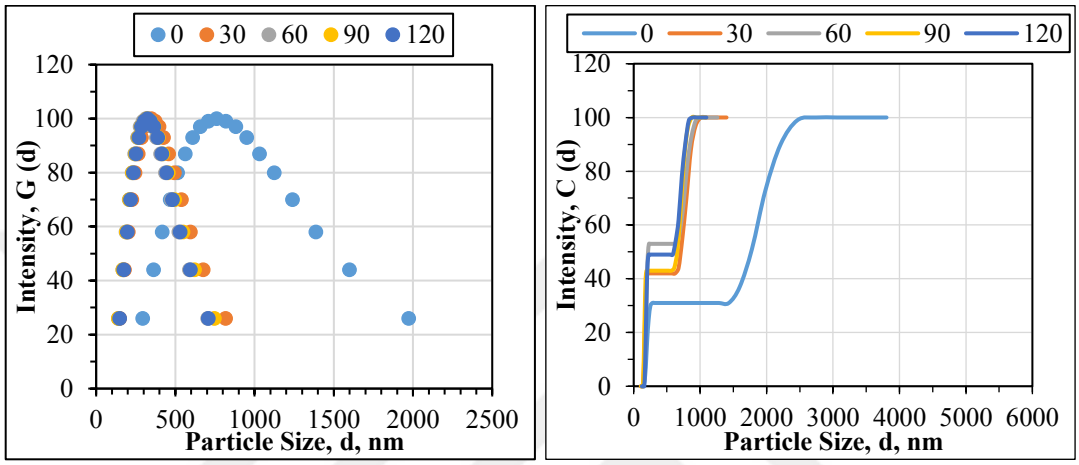


Figure 4.201. "Fe-TiO_2 and HA_{pho}" binary system following photolysis of organic matter intensity profile: Time dependent logN distribution G(d) and multi size distribution C(d).

Table 4.126. "Fe-TiO_2 and HA_{pho}" binary system following photolysis of organic matter intensity profile: Time dependent mean diameter, range and min-max diameter difference with respect to log normal and multi-size distribution.

Fe-TiO_2 and HA	time, min				
	0	30	60	90	120
Log Normal distribution					
Mean, nm	761.0	348.4	315.1	323.3	323.5
Range	293.7-1972.3	148.6-816.8	141.1-703.6	139.8-747.6	148.0-707.5
Difference	1678.6	668.2	562.5	607.8	559.5
Multi-size distribution					
Max 1, nm	202.8	171.0	198.3	166.9	196.3
Max 2, nm	1983.4	860.7	808.5	757.3	724.4
Range	117.8-3805.2	105.3-1397.7	118.2-1260.3	108.4-1085.5	121.3-1094.0
Difference	3687.4	1292.4	1142.1	977.1	972.7

Initial hydrodynamic size of "Fe-TiO_2 and HA_{pho}" following photolysis of organic matter was recorded as 761.0 nm and detected to 323.5 nm upon 120 min. Considering multi-size distribution, two max diameters were monitored upon period of 120 min. Time dependent comparative presentation of log Normal distribution and multi-size distribution of "Fe-TiO_2 and HA_{pho}" binary

system following photolysis of organic matter intensity profile was exhibited in Figure 4.202. Also, polydispersity of "Fe-TiO_2 and HA_{pho}" binary system following photolysis of organic matter was presented in Table 4.127. Simply an average value of 0.305 could be regarded as suitable for expressing polydispersity.

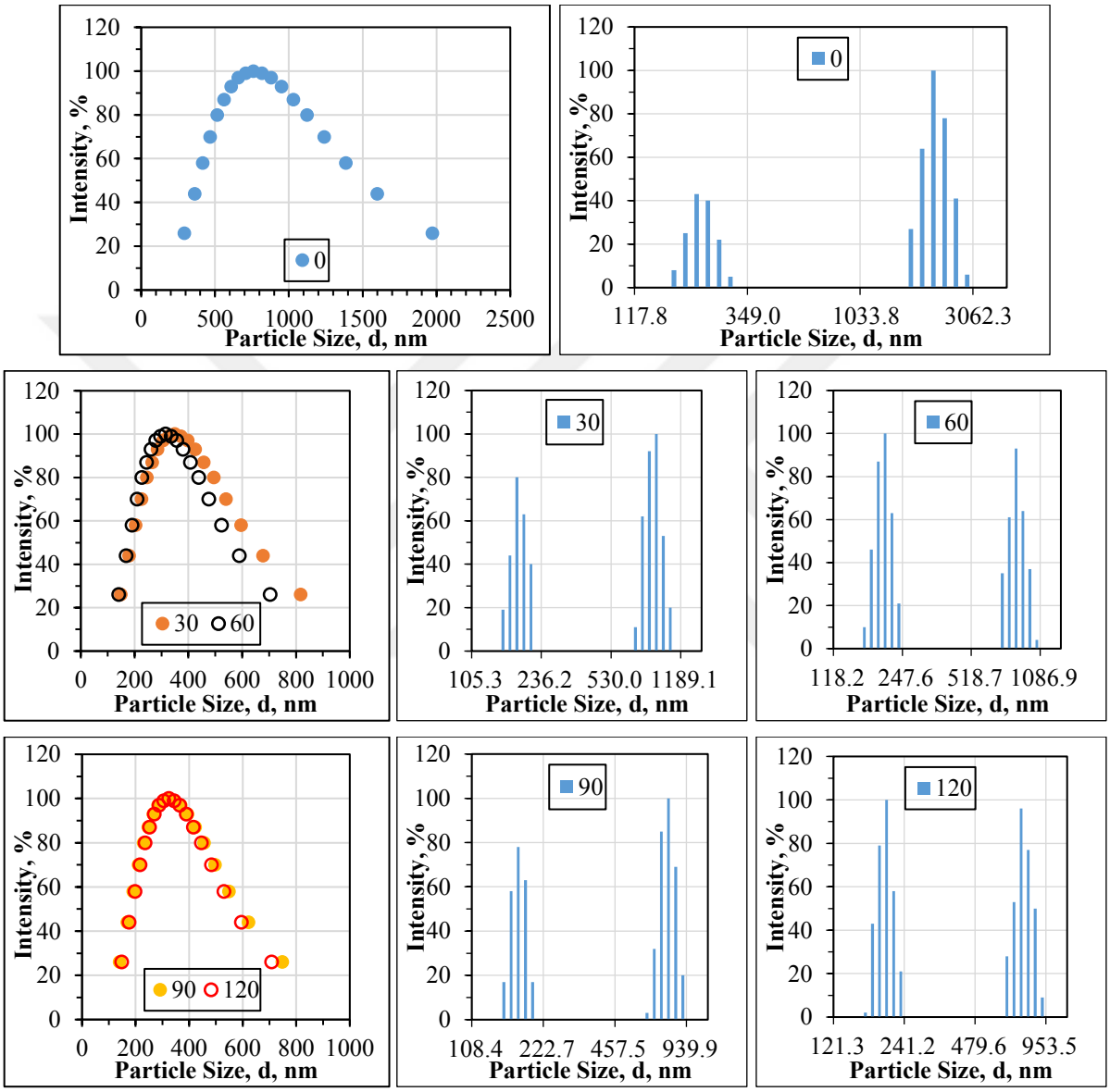


Figure 4.202. "Fe-TiO_2 and HA_{pho}" binary system following photolysis of organic matter intensity profile: Time dependent comparative presentation of log Normal distribution and multi-size distribution of "Fe-TiO_2 and HA_{pho}" binary system following photolysis of organic matter.

Table 4.127. Polydispersity of "Fe-TiO_2 and HA_{pho}" binary system following photolysis of organic matter.

Fe-TiO_2 and HA	Polydispersity				
	0	30	60	90	120
	0.398	0.308	0.269	0.297	0.254

4.1.6.18. "Fe-TiO_2 and HA_{pho}" binary system following photolysis of organic matter volume profile.

As described for "N-TiO_2 and HA_{pho}" binary system following photolysis of organic matter volume profile (Figure 4.187), a similar approach was followed for "Fe-TiO_2 and HA_{pho}" binary system following photolysis of organic matter. Time dependent logN distribution G(d) and multi size distribution C(d) of "Fe-TiO_2 and HA_{pho}" binary system following photolysis of organic matter volume profile was presented in Figure 4.203.

Time dependent mean diameter, range and min-max diameter difference with respect to log normal and multi-size distribution of "Fe-TiO_2 and HA_{pho}" binary system following photolysis of organic matter volume profile was given in Table 4.128.

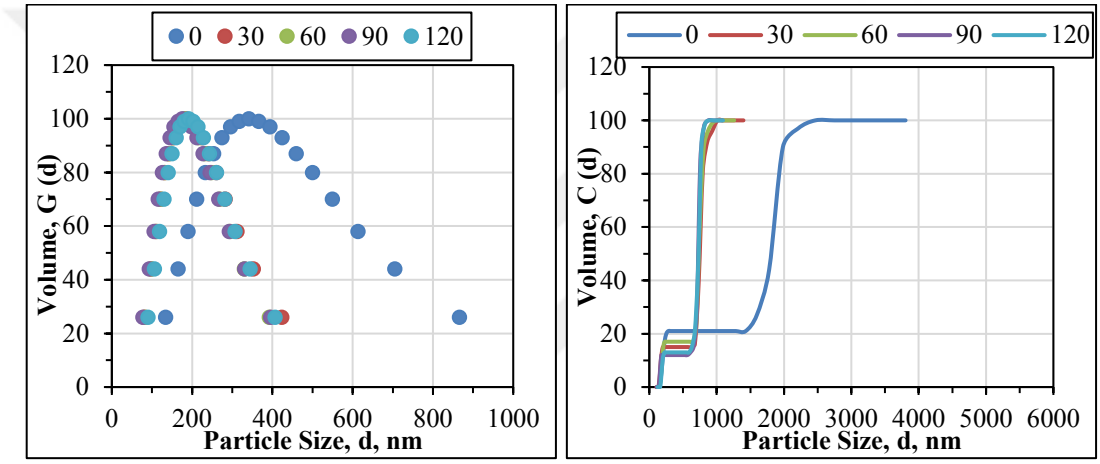


Figure 4.203. "Fe-TiO_2 and HA_{pho}" binary system following photolysis of organic matter volume profile: Time dependent logN distribution G(d) and multi size distribution C(d).

Table 4.128. "Fe-TiO_2 and HA_{pho}" binary system following photolysis of organic matter volume profile: Time dependent mean diameter, range and min-max diameter difference with respect to log normal and multi-size distribution.

Fe-TiO_2 and HA	time, min				
	0	30	60	90	120
Log Normal distribution					
Mean, nm	341.3	185.1	180.6	175.6	191.3
Range	134.5-866.5	80.9-423.4	83.1-392.4	77.9-395.8	90.0-406.7
Difference	732.0	342.5	309.3	317.9	316.7
Multi-size distribution					
Max 1, nm	202.8	171.0	184.2	166.9	196.3
Max 2, nm	1983.4	793.9	198.3	757.3	775.9
Max 3, nm	-	-	750.9	-	-
Range	117.8-3805.2	105.3-1397.7	118.2-1260.3	108.4-1085.5	121.3-1094.0
Difference	3687.4	1292.4	1142.1	977.1	972.7

In terms of volume profile, it could be inferred that hydrodynamic particle size of "Fe-TiO_2 and HA_{pho}" binary system that was performed by succeeding photolysis of organic matter displayed a rapid decrease following initial period of time. Initial hydrodynamic particle size of the "Fe-TiO_2 and HA_{pho}" binary system was recorded as 341.3 nm and decreased to 185.1 nm upon 30 min. According to particle size log normal distribution, initial size difference between max and min hydrodynamic diameter was observed as 732.0 nm. Upon 30 min, roughly 50 % decrease was observed in size difference and detected to 342.5 nm. Upon further 60 min duration, continuously decreasing trend was monitored until the end of 120 min period. In terms of volume profile multi-size distribution, two peaks (at around 202.8 nm and 1983.4 nm, respectively) were observed until 60 min. Upon 60 min, three max diameters were monitored, and two max diameters remained until the end of 120 min. Considering multi-size distribution, size difference revealed a sharp decrease following initial period of time. Initial size difference was recorded as 3687.4 nm and detected to 972.7 nm at the end of 120 min.

For comparison purposes, it could be deduced that lower hydrodynamic particle sizes were observed for "Fe-TiO_2 and HA_{pho}" binary system following photolysis of organic matter contrary to "Fe-TiO_2 and HA" binary system under "as-is" conditions (Table 4.66) over period of 120 min. Hydrodynamic particle size of "Fe-TiO_2 and HA" binary system under "as-is" conditions displayed variations between 764.4 nm and 315.7 nm along 120 min. However, under the specified conditions following photolysis of organic matter conditions represented by volume profile, hydrodynamic particle size variations were attained between 341.3 nm and 191.3 nm over period of 120 min. On the other hand, in terms of log normal distribution, size differences of "Fe-TiO_2 and HA_{pho}" binary system following photolysis of organic matter and "Fe-TiO_2 and HA" binary system under "as-is" conditions revealed similar tendencies with respect to time. It could be asserted that size difference revealed more than 50 % decrease until the end of 120 min period.

Nevertheless, considering volume profile multi-size distribution, initially two max diameters as mentioned 202.8 nm and 1983.4 nm were obtained for "Fe-TiO_2 and HA_{pho}" binary system following photolysis of organic matter whereas three max diameters were attained for "Fe-TiO_2 and HA" binary system under "as-is" conditions (Table 4.66).

It could be inferred that the role of photolytic treatment of HA resulted in diverse particle size distribution profiles of binary systems composed of Fe-TiO_2 in relation to the structural changes of humic fractions rather than the type of the doping of TiO_2.

Time dependent comparative presentation of log Normal distribution and multi-size distribution of "Fe-TiO_2 and HA_{pho}" binary system following photolysis of organic matter volume profile was displayed in Figure 4.204.

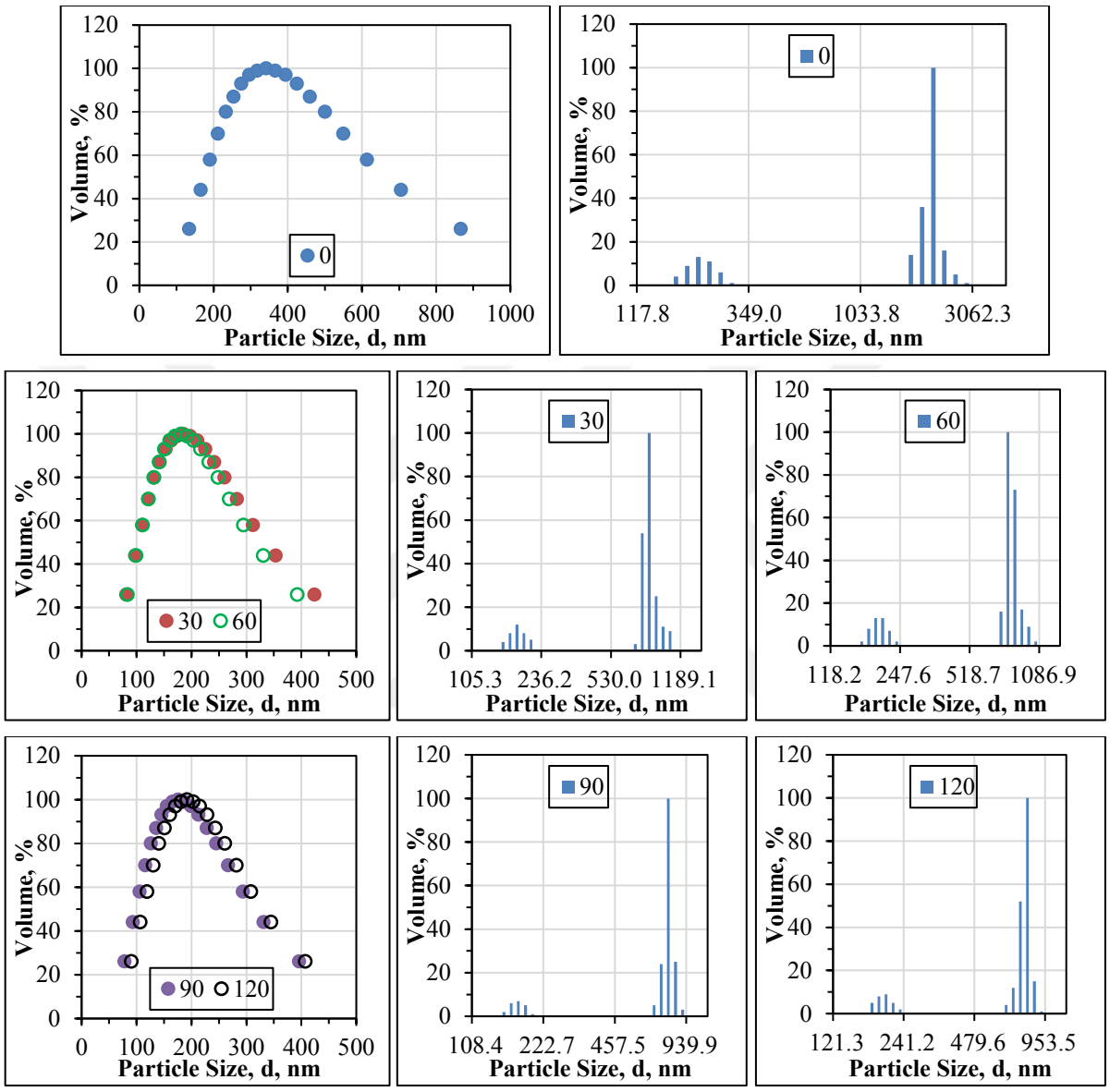


Figure 4.204. "Fe-TiO_2 and HA_{pho}" binary system following photolysis of organic matter volume profile: Time dependent comparative presentation of log Normal distribution and multi-size distribution of "Fe-TiO_2 and HA_{pho}" binary system following photolysis of organic matter.

As previously explained in the aforementioned sections along with the intensity and volume profile evaluation of "Fe-TiO_2 and HA_{pho}" binary system upon exposure to irraditaion of organic matter selected as HA, the system was further assessed in terms of surface area profiles under the specified experimental conditions.

4.1.6.19. "Fe-TiO_2 and HA_{pho}" binary system following photolysis of organic matter surface area profile. In a similar manner to data described "Fe-TiO_2 and HA_{pho}" binary system following photolysis of organic matter volume profile (Figure 4.203), time dependent logN distribution G(d) and multi size distribution C(d) of "Fe-TiO_2 and HA_{pho}" binary system following photolysis of organic matter surface area profile was demonstrated in Figure 4.205. Time dependent mean diameter, range and min-max diameter difference with respect to log normal and multi-size distribution of "Fe-TiO_2 and HA_{pho}" binary system following photolysis of organic matter surface area profile was exhibited in Table 4.129.

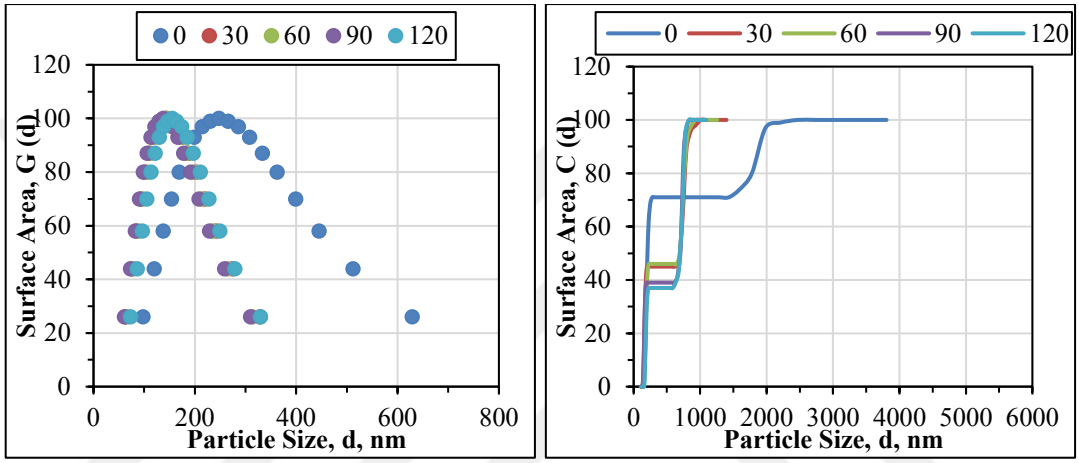


Figure 4.205. "Fe-TiO_2 and HA_{pho}" binary system following photolysis of organic matter surface area profile: Time dependent logN distribution G(d) and multi size distribution C(d).

Table 4.129. "Fe-TiO_2 and HA_{pho}" binary system following photolysis of organic matter surface area profile: Time dependent mean diameter, range and min-max diameter difference with respect to log normal and multi-size distribution.

Fe-TiO_2 and HA	time, min				
	0	30	60	90	120
Log Normal distribution					
Mean, nm	247.7	143.8	144.5	137.5	155.1
Range	97.6-628.8	62.9-328.8	66.5-314.1	61.0-310.1	72.9-329.6
Difference	531.2	265.9	247.6	249.1	256.7
Multi-size distribution					
Max 1, nm	202.8	171.0	184.2	166.9	196.3
Max 2, nm	1983.4	793.9	750.9	757.3	775.9
Range	117.8-3805.2	105.3-1397.7	118.2-1260.3	108.4-1085.5	121.3-1094.0
Difference	3687.4	1292.4	1142.1	977.1	972.7

According to log normal distribution and in terms of surface area profile, it could be deduced that approximately 40 % decrease was monitored in hydrodynamic particle size of "Fe-TiO_2 and

HA_{pho}" binary system following photolysis of organic matter until 30 min. Initial hydrodynamic particle size was recorded as 247.7 nm and decreased to 143.8 nm during 30 min. Upon 30 min, slight variations were observed until the end of 120 min. Size difference revealed drastic changes along 120 min, initial size difference was monitored as 531.2 nm and detected to 256.7 at the end of 120 min period. For comparison purposes, considering multi-size distribution, it could be deduced that two max diameters were attained along 120 min period.

Time dependent comparative presentation of log Normal distribution and multi-size distribution of "Fe-TiO_2 and HA_{pho}" binary system following photolysis of organic matter surface area profile was presented in Figure 4.206.

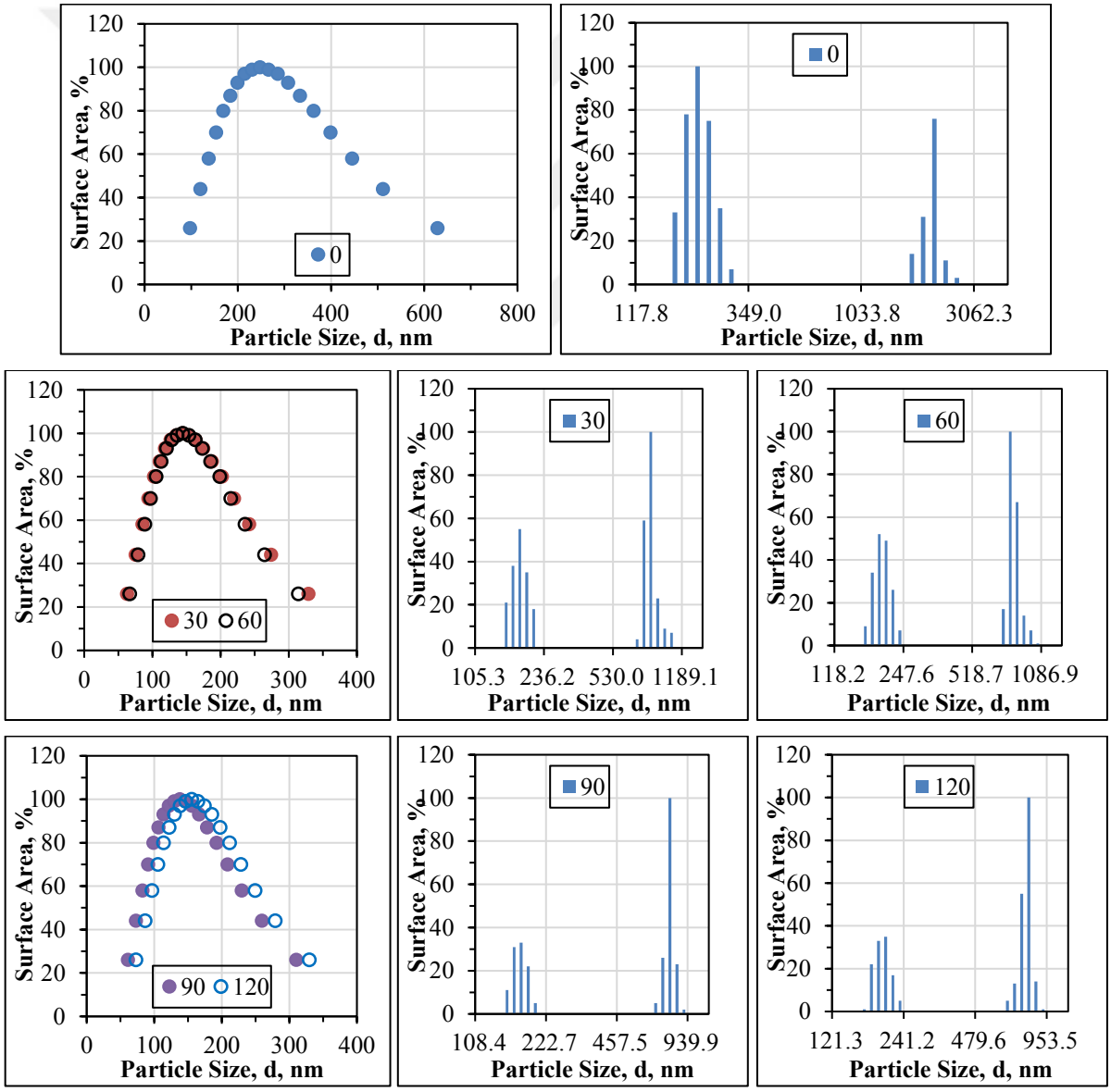


Figure 4.206. "Fe-TiO_2 and HA_{pho}" binary system following photolysis of organic matter surface area profile: Time dependent comparative presentation of log Normal distribution and multi-size distribution of "Fe-TiO_2 and HA_{pho}" binary system following photolysis of organic matter.

4.1.6.20. "Fe-TiO_2 and HA_{pho}" binary system following photolysis of organic matter number profile. Likewise expressed so far, time dependent logN distribution G(d) and multi size distribution C(d) of "Fe-TiO_2 and HA_{pho}" binary system following photolysis of organic matter number profile was demonstrated in Figure 4.207. Accordingly, time dependent mean diameter, range and min-max diameter difference with respect to log normal and multi-size distribution of "Fe-TiO_2 and HA_{pho}" binary system following photolysis of organic matter number profile was demonstrated in Table 4.130.

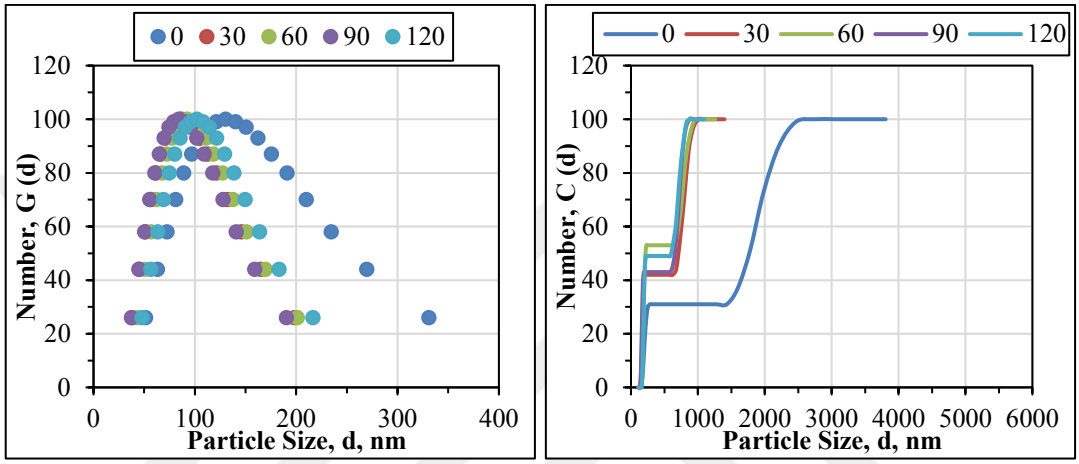


Figure 4.207. "Fe-TiO_2 and HA_{pho}" binary system following photolysis of organic matter number profile: Time dependent logN distribution G(d) and multi size distribution C(d).

Table 4.130. "Fe-TiO_2 and HA_{pho}" binary system following photolysis of organic matter number profile: Time dependent mean diameter, range and min-max diameter difference with respect to log normal and multi-size distribution.

Fe-TiO_2 and HA	time, min				
	0	30	60	90	120
Log Normal distribution					
Mean, nm	130.4	86.7	92.6	84.4	101.9
Range	51.4-331.1	37.9-198.3	42.6-201.2	37.4-190.3	47.9-216.5
Difference	279.7	160.4	158.6	152.9	168.6
Multi-size distribution					
Max 1, nm	202.8	171.0	198.3	166.9	196.3
Max 2, nm	1983.4	860.7	808.5	757.3	724.4
Range	117.8-3805.2	105.3-1397.7	118.2-1260.3	108.4-1085.5	121.3-1094.0
Difference	3687.4	1292.4	1142.1	977.1	972.7

In terms of number profile, hydrodynamic particle size of "Fe-TiO_2 and HA_{pho}" binary system following photolysis of organic matter was attained as 130.4 nm. Upon 30 min, approximately 35 % decrease was monitored and slight variations remained until the end of 120 min. On the other hand,

in the first 30 min, roughly 40 % decrease was observed in size difference between max and min diameter. Initial size difference was obtained as 279.7 nm and detected to 160.4 nm in the first 30 min. Upon 30 min, minor variations were observed until the end of 120 min. For comparison purposes, in terms of multi-size distribution, two max diameters were obtained along 120 min. Also, according to multi-size distribution, size difference was attained between 3687.4 nm and 972.7 nm along 120 min period.

Time dependent comparative presentation of log Normal distribution and multi-size distribution of "Fe-TiO_2 and HA_{pho}" binary system following photolysis of organic matter number profile was displayed in Figure 4.208.

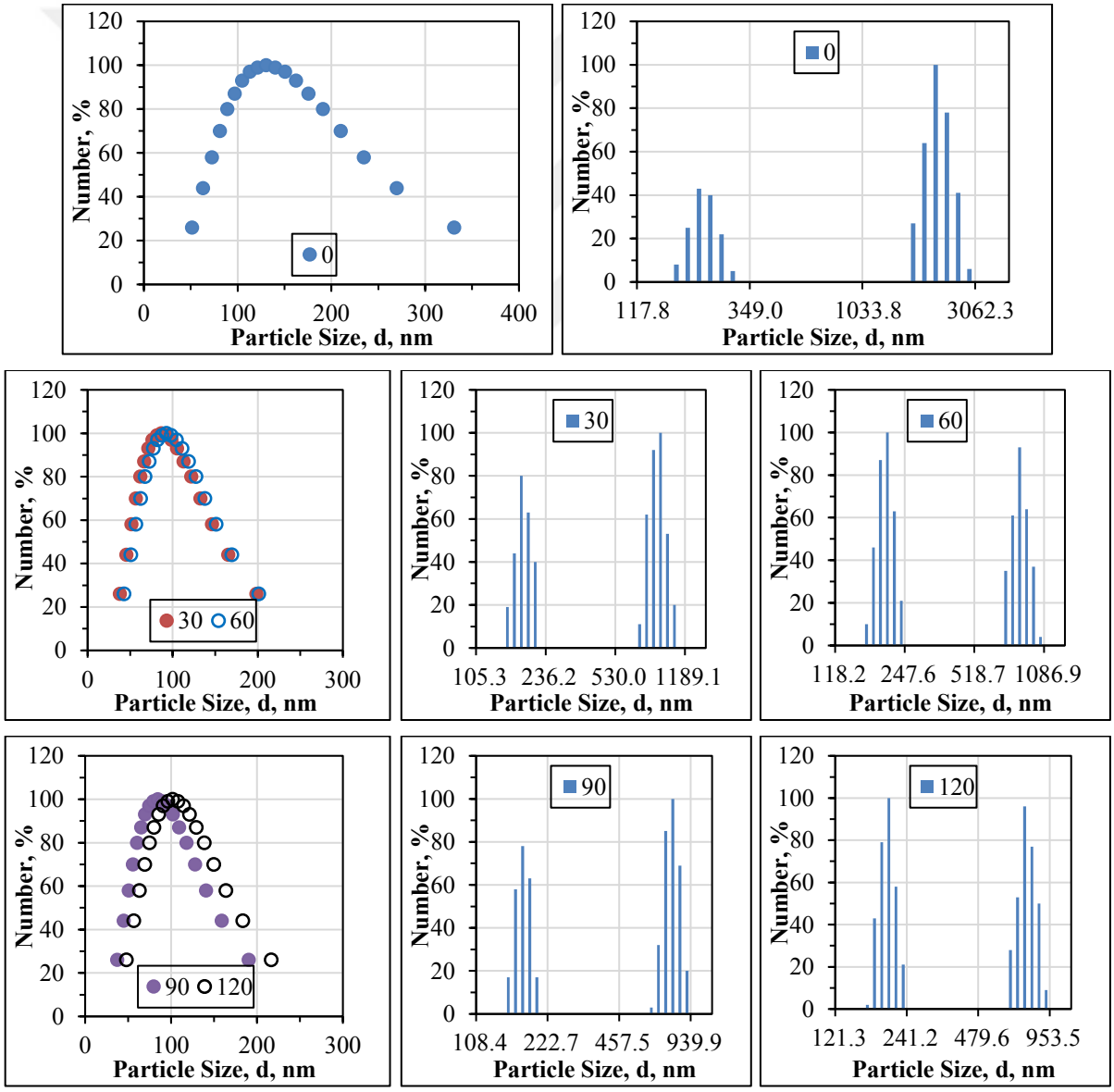


Figure 4.208. "Fe-TiO_2 and HA_{pho}" binary system following photolysis of organic matter number profile: Time dependent comparative presentation of log Normal distribution and multi-size distribution of "Fe-TiO_2 and HA_{pho}" binary system following photolysis of organic matter.

4.1.6.21. "Fe-TiO_2 and $SRNOM_{pho}$" binary system following photolysis of organic matter intensity profile. Time dependent logN distribution G(d) and multi size distribution C(d) of "Fe-TiO_2 and $SRNOM_{pho}$" binary system following photolysis of organic matter intensity profile was displayed in Figure 4.209. Time dependent mean diameter, range and min-max diameter difference with respect to log normal and multi-size distribution of "Fe-TiO_2 and $SRNOM_{pho}$" binary system following photolysis of organic matter intensity profile was demonstrated in Table 4.131.

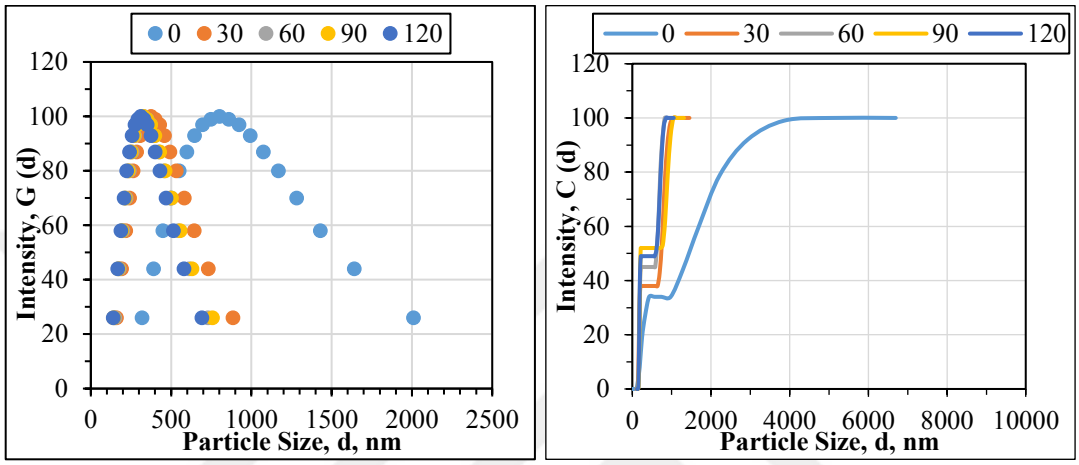


Figure 4.209. "Fe-TiO_2 and $SRNOM_{pho}$" binary system following photolysis of organic matter intensity profile: Time dependent logN distribution G(d) and multi size distribution C(d).

Table 4.131. "Fe-TiO_2 and $SRNOM_{pho}$" binary system following photolysis of organic matter intensity profile: Time dependent mean diameter, range and min-max diameter difference with respect to log normal and multi-size distribution.

Fe-TiO_2 and SRNOM	time, min				
	0	30	60	90	120
Log Normal distribution					
Mean, nm	801.7	375.4	330.4	328.4	311.3
Range	319.7-2010.0	159.2-885.3	149.7-729.4	142.4-757.4	140.1-691.8
Difference	1690.3	726.1	579.7	615.0	551.7
Multi-size distribution					
Max 1, nm	246.1	173.4	190.7	197.7	188.9
Max 2, nm	2226.5	819.3	717.0	899.3	746.6
Range	1.0-6696.5	106.2-1451.7	117.1-1089.4	116.3-1313.4	116.7-1052.8
Difference	6695.5	1345.5	972.3	1197.1	936.1

Initial hydrodynamic size of "Fe-TiO_2 and $SRNOM_{pho}$" following photolysis of organic matter was detected as 801.7 nm. Upon 30 min, a sharp decrease was observed and remained until 120 min. Considering multi-size distribution, two peaks were observed along 120 min. Time dependent comparative presentation of log Normal distribution and multi-size distribution of "Fe-TiO_2 and

SRNOM$_{pho}$" binary system following photolysis of organic matter intensity profile was given in Figure 4.210. Polydispersity of "Fe-TiO$_2$ and SRNOM$_{pho}$" binary system following photolysis of organic matter was demonstrated in Table 4.132, an average value of 0.300 could be regarded as suitable.

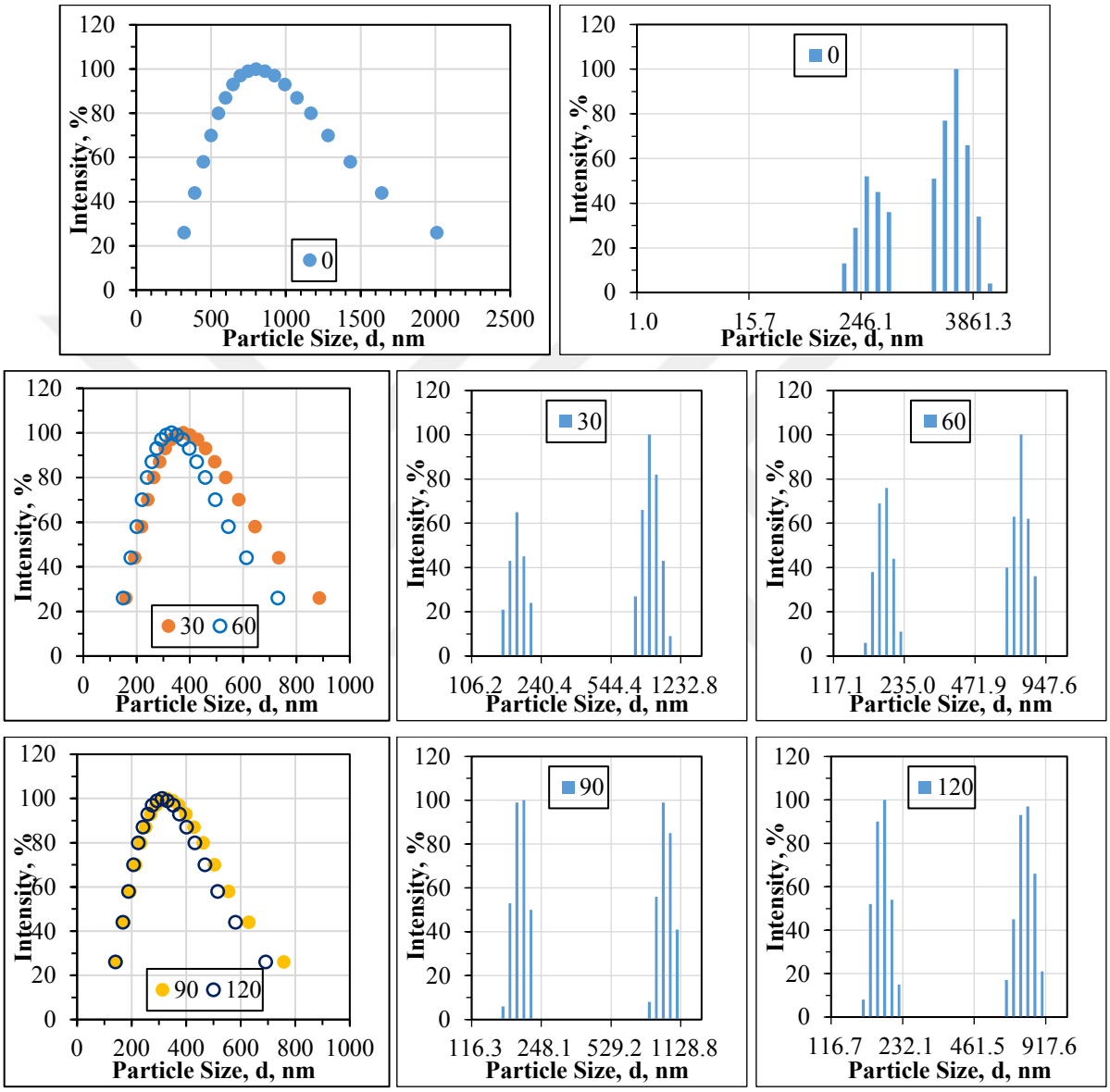


Figure 4.210. "Fe-TiO$_2$ and SRNOM$_{pho}$" binary system following photolysis of organic matter intensity profile: Time dependent comparative presentation of log Normal distribution and multi-size distribution of "Fe-TiO$_2$ and SRNOM$_{pho}$" binary system following photolysis of organic matter.

Table 4.132. Polydispersity of "Fe-TiO$_2$ and SRNOM$_{pho}$" binary system following photolysis of organic matter.

Fe-TiO$_2$ and SRNOM	Polydispersity				
	0	30	60	90	120
	0.366	0.313	0.261	0.295	0.266

4.1.6.22. "Fe-TiO_2 and $SRNOM_{pho}$" binary system following photolysis of organic matter volume profile. Time dependent logN distribution G(d) and multi size distribution C(d) of "Fe-TiO_2 and $SRNOM_{pho}$" binary system following photolysis of organic matter volume profile was shown in Figure 4.211. Time dependent mean diameter, range and min-max diameter difference with respect to log normal and multi-size distribution of "Fe-TiO_2 and $SRNOM_{pho}$" binary system following photolysis of organic matter volume profile was exhibited in Table 4.133.

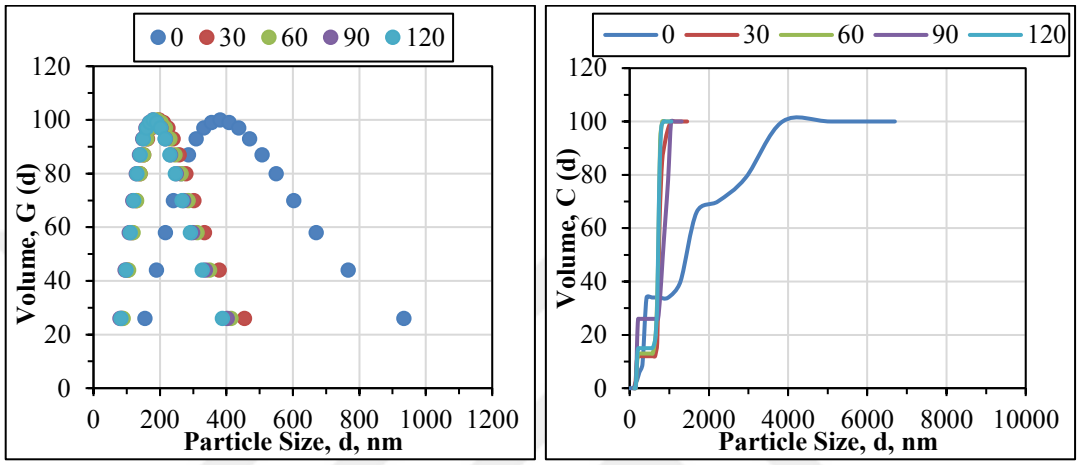


Figure 4.211. "Fe-TiO_2 and $SRNOM_{pho}$" binary system following photolysis of organic matter volume profile: Time dependent logN distribution G(d) and multi size distribution C(d).

Table 4.133. "Fe-TiO_2 and $SRNOM_{pho}$" binary system following photolysis of organic matter volume profile: Time dependent mean diameter, range and min-max diameter difference with respect to log normal and multi-size distribution.

Fe-TiO_2 and SRNOM	time, min				
	0	30	60	90	120
Log Normal distribution					
Mean, nm	381.1	197.6	192.7	179.1	179.8
Range	155.4-934.7	85.9-454.7	89.8-413.7	79.6-402.6	83.2-388.6
Difference	779.3	368.8	323.9	323.0	305.4
Multi-size distribution					
Max 1, nm	426.8	173.4	177.8	183.3	176.3
Max 2, nm	1690.7	755.0	190.7	833.7	188.9
Max 3, nm	3861.3	-	768.8	1046.4	746.6
Range	1.0-6696.5	106.2-1451.7	117.1-1089.4	116.3-1313.4	116.7-1052.8
Difference	6695.5	1345.5	972.3	1197.1	936.1

Considering log normal distribution, initial hydrodynamic particle size of "Fe-TiO_2 and $SRNOM_{pho}$" binary system following photolysis of organic matter was observed as 381.1 nm. Upon 30 min, roughly 50 % decrease was monitored and hydrodynamic size was detected as 197.6 nm. On

the other hand, it could be asserted that hydrodynamic size difference decreased from 779.3 nm to 305.4 nm according to time variations. For comparison purposes, in terms of multi-size distribution it could also be deduced that three peaks were monitored as 426.8 nm, 1690.7 nm, and 3861.3 nm for "Fe-TiO_2 and $SRNOM_{pho}$" binary system following photolysis of organic matter following initial period of time. Upon 30 min, two max diameters were obtained as 173.4 nm and 755.0 nm. Also, hydrodynamic size difference was attained between 6695.5 nm and 936.1 nm with respect to time.

Time dependent comparative presentation of log Normal distribution and multi-size distribution of "Fe-TiO_2 and $SRNOM_{pho}$" binary system following photolysis of organic matter volume profile was displayed in Figure 4.212.

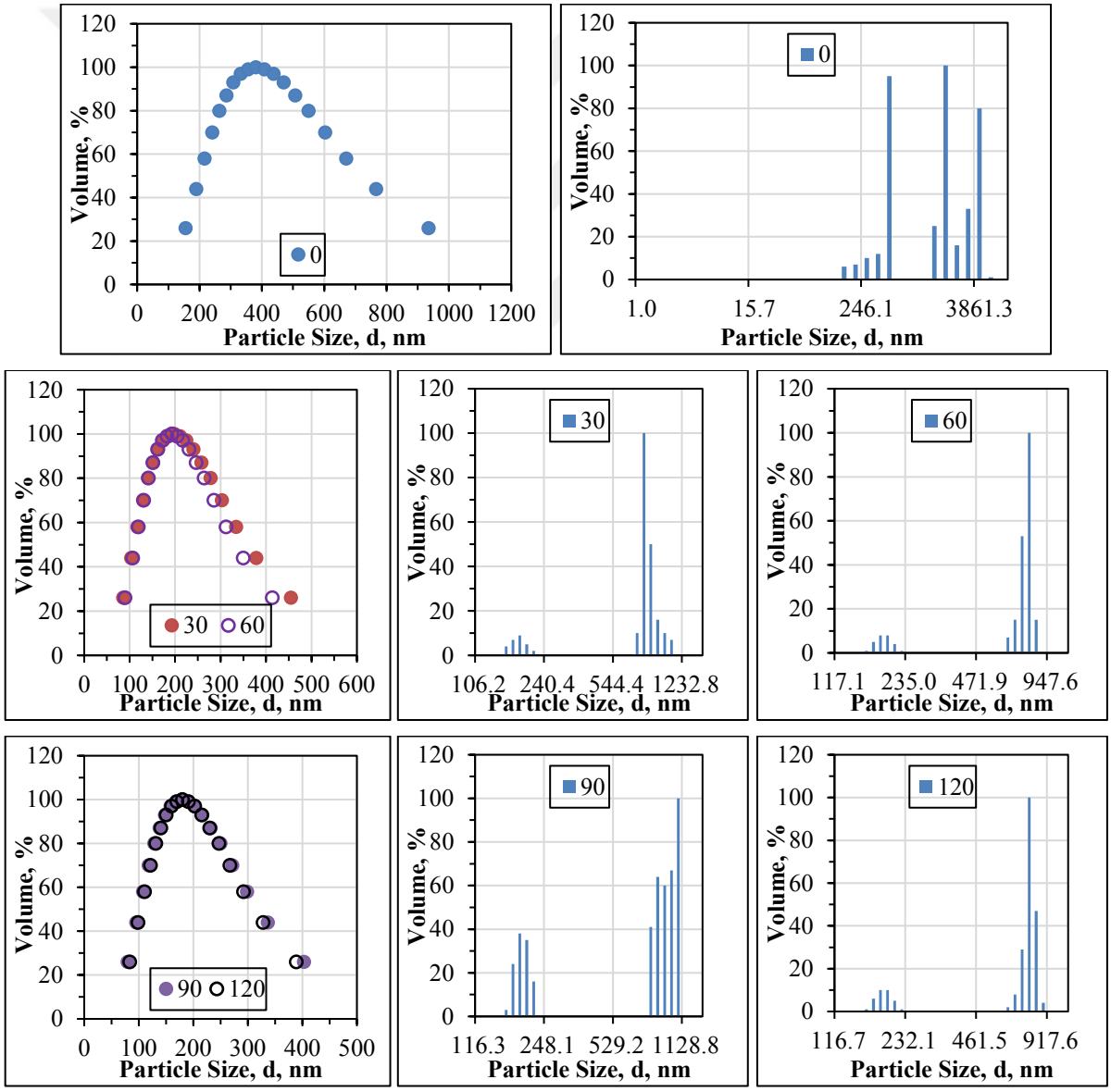


Figure 4.212. "Fe-TiO_2 and $SRNOM_{pho}$" binary system following photolysis of organic matter volume profile: Time dependent comparative presentation of log Normal distribution and multi-size distribution of "Fe-TiO_2 and $SRNOM_{pho}$" binary system following photolysis of organic matter.

4.1.6.23. "Fe-TiO_2 and $SRNOM_{pho}$" binary system following photolysis of organic matter surface area profile. In a similar manner to data depicted "Fe-TiO_2 and $SRNOM_{pho}$" binary system following photolysis of organic matter volume profile (Figure 4.211), time dependent logN distribution G(d) and multi size distribution C(d) of "Fe-TiO_2 and $SRNOM_{pho}$" binary system following photolysis of organic matter surface area profile was exhibited in Figure 4.213. Time dependent mean diameter, range and min-max diameter difference with respect to log normal and multi-size distribution of "Fe-TiO_2 and $SRNOM_{pho}$" binary system following photolysis of organic matter surface area profile was presented in Table 4.134.

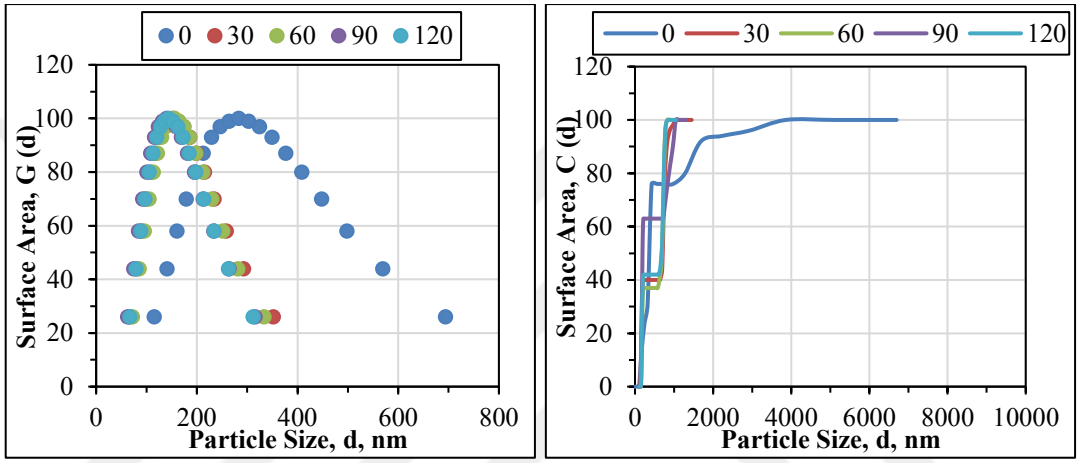


Figure 4.213. "Fe-TiO_2 and $SRNOM_{pho}$" binary system following photolysis of organic matter surface area profile: Time dependent logN distribution G(d) and multi size distribution C(d).

Table 4.134. "Fe-TiO_2 and $SRNOM_{pho}$" binary system following photolysis of organic matter surface area profile: Time dependent mean diameter, range and min-max diameter difference with respect to log normal and multi-size distribution.

Fe-TiO_2 and SRNOM	time, min				
	0	30	60	90	120
Log Normal distribution					
Mean, nm	283.0	152.9	155.3	140.5	144.3
Range	115.4-694.2	66.4-351.8	72.4-333.5	62.5-315.9	66.8-312.0
Difference	578.8	285.4	261.1	253.4	245.2
Multi-size distribution					
Max 1, nm	141.9	173.4	177.8	183.3	176.3
Max 2, nm	246.1	755.0	768.8	833.7	746.6
Max 3, nm	426.8	-	-	1046.4	-
Max 4, nm	1690.7	-	-	-	-
Max 5, nm	3861.3	-	-	-	-
Range	1.0-6696.5	106.2-1451.7	117.1-1089.4	116.3-1313.4	116.7-1052.8
Difference	6695.5	1345.5	972.3	1197.1	936.1

In terms of surface area profile, hydrodynamic particle size of "Fe-TiO_2 and $SRNOM_{pho}$" binary system following photolysis of organic matter was recorded as 283.0 nm following initial period of time. Upon 30 min, a rapid decrease was monitored and minor variations remained until the end of 120 min. On the other hand, size difference between max and min diameter revealed approximately 50 % decrease in the first 30 min and slight variations were observed until 120 min. However, in terms of multi-size distribution, five peaks were obtained following initial period of time. Upon 30 min, two peaks were monitored until 90 min. Upon 90 min, three peaks were obtained and two peaks were observed upon period of 120 min. Time dependent comparative presentation of log Normal distribution and multi-size distribution of "Fe-TiO_2 and $SRNOM_{pho}$" binary system following photolysis of organic matter surface area profile was exhibited in Figure 4.214.

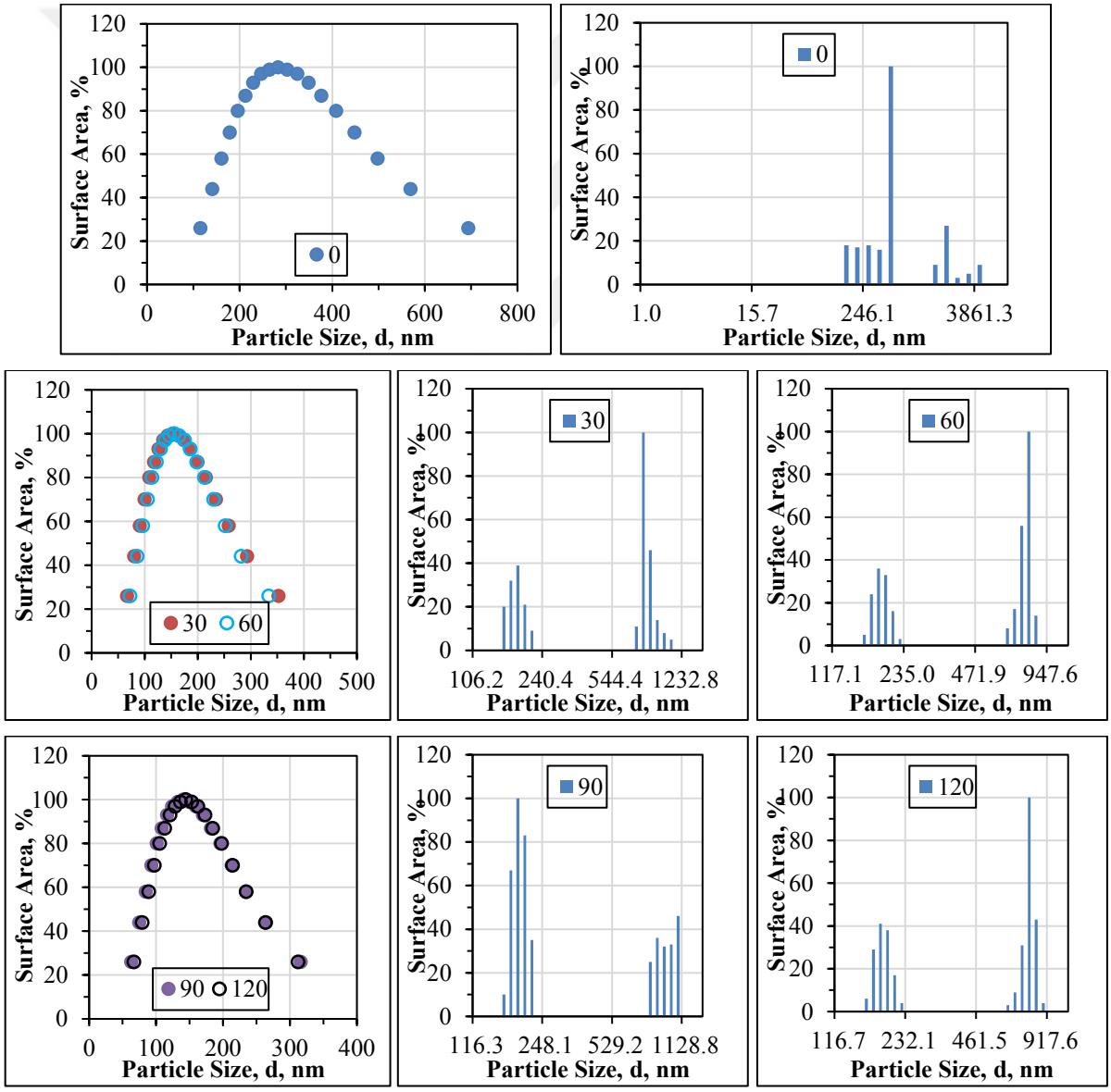


Figure 4.214. "Fe-TiO_2 and $SRNOM_{pho}$" binary system following photolysis of organic matter surface area profile: Time dependent comparative presentation of log Normal distribution and multi-size distribution of "Fe-TiO_2 and $SRNOM_{pho}$" binary system following photolysis of organic matter.

4.1.6.24. "Fe-TiO_2 and $SRNOM_{pho}$" binary system following photolysis of organic matter number profile. Time dependent logN distribution G(d) and multi size distribution C(d) of "Fe-TiO_2 and $SRNOM_{pho}$" binary system following photolysis of organic matter number profile was demonstrated in Figure 4.215. Time dependent mean diameter, range and min-max diameter difference with respect to log normal and multi-size distribution of "Fe-TiO_2 and $SRNOM_{pho}$" binary system following photolysis of organic matter number profile was given in Table 4.135.

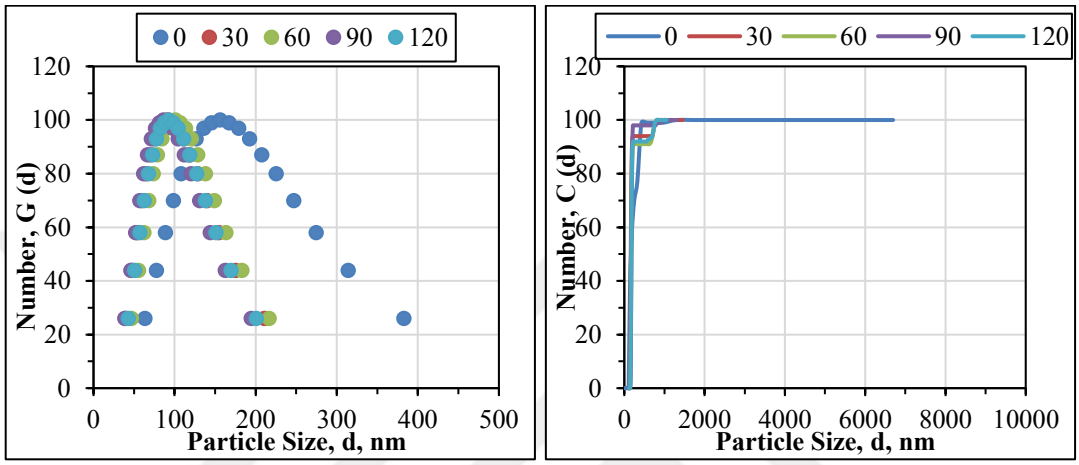


Figure 4.215. "Fe-TiO_2 and $SRNOM_{pho}$" binary system following photolysis of organic matter number profile: Time dependent logN distribution G(d) and multi size distribution C(d).

Table 4.135. "Fe-TiO_2 and $SRNOM_{pho}$" binary system following photolysis of organic matter number profile: Time dependent mean diameter, range and min-max diameter difference with respect to log normal and multi-size distribution.

Fe-TiO_2 and SRNOM	time, min				
	0	30	60	90	120
Log Normal distribution					
Mean, nm	156.1	91.5	100.9	86.5	93.0
Range	63.6-382.9	39.8-210.6	47.0-216.6	38.5-194.4	43.0-201.1
Difference	319.3	170.8	169.6	155.9	158.1
Multi-size distribution					
Max 1, nm	141.9	173.4	177.8	183.3	176.3
Max 2, nm	426.8	755.0	768.8	833.7	746.6
Max 3, nm	1283.8	-	-	-	-
Max 4, nm	1690.7	-	-	-	-
Range	1.0-6696.5	106.2-1451.7	117.1-1089.4	116.3-1313.4	116.7-1052.8
Difference	6695.5	1345.5	972.3	1197.1	936.1

According to number profile, it could be deduced that hydrodynamic particle size of "Fe-TiO_2 and $SRNOM_{pho}$" binary system following photolysis of organic matter displayed a fluctuating trend

according to time variations. In terms of log normal distribution, it could be asserted that initial hydrodynamic particle size was attained as 156.1 nm and detected to 93.0 nm upon 120 min. Based on the presented data, size difference decreased from 319.3 nm to 158.1 nm upon 120 min (Table 4.135). For comparison purposes, in terms of multi-size distribution, initially max diameters as 141.9 nm, 426.8 nm, 1283.8 nm, 1690.7 nm were monitored and two peaks were obtained until the end of 120 min period. In a similar manner to data depicted "Fe-TiO_2 and $SRNOM_{pho}$" binary system following photolysis of organic matter surface area profile (Figure 4.214), time dependent comparative presentation of log Normal distribution and multi-size distribution of "Fe-TiO_2 and $SRNOM_{pho}$" binary system following photolysis of organic matter number profile was given in Figure 4.216.

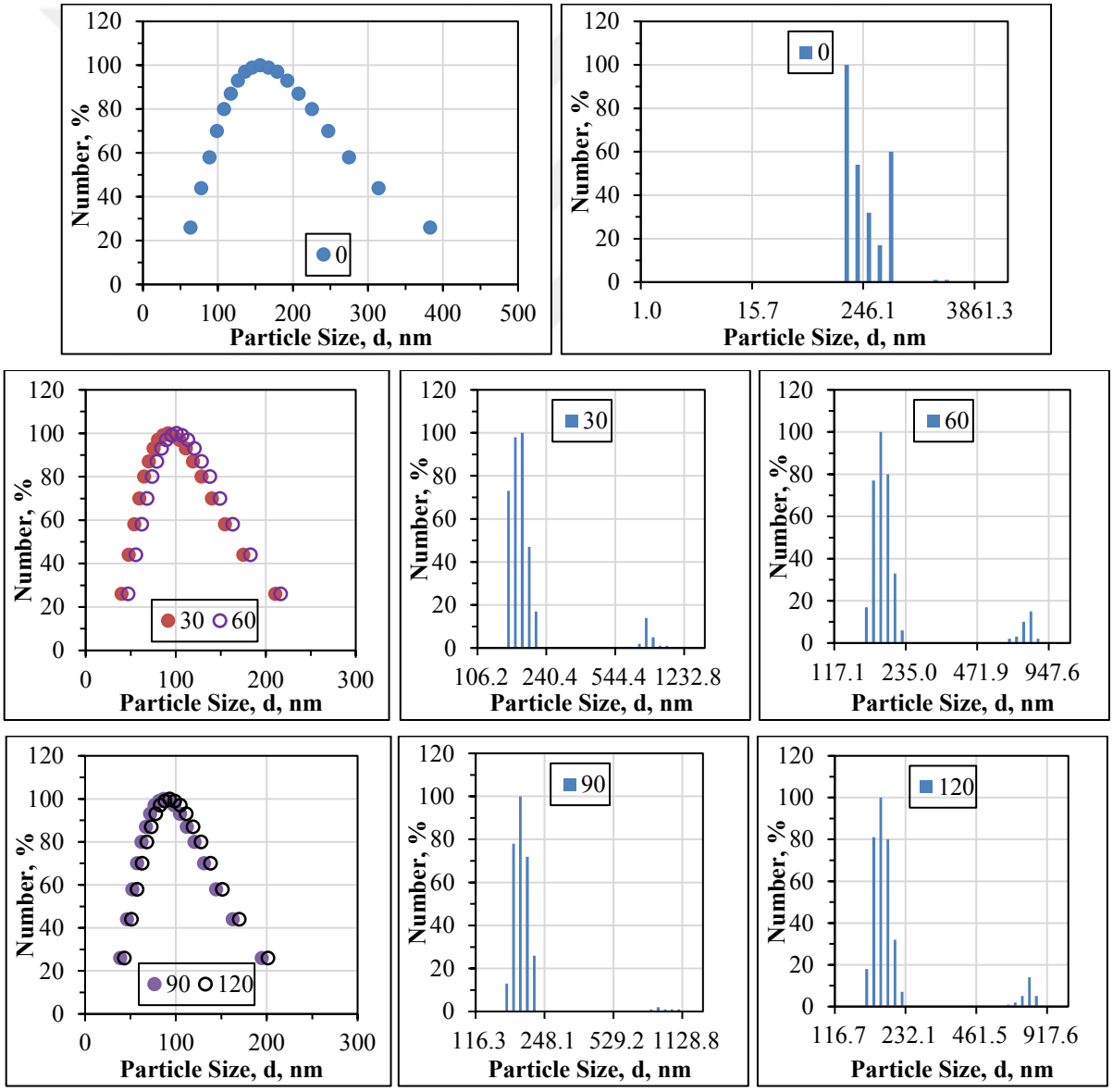


Figure 4.216. "Fe-TiO_2 and $SRNOM_{pho}$" binary system following photolysis of organic matter number profile: Time dependent comparative presentation of log Normal distribution and multi-size distribution of "Fe-TiO_2 and $SRNOM_{pho}$" binary system following photolysis of organic matter.

4.1.7. Binary System: As-is Under Irradiation

As explained for binary system under "as-is" conditions (Section 4.1.4), a similar approach was followed for elucidation of the hydrodynamic size of binary system "as-is" under irradiation.

4.1.7.1. "TiO_2 and HA" binary system "as-is" under irradiation intensity profile. Time dependent logN distribution G(d) and multi size distribution C(d), and time dependent mean diameter, range and min-max diameter difference with respect to log normal and multi-size distribution of "TiO_2 and HA" binary system "as-is" under irradiation intensity profile was presented in Figure 4.217 and Table 4.136, respectively.

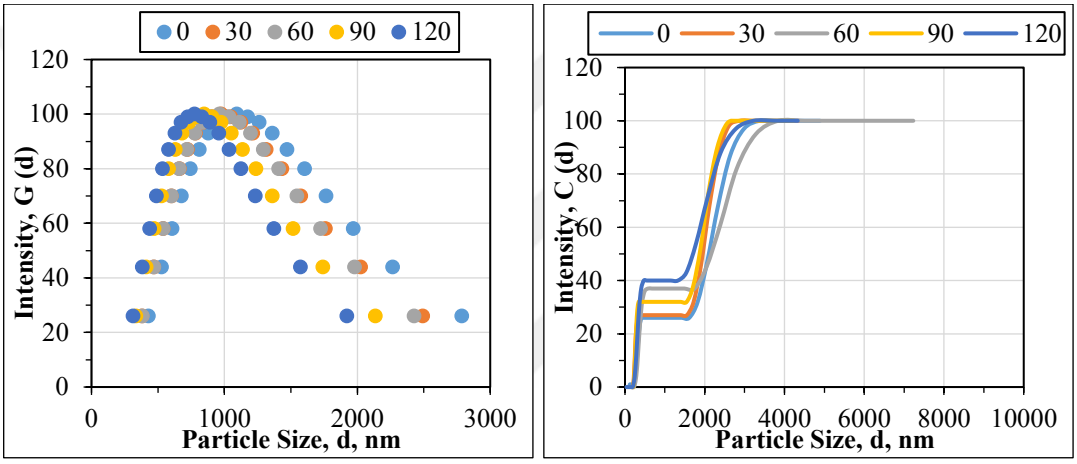


Figure 4.217. "TiO_2 and HA" binary system "as-is" under irradiation intensity profile: Time dependent logN distribution G(d) and multi size distribution C(d).

Table 4.136. "TiO_2 and HA" binary system "as-is" under irradiation intensity profile: Time dependent mean diameter, range and min-max diameter difference with respect to log normal and multi-size distribution.

TiO_2 and HA	time, min				
	0	30	60	90	120
Log Normal distribution					
Mean, nm	1092.9	974.2	964.1	846.5	775.7
Range	428.8-2785.4	380.7-2492.6	382.9-2427.5	335.5-2135.7	313.2-1920.7
Difference	2356.6	2111.9	2044.6	1800.2	1607.5
Multi-size distribution					
Max 1, nm	120.8	268.6	74.0	279.9	59.4
Max 2, nm	324.1	2116.2	359.1	2093.0	350.5
Max 3, nm	2332.4	-	2801.6	-	2068.0
Range	94.4-4889.2	160.3-4358.2	46.0-7230.7	169.3-4232.3	38.1-4332.2
Difference	4794.8	4197.9	7184.7	4063.0	4294.1

Initial hydrodynamic size of "TiO_2 and HA" binary system "as-is" under irradiation was detected as 1092.9 nm. Considering multi-size distribution, initially three peaks were observed. Time dependent comparative presentation of log Normal distribution and multi-size distribution and also polydispersity of "TiO_2 and HA" binary system "as-is" under irradiation was given in Figure 4.218 and Table 4.137, respectively. An average value of 0.373 could be regarded as suitable.

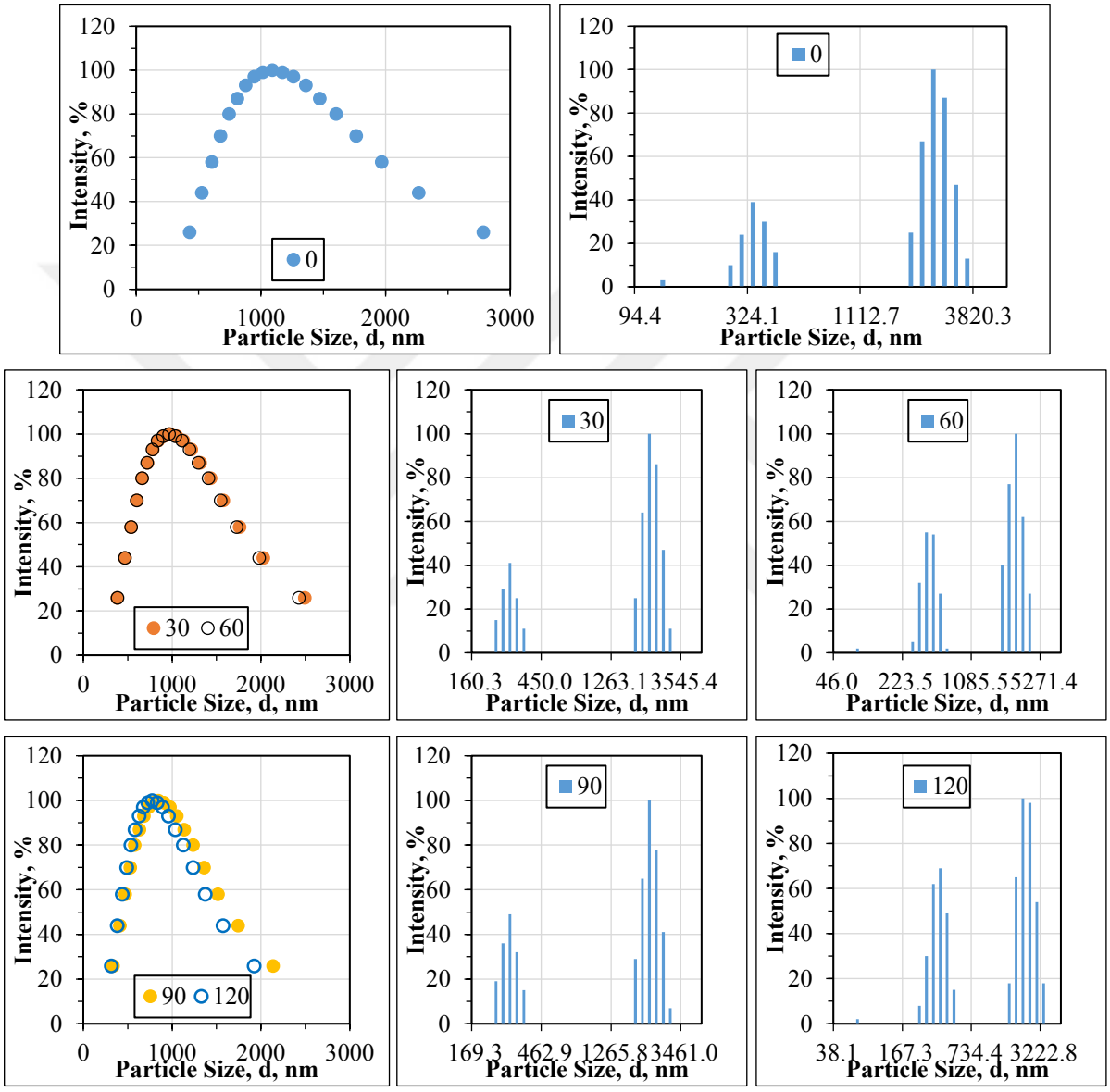


Figure 4.218. "TiO_2 and HA" binary system "as-is" under irradiation intensity profile: Time dependent comparative presentation of log Normal distribution and multi-size distribution of "TiO_2 and HA" binary system "as-is" under irradiation.

Table 4.137. Polydispersity of "TiO_2 and HA" binary system "as-is" under irradiation.

TiO_2 and HA	Polydispersity				
	0	30	60	90	120
	0.382	0.386	0.370	0.372	0.355

4.1.7.2. "TiO_2 and HA" binary system "as-is" under irradiation volume profile. Likewise expressed so far, time dependent logN distribution G(d) and multi size distribution C(d) of "TiO_2 and HA" binary system "as-is" under irradiation volume profile was exhibited in Figure 4.219. Time dependent mean diameter, range and min-max diameter difference with respect to log normal and multi-size distribution of "TiO_2 and HA" binary system "as-is" under irradiation volume profile was presented in Table 4.138.

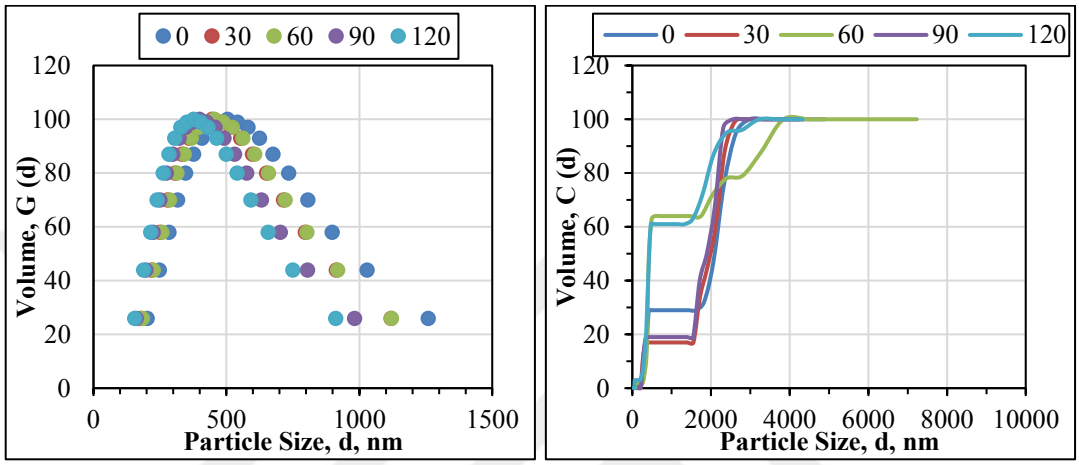


Figure 4.219. "TiO_2 and HA" binary system "as-is" under irradiation volume profile: Time dependent logN distribution G(d) and multi size distribution C(d).

Table 4.138. "TiO_2 and HA" binary system "as-is" under irradiation volume profile: Time dependent mean diameter, range and min-max diameter difference with respect to log normal and multi-size distribution.

TiO_2 and HA	time, min				
	0	30	60	90	120
Log Normal distribution					
Mean, nm	504.9	446.9	454.9	398.0	376.7
Range	202.4-1259.6	178.4-1119.7	184.7-1120.8	161.2-982.6	155.6-912.0
Difference	1057.2	941.3	936.1	821.4	756.4
Multi-size distribution					
Max 1, nm	120.8	268.6	74.0	279.9	59.4
Max 2, nm	414.8	1721.5	420.6	1711.6	406.4
Max 3, nm	2332.4	2346.2	2042.5	2314.5	2068.0
Max 4, nm	-	-	3843.0	-	3222.8
Range	94.4-4889.2	160.3-4358.2	46.0-7230.7	169.3-4232.3	38.1-4332.2
Difference	4794.8	4197.9	7184.7	4063.0	4294.1

In a similar manner to data represented "TiO_2 and HA" binary system "as-is" under irradiation intensity profile (Figure 4.217), log normal distribution G(d) and multi size distribution C(d) of "TiO_2

and HA" binary system "as-is" under irradiation intensity profile was demonstrated according to time variations. It could be seen that hydrodynamic particle size of "TiO_2 and HA" binary system "as-is" under irradiation displayed a rapid decrease following initial period of time and continuous decrease remained until 120 min. Initial hydrodynamic particle size was attained as 504.9 nm and decreased to 376.7 at the end of 120 min. In terms of log normal distribution, size difference revealed a sharp decrease in the first 30 min and continuous decrease was observed until the end of 120 min. However, in terms of multi-size distribution, three peaks were monitored until 60 min. Upon 60 min, four peaks were observed and remained until the end of 120 min. Time dependent comparative presentation of log Normal distribution and multi-size distribution of "TiO_2 and HA" binary system "as-is" under irradiation volume profile was exhibited in Figure 4.220.

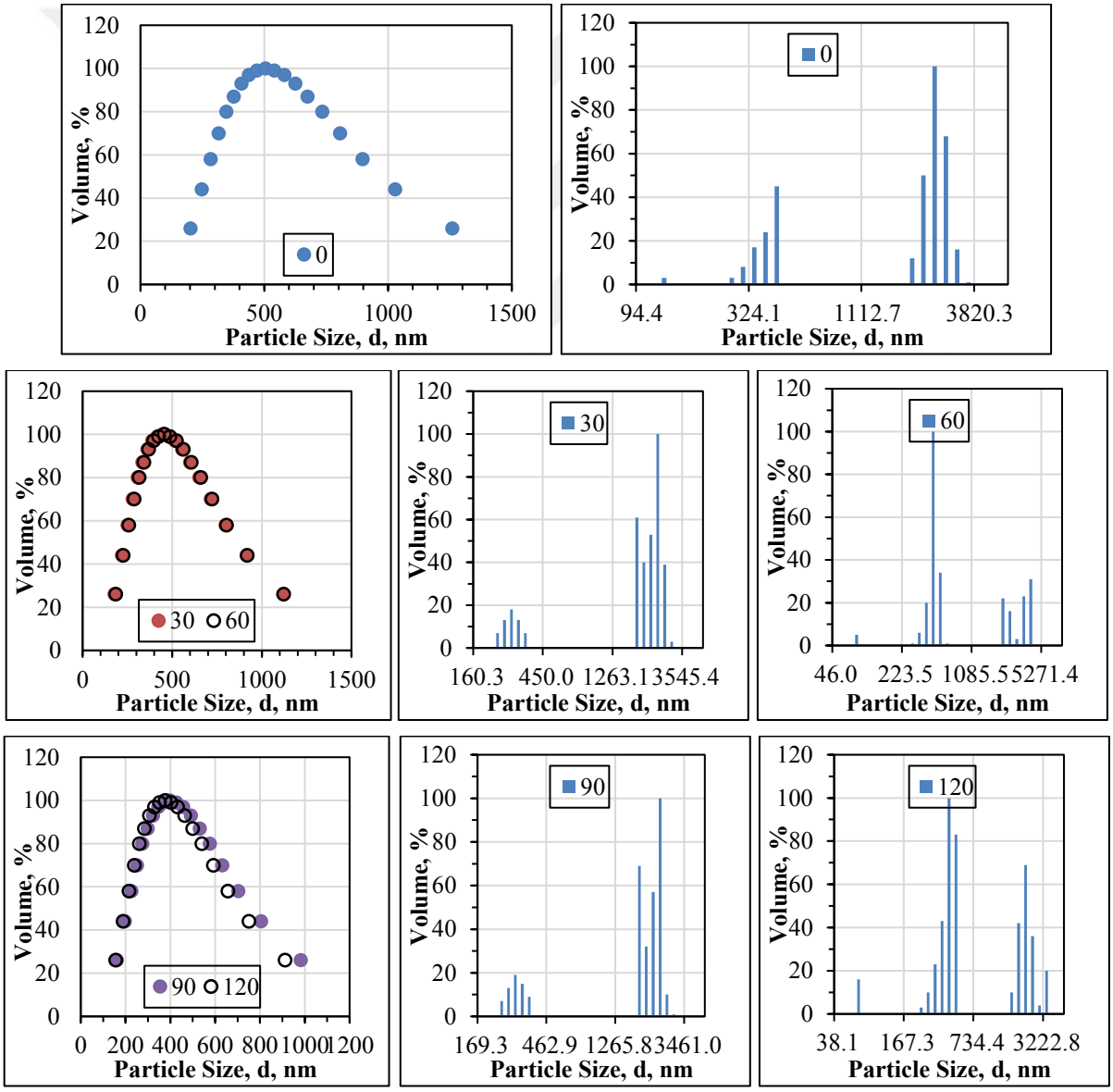


Figure 4.220. "TiO_2 and HA" binary system "as-is" under irradiation volume profile: Time dependent comparative presentation of log Normal distribution and multi-size distribution of "TiO_2 and HA" binary system "as-is" under irradiation.

4.1.7.3. "TiO_2 and HA" binary system "as-is" under irradiation surface area profile. As explained for "TiO_2 and HA" binary system "as-is" under irradiation intensity profile (Figure 4.217) and volume profile (Figure 4.219), a similar approach was followed for "TiO_2 and HA" binary system "as-is" under irradiation surface area profile. Time dependent logN distribution G(d) and multi size distribution C(d) of "TiO_2 and HA" binary system "as-is" under irradiation surface area profile was shown in Figure 4.221. Time dependent mean diameter, range and min-max diameter difference with respect to log normal and multi-size distribution of "TiO_2 and HA" binary system "as-is" under irradiation surface area profile was displayed in Table 4.139.

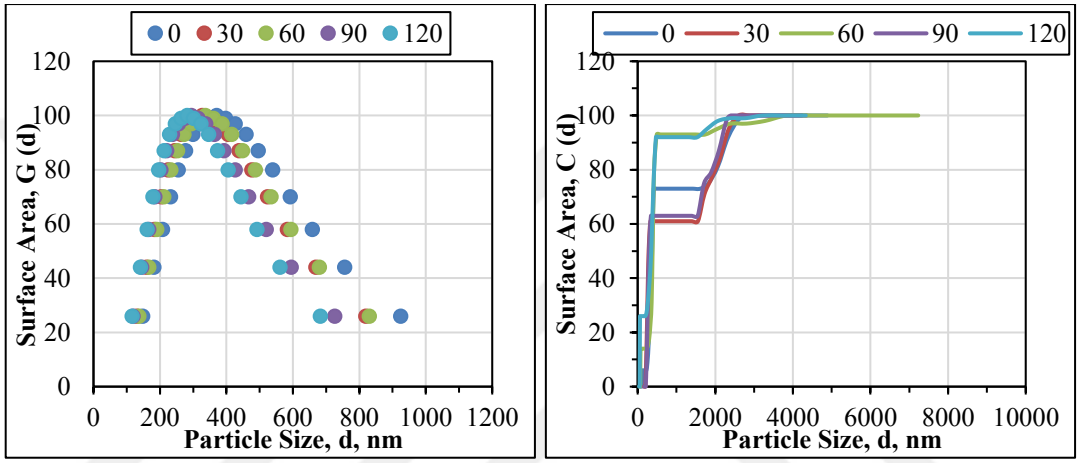


Figure 4.221. "TiO_2 and HA" binary system "as-is" under irradiation surface area profile: Time dependent logN distribution G(d) and multi size distribution C(d).

Table 4.139. "TiO_2 and HA" binary system "as-is" under irradiation surface area profile: Time dependent mean diameter, range and min-max diameter difference with respect to log normal and multi-size distribution.

TiO_2 and HA	time, min				
	0	30	60	90	120
Log Normal distribution					
Mean, nm	370.7	327.3	336.9	294.3	282.1
Range	148.6-924.9	130.6-819.9	136.7-829.9	119.2-726.6	116.5-683.1
Difference	776.3	689.3	693.2	607.4	566.6
Multi-size distribution					
Max 1, nm	120.8	268.6	74.0	279.9	59.4
Max 2, nm	414.8	1721.5	420.6	1711.6	406.4
Max 3, nm	2332.4	2346.2	2042.5	2314.5	2068.0
Max 4, nm	-	-	3281.3	-	3222.8
Max 5, nm	-	-	3843.0	-	-
Range	94.4-4889.2	160.3-4358.2	46.0-7230.7	169.3-4232.3	38.1-4332.2
Difference	4794.8	4197.9	7184.7	4063.0	4294.1

Considering log normal distribution, initial hydrodynamic particle size of "TiO_2 and HA" "as-is" under irradiation was detected as 370.7 nm. Along 120 min, hydrodynamic particle size of "TiO_2 and HA" binary system "as-is" under irradiation exhibited a continuously decreasing trend and detected to 282.1 nm at the end of 120 min period. In terms of multi-size distribution, initially three peaks were observed, upon 60 min five peaks were monitored, and four peaks were obtained upon 120 min.

Time dependent comparative presentation of log Normal distribution and multi-size distribution of "TiO_2 and HA" binary system "as-is" under irradiation surface area profile was presented in Figure 4.222.

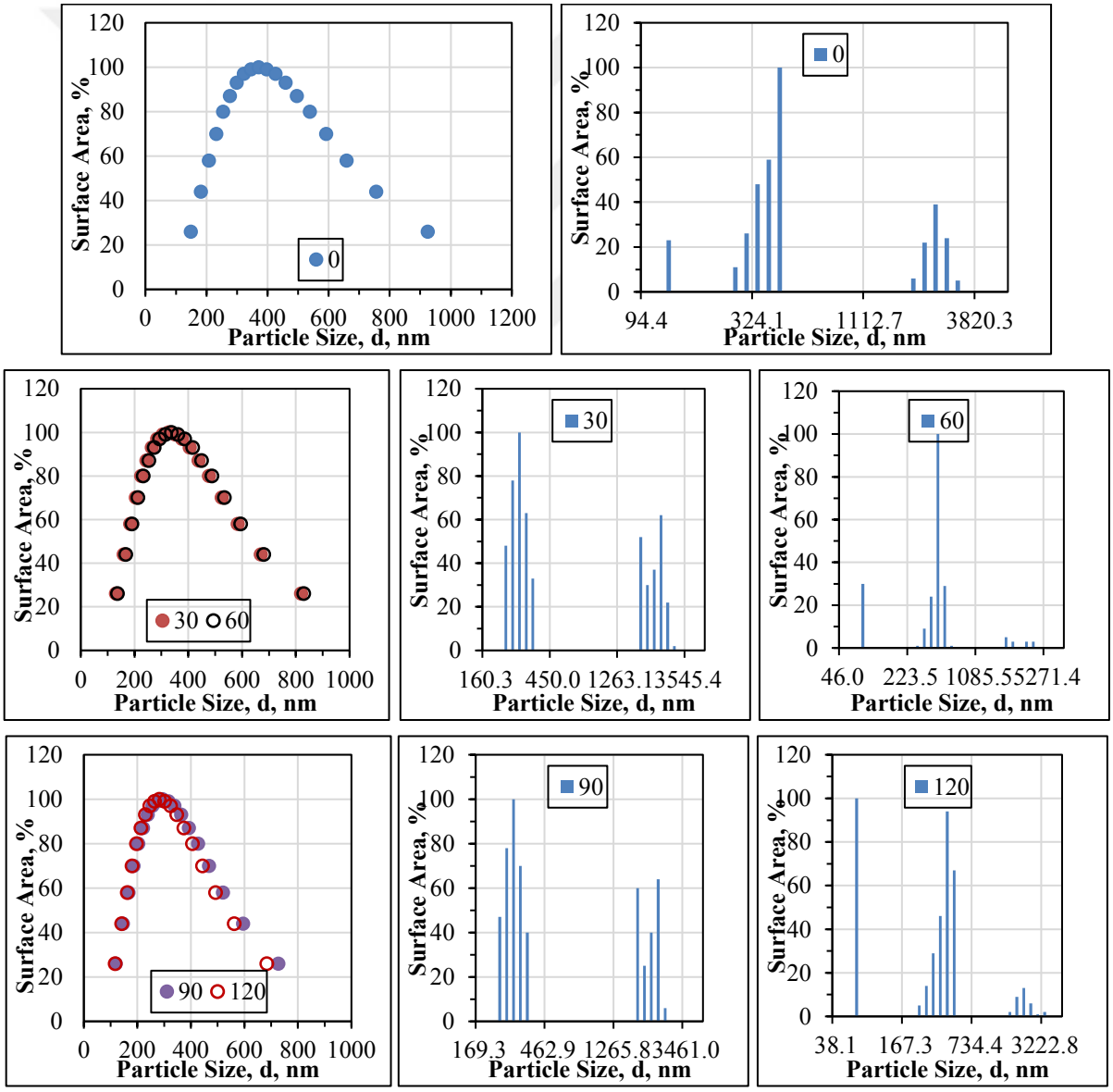


Figure 4.222. "TiO_2 and HA" binary system "as-is" under irradiation surface area profile: Time dependent comparative presentation of log Normal distribution and multi-size distribution of "TiO_2 and HA" binary system "as-is" under irradiation.

4.1.7.4. "TiO_2 and HA" binary system "as-is" under irradiation number profile. As elucidated for "TiO_2 and HA" binary system "as-is" under irradiation intensity profile (Figure 4.217), volume profile (Figure 4.219), and surface area profile (Figure 4.221), a similar approach was followed for "TiO_2 and HA" binary system "as-is" under irradiation number profile. Time dependent logN distribution G(d) and multi size distribution C(d) of "TiO_2 and HA" binary system "as-is" under irradiation number profile was given in Figure 4.223. Time dependent mean diameter, range and min-max diameter difference with respect to log normal and multi-size distribution of "TiO_2 and HA" binary system "as-is" under irradiation number profile was presented in Table 4.140.

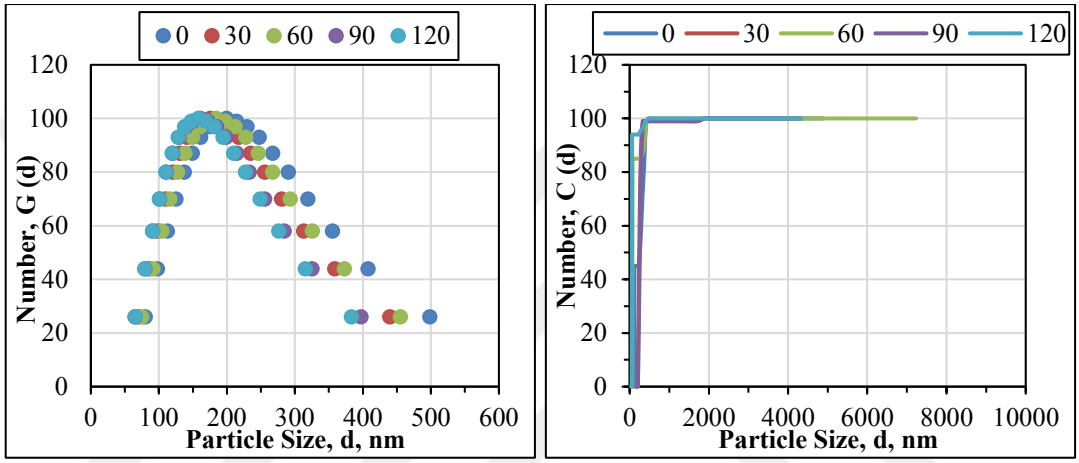


Figure 4.223. "TiO_2 and HA" binary system "as-is" under irradiation number profile: Time dependent logN distribution G(d) and multi size distribution C(d).

Table 4.140. "TiO_2 and HA" binary system "as-is" under irradiation number profile: Time dependent mean diameter, range and min-max diameter difference with respect to log normal and multi-size distribution.

TiO_2 and HA	time, min				
	0	30	60	90	120
Log Normal distribution					
Mean, nm	199.8	175.5	184.7	160.9	158.3
Range	80.1-498.6	70.0-439.6	75.0-455.1	65.2-397.3	65.4-383.3
Difference	418.5	369.6	380.1	332.1	317.9
Multi-size distribution					
Max 1, nm	120.8	268.6	74.0	279.9	59.4
Max 2, nm	414.8	1721.5	420.6	1711.6	406.4
Max 3, nm	-	1908.6	-	-	-
Max 4, nm	-	2116.2	-	-	-
Max 5, nm	-	2346.2	-	-	-
Range	94.4-4889.2	160.3-4358.2	46.0-7230.7	169.3-4232.3	38.1-4332.2
Difference	4794.8	4197.9	7184.7	4063.0	4294.1

According to log normal distribution and in terms of number profile, hydrodynamic particle size of "TiO_2 and HA" binary system "as-is" under irradiation revealed minor variations with respect to time. Initial hydrodynamic size was obtained as 199.8 nm and detected to 158.3 nm upon 120 min. In terms of multi-size distribution, initially two peaks were attained, five peaks were observed upon 30 min and two peaks remained until the end of 120 min.

In a similar manner to data depicted "TiO_2 and HA" binary system "as-is" under irradiation surface area profile (Figure 4.222), time dependent comparative presentation of log Normal distribution and multi-size distribution of "TiO_2 and HA" binary system "as-is" under irradiation number profile was demonstrated in Figure 4.224.

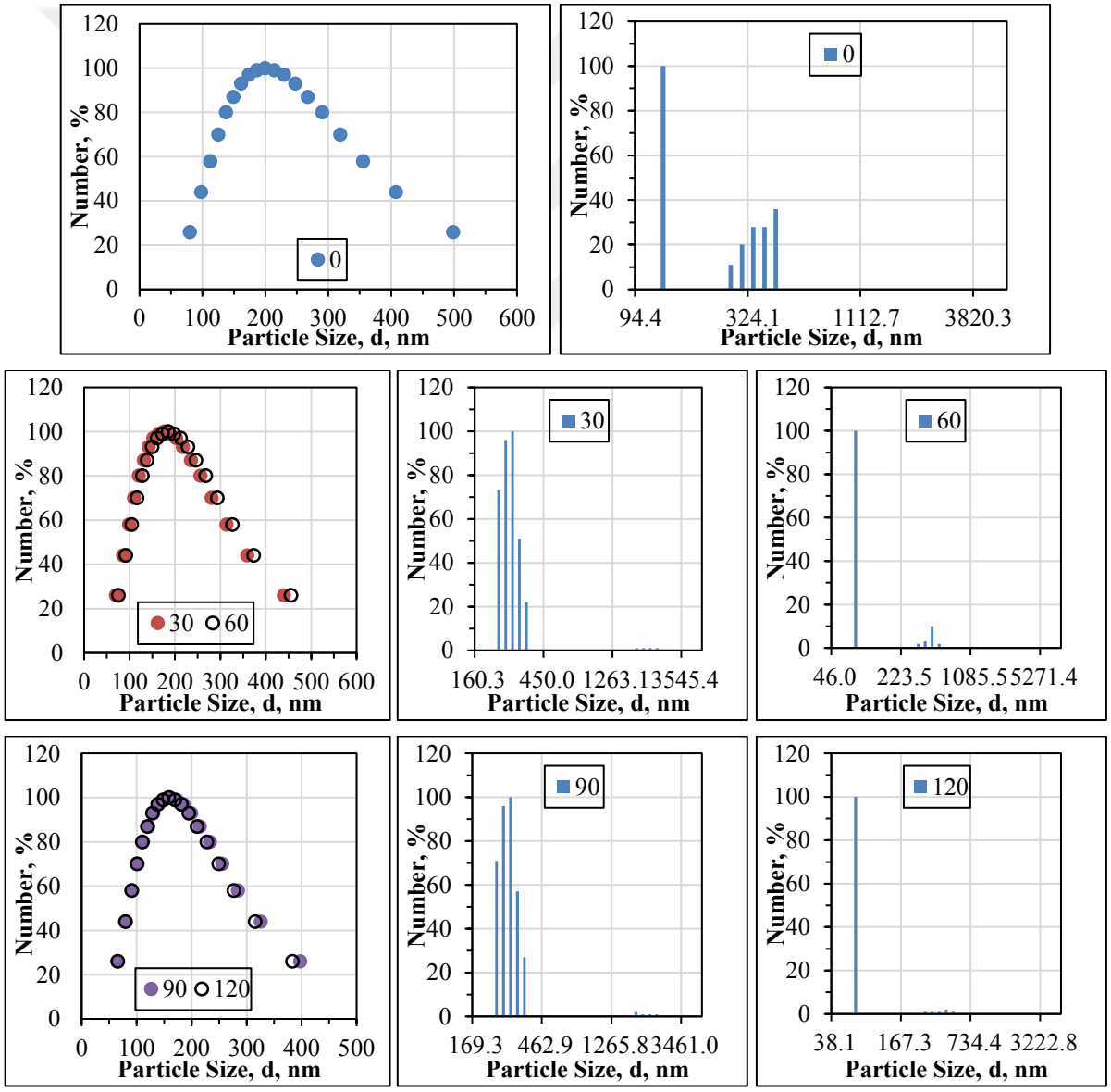


Figure 4.224. "TiO_2 and HA" binary system "as-is" under irradiation number profile: Time dependent comparative presentation of log Normal distribution and multi-size distribution of "TiO_2 and HA" binary system "as-is" under irradiation.

4.1.7.5. "TiO_2 and SRNOM" binary system "as-is" under irradiation intensity profile. Time dependent logN distribution G(d) and multi size distribution C(d) of "TiO_2 and SRNOM" binary system "as-is" under irradiation intensity profile was exhibited in Figure 4.225. Time dependent mean diameter, range and min-max diameter difference with respect to log normal and multi-size distribution of "TiO_2 and SRNOM" binary system "as-is" under irradiation intensity profile was demonstrated in Table 4.141.

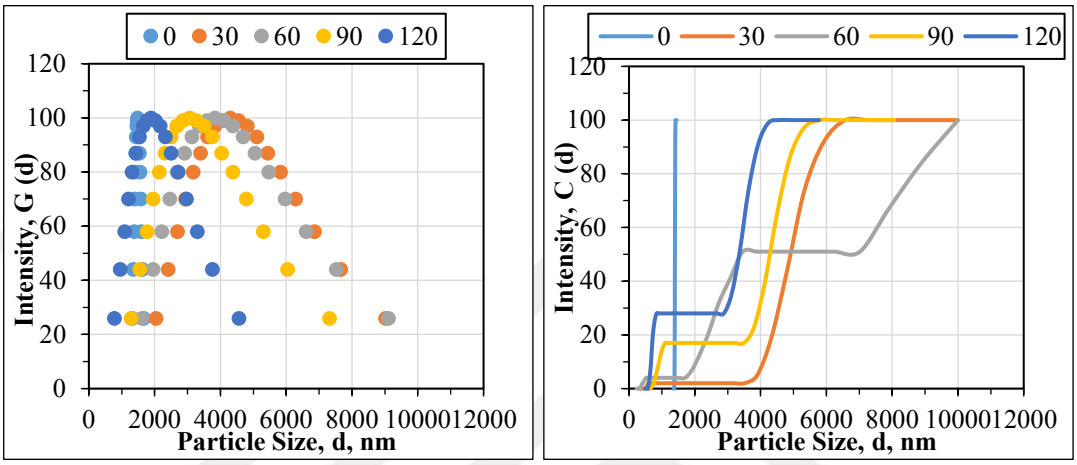


Figure 4.225. "TiO_2 and SRNOM" binary system "as-is" under irradiation intensity profile: Time dependent logN distribution G(d) and multi size distribution C(d).

Table 4.141. "TiO_2 and SRNOM" binary system "as-is" under irradiation intensity profile: Time dependent mean diameter, range and min-max diameter difference with respect to log normal and multi-size distribution.

TiO_2 and SRNOM	time, min				
	0	30	60	90	120
Log Normal distribution					
Mean, nm	1484.9	4301.2	3835.4	3064.2	1893.7
Range	1322.0-1667.8	2049.9-9025.2	1614.7-9110.2	1282.3-7322.1	785.2-4567.2
Difference	345.8	6975.3	7495.5	6039.8	3782.0
Multi-size distribution					
Max 1, nm	1397.9	5337.4	414.4	948.4	718.7
Max 2, nm	-	-	2733.5	4498.8	3635.4
Max 3, nm	-	-	8887.8	-	-
Range	1349.9-1446.5	351.4-10.000	229.8-10.000	607.8-8067.8	488.6-5776.8
Difference	96.6	9648.6	9770.2	7460.0	5288.2

In terms of intensity profile, initial hydrodynamic particle size of "TiO_2 and SRNOM" binary system "as-is" under irradiation was attained as 1484.9 nm. Upon 30 min, a rapid increase was observed and drastic changes monitored during 120 min. In terms of multi-size distribution, one peak

was attained until 60 min. Upon 60 min, three peaks were observed and two peaks remained until the end of 120 min. Time dependent comparative presentation of log Normal distribution and multi-size distribution of "TiO_2 and SRNOM" binary system "as-is" under irradiation intensity profile was presented in Figure 4.226. Polydispersity of "TiO_2 and SRNOM" binary system "as-is" under irradiation was given in Table 4.142 and dramatic changes were observed along 120 min.

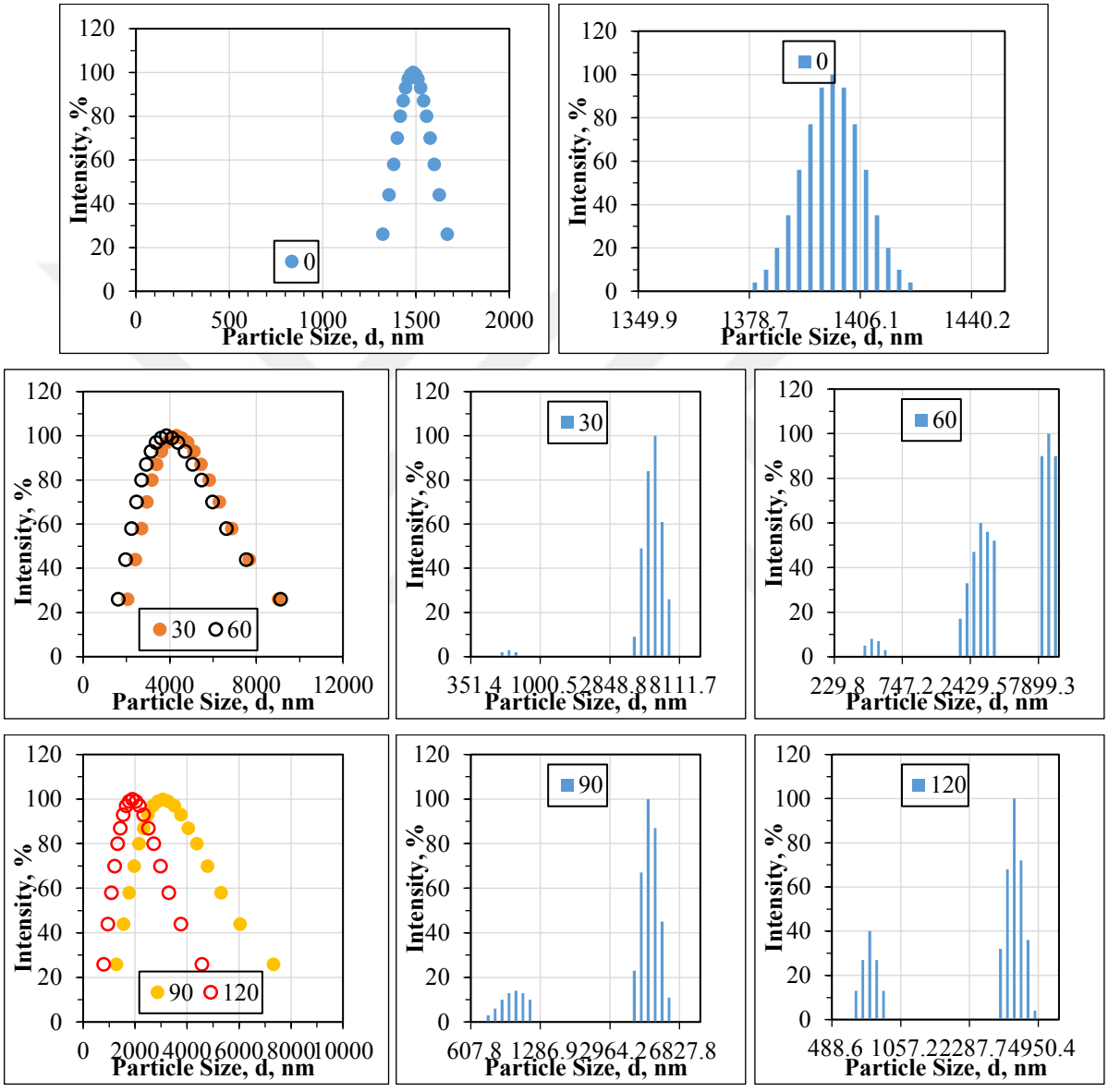


Figure 4.226. "TiO_2 and SRNOM" binary system "as-is" under irradiation intensity profile: Time dependent comparative presentation of log Normal distribution and multi-size distribution of "TiO_2 and SRNOM" binary system "as-is" under irradiation.

Table 4.142. Polydispersity of "TiO_2 and SRNOM" binary system "as-is" under irradiation.

TiO_2 and SRNOM	Polydispersity				
	0	30	60	90	120
	0.328	0.225	0.319	0.324	0.332

4.1.7.6. "TiO_2 and SRNOM" binary system "as-is" under irradiation volume profile. Time dependent logN distribution G(d) and multi size distribution C(d) of "TiO_2 and SRNOM" binary system "as-is" under irradiation volume profile was presented in Figure 4.227. Time dependent mean diameter, range and min-max diameter difference with respect to log normal and multi-size distribution of "TiO_2 and SRNOM" binary system "as-is" under irradiation volume profile was displayed in Table 4.143.

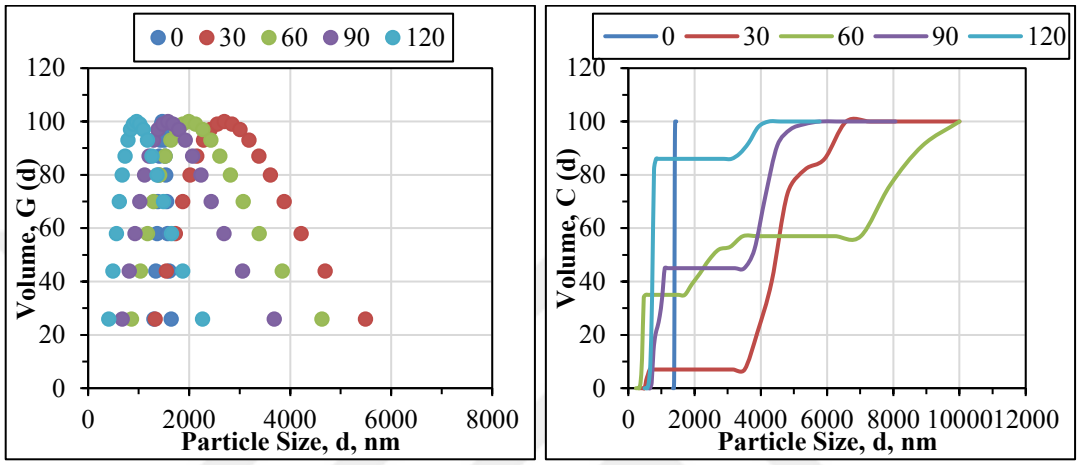


Figure 4.227. "TiO_2 and SRNOM" binary system "as-is" under irradiation volume profile: Time dependent logN distribution G(d) and multi size distribution C(d).

Table 4.143. "TiO_2 and SRNOM" binary system "as-is" under irradiation volume profile: Time dependent mean diameter, range and min-max diameter difference with respect to log normal and multi-size distribution.

TiO_2 and SRNOM	time, min				
	0	30	60	90	120
Log Normal distribution					
Mean, nm	1466.5	2698.3	1995.8	1579.0	961.1
Range	1305.6-1647.1	1326.0-5490.6	860.8-4627.0	676.8-3683.8	408.0-2264.0
Difference	341.5	4164.6	3766.2	3007.0	1856.0
Multi-size distribution					
Max 1, nm	1397.9	539.8	466.2	759.2	776.4
Max 2, nm	-	4807.1	2429.5	1100.1	3927.1
Max 3, nm	-	6579.9	3460.5	4138.6	-
Max 4, nm	-	-	7899.3	-	-
Range	1349.9-1446.5	351.4-10.000	229.8-10.000	607.8-8067.8	488.6-5776.8
Difference	96.6	9648.6	9770.2	7460.0	5288.2

According to log normal distribution and in terms of volume profile, it could be asserted that hydrodynamic particle size of "TiO_2 and SRNOM" binary system "as-is" under irradiation was

detected as 1466.5 nm following initial period of time and decreased to 961.1 nm upon period of 120 min. For comparison purposes, in terms of multi-size distribution, initially three max diameters were attained. Upon 30 min, one peak was observed and one peak was observed, upon 60 min, four peaks were monitored. However, two peaks were attained upon 120 min.

As described for "TiO_2 and SRNOM" binary system "as-is" under irradiation intensity profile (Figure 4.226), a similar approach was followed for "TiO_2 and SRNOM" binary system "as-is" under irradiation volume profile. Time dependent comparative presentation of log Normal distribution and multi-size distribution of "TiO_2 and SRNOM" binary system "as-is" under irradiation volume profile was exhibited in Figure 4.228.

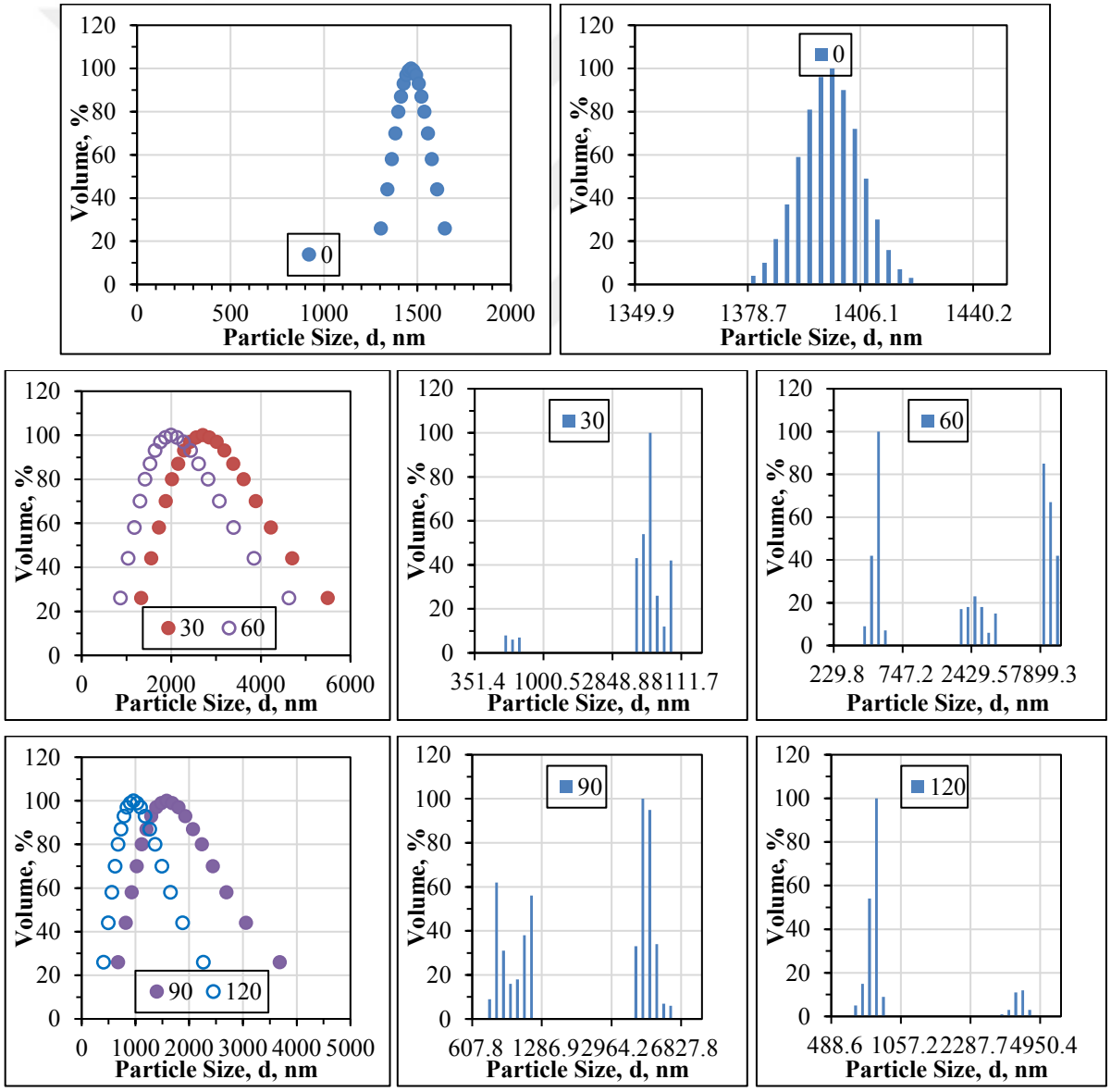


Figure 4.228. "TiO_2 and SRNOM" binary system "as-is" under irradiation volume profile: Time dependent comparative presentation of log Normal distribution and multi-size distribution of "TiO_2 and SRNOM" binary system "as-is" under irradiation.

4.1.7.7. “TiO_2 and SRNOM” binary system “as-is” under irradiation surface area profile. In a similar manner to data represented “TiO_2 and SRNOM” binary system “as-is” under irradiation volume profile (Figure 4.227), time dependent logN distribution G(d) and multi size distribution C(d) of “TiO_2 and SRNOM” binary system “as-is” under irradiation surface area profile was demonstrated in Figure 4.229. Time dependent mean diameter, range and min-max diameter difference with respect to log normal and multi-size distribution of “TiO_2 and SRNOM” binary system “as-is” under irradiation surface area profile was presented in Table 4.144.

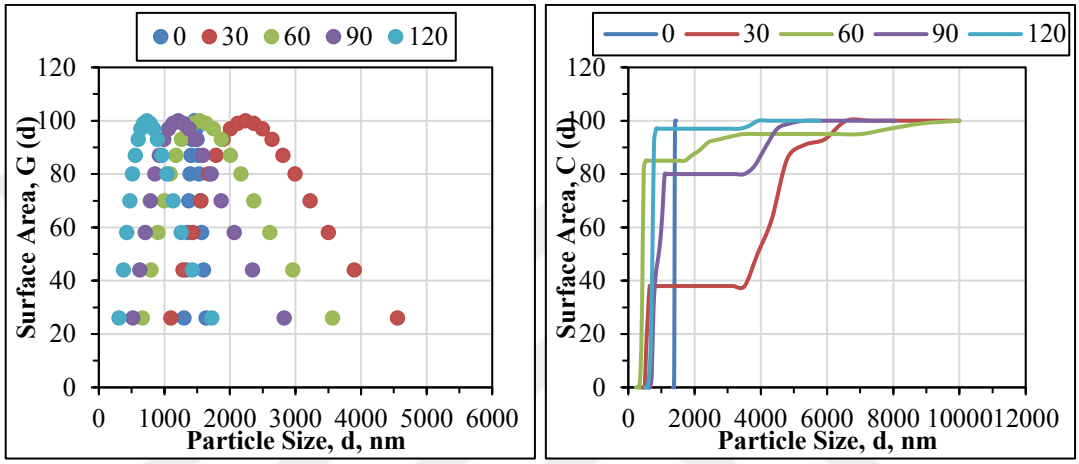


Figure 4.229. “TiO_2 and SRNOM” binary system “as-is” under irradiation surface area profile: Time dependent logN distribution G(d) and multi size distribution C(d).

Table 4.144. “TiO_2 and SRNOM” binary system “as-is” under irradiation surface area profile: Time dependent mean diameter, range and min-max diameter difference with respect to log normal and multi-size distribution.

TiO_2 and SRNOM	time, min				
	0	30	60	90	120
Log Normal distribution					
Mean, nm	1459.2	2239.2	1536.9	1211.2	732.7
Range	1299.1-1638.9	1100.4-4556.4	662.9-3563.1	519.2-2825.6	311.1-1726.1
Difference	339.8	3456.0	2900.2	2306.4	1415.0
Multi-size distribution					
Max 1, nm	1397.9	539.8	466.2	759.2	776.4
Max 2, nm	-	645.8	1919.1	1100.1	3635.4
Max 3, nm	-	4807.1	2159.3	4138.6	3927.1
Max 4, nm	-	6579.9	2429.5	-	-
Max 5, nm	-	-	3460.5	-	-
Max 6, nm	-	-	7899.3	-	-
Range	1349.9-1446.5	351.4-10.000	229.8-10.000	607.8-8067.8	488.6-5776.8
Difference	96.6	9648.6	9770.2	7460.0	5288.2

In terms of surface area profile, initial hydrodynamic particle size of "TiO_2 and SRNOM" binary system "as-is" under irradiation detected as 1459.2 nm and revealed a rapid increase in the first 30 min. Upon 30 min, a sharp increase was monitored in hydrodynamic particle size and continuous decrease was observed until 120 min. Considering multi-size distribution, initially one peak was observed and four peaks were attained upon 30 min. Upon 60 period of min, six max diameters were obtained and three peaks remained until the end of 120 min. In a similar manner to data described "TiO_2 and SRNOM" binary system "as-is" under irradiation volume profile (Figure 4.228), time dependent comparative presentation of log Normal distribution and multi-size distribution of "TiO_2 and SRNOM" binary system "as-is" under irradiation surface area profile was displayed in Figure 4.230.

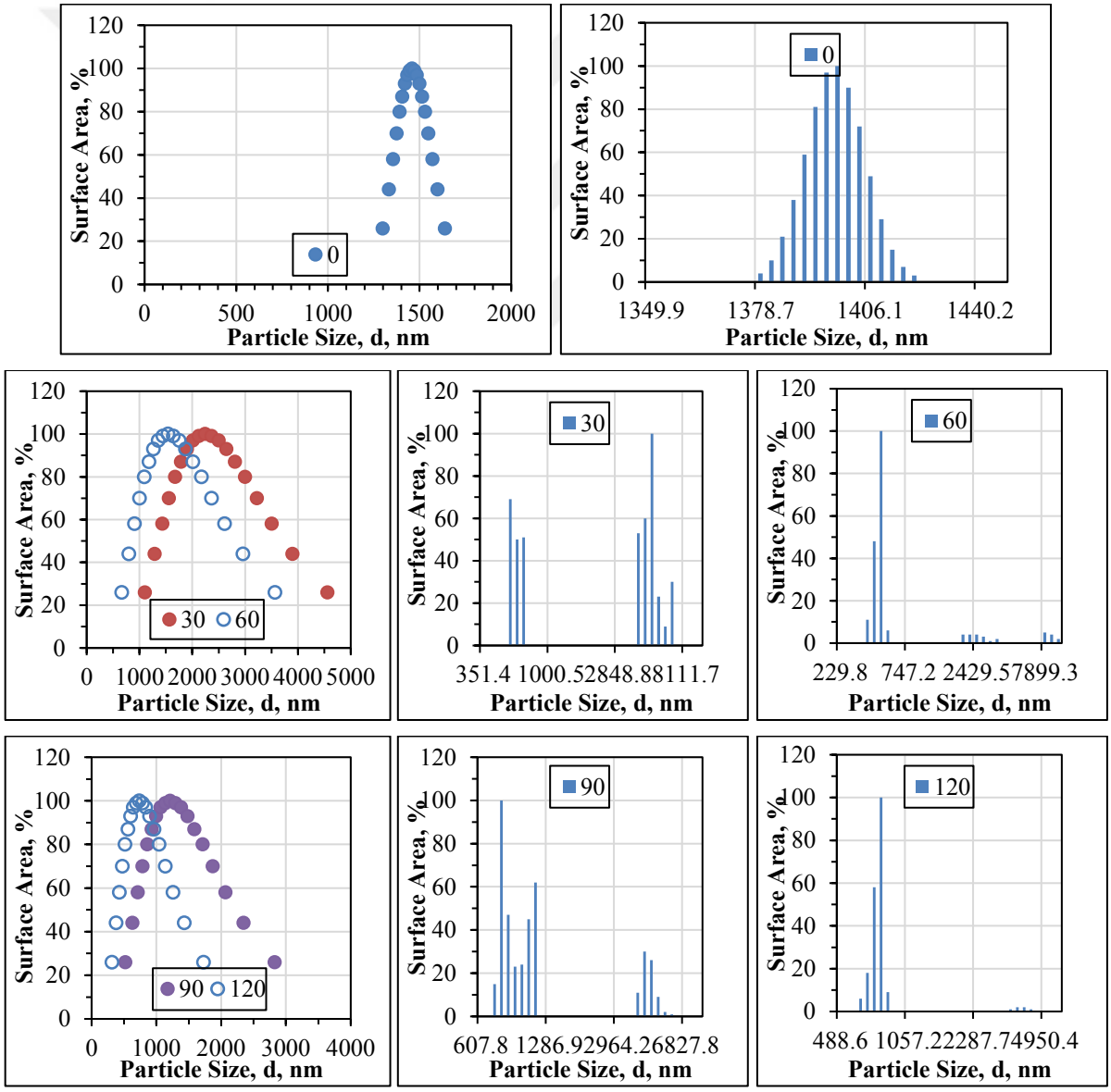


Figure 4.230. "TiO_2 and SRNOM" binary system "as-is" under irradiation surface area profile: Time dependent comparative presentation of log Normal distribution and multi-size distribution of "TiO_2 and SRNOM" binary system "as-is" under irradiation.

4.1.7.8. “TiO_2 and SRNOM” binary system “as-is” under irradiation number profile. Time dependent logN distribution G(d) and multi size distribution C(d) of “TiO_2 and SRNOM” binary system “as-is” under irradiation number profile was given in Figure 4.231. Time dependent mean diameter, range and min-max diameter difference with respect to log normal and multi-size distribution of “TiO_2 and SRNOM” binary system “as-is” under irradiation number profile was exhibited in Table 4.145.

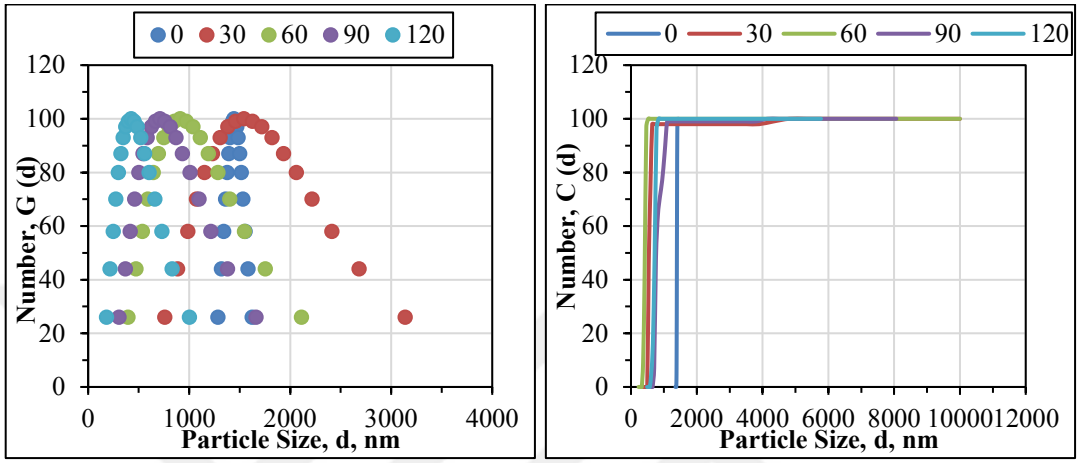


Figure 4.231. “TiO_2 and SRNOM” binary system “as-is” under irradiation number profile: Time dependent logN distribution G(d) and multi size distribution C(d).

Table 4.145. “TiO_2 and SRNOM” binary system “as-is” under irradiation number profile: Time dependent mean diameter, range and min-max diameter difference with respect to log normal and multi-size distribution.

TiO_2 and SRNOM	time, min				
	0	30	60	90	120
Log Normal distribution					
Mean, nm	1444.7	1542.0	911.3	712.6	425.9
Range	1286.2-1622.7	757.8-3137.7	393.1-2112.8	305.5-1662.5	180.8-1003.3
Difference	336.5	2379.9	1719.7	1357.0	822.5
Multi-size distribution					
Max 1, nm	1397.9	539.8	466.2	759.2	776.4
Max 2, nm	-	4807.1	-	1100.1	-
Max 3, nm	-	-	-	4138.6	-
Max 4, nm	-	-	-	4498.8	-
Range	1349.9-1446.5	351.4-10.000	229.8-10.000	607.8-8067.8	488.6-5776.8
Difference	96.6	9648.6	9770.2	7460.0	5288.2

In a similar manner to data represented “TiO_2 and SRNOM” binary system “as-is” under irradiation surface area profile (Figure 4.230), log normal distribution G(d) and multi size distribution C(d) of “TiO_2 and SRNOM” binary system “as-is” under irradiation number profile was presented

according to time variations. It could be stated that hydrodynamic particle size of "TiO_2 and SRNOM" binary system "as-is" under irradiation displayed a rapid increase following initial period of time and continuous decrease was observed until the end of 120 min. Size difference revealed drastic changes upon 120 min. However, in terms of multi-size distribution, initially one peak was observed, upon 30 min, two peaks were attained. Upon 60 min, one peak was obtained and upon 90 min, four peaks were monitored. Upon 120 min, one peak was attained. As described for "TiO_2 and SRNOM" binary system "as-is" under irradiation surface area profile (4.230), following a similar manner, time dependent comparative presentation of log Normal distribution and multi-size distribution of "TiO_2 and SRNOM" binary system "as-is" under irradiation number profile was displayed in Figure 4.232.

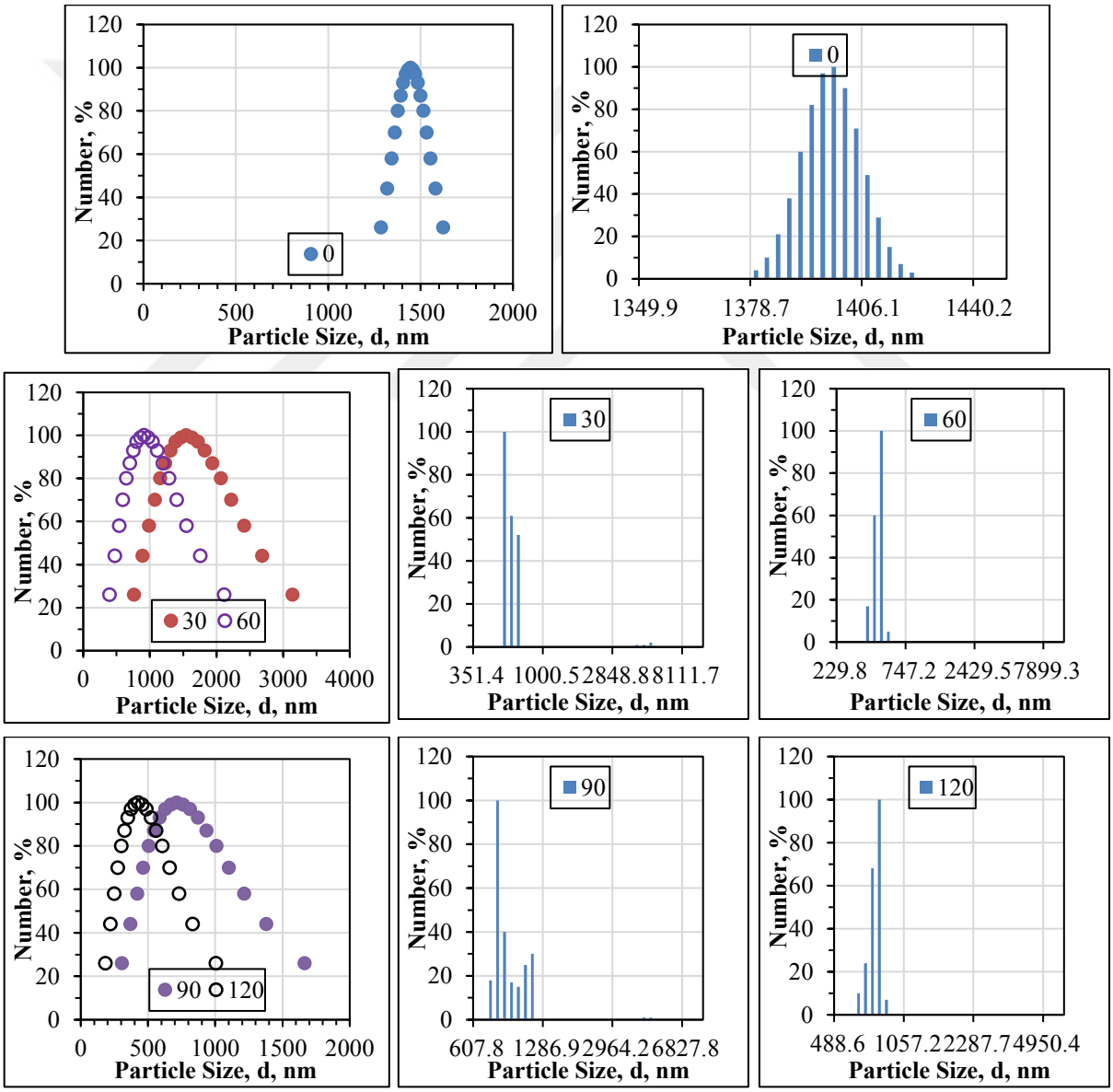


Figure 4.232. "TiO_2 and SRNOM" binary system "as-is" under irradiation number profile: Time dependent comparative presentation of log Normal distribution and multi-size distribution of "TiO_2 and SRNOM" binary system "as-is" under irradiation.

4.1.7.9. "N-TiO_2 and HA" binary system "as-is" under irradiation intensity profile. Time dependent logN distribution G(d) and multi size distribution C(d) of "N-TiO_2 and HA" binary system "as-is" under irradiation intensity profile was presented in Figure 4.233. Time dependent mean diameter, range and min-max diameter difference with respect to log normal and multi-size distribution of "N-TiO_2 and HA" binary system "as-is" under irradiation intensity profile was given in Table 4.146. Polydispersity of "N-TiO_2 and HA" binary system "as-is" under irradiation was shown in Table 4.147, and a continuous decrease was monitored until the end of 120 min period.

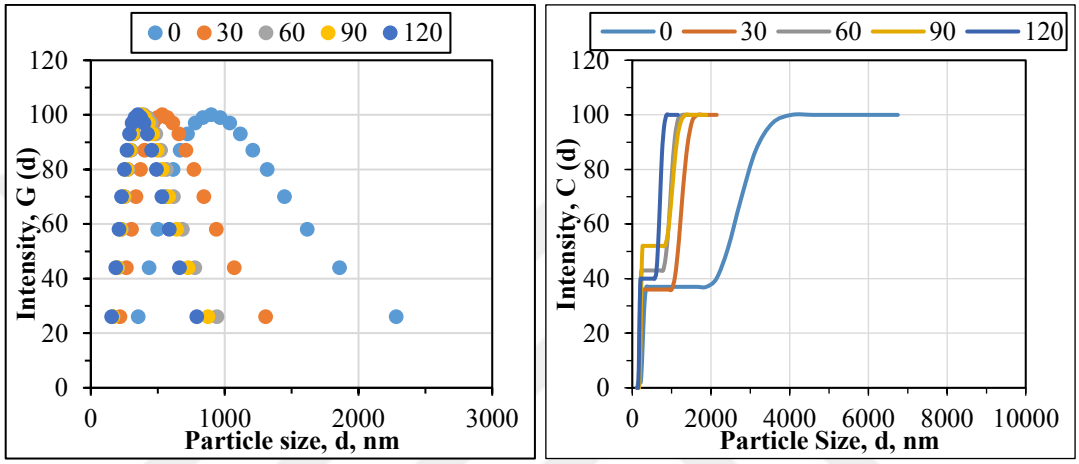


Figure 4.233. "N-TiO_2 and HA" binary system "as-is" under irradiation intensity profile: Time dependent logN distribution G(d) and multi size distribution C(d).

Table 4.146. "N-TiO_2 and HA" binary system "as-is" under irradiation intensity profile: Time dependent mean diameter, range and min-max diameter difference with respect to log normal and multi-size distribution.

N-TiO_2 and HA	time, min				
	0	30	60	90	120
Log Normal distribution					
Mean, nm	899.9	534.6	396.4	380.0	351.1
Range	354.9-2281.9	218.8-1306.2	166.8-942.2	165.0-875.2	155.5-792.9
Difference	1927.0	1087.4	775.4	710.2	637.4
Multi-size distribution					
Max 1, nm	146.1	216.9	195.5	220.7	180.7
Max 2, nm	276.8	1289.0	999.3	1057.3	754.0
Max 3, nm	2759.8	-	-	-	-
Range	113.2-6749.4	141.9-2144.9	119.8-1630.4	134.6-1882.8	117.7-1157.5
Difference	6636.2	2003.0	1510.6	1748.2	1039.8

In terms of intensity profile, hydrodynamic size of "N-TiO_2 and HA" binary system "as-is" under irradiation displayed a rapidly decreasing trend until 90 min. Upon 90 min, minor variations remained

until the end of 120 min. Considering multi-size distribution, initially three peaks were attained. Upon 30 min, two peaks remained until the end of 120 min. Time dependent comparative presentation of log Normal distribution and multi-size distribution of "N-TiO_2 and HA" binary system "as-is" under irradiation intensity profile was given in Figure 4.234.

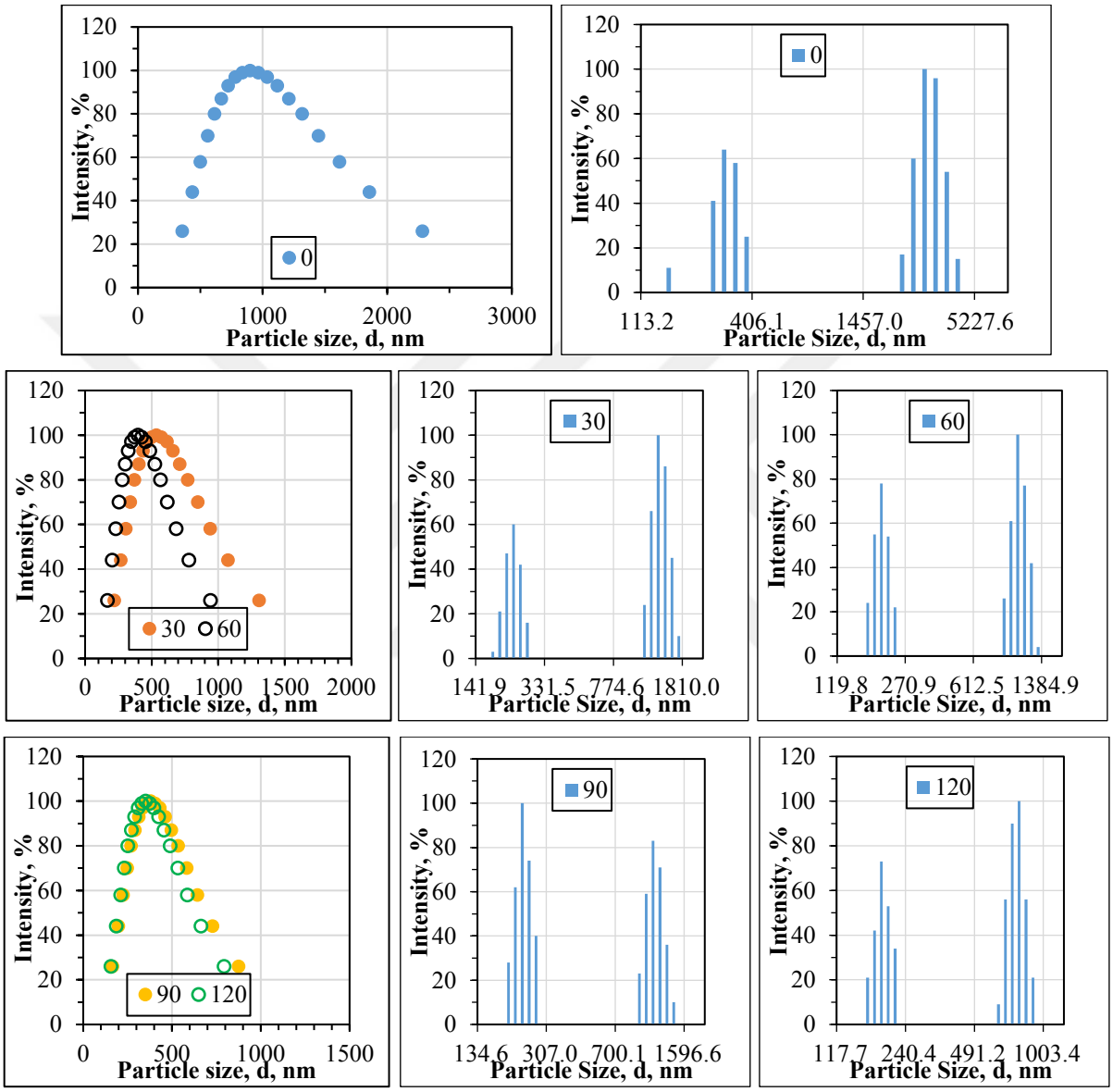


Figure 4.234. "N-TiO_2 and HA" binary system "as-is" under irradiation intensity profile: Time dependent comparative presentation of log Normal distribution and multi-size distribution of "N-TiO_2 and HA" binary system "as-is" under irradiation intensity profile.

Table 4.147. Polydispersity of "N-TiO_2 and HA" binary system "as-is" under irradiation intensity profile.

N-TiO_2 and HA	Polydispersity				
	0	30	60	90	120
	0.377	0.343	0.319	0.293	0.278

4.1.7.10. "N-TiO_2 and HA" binary system "as-is" under irradiation volume profile. Time dependent logN distribution G(d) and multi size distribution C(d) of "N-TiO_2 and HA" binary system "as-is" under irradiation volume profile was exhibited in Figure 4.235. Time dependent mean diameter, range and min-max diameter difference with respect to log normal and multi-size distribution of "N-TiO_2 and HA" binary system "as-is" under irradiation volume profile was demonstrated in Table 4.148.

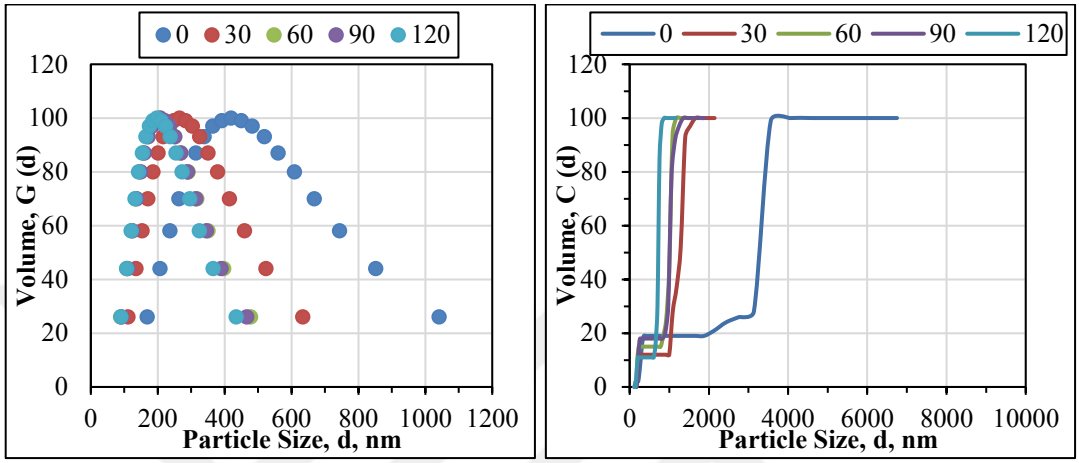


Figure 4.235. "N-TiO_2 and HA" binary system "as-is" under irradiation volume profile: Time dependent logN distribution G(d) and multi size distribution C(d).

Table 4.148. "N-TiO_2 and HA" binary system "as-is" under irradiation volume profile: Time dependent mean diameter, range and min-max diameter difference with respect to log normal and multi-size distribution.

N-TiO_2 and HA	time, min				
	0	30	60	90	120
Log Normal distribution					
Mean, nm	419.5	265.6	206.1	207.7	197.8
Range	169.0-1041.0	111.2-634.1	88.8-478.1	92.5-466.2	90.0-435.0
Difference	872.0	522.9	389.3	373.7	345.0
Multi-size distribution					
Max 1, nm	146.1	216.9	195.5	220.7	180.7
Max 2, nm	314.5	1087.7	1084.2	1057.3	754.0
Max 3, nm	2428.9	1403.2	-	-	-
Max 4, nm	3563.3	-	-	-	-
Range	113.2-6749.4	141.9-2144.9	119.8-1630.4	134.6-1882.8	117.7-1157.5
Difference	6636.2	2003.0	1510.6	1748.2	1039.8

In terms of volume profile, it could be asserted that hydrodynamic particle size of "N-TiO_2 and HA" binary system "as-is" under irradiation exhibited a dramatically decreasing trend upon 30 min. Hydrodynamic particle size was recorded as 419.5 nm following initial period of time and detected

to 265.6 nm upon period of 30 min. Upon 60 min, continuous decrease was observed until the end of 120 min. Correspondingly, according to log normal distribution, size difference was attained between 872.0 nm and 345.0 nm along 120 min. However, in terms of multi-size distribution, four peaks were monitored following initial period of time. Upon 30 min, three peaks were obtained and two peaks remained until the end of 120 min. Also, according to multi-size distribution, size difference was obtained between 6636.2 nm and 1039.8 nm during 120 min.

Time dependent comparative presentation of log Normal distribution and multi-size distribution of "N-TiO_2 and HA" binary system "as-is" under irradiation volume profile was displayed in Figure 4.236.

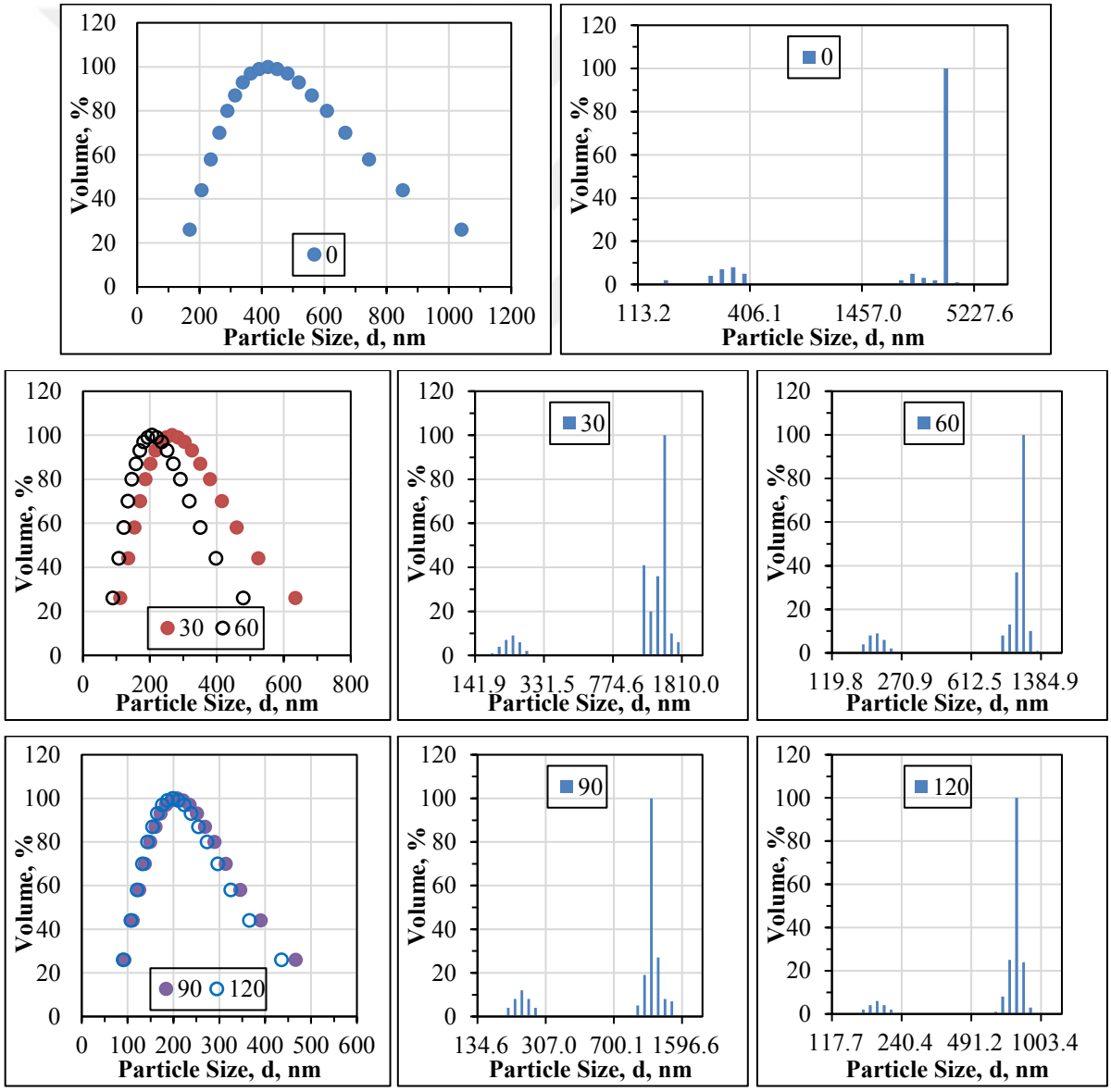


Figure 4.236. "N-TiO_2 and HA" binary system "as-is" under irradiation volume profile: Time dependent comparative presentation of log Normal distribution and multi-size distribution of "N-TiO_2 and HA" binary system "as-is" under irradiation.

4.1.7.11. "N-TiO_2 and HA" binary system "as-is" under irradiation surface area profile. Time dependent logN distribution G(d) and multi size distribution C(d) of "N-TiO_2 and HA" binary system "as-is" under irradiation surface area profile was given in Figure 4.237. Time dependent mean diameter, range and min-max diameter difference with respect to log normal and multi-size distribution of "N-TiO_2 and HA" binary system "as-is" under irradiation surface area profile was presented in Table 4.149.

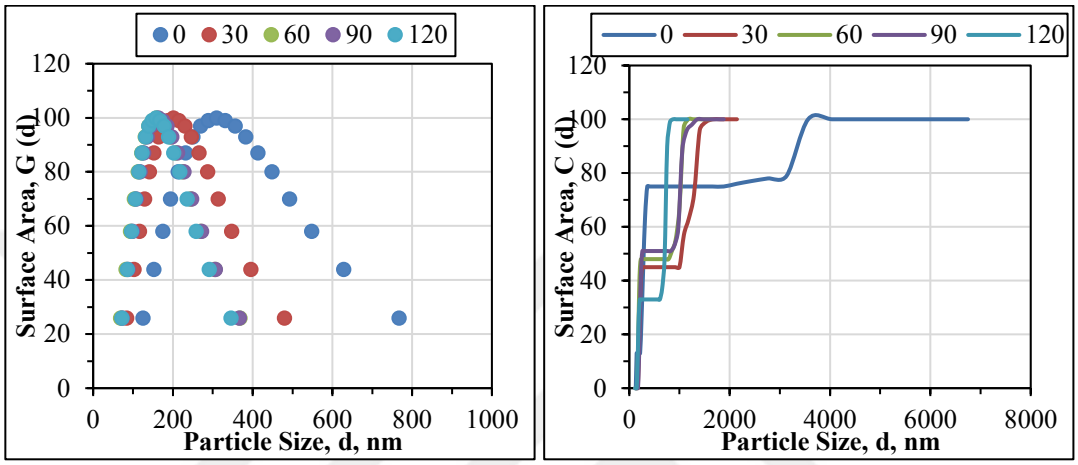


Figure 4.237. "N-TiO_2 and HA" binary system "as-is" under irradiation surface area profile: Time dependent logN distribution G(d) and multi size distribution C(d).

Table 4.149. "N-TiO_2 and HA" binary system "as-is" under irradiation surface area profile: Time dependent mean diameter, range and min-max diameter difference with respect to log normal and multi-size distribution.

N-TiO_2 and HA	time, min				
	0	30	60	90	120
Log Normal distribution					
Mean, nm	309.1	200.7	158.6	163.1	157.3
Range	124.6-767.2	84.1-479.3	68.4-368.0	72.6-366.1	71.5-345.8
Difference	642.6	395.2	299.6	293.5	274.3
Multi-size distribution					
Max 1, nm	146.1	216.9	195.5	220.7	180.7
Max 2, nm	276.8	1087.7	1084.2	1057.3	754.0
Max 3, nm	2428.9	1403.2	-	-	-
Max 4, nm	3563.3	-	-	-	-
Range	113.2-6749.4	141.9-2144.9	119.8-1630.4	134.6-1882.8	117.7-1157.5
Difference	6636.2	2003.0	1510.6	1748.2	1039.8

In a similar manner to data depicted "N-TiO_2 and HA" binary system "as-is" under irradiation volume profile (Figure 4.235), log normal distribution G(d) and multi size distribution C(d) of "N-

TiO_2 and HA" binary system "as-is" under irradiation surface area profile was exhibited according to time variations. It could be stated that hydrodynamic particle size of "N-TiO_2 and HA" binary system "as-is" under irradiation displayed a sharp decrease following initial period of time. Upon 30 min, hydrodynamic particle size displayed a slowly decreasing trend until the end of 120 min. Also, size difference was detected between 642.6 nm and 274.3 nm upon 120 min. In terms of multi-size distribution, four max diameters were attained following initial period of time. Upon 60 min, three peaks were monitored and two peaks remained until 120 min. Time dependent comparative presentation of log Normal distribution and multi-size distribution of "N-TiO_2 and HA" binary system "as-is" under irradiation surface area profile was demonstrated in Figure 4.238.

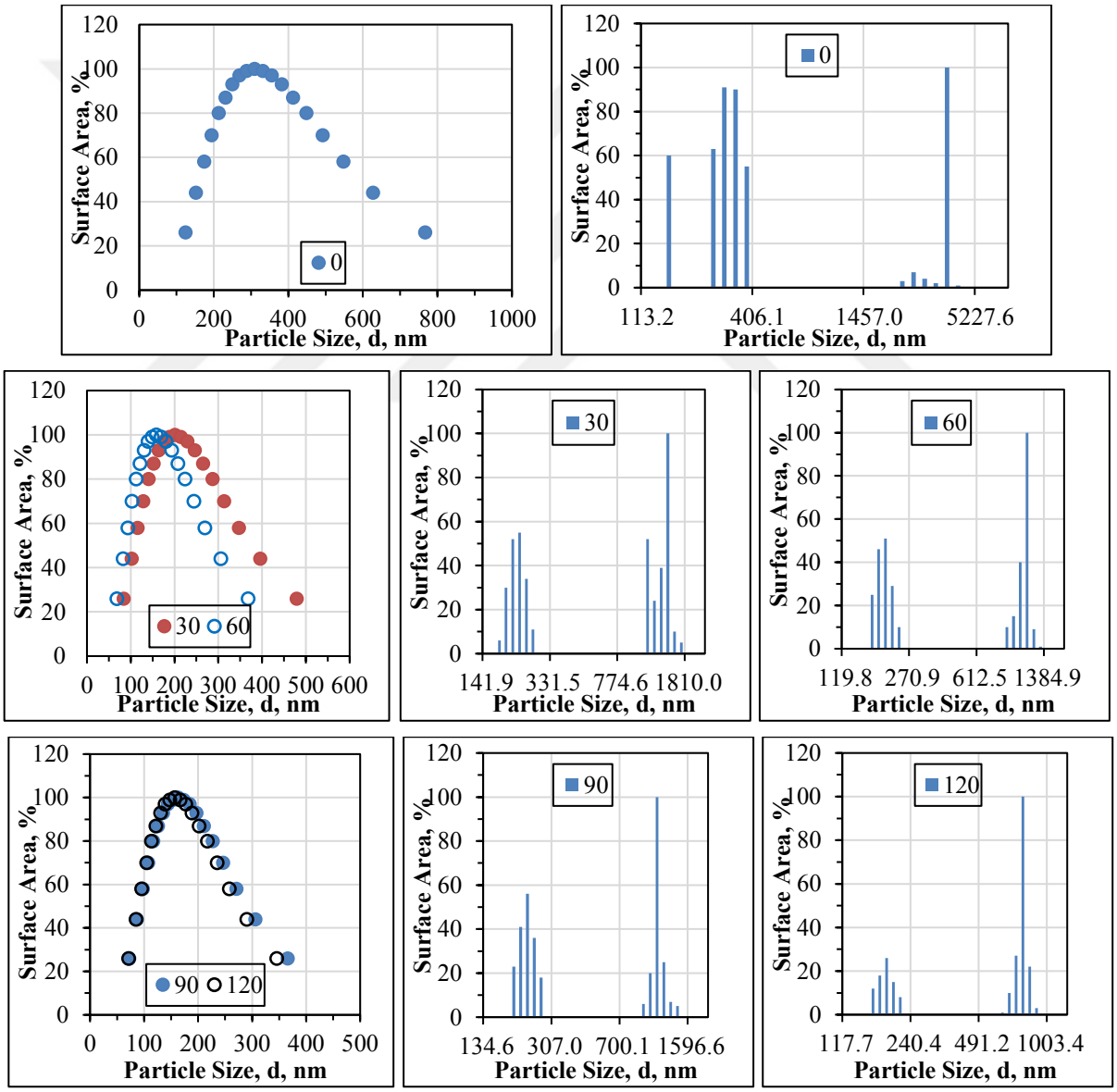


Figure 4.238. "N-TiO_2 and HA" binary system "as-is" under irradiation surface area profile: Time dependent comparative presentation of log Normal distribution and multi-size distribution of "N-TiO_2 and HA" binary system "as-is" under irradiation.

4.1.7.12. "N-TiO_2 and HA" binary system "as-is" under irradiation number profile. In a similar manner to data represented "N-TiO_2 and HA" binary system "as-is" under irradiation surface area profile (Figure 4.237), time dependent logN distribution G(d) and multi size distribution C(d) of "N-TiO_2 and HA" binary system "as-is" under irradiation number profile was presented in Figure 4.239. Time dependent mean diameter, range and min-max diameter difference with respect to log normal and multi-size distribution of "N-TiO_2 and HA" binary system "as-is" under irradiation number profile was exhibited in Table 4.150.

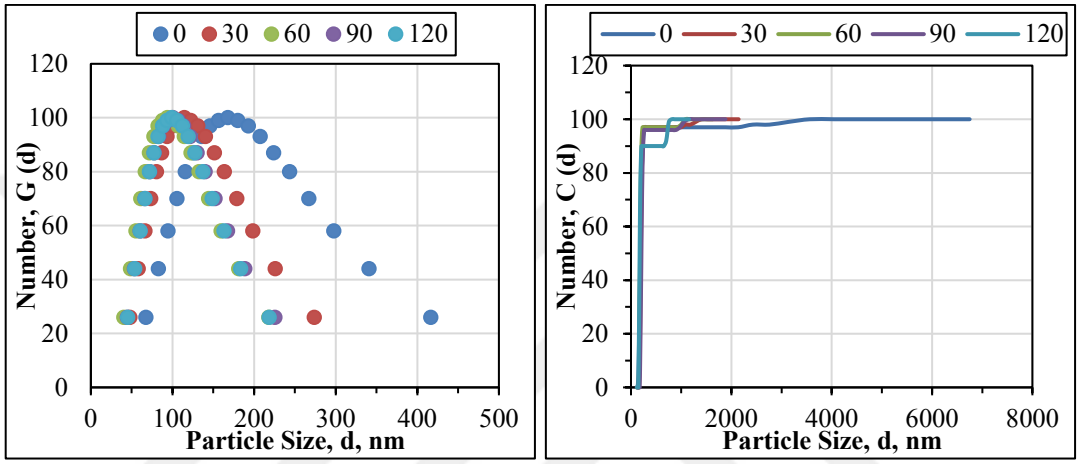


Figure 4.239. "N-TiO_2 and HA" binary system "as-is" under irradiation number profile: Time dependent logN distribution G(d) and multi size distribution C(d).

Table 4.150. "N-TiO_2 and HA" binary system "as-is" under irradiation number profile: Time dependent mean diameter, range and min-max diameter difference with respect to log normal and multi-size distribution.

N-TiO_2 and HA	time, min				
	0	30	60	90	120
Log Normal distribution					
Mean, nm	167.9	114.7	94.0	100.6	99.4
Range	67.6-416.6	48.0-273.8	40.5-218.1	44.8-225.8	45.2-218.5
Difference	349.0	225.8	177.6	181.0	173.3
Multi-size distribution					
Max 1, nm	146.1	199.2	180.2	220.7	180.7
Max 2, nm	276.8	1087.7	1084.2	1057.3	754.0
Max 3, nm	-	1403.2	-	-	-
Range	113.2-6749.4	141.9-2144.9	119.8-1630.4	134.6-1882.8	117.7-1157.5
Difference	6636.2	2003.0	1510.6	1748.2	1039.8

In terms of number profile, initial hydrodynamic particle size of "N-TiO_2 and HA" binary system "as-is" under irradiation was recorded as 167.9 nm. Upon 30 min, roughly 30 % decrease was

observed and minor variations remained until 120 min. On the other hand, in terms of size difference, approximately 35 % decline was monitored in the first 30 min and continuous decrease remained until the end of 120 min. For comparison purposes, in terms of multi-size distribution, initially two peaks were attained as 146.1 nm and 276.8 nm. Upon 30 min, three peaks were monitored as 199.2 nm, 1087.7 nm, and 1403.2 nm, and two peaks remained until the end of 120 min period. As explained for "N-TiO_2 and HA" binary system "as-is" under irradiation surface area profile (Figure 4.238), a similar approach was followed for "N-TiO_2 and HA" binary system "as-is" under irradiation number profile. Time dependent comparative presentation of log Normal distribution and multi-size distribution of "N-TiO_2 and HA" binary system "as-is" under irradiation number profile was displayed in Figure 4.240.

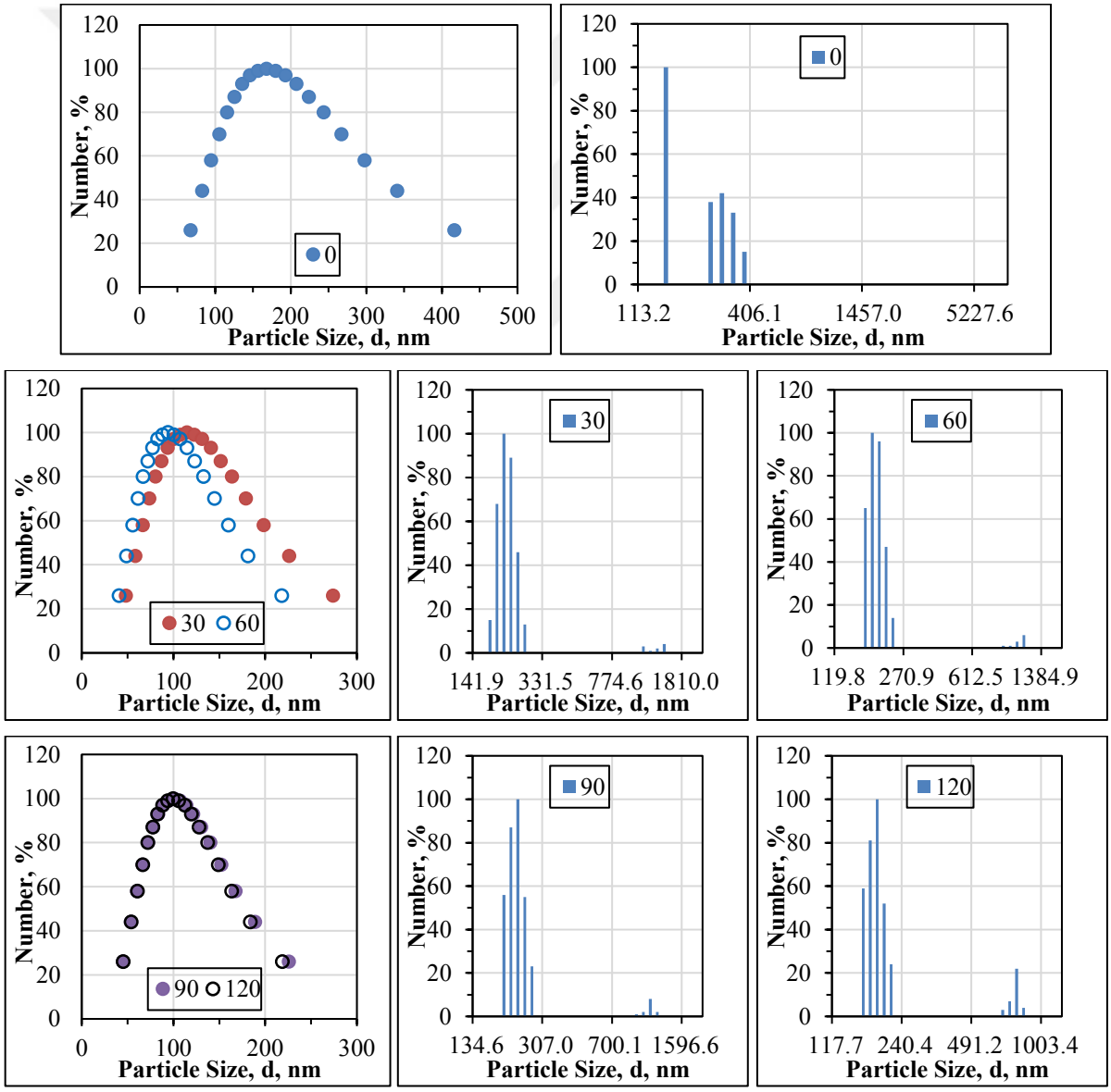


Figure 4.240. "N-TiO_2 and HA" binary system "as-is" under irradiation number profile: Time dependent comparative presentation of log Normal distribution and multi-size distribution of "N-TiO_2 and HA" binary system "as-is" under irradiation.

4.1.7.13. "N-TiO_2 and SRNOM" binary system "as-is" under irradiation intensity profile. In a similar manner to data represented "N-TiO_2 and HA" binary system "as-is" under irradiation intensity profile (Figure 4.233), time dependent logN distribution G(d) and multi size distribution C(d) of "N-TiO_2 and SRNOM" binary system "as-is" under irradiation intensity profile was exhibited in Figure 4.241. Time dependent mean diameter, range and min-max diameter difference with respect to log normal and multi-size distribution of "N-TiO_2 and SRNOM" binary system "as-is" under irradiation intensity profile was displayed in Table 4.151.

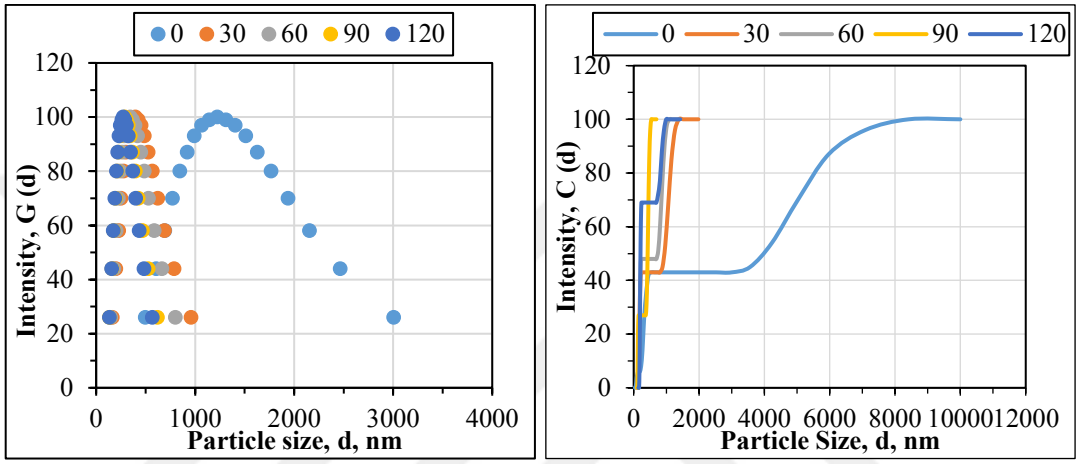


Figure 4.241. "N-TiO_2 and SRNOM" binary system "as-is" under irradiation intensity profile: Time dependent logN distribution G(d) and multi size distribution C(d).

Table 4.151. "N-TiO_2 and SRNOM" binary system "as-is" under irradiation intensity profile: Time dependent mean diameter, range and min-max diameter difference with respect to log normal and multi-size distribution.

N-TiO_2 and SRNOM	time, min				
	0	30	60	90	120
Log Normal distribution					
Mean, nm	1223.4	396.3	344.8	288.3	274.7
Range	497.9-3006.2	163.8-958.8	148.8-799.0	133.9-620.5	132.9-567.8
Difference	2508.3	795.0	650.2	486.6	434.9
Multi-size distribution					
Max 1, nm	96.3	192.1	192.4	134.0	205.8
Max 2, nm	321.0	1156.4	875.4	447.2	863.0
Max 3, nm	5970.1	-	-	-	-
Range	40.8-10.000	112.1-1981.5	122.1-1379.1	91.6-697.1	143.8-1425.1
Difference	9959.2	1869.4	1257.0	605.5	1281.3

In terms of intensity profile, initial hydrodynamic size of "N-TiO_2 and SRNOM" binary system "as-is" under irradiation was detected as 1223.4 nm. Upon 30 min, ~65 % decrease was observed. In

terms of multi-size distribution, initially three peaks were obtained and two peaks remained until the end of 120 min. Time dependent comparative presentation of log Normal distribution and multi-size distribution of "N-TiO_2 and SRNOM" binary system "as-is" under irradiation intensity profile was displayed in Figure 4.242. Polydispersity of "N-TiO_2 and SRNOM" binary system "as-is" under irradiation was given in Table 4.152, continuous decrease was observed along 120 min.

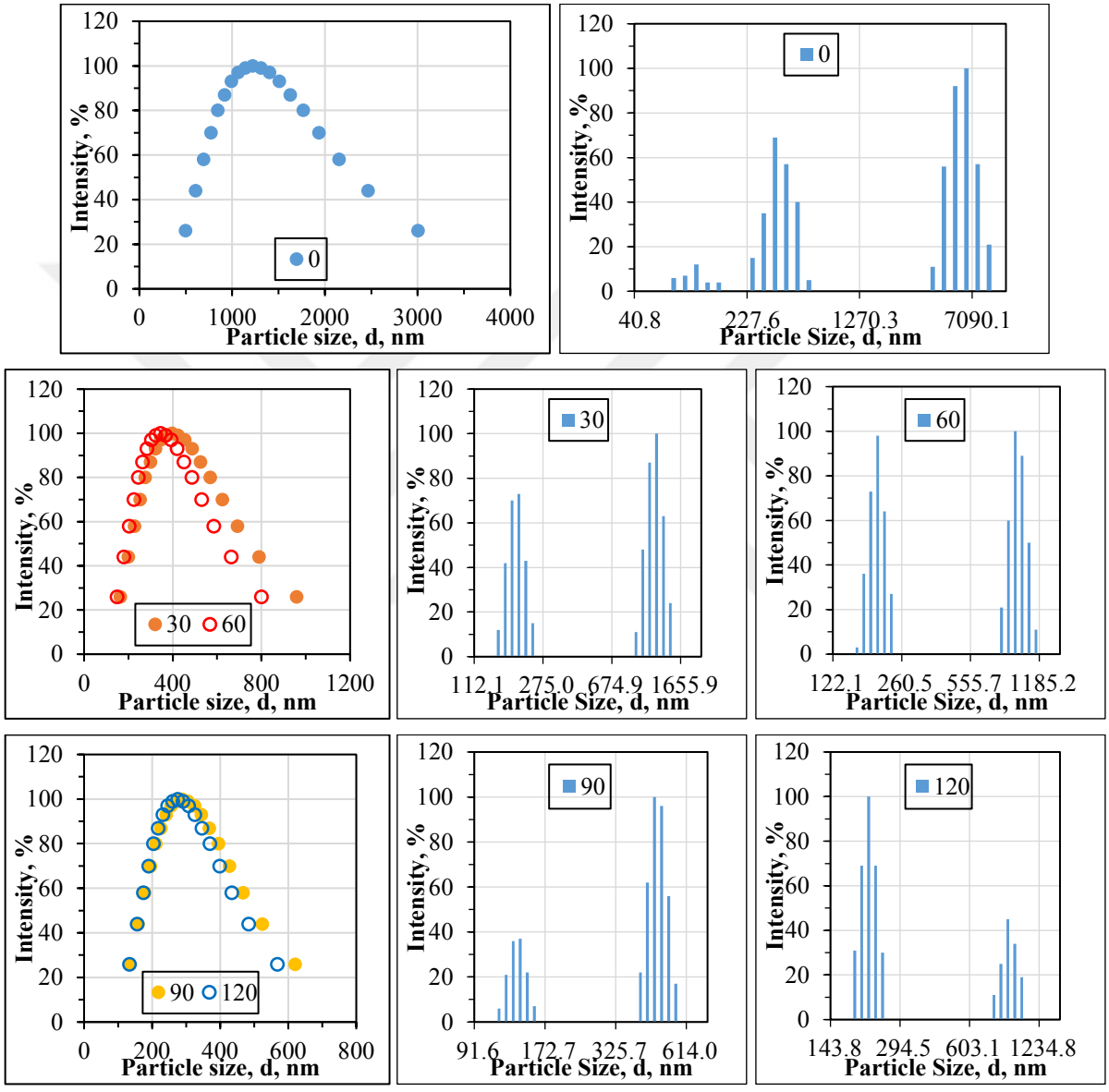


Figure 4.242. "N-TiO_2 and SRNOM" binary system "as-is" under irradiation intensity profile: Time dependent comparative presentation of log Normal distribution and multi-size distribution of "N-TiO_2 and SRNOM" binary system "as-is" under irradiation.

Table 4.152. Polydispersity of "N-TiO_2 and SRNOM" binary system "as-is" under irradiation.

N-TiO_2 and SRNOM	Polydispersity				
	0	30	60	90	120
	0.348	0.334	0.298	0.243	0.215

4.1.7.14. "N-TiO_2 and SRNOM" binary system "as-is" under irradiation volume profile. As elucidated for "N-TiO_2 and SRNOM" binary system "as-is" under irradiation intensity profile (Figure 4.241), a similar approach was followed for "N-TiO_2 and SRNOM" binary system "as-is" under irradiation volume profile. Time dependent logN distribution G(d) and multi size distribution C(d) of "N-TiO_2 and SRNOM" binary system "as-is" under irradiation volume profile was demonstrated in Figure 4.243. Time dependent mean diameter, range and min-max diameter difference with respect to log normal and multi-size distribution of "N-TiO_2 and SRNOM" binary system "as-is" under irradiation volume profile was displayed in Table 4.153.

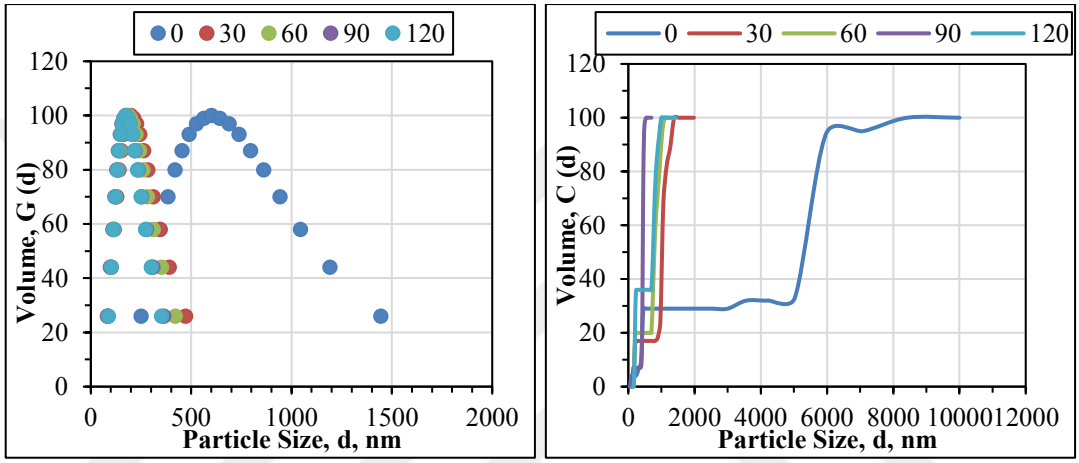


Figure 4.243. "N-TiO_2 and SRNOM" binary system "as-is" under irradiation volume profile: Time dependent logN distribution G(d) and multi size distribution C(d).

Table 4.153. "N-TiO_2 and SRNOM" binary system "as-is" under irradiation volume profile: Time dependent mean diameter, range and min-max diameter difference with respect to log normal and multi-size distribution.

N-TiO_2 and SRNOM	time, min				
	0	30	60	90	120
Log Normal distribution					
Mean, nm	601.9	200.1	186.6	174.5	175.9
Range	250.6-1445.6	84.7-472.9	82.6-421.7	83.5-364.7	87.9-352.3
Difference	1195.0	388.2	339.1	281.2	264.4
Multi-size distribution					
Max 1, nm	68.3	175.6	192.4	125.8	205.8
Max 2, nm	452.8	1057.1	811.5	447.2	803.3
Max 3, nm	3564.2	1383.8	1018.6	-	-
Max 4, nm	5970.1	-	-	-	-
Max 5, nm	8420.3	-	-	-	-
Range	40.8-10.000	112.1-1981.5	122.1-1379.1	91.6-697.1	143.8-1425.1
Difference	9959.2	1869.4	1257.0	605.5	1281.3

Considering log normal distribution and in terms of volume profile, hydrodynamic particle size of "N-TiO_2 and SRNOM" binary system "as-is" under irradiation exhibited a rapidly decreasing trend following initial period of time. Upon period of 30 min, continuous decrease was observed and remained until the end of 120 min. Considering multi-size distribution, five peaks were attained as 68.3 nm, 452.8 nm, 3564.2 nm, 5970.1 nm, and 8420.3 nm following initial period of time. Upon 30 min and 60 min, three peaks were observed and two peaks were monitored until 120 min period.

Time dependent comparative presentation of log Normal distribution and multi-size distribution of "N-TiO_2 and SRNOM" binary system "as-is" under irradiation volume profile was presented in Figure 4.244.

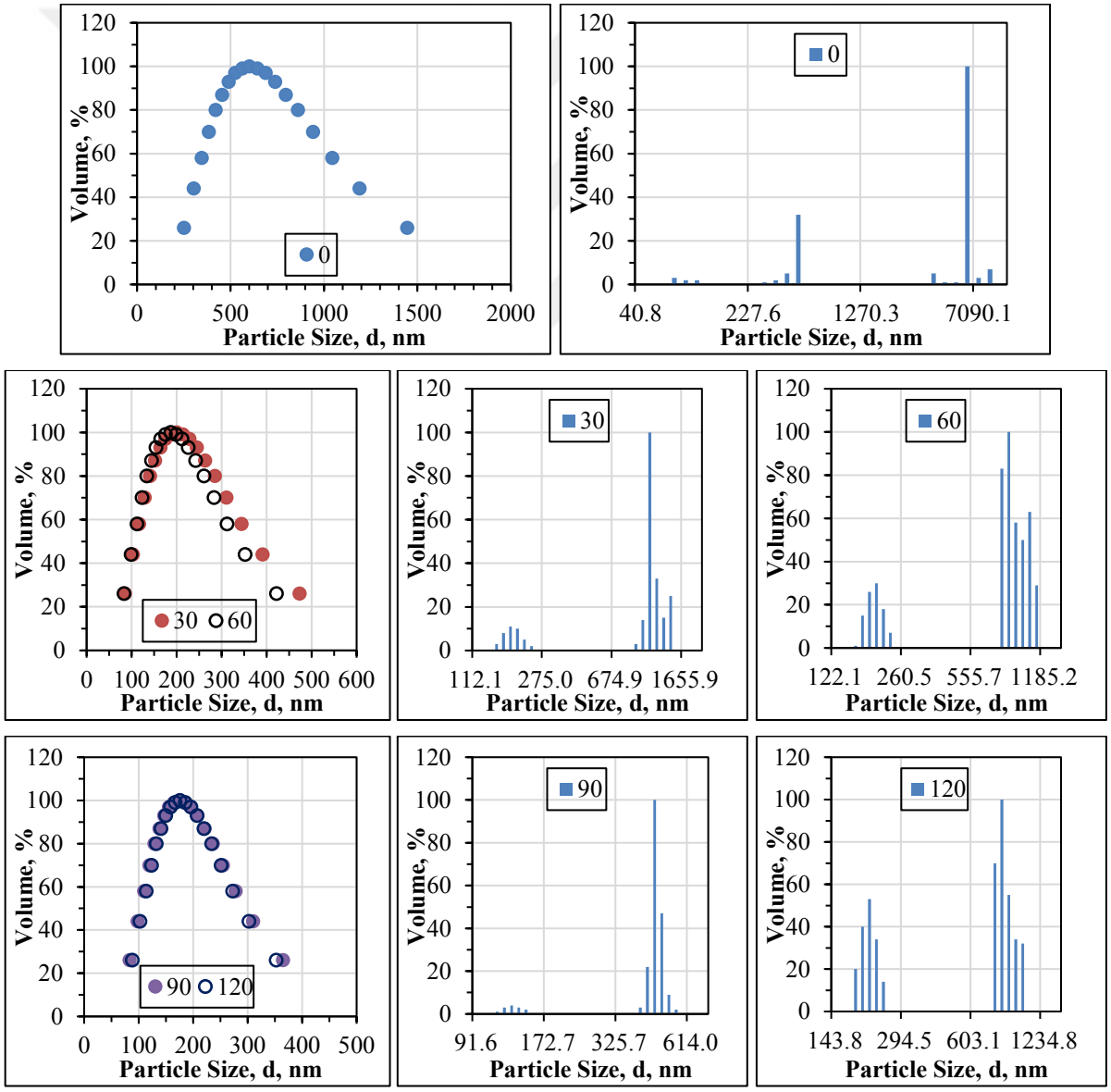


Figure 4.244. "N-TiO_2 and SRNOM" binary system "as-is" under irradiation volume profile: Time dependent comparative presentation of log Normal distribution and multi-size distribution of "N-TiO_2 and SRNOM" binary system "as-is" under irradiation.

4.1.7.15. "N-TiO_2 and SRNOM" binary system "as-is" under irradiation surface area profile. Time dependent logN distribution G(d) and multi size distribution C(d) of "N-TiO_2 and SRNOM" binary system "as-is" under irradiation surface area profile was exhibited in Figure 4.245. Time dependent mean diameter, range and min-max diameter difference with respect to log normal and multi-size distribution of "N-TiO_2 and SRNOM" binary system "as-is" under irradiation surface area profile was presented in Table 4.154.

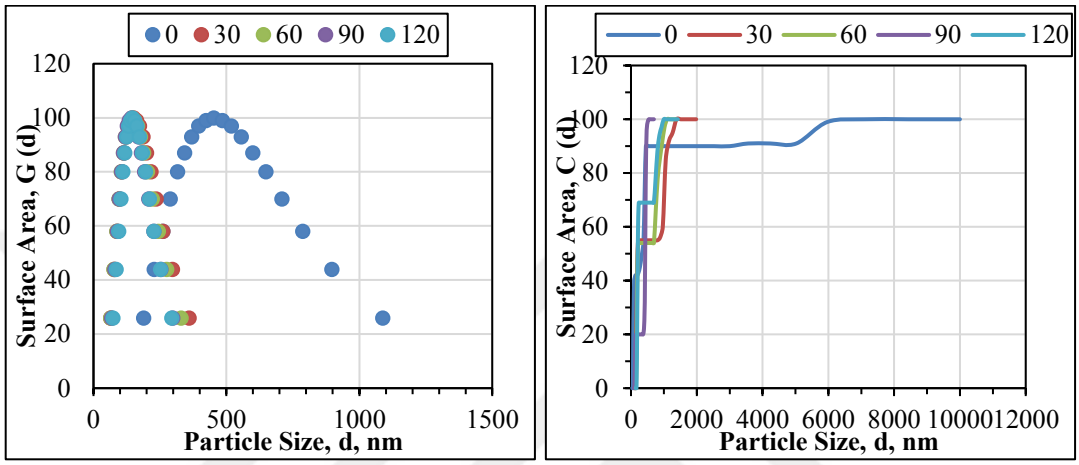


Figure 4.245. "N-TiO_2 and SRNOM" binary system "as-is" under irradiation surface area profile: Time dependent logN distribution G(d) and multi size distribution C(d).

Table 4.154. "N-TiO_2 and SRNOM" binary system "as-is" under irradiation surface area profile: Time dependent mean diameter, range and min-max diameter difference with respect to log normal and multi-size distribution.

N-TiO_2 and SRNOM	time, min				
	0	30	60	90	120
Log Normal distribution					
Mean, nm	453.2	152.2	146.0	142.7	147.2
Range	188.7-1088.5	64.4-359.8	64.6-329.9	68.3-298.3	73.5-294.8
Difference	899.8	295.4	265.3	230.0	221.3
Multi-size distribution					
Max 1, nm	68.3	175.6	192.4	125.8	205.8
Max 2, nm	452.8	1057.1	811.5	447.2	803.3
Max 3, nm	3564.2	1383.8	1018.6	-	-
Max 4, nm	5970.1	-	-	-	-
Range	40.8-10.000	112.1-1981.5	122.1-1379.1	91.6-697.1	143.8-1425.1
Difference	9959.2	1869.4	1257.0	605.5	1281.3

In terms of surface area profile, initial hydrodynamic particle size of "N-TiO_2 and SRNOM" binary system "as-is" under irradiation was recorded as 453.2 nm. Upon period of 30 min, roughly

65 % decrease was detected and slight variations remained until 120 min. On the other hand, initial size difference demonstrated a sharp decrease in the first 30 min and minor variations remained until 120 min. For comparison purposes, in terms of multi-size distribution, initially four max diameters were attained as 68.3 nm, 452.8 nm, 3564.2 nm, and 5970.1 nm, respectively. Upon 30 min and 60 min, three peaks were observed and two max diameters were monitored until the end of 120 min.

Time dependent comparative presentation of log Normal distribution and multi-size distribution of "N-TiO_2 and SRNOM" binary system "as-is" under irradiation surface area profile was presented in Figure 4.246.

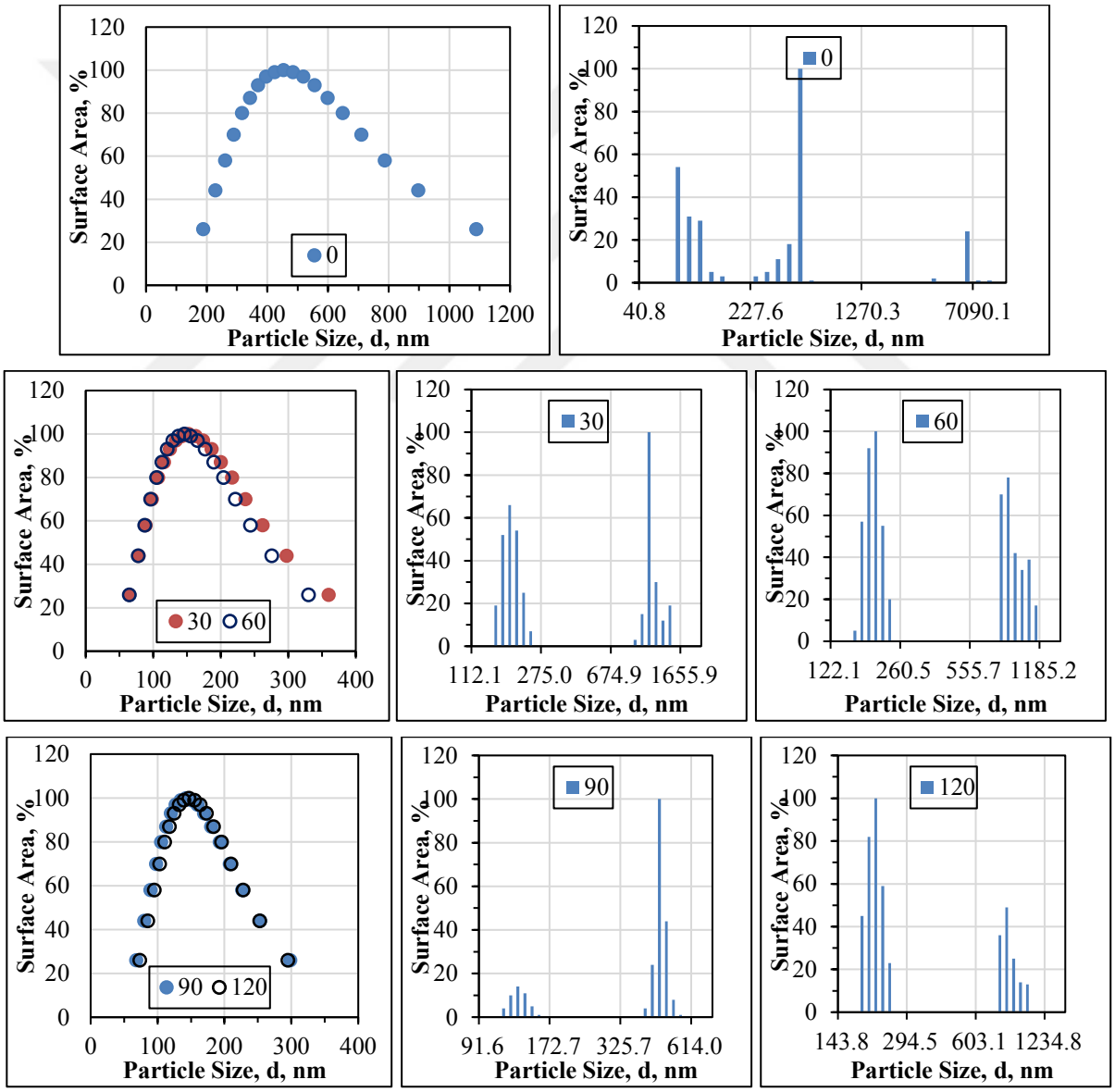


Figure 4.246. "N-TiO_2 and SRNOM" binary system "as-is" under irradiation surface area profile: Time dependent comparative presentation of log Normal distribution and multi-size distribution of "N-TiO_2 and SRNOM" binary system "as-is" under irradiation.

4.1.7.16. "N-TiO_2 and SRNOM" binary system "as-is" under irradiation number profile. Time dependent logN distribution G(d) and multi size distribution C(d) of "N-TiO_2 and SRNOM" binary system "as-is" under irradiation number profile was shown in Figure 4.247. Time dependent mean diameter, range and min-max diameter difference with respect to log normal and multi-size distribution of "N-TiO_2 and SRNOM" binary system "as-is" under irradiation number profile was given in Table 4.155.

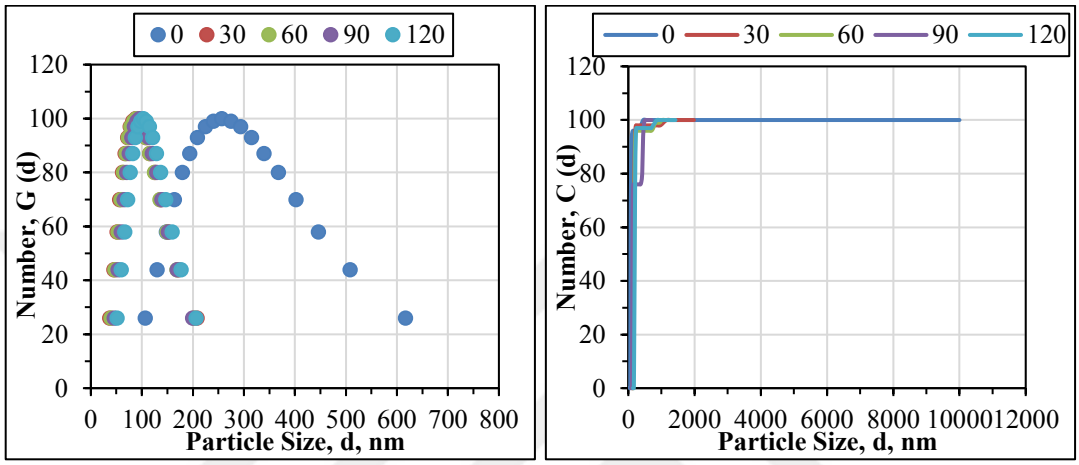


Figure 4.247. "N-TiO_2 and SRNOM" binary system "as-is" under irradiation number profile: Time dependent logN distribution G(d) and multi size distribution C(d).

Table 4.155. "N-TiO_2 and SRNOM" binary system "as-is" under irradiation number profile: Time dependent mean diameter, range and min-max diameter difference with respect to log normal and multi-size distribution.

N-TiO_2 and SRNOM	time, min				
	0	30	60	90	120
Log Normal distribution					
Mean, nm	256.9	88.1	89.4	95.5	103.1
Range	107.0-617.1	37.3-208.3	39.5-201.9	45.7-199.6	51.5-206.4
Difference	510.1	171.0	162.4	153.9	154.9
Multi-size distribution					
Max 1, nm	68.3	175.6	178.4	125.8	205.8
Max 2, nm	452.8	1057.1	752.3	447.2	747.7
Max 3, nm	-	-	811.5	-	803.3
Range	40.8-10.000	112.1-1981.5	122.1-1379.1	91.6-697.1	143.8-1425.1
Difference	9959.2	1869.4	1257.0	605.5	1281.3

In terms of number profile, initial hydrodynamic particle size of "N-TiO_2 and SRNOM" binary system "as-is" under irradiation was recorded as 256.9 nm. Upon 30 min, approximately 65 % decline was monitored and slight variations remained until the end of 120 min. On the other hand, initial size

difference displayed a dramatically decreasing trend and decreased from 510.1 nm to 171.0 nm in the first 30 min. Upon 30 min, minor alterations were observed until the end of 120 min. For comparison purposes, in terms of multi-size distribution, two peaks were obtained until 60 min. Upon 60 min, three max diameters were observed until 90 min. Upon 90 min, two peaks were attained until 120 min. Upon 120 min, three peaks were obtained.

In a similar manner to data represented "N-TiO_2 and SRNOM" binary system "as-is" under irradiation surface area profile (Figure 4.246), time dependent comparative presentation of log Normal distribution and multi-size distribution of "N-TiO_2 and SRNOM" binary system "as-is" under irradiation number profile was shown in Figure 4.248.

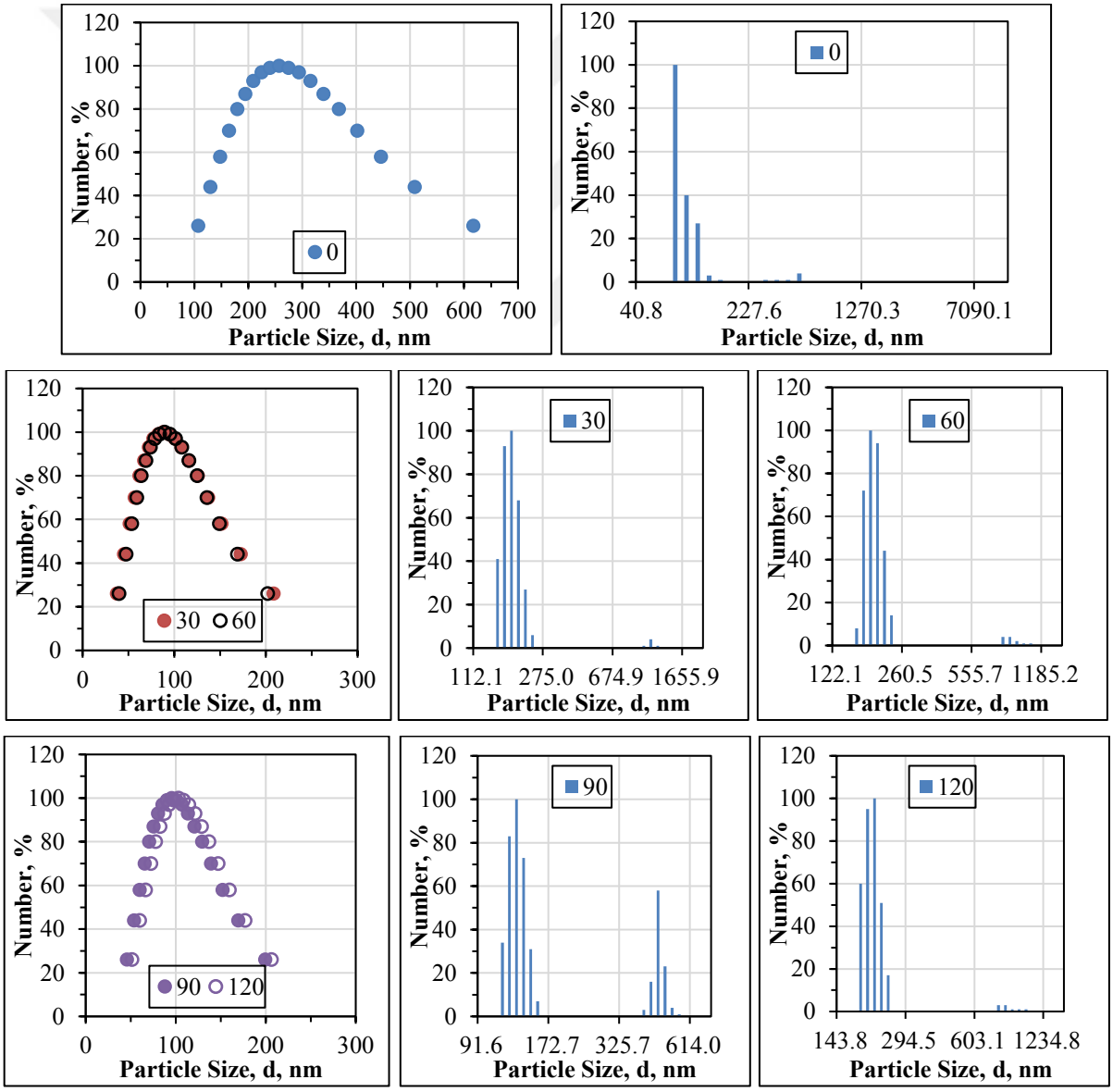


Figure 4.248. "N-TiO_2 and SRNOM" binary system "as-is" under irradiation number profile: Time dependent comparative presentation of log Normal distribution and multi-size distribution of "N-TiO_2 and SRNOM" binary system "as-is" under irradiation.

4.1.7.17. "Fe-TiO_2 and HA" binary system "as-is" under irradiation intensity profile. Time dependent logN distribution G(d) and multi size distribution C(d) of "Fe-TiO_2 and HA" binary system "as-is" under irradiation intensity profile was demonstrated in Figure 4.249. Time dependent mean diameter, range and min-max diameter difference with respect to log normal and multi-size distribution of "Fe-TiO_2 and HA" binary system "as-is" under irradiation intensity profile was exhibited in Table 4.156.

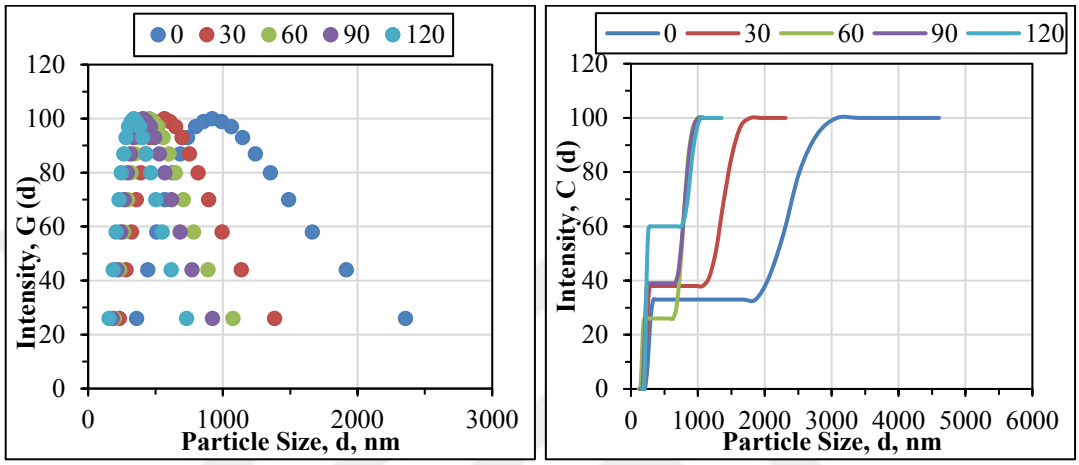


Figure 4.249. "Fe-TiO_2 and HA" binary system "as-is" under irradiation intensity profile: Time dependent logN distribution G(d) and multi size distribution C(d).

Table 4.156. "Fe-TiO_2 and HA" binary system "as-is" under irradiation intensity profile: Time dependent mean diameter, range and min-max diameter difference with respect to log normal and multi-size distribution.

Fe-TiO_2 and HA	time, min				
	0	30	60	90	120
Log Normal distribution					
Mean, nm	920.7	566.0	456.0	407.9	338.5
Range	359.6-2357.6	231.2-1385.5	193.2-1076.2	180.0-924.3	156.8-730.9
Difference	1998.0	1154.3	883.0	744.3	574.1
Multi-size distribution					
Max 1, nm	275.4	250.7	171.8	209.9	227.9
Max 2, nm	2517.6	1506.9	790.9	815.5	911.4
Range	184.1-4603.6	150.2-2309.5	117.3-1349.6	136.7-1344.7	163.9-1354.2
Difference	4419.5	2159.3	1232.3	1208.0	1190.3

Hydrodynamic particle size of "Fe-TiO_2 and HA" binary system "as-is" under irradiation exhibited a continuously decreasing trend according to time variations. In terms of log normal distribution, initial hydrodynamic size was obtained as 920.7 nm and detected to 338.5 nm upon 120

min. In terms of multi-size distribution, two peaks were observed during 120 min. Time dependent comparative presentation of log Normal distribution and multi-size distribution of "Fe-TiO_2 and HA" binary system "as-is" under irradiation intensity profile was given in Figure 4.250. Polydispersity of "Fe-TiO_2 and HA" binary system "as-is" under irradiation was presented in Table 4.157. An average value of 0.314 could be accepted as appropriate for expressing polydispersity.

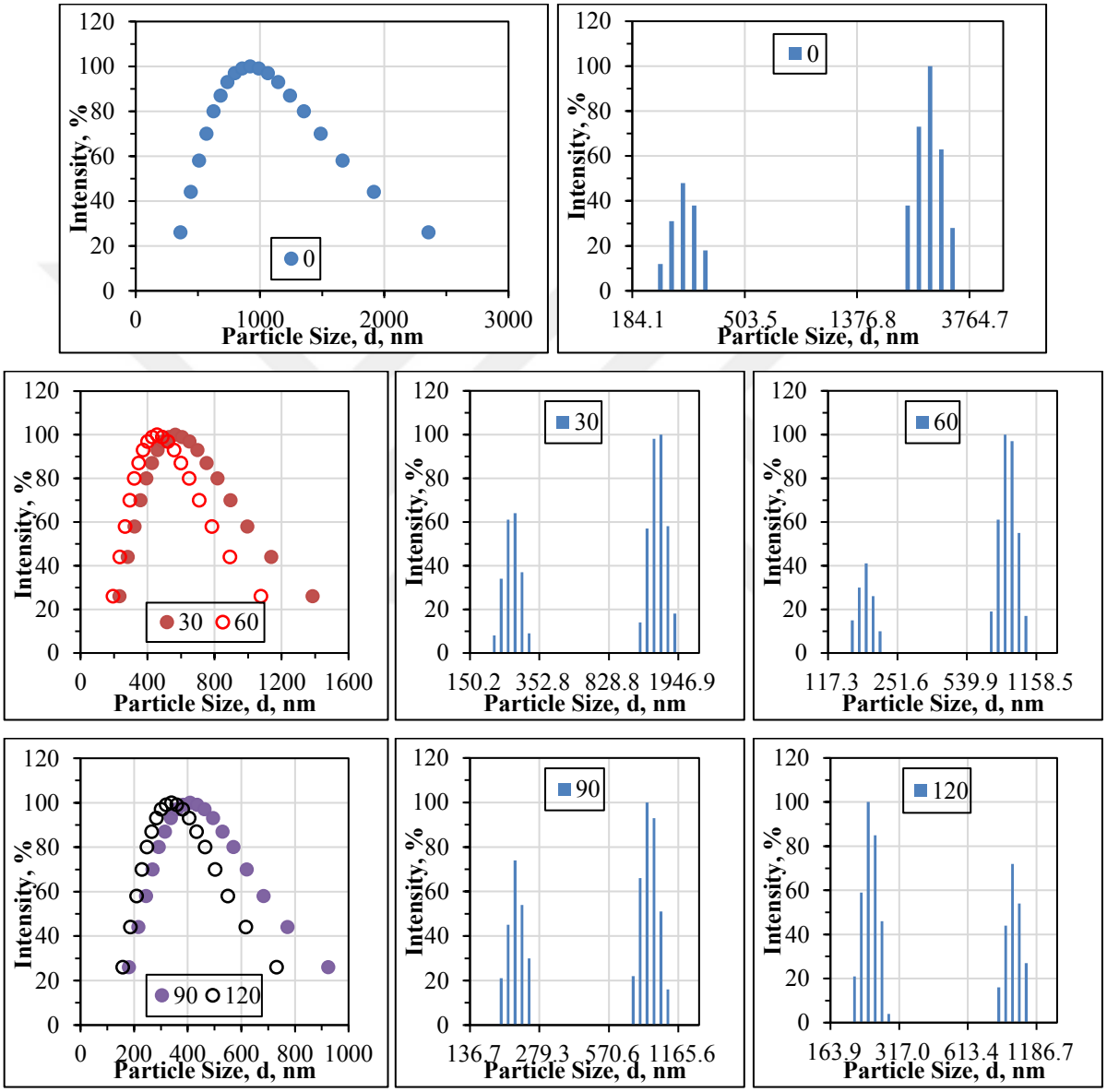


Figure 4.250. "Fe-TiO_2 and HA" binary system "as-is" under irradiation intensity profile: Time dependent comparative presentation of log Normal distribution and multi-size distribution of "Fe-TiO_2 and HA" binary system "as-is" under irradiation.

Table 4.157. Polydispersity of "Fe-TiO_2 and HA" binary system "as-is" under irradiation.

Fe-TiO_2 and HA	Polydispersity				
	0	30	60	90	120
	0.386	0.345	0.313	0.281	0.245

4.1.7.18. "Fe-TiO_2 and HA" binary system "as-is" under irradiation volume profile. In a similar manner to data described "Fe-TiO_2 and HA" binary system "as-is" under irradiation intensity profile (Figure 4.249), time dependent logN distribution G(d) and multi size distribution C(d) of "Fe-TiO_2 and HA" binary system "as-is" under irradiation volume profile was shown in Figure 4.251. Time dependent mean diameter, range and min-max diameter difference with respect to log normal and multi-size distribution of "Fe-TiO_2 and HA" binary system "as-is" under irradiation volume profile was presented in Table 4.158.

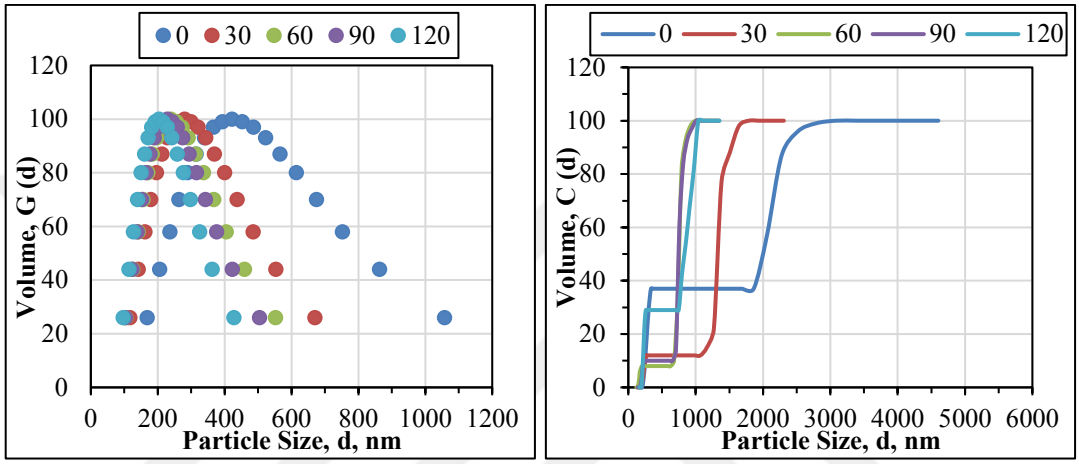


Figure 4.251. "Fe-TiO_2 and HA" binary system "as-is" under irradiation volume profile: Time dependent logN distribution G(d) and multi size distribution C(d).

Table 4.158. "Fe-TiO_2 and HA" binary system "as-is" under irradiation volume profile: Time dependent mean diameter, range and min-max diameter difference with respect to log normal and multi-size distribution.

Fe-TiO_2 and HA	time, min				
	0	30	60	90	120
Log Normal distribution					
Mean, nm	421.9	280.3	239.7	228.6	204.0
Range	168.3-1057.7	117.2-670.5	104.1-552.1	103.6-504.5	97.3-427.8
Difference	889.4	553.3	448.0	400.9	330.5
Multi-size distribution					
Max 1, nm	275.4	250.7	171.8	209.9	227.9
Max 2, nm	2276.6	1383.5	790.9	759.3	798.7
Max 3, nm	-	-	-	-	1040.0
Range	184.1-4603.6	150.2-2309.5	117.3-1349.6	136.7-1344.7	163.9-1354.2
Difference	4419.5	2159.3	1232.3	1208.0	1190.3

As explicated for "Fe-TiO_2 and HA" binary system "as-is" under irradiation intensity profile (Table 4.156), a similar approach was followed for "Fe-TiO_2 and HA" binary system "as-is" under

irradiation volume profile. Hydrodynamic particle size roughly 50 % decreased in the first 30 min. Initial hydrodynamic particle size was detected as 421.9 nm and decreased to 280.3 nm upon 30 min and slowly decreasing trend was observed until the end of 120 min. Also, size difference between max and min diameter decreased from 889.4 nm to 330.5 nm along 120 min. In terms of multi-size distribution, initially peaks were monitored until 120 min. Upon 120 min, three peaks were observed.

As described for "Fe-TiO_2 and HA" binary system "as-is" under irradiation intensity profile (Figure 4.250), in a similar manner, time dependent comparative presentation of log Normal distribution and multi-size distribution of "Fe-TiO_2 and HA" binary system "as-is" under irradiation volume profile was demonstrated in Figure 4.252.

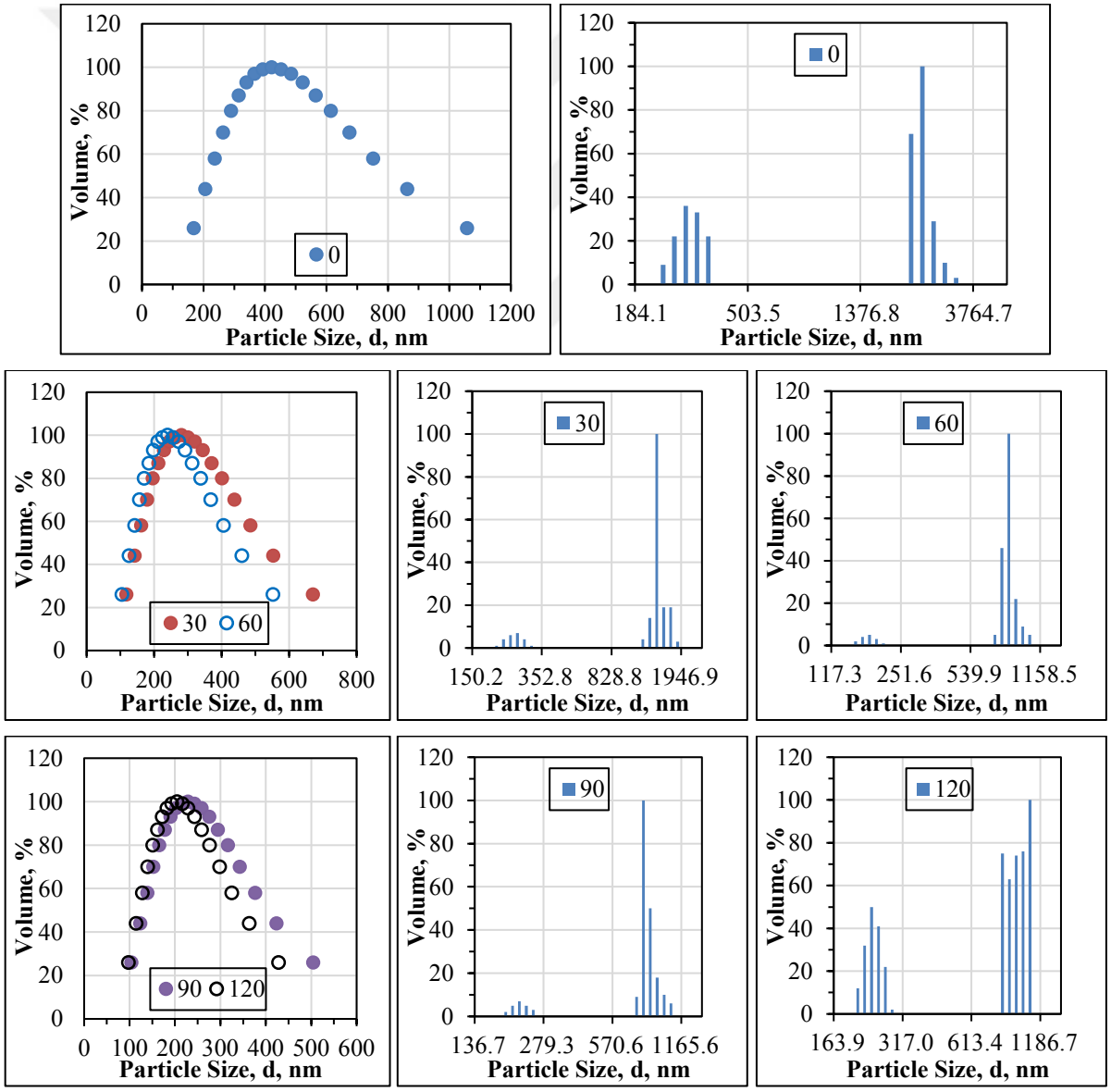


Figure 4.252. "Fe-TiO_2 and HA" binary system "as-is" under irradiation volume profile: Time dependent comparative presentation of log Normal distribution and multi-size distribution of "Fe-TiO_2 and HA" binary system "as-is" under irradiation.

4.1.7.19. "Fe-TiO_2 and HA" binary system "as-is" under irradiation surface area profile. Time dependent logN distribution G(d) and multi size distribution C(d) of "Fe-TiO_2 and HA" binary system "as-is" under irradiation surface area profile was demonstrated in Figure 4.253. Time dependent mean diameter, range and min-max diameter difference with respect to log normal and multi-size distribution of "Fe-TiO_2 and HA" binary system "as-is" under irradiation surface area profile was displayed in Table 4.159.

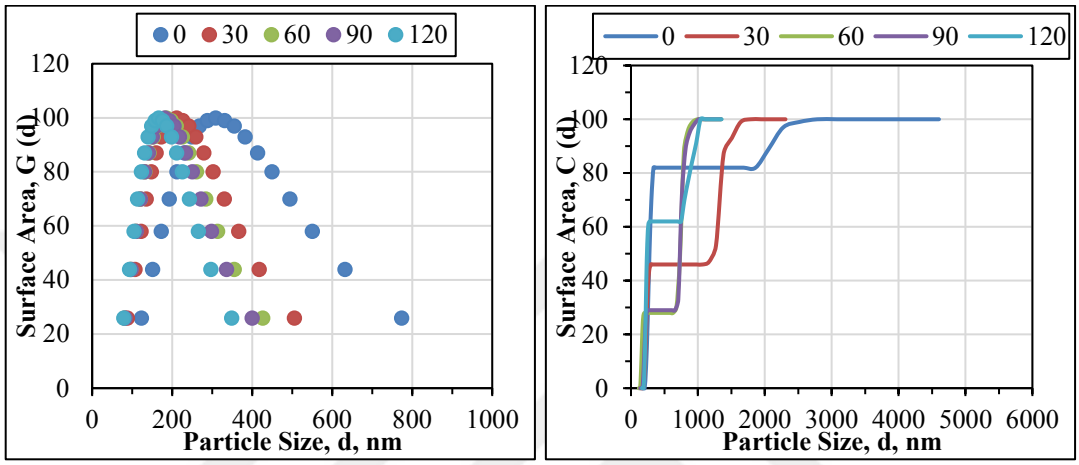


Figure 4.253. "Fe-TiO_2 and HA" binary system "as-is" under irradiation surface area profile: Time dependent logN distribution G(d) and multi size distribution C(d).

Table 4.159. "Fe-TiO_2 and HA" binary system "as-is" under irradiation surface area profile: Time dependent mean diameter, range and min-max diameter difference with respect to log normal and multi-size distribution.

Fe-TiO_2 and HA	time, min				
	0	30	60	90	120
Log Normal distribution					
Mean, nm	308.8	211.6	185.4	181.3	166.5
Range	123.2-774.1	88.4-506.1	80.5-426.9	82.2-400.2	79.4-349.3
Difference	650.9	417.7	346.4	318.0	269.9
Multi-size distribution					
Max 1, nm	275.4	230.2	171.8	209.9	227.9
Max 2, nm	2276.6	1383.5	790.9	759.3	798.7
Max 3, nm	-	-	-	-	911.4
Max 4, nm	-	-	-	-	1040.0
Range	184.1-4603.6	150.2-2309.5	117.3-1349.6	136.7-1344.7	163.9-1354.2
Difference	4419.5	2159.3	1232.3	1208.0	1190.3

As explicated for "Fe-TiO_2 and HA" binary system "as-is" under irradiation volume profile (Table 4.158), a similar approach was followed for "Fe-TiO_2 and HA" binary system "as-is" under

irradiation surface area profile. According to log normal distribution, initial hydrodynamic particle size was recorded as 308.8 nm and continuous decrease was monitored with minor variations until the end of 120 min. However, in terms of multi-size distribution, initially two peaks were observed and remained until 120 min. Upon 120 min, four max diameters were obtained as 227.9 nm, 798.7 nm, 911.4 nm, and 1040.0 nm, respectively.

As explained for "Fe-TiO_2 and HA" binary system "as-is" under irradiation volume profile (Figure 4.252), time dependent comparative presentation of log Normal distribution and multi-size distribution of "Fe-TiO_2 and HA" binary system "as-is" under irradiation surface area profile was presented in Figure 4.254.

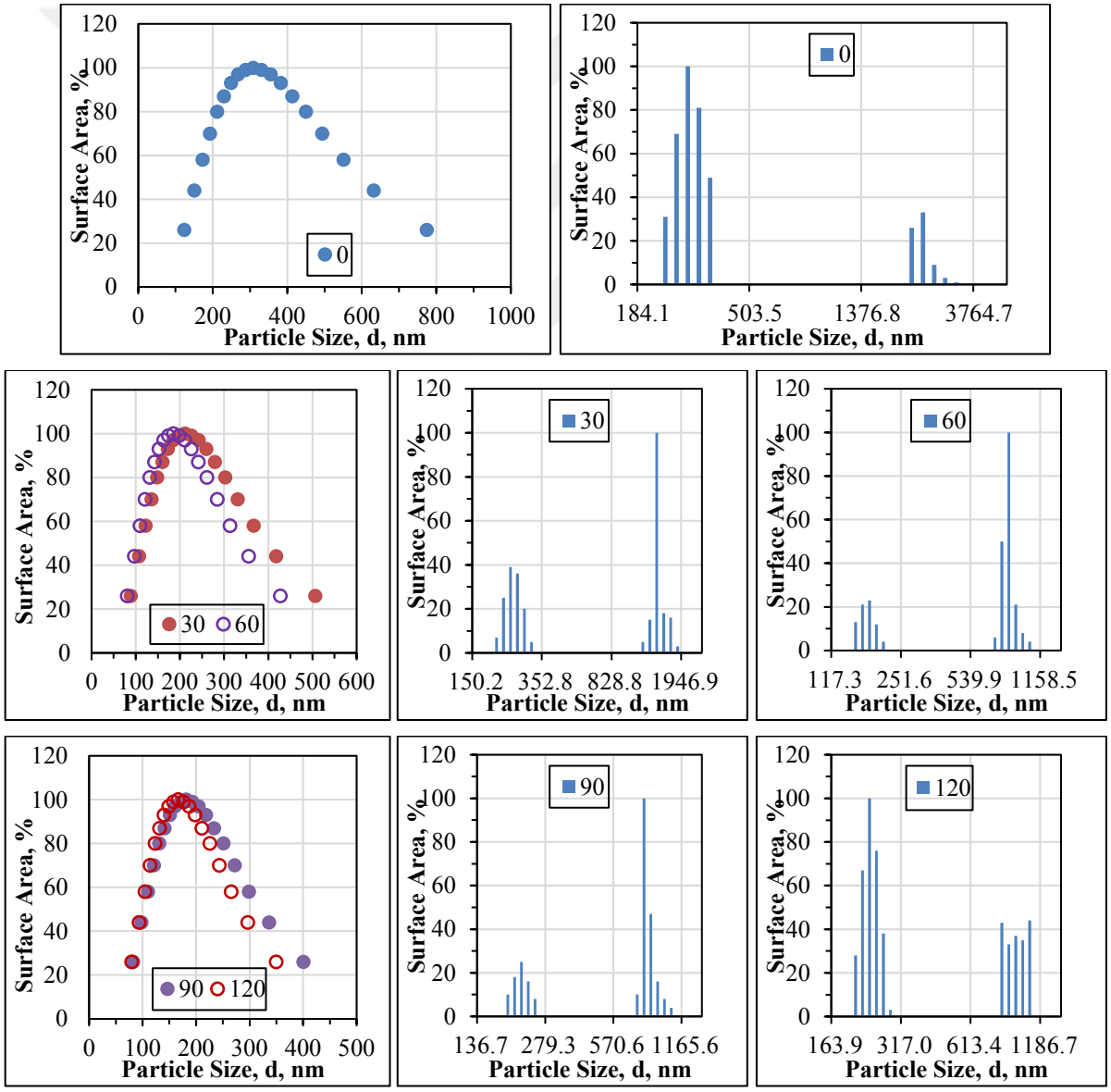


Figure 4.254. "Fe-TiO_2 and HA" binary system "as-is" under irradiation surface area profile: Time dependent comparative presentation of log Normal distribution and multi-size distribution of "Fe-TiO_2 and HA" binary system "as-is" under irradiation.

4.1.7.20. "Fe-TiO_2 and HA" binary system "as-is" under irradiation number profile. In a similar manner to data depicted "Fe-TiO_2 and HA" binary system "as-is" under irradiation surface area profile (Figure 4.253), time dependent logN distribution G(d) and multi size distribution C(d) of "Fe-TiO_2 and HA" binary system "as-is" under irradiation number profile was presented in Figure 4.255. Time dependent mean diameter, range and min-max diameter difference with respect to log normal and multi-size distribution of "Fe-TiO_2 and HA" binary system "as-is" under irradiation number profile was displayed in Table 4.160.

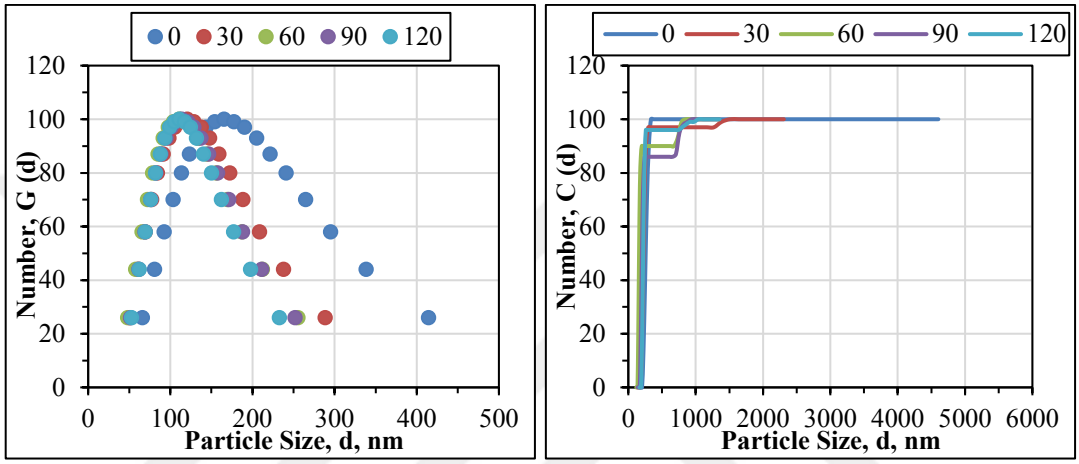


Figure 4.255. "Fe-TiO_2 and HA" binary system "as-is" under irradiation number profile: Time dependent logN distribution G(d) and multi size distribution C(d).

Table 4.160. "Fe-TiO_2 and HA" binary system "as-is" under irradiation number profile: Time dependent mean diameter, range and min-max diameter difference with respect to log normal and multi-size distribution.

Fe-TiO_2 and HA	time, min				
	0	30	60	90	120
Log Normal distribution					
Mean, nm	165.4	120.6	110.8	114.1	111.0
Range	66.0-414.6	50.4-288.4	48.1-255.3	51.7-251.8	52.9-232.9
Difference	348.6	238.0	207.2	200.1	180.0
Multi-size distribution					
Max 1, nm	275.4	230.2	159.2	209.9	227.9
Max 2, nm	-	1383.5	790.9	759.3	798.7
Range	184.1-4603.6	150.2-2309.5	117.3-1349.6	136.7-1344.7	163.9-1354.2
Difference	4419.5	2159.3	1232.3	1208.0	1190.3

As explained for "Fe-TiO_2 and HA" binary system "as-is" under irradiation surface area profile (Table 4.159), a similar approach was followed for "Fe-TiO_2 and HA" binary system "as-is" under

irradiation number profile. It could be stated that a slight decrease was observed along 120 min period. Initial hydrodynamic particle size was recorded as 165.4 nm and detected to 120.6 nm upon 30 min. Upon 120 min, hydrodynamic particle size was detected as 111.0 nm. Also, according to log normal distribution, initial size difference between max and min diameter was obtained as 348.6 nm and decreased to 180.0 nm during 120 min. In terms of multi-size distribution, initially one peak was monitored and two peaks were obtained until the end of 120 min. As explained for "Fe-TiO_2 and HA" binary system "as-is" under irradiation surface area profile (Figure 4.254), time dependent comparative presentation of log Normal distribution and multi-size distribution of "Fe-TiO_2 and HA" binary system "as-is" under irradiation number profile was shown in Figure 4.256.

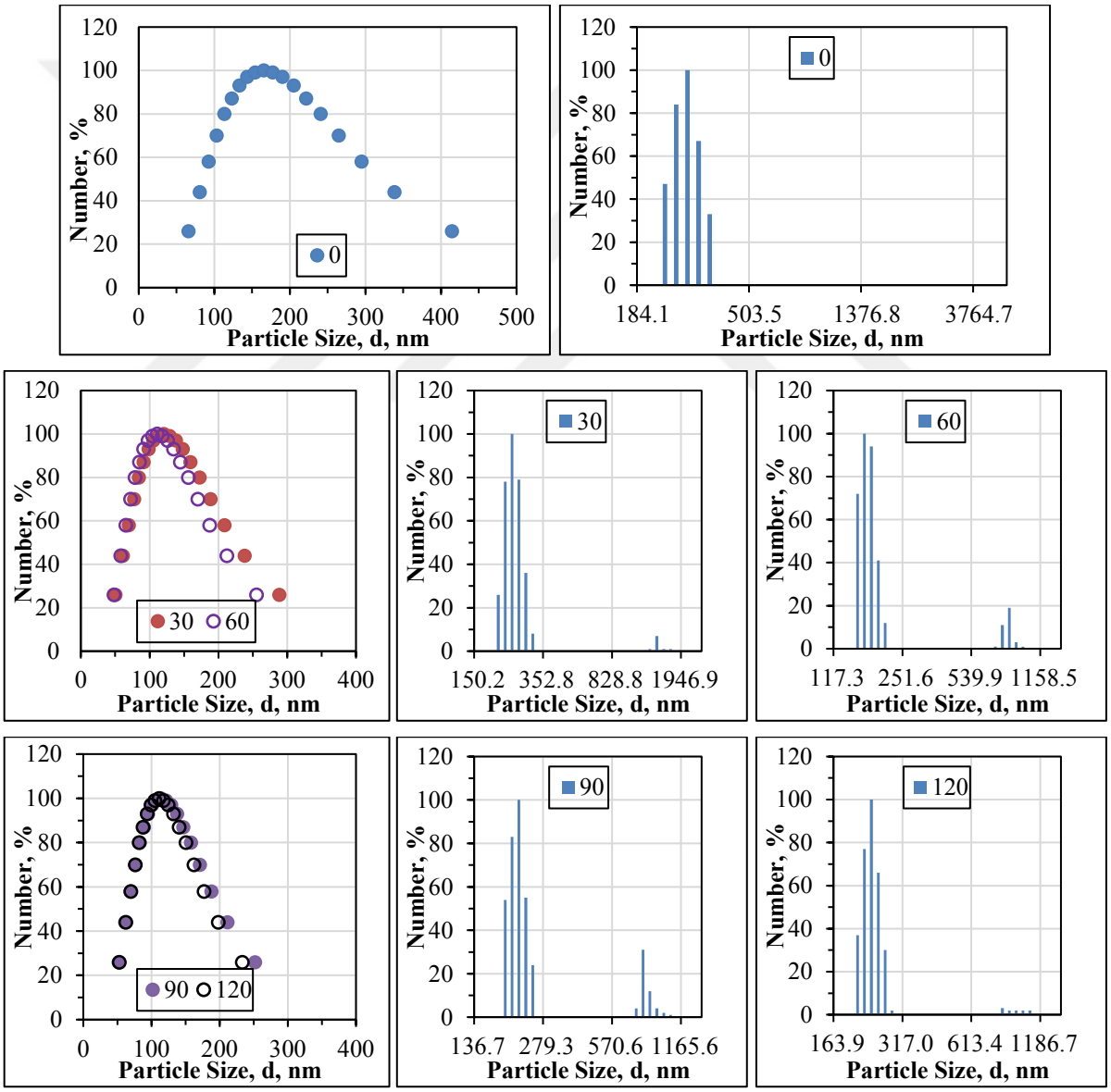


Figure 4.256. "Fe-TiO_2 and HA" binary system "as-is" under irradiation number profile: Time dependent comparative presentation of log Normal distribution and multi-size distribution of "Fe-TiO_2 and HA" binary system "as-is" under irradiation.

4.1.7.21. "Fe-TiO_2 and SRNOM" binary system "as-is" under irradiation intensity profile. In a similar manner to data depicted "Fe-TiO_2 and HA" binary system "as-is" under irradiation intensity profile (Figure 4.249), time dependent logN distribution G(d) and multi size distribution C(d) of "Fe-TiO_2 and SRNOM" binary system "as-is" under irradiation intensity profile was presented in Figure 4.257. Time dependent mean diameter, range and min-max diameter difference with respect to log normal and multi-size distribution of "Fe-TiO_2 and SRNOM" binary system "as-is" under irradiation intensity profile was displayed in Table 4.161.

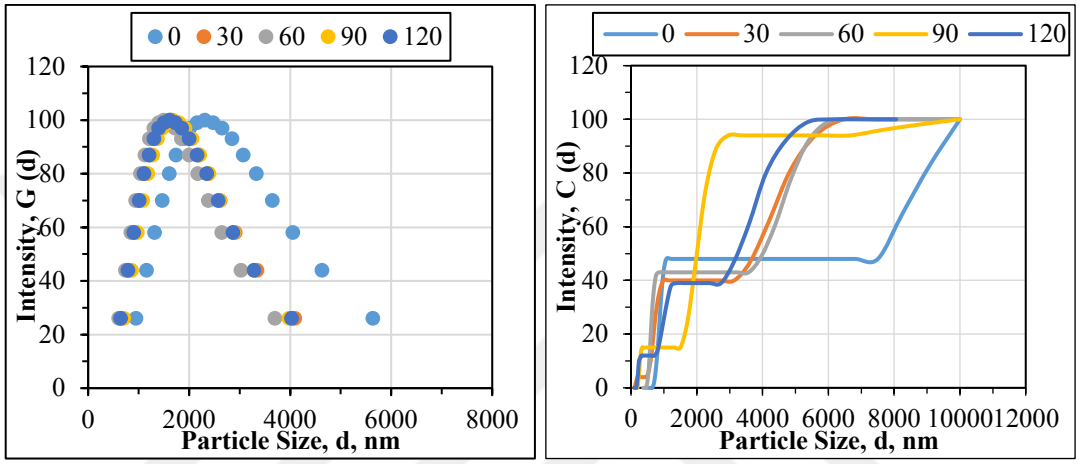


Figure 4.257. "Fe-TiO_2 and SRNOM" binary system "as-is" under irradiation intensity profile: Time dependent logN distribution G(d) and multi size distribution C(d).

Table 4.161. "Fe-TiO_2 and SRNOM" binary system "as-is" under irradiation intensity profile: Time dependent mean diameter, range and min-max diameter difference with respect to log normal and multi-size distribution.

Fe-TiO_2 and SRNOM	time, min				
	0	30	60	90	120
Log Normal distribution					
Mean, nm	2311.7	1634.4	1497.6	1679.6	1612.5
Range	947.8-5638.5	652.5-4094.2	606.5-3697.9	709.5-3976.0	645.9-4025.3
Difference	4690.7	3441.7	3091.4	3266.5	3379.4
Multi-size distribution					
Max 1, nm	906.7	173.1	623.0	296.6	241.2
Max 2, nm	9087.7	736.9	4869.3	2257.5	1064.5
Max 3, nm	-	4846.1	-	8734.5	4105.4
Range	468.3-10.000	96.9-10.000	372.6-10.000	131.7-10.000	107.3-8062.4
Difference	9531.7	9903.1	9627.4	9868.3	7955.1

In terms of intensity profile, initial hydrodynamic size was attained as 2311.7 nm and detected to 1612.5 nm upon 120 min. In terms of multi-size distribution, initially two peaks were attained and

upon 30 min, three peaks were obtained. Time dependent comparative presentation of log Normal distribution and multi-size distribution of "Fe-TiO_2 and SRNOM" binary system "as-is" under irradiation intensity profile was given in Figure 4.258. Polydispersity of "Fe-TiO_2 and SRNOM" binary system "as-is" under irradiation was given in Table 4.162. An average value of 0.348 could be regarded as suitable for expressing polydispersity.

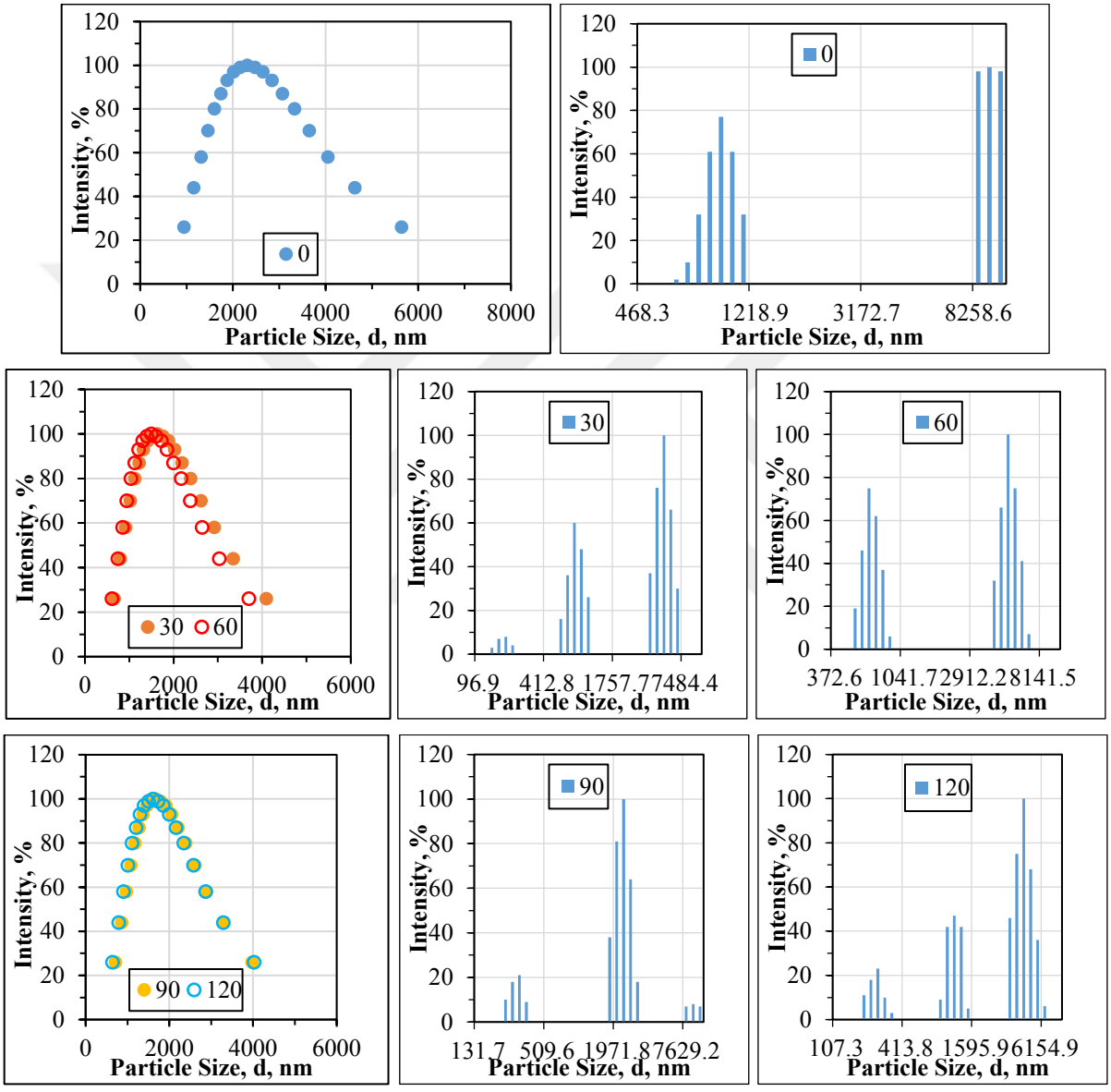


Figure 4.258. "Fe-TiO_2 and SRNOM" binary system "as-is" under irradiation intensity profile: Time dependent comparative presentation of log Normal distribution and multi-size distribution of "Fe-TiO_2 and SRNOM" binary system "as-is" under irradiation.

Table 4.162. Polydispersity of "Fe-TiO_2 and SRNOM" binary system "as-is" under irradiation.

Fe-TiO_2 and SRNOM	Polydispersity				
	0	30	60	90	120
	0.342	0.366	0.352	0.316	0.362

4.1.7.22. "Fe-TiO_2 and SRNOM" binary system "as-is" under irradiation volume profile. Time dependent logN distribution G(d) and multi size distribution C(d) of "Fe-TiO_2 and SRNOM" binary system "as-is" under irradiation volume profile was displayed in Figure 4.259. Time dependent mean diameter, range and min-max diameter difference with respect to log normal and multi-size distribution of "Fe-TiO_2 and SRNOM" binary system "as-is" under irradiation volume profile was presented in Table 4.163.

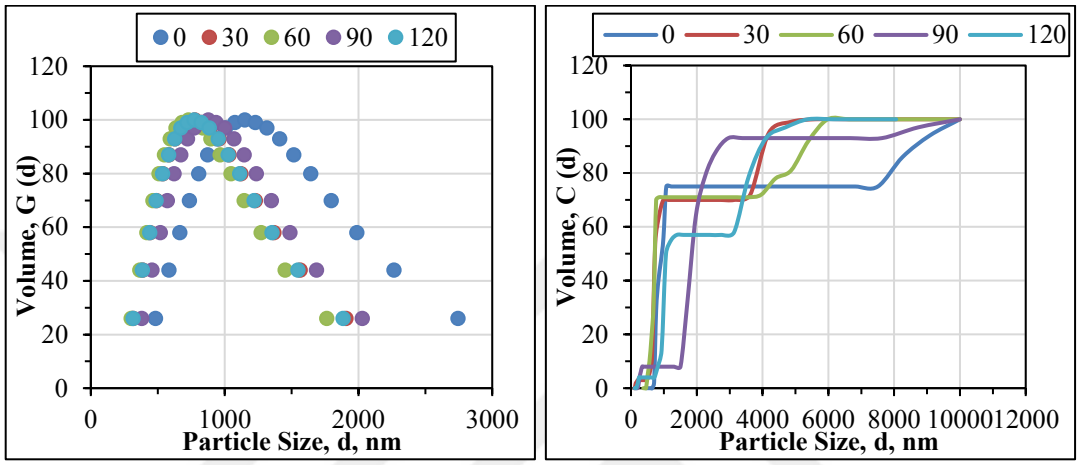


Figure 4.259. "Fe-TiO_2 and SRNOM" binary system "as-is" under irradiation volume profile: Time dependent logN distribution G(d) and multi size distribution C(d).

Table 4.163. "Fe-TiO_2 and SRNOM" binary system "as-is" under irradiation volume profile: Time dependent mean diameter, range and min-max diameter difference with respect to log normal and multi-size distribution.

Fe-TiO_2 and SRNOM	time, min				
	0	30	60	90	120
Log Normal distribution					
Mean, nm	1151.5	778.1	730.7	878.8	772.2
Range	483.1-2744.5	317.5-1906.7	302.7-1764.0	380.4-2030.2	316.3-1885.6
Difference	2261.4	1589.2	1461.3	1649.8	1569.3
Multi-size distribution					
Max 1, nm	764.9	149.7	765.2	296.6	210.7
Max 2, nm	1074.8	173.1	4393.5	1971.8	241.2
Max 3, nm	8258.6	736.9	5396.5	8734.5	1064.5
Max 4, nm	-	4192.5	-	-	3587.0
Range	468.3-10.000	96.9-10.000	372.6-10.000	131.7-10.000	107.3-8062.4
Difference	9531.7	9903.1	9627.4	9868.3	7955.1

In terms of volume profile, hydrodynamic particle size of "Fe-TiO_2 and SRNOM" binary system "as-is" under irradiation was recorded as 1151.5 nm following initial period of time. Upon 30 min, a

rapid decrease was observed and minor alterations remained until the end of 120 min. On the other hand, in the first 30 min, ~ 30 % decrease was attained in terms of size difference. Upon 30 min, slight variations were observed until the end of 120 min. However, in terms of multi-size distribution, initially three peaks were obtained, and upon 30 min, four peaks were observed. Upon period of 60 min and 90 min, three max diameters were attained and four peaks were monitored upon period of 120 min.

Time dependent comparative presentation of log Normal distribution and multi-size distribution of "Fe-TiO_2 and SRNOM" binary system "as-is" under irradiation volume profile was demonstrated in Figure 4.260.

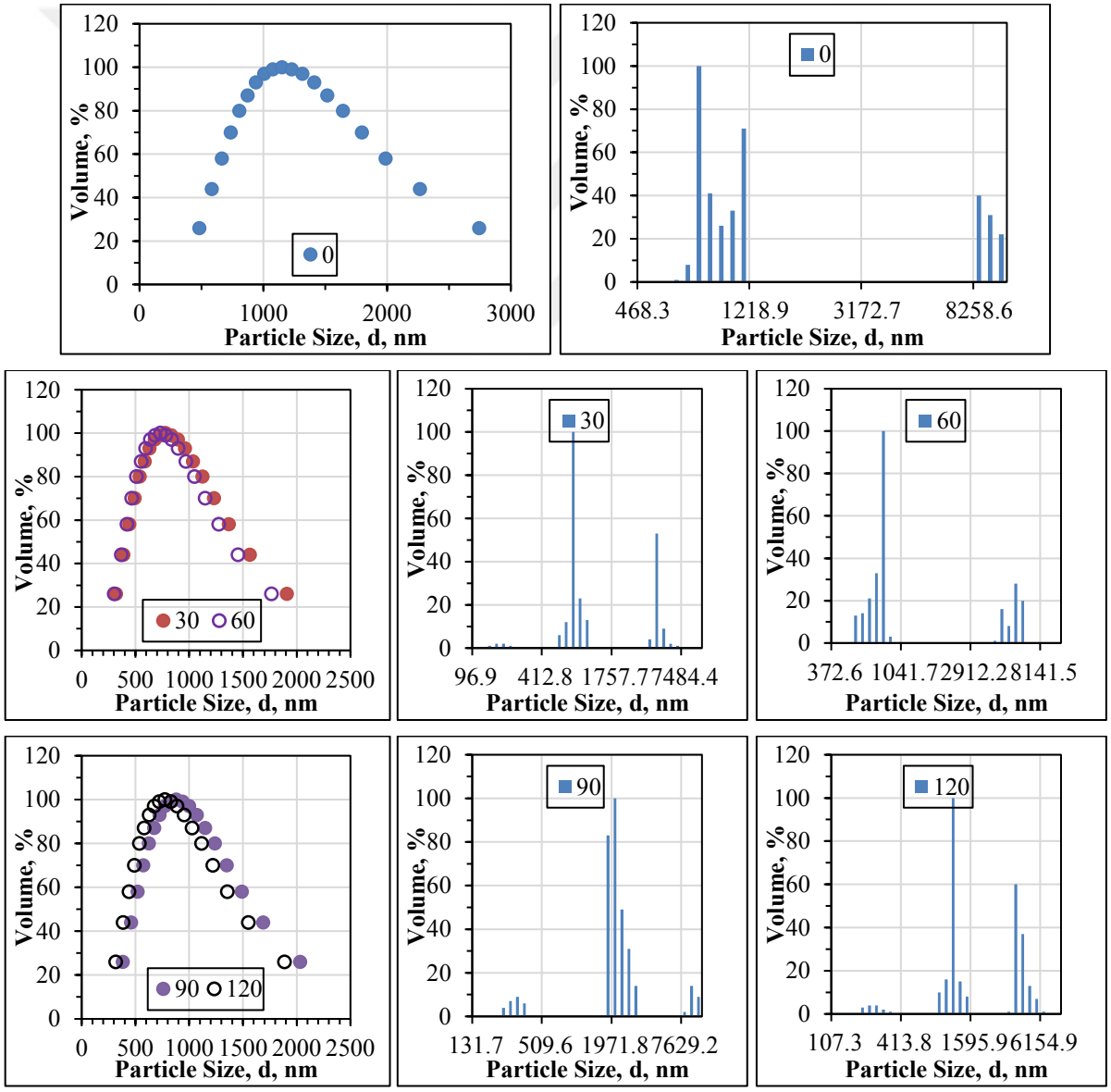


Figure 4.260. "Fe-TiO_2 and SRNOM" binary system "as-is" under irradiation volume profile: Time dependent comparative presentation of log Normal distribution and multi-size distribution of "Fe-TiO_2 and SRNOM" binary system "as-is" under irradiation.

4.1.7.23. "Fe-TiO_2 and SRNOM" binary system "as-is" under irradiation surface area profile. Time dependent logN distribution G(d) and multi size distribution C(d) of "Fe-TiO_2 and SRNOM" binary system "as-is" under irradiation surface area profile was given in Figure 4.261. Time dependent mean diameter, range and min-max diameter difference with respect to log normal and multi-size distribution of "Fe-TiO_2 and SRNOM" binary system "as-is" under irradiation surface area profile was exhibited in Table 4.164.

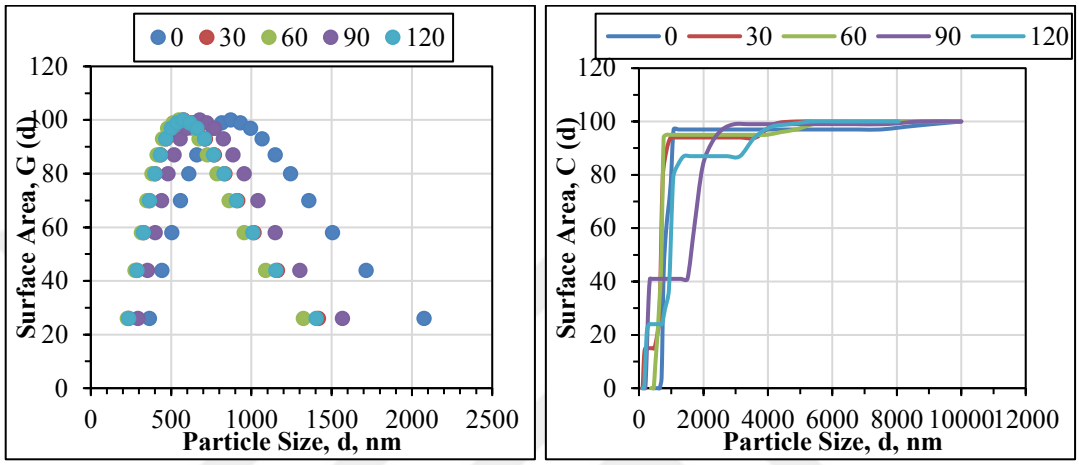


Figure 4.261. "Fe-TiO_2 and SRNOM" binary system "as-is" under irradiation surface area profile: Time dependent logN distribution G(d) and multi size distribution C(d).

Table 4.164. "Fe-TiO_2 and SRNOM" binary system "as-is" under irradiation surface area profile: Time dependent mean diameter, range and min-max diameter difference with respect to log normal and multi-size distribution.

Fe-TiO_2 and SRNOM	time, min				
	0	30	60	90	120
Log Normal distribution					
Mean, nm	871.3	578.2	548.4	678.2	575.3
Range	365.6-2076.8	236.0-1417.0	227.2-1323.8	293.6-1566.8	235.6-1404.6
Difference	1711.2	1181.0	1096.6	1273.2	1169.0
Multi-size distribution					
Max 1, nm	764.9	149.7	507.2	296.6	210.7
Max 2, nm	1074.8	736.9	765.2	1971.8	1064.5
Max 3, nm	8258.6	4192.5	4393.5	8734.5	3587.0
Max 4, nm	-	-	5396.5	-	-
Range	468.3-10.000	96.9-10.000	372.6-10.000	131.7-10.000	107.3-8062.4
Difference	9531.7	9903.1	9627.4	9868.3	7955.1

In a similar manner to data represented "Fe-TiO_2 and SRNOM" binary system "as-is" under irradiation volume profile (Table 4.163), time dependent mean diameter, range and min-max diameter

difference with respect to log normal and multi-size distribution of "Fe-TiO_2 and SRNOM" binary system "as-is" under irradiation surface area profile was displayed. It could be stated that hydrodynamic particle size of "Fe-TiO_2 and SRNOM" binary system "as-is" under irradiation exhibited drastic changes according to time variations. Initial hydrodynamic particle size was detected as 871.3 nm and decreased to 575.3 nm during 120 min. Also, size difference decreased from 1711.2 nm to 1169.0 nm. However, in terms of multi-size distribution, three peaks were obtained until 60 min. Upon 60 min, four peaks were attained, and three peaks were obtained until the end of 120 min period. Time dependent comparative presentation of log Normal distribution and multi-size distribution of "Fe-TiO_2 and SRNOM" binary system "as-is" under irradiation surface area profile was displayed in Figure 4.262.

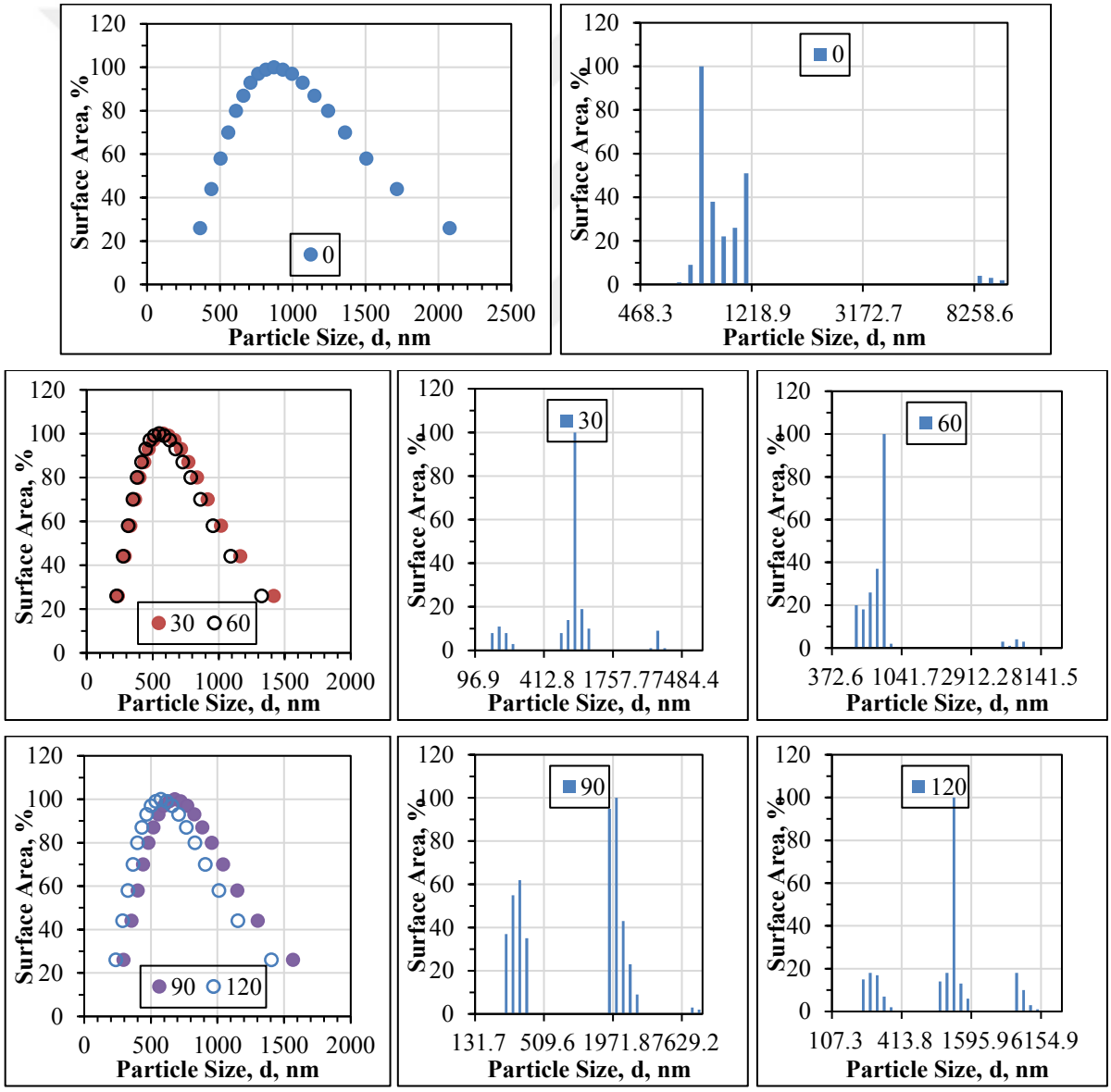


Figure 4.262. "Fe-TiO_2 and SRNOM" binary system "as-is" under irradiation surface area profile: Time dependent comparative presentation of log Normal distribution and multi-size distribution of "Fe-TiO_2 and SRNOM" binary system "as-is" under irradiation.

4.1.7.24. "Fe-TiO_2 and SRNOM" binary system "as-is" under irradiation number profile. As described for "Fe-TiO_2 and SRNOM" binary system "as-is" under irradiation intensity profile (Figure 4.257), volume profile (Figure 4.259), and surface area profile (Figure 4.261), a similar approach was followed for "Fe-TiO_2 and SRNOM" binary system "as-is" under irradiation number profile. Time dependent logN distribution G(d) and multi size distribution C(d) of "Fe-TiO_2 and SRNOM" binary system "as-is" under irradiation number profile was exhibited in Figure 4.263.

Following a similar manner, time dependent mean diameter, range and min-max diameter difference with respect to log normal and multi-size distribution of "Fe-TiO_2 and SRNOM" binary system "as-is" under irradiation number profile was presented in Table 4.165.

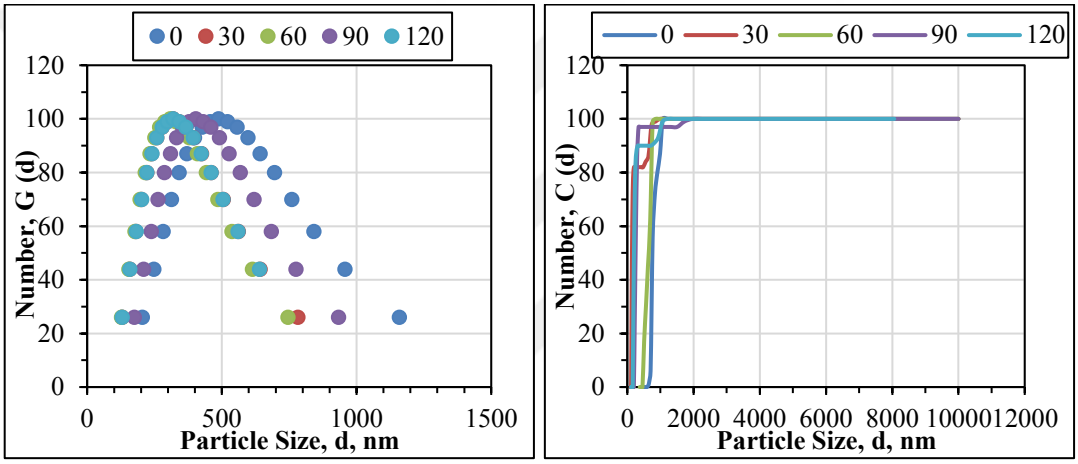


Figure 4.263. "Fe-TiO_2 and SRNOM" binary system "as-is" under irradiation number profile: Time dependent logN distribution G(d) and multi size distribution C(d).

Table 4.165. "Fe-TiO_2 and SRNOM" binary system "as-is" under irradiation number profile: Time dependent mean diameter, range and min-max diameter difference with respect to log normal and multi-size distribution.

Fe-TiO_2 and SRNOM	time, min				
	0	30	60	90	120
Log Normal distribution					
Mean, nm	487.7	319.3	308.9	403.9	319.2
Range	205.2-1159.4	130.3-782.5	127.9-745.6	174.8-933.1	130.7-779.4
Difference	954.2	652.2	617.7	758.3	648.7
Multi-size distribution					
Max 1, nm	764.9	129.5	507.2	259.1	184.1
Max 2, nm	1074.8	736.9	765.2	1722.3	1064.5
Range	468.3-10.000	96.9-10.000	372.6-10.000	131.7-10.000	107.3-8062.4
Difference	9531.7	9903.1	9627.4	9868.3	7955.1

According to log normal distribution and in terms of number profile, hydrodynamic particle size of "Fe-TiO_2 and SRNOM" binary system "as-is" under irradiation displayed a sharp decrease in the first 30 min. Upon period of 30 min, minor variations were observed until the end of 120 min. Initial hydrodynamic particle size was attained as 487.7 nm and decreased to 319.2 nm upon 120 min. Also, size difference decreased from 954.2 nm to 648.7 nm during 120 min. For comparison purposes, in terms of multi-size distribution, two max diameters were monitored until the end of 120 min period. In a similar manner to data represented "Fe-TiO_2 and SRNOM" binary system "as-is" under irradiation surface area profile (Figure 4.262), time dependent comparative presentation of log Normal distribution and multi-size distribution of "Fe-TiO_2 and SRNOM" binary system "as-is" under irradiation number profile was displayed in Figure 4.264.

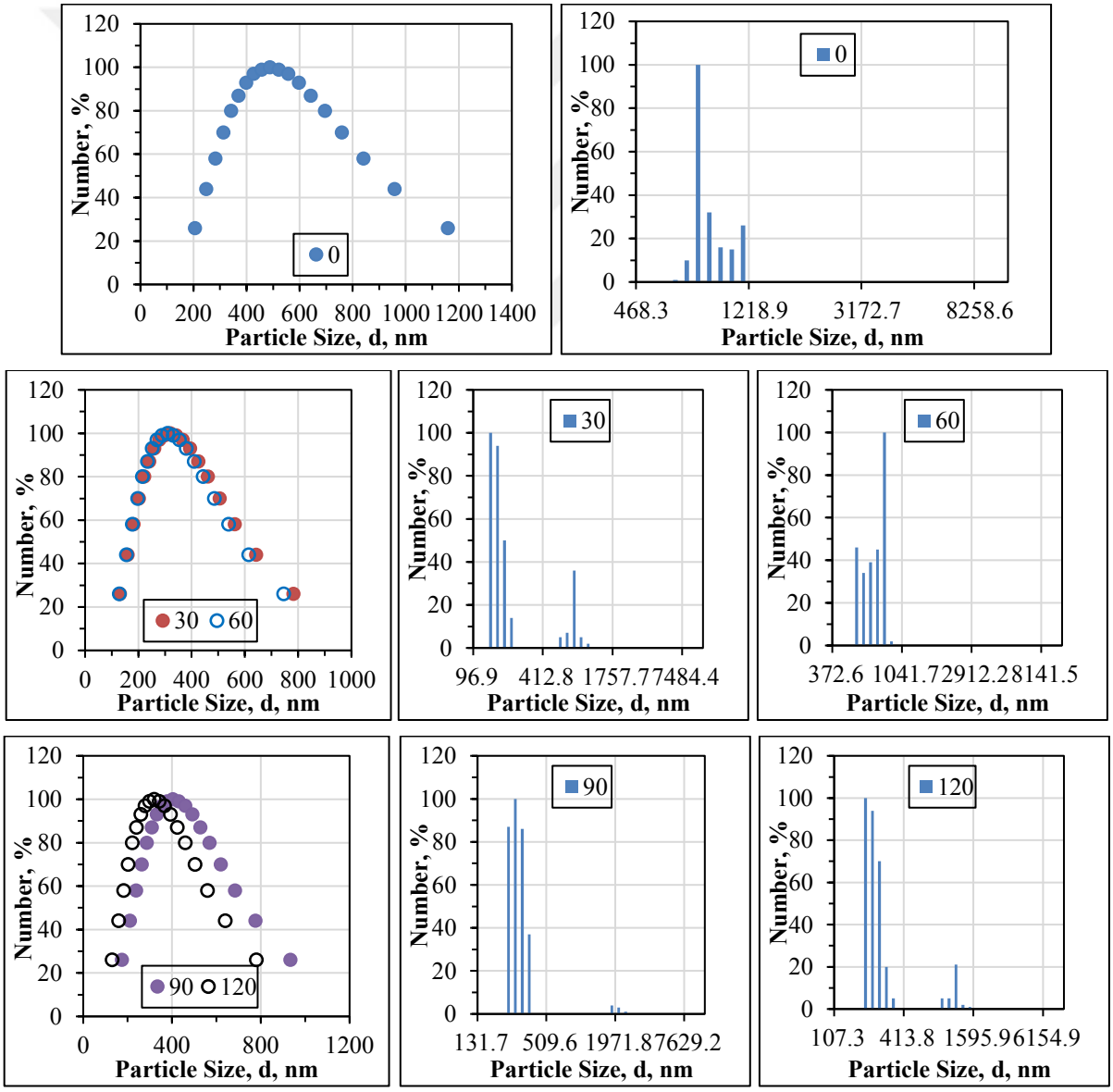


Figure 4.264. "Fe-TiO_2 and SRNOM" binary system "as-is" under irradiation number profile: Time dependent comparative presentation of log Normal distribution and multi-size distribution of "Fe-TiO_2 and SRNOM" binary system "as-is" under irradiation.

4.2. Sedimentation

Particle settling in the environment was investigated by various research groups (Joss et al. 2006; Keller et al. 2010; Phenrat et al. 2007; Quik et al. 2011, 2012; Starchevskii et al. 2009). Sedimentation profiles were attained as relative variation of with time of the absorbance recordings. Fluorescence spectrophotometer was employed as nephelometer, by setting $\lambda_{ex}=\lambda_{em}$ (Brunelli et al., 2013). Brunelli and colleagues further demonstrated that first order kinetics as an exponential model could explain the sedimentation behavior of TiO_2 (Aeroxide P25 Evonik) under various aqueous medium conditions covering the natural water constituents. As the nanoparticles aggregate and settle out of the suspension, the optical absorbance decreases. Therefore, change in optical absorbance with time can be measured, which can be related to the normalized nanoparticle concentration C/C_0, where C is the concentration in time, and C_0 is the initial concentration (*i.e.* the initial absorbance at time 0). The sedimentation rate becomes $d(C/C_0)/dt$ (Keller et al., 2010). Keller and co-workers also reported the sedimentation trend of TiO_2 (Evonik) in relation to the effect of initial concentration as well as aqueous medium characteristics.

Therefore, the sedimentation behavior of NPs either as sole particles in aqueous medium or NPs in the presence of organic matter could be monitored by UV-vis absorption spectroscopy. Following selection of effective and indicative wavelength, normalized absorbance variations could be modeled by exponential and/or linear kinetic models. The exponential model could be explained by the following equation;

$$-dA_\lambda/A_{\lambda o} = k\,dt \qquad (4.1)$$

A_λ: absorbance at specific wavelength at time t,
$A_{\lambda o}$: absorbance at specific wavelength at time 0,
k: rate constant.

On the other hand, depending on the data properties, linear model could also be applied using the following equation;

$$-A_\lambda/A_{\lambda o} = k\,t \qquad (4.2)$$

Where the terms were defined as presented above. Both models were applied and kinetic constants were comparatively evaluated.

Sedimentation performances of all NPs under the specified experimental conditions were elucidated via application of UV-vis absorbance spectroscopy. In a similar manner to particle size analysis, two main categories were defined;

1. Mono-systems as sole NPs in the absence of organic matter under various conditions;
2. Binary-systems as NPs in the presence of organic matter under various conditions.

Within each system the role of irradiation either to sole NPs or to organic matrix resulting in photolysis as well as for binary system leading to both photolysis and photocatalysis. It should be cited that all selected NPs possessed semiconductor properties expressing photocatalytic activities under solar irradiation. All selected TiO_2 specimens were subjected to sedimentation experiments that were performed under "as-is", "as-is" under dark" and "as-is under irradiation" conditions in the absence of organic matter in order to evaluate the sedimentation kinetics. As stated previously in Methodology Section UV-vis spectroscopic measurements were taken as the basis of assessment of suspension stability.

For this purpose, as a preliminary experiment for the assessment of the "indicative wavelength", time dependent UV-vis absorbance scan of each system was recorded between wavelength region of 200 and 600 nm. Although UV-vis spectral features of each specific NP could be considered as the basis of wavelength selection, due to the expected interference in the UV-vis region of organic matter as the aqueous medium constituent whole spectral region was recorded. The indicated interference would be more crucial in case of binary systems where irradiation effect would be prevailing in humic structure more specifically during photocatalysis. Selection of indicative wavelength held prime importance in case of the presence of humic matter displaying significant absorbance values as background effect. Therefore, NP specimens and humic relations either through aggregation or agglomeration could certainly affect the sedimentation behavior. As a baseline study, Erhayem and Sohn investigated the sedimentation profile of nano-TiO_2 (0.5 mg/mL) via time resolved optical absorbance measurements (Erhayem and Sohn, 2014a, b). Following an initial mixing period of 48 h, UV-vis absorbance at λ=378 nm of nano-TiO_2 suspended in different solutions both as sole and as binary systems *i.e.* in the presence of organic matter was recorded and considered as a suitable parameter for expressing sedimentation behavior. It was reported that nano-TiO_2 suspended in Milli-Q water at pH: 4.8 was stable for experimental time of 2h due to non-existence of any interfering components in the aqueous medium. Further discussion was extended to the role of pH_{zpc} as well to the effect of NOM compounds.

4.2.1. Sedimentation Behavior of Nanoparticles as TiO_2, N-TiO_2 and Fe-TiO_2 under "as-is" Conditions in the Absence of Organic Matter

4.2.1.1. TiO_2 specimen under "as-is" conditions. Time dependent UV-vis absorbance variations in the wavelength range of 200-600 nm were presented. Figure 4.265a displayed spectral variations that could be expressed by two regions as an inconsistent trend (200<λ<400 nm) followed by a consistent trend (400<λ<600 nm).

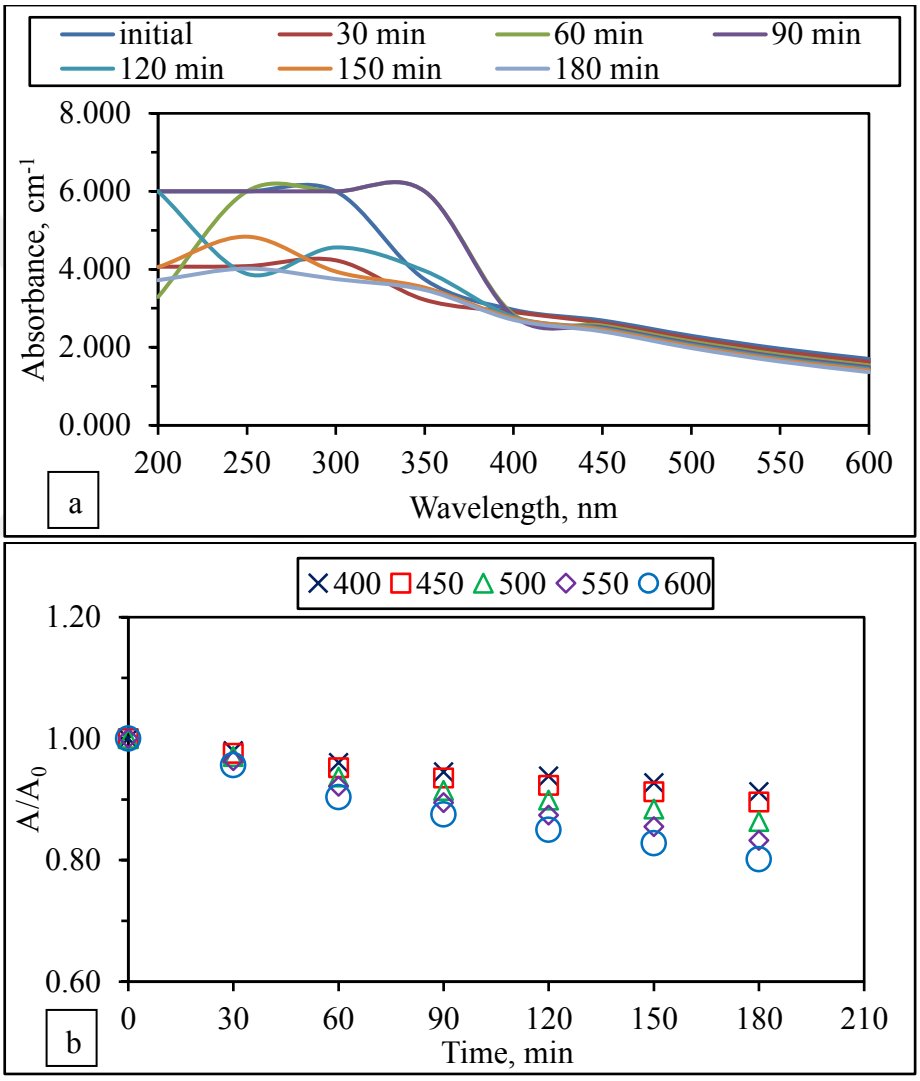


Figure 4.265. Sedimentation behavior of TiO_2 under "as-is" conditions in the absence of organic matter, a) UV-vis absorbance variations b) Normalized absorbance with respect to time.

Although absorbance recordings at λ=380 nm was selected in the previous literature reports, it could be visualized that absorbance variations expressed an inconsistent trend with respect to increasing time as stated. However, at longer wavelengths as 400 nm to 600 nm, a consistently decreasing trend was recorded. Therefore, time dependent absorbance values at selected wavelengths

as 400 nm, 450 nm, 500 nm, 550 nm and 600 nm were normalized to respective initial absorbance values and presented in Figure 4.265b. The variations were modeled by two approaches depending on the decreasing trend profiles. Exponential and linear models were applied and sedimentation kinetic constants were presented in Table 4.166. Both exponential and linear modeling revealed considerably high correlation coefficients as $R^2 > 0.972$.

Table 4.166. TiO_2 under "as-is" conditions, kinetic model parameters.

Kinetic model	Wavelength, nm				
	400	450	500	550	600
Exponential model					
k, min^{-1}	4.86×10^{-4}	5.91×10^{-4}	7.95×10^{-4}	1.00×10^{-3}	1.21×10^{-3}
R^2	0.979	0.981	0.982	0.982	0.981
Linear model					
k, min^{-1}	4.64×10^{-4}	5.59×10^{-4}	7.38×10^{-4}	9.13×10^{-4}	1.08×10^{-3}
R^2	0.976	0.977	0.976	0.975	0.972

Exponential model kinetics were expressed by kinetic constants (k, min^{-1}) in a decreasing order as $1.21 \times 10^{-3} > 1.00 \times 10^{-3} > 7.95 \times 10^{-4} > 5.91 \times 10^{-4} > 4.86 \times 10^{-4}$ for wavelengths of 600 nm, 550 nm, 500 nm, 450 nm, and 400 nm, respectively. Simply an average value of $k=8.16 \times 10^{-4}$ min^{-1} could be regarded as suitable for expressing sedimentation kinetics of sole TiO_2 using the exponential model.

In a similar manner, the linear trend as visualized by the decreasing trend of A/A_o revealed kinetic constants (min^{-1}) in a decreasing order as $1.08 \times 10^{-3} > 9.13 \times 10^{-4} > 7.38 \times 10^{-4} > 5.59 \times 10^{-4} > 4.64 \times 10^{-4}$ for wavelengths of 600 nm, 550 nm, 500 nm, 450 nm, and 400 nm, respectively. As expressed above an average of $k=7.51 \times 10^{-4}$ min^{-1} could be accepted as suitable for displaying sedimentation kinetics sole TiO_2 using the linear model. The average value resembled to the $k=7.38 \times 10^{-4}$ min^{-1} that was calculated for $\lambda=500$ nm.

Under the specified "as-is" conditions represented by selected wavelengths, it could be deduced that upon 60 min duration, approximately 10 % of sole TiO_2 were settled irrespective of the specified wavelength (excluding $\lambda=380$ nm) followed which a slight enhancement to ~20 % upon 180 min. The attained sedimentation profile could be regarded as comparable to the data reported by Erhayem and Sohn expressing stability of nano-TiO_2 (Erhayem and Sohn, 2014a, b). It should also be emphasized that UV-vis absorbance measurements excluded all spectroscopic interferences especially scattering effects due the presence of nanoparticles either as sole or in aggregate/agglomerate forms leading to settlement with respect to time.

4.2.1.2. N-TiO_2 specimen under "as-is" conditions. As explained for TiO_2, a similar approach was followed for elucidation of sedimentation behavior of N-TiO_2 under "as-is" conditions. Time dependent UV-vis absorbance variations in the wavelength range of 200-600 nm were presented (Figure 4.266a).

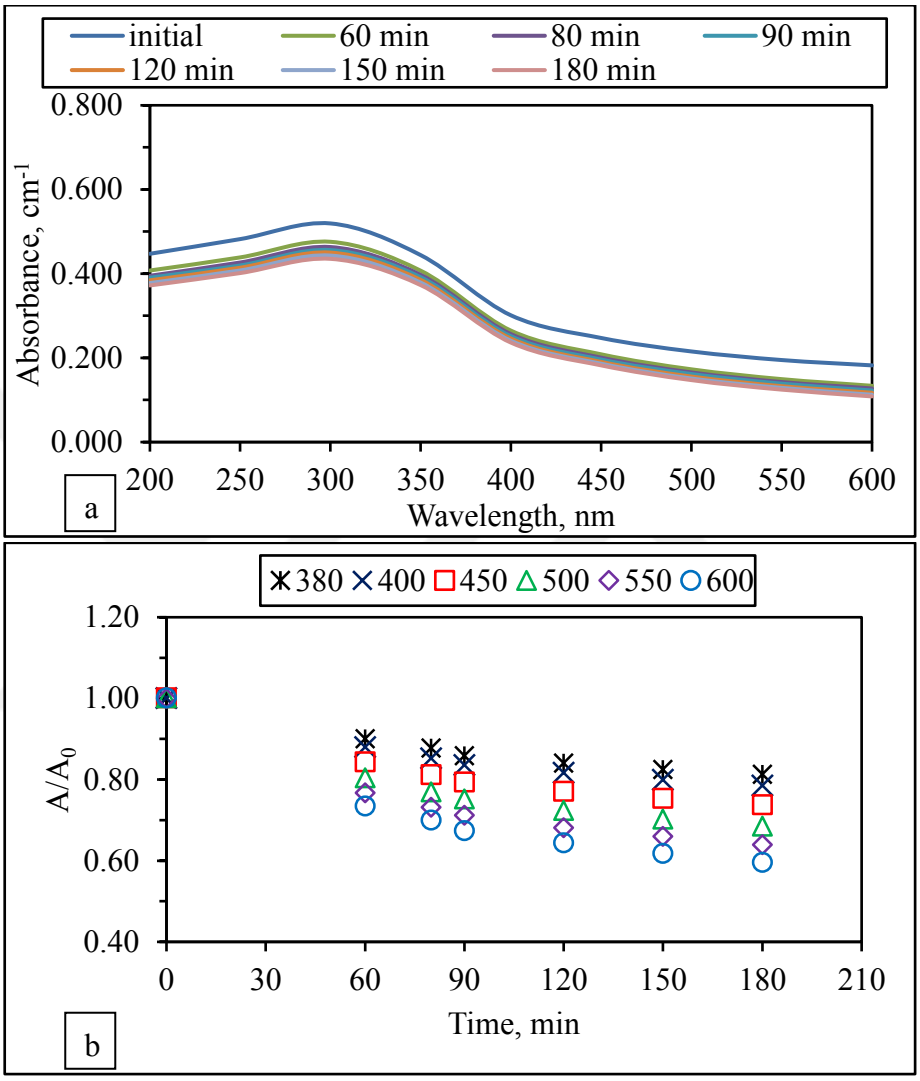


Figure 4.266. Sedimentation behavior of N-TiO_2 under "as-is" conditions in the absence of organic matter, a) UV-vis absorbance variations b) Normalized absorbance with respect to time.

Contrary to the two regional display of UV-vis spectra recorded for TiO_2 under as-is conditions, N-TiO_2 displayed a broad peak followed by an inclination that could be expressed as a consistent trend with respect to time. For comparison purposes, λ=380 nm was also considered for elimination of further expected effects due to system variations. Time dependent absorbance values at selected wavelengths were normalized to respective initial absorbance values and presented in Figure 4.266b. The variations were modeled by two approaches depending on the decreasing trend profiles. Exponential and linear models were applied and sedimentation kinetic constants were presented in

Table 4.167. Both exponential and linear modeling revealed considerably high correlation coefficients as $R^2 > 0.827$.

Table 4.167. N-TiO_2 under "as-is" conditions, kinetic model parameters.

Kinetic model	Wavelength, nm					
	380	400	450	500	550	600
Exponential model						
k, min^{-1}	1.13×10^{-3}	1.30×10^{-3}	1.63×10^{-3}	2.01×10^{-3}	2.35×10^{-3}	2.72×10^{-3}
R^2	0.924	0.909	0.890	0.886	0.877	0.878
Linear model						
k, min^{-1}	1.01×10^{-3}	1.15×10^{-3}	1.39×10^{-3}	1.65×10^{-3}	1.86×10^{-3}	2.09×10^{-3}
R^2	0.908	0.888	0.862	0.850	0.834	0.827

Exponential model kinetics were expressed by kinetic constant (min^{-1}) in a decreasing order as $2.72 \times 10^{-3} > 2.35 \times 10^{-3} > 2.01 \times 10^{-3} > 1.63 \times 10^{-3} > 1.30 \times 10^{-3} > 1.13 \times 10^{-3}$ for wavelengths of 600 nm, 550 nm, 500 nm, 450 nm, 400 nm, and 380 nm, respectively. It could be deduced that exponential model kinetic rate constants decreased steadily with respect to decreasing wavelength. Simply an average value of $k=1.86 \times 10^{-3}$ min^{-1} could be regarded as suitable for expressing sedimentation kinetics using the exponential model irrespective of the detection wavelength. It should also be considered that although the order of kinetic constant remained the same the coefficient was doubled with respect to the selected wavelength in UV to vis region.

In a similar manner, the linear trend as visualized by a decreasing trend of A/A_o revealed kinetic constants (min^{-1}) in a decreasing order as $2.09 \times 10^{-3} > 1.86 \times 10^{-3} > 1.65 \times 10^{-3} > 1.39 \times 10^{-3} > 1.15 \times 10^{-3} > 1.01 \times 10^{-3}$ for wavelengths of 600 nm, 550 nm, 500 nm, 450 nm, 400 nm, and 380 nm, respectively. As expressed above, an average of $k=1.53 \times 10^{-3}$ min^{-1} could be accepted as appropriate for displaying sedimentation kinetics using the linear model. As indicated above, a doubling effect in rate constant could also be considered.

Under the specified conditions represented by selected wavelengths, it could be deduced that upon 60 min duration, approximately 20 % removal was achieved with respect to increasing specified wavelengths followed which a slight enhancement that was observed as ~ 35 % upon 180 min. The attained steady decreasing trend could be accepted as minor variations revealing that sedimentation profiles of N-TiO_2 could be followed by any of the indicative wavelengths in vis-region (400 nm to 600 nm). It should also be indicated that both models could be successfully applied due to slight incremental decreases with respect to time.

4.2.1.3. Fe-TiO_2 specimen under "as-is" conditions. Similarly explained so far, a similar approach was also followed for elucidation of sedimentation behavior of Fe-TiO_2 under "as-is" conditions. Time dependent UV-vis absorbance variations in the wavelength range of 200-600 nm were presented (Figure 4.267a).

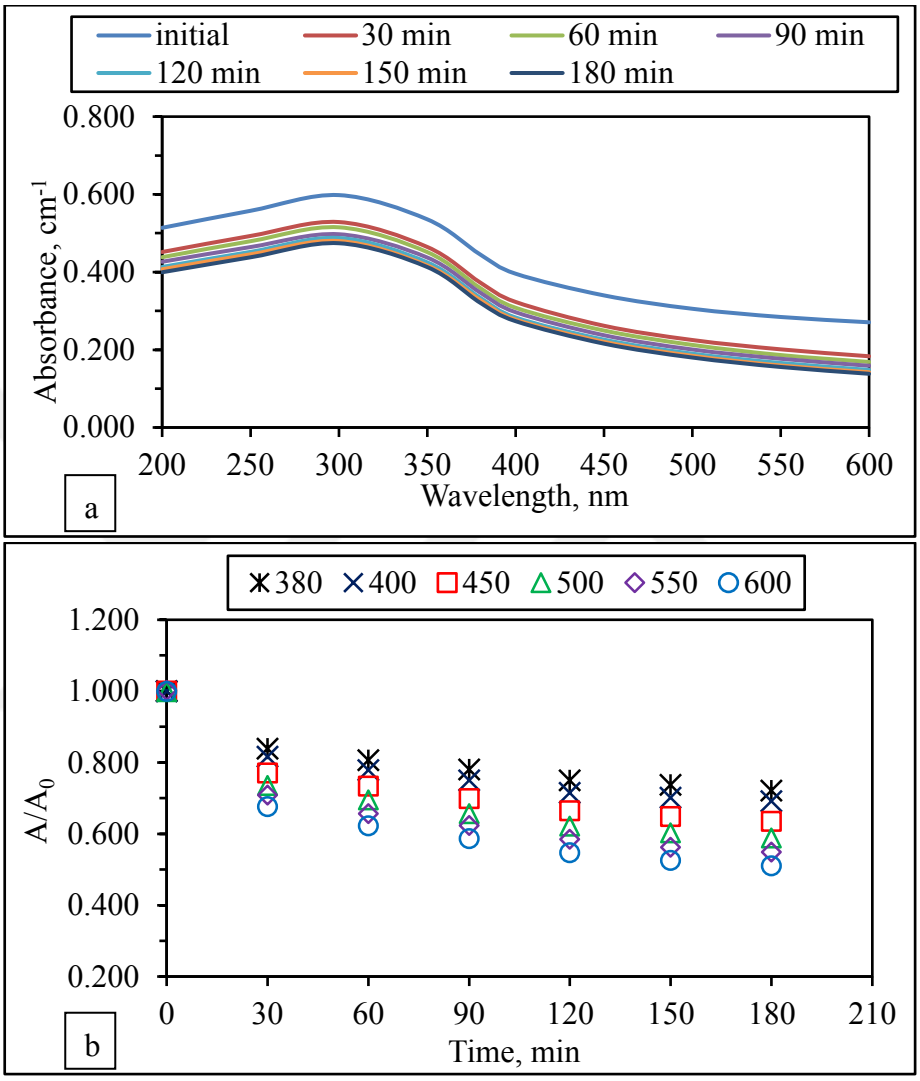


Figure 4.267. Sedimentation behavior of Fe-TiO_2 under "as-is" conditions in the absence of organic matter, a) UV-vis absorbance variations b) Normalized absorbance with respect to time.

Contrary to the two regional display of UV-vis spectra recorded for TiO_2 under "as-is" condition, and in a similar manner to N-TiO_2, Fe-TiO_2 expressed a broad peak followed by an inclination that could be expressed as a consistent trend with respect to time. Also, likewise to N-TiO_2, for comparison purposes, λ=380 nm was also considered for elimination of further expected effects due to system variations. Time dependent absorbance values at selected wavelengths were normalized to respective initial absorbance values and presented in Figure 4.267b. The variations were evaluated by two approaches as exponential and linear models depending on the decreasing trend profiles and

sedimentation kinetic constants were presented in Table 4.168. Both exponential and linear modeling revealed considerably high correlation coefficients as $R^2 > 0.706$.

Table 4.168. Fe-TiO_2 under "as-is" conditions, kinetic model parameters.

Kinetic model	Wavelength, nm					
	380	400	450	500	550	600
Exponential model						
k, min^{-1}	1.56×10^{-3}	1.78×10^{-3}	2.15×10^{-3}	2.50×10^{-3}	2.84×10^{-3}	3.16×10^{-3}
R^2	0.825	0.814	0.797	0.793	0.791	0.786
Linear model						
k, min^{-1}	1.31×10^{-3}	1.45×10^{-3}	1.68×10^{-3}	1.87×10^{-3}	2.05×10^{-3}	2.20×10^{-3}
R^2	0.787	0.771	0.744	0.731	0.720	0.706

Exponential model kinetics as expressed by kinetic constants (min^{-1}) revealed a decreasing order indicated as $3.16 \times 10^{-3} > 2.84 \times 10^{-3} > 2.50 \times 10^{-3} > 2.15 \times 10^{-3} > 1.78 \times 10^{-3} > 1.56 \times 10^{-3}$ for wavelengths of 600 nm, 550 nm, 500 nm, 450 nm, 400 nm, and 380 nm, respectively. Although an approximate average value of $k=2.33 \times 10^{-3}$ min^{-1} could be regarded as suitable for expressing sedimentation kinetics using the exponential model, the difference in min and max values should also be encountered as reported above for N-TiO_2 specimen.

In a similar manner, the linear trend as visualized by the decreasing trend of A/A_o revealed kinetic constants (min^{-1}) in a decreasing order as $2.20 \times 10^{-3} > 2.05 \times 10^{-3} > 1.87 \times 10^{-3} > 1.68 \times 10^{-3} > 1.45 \times 10^{-3} > 1.31 \times 10^{-3}$ for wavelengths of 600 nm, 550 nm, 500 nm, 450 nm, 400 nm, and 380 nm, respectively. As expressed above an average of $k=1.76 \times 10^{-3}$ min^{-1} could be accepted as suitable for displaying sedimentation kinetics using the linear model. The average value resembled to the $k=1.78 \times 10^{-3}$ min^{-1} that was calculated for $\lambda=400$ nm.

Under the specified conditions represented by selected wavelengths, it could be deduced that upon 60 min duration, approximately 35 % removals were achieved with respect to increasing specified wavelengths followed which a slight enhancement was also observed as approximately 45 % upon 180 min.

As achieved by UV-vis absorbance based kinetic modeling applied in two different approaches as exponential and linear models, simple removal data could not be accepted as significantly resembling the sedimentation behavior due to wavelength dependent differences recorded as a doubling effect by kinetic modeling. Therefore, two methods should be cautiously interpreted in case that sedimentation profiles should be addressed and compared.

4.2.2. Comparative Evaluation of Exponential and Linear Models of TiO_2, N-TiO_2, Fe-TiO_2 "as-is" Conditions

Based on the presented data for all of the NPs under as-is conditions, although similar sedimentation profiles were attained, a comparative evaluation was performed to elucidate the sample specific variations for suitability of application of UV-vis spectroscopic technique. For this purpose, kinetic model parameters attained at selected indicative wavelength of λ=550 nm were compiled from tables 4.166-4.168 and presented in Table 4.169.

Table 4.169. Comparative presentation of sedimentation kinetics of NPs under "as-is" conditions at λ=550 nm.

Kinetic model	Exponential model	
NP "as-is"	k, min^{-1}	R^2
TiO_2	1.00 x 10^{-3}	0.982
N-TiO_2	2.35 x 10^{-3}	0.877
Fe-TiO_2	2.84 x 10^{-3}	0.791
	Linear model	
	k, min^{-1}	R^2
TiO_2	9.13 x 10^{-4}	0.975
N-TiO_2	1.86 x 10^{-3}	0.834
Fe-TiO_2	2.05 x 10^{-3}	0.720

Sedimentation behavior of TiO_2, N-TiO_2, and Fe-TiO_2 "as-is" specimens that were fitted to the exponential kinetic equation gave the following rate constants (min^{-1}) as 2.84 x 10^{-3} for Fe-TiO_2 > 2.35 x 10^{-3} for N-TiO_2 > 1.00 x 10^{-3} for TiO_2. Fe-TiO_2 specimen expressed comparatively higher sedimentation rate in comparison to sole TiO_2 most probably as a result of Fe doping as replacement to oxygen vacancies in TiO_2 lattice. In a similar fashion, when sedimentation behavior of TiO_2, N-TiO_2, and Fe-TiO_2 specimens were fitted to linear model, rate constants (min^{-1}) were found as 2.05 x 10^{-3} for Fe-TiO_2 > 1.86 x 10^{-3} for N-TiO_2 > 9.13 x 10^{-4} for TiO_2.

Either exponential model or linear model could be regarded as suitable models for understanding the sedimentation behavior of TiO_2, N-TiO_2 and Fe-TiO_2 NPs each displaying different physico-chemical and morphological properties (Table A). It should be stated that these results refer only to "as-is" conditions in the absence of any contributing factors that cold resemble natural systems. Moreover, all NP specimens were subjected to sedimentation as followed by UV-vis spectroscopy primarily by scanning through the whole wavelength region (200 nm to 600 nm) to select to effective wavelength contrary to the indicated specific wavelength as 378 nm by Keller and colleagues (Keller et al., 2010).

4.2.3. Sedimentation Behavior of Nanoparticles as TiO_2, N-TiO_2 and Fe-TiO_2 "as-is under dark" Conditions in the Absence of Organic Matter

Following "as-is" conditions at which sonication for 1 minute and mixing for 4 minutes using a magnetic stirrer was provided, further experiments were conducted following 60 min mixing under dark in the solar simulator instrument.

4.2.3.1. TiO_2 specimen "as-is" under dark conditions. As explained so far, sedimentation behavior of TiO_2 specimen "as-is" under dark conditions was observed in a similar way. Time dependent UV-vis absorbance variations in the wavelength range of 200-600 nm were recorded and demonstrated in Figure 4.268a.

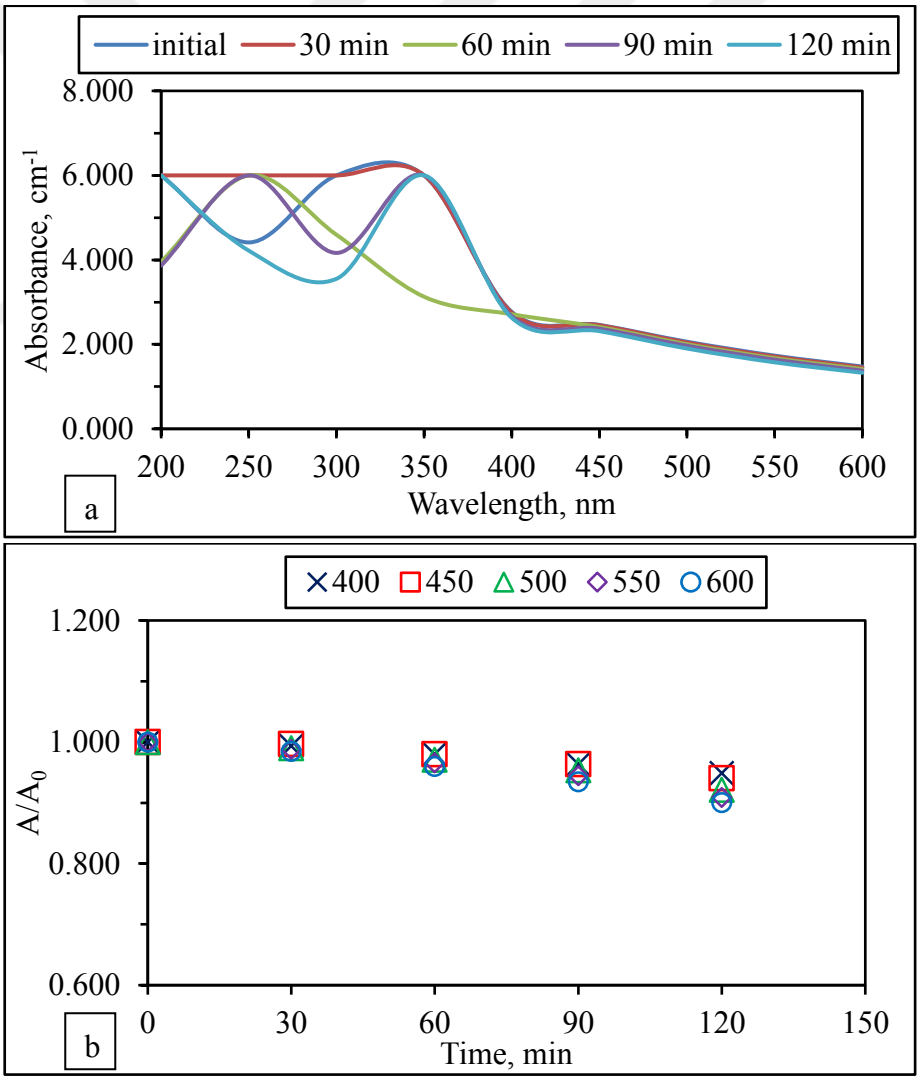


Figure 4.268. Sedimentation behavior of TiO_2 "as-is" under dark conditions in the absence of organic matter, a) UV-vis absorbance variations b) Normalized absorbance with respect to time.

UV-vis spectral variations that could also be expressed by two regions as an inconsistent trend ($200<\lambda<400$ nm) followed by a consistent trend ($400<\lambda<600$ nm). From a general perspective, the role of continuous mixing by a magnetic stirrer did not cause any alteration on sedimentation behavior of TiO_2 in comparison to TiO_2 "as-is" condition that was subjected to recording immediately after preparation (Figure 4.265). Due to the observed inconsistency, absorbance recordings at λ=380 nm were also excluded. No distinct separation could be visualized with respect to increasing time. Application of exponential and linear models revealed almost similar results as presented in Figure 4.268b and Table 4.170. Both exponential and linear modeling revealed considerably high correlation coefficients as $R^2 > 0.947$.

Table 4.170. TiO_2 "as-is" under dark conditions, kinetic model parameters.

Kinetic model	Wavelength, nm				
	400	450	500	550	600
Exponential model					
k, min^{-1}	5.00×10^{-4}	5.00×10^{-4}	7.00×10^{-4}	8.00×10^{-4}	9.00×10^{-4}
R^2	0.980	0.947	0.959	0.965	0.979
Linear model					
k, min^{-1}	4.40×10^{-4}	5.09×10^{-4}	6.43×10^{-4}	7.52×10^{-4}	8.32×10^{-4}
R^2	0.981	0.950	0.964	0.970	0.983

Exponential model kinetic constants expressed a decreasing order as $9.00 \times 10^{-4} > 8.00 \times 10^{-4} > 7.00 \times 10^{-4} > 5.00 \times 10^{-4} > 5.00 \times 10^{-4}$ for wavelengths of 600 nm, 550 nm, 500 nm, 450 nm, and 400 nm, respectively. Simply an average value of $k=1.25 \times 10^{-3}$ min^{-1} could be regarded as suitable for expressing sedimentation kinetics using the exponential model.

In a similar manner, the linear trend as visualized by the decreasing trend of A/A_o revealed kinetic constants (min^{-1}) in a decreasing order as $8.32 \times 10^{-4} > 7.52 \times 10^{-4} > 6.43 \times 10^{-4} > 5.09 \times 10^{-4} > 4.40 \times 10^{-4}$ for wavelengths of 600 nm, 550 nm, 500 nm, 450 nm, and 400 nm, respectively. As expressed above an average of $k=1.04 \times 10^{-3}$ min^{-1} could also be regarded as appropriate for displaying sedimentation kinetics using the linear model.

It could be deduced that for duration of 30 min very slight (< 5 %) removals were achieved with respect to increasing wavelengths followed which a slight enhancement was also observed as approximately 10 % upon 120 min. Although a similar trend was attained in UV-region, ten-fold decrease was attained under all conditions due to continuous mixing applied for 60 min prior to absorbance recordings. However, effect of wavelength dependency especially in near vis region should also be encountered (Table 4.166 and Table 4.169).

4.2.3.2. N-TiO_2 specimen "as-is" under dark conditions. As explained for N-TiO_2 under "as-is" conditions (Figure 4.266 and Table 4.167), a similar approach was followed for elucidation of sedimentation behavior of N-TiO_2 "as-is" under dark conditions. Time dependent UV-vis absorbance variations in the overall spectra covering the wavelength range of 200-600 nm were presented (Figure 269a). It could be easily visualized that N-TiO_2 specimen under "as-is" under dark conditions displayed quite similar tendency to N-TiO_2 "as-is" specimen and no direct effect of continuous mixing could be observed excluding the initial absorbance recordings. Moreover, the contribution of absorbance recordings at λ=380 nm could also be encountered.

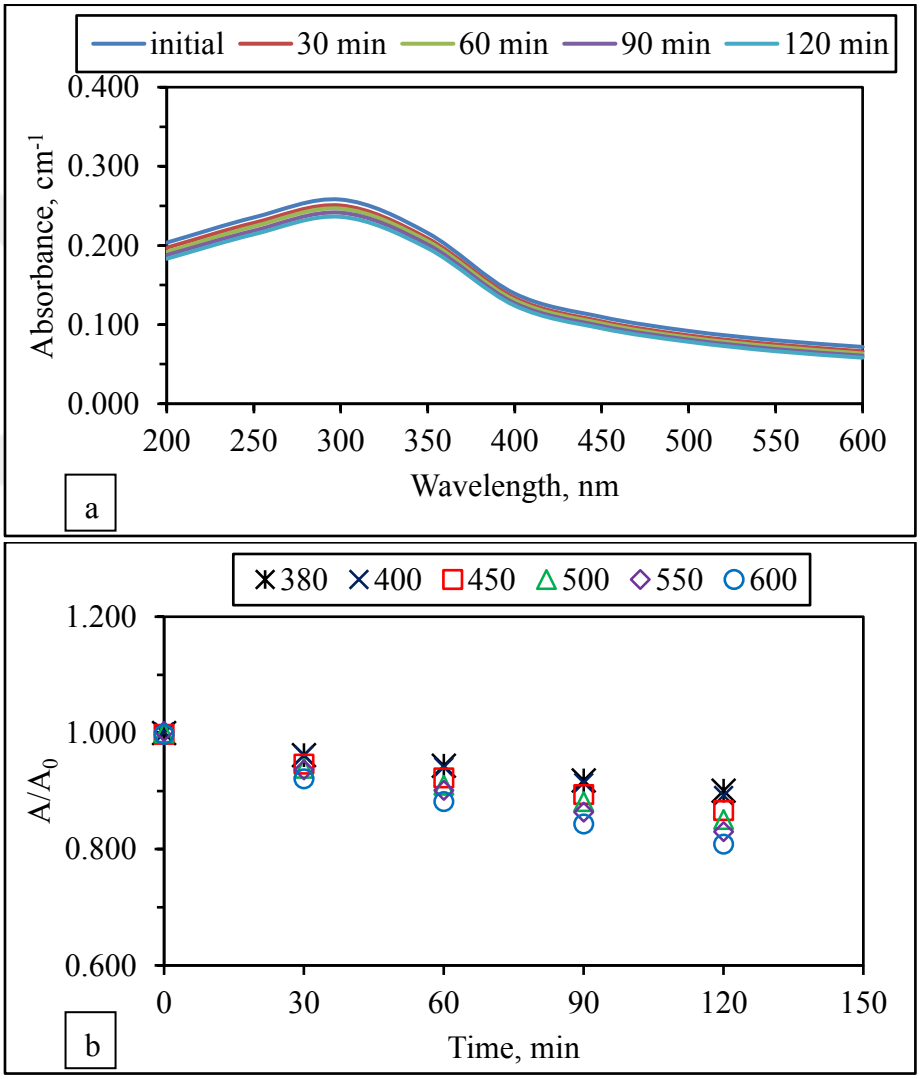


Figure 4.269. Sedimentation behavior of N-TiO_2 "as-is" under dark conditions in the absence of organic matter, a) UV-vis absorbance variations b) Normalized absorbance with respect to time.

On the other hand, normalized absorbance values in the wavelength range of 380 nm to 600 nm also revealed a decreasing profile that could be modeled by both exponential and linear models (Figure 4.269b and Table 4.171). Both exponential and linear modeling revealed considerably high correlation coefficients as $R^2 > 0.969$.

Table 4.171. N-TiO_2 "as-is" under dark conditions, kinetic model parameters.

Kinetic model	Wavelength, nm					
	380	400	450	500	550	600
Exponential model						
k, min^{-1}	8.49×10^{-4}	9.40×10^{-4}	1.13×10^{-3}	1.29×10^{-3}	1.53×10^{-3}	1.69×10^{-3}
R^2	0.984	0.990	0.984	0.977	0.986	0.980
Linear model						
k, min^{-1}	8.04×10^{-4}	8.87×10^{-4}	1.05×10^{-3}	1.18×10^{-3}	1.39×10^{-3}	1.52×10^{-3}
R^2	0.981	0.987	0.979	0.969	0.979	0.970

Exponential model kinetics as expressed by kinetic constants demonstrated a decreasing order as $1.69 \times 10^{-3} > 1.53 \times 10^{-3} > 1.29 \times 10^{-3} > 1.13 \times 10^{-3} > 9.40 \times 10^{-4} > 8.49 \times 10^{-4}$ for wavelengths of 600 nm, 550 nm, 500 nm, 450 nm, 400 nm, and 380 nm, respectively. Simply an average value of $k=1.24 \times 10^{-3}$ min^{-1} could be regarded as adequate for expressing sedimentation kinetics using the exponential model. The average value resembled to the $k=1.29 \times 10^{-3}$ min^{-1} that was calculated for λ=500 nm.

Following the same manner, the linear trend as visualized by the decreasing trend of A/A_o revealed kinetic constants (min^{-1}) in a decreasing order as $1.52 \times 10^{-3} > 1.39 \times 10^{-3} > 1.18 \times 10^{-3} > 1.05 \times 10^{-3} > 8.87 \times 10^{-4} > 8.04 \times 10^{-4}$ for wavelengths of 600 nm, 550 nm, 500 nm, 450 nm, 400 nm, and 380 nm, respectively. As expressed above, an average of $k=1.14 \times 10^{-3}$ min^{-1} could be accepted as appropriate for displaying sedimentation kinetics using the linear model. The average value resembled to the $k=1.18 \times 10^{-3}$ min^{-1} that was calculated for λ=500 nm. It could be indicated that an incremental increase in wavelength from 380 nm to 400 nm reflected as a slight increase in kinetic constants as approximately 10 % for both exponential and linear models. However, this insignificant increase could also be visualized for various deviations recorded for 50 nm changes in selected wavelengths.

Under the specified conditions represented by selected wavelengths, it could be indicated that upon 30 min duration approximately ≤ 10 % removals were achieved with respect to increasing specified wavelengths followed which a slight enhancement was also observed as ≤ 20 % upon 120 min period.

Although linear model revealed slightly lower kinetic constants, it could also be mentioned that both kinetic model constants were not significantly different from each other at the specified wavelengths (Table 4.171). Upon period of 120 min, wavelength dependent variation in removal efficiencies were obtained 10-20 % with respect to increasing detection wavelength.

4.2.3.3. Fe-TiO_2 specimen "as-is" under dark conditions. As explained for Fe-TiO_2 under "as-is" conditions (Figure 4.267 and Table 4.168), following a similar trend, sedimentation behavior of Fe-TiO_2 "as-is under dark" conditions was monitored. Time dependent UV-vis absorbance variations in the overall spectra covering the wavelength range of 200-600 nm were presented (Figure 4.270a).

For comparison purposes, Fe-TiO_2 specimen under "as-is" under dark conditions expressed quite similar tendency to Fe-TiO_2 under "as-is" conditions specimen. However, initial absorbance recordings of initial suspension had been significantly affected by continuous mixing following which no direct effect of continuous mixing could be observed. Moreover, the contribution of absorbance recordings at λ=380 nm should also be considered. Application of both exponential and linear modeling revealed considerably high correlation coefficients as $R^2 > 0.968$ (Figure 4.270b and Table 4.172).

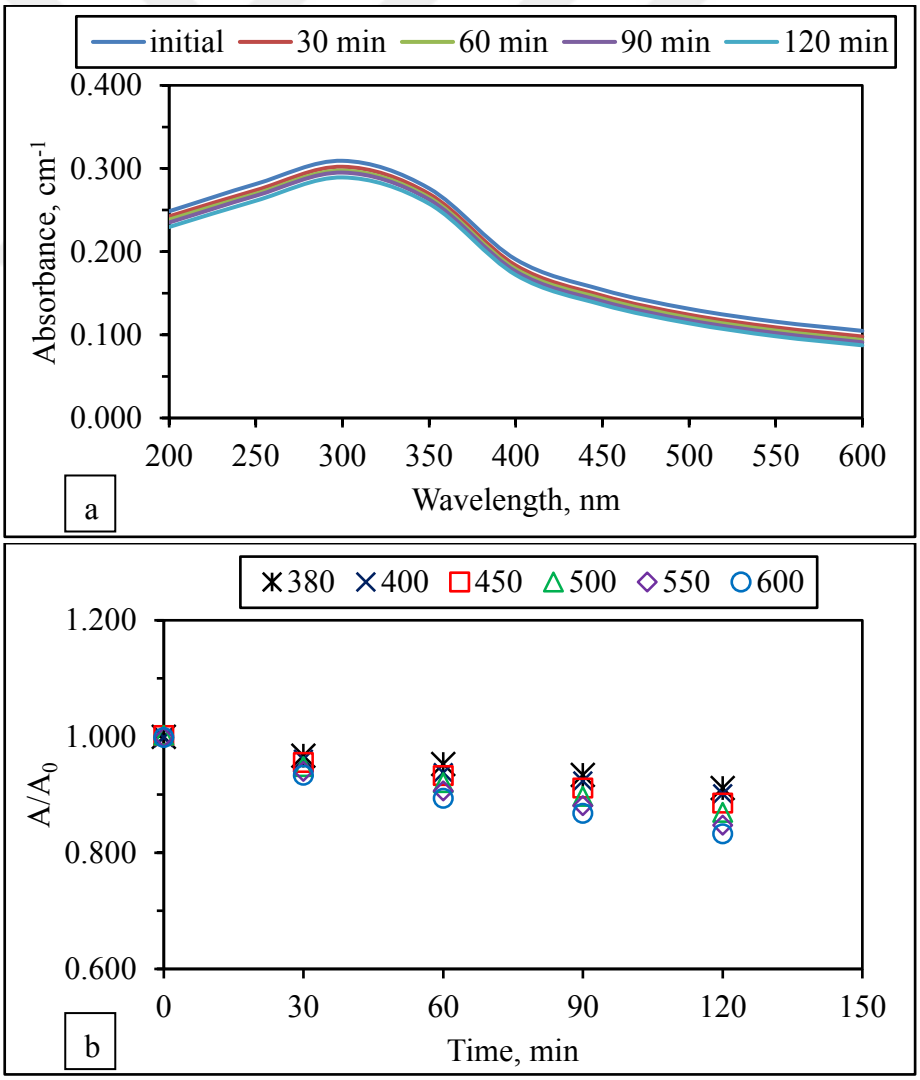


Figure 4.270. Sedimentation behavior of Fe-TiO_2 "as-is" under dark conditions in the absence of organic matter, a) UV-vis absorbance variations b) Normalized absorbance with respect to time.

Table 4.172. Fe-TiO_2 "as-is" under dark conditions, kinetic model parameters.

Kinetic model	Wavelength, nm					
	380	400	450	500	550	600
Exponential model						
k, min^{-1}	7.27×10^{-4}	8.18×10^{-4}	9.80×10^{-4}	1.13×10^{-3}	1.31×10^{-3}	1.45×10^{-3}
R^2	0.985	0.975	0.979	0.975	0.980	0.977
Linear model						
k, min^{-1}	6.94×10^{-4}	7.75×10^{-4}	9.22×10^{-4}	1.06×10^{-3}	1.20×10^{-3}	1.32×10^{-3}
R^2	0.983	0.971	0.974	0.968	0.973	0.969

Kinetic modeling of experimental data as expressed by kinetic constant (k, min^{-1}) expressed a decreasing order as $1.45 \times 10^{-3} > 1.31 \times 10^{-3} > 1.13 \times 10^{-3} > 9.80 \times 10^{-4} > 8.18 \times 10^{-4} > 7.27 \times 10^{-4}$ for wavelengths of 600 nm, 550 nm, 500 nm, 450 nm, 400 nm, and 380 nm, respectively. Although almost doubling effect could be encountered as $k=7.27 \times 10^{-4}$ min^{-1} at λ=380 nm to $k=1.45 \times 10^{-3}$ min^{-1} at λ=600 nm, an average value of $k=1.07 \times 10^{-3}$ min^{-1} could be regarded as appropriate for expressing sedimentation kinetics using the exponential model.

The linear trend as visualized by the decreasing trend of A/A_o deduced from data revealed kinetic constants (min^{-1}) in a decreasing order as $1.32 \times 10^{-3} > 1.20 \times 10^{-3} > 1.06 \times 10^{-3} > 9.22 \times 10^{-4} > 7.75 \times 10^{-4} > 6.94 \times 10^{-4}$ for wavelengths of 600 nm, 550 nm, 500 nm, 450 nm, 400 nm, and 380 nm, respectively. Although almost doubling effect could also be encountered as $k=6.94 \times 10^{-4}$ at λ=380 nm to $k=1.32 \times 10^{-3}$ min^{-1} at λ=600 nm, an average of $k=9.95 \times 10^{-4}$ min^{-1} could be accepted as suitable for displaying sedimentation kinetics using the linear model.

Under the specified conditions of continuous mixing for 60 min, Fe-TiO_2 NP specimen "as-is" under dark conditions behaved in an almost similar manner to respective TiO_2 and N-TiO_2 NPs. As represented by selected wavelengths, it could be deduced that upon 30 min duration, approximately 6 % removals were achieved with respect to increasing specified wavelengths followed which a slight enhancement was also observed as 15 % upon 120 min.

In spite of linear model expressing slightly lower kinetic constants, both kinetic model constants were not significantly different from each other at the specified wavelengths (Table 4.172). Upon period of 60 min, wavelength dependent variation in removal efficiencies were 5-10 % and further extended time period as 120 min displayed 10-20 % with respect to increasing detection wavelength. This slight incremental increase could also be followed by prolonged time intervals possibly leading to 40-60 % in 6 h as could be deduced by calculation using both exponential and linear models at λ=550 nm, respectively.

4.2.4. Comparative Evaluation of Exponential and Linear Models of TiO_2, N-TiO_2, Fe-TiO_2 "as-is" under dark Conditions

Regarding the presented data for all of the NPs under "as-is" under dark conditions, although similar sedimentation profiles were attained, a comparative evaluation could be useful in elucidation of the sample specific variations for suitability of application of UV-vis spectroscopic technique. To fulfill this purpose, kinetic model parameters attained at selected indicative wavelength of λ=550 nm were compiled from tables 4.170-4.172 and presented in Table 4.173.

Table 4.173. Comparative presentation of sedimentation kinetics of NPs under "as-is" under dark conditions at λ= 550 nm.

Kinetic model	Exponential model	
NP	k, min^{-1}	R^2
TiO_2	8.00 x 10^{-4}	0.965
N-TiO_2	1.53 x 10^{-3}	0.986
Fe-TiO_2	1.31 x 10^{-3}	0.980
	Linear model	
	k, min^{-1}	R^2
TiO_2	7.52 x 10^{-4}	0.970
N-TiO_2	1.39 x 10^{-3}	0.979
Fe-TiO_2	1.20 x 10^{-3}	0.973

Considering sedimentation behavior of TiO_2, N-TiO_2, and Fe-TiO_2 "as-is" under dark conditions in the absence of organic matter, normalized absorbance values recorded at λ=550 nm fitted to the exponential kinetic equation gave the following reaction rate constants (min^{-1}) as 1.53 x 10^{-3} for N-TiO_2 > 1.31 x 10^{-3} for Fe-TiO_2 > 8.00 x 10^{-4} for TiO_2 (Table 4.173).

When sedimentation behavior of TiO_2, N-TiO_2, and Fe-TiO_2 specimens were fitted to the linear model, rate constants (min^{-1}) were found as 1.39 x 10^{-3} for N-TiO_2 > 1.20 x 10^{-3} for Fe-TiO_2 > 7.52 x 10^{-4} for TiO_2 (Table 4.173).

A simple comparison to "as-is" conditions (Table 4.169) indicated that slightly lower kinetic constants were attained. Application of exponential model indicated preferential stability of TiO_2 in comparison to N-TiO_2 and Fe-TiO_2 all "as-is" under dark conditions, as also supported by linear modeling with minor differences. From a general perspective, both kinetic models revealed similar tendencies. The role of continuous mixing prior to absorbance recordings could be related to the possible disaggregation of the NPs in comparison to the applied sonication and magnetic stirring for a short duration of NP samples prepared under "as-is" conditions.

4.2.5. Sedimentation Behavior of Nanoparticles TiO_2, N-TiO_2 and Fe-TiO_2 "as-is" under irradiation in the Absence of Organic Matter

All selected NP specimens were subjected to irradiation in an ATLAS Suntest CPS+ simulator during a specific time of 30 min for TiO_2 and N-TiO_2, 60 min for Fe-TiO_2 and time dependent UV-vis absorbance measurements were recorded between wavelength region of 200 and 600 nm.

4.2.5.1. TiO_2 specimen "as-is" under irradiation. TiO_2 specimen "as-is" under irradiation was also subjected to irradiation during a specific time of 30 min for TiO_2 and N-TiO_2, 60 min for Fe-TiO_2. Time dependent UV-vis absorbance variations in the wavelength range of 200-600 nm were recorded and presented in Figure 4.271. Exponential and linear models were applied and sedimentation kinetic constants were exhibited in Table 4.174.

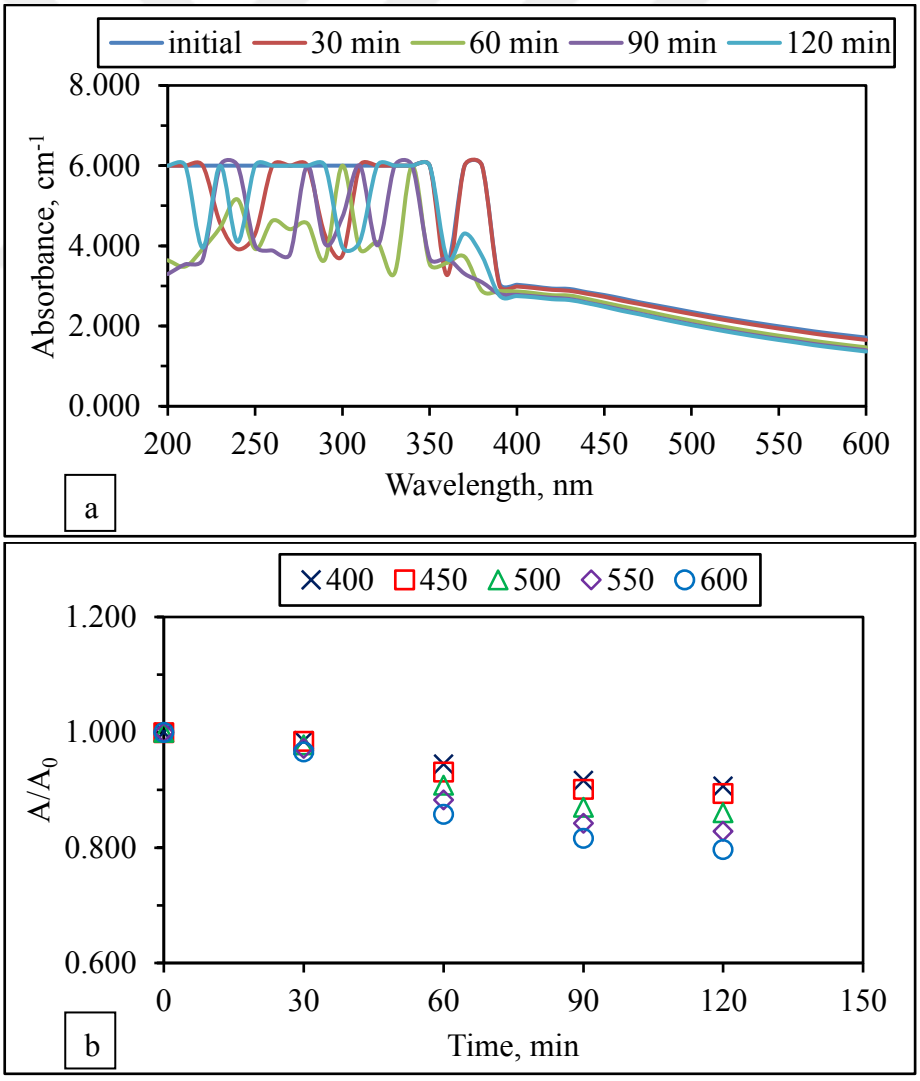


Figure 4.271. Sedimentation behavior of TiO_2 "as-is" under irradiation, a) UV-vis absorbance variations b) Normalized absorbance with respect to time.

The variations in exposure periods were related to the further application of binary systems *i.e.* photocatalysis. In a similar manner to data depicted under "as-is" (Figure 4.265a, b) and "as-is" under dark conditions (Figure 4.268a, b) UV-vis spectral variations could also be expressed by two regions as an inconsistent trend ($200<\lambda<400$ nm) followed by a consistent trend ($400<\lambda<600$ nm). Both exponential and linear modeling revealed considerably high correlation coefficients as $R^2 > 0.937$.

Table 4.174. TiO_2 "as-is" under irradiation, kinetic model parameters.

Kinetic model	Wavelength, nm				
	400	450	500	550	600
Exponential model					
k, min^{-1}	8.94×10^{-4}	1.04×10^{-3}	1.39×10^{-3}	1.73×10^{-3}	2.07×10^{-3}
R^2	0.965	0.945	0.945	0.943	0.943
Linear model					
k, min^{-1}	8.51×10^{-4}	9.82×10^{-4}	1.29×10^{-3}	1.58×10^{-3}	1.85×10^{-3}
R^2	0.964	0.942	0.942	0.939	0.937

Exponential model kinetic constants (min^{-1}) displayed a decreasing order as $2.07 \times 10^{-3} > 1.73 \times 10^{-3} > 1.39 \times 10^{-3} > 1.04 \times 10^{-3} > 8.94 \times 10^{-4}$ for wavelengths of 600 nm, 550 nm, 500 nm, 450 nm, and 400 nm respectively. An average value of $k=2.08 \times 10^{-3}$ min^{-1} could be regarded as suitable for expressing sedimentation kinetics of TiO_2 "as-is" under irradiation using the exponential model.

In a similar manner, the linear trend as visualized by the decreasing trend of A/A_o revealed kinetic constants (min^{-1}) in a decreasing order as $1.85 \times 10^{-3} > 1.58 \times 10^{-3} > 1.29 \times 10^{-3} > 9.82 \times 10^{-4} > 8.51 \times 10^{-4}$ for wavelengths of 600 nm, 550 nm, 500 nm, 450 nm, and 400 nm respectively. As expressed above an average of $k=1.78 \times 10^{-3}$ min^{-1} could be accepted as suitable for displaying sedimentation kinetics using the linear modeling with minor differences.

It could also be deduced that upon 30 min duration $\leq$ 5 % removals were achieved being considerably indifferent from each other with respect to increasing specified wavelengths followed which a slight enhancement was also observed as 5-15 % in 60 min representing between wavelength region of 400 nm and 600 nm. However, upon 120 min experimental duration, removal percentage increased to 20 % as detected at λ=600 nm being significantly different than the one attained for λ=400 nm. Wavelength dependent variations could not be related to the any physical phenomena rather than to the effect of instantaneous settling behavior of TiO_2 particles. On the other hand, light exposure under continuous mixing conditions could certainly affect the particle separation leading to disaggregation although this phenomenon should also be visualized by all absorbance recordings at all wavelength conditions.

4.2.5.2. N-TiO_2 specimen "as-is" under irradiation. As explained for N-TiO_2 "as-is under dark conditions (Figure 4.269 and Table 4.171), a similar approach was followed for elucidation of sedimentation behavior of N-TiO_2 "as-is" under irradiation conditions. Time dependent UV-vis absorbance variations in the overall spectra covering the wavelength range of 200-600 nm were presented (Figure 4.272a). N-TiO_2 "as-is" under irradiation conditions displayed quite similar tendency to N-TiO_2 "as-is" conditions and no direct effect of continuous mixing for 30 min could be observed excluding the initial absorbance recordings. Moreover, in a similar manner to N-TiO_2 under "as-is" (Figure 4.266a, b) and "as-is" under dark conditions (Figure 4.269a, b) the contribution of absorbance recordings at λ=380 nm could also be encountered.

Both kinetic models were applied revealing considerably high correlation coefficients as $R^2 >$ 0.755 and kinetic constants were tabulated (Table 4.175).

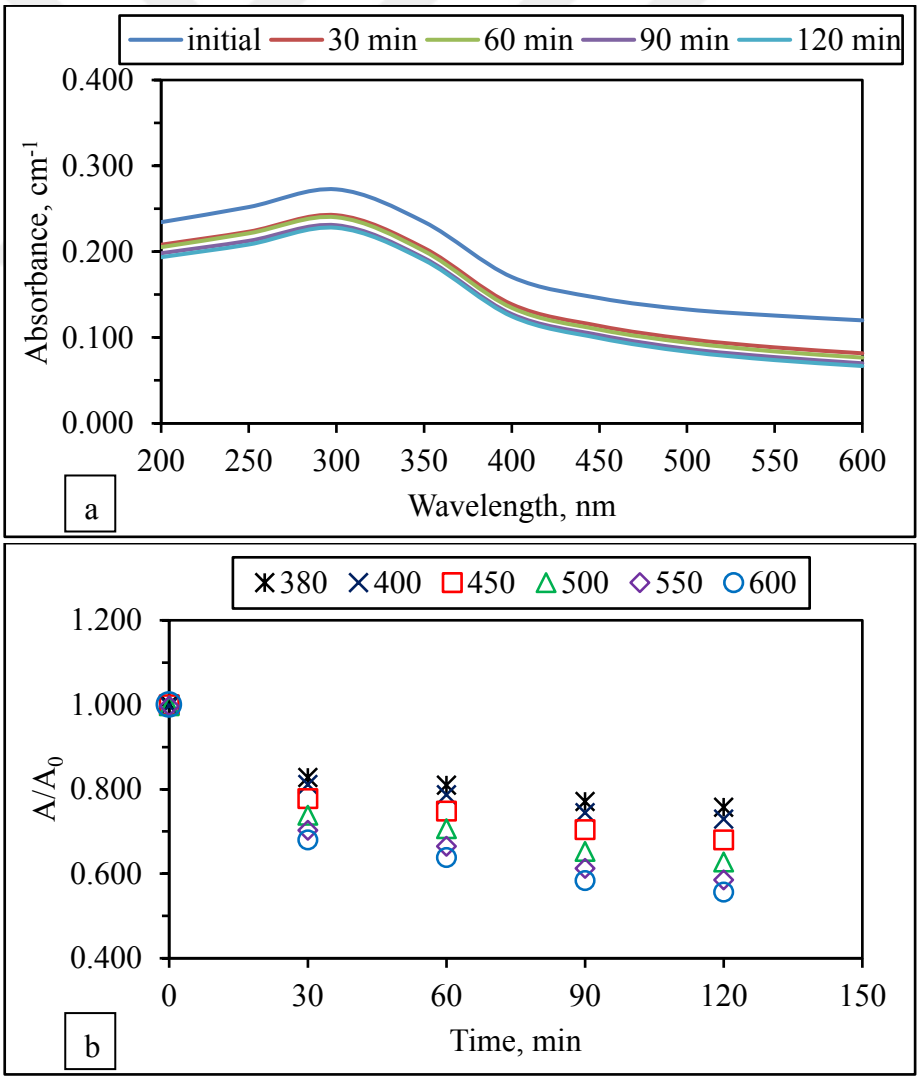


Figure 4.272. Sedimentation behavior of N-TiO_2 "as-is" under irradiation, a) UV-vis absorbance variations b) Normalized absorbance with respect to time.

Table 4.175. N-TiO_2 "as-is" under irradiation, kinetic model parameters.

Kinetic model	Wavelength, nm					
	380	400	450	500	550	600
Exponential model						
k, min^{-1}	2.09×10^{-3}	2.37×10^{-3}	2.90×10^{-3}	3.50×10^{-3}	4.01×10^{-3}	4.42×10^{-3}
R^2	0.797	0.814	0.819	0.823	0.815	0.812
Linear model						
k, min^{-1}	1.81×10^{-3}	2.01×10^{-3}	2.37×10^{-3}	2.75×10^{-3}	3.04×10^{-3}	3.28×10^{-3}
R^2	0.770	0.784	0.781	0.778	0.763	0.755

Exponential model kinetics expressed constants (min^{-1}) in a decreasing order as $4.42 \times 10^{-3} > 4.01 \times 10^{-3} > 3.50 \times 10^{-3} > 2.90 \times 10^{-3} > 2.37 \times 10^{-3} > 2.09 \times 10^{-3}$ for wavelengths of 600 nm, 550 nm, 500 nm, 450 nm, 400 nm, and 380 nm, respectively. Kinetic constants followed a steadily increasing trend with respect to increasing detection wavelengths. Still, an average value of $k=3.22 \times 10^{-3}$ min^{-1} could be regarded as suitable for expressing sedimentation kinetics using the exponential model. The average value resembled to the $k=3.50 \times 10^{-3}$ min^{-1} that was calculated for λ=500 nm.

Linear trend as visualized by the decreasing trend of normalized absorbance recordings as A/A_o revealed kinetic constants (min^{-1}) in a decreasing order as $3.28 \times 10^{-3} > 3.04 \times 10^{-3} > 2.75 \times 10^{-3} > 2.37 \times 10^{-3} > 2.01 \times 10^{-3} > 1.81 \times 10^{-3}$ for wavelengths of 600 nm, 550 nm, 500 nm, 450 nm, 400 nm, and 380 nm, respectively. As expressed above an average of $k=2.54 \times 10^{-3}$ min^{-1} could be accepted as suitable for displaying sedimentation kinetics using the linear model. The average value as $k=2.54 \times 10^{-3}$ min^{-1} could well be regarded as similar to the rate constant attained as 2.37×10^{-3} min^{-1} at λ=400 nm.

Under the specified conditions represented by selected wavelengths, it could be deduced that upon 30 min duration, 20 % removal at λ=380 nm and 30 % at λ=600 nm was obtained. Immediate settling profile could be distinctly visualized by absorbance recordings at various wavelengths in UV as well as in visible region. Further duration resulted in a continuous sedimentation tendency in a style expressing increasing difference between the absorbance recordings. Upon 120 min of duration, 30 % removal at λ=380 nm and 45 % removal at λ=600 nm were observed.

The differences in kinetic constants attained by application of both models as well as related removal percentages might indicate irradiation under continuous mixing conditions induced changes could predominate over mixing under "as-is" and "as-is" under dark conditions. However, no direct conclusion could be visualized with respect to wavelength variations.

4.2.5.3. Fe-TiO_2 specimen "as-is" under irradiation. Similarly, to Fe-TiO_2 under "as-is" (Figure 4.267 and Table 4.168) and "as-is" under dark conditions (Figure 4.270 and Table 4.172), a similar approach was followed for elucidation of sedimentation behavior of Fe-TiO_2 "as-is" under irradiation conditions. Time dependent UV-vis absorbance variations in the overall spectra covering the wavelength range of 200-600 nm were presented (Figure 4.273a). Fe-TiO_2 specimen under "as-is" under irradiation conditions displayed quite similar tendency to Fe-TiO_2 "as-is" conditions and no direct effect of continuous mixing for 60 min could be observed excluding the initial absorbance recordings.

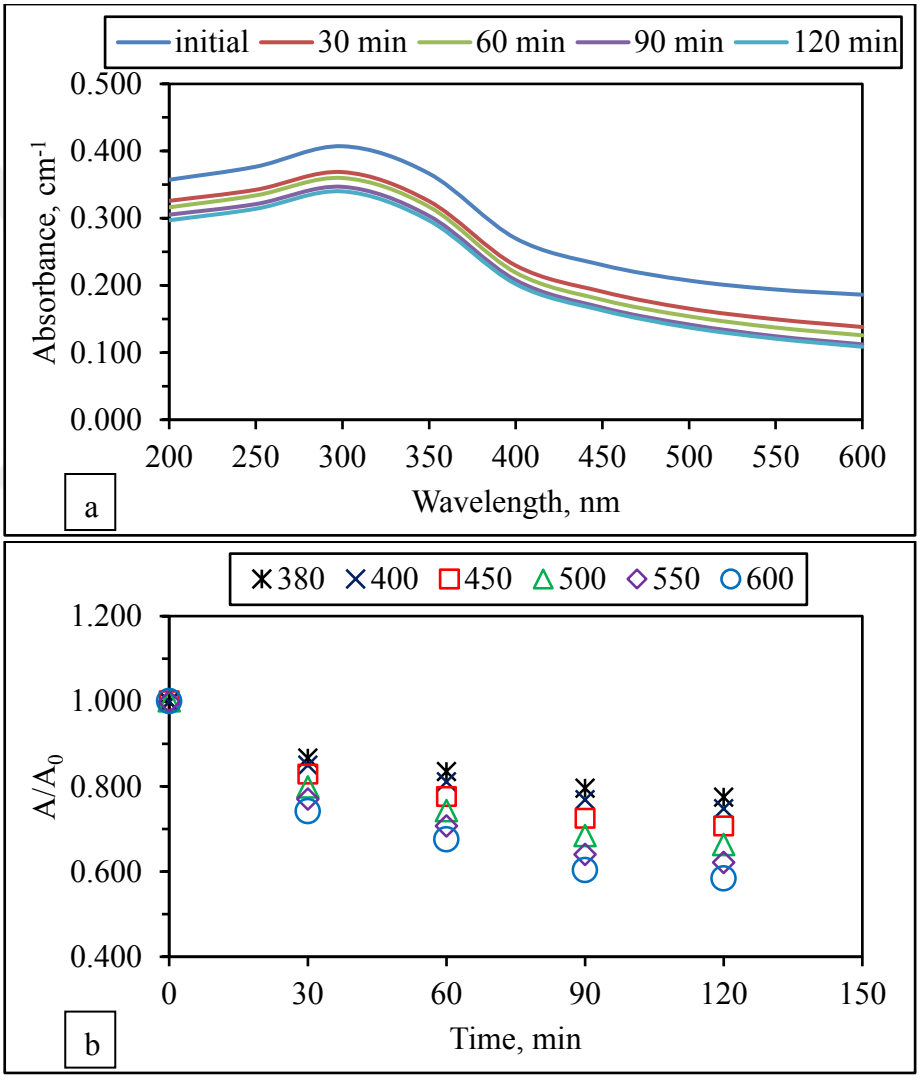


Figure 4.273. Sedimentation behavior of Fe-TiO_2 "as-is" under irradiation, a) UV-vis absorbance variations b) Normalized absorbance with respect to time.

Time dependent variations in UV-vis absorbance spectral features were distinctly different than the spectral features attained upon dark conditions revealing the significant effect of irradiation. Moreover, in a similar manner to Fe-TiO_2 under "as-is" (Figure 4.267a, b) and "as-is" under dark

conditions (Figure 4.270a, b) the contribution of absorbance recordings at λ=380 nm could also be encountered. Both kinetic models as exponential and linear models were applied revealing considerably high correlation coefficients as $R^2 > 0.834$ and kinetic constants were tabulated (Figure 4.273b and Table 4.176).

Table 4.176. Fe-TiO_2 "as-is" under irradiation, kinetic model parameters.

Kinetic model	Wavelength, nm					
	380	400	450	500	550	600
Exponential model						
k, min^{-1}	1.97×10^{-3}	2.26×10^{-3}	2.76×10^{-3}	3.26×10^{-3}	3.78×10^{-3}	4.28×10^{-3}
R^2	0.887	0.885	0.888	0.889	0.887	0.883
Linear model						
k, min^{-1}	1.73×10^{-3}	1.95×10^{-3}	2.30×10^{-3}	2.63×10^{-3}	2.95×10^{-3}	3.24×10^{-3}
R^2	0.863	0.858	0.857	0.852	0.845	0.834

Exponential model expressed kinetic constants (min^{-1}) in a decreasing order as $4.28 \times 10^{-3} > 3.78 \times 10^{-3} > 3.26 \times 10^{-3} > 2.76 \times 10^{-3} > 2.26 \times 10^{-3} > 1.97 \times 10^{-3}$ for wavelengths of 600 nm, 550 nm, 500 nm, 450 nm, 400 nm, and 380 nm, respectively. Simply an average value of $k=3.05 \times 10^{-3}$ min^{-1} could be regarded as suitable for expressing sedimentation kinetics using the exponential model. The average value resembled to the $k=3.26 \times 10^{-3}$ min^{-1} that was calculated from the data attained by absorbance recordings at λ=500 nm.

In a similar manner, the linear trend as visualized by the decreasing trend of A/A_o revealed kinetic constants (min^{-1}) in a decreasing order as $3.24 \times 10^{-3} > 2.95 \times 10^{-3} > 2.63 \times 10^{-3} > 2.30 \times 10^{-3} > 1.95 \times 10^{-3} > 1.73 \times 10^{-3}$ for wavelengths of 600 nm, 550 nm, 500 nm, 450 nm, 400 nm, and 380 nm, respectively. As expressed above an average of $k=2.47 \times 10^{-3}$ min^{-1} could be accepted as suitable for displaying sedimentation kinetics using a linear model. The average value resembled to the linear model kinetic constants calculated from the data attained by absorbance recordings at λ=450 and 500 nm.

It could be inferred that upon 60 min experimental duration, almost 40 % absorbance reduction was recorded at λ=600 nm. Further increase in duration did not significantly affect the removal percentage of Fe-TiO_2 "as-is" under irradiation reaching to slightly lower values. However, under similar conditions only 10 % enhancement was attained in case that the sedimentation efficiencies were expressed using absorbance recordings at λ=380 nm. Furthermore, a very slight difference was recorded in between sedimentation time scale of 90 min and 120 min resulting in almost expressing a plateau type behavior.

4.2.6. Comparative Evaluation of Exponential and Linear Models of TiO_2, N-TiO_2, Fe-TiO_2 "as-is" under irradiation Conditions

Regarding the presented data for all of the NPs under "as-is" under irradiation conditions, although similar sedimentation profiles were attained, a comparative evaluation could be convenient in clarification of the sample specific variations for suitability of application of UV-vis spectroscopic technique. To fulfill this purpose, kinetic model parameters attained at the selected indicative wavelength as λ=550 nm were compiled form tables 4.174-4.176 and presented in Table 4.177.

Table 4.177. Comparative presentation of sedimentation kinetics of NPs under "as-is" irradiation conditions at λ=550 nm.

Kinetic model	Exponential model	
NP "as-is"	k, min^{-1}	R^2
TiO_2	1.73 x 10^{-3}	0.943
N-TiO_2	4.01 x 10^{-3}	0.815
Fe-TiO_2	3.78 x 10^{-3}	0.887
	Linear model	
	k, min^{-1}	R^2
TiO_2	1.58 x 10^{-3}	0.939
N-TiO_2	3.04 x 10^{-3}	0.763
Fe-TiO_2	2.95 x 10^{-3}	0.845

Sedimentation behavior of TiO_2, N-TiO_2, and Fe-TiO_2 "as-is under irradiation" in the absence of organic matter was fitted to the exponential kinetic equation and gave the following reaction rate constants (min^{-1}) as 4.01 x 10^{-3} for N-TiO_2 > 3.78 x 10^{-3} for Fe-TiO_2 > 1.73 x 10^{-3} for TiO_2 (Table 4.177). However, when sedimentation behavior of TiO_2, N-TiO_2, and Fe-TiO_2 specimens were fitted to the linear model, reactions rate constants were found as 3.04 x 10^{-3} for N-TiO_2 > 2.95 x 10^{-3} for Fe-TiO_2 > 1.58 x 10^{-3} for TiO_2 (Table 4.177).

A simple comparison to "as-is" under dark conditions (Table 4.173) indicated that slightly higher kinetic constants were attained for NPs "as-is" under irradiation. Application of exponential model indicated preferential stability of TiO_2 in comparison to N-TiO_2 and Fe-TiO_2, as also supported by linear modeling with minor differences. From a general perspective, both kinetic models revealed similar tendencies as observed for "as-is" and "as-is" under dark conditions. The role of continuous mixing under irradiation prior to absorbance recordings could be related to the possible disaggregation of the NPs in comparison to the applied sonication and magnetic stirring for a short duration of NP samples prepared under "as-is" conditions and a constant mixing for 60 min under dark conditions.

4.2.7. Sedimentation Behavior of Nanoparticles as TiO_2, N-TiO_2 and Fe-TiO_2 under "as-is" Conditions in the Presence of Organic Matter

4.2.7.1. "TiO_2 and HA" binary system under "as-is" conditions. Time dependent UV-vis absorbance variations in the wavelength range of 200-600 nm were presented. Figure 4.274a exhibited spectral variations that could be stated by two regions as an inconsistent trend (200<λ<400 nm) followed by a consistent trend (400<λ<600 nm).

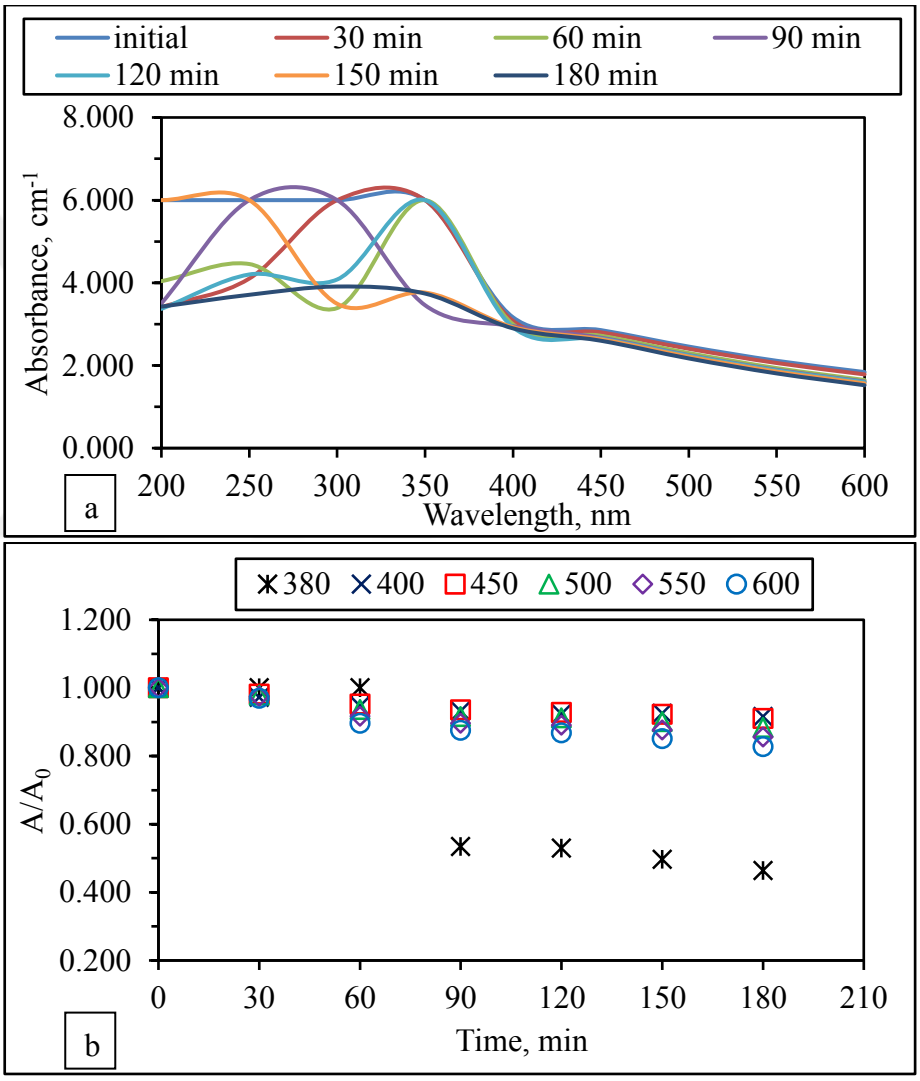


Figure 4.274. Sedimentation behavior of "TiO_2 and HA" under "as-is" conditions, a) UV-vis absorbance variations b) Normalized absorbance with respect to time.

Although absorbance recordings at λ=380 nm was not meaningful for TiO_2 under "as-is" conditions, absorbance recordings at λ=380 nm for "TiO_2 and HA" under "as-is" conditions were considered essential due to the interactions of nanoparticle and organic matter. Therefore, time dependent absorbance values at selected wavelengths as 380 nm, 400 nm, 450 nm, 500 nm, 550 nm

and 600 nm were normalized to respective initial absorbance values and presented in Figure 4.274b. The variations were modeled by two approaches depending on the decreasing trend profiles. Exponential and linear models were applied and sedimentation kinetic constants were presented in Table 4.178. Both exponential and linear modeling revealed considerably high correlation coefficients as $R^2 > 0.807$.

Table 4.178. "TiO_2 and HA" under "as-is" conditions, kinetic model parameters.

Kinetic model	Wavelength, nm					
	380	400	450	500	550	600
Exponential model						
k, min^{-1}	5.17×10^{-3}	4.64×10^{-4}	5.14×10^{-4}	6.71×10^{-4}	8.45×10^{-4}	1.03×10^{-3}
R^2	0.829	0.874	0.941	0.934	0.926	0.919
Linear model						
k, min^{-1}	3.67×10^{-3}	4.42×10^{-4}	4.90×10^{-4}	6.31×10^{-4}	7.81×10^{-4}	9.35×10^{-4}
R^2	0.807	0.867	0.936	0.927	0.917	0.908

Exponential model kinetics were expressed by kinetic constants (min^{-1}) in a decreasing order as $5.17 \times 10^{-3} > 1.03 \times 10^{-3} > 8.45 \times 10^{-4} > 6.71 \times 10^{-4} > 5.14 \times 10^{-4} > 4.64 \times 10^{-4}$ for wavelengths of 380 nm, 600 nm, 550 nm, 500 nm, 450 nm, and 400 nm, respectively. Simply an average value of $k=1.45 \times 10^{-3}$ min^{-1} could be regarded as suitable for explicating sedimentation kinetics of "TiO_2 and HA" under "as-is" conditions using the exponential model.

In a similar manner, the linear trend as visualized by the decreasing trend of A/A_o revealed kinetic constants (min^{-1}) in a decreasing order as $3.67 \times 10^{-3} > 9.35 \times 10^{-4} > 7.81 \times 10^{-4} > 6.31 \times 10^{-4} > 4.90 \times 10^{-4} > 4.42 \times 10^{-4}$ for wavelengths of 380 nm, 600 nm, 550 nm, 500 nm, 450 nm, and 400 nm, respectively. As expressed above, an average of kinetic model constant as $k=1.16 \times 10^{-3}$ min^{-1} could also be accepted as suitable for displaying sedimentation kinetics "TiO_2 and HA" under "as-is" conditions using the linear model.

Under the specified "as-is" conditions represented by selected wavelengths including λ=380 nm, it could be inferred that upon 60 min duration, approximately 10 % of "TiO_2 and HA" were settled irrespective of the specified wavelength. However, upon further experimental duration of 90 min, distinctly different behavior was observed in case that λ=380 nm was selected as the indicative wavelength. Under this condition ~ 45 % of "TiO_2 and HA" was settled followed by a slight enhancement to ~ 55 % upon 180 min experimental duration. Therefore, selection of indicative wavelength could be described as system dependent and should be assessed under the specified experimental conditions.

4.2.7.2. "TiO_2 and SRNOM" binary system under "as-is" conditions. As explained for "TiO_2 and HA" binary system under "as-is" conditions (Figure 4.274 and Table 4.178), following a similar trend, sedimentation behavior of "TiO_2 and SRNOM" binary system under "as-is" conditions was monitored. Time dependent UV-vis absorbance variations in the wavelength range of 200-600 nm were presented. Figure 4.275a exhibited spectral variations that could be stated by two regions as an inconsistent trend (200<λ<400 nm) followed by a consistent trend (400<λ<600 nm). Due to the observed inconsistency, absorbance recordings at λ=380 nm were excluded.

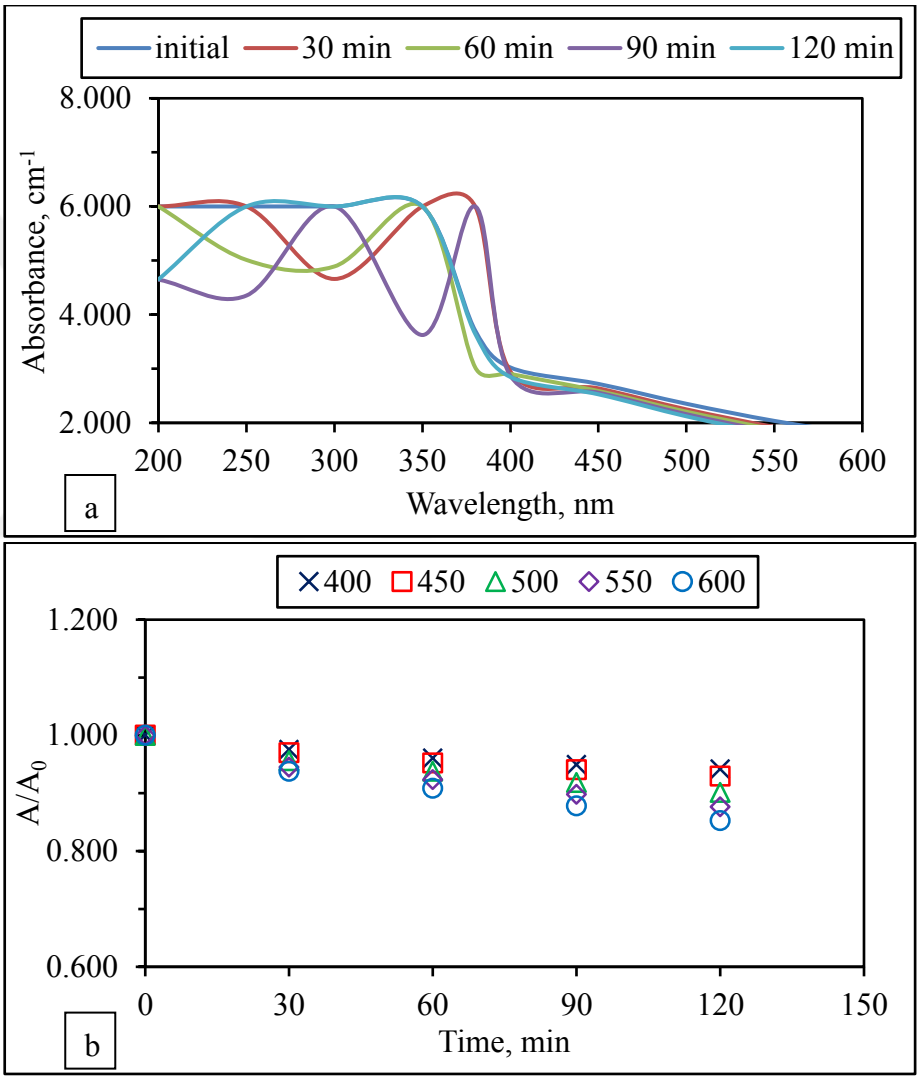


Figure 4.275. Sedimentation behavior of "TiO_2 and SRNOM" under "as-is" conditions, a) UV-vis absorbance variations b) Normalized absorbance with respect to time.

The variations were modeled by two approaches depending on the decreasing trend profiles. Exponential and linear models were applied and sedimentation kinetic constants were presented in Figure 4.275b and Table 4.179. Both exponential and linear modeling revealed considerably high correlation coefficients as $R^2 > 0.948$.

Table 4.179. "TiO_2 and SRNOM" under "as-is" conditions, kinetic model parameters.

Kinetic model	Wavelength, nm				
	400	450	500	550	600
Exponential model					
k, min^{-1}	4.90×10^{-4}	5.92×10^{-4}	8.26×10^{-4}	1.05×10^{-3}	1.28×10^{-3}
R^2	0.952	0.954	0.960	0.964	0.972
Linear model					
k, min^{-1}	4.75×10^{-4}	5.70×10^{-4}	7.83×10^{-4}	9.81×10^{-4}	1.18×10^{-3}
R^2	0.948	0.950	0.954	0.957	0.963

Exponential model kinetics as expressed by kinetic constants (min^{-1}) showed a decreasing order indicated as $1.28 \times 10^{-3} > 1.05 \times 10^{-3} > 8.26 \times 10^{-4} > 5.92 \times 10^{-4} > 4.90 \times 10^{-4}$ for wavelengths of 600 nm, 550 nm, 500 nm, 450 nm and 400 nm, respectively. Although an approximate average value of $k=8.48 \times 10^{-4}$ min^{-1} could be regarded as appropriate for expressing sedimentation kinetics using the exponential model, the average value resembled to the $k=8.26 \times 10^{-4}$ min^{-1} that was calculated at λ=500.

In a similar manner, the linear trend as visualized by the decreasing trend of A/A_o revealed kinetic constants (min^{-1}) in a decreasing order as $1.18 \times 10^{-3} > 9.81 \times 10^{-4} > 7.83 \times 10^{-4} > 5.70 \times 10^{-4} > 4.75 \times 10^{-4}$ for wavelengths of 600 nm, 550 nm, 500 nm, 450 nm and 400 nm, respectively. As expressed above, an average of $k=7.98 \times 10^{-4}$ min^{-1} could be accepted as suitable for demonstrating sedimentation kinetics of "TiO_2 and SRNOM" under "as-is" conditions" using the linear model. The average value resembled to the $k=7.83 \times 10^{-4}$ min^{-1} that was calculated at wavelength of λ=500. Under the specified "as-is" conditions represented by selected wavelengths, it could be inferred that upon 30 min duration, approximately 4 % removal (2 % and 6 % for λ=400 and 600 nm respectively) was attained.

Correspondingly, almost an average of 9 % removal (5 % and 12 % for λ=400 and 600 nm respectively) was attained upon 90 min experimental duration. However, upon further experimental duration of 120 min, it could be deduced that about 11 % removal (6 % and 15 % for λ=400 and 600 nm respectively) was accomplished. As explicated by UV-vis absorbance based kinetic modeling applied in two different approaches as exponential and linear models, a doubling effect could be seen between λ=400 and 600 nm in terms of removal efficiencies. Therefore, it could be concluded that selection of specific wavelengths displayed specific differences in evaluation of sedimentation kinetics. This slight incremental increase could also be followed by prolonged time intervals possibly leading to 35-65 % in 6 h as could be deduced by calculation using both exponential and linear models at λ=550 nm, respectively.

4.2.7.3. "N-TiO_2 and HA" specimen under "as-is" conditions. As explained for "TiO_2 and HA", a similar approach was followed for elucidation of sedimentation behavior of "N-TiO_2 and HA" under "as-is" conditions. Time dependent UV-vis absorbance variations in the wavelength range of 200-600 nm were presented (Figure 4.276a).

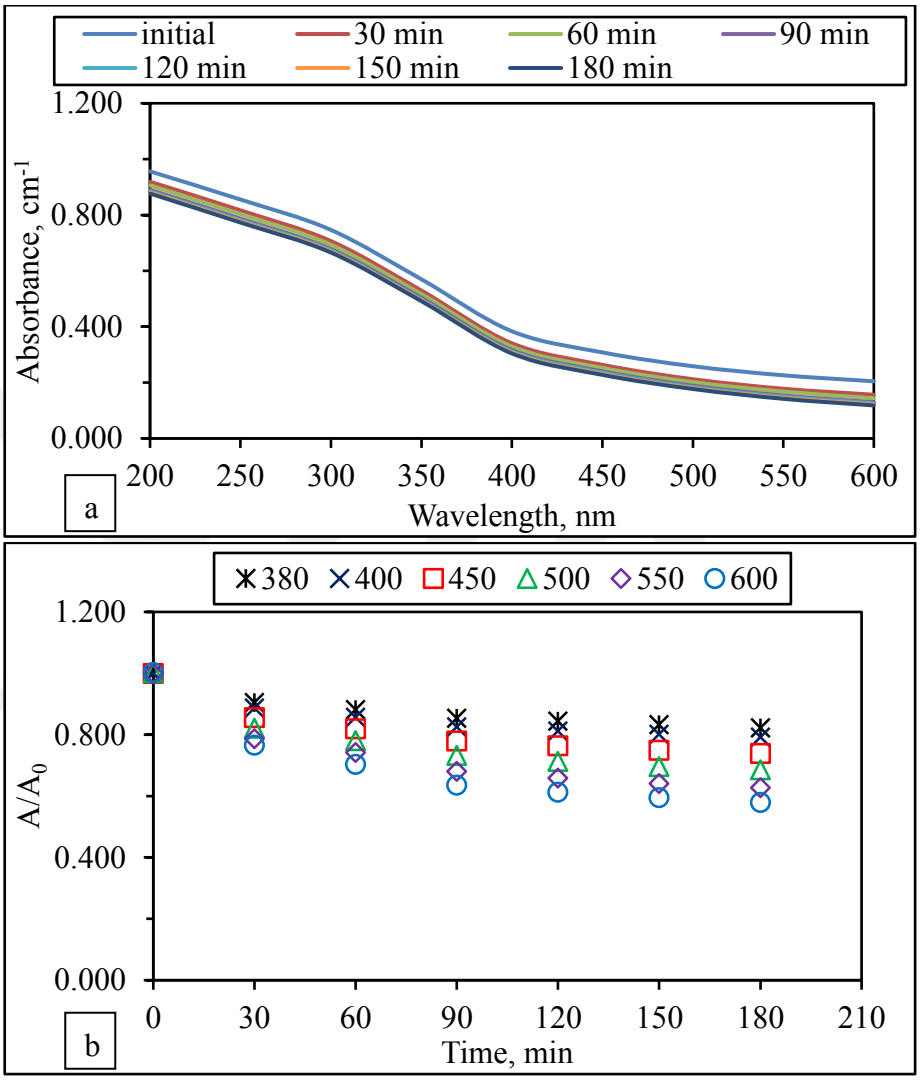


Figure 4.276. Sedimentation behavior of "N-TiO_2 and HA" under "as-is" conditions, a) UV-vis absorbance variations b) Normalized absorbance with respect to time.

Contrary to the two regional demonstration of UV-vis spectra recorded for "TiO_2 and HA" under as-is conditions (Figure 4.274), "N-TiO_2 and HA" spectral trend exhibited a substantially decreasing trend with respect to time irrespective of the experimental duration. Time dependent absorbance values at selected wavelengths were normalized to respective initial absorbance values and presented in Figure 4.276b. The variations were modeled by two approaches depending on the decreasing trend profiles. Exponential and linear models were applied and sedimentation kinetic constants were

presented in Table 4.180. Both exponential and linear modeling revealed considerably high correlation coefficients as $R^2 > 0.778$.

Table 4.180. "N-TiO_2 and HA" under "as-is" conditions, kinetic model parameters.

Kinetic model	Wavelength, nm					
	380	400	450	500	550	600
Exponential model						
k, min^{-1}	9.46×10^{-4}	1.14×10^{-3}	1.48×10^{-3}	1.86×10^{-3}	2.30×10^{-3}	2.73×10^{-3}
R^2	0.830	0.823	0.826	0.822	0.829	0.836
Linear model						
k, min^{-1}	8.49×10^{-4}	1.00×10^{-3}	1.25×10^{-3}	1.51×10^{-3}	1.78×10^{-3}	2.03×10^{-3}
R^2	0.809	0.798	0.793	0.780	0.779	0.778

Exponential model kinetics were expressed by kinetic constant (min^{-1}) in a decreasing order as $2.73 \times 10^{-3} > 2.30 \times 10^{-3} > 1.86 \times 10^{-3} > 1.48 \times 10^{-3} > 1.14 \times 10^{-3} > 9.46 \times 10^{-4}$ for wavelengths of 600 nm, 550 nm, 500 nm, 450 nm, 400 nm, and 380 nm, respectively. It could be inferred that exponential model kinetic rate constants decreased gradually with respect to decreasing wavelength. Simply an average value of $k=1.74 \times 10^{-3}$ min^{-1} could be regarded as suitable for expressing sedimentation kinetics using the exponential model irrespective of the detection wavelength.

In a similar manner, the linear trend as visualized by a decreasing trend of A/A_o revealed kinetic constants (min^{-1}) in a decreasing order as $2.03 \times 10^{-3} > 1.78 \times 10^{-3} > 1.51 \times 10^{-3} > 1.25 \times 10^{-3} > 1.00 \times 10^{-3} > 8.49 \times 10^{-4}$ for wavelengths of 600 nm, 550 nm, 500 nm, 450 nm, 400 nm, and 380 nm, respectively. As expressed above, an average of $k=1.40 \times 10^{-3}$ min^{-1} could be accepted as appropriate for displaying sedimentation kinetics using the linear model. It should also be indicated that both models could be successfully applied due to slight incremental decreases with respect to time.

Under the specified conditions represented by selected wavelengths, it could be deduced that upon 60 min duration, roughly 25 % removal (12 % and 30 % for λ=380 and 600 nm respectively) was achieved with respect to increasing specified wavelengths followed which a substantial enhancement that was observed as ~ 30 % (18 % and 42 % for λ=380 and 600 nm respectively) upon 180 min. Therefore, it could be inferred that in case that λ=380 nm was selected as the indicative wavelength, almost no change would be expressed.

However, considering the indicative wavelengths selected in vis region, variations in sedimentation efficiencies would be observed. "N-TiO_2 and HA" binary system also displayed the importance of the selection of the indicative wavelength for assessment of sedimentation efficiency.

4.2.7.4. "N-TiO_2 and SRNOM" binary system under "as-is" conditions. As explained for "N-TiO_2 and HA" binary system under "as-is" conditions, a similar approach was followed for elucidation of sedimentation behavior of "N-TiO_2 and SRNOM" binary system under "as-is" conditions. Time dependent UV-vis absorbance spectral variations in the wavelength range of 200-600 nm were recorded and presented in Figure 4.277a. Correspondingly, respective normalized absorbance values in the selected wavelengths were presented in Figure 4.277b.

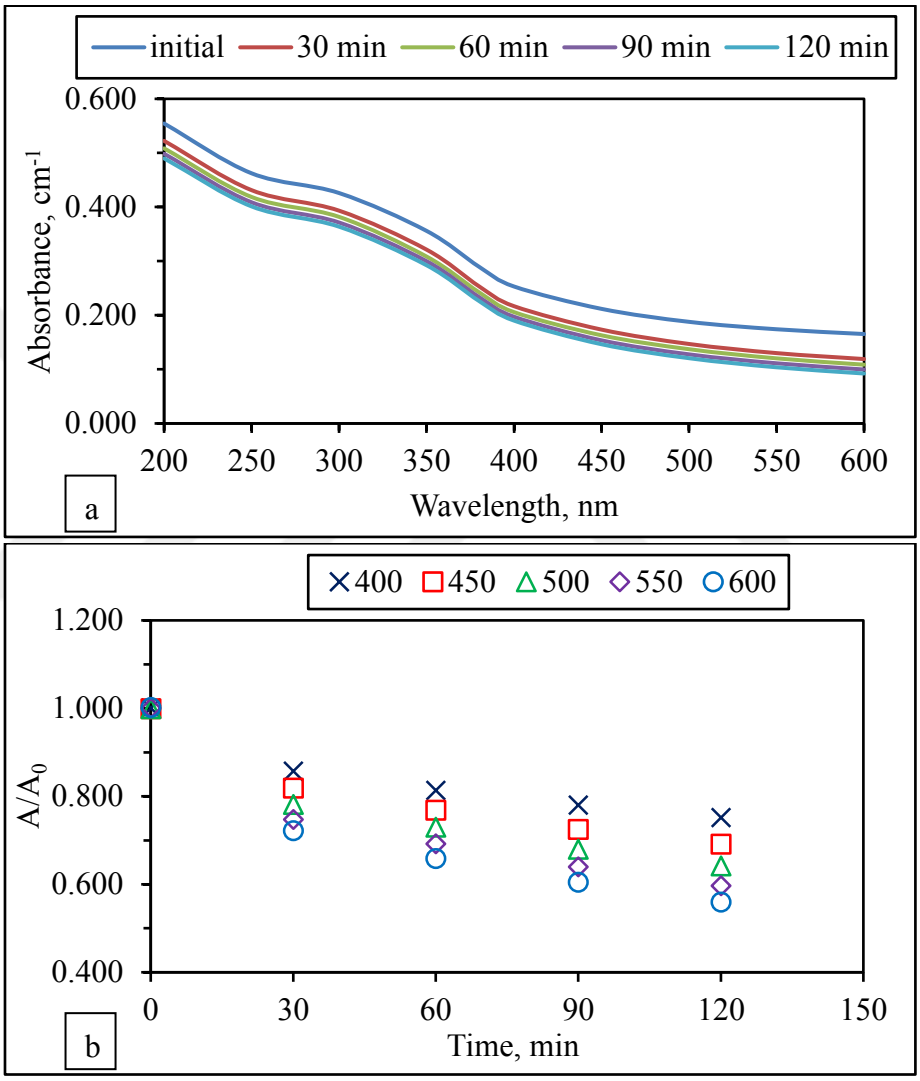


Figure 4.277. Sedimentation behavior of "N-TiO_2 and SRNOM" under "as-is" conditions, a) UV-vis absorbance variations b) Normalized absorbance with respect to time.

Contrary to the two regional demonstration of UV-vis spectra recorded for "TiO_2 and SRNOM" under "as-is" conditions (Figure 4.275), "N-TiO_2 and SRNOM" spectral trend demonstrated a substantially decreasing trend with respect to time irrespective of the experimental duration. Time dependent absorbance values at selected wavelengths were normalized to respective initial absorbance values and presented in Figure 4.277b. The variations were evaluated by two approaches

as exponential and linear models depending on the decreasing trend profiles and sedimentation kinetic constants were presented in Table 4.181. Due to the observed inconsistency absorbance recordings at λ=380 nm were excluded. Both exponential and linear modeling revealed considerably high correlation coefficients as $R^2 > 0.824$.

Table 4.181. "N-TiO_2 and SRNOM" under "as-is" conditions, kinetic model parameters.

Kinetic model	Wavelength, nm				
	400	450	500	550	600
Exponential model					
k, min^{-1}	2.22×10^{-3}	2.87×10^{-3}	3.42×10^{-3}	3.97×10^{-3}	4.47×10^{-3}
R^2	0.891	0.895	0.889	0.881	0.880
Linear model					
k, min^{-1}	1.92×10^{-3}	2.37×10^{-3}	2.72×10^{-3}	3.05×10^{-3}	3.34×10^{-3}
R^2	0.865	0.861	0.847	0.831	0.824

Exponential model kinetic constants expressed a decreasing order as $4.47 \times 10^{-3} > 3.97 \times 10^{-3} > 3.42 \times 10^{-3} > 2.87 \times 10^{-3} > 2.22 \times 10^{-3}$ for wavelengths of 600 nm, 550 nm, 500 nm, 450 nm, and 400 nm, respectively. Simply an average value of $k=3.39 \times 10^{-3}$ min^{-1} could be regarded as appropriate for expressing sedimentation kinetics using the exponential model. The average value resembled to the $k=3.42 \times 10^{-3}$ min^{-1} that was calculated at λ=500 nm.

Following the same manner, the linear trend as visualized by the decreasing trend of A/A_o revealed kinetic constants (min^{-1}) in a decreasing order as $3.34 \times 10^{-3} > 3.05 \times 10^{-3} > 2.72 \times 10^{-3} > 2.37 \times 10^{-3} > 1.92 \times 10^{-3}$ for wavelengths of 600 nm, 550 nm, 500 nm, 450 nm, and 400 nm, respectively. As expressed above an average of $k=2.68 \times 10^{-3}$ min^{-1} could also be regarded as suitable for displaying sedimentation kinetics using the linear model. The average value resembled to the $k=2.72 \times 10^{-3}$ min^{-1} that was calculated at λ=500 nm. Under the specified conditions represented by selected wavelengths, it could be inferred that upon 30 min duration, ~ 15 % removal at λ=400 nm and 30 % at λ=600 nm was attained. However, upon 90 min of duration, approximately 22 % removal at λ=400 nm and 40 % at λ=600 nm was obtained. Upon 120 min of duration 25 % removal at λ=400 nm and ~ 45 % removal at λ=600 nm were observed. This slight incremental increase could also be followed by prolonged time intervals possibly leading to 35-95 % in 6 h as could be inferred by calculation using linear model, respectively.

Despite the fact that linear model explicating slightly lower kinetic constants, both kinetic model constants revealed similar tendencies and were not significantly different from each other at the specified wavelengths (Table 4.181).

4.2.7.5. "Fe-TiO_2 and HA" binary system under "as-is" conditions. Likewise expressed so far, a similar approach was also followed for elucidation of sedimentation behavior of "Fe-TiO_2 and HA" under "as-is "conditions. Time dependent UV-vis absorbance variations in the wavelength range of 200-600 nm were presented (Figure 4.278a).

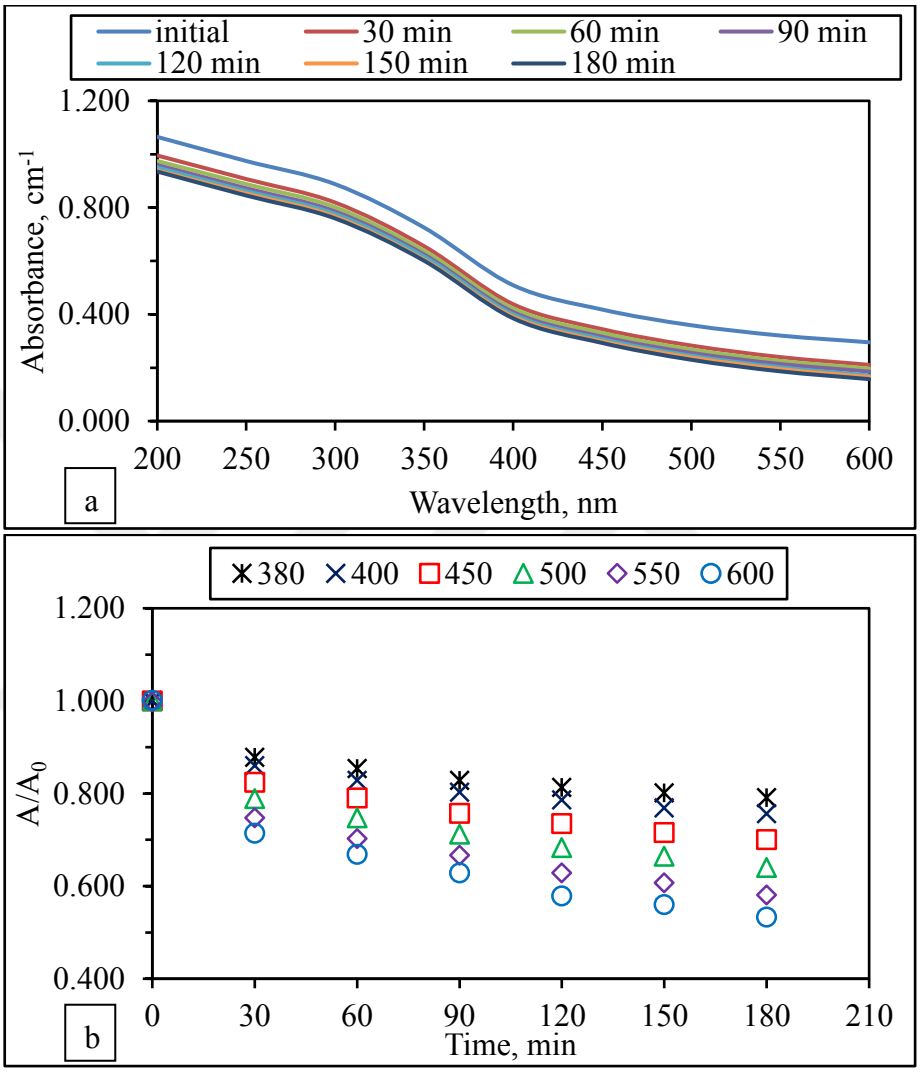


Figure 4.278. Sedimentation behavior of "Fe-TiO_2 and HA" under "as-is" conditions, a) UV-vis absorbance variations b) Normalized absorbance with respect to time.

Contrary to the two regional exhibition of UV-vis spectra recorded for "TiO_2 and HA" under "as-is" condition, and in a similar manner to "N-TiO_2 and HA", "Fe-TiO_2 and HA" also demonstrated a decreasing trend with respect to time. Time dependent absorbance values at selected wavelengths were normalized to respective initial absorbance values and presented in Figure 4.278b. The variations were evaluated by two approaches as exponential and linear models depending on the decreasing trend profiles and sedimentation kinetic constants were presented in Table 4.182. Both exponential and linear modeling revealed considerably high correlation coefficients as $R^2 > 0.761$.

Table 4.182. "Fe-TiO_2 and HA" under "as-is" conditions, kinetic model parameters.

Kinetic model	Wavelength, nm					
	380	400	450	500	550	600
Exponential model						
k, min^{-1}	1.11 x 10^{-3}	1.33 x 10^{-3}	1.69 x 10^{-3}	2.11 x 10^{-3}	2.56 x 10^{-3}	3.00 x 10^{-3}
R^2	0.806	0.816	0.821	0.828	0.831	0.835
Linear model						
k, min^{-1}	9.79 x 10^{-4}	1.14 x 10^{-3}	1.39 x 10^{-3}	1.66 x 10^{-3}	1.91 x 10^{-3}	2.15 x 10^{-3}
R^2	0.779	0.784	0.779	0.775	0.767	0.761

Exponential model kinetics as expressed by kinetic constants (min^{-1}) showed a decreasing order indicated as 3.00 x 10^{-3} > 2.56 x 10^{-3} > 2.11 x 10^{-3} > 1.69 x 10^{-3} > 1.33 x 10^{-3} > 1.11 x 10^{-3} for wavelengths of 600 nm, 550 nm, 500 nm, 450 nm, 400 nm, and 380 nm, respectively. Although an approximate average value of k=1.97 x 10^{-3} min^{-1} could be regarded as appropriate for expressing sedimentation kinetics using the exponential model, the difference in min and max values should also be considered more or less the same (1.74 x 10^{-3} min^{-1}) as reported above for "N-TiO_2 and HA" binary system (Table 4.180).

In a similar manner, the linear trend as visualized by the decreasing trend of A/A_o revealed kinetic constants (min^{-1}) in a decreasing order as 2.15 x 10^{-3} > 1.91 x 10^{-3} > 1.66 x 10^{-3} > 1.39 x 10^{-3} > 1.14 x 10^{-3} > 9.79 x 10^{-4} for wavelengths of 600 nm, 550 nm, 500 nm, 450 nm, 400 nm, and 380 nm, respectively. As expressed above an average of k=1.54 x 10^{-3} min^{-1} could be accepted as suitable for demonstrating sedimentation kinetics using the linear model.

Under the specified "as-is" conditions represented by selected wavelengths, it could be deduced that upon 30 min duration, approximately an average of 20 % removal (12 % and 29 % for λ=380 and 600 nm respectively) was obtained. Following a similar approach, relatively 30 % removal (17 % and 37 % for λ=380 and 600 nm respectively) was attained upon 90 min experimental duration. However, upon further experimental duration of 120 min, it could be inferred that about 35 % removal (19 % and 42 % for λ=380 and 600 nm respectively) was accomplished.

Furthermore, upon prolonged experimental duration of 180 min, roughly an approximate average of 40 % removal (21 % and 47 % for λ=380 and 600 nm respectively) was observed. As explicated by UV-vis absorbance based kinetic modeling applied in two different approaches as exponential and linear models, a doubling effect could be seen between λ=380 and 600 nm in terms of sedimentation removal efficiencies. Therefore, it could be concluded that specific wavelengths displayed specific differences in case of "Fe-TiO_2 and HA" under "as-is" conditions.

4.2.7.6. "Fe-TiO_2 and SRNOM" binary system under "as-is" conditions. As explained for "N-TiO_2 and SRNOM", a similar approach was followed for elucidation of sedimentation behavior of "Fe-TiO_2 and SRNOM" under "as-is" conditions. Time dependent UV-vis absorbance variations in the wavelength range of 200-600 nm were presented (Figure 4.279a).

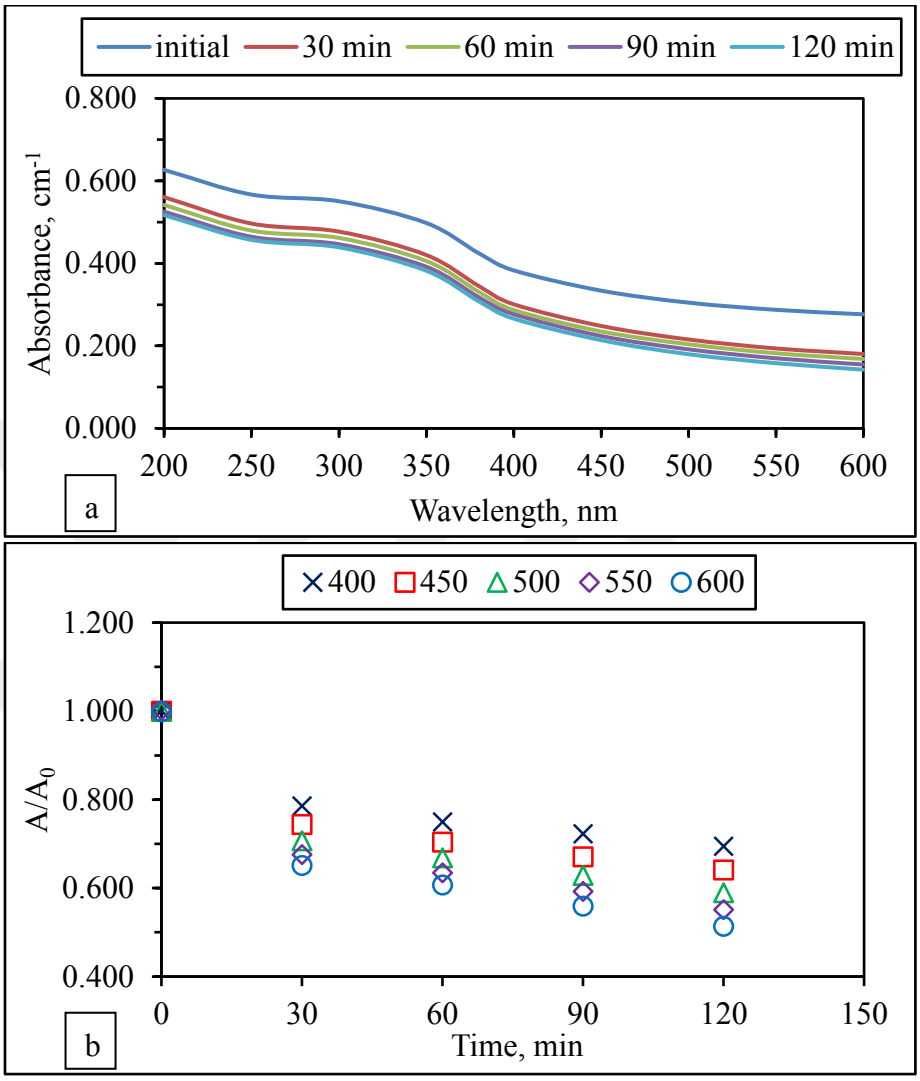


Figure 4.279. Sedimentation behavior of "Fe-TiO_2 and SRNOM" under "as-is" conditions, a) UV-vis absorbance variations b) Normalized absorbance with respect to time.

Contrary to the two regional exhibition of UV- vis spectra recorded for "TiO_2 and SRNOM" under "as-is" condition, and in a similar manner to "N-TiO_2 and SRNOM", "Fe-TiO_2 and SRNOM" also exhibited a decreasing trend with respect to time. The variations were modeled by two approaches depending on the decreasing trend profiles. Exponential and linear models were applied and sedimentation kinetic constants were presented in Table 4.183. Due to the observed inconsistency, absorbance recordings at λ=380 nm were excluded for interpretation of sedimentation

kinetics of "Fe-TiO_2 and SRNOM" under "as-is" conditions. Both exponential and linear modeling revealed considerably high correlation coefficients as $R^2 > 0.750$.

Table 4.183. "Fe-TiO_2 and SRNOM" under "as-is" conditions, kinetic model parameters.

Kinetic model	Wavelength, nm				
	400	450	500	550	600
Exponential model					
k, min^{-1}	2.71×10^{-3}	3.31×10^{-3}	3.91×10^{-3}	4.42×10^{-3}	4.94×10^{-3}
R^2	0.799	0.799	0.810	0.808	0.822
Linear model					
k, min^{-1}	2.25×10^{-3}	2.64×10^{-3}	2.99×10^{-3}	3.28×10^{-3}	3.54×10^{-3}
R^2	0.763	0.756	0.759	0.750	0.757

Exponential model kinetics as expressed by kinetic constants displayed a decreasing order as $4.94 \times 10^{-3} > 4.42 \times 10^{-3} > 3.91 \times 10^{-3} > 3.31 \times 10^{-3} > 2.71 \times 10^{-3}$ for wavelengths of 600 nm, 550 nm, 500 nm, 450 nm and 400 nm, respectively. An average value of $k=3.86 \times 10^{-3}$ min^{-1} could be regarded as adequate for expressing sedimentation kinetics using the exponential model. The average value resembled to the $k=3.91 \times 10^{-3}$ min^{-1} that was calculated at λ=500 nm.

Following the same manner, the linear trend as visualized by the decreasing trend of A/A_o revealed kinetic constants (min^{-1}) in a decreasing order as $3.54 \times 10^{-3} > 3.28 \times 10^{-3} > 2.99 \times 10^{-3} > 2.64 \times 10^{-3} > 2.25 \times 10^{-3}$ for wavelengths of 600 nm, 550 nm, 500 nm, 450 nm and 400 nm, respectively. As expressed above an average of $k=2.94 \times 10^{-3}$ min^{-1} could be accepted as suitable for displaying sedimentation kinetics using the linear model. The average value resembled to the $k=2.99 \times 10^{-3}$ min^{-1} that was calculated at λ=500 nm.

Under the specified conditions represented by selected wavelengths, it could be deduced that upon 30 min experimental duration, ~ 15 % removal at λ=400 nm and 35 % at λ=600 nm was obtained. However, upon 90 min of duration, approximately 20 % removal at λ=400 nm and 45 % at λ=600 nm was attained. Further increase in experimental duration did not significantly shift the removal percentage of "Fe-TiO_2 and SRNOM" under "as-is" conditions. Upon 120 min of duration 30 % removal at λ=400 nm and ~ 50 % removal at λ=600 nm were observed. This slight incremental increase could also be followed by prolonged time intervals possibly leading to 30-95 % in 6 h as could be deduced by calculation using linear model, respectively. Although linear model expressed slightly lower kinetic constants, both kinetic model constants followed a similar tendency and were not significantly different from each other at the specified wavelengths selected in the range from 400-600 nm as depicted in Table 4.183.

4.2.8. Comparative Evaluation of Exponential and Linear Models of "TiO_2 and HA", "N-TiO_2 and HA", "Fe-TiO_2 and HA" under "as-is" Conditions

Dependent on the presented data for all of the binary systems under as-is conditions, although similar sedimentation profiles were attained, a comparative evaluation was performed to elucidate the system specific variations for suitability of application of UV-vis spectroscopic technique. To this end, kinetic model parameters attained at selected indicative wavelength of λ=550 nm were compiled from tables 4.178-4.182 and presented in Table 4.184.

Table 4.184. Comparative presentation of sedimentation kinetics of NPs under "as-is" conditions at λ=550 nm.

Kinetic model	Exponential model	
NP "as-is"	k, min^{-1}	R^2
"TiO_2 and HA"	8.45 x 10^{-4}	0.926
"N-TiO_2 and HA"	2.30 x 10^{-3}	0.829
"Fe-TiO_2 and HA"	2.56 x 10^{-3}	0.831
	Linear model	
	k, min^{-1}	R^2
"TiO_2 and HA"	7.81 x 10^{-4}	0.917
"N-TiO_2 and HA"	1.78 x 10^{-3}	0.779
"Fe-TiO_2 and HA"	1.91 x 10^{-3}	0.767

Sedimentation behavior of "TiO_2 and HA", "N-TiO_2 and HA", and "Fe-TiO_2 and HA" "as-is" binary systems that were fitted to the exponential kinetic equation gave the following rate constants (min^{-1}) as 2.56 x 10^{-3} for "Fe-TiO_2 and HA" > 2.30 x 10^{-3} for "N-TiO_2 and HA" > 8.45 x 10^{-4} for "TiO_2 and HA". "Fe-TiO_2 and HA" binary system expressed comparatively higher sedimentation rate in comparison to "TiO_2 and HA" most probably as a result of surface interactions prevailing between Fe of the Fe-TiO_2 NP and humic sub-fractions through electrostatic interactions even leading to complexation. The reason could also be attributed to the surface area variations of the selected NPs (Table A) exposed to interactions with humic sub-fractions resulting in higher agglomeration and settlement tendency. Similarly, when sedimentation behavior of "TiO_2 and HA", "N-TiO_2 and HA", and "Fe-TiO_2 and HA" binary systems were fitted to linear model, rate constants (min^{-1}) were found as 1.91 x 10^{-3} for "Fe-TiO_2 and HA" > 1.78 x 10^{-3} for "N-TiO_2 and HA" > 7.81 x 10^{-4} for "TiO_2 and HA". Although slightly higher sedimentation rate constant was attained via exponential model, "Fe-TiO_2 and HA" binary system exhibited 45 % sedimentation percentage (λ=600 nm) in comparison to sole "Fe-TiO_2 as-is" as 49 % excluding any role of humic sub-fractions present in the aqueous medium. On the other hand, under similar conditions "TiO_2 and HA" binary system expressed 17 % efficiency in comparison to 20 % as achieved for sole TiO_2.

4.2.9. Comparative Evaluation of Exponential and Linear Models of "TiO_2 and SRNOM", "N-TiO_2 and SRNOM", "Fe-TiO_2 and SRNOM" under "as-is" Conditions

Dependent on the presented data for all of the binary systems under as-is conditions, though similar sedimentation profiles were obtained, a comparative evaluation was performed to elucidate the system specific variations for suitability of application of UV-vis spectroscopic technique. To that end, kinetic model parameters attained at selected indicative wavelength of λ=550 nm were compiled from tables 4.179-4.183 and presented in Table 4.185.

Table 4.185. Comparative presentation of sedimentation kinetics of NPs under "as-is" conditions at λ=550 nm.

Kinetic model	Exponential model	
NP "as-is"	k, min^{-1}	R^2
"TiO_2 and SRNOM"	1.05 x 10^{-3}	0.964
"N-TiO_2 and SRNOM"	3.97 x 10^{-3}	0.881
"Fe-TiO_2 and SRNOM"	4.42 x 10^{-3}	0.808
	Linear model	
	k, min^{-1}	R^2
"TiO_2 and SRNOM"	9.81 x 10^{-4}	0.957
"N-TiO_2 and SRNOM"	2.72 x 10^{-3}	0.847
"Fe-TiO_2 and SRNOM"	3.28 x 10^{-3}	0.750

Sedimentation behavior of "TiO_2 and SRNOM", "N-TiO_2 and SRNOM", and "Fe-TiO_2 and SRNOM" "as-is" binary systems that were fitted to the exponential kinetic equation gave the following rate constants (min^{-1}) as 4.42 x 10^{-3} for "Fe-TiO_2 and SRNOM" > 3.97 x 10^{-3} for "N-TiO_2 and SRNOM" > 1.05 x 10^{-3} for "TiO_2 and SRNOM". "Fe-TiO_2 and SRNOM" binary system expressed comparatively higher sedimentation rate in comparison to "TiO_2 and SRNOM" most probably as a result of surface interactions prevailing between Fe of the Fe-TiO_2 NP and humic sub-fractions through electrostatic interactions even leading to complexation. The reason could also be attributed to the surface area variations of the selected NPs (Table A) exposed to interactions with humic sub-fractions resulting in higher agglomeration and settlement tendency. Similarly, when sedimentation behavior of "TiO_2 and SRNOM", "N-TiO_2 and SRNOM", and "Fe-TiO_2 and SRNOM" binary systems were fitted to linear model, rate constants (min^{-1}) were found as 3.28 x 10^{-3} for "Fe-TiO_2 and SRNOM" > 2.72 x 10^{-3} for "N-TiO_2 and SRNOM" > 9.81 x 10^{-4} for "TiO_2 and SRNOM". "Fe-TiO_2 and SRNOM" binary system exhibited 49 % sedimentation percentage (λ=600 nm) in parallel with sole Fe-TiO_2 under "as-is" conditions. On the other hand, under similar conditions "TiO_2 and SRNOM" binary system expressed 15 % efficiency in comparison to 20 % as achieved for sole TiO_2.

4.2.10. Sedimentation Behavior of Nanoparticles as TiO_2, N-TiO_2 and Fe-TiO_2 "as-is under dark" Conditions in the Presence of Organic Matter

All selected NP binary systems were subjected to continuous mixing under dark in an ATLAS Suntest CPS+ simulator during a specific time of 30 min for "TiO_2 and HA" and "N-TiO_2 and HA" binary systems and 60 min for "Fe-TiO_2 and HA" binary system. Time dependent UV-vis absorbance measurements were recorded between wavelength region of 200 and 600 nm.

4.2.10.1. "TiO_2 and HA" binary system "as-is" under dark conditions. Following an initial mixing period of 30 min, "TiO_2 and HA" system was subjected to sedimentation as followed by time dependent UV-vis absorbance variations. Time dependent UV-vis absorbance variations in the overall spectra covering the wavelength range of 200-600 nm were displayed (Figure 4.280a).

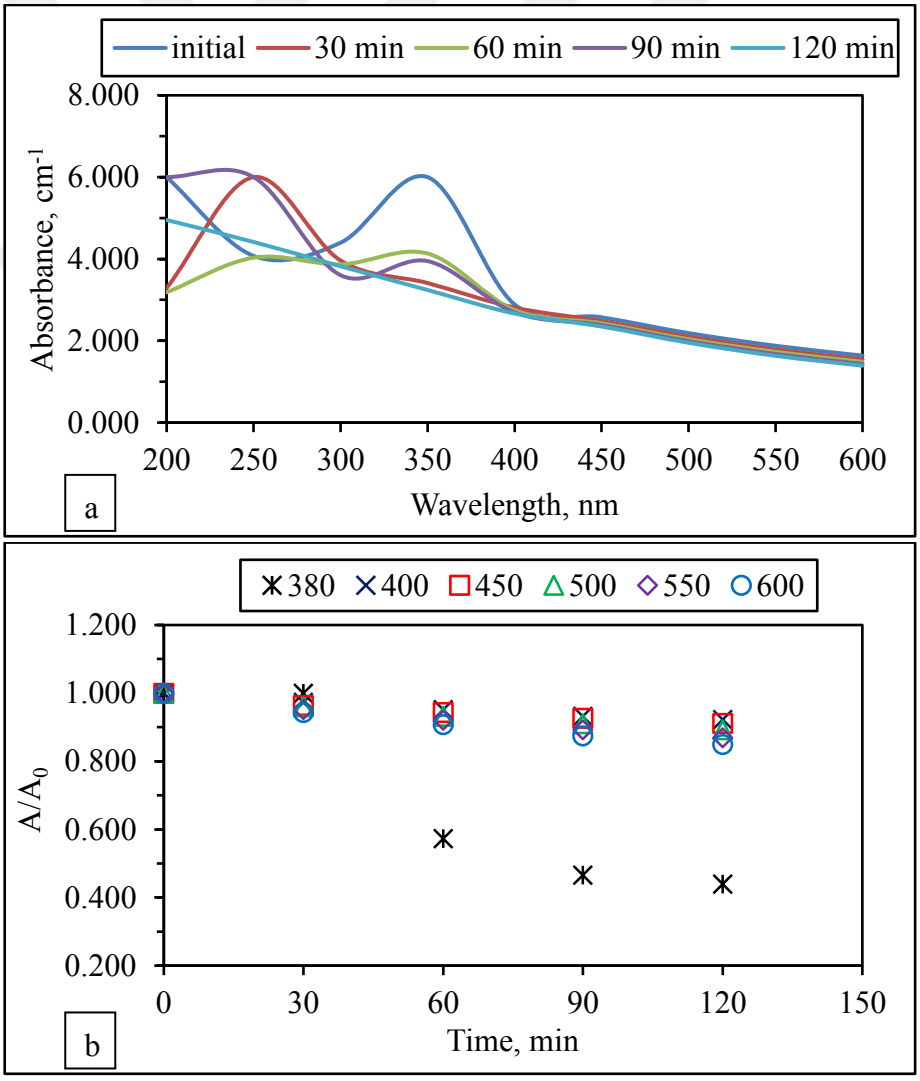


Figure 4.280. Sedimentation behavior of "TiO_2 and HA" binary system "as-is" under dark conditions, a) UV-vis absorbance variations b) Normalized absorbance with respect to time.

UV-vis spectral variations expressed two regions as an inconsistent trend (200<λ<400 nm) followed by a consistent trend (400<λ<600 nm). From a general perspective, the role of continuous mixing by a magnetic stirrer did not cause any alteration on sedimentation behavior of "TiO_2 and HA" in comparison to "TiO_2 and HA" under "as-is" conditions that was subjected to recording immediately after preparation (Figure 4.274). A distinct separation could be visualized at λ=380 nm with respect to increasing time. Application of exponential and linear models revealed almost similar results as presented in Figure 4.280b and Table 4.186. Both exponential and linear modeling revealed considerably high correlation coefficients as $R^2 > 0.860$.

Table 4.186. "TiO_2 and HA" "as-is" under dark conditions, kinetic model parameters.

Kinetic model	Wavelength, nm					
	380	400	450	500	550	600
Exponential model						
k, min^{-1}	8.02×10^{-3}	6.78×10^{-4}	7.46×10^{-4}	9.39×10^{-4}	1.15×10^{-3}	1.34×10^{-3}
R^2	0.891	0.977	0.969	0.979	0.986	0.984
Linear model						
k, min^{-1}	5.52×10^{-3}	6.50×10^{-4}	7.12×10^{-4}	8.85×10^{-4}	1.07×10^{-3}	1.23×10^{-3}
R^2	0.860	0.974	0.964	0.974	0.980	0.977

Exponential model kinetic constants expressed a decreasing order as $8.02 \times 10^{-3} > 1.34 \times 10^{-3} > 1.15 \times 10^{-3} > 9.39 \times 10^{-4} > 7.46 \times 10^{-4} > 6.78 \times 10^{-4}$ for wavelengths of 380 nm, 600 nm, 550 nm, 500 nm, 450 nm, and 400 nm, respectively. Simply an average value of $k=2.15 \times 10^{-3}$ min^{-1} could be regarded as appropriate for expressing sedimentation kinetics using the exponential model. However, fourfold higher rate constant was attained by using the data recorded at λ=380 nm.

In a similar manner, the linear trend as visualized by the decreasing trend of A/A_o revealed kinetic constants (min^{-1}) in a decreasing order as $5.52 \times 10^{-3} > 1.23 \times 10^{-3} > 1.07 \times 10^{-3} > 8.85 \times 10^{-4} > 7.12 \times 10^{-4} > 6.50 \times 10^{-4}$ for wavelengths of 380 nm, 600 nm, 550 nm, 500 nm, 450 nm, and 400 nm, respectively. As expressed above an average of $k=1.68 \times 10^{-3}$ min^{-1} could also be regarded as suitable for displaying sedimentation kinetics using the linear model.

Both models expressed quite similar average sedimentation rate constants revealing that indicative wavelength independent approach could be visualized. It could be concluded that for an experimental duration of 30 min very slight (~ 5 %) removals were achieved irrespective of the indicative wavelength followed a distinctly different profile was attained upon use of indicative wavelength as λ=380 nm. Changing mixing regime did not result in any significant change on sedimentation profile of "TiO_2 and HA" binary system "as-is under dark" and "as-is" conditions.

4.2.10.2. “TiO_2 and SRNOM” binary system “as-is” under dark conditions. As explained for “TiO_2 and HA”, a similar approach was followed for elucidation of sedimentation behavior of “TiO_2 and SRNOM” binary system “as-is” under dark conditions. Following an initial mixing period of 30 min, “TiO_2 and SRNOM” system was subjected to sedimentation as followed by time dependent UV-vis absorbance variations (Figure 4.281a).

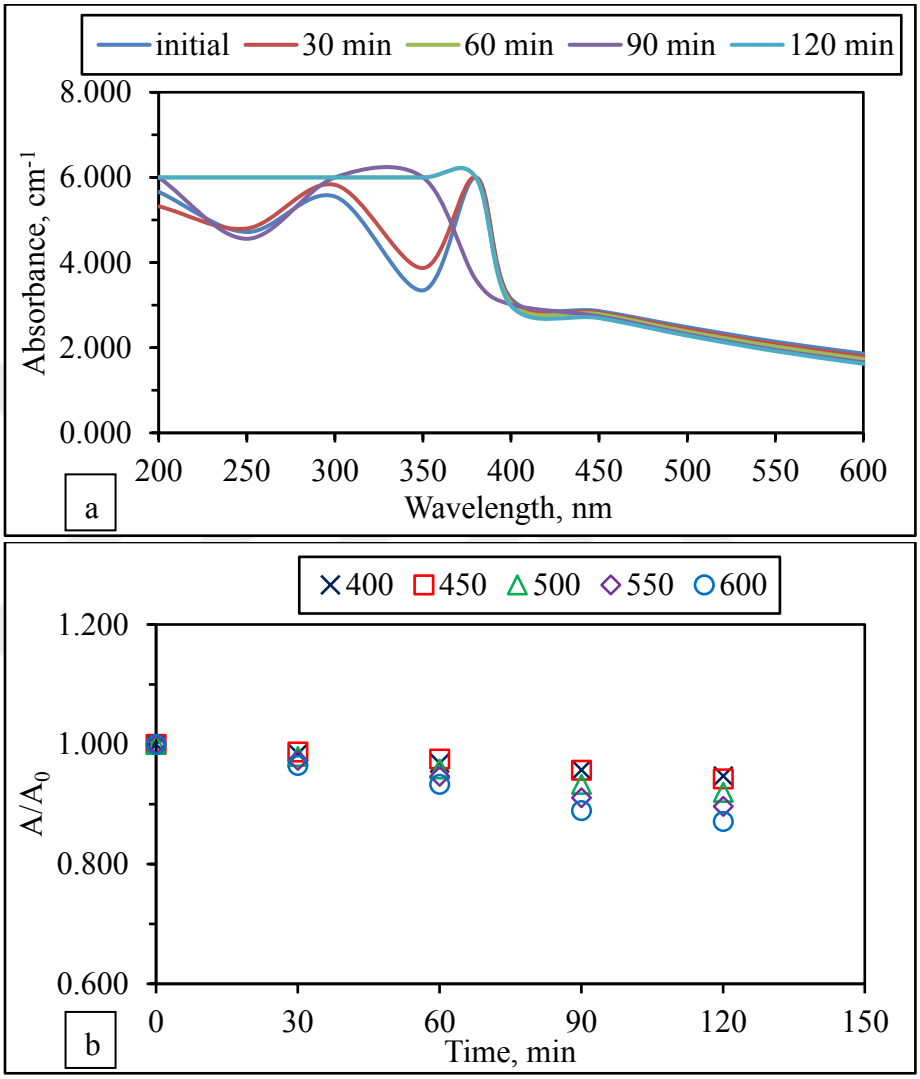


Figure 4.281. Sedimentation behavior of “TiO_2 and SRNOM” “as-is” under dark conditions, a) UV-vis absorbance variations b) Normalized absorbance with respect to time.

UV-vis spectral variations expressed two regions as an inconsistent trend ($200<\lambda<400$ nm) followed by a consistent trend ($400<\lambda<600$ nm). From a general perspective, the role of continuous mixing by a magnetic stirrer did not cause any alteration on sedimentation behavior of “TiO_2 and SRNOM” in comparison to “TiO_2 and SRNOM” under “as-is” condition that was subjected to recording immediately after preparation (Figure 4.275). Application of exponential and linear models

revealed almost similar results as presented in Figure 4.281b and Table 4.187. Both exponential and linear modeling revealed considerably high correlation coefficients as $R^2 > 0.988$.

Table 4.187. "TiO_2 and SRNOM" "as-is" under dark conditions, kinetic model parameters.

Kinetic model	Wavelength, nm				
	400	450	500	550	600
Exponential model					
k, min^{-1}	4.56×10^{-4}	4.99×10^{-4}	7.19×10^{-4}	9.50×10^{-4}	1.19×10^{-3}
R^2	0.991	0.992	0.994	0.989	0.989
Linear model					
k, min^{-1}	4.43×10^{-4}	4.85×10^{-4}	6.90×10^{-4}	8.99×10^{-4}	1.11×10^{-3}
R^2	0.990	0.993	0.993	0.988	0.989

Exponential model kinetics expressed constants (min^{-1}) in a decreasing order as $1.19 \times 10^{-3} > 9.50 \times 10^{-4} > 7.19 \times 10^{-4} > 4.99 \times 10^{-4} > 4.56 \times 10^{-4}$ for wavelengths of 600 nm, 550 nm, 500 nm, 450 nm, and 400 nm, respectively. Kinetic constants followed a continuously increasing trend with respect to increasing detection wavelengths. Still, an average value of $k=7.63 \times 10^{-4}$ min^{-1} could be regarded as suitable for expressing sedimentation kinetics using the exponential model. The average value resembled to the $k=7.19 \times 10^{-4}$ min^{-1} that was calculated for λ=500 nm.

Linear trend as visualized by the decreasing trend of normalized absorbance recordings as A/A_o revealed kinetic constants (min^{-1}) in a decreasing order as $1.11 \times 10^{-3} > 8.99 \times 10^{-4} > 6.90 \times 10^{-4} > 4.85 \times 10^{-4} > 4.43 \times 10^{-4}$ for wavelengths of 600 nm, 550 nm, 500 nm, 450 nm, and 400 nm, respectively. As expressed above an average of $k=7.25 \times 10^{-4}$ min^{-1} could be accepted as suitable for displaying sedimentation kinetics using the linear model. The average value as $k=7.25 \times 10^{-4}$ min^{-1} could well be regarded as similar to the rate constant attained by absorbance recordings at λ=500 nm and 550 nm.

Under the specified conditions represented by selected wavelengths, it could be inferred that upon 30 min duration, ~ 2 % removal at λ=400 nm and ~ 3 % at λ=600 nm was observed. However, upon 90 min experimental duration, roughly 4 % removal at λ=400 nm and 11 % at λ=600 nm was attained. Further increase in experimental duration did not significantly alter the removal percentage of "TiO_2 and SRNOM" "as-is under dark" conditions. Upon 120 min of duration ~ 5 % removal at λ=400 nm and ~ 13 % removal at λ=600 nm were observed. Despite the fact that linear model explicating slightly lower kinetic constants, both exponential and linear kinetic model constants revealed similar tendencies and were not significantly different from each other at the specified wavelengths (Table 4.187).

4.2.10.3. "N-TiO_2 and HA" binary system "as-is" under dark conditions. As explained for "N-TiO_2 and HA" binary system under "as-is" conditions (Figure 4.276 and Table 4.180), a similar approach was followed for elucidation of sedimentation behavior of "N-TiO_2 and HA" "as-is" under dark conditions. Time dependent UV-vis absorbance variations in the overall spectra covering the wavelength range of 200-600 nm were presented (Figure 4.282a). It could be easily visualized that "N-TiO_2 and HA" binary system under "as-is" under dark conditions displayed quite similar tendency to "N-TiO_2 and HA" "as-is" binary system and no direct effect of continuous mixing could be observed excluding the initial absorbance recordings.

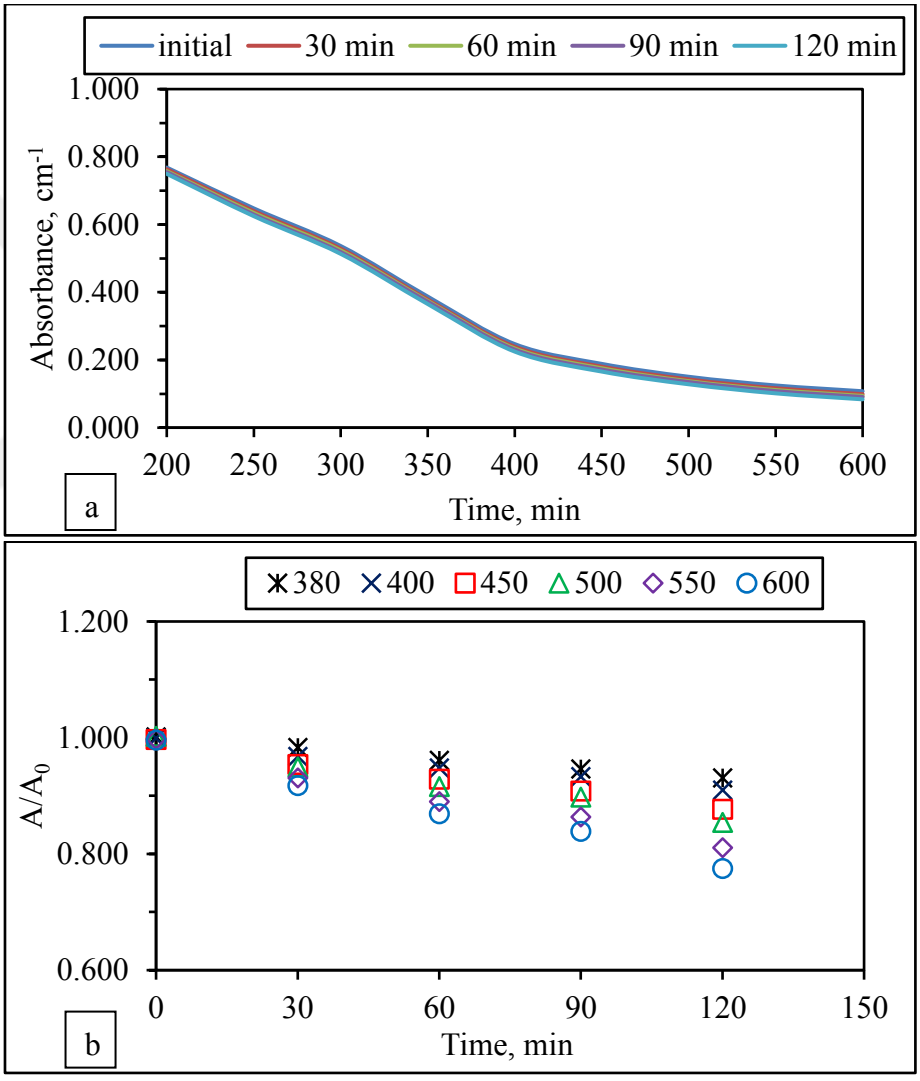


Figure 4.282. Sedimentation behavior of "N-TiO_2 and HA" "as-is" under dark conditions, a) UV-vis absorbance variations b) Normalized absorbance with respect to time.

As presented in Figure 4.282a almost overlapping behavior of the UV-vis absorbance profiles could simply imply that no difference could be observed upon kinetic modeling either by exponential model or linear model. Accordingly, normalized absorbance values in the selected wavelength range of 380 nm to 600 nm also revealed a decreasing profile that was modeled by both models (Figure

4.282b and Table 4.188). Both exponential and linear modeling revealed considerably high correlation coefficients as $R^2 > 0.976$.

Table 4.188. "N-TiO_2 and HA" "as-is" under dark conditions, kinetic model parameters.

Kinetic model	Wavelength, nm					
	380	400	450	500	550	600
Exponential model						
k, min^{-1}	6.10×10^{-4}	7.47×10^{-4}	1.02×10^{-3}	1.25×10^{-3}	1.63×10^{-3}	1.97×10^{-3}
R^2	0.996	0.987	0.986	0.979	0.984	0.983
Linear model						
k, min^{-1}	5.89×10^{-4}	7.13×10^{-4}	9.52×10^{-4}	1.16×10^{-3}	1.47×10^{-3}	1.74×10^{-3}
R^2	0.995	0.984	0.983	0.976	0.979	0.979

Exponential model kinetics as expressed by kinetic constants displayed a decreasing order as $1.97 \times 10^{-3} > 1.63 \times 10^{-3} > 1.25 \times 10^{-3} > 1.02 \times 10^{-3} > 7.47 \times 10^{-4} > 6.10 \times 10^{-4}$ for wavelengths of 600 nm, 550 nm, 500 nm, 450 nm, 400 nm, and 380 nm, respectively. Simply an average value of $k=1.20 \times 10^{-3}$ min^{-1} could be regarded as adequate for expressing sedimentation kinetics using the exponential model. The average value resembled to the $k=1.25 \times 10^{-3}$ min^{-1} that was calculated at λ=500 nm (Table 4.188).

Following the same manner, the linear trend as visualized by the decreasing trend of A/A_o revealed kinetic constants (min^{-1}) in a decreasing order as $1.74 \times 10^{-3} > 1.47 \times 10^{-3} > 1.16 \times 10^{-3} > 9.52 \times 10^{-4} > 7.13 \times 10^{-4} > 5.89 \times 10^{-4}$ for wavelengths of 600 nm, 550 nm, 500 nm, 450 nm, 400 nm, and 380 nm, respectively. As expressed above an average of $k=1.10 \times 10^{-3}$ min^{-1} could be accepted as suitable for displaying sedimentation kinetics using the linear model (Table 4.188). The average value resembled to the $k=1.16 \times 10^{-3}$ min^{-1} that was calculated at λ=500 nm.

Under the specified conditions represented by selected wavelengths, it could be indicated that upon 30 min duration approximately ≤ 10 % removals were achieved with respect to increasing specified wavelengths followed which a slight enhancement was also observed as ≤ 20 % upon 120 min. It should also be mentioned that both kinetic model constants were not significantly different from each other at the specified wavelengths (Table 4.188). Upon 120 min experimental duration, wavelength dependent variations in removal efficiencies were approximately 10-23 %.

Due to presence of humic sub-fractions expressing absorbances in the selected wavelength region, no direct discrimination could be assessed between sole N-TiO_2 under as-is conditions (dark and irradiation) and "N-TiO_2 and HA" binary system both under as-is and dark conditions.

4.2.10.4. "N-TiO_2 and SRNOM" binary system "as-is" under dark conditions. A similar approach was followed for elucidation of sedimentation behavior of "N-TiO_2 and SRNOM" binary system "as-is" under dark conditions considering "N-TiO_2 and HA" binary system "as-is" under dark conditions (Figure 4.282 and Table 4.188). Following an initial mixing period of 30 min, "N-TiO_2 and SRNOM" system was subjected to sedimentation as followed by time dependent UV-vis absorbance variations (Figure 4.283a).

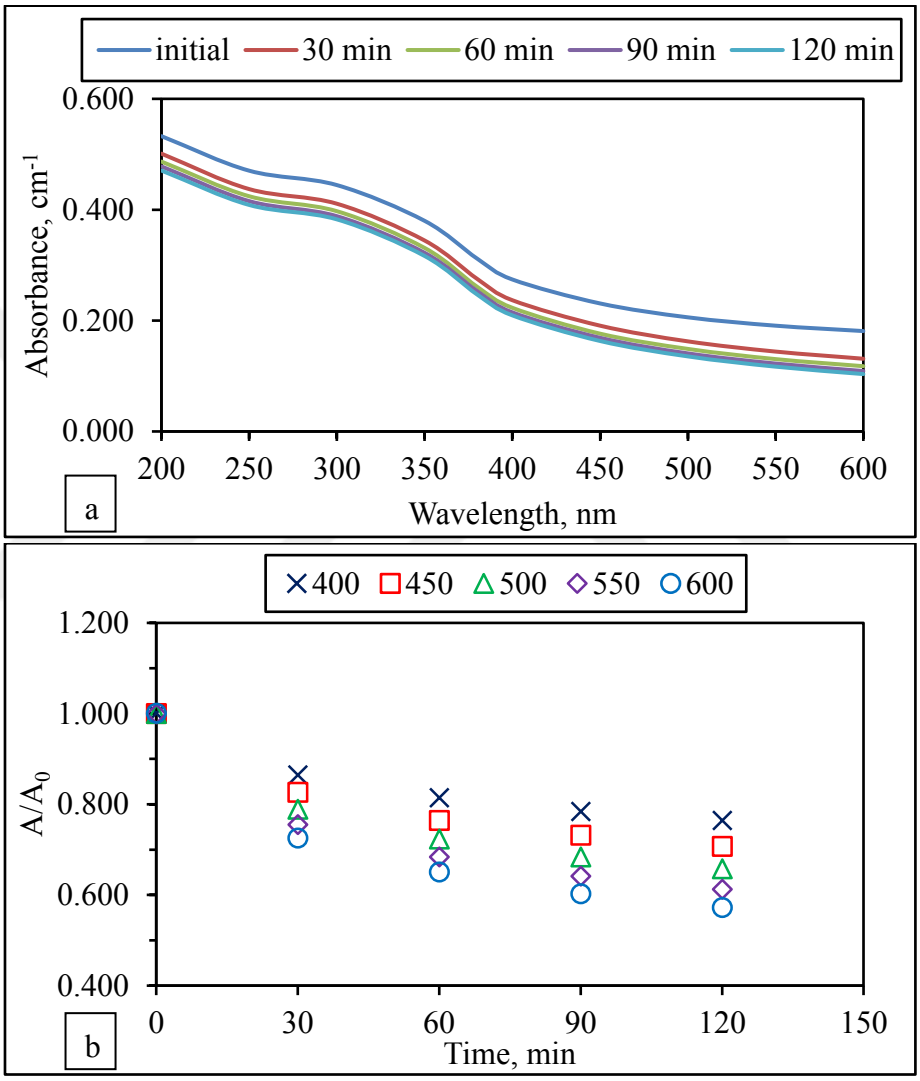


Figure 4.283. Sedimentation behavior of "N-TiO_2 and SRNOM" "as-is" under dark conditions, a) UV-vis absorbance variations b) Normalized absorbance with respect to time.

Contrary to the two regional demonstration of UV- vis spectra recorded for "TiO_2 and SRNOM" "as-is" under dark conditions (Figure 4.281), "N-TiO_2 and SRNOM" spectral trend displayed a decreasing trend with respect to time irrespective of the experimental duration. Time dependent absorbance values at selected wavelengths were normalized to respective initial absorbance values and presented in Figure 4.283b. The variations were modeled by two approaches depending on the

decreasing trend profiles. In a similar manner to data depicted "N-TiO_2 and SRNOM" under "as-is" conditions (Table 4.181), exponential and linear models were applied and sedimentation kinetic constants were presented in Table 4.189. Due to the observed inconsistency absorbance recordings at λ=380 nm were excluded. Both exponential and linear modeling revealed considerably high correlation coefficients as $R^2 > 0.808$.

Table 4.189. "N-TiO_2 and SRNOM" "as-is" under dark conditions, kinetic model parameters.

Kinetic model	Wavelength, nm				
	400	450	500	550	600
Exponential model					
k, min^{-1}	2.12×10^{-3}	2.72×10^{-3}	3.27×10^{-3}	3.81×10^{-3}	4.35×10^{-3}
R^2	0.878	0.872	0.866	0.861	0.861
Linear model					
k, min^{-1}	1.84×10^{-3}	2.27×10^{-3}	2.63×10^{-3}	2.96×10^{-3}	3.27×10^{-3}
R^2	0.854	0.841	0.827	0.815	0.808

Exponential model kinetics expressed constants (min^{-1}) in a decreasing order as $4.35 \times 10^{-3} > 3.81 \times 10^{-3} > 3.27 \times 10^{-3} > 2.72 \times 10^{-3} > 2.12 \times 10^{-3}$ for wavelengths of 600 nm, 550 nm, 500 nm, 450 nm, and 400 nm, respectively. Kinetic constants followed a gradually increasing trend with respect to increasing detection wavelengths. An average value of $k=3.25 \times 10^{-3}$ min^{-1} could be regarded as suitable for expressing sedimentation kinetics using the exponential model. The average value resembled to the $k=3.27 \times 10^{-3}$ min^{-1} that was calculated for λ=500 nm.

Linear trend as visualized by the decreasing trend of normalized absorbance recordings as A/A_o revealed kinetic constants (min^{-1}) in a decreasing order as $3.27 \times 10^{-3} > 2.96 \times 10^{-3} > 2.63 \times 10^{-3} > 2.27 \times 10^{-3} > 1.84 \times 10^{-3}$ for wavelengths of 600 nm, 550 nm, 500 nm, 450 nm, and 400 nm, respectively. Simply an average value of $k=2.59 \times 10^{-3}$ min^{-1} could be accepted as suitable for displaying sedimentation kinetics using the linear model. The average value as $k=2.63 \times 10^{-3}$ min^{-1} could well be regarded as similar to the rate constant obtained by absorbance recording at λ=500 nm.

Under the specified conditions represented by selected wavelengths, it could be concluded that upon 30 min experimental duration, roughly 14 % removal at λ=400 nm and 28 % at λ=600 nm was attained. Upon further experimental duration of 90 min, approximately 22 % removal at λ=400 nm and 40 % at λ=600 nm was obtained. However, upon 120 min of duration approximately 25 % removal at λ=400 nm and 45 % removal at λ=600 nm were observed. It should also be inferred that both kinetic model constants were not significantly different from each other at the specified wavelengths (Table 4.189).

4.2.10.5. "Fe-TiO_2 and HA" binary system "as-is" under dark conditions. As explained for "Fe-TiO_2 and HA" binary system under "as-is" conditions (Figure 4.278 and Table 4.182), following a similar trend, sedimentation behavior of "Fe-TiO_2 and HA" "as-is" under dark conditions was monitored. Time dependent UV-vis absorbance variations in the overall spectra covering the wavelength range of 200-600 nm were presented (Figure 4.284a). "Fe-TiO_2 and HA" binary system under "as-is" under dark conditions expressed quite similar tendency to "Fe-TiO_2 and HA" binary system under "as-is" conditions (Figure 4.278). However, initial absorbance recordings of the prepared suspension had been significantly affected by continuous mixing following which no direct after effect due to extended stirring under dark in solar simulator could be observed.

Application of both exponential and linear modeling revealed considerably high correlation coefficients as $R^2 > 0.983$ (Figure 4.284b and Table 4.190).

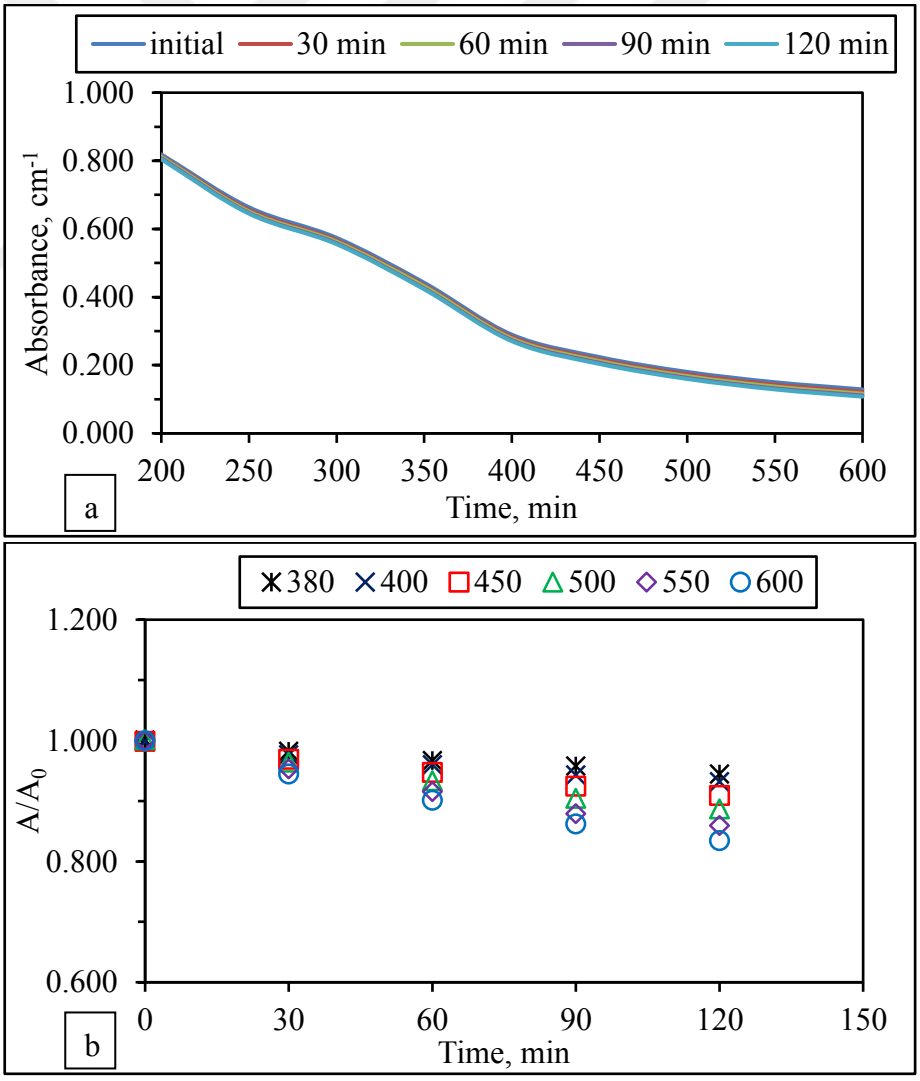


Figure 4.284. Sedimentation behavior of "Fe-TiO_2 and HA" "as-is" under dark conditions, a) UV-vis absorbance variations b) Normalized absorbance with respect to time.

Table 4.190. "Fe-TiO_2 and HA" "as-is" under dark conditions, kinetic model parameters.

Kinetic model	Wavelength, nm					
	380	400	450	500	550	600
Exponential model						
k, min^{-1}	4.66×10^{-4}	5.75×10^{-4}	7.85×10^{-4}	1.02×10^{-3}	1.28×10^{-3}	1.51×10^{-3}
R^2	0.986	0.989	0.991	0.988	0.987	0.991
Linear model						
k, min^{-1}	4.53×10^{-4}	5.54×10^{-4}	7.47×10^{-4}	9.63×10^{-4}	1.18×10^{-3}	1.38×10^{-3}
R^2	0.984	0.987	0.988	0.985	0.983	0.985

Exponential kinetics expressed by kinetic constants (min^{-1}) in a decreasing order as $1.51 \times 10^{-3} > 1.28 \times 10^{-3} > 1.02 \times 10^{-3} > 7.85 \times 10^{-4} > 5.75 \times 10^{-4} > 4.66 \times 10^{-4}$ for wavelengths of 600 nm, 550 nm, 500 nm, 450 nm, 400 nm, and 380 nm, respectively. Although almost trebling effect could also be encountered as $k=4.66 \times 10^{-4}$ min^{-1} at λ=380 nm to $k=1.51 \times 10^{-3}$ min^{-1} at λ=600 nm, an average value of $k=9.39 \times 10^{-4}$ min^{-1} could be regarded as appropriate for expressing sedimentation kinetics using the exponential model. The average value resembled to the $k=1.02 \times 10^{-3}$ min^{-1} that was calculated for λ=500 nm. The linear trend as visualized by the decreasing trend of A/A_o deduced from data revealed kinetic constants (min^{-1}) in a decreasing order as $1.38 \times 10^{-3} > 1.18 \times 10^{-3} > 9.63 \times 10^{-4} > 7.47 \times 10^{-4} > 5.54 \times 10^{-4} > 4.53 \times 10^{-4}$ for wavelengths of 600 nm, 550 nm, 500 nm, 450 nm, 400 nm, and 380 nm, respectively. Although nearly trebling effect could also be encountered as $k=4.53 \times 10^{-4}$ at λ=380 nm to $k=1.38 \times 10^{-3}$ min^{-1} at λ=600 nm, an average of $k=8.80 \times 10^{-4}$ min^{-1} could be accepted as suitable for displaying sedimentation kinetics using the linear model.

Under the specified conditions of continuous mixing for 60 min, "Fe-TiO_2 and HA" NP binary system "as-is" under dark conditions behaved in an almost similar manner to respective "TiO_2 and HA" and "N-TiO_2 and HA" NPs. As represented by selected wavelengths, it could be deduced that upon 30 min experimental duration approximately 5 % removals were achieved with respect to increasing specified wavelengths followed which a slight enhancement was also observed as 15 % upon 120 min experimental duration.

In spite of linear model expressing slightly lower kinetic constants, both kinetic model constants revealed quite similar tendencies and were not significantly different from each other at the specified wavelengths (Table 4.190). Upon 60 min experimental duration, wavelength dependent variation in removal efficiencies were 5-10 % and further extended time period as 120 min displayed 10-15 % with respect to increasing detection wavelength. This slight incremental increase could also be followed by prolonged time intervals possibly leading to 40-60 % in 6 h as could be deduced by calculation using both exponential and linear models at λ=550 nm, respectively.

4.2.10.6. "Fe-TiO_2 and SRNOM" binary system "as-is" under dark conditions. As explained for "Fe-TiO_2 and SRNOM" under "as-is" conditions (Figure 4.279 and Table 4.183), following a similar trend, sedimentation behavior of "Fe-TiO_2 and SRNOM" "as-is" under dark conditions was observed. Contrary to the initial mixing period of "TiO_2 and SRNOM" and "N-TiO_2 and SRNOM", an initial mixing period of 60 min was subjected for "Fe-TiO_2 and SRNOM" binary system "as-is" under dark conditions. Time dependent UV-vis absorbance variations in the overall spectra covering the wavelength range of 200-600 nm were presented (Figure 4.285a).

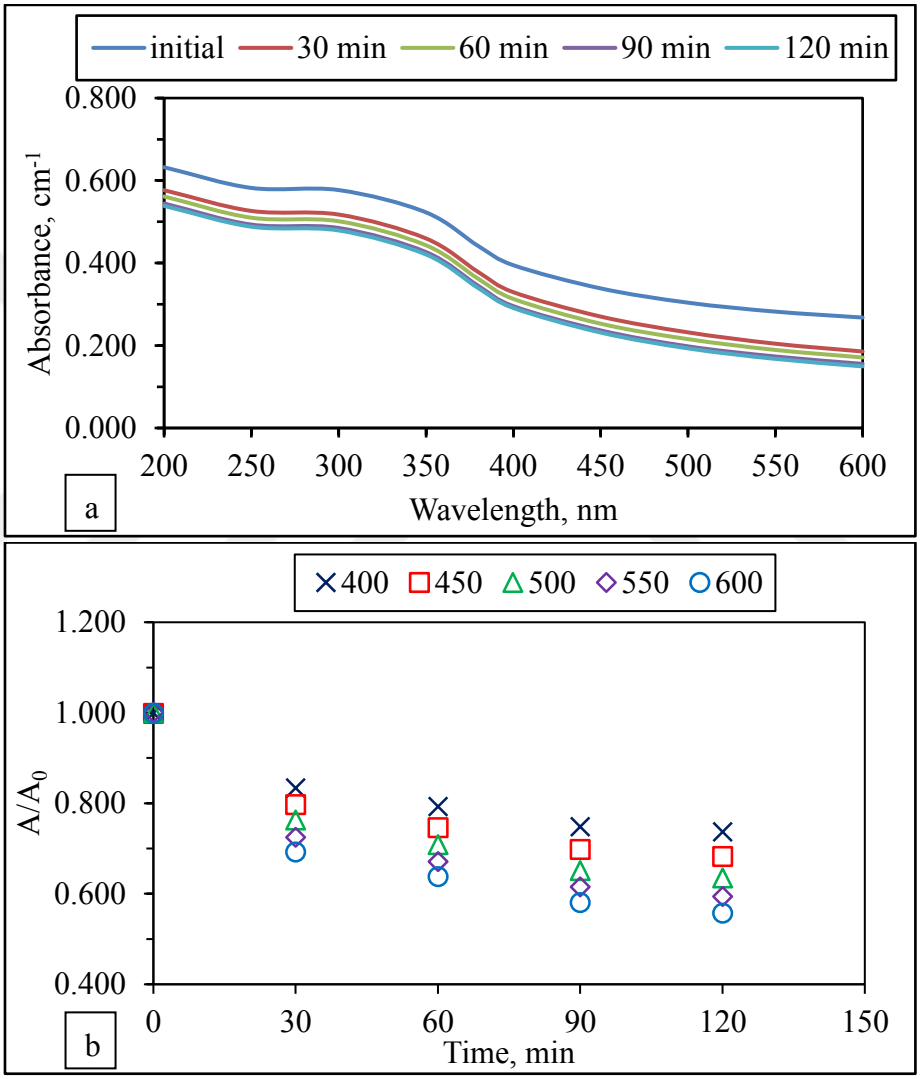


Figure 4.285. Sedimentation behavior of "Fe-TiO_2 and SRNOM" "as-is" under dark conditions, a) UV-vis absorbance variations b) Normalized absorbance with respect to time.

Contrary to the two regional exhibition of UV- vis spectra recorded for "TiO_2 and SRNOM" binary system "as-is" under dark conditions, and in a similar manner to "N-TiO_2 and SRNOM", "Fe-TiO_2 and SRNOM" also displayed a decreasing trend with respect to time. Also, likewise to "TiO_2 and SRNOM" and "N-TiO_2 and SRNOM", for comparison purposes, λ=380 nm was also considered

for elimination of further expected effects due to system variations. However, considering the indicative wavelengths selected in vis region, variations in sedimentation efficiencies would be monitored. Application of both exponential and linear modeling revealed considerably high correlation coefficients as $R^2 > 0.775$ (Figure 4.285b and Table 4.191).

Table 4.191. "Fe-TiO_2 and SRNOM" "as-is" under dark conditions, kinetic model parameters.

Kinetic model	Wavelength, nm				
	400	450	500	550	600
Exponential model					
k, min^{-1}	2.39×10^{-3}	2.98×10^{-3}	3.55×10^{-3}	4.02×10^{-3}	4.48×10^{-3}
R^2	0.854	0.854	0.854	0.838	0.832
Linear model					
k, min^{-1}	2.04×10^{-3}	2.44×10^{-3}	2.80×10^{-3}	3.08×10^{-3}	3.32×10^{-3}
R^2	0.826	0.818	0.811	0.788	0.775

Exponential model kinetics as expressed by kinetic constants displayed a decreasing order as $4.48 \times 10^{-3} > 4.02 \times 10^{-3} > 3.55 \times 10^{-3} > 2.98 \times 10^{-3} > 2.39 \times 10^{-3}$ for wavelengths of 600 nm, 550 nm, 500 nm, 450 nm, and 400 nm, respectively. Although almost doubling effect could also be encountered as $k=2.39 \times 10^{-3}$ min^{-1} at $\lambda=400$ nm to $k=4.48 \times 10^{-3}$ min^{-1} at $\lambda=600$ nm, an average value of $k=3.48 \times 10^{-3}$ min^{-1} could be regarded as appropriate for expressing sedimentation kinetics using the exponential model. The average value resembled to the $k=3.55 \times 10^{-3}$ min^{-1} that was calculated for $\lambda=500$ nm.

Following the same manner, the linear trend as visualized by the decreasing trend of A/A_o revealed kinetic constants (min^{-1}) in a decreasing order as $3.32 \times 10^{-3} > 3.08 \times 10^{-3} > 2.80 \times 10^{-3} > 2.44 \times 10^{-3} > 2.04 \times 10^{-3}$ for wavelengths of 600 nm, 550 nm, 500 nm, 450 nm, and 400 nm, respectively. As expressed above an average of $k=2.74 \times 10^{-3}$ min^{-1} could be accepted as suitable for demonstrating sedimentation kinetics using the linear model. The average value resembled to the $k=2.80 \times 10^{-3}$ min^{-1} that was calculated for $\lambda=500$ nm. Under the specified conditions represented by selected wavelengths, it could be deduced that upon 30 min experimental duration 15-30 % removals were achieved being considerably indifferent from each other with respect to increasing specified wavelengths followed which a slight enhancement was also observed as 20-35 % in 60 min representing between wavelength region of 400 nm and 600 nm. However, upon 120 min experimental duration, removal percentage increased to 45 % as detected at $\lambda=600$ nm being significantly different than the one obtained for $\lambda=400$ nm. It could also be concluded that both models could be successfully applied due to slight incremental decreases with respect to time for "Fe-TiO_2 and SRNOM" "as-is" under dark conditions (Table 4.191).

4.2.11. Comparative Evaluation of Exponential and Linear Models of "TiO_2 and HA", "N-TiO_2 and HA", "Fe-TiO_2 and HA" "as-is" under dark Conditions

Regarding the presented data for all of the NPs under "as-is under dark" conditions, although similar sedimentation profiles were attained, a comparative evaluation could be useful in elucidation of the sample specific variations for suitability of application of UV-vis spectroscopic technique. To fulfill this purpose, kinetic model parameters attained at selected indicative wavelength of λ=550 nm were compiled from tables 4.186-4.190 and presented in Table 4.192.

Table 4.192. Comparative presentation of sedimentation kinetics of NPs under "as-is" under dark conditions at λ=550 nm.

Kinetic model	Exponential model	
NP	k, min^{-1}	R^2
"TiO_2 and HA"	1.15 x 10^{-3}	0.986
"N-TiO_2 and HA"	1.63 x 10^{-3}	0.984
"Fe-TiO_2 and HA"	1.28 x 10^{-3}	0.987
	Linear model	
	k, min^{-1}	R^2
"TiO_2 and HA"	1.07 x 10^{-3}	0.980
"N-TiO_2 and HA"	1.47 x 10^{-3}	0.979
"Fe-TiO_2 and HA"	1.18 x 10^{-3}	0.983

Considering sedimentation behavior of "TiO_2 and HA", "N-TiO_2 and HA", and "Fe-TiO_2 and HA" "as-is under dark" conditions in the presence of organic matter, normalized absorbance values recorded at λ=550 nm fitted to the exponential kinetic equation gave the following reaction rate constants (min^{-1}) as 1.63 x 10^{-3} for "N-TiO_2 and HA" > 1.28 x 10^{-3} for "Fe-TiO_2 and HA" > 1.15 x 10^{-3} for "TiO_2 and HA" (Table 4.192). When sedimentation behavior of "TiO_2 and HA", "N-TiO_2 and HA", and "Fe-TiO_2 and HA" binary systems were fitted to the linear model, rate constants were found as 1.47 x 10^{-3} for "N-TiO_2 and HA" > 1.18 x 10^{-3} for "Fe-TiO_2 and HA" > 1.07 x 10^{-3} for "TiO_2 and HA" (Table 4.192).

A simple comparison to "as-is" conditions (Table 4.181) indicated that slightly lower kinetic constants were attained. Application of exponential model indicated preferential stability of "TiO_2 and HA" in comparison to "N-TiO_2 and HA" and "Fe-TiO_2 and HA" all "as-is" under dark conditions, as also supported by linear modeling with minor differences. From a general perspective, both kinetic models revealed similar tendencies. The role of continuous mixing prior to absorbance recordings could be related to the possible disaggregation of the NPs in comparison to the applied sonication and magnetic stirring for a short duration of NP samples prepared under "as-is" conditions.

4.2.12. Comparative Evaluation of Exponential and Linear Models of "TiO_2 and SRNOM", "N-TiO_2 and SRNOM", "Fe-TiO_2 and SRNOM" "as-is" under dark Conditions

Regarding the presented data for all of the NPs under "as-is" under dark conditions, although similar sedimentation profiles were obtained, a comparative evaluation could be useful in elucidation of the sample specific variations for suitability of application of UV-vis spectroscopic technique. To fulfill this aim, kinetic model parameters obtained at selected indicative wavelength of λ=550 nm were compiled from tables 4.187-4.191 and presented in Table 4.193.

Table 4.193. Comparative presentation of sedimentation kinetics of NPs under "as-is" under dark conditions at λ=550 nm.

Kinetic model	Exponential model	
NP	k, min^{-1}	R^2
"TiO_2 and SRNOM"	9.50 x 10^{-4}	0.989
"N-TiO_2 and SRNOM"	3.81 x 10^{-3}	0.861
"Fe-TiO_2 and SRNOM"	4.02 x 10^{-3}	0.838
	Linear model	
	k, min^{-1}	R^2
"TiO_2 and SRNOM"	8.99 x 10^{-4}	0.988
"N-TiO_2 and SRNOM"	2.96 x 10^{-3}	0.815
"Fe-TiO_2 and SRNOM"	3.08 x 10^{-3}	0.788

Considering sedimentation behavior of "TiO_2 and SRNOM", "N-TiO_2 and SRNOM", and "Fe-TiO_2 and SRNOM" "as-is" under dark conditions in the absence of organic matter, normalized absorbance values recorded at λ=550 nm fitted to the exponential kinetic equation gave the following reaction rate constants (min^{-1}) as 4.02 x 10^{-3} for "Fe-TiO_2 and SRNOM" > 3.81 x 10^{-3} for "N-TiO_2 and SRNOM" > 9.50 x 10^{-4} for "TiO_2 and SRNOM" (Table 4.193). When sedimentation behavior of "TiO_2 and SRNOM", "N-TiO_2 and SRNOM", and "Fe-TiO_2 and SRNOM" binary systems were fitted to the linear model, rate constants (min^{-1}) were found as 3.08 x 10^{-3} for "Fe-TiO_2 and SRNOM" > 2.96 x 10^{-3} for "N-TiO_2 and SRNOM" > 8.99 x 10^{-4} for "TiO_2 and SRNOM" (Table 4.193). A simple comparison to "as-is" conditions (Table 4.185) indicated that slightly lower kinetic constants were obtained. Application of exponential model indicated preferential stability of "TiO_2 and SRNOM" in comparison to "N-TiO_2 and SRNOM" and "Fe-TiO_2 and SRNOM" all "as-is" under dark conditions, as also supported by linear modeling with minor differences. From a general perspective, both kinetic models revealed similar tendencies. The role of continuous mixing prior to absorbance recordings could be related to the possible disaggregation of the NPs in comparison to the applied sonication and magnetic stirring for a short duration of NP samples prepared under "as-is" conditions.

4.2.13. Sedimentation Behavior of Nanoparticles TiO_2, N-TiO_2 and Fe-TiO_2 following photolysis of organic matter in the Presence of Organic Matter

Organic matter was subjected to irradiation in an ATLAS Suntest CPS+ simulator during a specific time of 60 min, mixed with NPs and time dependent UV-vis absorbance measurements were recorded between wavelength region of 200 and 600 nm.

4.2.13.1. "TiO_2 and HA_{pho}" binary system following photolysis of organic matter. As explained so far, a similar approach was also followed for "TiO_2 and HA_{pho}" binary system following photolysis of organic matter. Time dependent UV-vis absorbance spectral variations in the wavelength range of 200-600 nm were recorded and presented in Figure 4.286a. Accordingly, respective normalized absorbance values in the selected wavelengths were presented in Figure 4.286b.

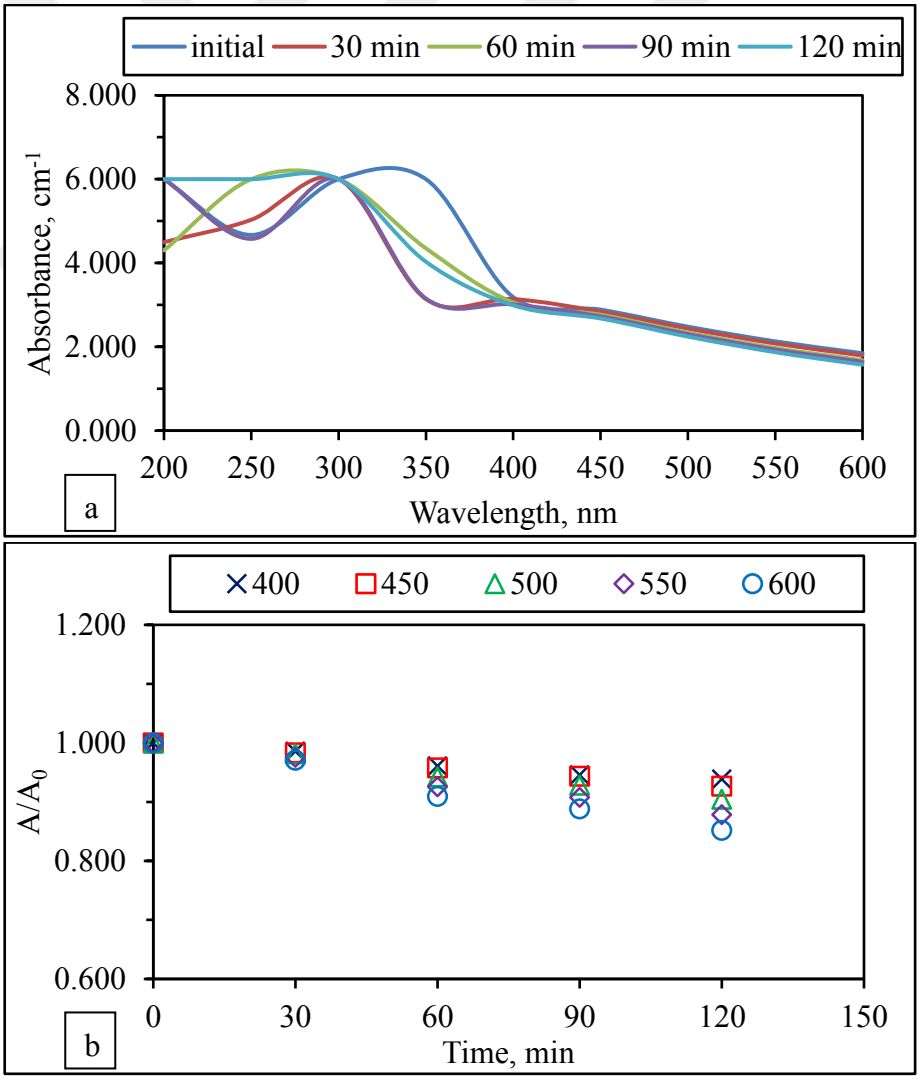


Figure 4.286. Sedimentation behavior of "TiO_2 and HA_{pho}" binary system following photolysis of organic matter, a) UV-vis absorbance variations b) Normalized absorbance with respect to time.

In a similar manner to data depicted under "as-is" (Figure 274a, b) and "as-is" under dark conditions (Figure 280a, b) UV-vis spectral variations could also be expressed by two regions as an inconsistent trend ($200<\lambda<400$ nm) followed by a consistent trend ($400<\lambda<600$ nm). Due to the observed inconsistency absorbance recordings at λ=380 nm were excluded. Both exponential and linear modeling revealed considerably high correlation coefficients as $R^2 > 0.967$ (Table 4.194).

Table 4.194. "TiO_2 and HA_{pho}" binary system following photolysis of organic matter, kinetic model parameters.

Kinetic model	Wavelength, nm				
	400	450	500	550	600
Exponential model					
k, min^{-1}	5.58×10^{-4}	6.44×10^{-4}	8.55×10^{-4}	1.10×10^{-3}	1.36×10^{-3}
R^2	0.969	0.993	0.982	0.982	0.982
Linear model					
k, min^{-1}	5.41×10^{-4}	6.20×10^{-4}	8.14×10^{-4}	1.03×10^{-3}	1.26×10^{-3}
R^2	0.967	0.992	0.980	0.980	0.979

Exponential model kinetic constants (min^{-1}) displayed a decreasing order as $1.36 \times 10^{-3} > 1.10 \times 10^{-3} > 8.55 \times 10^{-4} > 6.44 \times 10^{-4} > 5.58 \times 10^{-4}$ for wavelengths of 600 nm, 550 nm, 500 nm, 450 nm, and 400 nm, respectively. An average value of $k=9.03 \times 10^{-4}$ min^{-1} could be regarded as suitable for expressing sedimentation kinetics of "TiO_2 and HA_{pho}" following photolysis of organic matter using the exponential model. The average value resembled to the exponential model kinetic constants calculated from the data attained by absorbance recordings at λ=500 and 550 nm.

In a similar manner, the linear trend as visualized by the decreasing trend of A/A_o revealed kinetic constants (min^{-1}) in a decreasing order as $1.26 \times 10^{-3} > 1.03 \times 10^{-3} > 8.14 \times 10^{-4} > 6.20 \times 10^{-4} > 5.41 \times 10^{-4}$ for wavelengths of 600 nm, 550 nm, 500 nm, 450 nm, and 400 nm, respectively. As expressed above an average of $k=8.53 \times 10^{-4}$ min^{-1} could be accepted as suitable for displaying sedimentation kinetics using the linear model. The average value as $k=8.53 \times 10^{-4}$ min^{-1} could well be regarded as similar to the rate constant attained by absorbance recording at λ=500 nm. It could be inferred that upon 30 min duration ≤ 5 % removals were achieved being considerably indifferent from each other with respect to increasing specified wavelengths followed which a slight enhancement was also observed in 60 min representing wavelength dependent variations as 5-10 %. However, upon 120 min duration, 15 % removal percentage was observed and with 5 % increase, removal efficiency reached to 15 % at λ=600 nm. As previously recorded for all systems, absorbance values were recorded for 50 nm changes in selected wavelengths excluding λ=380 nm which was selected according to literature findings.

4.2.13.2. "TiO_2 and $SRNOM_{pho}$" binary system following photolysis of organic matter. Sedimentation behavior of "TiO_2 and $SRNOM_{pho}$" binary system following photolysis of organic matter was observed in a similar way. Time dependent UV-vis absorbance variations in the wavelength range of 200-600 nm were recorded and in Figure 4.287a.

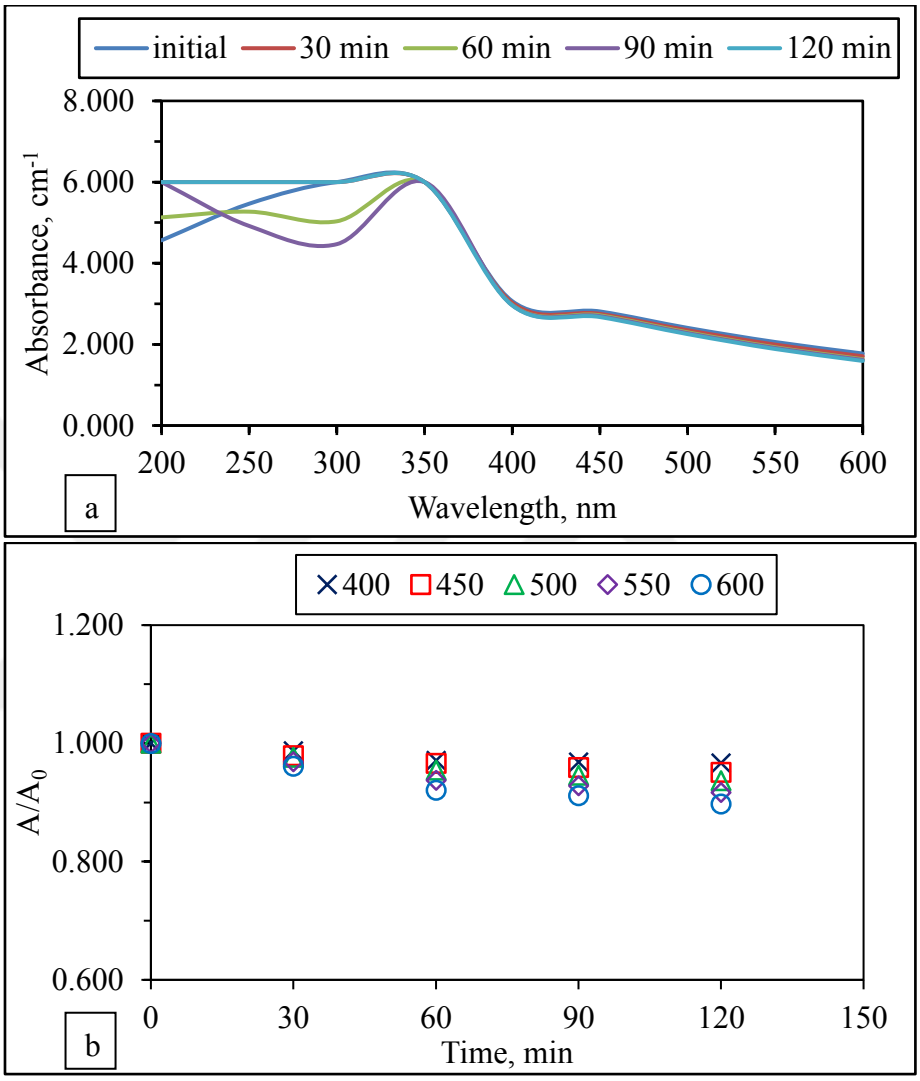


Figure 4.287. Sedimentation behavior of "TiO_2 and $SRNOM_{pho}$" binary system following photolysis of organic matter, a) UV-vis absorbance variations b) Normalized absorbance with respect to time.

In a similar manner to data depicted under "as-is" (Figure 11a, b) and "as-is" under dark conditions (Figure 17a, b) UV-vis spectral variations could also be expressed by two regions as an inconsistent trend ($200<\lambda<400$ nm) followed by a consistent trend ($400<\lambda<600$ nm). Due to the observed inconsistency, absorbance recordings at $\lambda=380$ nm were excluded. Exponential and linear models were applied and sedimentation kinetic constants were demonstrated in Table 4.195. Both exponential and linear modeling revealed considerably high correlation coefficients as $R^2 > 0.872$ (Table 4.195).

Table 4.195. "TiO_2 and $SRNOM_{pho}$" binary system following photolysis of organic matter, kinetic model parameters.

Kinetic model	Wavelength, nm				
	400	450	500	550	600
Exponential model					
k, min^{-1}	2.94×10^{-4}	4.03×10^{-4}	5.42×10^{-4}	7.24×10^{-4}	9.00×10^{-4}
R^2	0.874	0.946	0.950	0.936	0.930
Linear model					
k, min^{-1}	2.89×10^{-4}	3.93×10^{-4}	5.24×10^{-4}	6.92×10^{-4}	8.50×10^{-4}
R^2	0.872	0.943	0.947	0.932	0.924

Exponential model kinetic constants (min^{-1}) demonstrated a decreasing order as $9.00 \times 10^{-4} > 7.24 \times 10^{-4} > 5.42 \times 10^{-4} > 4.03 \times 10^{-4} > 2.94 \times 10^{-4}$ for wavelengths of 600 nm, 550 nm, 500 nm, 450 nm, and 400 nm, respectively. Simply an average value of $k=5.73 \times 10^{-4}$ min^{-1} could be regarded as suitable for expressing sedimentation kinetics of "TiO_2 and $SRNOM_{pho}$" binary system following photolysis of organic matter using the exponential model. The average value resembled to the $k=5.42 \times 10^{-4}$ min^{-1} that was calculated from the data attained by absorbance recordings at λ=500 nm.

Following the same manner, the linear trend as visualized by the decreasing trend of A/A_o revealed kinetic constants (min^{-1}) in a decreasing order as $8.50 \times 10^{-4} > 6.92 \times 10^{-4} > 5.24 \times 10^{-4} > 3.93 \times 10^{-4} > 2.89 \times 10^{-4}$ for wavelengths of 600 nm, 550 nm, 500 nm, 450 nm, and 400 nm, respectively. As expressed above an average of $k=5.50 \times 10^{-4}$ min^{-1} could be accepted as suitable for displaying sedimentation kinetics of "TiO_2 and $SRNOM_{pho}$" binary system following photolysis of organic matter using the linear model. The average value resembled to the $k=5.24 \times 10^{-4}$ min^{-1} that was calculated for λ=500 nm.

Under the specified conditions represented by selected wavelengths, it could be concluded that upon 30 min experimental duration, roughly $\leq$ 5 % removal at λ=400 nm and λ=600 nm was monitored. However, upon 90 min experimental duration, roughly $\leq$ 5 % removal at λ=400 nm and $\leq$ 10 % removal at λ=600 nm was observed. Further increase in experimental duration did not substantially alter the removal percentage of "TiO_2 and $SRNOM_{pho}$" following photolysis of organic matter. Upon 120 min of duration approximately $\leq$ 5 % removal at λ=400 nm and $\geq$ 10 % removal at λ=600 nm were obtained. This slight incremental increase could also be followed by prolonged time intervals possibly leading to 30-70 % in 6 h as could be inferred by calculation using both exponential and linear models, respectively. Although linear model explicating slightly lower kinetic constants, both kinetic model constants revealed similar tendencies and were not significantly different from each other at the specified wavelengths (Table 4.195).

4.2.13.3. "N-TiO_2 and HA_{pho}" binary system following photolysis of organic matter. Likewise expressed so far, a similar approach was followed for elucidation of sedimentation behavior of "N-TiO_2 and HA_{pho}" following photolysis of organic matter conditions in comparison to "N-TiO_2 and HA" under "as-is" conditions (Figure 4.276 and Table 4.180) and "as-is" dark conditions (Figure 4.282 and Table 4.188).

Time dependent UV-vis absorbance variations in the overall spectra covering the wavelength range of 200-600 nm were presented (Figure 4.288a). Accordingly, respective normalized absorbance values in the selected wavelengths were presented in Figure 4.288b. Both kinetic models were applied revealing considerably high correlation coefficients as $R^2 > 0.810$ and kinetic constants were presented in Table 4.196.

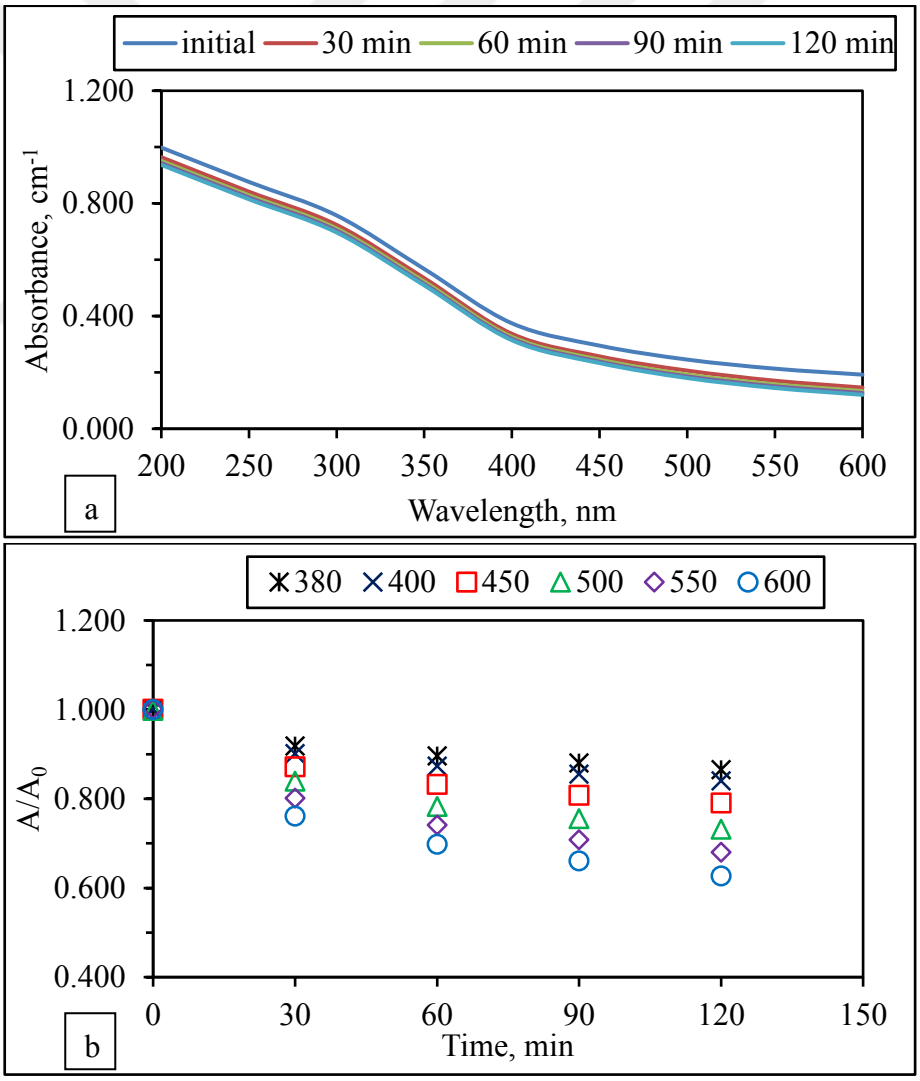


Figure 4.288. Sedimentation behavior of "N-TiO_2 and HA_{pho}" following photolysis of organic matter, a) UV-vis absorbance variations b) Normalized absorbance with respect to time.

Table 4.196. "N-TiO_2 and HA_{pho}" binary system following photolysis of organic matter, kinetic model parameters.

Kinetic model	Wavelength, nm					
	380	400	450	500	550	600
Exponential model						
k, min^{-1}	1.11 x 10^{-3}	1.34 x 10^{-3}	1.82 x 10^{-3}	2.42 x 10^{-3}	3.00 x 10^{-3}	3.59 x 10^{-3}
R^2	0.854	0.843	0.851	0.864	0.858	0.855
Linear model						
k, min^{-1}	1.03 x 10^{-3}	1.23 x 10^{-3}	1.61 x 10^{-3}	2.06 x 10^{-3}	2.46 x 10^{-3}	2.83 x 10^{-3}
R^2	0.840	0.827	0.829	0.836	0.821	0.810

Exponential model kinetics expressed constants (min^{-1}) in a decreasing order as 3.59 x 10^{-3} > 3.00 x 10^{-3} > 2.42 x 10^{-3} > 1.82 x 10^{-3} > 1.34 x 10^{-3} > 1.11 x 10^{-3} for wavelengths of 600 nm, 550 nm, 500 nm, 450 nm, 400 nm, and 380 nm, respectively. Kinetic constants followed a gradually increasing trend with respect to increasing detection wavelengths. Still, an average value of k=2.21 x 10^{-3} min^{-1} could be regarded as suitable for expressing sedimentation kinetics using the exponential model. The average value resembled to the k=2.42 x 10^{-3} min^{-1} that was calculated for λ=500 nm.

Linear trend as visualized by the decreasing trend of normalized absorbance recordings as A/A_o revealed kinetic constants (min^{-1}) in a decreasing order as 2.83 x 10^{-3} > 2.46 x 10^{-3} > 2.06 x 10^{-3} > 1.61 x 10^{-3} > 1.23 x 10^{-3} > 1.03 x 10^{-3} for wavelengths of 600 nm, 550 nm, 500 nm, 450 nm, 400 nm, and 380 nm, respectively. As expressed above an average of k=1.87 x 10^{-3} min^{-1} could be accepted as suitable for displaying sedimentation kinetics using the linear model. The average value resembled to the linear model kinetic constants calculated from the data attained by absorbance recordings at λ=450 nm and 500 nm.

Under the specified conditions represented by selected wavelengths, it could be concluded that upon 30 min duration, ~ 10 % removal at λ=380 nm and 25 % at λ=600 nm was obtained. However, upon 90 min experimental duration, roughly 12 % removal at λ=380 nm and 35 % at λ=600 nm was obtained. Further increase in experimental duration did not significantly alter the removal percentage of "N-TiO_2 and HA_{pho}" binary system following photolysis of organic matter. Upon 120 min of duration 15 % removal at λ=380 nm and ~ 40 % removal at λ=600 nm were observed. This slight incremental increase could also be followed by prolonged time intervals possibly leading to 70-95 % in 6 h as could be deduced by calculation using linear model, respectively. Despite the fact that linear model explicating slightly lower kinetic constants, both kinetic model constants revealed similar tendencies and were not significantly different from each other at the specified wavelengths (Table 4.196).

4.2.13.4. "N-TiO_2 and $SRNOM_{pho}$" binary system following photolysis of organic matter. A similar approach was followed for elucidation of sedimentation behavior of "N-TiO_2 and $SRNOM_{pho}$" binary system following photolysis of organic matter conditions considering "N-TiO_2 and SRNOM" under "as-is" conditions (Figure 4.117 and Table 4.81) and "as-is" under dark conditions (Figure 4.123 and Table 4.89). Time dependent UV-vis absorbance variations in the wavelength range of 200-600 nm were recorded and in Figure 4.289a.

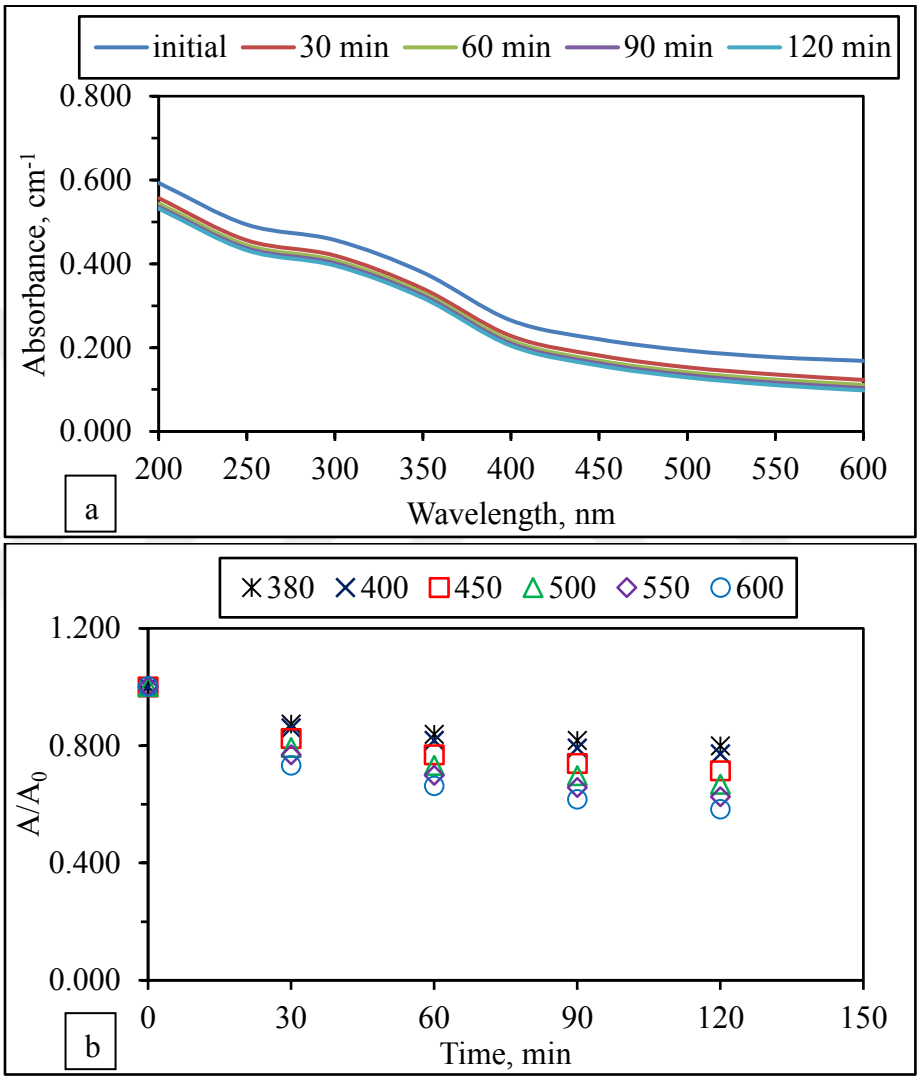


Figure 4.289. Sedimentation behavior of "N-TiO_2 and $SRNOM_{pho}$" following photolysis of organic matter, a) UV-vis absorbance variations b) Normalized absorbance with respect to time.

Contrary to the two regional demonstration of UV- vis spectra recorded for "TiO_2 and $SRNOM_{pho}$" following photolysis of organic matter (Figure 23), "N-TiO_2 and $SRNOM_{pho}$" spectral trend displayed a substantially decreasing trend with respect to time irrespective of the experimental duration. Time dependent absorbance values at selected wavelengths were normalized to respective initial absorbance values and presented in Figure 4.129b. The variations were modeled by two

approaches depending on the decreasing trend profiles. Exponential and linear models were applied and sedimentation kinetic constants were presented in Table 4.197. Both exponential and linear modeling revealed considerably high correlation coefficients as $R^2 > 0.809$.

Table 4.197. "N-TiO_2 and $SRNOM_{pho}$" binary system following photolysis of organic matter, kinetic model parameters.

Kinetic model	Wavelength, nm					
	380	400	450	500	550	600
Exponential model						
k, min^{-1}	1.72×10^{-3}	2.01×10^{-3}	2.61×10^{-3}	3.12×10^{-3}	3.66×10^{-3}	4.19×10^{-3}
R^2	0.837	0.855	0.858	0.859	0.870	0.861
Linear model						
k, min^{-1}	1.53×10^{-3}	1.75×10^{-3}	2.19×10^{-3}	2.54×10^{-3}	2.87×10^{-3}	3.18×10^{-3}
R^2	0.816	0.831	0.826	0.821	0.825	0.809

Exponential model kinetics as expressed by kinetic constants displayed a decreasing order as $4.19 \times 10^{-3} > 3.66 \times 10^{-3} > 3.12 \times 10^{-3} > 2.61 \times 10^{-3} > 2.01 \times 10^{-3} > 1.72 \times 10^{-3}$ for wavelengths of 600 nm, 550 nm, 500 nm, 450 nm, 400 nm, and 380 nm, respectively. An average value of $k=2.89 \times 10^{-3}$ min^{-1} could be regarded as suitable for expressing sedimentation kinetics using the exponential model. The average value resembled to the exponential model kinetic constants calculated from the data attained by absorbance recordings at λ=450 nm and 500 nm.

Following the same manner, the linear trend as visualized by the decreasing trend of A/A_o revealed kinetic constants (min^{-1}) in a decreasing order as $3.18 \times 10^{-3} > 2.87 \times 10^{-3} > 2.54 \times 10^{-3} > 2.19 \times 10^{-3} > 1.75 \times 10^{-3} > 1.53 \times 10^{-3}$ for wavelengths of 600 nm, 550 nm, 500 nm, 450 nm, 400 nm, and 380 nm, respectively. As expressed above an average of $k=2.34 \times 10^{-3}$ min^{-1} could be accepted as adequate for displaying sedimentation kinetics using the linear model.

Under the specified conditions represented by selected wavelengths, it could be inferred that upon 30 min duration 10-25 % removals were achieved with respect to increasing specified wavelengths followed which a slight enhancement was also observed as 15-35 % in 60 min representing between wavelength region of 380 nm and 600 nm. However, upon 120 min experimental duration, wavelength dependent variations in removal efficiencies increased to 40 % as detected at λ=600 nm being significantly different than the one attained for λ=380 nm. It should also be mentioned that both kinetic model constants were not significantly different from each other at the specified wavelengths (Table 4.197).

4.2.13.5. "Fe-TiO_2 and HA_{pho}" binary system following photolysis of organic matter. As explained for "Fe-TiO_2 and HA" under "as-is" (Figure 4.277 and Table 4.182) and "as-is" under dark conditions (Figure 4.283 and Table 4.190), a similar approach was followed for elucidation of sedimentation behavior of "Fe-TiO_2 and HA_{pho}" following photolysis of organic matter conditions. Time dependent UV-vis absorbance variations in the overall spectra covering the wavelength range of 200-600 nm were presented (Figure 4.290a). "Fe-TiO_2 and HA_{pho}" binary system under following photolysis of organic matter conditions demonstrated quite similar tendency to "Fe-TiO_2 and HA" under "as-is" conditions and no direct effect of photolysis for 60 min could be observed excluding the initial absorbance recordings.

Both kinetic models were applied revealing considerably high correlation coefficients as $R^2 >$ 0.824 and kinetic constants were tabulated (Figure 4.290b and Table 4.198).

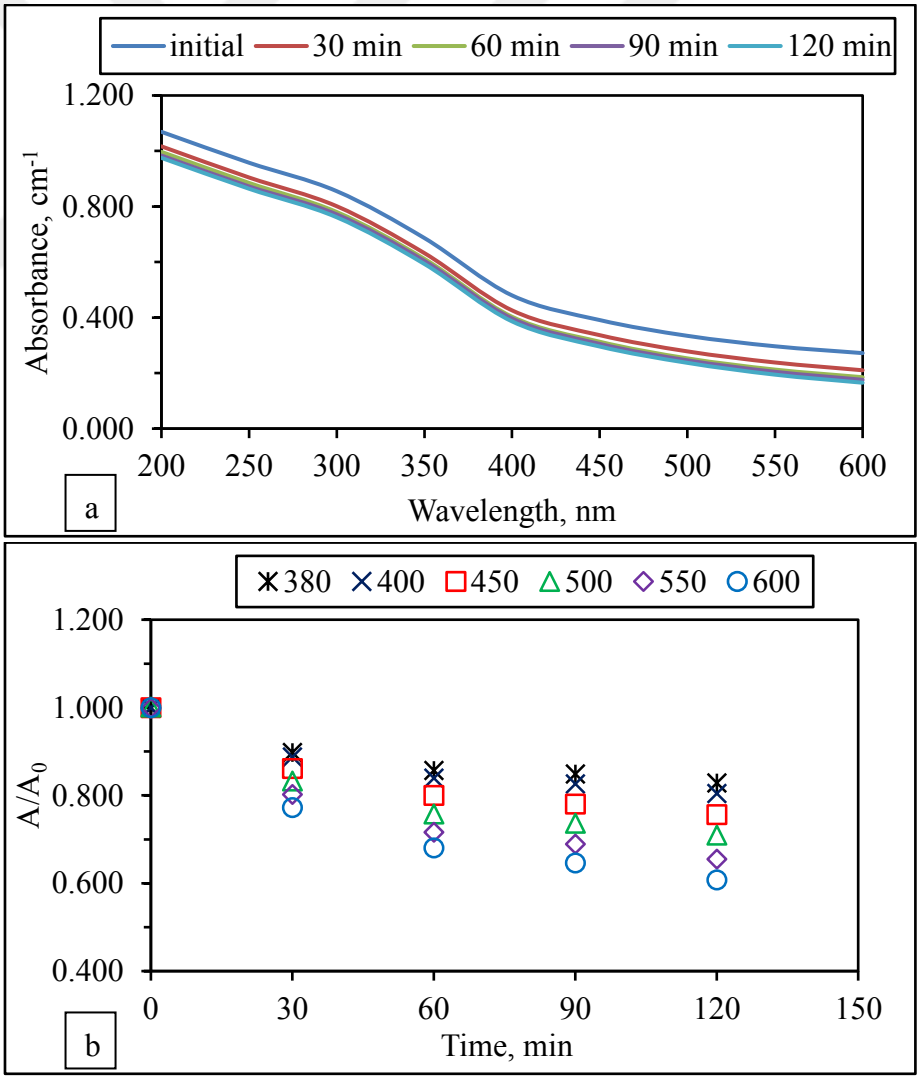


Figure 4.290. Sedimentation behavior of "Fe-TiO_2 and HA_{pho}" following photolysis of organic matter, a) UV-vis absorbance variations b) Normalized absorbance with respect to time.

Table 4.198. "Fe-TiO_2 and HA_{pho}" binary system following photolysis of organic matter, kinetic model parameters.

Kinetic model	Wavelength, nm					
	380	400	450	500	550	600
Exponential model						
k, min^{-1}	1.43×10^{-3}	1.68×10^{-3}	2.19×10^{-3}	2.71×10^{-3}	3.32×10^{-3}	3.91×10^{-3}
R^2	0.841	0.859	0.870	0.866	0.880	0.887
Linear model						
k, min^{-1}	1.30×10^{-3}	1.50×10^{-3}	1.89×10^{-3}	2.27×10^{-3}	2.67×10^{-3}	3.04×10^{-3}
R^2	0.824	0.840	0.845	0.837	0.843	0.843

Exponential model expressed kinetic constants (min^{-1}) in a decreasing order as $3.91 \times 10^{-3} > 3.32 \times 10^{-3} > 2.71 \times 10^{-3} > 2.19 \times 10^{-3} > 1.68 \times 10^{-3} > 1.43 \times 10^{-3}$ for wavelengths of 600 nm, 550 nm, 500 nm, 450 nm, 400 nm, and 380 nm, respectively. Simply an average value of $k=2.54 \times 10^{-3}$ min^{-1} could be regarded as suitable for expressing sedimentation kinetics using an exponential model. The average value resembled to the $k=3.26 \times 10^{-3}$ min^{-1} that was calculated from the data attained by absorbance recordings at λ=450 nm and 500 nm.

In a similar manner, the linear trend as visualized by the decreasing trend of A/A_o revealed kinetic constants (min^{-1}) in a decreasing order as $3.04 \times 10^{-3} > 2.67 \times 10^{-3} > 2.27 \times 10^{-3} > 1.89 \times 10^{-3} > 1.50 \times 10^{-3} > 1.30 \times 10^{-3}$ for wavelengths of 600 nm, 550 nm, 500 nm, 450 nm, 400 nm, and 380 nm, respectively. As expressed above an average of $k=2.11 \times 10^{-3}$ min^{-1} could be accepted as suitable for displaying sedimentation kinetics using a linear model. The average value resembled to the linear model kinetic constants calculated from the data attained by absorbance recordings at λ=450 nm and 500 nm.

It could also be inferred that an incremental increase in wavelength from 380 nm to 400 nm reflected as a minor increase in kinetic constants as roughly 15 % for both exponential and linear models. However, this insignificant increase could also be visualized for various deviations recorded for 50 nm changes in selected wavelengths. Under the specified conditions represented by selective wavelengths, it could be indicated that upon 30 min duration approximately 10 % removal was recorded at λ=400 nm and ~ 25 % at λ=600 nm. Nevertheless, upon 60 min experimental duration, 15 % removal was obtained at λ=400 nm and 30 % at λ=600 nm. As explained for "N-TiO_2 and HA_{pho}" binary system following photolysis of organic matter, further increase in experimental duration did not significantly change the removal percentage of "Fe-TiO_2 and HA_{pho}" binary system following photolysis of organic matter. Upon 120 min of duration 40 % removal at λ=600 nm was observed.

4.2.13.6. "Fe-TiO_2 and $SRNOM_{pho}$" binary system following photolysis of organic matter. As explained for "Fe-TiO_2 and SRNOM" under "as-is" (Figure 4.278 and Table 4.183) and "as-is" under dark conditions (Figure 4.285 and Table 4.191), a similar approach was followed for elucidation of sedimentation behavior of "Fe-TiO_2 and $SRNOM_{pho}$" following photolysis of organic matter conditions.

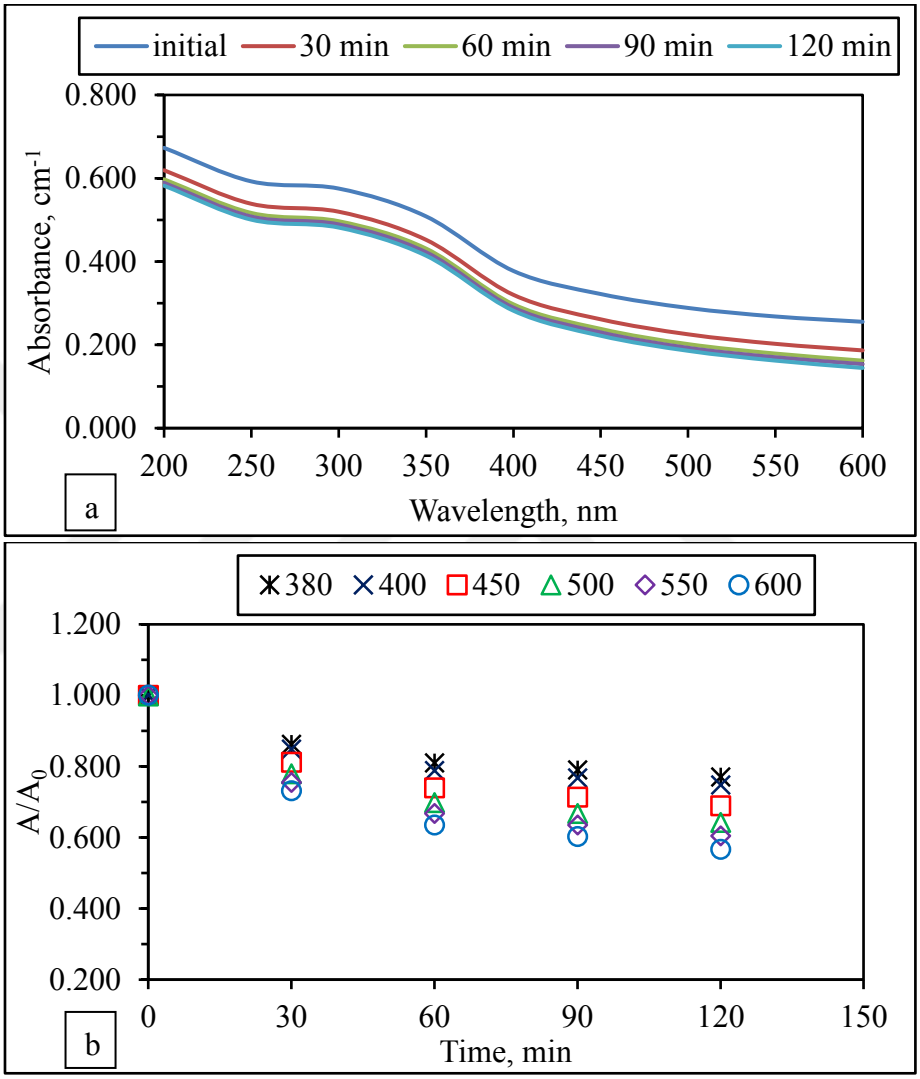


Figure 4.291. Sedimentation behavior of "Fe-TiO_2 and $SRNOM_{pho}$" following photolysis of organic matter, a) UV-vis absorbance variations b) Normalized absorbance with respect to time.

Contrary to the two regional demonstration of UV-vis spectra recorded for "TiO_2 and $SRNOM_{pho}$" following photolysis of organic matter (Figure 4.287), "Fe-TiO_2 and $SRNOM_{pho}$" spectral trend exhibited a substantially decreasing trend with respect to time irrespective of the experimental duration. Time dependent UV-vis absorbance variations in the overall spectra covering the wavelength range of 200-600 nm were presented (Figure 4.291a). Both kinetic models were

applied revealing considerably high correlation coefficients as $R^2 > 0.811$ and kinetic constants were tabulated (Figure 4.291b and Table 4.199).

Table 4.199. "Fe-TiO_2 and $SRNOM_{pho}$" binary system following photolysis of organic matter, kinetic model parameters.

Kinetic model	Wavelength, nm					
	380	400	450	500	550	600
Exponential model						
k, min^{-1}	2.02×10^{-3}	2.28×10^{-3}	2.91×10^{-3}	3.46×10^{-3}	3.93×10^{-3}	4.44×10^{-3}
R^2	0.852	0.849	0.855	0.853	0.858	0.862
Linear model						
k, min^{-1}	1.76×10^{-3}	1.96×10^{-3}	2.40×10^{-3}	2.75×10^{-3}	3.04×10^{-3}	3.33×10^{-3}
R^2	0.828	0.823	0.821	0.814	0.812	0.811

Exponential model kinetic constants (min^{-1}) demonstrated a decreasing order as $4.44 \times 10^{-3} > 3.93 \times 10^{-3} > 3.46 \times 10^{-3} > 2.91 \times 10^{-3} > 2.28 \times 10^{-3} > 2.02 \times 10^{-3}$ for wavelengths of 600 nm, 550 nm, 500 nm, 450 nm, 400 nm, and 380 nm, respectively. Simply an average value of $k=3.17 \times 10^{-3}$ min^{-1} could be regarded as adequate for displaying sedimentation kinetics of "Fe-TiO_2 and $SRNOM_{pho}$" following photolysis of organic matter using the exponential model. The average value resembled to the $k=3.46 \times 10^{-3}$ min^{-1} that was calculated from the data obtained by absorbance recordings at λ=500 nm.

Following the same manner, the linear trend as visualized by the decreasing trend of A/A_o revealed kinetic constants (min^{-1}) in a decreasing order as $3.33 \times 10^{-3} > 3.04 \times 10^{-3} > 2.75 \times 10^{-3} > 2.40 \times 10^{-3} > 1.96 \times 10^{-3} > 1.76 \times 10^{-3}$ for wavelengths of 600 nm, 550 nm, 500 nm, 450 nm, 400 nm, and 380 nm, respectively. As expressed above an average of $k=2.54 \times 10^{-3}$ min^{-1} could be accepted as suitable for expressing sedimentation kinetics using the linear model. The average value resembled to that was calculated from the data attained by absorbance recordings between λ=450 nm and 500 nm.

Under the specified conditions represented by selected wavelengths, it could be deduced that upon 30 min of duration, roughly ≤ 15 % removal at λ=380 nm and ≤ 30 % removal at λ=600 nm was observed. However, upon 90 min of duration, roughly ≤ 20 % removal at λ=380 nm and ≤ 40 % removal at λ=600 nm was monitored. Upon 120 min of duration approximately ≤ 25 % removal at λ=380 nm and ≥ 40 % removal at λ=600 nm were monitored. Although linear model explicating slightly lower kinetic constants, both kinetic model constants revealed similar tendencies and were not significantly different from each other at the specified wavelengths (Table 4.199).

4.2.14. Comparative Evaluation of Exponential and Linear Models of "TiO_2 and HA_{pho}", "N-TiO_2 and HA_{pho}", "Fe-TiO_2 and HA_{pho}" following photolysis of organic matter Conditions

Based on the presented data for all of the NPs under "following photolysis of organic matter" conditions, although similar sedimentation profiles were attained, a comparative evaluation could be beneficial in elucidation of the sample specific variations for suitability of application of UV-vis spectroscopic technique. To fulfill this aim, kinetic model parameters attained at selected indicative wavelength of λ=550 nm were compiled from tables 4.194-4.198 and presented in Table 4.200.

Table 4.200. Comparative presentation of sedimentation kinetics of NPs under following photolysis of organic matter conditions at λ=550 nm.

Kinetic model	Exponential model	
NP	k, min^{-1}	R^2
"TiO_2 and HA_{pho}"	1.10 x 10^{-3}	0.982
"N-TiO_2 and HA_{pho}"	3.00 x 10^{-3}	0.858
"Fe-TiO_2 and HA_{pho}"	3.32 x 10^{-3}	0.880
	Linear model	
	k, min^{-1}	R^2
"TiO_2 and HA_{pho}"	1.03 x 10^{-3}	0.980
"N-TiO_2 and HA_{pho}"	2.46 x 10^{-3}	0.821
"Fe-TiO_2 and HA_{pho}"	2.67 x 10^{-3}	0.843

Considering sedimentation behavior of "TiO_2 and HA_{pho}", "N-TiO_2 and HA_{pho}", and "Fe-TiO_2 and HA_{pho}" following photolysis of organic matter conditions, normalized absorbance values recorded at λ=550 nm fitted to the exponential kinetic equation gave the following reaction rate constants (min^{-1}) as 3.32 x 10^{-3} for "Fe-TiO_2 and HA_{pho}" > 3.00 x 10^{-3} for "N-TiO_2 and HA_{pho}" > 1.10 x 10^{-3} for "TiO_2 and HA_{pho}" (Table 4.200).

When sedimentation behavior of "TiO_2 and HA_{pho}", "N-TiO_2 and HA_{pho}", and "Fe-TiO_2 and HA_{pho}" binary systems were fitted to the linear model, rate constants (min^{-1}) were found as 2.67 x 10^{-3} for "Fe-TiO_2 and HA_{pho}" > 2.46 x 10^{-3} for "N-TiO_2 and HA_{pho}" > 1.03 x 10^{-3} for "TiO_2 and HA_{pho}" (Table 4.200). Application of exponential model indicated preferential stability of "TiO_2 and HA_{pho}" in comparison to "N-TiO_2 and HA_{pho}" and "Fe-TiO_2 and HA_{pho}" all following photolysis of organic matter conditions, as also supported by linear modeling with minor differences. From a general perspective, both kinetic models revealed similar tendencies. The role of photolysis prior to absorbance recordings could be related to the possible aggregation of the NPs in comparison to the applied sonication and magnetic stirring for a short duration of NP samples prepared under "as-is" conditions.

4.2.15. Comparative Evaluation of Exponential and Linear Models of "TiO_2 and $SRNOM_{pho}$", "N-TiO_2 and $SRNOM_{pho}$", "Fe-TiO_2 and $SRNOM_{pho}$" following photolysis of organic matter Conditions

Based on the presented data for all of the NPs under following photolysis of organic matter conditions, although similar sedimentation profiles were obtained, a comparative evaluation could be beneficial in elucidation of the sample specific variations for suitability of application of UV-vis spectroscopic technique. To fulfill this purpose, kinetic model parameters attained at selected indicative wavelength of λ=550 nm were compiled from tables 4.195-4.199 and presented in Table 4.201.

Table 4.201. Comparative presentation of sedimentation kinetics of NPs under following photolysis of organic matter conditions at λ=550 nm.

Kinetic model	Exponential model	
NP	k, min^{-1}	R^2
"TiO_2 and $SRNOM_{pho}$"	7.24 x 10^{-4}	0.936
"N-TiO_2 and $SRNOM_{pho}$"	3.66 x 10^{-3}	0.870
"Fe-TiO_2 and $SRNOM_{pho}$"	3.93 x 10^{-3}	0.858
	Linear model	
	k, min^{-1}	R^2
"TiO_2 and $SRNOM_{pho}$"	6.92 x 10^{-4}	0.932
"N-TiO_2 and $SRNOM_{pho}$"	2.87 x 10^{-3}	0.825
"Fe-TiO_2 and $SRNOM_{pho}$"	3.04 x 10^{-3}	0.812

Considering sedimentation behavior of "TiO_2 and $SRNOM_{pho}$", "N-TiO_2 and $SRNOM_{pho}$", and "Fe-TiO_2 and $SRNOM_{pho}$" following photolysis of organic matter conditions, normalized absorbance values recorded at λ=550 nm fitted to the exponential kinetic equation gave the following reaction rate constants (min^{-1}) as 3.93 x 10^{-3} for "Fe-TiO_2 and HA_{pho}" > 3.66 x 10^{-3} for "N-TiO_2 and HA_{pho}" > 7.24 x 10^{-4} for "TiO_2 and $SRNOM_{pho}$" (Table 4.201).

When sedimentation behavior of "TiO_2 and $SRNOM_{pho}$", "N-TiO_2 and $SRNOM_{pho}$", and "Fe-TiO_2 and $SRNOM_{pho}$" binary systems were fitted to the linear model, rate constants (min^{-1}) were found as 3.04 x 10^{-3} for "Fe-TiO_2 and $SRNOM_{pho}$" > 2.87 x 10^{-3} for "N-TiO_2 and $SRNOM_{pho}$" > 6.92 x 10^{-4} for "TiO_2 and $SRNOM_{pho}$" (Table 4.201). Application of exponential model indicated preferential stability of "TiO_2 and $SRNOM_{pho}$" in comparison to "N-TiO_2 and $SRNOM_{pho}$" and "Fe-TiO_2 and $SRNOM_{pho}$" all following photolysis of organic matter conditions, as also supported by linear modeling with minor differences. From a general perspective, both kinetic models revealed similar tendencies.

4.2.16. Sedimentation Behavior of Nanoparticles TiO_2, N-TiO_2 and Fe-TiO_2 "as-is under irradiation" in the Presence of Organic Matter

All selected NP binary systems were subjected to irradiation in an ATLAS Suntest CPS+ simulator during a specific time of 30 min for "TiO_2 and HA" and "N-TiO_2 and HA", 60 min for "Fe-TiO_2 and HA" and time dependent UV-vis absorbance measurements were recorded between wavelength region of 200 and 600 nm.

4.2.16.1. "TiO_2 and HA" binary system "as-is" under irradiation. Following a similar manner, time dependent UV-vis absorbance variations in the wavelength range of 200-600 nm were recorded and presented in Figure 4.292a. Exponential and linear models were applied and sedimentation kinetic constants were displayed in Table 4.202.

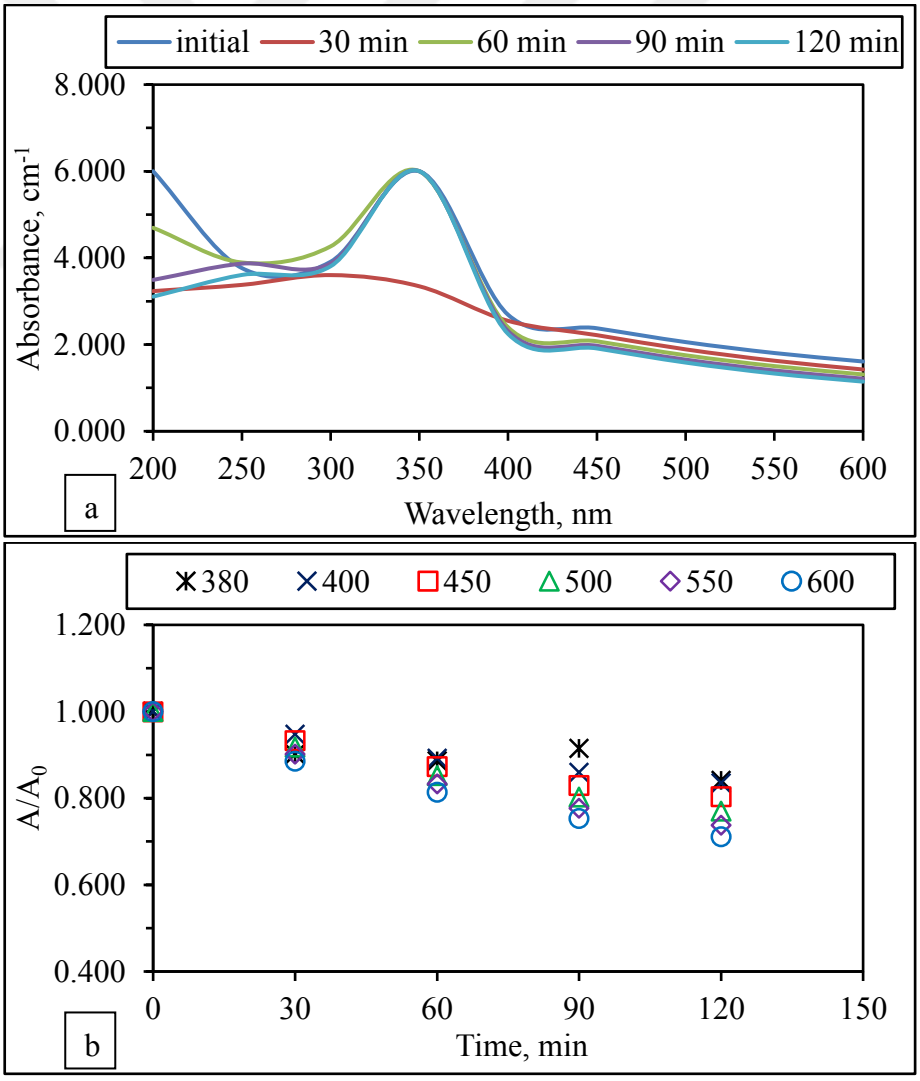


Figure 4.292. Sedimentation behavior of "TiO_2 and HA" "as-is" under irradiation, a) UV-vis absorbance variations b) Normalized absorbance with respect to time.

The variations in exposure periods were related to the further application of binary systems *i.e.* photocatalysis. In a similar manner to data depicted under "as-is" (Figure 4.274a, b), "as-is" under dark (Figure 4.280a, b) and "following photolysis of organic matter" conditions (Figure 4.286a, b) UV-vis spectral variations could also be expressed by two regions as an inconsistent trend ($200<\lambda<400$ nm) followed by a consistent trend ($400<\lambda<600$ nm). Both exponential and linear modeling revealed considerably high correlation coefficients as $R^2 > 0.686$ (Figure 4.292b and Table 4.202).

Table 4.202. "TiO_2 and HA" "as-is" under irradiation, kinetic model parameters.

Kinetic model	Wavelength, nm					
	380	400	450	500	550	600
Exponential model						
k, min^{-1}	1.10×10^{-3}	1.52×10^{-3}	1.84×10^{-3}	2.19×10^{-3}	2.53×10^{-3}	2.81×10^{-3}
R^2	0.692	0.980	0.980	0.983	0.984	0.981
Linear model						
k, min^{-1}	1.01×10^{-3}	1.39×10^{-3}	1.65×10^{-3}	1.92×10^{-3}	2.17×10^{-3}	2.37×10^{-3}
R^2	0.686	0.973	0.972	0.972	0.971	0.965

Exponential model kinetic constants (min^{-1}) displayed a decreasing order as $2.81 \times 10^{-3} > 2.53 \times 10^{-3} > 2.19 \times 10^{-3} > 1.84 \times 10^{-3} > 1.52 \times 10^{-3} > 1.10 \times 10^{-3}$ for wavelengths of 600 nm, 550 nm, 500 nm, 450 nm, 400 nm, and 380 nm, respectively. An average value of $k=2.00 \times 10^{-3}$ min^{-1} could be regarded as suitable for expressing sedimentation kinetics of "TiO_2 and HA" "as-is" under irradiation using the exponential model. The average value resembled to the exponential model kinetic constants calculated from the data obtained by absorbance recordings at λ=450 nm and 500 nm.

In a similar manner, the linear trend as visualized by the decreasing trend of A/A_o revealed kinetic constants (min^{-1}) in a decreasing order as $2.37 \times 10^{-3} > 2.17 \times 10^{-3} > 1.92 \times 10^{-3} > 1.65 \times 10^{-3} > 1.39 \times 10^{-3} > 1.01 \times 10^{-3}$ for wavelengths of 600 nm, 550 nm, 500 nm, 450 nm, 400 nm, and 380 nm, respectively. As expressed above an average of $k=1.75 \times 10^{-3}$ min^{-1} could be accepted as suitable for displaying sedimentation kinetics of "TiO_2 and HA" "as-is" under irradiation using the linear model. The average value resembled to the linear model kinetic constants calculated from the data attained by absorbance recordings at λ=450 nm and 500 nm. It could also be deduced that upon 30 min duration $\leq$ 10 % removals were achieved being considerably indifferent from each other with respect to increasing specified wavelengths followed which a slight enhancement was also observed in 60 min representing wavelength dependent variations as 15-20 %. However, upon 120 min duration, removal percentage increased to 25 % as detected at λ=600 nm being significantly different than the one attained for λ=380 nm.

4.2.16.2. "TiO_2 and SRNOM" binary system "as-is" under irradiation. As explained for "TiO_2 and HA" binary system "as-is" under irradiation, a similar approach was followed for elucidation of sedimentation behavior of "TiO_2 and SRNOM" binary system "as-is" under irradiation. Following an initial mixing period of 30 min, "TiO_2 and SRNOM" system was subjected to sedimentation as followed by time dependent UV-vis absorbance variations (Figure 4.293a).

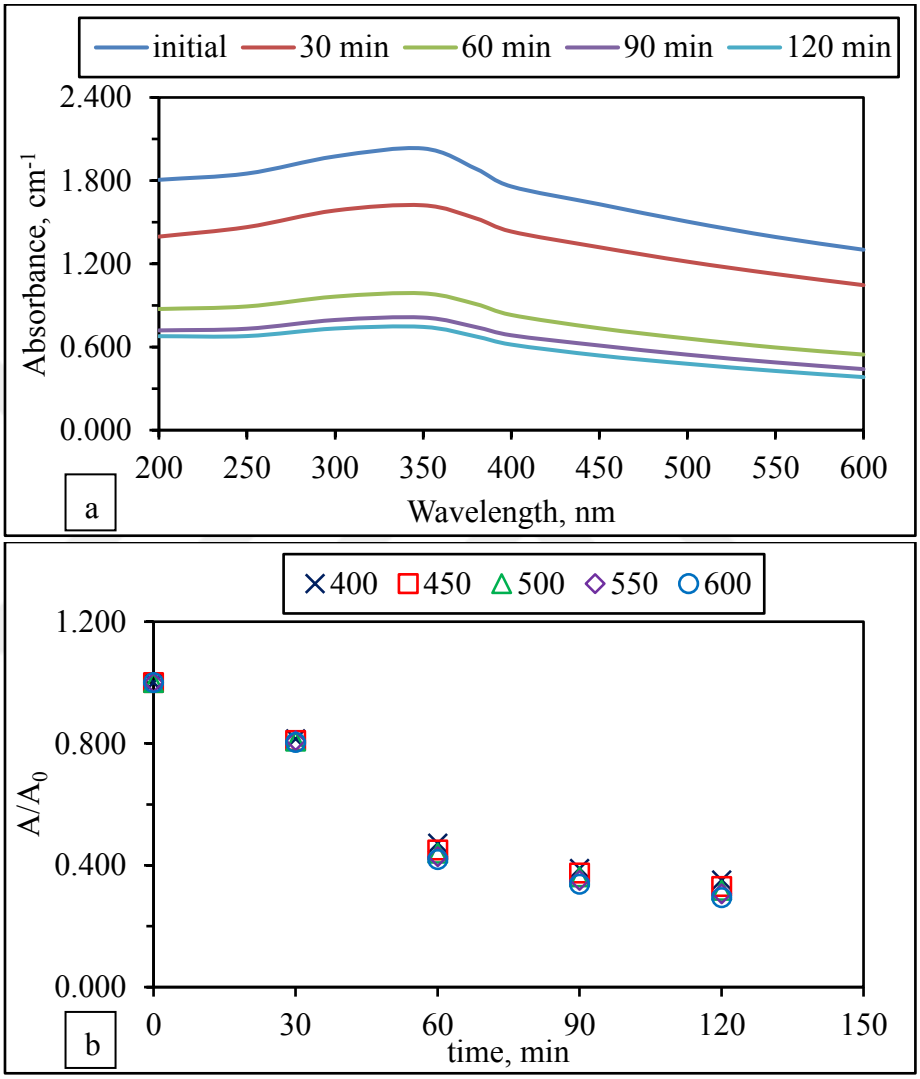


Figure 4.293. Sedimentation behavior of "TiO_2 and SRNOM" "as-is" under irradiation, a) UV-vis absorbance variations b) Normalized absorbance with respect to time.

Contrary to the two regional demonstration of UV-vis spectra recorded for "TiO_2 and HA" "as-is" under irradiation (Figure 4.292), "TiO_2 and SRNOM" "as-is" under irradiation spectral trend demonstrated a substantially decreasing trend with respect to time. Time dependent UV-vis absorbance variations in the overall spectra covering the wavelength range of 200-600 nm were presented (Figure 4.293a). Due to the observed inconsistency absorbance recordings at λ=380 nm were excluded.

Exponential and linear models were applied and sedimentation kinetic constants were presented in Figure 4.293b and Table 4.203. Both exponential and linear modeling revealed considerably high correlation coefficients as $R^2 > 0.898$.

Table 4.203. "TiO_2 and SRNOM" "as-is" under irradiation, kinetic model parameters.

Kinetic model	Wavelength, nm				
	400	450	500	550	600
Exponential model					
k, min^{-1}	9.44×10^{-3}	9.95×10^{-3}	1.03×10^{-2}	1.07×10^{-2}	1.10×10^{-2}
R^2	0.938	0.937	0.937	0.936	0.938
Linear model					
k, min^{-1}	5.74×10^{-3}	5.91×10^{-3}	6.03×10^{-3}	6.15×10^{-3}	6.26×10^{-3}
R^2	0.904	0.901	0.899	0.898	0.899

Exponential model kinetics expressed constants (min^{-1}) in a decreasing order as $1.10 \times 10^{-2} > 1.07 \times 10^{-2} > 1.03 \times 10^{-2} > 9.95 \times 10^{-3} > 9.44 \times 10^{-3}$ for wavelengths of 600 nm, 550 nm, 500 nm, 450 nm, and 400 nm, respectively. Kinetic constants followed a slightly increasing trend with respect to increasing detection wavelengths. Still, an average value of $k=1.03 \times 10^{-2}$ min^{-1} could be regarded as adequate for expressing sedimentation kinetics of "TiO_2 and SRNOM" "as-is" under irradiation using the exponential model. The average value resembled to the $k=1.03 \times 10^{-2}$ min^{-1} that was calculated for λ=500 nm.

Linear trend as visualized by the decreasing trend of normalized absorbance recordings as A/A_o revealed kinetic constants (min^{-1}) in a decreasing order as $6.26 \times 10^{-3} > 6.15 \times 10^{-3} > 6.03 \times 10^{-3} > 5.91 \times 10^{-3} > 5.74 \times 10^{-3}$ for wavelengths of 600 nm, 550 nm, 500 nm, 450 nm, and 400 nm, respectively. As expressed above an average of $k=6.02 \times 10^{-3}$ min^{-1} could be accepted as suitable for expressing sedimentation kinetics of "TiO_2 and SRNOM" "as-is" under irradiation using the linear model. The average value as $k=6.03 \times 10^{-3}$ min^{-1} could well be regarded as similar to the rate constant obtained by absorbance recording at λ=500 nm.

Under the specified conditions represented by selected wavelengths, it could also be inferred that upon 30 min experimental duration, ~ 18 % removal at λ=400 nm and 20 % at λ=600 nm was observed. However, upon further experimental duration of 90 min, roughly 60 % removal at λ=400 nm and 65 % at λ=600 nm was monitored. Further increase in experimental duration significantly shifted the removal percentage of "TiO_2 and SRNOM" "as-is" under irradiation. Correspondingly, upon 120 min of duration 65 % removal at λ=400 nm and approximately 70 % removal at λ=600 nm were recorded.

4.2.16.3. "N-TiO_2 and HA" binary system "as-is" under irradiation. As explained for "N-TiO_2 and HA_{pho}" binary system following photolysis of organic matter (Figure 4.288 and Table 4.196), a similar approach was followed for elucidation of sedimentation behavior of "N-TiO_2 and HA" "as-is" under irradiation conditions. Time dependent UV-vis absorbance variations in the overall spectra covering the wavelength range of 200-600 nm were presented (Figure 4.294a). Accordingly, normalized absorbance variations in the selected wavelengths were presented in Figure 4.294b. "N-TiO_2 and HA" binary system under "as-is" under irradiation conditions displayed quite similar tendency to "N-TiO_2 and HA" "as-is" conditions and no direct effect of continuous mixing for 30 min could be observed excluding the initial absorbance recordings.

Exponential and linear kinetic models were applied revealing considerably high correlation coefficients as $R^2 > 0.802$ and kinetic constants were tabulated (Table 4.204).

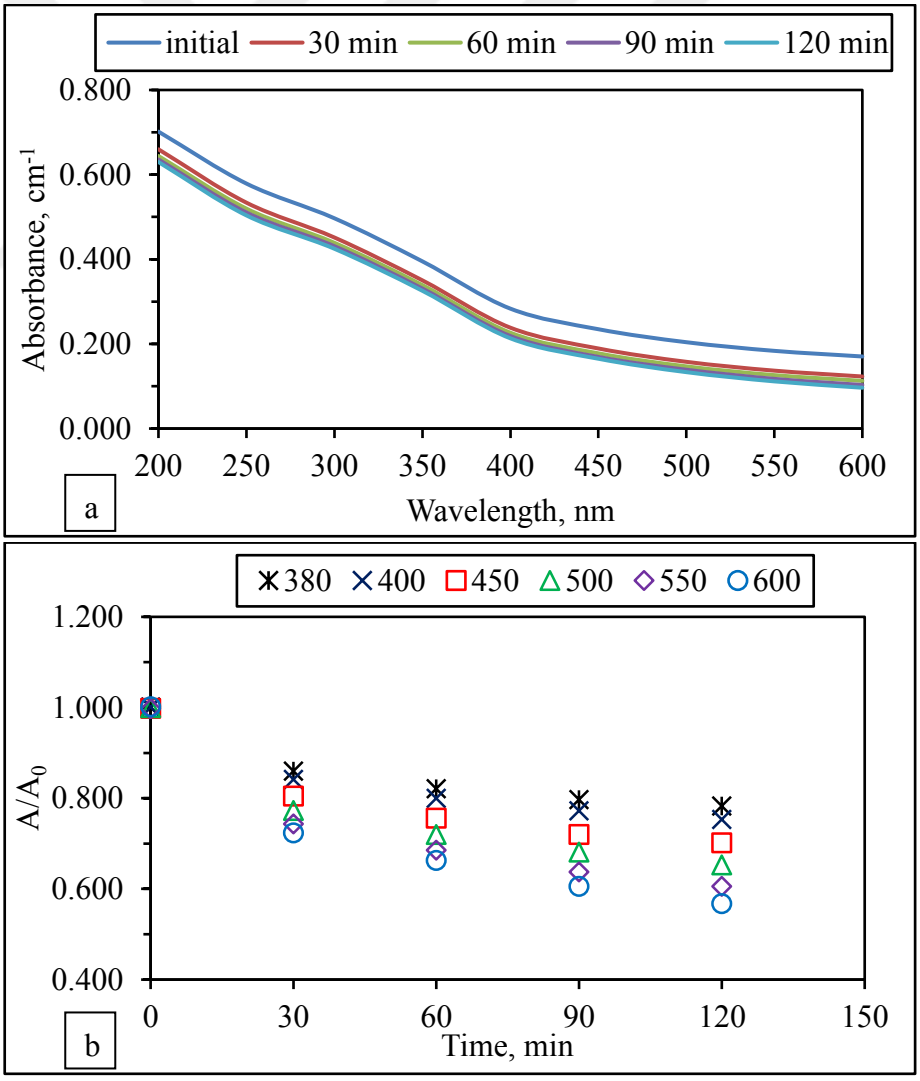


Figure 4.294. Sedimentation behavior of "N-TiO_2 and HA" "as-is" under irradiation, a) UV-vis absorbance variations b) Normalized absorbance with respect to time.

Table 4.204. "N-TiO_2 and HA" "as-is" under irradiation, kinetic model parameters.

Kinetic model	Wavelength, nm					
	380	400	450	500	550	600
Exponential model						
k, min^{-1}	1.89 x 10^{-3}	2.18 x 10^{-3}	2.72 x 10^{-3}	3.26 x 10^{-3}	3.83 x 10^{-3}	4.38 x 10^{-3}
R^2	0.825	0.837	0.836	0.844	0.859	0.875
Linear model						
k, min^{-1}	1.66 x 10^{-3}	1.88 x 10^{-3}	2.26 x 10^{-3}	2.62 x 10^{-3}	2.96 x 10^{-3}	3.29 x 10^{-3}
R^2	0.802	0.810	0.802	0.803	0.810	0.820

Exponential model kinetics expressed constants (min^{-1}) in a decreasing order as 4.38 x 10^{-3} > 3.83 x 10^{-3} > 3.26 x 10^{-3} > 2.72 x 10^{-3} > 2.18 x 10^{-3} > 1.89 x 10^{-3} for wavelengths of 600 nm, 550 nm, 500 nm, 450 nm, 400 nm, and 380 nm, respectively. Kinetic constants followed a gradually increasing trend with respect to increasing detection wavelengths. Still, an average value of k=3.04 x 10^{-3} min^{-1} could be regarded as suitable for expressing sedimentation kinetics of "N-TiO_2 and HA" "as-is" under irradiation using the exponential model. The average value resembled to the k=3.26 x 10^{-3} min^{-1} that was calculated for λ=500 nm.

Linear trend as visualized by the decreasing trend of normalized absorbance recordings as A/A_o revealed kinetic constants (min^{-1}) in a decreasing order as 3.29 x 10^{-3} > 2.96 x 10^{-3} > 2.62 x 10^{-3} > 2.26 x 10^{-3} > 1.88 x 10^{-3} > 1.66 x 10^{-3} for wavelengths of 600 nm, 550 nm, 500 nm, 450 nm, 400 nm, and 380 nm, respectively. As expressed above an average of k=2.45 x 10^{-3} min^{-1} could be accepted as suitable for displaying sedimentation kinetics using the linear model. The average value resembled to the linear model kinetic constants calculated from the data attained by absorbance recordings at λ=450 nm and 500 nm.

Under the specified conditions represented by selected wavelengths, it could be deduced that upon 30 min duration, 15 % removal at λ=380 nm and 30 % at λ=600 nm was obtained. Immediate settling profile could be distinctly visualized by absorbance recordings at various wavelengths in UV as well as in visible region. Further duration resulted in a continuous sedimentation tendency in a style expressing increasing difference between the absorbance recordings. Upon 120 min of duration 22 % removal at λ=380 nm and 43 % removal at λ=600 nm were observed.

The differences in kinetic constants attained by application of both models as well as related removal percentages might indicate irradiation under continuous mixing conditions induced changes could predominate over mixing under "as-is" and "as-is" under dark conditions. However, no direct conclusion could be visualized with respect to wavelength variations.

4.2.16.4. "N-TiO_2 and SRNOM" binary system "as-is" under irradiation. As explained for "TiO_2 and SRNOM" binary system "as-is" under irradiation (Figure 4.293a), a similar approach was followed for elucidation of sedimentation behavior of "N-TiO_2 and SRNOM" binary system "as-is" under irradiation. Following an initial mixing period of 30 min, "TiO_2 and SRNOM" system was subjected to sedimentation and time dependent UV-vis absorbance variations in the wavelength range of 200-600 nm were presented (Figure 4.295a).

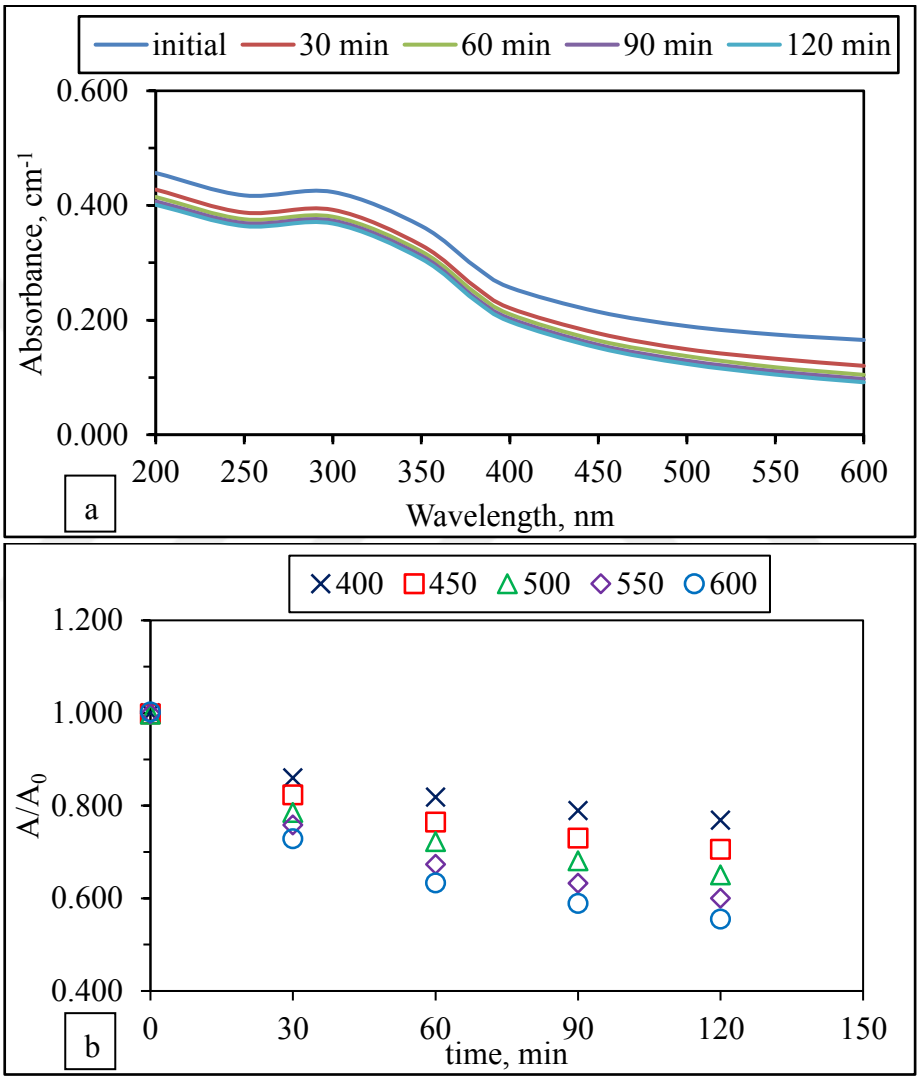


Figure 4.295. Sedimentation behavior of "N-TiO_2 and SRNOM" "as-is" under irradiation, a) UV-vis absorbance variations b) Normalized absorbance with respect to time.

The variations were modeled by two approaches depending on the decreasing trend profiles. Exponential and linear models were applied and sedimentation kinetic constants were presented in Figure 4.295b and Table 4.205. Due to the observed inconsistency absorbance recordings at λ=380 nm were excluded. Both exponential and linear modeling revealed considerably high correlation coefficients as $R^2 > 0.823$.

Table 4.205. "N-TiO_2 and SRNOM" "as-is" under irradiation, kinetic model parameters.

Kinetic model	Wavelength, nm				
	400	450	500	550	600
Exponential model					
k, min^{-1}	2.04×10^{-3}	2.71×10^{-3}	3.33×10^{-3}	4.00×10^{-3}	4.64×10^{-3}
R^2	0.865	0.871	0.874	0.877	0.877
Linear model					
k, min^{-1}	1.78×10^{-3}	2.26×10^{-3}	2.66×10^{-3}	3.08×10^{-3}	3.44×10^{-3}
R^2	0.840	0.839	0.834	0.830	0.823

Exponential model kinetics as expressed by kinetic constants displayed a decreasing order as $4.64 \times 10^{-3} > 4.00 \times 10^{-3} > 3.33 \times 10^{-3} > 2.71 \times 10^{-3} > 2.04 \times 10^{-3}$ for wavelengths of 600 nm, 550 nm, 500 nm, 450 nm, and 400 nm, respectively. Despite the fact that almost doubling effect could also be encountered as $k=2.04 \times 10^{-3}$ min^{-1} at $\lambda=400$ nm to $k=4.64 \times 10^{-3}$ min^{-1} at $\lambda=600$ nm, an average value of $k=3.34 \times 10^{-3}$ min^{-1} could be regarded as suitable for expressing sedimentation kinetics using the exponential model. The average value resembled to the $k=3.33 \times 10^{-3}$ min^{-1} that was calculated for $\lambda=500$ nm.

Following the same manner, the linear trend as visualized by the decreasing trend of A/A_o revealed kinetic constants (min^{-1}) in a decreasing order as $3.44 \times 10^{-3} > 3.08 \times 10^{-3} > 2.66 \times 10^{-3} > 2.26 \times 10^{-3} > 1.78 \times 10^{-3}$ for wavelengths of 600 nm, 550 nm, 500 nm, 450 nm, and 400 nm, respectively. Despite the fact that almost doubling effect could be encountered as $k=1.78 \times 10^{-3}$ min^{-1} at $\lambda=400$ nm to $k=3.44 \times 10^{-3}$ min^{-1} at $\lambda=600$ nm, an average value of $k=2.64 \times 10^{-3}$ min^{-1} could be regarded as suitable for expressing sedimentation kinetics using the linear model. The average value resembled to the $k=2.66 \times 10^{-3}$ min^{-1} that was calculated for $\lambda=500$ nm.

Under the specified conditions represented by selected wavelengths, it could be concluded that upon 30 min experimental duration approximately 14-27 % removals were achieved being considerably indifferent from each other with respect to increasing specified wavelengths followed which a slight enhancement was also observed as 18-37 % in 60 min representing between wavelength region of 400 nm and 600 nm. However, upon 120 min experimental duration, removal percentage reached to 45 % as detected at $\lambda=600$ nm being significantly different than the one attained for $\lambda=400$ nm. In a similar manner to data described "TiO_2 and SRNOM" "as-is" under irradiation (Table 4.203), for comparison purposes, further increase in experimental duration substantially altered the removal percentage of "N-TiO_2 and SRNOM" "as-is" under irradiation. It could also be concluded that both models could be successfully applied due to slight incremental decreases with respect to time (Table 4.205).

4.2.16.5. "Fe-TiO_2 and HA" binary system "as-is" under irradiation. In a similar fashion to "Fe-TiO_2 and HA" under "as-is" (Figure 4.278 and Table 4.182), "as-is" under dark conditions (Figure 4.284 and Table 4.190), and following photolysis of organic matter conditions (Figure 4.290 and Table 4.198), an identical approach was followed for elucidation of sedimentation behavior of "Fe-TiO_2 and HA" "as-is" under irradiation conditions.

Time dependent UV-vis absorbance variations in the overall spectra covering the wavelength range of 200-600 nm were presented (Figure 4.296a). Accordingly, respective normalized absorbance variations in the selected wavelengths were presented in Figure 4.296b. "Fe-TiO_2 and HA" binary system under "as-is" under irradiation exhibited quite similar tendency to "Fe-TiO_2 and HA" under "as-is" conditions and no direct effect of continuous mixing for 60 min could be observed excluding the initial absorbance recordings.

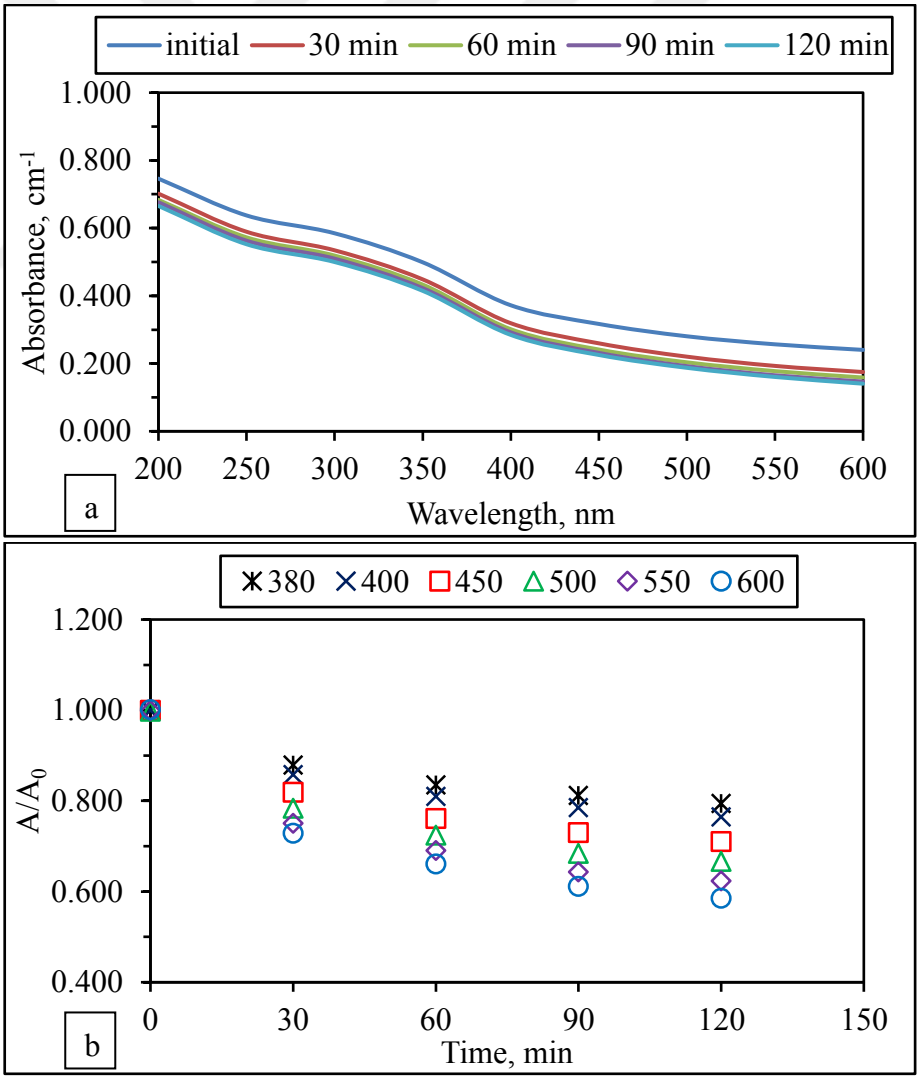


Figure 4.296. Sedimentation behavior of "Fe-TiO_2 and HA" "as-is" under irradiation, a) UV-vis absorbance variations b) Normalized absorbance with respect to time.

Time dependent variations in UV-vis absorbance spectral features were distinctly different than the spectral features obtained upon dark conditions revealing the significant effect of irradiation. Both kinetic models were applied revealing considerably high correlation coefficients as $R^2 > 0.796$ and kinetic constants were tabulated (Figure 4.296b and Table 4.206).

Table 4.206. "Fe-TiO_2 and HA" "as-is" under irradiation, kinetic model parameters.

Kinetic model	Wavelength, nm					
	380	400	450	500	550	600
Exponential model						
k, min^{-1}	1.80×10^{-3}	2.08×10^{-3}	2.66×10^{-3}	3.14×10^{-3}	3.65×10^{-3}	4.16×10^{-3}
R^2	0.864	0.858	0.848	0.842	0.841	0.852
Linear model						
k, min^{-1}	1.60×10^{-3}	1.81×10^{-3}	2.23×10^{-3}	2.54×10^{-3}	2.86×10^{-3}	3.16×10^{-3}
R^2	0.843	0.833	0.816	0.804	0.796	0.800

Exponential model expressed kinetic constants (min^{-1}) in a decreasing order as $4.16 \times 10^{-3} > 3.65 \times 10^{-3} > 3.14 \times 10^{-3} > 2.66 \times 10^{-3} > 2.08 \times 10^{-3} > 1.80 \times 10^{-3}$ for wavelengths of 600 nm, 550 nm, 500 nm, 450 nm, 400 nm, and 380 nm, respectively. Simply an average value of $k = 2.92 \times 10^{-3}$ min^{-1} could be regarded as suitable for expressing sedimentation kinetics using an exponential model. The average value resembled to the $k=3.14 \times 10^{-3}$ min^{-1} that was calculated from the data attained by absorbance recordings at λ= 500 nm.

In a similar manner, the linear trend as visualized by the decreasing trend of A/A_o revealed kinetic constants (min^{-1}) in a decreasing order as $3.16 \times 10^{-3} > 2.86 \times 10^{-3} > 2.54 \times 10^{-3} > 2.23 \times 10^{-3} > 1.81 \times 10^{-3} > 1.60 \times 10^{-3}$ for wavelengths of 600 nm, 550 nm, 500 nm, 450 nm, 400 nm, and 380 nm, respectively. As expressed above an average of $k=2.37 \times 10^{-3}$ min^{-1} could be accepted as appropriate for demonstrating sedimentation kinetics using a linear model. The average value resembled to the linear model kinetic constants calculated from the data attained by absorbance recordings at λ=450 nm and 500 nm.

Under the specified conditions represented by selected wavelengths, it could be concluded that upon 30 min experimental duration, ~ 15 % removal at λ=380 nm and ~ 25 % at λ=600 nm was observed. Upon 60 min duration approximately 35 % removal was recorded at λ=600 nm. Further increase in experimental duration did not significantly affect the removal percentage of "Fe-TiO_2 and HA" "as-is" under irradiation reaching to slightly lower values. Correspondingly, upon 120 min experimental duration 15 % removal at λ=380 nm and roughly 40 % removal at λ=600 nm were observed.

4.2.16.6. "Fe-TiO_2 and SRNOM" binary system "as-is" under irradiation. In a similar fashion to "Fe-TiO_2 and SRNOM" under "as-is" conditions (Figure 4.279 and Table 4.183), "as-is" under dark conditions (Figure 4.285 and Table 4.191), and following photolysis of organic matter conditions (Figure 4.291 and Table 4.199), a similar approach was followed for elucidation of sedimentation behavior of "Fe-TiO_2 and SRNOM" "as-is" under irradiation. Contrary to the initial mixing period of "TiO_2 and SRNOM" and "N-TiO_2 and SRNOM", an initial mixing period of 60 min was subjected for "Fe-TiO_2 and SRNOM" binary system "as-is" under irradiation.

Time dependent UV-vis absorbance variations in the overall spectra covering the wavelength range of 200-600 nm were presented in Figure 4.297a. Correspondingly, respective normalized absorbance values in the selected wavelength range of 380-600 nm were demonstrated in Figure 4.297b.

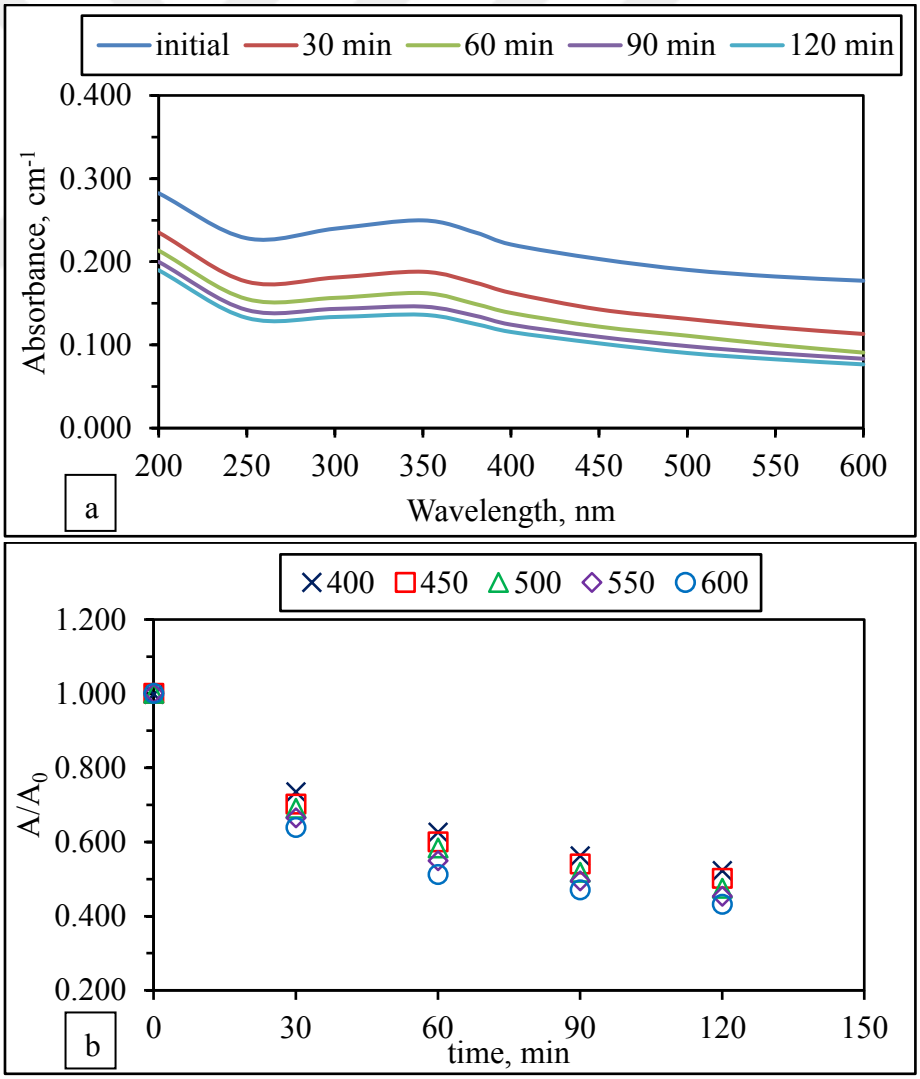


Figure 4.297. Sedimentation behavior of "Fe-TiO_2 and SRNOM" "as-is" under irradiation, a) UV-vis absorbance variations b) Normalized absorbance with respect to time.

The variations were modeled by two approaches depending on the decreasing trend profiles. Exponential and linear models were applied and sedimentation kinetic constants were presented in Figure 4.297b and Table 4.207. Due to the observed inconsistency absorbance recordings at λ=380 nm were excluded. Both exponential and linear modeling revealed considerably high correlation coefficients as $R^2 > 0.796$.

Table 4.207. "Fe-TiO_2 and SRNOM" "as-is" under irradiation, kinetic model parameters.

Kinetic model	Wavelength, nm				
	400	450	500	550	600
Exponential model					
k, min^{-1}	5.21×10^{-3}	5.48×10^{-3}	5.92×10^{-3}	6.26×10^{-3}	6.61×10^{-3}
R^2	0.922	0.901	0.913	0.893	0.871
Linear model					
k, min^{-1}	3.75×10^{-3}	3.87×10^{-3}	4.08×10^{-3}	4.22×10^{-3}	4.35×10^{-3}
R^2	0.869	0.839	0.847	0.821	0.796

Exponential model kinetics expressed constants (min^{-1}) in a decreasing order as $6.61 \times 10^{-3} > 6.26 \times 10^{-3} > 5.92 \times 10^{-3} > 5.48 \times 10^{-3} > 5.21 \times 10^{-3}$ for wavelengths of 600 nm, 550 nm, 500 nm, 450 nm, and 400 nm, respectively. Kinetic constants followed a continuously increasing trend with respect to increasing detection wavelengths. An average value of $k=5.90 \times 10^{-3}$ min^{-1} could be regarded as adequate for expressing sedimentation kinetics using the exponential model. The average value resembled to the $k=5.92 \times 10^{-4}$ min^{-1} that was calculated for λ=500 nm.

Linear trend as visualized by the decreasing trend of normalized absorbance recordings as A/A_o revealed kinetic constants (min^{-1}) in a decreasing order as $4.35 \times 10^{-3} > 4.22 \times 10^{-3} > 4.08 \times 10^{-3} > 3.87 \times 10^{-3} > 3.75 \times 10^{-3}$ for wavelengths of 600 nm, 550 nm, 500 nm, 450 nm, and 400 nm, respectively. As expressed above an average of $k=4.05 \times 10^{-3}$ min^{-1} could be accepted as suitable for displaying sedimentation kinetics using the linear model. The average value as $k=4.05 \times 10^{-3}$ min^{-1} could well be regarded as similar to the rate constant obtained by absorbance recordings at λ=500 nm.

Under the specified conditions represented by selected wavelengths, it could be concluded that upon 30 min duration, ~ 25 % removal at λ=400 nm and ~ 35 % at λ=600 nm was monitored. However, upon further experimental duration of 90 min, roughly 45 % removal at λ=400 nm and 50 % at λ=600 nm was obtained. Upon 120 min of duration ~ 50 % removal at λ=400 nm and ~ 55 % removal at λ=600 nm were observed. It could also be concluded that both models could be successfully applied due to slight incremental decreases with respect to time.

4.2.17. Comparative Evaluation of Exponential and Linear Models of "TiO_2 and HA", "N-TiO_2 and HA", "Fe-TiO_2 and HA" "as-is" under irradiation Conditions

Regarding the presented data for all of the NPs under "as-is" under irradiation conditions, although similar sedimentation profiles were attained, a comparative evaluation could be convenient in clarification of the sample specific variations for suitability of application of UV-vis spectroscopic technique. To fulfill this purpose, kinetic model parameters attained at the selected indicative wavelength as λ=550 nm were compiled from tables 4.202-4.206 and presented in Table 4.208.

Table 4.208. Comparative presentation of sedimentation kinetics of NPs under "as-is" irradiation conditions at λ=550 nm.

Kinetic model	Exponential model	
NP "as-is"	k, min^{-1}	R^2
"TiO_2 and HA"	2.53 x 10^{-3}	0.984
"N-TiO_2 and HA"	3.83 x 10^{-3}	0.859
"Fe-TiO_2 and HA"	3.65 x 10^{-3}	0.841
	Linear model	
	k, min^{-1}	R^2
"TiO_2 and HA"	2.17 x 10^{-3}	0.971
"N-TiO_2 and HA"	2.96 x 10^{-3}	0.810
"Fe-TiO_2 and HA"	2.86 x 10^{-3}	0.796

Sedimentation behavior of "TiO_2 and HA", "N-TiO_2 and HA", and "Fe-TiO_2 and HA" "as-is" under irradiation was fitted to the exponential kinetic equation and gave the following reaction rate constants (min^{-1}) as 3.83 x 10^{-3} for "N-TiO_2 and HA" > 3.65 x 10^{-3} for "Fe-TiO_2 and HA" > 2.53 x 10^{-3} for "TiO_2 and HA" (Table 4.208). However, when sedimentation behavior of "TiO_2 and HA", "N-TiO_2 and HA", and "Fe-TiO_2 and HA" binary systems were fitted to the linear model, reactions rate constants (min^{-1}) were found as 2.96 x 10^{-3} for "N-TiO_2 and HA" > 2.86 x 10^{-3} for "Fe-TiO_2 and HA" > 2.17 x 10^{-3} for "TiO_2 and HA" (Table 4.208). A simple comparison to "as-is" under dark conditions (Table 4.192) indicated that slightly higher kinetic constants were attained for NPs "as-is under irradiation" (Table 4.208). Application of exponential model indicated preferential stability of "TiO_2 and HA" in comparison to "N-TiO_2 and HA" and "Fe-TiO_2 and HA", as also supported by linear modeling with minor differences. From a general perspective, both kinetic models revealed similar tendencies as observed for "as-is" and "as-is" under dark conditions. The role of continuous mixing under irradiation prior to absorbance recordings could be related to the possible disaggregation of the NPs in comparison to the applied sonication and magnetic stirring for a short duration of NP samples prepared under "as-is" conditions and a constant mixing for 60 min under dark conditions.

4.2.18. Comparative Evaluation of Exponential and Linear Models of "TiO_2 and SRNOM", "N-TiO_2 and SRNOM", "Fe-TiO_2 and SRNOM" "as-is" under irradiation Conditions

Dependent on the presented data for all of the binary systems under as-is conditions, although similar sedimentation profiles were obtained, a comparative evaluation was performed to elucidate the system specific variations for suitability of application of UV-vis spectroscopic technique. To this end, kinetic model parameters attained at selected indicative wavelength of λ=550 nm were compiled from tables 4.203-4.207 and presented in Table 4.209.

Table 4.209. Comparative presentation of sedimentation kinetics of NPs under "as-is" irradiation conditions at λ=550 nm.

Kinetic model	Exponential model	
NP "as-is" under irradiation	k, min^{-1}	R^2
"TiO_2 and SRNOM"	1.07×10^{-2}	0.936
"N-TiO_2 and SRNOM"	4.00×10^{-3}	0.877
"Fe-TiO_2 and SRNOM"	6.26×10^{-3}	0.893
	Linear model	
	k, min^{-1}	R^2
"TiO_2 and SRNOM"	6.15×10^{-3}	0.898
"N-TiO_2 and SRNOM"	3.08×10^{-3}	0.830
"Fe-TiO_2 and SRNOM"	4.22×10^{-3}	0.821

Sedimentation behavior of "TiO_2 and SRNOM", "N-TiO_2 and SRNOM", and "Fe-TiO_2 and SRNOM" "as-is" under irradiation in the presence of organic matter was fitted to the exponential kinetic equation and gave the following reaction rate constants (min^{-1}) as 1.07×10^{-2} for "TiO_2 and SRNOM" > 6.26×10^{-3} for "Fe-TiO_2 and SRNOM" > 4.00×10^{-3} for "N-TiO_2 and SRNOM" (Table 4.209). However, when sedimentation behavior of "TiO_2 and SRNOM", "N-TiO_2 and SRNOM", and "Fe-TiO_2 and SRNOM" binary systems were fitted to the linear model, reactions rate constants (min^{-1}) were found as 6.15×10^{-3} for "TiO_2 and SRNOM" > 4.22×10^{-3} for "Fe-TiO_2 and SRNOM" > 3.08×10^{-3} for "N-TiO_2 and SRNOM" (Table 4.209).

A simple comparison to "as-is" conditions (Table 4.185) indicated that higher kinetic constants were obtained. However, a simple comparison to "as-is" under dark conditions (Table 4.193) displayed that substantially higher kinetic constants were attained for NPs "as-is" under irradiation. Application of exponential model indicated preferential stability of "TiO_2 and SRNOM" in comparison to "N-TiO_2 and SRNOM" and "Fe-TiO_2 and SRNOM", as also supported by linear modeling with minor differences. From a general perspective, both kinetic models revealed similar tendencies as observed for "as-is" and "as-is" under dark conditions.

4.3. Behavior of Nanoparticles as TiO_2, N-TiO_2, and Fe-TiO_2 under "as-is", "as-is" dark, and "as-is" irradiation Conditions in the Absence of Organic Matter

For comparison purposes, the elucidation of the particle size dynamics of the nanoparticles were compiled from the data presented in previous parts and presented separately under specific sub-headings *i.e.* TiO_2, N-TiO_2, and Fe-TiO_2. Basically, data represented time dependent hydrodynamic size variations, sedimentation kinetics and turbidity profiles under "as-is", "as-is" under dark, and "as-is" under irradiation conditions.

4.3.1. Behavior of TiO_2 under "as-is", "as-is dark", and "as-is irradiation" Conditions

Hydrodynamic size variations of TiO_2 under "as-is", "as-is dark" and "as-is irradiation" conditions were displayed in Figure 4.298. Under initial conditions, hydrodynamic sizes were 439.6 nm, 434.2 nm and 417.4 nm for mono system of TiO_2 designated as TiO_2 under "as-is" conditions, TiO_2 "as-is" under dark conditions, TiO_2 "as-is" under irradiation, respectively. Since no treatment was applied, the average hydrodynamic size could be accepted as 430.4 nm.

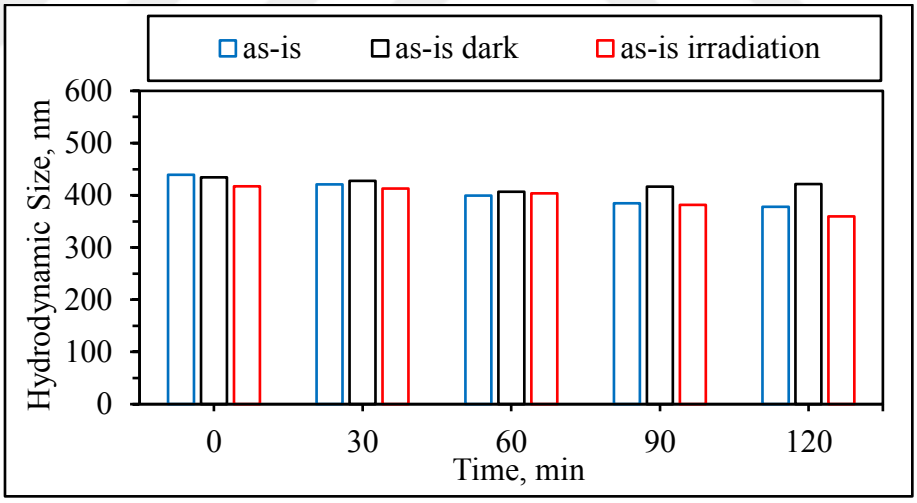


Figure 4.298. Hydrodynamic size variations of TiO_2 under "as-is", "as-is dark" and "as-is irradiation" conditions.

Upon treatment periods of 30 min and 60 min, no significant variations were attained under different conditions. However, alterations in hydrodynamic sizes became evident upon treatment period of 90 min and even slightly more apparent following a decreasing order of TiO_2 "as-is" under dark conditions > TiO_2 under "as-is" conditions > TiO_2 "as-is" under irradiation. Therefore, upon dark conditions *i.e.* continuously stirred sample for 60 min affected the particle size distribution of TiO_2 resulting in an average hydrodynamic size as 421.3 ± 10.5 nm. On the other hand, sample prepared

upon irradiation revealed an average hydrodynamic size as 404.0 ± 24.1 nm. However, TiO_2 under "as-is" conditions displayed an average hydrodynamic size as 399.2 ± 25.6 nm.

In a similar manner, sedimentation tendency profiles were presented in Figure 4.299. TiO_2 "as-is" under irradiation exhibited the most distinct decreasing trend along 120 min. Variations in sedimentation of TiO_2 under different conditions could be aligned in the order of TiO_2 "as-is" under irradiation > TiO_2 under "as-is" conditions > TiO_2 "as-is" under dark conditions. Turbidity variations of TiO_2 under the specified conditions reacted variously with respect to time (Figure 4.300). Alterations in turbidity of TiO_2 under different conditions decreased in the following order of TiO_2 "as-is" under irradiation > TiO_2 under "as-is" conditions > TiO_2 "as-is" under dark conditions.

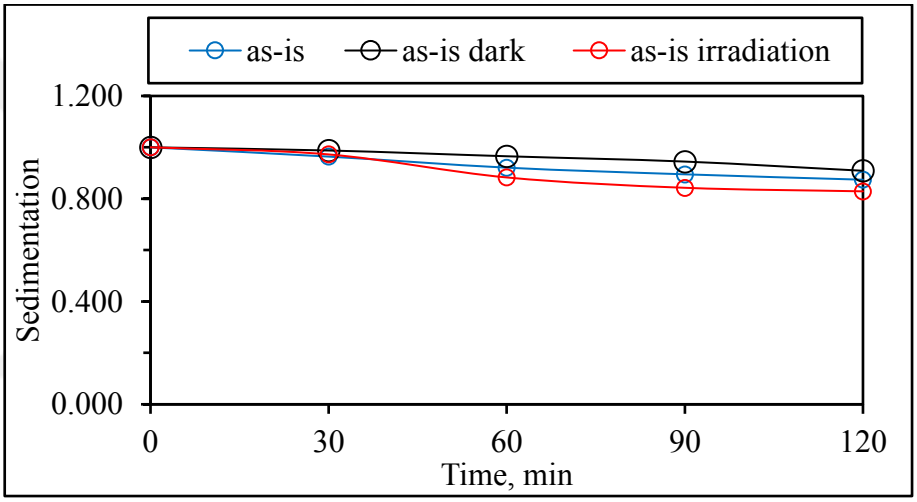


Figure 4.299. Sedimentation profiles of TiO_2 under "as-is", "as-is dark" and "as-is irradiation" conditions.

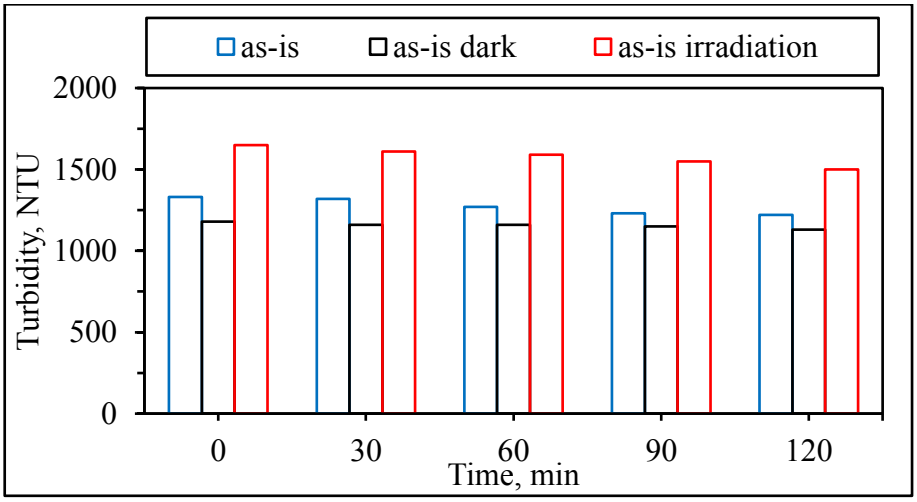


Figure 4.300. Turbidity profiles of TiO_2 under "as-is", "as-is dark" and "as-is irradiation" conditions.

4.3.1.1. Comparative evaluation of selected parameters as hydrodynamic size, hydrodynamic size difference, sedimentation and turbidity variations of TiO_2 under "as-is", "as-is" dark, and "as-is" irradiation conditions. For comparison purposes and with reference to the selected parameters as hydrodynamic size, hydrodynamic size difference, sedimentation and turbidity variations, the data attained for each NP were presented in the following figures 4.301-4.303 for TiO_2, N-TiO_2 and Fe-TiO_2 respectively. Comparative evaluation of selected parameters as hydrodynamic size, hydrodynamic size difference, sedimentation and turbidity variations of TiO_2 under "as-is" conditions was demonstrated in Figure 4.301. It could be asserted that TiO_2 under "as-is" conditions displayed a consistent slightly decreasing trend for all of the parameters during the whole span of the experiment. The observed non-different trend could only indicate the stability of the system composed of sole TiO_2 in aqueous medium in the absence of any interfering substances disturbing the colloidal stability.

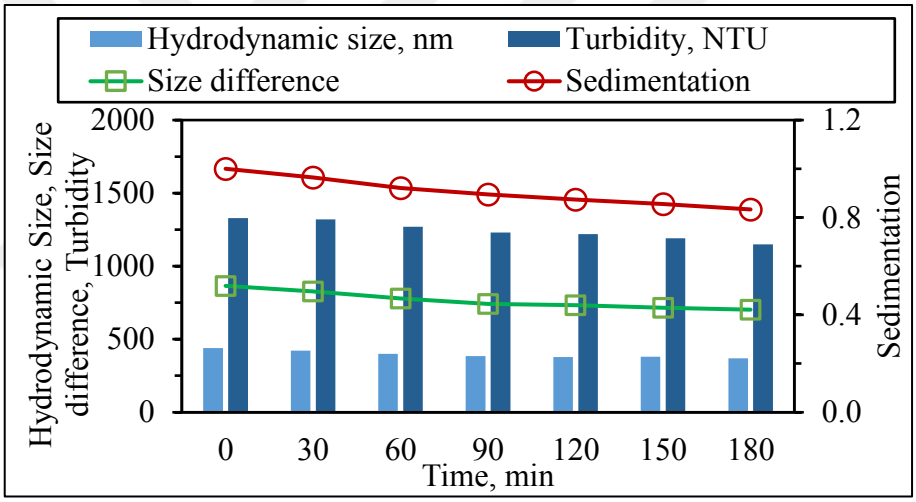


Figure 4.301. TiO_2 under "as-is" conditions. Comparative evaluation of selected parameters as hydrodynamic size, hydrodynamic size difference, sedimentation and turbidity variations.

Comparative evaluation of selected parameters as hydrodynamic size, hydrodynamic size difference, sedimentation and turbidity variations of TiO_2 "as-is" under dark conditions was demonstrated in Figure 4.302. It could be deduced that continuous mixing provided under dark distinctly affected the behavior of all parameters of TiO_2 under "as-is" conditions (Figure 4.301). The most significant variation was observed in sedimentation behavior that could be related to the disaggregation of the previously aggregated particles upon treatment of 60 min. However, this phenomenon was not supported by the other parameters that could also be expressed by light absorption as well as scattering of the aggregated particles. Hydrodynamic size difference remained almost similar under dark conditions in comparison to decreasing trend attained for TiO_2 under "as-is" conditions.

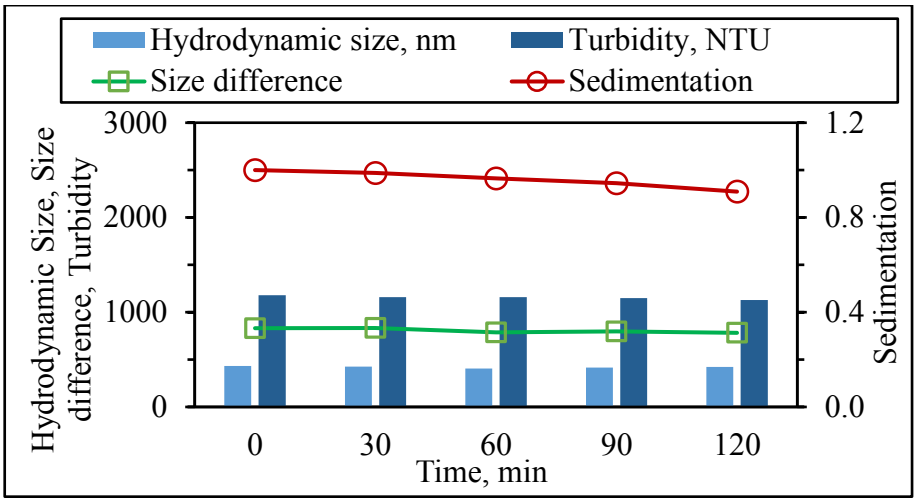


Figure 4.302. TiO_2 "as-is" under dark conditions. Comparative evaluation of selected parameters as hydrodynamic size, hydrodynamic size difference, sedimentation and turbidity variations.

Comparative evaluation of selected parameters as hydrodynamic size, hydrodynamic size difference, sedimentation and turbidity variations of TiO_2 "as-is" under irradiation conditions was presented in Figure 4.303. It could be inferred that the effect of mixing under irradiation was significantly different than the mixing under dark conditions.

From a general view, due to light absorption of TiO_2 NPs, particle-particle attractions could be significantly affected resulting in various photochemical reactions occurring in solution. Depending on the E_{bg} energies (Table A) of the NPs acting as photocatalysts, formation of various reactive species could directly affect the surface interactions via photochemical reactions depending on the type of the dopant.

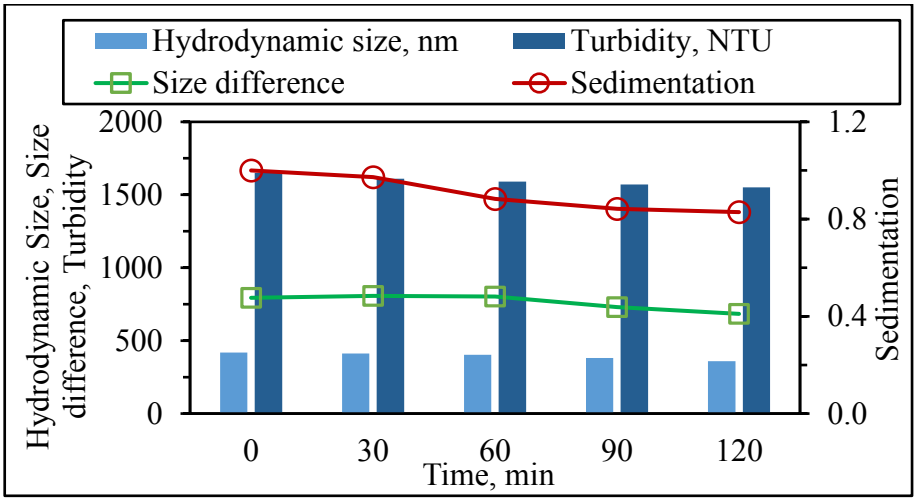


Figure 4.303. TiO_2 "as-is" under irradiation. Comparative evaluation of selected parameters as hydrodynamic size, hydrodynamic size difference, sedimentation and turbidity variations.

4.3.2. Behavior of N-TiO_2 under "as-is", "as-is" dark, and "as-is" irradiation Conditions

As explained for TiO_2 under "as-is", "as-is" dark, and "as-is" irradiation conditions (Section 4.3.1), a similar approach was followed for behavior of N-TiO_2 under "as-is", "as-is" dark, and "as-is" irradiation conditions. Hydrodynamic size variations of N-TiO_2 under "as-is", "as-is dark" and "as-is irradiation" conditions were exhibited in Figure 4.304. Hydrodynamic sizes of N-TiO_2 under different conditions behaved differently with respect to time. Variations in hydrodynamic sizes of N-TiO_2 under different conditions could be arrayed in the decreasing order of N-TiO_2 "as is" under irradiation > N-TiO_2 under "as-is" conditions > N-TiO_2 "as-is" under dark conditions. The most significant variation in terms of hydrodynamic sizes was observed for N-TiO_2 "as-is" under irradiation upon period of 120 min. It could be concluded that solar irradiation enhanced hydrodynamic sizes when compared to as is and as is dark conditions.

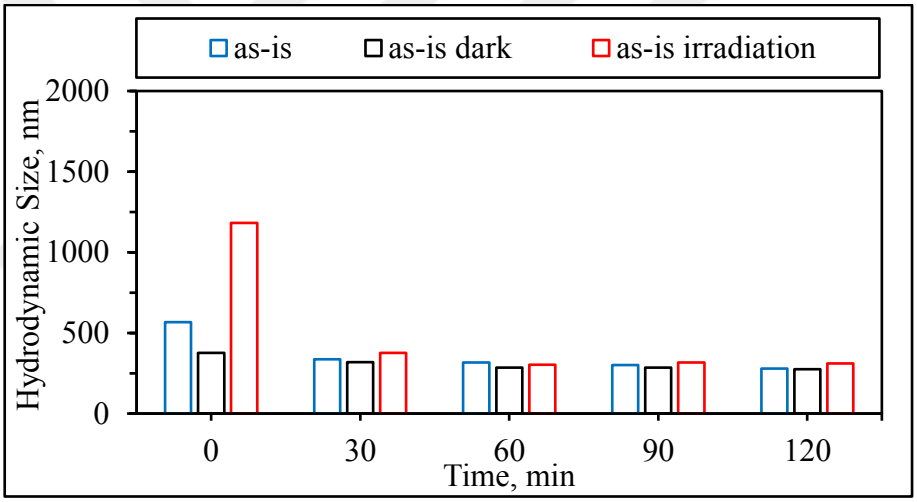


Figure 4.304. Hydrodynamic size variations of N-TiO_2 under "as-is", "as-is dark" and "as-is irradiation" conditions.

In a similar manner to data described TiO_2 under "as-is", "as-is" dark and "as-is" irradiation conditions (Figure 4.299), time dependent sedimentation profiles of N-TiO_2 under "as-is", "as-is" dark and "as-is" irradiation conditions were displayed in Figure 4.305. Alterations in sedimentation of N-TiO_2 aggregates under different conditions demonstrated similar trends over period of 120 min. Based on the presented data, it could be inferred that N-TiO_2 "as-is" under irradiation illustrated the most distinct decreasing trend at the end of the period. Accordingly, variations in sedimentation of N-TiO_2 under different conditions could be sorted in the decreasing order of N-TiO_2 "as-is" under irradiation > N-TiO_2 under "as-is" conditions > N-TiO_2 "as-is" under dark conditions. Therefore, it could be concluded that hydrodynamic size and sedimentation tendency profiles coincide with each other. For comparison purposes, it could be inferred that sedimentation profiles of TiO_2 under "as-

is", "as-is" dark and "as-is" irradiation conditions (Figure 4.299) and N-TiO_2 under "as-is", "as-is" dark and "as-is" irradiation conditions revealed similar tendencies over 120 min period.

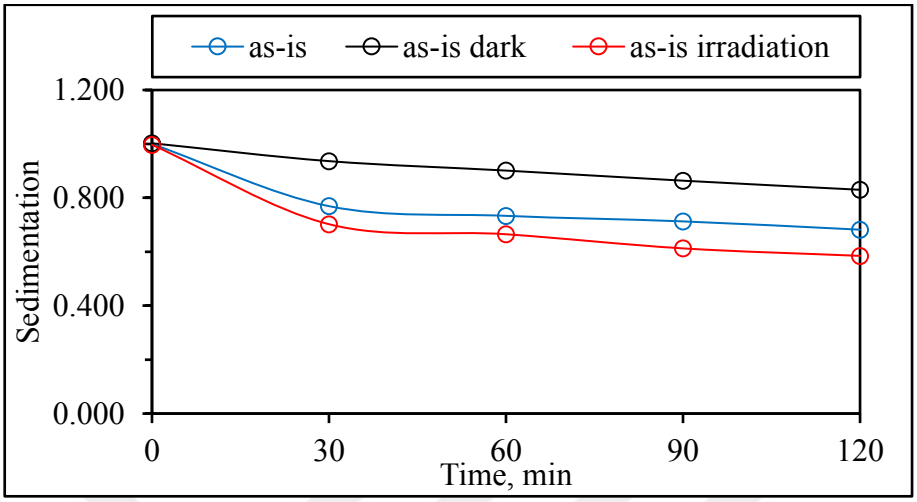


Figure 4.305. Sedimentation profiles of N-TiO_2 under "as-is", "as-is dark" and "as-is irradiation" conditions.

Following a similar manner, turbidity profiles of N-TiO_2 under "as-is", "as-is" dark and "as-is" irradiation conditions were exhibited in Figure 4.306. Based on the presented data, turbidity alterations of N-TiO_2 under different conditions displayed different behavior with respect to 120 min. Variations in turbidity of N-TiO_2 under different conditions decreased in the following order of N-TiO_2 under "as-is" conditions > N-TiO_2 "as-is" under irradiation > N-TiO_2 "as-is" under dark conditions. It could be concluded that the most significant alteration was monitored for N-TiO_2 under "as-is" conditions during 120 min period.

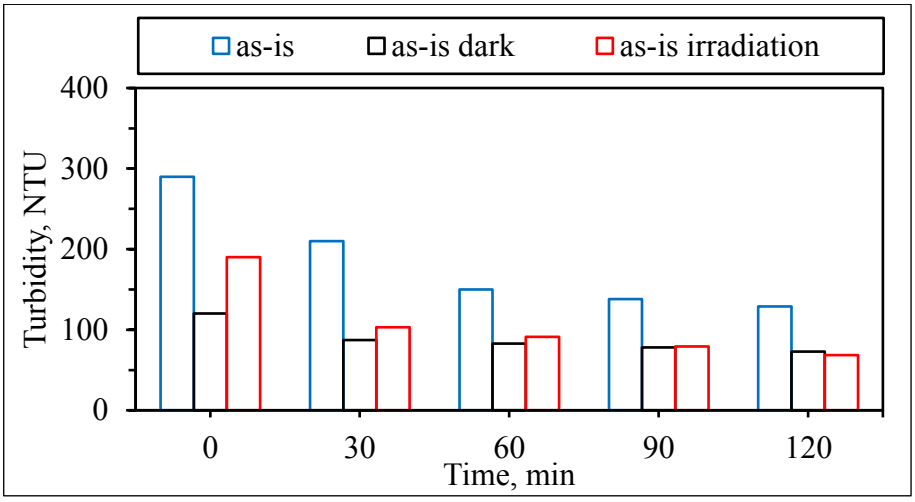


Figure 4.306. Turbidity profiles of N-TiO_2 under "as-is", "as-is dark" and "as-is irradiation" conditions.

4.3.2.1. Comparative evaluation of selected parameters as hydrodynamic size, hydrodynamic size difference, sedimentation and turbidity variations of N-TiO_2 under "as-is", "as-is" dark, and "as-is" irradiation conditions. As elucidated for N-TiO_2 under "as-is", "as-is" dark, and "as-is" irradiation conditions (Section 4.3.1.1), comparative evaluation of selected parameters as hydrodynamic size, hydrodynamic size difference, sedimentation and turbidity variations of N-TiO_2 under "as-is", "as-is" dark, and "as-is" irradiation conditions was presented in 4.307. It could be inferred that N-TiO_2 NP displayed comparatively lower turbidity values in relation to hydrodynamic size variations. Fluctuations could be observed in hydrodynamic size differences in accordance with the variations in the range although an average hydrodynamic size was attained as 341.2 ± 101.6 nm. Sedimentation profiles followed a similar trend to hydrodynamic size changes.

For comparison purposes, it should also be mentioned that primary particle size of TiO_2 was ~30 nm and N-TiO_2 was ~20 nm. However, aggregate sizes could be visualized as 439.6 nm and 567.9 nm for TiO_2 and N-TiO_2, respectively. The dominant effect could be related to the pH_{zpc} condition as 6.25 and 5.15 for TiO_2 and N-TiO_2, respectively (Table A). Correspondingly, it should be expressed that surface dominated electrostatic attractions could affect the interactions leading to aggregation formation.

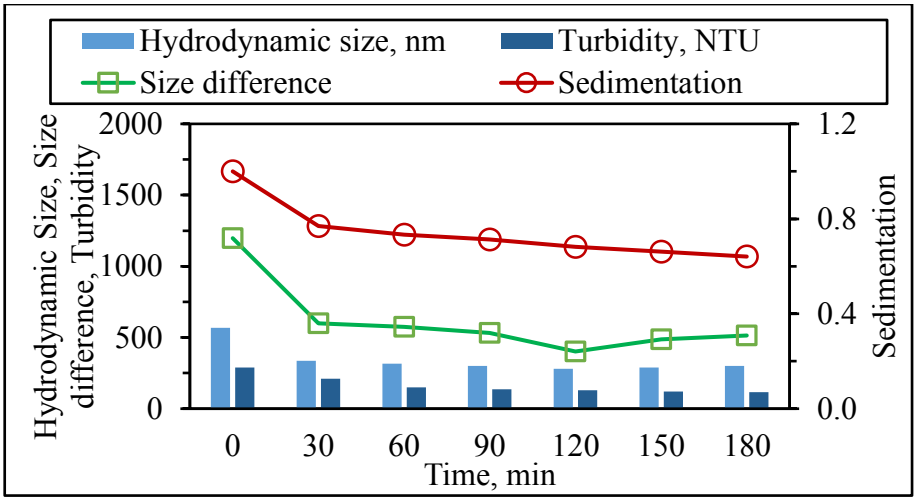


Figure 4.307. N-TiO_2 under "as-is" conditions. Comparative evaluation of selected parameters as hydrodynamic size, hydrodynamic size difference, sedimentation and turbidity variations.

Following a similar manner, comparative evaluation of selected parameters as hydrodynamic size, hydrodynamic size difference, sedimentation and turbidity variations of N-TiO_2 "as-is" under dark conditions was demonstrated in Figure 4.308. Under dark conditions, continuous mixing affected N-TiO_2 more significantly in hydrodynamic size difference trend in comparison to continuously

decreasing sedimentation profile. However, slight hydrodynamic size and turbidity variations could not be supported by sedimentation profiles.

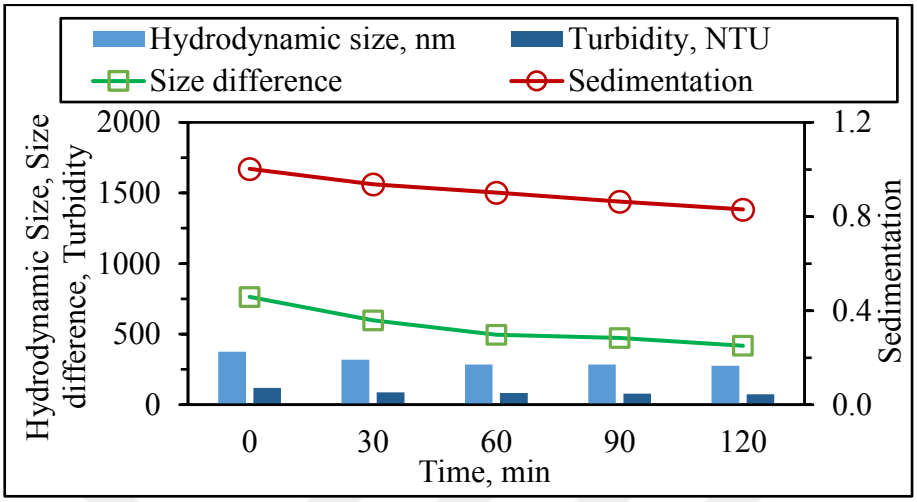


Figure 4.308. N-TiO_2 "as is" under dark conditions. Comparative evaluation of selected parameters as hydrodynamic size, hydrodynamic size difference, sedimentation and turbidity variations.

Likewise expressed so far, comparative evaluation of selected parameters as hydrodynamic size, hydrodynamic size difference, sedimentation and turbidity variations of N-TiO_2 "as-is" under irradiation was also displayed in Figure 4.309. Based on the presented data, it could be asserted that under the specified conditions, size difference revealed drastic changes in comparison to sedimentation profile with respect to time. On the other hand, it could be deduced that hydrodynamic size variations could be supported by sedimentation profiles whereas turbidity alterations did not demonstrate a similar trend upon period of 120 min. Also, minor turbidity values were attained when compared to hydrodynamic size variations along 120 min.

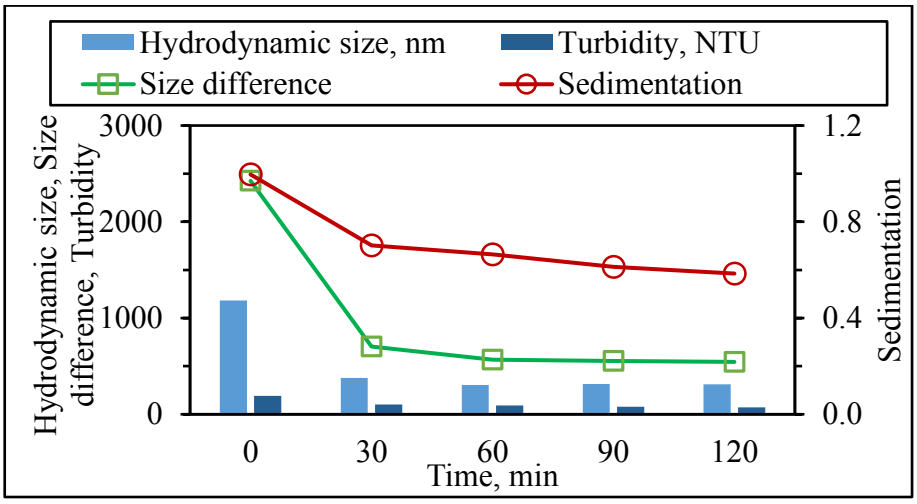


Figure 4.309. N-TiO_2 "as-is" under irradiation. Comparative evaluation of selected parameters as hydrodynamic size, hydrodynamic size difference, sedimentation and turbidity variations.

4.3.3. Behavior of Fe-TiO_2 under "as-is", "as-is" dark, and "as-is" irradiation Conditions

As described for TiO_2 under "as-is", "as-is" dark, and "as-is" irradiation conditions (Section 4.3.1) and N-TiO_2 under "as-is", "as-is" dark, and "as-is" irradiation conditions (Section 4.3.2), a similar approach was followed for behavior of Fe-TiO_2 under "as-is", "as-is" dark, and "as-is" irradiation conditions. Alterations in hydrodynamic sizes of Fe-TiO_2 under different conditions could be arranged in the decreasing order of Fe-TiO_2 "as-is" under irradiation > Fe-TiO_2 under "as-is" conditions > Fe-TiO_2 "as-is" under dark conditions (Figure 4.310). It could be asserted that sample prepared upon irradiation revealed higher hydrodynamic sizes in comparison to Fe-TiO_2 under "as-is" conditions and Fe-TiO_2 "as-is" under dark conditions.

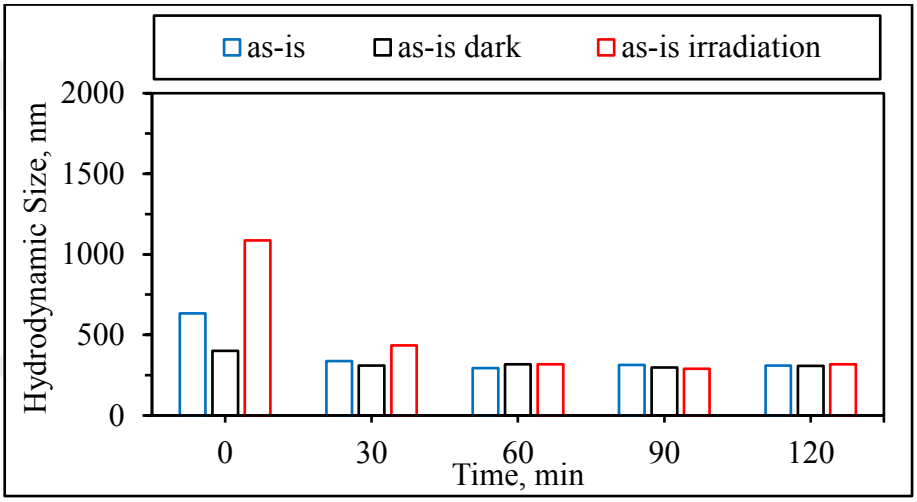


Figure 4.310. Hydrodynamic size variations of Fe-TiO_2 under "as-is", "as-is" dark and "as-is" irradiation conditions.

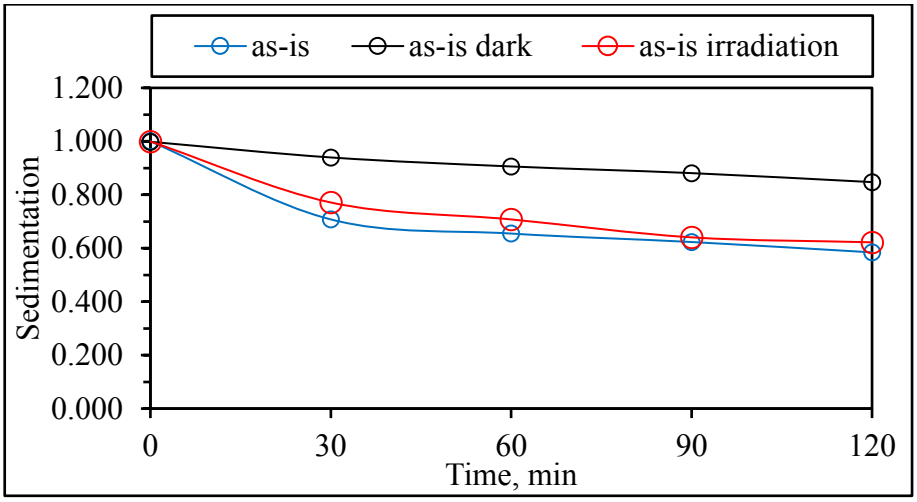


Figure 4.311. Sedimentation profiles of Fe-TiO_2 under "as-is", "as-is" dark and "as-is" irradiation conditions.

On the other hand, sedimentation profiles of Fe-TiO_2 under “as-is”, “as-is” dark and “as-is” irradiation conditions were demonstrated in Figure 4.311. It could be inferred that Fe-TiO_2 under “as-is” conditions and Fe-TiO_2 “as-is” under irradiation exhibited similar sedimentation tendency profiles whereas Fe-TiO_2 “as-is” under dark conditions revealed comparatively lower sedimentation tendency profile upon period of 120 min. As presented above, sedimentation profiles of Fe-TiO_2 specimens under different conditions could be aligned in the decreasing order of Fe-TiO_2 under “as-is” conditions > Fe-TiO_2 “as-is” under irradiation > Fe-TiO_2 “as-is” under dark conditions.

In a similar manner, turbidity profiles of Fe-TiO_2 under “as-is”, “as-is” dark and “as-is” irradiation conditions were demonstrated in Figure 4.312. It could be asserted that variations in turbidity profiles of Fe-TiO_2 under different conditions could be sorted in the decreasing order of Fe-TiO_2 under “as-is” conditions > Fe-TiO_2 “as-is” under irradiation > Fe-TiO_2 “as-is” under dark conditions.

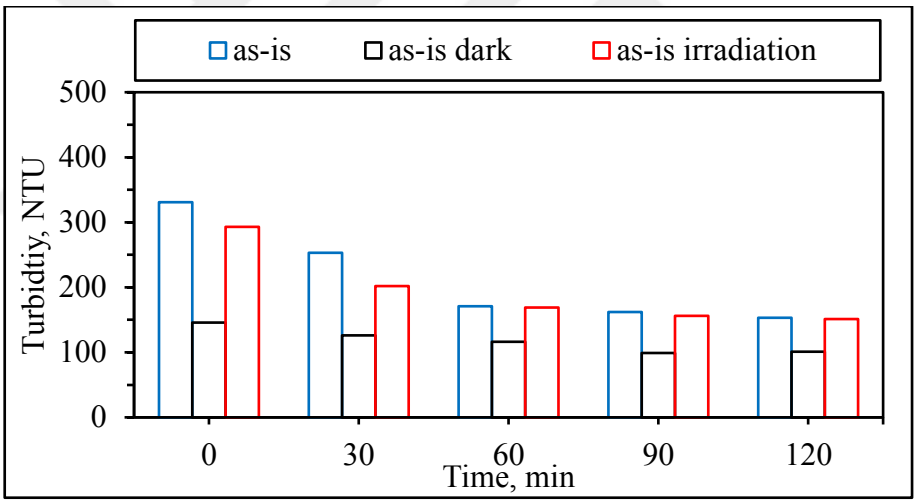


Figure 4.312. Turbidity profiles of Fe-TiO_2 under “as-is”, “as-is” dark and “as-is” irradiation conditions.

Fe-TiO_2 NPs expressed similar tendencies in all parameters in comparison to N-TiO_2 NPs. Turbidity values were all lower in accordance with the variations in hydrodynamic size differences whereas sedimentation profiles displayed a continuously decreasing trend as 45 % for Fe-TiO_2 being slightly higher than N-TiO_2 although almost half of these values as 20 % decrease were attained for sedimentation profile of TiO_2. The expected affect was more significant in N-TiO_2 and Fe-TiO_2 in comparison to sole TiO_2. More significantly turbidity changes were more affected by the presence of light resulting in comparatively lower values for N-TiO_2 in comparison to Fe-TiO_2. Under all conditions, sole TiO_2 displayed a sample specific tendency in all parameters.

4.3.3.1. Comparative evaluation of selected parameters as hydrodynamic size, hydrodynamic size difference, sedimentation and turbidity variations of Fe-TiO_2 under "as-is", "as-is" dark, and "as-is" irradiation conditions. From a general view, it could be stated that similar tendencies in all parameters were attained for both anion-doped TiO_2 as N-TiO_2 and cation as metal doped Fe-TiO_2 irrespective of the physicochemical parameters of these NPs (Table A). However, sole TiO_2 expressed a consistent stability behavior as shown in Figure 4.301. Comparative evaluation of selected parameters as hydrodynamic size, hydrodynamic size difference, sedimentation and turbidity variations of Fe-TiO_2 under "as-is", "as-is" dark, and "as-is" irradiation conditions was given in Figure 4.313. Relatively lower turbidity values were observed in comparison to hydrodynamic size variations. Although an average hydrodynamic size was obtained as 352.5 ± 125.2 nm, fluctuations could be monitored in hydrodynamic size differences in accordance with the variations in the range. Sedimentation profiles displayed a declining trend similar to hydrodynamic size changes with respect to time.

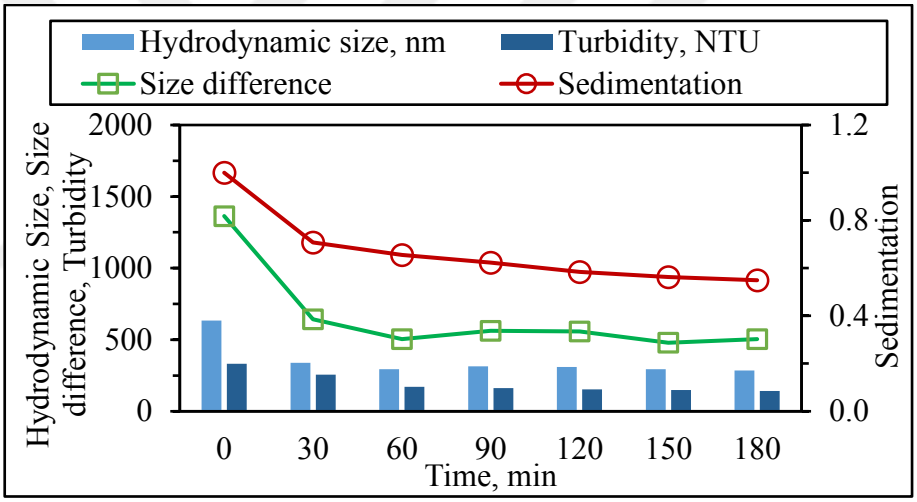


Figure 4.313. Fe-TiO_2 under "as-is" conditions. Comparative evaluation of selected parameters as hydrodynamic size, hydrodynamic size difference, sedimentation and turbidity variations.

Comparative evaluation of selected parameters as hydrodynamic size, hydrodynamic size difference, sedimentation and turbidity variations of Fe-TiO_2 "as-is" under dark conditions was given in Figure 4.314. Size difference followed a fluctuating trend similar to hydrodynamic size variations during 120 min. Turbidity values were attained comparatively lower than hydrodynamic size variations. Sedimentation profile revealed a continuously decreasing trend over period of 120 min. Also, comparative evaluation of selected parameters as hydrodynamic size, hydrodynamic size difference, sedimentation and turbidity variations of Fe-TiO_2 "as-is" under irradiation was exhibited in Figure 4.314. The most important change was observed in size difference upon treatment of 60 min. Solar irradiation affected Fe-TiO_2 more significantly in hydrodynamic size difference trend in comparison to continuously declining sedimentation profile.

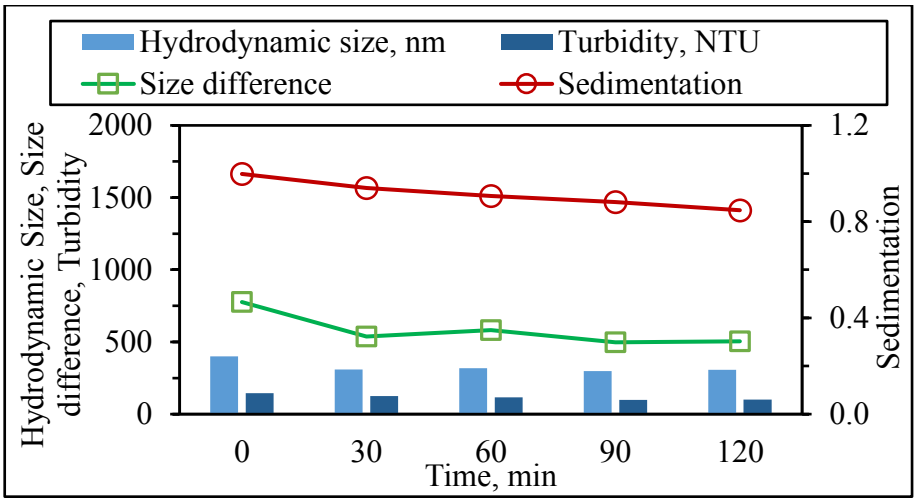


Figure 4.314. Fe-TiO_2 "as-is" under dark conditions. Comparative evaluation of selected parameters as hydrodynamic size, hydrodynamic size difference, sedimentation and turbidity variations.

The effect of continuous mixing could be accepted as more profound in Fe-TiO_2 displaying a similarity in all parameters in comparison to TiO_2 and N-TiO_2 under both "as-is" as well as "as-is" under dark conditions. From a general perspective, two main parameters as a hydrodynamic size and sedimentation profiles could not be regarded as surrogate parameters of aggregation that could be used for interchangeably understanding the system dynamics. Since these experiments were formed as baseline experiments for assessment of "binary systems under irradiation" as acting as true photocatalysis, sole particle behavior would be indicator of process efficiency.

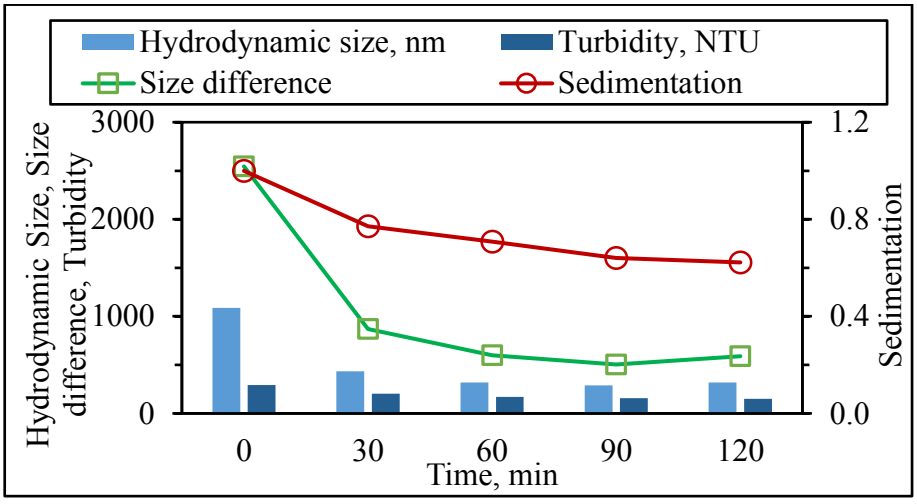


Figure 4.315. Fe-TiO_2 "as-is" under irradiation. Comparative evaluation of selected parameters as hydrodynamic size, hydrodynamic size difference, sedimentation and turbidity variations.

4.4. Behavior of Nanoparticles as TiO_2, N-TiO_2 and Fe-TiO_2 under "as-is", "as-is dark", "following photolysis of organic matter", and "as-is irradiation" Conditions in the Presence of Organic Matter

For comparison purposes, the elucidation of the particle size dynamics of the nanoparticles binary systems were compiled from the data presented in previous parts and presented separately under specific sub-headings *i.e.* TiO_2 and HA, TiO_2 and SRNOM, N-TiO_2 and HA, N-TiO_2 and SRNOM, Fe-TiO_2 and HA, Fe-TiO_2 and SRNOM. Basically, data represented time dependent hydrodynamic size variations, sedimentation kinetics and turbidity profiles under as-is; as-is under dark and as-is under irradiation conditions.

4.4.1. Behavior of "TiO_2 and HA" Binary System under "as-is", "as-is dark", "following photolysis of organic matter", and "as-is irradiation" Conditions

Hydrodynamic size variations of TiO_2 and HA binary system under "as-is", "as-is dark", "following photolysis of organic matter", and "as-is irradiation" conditions were presented in Figure 4.316. Under initial conditions, hydrodynamic sizes were 557.2 nm, 608.2 nm, 532.4 nm, and 1092.9 nm for binary system of TiO_2 and HA designated as "TiO_2 and HA" binary system under "as-is" conditions, "TiO_2 and HA" binary system "as-is" under dark conditions, "TiO_2 and HA_{pho}" binary system following photolysis of organic matter, "TiO_2 and HA" binary system "as-is" under irradiation, respectively. Since no treatment was applied, the average hydrodynamic size could be accepted as 697.7 nm.

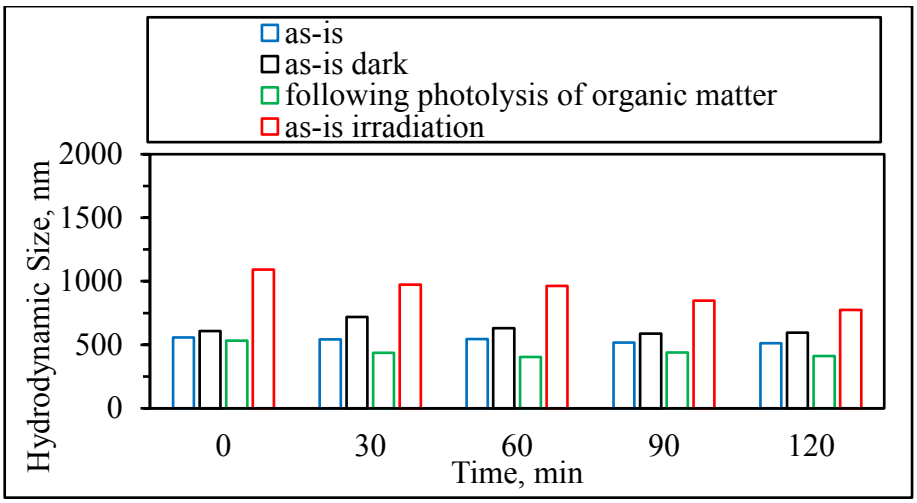


Figure 4.316. Hydrodynamic size variations of TiO_2 and HA binary system under "as-is", "as-is dark", "following photolysis of organic matter", and "as-is irradiation" conditions.

Upon treatment periods of 30 min and 60 min, no significant alterations were obtained under different conditions. However, variations in hydrodynamic sizes became evident upon treatment period of 90 min and even slightly more apparent following a decreasing order of "TiO_2 and HA" binary system "as-is under irradiation > "TiO_2 and HA" binary system "as-is" under dark conditions > "TiO_2 and HA" under "as-is" conditions > "TiO_2 and HA_{pho}" binary system following photolysis of organic matter. Upon dark conditions *i.e.* continuously stirred sample for 60 min affected the particle size distribution of TiO_2 and HA resulting in an average hydrodynamic size 628.3 ± 53.7 nm. "TiO_2 and HA_{pho}" binary system following photolysis of organic matter displayed an average hydrodynamic size as 444.8 ± 51.3 nm. On the other hand, sample prepared upon irradiation revealed an average hydrodynamic size as 930.7 ± 122.9 nm. However, "TiO_2 and HA" under "as-is" conditions demonstrated an average hydrodynamic size as 534.6 ± 19.2 nm. Therefore, it could be concluded that the biggest variance in terms of hydrodynamic size was monitored for "TiO_2 and HA" binary system "as-is" under irradiation over 120 min period.

Under similar experimental conditions, sedimentation tendency profiles were compiled and presented in Figure 4.317. Due to the fact that "TiO_2 and HA" binary system under "as-is" conditions and "TiO_2 and HA" binary system "as-is under dark" conditions revealed almost similar trends, "TiO_2 and HA_{pho}" binary system following photolysis of organic matter exhibited the most distinct decreasing trend over period of 120 min. Variations in sedimentation of TiO_2 and HA under different conditions could be arranged in the decreasing order of "TiO_2 and HA_{pho}" binary system following photolysis of organic matter > "TiO_2 and HA" binary system "as-is" under irradiation > "TiO_2 and HA" binary system "as-is" under dark conditions > "TiO_2 and HA" under "as-is" conditions.

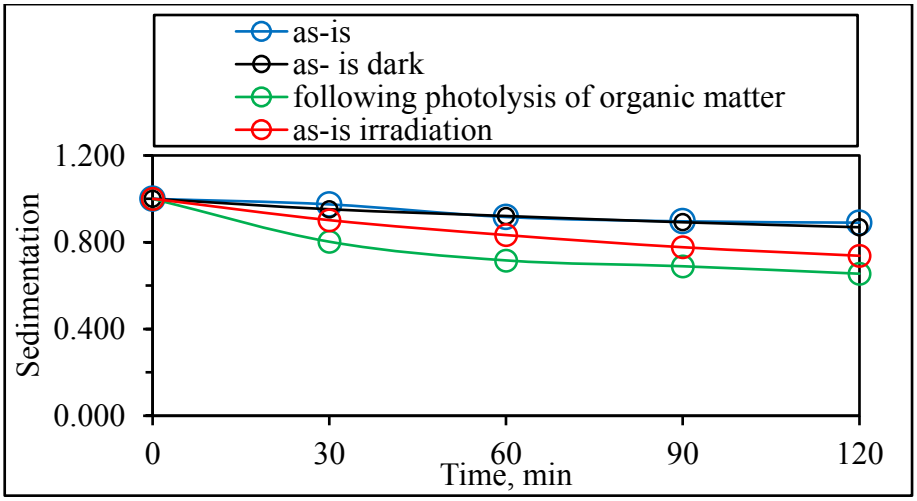


Figure 4.317. Sedimentation profiles of TiO_2 and HA binary system under "as-is", "as-is dark", "following photolysis of organic matter", and "as-is irradiation" conditions.

Turbidity profiles of TiO_2 and HA binary system under "as-is", "as-is dark", "following photolysis of organic matter", and "as-is irradiation" conditions were exhibited in Figure 4.318. Since turbidity symbolizes the presence and amount of the suspended particles, it could be correlated with sedimentation. Variations in turbidity of TiO_2 and HA under different conditions declined in the following order of "TiO_2 and HA" binary system "as-is" under irradiation > "TiO_2 and HA_{pho}" binary system following photolysis of organic matter > "TiO_2 and HA" binary system "as-is" under dark conditions > "TiO_2 and HA" binary system under "as-is" conditions.

Under the specified conditions, TiO_2 and HA" binary system "as-is" under irradiation, "TiO_2 and HA_{pho}" binary system following photolysis of organic matter, and "TiO_2 and HA" binary system "as-is" under dark conditions revealed almost similar trends contrary to "TiO_2 and HA" binary system under "as-is" conditions. Also, it could be asserted that "TiO_2 and HA" binary system under "as-is" conditions displayed the lowest turbidity values along 120 min period. The reason could be attributed to the effect of continuous mixing applied for TiO_2 and HA" binary system "as-is" under dark conditions revealed almost similar trends contrary to "TiO_2 and HA" binary system under "as-is" conditions.

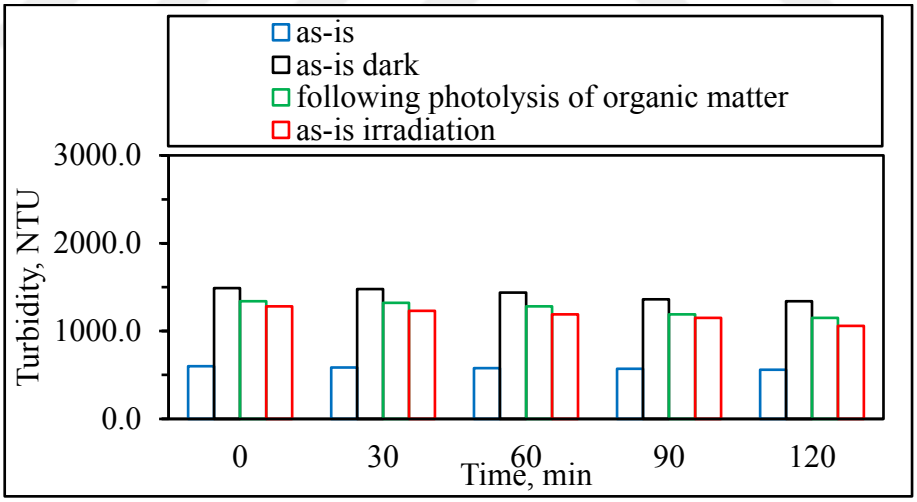


Figure 4.318. Turbidity profiles of TiO_2 and HA binary system under "as-is", "as-is dark", "following photolysis of organic matter", and "as-is irradiation" conditions.

For comparison purposes, it could be stated that upon irradiation period of 30 min, NPOC content decreased between initial 4.80 mg/L and detected to 1.12 mg/L (Table A). Therefore, organic content with TiO_2 particles attached on it decreased. In addition, specified UV-vis parameters also decreased under irradiation. Accordingly, hydrodynamic size of "TiO_2 and HA" binary system "as-is" under irradiation revealed higher hydrodynamic sizes in comparison to TiO_2 "as-is" under irradiation (Figure 4.298).

4.4.1.1. Comparative evaluation of selected parameters as hydrodynamic size, hydrodynamic size difference, sedimentation and turbidity variations of "TiO_2 and HA" binary system under "as-is", "as-is dark", "following photolysis of organic matter", and "as-is irradiation" conditions. For comparison purposes and with reference to the selected parameters as hydrodynamic size, hydrodynamic size difference, sedimentation and turbidity variations, the data obtained for each NP were demonstrated in the following figures 4.319-4.191 for "TiO_2 and HA", "TiO_2 and SRNOM", "N-TiO_2 and HA", "N-TiO_2 and SRNOM", "Fe-TiO_2 and HA", "Fe-TiO_2 and SRNOM", respectively. Comparative evaluation of selected parameters as hydrodynamic size, hydrodynamic size difference, sedimentation and turbidity variations for "TiO_2 and HA" binary system under "as-is" conditions was presented in Figure 4.319. It could be stated that TiO_2 and HA exhibited a consistent slightly decreasing trend for all of the parameters excluding hydrodynamic size difference during the whole span of the experiment. The observed inconsistent trend could only indicate the nonstability of the system composed of TiO_2 and HA in aqueous medium in the presence of any interfering substances disturbing the colloidal stability.

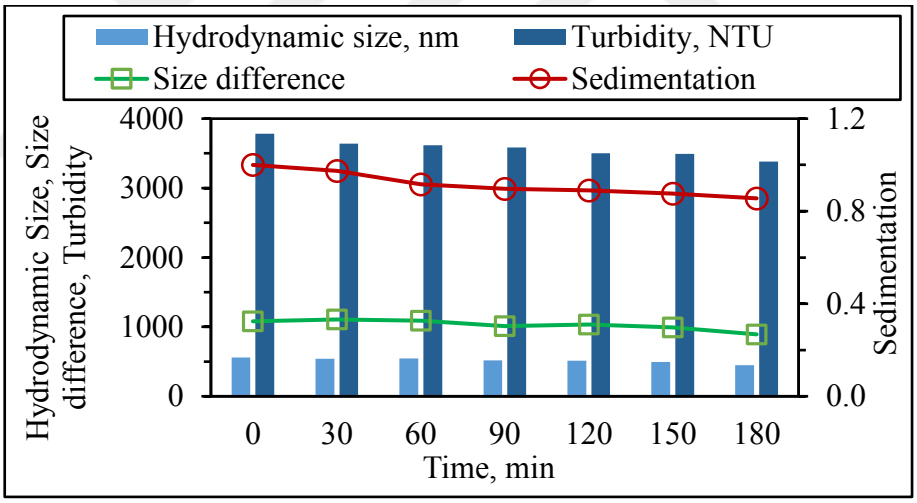


Figure 4.319. "TiO_2 and HA" binary system under "as-is" conditions. Comparative evaluation of selected parameters as hydrodynamic size, hydrodynamic size difference, sedimentation and turbidity variations.

Comparative evaluation of selected parameters as hydrodynamic size, hydrodynamic size difference, sedimentation and turbidity variations for "TiO_2 and HA" binary system "as-is" under dark conditions was demonstrated in Figure 4.320. It could be inferred that continuous mixing provided under dark did not significantly affect the behavior of all parameters of "TiO_2 and HA" binary system under "as-is" conditions excluding turbidity behavior. The most significant variation was monitored in turbidity behavior that could be related to the presence and number of suspended particles upon treatment of 60 min. Hydrodynamic size difference remained almost similar as-is under

dark conditions in comparison to inconsistent trend obtained for "TiO_2 and HA" binary system under "as-is" conditions.

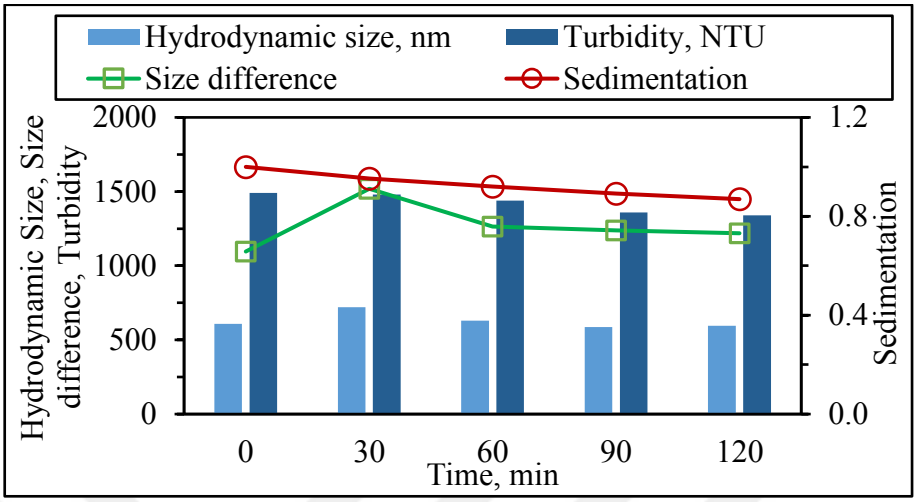


Figure 4.320. "TiO_2 and HA" binary system "as-is" under dark conditions. Comparative evaluation of selected parameters as hydrodynamic size, hydrodynamic size difference, sedimentation and turbidity variations.

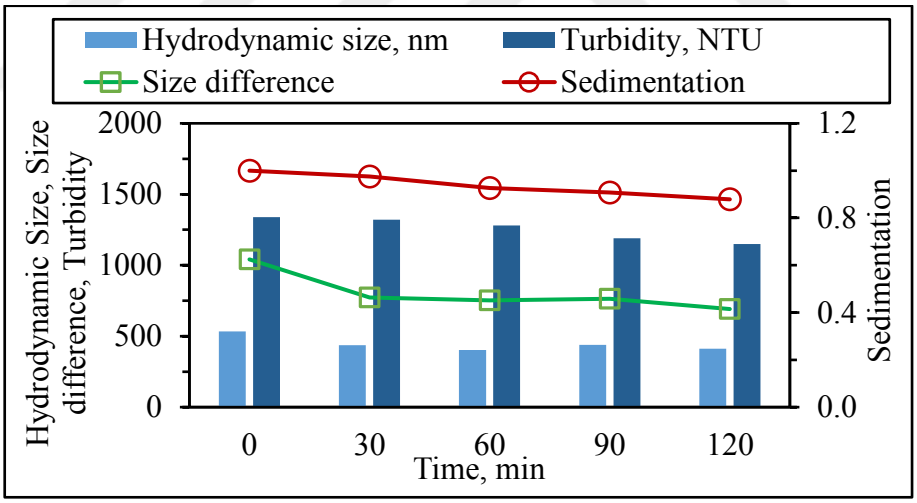


Figure 4.321. "TiO_2 and HA_{pho}" binary system following photolysis of organic matter. Comparative evaluation of selected parameters as hydrodynamic size, hydrodynamic size difference, sedimentation and turbidity variations.

Comparative evaluation of selected parameters as hydrodynamic size, hydrodynamic size difference, sedimentation and turbidity variations for "TiO_2 and HA_{pho}" binary system following photolysis of organic matter was presented in Figure 4.321. It could be deduced that photolysis of organic matter slightly affected the behavior of all parameters of "TiO_2 and HA" binary system under "as-is" conditions (Figure 4.319). The most significant change was monitored in size difference upon treatment of 60 min. It could be inferred that photolysis of organic matter affected TiO_2 and HA more

significantly in hydrodynamic size difference trend in comparison to continuously decreasing sedimentation profile. It could also be concluded that slight hydrodynamic size and turbidity variations could be supported by sedimentation profiles.

Comparative evaluation of selected parameters as hydrodynamic size, hydrodynamic size difference, sedimentation and turbidity variations of "TiO_2 and HA" binary system "as-is" under irradiation was presented in Figure 4.322. Dependent on the presented data for "TiO_2 and HA" binary system "as-is" under irradiation, it could be inferred that the effect of mixing under irradiation was significantly different than the mixing under dark conditions. It could be inferred that TiO_2 and HA indicated comparatively higher turbidity values in relation to hydrodynamic size variations.

Upon treatment of 30 min, continuous mixing under irradiation affected TiO_2 and HA more significantly in sedimentation profile in comparison to continuously decreasing hydrodynamic size difference profile. However, a doubling effect was observed for hydrodynamic size and hydrodynamic size difference alterations of "TiO_2 and HA" binary system under "as-is" conditions and "TiO_2 and HA" binary system "as-is" under irradiation. Therefore, it could be concluded that "TiO_2 and HA" binary system "as-is" under irradiation expressed higher hydrodynamic sizes and hydrodynamic size differences in comparison to under "as-is" conditions over period of 120 min. For comparison purposes, it could be concluded that upon irradiation of 30 min, hydrodynamic size and size difference values reached more than double whereas sedimentation and turbidity profiles were nearly stable during 120 min.

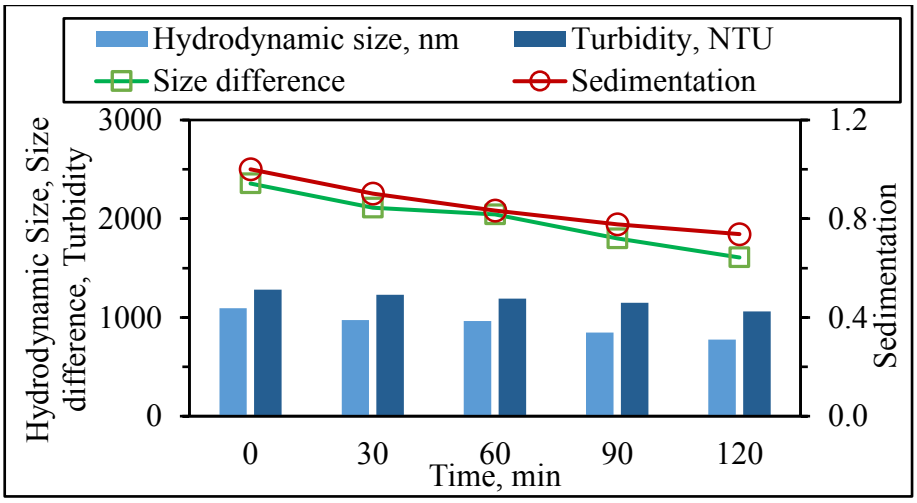


Figure 4.322. "TiO_2 and HA" binary system "as-is" under irradiation. Comparative evaluation of selected parameters as hydrodynamic size, hydrodynamic size difference, sedimentation and turbidity variations.

4.4.2. Behavior of "TiO_2 and SRNOM" Binary System under "as-is", "as-is dark", "following photolysis of organic matter", and "as-is irradiation" Conditions

Hydrodynamic sizes of TiO_2 and SRNOM under the specified conditions responded differently with minor variations excluding "as-is" under irradiation conditions along 120 min (Figure 4.323). Under initial conditions, hydrodynamic sizes were 527.8 nm, 362.4 nm, 428.7 nm, and 1484.9 nm for binary system of TiO_2 and SRNOM designated as "TiO_2 and SRNOM" binary system under "as-is" conditions, "TiO_2 and SRNOM" binary system "as-is under dark" conditions, "TiO_2 and $SRNOM_{pho}$" binary system following photolysis of organic matter, "TiO_2 and SRNOM" binary system "as-is" under irradiation, respectively.

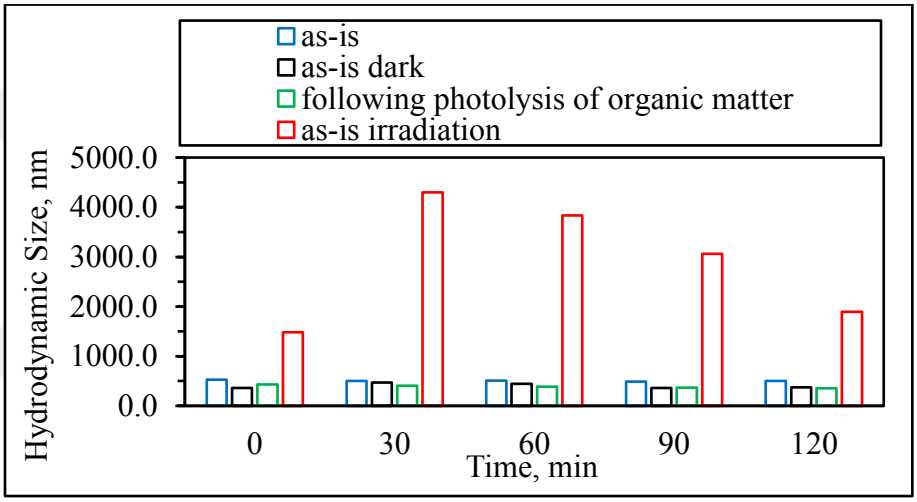


Figure 4.323. Hydrodynamic size variations of TiO_2 and SRNOM binary system under "as-is", "as-is dark", "following photolysis of organic matter", and "as-is irradiation" conditions.

As explained for TiO_2 and HA binary system under "as-is", "as-is dark", "following photolysis of organic matter", and "as-is irradiation" conditions (Figure 4.319), following a similar trend, hydrodynamic size variations of TiO_2 and SRNOM was monitored. Sample was subjected to recording immediately after preparation revealed an average hydrodynamic size as 505.2 ± 14.8 nm. Upon dark conditions, *i.e.* continuously stirred sample for 60 min affected the particle size distribution of TiO_2 and SRNOM demonstrated an average hydrodynamic size as 403.2 nm ± 50.8 nm. However, "TiO_2 and $SRNOM_{pho}$" binary system following photolysis of organic matter displayed an average hydrodynamic size as 387.6 ± 30.3 nm. On the other hand, sample prepared upon irradiation revealed an average hydrodynamic size as 2915.9 ± 1212.4 nm. Therefore, the biggest variance in terms of hydrodynamic size was observed for "TiO_2 and SRNOM" binary system "as-is" under irradiation upon 120 min. In a similar manner, sedimentation tendency profiles were presented in Figure 4.324. Although "TiO_2 and SRNOM" binary system under "as-is" conditions, "TiO_2 and SRNOM" binary

system “as-is” under dark conditions, and “TiO_2 and $SRNOM_{pho}$” binary system following photolysis of organic matter revealed almost similar trends, “TiO_2 and SRNOM” binary system “as-is” under irradiation displayed the most distinct decreasing trend along 120 min.

Turbidity profiles of TiO_2 and SRNOM binary system under “as-is”, “as-is dark” and “as-is irradiation” conditions were followed up to 120 min (Figure 4.325). Variations in turbidity behavior of TiO_2 and SRNOM binary system under “as-is”, “as-is dark” and “as-is irradiation” conditions could be aligned in the order of “TiO_2 and SRNOM” binary system “as-is” under irradiation > “TiO_2 and SRNOM” binary system “as-is” under dark conditions > “TiO_2 and $SRNOM_{pho}$” binary system following photolysis of organic matter > “TiO_2 and SRNOM” binary system under “as-is” conditions.

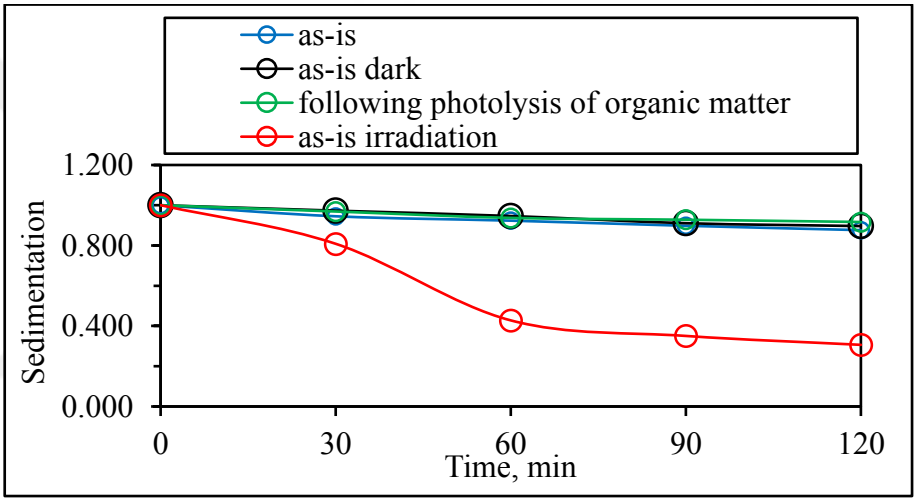


Figure 4.324. Sedimentation profiles of TiO_2 and SRNOM binary system under “as-is”, “as-is dark”, “following photolysis of organic matter”, and “as-is irradiation” conditions.

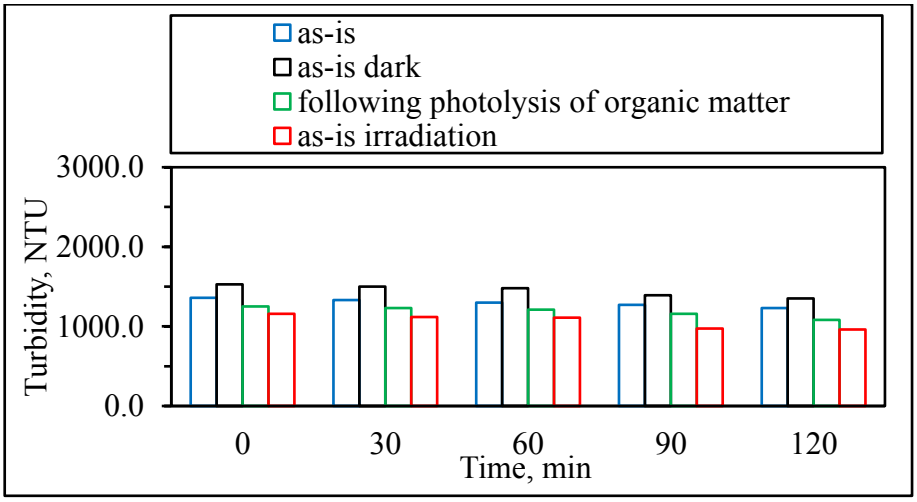


Figure 4.325. Turbidity profiles of TiO_2 and SRNOM binary system under “as-is”, “as-is dark” and “as-is irradiation” conditions.

4.4.2.1. Comparative evaluation of selected parameters as hydrodynamic size, hydrodynamic size difference, sedimentation and turbidity variations of "TiO_2 and SRNOM" binary system under "as-is", "as-is dark", "following photolysis of organic matter", and "as-is irradiation" conditions. Comparative evaluation of selected parameters as hydrodynamic size, hydrodynamic size difference, sedimentation and turbidity variations for "TiO_2 and SRNOM" binary system under "as-is" conditions was presented in Figure 4.326. "TiO_2 and SRNOM" binary system under "as-is" conditions indicated comparatively higher turbidity values in relation to hydrodynamic size variations. Slight fluctuations could be monitored in hydrodynamic size differences in accordance with the variations in the range although an average hydrodynamic size was obtained as 505.2 ± 14.8 nm. Also, sedimentation profiles followed a similar trend to hydrodynamic size variations.

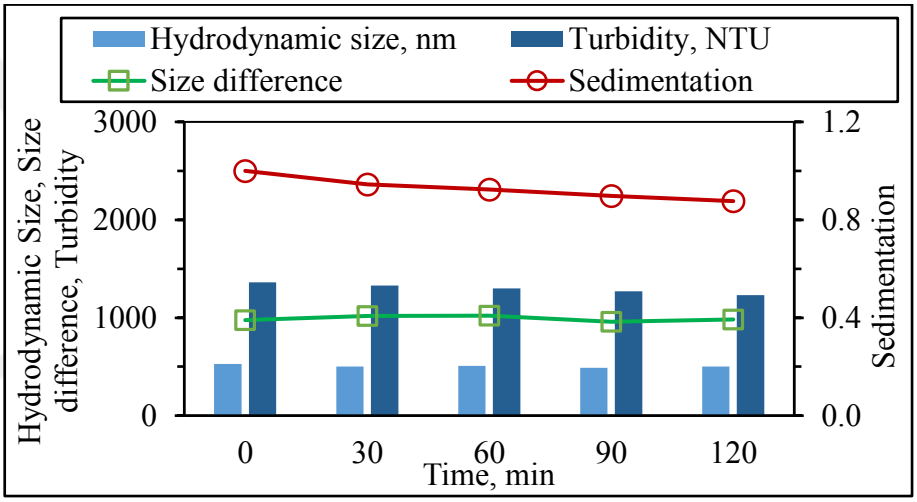


Figure 4.326. "TiO_2 and SRNOM" binary system under "as-is" conditions. Comparative evaluation of selected parameters as hydrodynamic size, hydrodynamic size difference, sedimentation and turbidity variations.

Comparative evaluation of selected parameters as hydrodynamic size, hydrodynamic size difference, sedimentation and turbidity variations for "TiO_2 and SRNOM" binary system "as-is" under dark conditions was presented in Figure 4.327. For comparison purposes, it could be inferred that continuous mixing provided under dark significantly affected the behavior of all parameters of "TiO_2 and SRNOM" binary system under "as-is" conditions (Figure 4.326). Upon dark conditions, TiO_2 and SRNOM indicated comparatively higher turbidity values in relation to hydrodynamic size variations. Also, a distinct fluctuation could be visualized in hydrodynamic size differences in accordance with the variations in the range although an average hydrodynamic size was obtained as 403.2 ± 50.8 nm. On the other hand, sedimentation profiles followed a parallel trend to turbidity variations.

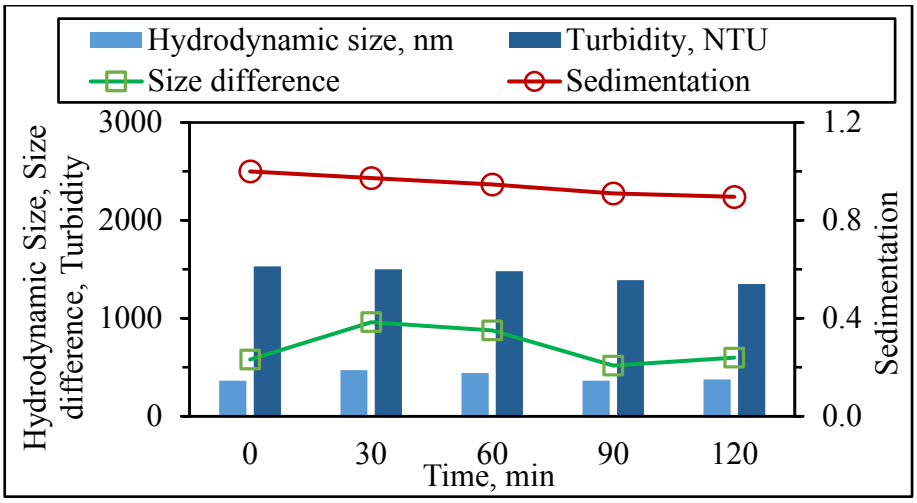


Figure 4.327. "TiO_2 and SRNOM" binary system "as-is" under dark conditions. Comparative evaluation of selected parameters as hydrodynamic size, hydrodynamic size difference, sedimentation and turbidity variations.

As explained for "TiO_2 and SRNOM" binary system under "as-is" conditions (Figure 4.326), comparative evaluation of selected parameters as hydrodynamic size, hydrodynamic size difference, sedimentation and turbidity variations for "TiO_2 and $SRNOM_{pho}$" binary system following photolysis of organic matter was also presented in Figure 4.328. The most significant change was observed in size difference upon treatment of 60 min. It could be deduced that photolysis of organic matter affected TiO_2 and SRNOM more significantly in hydrodynamic size difference trend in comparison to slightly decreasing sedimentation profile. Also, it could be concluded that slight hydrodynamic size and turbidity alterations could be supported by sedimentation profiles.

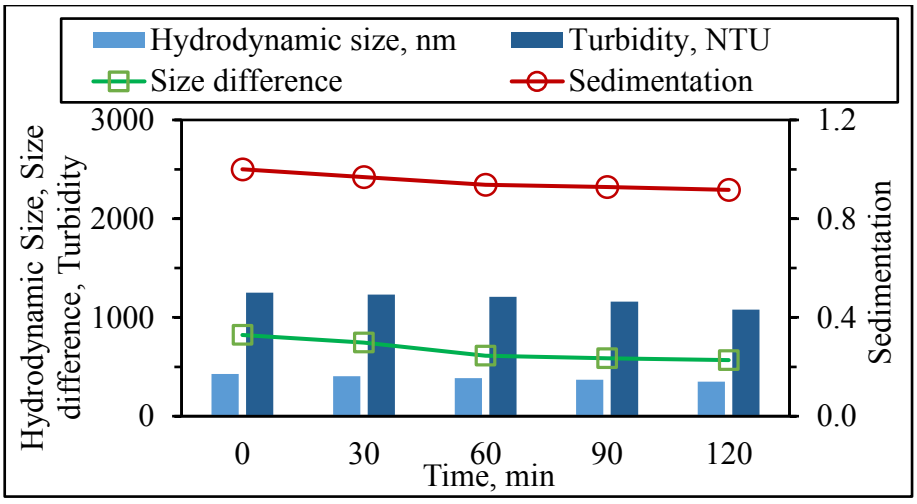


Figure 4.328. "TiO_2 and $SRNOM_{pho}$" binary system following photolysis of organic matter. Comparative evaluation of selected parameters as hydrodynamic size, hydrodynamic size difference, sedimentation and turbidity variations.

Likewise expressed so far, a similar approach was also followed for "TiO_2 and SRNOM" binary system "as-is" under irradiation. Comparative evaluation of selected parameters as hydrodynamic size, hydrodynamic size difference, sedimentation and turbidity variations were presented in Figure 4.329. For comparison purposes, it could be inferred that irradiation under continuous mixing conditions significantly affected the behavior of all parameters designated as hydrodynamic size, size difference, sedimentation and turbidity of "TiO_2 and SRNOM" binary system under "as-is" conditions (Figure 4.326). Upon treatment of 30 min, continuous mixing under irradiation affected TiO_2 and SRNOM more significantly in hydrodynamic size difference trend in comparison to continuously decreasing sedimentation profile. However, no significant change was observed for turbidity alterations of "TiO_2 and SRNOM" binary system under "as-is" conditions and "TiO_2 and SRNOM" binary system "as-is" under irradiation. On the other hand, "TiO_2 and SRNOM" binary system "as-is" under irradiation expressed higher hydrodynamic sizes in comparison to "TiO_2 and SRNOM" binary system under "as-is" conditions along 120 min.

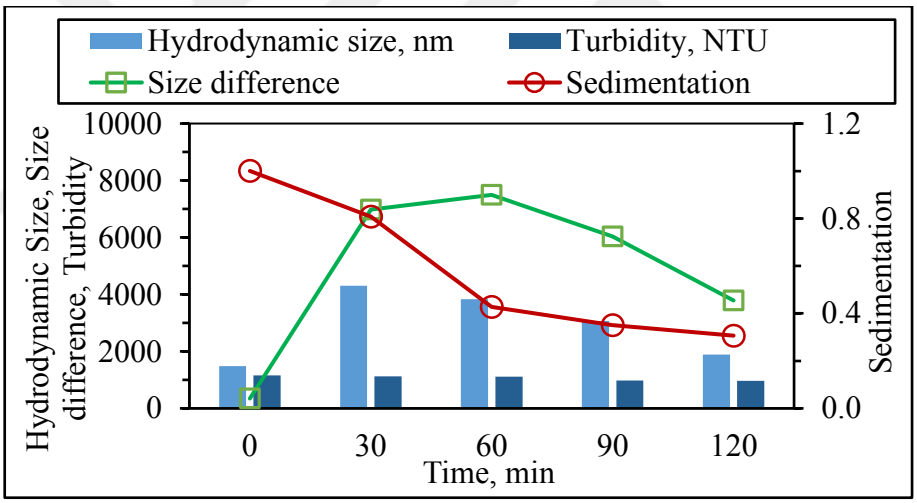


Figure 4.329. "TiO_2 and SRNOM" "as-is" under irradiation. Comparative evaluation of selected parameters as hydrodynamic size, hydrodynamic size difference, sedimentation and turbidity variations.

On the other hand, when compared to "TiO_2 and HA" "as-is" under irradiation (Figure 4.322), hydrodynamic size and size difference variations of "TiO_2 and SRNOM" "as-is" under irradiation revealed a fluctuating trend over period of 120 min. However, under similar experimental conditions, "TiO_2 and HA" "as-is" under irradiation displayed a continuously decreasing trend according to time variations. Due to photocatalytic activities under solar irradiation, NPOC content and organic matter content decreased (Table A), and therefore upon irradiation, hydrodynamic size variations of "TiO_2 and HA" and "TiO_2 and SRNOM" distinctly increased.

4.4.3. Behavior of "N-TiO_2 and HA" Binary System under "as-is", "as-is dark", "following photolysis of organic matter", and "as-is irradiation" Conditions

As explained for TiO_2 and HA, a similar approach was followed for elucidation of hydrodynamic sizes of N-TiO_2 and HA under "as-is", "as-is dark", "following photolysis of organic matter", and "as-is irradiation" conditions (Figure 4.330). Under initial conditions, hydrodynamic sizes were 715.9 nm, 544.5 nm, 747.4 nm, and 899.9 nm for binary system of N-TiO_2 and HA designated as "N-TiO_2 and HA" binary system under "as-is" conditions, "N-TiO_2 and HA" binary system "as-is" under dark conditions, "N-TiO_2 and HA_{pho}" binary system following photolysis of organic matter, "N-TiO_2 and HA" binary system "as-is" under irradiation, respectively. Since no treatment was applied, the average hydrodynamic size could be accepted as 726.9 nm.

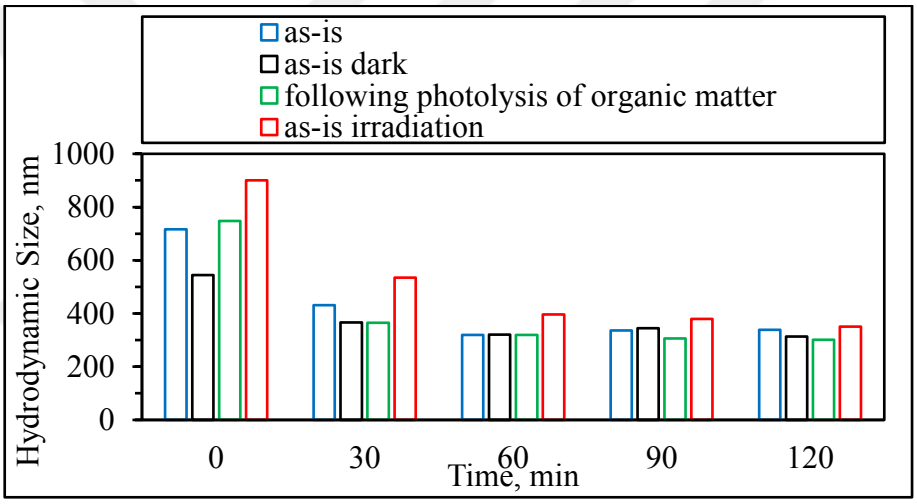


Figure 4.330. Hydrodynamic size variations of N-TiO_2 and HA binary system under "as-is", "as-is dark", "following photolysis of organic matter", and "as-is irradiation" conditions.

Hydrodynamic sizes of N-TiO_2 and HA binary system under the specified conditions behaved differently with respect to time. Variations in hydrodynamic sizes of N-TiO_2 and HA under "as-is", "as-is dark", "following photolysis of organic matter", and "as-is irradiation" conditions could be arranged in the decreasing order of "N-TiO_2 and HA" binary system "as-is" under irradiation > "N-TiO_2 and HA_{pho}" binary system following photolysis of organic matter > "N-TiO_2 and HA" binary system under "as-is" conditions > "N-TiO_2 and HA" binary system "as-is" under dark conditions.

Regarding the presented data for N-TiO_2 and HA binary system under "as-is", "as-is dark", "following photolysis of organic matter", and "as-is irradiation" conditions, similar sedimentation profiles were attained (Figure 4.331), "N-TiO_2 and HA" binary system "as-is" under irradiation demonstrated the most significant variation upon 120 min. Variations in sedimentation profiles of N-

TiO_2 and HA binary system under different conditions could be sorted in the decreasing order of "N-TiO_2 and HA" binary system "as-is" under irradiation > "N-TiO_2 and HA_{pho}" binary system following photolysis of organic matter > "N-TiO_2 and HA" binary system under "as-is" conditions > "N-TiO_2 and HA" binary system "as-is" under dark conditions. It could be concluded that hydrodynamic sizes and sedimentation profiles followed a similar trend.

Turbidity alterations of N-TiO_2 and HA under different conditions displayed different behavior with respect to increasing time and decreased in the following order of "N-TiO_2 and HA" binary system under "as-is" conditions > "N-TiO_2 and HA" binary system "as-is" under irradiation ≥ N-TiO_2 and HA_{pho}" binary system following photolysis of organic matter > "N-TiO_2 and HA" binary system "as-is" under dark conditions (Figure 4.332).

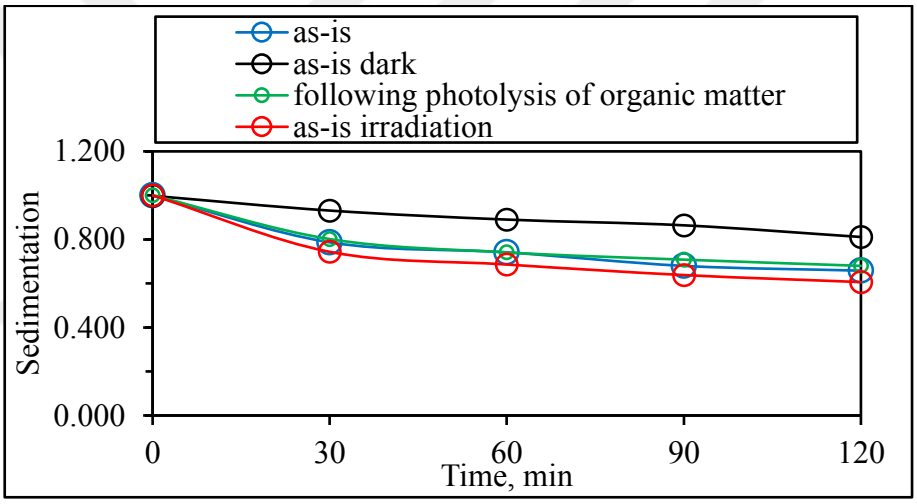


Figure 4.331. Sedimentation profiles of N-TiO_2 and HA binary system under "as-is", "as-is dark", "following photolysis of organic matter", and "as-is irradiation" conditions.

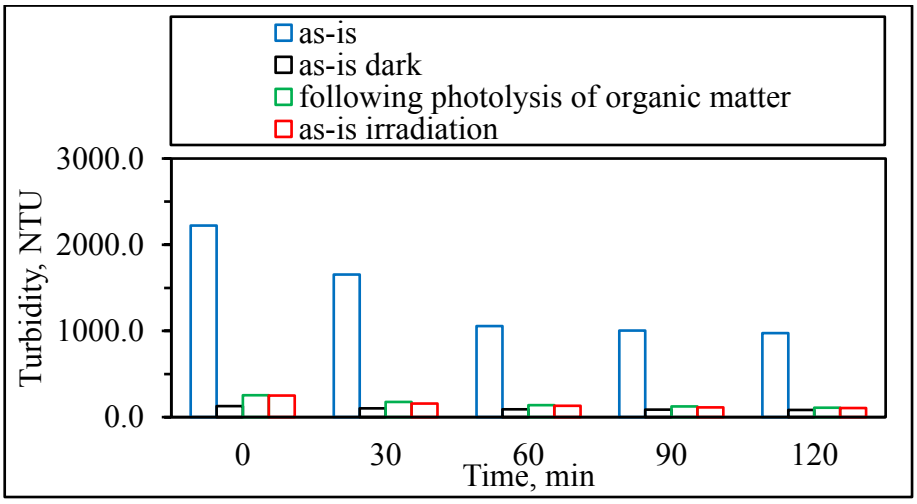


Figure 4.332. Turbidity profiles of N-TiO_2 and HA binary system under "as-is", "as-is dark" and "as-is irradiation" conditions.

4.4.3.1. Comparative evaluation of selected parameters as hydrodynamic size, hydrodynamic size difference, sedimentation and turbidity variations of "N-TiO_2 and HA" binary system under "as-is", "as-is dark", "following photolysis of organic matter", and "as-is irradiation" conditions. Comparative evaluation of selected parameters as hydrodynamic size, hydrodynamic size difference, sedimentation and turbidity variations for "N-TiO_2 and HA" binary system under "as-is" conditions was presented in Figure 4.333. N-TiO_2 and HA exhibited comparatively higher turbidity values in relation to hydrodynamic size variations. Fluctuations could be monitored in hydrodynamic size differences in accordance with the variations in the range even though an average hydrodynamic size was attained as 397.6 ± 146.0 nm. Sedimentation profiles followed a similar trend to hydrodynamic size variations.

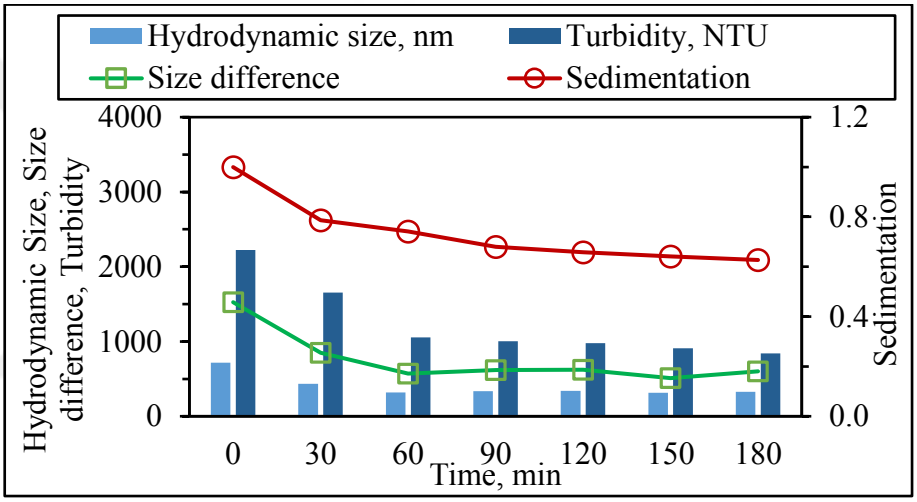


Figure 4.333. "N-TiO_2 and HA" binary system under "as-is" conditions. Comparative evaluation of selected parameters as hydrodynamic size, hydrodynamic size difference, sedimentation and turbidity variations.

Comparative evaluation of selected parameters as hydrodynamic size, hydrodynamic size difference, sedimentation and turbidity variations for "N-TiO_2 and HA" binary system "as-is" under dark conditions was displayed in Figure 4.334. Continuous mixing provided under dark obviously affected the behavior of all parameters of "N-TiO_2 and HA" binary system under "as-is" conditions. The most significant change was observed in turbidity behavior that could be related to the presence and number of suspended particles upon treatment of 30 min. Under dark conditions, continuous mixing affected N-TiO_2 and HA more significantly in hydrodynamic size difference trend in comparison to continuously decreasing sedimentation profile. However, slight hydrodynamic size and turbidity variations could not be supported by sedimentation profiles. Under the specified as-is under dark conditions, hydrodynamic size difference demonstrated similar trend in comparison to inconsistent trend attained for "N-TiO_2 and HA" binary system under "as-is" conditions.

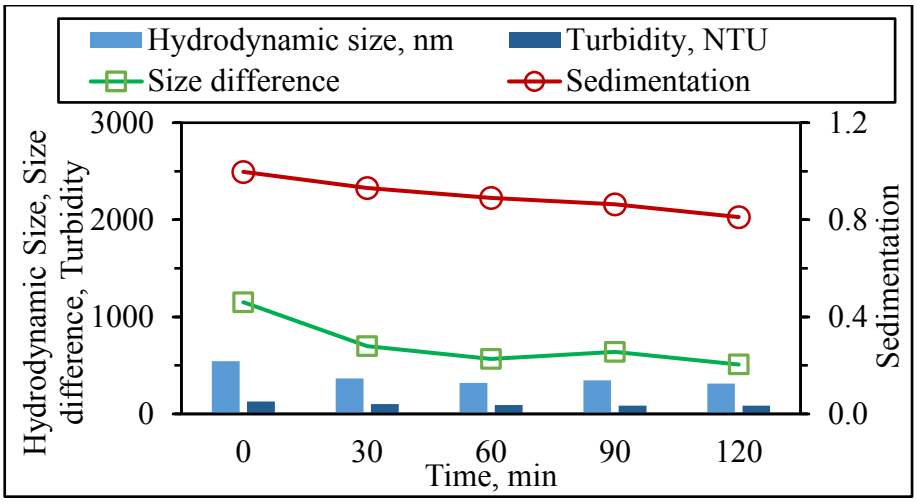


Figure 4.334. "N-TiO_2 and HA" binary system "as-is" under dark conditions. Comparative evaluation of selected parameters as hydrodynamic size, hydrodynamic size difference, sedimentation and turbidity variations.

Comparative evaluation of selected parameters as hydrodynamic size, hydrodynamic size difference, sedimentation and turbidity variations for "N-TiO_2 and HA" binary system following photolysis of organic matter was presented in Figure 4.335. Based on the presented data, due to photolysis of organic matter, a significant variation was not observed in NPOC of sole HA solution. However, minor variations were monitored in specified UV-vis parameters of sole HA solution (Table A). Depending upon changes in aromaticity of the organic content, interactions between N-TiO_2 and sole HA revealed minor difference in hydrodynamic size in comparison to "N-TiO_2 and HA" binary system under "as-is" conditions (Figure 4.333). Accordingly, an average diameter of "N-TiO_2 and HA" binary system under "as-is" conditions was attained as 397.6 ± 146.0 nm whereas average diameter of "N-TiO_2 and HA" binary system following photolysis of organic matter was obtained as 407.9 ± 191.5 nm.

On the other hand, lower turbidity values and sedimentation profiles were attained in comparison to "N-TiO_2 and HA" binary system under "as-is" conditions. Furthermore, approximately 50 % decrease was observed in hydrodynamic size variations during 120 min. Also, the most distinct decreasing trend was monitored in size difference over 120 min period. It could be concluded that sedimentation profiles followed a similar trend to hydrodynamic size variations. Following a similar manner, comparative evaluation of selected parameters as hydrodynamic size, hydrodynamic size difference, sedimentation and turbidity variations for "N-TiO_2 and HA" binary system "as-is" under irradiation was given in Figure 4.336.

For comparison purposes, it could be inferred that hydrodynamic size, hydrodynamic size difference, and sedimentation profiles of "N-TiO_2 and HA" binary system under "as-is" conditions and "N-TiO_2 and HA" binary system "as-is" under irradiation were not significantly different from each other. Under the specified "as-is" under irradiation conditions, size difference and sedimentation profiles followed a parallel trend, and turbidity values were observed comparatively lower in relation to hydrodynamic size variations. However, turbidity variations could be related to the possible disaggregation of the NPs due to continuous mixing under irradiation in comparison to the applied sonication and magnetic stirring under "as-is" conditions.

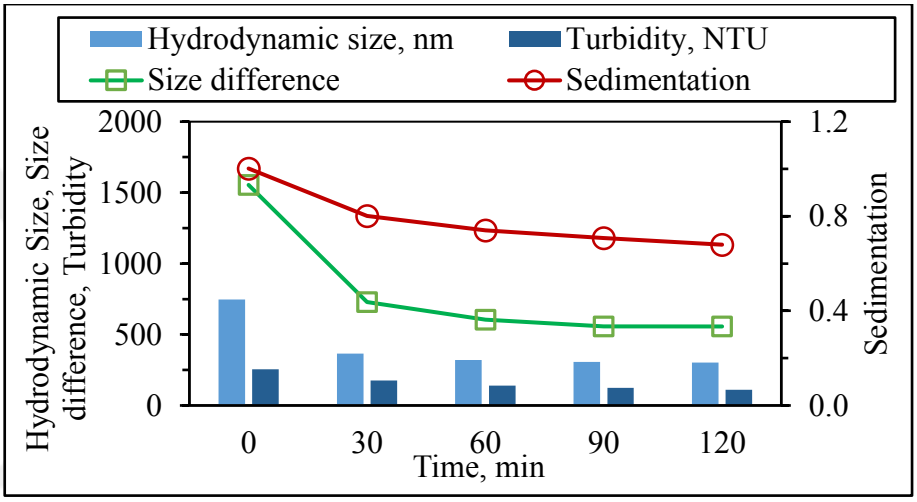


Figure 4.335. "N-TiO_2 and HA_{pho}" binary system following photolysis of organic matter. Comparative evaluation of selected parameters as hydrodynamic size, hydrodynamic size difference, sedimentation and turbidity variations.

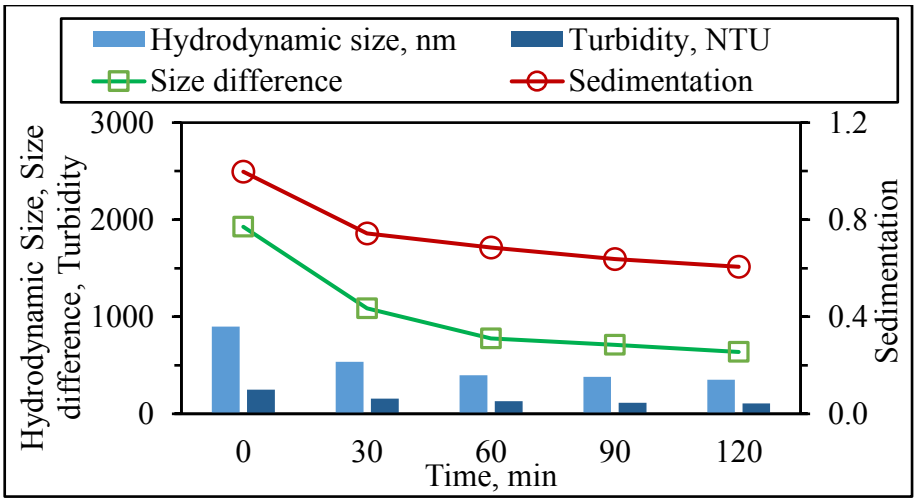


Figure 4.336. "N-TiO_2 and HA" binary system "as-is" under irradiation. Comparative evaluation of selected parameters as hydrodynamic size, hydrodynamic size difference, sedimentation and turbidity variations.

4.4.4. Behavior of "N-TiO_2 and SRNOM" Binary System under "as-is", "as-is dark", "following photolysis of organic matter", and "as-is irradiation" Conditions

Hydrodynamic size variations of N-TiO_2 and SRNOM binary system under "as-is", "as-is dark", "following photolysis of organic matter", and "as-is irradiation" conditions were exhibited in Figure 4.337. Under initial conditions, hydrodynamic sizes were detected as 1157.7 nm, 1365.3 nm, 801.2 nm, and 1223.4 nm for binary system of N-TiO_2 and SRNOM designated as "N-TiO_2 and SRNOM" binary system under "as-is" conditions, "N-TiO_2 and SRNOM" binary system "as-is" under dark conditions, "N-TiO_2 and $SRNOM_{pho}$" binary system following photolysis of organic matter, "N-TiO_2 and SRNOM" binary system "as-is" under irradiation, respectively.

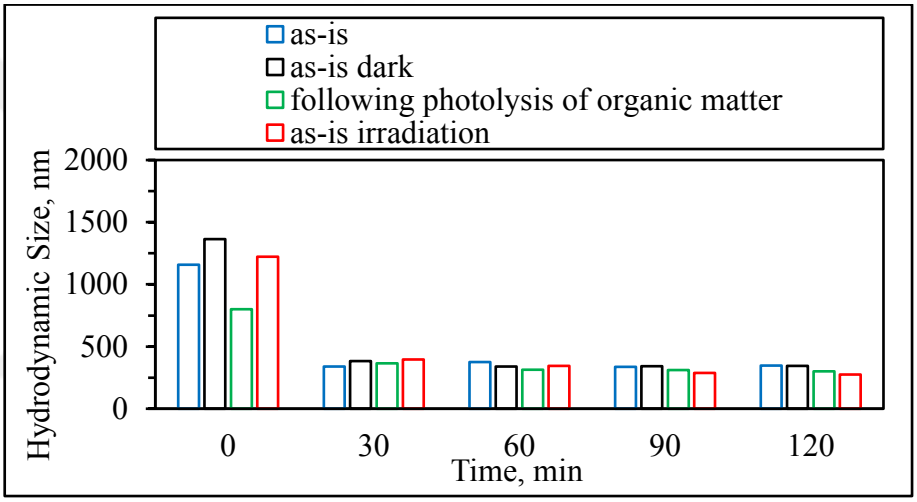


Figure 4.337. Hydrodynamic size variations of N-TiO_2 and SRNOM binary system under "as-is", "as-is dark", "following photolysis of organic matter", and "as-is irradiation" conditions.

Based on the presented data, alterations in hydrodynamic sizes of N-TiO_2 and SRNOM under "as-is", "as-is dark", "following photolysis of organic matter", and "as-is irradiation" conditions could be arranged in the decreasing order of "N-TiO_2 and SRNOM" binary system "as-is" under dark conditions > "N-TiO_2 and SRNOM" binary system "as-is" under irradiation > "N-TiO_2 and SRNOM" binary system under "as-is" conditions > "N-TiO_2 and $SRNOM_{pho}$" binary system following photolysis of organic matter. Upon dark conditions, N-TiO_2 and SRNOM demonstrated an average hydrodynamic size as 554.7 ± 453.5 nm. However, "N-TiO_2 and $SRNOM_{pho}$" binary system following photolysis of organic matter displayed an average hydrodynamic size as 418.4 ± 215.4 nm. On the other hand, sample prepared upon irradiation revealed an average hydrodynamic size as 505.5 ± 404.2 nm. Also, "N-TiO_2 and SRNOM" binary system under "as-is" conditions demonstrated an average hydrodynamic size as 511.6 ± 361.5 nm.

Sedimentation profiles of N-TiO_2 and SRNOM binary system under "as-is", "as-is dark", "following photolysis of organic matter", and "as-is irradiation" conditions were presented in Figure 4.338, and could be aligned in the order of "N-TiO_2 and $SRNOM_{pho}$" binary system following photolysis of organic matter > "N-TiO_2 and SRNOM" binary system "as-is" under dark conditions > "N-TiO_2 and SRNOM" binary system "as-is" under irradiation ≥ "N-TiO_2 and SRNOM" binary system under "as-is" conditions. Under similar conditions, turbidity alterations could be arranged in the order of "N-TiO_2 and $SRNOM_{pho}$" binary system following photolysis of organic matter > "N-TiO_2 and SRNOM" binary system "as-is" under irradiation > "N-TiO_2 and SRNOM" binary system under "as-is" conditions > "N-TiO_2 and SRNOM" binary system "as-is" under dark conditions (Figure 4.339).

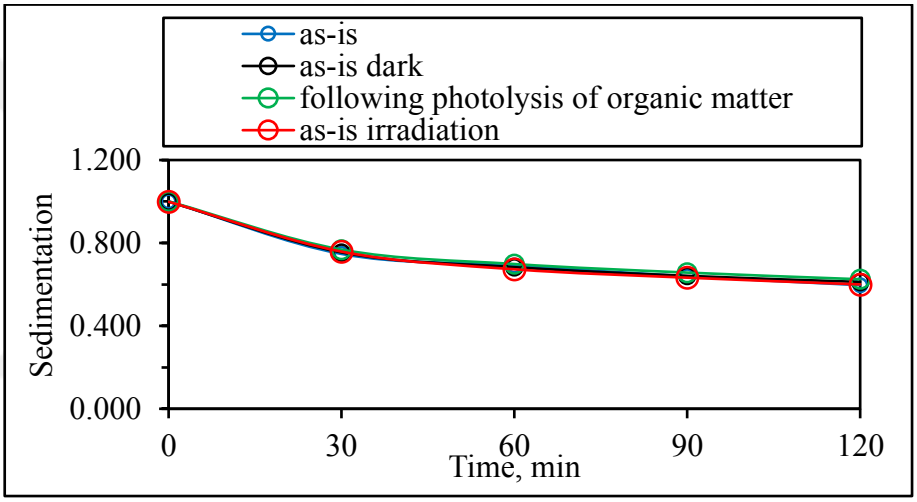


Figure 4.338. Sedimentation profiles of N-TiO_2 and SRNOM binary system under "as-is", "as-is dark", "following photolysis of organic matter", and "as-is irradiation" conditions.

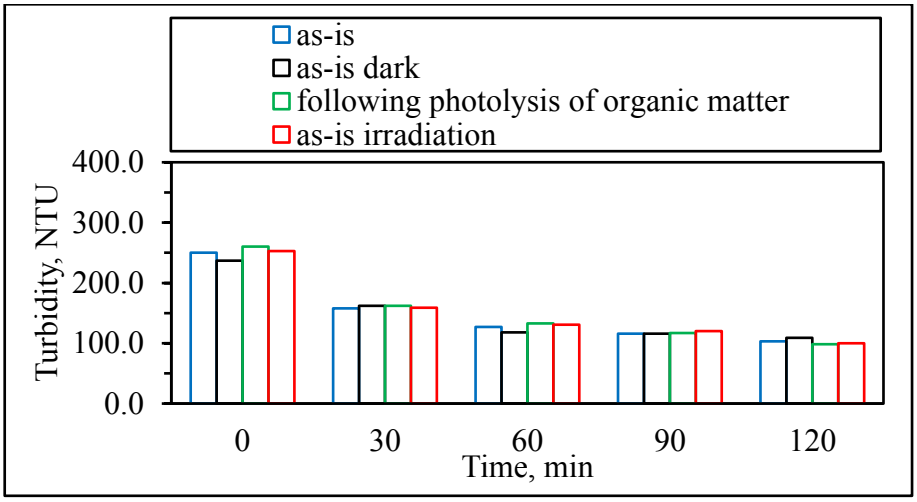


Figure 4.339. Turbidity profiles of N-TiO_2 and SRNOM binary system under "as-is", "as-is dark", "following photolysis of organic matter", and "as-is irradiation" conditions.

4.4.4.1. Comparative evaluation of selected parameters as hydrodynamic size, hydrodynamic size difference, sedimentation and turbidity variations of "N-TiO_2 and SRNOM" binary system under "as-is", "as-is dark", "following photolysis of organic matter", and "as-is irradiation" conditions. Comparative evaluation of selected parameters as hydrodynamic size, hydrodynamic size difference, sedimentation and turbidity variations was displayed in Figure 4.340. Based on the presented data, it could be inferred that N-TiO_2 and SRNOM binary system under "as-is" conditions demonstrated comparatively lower turbidity values in relation to hydrodynamic size variations. Fluctuations could be observed in hydrodynamic size differences in accordance with the variations in the range although an average hydrodynamic size was obtained as 511.6 ± 361.5 nm. On the other hand, sedimentation profiles followed a similar trend to hydrodynamic size variations over period of 120 min.

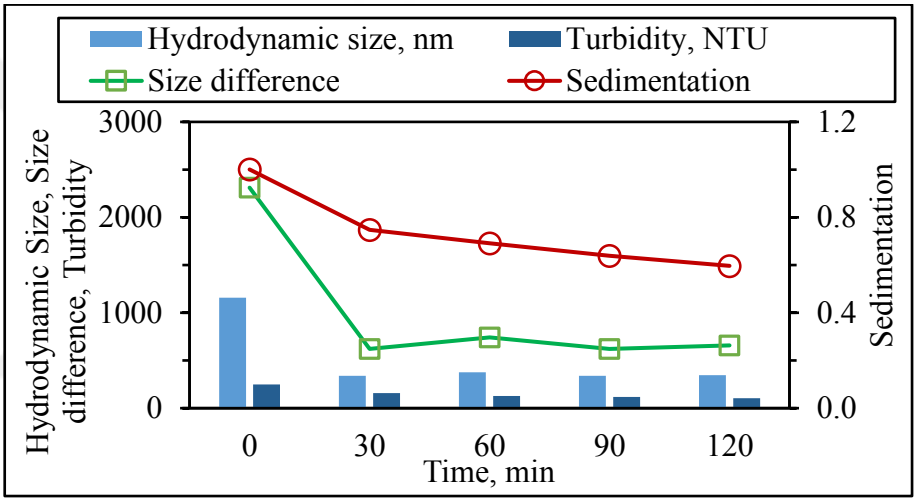


Figure 4.340. "N-TiO_2 and SRNOM" binary system under "as-is" conditions. Comparative evaluation of selected parameters as hydrodynamic size, hydrodynamic size difference, sedimentation and turbidity variations.

In a similar manner to data represented "N-TiO_2 and SRNOM" binary system under "as-is" conditions (Figure 4.340), comparative evaluation of selected parameters as hydrodynamic size, hydrodynamic size difference, sedimentation and turbidity variations for "N-TiO_2 and SRNOM" binary system "as-is" under dark conditions was also given in Figure 4.341. It could be asserted that continuous mixing provided under dark slightly affected the behavior of all parameters of "N-TiO_2 and SRNOM" binary system under "as-is" conditions over 120 min. Under the specified "as-is" under dark conditions, continuous mixing affected N-TiO_2 and SRNOM more significantly in hydrodynamic size difference in comparison to continuously decreasing sedimentation profile. On the other hand, hydrodynamic size difference displayed similar trend in comparison to inconsistent trend obtained for "N-TiO_2 and SRNOM" binary system under "as-is" conditions during 120 min.

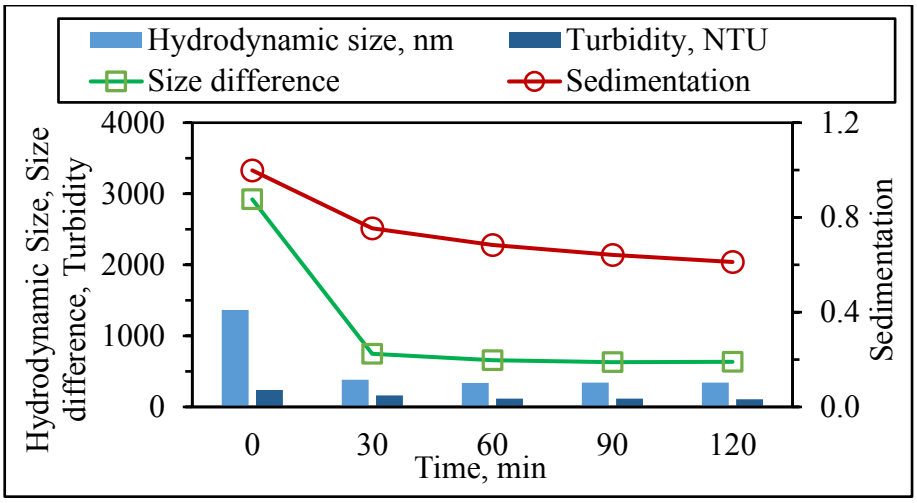


Figure 4.341. "N-TiO_2 and SRNOM" binary system "as-is" under dark conditions. Comparative evaluation of selected parameters as hydrodynamic size, hydrodynamic size difference, sedimentation and turbidity variations.

As explained for "N-TiO_2 and SRNOM" binary system under "as-is" conditions (Figure 4.340), comparative evaluation of selected parameters as hydrodynamic size, hydrodynamic size difference, sedimentation and turbidity variations of "N-TiO_2 and $SRNOM_{pho}$" binary system following photolysis of organic matter were presented in Figure 4.342. It could be deduced that upon photolysis of 60 min, a slight decrease in hydrodynamic size was observed for "N-TiO_2 and $SRNOM_{pho}$" binary system following photolysis of organic matter in comparison to "N-TiO_2 and SRNOM" binary system under "as-is" conditions. Based on the presented data, the most apparent alteration was monitored in size difference of "N-TiO_2 and $SRNOM_{pho}$" over 120 min period.

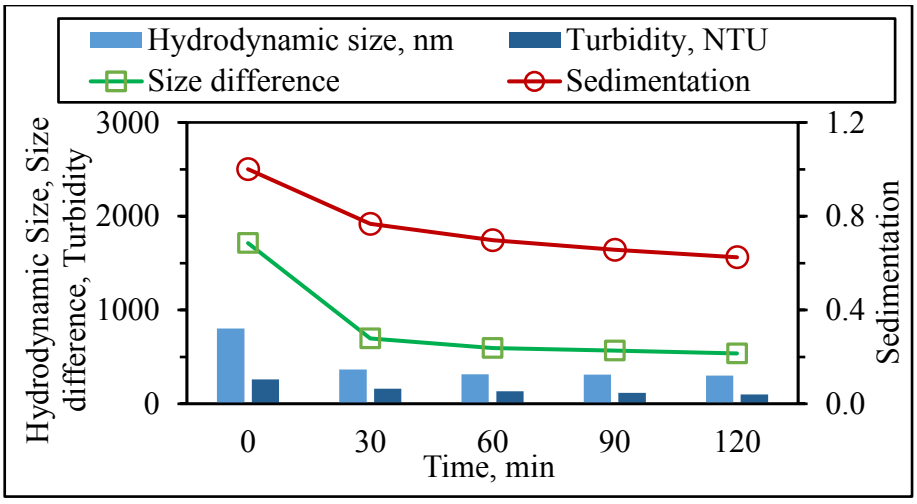


Figure 4.342. "N-TiO_2 and $SRNOM_{pho}$" binary system following photolysis of organic matter. Comparative evaluation of selected parameters as hydrodynamic size, hydrodynamic size difference, sedimentation and turbidity variations.

As elucidated for data "N-TiO_2 and $SRNOM_{pho}$" binary system following photolysis of organic matter (Figure 4.342), a similar approach was followed for "N-TiO_2 and SRNOM" binary system "as-is" under irradiation. Comparative evaluation of selected parameters as hydrodynamic size, hydrodynamic size difference, sedimentation and turbidity variations for "N-TiO_2 and SRNOM" binary system "as-is" under irradiation was presented in Figure 4.343. It could be inferred that sedimentation and turbidity profiles of "N-TiO_2 and SRNOM" binary system under "as-is" conditions and "as-is" under irradiation were not significantly different from each other. On the other hand, an increase in hydrodynamic size was monitored for "N-TiO_2 and SRNOM" binary system "as-is" under irradiation in comparison to "N-TiO_2 and SRNOM" binary system under "as-is" conditions. Therefore, it could be concluded that "N-TiO_2 and SRNOM" binary system "as-is" under irradiation expressed higher hydrodynamic sizes in comparison to "N-TiO_2 and SRNOM" binary system under "as-is" conditions along 120 min.

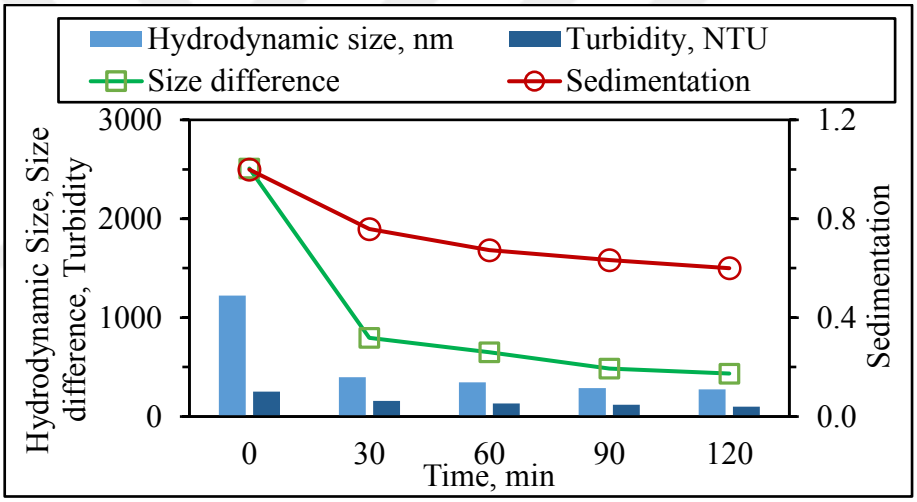


Figure 4.343. "N-TiO_2 and SRNOM" binary system "as-is" under irradiation. Comparative evaluation of selected parameters as hydrodynamic size, hydrodynamic size difference, sedimentation and turbidity variations.

For comparison purposes, it could be asserted that hydrodynamic size variations of "N-TiO_2 and SRNOM" binary system under "as-is", and "as-is dark" conditions was approximately doubled in comparison to "N-TiO_2 and HA" binary system under "as-is", and "as-is dark" conditions over period of 120 min (Figure 4.330). However, sedimentation profiles of "N-TiO_2 and SRNOM" binary system and "N-TiO_2 and HA" binary system were displayed similar tendencies. On the other hand, turbidity profiles of "N-TiO_2 and SRNOM" binary system and "N-TiO_2 and HA" binary system also demonstrated similarities excluding "N-TiO_2 and HA" binary system under "as-is" conditions over period of 120 min.

4.4.5. Behavior of "Fe-TiO_2 and HA" Binary System under "as-is", "as-is dark", "following photolysis of organic matter", and "as-is irradiation" Conditions

As described for TiO_2 and HA under "as-is", "as-is dark", "following photolysis of organic matter", and "as-is irradiation" conditions (Figure 4.316), a similar approach was followed for Fe-TiO_2 and HA under "as-is", "as-is dark", "following photolysis of organic matter", and "as-is irradiation" conditions (Figure 4.344). Under initial conditions, hydrodynamic sizes were 764.4 nm, 469.6 nm, 761.0 nm, and 920.7 nm for binary system of Fe-TiO_2 and HA designated as "Fe-TiO_2 and HA" binary system under "as-is" conditions, "Fe-TiO_2 and HA" binary system "as-is under dark" conditions, "Fe-TiO_2 and HA_{pho}" binary system following photolysis of organic matter, "Fe-TiO_2 and HA" binary system "as-is" under irradiation, respectively.

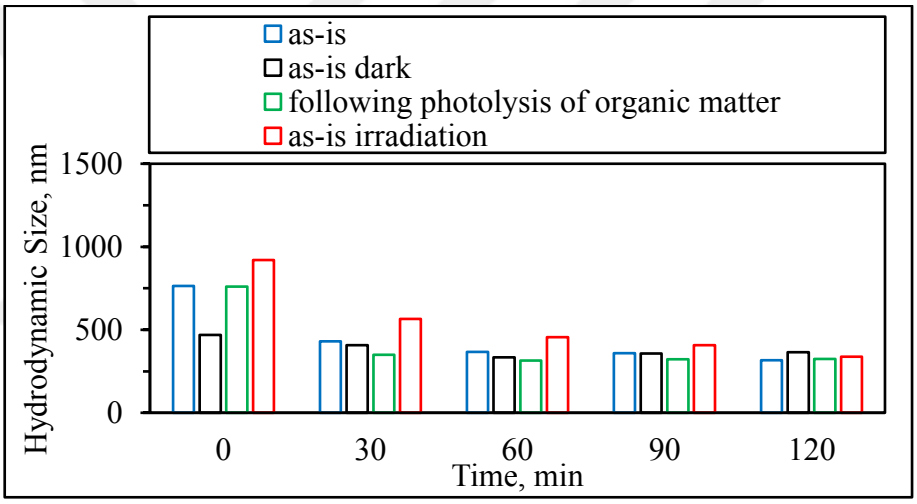


Figure 4.344. Hydrodynamic size variations of Fe-TiO_2 and HA binary system under "as-is", "as-is dark", "following photolysis of organic matter", and "as-is irradiation" conditions.

Variations in hydrodynamic sizes of Fe-TiO_2 and HA under various conditions could be aligned in the order of "Fe-TiO_2 and HA" binary system "as-is" under irradiation > "Fe-TiO_2 and HA" binary system under "as-is" conditions > "Fe-TiO_2 and HA_{pho}" binary system following photolysis of organic matter > "Fe-TiO_2 and HA" binary system "as-is" under dark conditions. Upon dark conditions, Fe-TiO_2 and HA displayed an average hydrodynamic size as 386.9 ± 53.3 nm. "Fe-TiO_2 and HA_{pho}" binary system following photolysis of organic matter demonstrated an average hydrodynamic size as 414.3 ± 194.2 nm. On the other hand, sample prepared upon irradiation revealed an average hydrodynamic size as 537.8 ± 229.5 nm. However, "Fe-TiO_2 and HA" binary system under "as-is" conditions exhibited an average hydrodynamic size as 447.2 ± 182.0 nm. It could be concluded that the biggest change was observed for "Fe-TiO_2 and HA" binary system "as-is" under irradiation.

Following the same manner, sedimentation tendency profiles were presented in Figure 4.345. Contrary to "Fe-TiO_2 and HA" binary system "as-is" under dark conditions, under "as-is" conditions, "following photolysis of organic matter", and "as-is under irradiation" conditions revealed almost similar trends.

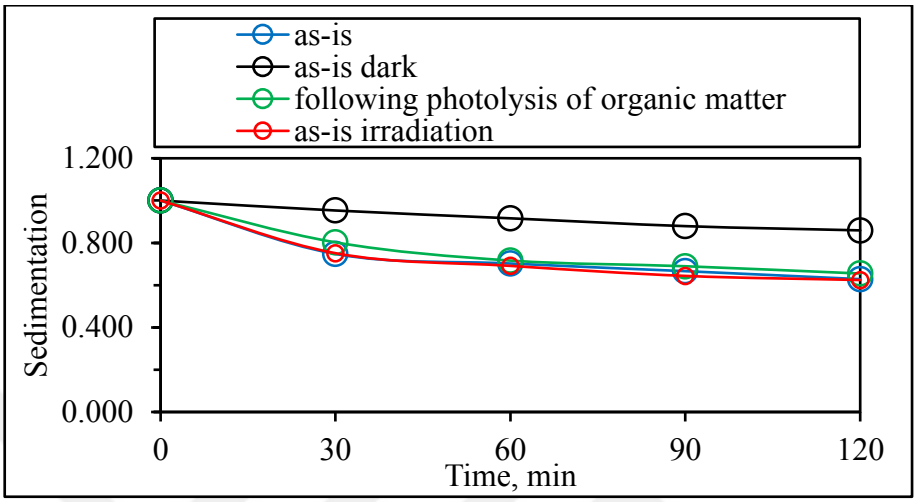


Figure 4.345. Sedimentation profiles of Fe-TiO_2 and HA binary system under "as-is", "as-is dark", "following photolysis of organic matter", and "as-is irradiation" conditions.

In a similar manner, alterations in turbidity of Fe-TiO_2 and HA under the specified conditions could be arrayed in the decreasing order of "Fe-TiO_2 and HA" binary system under "as-is" conditions > "Fe-TiO_2 and HA_{pho}" binary system following photolysis of organic matter > "Fe-TiO_2 and HA" binary system "as-is" under irradiation > "Fe-TiO_2 and HA" binary system "as-is" under dark conditions (Figure 4.346).

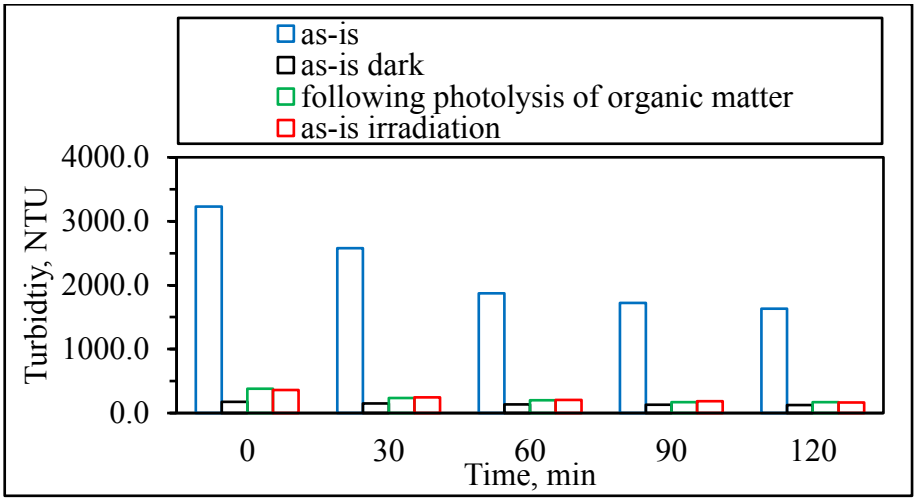


Figure 4.346. Turbidity profiles of Fe-TiO_2 and HA binary system under "as-is", "as-is dark", "following photolysis of organic matter", and "as-is irradiation" conditions.

4.4.5.1. Comparative evaluation of selected parameters as hydrodynamic size, hydrodynamic size difference, sedimentation and turbidity variations of "Fe-TiO_2 and HA" binary system under "as-is", "as-is dark", "following photolysis of organic matter", and "as-is irradiation" conditions. Comparative evaluation of selected parameters as hydrodynamic size, hydrodynamic size difference, sedimentation and turbidity variations for "Fe-TiO_2 and HA" binary system under "as-is" conditions was presented in Figure 4.347. "Fe-TiO_2 and HA" binary system under "as-is" conditions expressed comparatively higher turbidity values in relation to hydrodynamic size variations. Small fluctuations could be observed in hydrodynamic size differences in accordance with the variations in the range although an average hydrodynamic size was attained as 408.8 ± 162.6 nm. Sedimentation profiles followed a parallel trend to hydrodynamic size variations.

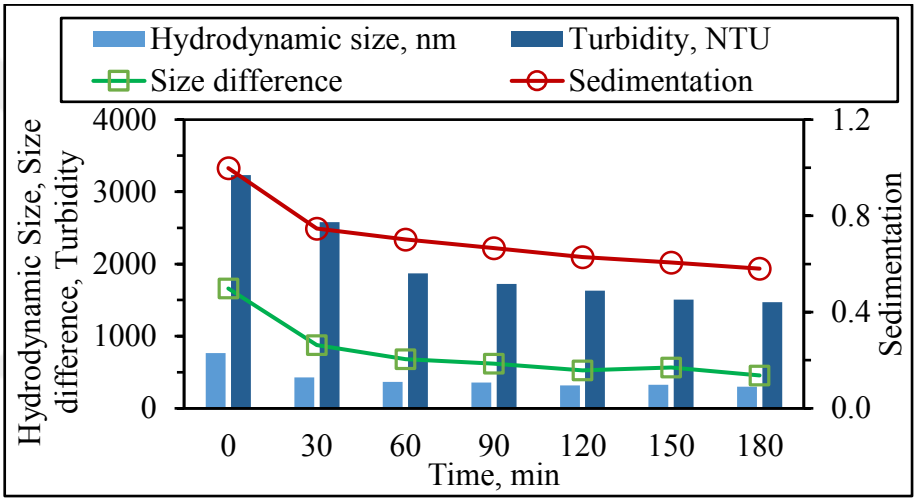


Figure 4.347. "Fe-TiO_2 and HA" binary system under "as-is" conditions. Comparative evaluation of selected parameters as hydrodynamic size, hydrodynamic size difference, sedimentation and turbidity variations.

Comparative evaluation of selected parameters as hydrodynamic size, hydrodynamic size difference, sedimentation and turbidity variations for "Fe-TiO_2 and HA" binary system "as-is" under dark conditions was demonstrated in Figure 4.348. For comparison purposes, it could be deduced that continuous mixing provided under dark significantly affected the behavior of all parameters of "Fe-TiO_2 and HA" binary system under "as-is" conditions (Figure 4.347). Although an average hydrodynamic size was obtained as 408.8 ± 162.6 nm for "Fe-TiO_2 and HA" binary system under "as-is" conditions, under the specified "as-is" under dark conditions, an average hydrodynamic size was attained as 386.9 ± 53.3 nm. Upon treatment of 60 min, continuous mixing under dark conditions affected Fe-TiO_2 and HA more significantly in hydrodynamic size difference trend in comparison to continuously decreasing sedimentation profile (Figure 4.348). Also, lower turbidity values were obtained in comparison to hydrodynamic size variations during 120 min.

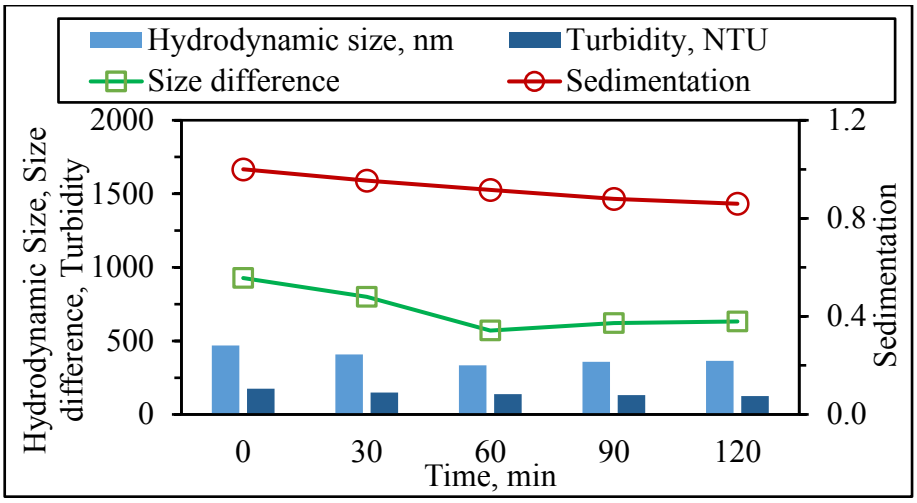


Figure 4.348. "Fe-TiO_2 and HA" binary system "as-is" under dark conditions. Comparative evaluation of selected parameters as hydrodynamic size, hydrodynamic size difference, sedimentation and turbidity variations.

Comparative evaluation of selected parameters as hydrodynamic size, hydrodynamic size difference, sedimentation and turbidity variations of "Fe-TiO_2 and HA_{pho}" binary system following photolysis of organic matter was demonstrated in Figure 4.349. It could be stated that the most distinct variation was observed in size difference upon treatment of 60 min. "Fe-TiO_2 and HA_{pho}" binary system following photolysis of organic matter expressed lower turbidity values in comparison to hydrodynamic size variations. On the other hand, sedimentation profiles of "Fe-TiO_2 and HA_{pho}" binary system following photolysis of organic matter followed a similar trend to hydrodynamic size alterations.

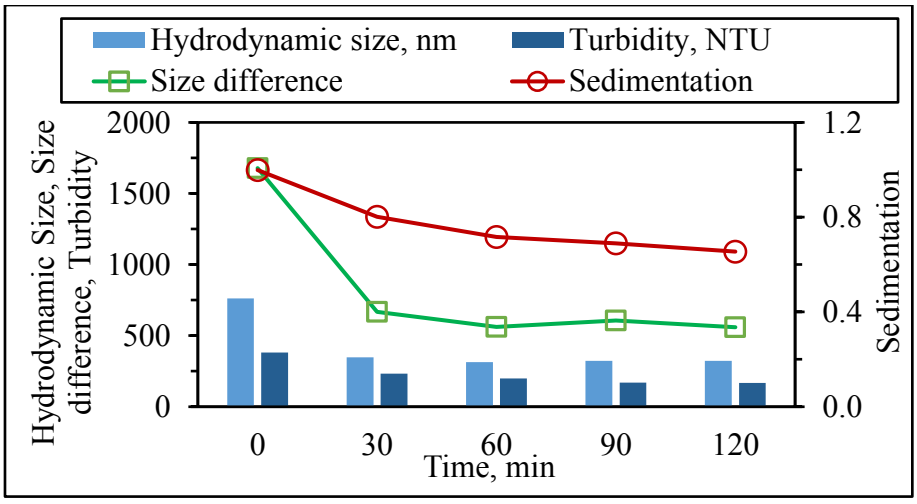


Figure 4.349. "Fe-TiO_2 and HA_{pho}" binary system following photolysis of organic matter. Comparative evaluation of selected parameters as hydrodynamic size, hydrodynamic size difference, sedimentation and turbidity variations.

From a general view, it should be mentioned that primary particle size of Fe-TiO_2 was ~15 nm. However, aggregate size could be visualized as 633.6 nm. The dominant effect could be related to the pH_{zpc} condition as 4.80 (Table A). Under the specified conditions, it should also be considered that irradiation effect would be prevailing in humic structure during photolysis. Therefore, it could be stated that an average diameter of "Fe-TiO_2 and HA" binary system under "as-is" conditions was obtained as 408.8 ± 162.6 nm whereas average diameter of "Fe-TiO_2 and HA" binary system following photolysis of organic matter was attained as 414.3 ± 194.2 nm.

In a similar manner, under similar experimental conditions, comparative evaluation of selected parameters as hydrodynamic size, hydrodynamic size difference, sedimentation and turbidity variations of "Fe-TiO_2 and HA" binary system "as-is" under irradiation was presented in Figure 4.350. It could be inferred that although similar decreasing trends were observed for size difference and sedimentation profiles, size difference revealed the most significant variations over period of 120 min. On the other hand, an average hydrodynamic diameter was obtained as 537.8 ± 229.5 nm and it could be concluded that "Fe-TiO_2 and HA" binary system "as-is" under irradiation expressed comparatively lower turbidity values in relation to hydrodynamic size variations. For comparison purposes, it could be deduced that hydrodynamic size, hydrodynamic size difference, and sedimentation profiles of "Fe-TiO_2 and HA" binary system under "as-is" conditions and "as-is" under irradiation revealed similar tendencies upon period of 120 min. However, turbidity variations under irradiation were distinctly different than alterations obtained upon "as-is" conditions proving the significant effect of irradiation.

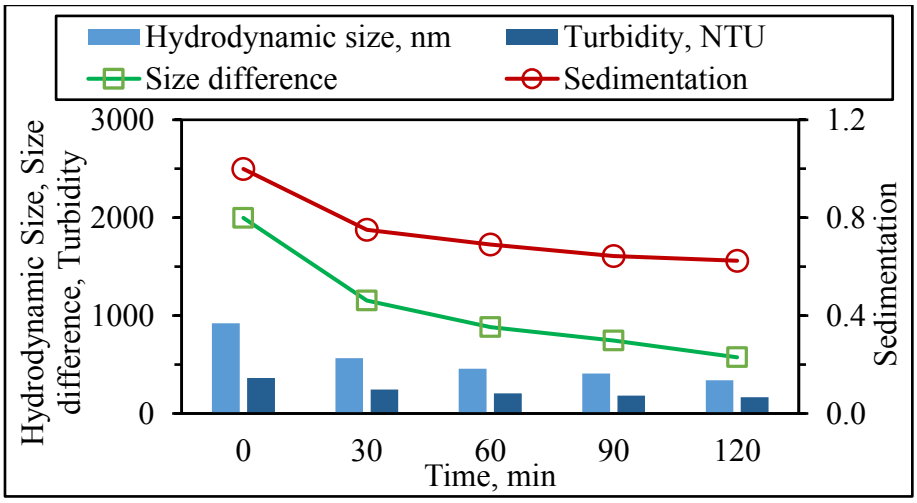


Figure 4.350. "Fe-TiO_2 and HA" binary system "as-is" under irradiation. Comparative evaluation of selected parameters as hydrodynamic size, hydrodynamic size difference, sedimentation and turbidity variations.

4.4.6. Behavior of "Fe-TiO_2 and SRNOM" Binary System under "as-is", "as-is dark", "following photolysis of organic matter", and "as-is irradiation" Conditions

As explained for Fe-TiO_2 and HA binary system under "as-is", "as-is dark", "following photolysis of organic matter", and "as-is irradiation" conditions (Figure 4.344), following a similar trend, hydrodynamic size variations of Fe-TiO_2 and SRNOM was observed (Figure 4.351). It could be inferred that sample was subjected to recording immediately after preparation revealed an average hydrodynamic size as 538.6 ± 310.4 nm. Upon dark conditions, *i.e.* continuously stirred sample for 60 min affected the particle size distribution of Fe-TiO_2 and SRNOM exhibited an average hydrodynamic size as 420.0 nm ± 99.2 nm. However, "Fe-TiO_2 and $SRNOM_{pho}$" binary system following photolysis of organic matter demonstrated an average hydrodynamic size as 429.4 ± 209.4 nm. On the other hand, sample prepared upon irradiation revealed an average hydrodynamic size as 1747.2 ± 322.6 nm.

Under initial conditions, hydrodynamic sizes were 1088.8 nm, 589.3 nm, 801.7 nm, and 2311.7 nm for binary system of Fe-TiO_2 and SRNOM designated as "Fe-TiO_2 and SRNOM" binary system under "as-is" conditions, "Fe-TiO_2 and SRNOM" binary system "as-is" under dark conditions, "Fe-TiO_2 and $SRNOM_{pho}$" binary system following photolysis of organic matter, "Fe-TiO_2 and SRNOM" binary system "as-is" under irradiation, respectively.

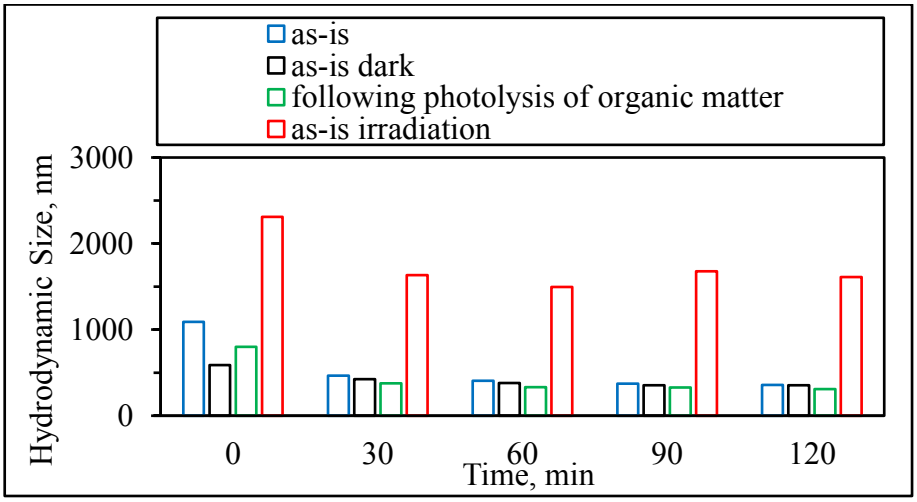


Figure 4.351. Hydrodynamic size variations of Fe-TiO_2 and SRNOM binary system under "as-is", "as-is dark", "following photolysis of organic matter", and "as-is irradiation" conditions.

Sedimentation profiles of Fe-TiO_2 and SRNOM binary system under "as-is", "as-is dark", "following photolysis of organic matter", and "as-is irradiation" conditions were displayed in Figure 4.352. Based on the presented data, sedimentation variations could be arranged in the decreasing

order of "Fe-TiO_2 and SRNOM" binary system under "as-is" conditions > "Fe-TiO_2 and SRNOM" binary system "as-is" under dark conditions > "Fe-TiO_2 and $SRNOM_{pho}$" binary system following photolysis of organic matter > "Fe-TiO_2 and SRNOM" binary system "as-is" under irradiation.

Also, turbidity profiles of Fe-TiO_2 and SRNOM binary system under "as-is", "as-is dark", "following photolysis of organic matter", and "as-is irradiation" conditions were exhibited in Figure 4.353 and could be aligned in the decreasing order of "Fe-TiO_2 and SRNOM" binary system "as-is" under dark conditions > "Fe-TiO_2 and SRNOM" "as-is" under irradiation > "Fe-TiO_2 and SRNOM" binary system under "as-is" conditions > "Fe-TiO_2 and $SRNOM_{pho}$" binary system following photolysis of organic matter.

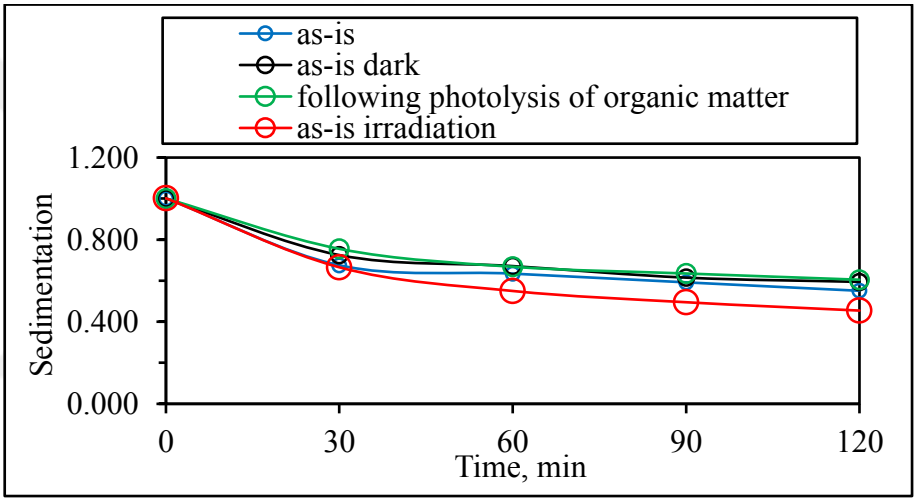


Figure 4.352. Sedimentation profiles of Fe-TiO_2 and SRNOM binary system under "as-is", "as-is dark", "following photolysis of organic matter", and "as-is irradiation" conditions.

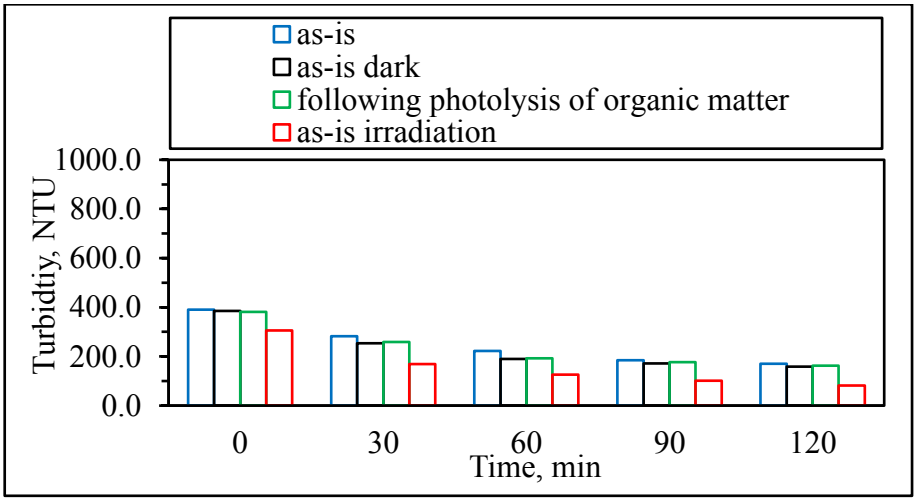


Figure 4.353. Turbidity profiles of Fe-TiO_2 and SRNOM binary system under "as-is", "as-is dark", "following photolysis of organic matter", and "as-is irradiation" conditions.

4.4.6.1. Comparative evaluation of selected parameters as hydrodynamic size, hydrodynamic size difference, sedimentation and turbidity variations of "Fe-TiO_2 and SRNOM" binary system under "as-is", "as-is dark", "following photolysis of organic matter", and "as-is irradiation" conditions. Comparative evaluation of selected parameters as hydrodynamic size, hydrodynamic size difference, sedimentation and turbidity variations for "Fe-TiO_2 and SRNOM" binary system under "as-is" conditions was presented in Figure 4.354. Fe-TiO_2 and SRNOM expressed comparatively lower turbidity values in relation to hydrodynamic size variations. In the first 30 min, a sharp decrease could be observed in hydrodynamic size differences in accordance with the variations in the range although an average hydrodynamic size was attained as 538.6 ± 310.4 nm. Also, sedimentation profiles followed a parallel trend to hydrodynamic size variations.

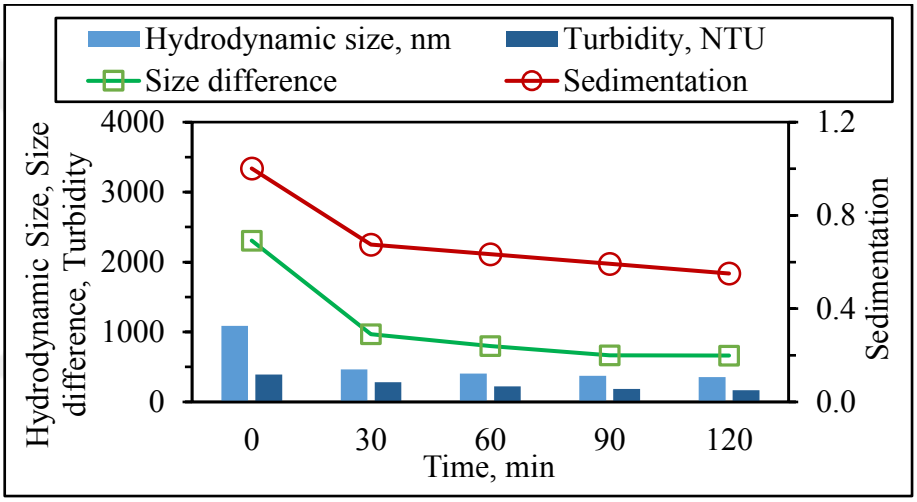


Figure 4.354. "Fe-TiO_2 and SRNOM" binary system under "as-is" conditions. Comparative evaluation of selected parameters as hydrodynamic size, hydrodynamic size difference, sedimentation and turbidity variations.

In a similar manner, comparative evaluation of selected parameters as hydrodynamic size, hydrodynamic size difference, sedimentation and turbidity variations of "Fe-TiO_2 and SRNOM" binary system "as-is" under dark conditions were demonstrated in Figure 4.355. It could be inferred that continuous mixing provided under dark significantly affected the hydrodynamic size of "Fe-TiO_2 and SRNOM" binary system under "as-is" conditions. Upon treatment of 60 min, continuous mixing under dark conditions affected Fe-TiO_2 and SRNOM more significantly in hydrodynamic size difference trend in comparison to continuously decreasing sedimentation profile. Under the specified "as-is" under dark conditions, although hydrodynamic size and size difference approximately 50 % decreased, sedimentation and turbidity profiles displayed almost similar trend in comparison to inconsistent trend obtained for "Fe-TiO_2 and SRNOM" binary system under "as-is" conditions (Figure 4.354).

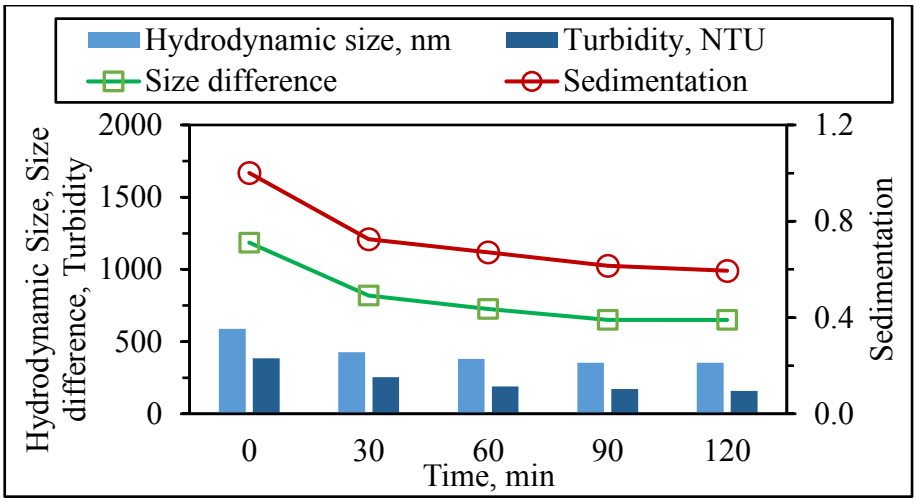


Figure 4.355. "Fe-TiO_2 and SRNOM" binary system "as-is" under dark conditions. Comparative evaluation of selected parameters as hydrodynamic size, hydrodynamic size difference, sedimentation and turbidity variations.

As explained for "Fe-TiO_2 and SRNOM" binary system under "as-is" conditions (Figure 4.354), following a similar trend, comparative evaluation of selected parameters as hydrodynamic size, hydrodynamic size difference, sedimentation and turbidity variations of "Fe-TiO_2 and $SRNOM_{pho}$" binary system following photolysis of organic matter were presented in Figure 4.356. It could be inferred that upon photolysis of 60 min, a slight decrease in hydrodynamic size and size difference was observed for "Fe-TiO_2 and $SRNOM_{pho}$" binary system following photolysis of organic matter in comparison to "Fe-TiO_2 and SRNOM" binary system under "as-is" conditions. On the other hand, sedimentation and turbidity alterations were substantially stabilized.

Following a similar manner to data described "Fe-TiO_2 and SRNOM" binary system under "as-is" conditions (Figure 4.354), comparative evaluation of selected parameters as hydrodynamic size, hydrodynamic size difference, sedimentation and turbidity variations of "Fe-TiO_2 and SRNOM" binary system "as-is" under irradiation was demonstrated in Figure 4.357. Size difference and sedimentation profiles followed a similar trend in the first 30 min, and the most distinct decreasing trend was observed for sedimentation profile. On the other hand, "Fe-TiO_2 and SRNOM" binary system "as-is" under irradiation demonstrated relatively minor turbidity values in relation to hydrodynamic size alterations. For comparison purposes, sedimentation and turbidity profiles of "Fe-TiO_2 and SRNOM" binary system under "as-is" conditions and "as-is" under irradiation revealed similar tendencies. However, hydrodynamic size and hydrodynamic size difference variations under irradiation were doubled, and distinctly different than alterations attained upon as-is conditions revealing the critical effect of irradiation.

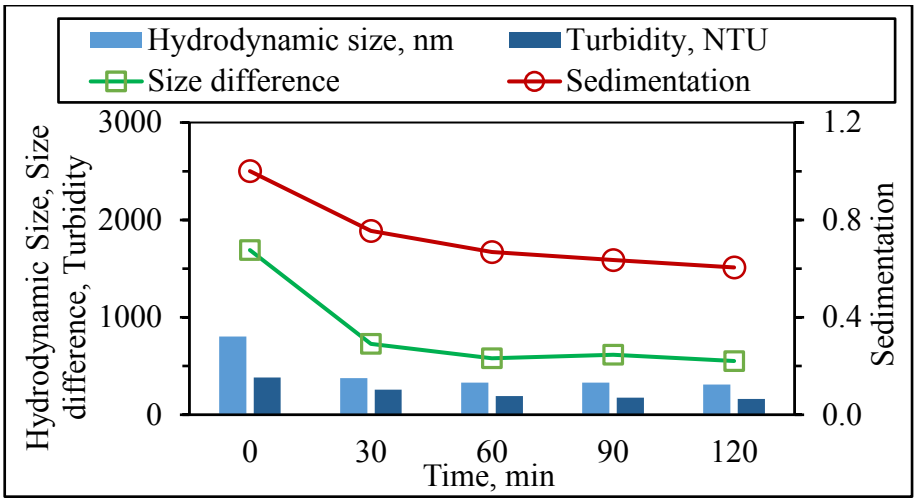


Figure 4.356. "Fe-TiO_2 and $SRNOM_{pho}$" binary system following photolysis of organic matter. Comparative evaluation of selected parameters as hydrodynamic size, hydrodynamic size difference, sedimentation and turbidity variations.

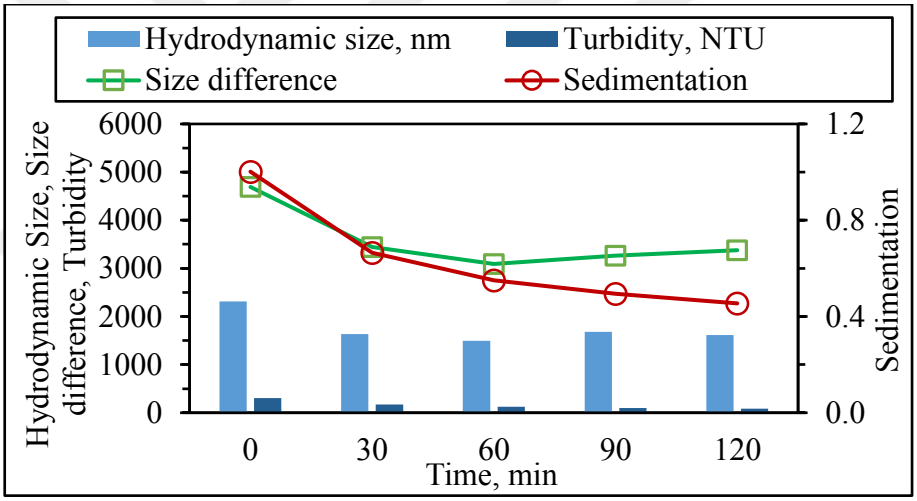


Figure 4.357. "Fe-TiO_2 and SRNOM" binary system "as-is" under irradiation. Comparative evaluation of selected parameters as hydrodynamic size, hydrodynamic size difference, sedimentation and turbidity variations.

For comparison purposes, it could be deduced that higher hydrodynamic size variations were attained for "Fe-TiO_2 and SRNOM" binary system under "as-is", "as-is dark", "following photolysis of organic matter", and "as-is irradiation" conditions in comparison to "Fe-TiO_2 and HA" binary system under "as-is", "as-is dark", "following photolysis of organic matter", and "as-is irradiation" conditions (Figure 4.344). On the other hand, similar sedimentation profiles were observed excluding "Fe-TiO_2 and HA" binary system under "as-is" conditions (Figure 4.345). Also, similar turbidity profiles were obtained excluding "Fe-TiO_2 and HA" binary system under "as-is" conditions and "as-is" under dark conditions upon 120 min period.

5. CONCLUSION

In this study, the colloidal behavior of the nanoparticles, namely bare TiO_2 and visible light active modified forms of TiO_2 *i.e.* N-TiO_2 and Fe-TiO_2 were investigated prior to, during and under post treatment conditions. Following individual assessments, binary systems composed of humic fractions and nanoparticles were subjected to evaluation by following basic experimental procedures, *i.e.* dynamic light scattering, sedimentation and turbidity. Aggregation and/or agglomeration behavior of both matrix components provided information on expected reactivity under irradiation during photocatalysis. Baseline experiments as photolysis and adsorption provided information on the partners prior to and post irradiation conditions. Adsorption properties of humic fractions onto bare TiO_2 and doped TiO_2 specimens were assessed and compared in terms of *i*. UV-vis spectroscopic parameters *i.e*. color forming moieties ($Color_{436}$) and UV absorbing centers (UV_{365}, UV_{280} and UV_{254}) *ii*. fluorescence spectroscopy acquired in emission and synchronous scan modes and *iii*. dissolved organic carbon.

Based on the information presented in the literature, it was clearly stated that colloidal behavior of both inorganic and organic components displayed various reactions under solar irradiation in nanoscale conditions. In this study the dynamic light scattering (DLS) technique has been used to characterize the particle size distribution of nanoparticles. Initial size distribution and time dependent homoaggregation kinetics of TiO_2 specimens were measured.

Comparative evaluation of behavior of nanoparticles under as-is conditions in the absence of organic matter indicated that doped TiO_2 nanoparticles tend to aggregate more than bare TiO_2. Although TiO_2 did not demonstrate big variations in terms of size differences, N-TiO_2 and Fe-TiO_2 displayed 50-60 % hydrodynamic size decrease with respect to time. The reason could be ascribed to the doping effect. Moreover, as well as sedimentation variations support turbidity measurements, they could not be assessed as a surrogate parameter. Considering removal efficiencies, TiO_2 specimens showed fewer tendencies than N-TiO_2 and Fe-TiO_2 specimens. Therefore, it could be concluded that turbidity alterations could be evaluated an evidence of this outcomes.

Comparative evaluation of behavior of nanoparticles as-is under dark conditions in the absence of organic matter displayed that relatively lower hydrodynamic sizes, sedimentation and turbidity variations were recorded compared to the alterations recorded under as-is conditions. The reason

could be attributed to the mixing effect under dark conditions. Samples were directly taken for the measurements under as-is conditions.

Comparative evaluation of behavior of nanoparticles as-is under irradiation in the absence of organic matter indicated that hydrodynamic size variations of TiO_2 could be assessed nearly stable, whereas N-TiO_2 and Fe-TiO_2 demonstrated more than 50 % decrease between 0 and 30 min and progressed almost stable until the end of 120 min period. Considering the hydrodynamic size differences between all conditions, the reason could also be ascribed to the preparation methodology, since 30 seconds ultrasonication was applied for irradiation, smaller hydrodynamic sizes could be seen compared to as-is and as-is under dark conditions of nanoparticles. Considering hydrodynamic size, sedimentation and turbidity variations, different behavior of TiO_2, N-TiO_2 and Fe-TiO_2 specimens could be attributed to the characterization of the photocatalysts.

Comparative evaluation of behavior of nanoparticles under as-is conditions in the presence of organic matter expressed "N-TiO_2 and HA" and "Fe-TiO_2 and HA" samples that were subjected to recording immediately after preparation revealed higher hydrodynamic sizes than "TiO_2 and HA". On the other hand, "TiO_2 and HA" did not exhibit significant variations in terms of hydrodynamic size and size differences, whereas hydrodynamic size and size difference of "N-TiO_2 and HA" and "Fe-TiO_2 and HA" fell almost by half upon 180 min experimental duration. The reason could be attributed to the surface interactions between nanoparticles and organic matter. Sedimentation profiles of "TiO_2 and HA", "N-TiO_2 and HA" and "Fe-TiO_2 and HA" binary system support turbidity measurements. Removal efficiencies of "N-TiO_2 and HA" and "Fe-TiO_2 and HA" were distinctly different than "TiO_2 and HA" removal efficiency along 180 min. It could be concluded that hydrodynamic size variations coincide with sedimentation variations of "TiO_2 and HA", "N-TiO_2 and HA" and "Fe-TiO_2 and HA" binary system under "as-is" conditions.

Comparative evaluation of behavior of nanoparticles as-is under dark conditions in the presence of organic matter demonstrated that comparatively lower hydrodynamic sizes, size differences, sedimentation and turbidity variations were recorded in comparison to the variations recorded under as-is conditions. The reason could be ascribed to the continuous mixing under dark conditions.

Comparative evaluation of behavior of nanoparticles following photolysis of organic matter conditions in the presence of organic matter displayed that photolysis of organic matter did not significantly affect the behavior of all parameters of "TiO_2 and HA" "N-TiO_2 and HA" and "Fe-TiO_2 and HA" under "as-is" conditions excluding turbidity behavior. For comparison purposes,

hydrodynamic size, size difference and sedimentation alterations of all samples revealed similar tendencies. However, turbidity profile of "TiO_2 and HA_{pho}" "following photolysis of organic matter" was comparatively higher than "N-TiO_2 and HA_{pho}" "following photolysis of organic matter" and "Fe-TiO_2 and HA_{pho}" "following photolysis of organic matter" samples upon 120 min experimental duration.

Comparative evaluation of behavior of nanoparticles as-is under irradiation in the presence of organic matter indicated that upon treatment of 30 min, continuous mixing under irradiation affected more significantly in hydrodynamic size and size difference of "TiO_2 and HA" under "as-is" conditions. On the other hand, no significant variation was observed in hydrodynamic size, size difference and sedimentation of "N-TiO_2 and HA" and "Fe-TiO_2 and HA" under "as-is" conditions. However, turbidity profiles of "TiO_2 and HA", "N-TiO_2 and HA" and "Fe-TiO_2 and HA" "as-is under irradiation" were significantly affected in comparison to "as-is" conditions. The reason could be attributed to the serious effect of irradiation upon treatment of 30 min.

In conclusion, this study represents the colloidal behavior of TiO_2, N-TiO_2, Fe-TiO_2 nanoparticles prior to, during and under post treatment conditions by the application of particle size distribution, sedimentation and turbidity experiments. It is clearly stated that colloidal behavior of both inorganic and organic components displayed various reactions under solar irradiation in nanoscale conditions. Overall evaluation of the systems provided information both during photocatalysis as well as light induced reactions under environmental conditions. In the light of these outcomes, an extensive insight was inferred on the fate of nanoparticles through photocatalysis.

REFERENCES

Abbas, Q., Yousaf, B., Amina, Ali, M.U., Munir, M.A.M., El-Naggar, A., Rinklebe, J., Naushad, M., 2020. Transformation pathways and fate of engineered nanoparticles (ENPs) in distinct interactive environmental compartments: A review. Environmental International, 138, 105646.

Al-Kattan, A., Wichser, A., Zuin, S., Arroyo, Y., Golanski, L., Ulrich, A., Nowack, B., 2014. Behavior of TiO_2 released from nano-TiO_2 containing paint and comparison to pristine nano-TiO_2. Environmental Science and Technology, 48, 6710-6718.

Bekbolet, M., Boyacioglu, Z., Ozkaraova, B., 1998. The influence of solution matrix on the photocatalytic removal of color from natural waters. Water Science and Technology, 38, 155-162.

Bekbolet, M., Suphandag A.S., Uyguner C.S., 2002. An investigation of the photocatalytic efficiencies of TiO_2 powders on the decolourisation of humic acids. Journal of Photochemistry and Photobiology, A: Chemistry, 148(1-3), 121-128.

Bekbolet, M., Sen-Kavurmaci, S., 2015. The effect of photocatalytic oxidation on molecular size distribution profiles of humic acid. Photochemical and Photobiological Sciences, 14, 576-582.

Benefield, L.D., Judkins, J.F., Weand, B.L., 1982. Process Chemistry for Water and Wastewater Treatment. Englewood Cliffs, Prentice-Hall, New Jersey, U.S.A.

Bharti, B. 2014. Adsorption, Aggregation and Structure Formation in Systems of Charged Particles, From Colloidal to Supracolloidal Assembly. Springer, Switzerland.

Birben, N.C., Uyguner-Demirel, C.S., Sen-Kavurmaci, S., Gurkan, Y.Y., Turkten, N., Cinar, Z., Bekbolet, M., 2015. Comparative evaluation of anion doped photocatalysts on the mineralization and decolorization of natural organic matter. Catalysis Today, 240, 125-131.

Birben N.C., Uyguner-Demirel C.S., Sen-Kavurmaci S., Gurkan Y.Y., Turkten N., Cinar Z., Bekbolet M., 2017. Application of Fe-doped TiO_2 specimens for the solar photocatalytic degradation of humic acid. Catalysis Today, 281, 78-84.

Budarz, J.F., Turolla, A., Piasecki, A.F., Bottero, J-Y., Antonelli, M., Wiesner, M.R., 2017. Influence of aqueous inorganic anions on the reactivity of nanoparticles in TiO_2 photocatalysis. Langmuir, 33, 2770-2779.

Buffle, J., 1988. Complexation Reactions in Aquatic Systems - An Analytical Approach. Ellis Harwood Series in Analytical Chemistry, 692, Chichester, U.K.

Chatterjee D., Dasgupta S., 2005. Visible light induced photocatalytic degradation of organic pollutants. Journal of Photochemistry and Photobiology, 6, 186-205.

Christian, P., Von der Kammer, F., Baalousha, M., Hoffmann, T., 2008. Nanoparticles: structure, properties, preparation and behavior in environmental media. Ecotoxicology, 17, 326-343.

Colombo, C., Palumbo, G., Angelico, R., Cho, H.G., Francisco, O., Ertani A., Nardi, S., 2015. Spontaneous aggregation of humic acid observed with AFM at different pH. Chemosphere, 138, 821-828.

Crittenden J.C., Trussell R.R., Hand D.W., Howe K.J., Tchobanoglous G., 2005. Water Treatment: Principles and Design, 2nd Edition, John Wiley & Sons, New Jersey, U.S.A.

Diaz, L., Peyrot, C., Wilkinson, K.J., 2015. Characterization of polymeric nanomaterials using analytical ultracentrifugation. Environmental Science and Technology, 49, 7302-7309.

Diebold, U., 2003. The surface science of titanium dioxide. Surface Science Reports, 48, 53-229.

Erhayem, M., Sohn, M., 2014a. Effect of humic acid source on humic acid adsorption onto titanium dioxide nanoparticles. Science of the Total Environment, 470-471, 92-98.

Erhayem, M., Sohn, M., 2014b. Stability studies for titanium dioxide nanoparticles upon adsorption of Suwannee River humic and fulvic acids and natural organic matter. Science of the Total Environment, 468-469, 249-257.

Gaffney J.S., Marley N.A., Clark S.B. (Eds.). 1996. Humic and fulvic acids: Isolation, Structure, and Environmental Role, ACS Symposium Series, U.S.A.

Gupta, S.M., Tripathi, M., 2011. A review of TiO_2 nanoparticles. Chinese Science Bulletin, 56, 1639-1657.

Hatcher, P.G., Schnitzer, M., Dennis, L.W., Maciel, G.E., 1981. Aromacity of humic substances in soils. Soil Science Society of America Journal, 45, 1089-1094.

Heilgeist, S., Sekine, R., Oz, S., Stewart, R.A., 2021. Finding Nano: Challenges involved in monitoring the presence and fate of engineered titanium dioxide nanoparticles in aquatic environments. Water, 13, 734.

Hendricks, D., 2006. Water Treatment Unit Processes, Physical and Chemical. CRC Press, Taylor and Francis, Florida, U.S.A.

Henglein A., 1861. Small-particle research: physicochemical properties of extremely small colloidal metal and semiconductor particles. Chemical Reviews, 89, 1861-1873.

Hufschmid, R., Newcomb, C.J., Grate, J.W., De Yoreo, J.J., Browning, N.D., Nikolla P. Qafoku, N.P., 2017. Direct visualization of aggregate morphology and dynamics in a model soil organic-mineral system. Environmental Science and Technology Letters. 4, 186-191.

Hotze, E.M., Bottero, J-Y., Wiesner, M.R., 2010. Theoretical framework for nanoparticle reactivity as a function of aggregation state. Langmuir, 26, 13, 11170-11175.

Jaffrezic-Renault, N., Pichat, P., Foissy, A., Mercier, R., 1986. Effect of Deposited Pt Particles on the Surface Charge of TiO_2 Aqueous suspensions by potentiometry, electrophoresis, and labeled ion adsorption. Journal of Physical Chemistry, 90, 2733-2738.

Jassby, D., Budarz, J.F., Wiesner, M., 2012. Impact of aggregate size and structure on the photocatalytic properties of TiO_2 and ZnO nanoparticles. Environmental Science and Technology, 46, 6934-6941.

Jiang, J., Oberdörster, G., Biswas, P., 2009. Characterization of size, surface charge, and agglomeration state of nanoparticle dispersions for toxicological studies. Nanoparticle Research, 11, 77-89.

Joo, S.H., Zhao, D., 2017. Environmental dynamics of metal oxide nanoparticles in heterogeneous systems: A review. Journal of Hazardous Materials, 322, 29-47.

Kisch, H., 2015. Semiconductor Photocatalysis: Principles and Applications. Wiley-VCH, Weinheim, Germany.

Kitis, M., Kaplan, S.S., 2007. Advanced oxidation of natural organic matter using hydrogen peroxide and iron-coated pumice particles. Chemosphere, 68, 1846-1853.

Kipton, H., Powell, J., Town, R.M., 1992. Solubility and fractionation of humic acid; Effect of pH and ionic medium. Analytica Chimica Acta, 267, 47-54.

Lee, J., Bartelt-Hunt, S.L., Li, Y., Gilrein, E.J., 2016. The influence of ionic strength and organic compounds on nanoparticle TiO_2 (n-TiO_2) aggregation. Chemosphere, 154, 187-193.

Li, Y., Yang, C., Guo, X., Dang, Z., Li, X., Zhang, Q., 2015. Effects of humic acids on the aggregation and sorption of nano-TiO_2. Chemosphere, 119, 171-176.

Loosli, F., Le Coustumer, P., Stoll, S., 2014. Effect of natural organic matter on the disagglomeration of manufactured TiO_2 nanoparticles. Environmental Science Nano, 1, 154.

Manahan, S.E., 2000. Environmental Chemistry, 6th Edition, Lewis Publishers, CRC Press, U.S.A.

Martínez, A.G., Barbosa S, Santos, I.P., Marzán, L.M.L., 2011. Nanostars shine bright for you: colloidal synthesis, properties and applications of branched metallic nanoparticles. Current Opinion in Colloid & Interface Science, 16, 118-127.

Matilainen, A., Sillanpää, M., 2010. Removal of natural organic matter from drinking water by advanced oxidation processes. Chemosphere, 80, 351-365.

Melcher, J., Barth, N., Schilde, C., Kwade, A., Bahnemann, D., 2017. Influence of TiO_2 agglomerate and aggregate sizes on photocatalytic activity. Journal of Material Science, 52, 1047-1056.

Melin, E.S., Ødegaard, H., 1999. Biofiltration of ozonated humic water in expanded clay aggregate filters. Water Science and Technology, 40, 165-172.

Modi, K.B., Bhalodia, J.A., Pathak, T.K., Raval, P.Y., Pansara, P.R., Vasoya, N.H., Kathad, C.R., Shah, S.J., 2018. Bimodal to unimodal particle size distribution transformation in nanocrystalline cobalt-ferri-chromites. International Journal of Scientific Research in Physics and Applied Sciences, 6, 1, 32-36.

Montes, M.O., Hanna, S.K., Lenihan, H.S., Keller, A.A., 2012. Uptake, accumulation, and biotransformation of metal oxide nanoparticles by a marine suspension-feeder. Journal of Hazardous Materials, 225-226, 139-145.

Murray, C.A., Parsons, S.A., 2004. Removal of NOM from drinking water: Fenton's and photo-Fenton's processes. Chemosphere, 54, 1017-1023.

Nikolaou, A., Rizzo, L., Selcuk, H., 2007. Control of Disinfection By-Products in Drinking Water Systems. Nova Science Publishers, Inc., New York.

Oppenländer, T., 2003. Photochemical Purification of Water and Air. Wiley VCH, Weinheim, Germany.

Peng, X., Luan, Z., Zhang, H., 2006. Montmorillonite-Cu (II)/Fe (III) oxides magnetic material as adsorbent for removal of humic acid and its thermal regeneration. Chemosphere, 63, 300-306.

Petala, M.D., Zouboulis, A.I., 2006. Vibratory shear enhanced processing membrane filtration applied for the removal of natural organic matter from surface waters. Journal of Membrane Science, 269, 1-14.

Petersen, E.J., Henry, T.B., Zhao, J., MacCuspie, R.I., Kirschling, T.L., Dobrovolskaia, M.A., Hackley, V., Xing, B., White, J.C., 2014. Identification and avoidance of potential artifacts and misinterpretations in nanomaterial ecotoxicity measurements. Environmental Science and Technology, 48, 4226-4246.

Petosa, A.R., Jaisi, D.P., Quevedo, I.R., Elimelech, M., Tufenkji, N., 2010. Aggregation and deposition of engineered nanomaterials in aquatic environments: Role of physicochemical interactions. Environmental Science and Technology, 44, 6532-6549.

Pichat, P., 2013. Photocatalysis and Water Purification: From Fundamentals to Recent Applications. Wiley-VCH, Weinheim, Germany.

Piccolo, A., 2001. The supramolecular structure of humic substances. Soil Science, 166, 810-832.

Rajeswari, R., Kanmani, S., 2009. A study on degradation of pesticide wastewater by TiO_2 photocatalysis. Journal of Scientific and Industrial Research, 68, 1063-1067.

Rashed, M.N., El-Amin, A.A., 2007. Photocatalytic degradation of methyl orange in aqueous TiO_2 under different solar irradiation sources. International Journal of Physical Sciences, 2(3), 073-081.

Raza, G., Amjad, M., Kaur, I., Wen, D., 2016. Stability and aggregation kinetics of titania nanomaterials under environmentally realistic conditions. Environmental Science and Technology, 50, 8462-8472.

Romanello, M.B., De Cortalezzi, M.M.F., 2013. An experimental study on the aggregation of TiO_2 nanoparticles under environmentally relevant conditions. Water Research, 47, 3887-3898.

SCENIHR, 2005. Request for a scientific opinion on the appropriateness of existing methodologies to assess the potential risks associated with engineered and adventitious nanotechnologies. SCENIHR/002/05.

Selcuk, H., Sene, J.J., Anderson, M.A., 2003. Photoelectrocatalytic humic acid degradation kinetics and effect of pH, applied potential and inorganic ions. Journal of Chemical Technology and Biotechnology, 78, 979-984.

Senesi, N., 1999. Aggregation patterns and macromolecular morphology of humic substances: a fractal approach. Soil Science, 164, 11, 841-856.

Sharpless, C.M., Aeschbacher, M., Page, S.E., Wenk, J., Sander, M., McNeill, K., 2014. Photooxidation-induced changes in optical, electrochemical, and photochemical properties of humic substances. Environmental Science and Technology, 48, 2688-2696.

Sillanpää, M., Paunu, T-M., Sainio, P., 2011. Aggregation and deposition of engineered TiO_2 nanoparticles in natural fresh and brackish waters. Journal of Physics: Conference Series, 304, 1-8.

Sobecka, S.B., Tomaszewska, M., Morawski, A.W., 2006. Removal of humic acids by the ozonation–biofiltration process. Desalination, 198, 265–273.

Stevenson, F.J., 1982. Humus Chemistry: Genesis, Composition, Reactions, Wiley and Sons, New York, Inc., U.S.A.

Sun, J., Guo, L-H., Zhang, H., Zhao, L., 2014. UV irradiation induced transformation of TiO_2 nanoparticles in water: Aggregation and photoreactivity. Environmental Science and Technology, 48, 11962-11968.

Suttiponparnit, K., Jiang, J., Sahu, M., Suvachittanont, S., Charinpanitkul, T., Biswas, P., 2011. Role of surface area, primary particle size, and crystal phase on titanium dioxide nanoparticle dispersion properties. Nanoscale Research Letters, 6, 27.

Uyguner, C.S., Bekbolet M., 2005a. Evaluation of humic acid photocatalytic degradation by UV-vis and fluorescence spectroscopy. Catalysis Today, 101, 267-274.

Uyguner, C.S., Bekbolet M., 2005b. Implementation of spectroscopic parameters for practical monitoring of natural organic matter. Desalination, 176, 47-55.

Uyguner, C.S., Bekbolet, M., 2007. Contribution of metal species to the heterogeneous photocatalytic degradation of natural organic matter. International Journal of Photoenergy, 23156, 1-8.

vanLoon, G.W., Duffy, S.J., 2000. Environmental Chemistry, Oxford University Press, Inc., New York.

Velev, O.D., Gupta, S., 2009. Materials fabricated by micro- and nanoparticle assembly. The challenging path from science to engineering. Advanced Materials, 21, 1897-1905.

Venkataraman, M., 2005. The effect of colloidal stability on the heat transfer characteristics of nanosilica dispersed fluids, M.Sc. Thesis, University of Central Florida, Orlando, Florida.

Wagoner, D.B., Christman, R.F., Cauchon, G., Paulson, R., 1997. Molar mass and size of Suwannee river natural organic matter using multi-angle laser light scattering. Environmental Science and Technology, 31, 937-941.

Wang, Y., 2000. Solar photocatalytic degradation of eight commercial dyes in TiO_2 suspension. Water Research, 34, 990-994.

Wang, G.S., Hsieh S.T., Hong C.S., 2000. Destruction of humic acid in water by UV light-catalyzed oxidation with hydrogen peroxide. Water Research, 34, 3882-3887.

Wang, P., Keller, A.A., 2009. Natural and engineered nano and colloidal transport: Role of zeta potential in prediction of particle deposition. Langmuir, 25, 12, 6856-6862.

Wang, P., Qi, N., Ao, Y., Hou, J., Wang, C., Qian, J., 2016. Effect of UV irradiation on the aggregation of TiO_2 in an aquatic environment: Influence of humic acid and pH. Environmental Pollution, 212, 178-187.

Wershaw, R.L., 1999. Molecular aggregation of humic substances. Soil Science, 164, 803-813.

Yalcin, Y., Kilic, M., Cinar, Z., 2010. Fe^{+3}-doped TiO_2: A combined experimental and computational approach to the evaluation of visible light activity. Applied Catalysis B: Environmental, 99, 469-477.

Young, C., Von Wandruszka, R., 2001. A Comparison of aggregation behavior in aqueous humic acids. Geochemical Transactions., 2001, 2.

Zhang, Q., Gao, L., Guo, J., 2000. Effects of calcination on the photocatalytic properties of nanosized TiO_2 powders prepared by $TiCl_4$ hydrolysis. Applied Catalysis B: Environmental, 26, 338-389.

Zhang, Y., Chen, Y., Westerhoff, P., Hristovski, K., Crittenden, J.C., 2008. Stability of commercial metal oxide nanoparticles in water. Water Research, 42, 2204-2212.

Zhao, T., Fang, M., Tang, Z., Zhao, X., Wu, F., Giesy, J.P., 2019. Adsorption, aggregation and sedimentation of titanium dioxide nanoparticles and nanotubes in the presence of different sources of humic acids. Science of the Total Environment, 692, 660-668.

Zhou, D., Abdel-Fattah, A.I., Keller, A.A., 2012. Clay particles destabilize engineered nanoparticles in aqueous environments. Environmental Science and Technology, 46, 7520-7526.

Zhou, D., Ji, Z., Jiang, X., Dunphy, D.R., Brinker, J., Keller, A.A., 2013. Influence of material properties on TiO_2 nanoparticle agglomeration. Plos One, 8, 11, e81239.

Zou, X-Y., Xu, B., Yu, C-P., Zhang, H-W., 2013. Imbalance between oxidative and antioxidative systems: Toward an understanding of visible light-induced titanium dioxide nanoparticles toxicity. Chemosphere, 93, 2451-2457.

APPENDIX A: PHYSICO-CHEMICAL AND MORPHOLOGICAL PROPERTIES OF NANOPARTICLES

Table A. Nanoparticle characterizations.

Photocatalyst	Band Gap Energy, eV	λ, nm	pH_{zpc}	Crystallite Size, nm	BET Surface Area, m^2g^{-1}	Reference
TiO_2	3.01	411	6.25	22.3	57.55	Birben et al., 2015
N-TiO_2	2.79	479	5.15	18.8	55.35	Birben et al., 2015
Fe-TiO_2	2.55	486	4.80	16.4	33.00	Birben et al., 2017

APPENDIX B: CHARACTERIZATION OF ORGANIC MATRIX

Table B. Specified and specific UV-vis spectroscopic parameters and NPOC of HA samples.

	Specified UV-vis parameters				NPOC, mg/L
HA	$Color_{436}$	UV_{365}	UV_{280}	UV_{254}	
initial	0.080	0.166	0.388	0.451	4.80
Photolysis	0.069	0.146	0.353	0.416	4.53
Photocatalysis					
TiO_2	0.001	0.002	0.011	0.013	1.12
N-TiO_2	0.023	0.058	0.149	0.175	1.92
Fe-TiO_2	0.039	0.105	0.279	0.341	5.08

	Specific UV-vis parameters, L/m mg				E2/E3	SFI
HA	$SCoA_{436}$	$SUVA_{365}$	$SUVA_{280}$	$SUVA_{254}$		
initial	1.67	3.45	8.08	9.41	2.71	1.17
Photolysis	1.52	3.22	7.79	9.18	2.85	1.08
Photocatalysis						
TiO_2	0.0892	0.179	0.981	1.16	6.50	1.25
N-TiO_2	1.21	3.02	7.76	9.11	3.01	1.24
Fe-TiO_2	0.768	2.07	5.49	6.71	3.24	1.11